Robert H. Cleveland
Edward Y. Lee
Editors

Imaging in Pediatric Pulmonology

Second Edition

Springer

Imaging in Pediatric Pulmonology

Robert H. Cleveland • Edward Y. Lee
Editors

Imaging in Pediatric Pulmonology

Second Edition

Springer

Editors
Robert H. Cleveland
Department of Radiology
Harvard Medical School Boston Children's Hospital
Boston, MA
USA

Edward Y. Lee
Department of Radiology
Harvard Medical School Boston Children's Hospital
Boston, MA
USA

ISBN 978-3-030-23978-7 ISBN 978-3-030-23979-4 (eBook)
https://doi.org/10.1007/978-3-030-23979-4

This Springer imprint is published by the registered company Springer Nature Switzerland AG
The registered company address is: Gewerbestrasse 11, 6330 Cham, Switzerland

Foreword

In pediatric radiology, whether in academic medical centers, or in private practice, the chest is the most frequently imaged part of the entire body. Millions of chest radiographs are taken across the country on infants and children, and read by radiologists of all levels of training, both in hospital and outpatient imaging sites. Adult radiologists are often called upon to read chest images from emergency departments or neonatal intensive care units. Most pediatric radiologists spend hours each week reading chest images, a task they will do their entire careers. As a result, having a well-grounded knowledge of pulmonary imaging in pediatrics is imperative for all image interpreters.

This updated text has taken on the challenge of providing this education. In the second edition of the book, *Imaging in Pediatric Pulmonology*, the authors cater to all possible readers. For general radiologists looking to enhance their knowledge of pediatric lung conditions, extensive information on neonatal conditions, pneumonia, and common diseases abounds. For pediatric radiologists who want to learn about rarer conditions, like plastic bronchitis, or who want to deepen their understanding of the complexities of pediatric pulmonary disease, chapters are there. The way in which the material is organized makes it easy to learn about conditions in a variety of ways. Cystic fibrosis, for instance, is discussed in its own chapter, but also in chapters on focal lung disease, interstitial lung disease, airway abnormalities, genetic lung conditions, lung transplantation, and others. This distribution of material throughout the book into carefully chosen disciplines allows readers with a specific bent to learn about disease processes in their contexts of interest.

Additionally, the authors have given readers detailed information about areas not typically covered. A whole chapter is dedicated to pleural effusions and pneumothoraces. Pulmonary lymphatic disorders, venous drainage conditions, pulmonary embolism, even "incidentalomas" – the list goes on and on. In this broad and extensive survey of pediatric lung diseases, the authors have truly provided a comprehensive reference that should be included in any radiology library.

Dr. Robert H. Cleveland, whose career has been dedicated to pulmonary imaging, both at Massachusetts General Hospital and Boston Children's Hospital, by this work, continues to enhance his legacy. The addition of Dr. Edward Y. Lee, a colleague at Boston Children's Hospital, and an acclaimed author and speaker on pediatric lung imaging, only adds to the prestige of this book. New images, new techniques, and new explanations abound throughout the revised text. Truly, reviewing this updated addition to *Imaging in Pediatric Pulmonary*, was an honor and an education.

Atlanta, GA, USA

Stephen F. Simoneaux, MD, FACR

Preface

Since the publication of the prior edition of this book, many advances have occurred in the performance of computed tomography (CT) and magnetic resonance imaging (MRI). For CT, examination performance times have diminished significantly, greatly enhancing the ability to perform CT on unsedated children. Possibly more important to pediatric practice, the radiation doses of CT have been significantly reduced. However, the concern of lifetime exposure to ionizing irradiation remains paramount, and therefore, the use of CT should be limited to instances where no other viable choice is available. MRI procedure times have also been shortened and resolution improved. Although this makes MRI a viable alternative or preferable imaging choice for questions of larger structures such as the central airway, cardiovascular system, lung parenchyma, and chest wall, it is still not able to accurately depict the smaller airways.

Consequently, this new edition again focuses on plain film imaging as well as advanced imaging. The material, in some instances, has been reorganized. In addition, there are three new chapters specifically addressing pediatric pulmonary embolism, thoracic MRI, and the genetics of pediatric pulmonary disorders.

The overall organization of the book remains the same with an initial chapter of clinical algorithms for the most common clinical scenarios presenting to pediatric pulmonologists or pediatricians. The branch points in the algorithms serve as references to diseases discussed elsewhere in the book. There are again several chapters dedicated to specific topics such as lung transplantation and fetal imaging.

Rather than assuming a priori knowledge or suspicion of the diagnosis, this text can lead the reader to a differential diagnosis based on clinical parameters and thus direct reading to the relevant diagnoses. If the readers know their topic of interest, the chapters are organized for easy access to a broad range of abnormalities. While radiologists may find this a new approach in organization of a textbook, clinicians hopefully find it a “user-friendly” imaging resource.

I would be remiss if I did not acknowledge, with much gratitude, the encouragement and assistance of the members of the New England Pulmonary Consortium who have been so much a part of my development as a pediatric pulmonary imager over the almost 40 years of our association.

Boston, MA, USA — Robert H. Cleveland

Acknowledgments

For this, the second edition of *Imaging in Pediatric Pulmonology*, I again would like to thank the members of the New England Pediatric Pulmonary Consortium for their nearly 40 years of friendship, teaching, and camaraderie. They have been the inspiration for this book.

Special thanks go to the many authors who have contributed to this second edition, both new and those who contributed previously. I am also deeply in debt to Dr. Ed Lee who has graciously provided his time and talent as coeditor for this edition.

The preparation of this edition has changed somewhat from the original textbook. As a part of this change, the editorial responsibilities have been assumed by my coeditor, Ed Lee, and myself. This does not diminish the tremendous gratitude I owe to the original associate editors, Claire Langston, Andrew Colin, and Ed Lee, or the assistant editor, Mei Mei Chow. I would also like to thank the several chapter authors of the original text who were not able to participate in this second edition.

Finally, I want to express sincere appreciation to all my clinical and imaging colleagues at the Massachusetts General Hospital and Boston Children's Hospital with whom it has been such a pleasure to work over the course of my career.

Bob Cleveland
Harvard Medical School
Boston, MA, USA
January 2019

Words cannot express my gratitude and appreciation to Dr. Bob Cleveland, a true pioneer in pediatric pulmonary imaging, who has been a main teacher and mentor for my career as an academic radiologist specialized in pediatric pulmonary imaging at Boston Children's Hospital.

Through this book, it is truly a great honor for me to be able to be a part of continuing Dr. Cleveland's lifelong dedication to academic radiology, enthusiasm for advancing the field of pediatric pulmonary imaging, and contribution to teaching and spreading his knowledge to others for pediatric patient care.

In addition, I would also like to acknowledge the trainees and clinicians that I have met during my academic career for sharing their enthusiasm for learning and the young patients of Boston Children's Hospital who always enlighten and remind us of the importance of advancing the field of pediatric pulmonary imaging.

Edward Y. Lee
Harvard Medical School
Boston, MA, USA
January 2019

Contents

Contributors

Mohammad Amarneh, MD Department of Pediatric and Interventional Radiology, University of Iowa Carver College of Medicine, Iowa City, IA, USA

Dorothy Bulas, MD Department of Diagnostic Imaging and Radiology, George Washington University Medical Center, Children's National Medical Center, Washington, DC, USA

Thomas Carraway, MD Department of Radiology, Maine Medical Center, Portland, ME, USA

Alicia Casey, MD Division of Pulmonary Medicine, Boston Children's Hospital, Harvard Medical School, Boston, MA, USA

Marilynn Chan, MD Department of Pediatric Pulmonology, University of California San Francisco Medical Center, San Francisco, CA, USA

Gulraiz Chaudry, MBChB, MRCP, FRCR Department of Radiology, Boston Children's Hospital and Harvard Medical School, Boston, MA, USA

Giuseppe Cicero, MD Department of Radiology and Nuclear Medicine, Sophia Children Hospital – Erasmus Medical Center, Rotterdam, The Netherlands

Department of Biomedical Sciences and Morphological and Functional Imaging, University of Messina, Messina, Italy

Pierluigi Ciet, MD, PhD Department of Radiology and Nuclear Medicine, Sophia Children Hospital – Erasmus Medical Center, Rotterdam, The Netherlands

Robert H. Cleveland, MD Department of Radiology, Harvard Medical School, Boston Children's Hospital, Boston, MA, USA

Anne C. Coates, MD Department of Pediatrics, Stanford School of Medicine/Lucille Packard Children's Hospital, Palo Alto, CA, USA

Andrew A. Colin, MD Miller School of Medicine, University of Miami, Miami, FL, USA

Alexia Egloff, MD Department of Radiology, Children's National Medical Center, Washington, DC, USA

Mary Shannon Fracchia, MD Department of Pediatric Pulmonary, Massachusetts General Hospital, Harvard Medical School, Boston, MA, USA

Charles K. Grimes, MD Department of Radiology, Maine Medical Center, Portland, ME, USA

Megan H. Hawley, MS, CGC Pediatric Pulmonary Division, Massachusetts General Hospital for Children, Boston, MA, USA

Monica Kahye Johnson, MD Department of Radiology, Harvard Medical School and Massachusetts General Hospital, Boston, MA, USA

Umakanth Katwa, MD Boston Children's Hospital and Harvard Medical School, Boston, MA, USA

T. Bernard Kinane, MD Pediatric Pulmonary Division, Massachusetts General Hospital for Children, Boston, MA, USA

Stella Kourembanas, MD Department of Newborn Medicine, Boston Children's Hospital, Boston, MA, USA

Katie Krone, MD Division of Pulmonary Medicine, Boston Children's Hospital, Harvard Medical School, Boston, MA, USA

Jason E. Lang, MD Division of Allergy, Immunology and Pulmonary Medicine, Duke University School of Medicine, Durham, NC, USA

Duke Children's Pulmonary Function Laboratory, Duke Clinical Research Institute, Duke Children's Health & Discovery Institute, Durham, NC, USA

Edward Y. Lee, MD, MPH Department of Radiology, Boston Children's Hospital and Harvard Medical School, Boston, MA, USA

Jonathan C. Levin, MD Department of Newborn Medicine and Respiratory Disease, Boston Children's Hospital, Boston, MA, USA

Mark C. Liszewski, MD Department of Radiology, Division of Pediatric Radiology, Montefiore Medical Center, Bronx, NY, USA

Raymond Liu, MD, FSIR Department of Radiology, Massachusetts General Hospital, Boston, MA, USA

Peter P. Moschovis, MD, MPH Pediatric Pulmonary Division, Massachusetts General Hospital for Children, Boston, MA, USA

Kara E. May, MD Department of Medicine, Division of Respiratory Diseases, Boston Children's Hospital and Harvard Medical School, Boston, MA, USA

Sanjay P. Prabhu, MBBS, FRCR Department of Radiology, Boston Children's Hospital and Harvard Medical School, Boston, MA, USA

Annabelle Quizon, MD Department of Respiratory Medicine, University of California San Diego- Rady Children's Hospital, San Diego, CA, USA

Dennis Rosen, MD Division of Pulmonary Medicine, Boston Children's Hospital and Harvard Medical School, Boston, MA, USA

Efraim Sadot, MD Department of Pediatric Intensive Care, Dana-Dwek Children's Hospital, Tel-Aviv Sourasky Medical Center and Sackler Faculty of Medicine, Tel-Aviv University, Tel Aviv-Yafo, Israel

Pallavi Sagar, MD Department of Radiology, Harvard Medical School and Massachusetts General Hospital, Boston, MA, USA

Ashraf Thabet, MD Department of Interventional Radiology, Massachusetts General Hospital, Harvard Medical School, Boston, MA, USA

Frédéric Thomas-Chaussé, MD FRCPC Department of Radiology, Radiation Oncology and Nuclear Medicine, University of Montreal, CHU Sainte-Justine, Montréal, QC, Canada

Gary Visner, DO Boston Children's Hospital, Harvard Medical School, Boston, MA, USA

Abbey J. Winant, MD, MFA Department of Radiology, Boston Children's Hospital and Harvard Medical School, Boston, MA, USA

Lael M. Yonker, MD Pediatric Pulmonary Division, Massachusetts General Hospital for Children, Boston, MA, USA

Clinical Algorithms

1

Dennis Rosen, Jason E. Lang, and Andrew A. Colin

Introduction

In medical practice, patients often present without a known diagnosis. Physicians move from a set of signs and symptoms to the formation of a differential diagnosis to a final diagnosis. This introductory chapter provides seven clinical algorithms that encompass a large part of the spectrum of pediatric pulmonary practice. By navigating through the appropriate algorithm, reference to possible relevant diagnoses may be encountered which will provide direction to further reading in the textbook.

The algorithms are as follows:

- Chest pain
- Chronic cough
- Cyanosis/hypoxia
- Shortness of breath
- Airway bleeding
- Noisy breathing
- Tachypnea

Chest Pain

See Fig. 1.1.

Chronic Cough

See Fig. 1.2.

Cyanosis and Hypoxia

Cyanosis is often associated with hypoxia, but the two do not always coexist (Fig. 1.3). *Acrocyanosis* is commonly associated with vasoconstriction, whereas *central cyanosis* is most often found in the perioral area and is reflective of at least 5 g/% of unsaturated hemoglobin. This can result from different causes, which will be reviewed systematically. In general, it is helpful to consider the causative mechanism of the cyanosis. These different mechanisms may include:

- Shunting of *blue* deoxygenated blood from the venous circulation to the arterial circulation, bypassing the alveolar capillary network
- Intrapulmonary shunting
- Ventilation/perfusion (V/Q) mismatching
- Inadequate ventilation
- Inadequate gas exchange at the level of the alveolus (diffusion defects)
- Inadequate bonding of O_2 to the red blood cells (hematologic causes)
- Inadequate perfusion

Shunting of blood can occur on many levels, primarily the heart, lung, and peripheral circulation. Cardiac causes may include cardiac malformations with right-to-left shunting, including primary heart lesions with right-to-left shunting (tetralogy of Fallot, transposition of great arteries, truncus arteriosus, pulmonic stenosis/atresia, aortic stenosis, Ebstein's anomaly, and hypoplastic left heart), and with lesions associated with pulmonary hypertension (either primary or secondary to increased pulmonary flow such as in Eisenmenger's syndrome), persistent fetal circulation, breath holding, and shunting through a patent foramen ovale.

D. Rosen (✉)
Division of Pulmonary Medicine, Boston Children's Hospital and Harvard Medical School, Boston, MA, USA
e-mail: Dennis.Rosen@childrens.harvard.edu

J. E. Lang
Division of Allergy, Immunology and Pulmonary Medicine, Duke University School of Medicine, Durham, NC, USA

Duke Children's Pulmonary Function Laboratory, Duke Clinical Research Institute, Duke Children's Health & Discovery Institute, Durham, NC, USA

A. A. Colin
Miller School of Medicine, University of Miami, Miami, FL, USA

R. H. Cleveland, E. Y. Lee (eds.), *Imaging in Pediatric Pulmonology*, https://doi.org/10.1007/978-3-030-23979-4_1

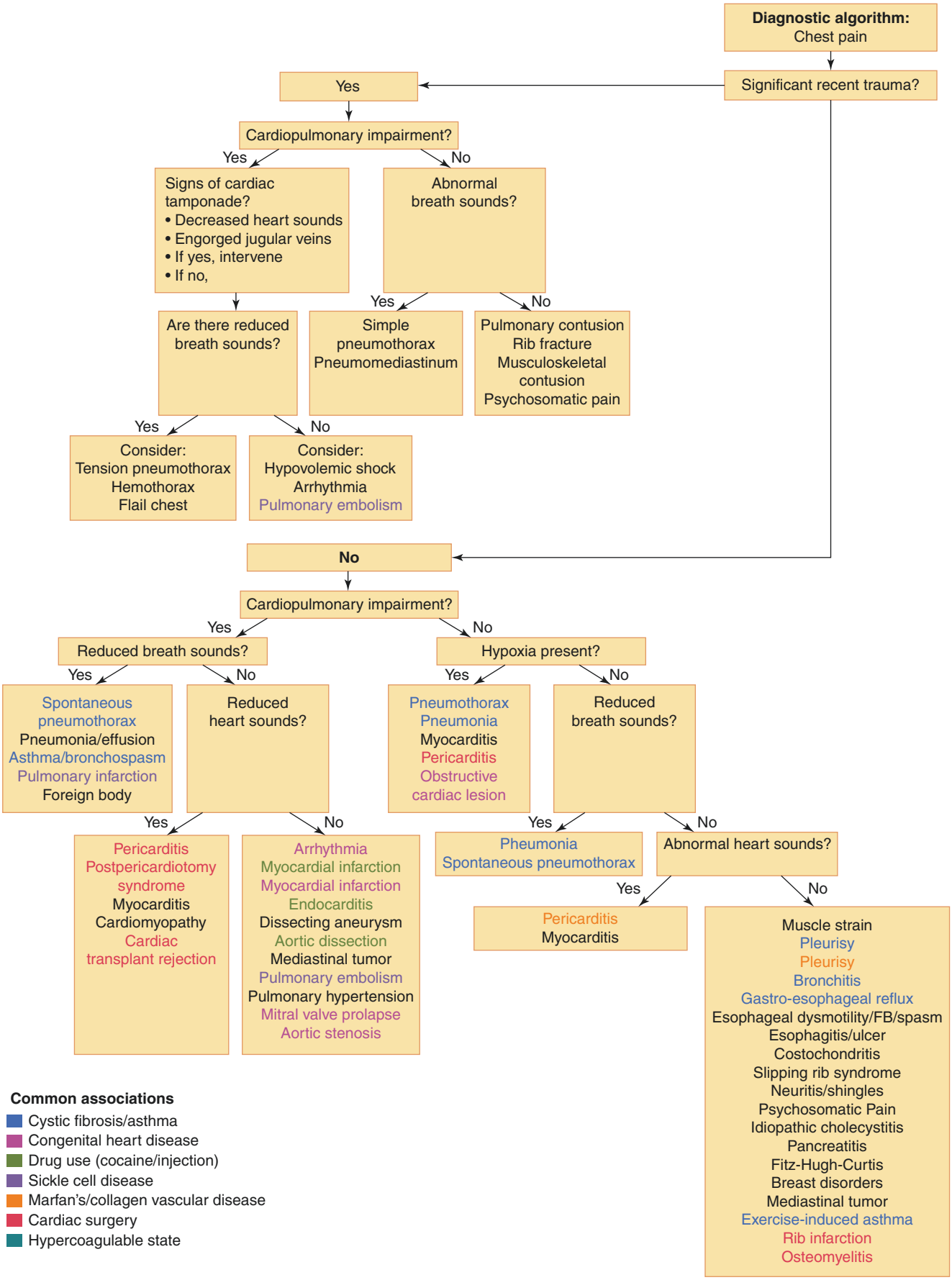

Fig. 1.1 Chest pain

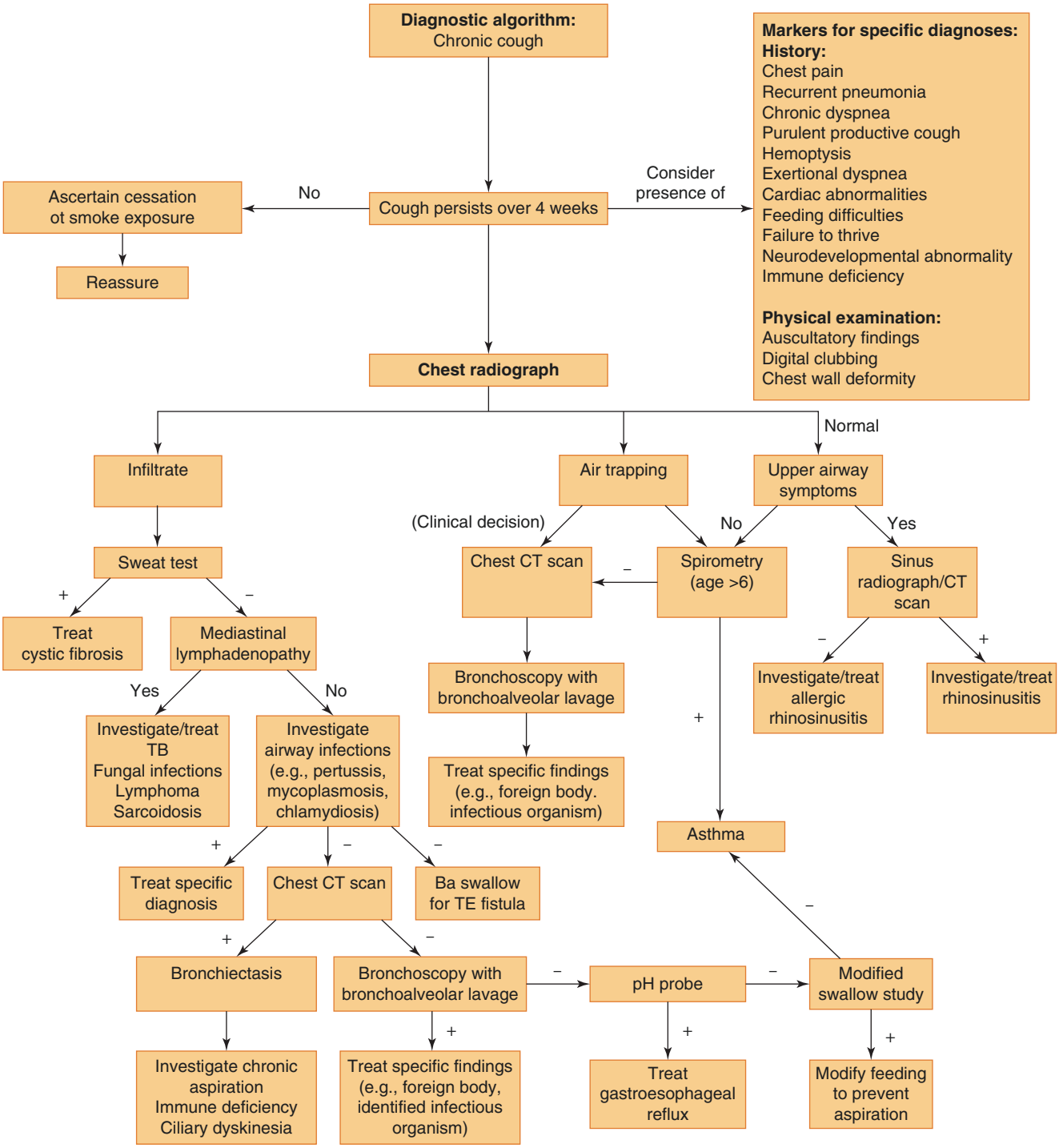

Fig. 1.2 Chronic cough

V/Q mismatching, in which there is good perfusion of under-ventilated lung, may occur with foreign body aspiration, in mucus plugging, atelectasis, in pneumonia with a large infiltrate, bronchiolitis, and pulmonary hemosiderosis. It is seen in cases of arteriovenous malformations (AVM), either primary or in the setting of liver failure and the hepatopulmonary syndrome. It can also be seen in restrictive lesions such as pneumothorax, pleural effusion, pulmonary fibrosis, pulmonary hemosiderosis, meconium aspiration, and respiratory distress syndrome (RDS) in neonates.

At the other end of the V/Q mismatching spectrum, in which there is under-perfusion of well-ventilated lung, may be found pulmonary emboli, pulmonary hypertension, and hyperinflative states such as asthma, bronchiolitis, and congenital lobar emphysema.

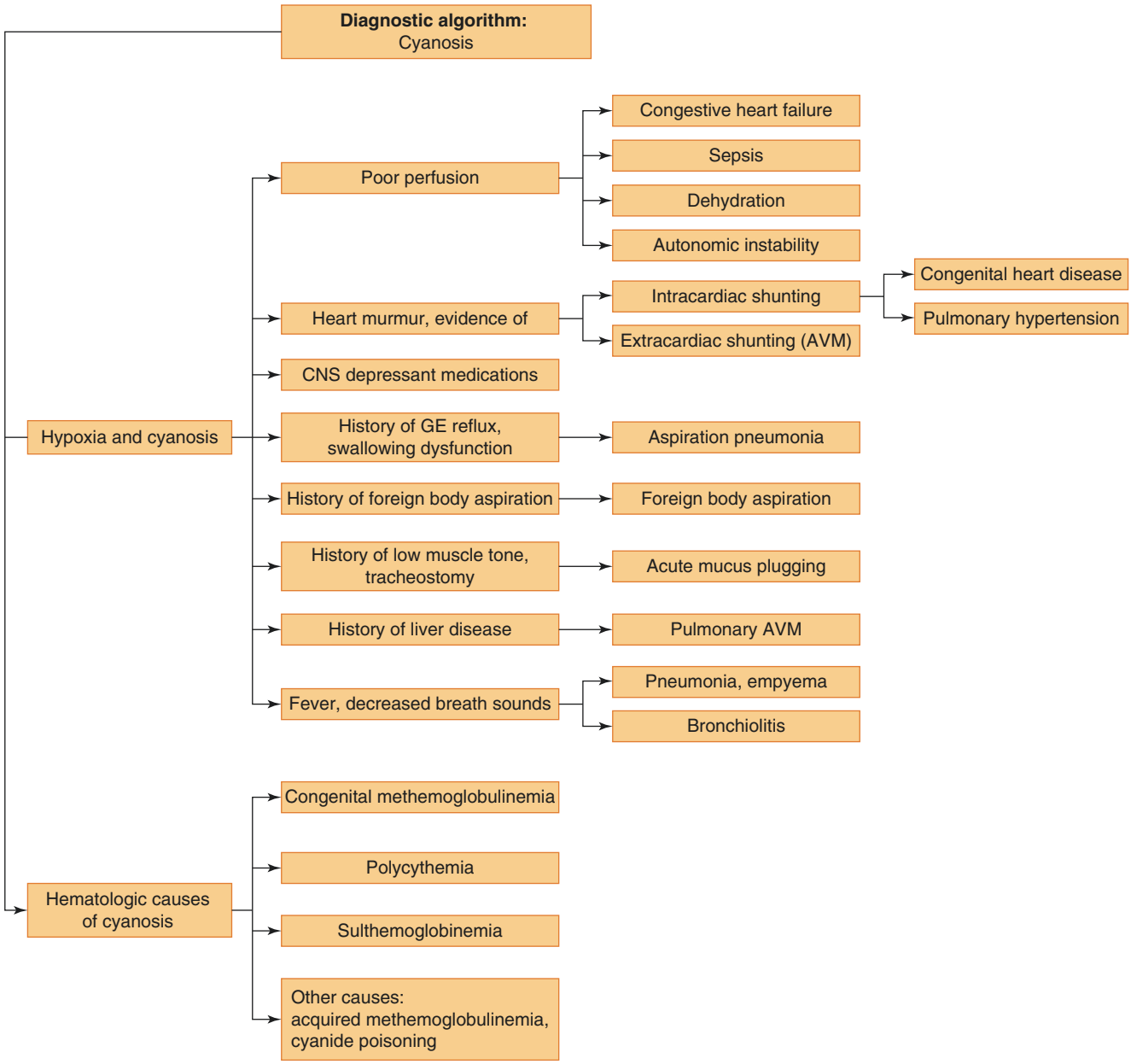

Fig. 1.3 Cyanosis

Inadequate ventilation may also result from restrictive defects such as pneumothorax, ribcage abnormalities, scoliosis, kyphosis, abdominal distention, and obesity, central control of breathing disorders such as congenital alveolar hypoventilation syndrome, and neuromuscular diseases such as muscular dystrophy, Werdnig–Hoffman, diaphragmatic paralysis, polio, and Guillain Barré. Obstructive processes such as nasal obstruction, retropharyngeal abscesses, tonsillar hypertrophy, severe croup, laryngeal webs, foreign body aspiration, obstructive sleep apnea, and hypoventilation syndrome. CNS depressant medications may also inhibit the respiratory drive.

Diffusion defects are caused by interstitial processes such as interstitial lung disease (ILD), bronchopulmonary dysplasia (BPD), pulmonary edema, hypersensitivity pneumonitis, and adult respiratory distress syndrome (ARDS).

Hematologic causes of cyanosis may include methemoglobinemia, either acquired (medication or nitrite ingestion) or congenital, polycythemia, and sulfhemoglobinemia. These are nonhypoxemic and can be distinguished by measurement of blood PaO_2 levels.

Poor perfusion leading to cyanosis may be cardiac in origin, stemming from congestive heart failure (primary, postischemia, secondary to myocarditis, arrhythmias, heart block, and pericarditis) or systemic causes, including shock, sepsis, autonomic instability, and medication effect.

Shortness of Breath

See Fig. 1.4.

Airway Bleeding

See Fig. 1.5.

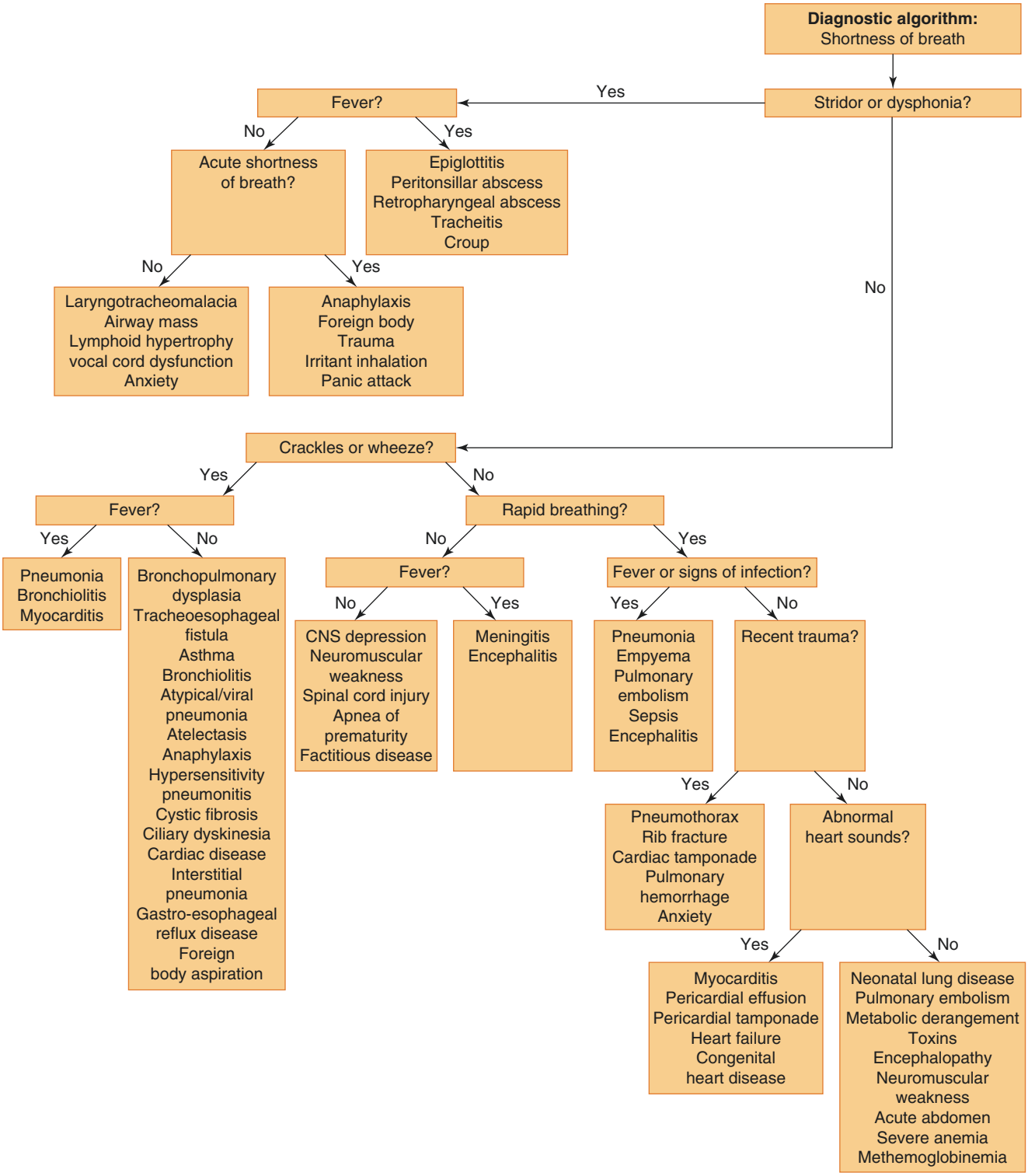

Fig. 1.4 Shortness of breath

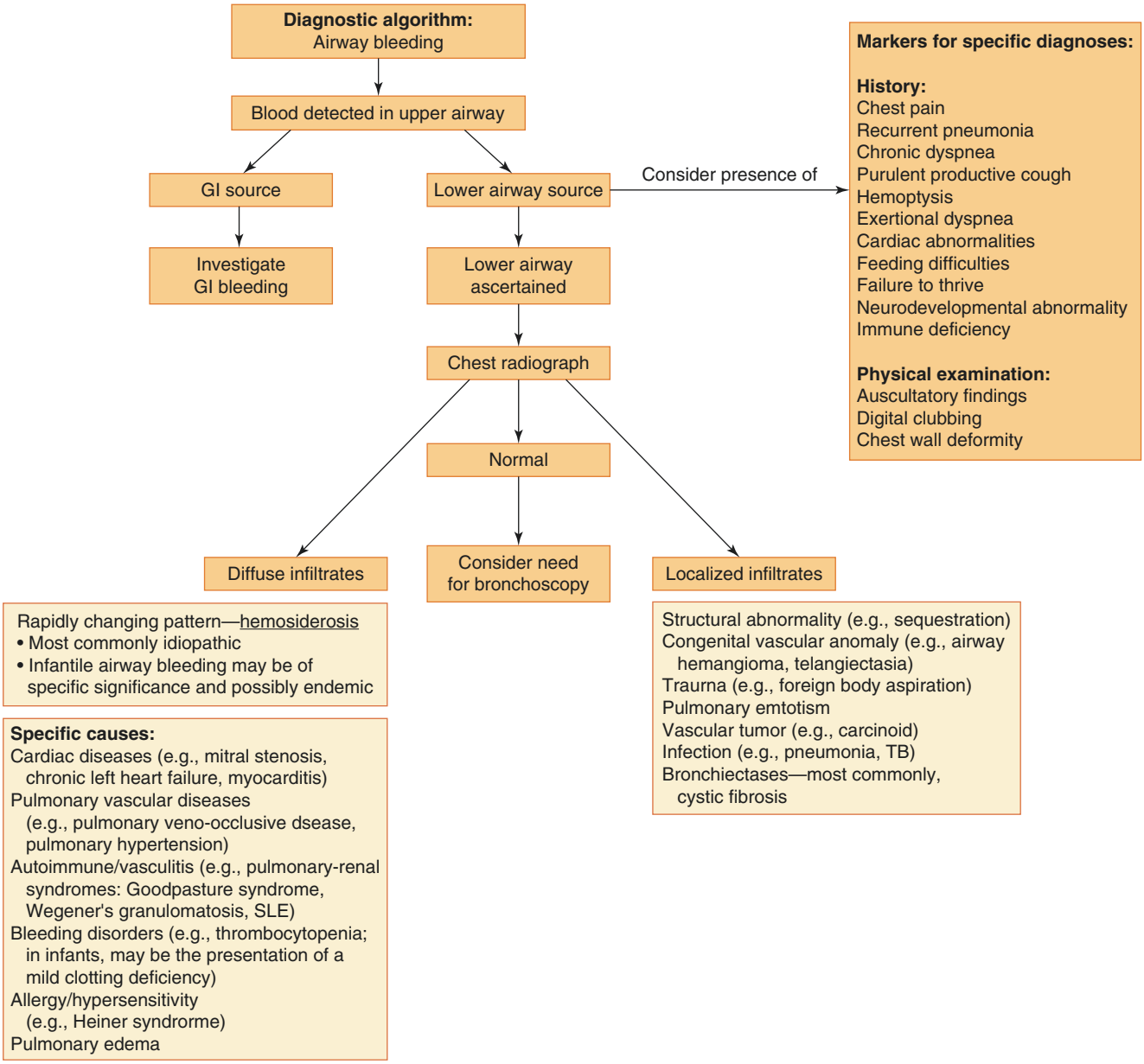

Fig. 1.5 Airway bleeding

Noisy Breathing

See Fig. 1.6a–c.

Tachypnea

Tachypnea is defined as a respiratory rate above the age-appropriate range, measured while the child is at rest (Fig. 1.7). The emphasis on age appropriateness is important, as infants may have resting respiratory rates ranging 30–60 breaths per minute, whereas children over the age of 2 will generally have resting respiratory rates ranging between 16 and 24 breaths per minute. This may be explained by a variety of factors, principal among which is the relatively high chest wall compliance of infants and toddlers, which decreases as children advance in age. Tachypnea may be a sign of an underlying disorder and in most cases represents an attempt by the body to improve gas exchange. It is detrimental as it results in increased energy expenditure, thus diverting calories away from other tasks such as growth. It may result in metabolic derangements, such as hyperventilation and respiratory alkalosis, and is difficult to sustain for a prolonged period of time because of progressive muscle fatigue. When caring for a child with tachypnea, it is important to identify and treat the underlying cause so as to prevent progression to respiratory failure.

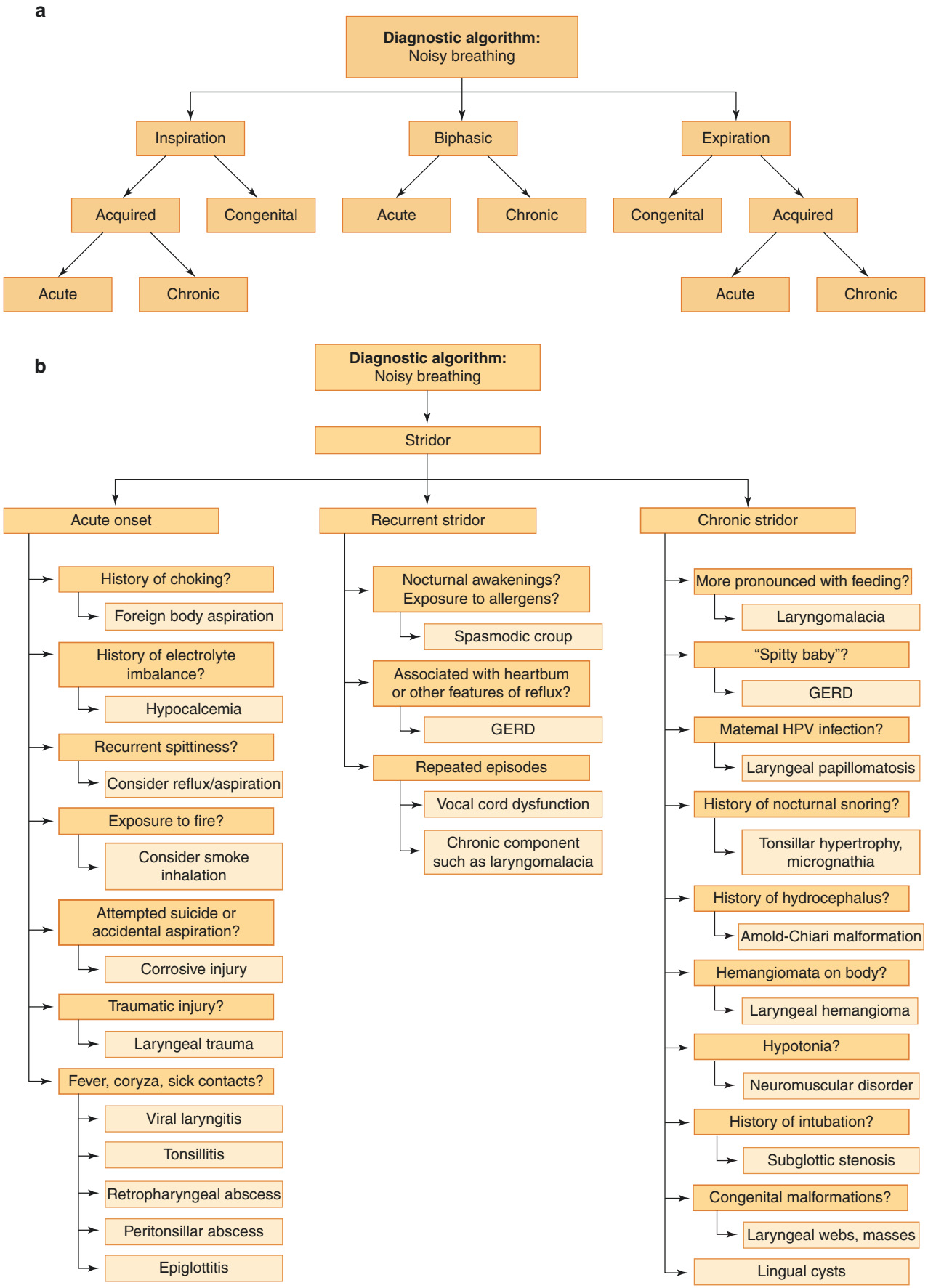

Fig. 1.6 Noisy breathing

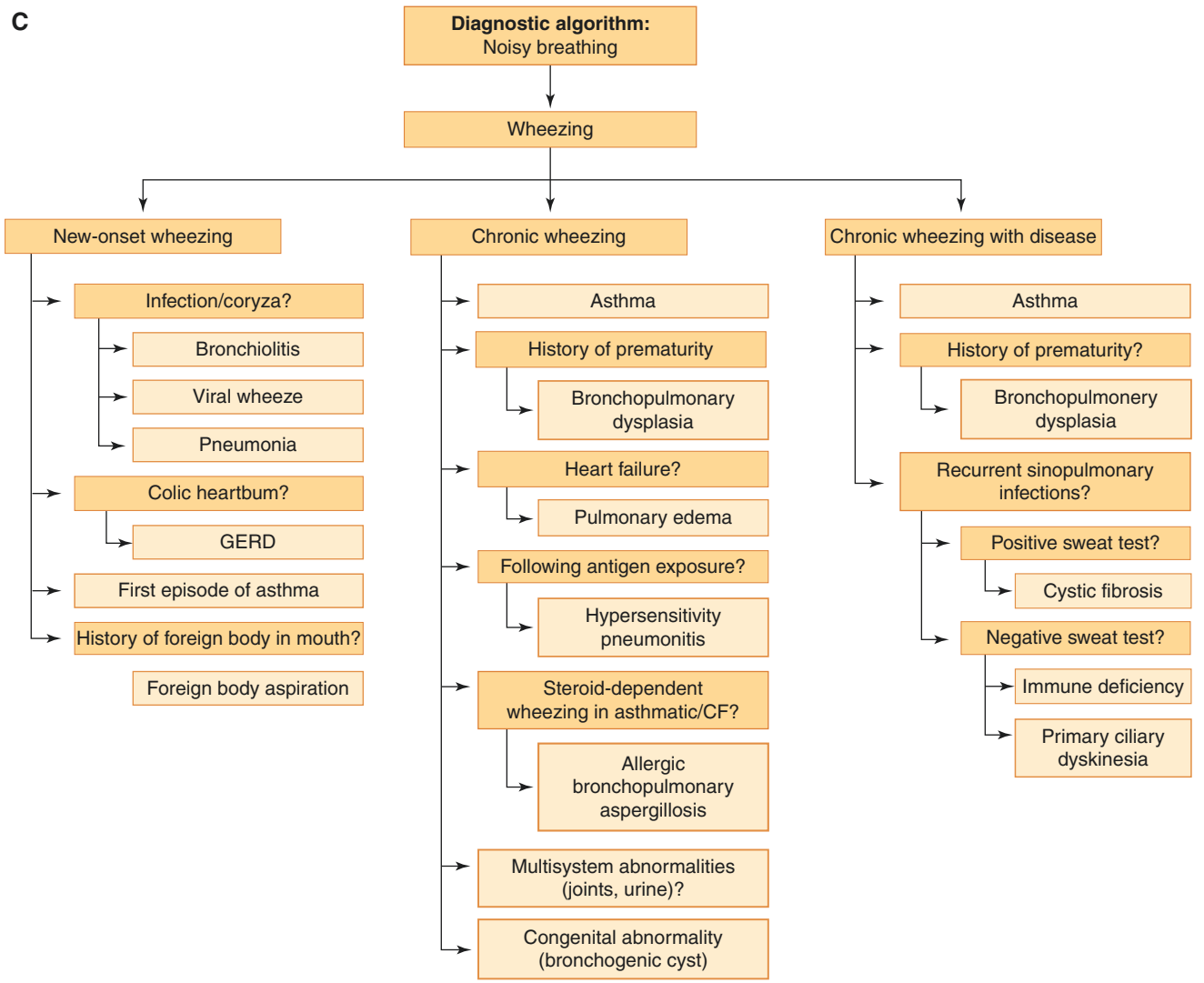

Fig. 1.6 (continued)

Causes of Tachypnea

There is a broad differential diagnosis for a child with tachypnea, encompassing not just pulmonary causes but also systemic, psychological, neurological, cardiac, and metabolic causes which are, for the most part, beyond the purview of this book.

Psychological

Emotional stress or anxiety can provoke tachypnea, often accompanied by hyperventilation, sometimes resulting in metabolic alkalosis and tetany.

Systemic

Pain and fever are both non-pulmonary causes of tachypnea. Poor perfusion accompanied by hypotension (such as in the case of dehydration or sepsis) can also lead to tachypnea, both as a compensatory mechanism to correct developing metabolic acidosis and as an attempt to improve oxygen delivery to end organs and tissues.

Metabolic

Both hypoxia and hypercarbia can increase the respiratory drive. Hypoxia may result from a decrease in the partial pressure of inspired oxygen, such as occurring at high altitudes, or from one or more of many pulmonary processes, which will be discussed shortly. Even when the intake and transport of oxygen are normal, in severe anemia, one can have a decrease in oxygen delivery to end organs and tissues and subsequently an increased respiratory rate.

There are many inborn errors of metabolism which can also bring about an increased basal respiratory rate, including urea cycle defects, methylmalonic acidemia, and isovaleric acidemia, to name but a few.

Acquired metabolic acidosis can induce hyperventilation with tachypnea as an attempt to correct the acidosis by increas-

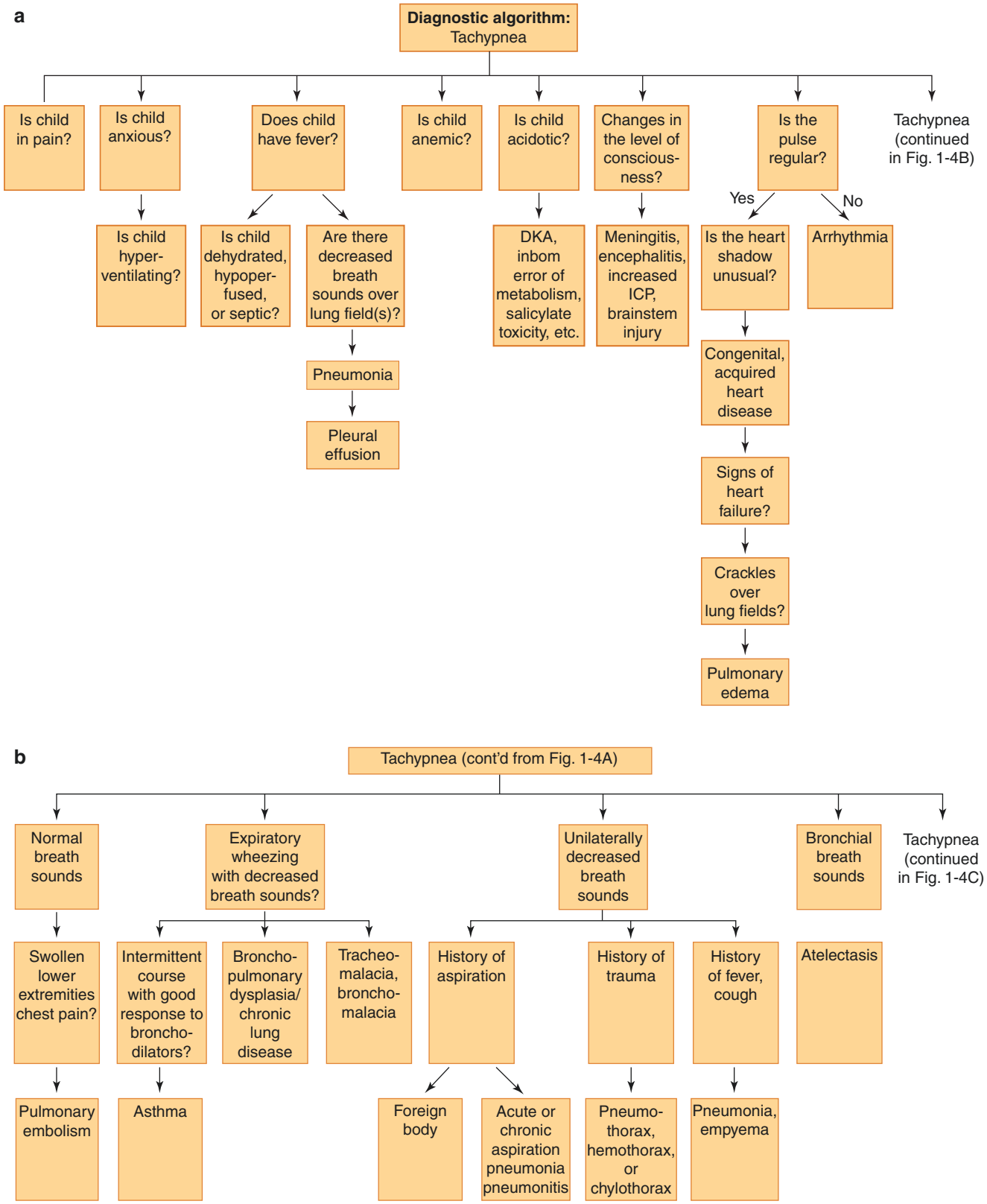

Fig. 1.7 Tachypnea

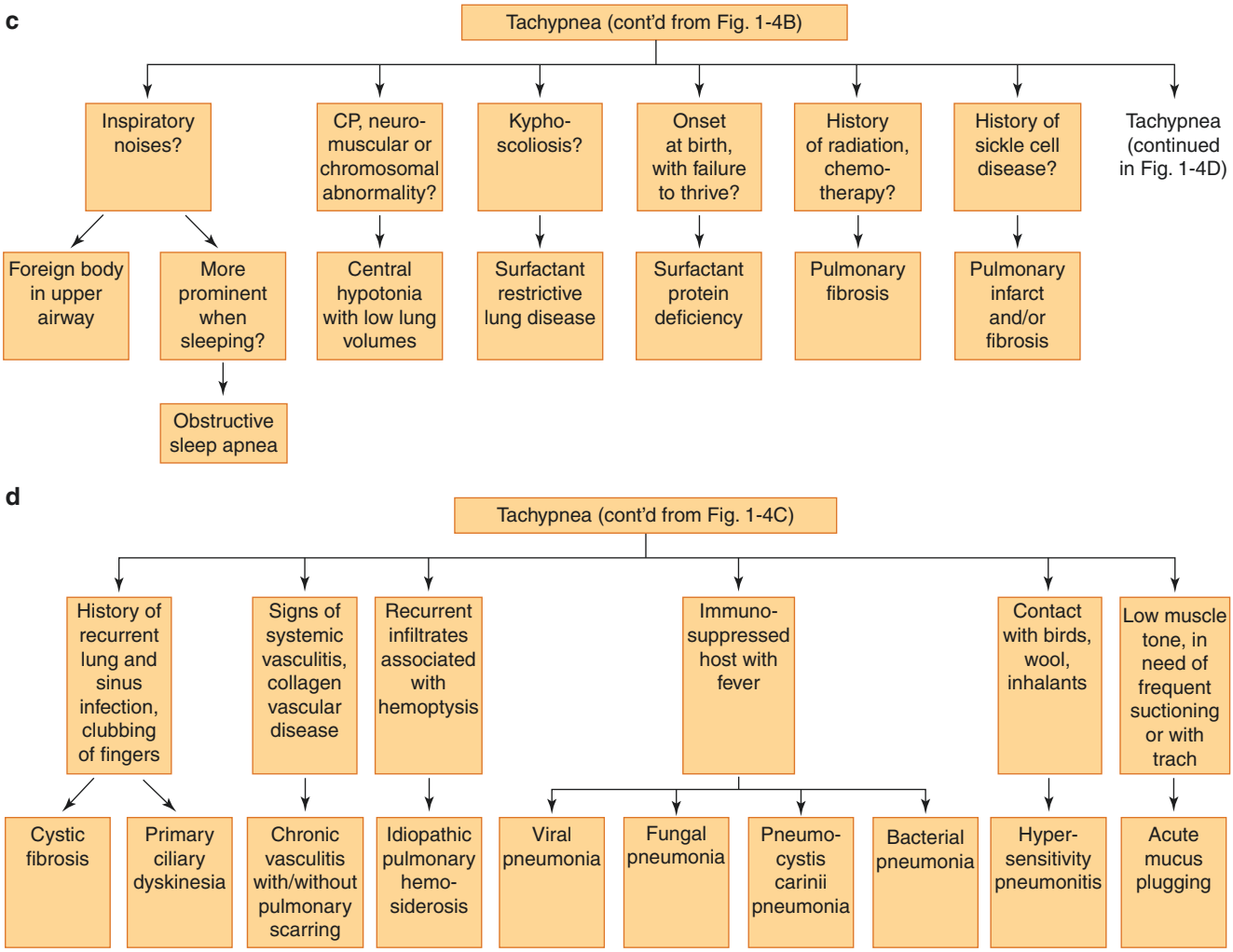

Fig. 1.7 (continued)

ing the clearance of CO_2 from the body, as described earlier. Causes of this include diabetic ketoacidosis, lactic acidosis, uremia, salicylate poisoning, dehydration, and sepsis.

Cardiac

Heart failure may cause tachypnea, either secondary to fluid accumulation in the lungs, such as in the case of pulmonary edema, or because of poor perfusion due to myocardial dysfunction. The presence of an irregular, weak, or rapid pulse, a murmur on physical exam, pulmonary edema, or an enlarged or abnormally shaped heart on chest X-ray should prompt a closer investigation of the heart and its function.

Neurological

Changes in intracranial pressure, encephalitis, and stroke are all recognized causes of tachypnea and should be considered in the context of the child's illness and presentation.

Pulmonary

Many types of pulmonary disease result in tachypnea because of a decrease in the proportion of tidal volume taking part in active gas exchange. In order to maintain minute ventilation, the respiratory rate needs to be increased. This can occur in obstructive processes, with air trapping; in restrictive processes, when the vital capacity is reduced, with the dead-space volume decreasing, remaining the same, or increasing; and in diffusion defects, when the amount of oxygen with any given breath traversing the alveolar membrane decreases. In cases of V/Q mismatching, such as pulmonary embolus, where tachypnea is one of the most common presenting signs, this is a result of the increase in functional dead space. Tachypnea also occurs in shunting, when a portion of the blood flow through the lungs is not exposed to the inspired air, resulting in hypoxemia, which in turn triggers a heightened respiratory drive.

Obstructive Processes

Obstructive processes can be subdivided into upper and lower airway obstruction, which refer to the location of the obstruction relative to the thoracic inlet. Examples of upper airway obstruction include acute laryngitis, foreign body aspiration, laryngomalacia, and obstructive sleep apnea. Lower airway obstruction may result from acute processes such as acute aspiration, or asthma exacerbation, and from chronic processes such as cystic fibrosis, bronchiectasis, bronchomalacia, tracheomalacia, BPD, chronic lung disease of prematurity, and chronic aspiration.

Restrictive Lung Disease

Restrictive lung disease may result from physical restriction of the lungs' capacity to insufflate, such as occurring chronically with kyphoscoliosis, neuromuscular disease, central hypotonia (in Down syndrome, Prader-Willi syndrome, other chromosomal disorders, and cerebral palsy), meningomyelocele, and congenital chest wall abnormality. It can be the result of an acute process that leads to physical restriction of the lungs' capacity to insufflate, such as chest wall injury, pneumo/hemo/chylothorax, or pleural effusion. It can also be the result of fibrosis of the lungs that occurs during the recovery phase from acute lung injury, such as radiation or drug injury, or pulmonary infarction secondary to pulmonary vascular disease, such as occurring with sickle cell disease. Fibrosis can also be caused as the result of chronic inflammation, such as is caused by some collagen vascular diseases.

Reversible Shunting

Reversible shunting may occur with atelectasis, which can result from mucus plugging, foreign body aspiration, and asthma. It can also occur in lobar pneumonia and pulmonary hemosiderosis. Chronic shunting can occur on the cardiac level, or the pulmonary level, via AVMs, which can be either congenital or acquired, such as in the case of the hepatopulmonary syndrome.

Diffusion Defects

Diffusion defects, stemming from ILD, can be acute processes, such as in the case of infectious pneumonitis, caused by viruses, fungi, or PCP, hypersensitivity pneumonitis, or chronic aspiration. Acute ILD can also be caused by radiation or drug injury. Pulmonary edema, which can be caused by a number of mechanisms, such as cardiogenic, neurologic, or postobstructive, will also reduce diffusion capacity and thus lead to tachypnea.

Normal Growth and Physiology

2

Andrew A. Colin and Dennis Rosen

Overview of Respiratory Physiology

In analyzing a chest radiograph, it is important to have an understanding of some of the basic principles of respiratory physiology and to appreciate how certain pathophysiological processes can cause distinct disease states, each with its own specific clinical signs and symptoms [1, 2]. These can be divided into broad categories, which include obstructive lung disorders, restrictive lung disorders, disorders of gas diffusion, shunts, and ventilation-perfusion abnormalities. The following is a short overview of the physiologic considerations of these complex disorders. For more detail, the reader is advised to refer to the references below.

Obstructive Lung Disorders

Obstructive lung disorders affect the conducting airways and result from increased resistance to airflow within the airways and/or increased compliance of the airways. These disorders can be diffuse or localized. They can be caused by the presence of congenitally narrowed bronchi, scarred bronchi (such as in postinfectious bronchiolitis obliterans), intraluminal lesions, debris, or secretions (such as in acute bronchiolitis), dynamic airway wall changes leading to increased resistance to airflow as seen with bronchoconstriction or increased compliance as is seen in bronchomalacia or bronchiectasis, and extraluminal compression by a blood vessel or mass. Depending upon which segment of the conducting airways the obstruction is located in, the mechanism involved, and its severity, different phases of the respiratory cycle can be affected. Extrathoracic obstruction primarily causes problems in the inspiratory phase (stridor), though the expiratory phase can be affected as well, and intrathoracic obstruction will cause predominantly expiratory abnormalities (though here too, the wheezing, inspiratory phase can be affected). The underlying mechanism of this variable behavior is that during inspiration, negative intrathoracic pressure is generated by the inspiratory muscles, drawing air and the walls of the extrathoracic airways inward while the intrathoracic airways expand. During expiration, positive pressure is generated within the chest, propelling air outward, narrowing the intrathoracic airways lumina, and expanding the extrathoracic airways. When intrathoracic obstruction is significant enough to cause inhomogeneity in the rate of emptying in some or many parts of the lung, the chest radiograph shows hyperinflation and air trapping. Examples of common diffuse obstructive lung disorders include asthma, cystic fibrosis (CF), bronchiolitis obliterans, bronchiectasis, and bronchopulmonary dysplasia. A bronchial foreign body represents a localized obstructive defect. Spirometry, which measures airflow, can quantify the degree of obstruction and is the standard pulmonary function test.

Restrictive Lung Disorders

Restrictive lung disorders occur when the lungs are unable to inflate to normal volumes. They can occur with congenital or acquired loss of lung mass (e.g., agenesis of the lung or lobectomy/pulmonectomy, respectively) and parenchymal abnormalities, such as interstitial lung disease (idiopathic or secondary to an underlying disorder, such as a surfactant protein deficiency). They can also be caused by a musculoskeletal or neuromuscular abnormality which prevents the chest wall from expanding to full capacity during a maximal inspiratory effort. Examples of this type of restrictive process include congenital myopathies and neuromuscular disorders (such as spinal muscular atrophy) and more rarely diseases affecting the diaphragm. Bony chest wall abnormalities (such as thoracic dysplasia and scoliosis) inhibit lung

A. A. Colin
Miller School of Medicine, University of Miami, Miami, FL, USA

D. Rosen (✉)
Division of Pulmonary Medicine, Boston Children's Hospital and Harvard Medical School, Boston, MA, USA
e-mail: Dennis.Rosen@childrens.harvard.edu

R. H. Cleveland, E. Y. Lee (eds.), *Imaging in Pediatric Pulmonology*, https://doi.org/10.1007/978-3-030-23979-4_2

growth and expansion, as do intrathoracic space occupying processes (such as a diaphragmatic hernia, large pleural effusion, or tumor). The chest radiograph may show reduced lung volumes, albeit this may be difficult to pick up in the young child with a limited inspiratory effort. More obvious are distorted or bell-shaped chest walls (e.g., Jeune syndrome), scoliosis, or an abnormally diffuse parenchymal process, depending upon the underlying disorder. Physiologic assessment of these disorders is made by thoracic gas volumes measurement using plethysmography and gas (e.g., helium) dilution methods to quantify fractional lung volumes and assess the degree of restriction and measurement of maximal respiratory muscle pressures to assess muscle weakness. With a few exceptions, these methods require patient cooperation and are therefore limited in the young child. While the regular chest radiograph has limited value for quantification of restriction, algorithms exist to assess lung volumes using chest computed tomography (CT) scans.

Gas Diffusion Disorders

Gas diffusion disorders affect the absorption of oxygen into the bloodstream with resulting hypoxemia. This typically occurs due to a structural abnormality or thickening of the alveolar wall through which the gas exchange between the alveolus and the adjacent capillary occurs, resulting in hampered gas exchange. This can be seen in disease states such as interstitial lung diseases and pulmonary fibrosis. Gas diffusion disorders may present symptomatically with dyspnea upon exertion or at rest, tachypnea, and/or hypoxemia. The chest radiograph often shows an abnormally diffuse parenchymal process. Measurement of the diffusion capacity of the lung with carbon monoxide (DLCO) is diagnostic.

Ventilation Perfusion Mismatch and Shunt

Ventilation perfusion mismatching refers to a discrepancy between blood flow and aeration within a given lung unit. A greater perfusion-to-ventilation ratio is also known as a shunt and results in the return of unoxygenated blood to the left side of the heart and outward into the arterial blood stream, resulting in hypoxemia. The hypoxemia caused by shunts does not typically respond to the administration of oxygen, as the shunted blood does not come in contact with the supplemental oxygen, whereas the blood flowing through the other, normally perfused, lung units is already well-saturated. Fixed shunts can be seen with arteriovenous malformations, whereas intermittent shunting can occur with low lung volumes, retention of secretions, and in acute atelectasis. The chest radiograph may reveal the underlying pathology; however, vascular malformation in the lungs is usually elusive to the standard chest radiograph and requires more advanced radiologic modalities such as chest CT or MRI imaging. Intrapulmonary shunts are much less common than right-to-left shunts of cardiac origin and are typically addressed once an underlying cardiac abnormality has been ruled out.

A greater ventilation-to-perfusion ratio can occur in congenital disorders, such as the absent development of a pulmonary artery, or in intravascular processes such as a pulmonary embolism. The physiologic/clinical effect of these disorders that result in relative "wasted ventilation" or in the extreme dead-space ventilation is mild relative to shunt, in particular with the long-standing circumstances such as congenital vascular anomalies, often with absence or minor hypoxic effects. The common chest radiograph often is of limited diagnostic value. Thus, when a V/Q mismatch is suspected, a ventilation-perfusion scan may be useful, and, in cases where a pulmonary embolus is suspected, a CT with IV contrast can be diagnostic.

Lung Development and Effects on Lung Physiology

For the pediatric radiologist, lung mechanics and in particular those related to changes in lung volume are of crucial significance. One has to keep in mind that the radiograph of the noncooperative young child is rarely obtained at the optimal full inflation typical for the older person who inhales to full lung capacity (thus, total lung capacity or TLC) and breath-holds. The lung volumes reflected in the pediatric radiograph (assuming quiet breathing) span a volume range from functional residual capacity (FRC) (the volume at end expiration) to peak of tidal volume (the volume at end inspiration). Thus, by definition, the volume of the usual pediatric radiograph is almost always well below the lung volume of the cooperative patient, with all the implications that this has on the quality of the radiograph. Obviously, the lower the lung volume, the less reliable is the interpretation of pathology.

Stages of Lung Development

Early growth and development of the human lung is a continuous process that is highly variable between individuals and has traditionally been divided into five stages [3]. The first is the embryonic phase (26 days to 6 weeks of gestational age [wGA]), followed by the pseudoglandular (6–16 wGA) stage. At the end of this stage, the major elements of the bronchial tree complete their branching. The third is the canalicular stage (16–28 wGA). In the later phase of this stage, the prealveolar elements may allow infant survival. The saccular stage (28–36 wGA) is the one in which most premature infants are born and is followed by the alveolar (36 wGA–term) phase, which continues into childhood. The

saccular period, 28–36 wGA, is a transitional phase before full maturation of alveoli occurs. The primitive alveoli that become gradually more effective as gas exchangers have alveolar walls that are more compact and thicker than the final thin walls of alveoli; they also have an immature capillary structure. However, this partially developed structure is capable of carrying out a limited function of gas exchange that fully matures in the alveolar phase. Mature alveoli are not uniformly present until 36 wGA at which time the epithelium and interstitium decrease in thickness, air space walls proliferate, and the capillary network matures to its final single capillary network. Alveolar proliferation represents the predominant element of lung growth after birth. The alveolar proliferation rate is maximal in the first 2 years of life and subsequently decelerates. However, it is not well established to what age alveolar proliferation is maintained, and it may continue into later childhood or early adulthood.

The structural changes associated with the transition to mature alveoli through the alveolar stage and the following alveolar proliferation account for the subsequent gains in lung volume. Physiologically, these maturational changes not only affect gas exchange but together with the changes in the chest wall that will be discussed below have profound effects on the mechanical properties of the respiratory system and as such on the radiographic characteristics that are affected by these structural and mechanical considerations.

Changes in Lung Volume During the Last Trimester of Gestation

Calculations by Langston et al. [3] revealed that total lung volume undergoes rapid changes during the last trimester of gestation. At 30 wGA, the lung volume is only 34% of the ultimate lung volume at mature birth and at 34 weeks only reaches 47% of the final volume at maturity. In contrast, the air space (future alveolus) walls decrease in thickness such that at 30 and 34 weeks, they are 164% (28 μm) and 135% (23 μm), respectively, relative to the ultimate wall thickness at mature birth (17 μm). In parallel, dramatic increases in air space surface area occur. Surface area increases from 1.0–2.0 m^2 at 30–32 wGA to 3.0–4.0 m^2 at term. These volume changes likely have direct mechanical implications in reducing the vulnerability caused by a low and unstable FRC. Maturation of the alveolar network improves parenchymal elastance and therefore airway tethering.

Functional Residual Capacity (FRC) Tends to Be Low and Unstable in Infancy

Maintenance of a stable and adequate functional residual capacity (FRC) is important to secure effective gas exchange. FRC is determined by the balance between the opposing forces of the chest wall and lung and is thus a direct function of their respective mechanical properties. In early life, a compliant chest wall offers little outward recoil to the respiratory system, and thus the elastic characteristics of the respiratory system approximate those of the lung. The lung is also more compliant (i.e., has less elastance) in premature and newborn infants. The lung becomes less compliant (i.e., increases in elastance) as it undergoes alveolization, and the interstitial network becomes more intricately woven. (*Note*: the interstitium here represents the alveolar wall; a different concept from the same term utilized in radiology.) Compliance of the chest wall is extremely high in premature infants and undergoes rapid stiffening in late intrauterine life [4], but this stiffening (or decline in compliance) continues over the first 2 years of life [5]. Therefore, in early life (and more so in premature infants), the almost absent elastic recoil of the chest wall leads to a lung–chest wall equilibrium that results in a mechanically determined FRC that is low relative to older children and adults.

Thus, the baseline FRC in the young infant tends to drive itself to low volumes because of the mechanical characteristics discussed above. To circumvent this limitation, infants, unlike older children, actively elevate their end-expiratory volume (EEV), to a level that is higher than the mechanically determined FRC. At least three mechanisms are involved in the protection of a high end-expiratory volume: (a) a timing mechanism that initiates inspiration at an end-expiratory volume above that determined by the mechanical properties of the chest wall and lung [6], the other two mechanisms modulate the expiratory flow; (b) laryngeal braking during tidal expiration, a variable resistor mechanism [7]; and (c) persistence of inspiratory muscle activity into the expiratory phase [8].

The age at which transition to an *adult* pattern and cessation of these series of protective mechanisms has not been established for all of them, but based on one study [9], they persist at least into late in the first year and into the second year of life. It is likely that for a premature infant, the transition may be delayed. Interference with these active protective mechanisms, such as apnea or sedation, immediately drives the system toward low lung volumes. Also to be kept in mind is that the infant's sleeping state, supine position, and REM sleep (predominant in infancy) all substantially reduce lung volumes [10].

Airway Tethering

An additional crucial mechanism that secures airway patency and thus adequate maintenance of FRC is airway tethering. Tethering is the mechanism coupling lung volume to airway patency and is mediated through the elastic components in alveolar walls that surround bronchi. These elastic fibers are anchored to each other creating an extended mesh that exerts

a circumferential pull on the intraparenchymal airways. This complex elastic network that in its entirety reflects the elastic recoil of the lung transmits tension from the pleural surface to individual bronchi; thus, tethering links (couples) lung volume changes to airway caliber. The tension oscillates with the inspiratory cycle and increases during inspiration, increasing airway caliber. The cross-sectional area of the airway decreases with decline in lung volume, and airways may close if the lung volume is driven to critically low ranges of FRC (as may occur through the processes described in the previous segment). Tethering of airways was shown to be absent or less effective in young experimental animals [11] and most likely in infants in whom alveolization and the associated parenchymal elastic network are still in early stages of development. The effect of reduced tethering is decreased airway stability, increased tendency to airway closure, increased airway resistance, and, ultimately, a tendency to collapse alveolar units in the lung periphery.

Lessons for the Pediatric Radiologist

With the above observations, the radiologist needs to keep in mind that the predictable deficiencies in lung volume in infants and in particular when interference occurs with the mechanisms that protect lung volume (e.g., sedation) have an immediate effect on the quality of imaging. Chest radiographs and in particular chest CT scans obtained at low lung volumes have artifactual "infiltrates" in the lung fields that result from closure of airways and atelectases. This occurs in particular in the periphery of the lung and in dependent areas of the lung that are subjected to gravitational effects. To overcome these effects inflation of the lungs during the acquisition of the imaging is desirable. Most attractive for this purpose is the methodology developed by Long and Castile [12].

Some further physiological concepts related to pediatric respiratory physiology may be of use to the pediatric radiologist. Lung emptying in expiration is under normal circumstances a passive maneuver. Expiratory flow rate is determined by the interplay between a force that expels the air from the lung and the properties of the airways through which this exhaled air traverses. This flow rate is termed the expiratory time constant (τ) and is indeed a product of the compliance of the respiratory system (C) and the resistance of the airways (R) (thus, $\tau = C \times R$). To clarify, the force driving the air out upon relaxation at end inspiration is the elastance of the respiratory system (combined elastic properties of the lung and chest wall); this term is the reciprocal of the previously discussed compliance. In other words, compliant structures such as the chest wall and the lung in the very young, as discussed above, offer little driving force in exhalation. Small airways, the patency of which is impaired because of relatively small lung volumes and insufficient tethering, offer relatively high resistance to flow. This may be complicated in conditions of uneven structures of airways and parenchyma, because of damage related to trauma to the lung, e.g., by mechanical ventilation, or infection, creating regions that offer uneven emptying profiles, or uneven expiratory time constants, bringing about inhomogeneity in lung emptying.

The need to protect lung volumes through the mechanisms described above results in a rapid breathing rate, short expiratory time, and absent expiratory pauses (rapid transition from expiration to inspiration). In such circumstances, when the breathing rate increases (for reasons such as hypoxia, fever, or infection), there may be insufficient time for full lung emptying, in particular when emptying inhomogeneity is present. This may result in air trapping and a radiological interpretation of *hyperinflation*. While no systematic studies exist on the duration of this phenomenon, it is likely to resolve within the second year of life when the maturational processes bring about a shift to the "adult" pattern of breathing.

References

1. Bryan AC, Wohl ME. Respiratory mechanics in children. In: Macklem P, Mead J, editors. Handbook of physiology, Sect. 3, Vol. 111: Part 1: Mechanics of Breathing, Chap. 12. Bethesda: American Physiological Society; 1986.
2. West JB. Respiratory physiology: the essentials. 8th ed. Philadelphia: Lippincott Williams & Wilkins; 2008.
3. Langston C, Kida K, Reed M, et al. Human lung growth in late gestation and in the neonate. Am Rev Respir Dis. 1984;129(4):607–13.
4. Gerhardt T, Bancalari E. Chestwall compliance in full-term and premature infants. Acta Paediatr Scand. 1980;69(3):359–64.
5. Papastamelos C, Panitch HB, England SE, et al. Developmental changes in chest wall compliance in infancy and early childhood. J Appl Physiol. 1995;78(1):179–84.
6. Kosch PC, Davenport PW, Wozniak JA, et al. Reflex control of expiratory duration in newborn infants. J Appl Physiol. 1985;58(2):575–81.
7. Kosch PC, Hutchinson AA, Wozniak JA, et al. Posterior cricoarytenoid and diaphragm activities during tidal breathing in neonates. J Appl Physiol. 1988;64(5):1968–78.
8. Mortola JP, Milic-Emili J, Noworaj A, et al. Muscle pressure and flow during expiration in infants. Am Rev Respir Dis. 1984;129(1):49–53.
9. Colin AA, Wohl ME, Mead J, et al. Transition from dynamically maintained to relaxed end-expiratory volume in human infants. J Appl Physiol. 1989;67(5):2107–11.
10. Henderson-Smart DJ, Read DJ. Reduced lung volume during behavioral active sleep in the newborn. J Appl Physiol. 1979;46(6):1081–5.
11. Gomes RF, Shardonofsky F, Eidelman DH, et al. Respiratory mechanics and lung development in the rat from early age to adulthood. J Appl Physiol. 2001;90(5):1631–8.
12. Long FR, Castile RG. Technique and clinical applications of full-inflation and end-exhalation controlled-ventilation chest CT in infants and young children. Pediatr Radiol. 2001;31(6):413–22.

Normal Pediatric Chest and Role of Advanced Imaging

3

Monica Kahye Johnson, Pallavi Sagar, and Robert H. Cleveland

The Normal Chest Radiograph and Clues to Cardiovascular Disease

Patients with respiratory and cardiovascular diseases often have overlapping symptoms. One of the first tests for patients with respiratory distress is a chest radiograph, which can frequently distinguish between primary lung disease and congenital heart disease.

The purpose of this chapter is to understand the appearance of a normal chest radiograph and which abnormalities point to cardiovascular disease. This chapter provides a simple approach to chest radiography and to distinguish patients with cardiovascular disease as the cause of their respiratory symptoms so that further appropriate testing can be performed.

We recommend a standard approach in evaluating a chest radiograph:

- Technical adequacy
- Cardiac chamber enlargement
- Pulmonary vascularity
- Situs and side of aortic arch
- Lung parenchyma
- Extra-cardiovascular structures

If the heart is enlarged or abnormally shaped, as well as there is abnormal pulmonary vascularity, pulmonary edema, pleural effusions, or an abnormally positioned aortic arch, then the patient may have a congenital or acquired cardiovascular disease. More importantly, a normal chest radiograph does not exclude congenital heart disease. Parenchymal abnormalities due to primary pulmonary disease are discussed in detail in other chapters.

M. K. Johnson (✉) · P. Sagar
Department of Radiology, Harvard Medical School and Massachusetts General Hospital, Boston, MA, USA
e-mail: mjohnson86@partners.org

R. H. Cleveland
Department of Radiology, Harvard Medical School, Boston Children's Hospital, Boston, MA, USA

Technical Adequacy

In infants, the frontal radiograph is frequently taken recumbent and in the AP (anterior–posterior) projection, while in older children, the film is obtained upright and in the PA (posterior–anterior) projection. In an optimal chest radiograph, the intervertebral disc spaces should be seen through the cardiomediastinal silhouette. An underexposed film (one that is too bright) may suggest pulmonary edema or pneumonia where it does not exist. On the contrary, an overexposed film (one that is too dark) may cause the interpreter to miss findings particularly in the lung parenchyma. These were common issues in the past, as radiographs were generated using screen film radiography. With the advent of digital radiography, which allows for post-processing, images which originally were improperly exposed may be remedied without re-exposing the child to ionizing radiation [1].

Patient motion, rotation, and angulation may also distort an otherwise normal appearing chest. In a well-centered film, the distance of the medial ends of the clavicles should be equidistant from the adjacent posterior spinous process. The anterior ribs should be equidistant from the lateral margins of the spine and posterior spinous processes of the vertebra. On the lateral view, there should be a very small distance between the posterior right and left rib margins. A slight rotation to the left may cause the appearance of enlargement of the left superior mediastinum and left cardiac structures. Conversely, right mediastinal and cardiac structures appear larger when the patient rotates to the right. A lordotic image can exaggerate the size of the cardiac apex.

The degree of inspiration should be assessed on every radiograph. Although the degree of inspiration can be measured indirectly, the amount of inspiration is best judged by experience. A good inspiratory image is one in which the anterior sixth or posterior eighth rib is visualized above the

R. H. Cleveland, E. Y. Lee (eds.), *Imaging in Pediatric Pulmonology*, https://doi.org/10.1007/978-3-030-23979-4_3

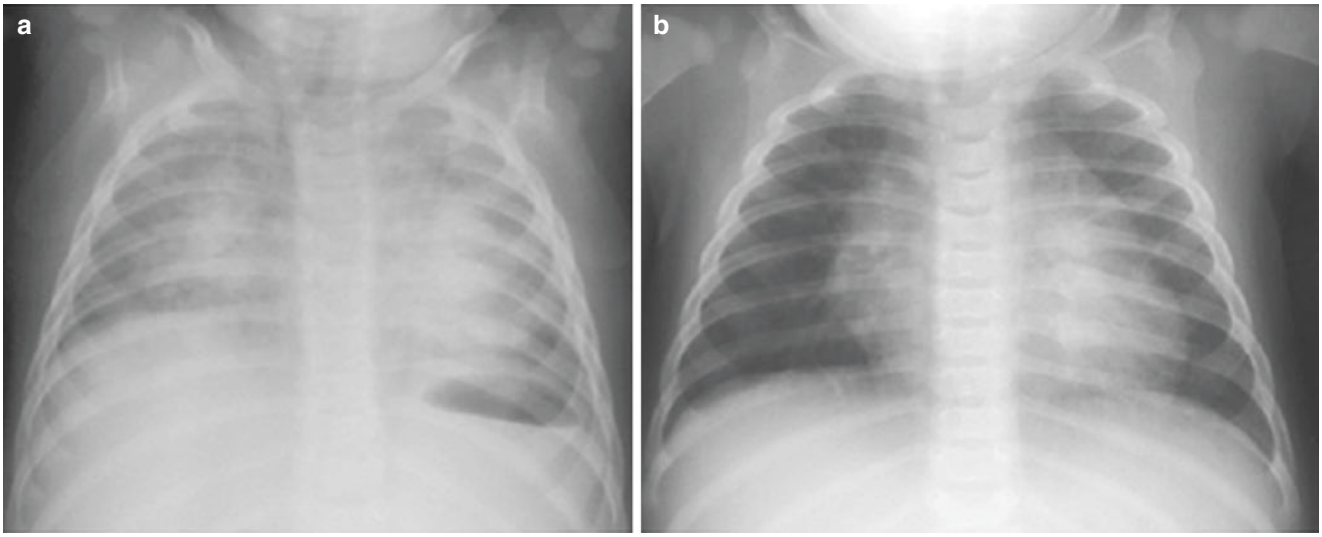

Fig. 3.1 (**a**, **b**) Expiratory and inspiratory radiographs with posterior rib fractures. These two frontal radiographs on the same patient emphasize the importance of lung volumes when interpreting a chest radiograph. The first frontal radiograph (**a**) is performed in expiration, as evidenced by low lung volumes, bilateral atelectasis, and tracheal deviation toward the right. The second radiograph (**b**) performed moments later in inspiration shows clear lungs and left posterior rib fractures in a patient with non-accidental trauma

apex of the left hemidiaphragm. In general, radiographs taken during expiration may show the dome of the left hemidiaphragm above this level. The lateral view and the appearance of flattened hemidiaphragms are also useful in determining the degree of inspiration. Many experienced radiologists rely on the degree of flattening of the diaphragm as the primary criterion of determining the degree of lung inflation.

Films obtained with very high lung volumes may produce an appearance of abnormal uplifting of the cardiac apex and thus be confused for right ventricular enlargement. Films obtained in expiration causes crowding of the normal bronchovascular structures and thus produce opacities suggesting edema, atelectasis, or pneumonia where it does not exist. Furthermore, these films may also obscure important lung parenchymal findings (Fig. 3.1a, b).

Normal Heart Size, Shape, and Position

In order to determine the size and position of cardiomediastinal structures, the appearance of the normal thymus must be understood. This is especially important in infants and toddlers where the normal thymus fills the anterior mediastinum and can obscure the superior cardiac border and mediastinum, the side and size of the great vessels, and the normal borders of the heart. Normally, the thymus involutes with increasing age and should be relatively inconspicuous by the end of the first decade.

The classic appearance of a newborn thymus is anterior superior mediastinal soft tissue that blends imperceptibly with the cardiac silhouette. A large thymus can simulate upper lobe atelectasis [2]. The other classic appearance is of the *sail sign*, which is more commonly seen on the right. The lateral edge of the thymus is often undulating, due to adjacent rib compression, *the thymic wave sign* [3]. On the lateral view, the thymus fills the anterior superior mediastinum and has a well-defined inferior border. Some of the different appearances of the thymus are pictured in Fig. 3.2.

There is a great variation in the size of the normal thymus [4]. The size varies during the respiratory cycle, e.g., inspiration (causing a small appearing thymus) and expiration (causing a larger appearing thymus). The thymus is also a dynamic organ and fluctuates in size during periods of prolonged illnesses. It may become smaller with infection or medications such as steroids or chemotherapeutic agents (stress atrophy) and rebound in size after recovery (rebound hypertrophy) [5–8]. A thymus may be pathologically enlarged if the enlargement persists into the second decade, if the borders are unusually lobular in contour, or if adjacent structures are displaced [9].

Both frontal and lateral views are necessary to adequately assess the position, shape, and size of the heart. On a well-centered frontal view of the chest, the normal heart and cardiac apex are centered to the left of the spine. From superior to inferior, the right cardiac margin is formed by the superior vena cava (upper one third) and right atrium (lower two thirds). The right atrium borders the right middle lobe. The ascending aorta is not normally seen in children. The soft tissue border of the superior vena cava often extends more laterally from the spine in young children than in adults.

The border of the left cardiomediastinal silhouette from superior to inferior is formed by the aortic arch (Fig. 3.3a,

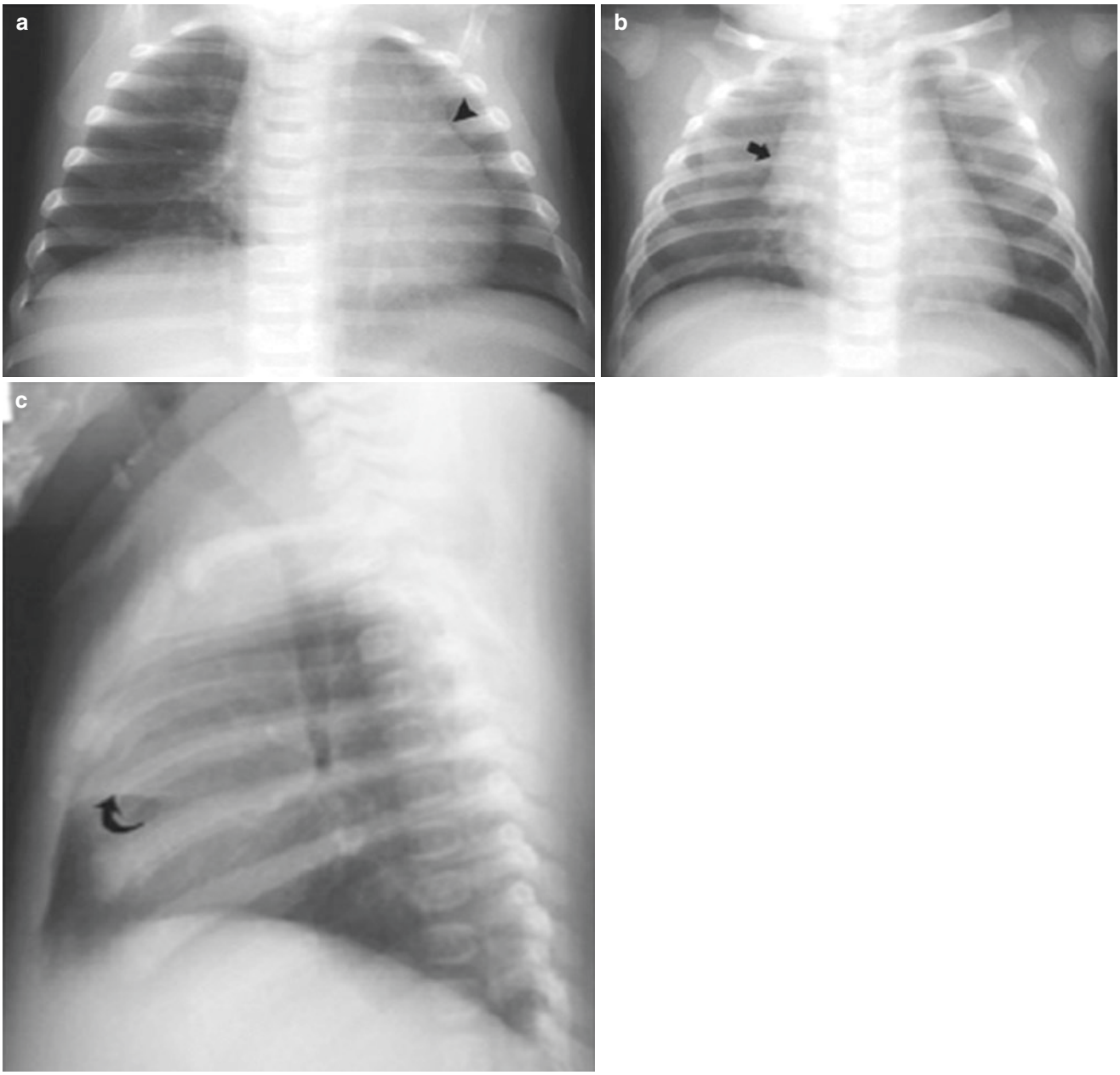

Fig. 3.2 (**a**–**c**) Normal thymus. These three images demonstrate the normal appearance of the thymus in infancy. The first image (**a**) demonstrates a thymus nearly completely filling the left upper chest with a smooth wavy contour (*arrowhead*) due to compression of the adjacent ribs. The thymus blends imperceptibly with the superior and lateral margin of the heart and superior mediastinum. The second image demonstrates the *sail sign* of the thymus. The thymus (*arrow*) blends in with the right superior cardiac and mediastinal borders and forms a sharp lateral border mimicking a sail. On the lateral view of the chest (**c**), the thymus fills the retrosternal clear space and has a sharply defined inferior margin (*curved arrow*)

arrowhead), main pulmonary artery (arrow), left atrial appendage (wavy arrow), and left ventricle (curved gray arrow). The left atrial appendage may not be seen in a normal heart. Normally, the borders of the left atrium and right ventricle do not contribute to the borders of the cardiac silhouette on the frontal view. The borders of the left atrium can be normally seen though the silhouette of the heart in 30% of children (Fig. 3.4, arrow) [10].

On the lateral view of the chest, the anterior cardiomediastinal border is formed (from superior to inferior) by the ascending aorta (arrowhead), main pulmonary artery (arrow), and right ventricle (curved arrow). The retrosternal clear space, or relatively lucent area cephalad to the right ventricle and posterior to the sternum, typically occupies one third to one half of the anterior chest (Fig. 3.3b). In infants, the thymus occupies the anterior mediastinum and may fill the

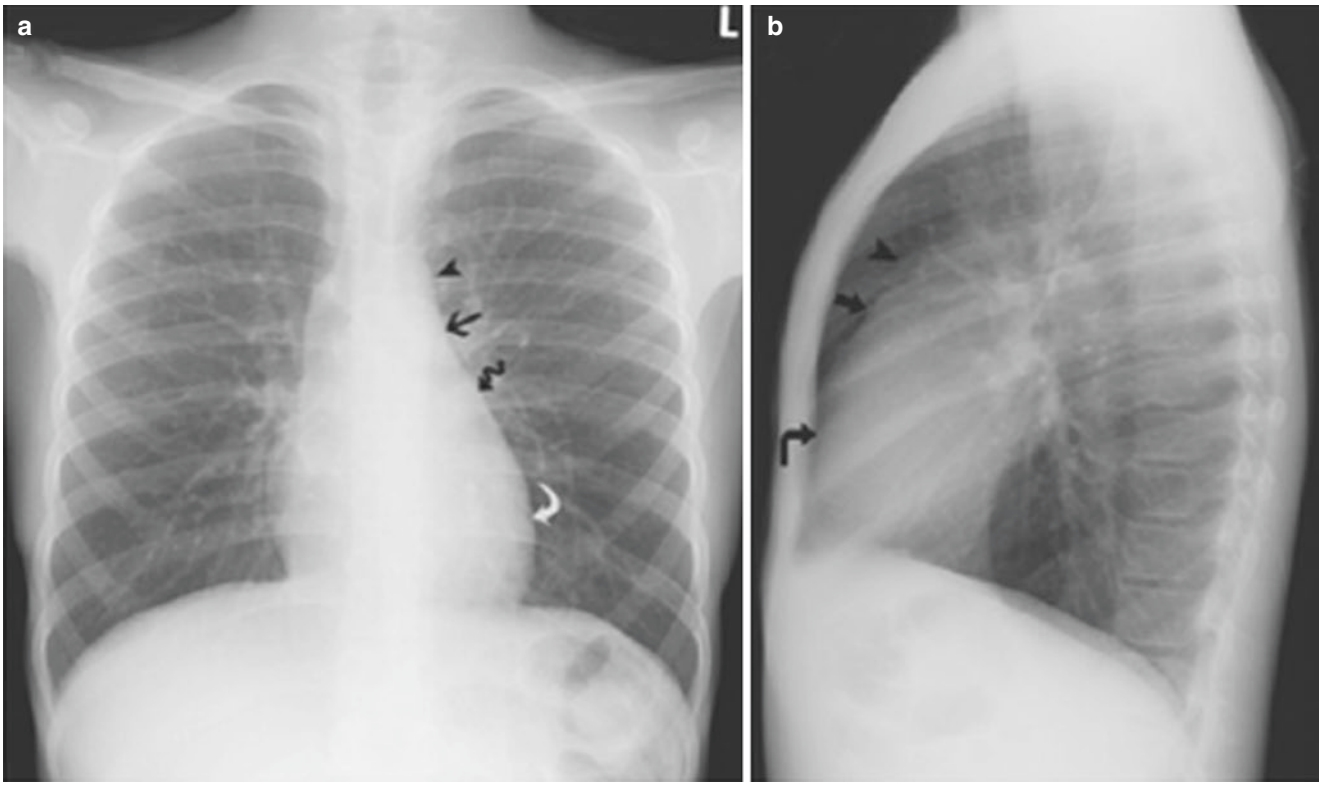

Fig. 3.3 (**a**, **b**) Normal PA and lateral radiographs of the chest in a 10-year-old

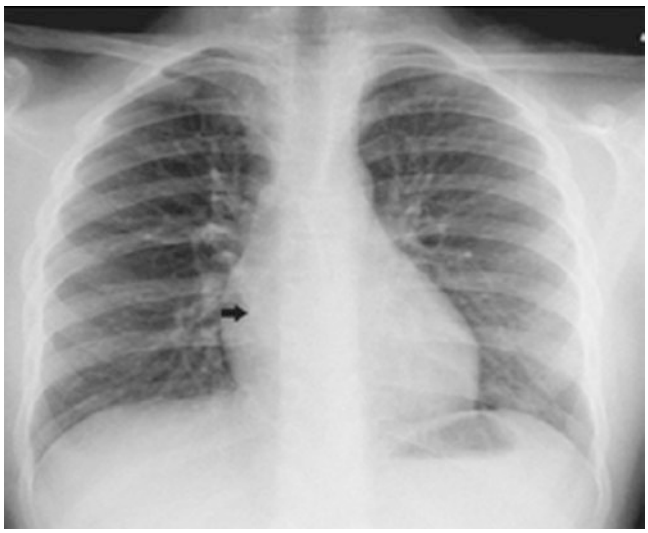

Fig. 3.4 Normal PA radiograph in a 10-year-old showing the normal left atrial shadow (*arrow*)

retrosternal clear space obscuring the anterior superior border of the heart and great vessels.

The posterior cardiomediastinal margin from superior to inferior is composed of the left atrium, left ventricle, and inferior vena cava on the lateral view. Normally, the posterior margin of the left atrium is anterior to the left mainstem bronchus and should not displace the bronchus or extend posterior to the inferior vena cava.

The normal heart size can be judged qualitatively and quantitatively. One index, the cardiothoracic ratio, is the ratio between the widest transverse cardiac diameter and the widest internal thoracic diameter. Normal values during quiet respiration are less than 60% for newborns and less than 50% for all children greater than 1 month of age [11, 12]. However, neither the left atrium nor the right ventricle is represented in the transverse dimension of the heart, making this measurement unreliable. Thus, a subjective evaluation of the heart size, based on the frontal and lateral views, with attention to each chamber of the heart and the overall cardiac size is preferred. Comparison to prior films is also valuable.

Judging heart size or specific chamber enlargement on an AP view of the chest in an infant with a large thymus is very challenging (Fig. 3.5a, b). The lateral view is particularly helpful. If the posterior aspect of the cardiac silhouette extends over the vertebral bodies, then the heart is enlarged. If the posterior margin of the heart extends posterior to the anterior line of the trachea, the heart may be enlarged. Another way of judging cardiomegaly is if the posterior border of the heart is closer to the anterior edge of the spine than the AP width of the adjacent vertebra.

Cardiac silhouette enlargement may be due to global chamber enlargement or due to specific chamber enlargement. Determining which chambers are enlarged provides clues to the type of cardiac abnormality. For example, global cardiac enlargement may be due to a cardiomyopathy or peripheral arterial to venous shunting due to tumors

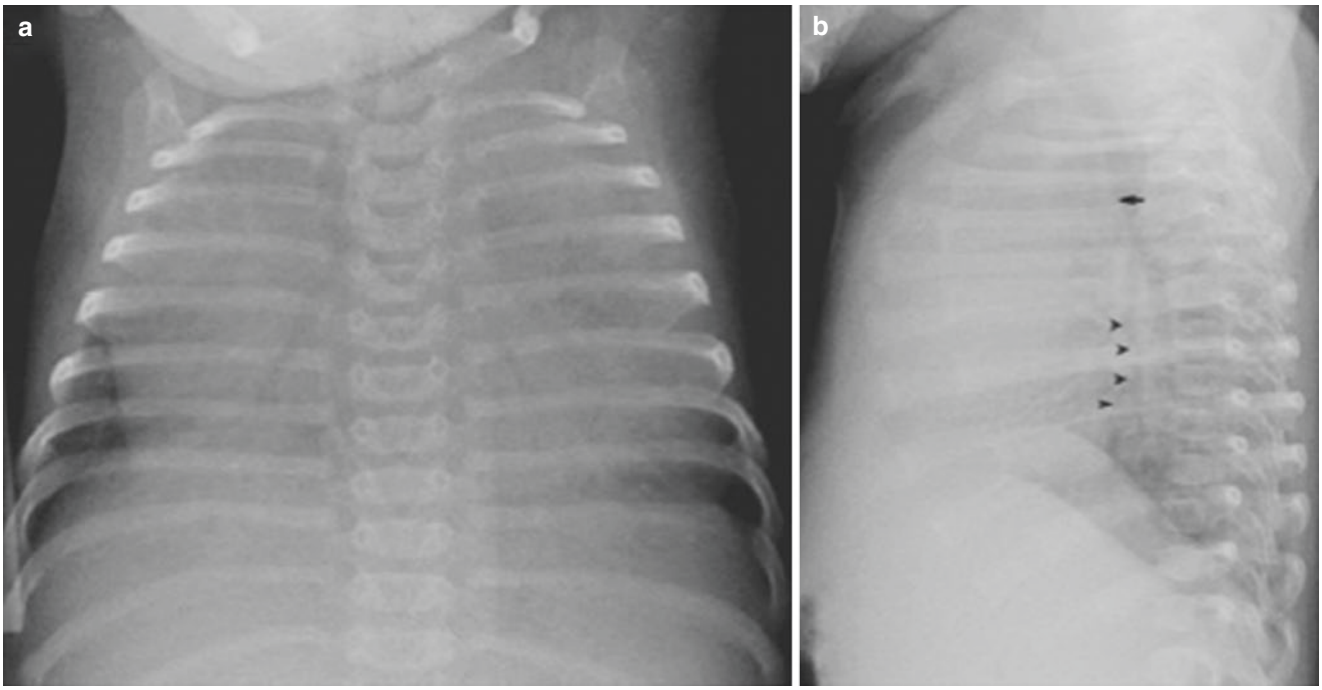

Fig. 3.5 (**a**, **b**) AP and lateral radiographs in an infant with a large central soft tissue which nearly opacifies both hemithoraces. The lateral radiograph demonstrates that the posterior margin of the heart (*arrowheads*) does not extend posterior to the anterior margin of the trachea (*arrow*). Ultrasound showed that this mass is a normal large thymus, and the heart was normal

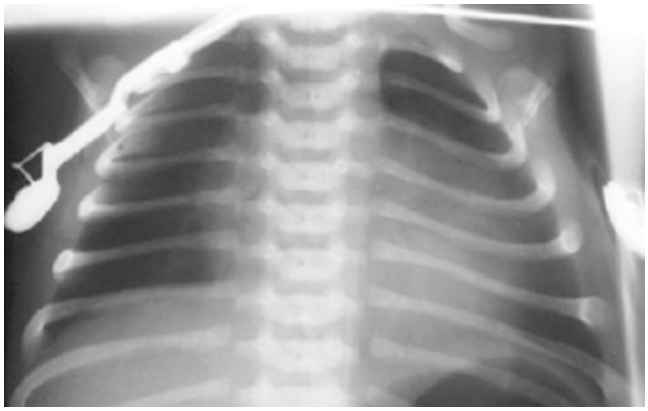

Fig. 3.6 Ebstein anomaly. This frontal view of the chest in an infant with Ebstein anomaly demonstrates an enlarged box-shaped cardiac silhouette due to a massively enlarged right atrium. The lungs appear hyperlucent because of decreased pulmonary blood flow

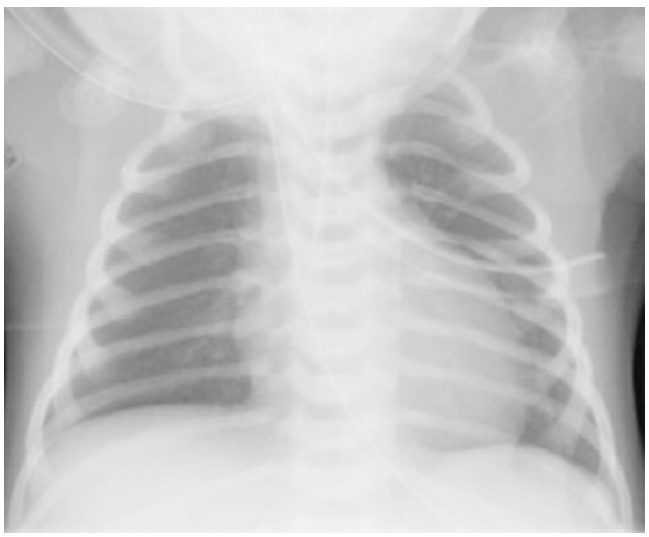

Fig. 3.7 Valvar pulmonary stenosis. This radiograph in a cyanotic infant demonstrates right ventricular enlargement as evidenced by an enlarged left cardiac margin in a patient with pulmonary valve stenosis. This image also demonstrates pulmonary vascular oligemia

(e.g., hemangioendothelioma) or vascular malformations (e.g., vein of Galen aneurysm).

The size and shape of the normal right atrium are variable; thus, mild to moderate enlargement of this chamber can be missed. Two signs of right atrial enlargement on the frontal projection are that the border is laterally displaced more than a few centimeters from the spine. When the right atrium is enlarged, the right heart border becomes squared, and the entire heart assumes a box-like appearance. The most common causes of right atrial enlargement in newborns are pulmonary atresia with an intact septum or Ebstein anomaly (Fig. 3.6).

When the right ventricle is enlarged, the retrosternal clear space becomes smaller. When the right ventricle enlarges, there is a clockwise rotation of the heart, and the cardiac apex can point upward (Fig. 3.7). In infants and young children, evaluation of the right ventricle on the lateral view may be impossible due to the thymus.

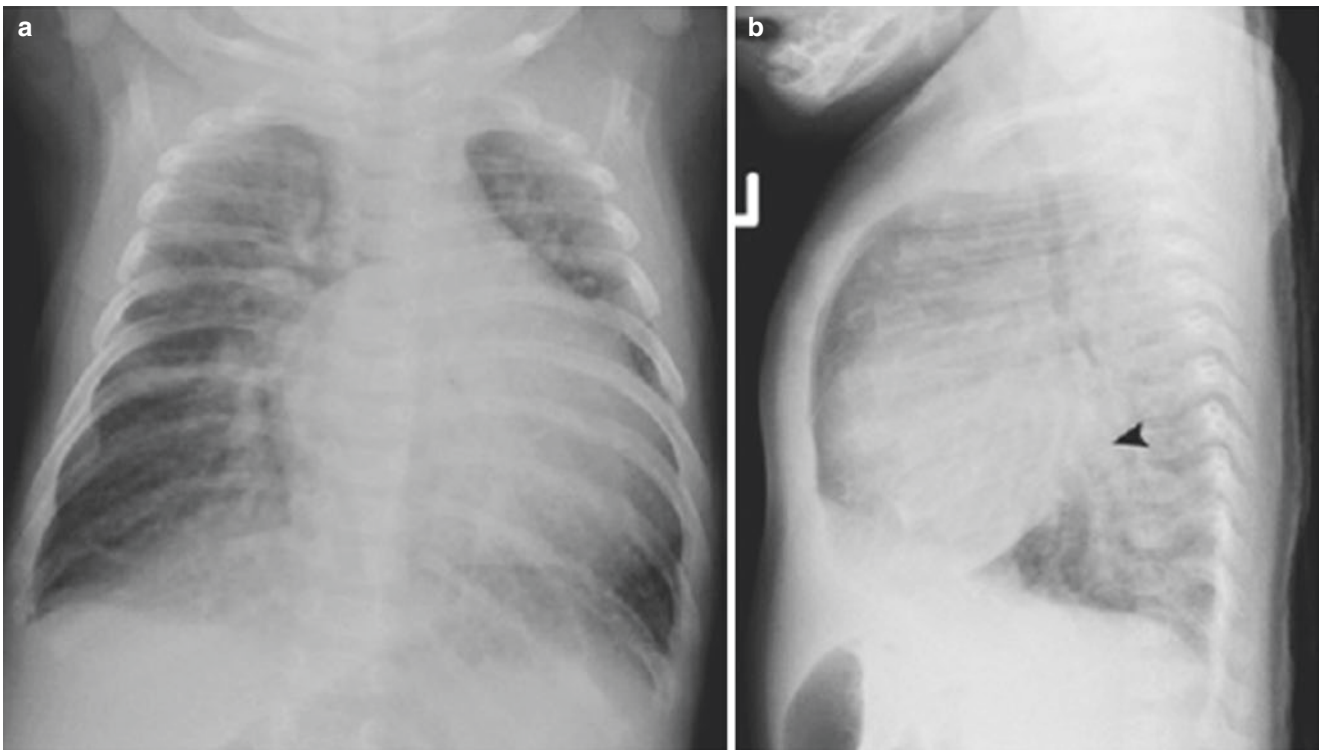

Fig. 3.8 (**a**, **b**) AV canal. Frontal and lateral views of the chest in a patient with trisomy 21 and an unrepaired AV canal defect demonstrate hyperinflation, cardiomegaly, and increased pulmonary vascularity. The lateral view shows left atrial enlargement as evidenced by the posterior margin of the left atrium (*arrowhead*) extending posterior to the inferior vena cava and pushing the left mainstem bronchus posteriorly. Notice that the angle between the left mainstem bronchus and axis of the trachea/right mainstem bronchus increases with left atrial enlargement

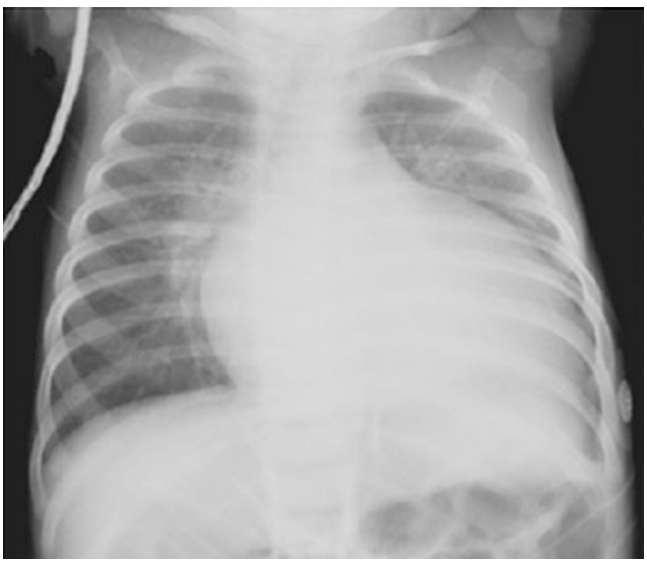

Fig. 3.9 Aberrant coronary artery. This infant presented to the ER with respiratory distress. The frontal radiograph demonstrates cardiomegaly, mainly due to left ventricular dilatation. The patient was found to have an aberrant left coronary artery arising from the left pulmonary artery on echocardiography

Left atrial enlargement is best seen on the lateral view. An enlarged left atrium extends posterior to the inferior vena cava and pushes the left mainstem bronchus posteriorly. In children, left atrial enlargement may be due to ventricular septal defect (Fig. 3.8a, b), patent ductus arteriosus, mitral stenosis, or mitral insufficiency.

Left ventricular enlargement is best seen on the frontal view and is demonstrated by enlargement of the left side of the heart. Left ventricular dilatation may produce a downward pointing cardiac apex. In this patient with an anomalous coronary artery (Fig. 3.9), both the left atrium and left ventricle were enlarged by echocardiography.

Vascular Pattern

Determining normal and abnormal pulmonary vascularity may be the most difficult aspect of evaluating a chest radiograph, but is very important to generating the appropriate diagnosis of congenital heart disease. Pulmonary vascularity can be normal and demonstrate increased pulmonary arterial flow, increased pulmonary venous distention, or decreased pulmonary flow. Normally, the right interlobar pulmonary artery is the same size as the trachea at the level of the aortic arch (Fig. 3.10).

The peripheral arteries normally taper gradually from the hilum to the periphery of the lung (see image normal PA of the chest). If the patient is upright, the width of the vessels in

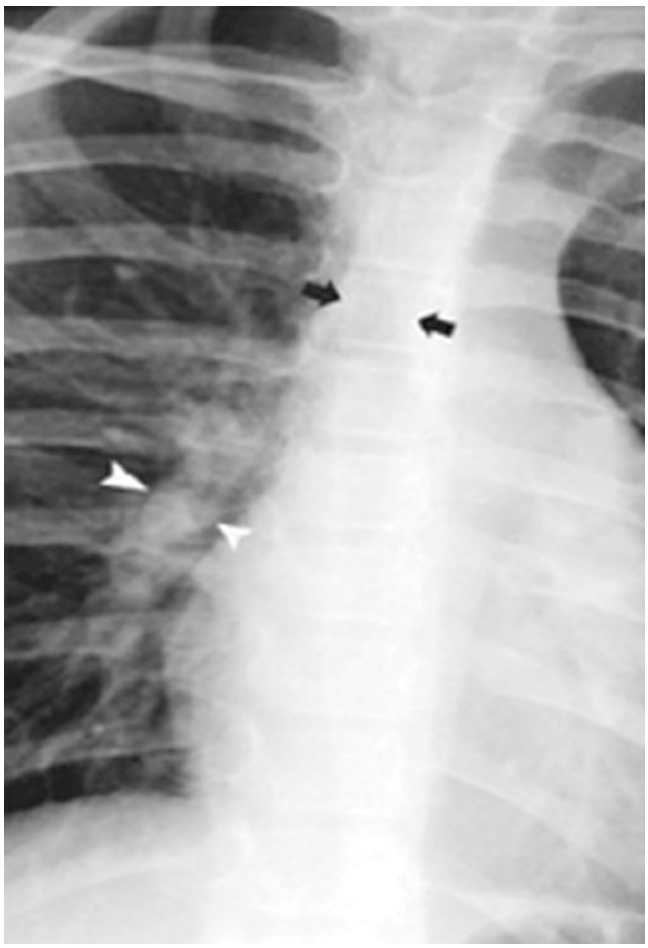

Fig. 3.10 Normal diameter of the right interlobar pulmonary artery relative to the trachea. This magnified view of the chest demonstrates that the width of the normal right interlobar pulmonary artery (*arrowheads*) is the same as the trachea (*arrows*) at the level of the aortic arch. The spinal curvature allows the right hilar structures to be better visualized

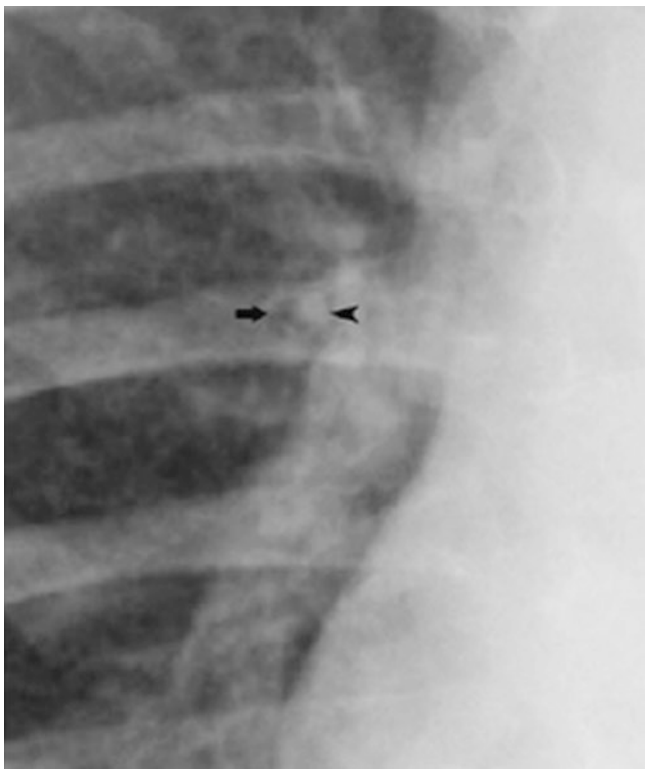

Fig. 3.11 Pulmonary artery on end with bronchus. This magnified view of the chest demonstrates a pulmonary artery (*arrowhead*) and adjacent bronchus (*arrow*) in cross section. Normally the diameter of these two structures is similar

the upper lobes is smaller than that of the lower lobes at comparable branch level. If the patient is recumbent, pulmonary vascular markings are more evenly distributed in size. Normally, the margins of the peripheral arteries (seen on end) are approximately the same size as the adjacent bronchi (Fig. 3.11). The borders of the peripheral arteries are normally sharp.

When pulmonary arterial flow is increased, the right interlobar artery will be larger than the trachea, and the apparent number and size of pulmonary arteries will increase. The pulmonary artery seen on end will be larger than the adjacent bronchus (Fig. 3.12). With increased pulmonary venous flow and edema, the margins of the enlarged vessels will become poorly defined. Increased pulmonary venous flow is often confused with peribronchial cuffing as seen in viral pneumonia.

Decreased pulmonary vascularity reflects diminished pulmonary blood flow. The main pulmonary artery segment may be decreased in size, the blood vessels appear thin, and the sparseness of the vessels gives an appearance of hyperlucency of the lungs (Fig. 3.6, Ebstein anomaly).

The Side of the Aortic Arch and Situs

The aorta is normally to the left of the spine, cephalad to the main pulmonary artery. In children, the thymus often obscures direct visualization of the aorta, and the position of the aortic arch is inferred by the deviation of the trachea. The trachea deviates to the opposite side of the aortic arch, especially during expiration [13, 14]. (For an image, refer to the expiratory radiograph in the patient with rib fractures.)

A right aortic arch serves as a warning for the presence of congenital heart disease. In the general population, right-sided aortic arch is associated with congenital heart disease in 5% of patients, especially truncus arteriosus, tetralogy of Fallot (Fig. 3.13), and pulmonary atresia with ventricular septal defect [15]. Right-sided aortic arches may also indicate the presence of variant arch anatomy or a vascular ring, most commonly due to an aberrant left subclavian or double aortic arch [15, 16].

Situs refers to the position of the chambers of the heart and tracheobronchial tree relative to abdominal organs (the

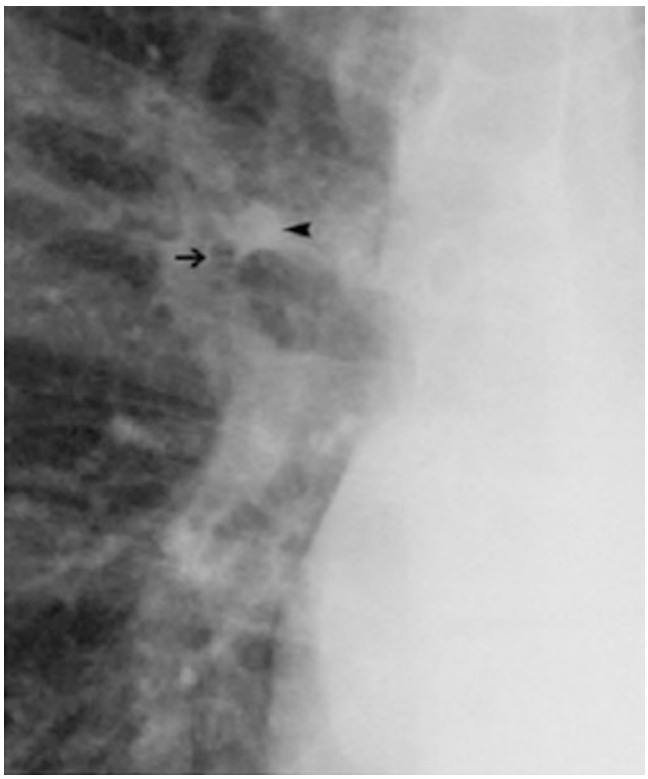

Fig. 3.12 Increased pulmonary arterial flow. A magnified view demonstrates that the pulmonary artery (*arrowhead*) is larger than the adjacent bronchiole (*arrow*). Increased pulmonary vascularity is also demonstrated in the previous patient with trisomy 21 and an AV canal

liver, spleen, stomach). Situs solitus is the normal position of the thoracic and abdominal organs, while situs inversus is its mirror image (i.e., the heart on the right, the liver on the left). Levocardia is when the heart points to the left chest (normal anatomy), while dextrocardia is when the heart points toward the right. The importance of situs and the position of the heart is that there is an increased incidence of congenital heart disease in patients with situs abnormalities. The frequency of congenital heart disease in patients with normal anatomy is 1%. In patients with situs solitus and dextrocardia or situs inversus and levocardia, the incidence of congenital heart disease approaches 100%.

Practically speaking, the cardiac apex, stomach, and spleen should be on the left, and the liver should be centered in the right upper abdomen. If there is discordance between the location of the cardiac apex and the gastric bubble, there is a very high incidence of congenital heart disease.

Extra-cardiovascular Structures

Pleural

Cardiovascular disease is one of the many causes of pleural effusions. On the standard PA and lateral chest radiographs, the costophrenic angles should be well visualized and sharp. The lateral view is the most sensitive view of detecting effusions and is represented by blunting of the costophrenic sulci. A lateral decubitus view may be sensitive for showing effusions and if large effusions are free flowing or loculated. Fluid may also track along the fissures so that the fissures appear thickened.

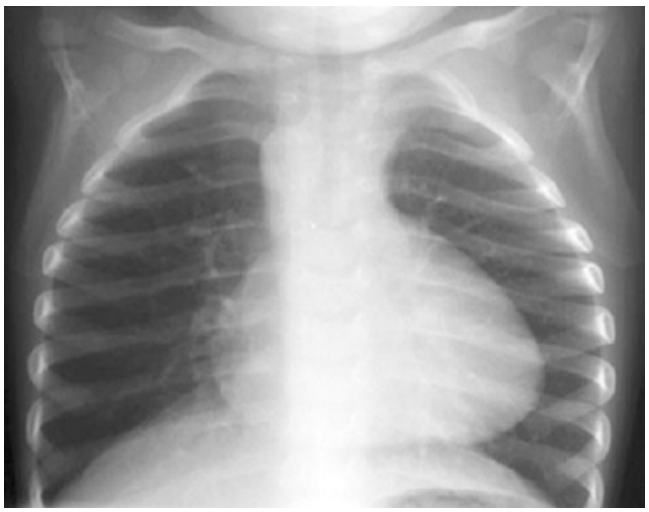

Fig. 3.13 Tetralogy of Fallot with right aortic arch. This radiograph in a patient with tetralogy of Fallot demonstrates a right aortic arch and enlarged upturned cardiac apex. The appearance of the heart is due to an enlarged right ventricle which causes clockwise rotation of the heart. There is decreased pulmonary vascularity, due to subpulmonic stenosis with a ventricular septal defect allowing a right to left shunt

Diaphragm

The heights of the two hemidiaphragms vary somewhat from person to person and with positioning. The relative heights of the two hemidiaphragms may also vary. It has been suggested that in normal individuals, the right may be as much as 0.5–2 intercostal spaces higher than the left and that the left may be up to 0.5 interspace higher than the right [17].

Bony

Certain bony findings on a chest radiograph may also point to the presence of congenital heart disease. Scoliosis, particularly thoracic scoliosis, can be associated with congenital heart disease [18]. Patients with vertebral anomalies may also have the VATER association of anomalies, which include vertebral, anorectal, esophageal atresia, renal, or radial ray limb anomalies and congenital heart disease [19]. Inferior rib notching may be a very subtle sign of coarctation of the aorta and is mainly seen in older children. Eleven pairs of ribs or multiple manubrial ossification centers are seen in patients with Down syndrome who also have an increased incidence of congenital heart disease [20]. Thoracotomy changes, median sternotomy wires, and vascular coils may give clues to prior cardiothoracic surgery. Lack of calcification of the inferior segments of the sternum, the mesosternum, may also be associated with congenital heart disease (Fig. 3.14).

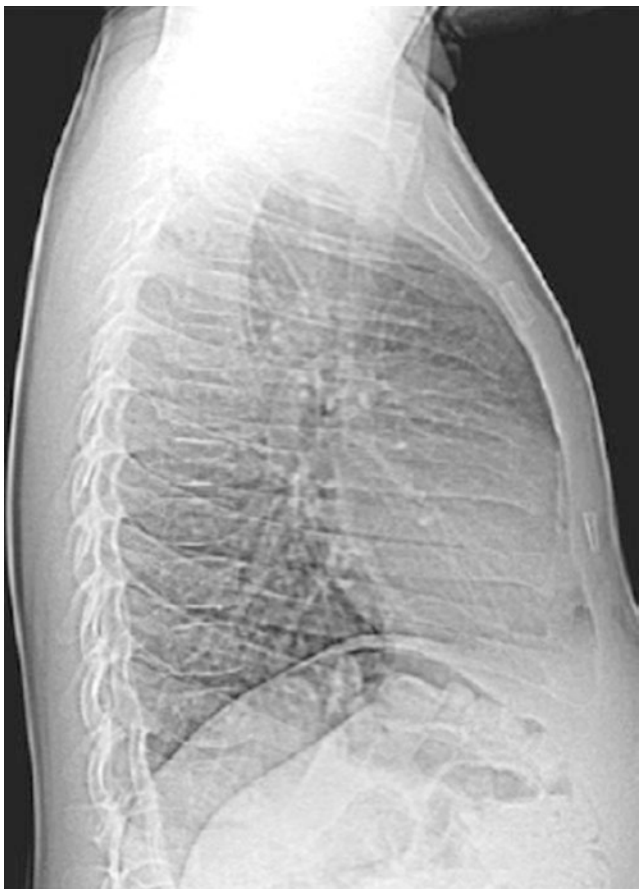

Fig. 3.14 Absent mesosternum

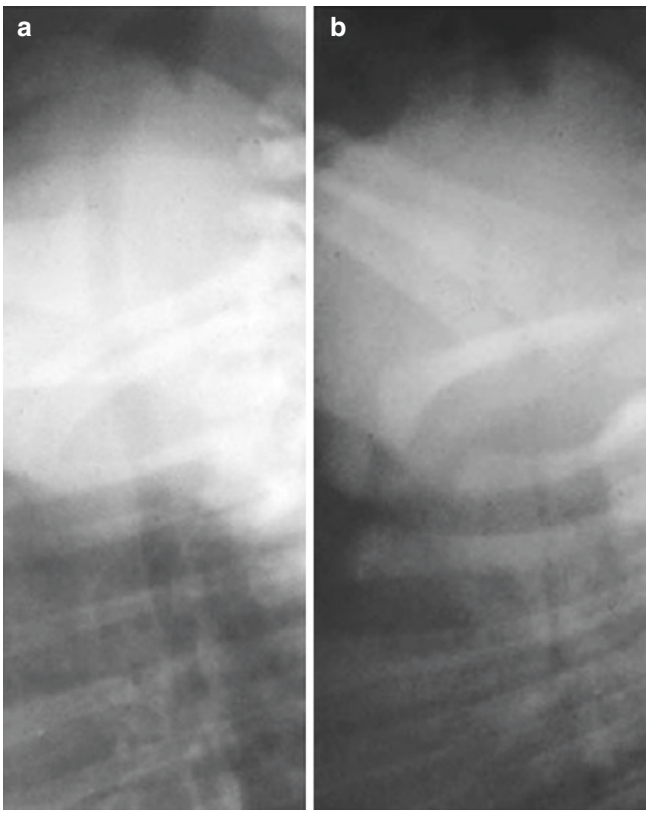

Fig. 3.15 (**a**) The configuration of the trachea in this 5-month-old on inspiration is as seen with a normal adult airway. The trachea assumes a straight, linear course from the infraglottic region to the carina. (**b**) Moments later on expiration, there is an angular posterior buckling just above the thoracic inlet and then an inferior buckling. The entire intrathoracic trachea is significantly narrowed. (Although image quality is diminished, using *the last image hold* option on fluoroscopy reduces patient radiation exposure and facilitates capturing transient images)

Conclusion

Using a standard approach to interpreting chest radiographs and understanding the normal and abnormal appearances in children can help distinguish primary pulmonary disease from cardiovascular disease.

Normal Upper Airway in Infants

There are two major differences in the infant's upper airway that differ from older children and adults. They are an exaggerated change in diameter of the intrathoracic trachea from inspiration to expiration and a change in course and configuration of the extrathoracic trachea from inspiration to expiration [21, 22].

The neonate's tracheal cartilages are less rigid and contribute to less of the circumference of the trachea than in older individuals. This results in significant narrowing of the AP diameter of the intrathoracic trachea on expiration. It is normal as a baby approaches end-expiratory volume with crying for the AP diameter of the entire intrathoracic trachea to nearly complete collapse (Fig. 3.15). However, if only a portion of the intrathoracic trachea narrows, it is abnormal, and focal tracheomalacia or compression from an extrinsic cause such as a vessel or mass should be suspected.

The normal extrathoracic trachea in infants assumes a very angular buckling on expiration. In frontal projection, this is usually seen as an angular rightward deviation and then inferior deviation just above the thoracic inlet (Fig. 3.16). The buckling is characteristically away from the side of the aortic arch and hence to the right. On lateral projection, the buckling is posterior and then inferior just above the thoracic inlet (Fig. 3.15b). This will be accompanied by an increased AP diameter of the retropharyngeal soft tissues as the buckling becomes more pronounced with increasing expiration.

Pediatric Chest Ultrasound

As previously discussed, most pediatric chest diseases are evaluated by plain radiographs. However, chest ultrasound (US) is an appealing modality particularly in children due to its inherent lack of ionizing radiation. Ultrasound machines

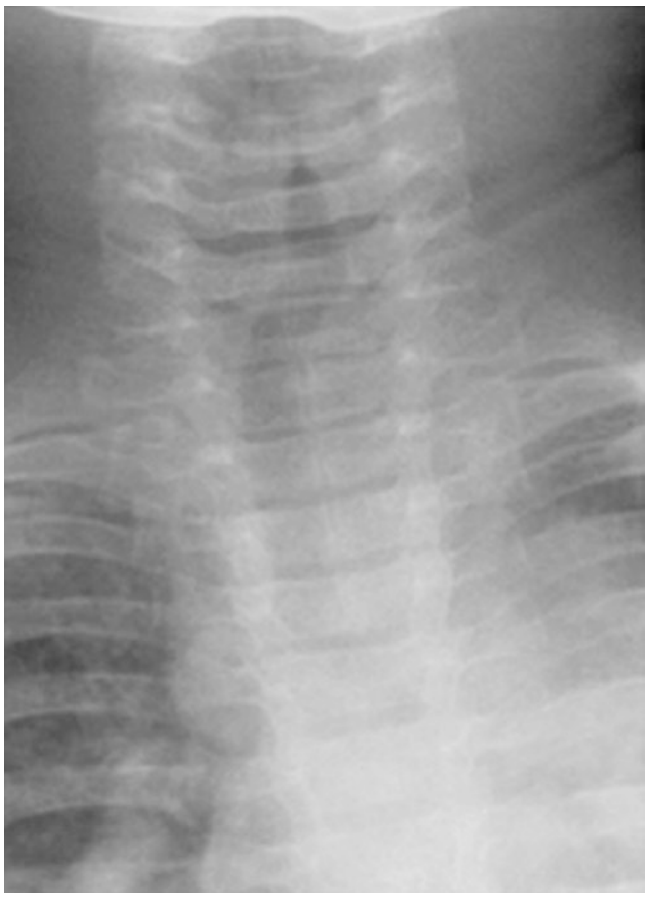

Fig. 3.16 AP image in expiration shows the normal angular buckling away from the side of the aortic arch and then inferiorly just above the thoracic inlet

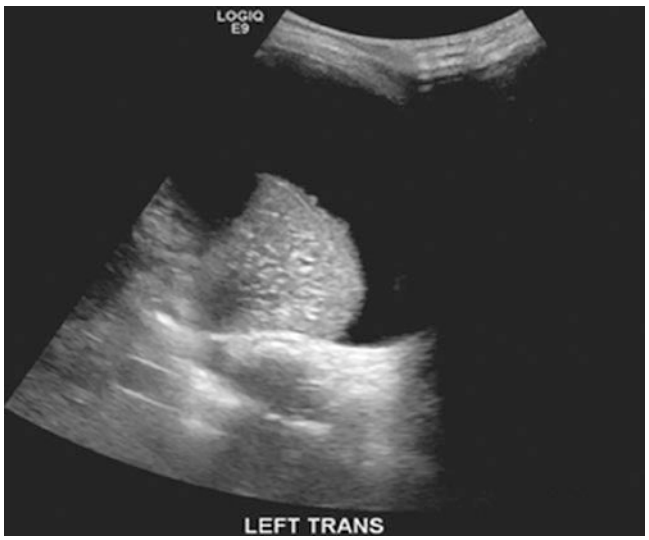

Fig. 3.17 Ultrasound of the left chest, transverse view, demonstrating a large simple pleural effusion with underlying collapsed left lower lobe

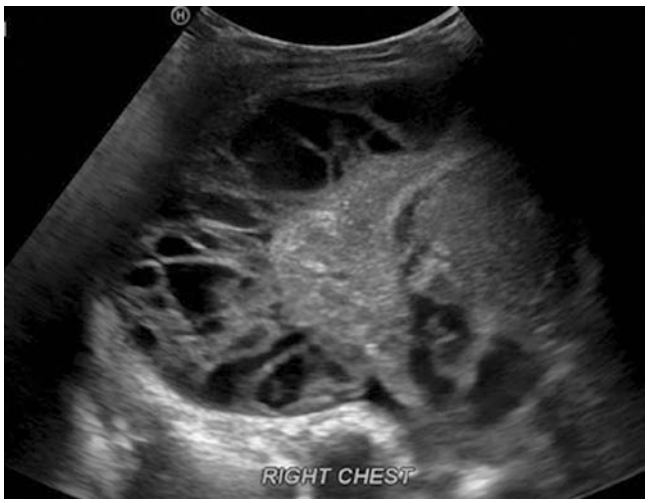

Fig. 3.18 Ultrasound of the right chest, transverse view, in a patient with complicated pneumonia. There is loculated pleural effusion with underlying consolidated lung with air bronchograms in the right lower lobe

are ubiquitous to the practice of medicine today and can be easily performed at the patient's bedside.

Chest US is commonly used in the pediatric intensive care setting for detecting and characterizing pleural effusions, including planning for possible thoracentesis and chest tube placement (Figs. 3.17 and 3.18). Although decubitus chest radiographs can be obtained to evaluate for pleural effusions, currently they are seldom performed and have been replaced by US due to its increased sensitivity, portability, and lack of ionizing radiation [23].

In addition to evaluating for pleural effusions, US is useful for evaluating mediastinal widening and palpable masses in the chest wall [23]. The unossified sternum in infants and costochondral junctions provide a good sonographic window to visualize the mediastinum. While CT and MRI are technically superior for evaluating the mediastinum, US is a good alternative in specific circumstances, e.g., differentiating normal thymus from mediastinal mass in an infant, as normal thymus has a distinctive appearance. It is mildly hypoechoic relative to the liver and thyroid gland and has homogeneous and finely granular echotexture and smooth, well-defined margins. Most importantly, it does not cause mass effect on the great vessels (Fig. 3.19).

In recent years, US has been studied as a promising alternative to chest radiographs in assessing the lung parenchyma when pneumonia is clinically suspected, especially in resource-limited areas. Typically, a linear probe is used and placed longitudinally perpendicular to the ribs. In between the shadowing ribs, normal lung parenchyma has a characteristic appearance with a peripheral echogenic pleural line, deeper to which are multiple gradually fading parallel horizontal lines called A-lines. These A-lines are reverberation artifacts due to changes in acoustic impedance at the pleural-lung interface (Fig. 3.20). Any alteration in this appearance may suggest replacement of aerated lung by

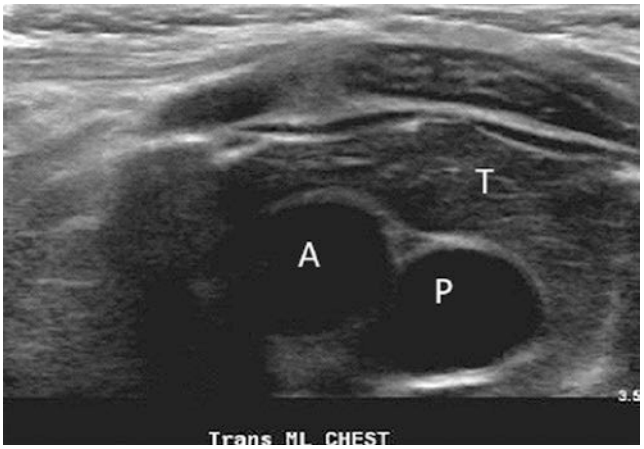

Fig. 3.19 Transverse ultrasound of the mediastinum, suprasternal approach, demonstrates a normal thymus (T) and normal underlying aorta (A) and main pulmonary artery (P)

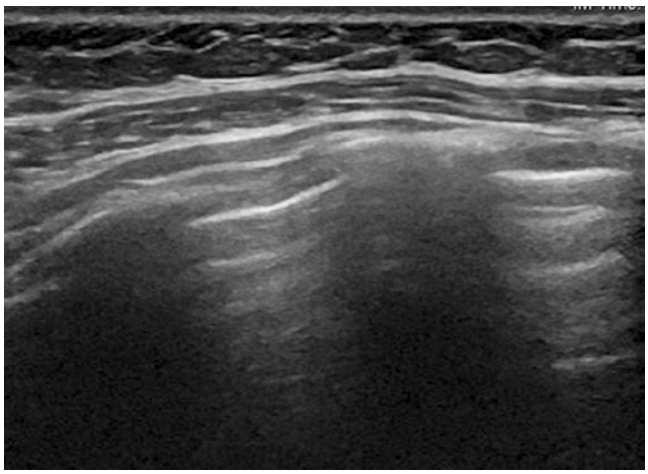

Fig. 3.20 Ultrasound of normal lung parenchyma using a linear array transducer. Structures of the chest wall include the subcutaneous soft tissues, muscles, and rib shadows. Between the ribs are horizontal dense lines representing the pleural line. Parallel to pleural lines are multiple echogenic horizontal lines called as A-Lines, which are evenly spaced representing reverberation artifacts from the pleural lines in normal lung tissue

fluid as in pulmonary edema or consolidation due to an underlying pneumonia. A randomized controlled trial published in 2016 showed that lung ultrasound was a safe and effective way to diagnose pneumonia [24].

Pediatric Chest Computed Tomography

CT chest is the modality of choice for a variety of cardiothoracic conditions in children but can be challenging to perform for multiple reasons. Logistically, CT examinations are often difficult, particularly in children less than 5 years of age, due to the child's limited ability to follow instructions and restrict movement. In the past, with older versions of CT technology, the overall scan times were relatively longer, and hence sedation or generalized anesthesia was often required. More recently, this practice is less desirable due to an understanding of side effects associated with sedation. Nowadays, with the significant advancement of CT technology, extremely short scan times are possible, and most CT examinations in younger preschool children can be attempted and performed without sedation.

Although CT technology has exponentially advanced in the last decade, it is important to emphasize that the tissues of children are relatively more radiosensitive to ionizing radiation compared to adults, as their cells are rapidly dividing. Furthermore, children have a longer life span and therefore a greater length of time to develop radiation-induced side effects. Although in general the risk of CT radiation-induced cancer for a given child may be small and remains undetermined, it is a serious health concern due to the extensive availability and potential overutilization of medical imaging.

The Image Gently campaign was launched in 2008, to consolidate the efforts to minimize radiation doses imparted to children via medical imaging. It emphasizes that each CT examination performed in a child should not only be strongly medically indicated and the CT imaging protocols should be optimized based on the child's age, weight, and body habitus in order to maximize the diagnostic yield using the minimal possible radiation dose. Hence, it is extremely important to triage all CT requisitions in children ahead of time to tailor the protocol and consider alternative imaging modalities such as US and MRI when appropriate.

Patient Preparation

Preparation of a patient and the family is critical to the success of pediatric CT examinations, as it helps with image quality and decreases the need for sedation. For younger children, it is especially important to alleviate anxiety and fear as much as possible with age and developmentally appropriate information. Child life specialists are very helpful in preparing a child for an imaging study and help minimize the need for sedation. It is also important that all members of the radiology team be adept at working with children and their families. In addition, a child-friendly CT suite and distraction techniques (i.e., electronic games, music) can help the child and his or her family feel more at ease and better able to cooperate during the entire length of the examination.

While sedation and general anesthesia may sometimes be required and the only available option in the evaluation of certain clinical conditions, it is important to exhaust all options without sedation first. For example, infants can be swaddled or placed in vacuum pillows to restrict their movement when performing chest CT.

Protocols

Pediatric CT protocols differ from adult protocols in many ways, for reasons of patient cooperation and radiation as previously discussed and for unique pediatric pathologies that require special considerations. Radiologists, medical physicists, and technologists should work together to obtain diagnostic quality images while following the as low as reasonably achievable (ALARA) principle.

As children usually have little body fat and poor natural soft tissue contrast, intravenous contrast is desired unless specifically contraindicated (e.g., renal failure) or not clinically indicated (e.g., pectus excavatum and surveillance imaging for pulmonary metastatic disease in osteosarcoma). Oral contrast is not normally needed for chest CT.

It is very important to confirm the clinical indication before acquiring images so that the correct protocol is used to answer the specific clinical question and the scan area is limited to the area of interest. For example, a chest CT for the evaluation of pectus excavatum primarily focuses on the bony thoracic cage for the calculation of the Haller index. This can be performed at an extremely low dose with significantly higher image noise than a usual chest CT and without intravenous contrast (Fig. 3.21). On the contrary, a two-phase ventilation-controlled, paired inspiratory and expiratory chest CT may be required in children to investigate tracheomalacia and interstitial lung disease. Occasionally, relatively higher radiation dose technique needs to be utilized, e.g., CT pulmonary angiography, to evaluate for pulmonary embolism.

There are various methods that can be employed to reduce radiation dose. CT protocols should be limited to the area of interest, and faster scan times decrease dosage and motion artifacts. Multiphase CT examinations (i.e., pre-contrast and post-contrast imaging) in children should be avoided. If necessary, dual-energy CT technology can be helpful due to its ability to create virtual non-contrast-enhanced images through image post-processing.

Although detailed discussion of CT parameters is outside the scope of this chapter, it is important to note that several factors can be customized for the patient according to body size and clinical indication. Factors like tube current (mAs) and peak kilovoltage (kVp) directly affect the image quality (i.e., noise) and radiation dose. It should be noted that mAs has a linear relationship with radiation dose, i.e., decreases in mAs cause increased image noise and decreased spatial resolution. Furthermore, kVp can have the greatest impact on patient radiation dose, due to a nonlinear relationship [25]. In adults, 120 kVp is generally used, and for smaller children, the optimal kVp is around 80. More recently, studies have found acceptable image quality for chest CT performed at 70 kVp in children up to 5 years of age [26].

Adjusting pitch and using tube current modulation and iterative reconstruction algorithms are specific techniques that allow imaging children at lower radiation dose and correcting for image noise. For example, recent studies demonstrate that high-pitch CT does not require breath holds (therefore minimizing sedation) and results in excellent image quality and lower radiation exposure compared to standard pitch (Fig. 3.22) [27].

Dual-energy CT uses photon spectra generated from different tube voltages which allow for material decomposition of tissues in the same acquisition. It is useful in metallic artifact reduction, e.g., after posterior spinal fixation for scoliosis repair. It can also create virtual non-contrast images from a contrast-enhanced study. One of its most powerful features is in vascular imaging, e.g., evaluating pulmonary arteriovenous malformations (AVM) with exceptional vascular enhancement at low kVp (Fig. 3.23). Its high diagnostic performance has overall decreased the incidence of nondiagnostic studies requiring optimal vascular enhancement which is frequently encountered during CT pulmonary angiography

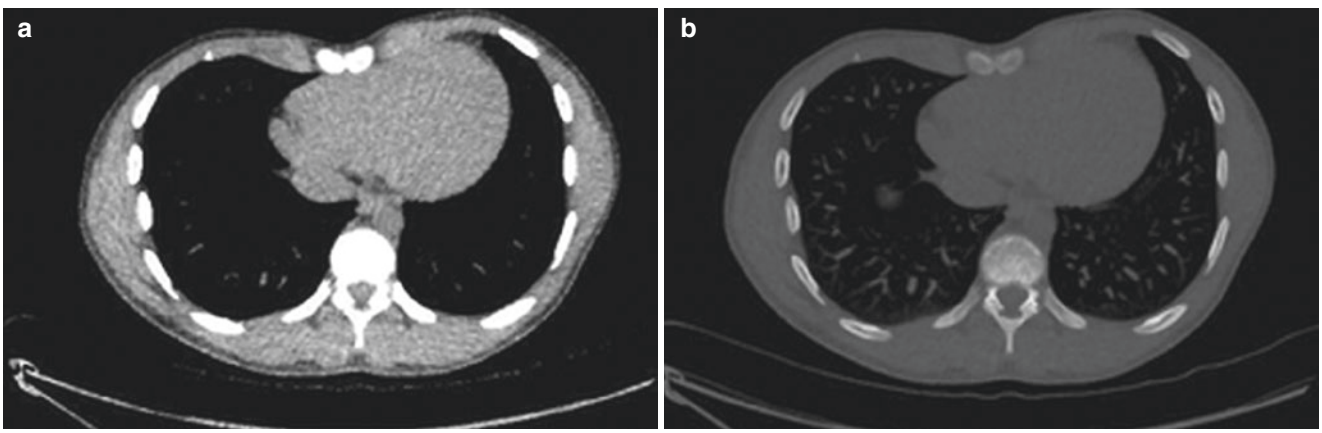

Fig. 3.21 (**a**, **b**) Axial CT views of the chest in a patient with pectus excavatum, low-dose protocol with soft tissue (**a**) and bone (**b**) windows. There is significant image noise seen in the soft tissues of the chest wall

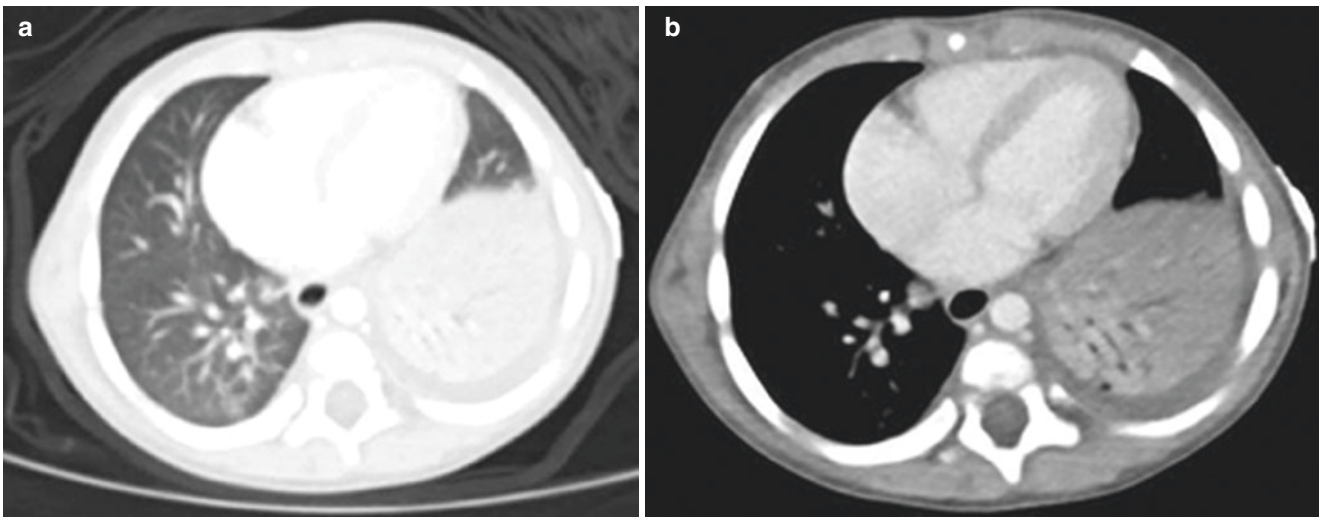

Fig. 3.22 (**a**, **b**) Axial CT views of the chest in a patient with necrotizing pneumonia in the left lower lobe and a left pleural effusion, lung (**a**) and soft tissue (**b**) windows, using high-pitch protocol. Diagnostic quality images were obtained while minimizing radiation to the patient

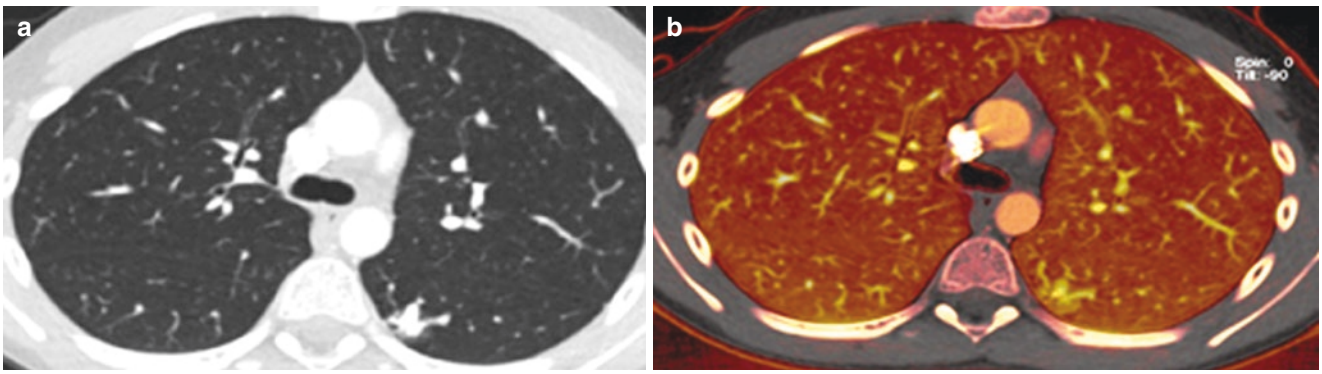

Fig. 3.23 (**a**, **b**) Dual-energy CT of the chest with monochromatic image at 60 kVp (**a**) and pulmonary blood volume/iodine distribution map (**b**) in a patient with pulmonary AVM in the superior segment of the left lower lobe. Note the feeding artery and draining vein in the nidus, with increased iodine distribution around the AVM, suggestive of surrounding vascular hyperplasia

by single-energy CT to evaluate for pulmonary embolism. While thus far, dual-energy CT has been shown to be dose neutral in the head and abdomen imaging, chest CT in young children may be associated with slightly higher radiation dose than single-energy photon protocols, though this topic needs further study [28].

Pediatric Magnetic Resonance Imaging

Although still in its early investigational stages, there has been extensive growth in chest MRI techniques in recent years. CT chest remains the workhorse of thoracic imaging, and MRI is an appealing alternative due to the lack of ionizing radiation, especially in the pediatric population. However, MRI is more time-intensive than CT and thus is more challenging with regard to patient comfort and cooperation. A typical MRI examination may range from 30 minutes to an hour compared to a few seconds in CT, and most children under 5 or 6 years of age may require sedation and/or general anesthesia. Furthermore, while MRI's performance to evaluate the mediastinum and chest wall is arguably similar or possibly better than CT, imaging of the lungs remains challenging due to artifacts and poor resolution from low-proton density and artifacts related to the magnetic susceptibility differences between air and soft tissues (Fig. 3.24). Nevertheless, there is continual interest in this field, and new imaging techniques are constantly being investigated to improve and optimize MR lung imaging aiming to make it comparable to CT.

While CT is superior to MRI for anatomic imaging, MRI also allows for functional assessment of the chest, including lung perfusion and ventilation and diaphragmatic excursion, and newer techniques may increase its applicability for more routine indications. Studies have shown that rapid lung MRI was comparable to CT for evaluating patients with suspected

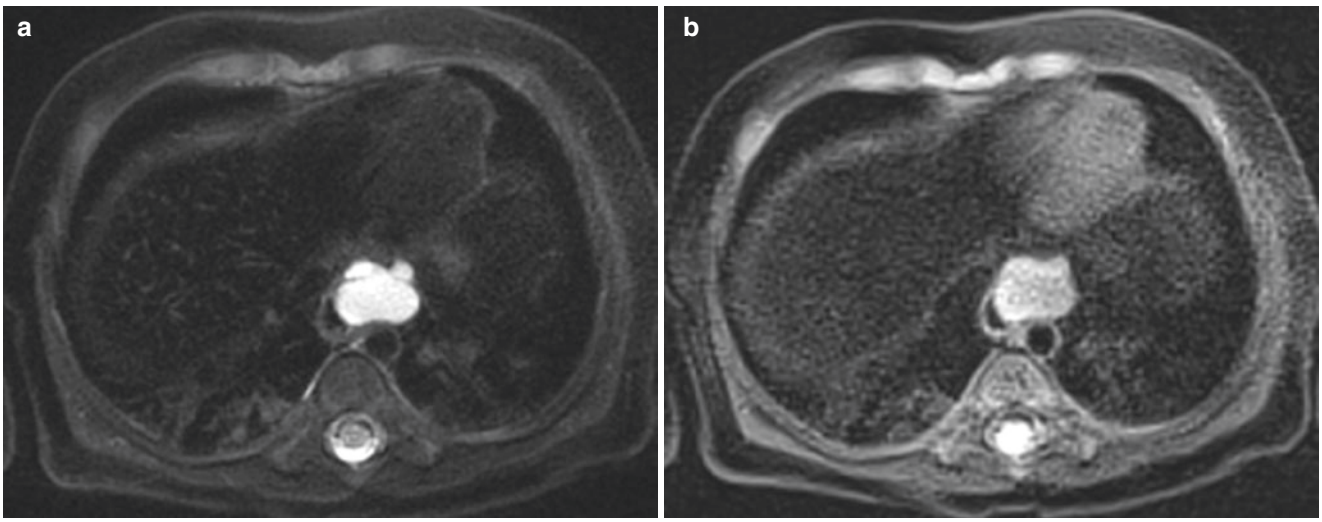

Fig. 3.24 (**a**, **b**) MRI of the chest. Axial T2-weighted image with fat saturation (**a**) and T2 post-gadolinium image (**b**) demonstrate a T2 bright cystic structure arising from the anterolateral wall of the esophagus, suggestive of esophageal duplication cyst

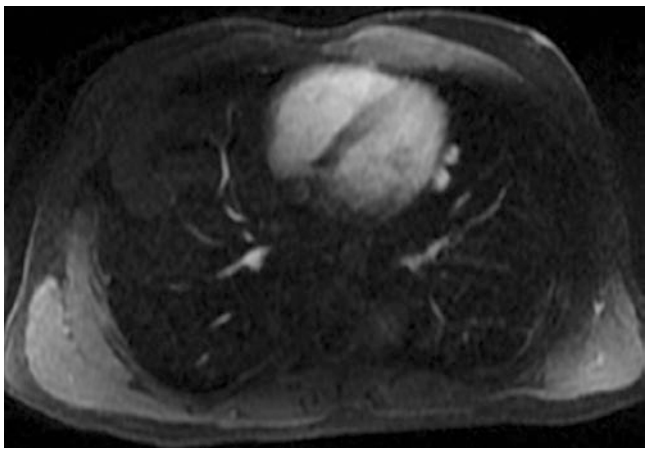

Fig. 3.25 MRI of the chest in a patient with metastatic Ewing's sarcoma. This post-contrast-enhanced fat-suppressed image demonstrates two pulmonary nodules in the lingula, adjacent to the pericardium

pulmonary infections [29]. Due to the lack of ionizing radiation, it also can play an important role in chronic lung diseases that require a long-term follow-up, i.e., cystic fibrosis [30–32]. Larger 1–2 cm pulmonary nodules can occasionally be seen (Fig. 3.25).

Patient Preparation

As with chest CT, proper patient preparation is essential for chest MRI, which can be more challenging for younger patients since the examination times are longer. A multidisciplinary approach including a pediatric anesthesiologist and child life specialist may be required as sedation is often required for younger children. Distraction techniques using MRI-compatible goggles can help put children at ease, improve their ability to follow instructions, and help avoid sedation in some cases.

Protocols

High-resolution images of the lungs are compromised by low signal intensity due to low-proton density, long examination times, and predilection of MRI for susceptibility artifacts from cardiac and respiratory motion. Children have difficulty with breath-holds, and young children are even more challenging due to high cardiac and respiratory rates, leading to motion artifacts.

When performing chest MRI, the smallest field of view focused on the area of concern should be used as much as possible, and sequences should be selected based on the type of contrast required (T1, T2, or proton density), signal-to-noise ratio, contrast-to-noise ratio, tissue characterization, and spatial and temporal resolution [33]. For example, chest wall lesions can be evaluated using standard spin echo and inversion recovery sequences. Image sequences like free-breathing Propeller (BLADE with navigator) allow images to be taken without breath-holding, which increases patient comfort and image quality. Sodhi et al. [29] showed that four fast sequences with short acquisition times can be used to assess pulmonary infections, for a total scan time of 2 minutes, with the patient spending 14–20 minutes in the MRI suite.

Pediatric chest MRI remains challenging, but the lack of ionizing radiation gives it an important advantage over CT in the pediatric population. Recent advances that shorten image acquisition time and improve diagnostic image quality should be continued to be explored to make chest MRI

increasingly feasible for children. Finally, MRI plays an important role in decreasing lifelong radiation exposure for children with chronic respiratory conditions like cystic fibrosis where the need for follow-up to monitor disease progression is regularly required throughout their life span.

References

1. Franken EA Jr, Smith WL, Berbaum KS, et al. Comparison of a PACS workstation with conventional film for interpretation of neonatal examinations: a paired comparison study. Pediatr Radiol. 1991;21(5):336–40.
2. Lanning P, Heikkinen E. Thymus simulating left upper lobe atelectasis. Pediatr Radiol. 1980;9(3):177–8.
3. Mulvey RB. The thymic "wave" sign. Radiology. 1963;81:834–8.
4. Francis IR, Glazer GM, Bookstein FL, et al. The thymus: reexamination of age-related changes in size and shape. AJR Am J Roentgenol. 1985;145(2):249–54.
5. Chen CM, Yu KY, Lin HC, et al. Thymus size and its relationship to perinatal events. Acta Paediatr. 2000;89(8):975–8.
6. De Felice C, Latini G, Del Vecchio A, et al. Small thymus at birth: a predictive radiographic sign of bronchopulmonary dysplasia. Pediatrics. 2002;110(2. Pt 1):386–8.
7. Hendrickx P, Dohring W. Thymic atrophy and rebound enlargement following chemotherapy for testicular cancer. Acta Radiol. 1989;30(3):263–7.
8. Meyers A, Shah A, Cleveland RH, et al. Thymic size on chest radiograph and rapid disease progression in human immunodeficiency virus 1-infected children. Pediatr Infect Dis J. 2001;20(12):1112–8.
9. Shackelford GD, McAlister WH. The aberrantly positioned thymus: a cause of mediastinal or neck masses in children. Am J Roentgenol Radium Therapy, Nucl Med. 1974;120(2):291–6.
10. Rosario-Medina W, Strife JL, Dunbar JS. Normal left atrium: appearance in children on frontal chest radiographs. Radiology. 1986;161(2):345–6.
11. Walmsley R, Monkhouse WS. The heart of the newborn child: an anatomical study based upon transverse serial sections. J Anat. 1988;159:93–111.
12. Ablow R. Radiologic diagnosis of the newborn chest. Curr Probl Pediatr. 1971;1:1–55.
13. Strife JL, Matsumoto J, Bisset GS III, et al. The position of the trachea in infants and children with right aortic arch. Pediatr Radiol. 1989;19(4):226–9.
14. Chang LW, Lee FA, Gwinn JL. Normal lateral deviation of the trachea in infants and children. Am J Roentgenol Radium Therapy, Nucl Med. 1970;109(2):247–51.
15. Stewart JR, Kincaid OW, Titus JL. Right aortic arch: plain film diagnosis and significance. Am J Roentgenol Radium Therapy, Nucl Med. 1966;97(2):377–89.
16. Felson B, Palayew MJ. The two types of right aortic arch. Radiology. 1963;81:745–59.
17. Eisenberg RL. Elevation of the Diaphragm. In: Gastrointestinal radiology: a pattern approach. 4th ed. Philadelphia: Lippincott Williams & Wilkins; 2003. p. 153–9.
18. Luke MJ, McDonnell EJ. Congenital heart disease and scoliosis. J Pediatr. 1968;73(5):725–33.
19. Quan L, Smith DW. The VATER association. Vertebral defects, anal atresia, T-E fistula with esophageal atresia, radial and renal dysplasia: a spectrum of associated defects. J Pediatr. 1973;82(1):104–7.
20. Noonan JA. Association of congenital heart disease with syndromes or other defects. Pediatr Clin N Am. 1978;25(4):797–816.
21. Cleveland RH. The pediatric airway. Contemp Diagn Radiol. 1996;19:1–6.
22. Bramson RT, Griscom NT, Cleveland RH. Interpretation of chest radiographs in infants with cough and fever. Radiology. 2005;236:22–9.
23. Cox M, Soudack M, Podberesky DJ, Edelman M. Pediatric chest ultrasound: a practical approach. Pediatr Radiol. 2017;47:1058–68.
24. Jones BP, Tay ET, Elikashvili I, et al. Feasibility and safety of substituting lung ultrasonography for chest radiography when diagnosing pneumonia in children: a randomized controlled trial. Chest. 2016;150(1):131–8.
25. Ngo AV, Winant AJ, Lee Y, Phillips G. Strategies for reducing radiation dose in CT for pediatric patients: how we do it. Semin Roentgenol. 2018;53(2):124–31.
26. McDougall R, Kleinbahn P, Yu L, Lee EY. Pediatric thoracic CT angiography at 70 kV: a phantom study to investigate the effects on image quality and radiation dose. Pediatr Radiol. 2016;46(8):1114–9.
27. Bodelle B, Fischbach C, Booz C, et al. Free-breathing high-pitch 8 kVp dual-source computed tomography of the pediatric chest: Image quality, presence of motion artifacts and radiation dose. Eur J Radiol. 2017;89:208–14.
28. Zhu X, McCullough WP, Mecca P, Servaes S, Darge K. Dual-energy compared to single-energy CT in pediatric imaging: a phantom study for DECT clinical guidance. Pediatr Radiol. 2016;46:1671–9.
29. Sodhi KS, Kandelwal N, Saxena AK, et al. Rapid lung MRI in children with pulmonary infections. Time to change our diagnostic algorithms. J Magn Reson Imaging. 2016;43:1196–206.
30. Tiddens HAWM, Kuo W, van Straten M, et al. Paediatric lung imaging: the times they are a-changin. Eur Respir Rev. 2018;27:170097.
31. Tepper lA, Ciet P, Zaudre D, et al. Validating chest MRI to detect and monitor cystic fibrosis lung disease in a pediatric cohort. Pediatr Pulmonol. 2016;51(1):34–41.
32. Amaxopoulou C, Gnannt R, Higashigaito K, et al. Structural and perfusion magnetic resonance imaging of the lung in cystic fibrosis. Pediatr Radiol. 2018;48(2):165–75.
33. Ciet P, Tiddens HA, Wielopolski PA, et al. Magnetic resonance imaging in children: common problems and possible solutions for lung and airways imaging. Pediatr Radiol. 2015;45:1901–15.

Fetal Chest

4

Dorothy Bulas and Alexia Egloff

Ultrasonography (US) is the screening method of choice for the evaluation of the fetal airway and chest. It is safe, inexpensive, and easily performed. Advances in US technique including higher resolution transducers, Doppler, and 3D/4D imaging have allowed for improved assessment of the congenital thoracic masses. The assessment of the fetal chest by US, however, is operator dependent and evaluation may be limited due to fetal position, maternal obesity, overlying bone, and/or oligohydramnios. Ultrasound evaluation is sensitive in the diagnosis of many prenatal lung lesions but has low specificity [1].

Magnetic resonance imaging (MRI) is an alternative modality that uses no ionizing radiation, has excellent tissue contrast and a large field of view, is not limited by obesity or overlying bone, and can image the fetus in multiple planes regardless of fetal lie. Faster scanning techniques allow studies to be performed without sedation in the second and third trimester with minimal motion artifact. Fetal MRI helps confirm the presence of masses identified by US, can delineate anatomy such as the trachea not visualized by US, more accurately measure lung volumes, and may demonstrate additional subtle anomalies. Experts in fields such as pediatric surgery and neonatology not comfortable interpreting US imaging can provide additional expertise when reviewing MR images. This multidisciplinary approach is crucial for the success of handling these complex cases [2–5].

Thus, advances in both US and MRI have improved our ability to accurately diagnose fetal airway and chest anomalies and furthered our understanding of the evolution of fetal lung lesions.

D. Bulas (✉)
Department of Diagnostic Imaging and Radiology, George Washington University Medical Center, Children's National Medical Center, Washington, DC, USA
e-mail: dbulas@cnmc.org

A. Egloff
Department of Radiology, Children's National Medical Center, Washington, DC, USA

The prenatal and postnatal prognosis for fetuses with chest anomalies is quite variable. Fetal imaging not only is important for the initial diagnosis of the lesion but is also useful for follow-up in case nonimmune hydrops develops. Preparation for delivery at a tertiary institution is critical for the fetus with a large airway or chest mass. The decision to perform in utero intervention or an ex utero intrapartum treatment (EXIT) delivery places both the mother and fetus at risk and thus benefits from precise evaluation and accurate assessment of the situation. Prenatal evaluation not only allows for the planning of in utero therapy but can optimize postnatal therapeutic planning with reduction in neonatal imaging, useful when caring for the unstable infant [2–4].

Prenatal diagnosis does not always result in improved outcome as some cases are associated with lethal pulmonary hypoplasia. A small chest mass can be associated with severe chromosomal anomalies or other lethal anatomic abnormalities. Thus, accurate chromosomal and structural assessment of the entire fetus is also important for appropriate counseling and planning of in utero interventional procedures, delivery, and postnatal management.

Ultrasonography Imaging of the Fetal Neck and Chest

Ultrasonography of the Fetal Chest

Ultrasound is the initial imaging modality in the detection of fetal chest masses. On axial images, the normal fetal chest is oval or round. The heart is positioned within the anterior half of the left chest and bordered on both sides by lung tissue. The apex of the heart touches the wall of the left anterior chest, while the intersection of the atrial septum with the posterior heart border lies just to the right of center. The lungs, thorax, and heart grow proportionally, so the normal cardiothoracic ratio is constant throughout the pregnancy, and the cardiac position and axis should not change over time. The fetal ribs are echogenic and encompass more than

R. H. Cleveland, E. Y. Lee (eds.), *Imaging in Pediatric Pulmonology*, https://doi.org/10.1007/978-3-030-23979-4_4

half the chest circumference on either side. The ultrasound appearance of normal fetal lungs is typically homogeneous and echogenic. In early pregnancy, the lungs are less echogenic than the liver, but echogenicity increases through gestation as the lungs become more fluid filled. At times, the echogenicity of the lung may appear similar to the adjacent liver and bowel making it difficult to differentiate sonographically from the surrounding organs. Inferiorly, the diaphragms border the lungs and are dome shaped and hypoechoic. It is important to remember that visualization of a seemingly intact diaphragm does not exclude a diaphragmatic hernia as a small defect may be missed. The thymus, a homogeneous anterior mediastinal structure, is often not well seen because of overlying rib shadowing. Normal measurements for the fetal thymus have been published. A smaller than normal-sized thymus can be seen in fetuses with intrauterine growth restriction, Down syndrome, congenital heart defects in combination with 22q11 microdeletion, preeclampsia, and preterm rupture of membranes [6].

Different two-dimensional measurements have been used to assess lung development for age. The chest circumference measured at the level of the four-chamber view of the heart has been traditionally used. A recent study by Britto et al. suggests using 3D ultrasound to estimate chest circumference by using the fetal aorta and inferior angle of the scapula as anatomical landmarks [7]. This approach should provide a better assessment of lung and thorax development as landmarks are less likely to be affected or displaced by thoracic pathology compared to the heart. Three-dimensional US can also provide lung volumetry measurements [8]. Nomograms exist for chest circumference, 2D oblique lung diameter and 3D volumetry [7–9], and can be used to aid in the early diagnosis of pulmonary hypoplasia. Obtaining volume measurements, however, can be difficult in all three planes as oligohydramnios, maternal obesity, or fetal lie may make differentiation of the lung and surrounding structures difficult.

Sonographically, congenital lung masses can appear hypoechoic/cystic or hyperechoic/microcystic/solid and small or large (Fig. 4.1). When a solid lung mass is present, the echogenicity may be similar to adjacent liver and lung and, thus, difficult to identify. Shift of the heart and flattening of the diaphragms may be the first clue that a lung mass or diaphragmatic hernia is present (Fig. 4.2). Echogenic masses may become less visible later in gestation as the surrounding lung tissue becomes more echogenic and rib shadowing increases. The differential for lung masses includes congenital diaphragmatic hernia (CDH), congenital pulmonary airway malformation (CPAM/CCAM), bronchopulmonary sequestration (BPS), congenital lobar emphysema (CLE)/bronchial atresia, hybrid lesions, and congenital hydrothorax [10–12]. Ultrasound while sensitive in the identification of many lung lesions due to their abnormal echogenicity and/or mass affect has a low specificity [1].

Ultrasonography of the Fetal Neck

Ultrasound imaging the fetal neck is also important in the assessment of the fetal airway and lungs. Axial images of the neck may demonstrate the larynx and pharynx sonographically if they are fluid filled, but the trachea is typically not visualized. Axial images of the posterior neck are important for the identification of nuchal translucency at 11–14 weeks and nuchal thickening at 16–20 weeks both of which are markers for aneuploidy. The jugular vein and carotid artery can be identified by color Doppler and may be deviated if a mass is present. A detailed exam of the neck is not always possible by ultrasound when oligohydramnios, maternal obesity, or fetal lie prevents adequate visualization. If the neck is in fixed extension, there should be concern that a neck mass is present.

When a neck mass is identified, internal characteristics may help determine the diagnosis. There are a wide variety of neck masses which can be cystic (lymphatic malformation (lymphangioma/cystic hygroma), branchial cleft cyst, thyroglossal duct cyst, laryngocele, cervical meningomyelocele), solid (goiter, neuroblastoma, fibroma), or complex (teratoma, hemangioma, goiter). The two most common causes for neck masses are lymphangioma and teratomas [13] (Figs. 4.3 and 4.4).

The prognosis of a cervical mass is dependent on the amount of airway compression, presence of other anomalies, and development of hydrops. As the airway is not directly seen by US, secondary signs of airway compression such as polyhydramnios or a small stomach may suggest severity of airway compromise.

Magnetic Resonance Imaging of the Fetal Neck and Chest

Fetal Magnetic Resonance Technique

Advances in MR including single-shot rapid acquisition with relaxation enhancement sequences have significantly decreased movement artifact on 1.5 T and 3 T magnets. Slices are acquired individually with each slice obtained by a single excitation pulse taking less than 400 ms. A series can be obtained in less than 30–40 seconds with slices as thin as 2–3 mm. These T2-weighted images have excellent contrast and spatial resolution and good signal-to-noise ratios. Sequences available include single-slice fast spin echo, ssFSE (GE, Milwaukee, WI), and half-Fourier acquisition single-shot turbo spin echo, HASTE (Siemens, Erlangen, Germany) [14, 15]. Additional MR sequences include heavy T2w hydrography, fast T1w sequences including fast multiplanar spoiled gradient echo, diffusion-weighted sequences, and two-dimensional fast low angle shot. These sequences

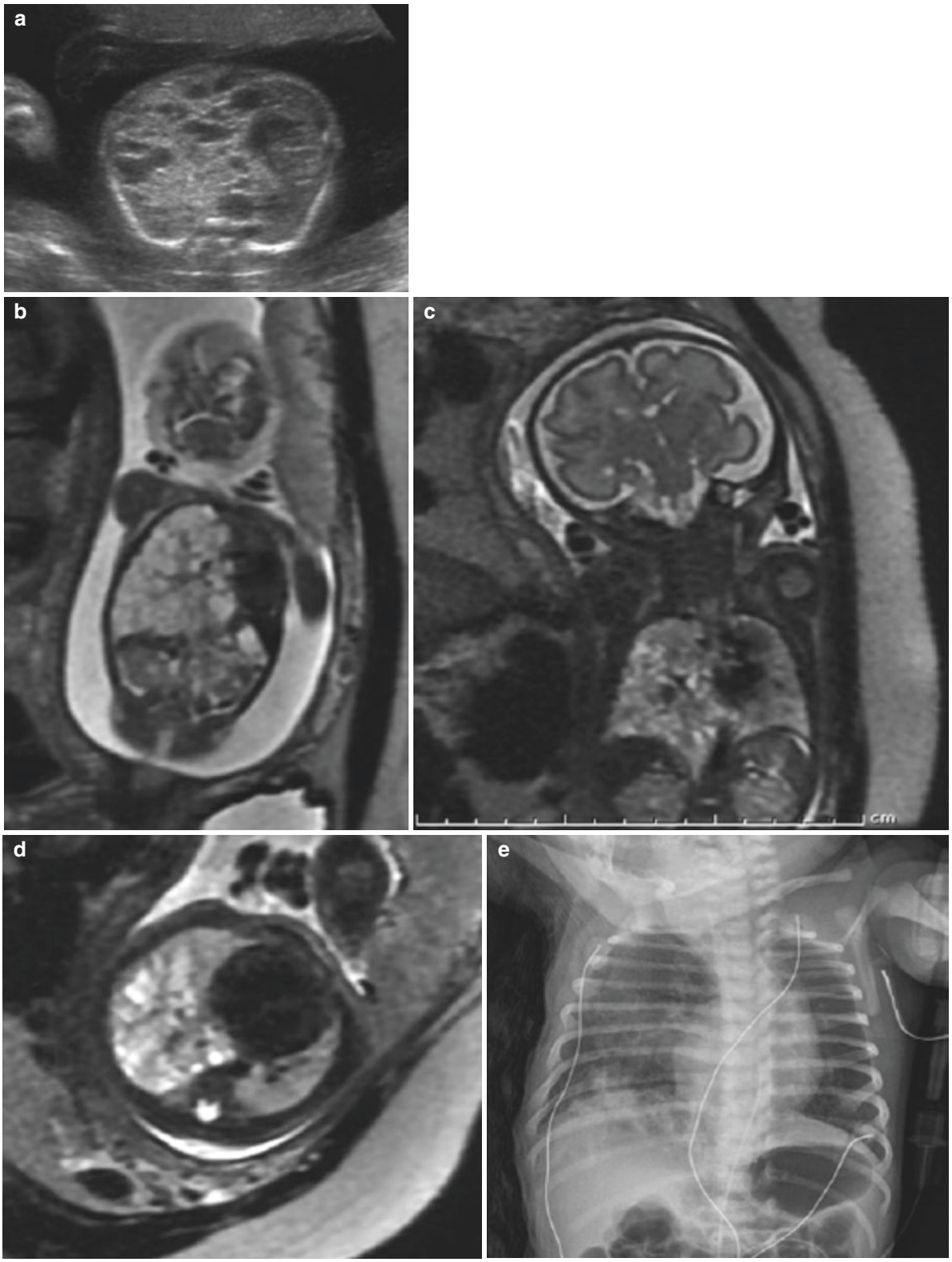

Fig. 4.1 Congenital pulmonary airway malformation. (**a**) Axial US at 21 weeks gestation demonstrates a large mixed macrocystic and microcystic mass in the right hemithorax with compression of normal left lung. (**b**) Coronal SSFSE T2w MR image also at 21 weeks confirms the presence of a large multicystic mass in the right hemithorax everting the diaphragm inferiorly and deviating the heart to the left. The CPAM volume ratio (CVR) measures 2.4 high risk for developing hydrops. Follow-up coronal (**c**) and axial (**d**) MR images at 30 weeks gestation demonstrates growth of the fetus with stable size of the right lung mass. The mass no longer everts the diaphragm nor deviates the heart to the left. The CVR has improved and now measures 1.4 low risk for developing hydrops. (**e**) At delivery, the infant had minimal respiratory distress. Chest radiograph demonstrates minimally heterogeneous right lower lobe

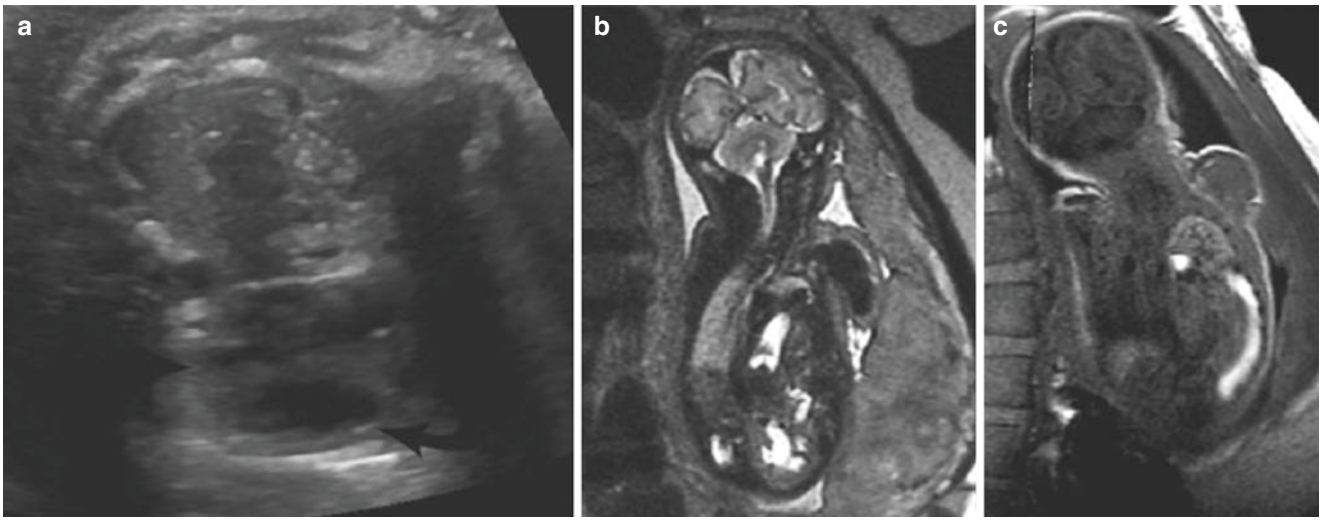

Fig. 4.2 Congenital diaphragmatic hernia. (**a**) Axial US of a fetal chest demonstrates a heterogeneous mass in the left hemithorax deviating the heart (*curved arrow*) to the right. (**b**) Coronal SSFSE T2w image of the fetal chest demonstrates that small and large bowel is herniated into the left hemithorax consistent with a diaphragmatic hernia rather than CPAM. (**c**) Coronal T1w image confirms that high-signal meconium filled bowel and liver are herniated into the left hemithorax

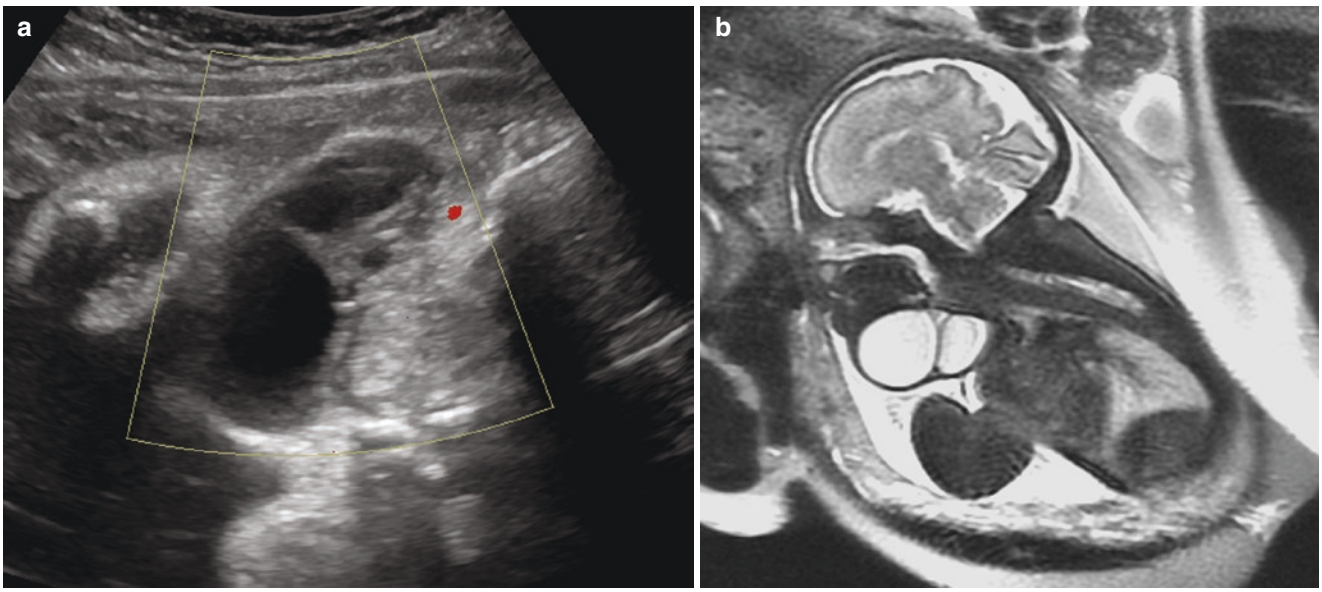

Fig. 4.3 Cervical lymphangioma. (**a**) Axial US image of the fetal neck demonstrates several macrocysts with no significant vascularity. (**b**) Sagittal SSFSE T2w MR image of the fetal neck at 30 weeks' gestation confirms the presence of a large multiseptated mass compressing the cervical trachea

take longer and may require breath holding and thicker slices for sufficient signal-to-noise ratios.

Total study time can average 20–40 min, depending on fetal movement which is particularly problematic in cases of polyhydramnios and younger gestations. Studies may be limited due to maternal size, claustrophobia, and maternal discomfort in the supine position. Left lateral decubitus position can be helpful in patients with back pain or with supine hypotension. A fast multiplanar spoiled gradient-echo sequence or large field of view (48 cm; section thickness 8 mm; intersection gap 2 mm) coronal ssFSE localizer is first performed to evaluate fetal position and select future imaging planes. Each subsequent plane is placed orthogonal to the previous sequence to account for fetal movement. Axial, sagittal, and coronal T2w images angled to the fetal chest are obtained at 3–5 mm thickness, 0 mm section gap. Planes angled to the fetal brain and abdomen are important for complete assessment of the fetus. Quiet maternal breathing is adequate for

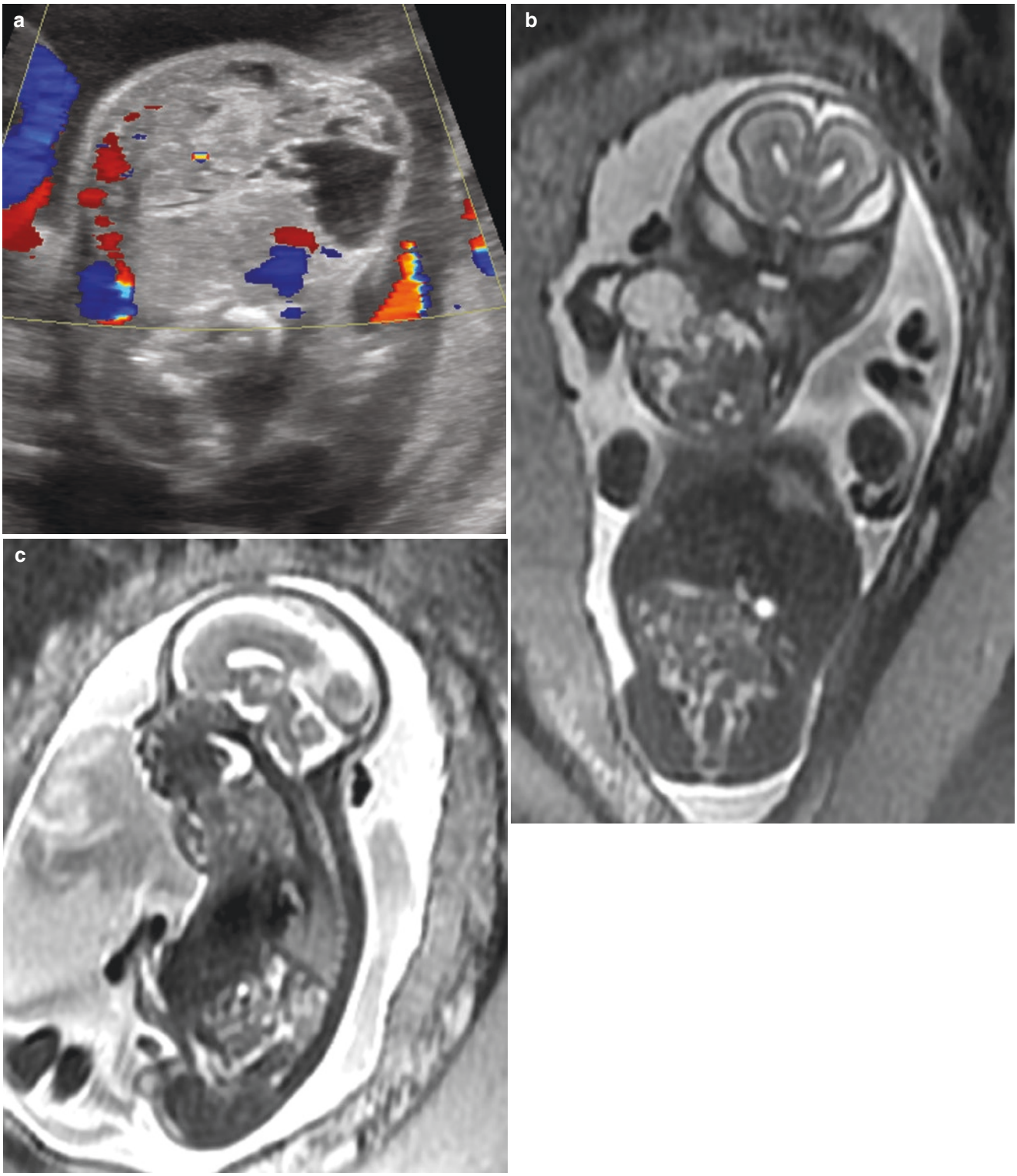

Fig. 4.4 Cervical teratoma. (**a**) Axial US image of the fetal neck at 21 weeks' gestation demonstrates a mixed cystic and solid mass with prominent vessels. Coronal (**b**) and sagittal (**c**) fetal T2w MR images confirm the presence of a large mass compressing the cervical trachea. The oropharynx was distended with fluid. Polyhydramnios was present

T2w images, with breath-hold T1w, echoplanar, and angiographic sequences added as needed. Fetal MRI provides improved anatomic evaluation of the airway and lungs, helps corroborate the diagnosis, and often provides additional information useful for management planning including fetal intervention [2, 3]. More specific diagnosis prenatally provides improved counseling, decreasing the level of stress that could result when a thoracic anomaly is diagnosed [5].

Fetal Magnetic Resonance Safety

There is no definitive evidence that MRI produces harmful effects on human embryos or fetuses using current clinical parameters. The long-term safety of MRI exposure to the fetus, however, has not been definitively demonstrated [16–18].There has been concern that prolonged exposure to high-field MRI may affect embryogenesis, chromosomal structure, or fetal development [3]. Animal studies on embryos have not demonstrated any growth abnormalities or genetic damage at clinical levels of exposure so far [19, 20]. There is concern that with higher strength units and prolonged scanning times, biological effects may occur if applied at sensitive stages of fetal development [21, 22]. Recently, the long-term safety after MRI exposure in the first trimester was assessed with a large retrospective study and demonstrated no significant increase in congenital anomalies, neoplasms, or vision or hearing loss [23].

Compliance with the US Food and Drug Administration (FDA) and International Commission on Nonionizing Radiation Protection (ICNIRP) guidelines requires control of specific absorption rate (SAR) values [24, 25]. Medical Device Agency (MDA) guidelines require control of the maximum SAR (10 g) within the fetus. The most frequently used sequences do operate at the SAR limit recommendations. These limits need to be carefully followed with higher field systems as well [26]. MR is not routinely recommended during the first trimester due to the small fetal size and significant fetal motion limiting imaging at this gestation .

Gadolinium should not be used with fetal imaging as it has been shown to cross the placenta. The fetus excretes and then swallows gadolinium which gets reabsorbed from the gastrointestinal tract. In animal studies, growth retardation has been reported after high doses of gadolinium (Magnevist product information, Berlex Labs, Wayne, NJ). A retrospective study demonstrated an increase in rheumatologic, inflammatory, or infiltrative skin conditions as well as stillbirths and neonatal death after gadolinium administration [23], Thus exposure of the fetus to gadolinium is not recommended.

MRI of the Fetal Chest

Fetal MRI is a useful adjunct in the assessment of the fetal airway and chest. Fluid in the trachea and larynx is high T2w and thus well delineated [27]. Fetal lungs are homogeneously brighter than muscle and increase in signal after 24 weeks' gestation due to the development of alveoli and production of alveolar fluid [28] in the third trimester. Normal lung when compressed by a mass may be slightly hypointense compared to noncompressed normal lung. Normal lung parenchyma is easily separated from abnormal lung masses which tend to be higher in signal.

The mediastinal structures, liver, and lung are easily differentiated by MR. The liver and spleen are low in signal on T2w with liver higher in signal on T1w than normal lung. On T2w, meconium is low in signal, while fluid-filled small bowel is high in signal. This reverses on T1w when meconium is bright and fluid-filled small bowel is low in signal and is easily distinguished from adjacent lung and liver in cases of CDH (Fig. 4.2). The thymus is homogeneous and of higher signal than the heart which appears as a flow void on T2w.

The ability to image in any plane and large field of view aids in the delineation of fetal lung masses. Lung volumes can be measured in any plane, and normative data are being accumulated for various gestational ages. Volumetric lung measurements appear to be reproducible and increase with gestational age. The right lung measures approximately 56% of the total lung volume. When oligohydramnios limits visualization of the fetus sonographically, MR can still demonstrate many anomalies, and lung volumes can be measured to assess for pulmonary hypoplasia. In complex cases, such as thoracopagus conjoined twins, the large field of view can be particularly helpful. Thus, while US is the initial modality in detecting chest masses, MRI is useful in confirming the presence of a mass, providing assessment of residual lung volume, and further characterizing the lesion increasing specificity.

MRI of the Fetal Airway

Prenatal evaluation of the fetal neck is difficult with complex embryology involving the development of vascular, lymphatic, musculoskeletal, and digestive systems. Masses such as teratomas and lymphangiomas can share both cystic and solid components, with precise histologic diagnosis difficult prenatally. If the neck mass is large and compresses the airway, death may occur at delivery if a patent airway is not established quickly. Thus, detection of a neck mass prenatally is important to prepare for the timing, location, and mode of delivery.

Fetal MRI is a useful adjunct in the evaluation of neck and thoracic masses which compress the fetal airway. The normal fetal airway can be visualized on T2w due to high-signal fluid within the larynx, trachea, and bronchi. The esophagus is not typically visualized but may be identified when distended by a distal obstruction. T1w images are useful for the diagnosis of a goiter which is of high signal on T1w.

When a neck mass is identified, MRI can delineate if the mass extends into the oropharynx. The amount of tracheal deviation and compression can be directly visualized. MRI is also useful for the evaluation of tracheal compression from thoracic masses. Mediastinal masses are rare and include foregut cysts, teratomas, esophageal duplication cysts, and bronchogenic cysts. Foregut cysts including bronchogenic, enteric, and neurenteric are typically fluid filled with high T2w homogeneous signal. Mediastinal teratomas have a complex heterogeneous appearance due to fat and fluid. These masses may compress the great vessels and result in hydrops and/or compress the esophagus and result in polyhydramnios [28].

The location of cystic and solid components of neck and mediastinal masses can be evaluated in three dimensions allowing the surgeon to plan for in utero intervention or post-delivery cyst aspiration or resection. If the fetus greater than 32 weeks' gestation with a large lesion expected to have difficulty breathing at delivery, EXIT may be considered. This partial delivery followed by intubation and intravenous access prior to clamping the umbilical cord can improve the survival of these difficult cases [29].

Prenatal Diagnosis and Management of Chest Anomalies

When an airway or chest abnormality is identified prenatally, several questions need to be answered:

- Are additional anomalies or hydrops present?
- Will there be pulmonary hypoplasia at delivery?
- Will there be airway obstruction at delivery?
- Can in utero intervention help?

The most common congenital thoracic lesions include CDH, congenital pulmonary airway malformation (CPAM/CCAM), BPS, congenital lobar overinflation/bronchial atresia, hybrid lesions, and congenital hydrothorax [30]. Pulmonary hypoplasia, agenesis, and aplasia are less common. A definitive diagnosis of a chest mass is usually possible only after surgical resection and histopathological evaluation [10–12].

In the fetus, the clinical importance of these lesions lies primarily in the mass effect on surrounding structures. This can result in compression of the airway, blood vessels, lymphatics and normal lung with development of pleural effusions, polyhydramnios, hydrops, and pulmonary hypoplasia. Outcome depends on the timing of secondary effects and severity of pulmonary hypoplasia. With improvement in fetal imaging, more aggressive fetal interventions have advanced. While the majority of cases with lung masses survive, masses that result in hydrops in the past were typically lethal. Now these masses may be amenable to fetal interventions such as maternal steroids, fetal thoracentesis, laser therapy, and in utero surgery [31–36].

Congenital Pulmonary Airway Malformation

Congenital pulmonary airway malformation (CPAM/CCAM) has varying appearances sonographically dependent on subtype. The pathologic classifications by Stocker et al. have no real prognostic value prenatally [37]. A simpler fetal classification by Adzick et al. [33] based on gross anatomy and imaging appearance has been recommended for prenatal assessment:

- Macrocystic – One or more macrocysts measuring >5 mm. These cysts are hypoechoic by ultrasound and high signal by MR. This subtype grows less rapidly but may develop hydrops and can require prenatal intervention (Fig. 4.5).

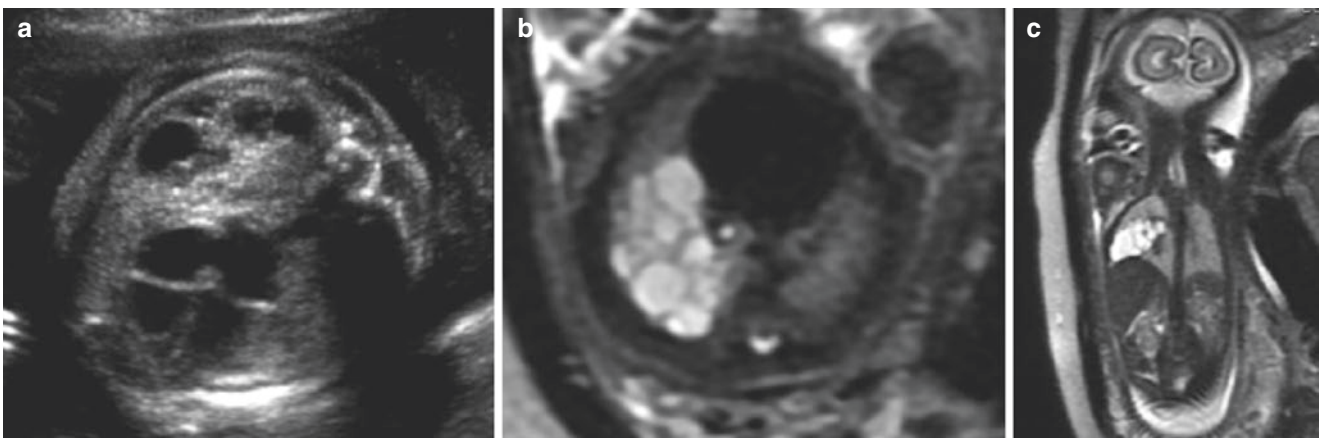

Fig. 4.5 Macrocystic CPAM. (**a**) Axial US image of the fetal chest demonstrates multiple macrocysts within the right hemithorax. Axial (**b**) and coronal (**c**) SSFSE T2w MR images confirm that the high-signal macrocysts are limited to the right middle lobe with normal intermediate signal right upper and lower lobe parenchyma

- Microcystic – Multiple microcysts <5 mm that appear homogeneously echogenic/solid by ultrasound and are high signal by MR. When large, they may be associated with mediastinal shift, pulmonary hypoplasia, polyhydramnios, and nonimmune hydrops requiring in utero intervention.

By ultrasound, macrocysts are well delineated from adjacent echogenic normal parenchyma. The microcystic subtype is echogenic as compared to normal lung but may become more difficult to visualize as gestational age advances due to the normal increase in echogenicity of surrounding normal lung as alveoli develop (Fig. 4.6). Shadowing from overlying ribs becomes more problematic in the third trimester limiting lung parenchymal visualization. When the mass is large, mediastinal shift can be identified by rotation and deviation of the heart axis.

When severe, vena cava and cardiac compression may result in hydrops, with pleural effusions, pericardial effusions, skin thickening, and ascites developing. Esophageal compression can result in a small stomach and polyhydramnios. Color and power Doppler imaging are useful in looking for a systemic feeding vessel [5], while 3D/4D imaging can be used to measure lung volumes [8].

By MR, CPAM are typically higher in signal than adjacent normal lung with mediastinal shift easily demonstrated. MR is particularly valuable when a rare bilateral CPAM is present. Lung volumes are easily measured in any plane by MR.

Prognosis does not depend on the type of lesion [33]; rather, it is dependent on the size of the mass, amount of mediastinal shift and pulmonary hypoplasia, fetal hemodynamics, associated anomalies, and gestational age at delivery [30, 33].

CPAM is rarely associated with chromosomal anomalies, but associated anomalies should still be searched for [34]. Karyotyping is not necessary if no other anomalies or risk factors are identified [34]. In the absence of hydrops, early survival without any intervention is higher than 95% [35].

Follow-up ultrasounds are critical to assess stability of mass size and the potential development of hydrops.]. The presence of hydrops is the most important indicator of poor outcome and can result in perinatal death approaching 100% without intervention [33].

A CPAM volume ratio (CVR) has been described as a predictor of hydrops and outcome [38]. It is obtained by calculating the volume of the lung mass and normalizing it by gestational age using the head circumference [38].

$$\text{CVR} = \frac{\text{height} \times \text{anteroposterior diameter} \times \text{transverse diameter} \times (\text{constant})}{\text{Head cirumference}}$$

If the CVR is less than 1.6, the risk of developing hydrops is low [38]. If the ratio is more than 1.6, the fetus is at high risk for developing hydrops, and intervention should be considered to increase survival.

CPAM typically show progressive growth between weeks 20 and 26 of gestation. By 26–28 weeks, growth begins to plateau. Usually, no hydrops develops after reaching the 28 weeks' growth plateau [38].

If hydrops develops and gestation is less than 32 weeks, various interventions have been attempted with the objective of decreasing fetal compromise and preventing lung hypoplasia [11]. Best approach is selected for each individual case depending on the presence of hydrops, the type of anomaly, and the consideration of potential risks of the various treatment options [39]. Interventions include maternal steroids, fetal thoracentesis, cyst aspiration, thoracoamniotic shunt, laser therapy, sclerotherapy, and in utero surgical resection [38–47].

Successful fetal surgery depends on surgical experience as well as optimal maternal anesthesia and uterine relaxation, hysterotomy, and fetal exposure techniques: intraoperative fetal monitoring, reliable amniotic membrane, and uterine closure. Close postoperative follow-up and early detection and treatment of preterm labor are fundamental. To undergo fetal surgery, maternal health needs to be considered to decrease the risk of complications [33].

Up to 50% of CPAM actually resolve prenatally [36]. Of the lesions that resolve in utero, 60% show no abnormality on postnatal imaging [36]. The remaining 40% with apparent prenatal resolution are still present postnatally but not well seen by follow-up prenatal imaging due to increase in normal lung echogenicity and difficulty in differentiating normal from abnormal lung [38]. When a persistent mass is seen, it is confirmed by postnatal imaging in over 95% of cases.

Persistent masses can decrease in size during the late second trimester [33] or have a relative decrease in size due to normal fetal growth. Some do actually increase in size. Implications for delivery and postnatal management include size of mass at delivery and the presence of hydrops. If the lesion is small with no hydrops, the obstetrician and neonatologist need to be aware of the potential need for respiratory support. However, the majority of these infants do well and can be delivered vaginally with no additional support required [48]. Following delivery, these infants should be assessed for respiratory stability and feeding tolerance. If stable, the infant can be discharged home. Follow-up may include radiographs

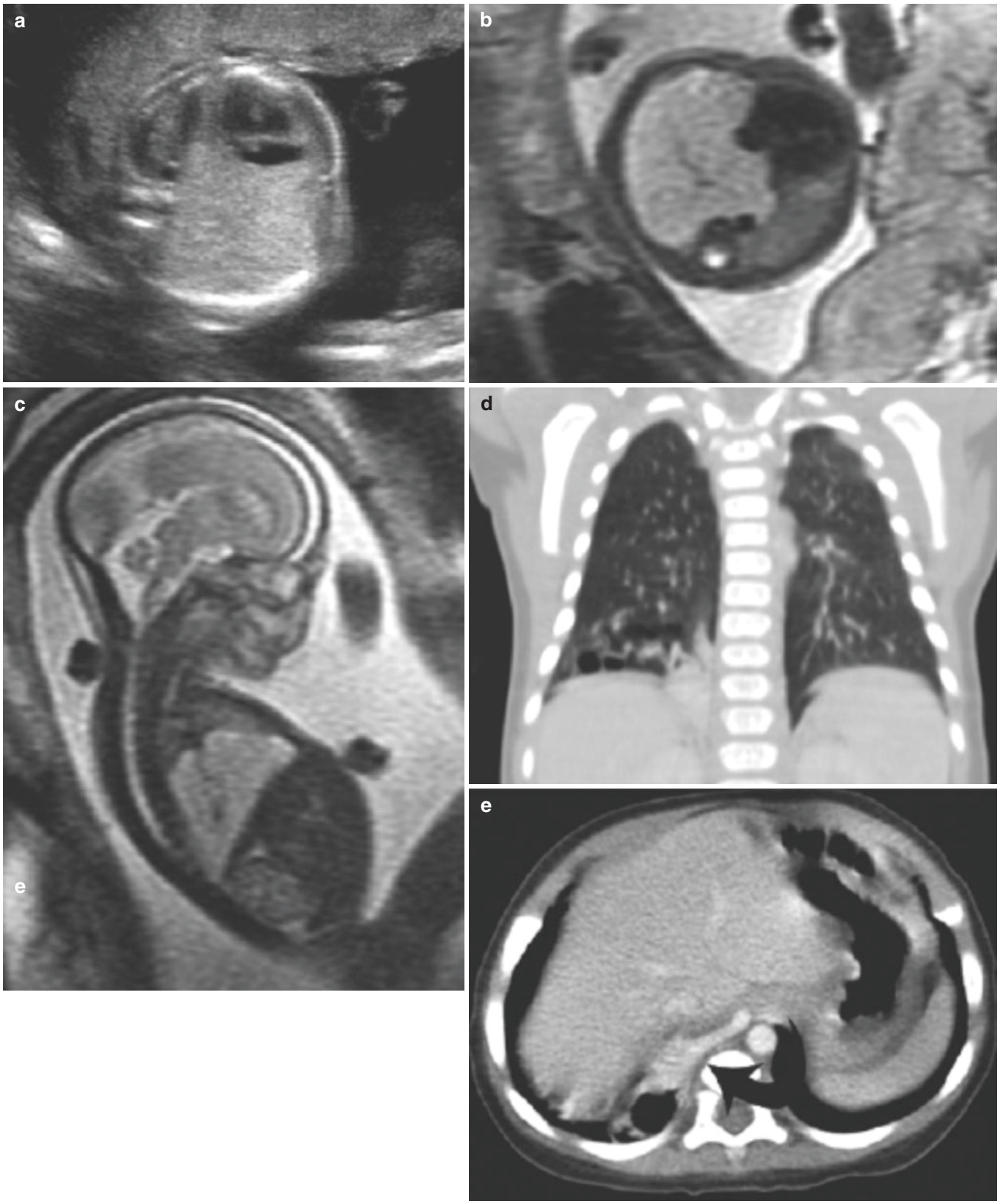

Fig. 4.6 Microcystic hybrid lung mass. (**a**) Axial US image of the fetal chest demonstrates a homogeneous echogenic mass deviating the heart to the left. Axial (**b**) and sagittal (**c**) SSFSE T2w MR confirm the presence of a high-signal right lower lobe mass. (**d**) Coronal reformatted image of a chest CT at 5 months of age demonstrates a small residual mixed cystic and solid mass in the right lower lobe. (**e**) Axial CT with intravenous contrast demonstrates the presence of a feeding systemic vessel (curved arrow) consistent with a hybrid sequestration

and CT scans, the timing of which should be dependent on whether the infant is symptomatic or not.

A recent pathologic analysis by Pogoriler et al. classified all surgically resected prenatally diagnosed lung lesions diagnosed over 2½ years [49]. In this study, lesions with large cysts (Stocker type I) were less common than those with small cysts and more likely to be symptomatic postnatally and thus need surgical management. They also found that clusters of mucinous cells are overall rare (present in 8% of congenital cystic lung lesions) but seen almost exclusively in cases with large cysts [49]. These results are useful when counseling during pregnancy.

For large masses that cause mediastinal shift and/or hydrops, delivery at a tertiary care center with an intensive care nursery capable of resuscitation of a neonate with respiratory difficulties, including capability of ECMO, should be planned [40, 46].

If the fetus is greater than 32 weeks' gestation with hydrops, delivery by EXIT should be prepared for with likely need of the mass to be resected at birth [46].

Bronchopulmonary Sequestration

Bronchopulmonary sequestration (BPS) typically has the appearance of a homogeneous triangular echogenic mass with well-defined borders by ultrasound. By definition, BPS have systemic feeding and draining vessels and consist of lung parenchyma without communication to the bronchial tree. The mass is often in the lower hemithorax adjacent to the diaphragm; most are left sided, but bilateral cases have been described [50]. Hybrid lesions can have a cystic component with feeding systemic vessels and typically have a better prognosis than patients with CPAM without systemic feeding vessels. Careful color and power Doppler assessment are critical to identify the vessel branching from the aorta below the diaphragm (Fig. 4.7). Even with careful assessment, the vascular supply may be difficult to demonstrate prenatally [32, 51].

MRI appearance is typically of a hyperintense T2w mass in the lower lobe [30, 32]. The feeding vessel may be a low-signal line coursing from the aorta into the mass. MRI does not always demonstrate the abnormal vessels but is helpful in delineating the mass, evaluating the contralateral lung, and assessing for other congenital abnormalities [32, 52]. It is particularly useful in assessing if the mass is thoracic, in the diaphragm or infradiaphragmatic. When infradiaphragmatic in location, BPS tend to be suprarenal and can mimic a neuroblastoma [32, 52].

Prognosis is favorable with only rare reports of associated hydrops. If hydrops develops after 32 weeks' gestation, early delivery is recommended. Prior to 32 weeks, in utero surgical resection or thoracentesis may be considered [53–57]. Other treatment options have been described for hydropic patients including radiofrequency ablation, laser ablation, and thrombogenic coil embolization of the feeding vessel but

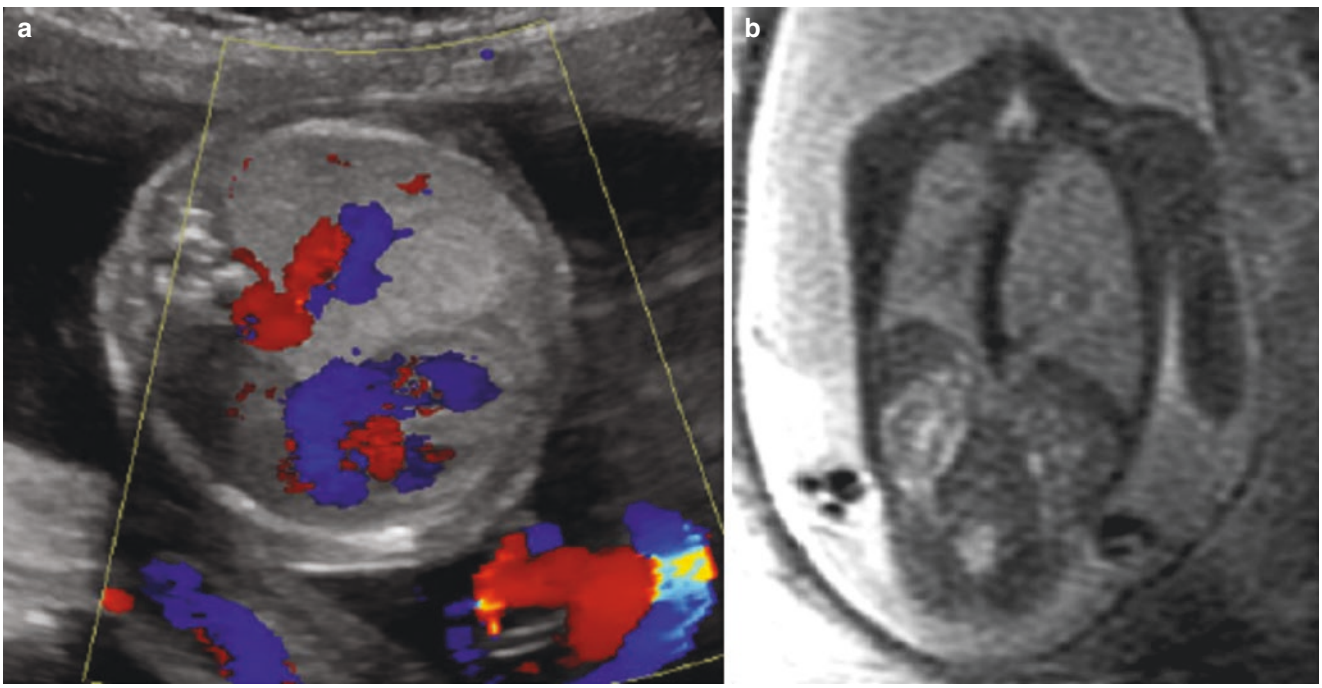

Fig. 4.7 Bronchopulmonary sequestration. (**a**) Axial US image of the fetal chest with power Doppler documents an echogenic mass in the left lung with systemic vessels coursing into the mass. (**b**) Coronal SSFSE T2w image confirms the presence of a low-signal line coursing to the high-signal mass consistent with a sequestration

thus far with increased morbidity and mortality [58, 59]. Lesions may appear to resolve in utero but are usually present on postnatal CT with contrast or MRI.

Congenital Lobar Overinflation/Congenital Lobar Emphysema/Bronchial Atresia

Intrinsic or extrinsic obstruction of the airway may result in overinflation of one or more lobes. CLO may affect one or more lobes and can be segmental or lobar. Bilateral cases have been described [60]. Criteria for the diagnosis of congenital lobar overinflation (CLO) include echogenic lung by ultrasound or high-signal T2w parenchyma with normal lung architecture and absence of macroscopic cysts. This diagnosis may be difficult to differentiate from microcystic CPAM prenatally (Fig. 4.8). The presence of normal pulmonary vascularity and lack of macrocysts can help suggest the diagnosis; confirmation is done with postnatal CT [61, 62].

By ultrasound, CLO is characterized as a homogeneous echogenic lung mass, thought to be secondary to accumulation of the pulmonary fluids within the lung due to a ball-valve mechanism occurring at the site of obstruction [60, 62]. MRI images demonstrate a homogeneous thoracic

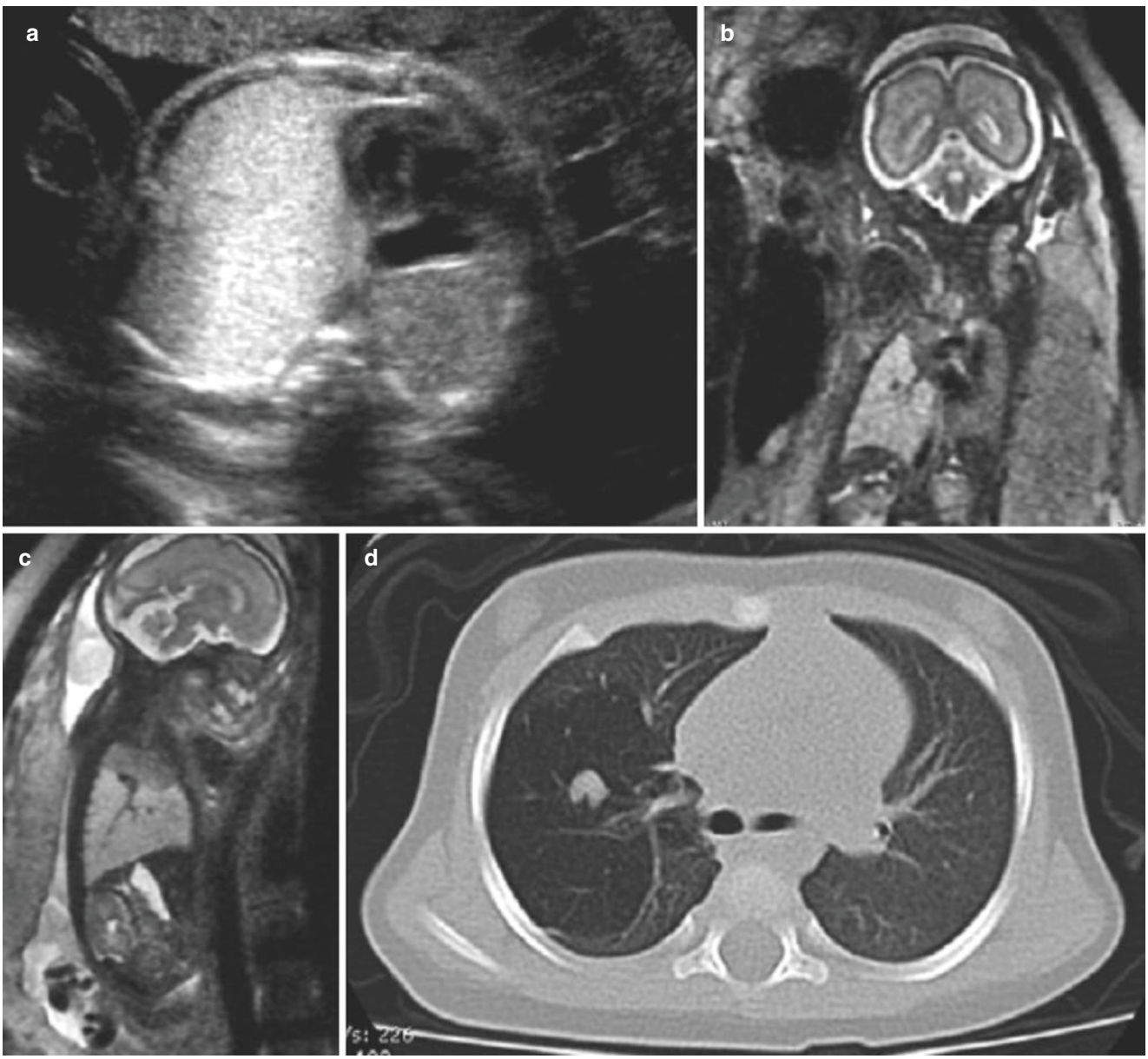

Fig. 4.8 Congenital lobar overinflation (CLO). (**a**) Axial US at 27 weeks' gestation demonstrates a large echogenic mass in the right hemithorax deviating the heart to the left. No systemic feeding vessel was identified. (**b**) Coronal and (**c**) sagittal SSFSE T2w MR image at 27 weeks gestation confirms the presence of a high-signal mass in the right lower lobe. (**d**) Axial chest CT scan at 5 months of age demonstrates an emphysematous lobe consistent with CLH

mass with increased T2 signal. Displacement of the mediastinum to the contralateral side, polyhydramnios and hydrops have been described especially secondary to bronchial atresia of lobar bronchi [61–63]. Many cases resolve in utero. When symptomatic, respiratory issues tend to occur early in life, 30% at birth, 50% in the first month, and almost all by the first 6 months of life ([60].

Diaphragmatic Hernia

Herniated bowel loops into the hemithorax can mimic a multicystic, heterogeneous lung mass by US (Fig. 4.2). Mediastinal and cardiac deviation may be the first hint that a CDH is present if the stomach remains infradiaphragmatic. When the stomach is herniated into the hemithorax, nonvisualization of stomach bubble within the abdomen is helpful for suggesting the diagnosis [32, 35]. Peristalsis of bowel loops in the thorax can sometimes be seen by ultrasound [32]. Deviation of the umbilical vein toward the side of the defect is appreciated in CDH, and an abnormal umbilical vein ratio is seen in 93% of right-sided and 98% of left-sided CDH. The umbilical vein ratio is obtained from a true axial image of the abdomen, where the umbilical vein is at its maximum lateral deviation. It is calculated by measuring the transverse diameter between the left internal rib margin and the left lateral vein edge and dividing it by the transverse diameter between the right inner rib margin and the right lateral border of the vein. This ratio is particularly useful in cases with subtle bowing, and when it is less than 0.4, it is highly predictive of liver herniation [64].

MRI helps by confirming the diagnosis, especially in right and bilateral CDH. It provides information regarding the amount of liver herniation and delineates location of small and large meconium-filled bowel in the chest. In cases with an intraabdominal stomach, it may be difficult by US to differentiate a CPAM from a CDH. MRI can easily distinguish abdominal contents within the chest from cystic lesions. MRI can provide specific information on hernia content, including the presence of the liver, size of diaphragmatic defect, and volume of ipsilateral and contralateral lung.

Congenital Hydrothorax

Pleural fluid may develop with or without an associated mass. It is considered abnormal at any gestational age and can be unilateral or bilateral.

Chylothorax is the most common cause of congenital hydrothorax and can be due to thoracic duct anomalies (Fig. 4.9). Secondary cases of hydrothorax include entities such as anemia, CPAM, BPS, lymphangiectasia, cardiac anomalies, Turner's syndrome, trisomy 21, cystic hygroma, and TORCH infection. Thus, careful assessment is required to identify associated anomalies, and karyotyping is recommended [65, 66].

Ultrasound will demonstrate anechoic fluid in the pleural space. MRI demonstrates high-signal fluid surrounding lung parenchyma and may help identify a cause for the hydrothorax such as an underlying CPAM.

Overall mortality can be as high as 50%. Natural evolution varies between spontaneous resolution and progression

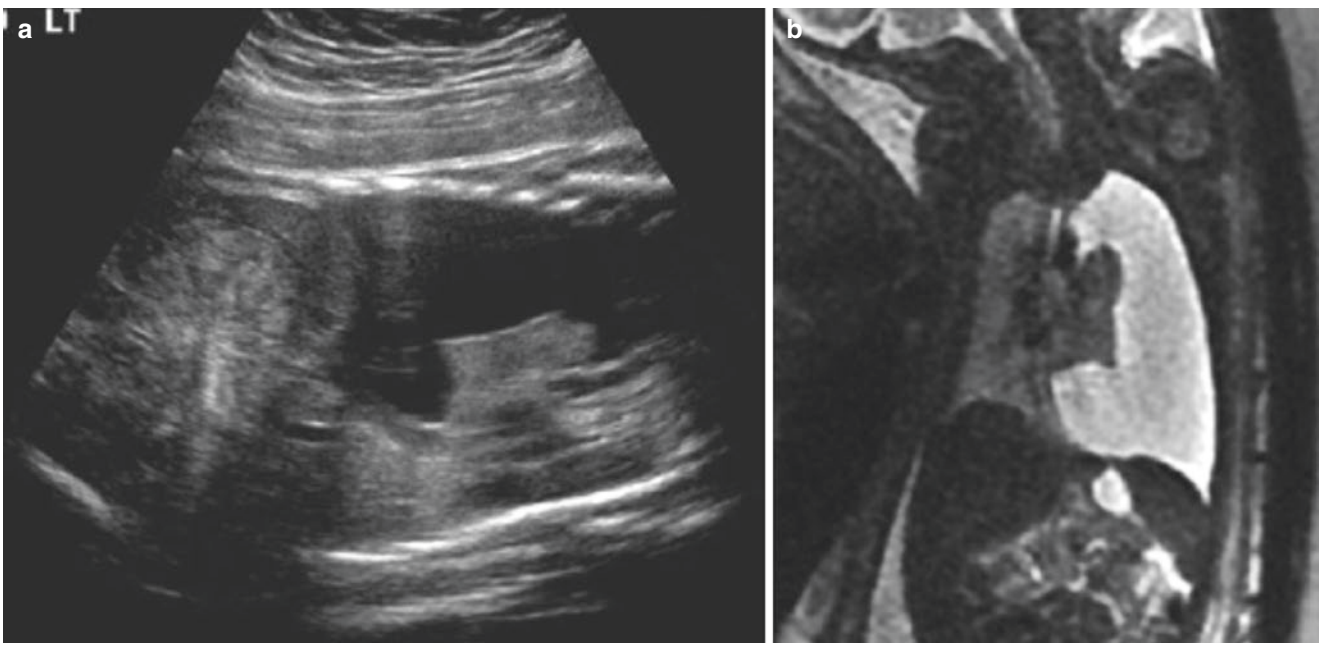

Fig. 4.9 Chylous effusion. (**a**) Coronal US of the chest demonstrates a large fluid collection in the left hemithorax compressing the left lung. (**b**) SSFSE coronal MR image confirms the presence of a large left pleural effusion with compressed lung parenchyma and no underlying lung mass

[67]. Outcome is best if the effusion is unilateral, and primary chylothorax may resolve spontaneously [65]. Prognosis is worst when hydrothorax presents before 30 weeks of gestation and is associated with hydrops [66]. If effusions progress, lung hypoplasia may occur with worsening morbidity and up to 75% mortality [67]. Patients with trisomy 21 and hydrops have a better prognosis; they can be treated later in pregnancy and require less interventions [68].

In cases with progression to hydrops, if the effusion is small, conservative observation is appropriate. If the effusion is large and the infant is less than 32 weeks' gestation, fetal thoracentesis and thoracoamniotic shunting are potential prenatal treatment options after balancing the benefits of the procedure and the possibility of prematurity and premature rupture of membranes [68]. Thoracentesis has the disadvantage of possible rapid re-accumulation after drainage but when done close to delivery may help with neonatal resuscitation [65, 68]. Complications after shunt placement also include shunt migration (20–65%), chest wall deformity secondary to altered rib growth and mechanical chest trauma during insertion (more common when shunts are placed early in gestation), and fetal demise (11% of cases) [67].

Congenital High Airway Obstruction

Congenital high airway obstruction (CHAOS) should be included in the differential when bilateral large echogenic lung masses are identified [35] (Fig. 4.10). This rare entity is usually sporadic but can be syndromic (Fraser syndrome) or as part of an association [69]. It can be secondary to laryngotracheal atresia, tracheal stenosis, or a thick web, laryngeal atresia being the most common etiology. Aberrant pulmonary budding off the foregut is present. Most cases have a connection with the esophagus. By ultrasound, both lungs are symmetrically enlarged and echogenic due to fluid trapping. The heart is compressed, usually small, and centrally located; the diaphragms flattened or inverted. Compression of the heart and great vessels may result in heart failure and hydrops. Compression of the esophagus may result in polyhydramnios [69].

MRI demonstrates abnormally large high-signal lungs on T2w that are enlarged causing eversion of the diaphragms. Identification of a dilated fluid-filled trachea and bronchi help to confirm the diagnosis and differentiate this diagnosis from bilateral CPAM. EXIT delivery with airway control is recommended but with prognosis poor [35].

Associated anomalies, such as urogenital defects, omphalocele, radial ray defects, syndactyly or polydactyly, and cryptophthalmos, should be closely looked for as this can provide useful information for future pregnancies [70]. Encephalocele and myelomeningocele have also been seen in patients with CHAOS [71]. Genetic analysis should also be performed to assess anomalies such as trisomy 9, trisomy 16, and chromosome 5p deletion [70].

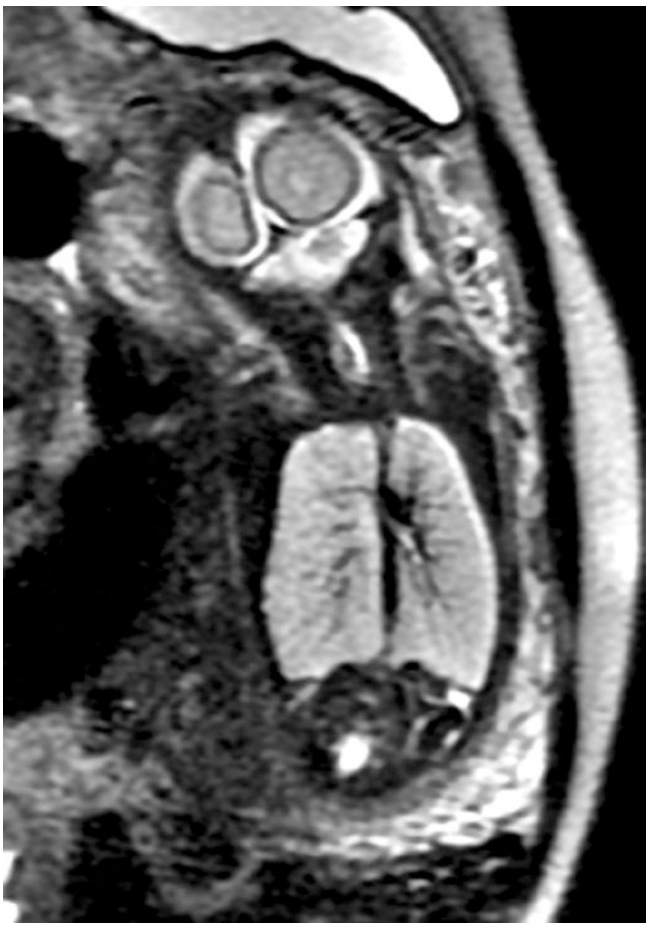

Fig. 4.10 Congenital high airway obstruction. Coronal T2w MR image of the fetal chest at 27 weeks gestation demonstrates overinflated high-signal lungs with flattened diaphragms due to cervical tracheal web causing obstruction. The left bronchus is abnormally dilated with fluid. There is oligohydramnios with bilateral renal agenesis. The infant died at delivery

Pulmonary Hypoplasia

Pulmonary hypoplasia is a wide spectrum diagnosis which includes agenesis, aplasia, as well as hypoplasia. Agenesis is the actual absence of lung parenchyma and bronchi (Fig. 4.11). Aplasia is the absence of lung tissue with rudimentary bronchi. Hypoplasia is the presence of alveoli and bronchi that are underdeveloped with a decreased number of airways and alveoli resulting in a decrease in size and weight of the lungs. Alveoli and pulmonary vascularity develop concomitantly, so associated anomalies of pulmonary vessels are common.

Pulmonary hypoplasia causes severe respiratory failure at birth often resulting in rapid death. Hypoplasia can be secondary to premature rupture of membranes, renal anomalies,

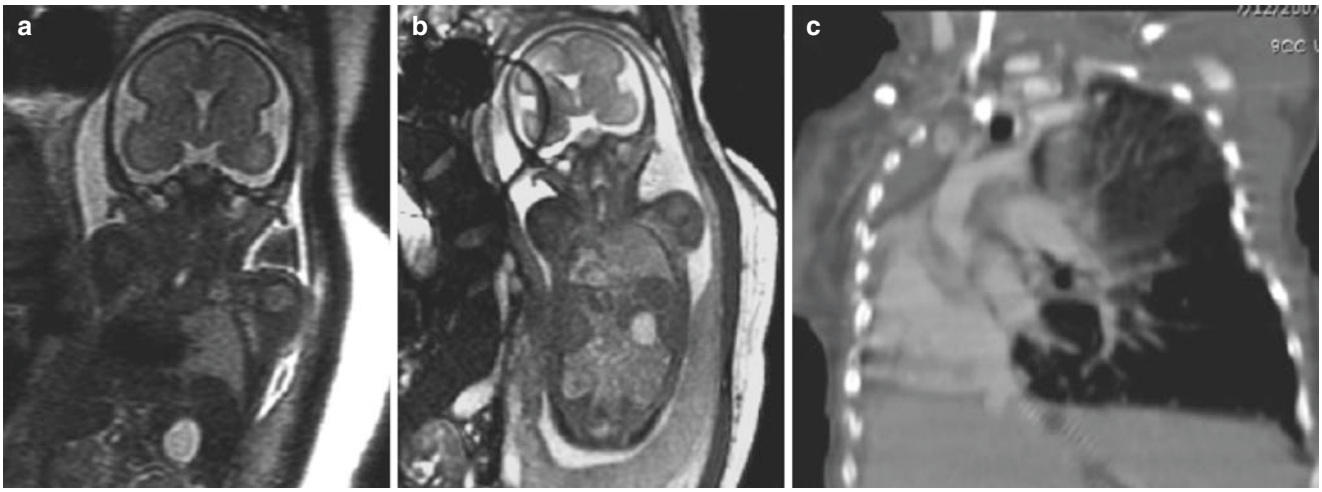

Fig. 4.11 Right lung agenesis. (**a**) Coronal SSFSE and (**b**) FIESTA T2w images at 21 weeks' gestation demonstrate shift of the heart to the right with no right lung parenchyma or right mainstem bronchus identified. (**c**) Contrast chest CT after delivery confirms the diagnosis of agenesis of the right lung

lung masses, or a severe skeletal dysplasia. Severity of the hypoplasia is dependent of gestation age at onset.

Prenatal US diagnosis of pulmonary hypoplasia is often limited. Various measurements have been proposed to predict pulmonary hypoplasia including lung area, ratio of the lung to thoracic area, thoracic to abdominal circumference, and volumetric measurements. High resistance patterns in peripheral pulmonary arteries have been reported in fetuses with pulmonary hypoplasia [72]. Both 2D diameter measurements and 3D volumetry can be performed, even before 24 weeks of gestation, for the diagnosis of hypoplasia, but follow-up assessment might be needed to assess outcome and differentiate lethal versus nonlethal forms [73]. Oligohydramnios and maternal obesity, however, limit US evaluation, so prognosis is often difficult to predict.

Fetal lung volume by MR is also being used to assess pulmonary hypoplasia [74–81] (Fig. 4.12). Relative lung volume based on gestational age and lung volume to body weight ratios have been evaluated. Normal lungs are progressively hyperintense on T2w with maturation. Decreased signal has been described in hypoplastic lungs. Relative lung signal intensity and spectroscopy are potential methods for further assessing the severity of hypoplasia [79, 80].

Several methods have been described to measure the lung volumes. One of the most common techniques is done by tracing the lung on each MRI slice, adding all the areas together, and then multiplying by the slice thickness. Using this method, normal results are highly variable. To decrease the variability, the percentage predicted lung volume (PPLV) can be used where the residual lung volume is divided by the predicted lung volume. The observed-to-expected lung volume ratio is better at predicting outcome in fetuses with CDH [82].

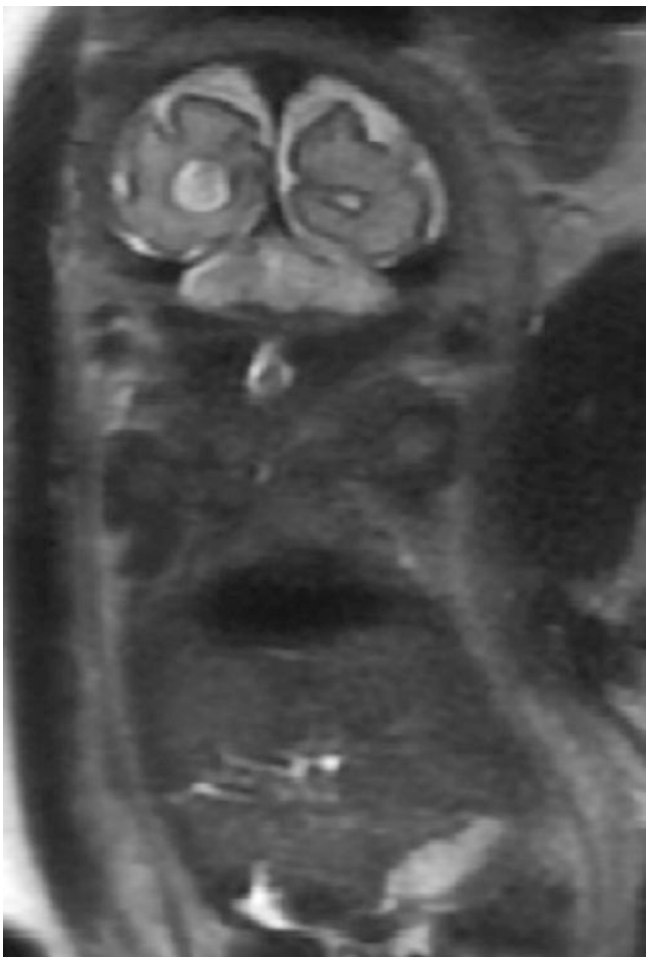

Fig. 4.12 Pulmonary hypoplasia. Coronal SSFSE MR image of the fetal chest demonstrates small low-signal pulmonary parenchyma in this fetus with renal anomalies resulting in oligohydramnios

Congenital Lung Tumors

Primary lung tumors are extremely rare compared to developmental anomalies of the lung and include cystic pleuropulmonary blastoma (cystic PPB), fetal lung interstitial tumor (FLIT), congenital peribronchial myofibroblastic tumor (CPMT), and congenital fibrosarcoma [83].

Even though the biological behavior of a tumor compared to a developmental anomaly is extremely different, the ability to differentiate them by imaging has been considered very difficult to impossible (Fig. 4.13). A recent study by Waelti et al. suggests that nonvisualization of a lung lesion in the mid-second trimester ultrasound should raise the concern for a tumor. In the presence of a multicystic lesion, knowledge of a normal mid-second trimester ultrasound is highly suggestive of PPB [83]. Differentiating imaging characteristics between solid tumors have not been identified.

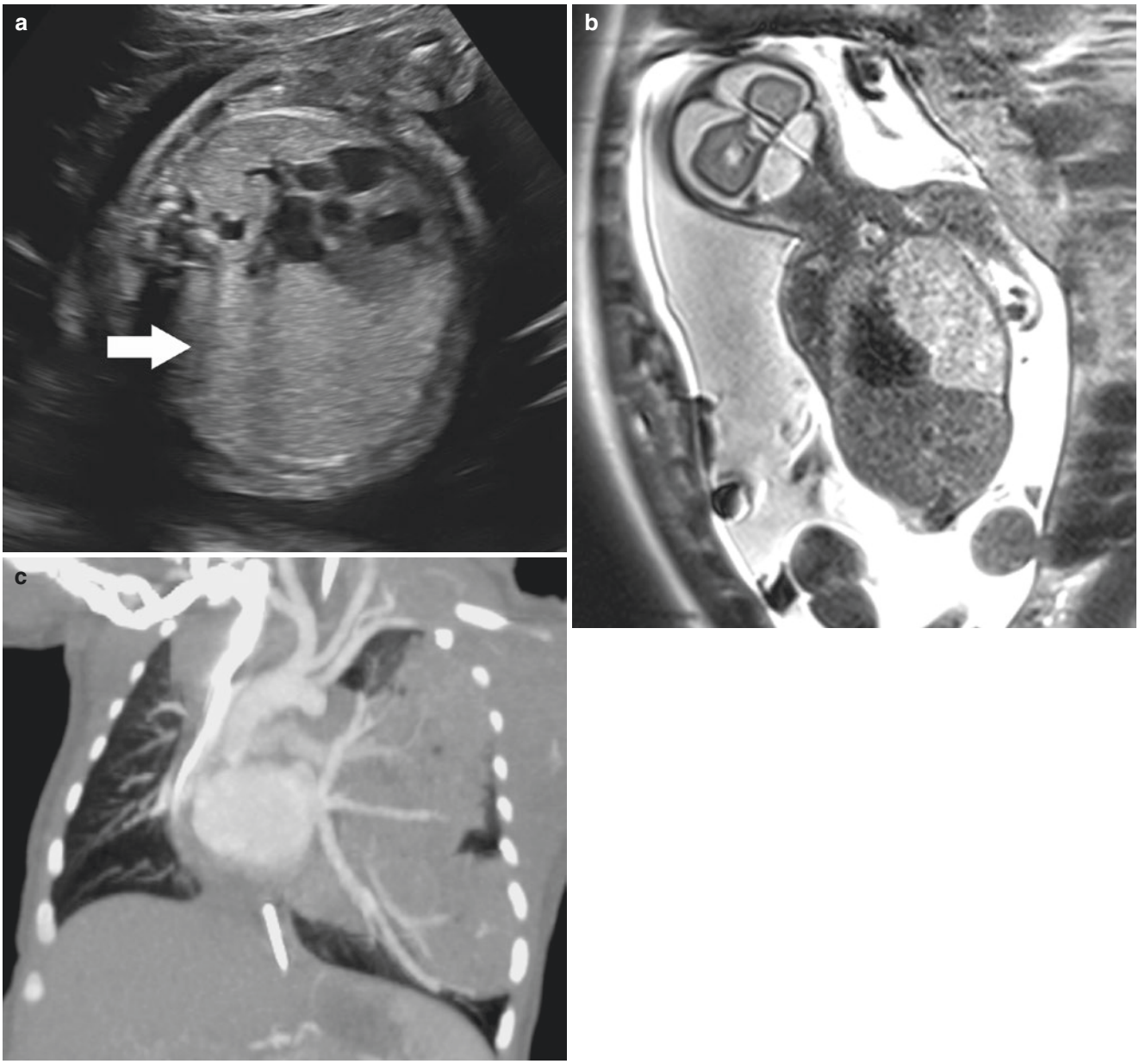

Fig. 4.13 Fetal lung interstitial tumor (FLIT). (**a**) Axial US image at 27 weeks gestation demonstrates an echogenic mass (arrow) deviated the heart to the right. (**b**) Coronal T2w MR image on the same date confirms the presence of a heterogeneous mass compressing the diaphragm inferiorly and shifting the mediastinum to the right. This was thought to be a CPAM prenatally, but the mass did not involute in the third trimester. (**c**) Following delivery, the infant was in respiratory distress. Coronal reformatted image of the chest demonstrates pulmonary vessels coursing through a solid-appearing mass. The mass was resected, and FLIT was confirmed

Pulmonary Lymphangiectasia

Pulmonary lymphangiectasia is the result of dilatation of lymphatics draining the pulmonary interstitial and subpleural spaces. This can develop prenatally resulting in enlarged, noncompliant lung parenchyma with effusions that can lead to respiratory distress at delivery [84, 85].

Lymphangiectasia can be primary or secondary. Primary pulmonary lymphangiectasia has been associated with several genetic syndromes (FOXC2) with failure of the normal regression of connective tissue elements after 16 weeks gestation. Secondary lymphangiectasia can be the result of congenital heart disease causing poor venolymphatic return. Hypoplastic left heart syndrome and total anomalous pulmonary venous return are most commonly associated with fetal lymphangiectasia [85, 86].

Prenatal ultrasound images will demonstrate small bilateral pleural effusions and heterogeneous lung parenchyma (Fig. 4.14).

Fetal MRI also can demonstrate pleural effusions and lung heterogeneity. A typical heterogeneous pattern termed the "nutmeg lung" exhibits branching tubular T2w high-signal structures radiating from the hila, providing a more specific diagnosis. MRI is also helpful in excluding other lung masses [85].

Cardiac echo is important to exclude cardiac anomalies. Not all restrictive lesions will develop the nutmeg lung pattern. In a study by Saul et al., the finding of "nutmeg lung" in fetuses with hypoplastic left heart syndrome was associated with increased mortality [87]. Fetal MRI, thus, may be a useful guide in prognosticating severity of HLHS and counseling families.

Postnatal management includes various attempts at decreasing pulmonary lymph burden such as restriction of dietary fats, pleural effusion drainage, pleurodesis, and more invasive procedures such as thoracic duct ligation. Recent experimental treatment using ethiodized oil to embolize the patulous pulmonary lymphatics has shown some success [84].

Conclusion

Congenital lung malformations are rare and often involute prenatally with a small percentage developing hydrops in utero. A majority have no respiratory symptoms at delivery. Ultrasound is the initial study to identify a congenital lung malformation which can be cystic, solid, or mixed. Fetal MRI can be a useful adjunct in the assessment of large lung masses for improved counseling and management planning. While rare, hydrops can develop with congenital pulmonary masses, is a sign of impending demise, and may be an indication for fetal intervention.

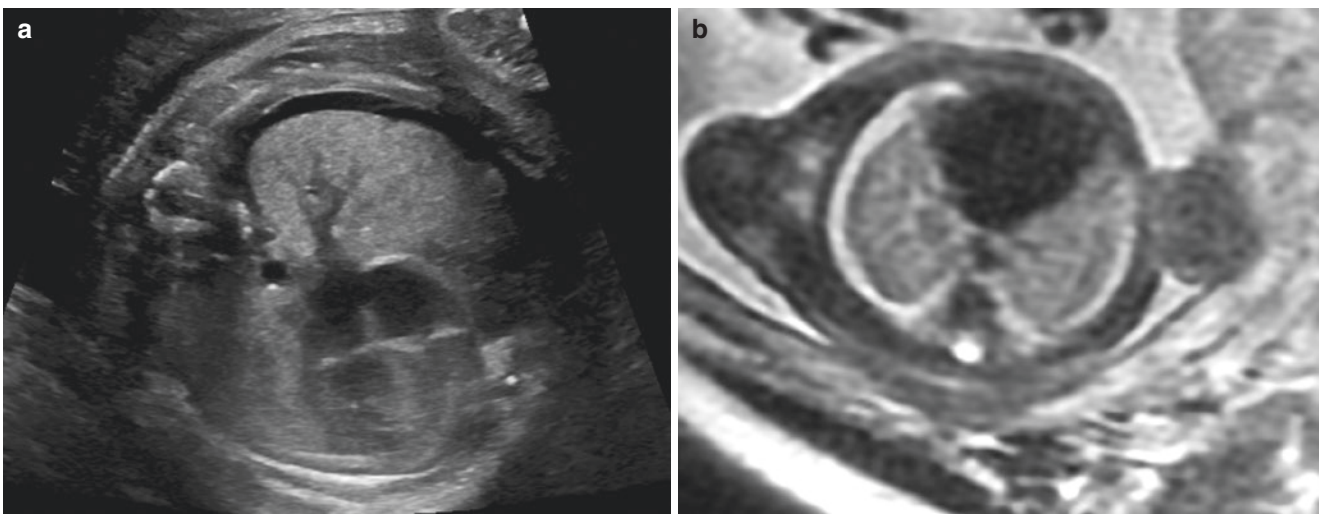

Fig. 4.14 Pulmonary lymphangiectasia. (**a**) Axial US images of the fetal chest at 28 weeks' gestation demonstrate small pleural effusions and heterogeneous parenchyma. The heart was normal. (**b**) Axial T2w MR image of the fetal chest on the same date confirms the presence of small effusions and high-signal tubular structures radiating from the hilum. At delivery primary lymphangiectasia was confirmed

References

1. Kline-Fath BM. Is prenatal sonography accurate in identification of congenital lung lesions? Scientific paper presented at SPR, Boston, MA. April 15; 2010.
2. Breysem L, Bosmans H, Dymarkowski S, et al. The value of fast MR imaging as an adjunct to ultrasound in prenatal diagnosis. Eur Radiol. 2003;13:1538–48.
3. Quinn TM, Hubbard AM, Adzick NS. Prenatal MRI enhance fetal diagnosis. J Pediatr Surg. 1998;33:553–8.
4. Bulas DI. Fetal magnetic resonance imaging as a complement to fetal ultrasonography. Ultrasound Q. 2007;23(1):3–22.
5. Aite L, Zaccara A, Trucchi A, et al. When uncertainty generates more anxiety than severity: the prenatal experience with cystic adenomatoid malformation of the lung. J Perinat Med. 2009;37:539–42.
6. Warby AC, et al. Fetal thymus and pregnant women with rheumatic disease. J Perinat Med. 2014;42(5):635–9.
7. Britto ISW, et al. New anatomical landmarks to study the relationship between fetal lung area and thoracic circumference by three-dimensional ultrasonography. J Matern Fetal Neonatal Med. 2012;25(10):1927–32.
8. Ruano R, Joubin L, Abry MC, et al. A nomogram of fetal lung volumes estimated by 3D US using the rotaional technique (virtual organ computer aided analysis). J Ultrasound Med. 2006;35:701–9.
9. Mirik Tesanic D, Merz E, Wellek S. Fetal lung volume measurements using 3D ultrasonography. Ultraschall Med. 2011;32:373–80.
10. Harmath A, Csaba A, Hauzman E, et al. Congenital lung malformations in the second trimester: prenatal ultrasound diagnosis and pathologic findings. J Clin Ultrasound. 2007;35(5):250–5.
11. Lecompte B, Hadden H, Coste K, et al. Hyperechoic congenital lung lesions in a non-selected population: from prenatal detection till perinatal management. Prenat Diagn. 2009;29:1222–30.
12. Ankerman T, Oppermann HC, Engler S, et al. Congenital masses of the lung, cystic adenomatoid malformation versus congenital lobar emphysema: prenatal diagnosis and implications for postnatal treatment. J Ultrasound Med. 2004;23:1379–84.
13. Johnson AM, Hubbard AM. Congenital anomalies of the fetal/neonatal chest. Semin Roentgenol. 2004;39:197–214.
14. Coakley FV, Glenn OA, Qayyam A, et al. Fetal MRI: a developing technique for the developing patient. AJR. 2004;182:243–52.
15. Prayer D, Brugger PC, Prayer L. Fetal MRI: techniques and protocols. Pediatr Radiol. 2004;34:685–93.
16. Baker PN, Johnson IR, Harvey PR, et al. A three year follow up children imaged in utero with echoplanar magnetic resonance. Am J Obstet Gynecol. 1994;170:32–3.
17. De Wilde JP, Rivers AW, Price DU, et al. A review of the current use of magnetic resonance imaging in pregnancy and safety implications for the fetus. Prog Biophys Mol Biol. 2005;87:335.
18. Committee of Obstetric Practice. Committee opinion no. 723: guidelines for diagnostic imaging during pregnancy and lactation. Obstet Gynecol. 2017;130(4):e210–6.
19. Yip YP, Capriotti C, Tlagala SL, et al. Effects of MR exposure at 1.5 T on early embryonic development of the chick. J Magn Reson Imaging. 1994;4:742–8.
20. Yip YP, Capriotti C, Yip JW. Effects of MR exposure on axonal outgrowth in the sympathetic nervous system of the chick. J Magn Reson Imaging. 1995;5:457–62.
21. Vadeyar SH, Moore RJ, Strachan BK, et al. Effect of fetal magnetic resonance imaging on fetal heart rate patterns. Am J Obstet Gynecol. 2000;182:666–9.
22. Mevissen M, Buntenkotter S, Loscher W. Effect of static and time varying magnetic field on reproduction and fetal development in rats. Teratology. 1994;50:229–37.
23. Ray JG, Vermeulen MJ, Bharatha A, et al. Association between MRI exposure during pregnancy and fetal and childhood outcomes. JAMA. 2016;316(9):952–61.
24. Shellock FG, Kanal E. Policies, guidelines and recommendations for MR imaging safety and patient management. JMRI. 1991;1:97–101.
25. United Nations Scientific Committee on the effects of atomic radiation. Ionizing radiation levels and effects. 1972 report to the general assembly Vol 2 effects New York; 1972.
26. Hand JW, Li Y, Thomas EL, et al. Prediction of specific absorption rate in mother and fetus associated with MRI examinations during pregnancy. Magn Reson Med. 2006;55:883–93.
27. Frates MC, Kumar AJ, Benson CB, et al. Fetal anomalies: comparison of MR imaging and US for diagnosis. Radiology. 2004;232:398–404.
28. Levine D, Barnewolt CE, Mehta TS, et al. Fetal thoracic abnormalities: MR imaging. Radiology. 2003;228:379–88.
29. Kunisaki SM, Fauza DO, Barnewolt CE, et al. Ex utero intrapartum treatment with placement of extracorporeal membrane oxygenation for fetal thoracic masses. J Pediatr Surg. 2007;42(2):420–5.
30. Daltro P, Werner H, Gasparetto TD, et al. Congenital chest malformations: a multimodality approach with emphasis on fetal MR imaging. Radiographics. 2010;30:385–95.
31. Curran PF, Jelin EB, Rand L, et al. Prenatal steroids for microcystic congenital cystic adenomatoid malformations. J Pediatr Surg. 2010;45:145–50.
32. Azizkhan RG, Crombleholme TM. Congenital cystic lung disease: contemporary antenatal and postnatal management. Pediatr Surg Int. 2008;24:643–57.
33. Adzick NS. Management of fetal lung lesions. Clin Perinatol. 2009;36:363–76.
34. Kumar AN. Perinatal management of common neonatal thoracic lesions. Indian J Pediatr. 2008;75:931–7.
35. Bush A, Hogg J, Chitty LS. Cystic lung lesions – prenatal diagnosis and management. Prenat Diagn. 2008;28:604–11.
36. Cavoretto P, Molina F, Poggi S, et al. Prenatal diagnosis and outcome of echogenic fetal lung lesions. Ultrasound Obstet Gynecol. 2008;32:769–83.
37. Stocker TJ, Manewell JE, Drake RM. Congenital cystic adenomatoid malformation of the lung: classification and morphologic spectrum. Hum Pathol. 1977;8:155–71.
38. Crombleholme TM, Coleman B, Hedrick H, et al. Cystic adenomatoid malformation volume ratio predicts outcome in prenatally diagnosed cystic adenomatoid malformation of the lung. J Pediatr Surg. 2002;37(3):331–8.
39. H Chon A, et al. A complication of percutaneous sclerotherapy for congenital pulmonary airway malformation: intravascular injection and cardiac necrosis. Fetal Pediatr Pathol. 2017;36(6):437–44.
40. Mann S, Wilson RD, Bebbington MW, et al. Antenatal diagnosis and management of congenital cystic adenomatoid malformation. Semin Fetal Neonatal Med. 2007;12:477–81.
41. Coleman BG, Adzick NS, Crombleholme TM, et al. Fetal therapy: state of the art. J Ultrasound Med. 2002;21:1257–88.
42. Morris LM, Lim FY, Livingston JC, et al. High-risk fetal congenital pulmonary airway malformations have a variable response to steroids. J Pediatr Surg. 2009;2004:60–5.
43. Kunisaki SM, Barnewolt CE, Estroff JA, et al. Large fetal congenital cystic adenomatoid malformations: growth trends and patient survival. J Pediatr Surg. 2007;42(2):404–10.
44. Knox EM, Kilby MD, Martin WL, et al. In-utero pulmonary drainage in the management of primary hydrothorax and congenital cystic lung lesion: a systematic review. Ultrasound Obstet Gynecol. 2006;28:726–34.

45. Fortunato S, Lombardo S, Dantrell J. Intrauterine laser ablation of a fetal cystic adenomatoid malformation with hydrops: the application of minimally invasive surgical techniques to fetal surgery. Am J Obstet Gynecol. 1997;177:S84.
46. Adzick NS. Open fetal surgery for life-threatening fetal anomalies. Semin Fetal Neonatal Med. 2009;15(1):1–8. (epub ahead of print).
47. Bermudez C, Perez-Wulff J, Arcadipane M, et al. Percutaneous fetal sclerotherapy for congenital cystic adenomatoid malformation of the lung. Fetal Diagn Ther. 2008;24:237–40.
48. Marshall KW, Blane CE, Teitelbaum DH, et al. Congenital cystic adenomatoid malformation: impact of prenatal diagnosis and changing strategies in the treatment of the asymptomatic patient. AJR. 2000;175:1551–4.
49. Pogoriler J, et al. Congenital Cystic Lung Lesions. Redefining the natural distribution of subtypes and assessing the risk of malignancy. Am J Surg Pathol. 2017; https://doi.org/10.1097/PAS.0000000000000992. [Epub ahead of print].
50. Hong C, Yu G, Tang J, et al. Risk analysis and outcomes of bronchopulmonary sequestrations. Padiatr Surg Int. 2017;33(9):971–5. Published online 19 June 2017.
51. Vijayaraghavan SB, Rao PS, Selvarasu CD, et al. Prenatal sonographic features of intralobar bronchopulmonary sequestration. J Ultrasound Med. 2003;22:541–4.
52. Sepulveda W. Perinatal imaging in bronchopulmonary sequestration. J Ultrasound Med. 2009;28:89–94.
53. Zeidan S, Gorincour G, Potier A, et al. Congenital lung malformation: evaluation of prenatal and postnatal radiologic findings. Respirology. 2009;14:1005–11.
54. Witlox RS, Lopriore E, Rikkers-Mutsaerts ER, et al. Single-needle laser treatment with drainage of hydrothorax in fetal bronchopulmonary sequestration with hydrops. Ultrasound Obstet Gynecol. 2009;34:355–7.
55. Oepkes D, Devlieger R, Lopriore E, et al. Successful ultrasound-guided laser treatment of fetal hydrops caused by pulmonary sequestration. Ultrasound Obstet Gynecol. 2007;29:457–9.
56. Ruano R, de A Pimenta EJ, Marques da Silva M, et al. Percutaneous intrauterine laser ablation of the abnormal vessel in pulmonary sequestration with hydrops at 29 weeks' gestation. J Ultrasound Med. 2007;26:1235–41.
57. Becmeur F, Horta-Geraud P, Donato L, et al. Pulmonary sequestrations: prenatal ultrasound diagnosis, treatment and outcome. J Pediatr Surg. 1998;33:492–6.
58. Mathis J, Raio L, Baud D. Fetal laser therapy: applications in the management of fetal pathologies. Prenat Diagn. 2015;35(7):623–36.
59. Baud D, et al. Minimally invasive fetal therapy for hydropic lung masses: three different approaches ad review of the literature. Ultrasound Obstet Gynecol. 2013;42:440–8.
60. Perea L, Blinman T, Piccione J, Laje P. Bilateral congenital lobar emphysema: staged management. J Pediatr Surg. 2017;52(9):1442–5.
61. Seo T, Ando H, Kaneko K, et al. Two cases of prenatally diagnosed congenital lobar emphysema caused by lobar bronchial atresia. J Pediatr Surg. 2006;41:E17–20.
62. Pariente G, Aviram M, Landau D, et al. Prenatal diagnosis of congenital lobar emphysema: case report and review of the literature. J Ultrasound Med. 2009;28:1081–4.
63. Peranteau WH, Merchant AM, Hedrick HL, et al. Prenatal course and postnatal management of peripheral bronchial atresia: association with congenital cystic adenomatoid malformation of the lung. Fetal Diagn Ther. 2008;24:190–6.
64. Richards DS, Kays DM. Fetal umbilical vein deviation in congenital diaphragmatic hernia. J Ultrasound Med. 2013;32:263–8.
65. Aubard Y, Derouineau I, Aubard V, et al. Primary fetal hydrothorax: a literature review and proposed antenatal clinical strategy. Fetal Diagn Ther. 1998;13:325–33.
66. Wada S, et al. The prognostic factors and outcomes of primary fetal hydrothorax with the effects of fetal intervention. Prenatal Diagn. 2017;37(2):184–92.
67. Mon RA, et al. Outcomes of foetuses with primary hydrothorax that undergo prenatal intervention (prenatal intervention for hydrothorax). J Surg Res. 2018;221:121–7.
68. Mallman MR, et al. Thoracoamniotic shunting for fetal hydrothorax: predictors of intrauterine course and postnatal outcome. Fetal Diagn Ther. 2017;41(1):58–65.
69. Gowda M, Gupta S, Ali A, Paranthaman S. Locating the level of congenital high airway obstruction: fluid in the airway tract as reference points. J Ultrasound Med. 2017;36(10):2179–85.
70. Gosavi M, Kumar L, Ratnakar A, Bannur H. Congenital High Airway Obstruction Syndrome (CHAOS): A perinatal autopsy case report. Pathol Res Pract. 2017;213(2):170–5.
71. Adin M. CHAOS associated with cervical myelomeningocele. J Clin US. 2017;45(8):507–10.
72. Chaoui R, Kalache K, Tennstedt C, et al. Pulmonary arterial Doppler velocimetry in fetuses with lung hypoplasia. Eur J Obstet Gynecol Repord Biol. 1999;84:179–85.
73. Miric TD, Merz E, Wellek S. Fetal lung volume measurements using 3DUS. Ultraschall Med. 2011;32:373–89.
74. Keller TM, Rake A, Michel SC, Seifert B, et al. MR assessment of fetal lung development using lung volumes and signal intensities. Eur Radiol. 2004;14(6):984–9.
75. Osada H, Kaku K, Masuda K, Iitsuka Y, Seki K, Sekiya S. Quantitative and qualitative evaluations of fetal lung with MR imaging. Radiology. 2004;231:887–92.
76. Tanigaki S, Miyakoshi K, Tanaka M, et al. Pulmonary hypoplasia: prediction with use of ratio of MRI measured fetal lung volume to US estimated fetal body weight. Radiology. 2004;232:767–72.
77. Ward VL, Nishino M, Hatabu H, et al. Fetal lung volume measurements: determination with MR imaging – effect of various factors. Radiology. 2006;240(1):187–93.
78. Williams G, Coakley FV, Qayyum A, et al. Fetal relative lung volume: quantification by using prenatal MR imaging lung volumetry. Radiology. 2004;233:457–62.
79. Keller TM, Rake A, Michel SC, Seifert B, Wisser J, et al. MR assessment of fetal lung development using lung volumes and signal intensities. Eur Radiol. 2004;14(6):984–9.
80. Kuwashima S, Nishimura G, Limura F, et al. Low intensity fetal lungs on MRI may suggest the diagnosis of pulmonary hypoplasia. Pediatr Radiol. 2001;31:669–72.
81. Zaretsky M, Ramus R, McIntire D, et al. MR calculation of lung volumes to predict outcome in fetuses with genitourinary abnormalities. Am J Roentgenol. 2005;185(5):1328–34.
82. Rubesova E. Why do we need more data on MR volumetric measurements of the fetal lung? Pediatr Radiol. 2016;46:167–71.
83. Waelti SL, Garel L, Soglio DD, et al. Neonatal congenital lung tumors – the importance of mid-second-trimester ultrasound as a diagnostic clue. Pediatr Radiol. 2017;47:1766.
84. Raman SP, Pipavath SN, Raghu G, et al. Imaging of thoracic lymphatic diseases. Am J Roentgen. 2009;193(6):1504–13.
85. Victoria T, Andronikou S. The fetal MR appearance of 'nutmeg lung': findings in 8 cases linked to pulmonary lymphangiectasia. Pediatr Radiol. 2014;44(10):1237–42.
86. Seed M. Antenatal MR imaging of pulmonary lymphangiectasia secondary to hypoplastic left heart syndrome. Pediatr Radiol. 2009;39:747–50.
87. Saul D, Degenhardt K, Iyoob SD, et al. Hypoplastic left heart syndrome and the nutmeg lung pattern in utero: a cause and effect relationship or prognostic indicator? Pediatr Radiol. 2016;48(4):483–9.

Newborn Chest

5

Jonathan C. Levin, Robert H. Cleveland, and Stella Kourembanas

Respiratory Distress Syndrome

RDS, also known by its histological name hyaline membrane disease (HMD), is the clinical manifestation of pulmonary immaturity seen predominantly in infants less than 36 weeks of gestational age weighing less than 2.5 kg. Rates of RDS are inversely proportional to gestational age and birth weight. However, while RDS today is most common in the extremely premature infant, RDS due to relative surfactant deficiency in the late preterm or even term infant is also observed. Term infants of mothers with poorly controlled diabetes may present with RDS because fetal hyperinsulinism interferes with the glucocorticoid axis that governs surfactant biosynthesis. Other risk factors include multiple births, cesarean delivery, precipitous delivery, fetal asphyxia, cold stress, and a maternal history of previously affected infants. Incidence is higher in male and white infants. In 1979, RDS was the second-ranking cause of death in infants, but because of the progress made in prenatal and postnatal care, it dropped to eighth place in 2014, when RDS accounted for only 10.5 deaths per 100,000 live births [3].

In 1959, Avery and Mead reported that RDS resulted from deficiency of surfactant in the lungs, which leads to the inability to maintain acinar distention [4]. Exposure to air can then rapidly lead to the development of hyaline membranes containing fibrin and cellular debris. There frequently is epithelial necrosis beneath the hyaline membranes. Deficient surfactant production or deficient release of surfactant into the immature respiratory alveoli results in an increase in surface forces and lung elastic recoil. Coupled with the extremely compliant chest wall of a preterm infant, this leads to a reduced alveolar recruitment (atelectasis). This condition is characterized by decreased functional residual capacity (FRC), decreased pulmonary compliance, increased pulmonary resistance, and ventilation–perfusion mismatch. By the second day of life, repair has begun with proliferation of type 2 pneumocytes (which produce surfactant) and increased secretions [5]. Thus, without exogenous surfactant administration, the disease will typically progress over 48–72 hours, with subsequent improvement as endogenous surfactant production is increased and a marked diuresis occurs, with improvement in pulmonary function usually by 1 week of age. In the current era of available surfactant replacement and/or early use of continuous positive airway pressure (CPAP), most cases of RDS improve and resolve more quickly.

Infants that survive RDS but go on to require continued ventilatory support, including positive pressure ventilation and supplemental oxygen, have a significant chance of developing BPD, which is discussed in further detail in a later section. However, infants without significant RDS may also go on to develop BPD as well.

Clinically, infants with RDS are usually symptomatic within minutes of birth, with grunting, nasal flaring, retractions, tachypnea, and cyanosis. Although the initial radiographic findings may be noted minutes after birth, an early CXR within the first hour of birth may not be diagnostic of RDS due to the persistence of fetal lung fluid that has not yet cleared. Occasionally the maximum radiographic findings are not present until 12–24 h of life particularly in the late-preterm infants. For most premature infants with RDS, the radiographic finding is an evenly distributed, finely granular

Portions of this chapter are reprinted from Cleveland RH. A radiologic update on medical diseases of the newborn chest. Pediatr Radiol. 1995;25:631–7; Cleveland R, Donoghue V. Imaging of the newborn chest. Syllabus IDKD: diseases of the heart, chest & breast. Milan: Springer-Verlag Italia; 2007. p. 55–62, with permission.

J. C. Levin (✉)
Department of Newborn Medicine and Respiratory Disease, Boston Children's Hospital, Boston, MA, USA
e-mail: jonathan.levin@childrens.harvard.edu

R. H. Cleveland
Department of Radiology, Harvard Medical School, Boston Children's Hospital, Boston, MA, USA

S. Kourembanas
Department of Newborn Medicine, Boston Children's Hospital, Boston, MA, USA

R. H. Cleveland, E. Y. Lee (eds.), *Imaging in Pediatric Pulmonology*, https://doi.org/10.1007/978-3-030-23979-4_5

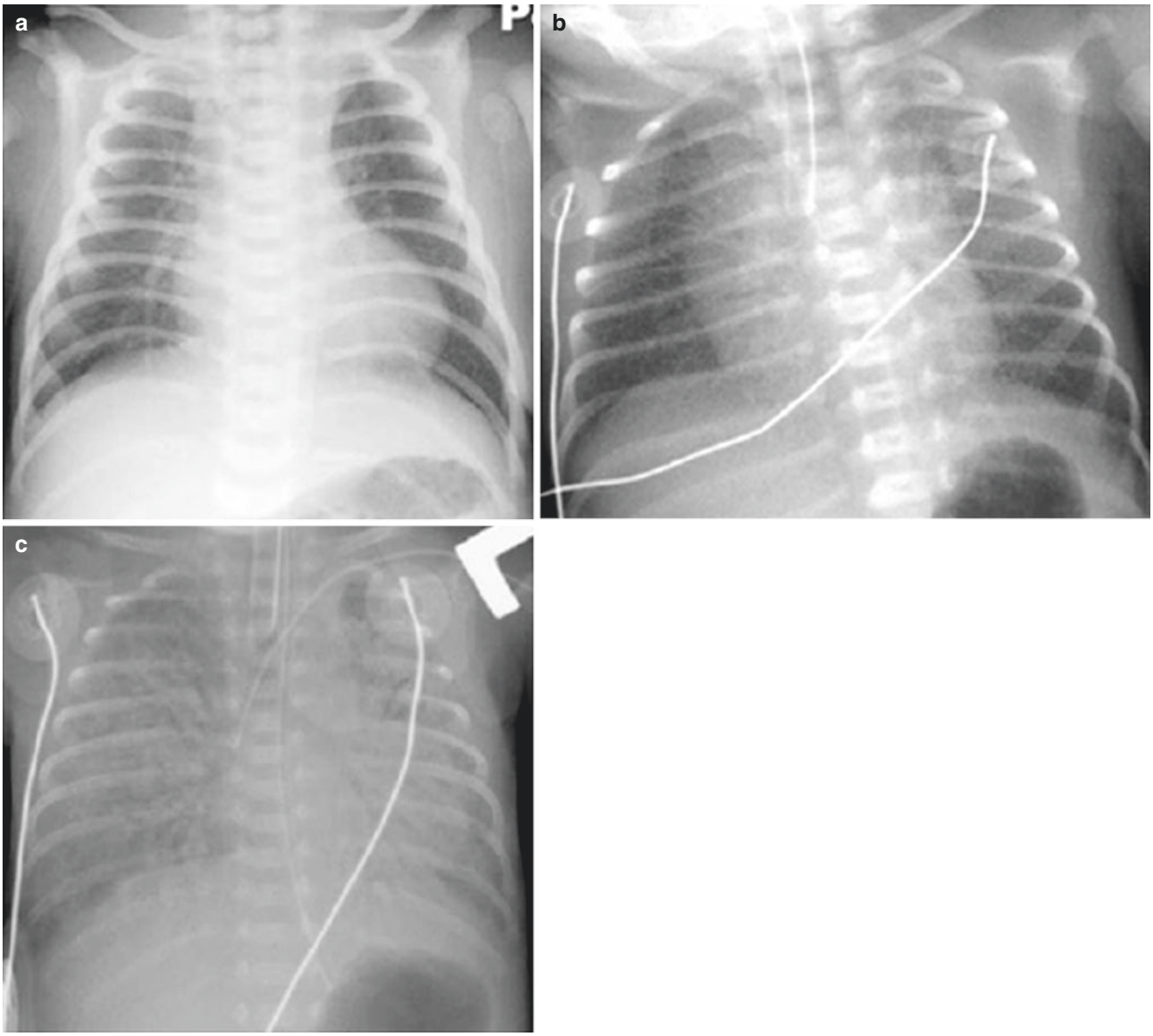

Fig. 5.1 Uncomplicated RDS is an evenly distributed, fine granular opacification. It may vary from patient to patient in its clinical and imaging severity. (**a**) Mild RDS. (**b**) Moderate RDS. (**c**) Severe RDS

opacification seen throughout both the lungs (Fig. 5.1). This is so characteristic that if the opacification is uneven, it suggests a different or multiple etiologies, such as TTN or neonatal pneumonia. The exception is seen occasionally in late-preterm infants and, in particular, near-term boys where there may be uneven distribution of lung disease, at times with mild accentuation of opacification in the lung bases (Fig. 5.2). Bile acid pneumonia (a rare diagnosis) [6] may produce a pattern identical to RDS. This diagnosis may be suspected in newborns of mothers with severe intrahepatic cholestasis of pregnancy. This is especially true if indices of lung maturity are good and the baby has high serum bile acid levels.

The rigid, noncompliant lungs and the associated hypoxia and acidosis of RDS often result in pulmonary artery constriction and pulmonary hypertension. As pulmonary resistance decreases, there may be the onset of left-to-right shunting across a patent ductus arteriosus (Fig. 5.3). This may be recognized radiographically before clinical symptoms of a murmur develop. It is heralded by the development of pulmonary edema and, on occasion, a suddenly enlarging heart size. In the premature newborn with RDS, the patency of the ductus arteriosus may be maintained by hypoxia, acidosis, and high levels of prostaglandin E1 and E2 [7]. Soon after birth, the pulmonary and systemic pressures may be equal, or the pulmonary pressure may exceed systemic,

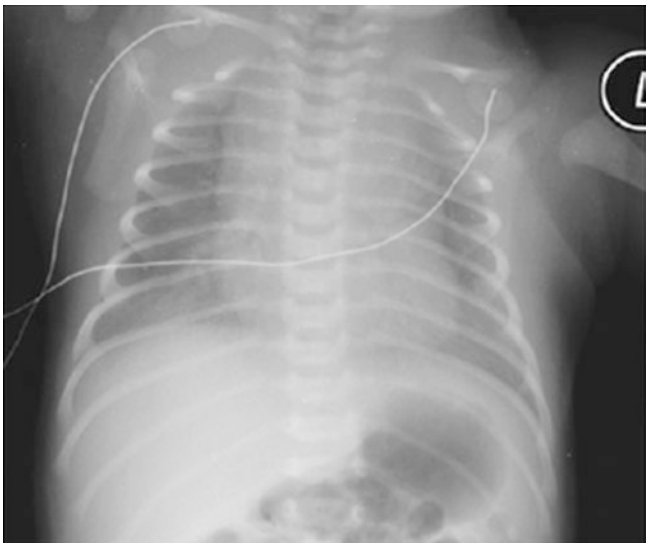

Fig. 5.2 HMD in near-term boys may be irregular in its distribution, usually accentuated in the lung bases as in this 36-week gestational age newborn boy

precluding left-to-right shunting. By several days of life, as the pulmonary resistance drops, if the ductus is not responsive or the stimuli are not present, the ductus arteriosus will remain open in most premature infants, although its clinical significance remains questionable. Treatment with cyclooxygenase inhibitors such as ibuprofen or indomethacin (by inhibiting production of prostaglandin) may produce ductal closure but also increase the risk of inducing gastrointestinal perforation especially if corticosteroids have also been administered as in cases of persistent hypotension [8]. Surgery may be required to close a persistent patent ductus arteriosus (PDA) although surgical closure of PDA is becoming less common across NICUs due to the accumulating evidence that it may not improve long-term outcomes but could have surgical complications [9].

Sudden diffuse opacification of the lungs in RDS may be seen with other conditions in addition to pulmonary edema from a PDA or fluid overload (Fig. 5.4). A frequent cause is atelectasis due to decreasing ventilatory support. Less commonly, diffuse pulmonary hemorrhage may be a cause. Rarely, sudden catastrophic intracranial hemorrhage may produce pulmonary edema that is central nervous system-mediated.

Changes in perinatal care, such as the use of antenatal steroids, exogenous surfactant administration, early CPAP, and lung protective strategies of mechanical ventilation (patient-triggered modalities, volume-controlled modes, and high-frequency ventilation), have led to improvement in survival and outcomes of infants with RDS over the past 30 years.

The efficacy and safety of surfactant replacement therapy to improve oxygenation, decrease the need for mechanical ventilation, and reduce mortality in neonates with respiratory failure from RDS have been established in multiple randomized controlled clinical trials. However, the long-term consequences of RDS, such as BPD, have not been clearly altered [10–12]. The use of exogenous surfactant has produced several significant changes in radiographic configurations. The surfactant is given as liquid boluses via an ET tube and can dramatically improve pulmonary compliance, oxygenation, and radiographic expansion.

It is possible for surfactant to be unevenly distributed throughout the lungs, resulting in a radiograph pattern of areas with improved aeration alternating with areas of atelectasis. The uneven distribution produces a radiograph that may simulate other entities such as neonatal pneumonia or MAS.

A consequence of RDS is air leak syndromes, including pulmonary interstitial emphysema (PIE), pneumothorax, pneumomediastinum, or pneumopericardium (Fig. 5.5). This is caused by overdistention of terminal air spaces or airways resulting from uneven alveolar ventilation, air trapping, or high alveolar distending pressure in infants on ventilatory support, particularly in noncompliant lungs (such as those with RDS). As lung volume exceeds physiological limits, mechanical stresses occur in all planes of the alveolar or respiratory bronchial wall, with eventual tissue rupture once pressures have exceeded tensile strength of the noncartilaginous terminal airway and alveolar tissues. Air leak syndromes are managed using high-frequency ventilation (which minimizes volutrauma), needle thoracentesis, and sometimes chest tube insertion [13].

The location of a pneumothorax in a newborn, as is true for all individuals imaged in supine position, may best be seen medially, along the mediastinal border [14]. The anterior medial chest in a supine patient is the most superior portion of the thorax. Without pleural adhesions to restrict free flow of air in the pleural space, the air will accumulate anteriorly and first be apparent as an air/pleural interface medially adjacent to the heart border [15]. As the pneumothorax enlarges, it will become apparent inferiorly, subpulmonic. As it further increases, it will be seen laterally and inferiorly and finally over the pulmonary apex.

Surfactant may reach the level of the acinae causing sudden and effective distention of multiple acinar units producing a radiographic configuration quite suggestive of PIE [16]. In these situations, close communication with the neonatologist to ascertain clinical status is mandatory to the intelligent interpretation of the radiograph. Babies with positive response to surfactant generally improve at this point, while those with PIE deteriorate.

Those babies with PIE usually resolve the interstitial air over a period of a few days. However, rarely, the interstitial air may persist and enlarge. This may be severe enough to expand the involved segment of the lung causing mass

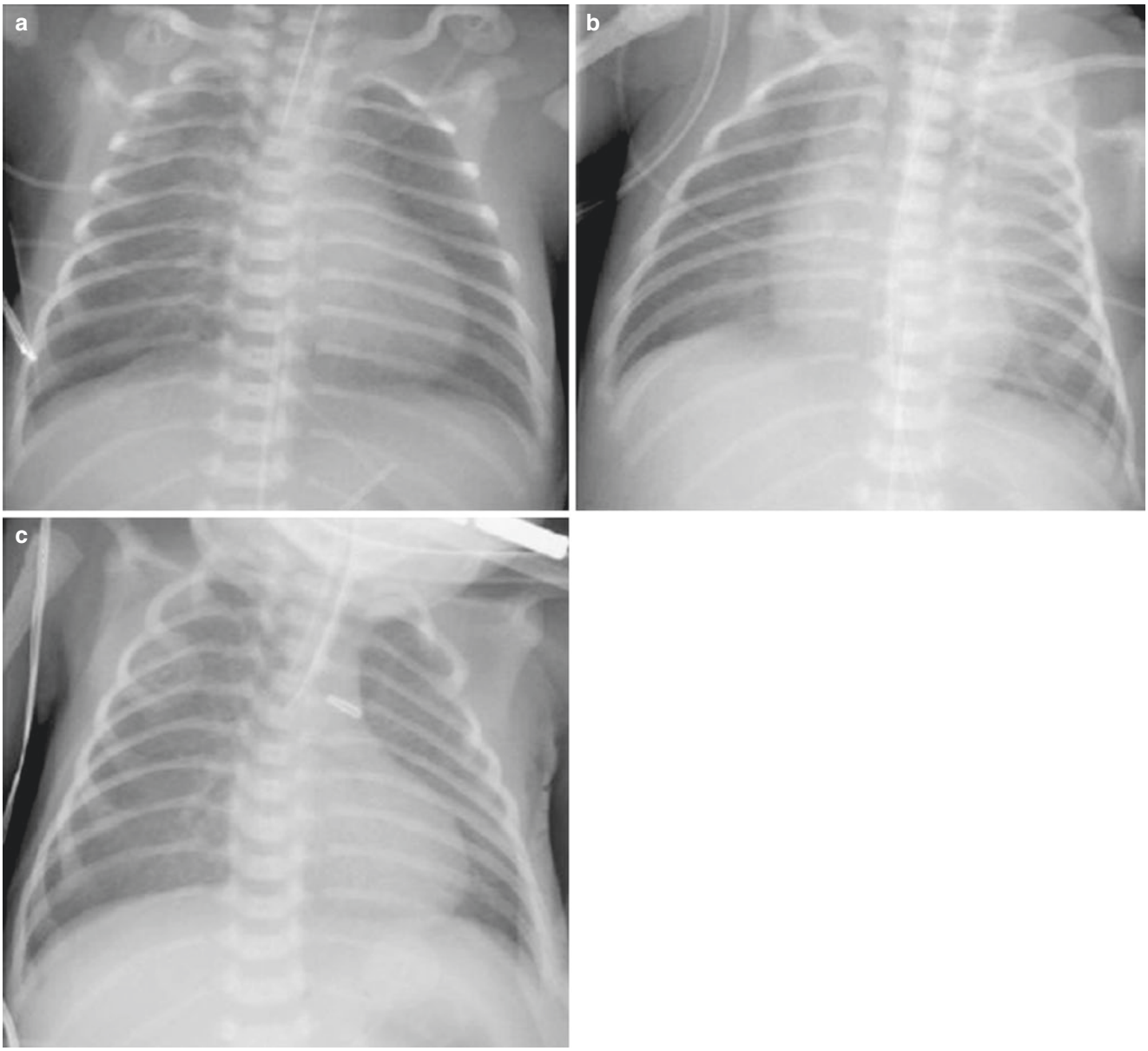

Fig. 5.3 Pulmonary edema, usually the result of left-to-right shunting across a patient ductus arteriosus, is a relatively common complication in premature infants. (**a**) Moderately severe RDS in a 1-day-old. (**b**) Increased hazy opacification, accentuated centrally, on the third day of life consistent with the interval development of pulmonary edema. (**c**) The edema has diminished following surgical closure of the PDA (a ductus clip overlies the left hilus)

effect and further respiratory distress. Occasionally the PIE may coalesce into a giant interstitial bleb. Many of these eventually resolve spontaneously, but some will require surgical resection. Although not usually necessary to establish the diagnosis, CT may show a characteristic *line and dot* pattern [17].

High-frequency ventilation (10–15 Hz, 600–900 cycles/min) has also been employed to reduce the incidence of barotrauma. It is typically used as a rescue therapy for infants failing conventional ventilation or those with air leak syndrome, as current evidence does not support the use of high-frequency ventilation as initial therapy in extremely premature infants [18]. The radiographs of babies receiving high-frequency ventilation are not significantly altered from that noted with conventional ventilator therapy. However, the degree of pulmonary inflation is used to adjust mean airway pressure (MAP). Ideally, the dome of the diaphragm should project over the 8–10 posterior rib if MAP is appropriately adjusted.

In children successfully managed with short courses of assisted ventilation, the usual radiographic course is to evolve from RDS to a hazy diffuse opacification of the lungs to normal over a period of several days to 2 or 3 weeks (Fig. 5.6).

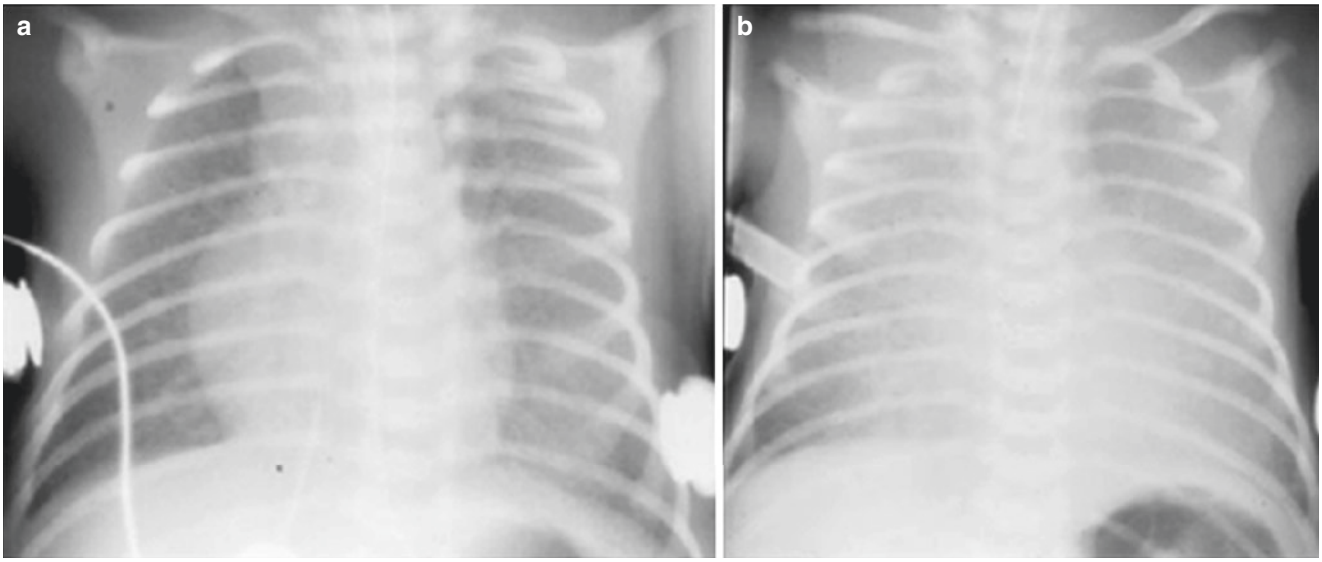

Fig. 5.4 Sudden onset of a *white out* has several possible explanations. (**a**) Moderately severe HMD on day 2 of life. (**b**) This image was obtained 2 days later, approximately 15 min after a moderate decrease in peak end-expiratory pressure (PEEP). There is a dramatic increase in diffuse pulmonary opacification. The baby was stable at this time with a subsequent image no longer showing the *white out*

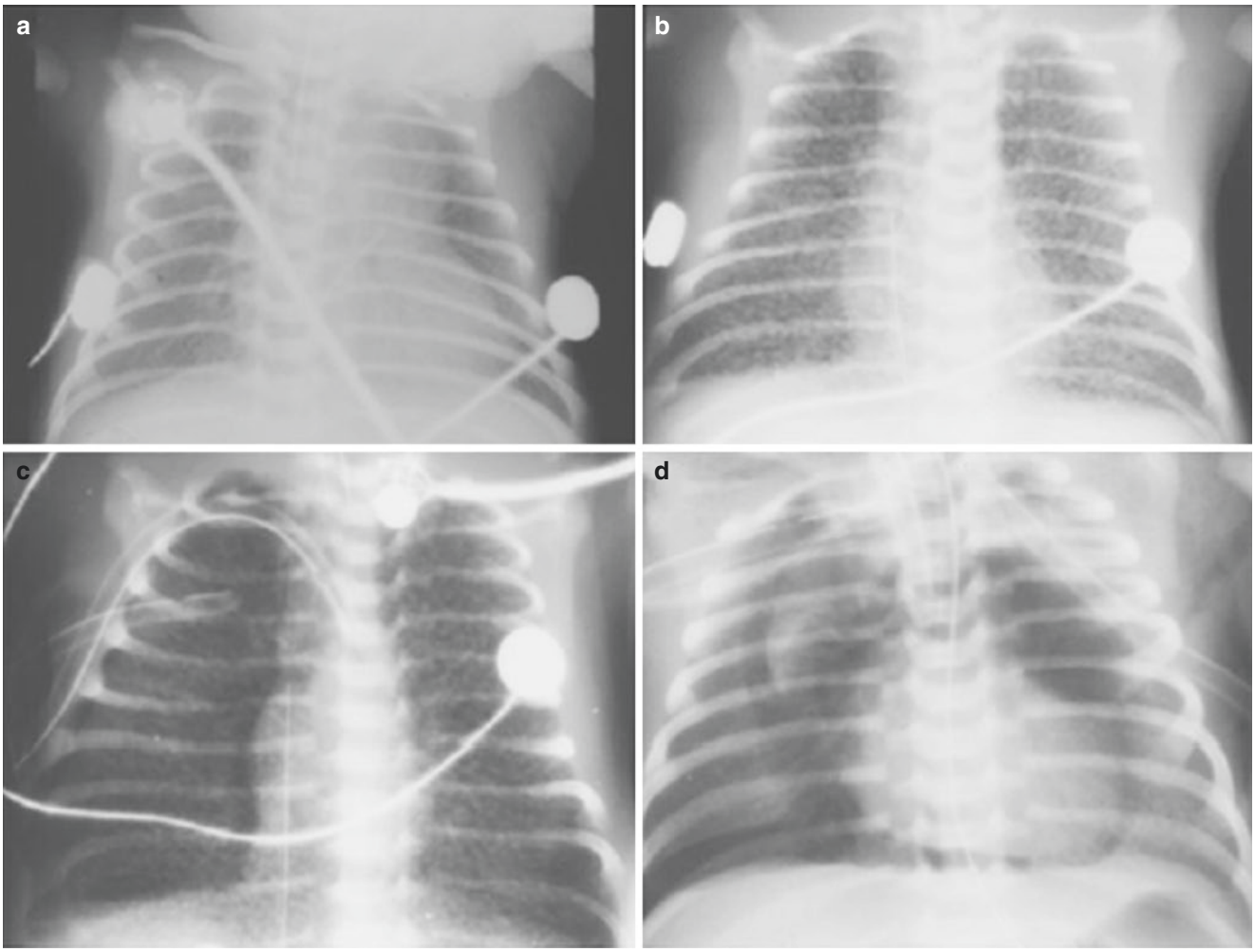

Fig. 5.5 Air leak phenomenon is a complication of RDS, which can be treated with high-frequency ventilation. (**a**) Moderate RDS on day 1 of life. (**b**) Diffuse PIE has developed by day 3. (**c**) Right pneumothorax developed shortly afterward. (**d**) Air surrounding the heart, lifting the right lobe of the thymus off the heart indicates the presence of a pneumomediastinum or pneumopericardium. Air outlining the inferior heart is more commonly seen in pneumopericardium but may be seen with a pneumomediastinum as is the case in this baby with air in the subcutaneous tissues of the right shoulder/neck

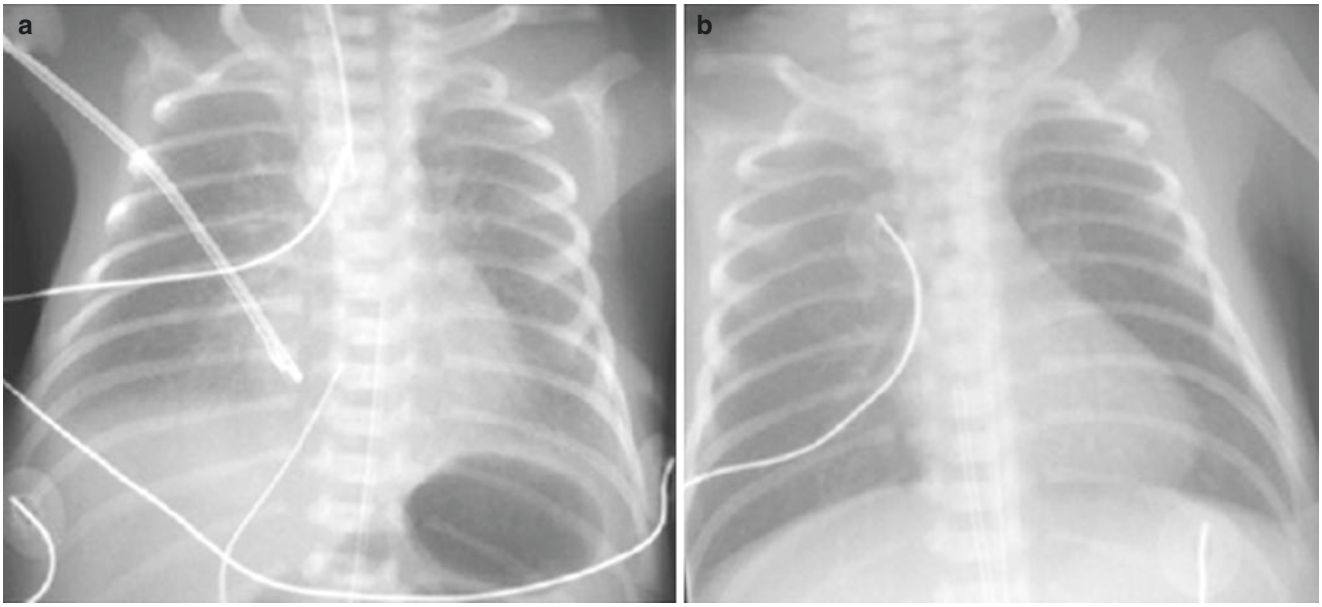

Fig. 5.6 Most cases of mild to moderate RDS resolve without developing BPD. (**a**) Moderate HMD on day 1. (**b**) By day 6, the crisp, finely granular appearance of HMD RDS on day 1 has become less distinctly defined and is now irregular in its distribution. The baby's RDS resolved without pulmonary sequelae

Bronchopulmonary Dysplasia

Bronchopulmonary dysplasia (BPD) is a chronic lung injury in premature infants who survive RDS after treatment with mechanical ventilation and oxygen. It is the most common long-term complication of prematurity and results in significant morbidity and mortality. Since Northway's original description of BPD in 1967 [6], many changes have occurred in the management and outcome of children with RDS, as well as in the definition of BPD itself. In 2001, a workshop conducted by the National Institutes of Child Health and Human Development (NICHD) proposed a definition for BPD diagnosis and severity based on oxygen requirement at 28 postnatal days for infants born <32 weeks and at 29–55 postnatal days or discharge to home (whichever comes first) for infants born ≥32 weeks [19]. Radiology was not imcluded in the workshop definition because of lack of consistent readings. BPD is a lung injury syndrome resulting from interactions of antenatal exposures and postnatal trauma from oxygen, mechanical ventilation, infection, as well as other inflammation-associated injuries impacting the immature and developing lung [20]. Practices changes including the use of noninvasive ventilation, favoring early extubation, minimizing ventilator pressures and barotrauma, and minimizing oxygen toxicity have been implemented to reduce the development of BPD. Infants at greatest risk for developing severe BPD are the profoundly premature who require longer courses of assisted ventilation at greater pressures and rate and higher inspired oxygen concentration (FiO_2 of 0.6–1.0). With the above improvements in neonatal intensive care, it is now rare to see the development of the classic four stages of BPD as described by Northway et al. [21] (Fig. 5.7). This form of BPD, referred to as "old BPD," is characterized by airway injury, bronchial smooth muscle hypertrophy and peribronchial inflammation, and parenchymal fibrosis and due to volutrauma, barotrauma, and oxygen toxicity to the lungs during mechanical ventilation for RDS.

In contrast, "new BPD" can occur in premature infants with minimal lung disease after birth who required brief or even no ventilator support and relatively low FiO2 in the early postnatal period. Symptoms often develop after the first week of life. The disease is attributed to aberrant lung development with inhibition of alveolar and vascular development resulting in alveolar hypoplasia, decreased septation, and reduction of areas for gas exchange. Some suspect that this *new BPD* is in fact what has been previously referred to as Wilson–Mikity syndrome or chronic pulmonary insufficiency of prematurity [22, 23]. Radiographically, BPD and *new* BPD and Wilson–Mikity syndrome are indistinguishable.

However, the classic radiographic changes seen with new BPD are more subtle. First the radiograph may reveal a diffuse haziness, corresponding with a worsening ventilatory or oxygen requirements. This over the next

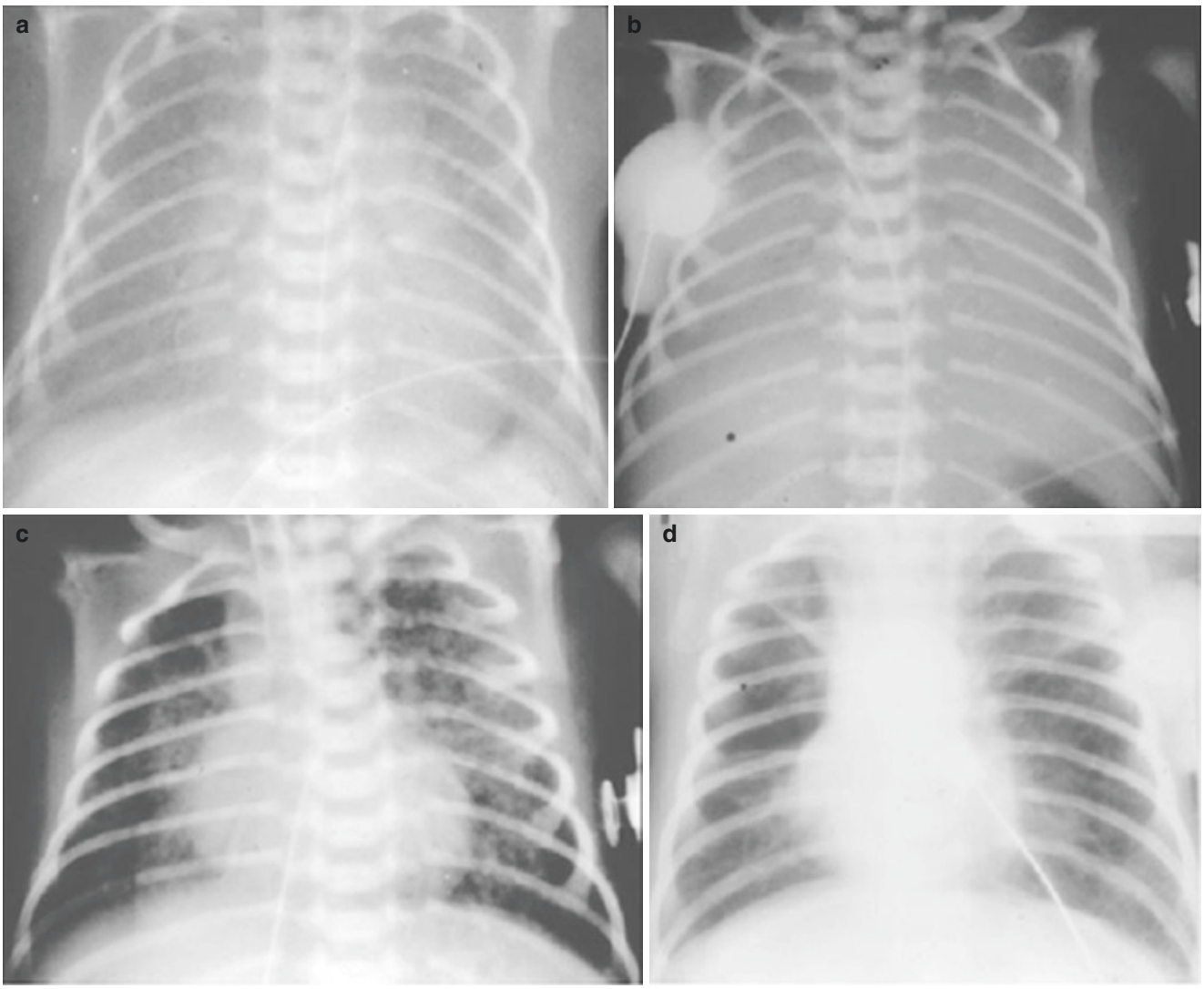

Fig. 5.7 With modern management of RDS, the four stages of BPD as originally described by Northway [6] is rarely encountered. (**a**) Stage 1, RDS on day 1. (**b**) Stage 2, *white out* on day 3. (**c**) Stage 3, BPD on day 21. (**d**) Stage 4, BPD at 6 weeks

1–2 months evolves into increasing heterogeneity and differential areas of atelectasis and edema. By 3–4 months of age, the radiograph is notable for a diffuse coarseness and low lung volumes, with or without some cystic components seen (Fig. 5.8). Although CT is not used as a primary modality for making the diagnosis of BPD, over time characteristic changes include areas of linear and triangular densities (representing segmental atelectasis), mosaic hypoattenuation (indicating air trapping), emphysema, and bronchial wall thickening and bronchiectasis [24]. New imaging techniques using magnetic resonance imaging can now define structural lung changes with remarkable resolution [25].

Strategies to improve outcomes of RDS have not necessarily changed outcomes with regard to BPD. While randomized controlled trials have shown that antenatal corticosteroid administration reduces the incidence of RDS by accelerating lung maturation, the practice has not impacted rates of BPD. This may be due to the survival of sicker infants.

Similarly, the prophylactic use of CPAP after delivery to maintain acinar distention, without intubation and prophylactic surfactant administration, in order to avoid the consequences of mechanical ventilation (barotrauma and volutrauma) has been suggested to improve pulmonary outcomes of prematurity and BPD [26]. However, more recent data has also suggested that despite changes in delivery room management, the long-term pulmonary function has not significantly improved over comparisons of large historical cohorts of former premature infants [27].

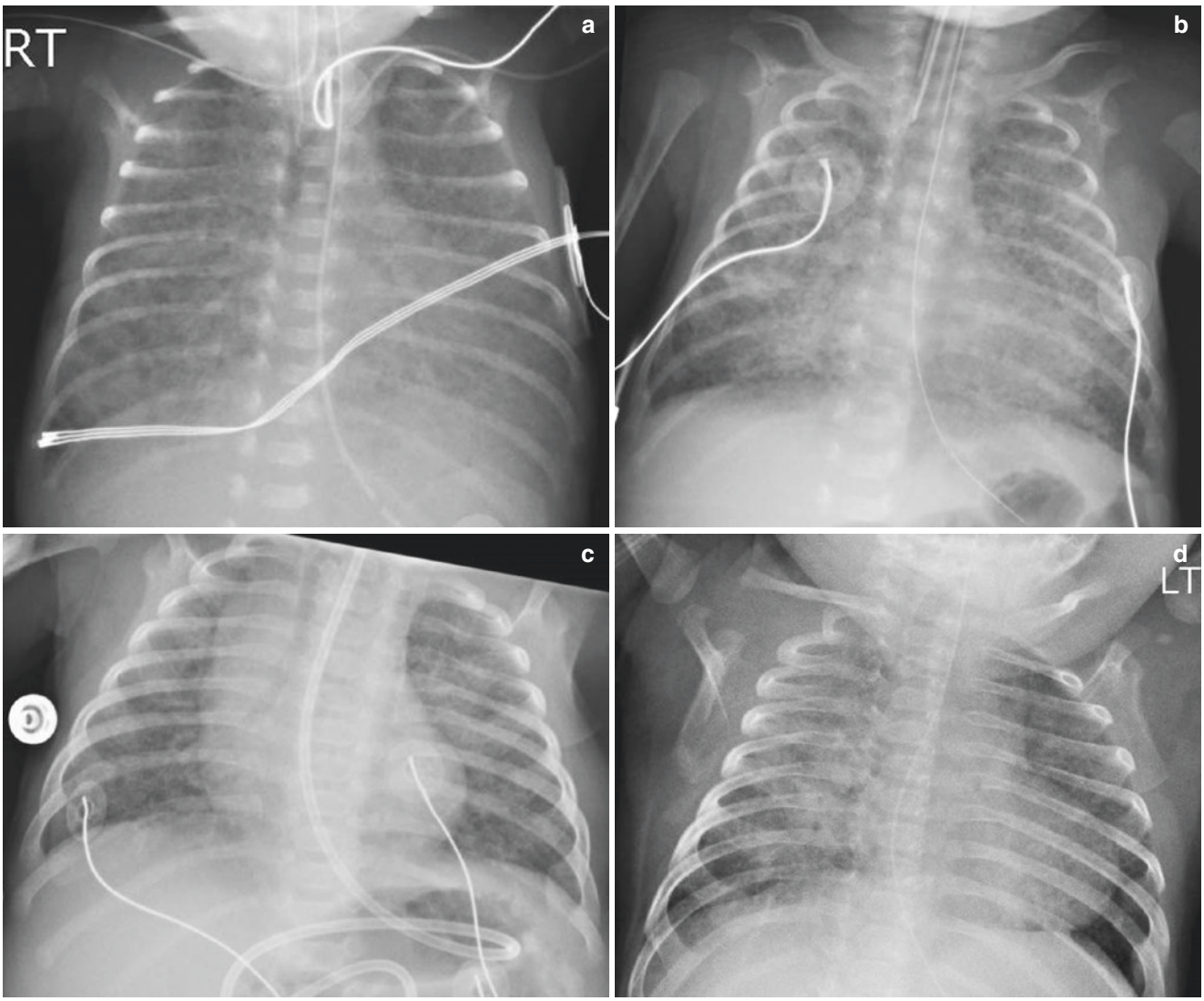

Fig. 5.8 These images are of an infant born at 27 weeks' gestation, with respiratory distress syndrome RDS. They represent progression of lung disease into "new" bronchopulmonary dysplasia over time. These images differ than "old" BPD, in which radiographs showed developing cystic changes and hyperinflation. The images are taken at (**a**) 2 weeks of age, with developing coarseness to lung disease (also note endotracheal tube in upper trachea); (**b**) 1 month of age, with increasing heterogeneity and differential areas of atelectasis and edema (again, patient remains intubated); (**c**) 3 months of age, with coarseness and low lung volumes (also note post-pyloric feeding tube which is partially visualized); and (**d**) at 5 months of age, with edema and some small cystic changes noted

In spite of the advances in management of these babies, many of the survivors develop the chronic pulmonary manifestations of Northway's stage 4 BPD [21]. This consists of alternating areas of fibrosis/atelectasis and focal overexpansion of the lung. These findings have been documented by CT in older children and adults and expectedly are represented by areas of linear opacities and areas of ground-glass opacification alternating with areas of decreased attenuation and perfusion (focal overinflation). There is diffuse bronchial wall thickening and decreased bronchus to pulmonary artery diameter ratios [28].

Meconium Aspiration Syndrome

Meconium aspiration syndrome (MAS) is the result of intrapartum or intrauterine aspiration of meconium. It most commonly occurs in babies who are postmature; the mean gestational age for MAS has been reported as 290 days or 10 days past the expected date of delivery. MAS may also occur in infants who are small for gestational age or in infants that have been exposed to intrauterine stress causing hypoxemia. Although there is meconium staining of the amniotic fluid in approximately 10–15% of live births, MAS is seen in 1–5% of newborns.

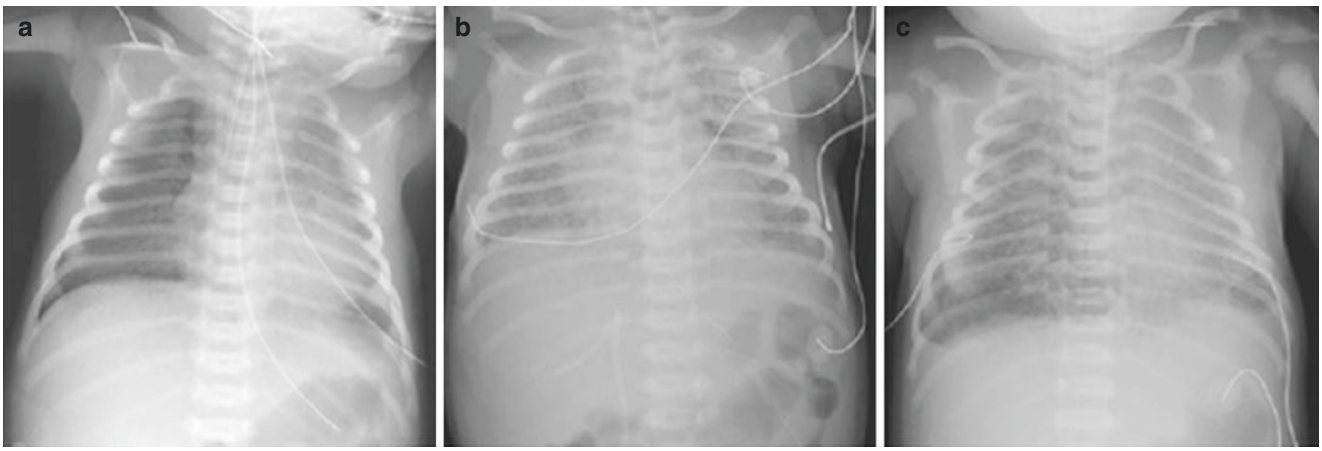

Fig. 5.9 MAS may present radiographically in several manners. (**a**) It may present as ill-defined focal opacifications as in this baby's left lower lobe and to a lesser degree the right lower lobe. There is a right pneumothorax seen as a lucent line paralleling the superior mediastinum (medial pneumothorax) and inferolaterally. (**b**) More typically, MAS may present as course irregular opacification. (**c**) There may be a combination of coarse, irregular opacifications and focal consolidations (left lower lobe in this baby). There is a right pneumothorax

The radiographic findings in MAS vary, in part secondary to the severity of the aspiration. The tenacious meconium often will cause both medium and small airway obstruction. This typically will cause areas of atelectasis alternating with areas of overinflation (Fig. 5.9). The meconium is an irritant to bronchial mucosa and may cause a chemical pneumonia, as well as inactivate surfactant. Though meconium is sterile, there is increased risk for concurrent pneumonia.

Hypoxia usually results, with all factors combining to produce persistent pulmonary hypertension of the newborn (PPHN). Air leak syndromes including pneumothorax are present in 10% of cases, due to both the need for mechanical ventilation and air trapping from ball-valve effects of the meconium.

Occasionally, babies with MAS requiring ventilatory support will have a normal chest X-ray or possibly only a pneumothorax. Small pleural effusions are also seen in approximately 10% of cases. The chest X-rays of infants with MAS may be indistinguishable from children with neonatal pneumonia. Because of the difficulty in excluding neonatal pneumonia and the possibility of developing a superimposed pneumonia in MAS, most of these infants are treated with antibiotics. On rare occasions, an early follow-up radiograph will show dramatic improvement in pulmonary opacifications (possibly mimicking the clearing of transient tachypnea of the newborn). However, in these cases of MAS, the clinical condition does not improve in parallel with the radiograph, and subsequent images fail to show similar continued rapid clearing of the abnormality (as would be expected with transient tachypnea of the newborn), possibly due to PPHN. In other cases, the radiographic abnormalities and clinical symptoms persist for several days and are likely the result of secondary MAS pneumonitis.

In spite of optimal care, there is a persistent mortality rate of up to 5–10% in babies with MAS. This has been partly mitigated by the use of inhaled nitric oxide (iNO) to treat severe pulmonary hypertension and extracorporeal membrane oxygenation (ECMO). Inhaled NO has been shown to decrease the need for ECMO in babies with severe PPHN [29–31]. Surfactant replacement therapy has also been shown to decrease need for ECMO in babies with MAS [32].

Since ECMO has potentially life-threatening side effects including cerebral hemorrhage, its use is limited to babies who have failed conventional therapy including iNO. Survival rates with ECMO have been excellent [33]. The most critical factor in weaning from ECMO is not simply improved pulmonary mechanics but reduction of pulmonary vascular pressure to below systemic. Some have postulated a primary abnormality of pulmonary microcirculation in MAS. However, others feel that the increased pressures within the airways, produced by assisted ventilation, are the cause of PPHN in these babies. ECMO, which bypasses the lungs, allows pulmonary inflation to be at a minimum while maintaining physiologic levels of oxygen tension and saturation [34–36]. In addition, there is significant third space fluid deposition while on ECMO. Therefore, on ECMO the lungs are usually nearly or completely airless (Fig. 5.10).

Neonatal Pneumonia

Neonatal pneumonia is seen in less than 1% of live born full-term infants, though it can occur in more than 10% of infants admitted to the NICU. Premature infants are at increased risk. It may be acquired in utero, during labor, at delivery, or shortly after birth. The major risk factor for intrauterine development of pneumonia is prolonged rupture of the mem-

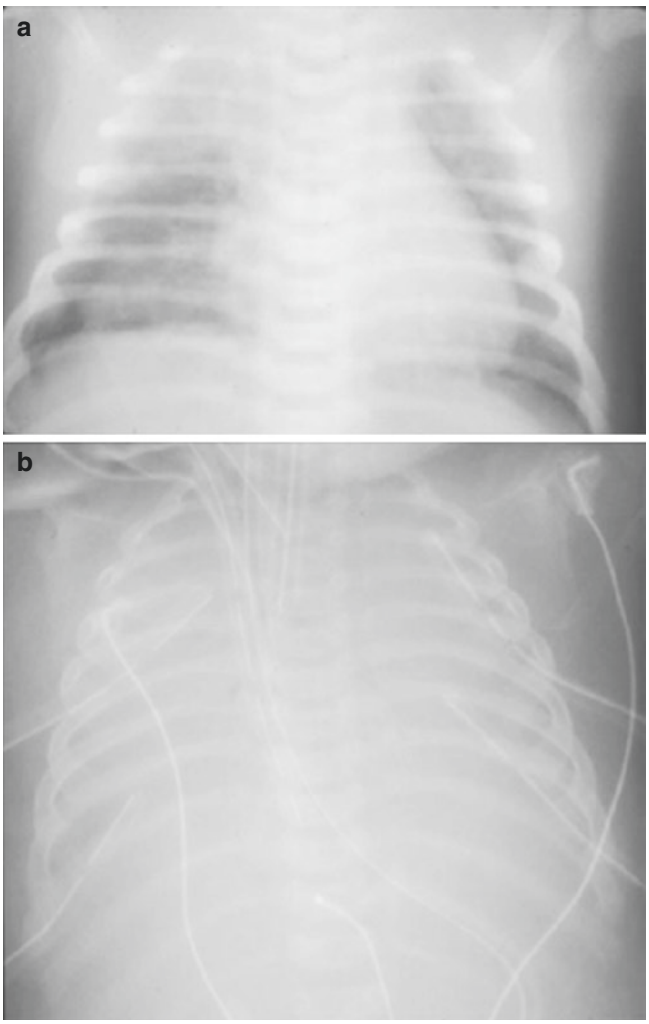

Fig. 5.10 The survival of infants with MAS may require the use of ECMO. (**a**) Eight-hour old with severe MAS. (**b**) Once this baby was placed on ECMO, the lungs became airless. The ECMO cannulae are appropriately placed with the venous line tip in the right atrium and the arterial line tip in the distal aortic arch

branes, particularly if labor is active during this period. Some organisms, particularly viruses, may cross the placenta. Prior to universal maternal screening and chemoprophylaxis, group B streptococcus (GBS) infections were the most common cause of pneumonia in the newborn with an incidence of 3/1000 live births and are acquired in utero or during labor and delivery [37]. Both clinically and radiographically, it may be difficult to distinguish GBS pneumonia from RDS. In premature infants, *Escherichia coli* has now become the most common bacterial isolate in neonatal sepsis [38].

Chest radiographs may reveal lung disease identical to RDS; however, pleural effusions are more commonly associated with pneumonia (in up to 67%) and essentially never with uncomplicated RDS [19]. Small effusions are most apparent over the pulmonary apex and in the medial, inferior costophrenic sulcus. In neonatal pneumonia, the lungs may reveal irregular patchy infiltrates (Fig. 5.11) or occasionally be normal. There may be mild cardiac enlargement with pneumonia, but it is unusual with uncomplicated RDS (Fig. 5.12) [39]. In addition, RDS and neonatal pneumonia frequently coexist.

Infections with other bacterial organisms may produce radiographic findings identical to those described above in group B streptococcal infections, including *Klebsiella* species, *Listeria monocytogenes*, pneumococci, and *mycoplasma* [40, 41]. An unusual clinical and imaging course has been described with *Ureaplasma urealyticum*. This has been characterized as having a milder acute course but early onset of chronic lung disease, and its isolation from the upper and lower respiratory tract of premature infants has been shown to be associated with BPD [42].

Both neonatal pneumonia and MAS most commonly present with irregularly distributed, somewhat coarse airspace opacifications. Generally the coarseness of the opacifications is more accentuated in MAS, but not consistently enough to allow precise differentiation. These imaging findings may also be seen with transient tachypnea of the newborn. However, with transient tachypnea of the newborn, the radiographic and clinical courses improve rapidly in parallel over the first 1–3 days of life.

Chlamydia Pneumonia

Chlamydia pneumonia is caused by a bacterial-like intracellular parasite, *C. trachomatis* [47–49], which is acquired from the mother by direct contact during vaginal delivery. This organism is widely distributed, having been identified in the vagina of up to 13% of women tested. Up to 50% of babies infected become symptomatic with conjunctivitis. This most common manifestation usually appears around 5–14 days of life. Pneumonia develops in 10–20% of infected babies, appearing between 2 weeks and 3 months of age. However, the average age of onset is 6 weeks; therefore, Chlamydia pneumonia is somewhat unusual in the neonatal age group. Cough, sometimes paroxysmal and associated with tachypnea, is the most common symptom of this disease. It may be preceded by nasal obstruction or discharge. Up to 50% of infants with Chlamydia pneumonia will have conjunctivitis, and up to 50% will have peripheral eosinophilia with absolute blood eosinophil levels in excess of 300/mm^3. Definitive diagnosis may be made by nasopharyngeal culture, which must be specially processed. Nucleic acid amplification testing is also available but is not approved for nasopharyngeal swabs. Not uncommonly, the findings on chest radiograph are far worse than would be predicted by physical examination (Fig. 5.13). The findings may range from a purely interstitial process to a focal alveolar infiltrate. Hyperinflation is generalized, and pleural effusions are

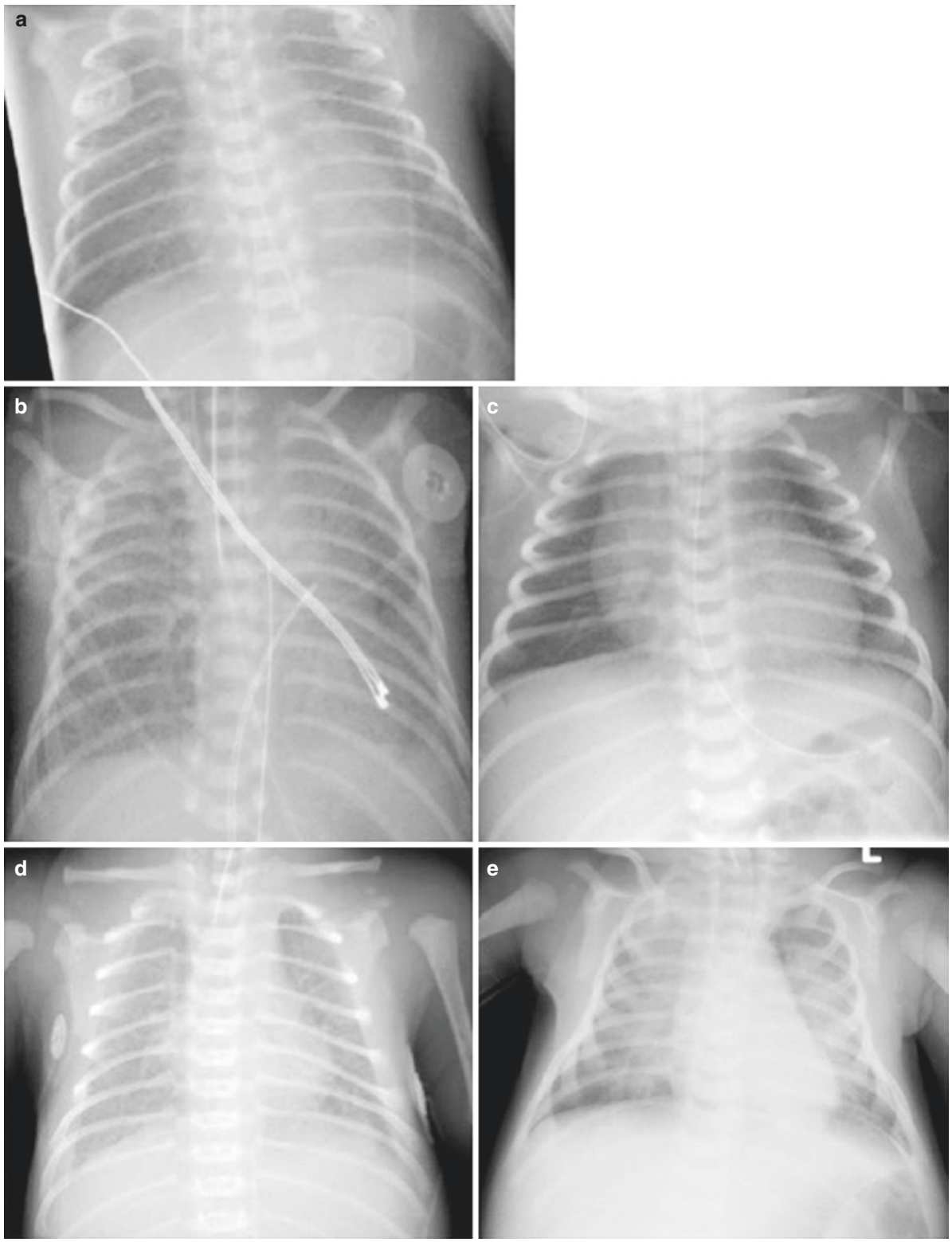

Fig. 5.11 Neonatal pneumonia has variable radiographic characteristics. (**a**) It may simulate mild RDS, except in this patient it is somewhat accentuated in the left lower lobe. (**b**) It may simulate severe RDS, except in this baby there are slightly accentuated focal opacities in the left upper lobe and left lower lobe. (**c**) It may present as a focal infiltrate as in this baby's left lower lobe. (**d**) The opacification may be coarse and irregularly distributed. There are bilateral effusions as well. (**e**) The opacifications may be classically alveolar

uncommon. Occasionally there will be a diffuse linear opacification closely mimicking congenital lymphangiectasia, obstructed pulmonary venous return, or possibly bacterial pneumonia or meconium aspiration.

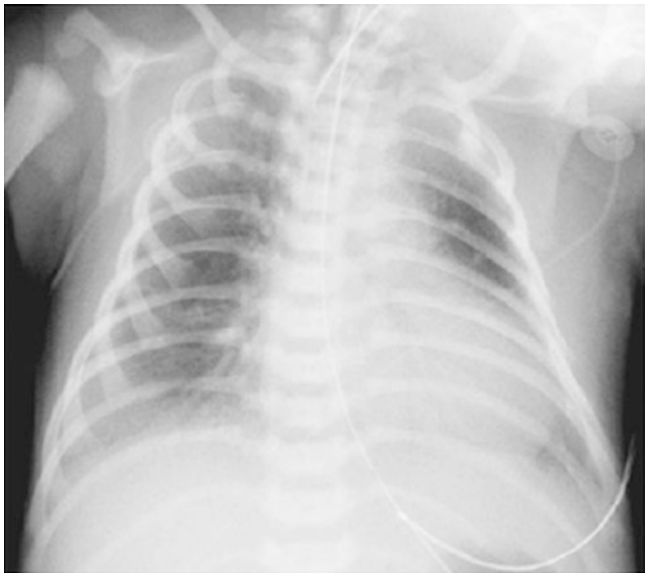

Fig. 5.12 The presence of moderate cardiac enlargement in a baby with coarse, irregularly distributed disease (left lower and right lower lobes) suggests neonatal pneumonia

Transient Tachypnea of the Newborn

Transient tachypnea of the newborn (TTN) is also referred to as retained fetal lung liquid. Fetal lung liquid is an ultrafiltrate of fetal serum. Under normal circumstances, it is cleared from the lungs during the process of labor via the tracheobronchial system (30%), the interstitial lymphatics (30%), and the capillaries (40%), mediated by catecholamines and endogenous glucocorticoids. TTN is most commonly seen in infants born by cesarean section but may also be identified in infants who have experienced a precipitous delivery or macrosomia.

Infants with TTN typically present with tachypnea and cyanosis within the first few hours after birth. Often the tachypnea is described as "comfortable," though it can be accompanied by grunting, retractions, and nasal flaring. Chest radiographs may show pulmonary vascular congestion, prominent perihilar streaking, fluid in the interlobular fissures, hyperexpansion, and a flat diaphragm (Fig. 5.14). Mild cardiomegaly and pleural effusions may also be present [13]. The hallmark of this process is a relatively benign clinical course (i.e., tachypnea) as compared to the overall severity of disease suggested by chest X-ray, i.e., if there is no endotracheal tube (ETT) or other ventilatory support in a child with significant lung abnormalities on chest X-ray (Fig. 5.15).

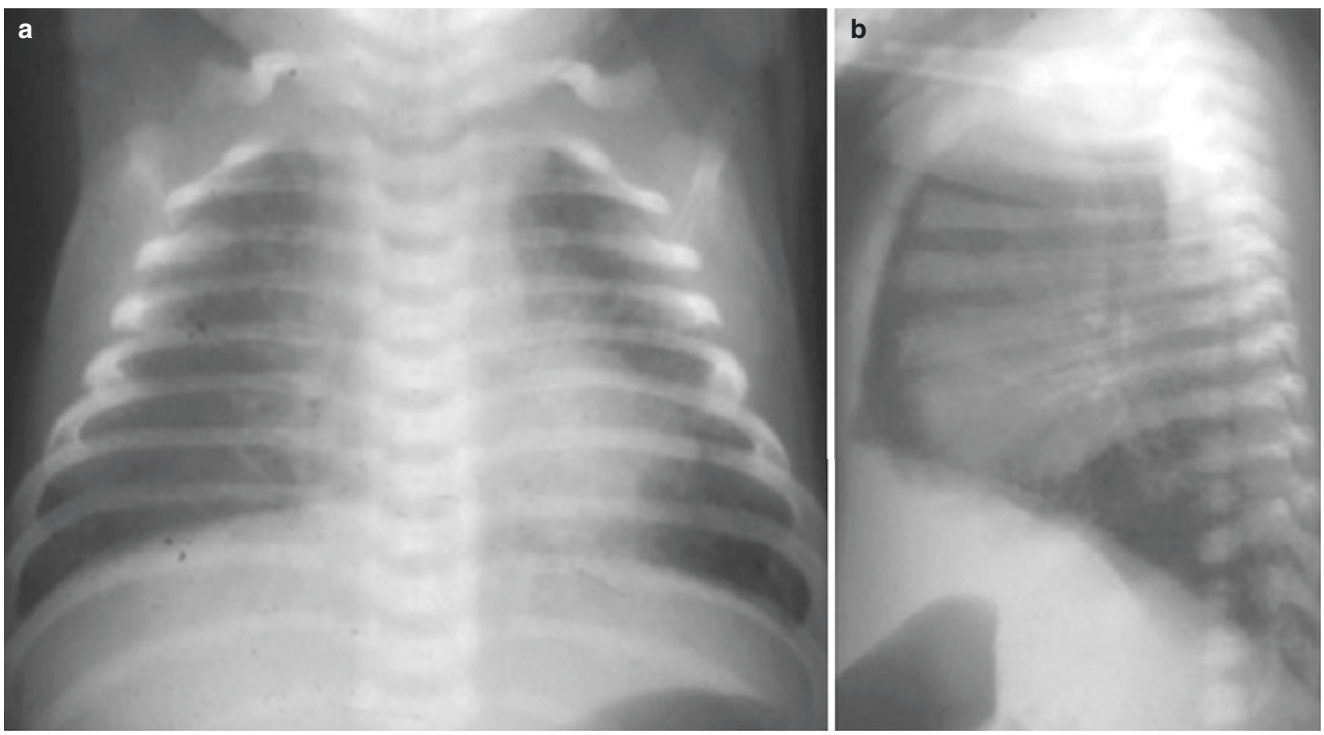

Fig. 5.13 This 26-day-old girl presented at the time of a well-baby checkup with no symptoms but faint crackles heard in both the lungs. There is a diffuse interstitial infiltrate, bibasilar ill-defined alveolar opacifications, and hyperinflation. The imaging findings are worse than anticipated based on the clinical findings. (**a**) PA image. (**b**) Lateral image

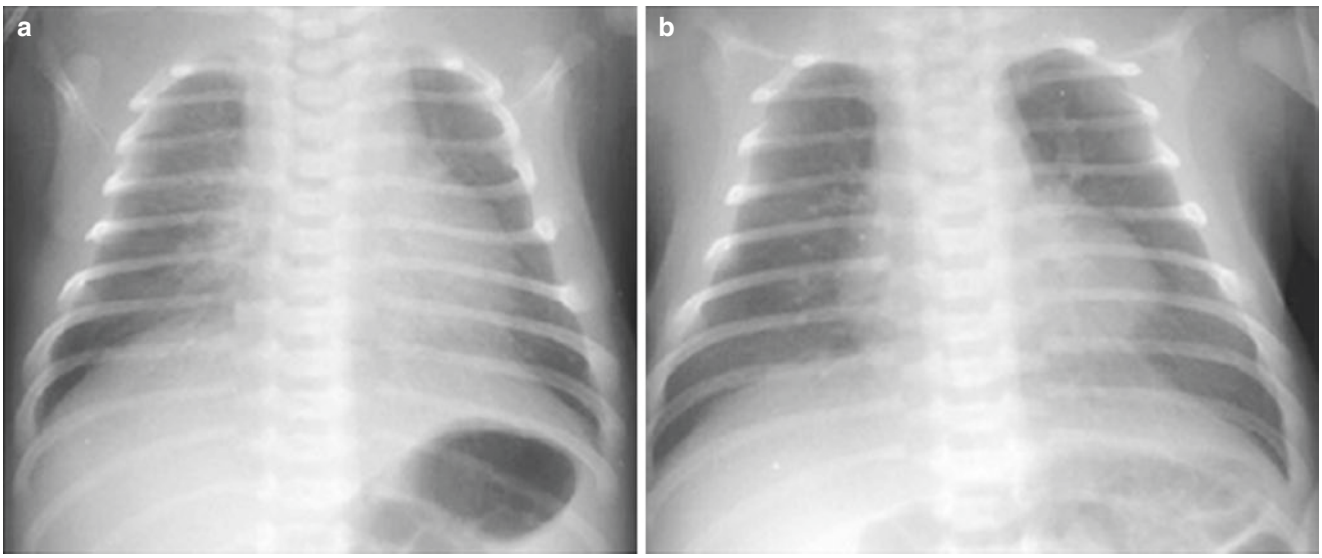

Fig. 5.14 TTN may feature pulmonary vascular congestion, prominent perihilar streaking, fluid in the interlobular fissures. (**a**) At 1.5 h of age, there is a diffuse granular opacification with bibasilar alveolar accentuation, but no ET tube. (**b**) By 10 h, the opacifications have almost resolved. No pleural fluid was noted in this infant

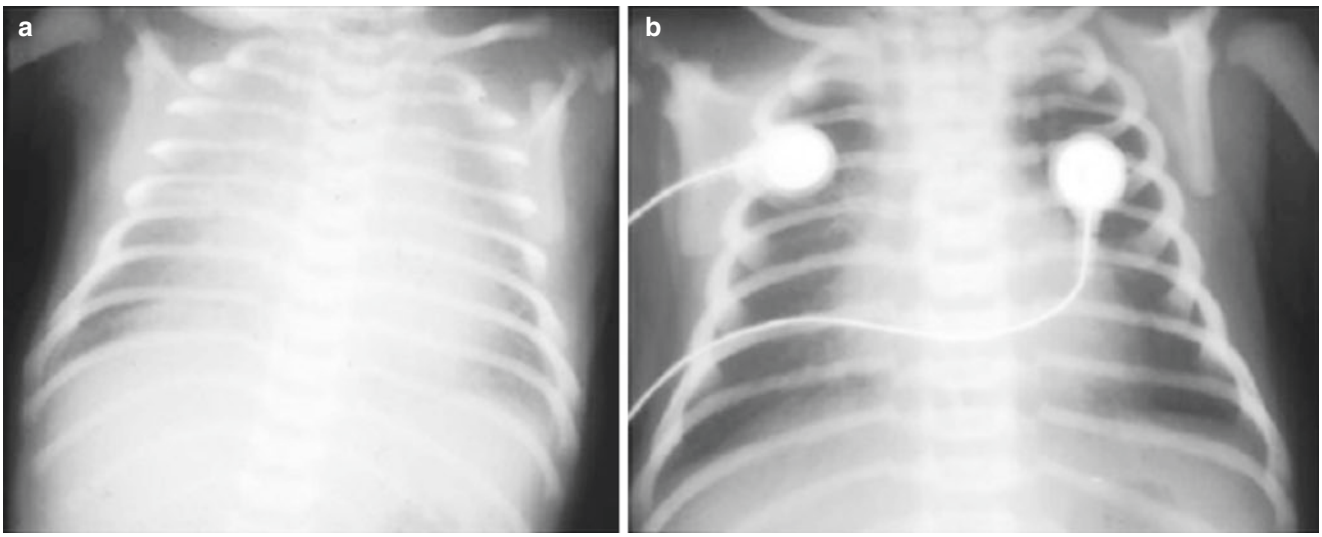

Fig. 5.15 Severe TTN may mimic MAS or alveolar infiltrates of neonatal pneumonia. (**a**) At 3 h of age, there are dense multifocal alveolar opacifications, bilateral effusions, and possible heart enlargement, but no ET tube. (**b**) By the third day of life, the focal opacifications have markedly improved, the effusions have resolved, and the heart is at the upper limits of normal

Clearing of the process should occur rapidly (1–2 days). In particularly severe cases, where clearing may require up to 3 days, there should be a rapid improvement on each successive image.

Focal retention of fetal lung liquid within congenital lobar emphysema has been recognized for several years. One publication suggests that the focal retention of fetal lung liquid occurs only, or mainly, within polyalveolar lobes rather than classic congenital lobar emphysema [43].

Congenital Lymphangiectasia

Babies with congenital lymphangiectasia may present with respiratory distress and chylous pleural effusions. The lungs may be normal or reveal a course interstitial infiltrate secondary to the distended and abnormally draining lymphatics. There may be generalized overinflation. Pleural effusions may be present [44]. A particularly large pleural effusion should suggest this diagnosis or may be related to a traumatic chylous or hemorrhagic effusion (Fig. 5.16), as can occur

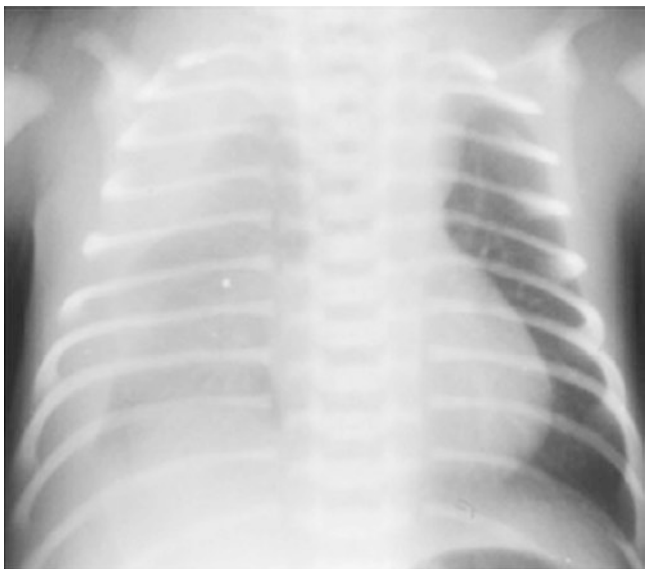

Fig. 5.16 The presence of the large right effusion suggests hemothorax or chylothorax

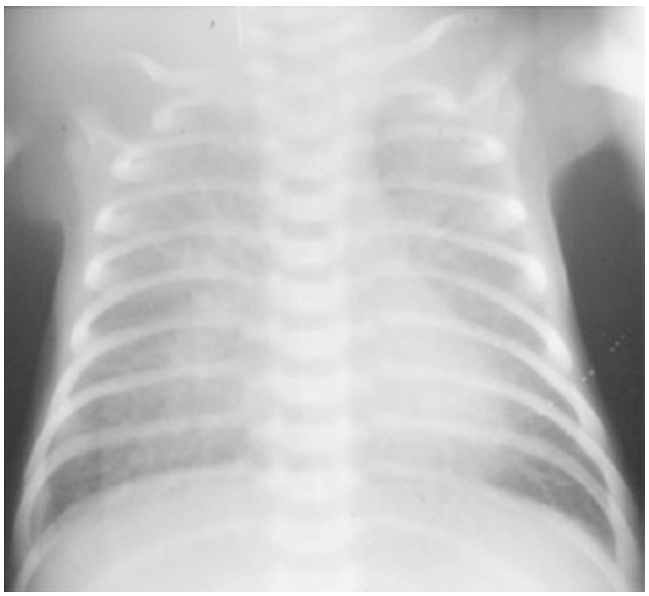

Fig. 5.17 The presence of pulmonary edema with a normal-sized heart suggests mechanical obstruction of pulmonary venous return. In this child with cor triatriatum, there is also a small right effusion. In the correct clinical setting, this image could have represented TTN, neonatal pneumonia, or MAS

during cardiothoracic surgery by injury to the thoracic duct. The presence of a chylous effusion without a history of trauma is suggestive of congenital lymphangiectasia although isolated chylous effusions do occur, particularly in the setting of genetic abnormalities (trisomy 21, Noonan syndrome, and Turner's syndrome). This diagnosis is best made by sampling of the pleural effusion for triglyceride content following the administration of enteral fat-containing feeds. Although prominent interlobular septae, ground glass opacifications, and subpleural fluid/pleural fluid demonstrated on CT are suggestive of this diagnosis [45], the findings are very nonspecific. Although historical descriptions of neonatal congenital pulmonary lymphangiectasia suggested that it was uniformly fatal, more recent experience suggests that a milder form exists. Conservative nutritional management with parenteral nutrition, high-MCT formula feeding, and gradual transition to normal feeds may be successful in such cases.

Congenital Heart Disease

Cases of congenital heart disease may closely mimic several of the entities mentioned previously. The presence of pulmonary interstitial edema may be difficult to distinguish from RDS, neonatal pneumonia, or TTN. However, typically the clinical presentation of congenital cardiac disease is one of profound cyanosis out of proportion to respiratory distress.

A particularly confusing constellation of chest findings may occur in congenital heart lesions producing obstruction to pulmonary venous return but without significant cardiac enlargement. This includes congenital obstructing lesions which occur at the level of the mitral valve or between the mitral valve and the pulmonary venous system. Specifically, these lesions include mitral valve stenosis, supravalvular mitral stenosis, cor triatriatum, stenosis of a common pulmonary vein, or total anomalous pulmonary venous connection (TAPVC) with obstruction. TAPVC physiologically may present with or without obstruction. If obstruction is sufficient, children will present in the first week of life with cyanosis (in severe cases) or with signs of pulmonary edema, dyspnea, and feeding difficulties (in less severe cases). A chest radiograph will show evidence of pulmonary venous hypertension but without an enlarged heart (Fig. 5.17). If there is little or no obstruction to venous return, the children usually present with high-output failure at 6–12 months of age with a radiograph suggestive of congestive heart failure. Several reviews have revealed an overall incidence of obstruction in TAPVC of 50–65%. With supradiaphragmatic draining veins, obstruction has been noted in up to 53% of cases. Essentially, all subdiaphragmatic draining veins are obstructed [37].

If the heart is significantly enlarged, the likelihood that the baby has true congestive heart failure is suggested. Within the first week of life, before the pulmonary vascular resistance drops sufficiently to allow left-to-right shunting, congestive heart failure is usually secondary to pressure overload, obligatory volume overload, or myocardial dysfunction. The lesions most commonly producing this phenomenon include critical aortic stenosis, hypoplastic left

heart syndrome, coarctation of the aorta (interruption of the aortic arch), myocarditis, dysrhythmias, myocardial ischemia, and arterial venous fistula. Significant arterial shunting outside the heart, such as vein of Galen aneurysm, hepatic hemangioma, or hemangioendothelioma may also produce congestive failure in this time period. By the second week of life, after pulmonary resistance has dropped sufficiently, volume overload lesions are the predominant cause for congestive failure. This includes ventricular septal defect, endocardial cushion defect, patent ductus arteriosus, aortopulmonic window, as well as milder forms of those lesions potentially presenting within the first week of life [46].

Lines and Tubes

What is considered to be the *correct* position of various lines and tubes used for support purposes varies from institution to institution. The following discussions reflect the current practice in our institution. Since opinion concerning *safe and appropriate* positioning changes frequently and varies from institution to institution and physician to physician, the following should not be taken as recommendations but merely a reporting of current practice at the author's institution.

Endotracheal Tubes

ETTs in neonates commonly do not have inflatable cuffs. Therefore many neonatalogists attempt to maintain the ETT tip within the intrathoracic trachea, i.e., between the thoracic inlet and the carina. The thoracic inlet is anatomically defined as a plane extending from the first thoracic vertebral body (T1) to the medial end of the clavicles. At the level of the thoracic inlet, the trachea is midway between the T1 vertebral body and the medial end of the clavicles. Therefore, for purposes of chest X-ray assessment, the level of the thoracic inlet in reference to the trachea is the midpoint between the body of T1 and the medial end of the clavicles.

It has been demonstrated that the tip of the ETT in neonates may move a distance equal to the length of the intrathoracic trachea when the head is moved from complete flexion to complete extension. Therefore, the *correct* position of an ETT must relate to head position and the level of the ETT tip. The ETT tip moves inferiorly with flexion of the head and superiorly with extension of the head [50]. Therefore, if the chin is flexed upon the chest wall, the ETT tube tip should be very slightly above the carina. If the head is quite extended and rotated laterally, the ETT tip should be slightly below a point midway between the T1 vertebral body and the clavicles. Some institutions will reference the ETT tip to a vertebral body. Since differences in X-ray beam angle, i.e., straight anterior–posterior vs. lordotic, will alter the way the ETT tip projects over the spine, using only the vertebral level is a less accurate means of assessment.

Enteric Tubes

Nasogastric and orogastric tubes should be positioned so that the tip projects in the expected region of the stomach. Transpyloric tubes are often placed into the small bowel for feeding purposes when dysmotility, gastroesophageal reflux, and lung disease are concerns. Ideally these tubes should follow a course that corresponds to the normal positioning of the stomach, pylorus, duodenum, and proximal jejunum, with the duodenal–jejunal junction (DJJ) (also referred to as the ligament of Treitz) in the left upper quadrant of the abdomen, roughly at the craniocaudal level of the pylorus. Transpyloric tubes can develop a straightening of their course, mimicking the positioning of midgut malrotation. In these situations, it may be prudent to slightly withdraw the tube to proximal to the DJJ and perform a bedside injection of opaque contrast material to document the placement of the DJJ.

Central Venous Lines

The *correct* position of central venous lines (CVLs), including peripherally inserted central catheters (PICC), is the cavo-atrial junction (junction of the right atrium and the superior vena cava (SVC)) if placed in an upper extremity or within the inferior vena cava if placed in the lower extremity. PICC lines should not be left within the right atrium (RA), where it can cause erosion of the endothelium with subsequent development of pericardial effusion and cardiac tamponade. Arrhythmias have also been attributed to incorrect CVL placement.

The junction of the SVC and right atrium has been estimated by projecting the lateral margin of the right atrium to its junction with the SVC. However, the most precise localization, based on CT evidence, places the SVC/RA junction two vertebral bodies (±0.4 vertebral body) below the carina on frontal CXR imaging [33]. PICCs placed via the lower extremity optimally will have the tip situated at the inferior vena cava/right atrium (IVC/RA) junction. As discussed in the section concerning ETT, some institutions use the thoracic spine level as the point of reference; however, because of reasons discussed in connection with ETT position, this is felt by many to be a less accurate method of determining intravascular position. The position of a PICC tip will move as many as several centimeters with changes in position of the extremity into which the line is placed (Fig. 5.18).

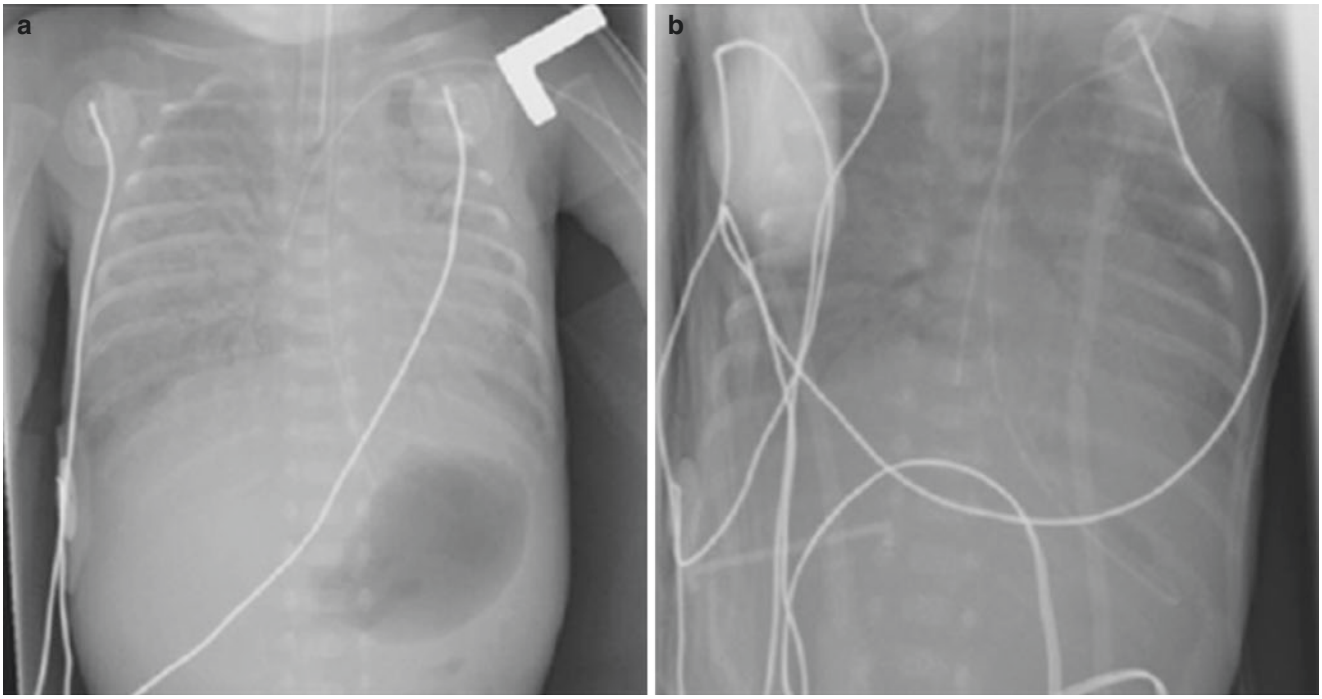

Fig. 5.18 Vascular catheter tip positions change with changing position of the body part into which the catheter is inserted. (**a**) With the left arm slightly abducted, the left arm PICC tip is perfectly positioned at the SVC–RA junction. (**b**) Five hours later, without the PICC having been manipulated, but with the left arm now elevated above the baby's head, the PICC tip in deep within the RA

Umbilical Arterial Catheters

There are two commonly used practices for umbilical arterial catheter (UAC) placement. Both are meant to minimize the potential for development of thromboembolic propagation into the main branches of the aorta. These are the *high line* position and *low line* position. Occasionally there may be the need or preference for placement of peripheral arterial lines.

Since the aorta lies adjacent to the spine, UAC tip position can be reliably referenced to the vertebral level. The branching of the aorta in newborns is slightly different from that of older children and adults. The ductus arteriosus is frequently initially open in both full-term and premature newborns. It joins with the aorta at the level of the fourth thoracic vertebra (T4). The expected level of abdominal aortic branching in newborns is two vertebral bodies higher than in adults. In newborns, the best assumptions are that the celiac axis arises at T10–11, the superior mesenteric artery at T11, the renal arteries at T12–L1, the inferior mesenteric artery at L1, and the iliac bifurcation at L3.

The goal of UAC placement following a *high line* positioning is to have the tip between the ductus arteriosus and the celiac axis, i.e., between T4 and T10. Most neonatologists, therefore, attempt to have the tip between T6 and T9.

For *low line* placement, the tip should be at or below L3. However, the iliac bifurcation lies roughly at L3. Lines with their tips in the iliac artery risk being displaced. As a result, most institutions follow a *high line* policy.

Umbilical Venous Catheters

Unlike for UAC, umbilical venous catheter (UVC) tip position is not reliably referenced to the vertebral level. The explanation is as explained for ETT and CVL. Since the venous anatomy is not adjacent to the spine, variability in patient positioning and X-ray beam angle will significantly alter the projected UVC tip position in relation to the spine. Therefore, reference should be to the venous anatomy. This may be stated as below the liver, within the liver, or above the liver. Rarely the UVC will descend in the inferior vena cava. Most consider the preferred UVC tip position to be at the inferior vena cava and right atrial junction (IVC/RA junction). When the catheter extends more superiorly, a statement should be made as to where the tip resides, i.e., in the right atrium, the right ventricle, the pulmonary artery, across the foramen ovale into the left atrium or pulmonary veins, up the SVC, into the neck, etc. Ultrasound has been demonstrated as a reliable alternative to confirming UVC position that can decrease insertion time and line manipulations, as well as decrease radiographic exposure [51].

References

1. Cleveland RH. A radiologic update on medical diseases of the newborn chest. Pediatr Radiol. 1995;25:631–7.
2. Cleveland R, Donoghue V. Imaging of the newborn chest. Diseases of the heart, chest & breast. Milan: Springer. p. 55–62.
3. Heron M. Deaths: leading causes for 2014, Natl Vital Stat Rep. 2016;65:1–96.
4. Avery ME, Mead J. Surface properties in relation to atelectasis and hyaline membrane disease. AMA J Dis Child. 1959;97:517–23.
5. Welty S, Hansen TN, Corbet A. Respiratory distress in the preterm infant. In: Avery's diseases of the newborn: Elsevier; 2005. p. 687–703.
6. Zecca E. Bile acid pneumonia: a "new" form of neonatal respiratory distress syndrome? Pediatrics. 2004;114:269–72.
7. Clyman RI. Patent ductus arteriosus in the premature infant. In: Avery's diseases of the newborn: Elsevier; 2005. p. 816–26.
8. Watterberg KL, Gerdes JS, Cole CH, et al. Prophylaxis of early adrenal insufficiency to prevent bronchopulmonary dysplasia: a multicenter trial. Pediatrics. 2004;114:1649–57.
9. Weisz DE, More K, McNamara PJ, et al. PDA ligation and health outcomes: a meta-analysis. Pediatrics. 2014;133:e1024–46.
10. Couser RJ, Ferrara TB, Ebert J, et al. Effects of exogenous surfactant therapy on dynamic compliance during mechanical breathing in preterm infants with hyaline membrane disease. J Pediatr. 1990;116:119–24.
11. Liechty EA, Donovan E, Purohit D, et al. Reduction of neonatal mortality after multiple doses of bovine surfactant in low birth weight neonates with respiratory distress syndrome. Pediatrics. 1991;88:19–28.
12. Polin RA, Carlo WA. Surfactant replacement therapy for preterm and term neonates with respiratory distress. Pediatrics. 2013;133:156–63.
13. Hansen A, Levin J. Neonatal pulmonary disorders. In: Walsh BK, editor. Neonatal and pediatric respiratory care. 5th ed. St Louis: Elsevier; 2019.
14. Cleveland RH, Weber B. Retained fetal lung liquid in congenital lobar emphysema: a possible predictor of polyalveolar lobe. Pediatr Radiol. 1993;23:291–5.
15. Moskowitz PS, Griscom NT. The medial pneumothorax. Radiology. 1976;120:143–7.
16. Jackson JC, Truog WE, Standaert TA, et al. Effect of high-frequency ventilation on the development of alveolar edema in premature monkeys at risk for hyaline membrane disease. Am Rev Respir Dis. 1991;143:865–71.
17. Donnelly LF, Lucaya J, Ozelame V, et al. CT findings and temporal course of persistent pulmonary interstitial emphysema in neonates:a multiinstitutional study. Am J Roentgenol. 2003;180:1129–33.
18. Cools F, Henderson-Smart DJ, Offringa M, et al. Elective high frequency oscillatory ventilation versus conventional ventilation for acute pulmonary dysfunction in preterm infants. Cochrane Database Syst Rev (John Wiley & Sons, Ltd). 2009;3:CD000104.
19. Jobe AH, Bancalari E. Bronchopulmonary dysplasia. Am J Respir Crit Care Med. 2001;163:1723–9.
20. McEvoy CT, Jain L, Schmidt B, et al. Bronchopulmonary dysplasia: NHLBI workshop on the primary prevention of chronic lung diseases. Ann Am Thorac Soc. 2014;11(Suppl 3):S146–53.
21. Northway WH, Rosan RC, Porter DY. Pulmonary disease following respirator therapy of hyaline-membrane disease. N Engl J Med. 1967;276:357–68.
22. Hodgman JE. Relationship between Wilson-Mikity syndrome and the new bronchopulmonary dysplasia. Pediatrics. 2003;112:1414–5.
23. Jobe AJ. The new BPD: an arrest of lung development. Pediatr Res. 1999;46:641.
24. Tonson la Tour A, Spadola L, Sayegh Y, et al. Chest CT in bronchopulmonary dysplasia: clinical and radiological correlations. Pediatr Pulmonol. 2013;48:693–8.
25. Walkup LL, Tkach JA, Higano NS, et al. Quantitative magnetic resonance imaging of bronchopulmonary dysplasia in the neonatal intensive care unit environment. Am J Respir Crit Care Med. 2015;192:1215–22.
26. Respiratory support in preterm infants at birth. Pediatrics. 2014;133:171–4.
27. Doyle LW, Carse E, Adams AM, et al. Ventilation in extremely preterm infants and respiratory function at 8 years. N Engl J Med. 2017;377:329–37.
28. Howling SJ, Northway WH, Hansell DM, et al. Pulmonary sequelae of bronchopulmonary dysplasia survivors. Am J Roentgenol. 2000;174:1323–6.
29. Neonatal Inhaled Nitric Oxide Study Group. Inhaled nitric oxide in full-term and nearly full-term infants with hypoxic respiratory failure. N Engl J Med. 1997;336:597–604.
30. Roberts JD Jr, Fineman JR, Morin FC 3rd, et al. Inhaled nitric oxide and persistent pulmonary hypertension of the newborn. The Inhaled Nitric Oxide Study Group. N Engl J Med. 1997;336:605–10.
31. Christou H, Van Marter LJ, Wessel DL, et al. Inhaled nitric oxide reduces the need for extracorporeal membrane oxygenation in infants with persistent pulmonary hypertension of the newborn. Crit Care Med. 2000;28:3722–7.
32. Wiswell TE, Knight GR, Finer NN, et al. A multicenter, randomized, controlled trial comparing Surfaxin (Lucinactant) lavage with standard care for treatment of meconium aspiration syndrome. Pediatrics. 2002;109:1081–7.
33. Lazar DA, Cass DL, Olutoye OO, et al. The use of ECMO for persistent pulmonary hypertension of the newborn: a decade of experience. J Surg Res. 2012;177:263–7.
34. Brudno DS, Boedy RF, Kanto WP. Compliance, alveolar–arterial oxygen difference, and oxygenation index changes in patients managed with extracorporeal membrane oxygenation. Pediatr Pulmonol. 1990;9:19–23.
35. Gregory GA, Gooding CA, Phibbs RH, et al. Meconium aspiration in infants—a prospective study. J Pediatr. 1974;85:848–52.
36. Lung function in children after neonatal meconium aspiration. Lancet. 1988;332:317–8.
37. Cleveland R. Total anomalous pulmonary venous connection: case 10. ACR pediatric disease (4th series) test and syllabus American College of Radiology. Reston. 1993:272–302.
38. Stoll BJ, Hansen NI, Sanchez PJ, et al. Early onset neonatal sepsis: the burden of group B streptococcal and E. coli disease continues. Pediatrics. 2011;127:817–26.
39. Leonidas JC, Hall RT, Beatty EC, et al. Radiographic findings in early onset neonatal group b streptococcal septicemia. Pediatrics. 1977;59(Suppl):1006–11.
40. Ursi D, Ursi JP, Ieven M, et al. Congenital pneumonia due to Mycoplasma pneumoniae. Arch Dis Child Fetal Neonatal Ed. 1995;72:F118–20.
41. Theilen U. Infection with Ureaplasma urealyticum: is there a specific clinical and radiological course in the preterm infant? Arch Dis Child Fetal Neonatal Ed. 2004;89:163F–167.
42. Lowe J, Watkins WJ, Edwards MO, et al. Association between pulmonary ureaplasma colonization and bronchopulmonary dysplasia in preterm infants: updated systematic review and meta-analysis. Pediatr Infect Dis J. 2014;33:697–702.
43. Hagmann C, Berger TM. Congenital pulmonary Lymphangiectasia. N Engl J Med. 2003;349:e21.
44. Chung CJ, Fordham LA, Barker P, et al. Children with congenital pulmonary lymphangiectasia: after infancy. Am J Roentgenol. 1999;173:1583–8.

45. Freed M. Congenital cardiac malformations. Schaffer's disease of the newborn. Philadelphia: WB Saunders Company; 1984.
46. Schachter J. Chlamydial infections. N Engl J Med. 1978;298:428–35.
47. Schachter J. Chlamydial infections. N Engl J Med. 1978;298:490–5.
48. Schachter J. Chlamydial infections. N Engl J Med. 1978;298:540–9.
49. Todres ID, deBros F, Kramer SS, et al. Endotracheal tube displacement in the newborn infant. J Pediatr. 1976;89:126–7.
50. Baskin KM, Jimenez RM, Cahill AM, et al. Cavoatrial junction and central venous anatomy: implications for central venous access tip position. J Vasc Interv Radiol. 2008;19:359–65.
51. Fleming SE, Kim JH. Ultrasound-guided umbilical catheter insertion in neonates. J Perinatol: official journal of the California Perinatal Association. 2011;31:344–9.

Pediatric Congenital and Miscellaneous Lung Abnormalities

6

Edward Y. Lee, Jason E. Lang, Kara E. May, and Umakanth Katwa

The Spectrum of Congenital Lung Malformations

Although clinical presentation of pediatric patients with various congenital lung malformations is typically related to compression or mass effect upon the tracheobronchial tree, imaging appearance of congenital lung masses varies widely similar to other congenital anomalies involving other body parts. For the purpose of evaluation and diagnosis, congenital pulmonary masses can be classified into two major categories: (1) congenital lung malformations with normal vasculature and (2) congenital lung malformations with anomalous vasculature [1]. Additionally, congenital lung masses can also present as a combination of more than one entity such as in cases of congenital pulmonary airway malformation (CPAM) and pulmonary sequestration, which is known as a mixed or hybrid lesion [1, 2].

E. Y. Lee (✉)
Department of Radiology, Boston Children's Hospital and Harvard Medical School, Boston, MA, USA
e-mail: Edward.Lee@childrens.harvard.edu

J. E. Lang
Division of Allergy, Immunology and Pulmonary Medicine, Duke University School of Medicine, Durham, NC, USA

Duke Children's Pulmonary Function Laboratory, Duke Clinical Research Institute, Duke Children's Health & Discovery Institute, Durham, NC, USA

K. E. May
Department of Medicine, Division of Respiratory Diseases, Boston Children's Hospital and Harvard Medical School, Boston, MA, USA

U. Katwa
Boston Children's Hospital and Harvard Medical School, Boston, MA, USA

Congenital Lung Malformations with Normal Vasculature

Congenital Bronchial Atresia

Congenital bronchial atresia is a relatively rare congenital anomaly which typically presents as a focal, round, or oval-shaped pulmonary lesion. It is also known as congenital bronchocele or mucocele. It results from developmental disconnection of a segmental or subsegmental bronchus from the central airway [3, 4]. Such disconnection of the bronchus results in subsequent mucus accumulation in the segments of bronchus distal to the atretic regions. Air trapping adjacent to the bronchial atresia results from the unilateral collateral air-drift through pores of Kohn and canals of Lambert from the adjacent normal lung [1, 5]. These collateral channels act as a check-valve mechanism only allowing air to enter and not leave from the distal lung. Bronchial atresia is typically an incidental finding in asymptomatic children on chest radiographs obtained for other indications. However, up to 42% of patients may present with symptoms such as cough, wheezing, hemoptysis, shortness of breath, or recurrent pulmonary infection [6].

On chest radiographs, bronchial atresia typically presents as a round, ovoid, or tubular opacity with or without an associated fluid level [1]. Bronchial atresia is most commonly located in the apico-posterior segment of the left upper lobe followed by the right upper lobe, right middle lobe, and right lower lobe. Due to its typical radiographic findings, bronchial atresia can be sometimes confused with a pulmonary nodule or other focal lung abnormalities in children. Although CT is not usually obtained for further evaluation when typical imaging findings of bronchial atresia are seen on chest radiographs, CT can be helpful for confirming and further characterizing bronchial atresia. On CT, bronchial atresia is a central mass-like opacity near the hilum that usually has a round, ovoid, or tubular shape [1] (Fig. 6.1). It typically exhibits an attenuation value of 10–25 HU due to internal mucoid contents [6]. After administration of

R. H. Cleveland, E. Y. Lee (eds.), *Imaging in Pediatric Pulmonology*, https://doi.org/10.1007/978-3-030-23979-4_6

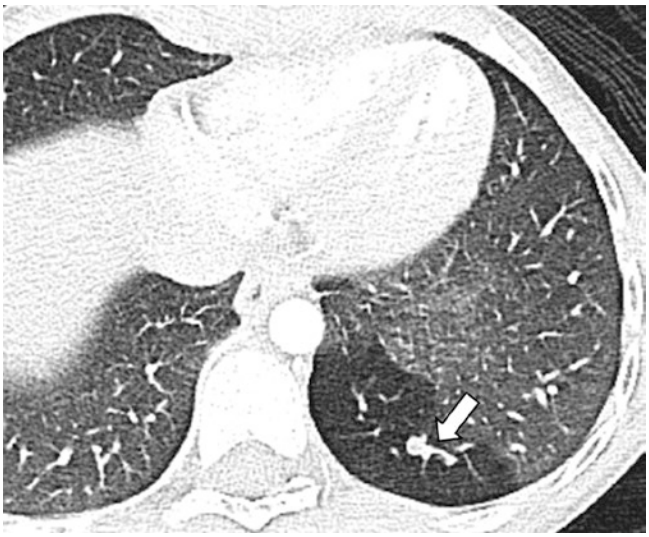

Fig. 6.1 An 8-year-old girl with an incidental detection of bronchial atresia. Axial lung window CT image shows an oval-shaped opacity (arrow) located in the left lower lobe with adjacent surrounding air trapping

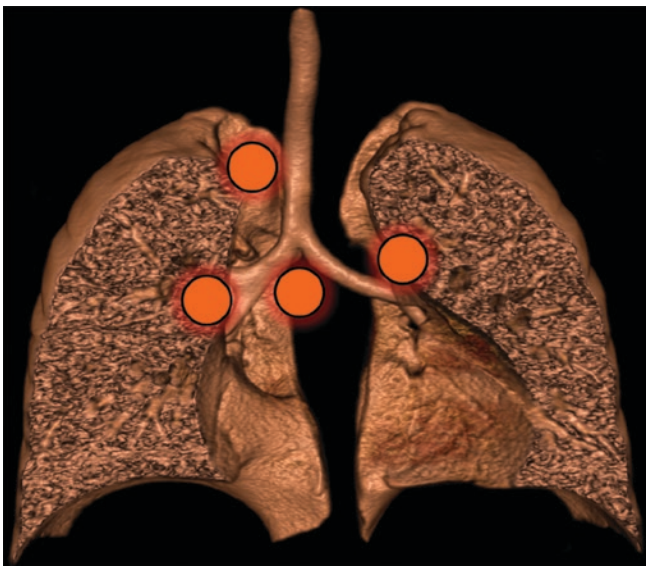

Fig. 6.2 Diagram shows common locations of bronchogenic cysts marked with circles in the right paratracheal, subcarinal, and hilar regions

intravenous contrast, there is usually no internal contrast enhancement. Multidetector CT (MDCT) with 2D reconstructions can provide a comprehensive evaluation of spatial relationship of the bronchial atresia and adjacent surrounding air trapping. Although magnetic resonance imaging (MRI) is not currently used for evaluation of bronchial atresia, it has been reported that bronchial atresia shows high T2 signal intensity due to underlying mucoid contents [7]. Unlike CT, MRI cannot reliably demonstrate surrounding air trapping often seen adjacent to the bronchial atresia.

Although no treatment is necessary for an incidentally detected bronchial atresia in asymptomatic children, surgical resection may be necessary in symptomatic children particularly with recurrent pulmonary infections.

Bronchogenic Cysts

Bronchogenic cysts are developmental anomalies of airways. They result from abnormal ventral budding or branching of the embryonic foregut and tracheobronchial tree which occurs between 26th and 40th days of gestation [8–10]. Other foregut duplication cysts include enteric cysts and neurenteric cysts. They account for an approximately 40–50% of all congenital mediastinal cystic masses [5]. Histologically, bronchogenic cysts are characterized by mucoid material collection lined by respiratory ciliated columnar or cuboidal epithelium. Children with small bronchogenic cysts are usually asymptomatic [5]. However, large bronchogenic cysts can result in mass effect upon adjacent airways and the esophagus. Affected children in such situations can present with a variety of clinical symptoms such as respiratory distress, dysphagia, and chest pain.

On chest radiographs, bronchogenic cysts usually present as round opacity located within the mediastinum (~67%) or lung parenchyma (~33%) [1, 5]. If they are located in the mediastinum, the most common location of the bronchogenic cysts is the subcarinal region, followed by the right paratracheal region and hilar region [1, 5] (Fig. 6.2). Intraparenchymal bronchogenic cysts are typically located in the medial third of the lung [5]. On CT, bronchogenic cysts are characteristically well-circumscribed round or ovoid cystic solitary mass with uniform attenuation (Fig. 6.3a). The attenuation value of the bronchogenic cysts is variable due to variable amount of internal proteinaceous materials and calcium. Approximately 50% of bronchogenic cysts show 0–20 HU on CT images [10–12]. High contents of internal proteinaceous materials and calcium within bronchogenic cysts can result in increased HU of the cysts, which may mimic possible solid masses. In this situation, MRI can be a helpful imaging study for confirmation and further characterization. Although signal intensity of bronchogenic cysts on T1-weighted images may be variable due to variable amount of internal proteinaceous materials [13], the bronchogenic cysts are typically high in signal intensity on T2-weighted images (Fig. 6.3b) [11, 14]. With intravenous contrast, no internal contrast enhancement is typically seen, although wall enhancement may be seen when they are infected.

For symptomatic pediatric patients, the current treatment of choice of bronchogenic cysts is surgical resection.

Congenital Lobar Emphysema

Congenital lobar emphysema is also known as infantile lobar emphysema or congenital lobar hyperinflation [1]. Although

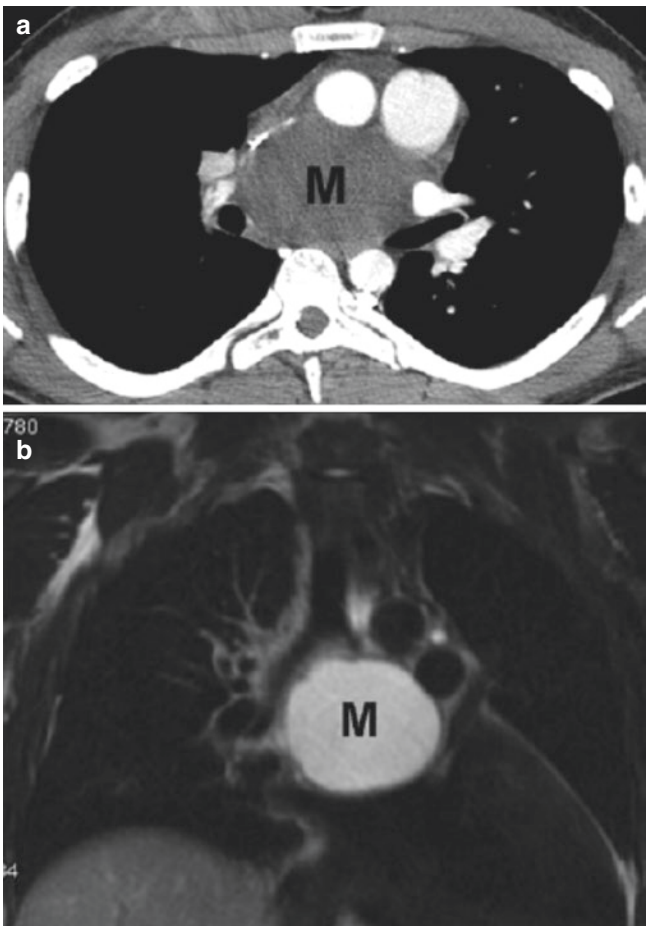

Fig. 6.3 An 18-year-old male with chest pain and respiratory distress. Surgical pathology of the mediastinal cystic mass was consistent with bronchogenic cyst. (**a**) Enhanced axial CT image shows a large round cystic mass (M) located in the subcarinal region. (**b**) Coronal T2-weighted MR image demonstrates a large round cystic mass (M) with high MR signal intensity

the etiology of congenital lobar emphysema is currently unknown, it has been presumed that underlying airway malacia or stenosis may be the cause of congenital lobar emphysema [5, 9, 12, 15–18]. Such airway malacia or stenosis can cause progressive hyperinflation of the lung by allowing more air to enter the involved lung on inspiration than leaves on expiration as a check-valve mechanism. This results in hyperinflation of an affected lobe without destruction of alveolar walls or septa [1]. Most pediatric patients with congenital lobar emphysema present during the neonatal period with respiratory distress due to mass effect upon adjacent airway and lung from the hyperinflated lobe. Congenital lobar emphysema is associated with other congenital anomalies such as cardiovascular anomalies in up to 12–14% of patients [19, 20].

On newborns' chest radiographs, congenital lobar emphysema may present as an opacity due to retention of fetal lung fluid just after birth. However, the affected lobe typically shows hyperlucency as fetal lung fluid is cleared by subsequent lymphatic resorption and replaced by air (Fig. 6.4a). The most common location of congenital lobar emphysema is the left upper lobe followed by the right middle lobe and lower lobes [5]. Occasionally, more than one lobe can be affected. Due to hyperinflation of the affected lobe, adjacent lobes may be compressed or atelectatic. Large and markedly hyperinflated congenital lobar emphysema can result in separation of ipsilateral ribs and hemidiaphragm depression. Due to hyperlucency on chest radiographs, congenital lobar emphysema may be confused with pneumothorax or cystic lung abnormalities. In this situation, CT can be a helpful imaging modality which can show a hyperinflated lobe with attenuating and displaced pulmonary vessels (Fig. 6.4b, c) [1].

Surgical resection is the current management of choice for symptomatic infants and children with congenital lobar emphysema.

Congenital Pulmonary Airway Malformation

CPAM is a congenital lung mass, which results from disorganized adenomatoid and hamartomatous proliferation of bronchioles that are in communication with the adjacent normal bronchial tree [1, 5, 9, 12, 20–25]. The etiology of CPAM is currently unknown. In the past, CPAM has been referred to as congenital cystic adenomatoid malformation (CCAM) of the lung and classified into three different types by Stocker et al. based on its radiological, gross pathological, and histological findings. However, it has been recently reclassified into five types (types 0–4) based on the location or stage of development of the abnormality involving the tracheobronchial airway [26, 27].

Type 0 CPAM is the rarest type which involves an abnormality of the trachea and main stem bronchi. While type 1 CPAM, which is the most common type (60–70%), involves an abnormality of the bronchial and/or proximal bronchiolar region, type 2 CPAM (15–20%) involves an abnormality of the bronchiolar region. Type 3 CPAM (5–10%) involves an abnormality of the terminal bronchiolar/alveolar duct region. Type 4 CPAM involves an abnormality of the distal acinus or alveolar saccular/alveolus region. Affected children with small CPAM are typically asymptomatic. However, pediatric patients with large CPAM usually present with respiratory distress or superimposed infection if left untreated.

On chest radiographs, CPAMs typically present as solitary or multiple air-filled thin-walled cysts that vary in size [1, 25]. Additionally, they may also present as a focal mass-like opacity. CT is a helpful imaging modality for identifying CPAMs, characterizing CPAMs, evaluating mass effect on adjacent structures, and distinguishing CPAMs from other congenital lung anomalies. On CT, CPAMs are usually solitary or multiple air-filled cystic masses (Fig. 6.5) [1, 25]. However, it may also present as a solid soft tissue mass without associated anomalous vasculature.

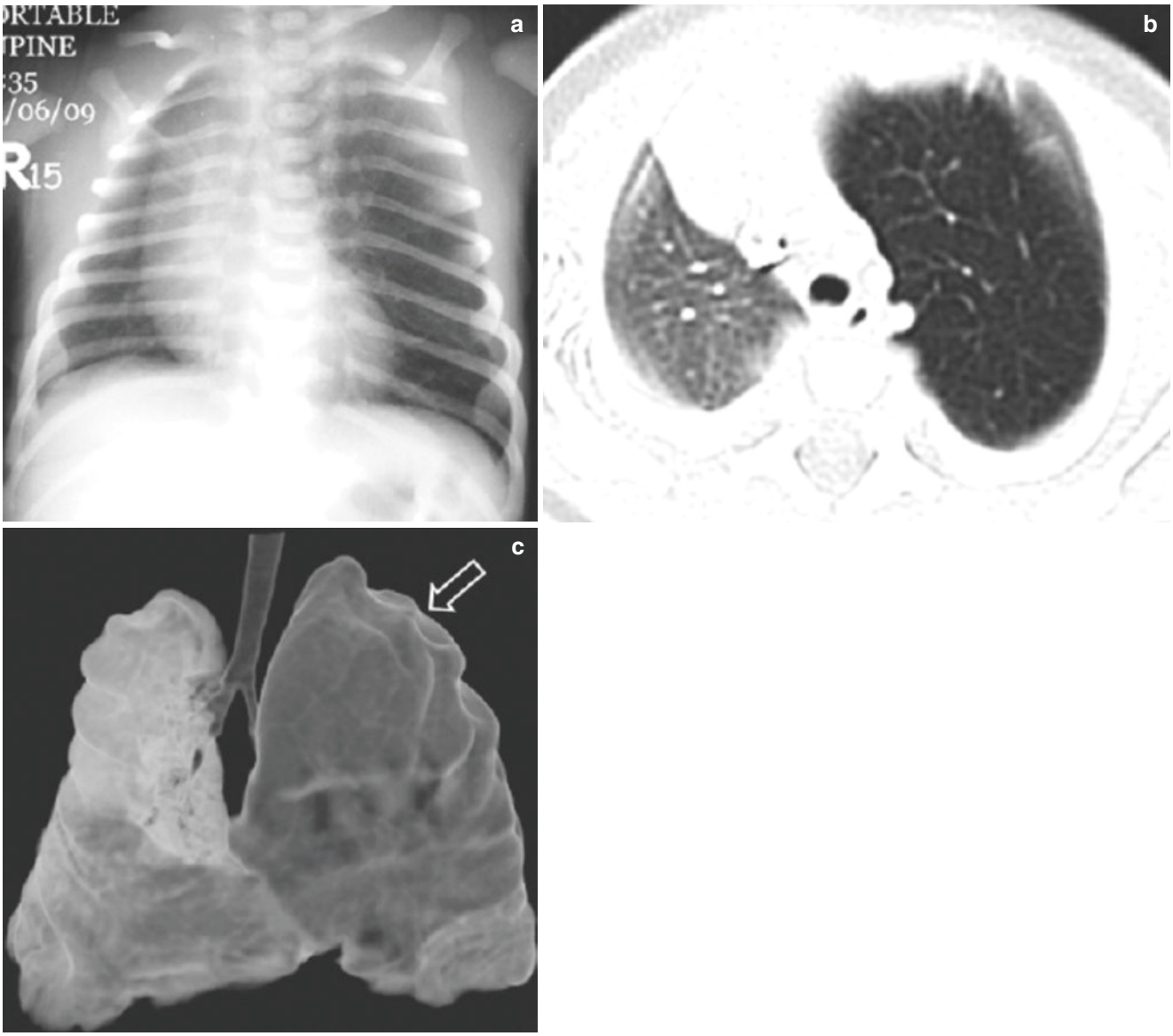

Fig. 6.4 A 3-day-old boy presented with respiratory distress. Surgical pathology was consistent with congenital lobar emphysema. (**a**) Frontal chest radiograph shows increased lucency and hyperinflation of the left upper lobe. Also noted is mass effect upon mediastinum. (**b**) Axial lung window CT image demonstrates markedly hyperinflated left upper lobe with attenuating and displaced pulmonary vessels. (**c**) 3D volume-rendered image of the lung shows hyperinflated left upper lobe (*arrow*)

Surgical resection is the current management of choice particularly due to an increased risk of superimposed infection, if left untreated, or rare but potential development of pulmonary neoplasms such as bronchoalveolar carcinoma or pleuropulmonary blastoma [1].

Congenital Lung Masses with Abnormal Vasculature

Pulmonary Sequestration

Pulmonary sequestration is an aberrant lung mass, which is characterized by dysplastic and nonfunctioning pulmonary tissue without a normal connection with the tracheobronchial tree [1, 25]. Traditionally, pulmonary sequestration is divided into two types: extralobar sequestration (25%) and intralobar sequestration (75%) [1, 25, 28–34] (Table 6.1). Histologically, extralobar sequestration has its own lung pleura, while intralobar sequestration is located within the lung parenchyma without its own lung pleura. Both extralobar and intralobar sequestrations have anomalous arterial supply generally arising from the descending aorta. However, intralobar sequestration may have an arterial supply from secondary or tertiary branches, possibly relating to prior infection. Anomalous venous drainage associated with extralobar and intralobar sequestrations differs. While anomalous venous drainage of the intralobar sequestration is into a pulmonary vein, extralobar sequestration

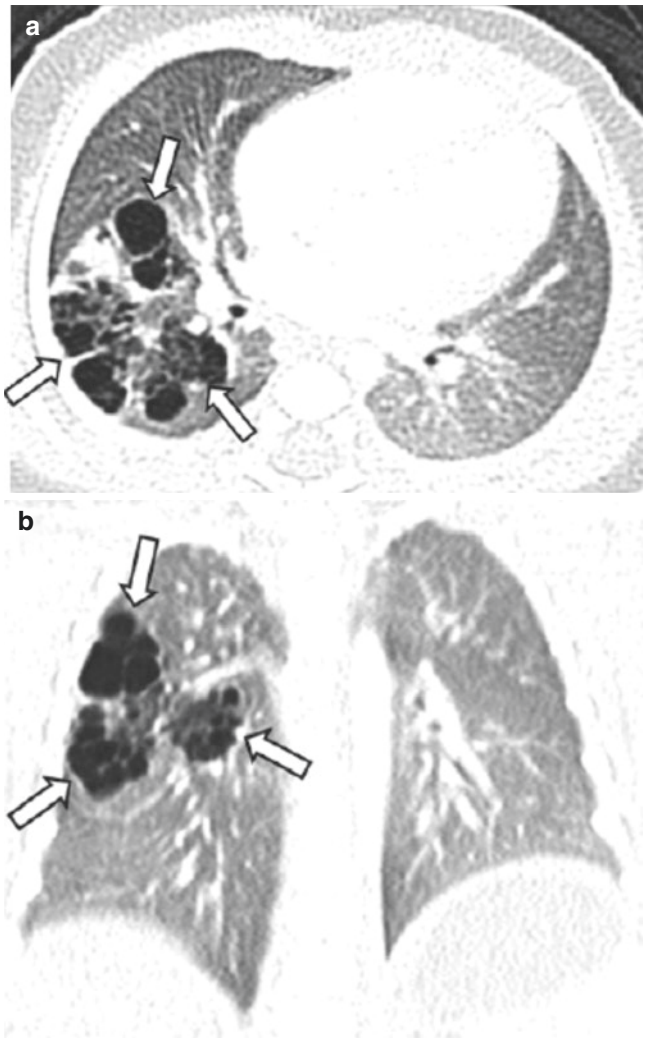

Fig. 6.5 One-month-old girl with prenatal diagnosis of right lung mass is shown. Surgical pathology confirmed congenital pulmonary airway malformation (CPAM). (**a**) Axial lung window CT image shows type 2 CPAM (*arrows*) manifested as multiple small cystic lesions within the right upper lobe. (**b**) Coronal lung window CT image again demonstrates type 2 CPAM (*arrows*)

Table 6.1 Characteristics of extralobar and intralobar sequestrations

	Extralobar sequestration	Intralobar sequestration
Cause	Congenital	Acquired (postinfectious) vs. congenital
Patient age	Infants or young children	Older children
Presentation	Focal lung mass	Recurrent infection
Morphology	With its own lung pleura	Without its own lung pleura
Common location	Lower lobes (L > R)	Lower lobes (L > R)
Arterial supply	Abdominal aorta	Thoracic/abdominal aorta/ branch arteries
Venous drainage	Systemic veins	Pulmonary veins

has an anomalous venous drainage into systemic veins such as the azygos vein, portal vein, or subclavian vein [1, 25]. Occasionally, extralobar sequestration can coexist with CPAM and appear as a hybrid lesion [1, 2]. Clinical presentation of pediatric patients with intralobar and extralobar sequestrations also often differs. While extralobar sequestration typically presents in neonates or young children with a focal lung mass, intralobar sequestration typically presents in older children with recurrent pulmonary infection in the lower lobes [1, 25].

On chest radiographs, a focal lung opacity in the lower lobes, left side more often than right side, is typically seen [1, 25]. When there is superimposed infection, associated lung parenchymal inflammation and/or even abscess formation may be present. CT is a helpful imaging modality in diagnosing pulmonary sequestration by demonstrating the abnormally sequestrated portion of the lung and associated anomalous vessels (Fig. 6.6). It has been reported that MDCT with 3D imaging can help radiologists to make a correct detection of anomalous arterial supply and anomalous venous drainage associated with pulmonary sequestration in 100 and 100% of cases, respectively [35, 36]. Such information regarding anomalous venous drainage associated with pulmonary sequestration can help in differentiating the two types of pulmonary sequestration for preoperative evaluation [1, 37]. While most intralobar sequestrations require lobectomy, extralobar sequestration can be surgically removed via segmentectomy without excising adjacent normal lung tissue [1, 35].

Surgical resection is the current management of choice for infants and children with pulmonary sequestrations.

Pulmonary Arteriovenous Malformation

Pulmonary arteriovenous malformation (AVM) is due to a congenital anomalous direct connection between pulmonary veins and arteries caused by an underlying defect in the formation of normal pulmonary capillaries [1]. In children, pulmonary AVM is usually congenital in etiology. However, pulmonary AVM can also be acquired typically in children with prior congenital cyanotic heart surgeries (i.e., Glenn and Fontan procedures) or chronic liver disease [28, 38–43]. If there are multiple pulmonary AVMs, hereditary hemorrhagic telangiectasis, also known as Rendu–Osler–Weber syndrome, should be considered. Hereditary hemorrhagic telangiectasis is an autosomal dominant syndrome, which is characterized by a clinical triad of epistaxis, telangiectasis, and a family history of pulmonary AVMs [28, 44, 45]. Although pediatric patients may be asymptomatic if the size of pulmonary AVM is less than 2 cm, however, a large pulmonary AVM (>2 cm) or multiple pulmonary AVMs in children likely result in anatomic right-to-left shunts [1]. Affected children can present with symptoms such as hemoptysis, dyspnea, chest pain, palpitations, and cyanosis [1]. Rarely, serious complications such as stroke or brain abscess

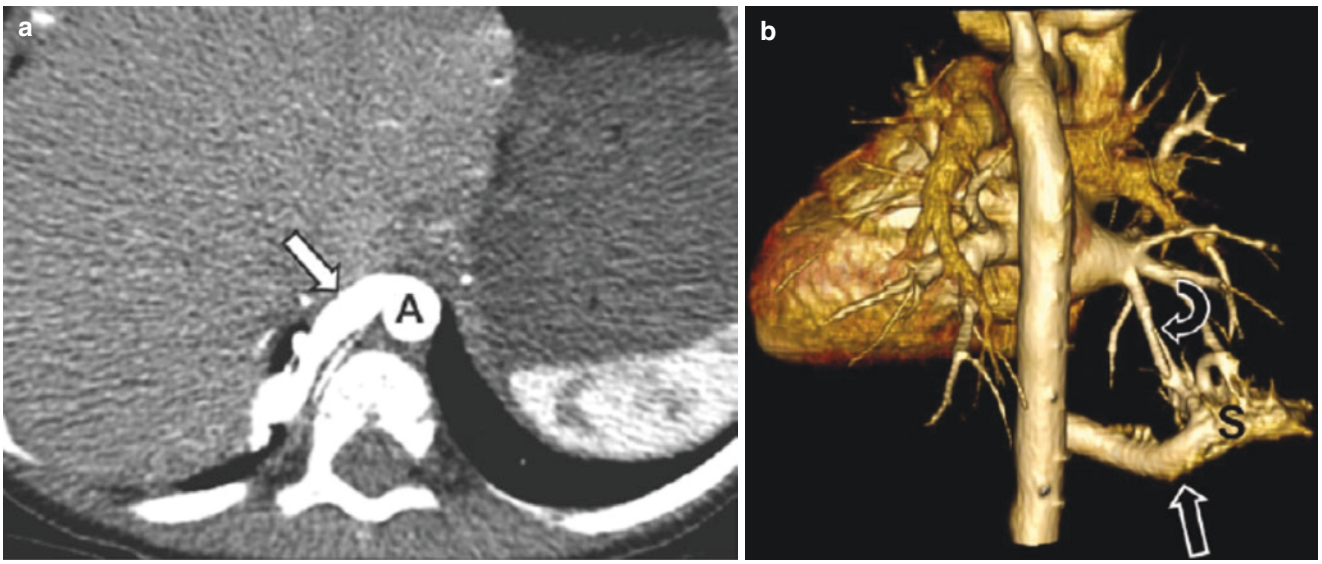

Fig. 6.6 A 5-week-old girl with prenatal diagnosis of focal lung mass located in the right lower hemithorax. Surgical pathology was consistent with pulmonary sequestration. (**a**) Enhanced axial CT image shows an anomalous artery (*arrow*) arising from the descending aorta (letter A). (**b**) 3D volume-rendered image demonstrates a pulmonary sequestration (letter S) with associated anomalous artery (*arrow*) and anomalous vein (*curved arrow*)

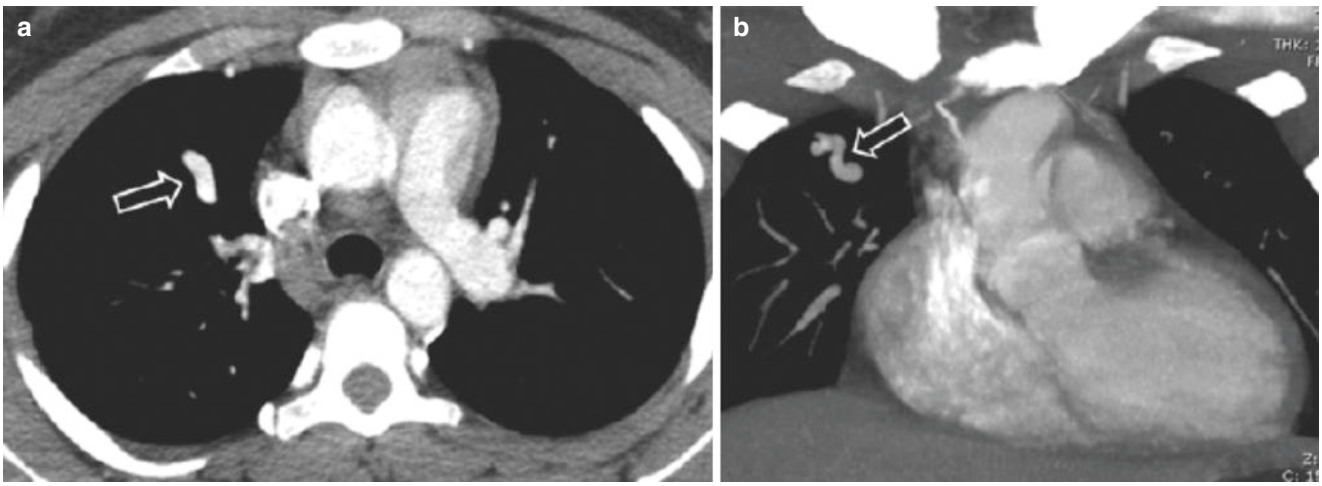

Fig. 6.7 A 17-year-old girl with an abnormal chest radiograph showing possible nodular opacity in the right upper lobe. (**a**) Enhanced axial CT image shows a vascular tubular structure mass (*arrow*) located in the right upper lobe. (**b**) Enhanced coronal CT image demonstrates a tubular structure (*arrow*) with contrast enhancement, consistent with pulmonary arteriovenous malformation

due to paradoxical embolization or pulmonary hemorrhage may also occur [28, 45–47].

On chest radiographs, round or oval-shaped opacities often with associated curvilinear opacities representing a feeding artery and a draining vein may be seen. They are often located in the lower lobe in 50–70% of cases [27, 45]. In the past, conventional catheter-based pulmonary angiography has been used for the evaluation of pulmonary AVM. However, in recent years, MDCT has become an imaging modality of choice for assessing pulmonary AVM in children (Fig. 6.7). MDCT with 3D imaging is particularly useful in detecting and characterizing the angioarchitecture of the feeding arteries and draining veins [1]. Small pulmonary AVMs can be particularly best detected with maximum intensity projection (MIP) reconstruction of CT images (Fig. 6.8).

For pulmonary AVMs larger than 2 cm, the current treatment of choice is endovascular coil embolization or balloon occlusion [45–47].

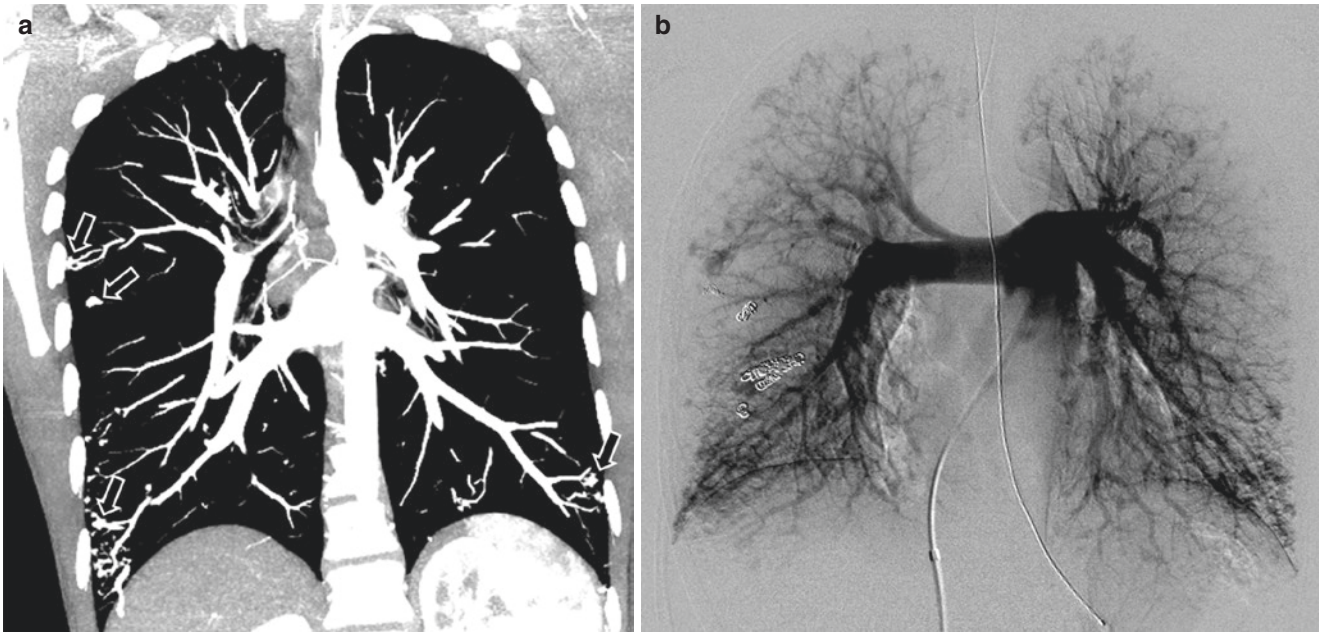

Fig. 6.8 (**a**, **b**) A 15-year-old girl with Rendu–Osler–Weber syndrome with multiple small pulmonary arteriovenous malformations. (**a**) Coronal maximum intensity projection reconstruction of CT image shows multiple small pulmonary arteriovenous malformations (AVMs). (**b**) Coronal projection image of conventional pulmonary artery angiogram demonstrates bilateral multiple small pulmonary arteriovenous malformations (arrows). Previously placed several embolization coils are also seen in the right hemithorax

Pulmonary Varix

Pulmonary varix is a localized enlarged segmental pulmonary vein, which anatomically enters the left atrium normally [1]. It may present as a pulmonary mass-like opacity on chest radiographs. It can be congenital or acquired. Chronic pulmonary hypertension and mitral valvular disease are often associated with acquired pulmonary varix [3, 28]. Pulmonary varix is usually discovered incidentally in asymptomatic patients. However, it may also result in serious complications such as systematic embolus from a clot in the varix and rupture leading to death [28, 48].

On chest radiographs, pulmonary varix typically presents as a well-defined round mass-like opacity near the heart border [1]. Pulmonary varix is usually not clinically significant, and it is important not to confuse it with a true pulmonary mass. CT is currently the best imaging modality for diagnosing pulmonary varix and in differentiating it from other possible diagnostic considerations such as pulmonary AVM or nodule [1]. Confirmation of pulmonary varix can be made when contiguity of pulmonary varix with the adjacent pulmonary vein is visualized on contrast-enhanced CT (Fig. 6.9). It is typically located near its point of entry into the left atrium.

While asymptomatic children should be closely followed with periodic chest radiographs, symptomatic patients require urgent surgical resection of the pulmonary varix.

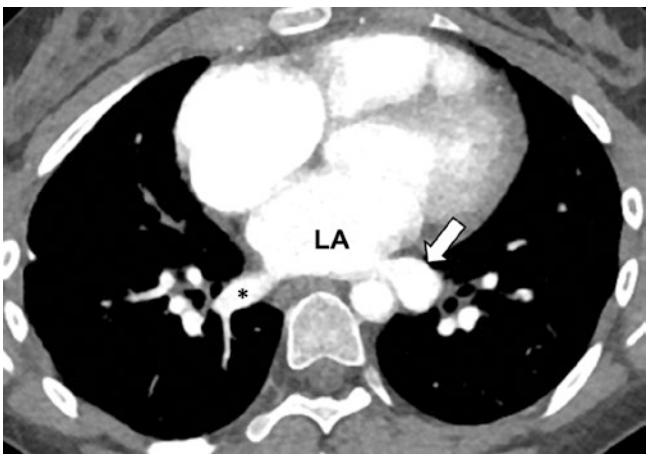

Fig. 6.9 A 16-year-old girl who underwent CT study for evaluation of lung infection and an incidental detection of pulmonary varix. Enhanced axial CT image shows a dilated left inferior pulmonary vein (arrow). Normal-size right inferior pulmonary vein (asterisk) is also seen. LA = Left atrium

Horseshoe Lung Malformation

Horseshoe lung is a rare congenital lung anomaly first described in 1962 by Spencer, who reported a lung malformation characterized by the fusion of two lungs via a posterior midline isthmus associated with unilateral lung hypoplasia (Fig. 6.10) [49]. In this condition, the posteroinferior bases of the right and left lungs are fused by a narrow band of normal

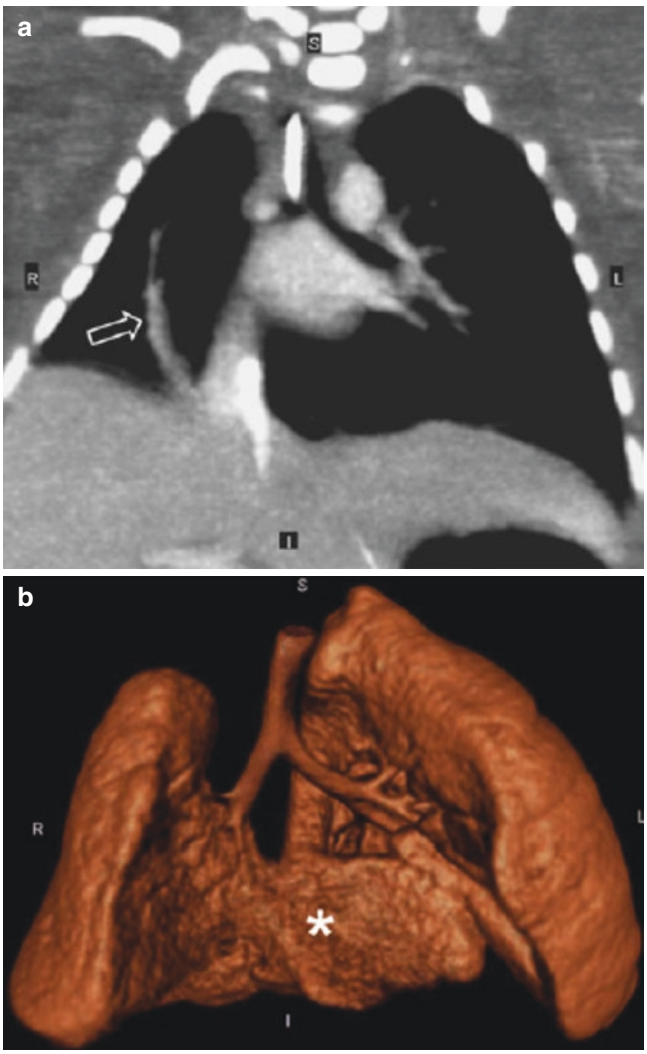

Fig. 6.10 Hypogenetic lung syndrome (scimitar syndrome) with horseshoe lung in a young child. (**a**) Enhanced coronal CT image shows a scimitar vein (*arrow*) and hypoplastic right lung. (**b**) Anterior view of 3D volume-rendered image of the central airway and lungs demonstrates a horseshoe lung. Inferior medial portions (*asterisk*) of both lungs are fused. (Case courtesy of David Stringer, M.D. From Lee et al. [112])

lung tissue referred to as an *isthmus* without an intervening pleural fissure. The isthmic portion of the horseshoe lung originates from the hypoplastic sides of the lung; it is located posterior to the heart, but anterior to the aorta and to the esophagus. The blood supply for the isthmus usually originates from the right pulmonary artery and is aerated by a bronchial extension from the right bronchus [49, 50].

Classification

Some investigators believe that horseshoe lung represents one variation on the spectrum of a single lung malformation complex, specifically an example of *pair organ* maldevelopment associated with various other anomalies of the tracheobronchial tree and pulmonary vasculature including scimitar syndrome and *crossover lung segment* [50]. In particular, horseshoe lung malformation association with scimitar syndrome (80%) is well reported [49, 51–53]. The horseshoe lung and scimitar syndrome share several features including hypoplasia of the right lung, anomalous systemic arterial supply to the right lung, and absence or hypoplasia of the bronchus and artery to the right lung. The horseshoe lung is also morphologically similar to crossover lung segment [50]. In the case of *crossover lung*, part of one lung extends into the contralateral side thorax without connection; this displaced pulmonary segment is referred to as the *crossover segment*. Similar to horseshoe lung, the blood supply for the crossover isthmus usually originates from an ipsilateral pulmonary artery and is aerated by a bronchial extension from an ipsilateral bronchus. In addition to scimitar syndrome and crossover lung segment, bilateral pulmonary sequestrations with a bridging isthmus also may mimic horseshoe lung [50, 54, 55].

Table 6.2 Tracheobronchial anomalies associated with horseshoe lung malformation

1. Disorganized bronchial branching
2. Abnormal bronchial bifurcation
3. Bridging bronchus
4. Bronchial stenosis
5. Tracheal stenosis
6. Tracheal dilatation
7. Tracheoesophageal fistula
8. Persistent foregut (common esophagotrachea)

Table 6.3 Cardiac anomalies associated with horseshoe lung malformation

1. Dextroposition
2. ASD
3. VSD
4. Patent foramen ovale
5. Persistent left superior vena cava
6. Pulmonary valvular stenosis
7. Hypoplastic left heart syndrome

Horseshoe lung malformation is associated with various tracheobronchial anomalies as listed in Table 6.2 [50]. Horseshoe lung is also associated with various cardiac anomalies; the most common among these is dextroposition of the heart (Table 6.3). Other reported anomalies include hypoplastic right thorax, diaphragmatic eventration, diaphragmatic hernia, horseshoe kidney hemivertebrae, and absent radius [50].

Clinical Presentation

The age of presentation in patients with horseshoe lung varies greatly (from neonates to adults) and depends on the

extent of other associated malformations such as congenital heart disease [49, 50, 53]. Patients with horseshoe lung malformation are commonly symptomatic in the neonatal period (50%), and the diagnosis is usually made by year one (75%). There is greater prevalence among females [50]. In symptomatic patients, the most common presenting symptom is respiratory distress manifested by tachypnea, tachycardia, chest retraction, dyspnea, coughing, wheezing, hypoxia, and cyanosis. Less common symptoms include heart murmur, failure to thrive, chest wall asymmetry, and pulmonary hypertension. Following the neonatal period, recurrent respiratory tract infections (i.e., pneumonia, bronchitis, and empyema) are most frequently reported [50]. In asymptomatic children, diagnosis is often made incidentally when routine chest radiographs show abnormalities associated with horseshoe lung such as unilateral lung haziness and dextroposition of the heart [56].

Radiological Findings

No plain radiographic findings are pathognomonic of horseshoe lung malformation. The most common radiographic findings in patients with horseshoe lung include rightward shift of the heart (dextroposition), mediastinal structures (75%), lung hypoplasia (50%), and scimitar shadow (40%) [49, 50]. As unilateral pulmonary hypoplasia is a constant finding, horseshoe lung should be looked for in every case of hypoplasia. Other less common plain radiographic findings include eventration of the right diaphragm, hypoplastic right thorax, fusion of ribs, and varying degrees of lung density suggestive of pulmonary sequestration [49, 50, 56]. In the past, bronchography has been used to detect abnormal bronchial branching patterns with an oblique bronchus coursing from the right main stem bronchus to the isthmus of the horseshoe lung. Conventional pulmonary angiography (in frontal projection) has also been utilized in evaluating the vascular supply to the isthmus of the horseshoe lung since it accurately depicts the variable degree of hypoplasia, the decreased number of hypoplastic cells, and the abnormal distribution of the segmental branches. Scintigraphy lung perfusion imaging can also show perfusion defects throughout the right lung if these areas are supplied by the systemic arteries [50, 52].

However, in recent years, especially with development of MDCT which clearly depicts lung parenchymal and associated vascular anomalies in congenital lung disease, the diagnosis of horseshoe lung malformation is most often made by CT, thus obviating the need for invasive bronchography and angiography (Fig. 6.10) [50, 57]. Although abnormal lung parenchyma and associated vascular anomalies can be evaluated with axial CT images alone, multiplanar reformations and 3D imaging have proven particularly helpful in confirming the diagnosis as well as in further characterizing the anomalous locations and courses of vessels and airways associated with horseshoe lung. 2D and 3D CT imaging have also been established as effective tools in generating useful preoperative evaluations that ultimately improve surgical outcomes and enhance physician–patient/parent communication.

Management

The management of patients with horseshoe lung malformation depends on their clinical symptoms. While asymptomatic patients are managed conservatively, surgery is generally recommended for cases of horseshoe lung malformation (with or without scimitar syndrome) in the presence of functional impairment and chronic infection, left-to-right shunt ($Qp/Qs > 2$), congenital heart disease, recurrent pneumonias, and progressive pulmonary hypertension [49, 50].

Hepatopulmonary Fusion

Primary hepatopulmonary fusion is an extremely rare condition in patients with a right-sided CDH, in which there is a fusion between the right lung and the herniated liver parenchyma through a defect in the diaphragm [58, 59]. There may be varying degrees of pulmonary hypoplasia associated with this condition [60]. Although the etiology for the development of hepatopulmonary fusion is currently not clearly known, it is speculated that incomplete fusion of the diaphragm may contribute to the fusion between the liver and lung.

Fusion of Four Embryonic Components

Development of an intact diaphragm requires a complete fusion between the four embryonic components: septum transversum, pleuroperitoneal membrane, muscular component, and dorsal mesentery [61]. Among these four embryonic components of the diaphragm, the septum transversum may be hypoplastic, which leads to incomplete formation of the diaphragm preventing separation between the liver and lung during embryogenesis [61]. On the other hand, others suspect that hepatopulmonary fusion may be due to the intrauterine inflammatory or ischemic events during organogenesis [62]. Secondary hepatopulmonary fusion which occurs after primary right-sided CDH repair is also a rare condition. In this condition, the liver herniates through the recurrent diaphragmatic defect resulting in a fusion of the herniated liver and lung parenchyma. Postoperative inflammatory changes and scar formation may be a nidus for a fusion of the herniated liver and lung parenchyma.

Clinical Presentation

There are very few reports consisting of a small patient size or case reports of hepatopulmonary fusion in the literature, limiting the clear understanding of how these patients present clinically [59, 61, 63, 64]. However, patients in the reported literature with hepatopulmonary fusion present with similar symptoms as patients with CDH without hepatopulmonary fusion. Typical symptoms include severe respiratory distress, cyanosis, and retraction with scaphoid abdomen immediately following birth [59, 62]. However, patients with small CDH defect and hepatopulmonary fusion may be asymptomatic at birth [64, 65]. They may later present with recurrent respiratory distress.

Radiological Finding

The most reported common radiological finding of hepatopulmonary fusion is the opacification of the right hemithorax without (more common) or with mediastinal shift to the contralateral hemithorax or toward the lesion [60]. Bowel loops, sometimes seen within the right hemithorax in patients with right congenital diaphragm, are not usually seen. Hepatic and pulmonary tissue fused by a fibrous band [62] and bronchobiliary fistula formation [66] are other reported findings associated with hepatopulmonary fusion. Anomalous venous drainage from the right lung to the intrahepatic inferior vena cava (IVC) was also reported in one patient who was evaluated with MRI [60].

Diagnosis

An early and correct diagnosis of hepatopulmonary fusion is difficult due to its rarity; however, high clinical suspicion coupled with the familiarity of this condition is important for correct diagnosis and for proper patient management [67]. It has been reported that reducing the herniated liver into the peritoneal cavity in patients with hepatopulmonary fusion can be particularly challenging during surgical repair, requiring more operation time than the repair of a typical right-sided CDH [58, 59]. Furthermore, intraoperative complication such as kinking of the inferior vena cava and associated intractable hypotension has been reported during hepatopulmonary fusion repair [58].

Once possible hepatopulmonary fusion is suspected in a neonate with a right-sided CDH, a complete preoperative evaluation of the precise anatomy is paramount in order to plan for surgical repair and to minimize possible intraoperative complications. Although plain radiographs are typically an initial postnatal diagnostic imaging study, findings are often nonspecific in patients with hepatopulmonary fusion. MRI has been reported to be useful for evaluation of the fused portion of lung parenchyma and its associated abnormal venous drainage into the intrahepatic inferior vena cava [60]. However, with the advent of multidetector CT (MDCT), MDCT with multiplanar and 3D imaging can be helpful for the preoperative evaluation of hepatopulmonary fusion. Although there is an ionizing radiation exposure associated with MDCT, CT has several advantages over MRI due to its fast scan time and decreased sedation rate. Furthermore, a precise evaluation of lung parenchyma and central airway with axial, multiplanar, and 3D imaging can be achieved with MDCT, unlike MRI, which provides a limited evaluation of the lung parenchyma and central airway. Furthermore, in patients with hepatopulmonary fusion, an evaluation of possible anomalous arterial and venous vessels is crucial for preoperative evaluation. MDCT with multiplanar and 3D imaging has proven to be useful and diagnostic in the evaluation of small anomalous vascular structures in children [68–70].

Management

Treatment of CDH with hepatopulmonary fusion is surgical repair, which may require partial hepatectomy and/or pneumonectomy [58]. Due to the complexity of abnormal anatomy, some patients may need several staged surgical procedures. Unfortunately, the prognosis of patients with hepatopulmonary fusion is poor. Most affected patients usually die during the perioperative period due to various complications including respiratory distress, right heart failure, persistent pulmonary hypertension, and thrombosis of the inferior vena cava [58, 59, 62].

Bronchobiliary Fistula

Bronchobiliary fistula (BBF) is a rare condition characterized by communication between the tracheobronchial and biliary ductal systems. When BBF occurs, it typically is associated with trauma, cancer, or liver infection, although congenital BBF has been described [66, 71, 72].

Congenital Bronchobiliary Fistula

Congenital bronchobiliary fistula (cBBF) was first described in 1952 by Neuhauser. From histologic examination of cases, cBBF appears to result from anomalous liver and bronchial buds connecting and remaining connected after birth [73]. The fistula nearest to the lung often displays respiratory histology such as cartilaginous rings, respiratory epithelium, and airway smooth muscle. Likewise, the fistula closest to the

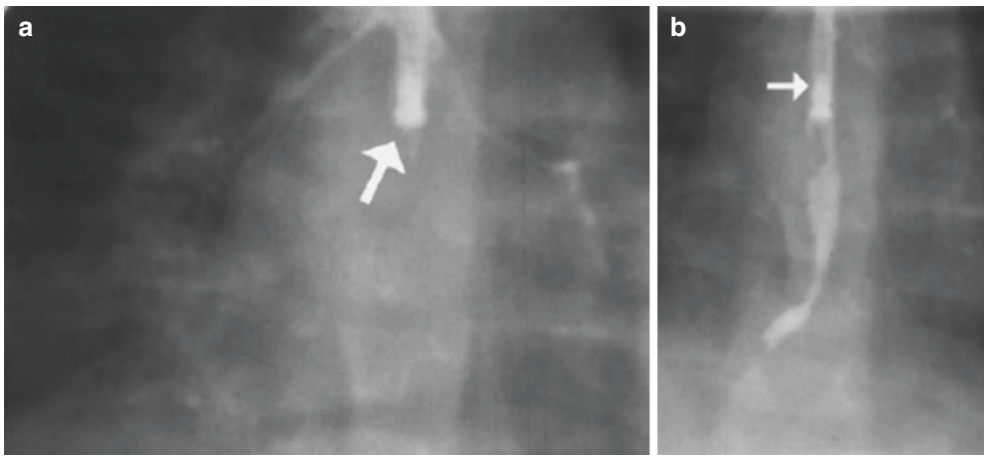

Fig. 6.11 An infant with bronchobiliary fistula. (**a**) The *arrow* points to the biliary proximal fistula arising from the carina (the two main bronchi are seen partially opacified by contrast material arising from the carina at the uppermost limit of the image). (**b**) The contrast is seen to fill more of the fistula extending to the level of the liver (*arrow* points to the more superior portion of the fistula)

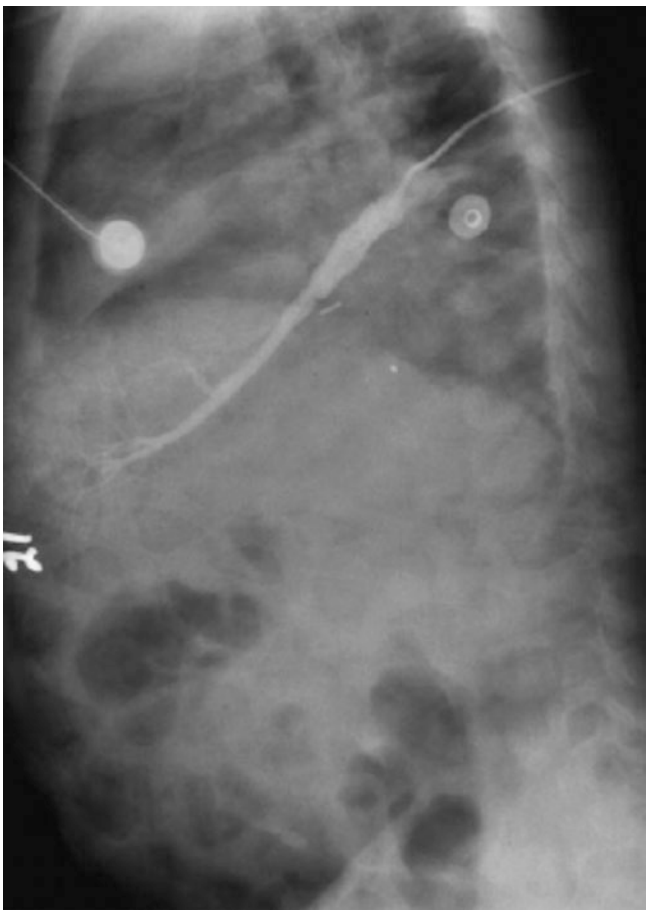

Fig. 6.12 An infant with bronchobiliary fistula. This lateral projection from a percutaneous fistulogram demonstrates the fistula communicating with the intrahepatic branching biliary system

biliary tract displays stratified squamous epithelium of the GI tract. Congenital BBF has been associated with malformations in the biliary tree, diaphragmatic hernia, and esophageal atresia [74–76]. The fistula typically arises from the left hepatic lobe and connects to the distal main trachea or proximal right main stem bronchus [71] (Figs. 6.11 and 6.12).

Presentation typically occurs within the first year of life with a median age of 4 months; however, adult presentation has also been described [72, 77]. Infants most commonly present with respiratory distress, bilious vomiting or expectoration (biliptysis), and the notable absence of intestinal obstruction [71]. Symptoms in this age group might be mistaken for gastroesophageal reflux, tracheoesophageal fistula, malrotation, or aspiration pneumonia and should be included in the differential diagnosis.

Helpful diagnostic testing for BBF includes CT, bronchoscopy, and hepatobiliary scintigraphy (HS). Hepatobiliary scintigraphy (HS) has been recommended to determine adequacy of hepatic drainage and to define associated biliary tract malformations [73, 75]. HS also allows detection of bilious drainage to the respiratory tract. Reconstruction of CT images may also provide virtual bronchoscopy that may be more useful and feasible than traditional bronchoscopy. Recommended treatment includes total surgical removal of the BBF. Prognosis related to cBBF is generally good when not associated with more severe congenital anomalies. Typically, if the left hepatic duct can drain normally, total resection of the fistula is performed. Other surgical options may be considered in cases with impaired left hepatic drainage. These can include anastomoses such as a Roux-en-Y or a type of fistula-enteric procedure.

Acquired Bronchobiliary Fistula

Acquired bronchobiliary fistula (aBBF) was first described in 1850 by Peacock complicating hydatid cystic disease of the liver [78]. Most cases of noncongenital BBF occur as a result of acquired hepatic lesions such as hepatobiliary abscess (with or without biliary stones), hydatid disease, hepatic tumors, or recurrent pancreatic, blunt or penetrating thoracoabdominal trauma or following liver surgery [79–82]. Hepatic infections from tuberculosis [83], echinococcus [84], and ameba have all been described. Overall, aBBF is

rare and can prove difficult to diagnose. A common mechanism of liver disease-associated BBF involves erosion through the diaphragm into the apposing bronchial tree. In cases of trauma with both diaphragmatic and hepatic injury, impaired biliary drainage may act as a nidus for fistula formation.

Acquired BBF should be considered in cases involving liver disease or thoracoabdominal trauma with biliptysis (bilious expectoration). Acquired BBF is associated with significant morbidity and mortality due in part to associated comorbidities and bilious pneumonitis due to the fact that bile is caustic to the respiratory tract. Other common presenting signs and symptoms include respiratory distress, cough, abdominal or chest pain, and fever. When presenting in a subacute manner, symptoms typically include chronic congestion, cough, recurrent pneumonia, and fever. Delayed diagnosis and treatment of BBF can lead to lower lobe bronchiectasis and in some cases the need for lung resection.

Several diagnostic imaging studies have been helpful in diagnosis including bronchoscopy [81], hepatobiliary iminodiacetic acid (HIDA) scan [82], ERCP [85, 86], MR cholangiopancreatography [86], or percutaneous transhepatic cholangiographic fistulogram. Case reports suggest that ERCP with stent- or sphincterotomy-induced bile drainage may be therapeutic by preventing continued intrathoracic bile drainage through the acquired fistula [80, 85, 87]. Additionally, sputum analysis for bilirubin may be helpful. An immediate complication of acquired BBF is bile chemical pneumonitis, which can be severe, leading to respiratory failure. With trauma-induced BBF, both surgical and conservative management approaches are warranted depending on severity and associated complications. No management guidelines have yet been established; however, resolving biliary obstruction is a well-accepted priority following diagnosis. In cases with severe trauma or pulmonary injury, more definitive surgical resection of BBF may be needed [88].

Cast Bronchitis

Cast or plastic bronchitis is a potentially fatal disorder seen relatively rarely in children. It derives its name from mucoid material which forms within the tracheobronchial tree in the form of a branching tubular cast of the airway (Fig. 6.13). It characteristically has a rubbery consistency. These may be expectorated piecemeal or removed at bronchoscopy as extensive casts of the airway.

Classification of Cast Bronchitis

There are several classification systems for cast bronchitis [89]. The original system, proposed by Seear [90], described two types. Type 1, inflammatory casts, is comprised mainly of fibrin, eosinophils, polymorphonuclear leukocytes, and Charcot–Leyden crystals [89–91]. This form is associated with allergic and inflammatory conditions, most commonly asthma and CF [89, 90]. Type 2, noninflammatory casts, is comprised mainly of mucin. This form is associated mainly with cyanotic congenital heart disease, notably with single-ventricle physiology, most particularly following the Fontan procedure (right atrium to pulmonary artery conduit). Others have felt this classification to be too restrictive. Brogan [92] has proposed an expanded classification, among other reasons, to include the idiopathic cases. This classification is based on clinical presentation and includes the following three groups: allergic and asthmatic, cardiac, and idiopathic [89, 92]. Although these classifications include the majority of associated diseases, several other causative or related conditions have been recognized. These include acute chest syndrome of sickle cell disease [89], allergic bronchopulmonary aspergillosis (ABPA) [93], pneumonia [93, 94], lymphangiomatosis [94], bronchiectasis [91, 94], and smoke inhalation [94]. Cases of cast bronchitis have been reported in patients with rheumatoid arthritis, amyloidosis, and membranous colitis and those with large thymuses [91]. In addition to heart disease with single-ventricle physiology, isolated cases of associated tetralogy of Fallot, atrial septal defect with partial anomalous pulmonary venous return, constrictive pericarditis [94], and chronic pericardial effusion [91] have been reported.

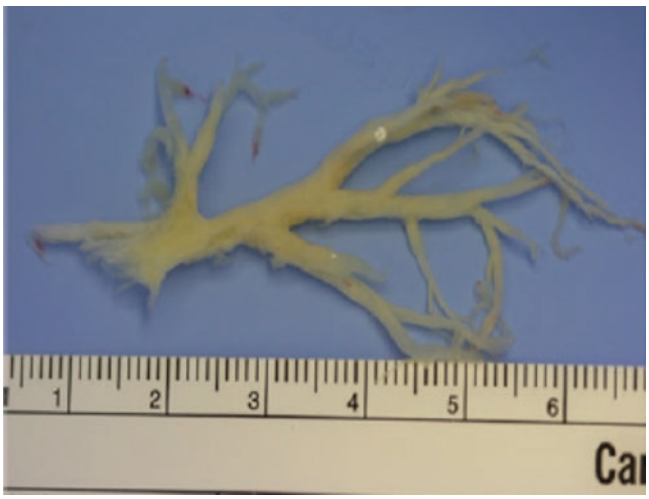

Fig. 6.13 This cast of much of the left bronchial system was retrieved at bronchoscopy

The cause of cast formation is unknown. Type 1 casts are generally acute and occur in association with an acute inflammatory process [93]. Type 2 casts are generally recurrent or chronic [93]. It has been theorized that type 2 casts are caused by disturbances in lymphatic drainage [93] with endobronchial lymph leakage [94] and elevated pulmonary venous pressure [91]. Whereas type 1 casts may resolve with

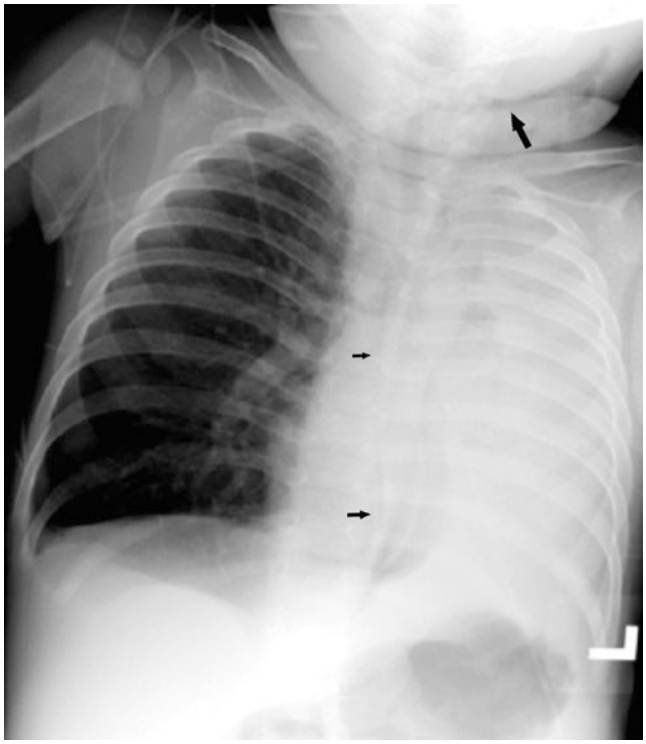

Fig. 6.14 Young child with cast bronchitis. Initial chest radiograph reveals collapse of the left lung. There is subcutaneous air in the left aspect of the neck (*large arrow*) consistent with a pneumomediastinum (*small arrows*). There is compensatory overinflation of the right lung; the mediastinum is shifted to the left

airway clearance and treatment of the underlying disorder, type 2 casts have a worse prognosis [93].

Clinical Presentation

Clinical presentation in pediatric patients with cast bronchitis is nonspecific and varied. Signs include dyspnea, wheezing, fever, and cough [89, 91, 93]. As such, presentation may mimic status asthmaticus or foreign body aspiration [89]. A classic adult finding of a *bruit de drapeau* (the sound produced by a flapping flag) has not been reported in children [89, 91].

Radiological Findings

Imaging findings, likewise, are nonspecific. Findings include atelectasis (sometimes of an entire lung) or airspace consolidation, obstructive emphysema, or compensatory hyperinflation (Figs. 6.14 and 6.15) [89, 91]. An elongated endobronchial opacity with undulating borders may be apparent [89]. Air leakage may rarely occur, including, rarely, pneumomediastinum (Fig. 6.14) [89, 91].

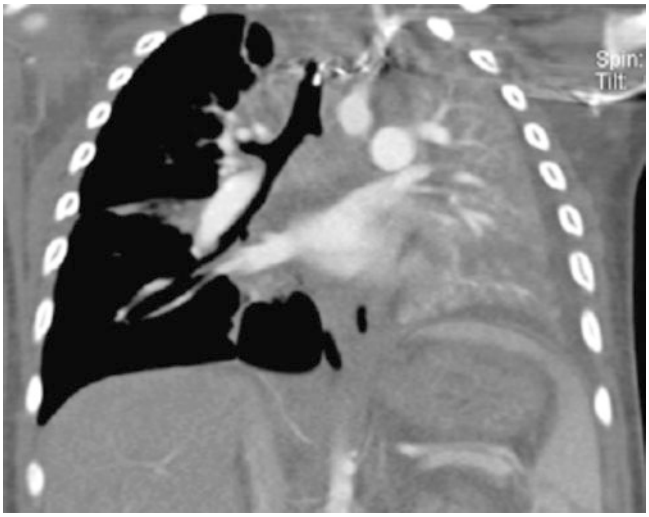

Fig. 6.15 Young children with cast bronchitis. Enhanced coronal CT image confirmed a complete obstruction of the proximal left main bronchus, but did not show the exact nature of the obstructing process

Diagnosis

As presenting signs and symptoms and imaging findings are nonspecific, a high index of suspicion is necessary to make the correct diagnosis, particularly in the absence of an expectorated cast which may be mistaken for aspirated food [91, 94]. Acute respiratory failure, with wheezing which is refractory to asthmatic therapy, should raise concern for the diagnosis of cast bronchitis, particularly if an aspirated foreign body is not suspected [89]. A low threshold for bronchoscopy is warranted under these circumstances [93]. With the presence of an air leak, emergency bronchoscopy should be performed [89].

Management

Treatment of cast bronchitis has had mixed results, frequently with limited poor response and continued high mortality rate (as high as 50% for type 1 casts), with asphyxiation secondary to airway obstruction as the primary cause of death [93, 94]. Mechanical removal by simple expectoration may be effective; however, bronchoscopic removal may be required and remains the most effective current intervention [89]. Bronchial lavage, hydration, and physical therapy may aid in expectoration of casts [91]. Treatment aimed at cast destruction or disruption has been used with limited success including endobronchial administration of tissue plasminogen activator [93, 94], acetylcysteine [94], urokinase, oral and endobronchial steroids, mucolytic agents, anticoagulants [89, 93], bronchodilators, and azithromycin [93]. Although type 1 casts may respond

to these therapeutic maneuvers, type 2 casts, which may be caused by disturbances in lymphatic drainage, may respond to thoracic duct ligation or diet [93, 94]. Pericardiectomy may be effective [94].

Congenital Diaphragmatic Hernia

CDH describes an inborn defect in the diaphragm which allows protrusion of abdominal fat and/or viscera through the opening into the thoracic cavity. The cause of this defect is not fully understood and likely is multifactorial. Patients with diaphragmatic hernias suffer from severe, often lethal, pulmonary hypoplasia. The prevalence of CDH has been reported from 1:2500 to 1:4000 live births [95, 96]. Mortality rates are upward of 60% and have arguably remained relatively unaffected by the adoption of new therapies [97]. In addition to the startlingly high mortality despite medical advances, short- and long-term morbidity is significant. Although a majority of cases are sporadic, some cases of CDH are associated with other anomalies or syndromes. Association with another malformation portends a worse prognosis [98].

Embryology and Pathophysiology

Lung formation begins during the third gestational week and continues throughout fetal life. Lung development is often divided into five overlapping stages: embryonic, pseudoglandular, canalicular, saccular, and alveolar. The reader is directed to Chap. 2, for a more detailed examination of pulmonary embryogenesis.

The diaphragm forms between the 4th and 12th gestational weeks. Until recently, the accepted hypothesis of diaphragmatic formation was based upon a developmental scheme in which four separate substrata contributed to the overall structure. The widely taught theory held that the central portion of the diaphragm was formed by the septum transversum, the dorsal esophageal mesentery contributed to the posterior aspect of the structure, the posterolateral portions arose from the pleuroperitoneal folds, and the periphery was formed by contributions from the adjacent body wall [99, 100]. Recent research in a rodent model, however, has questioned the contributions of all elements but the pleuroperitoneal folds [101]. Myogenic cells and axons appear to coalesce within the pleuroperitoneal folds and expand to form the diaphragm. There is compelling evidence to suggest that abnormal formation of the nonmuscular mesenchyme of the pleuroperitoneal folds leads to CDH in rodents and humans [102].

The exact etiology of CDH and the associated pulmonary hypoplasia is not yet fully understood. Interference with the retinoid signaling pathway has been implicated as a possible causative factor. Retinoids are known to play an important part in all stages of lung development ranging from formation of the lung buds to proliferation of type 2 pneumocytes, stimulation of phospholipid synthesis, and alveologenesis [103]. When evaluating the retinoid pathway's potential link to CDH, it is helpful to consider the nitrofen rat model. Fetal rodents exposed to nitrofen between the 8th and 11th days post-conception experience a high rate of CDH and pulmonary hypoplasia [104]. Although the similarity of this model to human CDH has been questioned [105], nitrofen has recently been shown to decrease retinoic acid levels [106]. Furthermore, retinol and retinol-binding protein have been shown to be decreased in the cord blood of newborns with CDH and increased in their mothers, suggesting a failure of placental transport [107].

The final pathophysiologic theory worthy of consideration is the "dual-hit hypothesis." This concept holds that the pulmonary hypoplasia present in patients with CDH stems not only from compression of the lung by herniated abdominal viscera but also from a direct insult to the developing lung. This is supported by the nitrofen model in which pulmonary hypoplasia is evident prior to normal diaphragm closure [108]. The importance of retinol in the formation of not only the diaphragm but also the lung helps to explain the severity of pulmonary disease experienced in this population.

Types of Hernias

Diaphragmatic hernias can be subcategorized according to location. The most common form of hernia occurs posterolaterally (Fig. 6.16). Though reported by McCauley in 1754, the Czech anatomist Bochdalek's 1848 description yields the eponymous title of a posterolateral defect. It is postulated that this type of hernia results when the pleuroperitoneal folds fail to fuse to the adjacent body wall. Bochdalek hernias are the most common form of congenital diaphragmatic defect accounting for greater than 80% in most series [109, 110]. Of these, a majority are left sided. True hernia sacs are found in only a minority (~15%) of Bochdalek hernias.

Named for the sixteenth-century Italian anatomist and pathologist, Morgagni hernias occur anteriorly between the sternum and eighth rib where the internal mammary artery normally traverses the diaphragm (Fig. 6.17). This type of defect is seen in less than 5% of cases of CDH in many series [95, 110]. Morgagni hernias, though, likely account for a greater percent of CDH in some geographic regions and in patient populations presenting outside the neonatal period [111]. The defect is more often right sided and typically is contained within a true hernia sac. A less common form of retrosternal hernia is seen in patients with pentalogy of

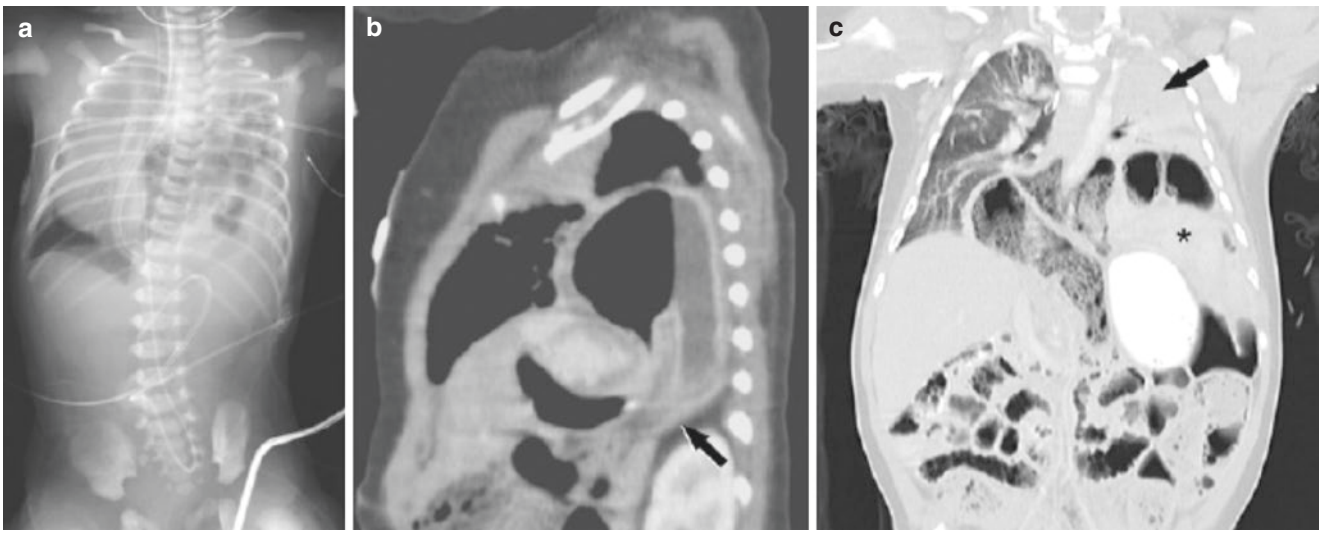

Fig. 6.16 Bochdalek hernia. (**a**) Frontal view of the chest and abdomen showing numerous loops of air-filled bowel in the left hemithorax. There is significant mediastinal shift to the right. (**b**) Sagittal CT of the chest and abdomen reveals the posterior diaphragmatic defect (*arrow*) with herniation of bowel through the opening. (**c**) Coronal lung window image from the same CT shows herniation of bowel and spleen (*asterisk*) into the left thorax. The left lung is hypoplastic and collapsed (*arrow*)

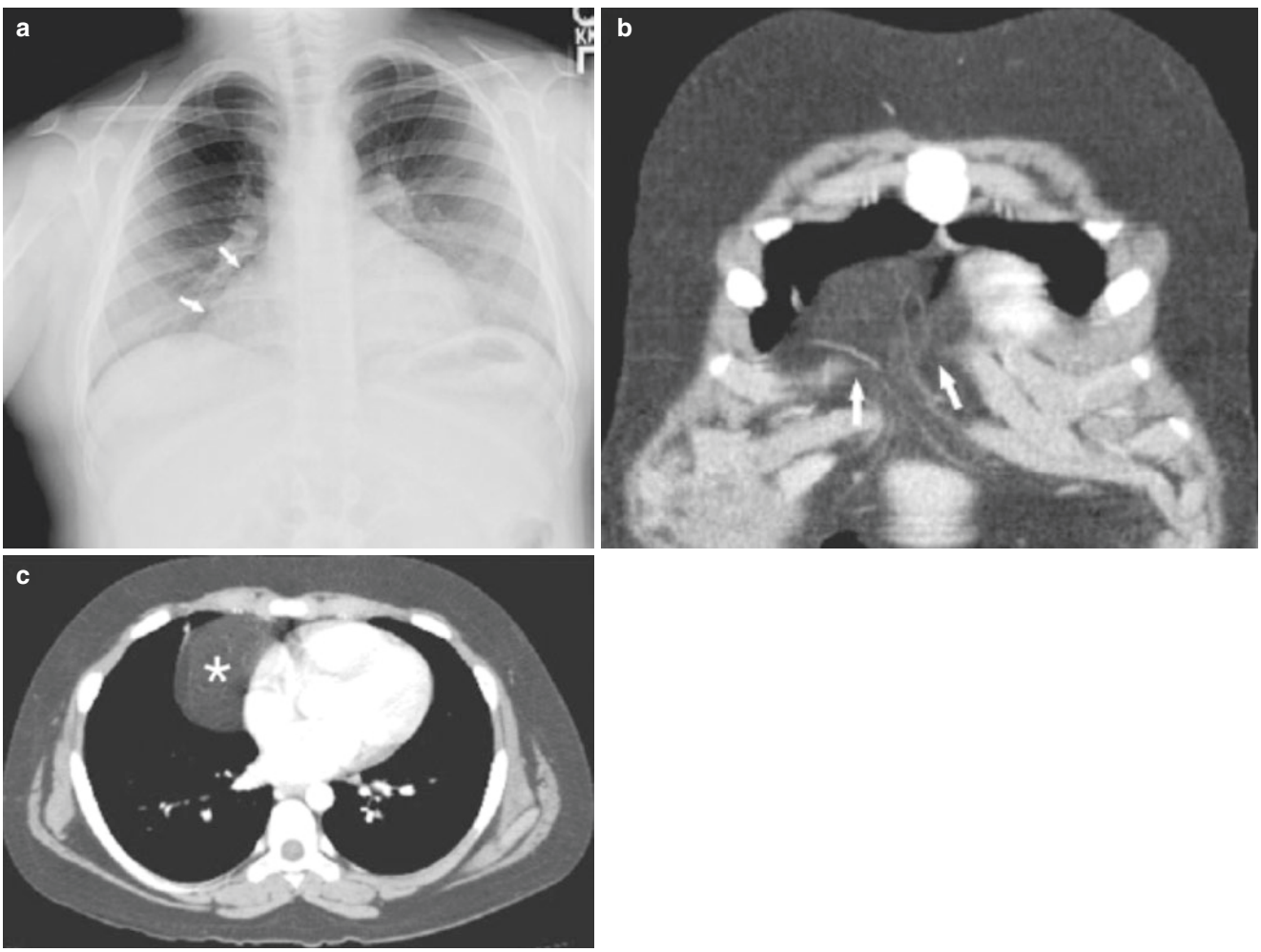

Fig. 6.17 Morgagni hernia. (**a**) Note the enlarged mediastinal silhouette with abnormal right atrial contour (*arrows*). (**b**) Coronal CT reveals defect in the anterior diaphragm (*arrows*) without herniation of mesenteric fat through the defect. (**c**) Axial CT image shows the fatty mass (*asterisk*) in the anterior mediastinum to the right of the heart

Cantrell. Originally described by J. Cantrell in 1958, the condition is typified by an inferior sternal cleft, adjacent anterior diaphragmatic defect, pericardial defect, and omphalocele [112]. The result is an anterior midline defect which permits extrusion of the heart (ectopia cordis). These patients also tend to suffer from complex congenital heart disease. Hiatal hernias constitute the remainder of congenital diaphragmatic defects. Like acquired hiatal hernias, the congenital defect may manifest as a sliding or paraesophageal hernia.

Prenatal

CDH is often detected on routine prenatal ultrasound exams. CDH is suggested when a complex cystic mass representing herniated bowel is noted in the chest. Similarly, the presence of abdominal viscera such as the liver or gallbladder adjacent to the fetal heart is indicative of diaphragmatic hernia. Color Doppler may reveal abnormal course or position of the umbilical or portal vein, particularly in hernias containing fetal liver. Often, there is ipsilateral pulmonary hypoplasia and displacement of the mediastinum into the contralateral thorax. Secondary signs such as decreased abdominal circumference and polyhydramnios may also be observed. One important differential consideration in a patient with apparent CDH is congenital diaphragmatic eventration. Congenital eventration implies cephalic displacement of an intact diaphragm and is associated with lower infant morbidity and mortality. Although the prenatal distinction can be difficult to make, high-resolution ultrasound or MRI may allow discrimination. The presence of a pleural and/or pericardial effusion has been suggested as a secondary sign favoring eventration [113].

The lung–heart ratio (LHR) has been used to prognosticate cases of diaphragmatic hernia [114–116]. The lung contralateral to the defect is measured in its axial dimensions at the atrial level, and this area is divided by the head circumference. A ratio less than 1 is associated with a poor prognosis, with 100% mortality in some series [115, 117]. Conversely, in the same studies, a ratio greater than 1.4 is associated with a routinely good prognosis (100% survival). Prognosis appears less predictable for fetuses with ratios between 1.0 and 1.4 [114, 115, 117]. Other studies have questioned the prognostic value of the LHR for survival prediction and the need for extracorporeal membrane oxygenation (ECMO) [118–120]. Recently, 3D ultrasonography [121, 122] and fetal MRI have been utilized to obtain fetal lung volumes [123, 124]. Percent predicted lung volumes derived from subtracting mediastinal volume from total thoracic volume on fetal MR have been shown to correlate with ECMO requirement, length of hospital stay, and overall survival [125]. MR fetal lung volume measurements appear to be particularly useful in estimating survival and ECMO requirements beyond 30 weeks' gestation [126].

Fetal MRI is also useful in the overall morphologic evaluation of fetuses suspected of having CDH. Presence of liver herniation has been shown to correlate with the need for prosthetic repair, and prenatal recognition of this may aid in counseling and surgical planning [127]. Not only can MRI provide information about herniated viscera; coexistent anomalies can be assessed. Fast spin echo T2-weighted sequences are the mainstay of fetal MRI and provide a detailed anatomic survey in standard imaging planes regardless of fetal position.

Fetal surgery, including CDH repair and tracheal occlusion, is technically possible but has not yet been shown to improve survival [128, 129]. Likewise, pharmacologic therapies such as late prenatal steroids have not demonstrated a benefit [130]. Recent data in an animal model has shown that prenatal treatment with retinoic acid stimulates alveologenesis in hypoplastic lung, leading to increased lung volumes in CDH [131].

Postnatal

The first postnatal imaging study in CDH is typically a frontal chest radiograph. Often, air-filled loops of bowel can be visualized in the chest with mass effect from the hernia resulting in contralateral mediastinal shift (Fig. 6.18). If the radiograph is acquired early after delivery, the herniated bowel may not yet be air filled, presenting as opacification of

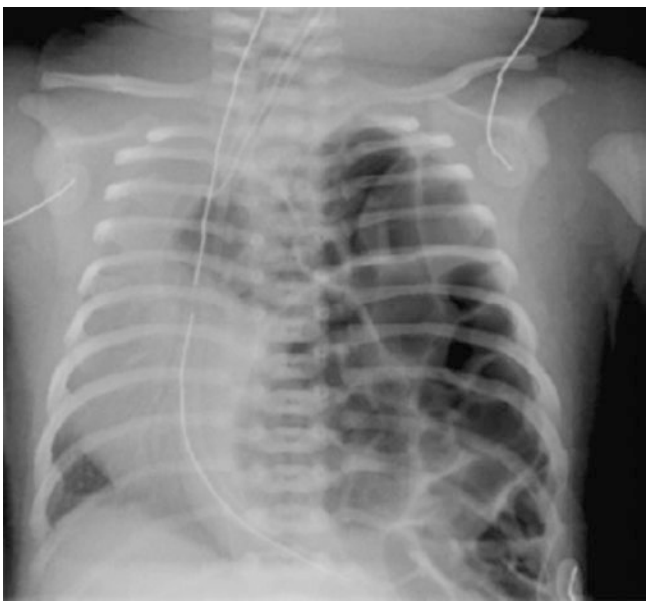

Fig. 6.18 Diaphragmatic hernia with mediastinal shift. Multiple loops of air-filled bowel are herniated into the left hemithorax resulting in marked contralateral mediastinal shift. Note the deviation of the endotracheal and enteric tubes to the right

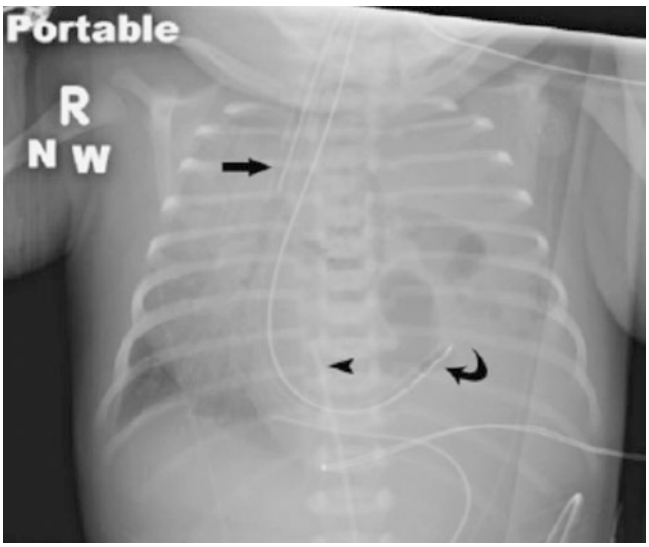

Fig. 6.19 Diaphragmatic hernia with abnormal tube positions. Typical appearance of a left-sided Bochdalek hernia. The endotracheal tube (*arrow*) and umbilical arterial catheter (*arrowhead*) are deviated to the right due to mass effect from the left-sided hernia. Also note the abnormal position of the enteric tube (*curved arrow*) which ends in the lower left hemithorax indicating herniation of the stomach through the defect

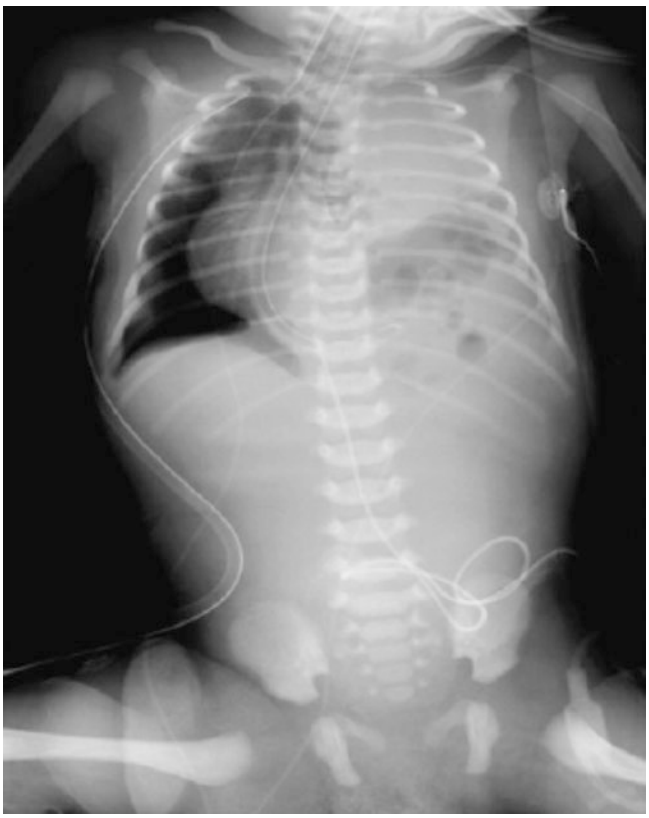

Fig. 6.20 Diaphragmatic hernia with pneumothorax. Left-sided diaphragmatic hernia with typical contralateral mediastinal shift. Note the increased lucency in the right mid- and lower thorax with sharply marginated right atrial margin and right diaphragm consistent with an anterior pneumothorax

the affected hemithorax. Secondary signs of CDH include abnormal positions or deviations of enteric tubes and umbilical catheters (Fig. 6.19). Severe respiratory failure at birth is common, and many patients require rapid ventilatory support. The inherent pulmonary hypoplasia coupled with aggressive ventilation may result in a pneumothorax (Fig. 6.20). The differential for cystic lucent masses within the chest in a newborn includes congenital cystic adenomatoid malformation (CCAM) and pulmonary sequestration. Often, continuity of bowel loops in the upper abdomen and chest makes the diagnosis of CDH obvious. Also, aberrant enteric tube and catheter positions help solidify the diagnosis. Chest and abdominal radiography is often the only preoperative imaging obtained. If question remains as to the etiology of the thoracic mass, computed tomography may be employed for more detailed anatomic depiction.

The inherent pulmonary and vascular hypoplasia results in low-volume, poorly compliant lungs in the perioperative period [132]. Due to the potential of iatrogenic lung injury, many institutions employ permissive hypercapnia and "gentle ventilation" techniques. High-frequency oscillatory ventilation and inhaled nitrous oxide are other practices commonly utilized. Despite these methods, approximately half of patients still require ECMO therapy. Preterm infants with CDH who receive ECMO have been shown to have decreased survival, more complications while on ECMO, and longer ECMO courses and hospital stays than similar late-term infants [133]. ECMO may be venovenous or arteriovenous. Venovenous systems are less commonly seen in CDH patients. The radiodense portion of the efferent catheter should be positioned within the superior vena cava (SVC) with a radiolucent portion extending into the right atrium. The blood is returned via a large-diameter venous catheter which may be placed within the femoral vein often extending into the IVC. With a venoarterial system, the venous cannula should extend into the SVC. A radiolucent portion of the catheter then extends into the atrium with a small radiopaque marker at its tip in the right atrium. The radiopaque portion of the arterial-side cannula should follow the expected path of the brachiocephalic artery and terminate at the aortic arch (Fig. 6.21).

Long-Term Pulmonary Function

While the early effects of severe pulmonary hypoplasia and pulmonary hypertension are well documented, the long-term pulmonary function of neonates surviving CDH repair is less well documented. Recent studies have shown that lung function does improve overtime with the most dramatic improvements occurring in the first 6 months of life [134]. Despite normal results on pulmonary function tests, though, there do

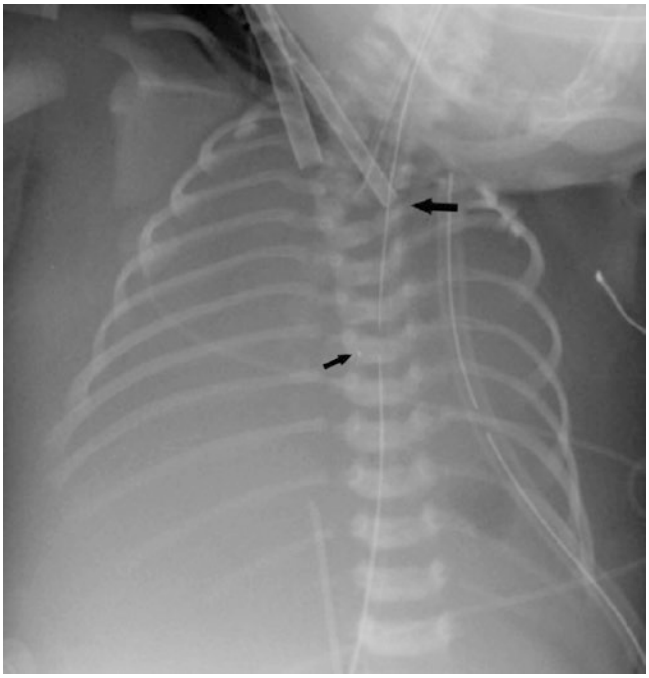

Fig. 6.21 Diaphragmatic hernia on ECMO. Patient with a left-sided hernia on ECMO. The arterial catheter (*large arrow*) courses through the brachiocephalic artery ending in the expected location of the distal aortic arch. The marker at tip of the venous cannula (*small arrow*) projects in the distribution of the right atrium. As expected, on ECMO, the lungs are almost completely airless

appear to be residual effects on ventilation distribution and airway patency at the end of the first year of life [135]. While varying degrees of chronic lung disease are encountered, long-term oxygen requirement after the second year is uncommon [136]. A recent study found that adult survivors of CDH repair suffered only mild pulmonary function impairment consistent with residual small airway disease [137]. Other studies, however, have shown that ventilatory impairment and thoracic deformities are common in adult survivors of CDH [138].

Associated Anomalies and Related Morbidity

Congenital Heart Disease

The most common anomaly associated with CDH is congenital heart disease, occurring in 10–35% of patients [139–144]. While the most frequent heart defect reported in association with CDH is a ventricular septal defect (VSD, 42%), aortic arch obstruction and hypoplastic left heart are also commonly seen [144, 145]. Other reported heart diseases include tetralogy of Fallot, double outlet right ventricle, total anomalous pulmonary venous connection, transposition of the great arteries, pulmonic stenosis, and tricuspid atresia. Overall, there appears to be approximately a 20-fold increase in heart disease in patients with CDH compared to the normal population with the incidence of hypoplastic left heart and obstructive arch lesions disproportionately inflated (100 and 75 times the general population, respectively) [145]. The coexistence of CDH in patients with heart disease yields a worse prognosis than experienced in isolated diaphragmatic hernia. The pulmonary vascular changes inherent in CDH aggravate, and are themselves exacerbated by, congenital heart disease. The effects of increased pulmonary resistance secondary to CDH are greatest in types of heart disease themselves governed by elevated pulmonary pressures. Therefore, patients with arch obstruction, transposition, or monoventricular morphology tend to have a worse prognosis than patients with VSD.

Gastrointestinal Morbidity

Gastrointestinal morbidity is ubiquitous in CDH. As with other malformations resulting in disruption of the normal contour and shape of the peritoneal cavity, intestinal malrotation is inherent in patients with diaphragmatic hernia resulting in intestinal displacement. Obstruction has been reported in up to 20% of patients with CDH [146]. Although the mechanisms are incompletely understood, gastroesophageal reflux disease (GERD) is commonly encountered in association with CDH. Whether due to abnormal formation of the gastroesophageal junction, esophageal ectasia, or altered thoracic-abdominal pressure gradients post-repair, GERD is frequently encountered in patients surviving surgery. The published incidence of GERD varies, but most studies report a prevalence exceeding 50% [147–149]. Reflux and oral aversion are thought to play a significant role in the poor growth and failure to thrive noted in CDH survivors. Other gastrointestinal abnormalities reported in association with CDH include small bowel atresia, colonic agenesis, and Meckel diverticula [150, 151].

Musculoskeletal Deformities

Musculoskeletal deformities are observed in a significant percentage of patients with CDH. Scoliosis has been described in up to 27% of CDH survivors [152]. Chest wall deformities ranging from asymmetry to pectus excavatum have also been reported [152–154]. The pulmonary hypoplasia and increased negative intrathoracic pressure intrinsic to CDH are felt to contribute to the chest wall deformities. The thoracic and spinal abnormalities in turn lead to long-term impairment of pulmonary function.

Neurologic Abnormalities

While morphologic abnormalities of the central nervous system may be seen, acquired neurologic disease secondary to hypoxia, ischemia, and/or hemorrhage is more frequently encountered. The immediate issues of anticoagulation are encountered in patients who require ECMO. These patients undergo regular cranial ultrasound to survey for germinal matrix and parenchymal bleeds. It has been shown that while CDH is not an independent risk factor for ECMO, patients

with CDH are more likely to have complications while on ECMO [155]. CDH requiring ECMO is associated with worse long-term cognitive outcome than seen in ECMO patients without CDH [155]. Also, patients with CDH who require ECMO have a poor neurologic outcome compared to CDH patients who are not treated with ECMO.

Associated Syndromes

Diaphragmatic defects are noted in association with a chromosomal anomaly or syndrome approximately 40% of the time in most series [98, 141], although occurred in over 60% of patients in one large review [156]. The most common chromosomal aberrations seen with CDH are the trisomies 13, 18, and 21 [157]. Turner syndrome (45,X) has also been reported in association with diaphragmatic defects [158]. A vast array of translocations, deletions, duplications, and inversions has been reported with CDH [99]. CDH has been identified as a defining feature of Fryns and Donnai–Barrow syndromes. Fryns syndrome (MIM 229850) is an autosomal recessive condition which consists of CDH, coarse facies, distal limb deformities, cleft lip or palate, congenital heart disease, and cerebral anomalies. Congenital diaphragmatic defect in association with omphalocele, agenesis of the corpus callosum, hypertelorism, and hearing loss constitutes Donnai–Barrow syndrome (MIM 222448), an autosomal recessive disorder linked to a mutation in the LRP2 gene (2q23-q31). Other syndromes which do not require, but may have, an associated diaphragmatic hernia include Beckwith–Wiedemann, Brachmann de Lange, CHARGE association, craniofrontonasal, Denys-Drash, Goldenhar, Fraser, Smith–Lemli–Opitz, Noonan, Pallister–Killian, Pierre Robin, Simpson–Golabi–Behmel, thoracoabdominal (including pentalogy of Cantrell), and multiple pterygium syndromes, spondylocostal dysostosis, and Wolf–Hirschhorn syndrome [95, 96, 99, 156].

Treatment and Outcome Prediction

As previously stated, although fetal repair is technically possible in some cases of CDH, there is no discernable improvement in morbidity or mortality compared to standard postnatal repair. Previously considered a surgical emergency, many institutions now employ a delayed surgical repair. The standard postnatal surgical repair of CDH is via subcostal incision, although thoracotomy may also be performed [159]. The herniated viscera are reduced to the abdominal cavity, and the defect is examined. If a hernia sac is present, it is excised to decrease the chance of recurrence. Depending on the extent of the defect, a primary closure or patch repair is then performed. The size of the diaphragmatic defect appears to be an important factor in the outcome of these patients. Infants with small defects which can be closed without a patch have improved survival when compared to patients having moderate-sized defects requiring patch closure or those with near-complete absence of the diaphragm necessitating a more extensive patch reconstruction [109] (Fig. 6.22).

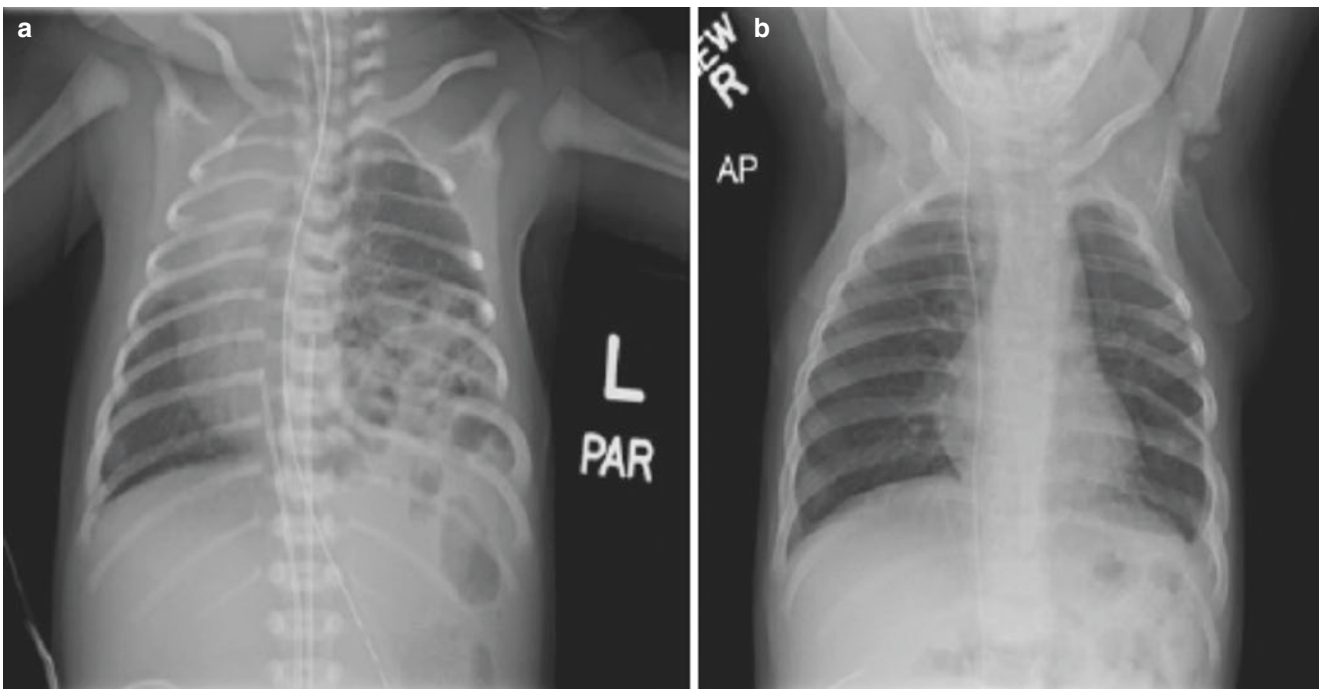

Fig. 6.22 Large diaphragmatic defect requiring patch graft. (**a**) Preoperative image showing left diaphragmatic hernia. (**b**) Postoperative image revealing a tight, flattened left hemidiaphragm with ipsilateral small lung. This combination is highly suggestive of prior diaphragmatic hernia repair

Conclusion

Congenital and miscellaneous lung anomalies, which can be incidental findings or may cause symptoms, are common in pediatric patients. Imaging evaluation can provide the precise information of the congenital and miscellaneous lung masses regarding their location, appearance, size, as well as connection to and mass effect upon the adjacent thoracic structures. Such information is crucial for early and correct diagnosis, which in turn can lead to optimal pediatric patient management.

References

1. Lee EY, Boiselle PM, Cleveland RH. Multidetector CT evaluation of congenital lung anomalies. Radiology. 2008;247(3):632–48.
2. McLean SE, Pfeifer JD, Siegel MJ, Jensen ER, Schuler PM, Hirsch R, et al. Congenital cystic adenomatoid malformation connected to an extralobar pulmonary sequestration in the contralateral chest: common origin? J Pediatr Surg. 2004;39(8):e13–7.
3. Fraser R, Colman N, Muller NL, Pare PD. Developmental and metabolic lung disease. In: Fraser R, Colman N, Muller NL, Pare PD, editors. Synopsis of diseases of the chest. 3rd ed. Philadelphia: Elsevier Saunders; 2005. p. 188–221.
4. Webb W, Higgins CB. Congenital bronchopulmonary lesions. In: Webb WR, editor. Thoracic imaging: pulmonary and cardiovascular radiology. Philadelphia: Lippincott Williams & Wilkins; 2005. p. 1–29.
5. Berrocal T, Madrid C, Novo S, Gutierrez J, Arjonilla A, Gomez-Leon N. Congenital anomalies of the tracheobronchial tree, lung, and mediastinum: embryology, radiology, and pathology. Radiographics. 2004;24(1):e17.
6. Rahalkar A, Rahalkar MD, Rahalkar MA. Pictorial essay: all about bronchial atresia. Ind J Radiol Imag. 2005;15(3):389–93.
7. Matsushima H, Takayagi N, Satoh M, Kurashima K, Kanauchi T, Hoshi T, et al. Congenital bronchial atresia: radiologic findings in nine patients. J Comput Assist Tomogr. 2002;26(5):860–4.
8. Chapman KR, Rebuck AS. Spontaneous disappearance of a chronic mediastinal mass. Chest. 1985;87:235–6.
9. Zylak CJ, Eyler WR, Spizarny DL, Stone CH. Developmental lung anomalies in the adult: radiologic-pathologic correlation. Radiographics. 2002;22.(Spec Issue:S25–43.
10. Aktogu S, Yuncu G, Halilcolar H, Ermete S, Buduneli T. Bronchogenic cysts: clinico-pathological presentation and treatment. Eur Respir J. 1996;9:2017–21.
11. McAdams HP, Kirejczyk WM, Rosado-de-Christenson ML, Matsumoto S. Bronchogenic cyst: imaging features with clinical and histopathologic correlation. Radiology. 2000;217:441–6.
12. Williams HJ, Johnson KJ. Imaging of congenital cystic lung lesions. Paediatr Respire Rev. 2002;3:120–7.
13. Ashizawa K, Okimoto T, Shirafuji T, Kusano H, Ayabe H, Hayashi K. Anterior mediastinal bronchogenic cysts: demonstration of complicating malignancy by CT and MRI. Br J Radiol. 2001;74:959–61.
14. Winters WD, Effmann EL. Congenital masses of the lung: prenatal and postnatal imaging evaluation. J Thoracic Imaging. 2001;16:196–206.
15. Karnak I, Senock ME, Ciftci AO, Buyukpamukcu N. Congenital lobar emphysema: diagnostic and therapeutic considerations. J Pediatr Surg. 1999;34:1347–51.
16. Olutoye OO, Coleman GB, Hubbard AM, Adzick NS. Prenatal diagnosis and management of congenital lobar emphysema. J Pediatr Surg. 2000;35:792–5.
17. Mei-Zahav M, Konen O, Manson D, Langer JC. Is congenital lobar emphysema a surgical disease? J Pediatr Surg. 2006;41:1058–61.
18. Ozcelik U, Gocmen A, Kiper N, Dogru D, Dilber E, Yalcin EG. Congenital lobar emphysema: evaluation and long-term follow up of thirty cases at a single center. Pediatr Pulmonol. 2003;35:384–91.
19. Kuga T, Inoue T, Sakano H, Zempo N, Oga A, Esato K. Congenital cystic adenomatoid malformation of the lung with an esophageal cyst: report of a case. J Pediatr Surg. 2001;36(6):E4.
20. Stocker J, Madewell J, Drake R. Congenital cystic adenomatoid malformation of the lung: classification and morphologic spectrum. Hum Pathol. 1977;8:155–71.
21. Wilson RD, Hedrick HL, Liechty KW, et al. Cystic adenomatoid malformation of the lung: review of genetics, prenatal diagnosis, and in utero treatment. Am J Med Genet A. 2006;140:151–5.
22. Sauvat F, Michel JL, Benachi A, Edmond S, Revillon Y. Management of asymptomatic neonatal cystic adenomatoid malformations. J Pediatr Surg. 2003;38:548–52.
23. Usui N, Kamata S, Sawai T, et al. Outcome predictors for infants with cystic lung disease. J Pediatr Surg. 2004;39:603–6.
24. Khosa JK, Leong SL, Borzi PA. Congenital cystic adenomatoid malformation of the lung: indications and timing of surgery. Pediatr Surg Int. 2004;20:505–8.
25. Yikilmaz A, Lee EY. CT imaging of mass-like nonvascular pulmonary lesions in children. Pediatr Radiol. 2007;37(12):1253–63.
26. Stocker J. Congenital pulmonary airway malformation: a new name and expanded classification of congenital cystic adenomatoid malformations of the lung. Histopathology. 2001;41(Suppl 2):424–58.
27. McSweeney F, Papagiannopoulos K, Goldstarw P, et al. An assessment of the expanded classification of congenital cystic adenomatoid malformations and their relationship to malignant transformation. Am J Surg Pathol. 2003;27:1139–46.
28. Remy-Jardin M, Remy J, Mayo JR, Muller NL. Vascular anomalies of the lung. In: Remy-Jardin M, Remy J, Mayo JR, Muller NL, editors. CT angiography of the chest. Philadelphia: Lippincott Williams & Wilkins; 2001. p. 97–114.
29. Corbett HJ, Humphrey GM. Pulmonary sequestration. Paediatr Respir Rev. 2004;5:59–68.
30. Freedom RM, Yoo SJ, Goo HW, Mikailian H, Anderson RH. The bronchopulmonary foregut malformation complex. Cardiol Young. 2006;16:229–51.
31. Frush DP, Donnelly LF. Pulmonary sequestration spectrum: a new spin with helicial CT. AJR Am J Roentgenol. 1997;169:679–82.
32. Bolca N, Topal U, Bayram S. Bronchopulmonary sequestration: radiologic findings. Eur J Radiol. 2004;52:185–91.
33. Ahmed M, Jacobi V, Vogl TJ. Multislice CT and CT angiography for non-invasive evaluation of bronchopulmonary sequestration. Eur Radiol. 2004;14:2141–3.
34. Lee EY, Dillon JE, Callahan MJ, Voss SD. 3D multidetector CT angiographic evaluation of extralobar pulmonary sequestration with anomalous venous drainage into the left internal mammary vein in a paediatric patient. Br J Radiol. 2006;79:e99–102.
35. Lee EY, Boiselle PM, Shamberger RC. Multidetector computed tomography and 3-dimensional imaging: preoperative evaluation of thoracic vascular and tracheobronchial anomalies and abnormalities in pediatric patients. J Pediatr Surg. 2010;45(4):811–21.
36. Kang M, Khandelwal N, Ojili V, Rao KL, Rana SS. Multidetector CT angiography in pulmonary sequestration. J Comput Assist Tomogr. 2006;30(6):926–32.
37. Lee EY, Tracy DA, Mahmood SA, Weldon CB, Zurakowski D, Boiselle PM. Preoperative MDCT evaluation of congenital lung anomalies in children: comparison of axial, multiplanar, and 3D images. AJR Am J Roentgenol. 2011;196(5):1040–6.
38. Srivastava D, Preminger T, Lock JE, et al. Hepatic venous blood and the development of pulmonary arteriovenous malformations in congenital heart disease. Circulation. 1995;92:1217–22.

39. Shah MJ, Rychik J, Fogel MA, Murphy JD, Jacobs ML. Pulmonary AV malformations after superior cavopulmonary connection: resolution after inclusion of hepatic veins in the pulmonary circulation. Ann Thorac Surg. 1997;63:960–3.
40. Schraufnagel DE, Kay JM. Structural and pathologic changes in the lung vasculature in chronic liver disease. Clin Chest Med. 1996;17:1–15.
41. Lee KN, Lee HJ, Shin WW, Webb WR. Hypoxemia and liver cirrhosis (hepatopulmonary syndrome) in eight patients: comparison of the central and peripheral pulmonary vasculature. Radiology. 1999;211:549–53.
42. Oh YW, Kang EY, Lee NJ, Suh WH, Godwin JD. Thoracic manifestations associated with advanced liver disease. J Comput Assist Tomogr. 2000;24:699–705.
43. McAdams HP, Erasmus J, Crockett R, Mitchell J, Godwin JD, McDermott VG. The hepatopulmonary syndrome: radiologic findings in 10 patients. AJR Am J Roentgenol. 1996;166:1379–85.
44. Shovlin CL, Letarte M. Hereditary haemorrhagic telangiectasia and pulmonary arteriovenous malformations: issues in clinical management and review of pathogenic mechanisms. Thorax. 1999;54:714–29.
45. Donnelly LF. Chest. In: Donnelly LF, editor. Diagnostic imaging pediatrics. Salt Lake City: Amirsys; 2005. p. 118–20.
46. White RI Jr, Lynch-Nyhan A, Terry P, et al. Pulmonary arteriovenous malformations: techniques and long-term outcome of embolotherapy. Radiology. 1988;169:663–9.
47. Lee DW, White RI Jr, Egglin TK, et al. Embolotheraphy of large pulmonary arteriovenous malformations: long-term results. Ann Thorac Surg. 1997;64:930–40.
48. Ferretti GR, Arbib A, Bertrand B, Coulomb M. Haemoptysis associated with pulmonary varices: demonstration using computed tomography angiography. Eur Respir J. 1998;12:989–92.
49. Frank JL, Poole CA, Rosas G. Horseshoe lung: clinical, pathologic, and radiologic features and a new plain film finding. Am J Roentgenol. 1986;146:217–26.
50. Kelly D, Mroczek EC, Galliani CA, et al. Horseshoe lung and cross over segment: a unifying concept. Perspect Pediatr Pathol. 1995;18:183–213.
51. Paterson A. Imaging evaluation of congenital lung anomalies in infants and children. Radiol Clin N Am. 2005;43:303–23.
52. Freedom RM, Burrows PE, Moes CA. Horseshoe lung: report of five cases. Am J Roentgenol. 1986;146:211–5.
53. Dupuis C, Remy J, Remy-Jardin M, et al. The "horseshoe" lung: six new cases. Pediatr Pulmonol. 1994;17(2):124–30.
54. Hawass ND, Badwai AM, Al-Muzrakehi M, et al. Horseshoe lung: differential diagnosis. Pediatr Radiol. 1990;20:580–4.
55. Chen SJ, Li YW, Wu MH, et al. Crossed ectopic left lung with fusion to the right lung: a variant of horseshoe lung? Am J Roentgenol. 1997;168:1347–8.
56. Takeda K, Kato N, Nakagawa T, et al. Horseshoe lung without respiratory distress. Pediatr Radiol. 1990;20(8):604.
57. Takahashi M, Murata K, Yamori M, et al. Horseshoe lung: demonstration by electron-beam CT. Br J Radiol. 1997;70:964–6.
58. Tanaka S, Kubota M, Yagi M, et al. Treatment of a case with right-sided diaphragmatic hernia associated with an abnormal vessel communication between a herniated liver and the right lung. J Pediatr Surg. 2006;41(3):E25–8.
59. Robertson DJ, Harmon CM, Goldberg S. Right congenital diaphragmatic hernia associated with fusion of the liver and the lung. J Pediatr Surg. 2006;41(6):E9–10.
60. Slovis TL, Farmer DL, Berdon WE, et al. Hepatic pulmonary fusion in neonates. Am J Radiol. 2000;174:229–33.
61. Kluth D, Tenbrinck R, Ekesparre M, et al. The natural history of congenital diaphragmatic hernia and pulmonary hypoplasia in embryo. J Pediatr Surg. 1993;28:456–63.
62. Katz S, Kidron D, Litmanovitz I, et al. Fibrous fusion between the liver and the lung: an unusual complication of right congenital diaphragmatic hernia. J Pediatr Surg. 1998;33(5):766–7.
63. Van MK, Lou SB. Congenital diaphragmatic hernia: the neonatologist's perspective. Pediatr Rev. 1999;20:e79–87.
64. Keller RL, Aaroz PA, Hawgoog S, et al. MR imaging of hepato pulmonary fusion in neonates. Am J Radiol. 2003;180:438–40.
65. Nadroo AM, Levshina R, Tugertimur A, et al. Congenital diaphragmatic hernia: atypical presentation. J Perinat Med. 1999;27(4):276–8.
66. Neuhauser E, Elkin M, Landing B. Congenital direct communication between biliary system and respiratory tract. AMA Am J Dis Child. 1952;83(5):654–9.
67. Bohn D. Congenital diaphragmatic hernia. Am J Respir Crit Care Med. 2002;166:911–5.
68. Lee EY, Siegel MJ, Hildebolt CF, Gutierrez FR, Fallah JH, Bhalla S. Evaluation of thoracic aortic anomalies in pediatric patients and young adults: comparison of axial, multiplanar, and 3D images. AJR. 2004;183:777–84.
69. Lee EY, Siegel MJ, Sierra LM, Foglia RP. Evaluation of angio architecture of pulmonary sequestration in pediatric patients using 3D MDCT angiography. AJR. 2004;183:183–8.
70. Lee EY, Dillon JE, Callahan MJ, Voss SD. 3D MDCT angiographic evaluation of extralobar sequestration with anomalous venous drainage into left internal mammary vein in a pediatric patient. Br J Radiol. 2006;79(945):e99–e102.
71. Tommasoni N, Gamba PG, Midrio P, Guglielmi M. Congenital tracheobiliary fistula. Pediatr Pulmonol. 2000;30(2):149–52.
72. de Carvalho CR, Barbas CS, Guarnieri RM, et al. Congenital bronchobiliary fistula: first case in an adult. Thorax. 1988;43(10):792–3.
73. Gunlemez A, Tugay M, Elemen L, et al. Surgical experience in a baby with congenital broncho-biliary fistula. Ann Thorac Surg. 2009;87(1):318–20.
74. Tekant GA, Joseph VT, Cheah SL. Congenital tracheobiliary fistula. J Pediatr Surg. 1994;29(5):594–5.
75. Egrari S, Krishnamoorthy M, Yee CA, et al. Congenital bronchobiliary fistula: diagnosis and postoperative surveillance with HIDA scan. J Pediatr Surg. 1996;31(6):785–6.
76. Kalayoglu M, Olcay I. Congenital bronchobiliary fistula associated with esophageal atresia and tracheo-esophageal fistula. J Pediatr Surg. 1976;11(3):463–4.
77. Bringas Bollada M, Cabezas Martin MH, Martinez Sagasti F, et al. Congenital bronchobiliary fistula diagnosed in adult age. Med Intensiva. 2006;30(9):475–6.
78. Peacock TB. Case in which hydatids were expectorated and one of suppuration of a hydatid cyst of the liver communicating with the lungs. Edinburgh Med Surg J. 1850;74:33–46.
79. Eryigit H, Urek S, Olgac G, et al. Management of acquired bronchobiliary fistula: 3 case reports and a literature review. J Cardiothorac Surg. 2007;2:52.
80. Gandhi N, Kent T, Kaban JM, et al. Bronchobiliary fistula after penetrating thoracoabdominal trauma: case report and literature review. J Trauma. 2009;67(5):E143–5.
81. Mitra S, Bhatia N, Dey N, Dalal U. Bronchobiliary fistula: an anesthetic challenge! J Clin Anesth. 2009;21(5):360–2.
82. Annovazzi A, Viceconte G, Romano L, et al. Detection of a suspected bronchobiliary fistula by hepatobiliary scintigraphy. Ann Nucl Med. 2008;22(7):641–3.
83. Flemma RJ, Anlyan WG. Tuberculous bronchobiliary fistula. Report of an unusual case with demonstration of the fistulous tract by percutaneous transhepatic cholangiography. J Thorac Cardiovasc Surg. 1965;49:198–201.
84. Borrie J, Shaw JH. Hepatobronchial fistula caused by hydatid disease. The Dunedin experience 1952–79. Thorax. 1981;36(1):25–8.

85. Singh B, Moodley J, Sheik-Gafoor MH, et al. Conservative management of thoracobiliary fistula. Ann Thorac Surg. 2002;73(4):1088–91.
86. Oettl C, Schima W, Metz-Schimmerl S, et al. Bronchobiliary fistula after hemihepatectomy: cholangiopancreaticography, computed tomography and magnetic resonance cholangiography findings. Eur J Radiol. 1999;32(3):211–5.
87. Sheik-Gafoor MH, Singh B, Moodley J. Traumatic thoracobiliary fistula: report of a case successfully managed conservatively, with an overview of current diagnostic and therapeutic options. J Trauma. 1998;45(4):819–21.
88. Chua HK, et al. Bronchobiliary fistula: principles of management. Ann Thorac Surg. 2000;70(4):1392–4.
89. Kruger J, Shpringer C, Picard E, Kerem E. Thoracic air leakage in the presentation of cast bronchitis. Chest. 2009;136:615–7.
90. Seear M, Hui H, Magee F, Bohn D, Cutz E. Bronchial cast in children: a proposed classification based on nine cases and a review of the literature. Am J Respir Crit Care Med. 1997;155: 364–70.
91. Bowen A'D, Oudjhane K, Odagiri K, Liston SL, Cumming WA, Oh KS. Plastic bronchitis: large, branching, mucoid bronchial casts in children. Am J Roentgenol. 1985;144:371–5.
92. Brogan TV, Finn LS, Pyskaty DJ, Redding GJ, Ricker D, Inglis A, et al. Plastic bronchitis in children: a case series and review of the medical literature. Pediatr Pulmonol. 2002;34:482–7.
93. Schultz KD, Oermann CM. Treatment of cast bronchitis with low-dose oral azithromycin. Pediatr Pulmonol. 2003;35:139–43.
94. Costello JM, Steinhorn D, McColley S, Gerber ME, Kumar SP. Treatment of plastic bronchitis in a Fontan patient with tissue plasminogen activator: a case report and review of the literature. Pediatrics. 2002;109:e67.
95. Wenstrom KD, Weiner CP, Hanson JW. A five-year statewide experience with congenital diaphragmatic hernia. Am J Obstet Gynecol. 1991;165:838–42.
96. Langham MR Jr, Kays DW, Ledbetter DJ, Frentzen B, Sanford LL, Richards DS. Congenital diaphragmatic hernia: epidemiology and outcome. Clin Perinatol. 1996;23:671–88.
97. Stege G, Fenton A, Jaffray B. Nihilism in the 1990s: the true mortality of congenital diaphragmatic hernia. Pediatrics. 2003;112:532–5.
98. Sweed Y, Puri P. Congenital diaphragmatic hernia: influence of associated malformations on survival. Arch Dis Child. 1993;69:68–70.
99. Holder AM, Klaassens M, Tibboel D, de Klein A, Lee B, Scott DA. Genetic factors in congenital diaphragmatic hernia. Am J Hum Genet. 2007;80:825–45.
100. Moore KL, Persaud TVN. The developing human: clinically oriented anatomy. 8th ed. Philadelphia: Saunders; 2008.
101. Babiuk RP, Zhang W, Clugston R, Allan DW, Greer JJ. Embryological origins and development of the rat diaphragm. J Comp Neurol. 2003;455:477–87.
102. Clugston RD, Klattig J, Englert C, Clagett-Dame M, Martinovic J, Benachi A, et al. Teratogen-induced, dietary and genetic models of congenital diaphragmatic hernia share a common mechanism of pathogenesis. Am J Pathol. 2006;169:1541–9.
103. Montedonico S, Nakazawa N, Puri P. Congenital diaphragmatic hernia and retinoids: searching for an etiology. Pediatr Surg Int. 2008;24:755–61.
104. Mortell A, Montedonico S, Puri P. Animal models in pediatric surgery. Pediatr Surg Int. 2006;22:111–28.
105. Baglaj SM, Czernik J. Nitrofen-induced congenital diaphragmatic hernia in rat embryo: what model? J Pediatr Surg. 2004;39: 24–30.
106. Noble BR, Babiuk RP, Clugston RD, Underhill TM, Sun H, Kawaguchi R. Mechanisms of action of the congenital diaphragmatic hernia-inducing teratogen nitrofen. Am J Physiol Lung Cell Mol Physiol. 2007;293:L1079–87.
107. Major D, Cadenas M, Fournier L, Leclerc S, Lefebvre M, Cloutier R. Retinol status of newborn infants with congenital diaphragmatic hernia. Pediatr Surg Int. 1998;13:547–9.
108. Keijer R, Liu J, Deimling J, Tibboel D, Post M. Dual-hit hypothesis explains pulmonary hypoplasia in the nitrofen model of congenital diaphragmatic hernia. Am J Pathol. 2000;156:1299–306.
109. The Congenital Diaphragmatic Hernia Study Group. Defect size determines survival in infants with congenital diaphragmatic hernia. Pediatrics. 2007;120:e651–7.
110. Torfs CP, Curry CJ, Bateson TF, Honore LH. A population-based study of congenital diaphragmatic hernia. Teratology. 1992;46:555–65.
111. Al-Salem AH, Nawaz A, Matta H, Jacobsz A. Herniation through the foramen of Morgagni: early diagnosis and treatment. Pediatr Surg Int. 2002;18:93–7.
112. Cantrell JR, Haller JA, Ravitch MM. A syndrome of congenital defects involving the abdominal wall, sternum, diaphragm, pericardium, and heart. Surg Gynecol Obstet. 1958;107:602–14.
113. Jeanty C, Nien JK, Espinoza J, Kusanovic JP, Goncalves LF, Qureshi F, et al. Pleural and pericardial effusion: a potential ultrasonographic marker for the prenatal differential diagnosis between congenital diaphragmatic eventration and congenital diaphragmatic hernia. Ultrasound Obstet Gynecol. 2007;29:378–87.
114. Metkus AP, Filly RA, Stringer MD, Harrison MR, Adzick NS. Sonographic predictors of survival in fetal diaphragmatic hernia. J Pediatr Surg. 1996;31:148–51.
115. Lipshutz GS, Albanese CT, Feldstein VA, Jennings RW, Housley HT, Beech R, et al. Prospective analysis of lung-to-head ratio predicts survival for patients with prenatally diagnosed congenital diaphragmatic hernia. J Pediatr Surg. 1997;32:1634–6.
116. Jani J, Keller RL, Benachi A, Nicolaides KH, Favre R, Gratacos E. Prenatal prediction of survival in isolated left-sided diaphragmatic hernia. Ultrasound Obstet Gynecol. 2006;27:18–22.
117. Laudy JA, Van Gucht M, Van Dooren MF, Wladimiroff JW, Tibboel D. Congenital diaphragmatic hernia: an evaluation of the prognostic value of the lung-to-head ratio and other prenatal parameters. Prenatal Diagn. 2003;23:634–9.
118. Sbragia L, Paek BW, Filly RA, Harrison MR, Farrell JA, Farmer DL, et al. Congenital diaphragmatic hernia without herniation of the liver: does the lung-to-head ratio predict survival? J Ultrasound Med. 2000;19:845–8.
119. Heling KS, Wauer RR, Hammer H, Bollman R, Chaoui R. Reliability of the lung-to-head ratio in predicting outcome and neonatal ventilation parameters in fetuses with congenital diaphragmatic hernia. Ultrasound Obstet Gynecol. 2005;25:112–8.
120. Arkovitz MS, Russo M, Devine P, Budhorick N, Stolar CJ. Fetal lung-head ratio is not related to outcome for antenatal diagnosed congenital diaphragmatic hernia. J Pediatr Surg. 2007;42:107–10.
121. Bahmaie A, Hughes SW, Clark T, Milner A, Saunders J, Tilling K, et al. Serial fetal lung volume measurements using three-dimensional ultrasound. Ultrasound Obstet Gynecol. 2000;16:154–8.
122. Ruano R, Joubin L, Sonigo P, Benachi A, Aubry MC, Thalabard JC, et al. Fetal lung volume estimated by 3-dimensional ultrasonography and magnetic resonance imaging in cases with isolated congenital diaphragmatic hernia. J Ultrasound Med. 2004;23:353–8.
123. Jani JC, Cannie M, Peralta CF, Deprest JA, Nicolaides KH, Dymarkowski S. Lung volumes in fetuses with congenital diaphragmatic hernia: comparison of 3D US and MR imaging assessments. Radiology. 2007;244:575–82.
124. Büsing KA, Kilian AK, Schaible T, Endler C, Schaffelder R, Neff KW. MR relative fetal lung volume in congenital diaphragmatic hernia: survival and need for extracorporeal membrane oxygenation. Radiology. 2008;248:240–6.
125. Barnewolt CE, Kunisaki SM, Fauza DO, Nemes LP, Estroff JA, Jennings RW. Percent predicted lung volumes as measured on

fetal magnetic resonance imaging: a useful biometric parameter for risk stratification in congenital diaphragmatic hernia. J Pediatr Surg. 2007;42:193–7.
126. Büsing KA, Kilian AK, Schaible T, Dinter DJ, Neff KW. MR lung volume in fetal congenital diaphragmatic hernia: logistic regression analysis – mortality and extracorporeal membrane oxygenation. Radiology. 2008;248:233–9.
127. Kunisaki SM, Barnewolt CE, Estroff JA, Nemes LP, Jennings RW, Wilson JM, et al. Liver position is a prenatal factor of prosthetic repair in congenital diaphragmatic hernia. Fetal Diagn Ther. 2008;23:258–62.
128. Harrison MR, Adzick NS, Bullard KM, Farrell JA, Howell LJ, Rosen MA, et al. Correction of congenital diaphragmatic hernia in utero VII: a prospective trial. J Pediatr Surg. 1997;32:1637–42.
129. Harrison MR, Keller RL, Hawgood SB, Kitterman JA, Sandberg PL, Farmer DL, et al. A randomized trial of fetal endoscopic tracheal occlusion for severe fetal congenital diaphragmatic hernia. N Engl J Med. 2003;349:1916–24.
130. Lally KP, Bagolan P, Hosie S, Lally PA, Stewart M, Cotton CM, et al. Corticosteroids for fetuses with congenital diaphragmatic hernia: can we show benefit? J Pediatr Surg. 2006;41:668–74.
131. Montedonico S, Sugimoto K, Felle P, Bannigan J, Puri P. Prenatal treatment with retinoic acid promotes pulmonary alveologenesis in the nitrofen model of congenital diaphragmatic hernia. J Pediatr Surg. 2008;43:500–7.
132. Nakayama DK, Motoyama EK, Mutich RL, Koumbourlis AC. Pulmonary function in newborns after repair of congenital diaphragmatic hernia. Pediatr Pulmonol. 1991;11:49–55.
133. Stevens TP, Chess PR, McConnochie KM, Sinkin RA, Guillet R, Maniscalco WM, et al. Survival in early- and late-term infants with congenital diaphragmatic hernia treated with extracorporeal membrane oxygenation. Pediatrics. 2002;110:590–6.
134. Koumbourlis AC, Wung JT, Stolar CJ. Lung function in infants after repair of congenital diaphragmatic hernia. J Pediatr Surg. 2006;41:1716–21.
135. Dotta A, Palamides S, Braguglia A, Crescenzi F, Ronchetti MP, Calzolari F, et al. Lung volumes and distribution of ventilation in survivors to congenital diaphragmatic hernia (CDH) during infancy. Pediatr Pulmonol. 2007;42:600–4.
136. Jaillard SM, Pierrat V, Dubois A, Truffert P, Lequien P, Wurtz AJ, et al. Outcome at 2 years of infants with congenital diaphragmatic hernia: a population-based study. Ann Thorac Surg. 2003;75:250–6.
137. Peetsold MG, Vonk-Noordegraaf A, Heij HH, Gemke R. Pulmonary function and exercise testing in adult survivors of congenital diaphragmatic hernia. Pediatr Pulmonol. 2007;42:325–31.
138. Vanamo K, Rintala R, Sovijärvi A, Jääskeläinen J, Turpeinen M, Lindahl H, et al. Long-term pulmonary sequelae in survivors of congenital diaphragmatic defects. J Pediatr Surg. 1996;31:1096–100.
139. Greenwood RD, Rosenthal A, Nadas AS. Cardiovascular abnormalities associated with congenital diaphragmatic hernia. Pediatrics. 1976;57:92–7.
140. Cuniff C, Jones KL, Jones MC. Patterns of malformation in children with congenital diaphragmatic defects. J Pediatr. 1990;116:258–61.
141. Fauza DO, Wilson JM. Congenital diaphragmatic hernia and associated anomalies: their incidence, identification, and impact on prognosis. J Pediatr Surg. 1994;29:1113–7.
142. Martínez-Frías ML, Prieto L, Urioste M, Bermejo E. Clinical/epidemiological analysis of congenital anomalies associated with diaphragmatic hernia. Am J Med Genet. 1996;62:71–6.
143. Migliazza L, Otten C, Xia H, Rodriguez JI, Diez-Pardo JA, Tovar JA. Cardiovascular malformations in congenital diaphragmatic hernia: human and experimental studies. J Pediatr Surg. 1999;34:1352–8.
144. Cohen MS, Rychik J, Bush DM, Tian ZY, Howell LJ, Adzick NS, et al. Influence of congenital heart disease on survival in children with congenital diaphragmatic hernia. J Pediatr. 2002;141:25–30.
145. Graziano JN. Cardiac anomalies in patients with congenital diaphragmatic heria and their prognosis: a report from the congenital diaphragmatic hernia study group. J Pediatr Surg. 2005;40:1045–50.
146. Vanamo K, Rintala RJ, Lindahl H, Louhimo I. Long-term gastrointestinal morbidity in patients with congenital diaphragmatic defects. J Pediatr Surg. 1996;31:551–4.
147. Koot VC, Bergmeijer JH, Bos AP, Molenaar JC. Incidence and management of gastroesophageal reflux after repair of congenital diaphragmatic hernia. J Pediatr Surg. 1993;28:48–52.
148. Kieffer J, Sapin E, Berg A, Beaudoin S, Bargy F, Helardot PG. Gastroesophageal reflux after repair of congenital diaphragmatic hernia. J Pediatr Surg. 1995;30:1330–3.
149. Su W, Berry M, Puligandla PS, Aspirot A, Flageole H, Laberge JM. Predictors of gastroesophageal reflux in neonates with congenital diaphragmatic hernia. J Pediatr Surg. 2007;42:1639–43.
150. van Dooren MF, Goemaere N, de Klein A, Tibboel D, de Krijger RR. Postmortem findings and clinicopathological correlation in congenital diaphragmatic hernia. Pediatr Dev Pathol. 2004;7:459–67.
151. Benjamin DR, Juul S, Siebert JR. Congenital posterolateral diaphragmatic hernia: associated malformations. J Pediatr Surg. 1988;23:899–903.
152. Vanamo K, Peltonen J, Rintala R, Lindahl H, Jääskeläinen J, Louhimo I. Chest wall and spinal deformities in adults with congenital diaphragmatic defects. J Pediatr Surg. 1996;31:851–4.
153. Lund DP, Mitchell J, Kharasch V, Quigley S, Kuehn M, Wilson JM. Congenital diaphragmatic hernia: the hidden morbidity. J Pediatr Surg. 1994;29:258–62.
154. Arena F, Romeo C, Calabrò MP, Antonuccio P, Arena S, Romeo G. Long-term functional evaluation of diaphragmatic motility after repair of congenital diaphragmatic hernia. J Pediatr Surg. 2005;40:1078–81.
155. Stolar C, Crisafi MA, Driscoll YT. Neurocognitive outcome for neonates treated with extracorporeal membrane oxygenation: are infants with congenital diaphragmatic hernia different? J Pediatr Surg. 1995;30:366–71.
156. Stoll C, Alembik Y, Dott B, Roth MP. Associated malformations in cases with congenital diaphragmatic hernia. Genet Couns. 2008;19:331–9.
157. Tibboel D, Gaag A. Etiologic and genetic factors in congenital diaphragmatic hernia. Clin Perinatol. 1996;23:689–99.
158. Cigdem MK, Onen A, Okur H, Otcu S. Associated malformations in Morgagni hernia. Pediatr Surg Int. 2007;23:1101–3.
159. Stolar CJ, Dillon PW. Pediatric surgery. 6th ed. Philadelphia: Mosby; 2006.

Focal Lung Disorders

7

Edward Y. Lee

Pulmonary Cysts

Pulmonary cysts seen on plain chest radiographs as completely or partially air-filled, round masses may be congenital, infectious/inflammatory, traumatic, or neoplastic in origin. The differential diagnosis can be refined based on the age of the patient (neonate and young infant vs. child) and distribution within the lungs (unilateral vs. bilateral), as well as the clinical presentation and the presence of other findings such as nodules or wedge-shaped opacities.

In neonates or young infants, unilateral findings most often represent bronchopulmonary foregut malformations, while bilateral involvement suggests chronic lung disease of prematurity (Table 7.1). Young children most commonly present with symptoms of infection with or without an underlying congenital anomaly. A solitary lesion suggests a congenital anomaly or bacterial infection in a previously healthy child. If findings are bilateral, a systemic disease should be considered. Langerhans histiocytosis and cystic fibrosis (CF) are bilateral upper lung zone predominant diseases early on, while septic emboli involve the lower lobes preferentially. The presence of nodules and cysts suggests conditions such as Langerhans cell histiocytosis (LCH), granulomatosis with polyangiitis (previously known as Wegener granulomatosis), cystic fibrosis, and papillomatosis. The presence of wedge-shaped opacities suggests a vascular etiology as in granulomatosis with polyangiitis or septic emboli (Table 7.2).

Table 7.1 Cystic lesions in neonate or young infant

Unilateral
Congenital malformations
Pulmonary
Congenital pulmonary airway malformation (CPAM)
Extralobar pulmonary sequestration
Congenital lobar emphysema
Diaphragm
Congenital diaphragmatic hernia (CDH)
Bilateral
Chronic lung disease of prematurity
Persistent pulmonary interstitial emphysema

Table 7.2 Cystic lesions in children

Unilateral
Infection
Complicated pneumonia – Abscess, cavitary necrosis, pneumatocele
Intralobar pulmonary sequestration
Hydatid disease
Trauma – Contusion/laceration – Pneumatocele
Neoplasm – Pleuropulmonary blastoma, type 1
Bilateral
Infectious/inflammatory
Cystic fibrosis/bronchiectasis
Septic emboli
Nonbacterial infections – Fungi, mycobacteria, opportunistic organisms
Vasculitides
Hydrocarbon pneumonitis – Pneumatocele
Neoplastic/proliferative
Laryngotracheal (juvenile) papillomatosis
Langerhans cell histiocytosis
Metastatic disease
Syndrome associated
Lymphangioleiomyomatosis with or without tuberous sclerosis
Proteus syndrome
Neurofibromatosis type 1
Marfan syndrome

E. Y. Lee (✉)
Department of Radiology, Boston Children's Hospital and Harvard Medical School, Boston, MA, USA
e-mail: Edward.Lee@childrens.harvard.edu

R. H. Cleveland, E. Y. Lee (eds.), *Imaging in Pediatric Pulmonology*, https://doi.org/10.1007/978-3-030-23979-4_7

Neonate or Young Infant

Unilateral Lesions

Congenital Lung Malformations

Congenital lung malformations are unilateral and most often discovered prenatally or in a neonate with respiratory distress [1–5]. Some present later with symptoms due to recurrent infection. Congenital lung malformations including congenital pulmonary airway malformation (CPAM), pulmonary sequestration (Fig. 7.1), and congenital lobar emphysema (CLE) can appear as a focal lung lesion. These congenital lung malformations are discussed in Chap. 6 of this book.

Persistent Pulmonary Interstitial Emphysema

Pulmonary interstitial emphysema (PIE) develops as a complication of barotrauma from positive-pressure ventilation and is usually, but not exclusively, encountered in premature neonates with surfactant deficiency. Rupture of alveoli results in dissection of air into the interstitium. For pediatric patients who survive, the interstitial air is usually resorbed, but the air may collect in an expanding radiolucent cyst termed *localized* or persistent PIE. Although the PIE is bilateral, persistent collections are most often unilateral [6] (Table 7.3). On plain radiographs and CT, persistent PIE appears as hyperexpanded collections of thin-walled cysts. CT shows the characteristic appearance of linear and punctate densities within the cyst, the so-called *line-and-dot* pat-

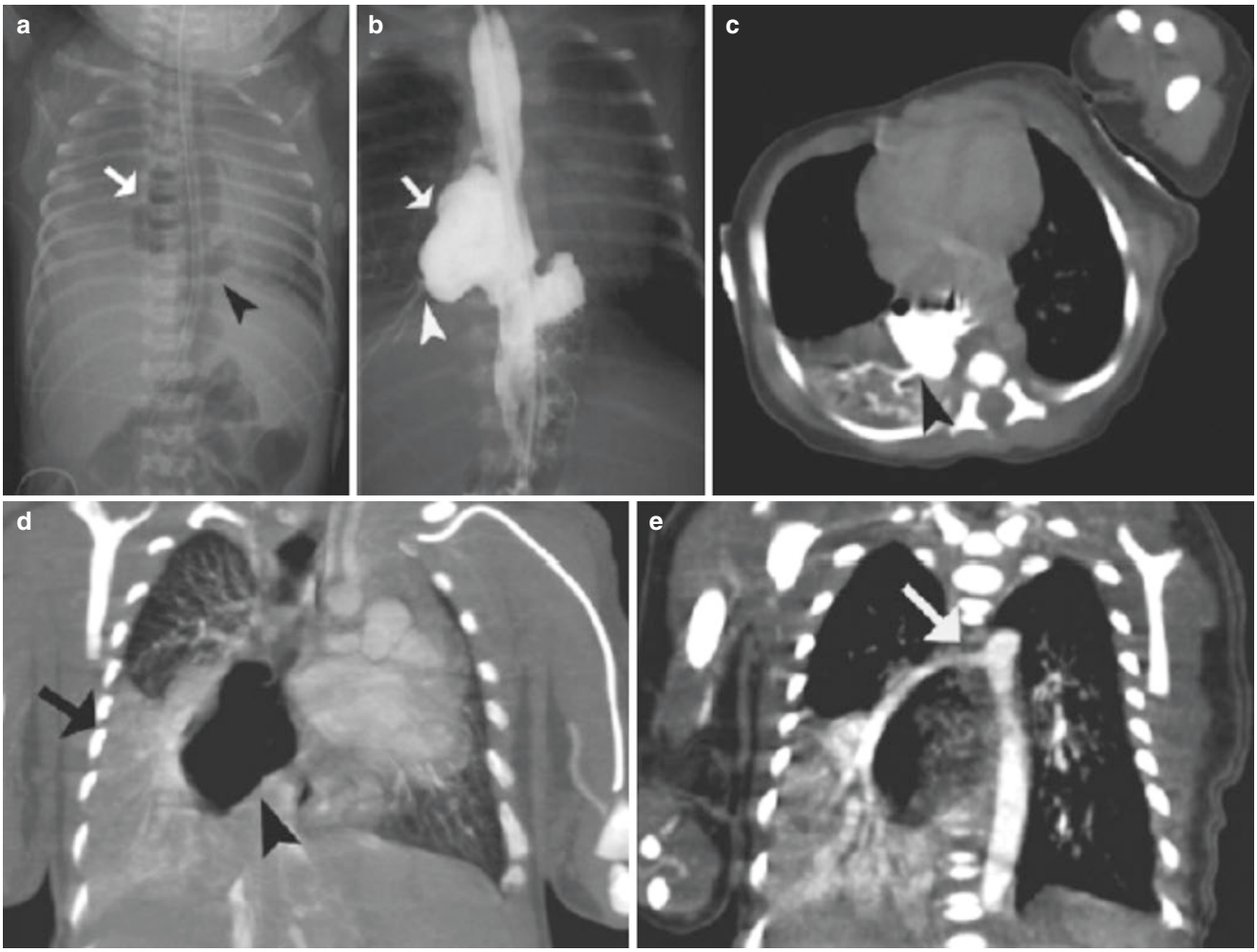

Fig. 7.1 A 3-day-old boy with bronchopulmonary foregut malformation with systemic arterial supply and bronchial connection to gastrointestinal tract. (**a**) Frontal radiograph of the chest and abdomen shows dense opacification of right lower lobe silhouetting the right hemidiaphragm. There is also right lateral pleural effusion. An air-filled cystic structure (arrow) is seen in the medial right hemithorax. Additionally, there appears to be a hiatus hernia (*arrowhead*). (**b**) Esophagram shows the right medial lucent cystic lesion (arrow) fills directly from the esophagus and the subdiaphragmatic stomach is small. Also seen is filling of a distal branching structure (arrowhead) extending to the right lower lobe opacity. (**c**) Axial CT image obtained after the esophagram without additional contrast shows that the branching structure is consistent with a bronchus (arrowhead) communicating via the cystic structure with the esophagus. (**d**) Coronal lung window CT image obtained after administration of intravenous iodinated contrast reveals enhancing mass (arrow) peripherally in lower right hemithorax and medial air-filled cystic structure (arrowhead). (**e**) Coronal enhanced CT image shows large artery (arrow) arising from the upper descending aorta to right lower lobe pulmonary sequestration

tern, which is thought to represent air in the interstitium surrounding the bronchovascular bundles [6] (Fig. 7.2). It is important to distinguish these from congenital pulmonary malformations which are treated surgically, as lesions of persistent pulmonary emphysema are at least initially managed conservatively.

Bilateral Lesions

Chronic Lung Disease of Prematurity (Bronchopulmonary Dysplasia, BPD)

In this age group, the most common cause of bilateral lung lesions is chronic lung disease of prematurity, which usually occurs in premature neonates as the sequela of surfactant deficiency disease, but may also occur in term or near-term infants with persistent pulmonary hypertension or meconium aspiration [7]. The etiology is not fully understood, but barotrauma from positive-pressure ventilation and oxygen toxicity is implicated [8]. Chronic lung disease does not cause cyst formation, and the classic *bubbly* appearance of stage 3 bronchopulmonary dysplasia (BPD) described by Northway is not commonly seen today; however, after the third week of life, findings of atelectasis and fibrosis appear adjacent to areas of hyperlucency and air trapping, and the juxtaposition of these may suggest a cystic appearance [9, 10]. Chest radiography is relatively insensitive to the early findings of chronic lung disease and does not correlate well with results of lung function studies. CT is abnormal in almost all survivors often demonstrating underlying lung parenchymal architectural distortion, atelectasis, and areas of hyperinflation [9, 10].

Table 7.3 Lucent lung and lung segments

Both lungs (air trapping)
Bronchiolitis
Hyperventilation
Asthma
Chronic lung disease
One lung
Obstruction
Hypoplasia/absence
Bronchiolitis obliterans
Postoperative congenital diaphragmatic hernia (CDH)
Contralateral increased opacity
Effusion
Asymmetric pulmonary edema
Asymmetric soft tissues
Pneumothorax
Poland's syndrome
Rotation
Lung segments
Congenital lobar emphysema (CLE)
Bronchial obstruction
Chronic lung disease of prematurity (CLD)
Peripheral pulmonary artery stenosis (PPS)

Child

In children, infection is the most common cause of pulmonary disease. Bacterial infections such as lobar pneumonia are generally unilateral. Atypical infections, infections that occur in patients with underlying predisposing conditions, and inflammatory conditions are likely to involve both lungs. Rare primary neoplasms of the lung are unilateral, while metastases are typically bilateral.

Unilateral Lesions

Complicated Pneumonia

Complicated pneumonia, while less common than in the past, is still a frequent cause of cystic lesions of the lung in young children [11]. These children are quite ill with productive cough, fever, and tachypnea progressing to respiratory distress despite adequate oral antibiotic therapy. Pneumonia

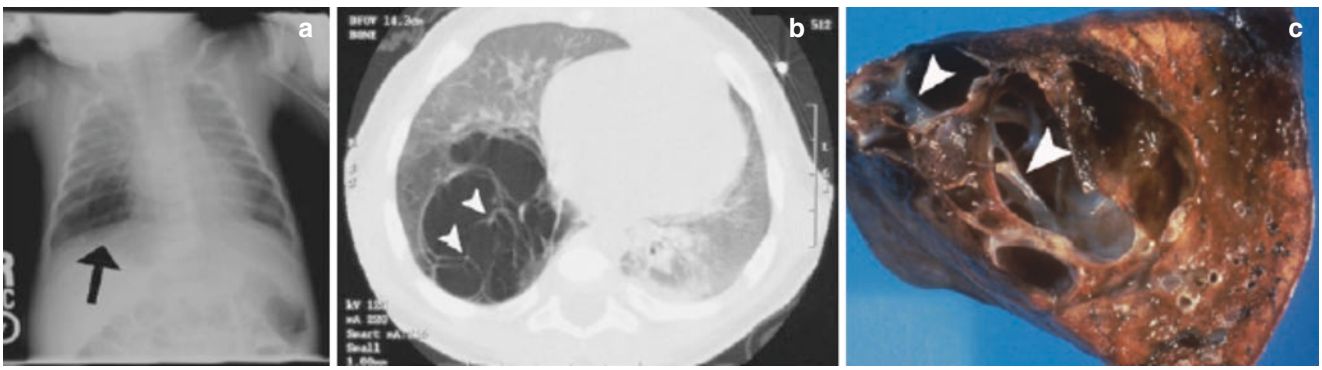

Fig. 7.2 A 14-month-old ex-27 week premature infant with persistent pulmonary interstitial emphysema who was found to have a persistent lucent lesion at right lung base at age 3 months. (**a**) Frontal chest radiograph shows a lucent cyst (arrow) at the right base. (**b**) Axial lung window CT image demonstrates a multilocular air-filled cyst with thin walls and septa. Line-and-dot pattern (arrowheads) is seen reflecting air collections surrounding bronchovascular bundles. (**c**) Photograph of the gross resected specimen reveals large air-filled cysts (arrowheads) surrounding bronchovascular bundles

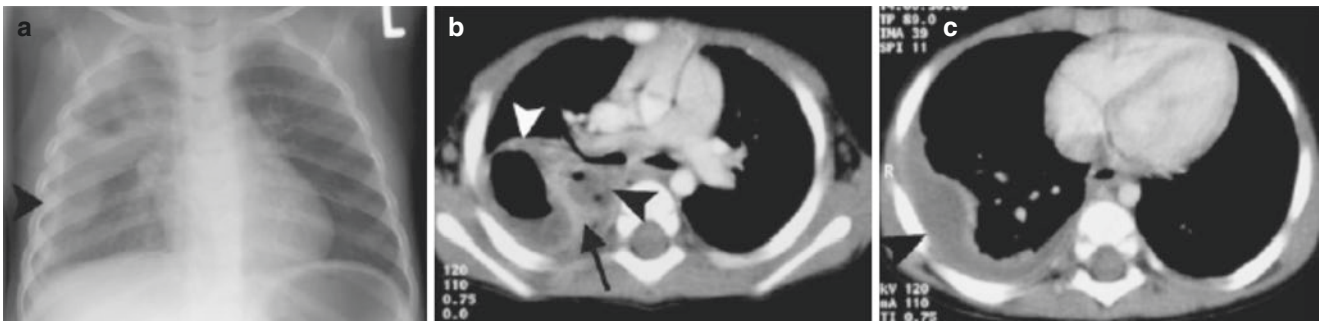

Fig. 7.3 A 22-month-old girl with complicated pneumonia who presented with fever and tachypnea. (**a**) Frontal chest radiograph shows round, soft tissue density masses containing air and adjacent pleural thickening (*arrowhead*) on the right. (**b**) Axial enhanced CT image of the chest demonstrates fluid- and air-filled cavities (arrowheads) in the right lung. Note that the surrounding lung parenchyma (arrow) enhances indicating viable, consolidated tissue as opposed to necrotic lung. (**c**) Axial enhanced CT image inferior to (**b**) shows adjacent nondependent pleural fluid (*arrowhead*) consistent with empyema

beyond the neonatal period is usually unilateral and lobar, but can be complicated by the development of abscess or cavitary necrosis. Both are more easily detected on CT than on plain radiography. They are fluid filled but may also contain air. With contrast-enhanced CT, the uncompromised, consolidated lung surrounding an abscess cavity enhances diffusely, while the parenchyma surrounding a necrotic cavity does not enhance [82]. In either case, an adjacent empyema is common (Fig. 7.3). The most common causative agent is pneumococcus in healthy children and *S. aureus* in immunocompromised children. The differential diagnosis includes an infected congenital cystic malformation. History of severe acute illness, prior normal chest radiograph, and near-complete resolution of the radiographic abnormalities after 40 days support a diagnosis of complicated pneumonia, as opposed to infected congenital cyst.

Staph and strep pneumonia can also be associated with pneumatocele formation as the infection resolves. Pneumatoceles are thought to result from alveolar rupture into the inflamed interstitium, which traps the air in a collection. The improving clinical status of the patient favors a diagnosis of pneumatocele over abscess formation. Pneumatoceles can also develop in tuberculous infection, hydrocarbon pneumonitis, LCH, and pulmonary contusion/laceration.

Hydatid Disease

Hydatid disease, or echinococcosis, is a parasitic infection caused by *Echinococcus granulosus* or *Echinococcus multilocularis.* The disease is prevalent in shepherding regions [12]. Humans contract the infection through contact with the definitive host, usually dogs, or by consuming contaminated food or water. Sheep or cattle serve as the intermediate host. Infection of the lung generally manifests as one or more large, well-circumscribed cysts which are generally fluid filled. If the lung cyst ruptures into the tracheobronchial tree, an air-fluid level develops (Fig. 7.4). The cyst membrane may be seen floating on top of the air-fluid level, producing the so-called *water lily* sign. The liver is another commonly involved organ, and liver cysts may be seen on chest CT [13–15].

Congenital Lung Malformations

Some congenital lung malformations are more likely to be discovered after infancy which include intralobar pulmonary sequestration, bronchogenic cyst, and bronchial atresia [1–5]. These congenital lung malformations are discussed in detail in Chap. 6 of this book; therefore, they are only discussed briefly in this chapter.

First, intralobar sequestration can be associated with clinical and pathologic features of chronic or recurrent infection/inflammation, an observation that, along with the fact that patients tended to present after infancy, has led to controversy regarding whether intralobar sequestration is a congenital lesion or rather acquired as the sequela of chronic infection, with shunting of blood flow from the pulmonary to the systemic supply. The question remains whether the infection causes part of the normal lung to be sequestered or whether the infection is secondary to an underlying congenital malformation. In young children as in neonates, the pulmonary sequestration generally appears as a solid or solid and cystic mass in one of the lower lobes, more often on the left. Air may be seen in the cysts perhaps as a result of infection. All sequestrations have systemic arterial supply, usually from the descending or upper abdominal aorta (Fig. 7.5). Venous drainage is to the inferior pulmonary vein in the setting of intralobar pulmonary sequestration and systemic veins for extralobar pulmonary sequestration [1–5]. Recent study showed that axial MDCT images allow accurate diagnosis of the types, location, associated mass effect, and anomalous arteries of congenital lung anomalies [16]. However, multiplanar (2D) or 3D MDCT images can add diagnostic value for the evaluation of congenital lung lesions associated with anomalous veins, thus improving diagnostic accuracy [16, 17].

Second, bronchogenic cyst may be diagnosed prenatally or later in infancy or childhood either incidentally or with

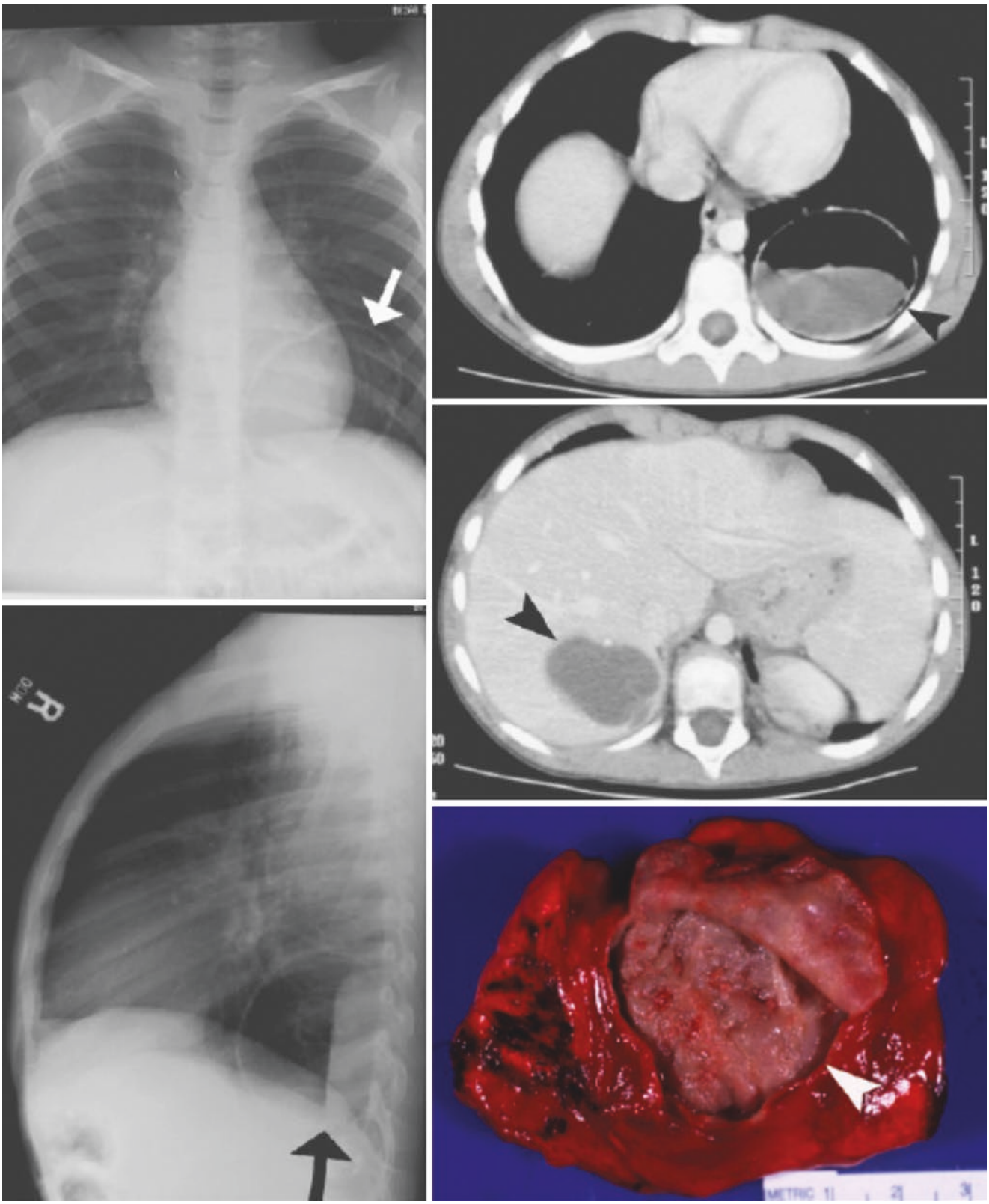

Fig. 7.4 A 7-year-old boy with hydatid disease from Kosovo. (**a**) Frontal chest radiograph shows large well-circumscribed, thin-walled, lucent cyst (arrow) on the left. (**b**) Cross-table lateral radiograph reveals a meniscus (arrow) within this cyst in the left lower lobe. (**c**) Axial enhanced CT image again shows the thin-walled, air-filled cyst with meniscus. There is also a small inverted crescent of air (arrowhead) behind the fluid density. (**d**) Axial enhanced CT image inferior to (**c**) demonstrates a cyst in the liver, a common site of hydatid disease. (**e**) Photograph of resected gross specimen shows the cyst with the roof retracted (*arrowhead*)

respiratory distress or dysphagia (Fig. 7.6). These are well-defined, typically unilocular cysts with very thin or imperceptible walls and homogeneous fluid content [1–5]. The fluid has the attenuation of proteinaceous fluid on CT. They appear solid on chest radiographs unless infected, when they may contain some internal air and associated adjacent lung parenchymal air-space changes [1–5].

Finally, bronchial atresia is usually asymptomatic and often diagnosed serendipitously in older children or young adults. In contrast to CLE, which is often caused by bronchial compression or stenosis, bronchial atresia has no check valve mechanism but rather complete obstruction of the bronchus [1–5, 18]. As a result, air reaches the lung parenchyma beyond the atresia via collateral drift only, so that the segment or lobe does not become large enough to cause mass effect. There is mild hyperlucency of the involved segment or lobe which may suggest the diagnosis. Additionally, the bronchus beyond the atretic segment is dilated; and mucoid secretions may become trapped within, forming an ovoid, tubular, or branching density. The dilated distal bronchus may also contain air and appear as a cystic lucency on radiographs (Fig. 7.7).

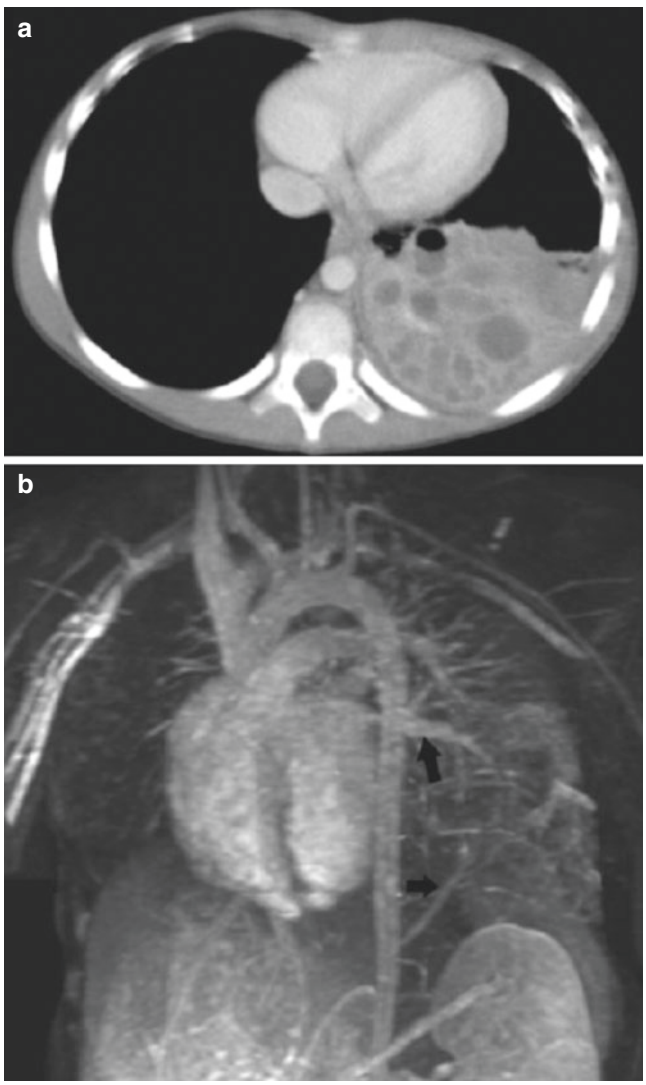

Fig. 7.5 Intralobar pulmonary sequestration in a 12-year-old boy who presented with pneumonia. (a) Axial enhanced CT image shows a complex left lower lobe mass with areas of fluid and enhancing septations by CT. (b) MRA shows two large feeding vessels (arrows) arising from the aorta. Pathology after surgical resection proved intralobar pulmonary sequestration

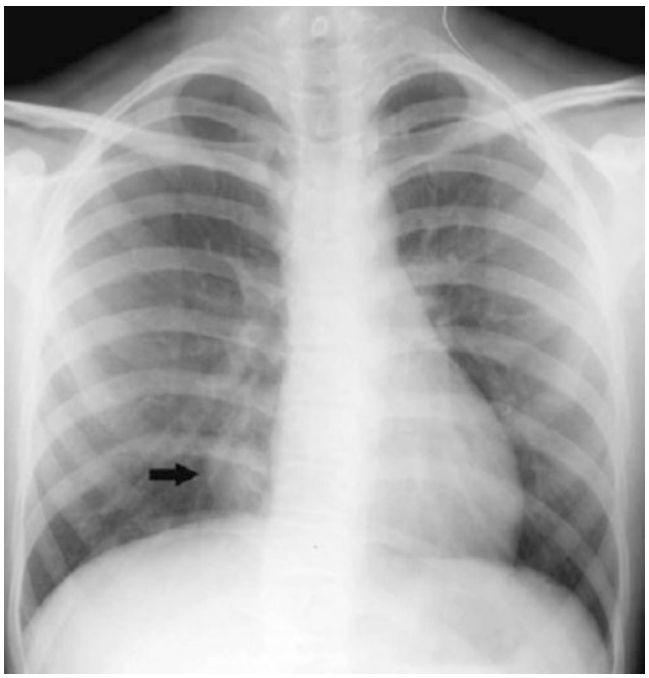

Fig. 7.6 This 11-year-old boy presented with a cough and was found to have a bronchogenic cyst. Frontal chest radiograph shows a well-defined solitary right middle lobe pulmonary lesion (arrow) in the right cardiophrenic angle. Surgical specimen after resection showed this to be a bronchogenic cyst

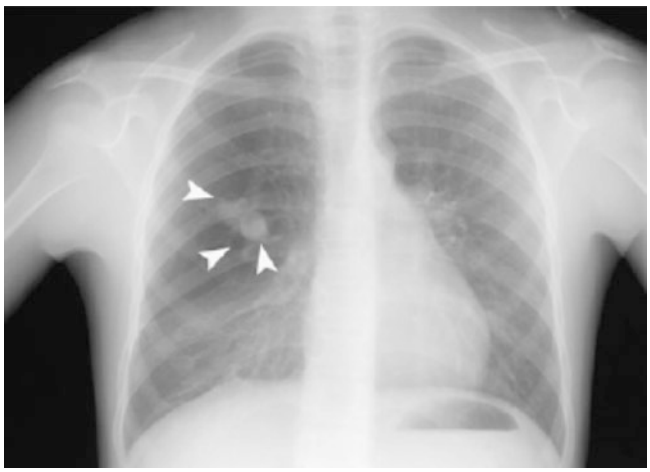

Fig. 7.7 Fourteen-year-old boy with bronchial atresia found incidentally. Frontal chest radiograph shows a round opacity that appears to branch (*arrowheads*). Additionally, the surrounding lung is hyperlucent and exerts mild mass effect on adjacent lung

Traumatic Lung Lesion

Pulmonary laceration or contusion from blunt trauma can produce an air-filled cyst or pseudocyst [19, 20]. Contusions appear as peripheral nonsegmental, dense opacities in the posterior or posteromedial lung. They are frequently crescentic in configuration, and a thin zone of subpleural sparing is a specific finding on CT [21]. Hemothorax or hemopneumothorax is also commonly seen with trauma. Adjacent rib fractures may also be present but are less common than in adults. Lacerations appear as opacities with areas of cavitation, which may contain air-fluid levels [22]. Also, as contusions resolve, pneumatoceles may develop within them.

Pleuropulmonary Blastoma (PPB), Type 1

Primary neoplasms of the lung are rare, but the most common of these is the childhood form of PPB, a blastemal tumor similar to Wilm's tumor [23, 24]. Mutations in the DICER gene have been described with PPB [25]. PPB has three different main subtypes: cystic [type 1], combined cystic and solid [type 2], and solid [type 3] [26]. The purely cystic form (type 1) of PPB may be indistinguishable on imaging from congenital cystic lesions, especially CPAM (Fig. 7.8). Type 1 PPB tends to occur in younger patients than the other types with a peak incidence at age 10 months. It also has a better prognosis for long-term survival than the

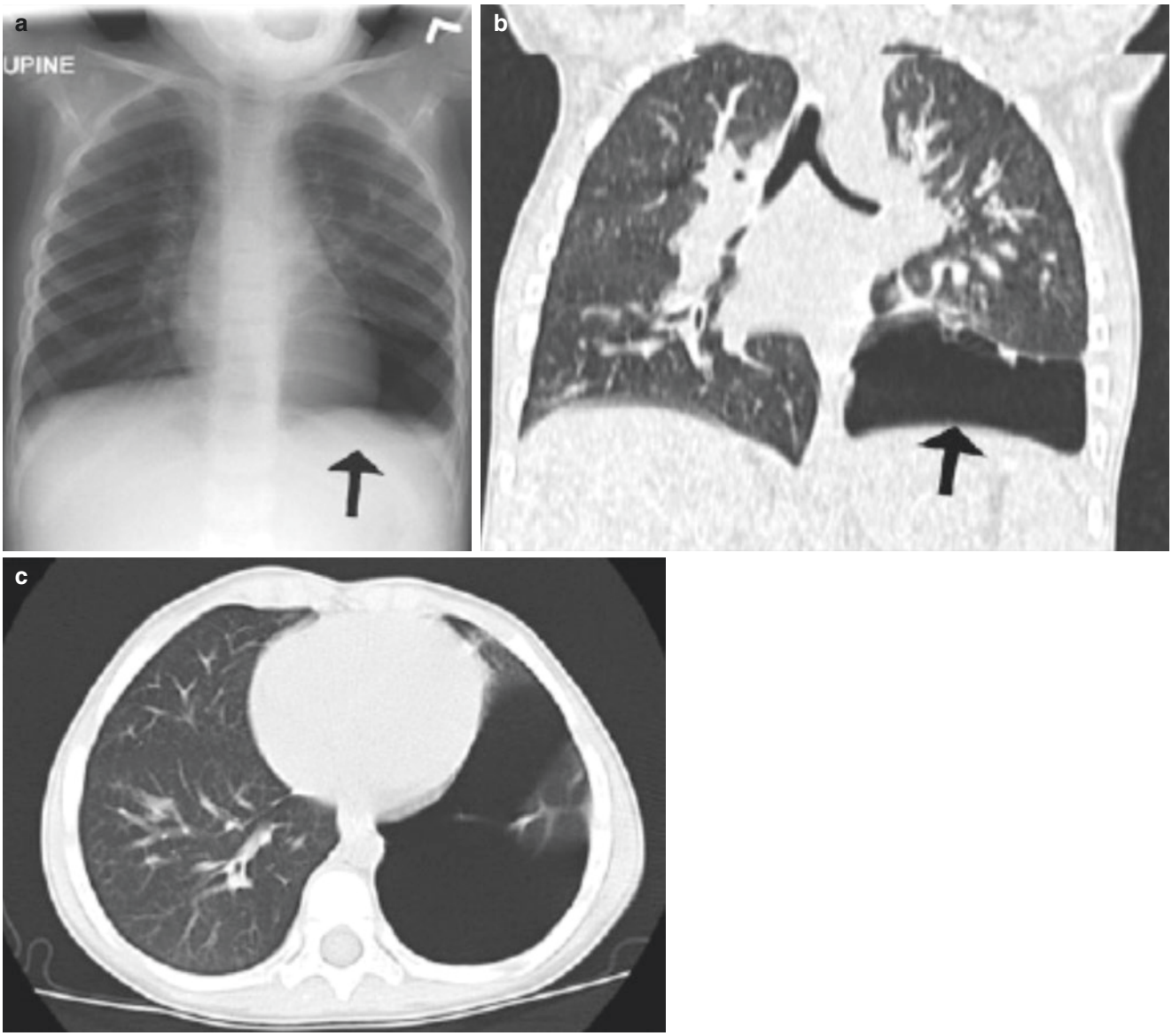

Fig. 7.8 Pleuropulmonary blastoma (PPB) type 1 in a 3-year-old boy. (**a**) Frontal chest radiograph shows solitary lucent cyst (arrow) at left lower hemithorax. (**b**, **c**) Axial lung window and coronal reformation CT images show large thin-walled cyst (arrow) at left lower hemithorax, which is indistinguishable from a large cystic congenital pulmonary airway malformation

other types. If it recurs after treatment, it tends to recur as a more aggressive subtype. Children with PPB are at increased risk of other childhood tumors [24–26]. Tumors associated with PPB include cystic nephroma, Sertoli-Leydig tumors of the ovaries, and small bowel polyps in the pediatric population [23–26].

Bilateral Lesions

Cystic Fibrosis (CF)/Bronchiectasis

Pediatric patients with cystic fibrosis may have cystic-appearing lesions due to abscesses, cystic or saccular bronchiectasis, and/or bullae [27]. CF patients have additional findings of bilateral diffuse lung disease with hyperinflation and linear and patchy, confluent opacities [28]. These changes may be initially upper lobe predominant. Hilar and paratracheal adenopathy are common. Additionally, 10% of CF patients also have findings of allergic bronchopulmonary aspergillosis (ABPA). Bullae may rupture, leading to intractable pneumothorax. CF is a multisystem disease; and findings of paranasal sinus disease, fatty liver and/or pancreas, and bowel obstruction may also be noted on radiographs or CT.

Other less common causes of bronchiectasis include asthma with ABPA, recurrent aspiration pneumonia (usually in patients with neuromuscular disorder), chronic aspirated foreign body, congenital immunodeficiency disorder (e.g., severe combined immunodeficiency and chronic granulomatous disease of childhood), HIV/AIDS, and immotile cilia syndrome, which may feature situs inversus totalis (Kartagener syndrome). Bronchiectasis is best evaluated with high-resolution chest CT (HRCT), which may reveal thick or beaded bronchial walls, bronchial diameter greater than that of the adjacent artery (signet ring appearance), and lack of distal tapering. Distal air trapping may also be seen.

Septic Pulmonary Emboli

Septic emboli typically appear as cavitary nodules which are bilateral and involve the lower and peripheral lungs. Such children are acutely ill and septic. The margins of the nodules may be ill defined, and feeding vessels are often noted. Air bronchograms may be seen within the nodules. The additional finding of peripheral wedge-shaped opacities suggests the diagnosis. Imaging often reveals the source of the infection such as a central venous catheter, cardiac valve vegetation, abscess, or jugular vein thrombosis due to pharyngitis (Lemierre syndrome) [29, 30] (Fig. 7.9). A situation as seen with Lemierre syndrome may also rarely be encountered with septic thrombosis of other veins remove from the head and neck.

Atypical Infections

Nonbacterial infections can produce pulmonary nodules or confluent consolidations, which may cavitate. These include fungal infections, such as *Aspergillus* (nodules may be surrounded by a ground-glass halo), mucormycosis, blastomycosis, and coccidioidomycosis [13]. These may form fungus balls within air-filled cavities (Fig. 7.10). Other considerations include opportunistic infections such as nocardiosis and candidiasis. Pneumocystis pneumonia, atypical mycobacterial infections, and lymphocytic interstitial pneumonitis in patients with HIV infection can also be associated with cyst formation [31].

In childhood tuberculosis, partially air-filled cavities can form via several different mechanisms. First, postprimary TB may be seen in older children in the typical upper lobe distribution commonly seen in adults. Second, in young or immunocompromised children, progressive endobronchial spread caused by rupture of the liquefied Ghon focus into a bronchus can lead to development of bilateral, multiple, and small cavitary lesions. Third, in children under 3 years of age, mediastinal adenopathy is a prominent manifestation of the infection. Secondary bronchial obstruction by enlarged lymph nodes can lead to caseous liquefaction distal to the obstruction. The cavity is thick walled with an air-fluid level and surrounding dense consolidation [32]. Finally, pneumatocele may form in the recovery phase of the disease.

Hydrocarbon Pneumonitis

Due to their low viscosity, ingestion of hydrocarbons such as lighter fluid, wood polish, gasoline, and kerosene typically leads to aspiration of these chemicals, which destroys surfactant and causes severe pneumonitis [33]. Affected young children typically show radiographic abnormalities by 12–24 hours, developing patchy and then confluent airspace opacities in both medial lower lung zones. Pneumothorax and pneumomediastinum may also be seen. Pneumatoceles may develop as the patient clinically improves. Resolution of radiographic abnormalities frequently lags behind rapid clinical improvement.

Vasculitides

Granulomatosis with polyangiitis is a small vessel vasculitis that affects multiple organ systems including the lungs, kidneys, nasopharynx, and paranasal sinuses [34]. The disease usually presents in the teenage years. Findings include pulmonary nodules and small masses, some of which are cavitary [35] (Fig. 7.11). Plain radiographs in children frequently show multifocal, ill-defined interstitial, and airspace opacities [36]. On CT, nodules are the most common finding. Also common are ground glass opacities and multifocal areas of airspace opacification [37, 38]. Vessels may be seen leading

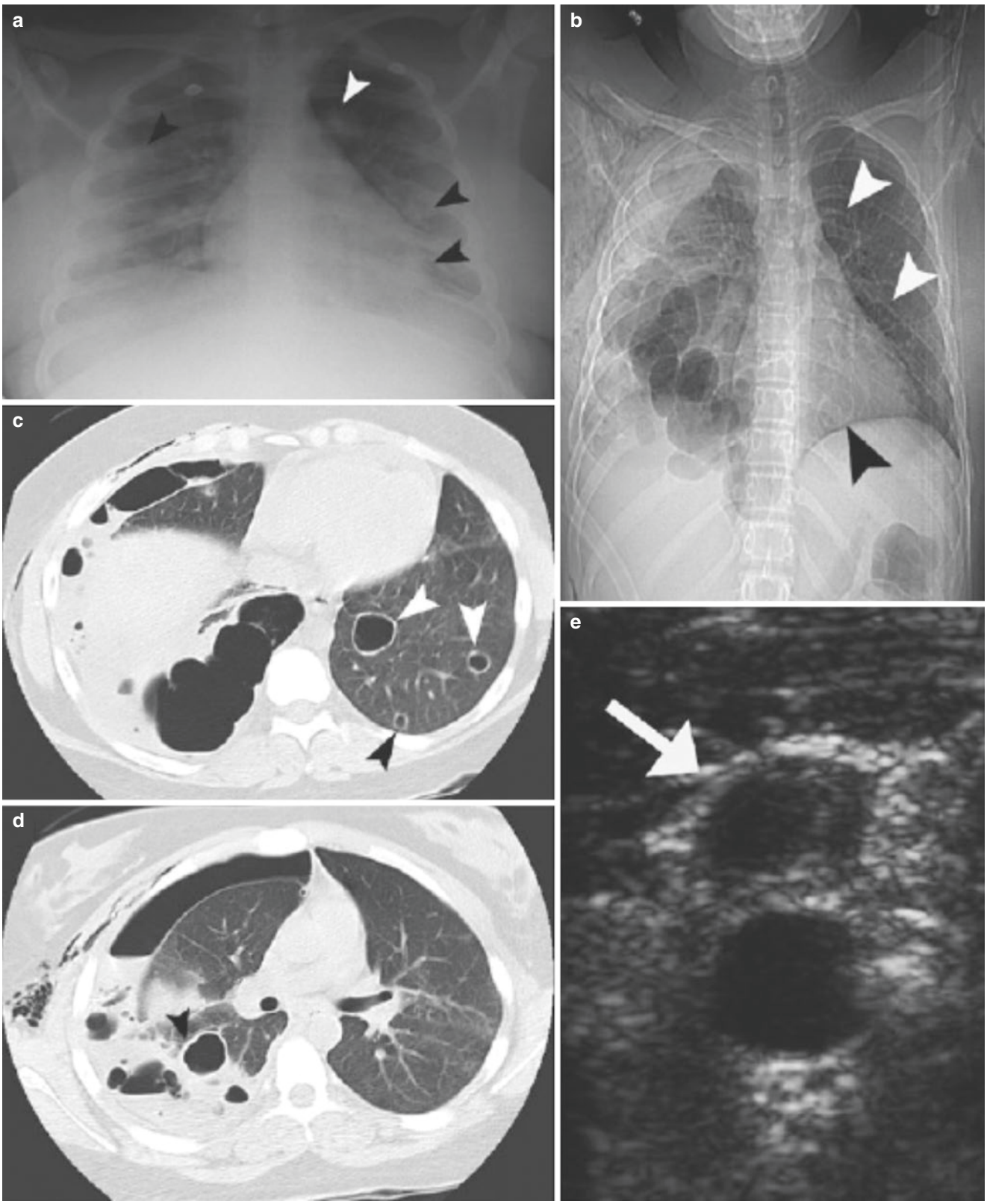

Fig. 7.9 Septic emboli in a 16-year-old girl with recent history of sore throat and fever. Blood cultures were positive for *Fusobacterium necrophorum*. (**a**) Initial frontal chest radiograph shows ill-defined, rounded opacities (*arrowheads*) and right peripheral pleural-based opacity consistent with pleural fluid. (**b**) Scout image from CT obtained 6 days later shows thin-walled lucent cysts (arrowheads) on the left and multiple air-filled cavities on the right with a chest tube. (**c**) Axial lung window CT image demonstrates thin-walled intraparenchymal cysts (arrowheads) on the left. The air collections on the right are loculated in the pleural space. (**d**) Axial CT image superior to (**c**) shows an intraparenchymal cyst (arrowhead) on the right with thicker wall and adjacent airspace opacity. (**e**) Ultrasound image demonstrates thrombosis (arrow) of the left internal jugular vein

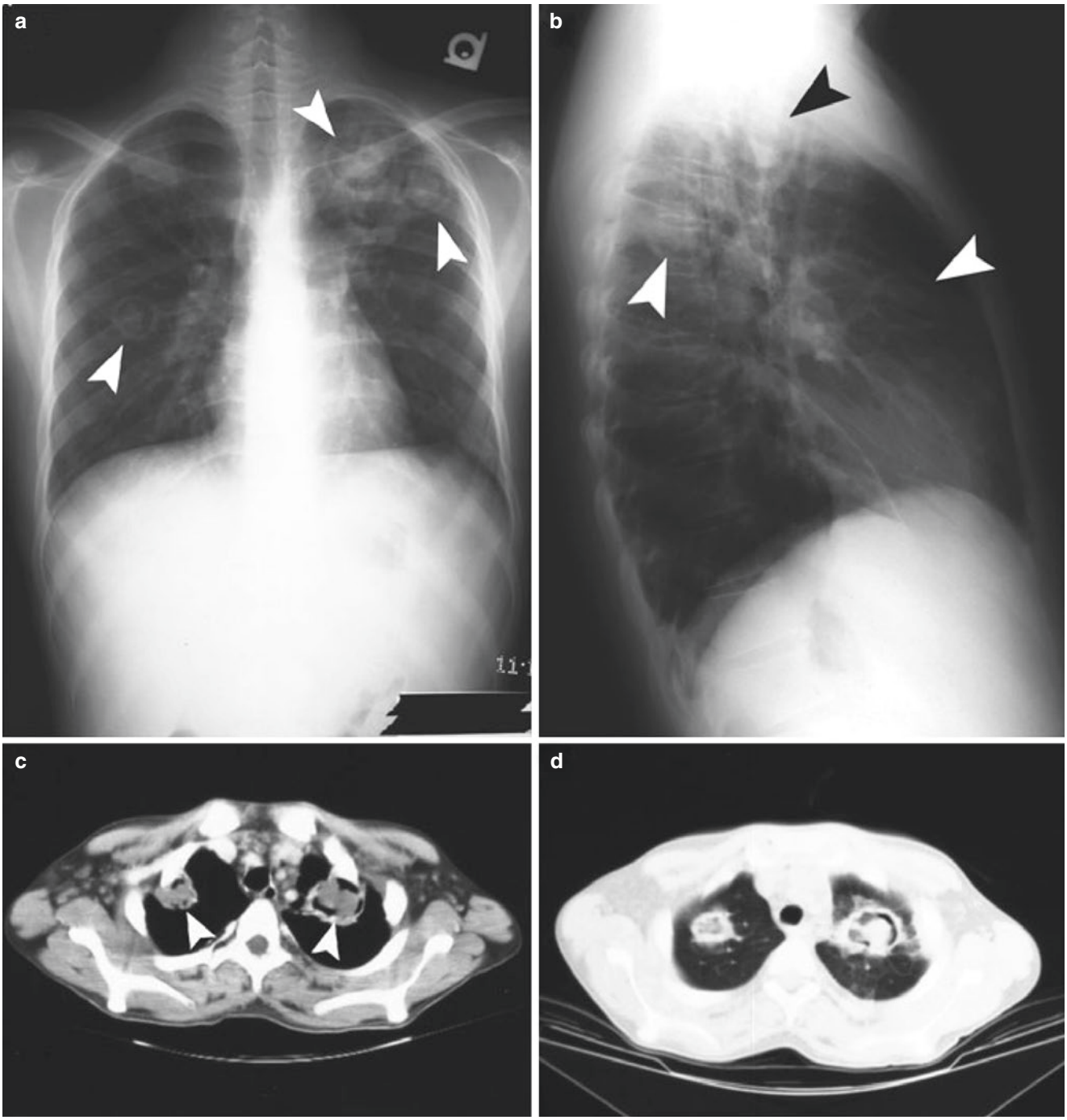

Fig. 7.10 Mucormycosis with fungus balls in a 14-year-old boy on chemotherapy for acute lymphoblastic leukemia. (**a**, **b**) Frontal and lateral radiographs show multiple bilateral upper lobe cysts (arrowheads) filled with soft tissue attenuation masses. (**c**, **d**) Enhanced axial soft tissue window and lung window CT images show an air-filled cyst with thick, ill-defined walls containing a fungus ball (arrowhead) on the left. On the *right*, a large cavitary nodule (arrowhead) is seen

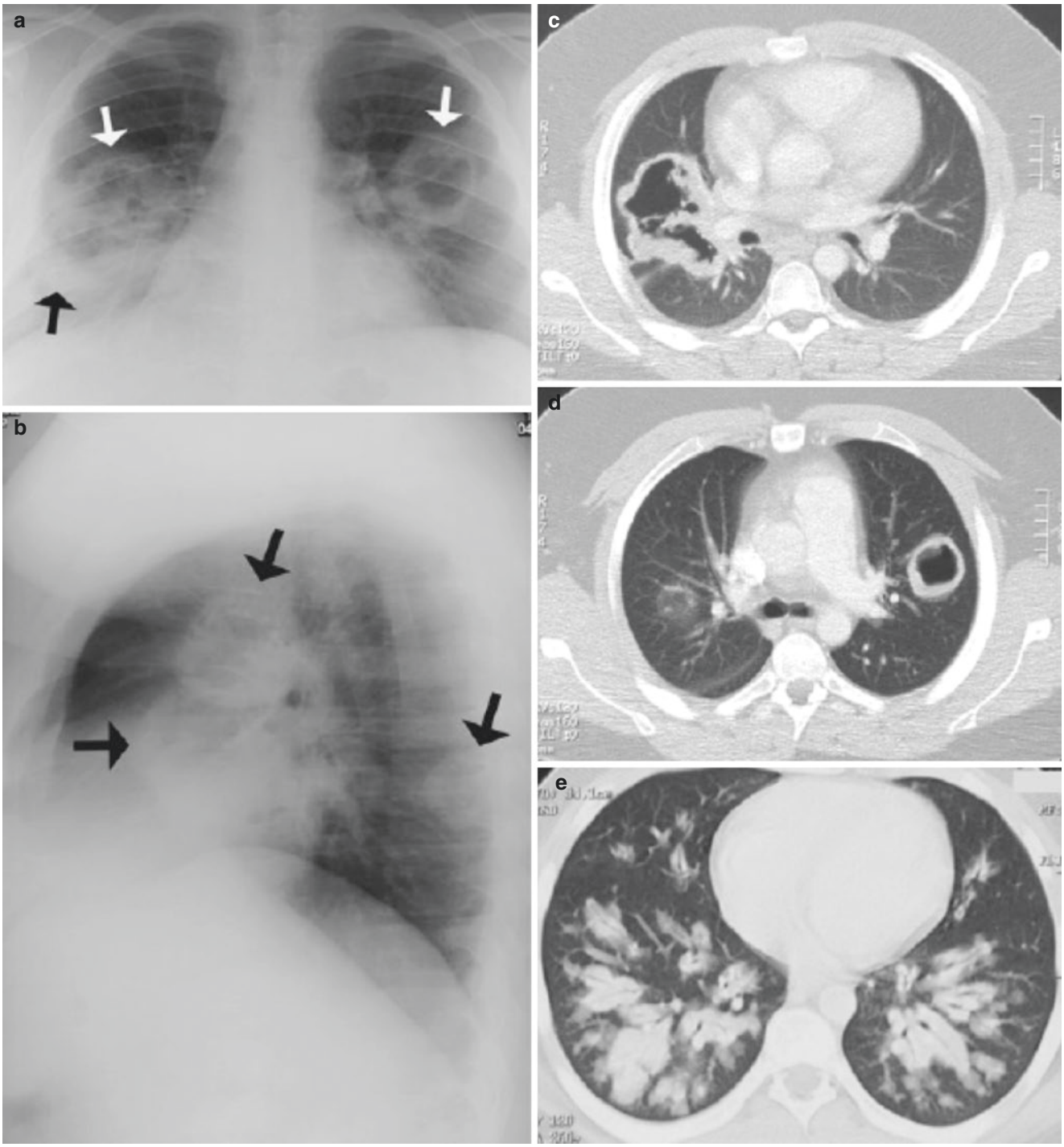

Fig. 7.11 Granulomatosis with polyangiitis (previously known as Wegener granulomatosis) in a 23-year-old man diagnosed 9 years prior. (**a**) Frontal and (**b**) lateral chest radiographs reveal bilateral cavitary round masses (*arrows*). (**c**, **d**) Axial lung window CT images demonstrate bilateral thick air-filled masses with thick, irregular walls. (**e**) Axial lung window CT image in a 14-year-old boy with granulomatosis with polyangiitis shows nodular opacities containing air bronchograms

to the nodules, and the margins of the nodules are often irregular or spiculated. Air bronchograms may be seen within the nodules (Fig. 7.11). Areas of consolidation are common, and peripheral wedge-shaped opacities may also be seen. Diffuse pulmonary hemorrhage may occur [37, 39]. Additional findings of paranasal sinus disease may be noted.

Collagen vascular diseases may also involve the lung, but less frequently in children than in adults. Systemic sclerosis, or scleroderma, may cause large, thin-walled cysts in the upper lung zones in addition to peripheral interstitial fibrosis and ground glass opacities on high-resolution chest CT [40]. A dilated esophagus may also be observed.

Laryngotracheal (Juvenile) Papillomatosis

Laryngotracheal papillomatosis consists of lobulated or sessile benign cellular proliferations of the larynx or trachea thought to be related to human papilloma virus (HPV) infection acquired from the mother in the perinatal period. The peak age at diagnosis is almost 4 years. The lesions grow and recur necessitating multiple repeated surgical debulking procedures. These procedures are thought to facilitate endobronchial spread of the lesions to the lungs. The tumors appear as bilateral nodules, some of which are cavitary, with thick or thin walls. Occasionally, papillary lesions may be seen in the airway on CT (Fig. 7.12). Malignant degeneration to squamous cell carcinoma occurs in less than 2% of patients and should be suspected when a large mass develops. Even without malignant degeneration, pulmonary involvement carries a poor prognosis, as the tumors grow slowly but relentlessly and destroy the adjacent lung [41].

Langerhans Cell Histiocytosis (LCH)

LCH is an idiopathic proliferative disorder of dendritic cells of the reticuloendothelial system. The disease may be localized to one organ system or disseminated. About 10% of children with localized or disseminated LCH have lung involvement at presentation [42]. In the lungs, peribronchiolar proliferations produce small nodules (1–10 mm) with irregular margins that often cavitate, forming thin- and thick-walled cysts best demonstrated on high-resolution chest CT [43–46]. The earliest manifestation is interstitial prominence. Later nodules predominate, and later yet cystic changes prevail [47]. The disease predominantly involves the upper lungs symmetrically with sparing of the bases and pleural margins. The finding of nodules and cysts in this distribution on high-resolution chest CT in the appropriate clinical setting allows a confident diagnosis [46]. Lung volumes are normal to increased. Spontaneous pneumothorax occurs in about 10% of patients (Fig. 7.13). In younger children in whom the disease is more likely to be disseminated and aggressive, additional findings in other organ systems, such as lytic bone lesions or hepatosplenomegaly, may suggest the diagnosis (Fig. 7.14).

Metastasis

Metastases are rarely cavitary. Squamous cell carcinoma commonly cavitates but is quite rare in children. Sarcomas, which are more common in children, may cavitate. These may also be associated with spontaneous pneumothorax. Metastatic angiosarcoma may rarely occur in children and may appear as multiple thin-walled cysts [48].

Lung Disease Associated with Syndromes

Lymphangioleiomyomatosis (LAM) is a rare interstitial lung disease with thin-walled cysts, affecting almost exclusively women of child-bearing age. The condition can be sporadic or associated with tuberous sclerosis. Affected pediatric patients most commonly present with progressive dyspnea.

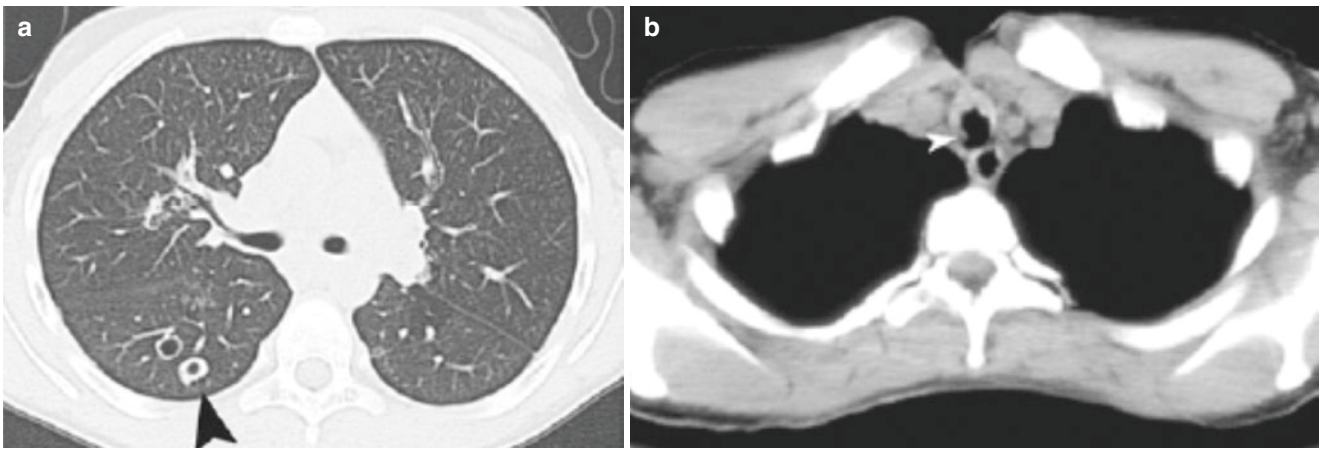

Fig. 7.12 Eleven-year-old girl with history of multiple surgical procedures for laryngotracheal papillomatosis. (**a**) Axial lung window CT image shows thin- and thick-walled pulmonary nodules (*arrowhead*). (**b**) Axial soft tissue CT image at the level of the trachea in another pediatric patient shows a small polypoid mass (arrowhead) projecting from the wall of the trachea

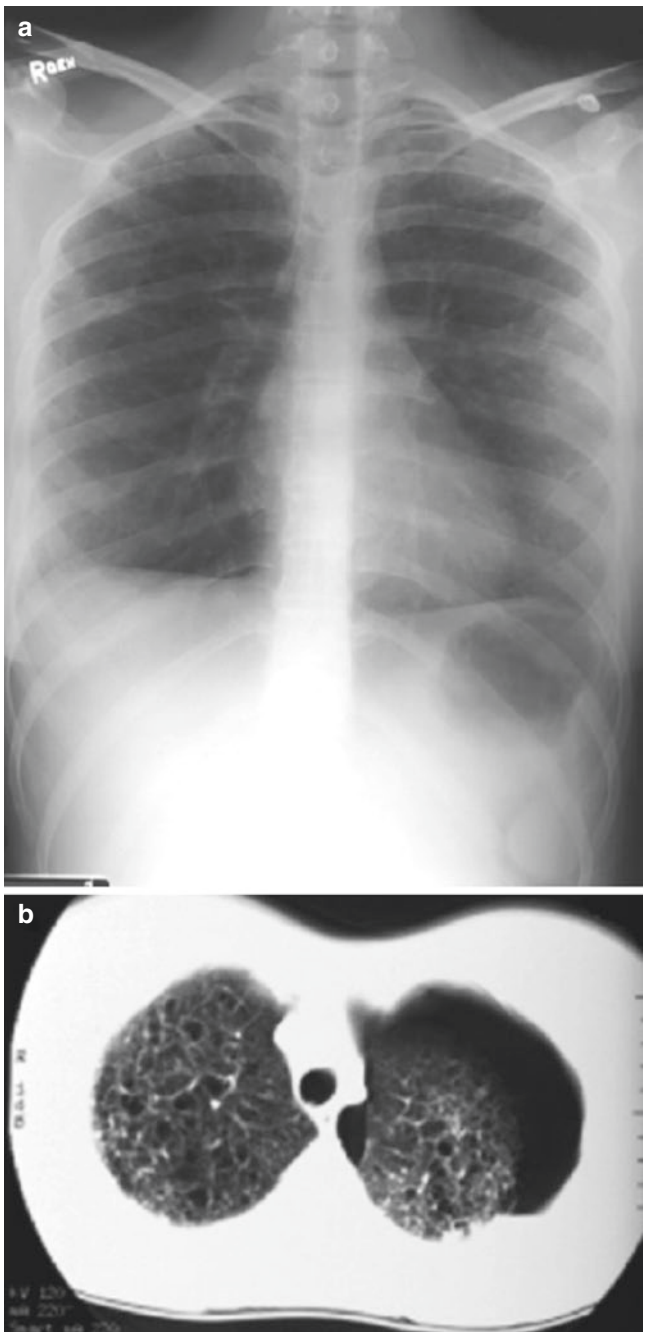

Fig. 7.13 Localized form of Langerhans cell histiocytosis in an 18-year-old male smoker. (**a**) Frontal radiograph shows upper lobe-predominant interstitial lung disease. (**b**) Axial non-enhanced lung window CT image shows diffuse small lucent cysts throughout the upper lobes and a left spontaneous pneumothorax

Cough and chest pain are also common complaints. Chest pain is due to spontaneous pneumothorax, which is found in about half of patients at initial presentation. Affected pediatric patients may also develop chylous effusion.

Radiographs typically show hyperinflation and linear, reticular opacities and apical sparing. Cysts may be visible on plain radiographs, particularly when the disease is severe. Pneumothorax and pleural effusion are also common findings (Fig. 7.15). On CT, thin-walled cysts are seen virtually in all patients. They are usually small (2–5 mm) and uniformly distributed throughout the parenchyma, although there may be relative sparing of the apices (Fig. 7.16). In severe disease, there are larger cysts, which may replace most of the parenchyma. High-resolution chest CT may demonstrate interlobular septal thickening. Nodules are generally not identified. Pleural effusion with an attenuation coefficient less than zero may also be observed.

Extrapulmonary manifestations may be noted in patients with sporadic LAM as well as in tuberous sclerosis. Affected pediatric patients may have one or more renal angiomyolipomas, chylous ascites, and masses along the lymph node chains of the mediastinum, retroperitoneum, and pelvis. Affected pediatric patients with tuberous sclerosis may also have dermatologic manifestations, neurologic stigmata, renal cysts and angiomyolipomas, and cardiac rhabdomyomas (Fig. 7.16).

The imaging differential diagnosis for pulmonary LAM includes LCH, but the latter is distinguished by the finding of nodules as well as cysts and a predilection for the upper lobes. Additionally, LCH occurs in males as well as females. Pneumothorax occurs in both LAM and LCH, but is more common in LAM. The natural history of sporadic LAM is usually progression to respiratory failure and cor pulmonale frequently requiring heart-lung transplant. Affected pediatric patients with LAM and tuberous sclerosis typically remain relatively asymptomatic for their lung disease [49].

Proteus syndrome is a rare congenital hamartomatous disorder characterized by hemihyperplasia, decreased subcutaneous fat, palmar and plantar overgrowth, cutaneous and subcutaneous masses including vascular lesions, and kyphoscoliosis. Approximately 10% of affected patients may develop lung cysts consisting of hyperexpanded airspaces [50]. The cysts are usually large and multiple. The course of the lung disease is progressive and may require heart-lung transplant for survival [50].

Other congenital syndromes may also be associated with cystic changes in the lung. Patients with Down syndrome may have subpleural lung cysts, which are best detected with CT. A study of 25 patients revealed a prevalence of 36% [51]. They occur independent of congenital heart disease and may reflect reduced postnatal development of peripheral alveoli and peripheral airways [52]. These are most commonly found in the anteromedial lungs and may also be found along fissures or surrounding bronchovascular bundles [51, 52].

Pediatric patients with neurofibromatosis type 1 typically have apical bullae and thin-walled cysts in their lungs, along with reticular disease and fibrosis. The pulmonary abnormalities are usually diagnosed in adulthood [53]. Additionally, Marfan syndrome may be associated with diffuse or apical

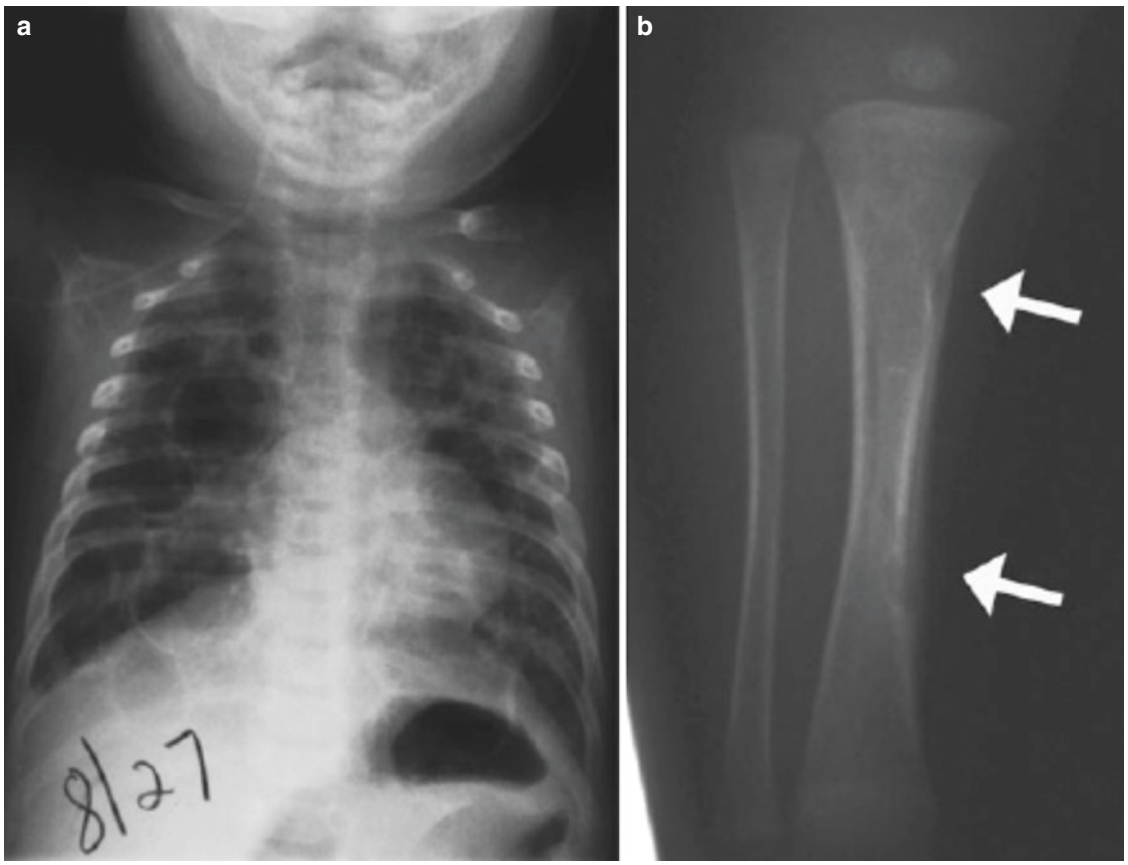

Fig. 7.14 Disseminated form of Langerhans cell histiocytosis in a 3-year-old boy involving the pulmonary and musculoskeletal systems. (**a**) Frontal chest radiograph shows extensive lucent cysts throughout both lungs. (**b**) Frontal radiograph of the right leg shows eccentric lucent lesions of the medial diaphysis of the tibia with adjacent periosteal thickening (*arrows*)

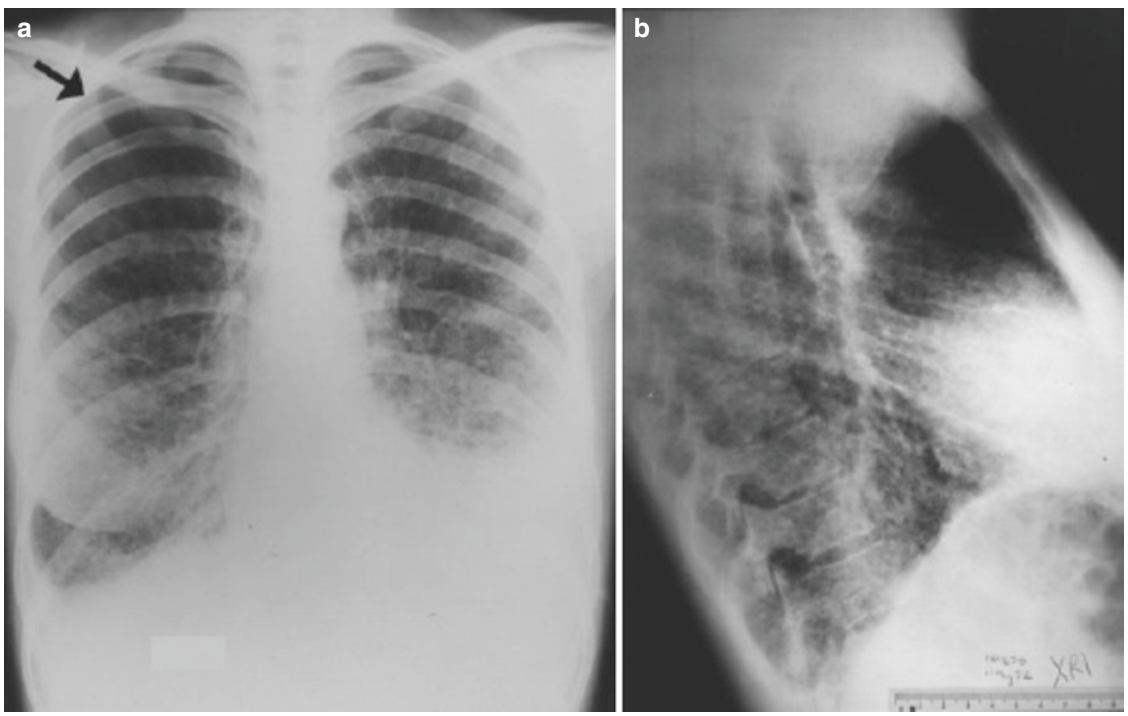

Fig. 7.15 Lymphangioleiomyomatosis in a 22-year-old woman with history of normal chest radiographs 2 years prior. (**a**) Frontal radiograph shows diffuse interstitial lung disease with small round lucent foci with apical sparing. Additional findings include right pneumothorax (arrow) and bilateral effusions, which along with the age and gender of the patient suggest the diagnosis. (**b**) Lateral radiograph obtained 8 months prior shows to better advantage the diffuse reticular opacities and interposed small round lucencies. Note mild hyperinflation

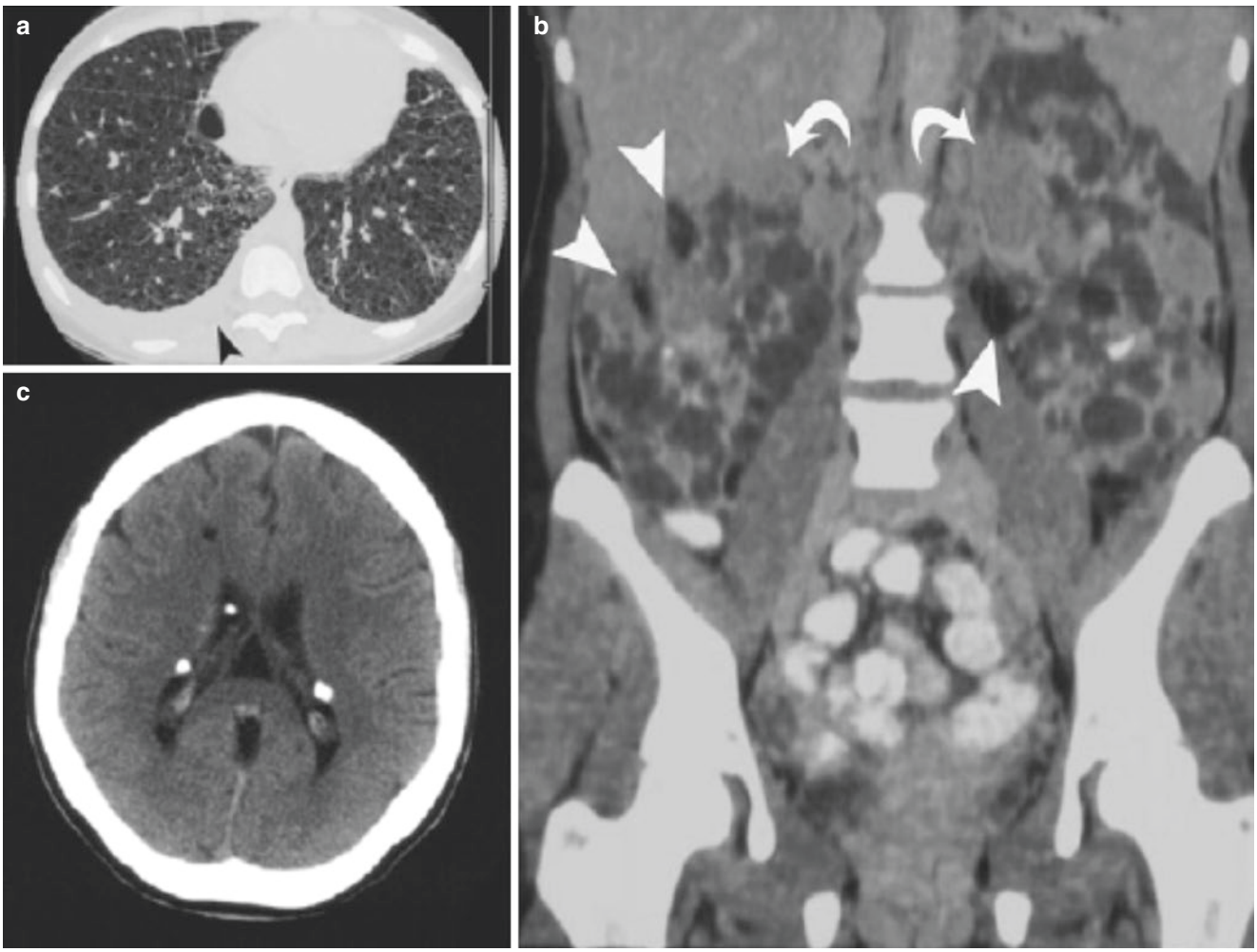

Fig. 7.16 Lymphangioleiomyomatosis in a 29-year-old woman with tuberous sclerosis. (**a**) Axial HRCT image shows diffuse small cysts with imperceptible walls throughout both lungs. Note also the right pleural effusion (*arrowhead*). (**b**) Coronal enhanced CT image shows multiple fluid attenuation cysts throughout both kidneys along with foci of fat attenuation (*arrowheads*) and soft tissue attenuation (*curved arrows*) indicating angiomyolipomas. (**c**) Axial CT image through the lateral ventricles of the brain reveals calcified subependymal nodules of tuberous sclerosis

bullous disease and cyst formation, particularly in males. Upper lobe fibrosis may also be seen. Affected pediatric patients often develop recurrent spontaneous pneumothorax (11%) which may present in adolescence [54].

In summary, lucent cystic lesions on imaging may be distinguished based on age at presentation and on the distribution of the findings in the lungs. Additional features, such as the presence of nodules or peripheral wedge-shaped opacities, and clinical signs and symptoms, such as fever and systemic illness or underlying chronic condition, can further narrow the differential diagnosis.

Nodular Lung Disease

This section, which incorporates a conglomerate of different entities based on the common radiographic appearance of solitary or multiple pulmonary nodules, is divided into anomalies that tend to cause solitary nodules and those that cause multiple nodules. Because developmental, infectious, inflammatory, hemorrhagic, and neoplastic disorders can all give the appearance of pulmonary nodules, many different disease entities are touched upon or discussed in this chapter or discussed elsewhere in this textbook in greater detail. Each section describes the clinical or radiological traits of the various diseases characterized by pulmonary nodules.

A pulmonary nodule is a round opacity surrounded by normal lung tissue. Pulmonary nodules that arise close to the pleural surface may be difficult to distinguish from masses arising from the pleura or chest wall; however, an acute angle between the nodule and the chest wall suggests it may have originated from within the lung parenchyma. Radiographically, a *nodule* is defined as an opacity measuring 3 cm or smaller in size. *Masses* are defined as 3 cm or larger in size. In this chapter, the term nodule is used more loosely and may include rounded opacities larger than 3 cm.

An *opacity* is a general radiographic term for any soft tissue density lesion in the lung. Unfortunately, radiographs cannot discern the composition of the opacity, whether fluid, blood, or cellular; and many entities that give rise to nodules may be comprised of a combination of these substances. Computed tomography (CT) and MRI are more specific in determining the underlying composition of nodules. Nodules are also characterized by growth rate, margins, and various internal characteristics. Additional clinical history, physical examination, and laboratory tests are crucial in determining a differential or specific diagnosis for lung nodules. Finally, results from a percutaneous or open biopsy provide a specific pathological diagnosis. Nuclear medicine studies, including PET, are not currently used to characterize pulmonary nodules but primarily to follow primary or metastatic tumors.

Solitary Pulmonary Nodules

Unlike the case in adults, a solitary pulmonary nodule in a child is generally not a harbinger of malignancy. In the absence of a known underlying malignancy, solitary pulmonary nodules in children are generally benign and congenital or infectious in nature. Primary pulmonary malignancies are extremely rare [26]. This section classifies solitary pulmonary nodules into of underlying congenital, infectious, neoplastic, and vascular causes. Because congenital lung malformations are discussed in Chap. 6 of this book, this chapter focuses on infectious, neoplastic, and vascular causes of solitary pulmonary nodules.

Infectious Lesions

Infections are likely the most common cause of nodules in the pediatric population.

Round Pneumonia

One of the most common causes of a pulmonary nodule or a mass-like opacity on chest radiography in a child is bacterial pneumonia [55, 56]. In children younger than 8 years of age whose collateral pathways of circulation have not yet developed, some bacterial pneumonias appear round and may mimic a mass. However, unlike classical bacterial pneumonias, round pneumonias may not have air bronchograms and tend to resolve on follow-up imaging. They are most commonly found posteriorly. In a pediatric patient with the appropriate clinical history, a round mass in the chest is most likely to be due to pneumonia (Fig. 7.17). The most common pathogen causing round pneumonia is *S. pneumoniae* [55, 56]. In cases where round pneumonia becomes necrotic and cavitates, an air-fluid level may be seen on upright views of the chest or by CT. Pneumonias are discussed more thoroughly in the section on pneumonia in this textbook.

Tuberculosis

Tuberculosis (TB) is an infection caused by any of the *Mycobacterium* complex mycobacteria (*Mycobacterium*

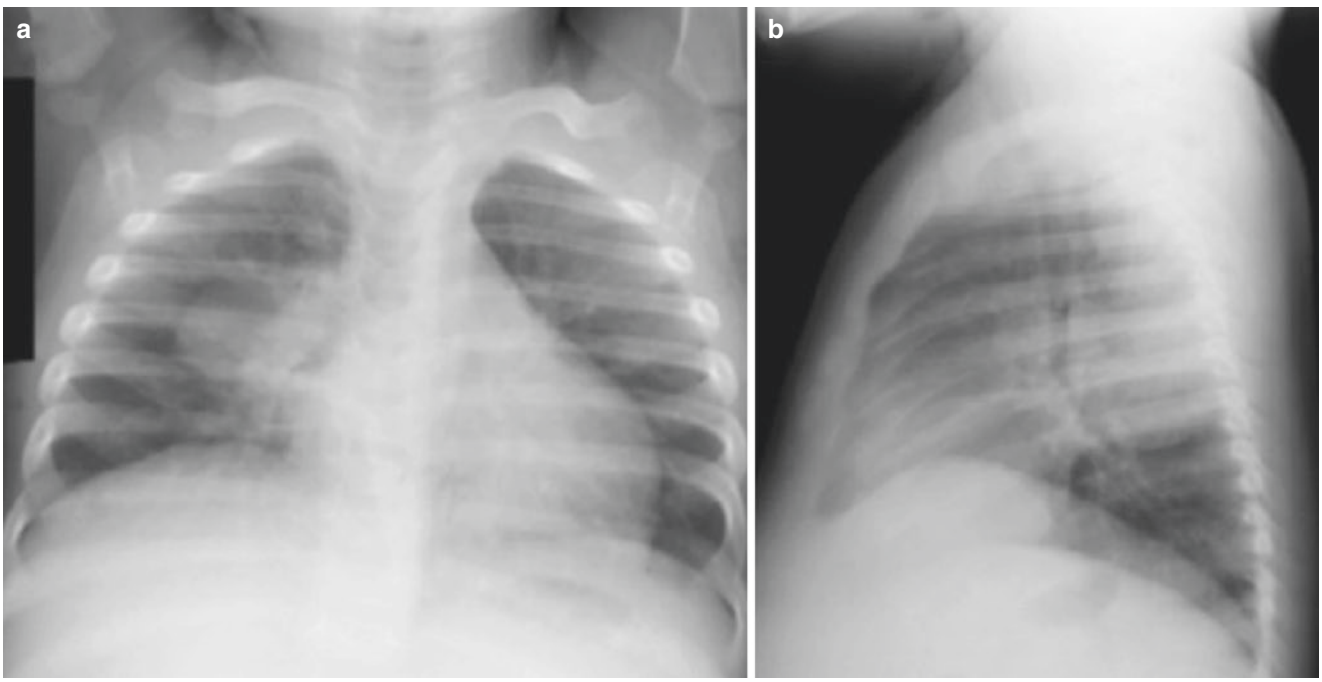

Fig. 7.17 Round pneumonia in a 5-year-old boy who presented with cough and fever. (**a**) Frontal radiograph and (**b**) lateral radiograph show a round mass-like opacity located in the superior segment of the right upper lobe. Subsequently obtained chest radiograph after treatment showed complete interval resolution

tuberculosis, *Mycobacterium bovis*, *Mycobacterium africanum*, *Mycobacterium microti*, and *Mycobacterium canettii*). *M. tuberculosis* is the most common cause of this disease worldwide [57].

The lungs are the most commonly affected organ because most tuberculous infections are caused by aspiration or inhalation of the tubercle bacillus. From the lungs, the bacilli may spread hematogenously to infect any part of the body. Affected children appear to have a higher risk of developing extrapulmonary TB than adults [57, 58]. Primary pulmonary tuberculosis occurs after a 2–10-week incubation period. The most classic finding of primary pulmonary tuberculosis is the "primary complex," which consists of a solitary peripheral parenchymal opacity, resembling bacterial lobar pneumonia, and enlargement of mediastinal and regional lymph nodes (92%) (Fig. 7.18) [57–59]. Lymphadenopathy is a more common finding in primary tuberculosis in children than parenchymal opacity [57–60]. If the pulmonary focus abuts or affects the pleura, pleural thickening and effusion often results. Affected pediatric patients may also present with signs of air trapping as the primary infection may affect the airway directly or surrounding hilar lymph nodes, causing airway obstruction [57–62]. Six months following the initial formation of the primary lung infection, greater than 50% of the pulmonary opacities and lymph nodes calcify, thus creating the radiographic findings of prior TB infection commonly seen in adults [57–62].

Miliary tuberculosis may develop within 6 months of the primary infection and results from hematogenous spread. The result is innumerable tiny nodules scattered throughout the lungs and other organs, particularly the liver and spleen [57–63].

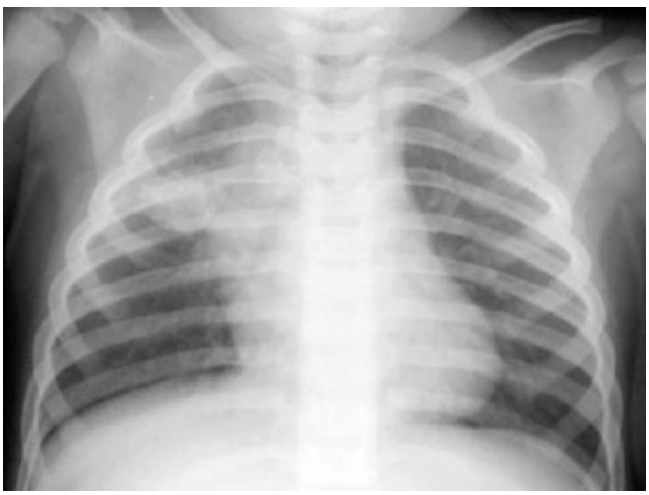

Fig. 7.18 An infant boy who presented with fever and history of a mother who died of tuberculosis. Frontal chest radiograph demonstrates a right upper lobe partially calcified opacity and right hilar and paratracheal adenopathy, consistent with primary tuberculosis

Primary tuberculosis may be treated successfully or may progress or recur as postprimary tuberculosis. Postprimary tuberculosis results from the growth of previously dormant bacilli in the apices of the lung. The reactivated lesions typically found in the apical and posterior segments of the upper lobes are necrotic and often appear cavitary. The cavities have irregular thick walls readily seen on radiographs. Unlike primary tuberculosis, however, adenopathy is rare in postprimary TB. Reactivation tuberculosis is extremely uncommon in children, especially if the primary infection occurs before 2 years of age [57–64].

Fungal Infections and Certain Bacterial Infections That Resemble Fungi

Fungal infections can have a variety of appearances but, in general, mimic tuberculosis radiographically. Fungal infections and tuberculosis can be distinguished by history, clinical examination, skin, and laboratory tests. Most pulmonary fungal infections are caused by aspiration and are especially virulent in immunocompromised pediatric patients. Histoplasmosis, coccidioidomycosis, and blastomycosis also cause pulmonary infections in immunocompetent hosts. Actinomycosis and *Nocardia*, two types of bacterial infections, are also discussed in this section as they mimic fungal infections.

Histoplasmosis is a fungal infection caused by inhaling *Histoplasma capsulatum*, a fungus endemic to the Ohio and Mississippi River valleys, spread by contaminated bird and bat feces. Ninety-five percent of affected patients are asymptomatic during the initial infection, and the radiographic manifestations are often not documented during this period because the disease is occult [65]. Radiographic manifestations of remote infection include multiple calcified nodules in the lungs, liver, and spleen and are often found incidentally [129]. Chronic histoplasmosis may develop in pediatric patients with underlying lung disease and, like tuberculosis, presents as a cavitary mass in the lungs. Progressive disseminated histoplasmosis occurs in immunocompromised hosts and results from hematogenous spread of infection to anywhere in the body (Fig. 7.19) [66, 67].

Coccidioidomycosis, also called valley fever or desert rheumatism, is caused by aspiration of the *Coccidioides immitis* spores, a fungus endemic to California, Arizona, New Mexico, and Texas. Blastomycosis is an infection caused by inhaling *Blastomyces dermatitidis*, a fungus commonly found in the soil. This fungus is distributed throughout the world and in the United States; it is endemic to Mississippi, Kentucky, Arkansas, and Wisconsin. Most cases of coccidioidomycosis and blastomycosis are asymptomatic. On radiographs, chest abnormalities in acute and chronic infection mimic those seen in tuberculosis, although the adenopathy and effusions reported in 20% of adult cases have not been noted in neonates and infants [68, 69]. Approximately, 5% of patients with primary disease are left with chronic, residual lesions of the lung.

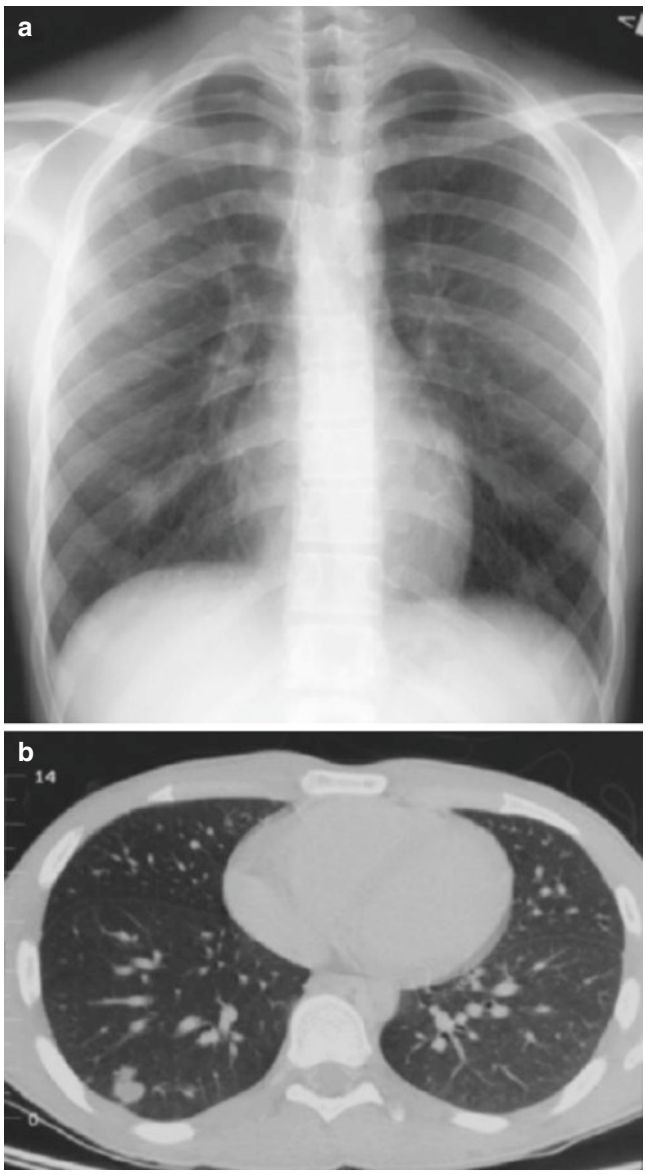

Fig. 7.19 A 16-year-old girl with a history of treated neuroblastoma who presented with right chest pain. (**a**) Chest radiograph and (**b**) axial lung window CT image show multiple bilateral pulmonary nodules, with the largest seen in the right lower lobe. Open biopsy of the right lower lobe nodule demonstrated histoplasmosis

Cryptococcus neoformans is a fungus that causes infections primarily in immunocompromised patients, especially patients with AIDS [70]. The most common form of this fungus is found in aged pigeon droppings. The inhaled spores most commonly cause infections in the lungs and may spread hematogenously resulting in meningitis. The initial pulmonary infection often has the appearance of a bacterial pneumonia or of solitary or multiple pulmonary nodules. Nodules may cavitate. In chronic or treated pulmonary infections, lymph nodes may calcify [70].

Candida albicans, the most common cause of pulmonary candidiasis, results from inhalation or aspiration of this yeast, which normally colonizes the upper respiratory tract. Hematogenous infection may occur in patients who are immunocompromised, have a history of prolonged antibiotic therapy, or have indwelling catheters. *Candida* infections acquired through aspiration appear as a focal opacity, similar to bacterial pneumonia, or as multiple nodules. Hematogenous candidiasis is characterized by microabscesses in the lungs, liver, spleen, and kidneys. In the lungs, these appear as tiny diffuse nodules [71, 72].

Infections caused by *Aspergillus fumigatus*, a ubiquitous mold, have a wide variety of appearances, which depend on the patient's immune status and the presence or absence of preexisting disease. The pulmonary disease is separated into four categories: ABPA, fungal balls or mycetomas, semi-invasive aspergillosis, and invasive aspergillosis. *Aspergillus* infections may present as solitary or multiple pulmonary nodules [73, 74].

ABPA is caused by a hypersensitivity reaction to *Aspergillus* colonizing the airways, occurring in 1–2% of patients with asthma and 7–9% of individuals with cystic fibrosis [75, 76]. The classical appearance of finger-like, tubular densities radiating from the hilum represents central dilated bronchi filled with mucus. Mucus plugging also causes areas of atelectasis or consolidation radiating from the hilum peripherally. Smaller airway mucus plugging causes additional peripheral opacities to form. Findings are often bilateral. *Aspergillus* may parasitize a preexisting pulmonary cavity or cyst, forming a mycetoma or fungus ball. Thus, the finding of a known pulmonary cystic lucency that becomes opacified should raise the possibility of a superimposed fungal infection.

Invasive aspergillosis is a severe, rapidly progressive, often fatal infection that occurs in immunocompromised neutropenic patients. In these patients, *Aspergillus* aggressively invades the airways and blood vessels, causing airway obstruction or hemorrhage, both of which can give the appearance of bilateral diffuse pulmonary nodules (Fig. 7.20). CT shows that the borders of the nodules are poorly defined forming a *halo* around the nodule. As the patient's neutropenia and the infection begin to resolve, the nodule cavitates [77]. Semi-invasive aspergillosis occurs in mildly immunocompromised patients and is a less severe disease than invasive aspergillosis [78].

Actinomycosis is caused by an anaerobic organism that combines traits of bacteria and fungi [79]. This is primarily an opportunistic infection that affects immunocompromised hosts. Chest wall invasion and enlarged lymph nodes, in addition to solitary or multiple pulmonary nodules, distinguish this infection from the others discussed in this section [79, 80].

Nocardia is an infection most commonly caused by *Nocardia asteroides*, with a small minority caused by *Nocardia brasiliensis* and *Nocardia farcinica*. Lung infec-

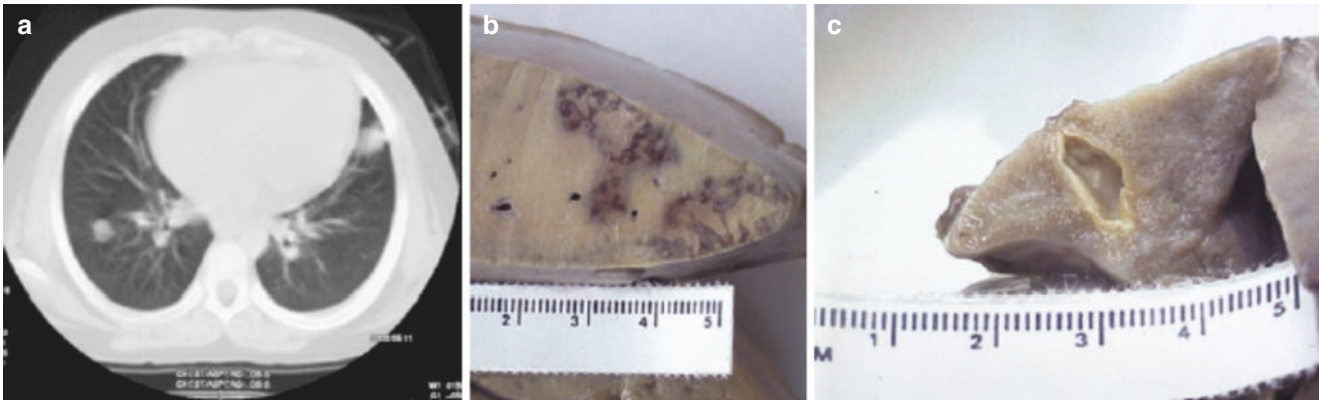

Fig. 7.20 A 7-year-old boy with presumed immunodeficiency who presented with 4 months of headache and was found to have a posterior fossa mass. Biopsy of the mass in the cerebellum revealed *Aspergillus*. (**a**) Axial lung window CT image demonstrates bilateral pulmonary nodules, which at (**b**, **c**) autopsy were found to be invasive aspergillosis

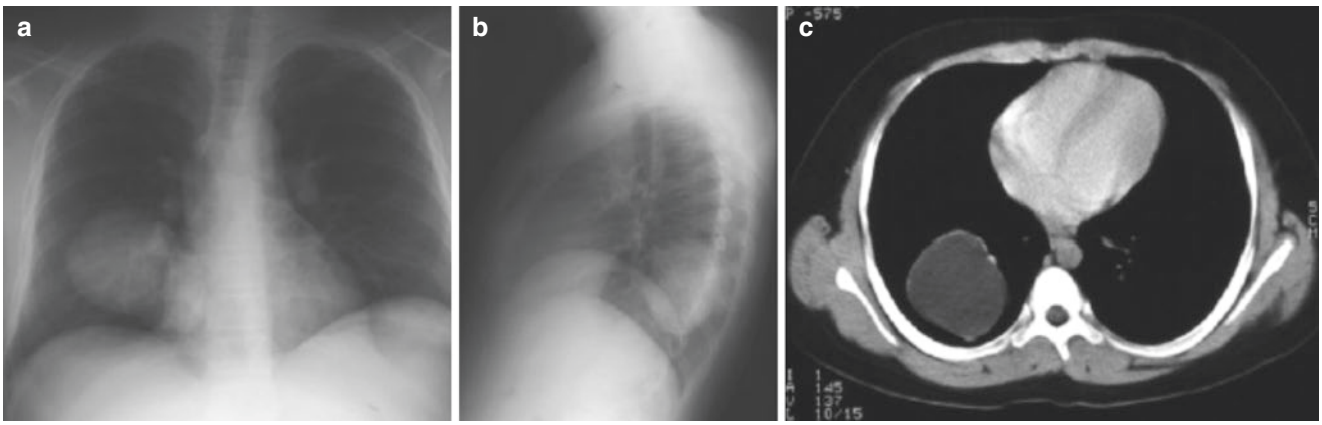

Fig. 7.21 A 7-year-old daughter of an Australian sheep farmer who presented with fever and chills. (**a**) Frontal and (**b**) lateral radiographs demonstrate a well-circumscribed right lower lobe mass which was found to be primarily cystic on (**c**) axial CT image. Surgical resection revealed a hydatid cyst

tion typically occurs in immunocompromised hosts [81]. Cavitation is a very common feature, both of consolidations and of multiple nodules [81–83], which are manifestations of the pulmonary disease.

Hydatid Cyst

In the endemic sheep- and cattle-raising areas around the world, larvae from the tapeworm *Echinococcus* are swallowed and may disseminate hematogenously throughout the body. The most commonly affected organs are the liver and lungs. As the hydatid enlarges, a round well-circumscribed cyst forms in the lung parenchyma. Between 7 and 38% of patients with lung disease have multiple cysts. As the cysts enlarge, they may cause mass effect on adjacent bronchi with resulting atelectasis or may erode into nearby structures. Up to 30% of lung cysts may be complicated by rupture into the pleural space or bronchus. CT is helpful in confirming the diagnosis and in better assessing complications (Fig. 7.21) [14].

Neoplastic Lesions

Tumors of the lung, both benign and malignant, are unusual in children. In a review of the files of the Armed Forces Institute of Pathology, over a 40-year period, 166 pulmonary tumors were found in patients 21 years of age or younger, and the ratio of benign to malignant tumors was 1:1.68. The most common tumor was the benign inflammatory pseudotumor, followed by three malignant tumors, bronchial adenoma, bronchogenic carcinoma, and mesenchymal tumors in order of frequency [26]. Some of these tumors are also discussed elsewhere in this textbook.

Inflammatory Pseudotumor

Inflammatory pseudotumor (inflammatory myofibroblastic tumor, plasma cell granuloma, histiocytoma, and xanthofibroma) is a distinctive but controversial lesion, usually occurring during childhood [84, 85]. Although rare, these are the most frequent primary lung tumors in childhood and are

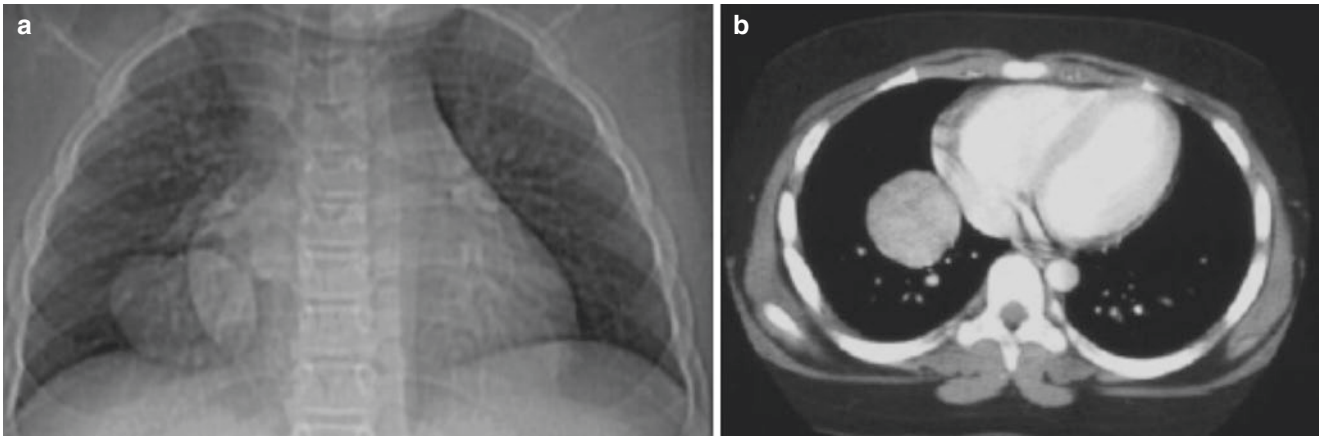

Fig. 7.22 A 17-year-old boy with an inflammatory pseudotumor confirmed upon surgical resection and pathological analysis. (**a**) Scout and (**b**) axial CT images show a well-circumscribed mass located in the right lower lobe

most commonly seen in older children [26, 84, 85]. The masses are composed of fascicles of bland myofibroblastic cells admixed with a prominent inflammatory infiltrate consisting of lymphocytes, plasma cells, and eosinophils. This lesion has been variously termed plasma cell granuloma, inflammatory myofibroblastic tumor, histiocytoma, xanthofibroma, inflammatory myofibrohistiocytic proliferation, and inflammatory fibrosarcoma, reflecting divergent views concerning its pathogenesis and malignant potential.

Pediatric patients with pseudotumor typically present with respiratory symptoms, chiefly cough, chest pain, fever, or hemoptysis. On radiographs, the lesions are typically solitary, well-defined nodules, but they may be multiple (Fig. 7.22). They are most commonly found in the lung parenchyma, although these lesions have also been found within the bronchi and trachea [84, 85]. Tumors arising within the airway can cause obstruction and likely contribute to the high percentage of patients presenting with respiratory symptoms. These tumors can invade adjacent non-pulmonary structures including the mediastinum, heart, and pulmonary artery [84–91]. Lesions may partially calcify; this can be seen on radiography and CT. The attenuation coefficient measured by CT is variable, however. Some lesions are uniform, while others are heterogeneous and demonstrate a variable amount of enhancement following the administration of intravenous contrast [87].

Inflammatory pseudotumors can cause secondary hypertrophic osteoarthropathy (HOA). HOA is a clinical syndrome of clubbing of the fingers and toes, enlargement of the extremities, and painful swollen joints. Radiographs typically show symmetric periostitis, an inflammatory reaction of the bones, involving the radius and fibula and, to a lesser extent, the femur, humerus, metacarpals, and metatarsals. After the lesion is removed, the bone findings resolve [92, 93]. The treatment of inflammatory pseudotumor is limited to complete resection [94, 95].

Hamartoma

Pulmonary hamartomas are congenital tumors composed of normal lung tissue in abnormal proportions. These pulmonary masses, composed of pulmonary, bronchial, and cartilaginous elements, are usually found incidentally. They are most commonly located in the right lower lobe. Rarely are these tumors endobronchial. These well-defined lesions are smoothly marginated and lobular in contour. The additional presence of coarse, large "popcorn"-shaped calcifications is clearly defined on plain radiographs or CT, which are helpful in making a confident diagnosis (Fig. 7.23). These benign lesions may grow slowly overtime [96, 97]. They can become quite large and may even simulate chest tumors of extrapulmonary origin [98].

Because pulmonary hemangiomas and chondromas contain bronchial and other pulmonary elements, these too can be considered hamartomas [99]. Occasionally, hemangiomas may be multiple. Chondromas are usually solitary and nearly half calcify (Fig. 7.24). Chondromas occur in 76% of patients with Carney's triad of pulmonary chondromas, gastric smooth muscle tumors, and extra-adrenal paragangliomas. In association with Carney's triad, chondromas are often multiple [100]. Choristomas are another type of pulmonary tumors that consist of non-pulmonary as well as pulmonary elements of hamartomas; but unlike hamartomas, these have no known growth potential. Confidently diagnosed hamartomas can be treated expectantly [101].

Bronchial Adenomas

Bronchial adenoma is the broad term for a group of malignant tumors arising from neuroendocrine cells in the lungs [1–4]. This group includes bronchial carcinoid, adenoid cystic carcinoma, and mucoepidermoid carcinoma; these lesions account for nearly 45% of primary malignant tumors of the lung [26]. Carcinoids comprise 80% of bronchial adenomas and are the most common primary malignant tumors of the

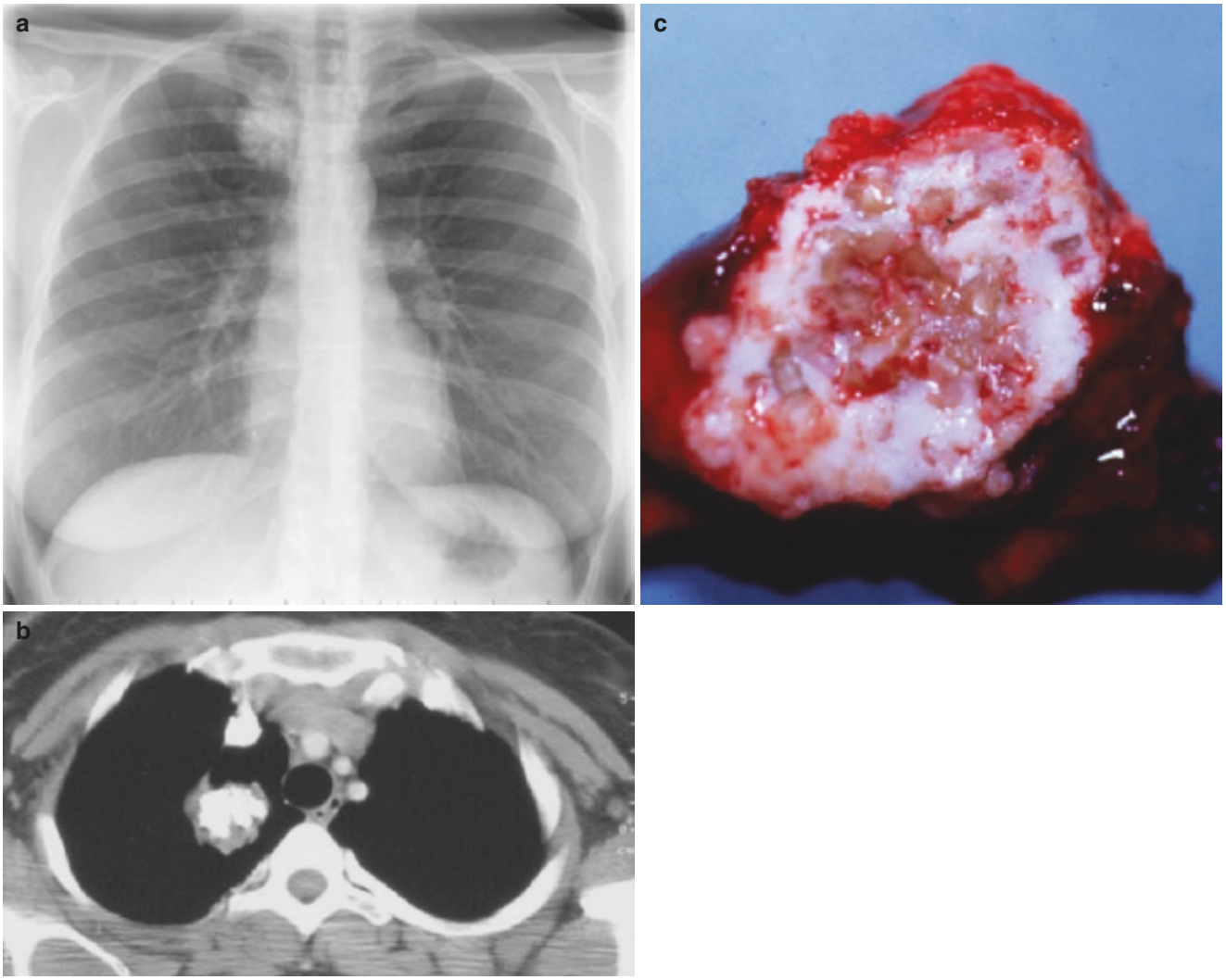

Fig. 7.23 An 18-year-old girl with pulmonary hamartoma. (**a**) Frontal radiograph demonstrates a right upper lobe well-circumscribed mass with multiple calcifications. (**b**) Axial enhanced CT image shows the large *popcorn* calcifications which are typical of hamartoma. (**c**) Pathology after surgical resection confirmed the diagnosis of pulmonary hamartoma

lung in children and adolescents. They typically arise in the lobar bronchi and cause airway obstruction. On radiographs, these lesions may be detected as filling defects in large airways, but more commonly result in radiographic findings of airway obstruction (i.e., air trapping, atelectasis, or postobstructive pneumonia). CT is helpful in further defining the underlying endobronchial lesion revealed by the radiographic findings or in further evaluating the clinical symptoms of airway obstruction (Fig. 7.25). Tumors are slow growing and rarely show malignant transformation. These tumors generally present as endobronchial lesions, but rarely may occur peripherally in the lung parenchyma as pulmonary nodules [102].

Bronchogenic Carcinoma

Unlike adults, bronchogenic carcinomas are relatively rare in childhood and account for 25% of the primary malignant tumors of the lung [26, 103] [112]. Tumors present as nodules and show very rapid growth and early metastases [104].

Primary Mesenchymal Tumors

Primary mesenchymal tumors or sarcomas of lungs are composed of primitive mesenchymal tissue and contain varying quantities of cartilage, skeletal and smooth muscle, and fibrous tissue. Sarcomas are named for the predominant tissue composition, including rhabdomyosarcoma, malignant mesenchymoma, leiomyosarcoma, fibrosarcoma, mesenchymal sarcoma, and pleuropulmonary blastoma (PPB).

PPB, the largest subgroup of the mesenchymal tumors, is derived from primitive lung tissue or pulmonary blastoma, and shares many features with Wilm's tumor or nephroblastoma. Both tumors arise from primitive developmental tissue that normally regresses after birth. The

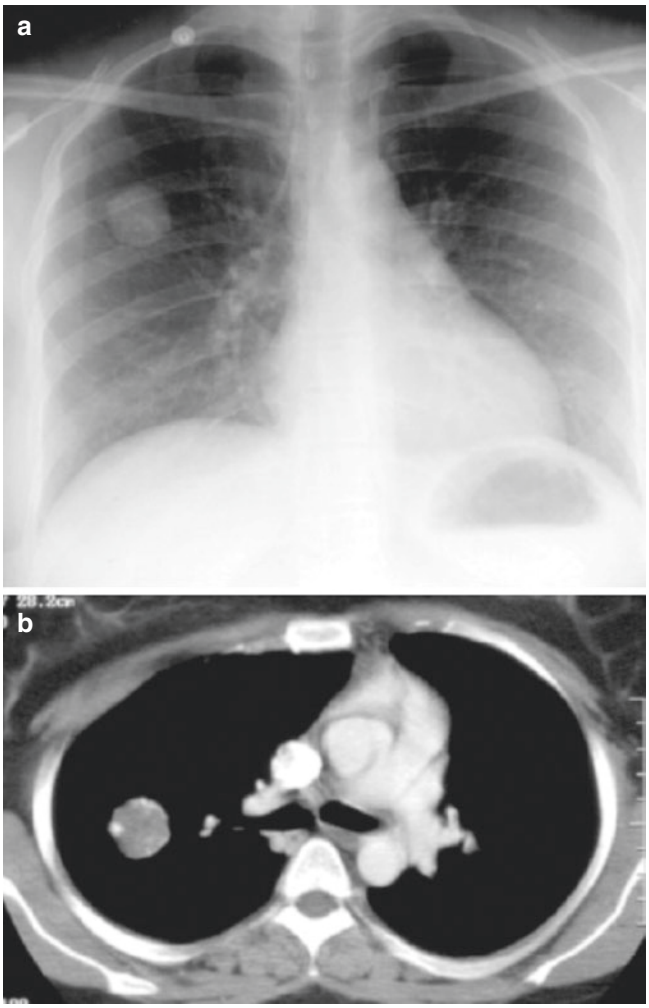

Fig. 7.24 An 18-year-old girl with a pulmonary chondroma. (**a**) Routine preoperative chest radiograph and (**b**) axial enhanced CT image show a well-circumscribed soft tissue mass with a coarse calcification in the periphery of the nodule

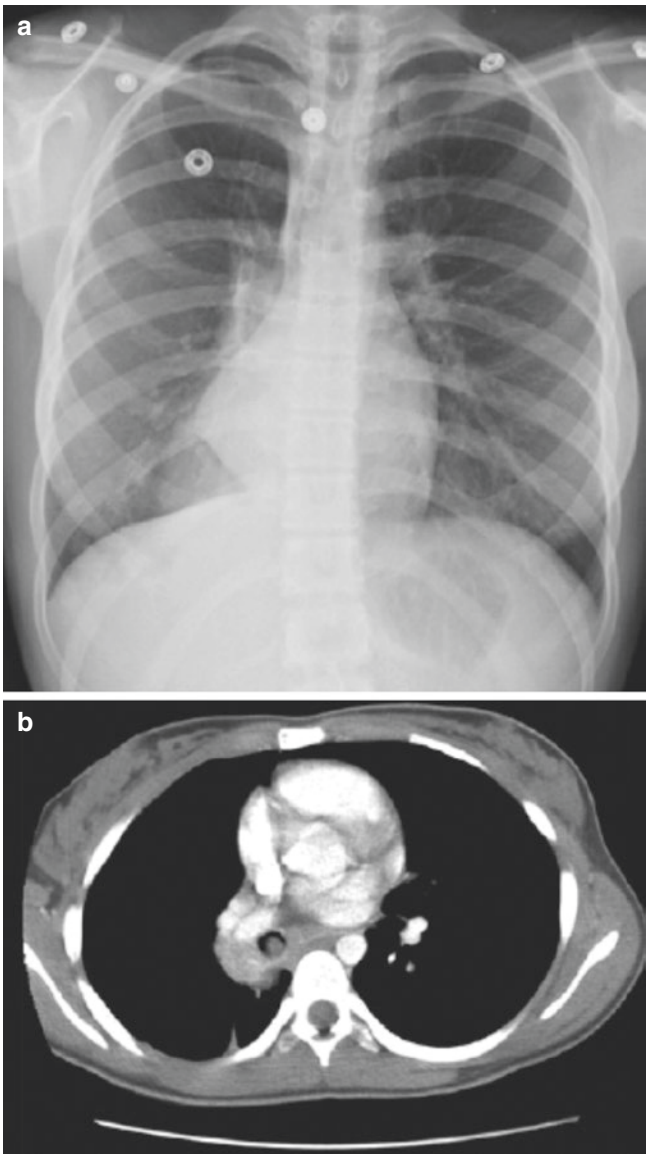

Fig. 7.25 A 15-year-old girl with an endobronchial carcinoid tumor who presented with cough. (**a**) Frontal chest radiograph shows an opacity in the right lower lobe with volume loss likely representing atelectasis. (**b**) Axial enhanced CT image shows a well-circumscribed endobronchial mass. At bronchoscopy, the patient was found to have an endobronchial carcinoid tumor

presence of persistent, primitive pluripotent mesoderm is thought to be related to the development of malignancy [26, 105]. Histologically, PPB and nephroblastoma are similar. Both are composed of a stroma of spindle cells and glandular elements. In addition, PPB and cystic nephroma have been reported to occur synchronously in the same patients, providing further evidence of their close relationship [106, 107]. This tumor is histologically different from a tumor of the same name, which occurs in adults.

These aggressive tumors often present as large pulmonary masses composed of a mixture of solid and cystic components. A variable appearance is seen on CT (Fig. 7.26). Some are solid and hemorrhagic, similar to nephroblastoma, while others such as PPB type 1 are primarily cystic, mimicking CPAM [108]. Calcifications are uncommon, but have been reported on CT [109]. Hilar lymph nodes are not typically enlarged. Because these tumors are so rare and often fatal, the usefulness of additional radiation or chemotherapy following surgical excision is unknown.

Vascular Lesions

Vascular lesions such as arteriovenous malformations or pulmonary vein (or venous) varices may give the appearance of a solitary or multiple pulmonary nodules in children (Fig. 7.27). Pulmonary arteriovenous malformations (PAVMs) are congenital anomalous connections between a pulmonary artery and veins [110]. Although congenital PAVMs are more common, these can occasionally develop

following infection or trauma in the pediatric population. Associated clinical symptoms include hemoptysis, clubbing, cyanosis, and polycythemia [111]. Major complications include massive hemoptysis and paradoxical embolization to the brain resulting in either stroke or abscess. Two-thirds of pulmonary AVMs are associated with hereditary hemorrhagic telangiectasia or Osler-Weber-Rendu syndrome, an autosomal dominant condition in which telangiectatic lesions involve the mucous membranes, skin, and lungs. In these patients, PAVMs are often multiple, and screening for pulmonary AVMs in an asymptomatic first-degree relative may be needed [112].

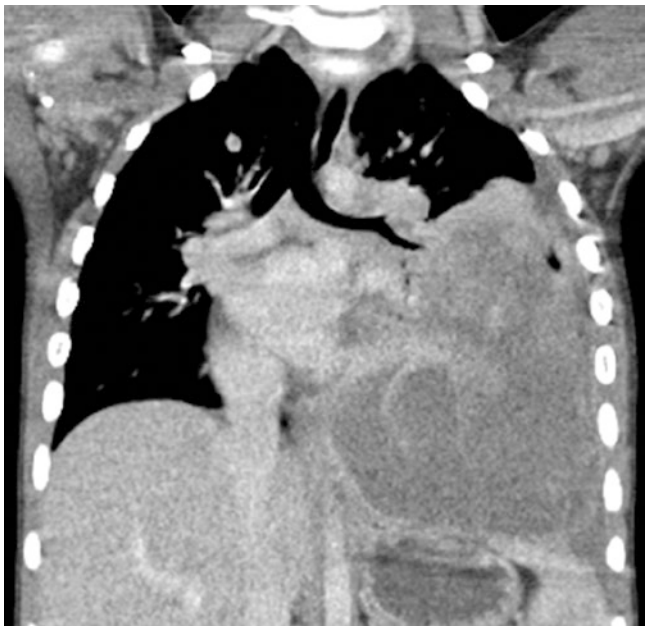

Fig. 7.26 A 3-year-old boy with pleuropulmonary blastoma who presented with respiratory distress and left-sided chest pain. Coronal enhanced CT image shows a large heterogeneously enhancing soft tissue mass which occupies the left hemithorax

In contrast to arteriovenous fistulas, pulmonary varices typically cause no symptoms. These are abnormally dilated pulmonary veins that tend to have a smoother, more regular contour than PAVMs and are most commonly solitary. In the past, the diagnosis of either type of vascular malformation was used to be made with conventional arteriography, which can show a dilated vessel or tangle of vessels characteristic of the lesion [113–116]. However, in recent years, CTA with 2D and 3D postprocessing techniques became the imaging study and technique of choice for evaluating PAVMs and pulmonary varices [5]. Following embolization or surgical procedure for management of these vascular lesions, CT, as a noninvasive imaging modality, can also aid in confirming the presence or absence of residual PAVMs and pulmonary varices. In addition, the recent study highlighted the usefulness of CT as an efficient approach to detect nonsymptomatic PAVMs in children carrying the diagnosis of hereditary hemorrhagic telangiectasia or Osler-Weber-Rendu syndrome [117].

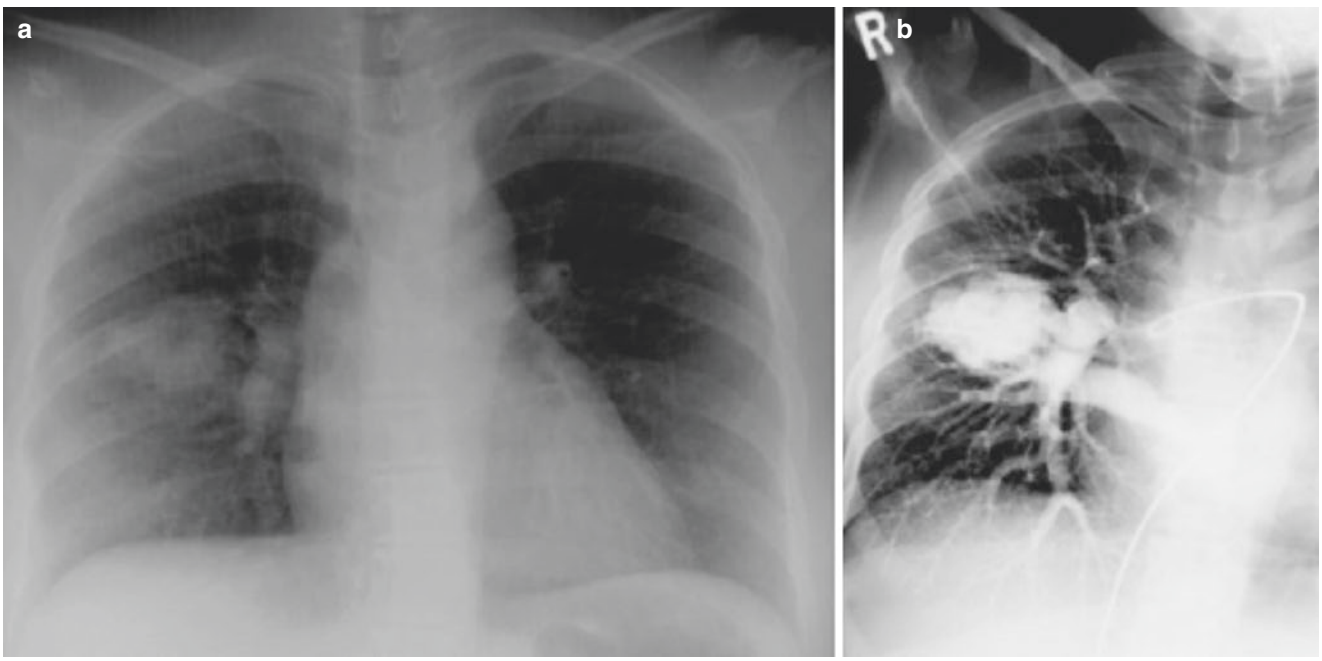

Fig. 7.27 A 15-year-old girl with a pulmonary arteriovenous malformation who presented with hemoptysis. (**a**) Frontal chest radiograph shows a right parahilar nodular opacity. (**b**) Angiography demonstrates a mass-like tangle of vessels forming a pulmonary arteriovenous malformation

Multiple Pulmonary Nodules

Multiple nodules are caused by processes that proliferate diffusely throughout the lungs. These processes may reach the lungs by aspiration or hematogenous spread or may have a particular affinity for lung tissue. In addition, many of the disorders that cause diffuse pulmonary nodules are a part of a multiorgan system disease, having manifestations in other organs as well. Infections and inflammatory disorders are the most common cause of multiple pulmonary nodules. Knowledge of the patient's clinical history is crucial in distinguishing the disparate causes of multiple nodules because the radiographic appearances often overlap. This section classifies multiple pulmonary nodules into infections, neoplasms, systemic autoimmune disease, and noninfectious inflammatory disorders.

Infectious Lesions

Infections are one of the most common causes of multiple pulmonary nodules in the pediatric population [171]. Many infections may also present as a solitary pulmonary nodule and were discussed in the prior section. Naturally, pediatric patients with immunodeficiency, either congenital or acquired, are more likely to have severe systemic and respiratory infections, both of which may lead to the appearance of bilateral pulmonary nodules.

Tuberculosis and Disseminated Fungal Infections

The classical description of hematogenously disseminated tuberculosis in the lung is miliary tuberculosis [118]. The tiny, uniformly sized abscesses have the appearance of millet seeds and are scattered diffusely throughout the lungs giving a "snowstorm" appearance to the lung parenchyma (Fig. 7.28). Miliary tuberculosis typically occurs within 6 months of the original infection and is rare in children. Hematogenously disseminated fungal infections may cause diffuse bilateral pulmonary nodules. These nodules may be as small as those seen in miliary tuberculosis or larger. In treated or chronic tuberculosis and fungal infections, the nodules often calcify.

Varicella and Measles

Pneumonia is a relatively rare complication of infections caused by the viruses varicella zoster and measles in normal immunocompetent children [119, 120]. However, in those patients who are hospitalized for varicella, 17% of patients also have pneumonia [121]. Both viruses are more virulent in immunocompromised children and can cause pneumonia, meningitis, and hepatitis [122]. Children inoculated with the inactivated measles virus vaccine who are then exposed to a natural measles virus rarely develop pneumonia [123].

Both measles and varicella pneumonias are also heralded by typical rashes on the skin [124]; only rarely do these viral pneumonias occur without the telltale rash [125]. In the acute phase, the classic radiographic findings of both pneumonias are bilateral small pulmonary nodules and interstitial thickening (Fig. 7.29). Occasionally, the radiographic pattern resembles that of bronchopneumonia. Residual calcified nodules may remain after treatment [126]. Adenopathy is rarely seen.

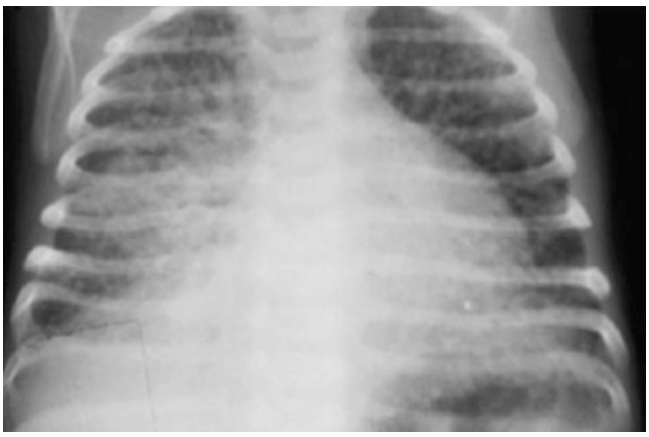

Fig. 7.28 An infant girl with miliary tuberculosis. Frontal chest radiograph shows bilateral diffuse tiny nodular densities resemble a snowstorm, and these radiographic findings are compatible with military tuberculosis

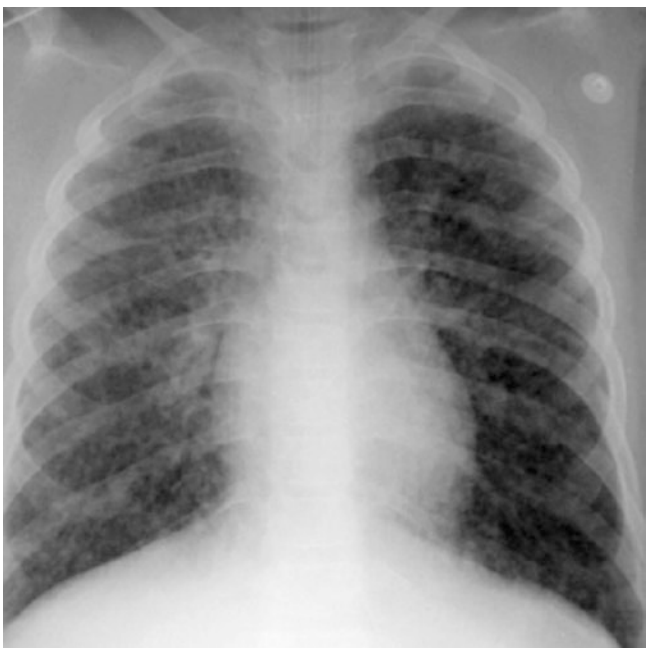

Fig. 7.29 A 9-year-old boy who presented with a classical maculopapular rash of varicella and was admitted to the hospital for high fever and seizures. Frontal chest radiograph demonstrates diffuse bilateral small nodular densities characteristic of varicella pneumonia

Septic Emboli

Infected thrombi that seed the lungs via the pulmonary arteries cause septic emboli. The most common predisposing factors include indwelling catheters, prosthetic heart valves [127], endocarditis, skin infections, and osteomyelitis [128]. In addition, children with bacterial pharyngitis may develop thrombophlebitis of the internal jugular vein (Lemierre syndrome). The most common complication of Lemierre syndrome is septic emboli to the lungs [129]. *S. aureus* and *S. pneumoniae* are the most common bacteria associated with septic emboli [130].

The appearance of septic emboli tends to evolve from well-defined, round, wedge-shaped, or diffuse nodular opacities, measuring less than 2 cm, to thick-walled cavities (Fig. 7.30). Septic emboli have a predilection for the periphery and lower lobes of the lungs. A feeding vessel may be seen abutting (or leading to) the nodule, although this sign is not specific for septic emboli [131]. The frequently associated enlarged hilar and mediastinal lymph nodes are expected, as the emboli are due to the spread of an infection.

Neoplastic Lesions

Metastasis

Because primary lung cancers are so uncommon in the pediatric population, lung metastases are the most common cause of malignant pulmonary nodules in children [26]. Most metastases are spread hematogenously, via the pulmonary arterial supply, but occasionally may spread via the lymphatics or the airways. The most common primary tumors that cause pulmonary metastases are Wilm's tumor and sarcomas. A history of primary malignancy suggests the proper diagnosis. In rare instances, multiple pulmonary metastases are the initial manifestation of an unknown malignancy.

Metastatic lesions, unlike infectious causes of multiple pulmonary nodules, tend to vary in size. Nodules are commonly spherical, well defined, and located in the peripheral two-thirds of the lungs. Certain metastases do have characteristic appearances. The metastases of osteogenic sarcoma can ossify, cavitate, and cause pneumothorax [132]. Thyroid metastases manifest with innumerable tiny nodules, mimicking the appearance of miliary tuberculosis. Unfortunately, the majority of pulmonary nodules caused by metastases cannot be distinguished from other causes of pulmonary nodules. In a patient with primary cancer and other causes of and concern for metastases, computed tomography is much more sensitive than chest radiography for the detection of nodules and is generally the means by which diagnosis is reached and follow-up is conducted.

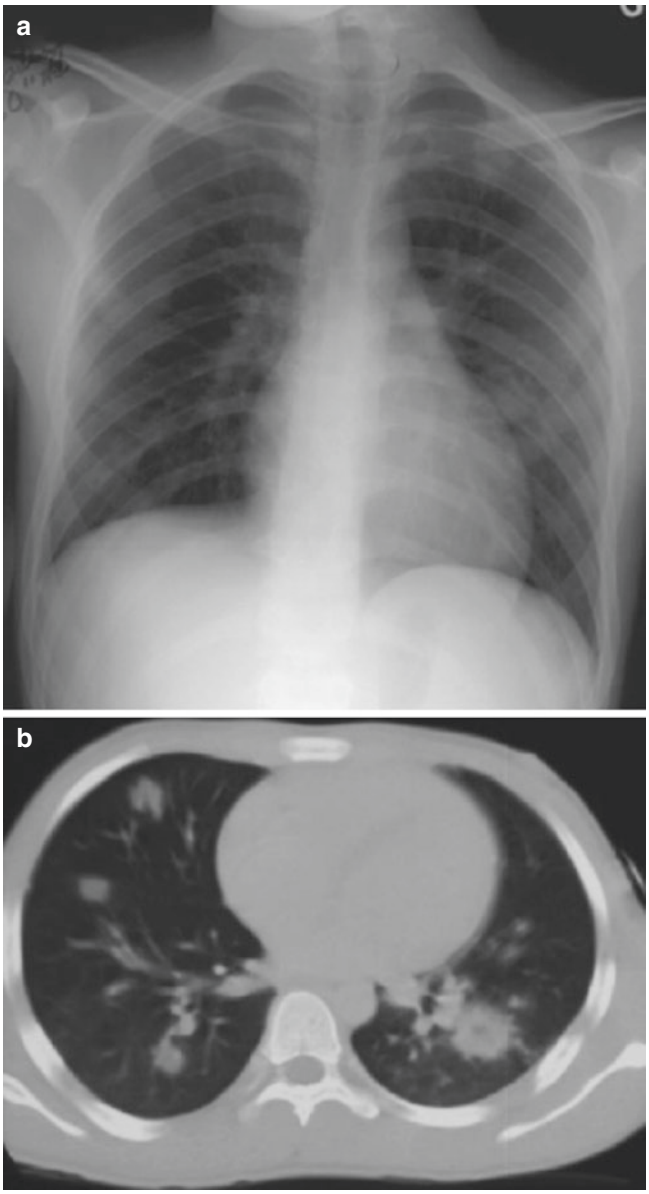

Fig. 7.30 A 7-year-old boy with thrombophlebitis of the internal jugular vein with septic emboli. (**a**) Frontal chest radiograph and (**b**) axial lung window CT image show ill-defined bilateral pulmonary opacities on chest radiograph, which are better visualized on CT. On CT, there is cavitation of the left posterior pulmonary nodule. These pulmonary nodules are most consistent with septic emboli

Leukemia

Leukemia may present with diffuse bilateral nodular or interstitial abnormality even before clinical disease is evident. Lung disease is most commonly seen in acute monocytic and myelogenous leukemias [133]; however, the most common cause of pulmonary nodules in children with leukemia is infection, often opportunistic, related to systemic neutropenia [134, 135]. Reactions or infections related to bone marrow transplantation, immunosuppression, and chemotherapy

toxicity are other causes of pulmonary abnormalities in these children.

Lymphoma

Neither Hodgkin's nor non-Hodgkin's lymphomas typically involve the lung. Only 12% of patients with Hodgkin's disease and 4% of patients with non-Hodgkin's lymphoma present with lung abnormalities [136]. Hodgkin's disease is always associated with mediastinal or hilar adenopathy; non-Hodgkin's lymphoma, by contrast, is characterized by parenchymal lung disease (Fig. 7.31). Primary disease may develop from lymphoid tissue and cause interlobular septal thickening, nodules, and pulmonary masses. Lung disease may be present at initial presentation, during relapse, or both [137].

Papillomatosis

Recurrent respiratory papillomatosis (RRP) is a generally benign neoplasm caused by the human papilloma virus (HPV) transmitted from mother to infant during vaginal delivery. Papillomatosis is characterized by multiple warty excrescences composed of stratified squamous epithelium covering a fibrovascular stalk on the mucosal surface of the respiratory tract. Papillomas are the most common laryngeal tumors in children [138]. These are commonly recurrent throughout childhood, necessitating multiple procedures to remove them. Lung parenchymal involvement occurs in approximately 20% of cases [138]. Surgical procedures, intubation, or tracheostomy placement augments spread into the lung parenchyma. Once they reach the lungs, they find a rich vascular supply to support their growth. Continued growth and desquamation of the epithelium may lead to respiratory insufficiency or even death. Very rarely, malignant transformation to pulmonary carcinoma has been reported [139].

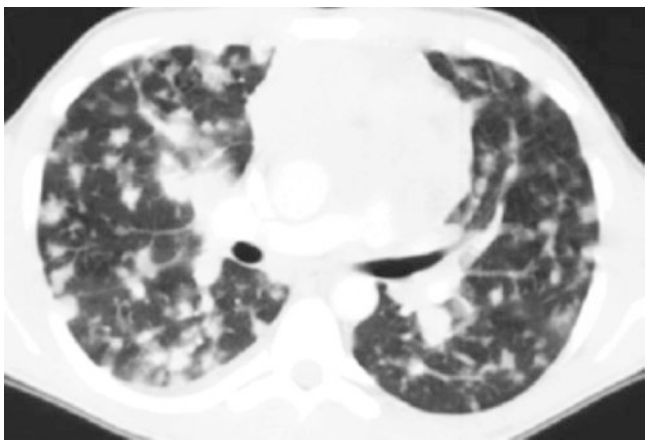

Fig. 7.31 A child who presented with multiple ill-defined bilateral pulmonary nodules at the time of the diagnosis of B-cell lymphoma. Axial lung window CT image shows scattered ill-defined bilateral pulmonary nodules

When the tumor spreads into the distal airway, the radiographic appearance depends on the site of involvement. Endobronchial tumors cause airway obstruction and atelectasis. Distal bronchiole and pulmonary lesions appear as multiple nodules, often with central cavitation in the dependent portions of the lower lobes (Fig. 7.32) [140]. Bronchiectasis may also be a sign of distal airway involvement and repeated infections due to chronic obstruction. Calcification is not a common feature [41, 141].

Systemic Autoimmune Diseases

Systemic autoimmune diseases include collagen vascular disease and the syndromes of pulmonary angiitis and granulomatosis. Because lymphocytic interstitial pneumonia (LIP) is associated with autoimmune disorders, it is also discussed in this section. These diseases cause a variety of pulmonary parenchymal, airway, vascular, and pleural abnormalities. HRCT is a useful adjunct to chest radiography for determining the extent of these pulmonary abnormalities [142]. These diseases are far more common in adults than children.

Collagen Vascular Diseases

Collagen vascular diseases are a subgroup of autoimmune connective tissue disorders, including juvenile idiopathic arthritis (JIA, previously referred to as juvenile rheumatoid arthritis), systemic lupus erythematous (SLE), progressive systemic sclerosis (scleroderma), dermatomyositis, polyarteritis nodosa, and mixed connective tissue disorders. All share common features including inflammation or fragility of the connective tissues. Of all of the disorders, juvenile idiopathic arthritis (JIA) most commonly affects children.

Intrathoracic disease is characterized by pleural effusions associated with lung disease (Fig. 7.33) [143, 144]. By contrast, SLE and systemic sclerosis are more common in adults than in children and also are often associated with pleural effusions. SLE is particularly associated with pericardial effusions. This diverse group of collagen vascular diseases may cause various lung abnormalities, including hemorrhage due to vasculitis, usual interstitial pneumonia, nonspecific interstitial pneumonia, organizing pneumonia, diffuse alveolar damage, lymphoid interstitial pneumonia, bronchiectasis, bronchiolitis, and, ultimately, pulmonary fibrosis and hypertension. The radiographic manifestations of these several entities can resemble pulmonary nodules, as well as diffuse ground glass opacities and diffuse alveolar parenchymal opacities [145, 146]. Overall, collagen vascular diseases affect the lungs less frequently in children than adults. Pulmonary fibrosis, a common finding in adults, is uncommon in children.

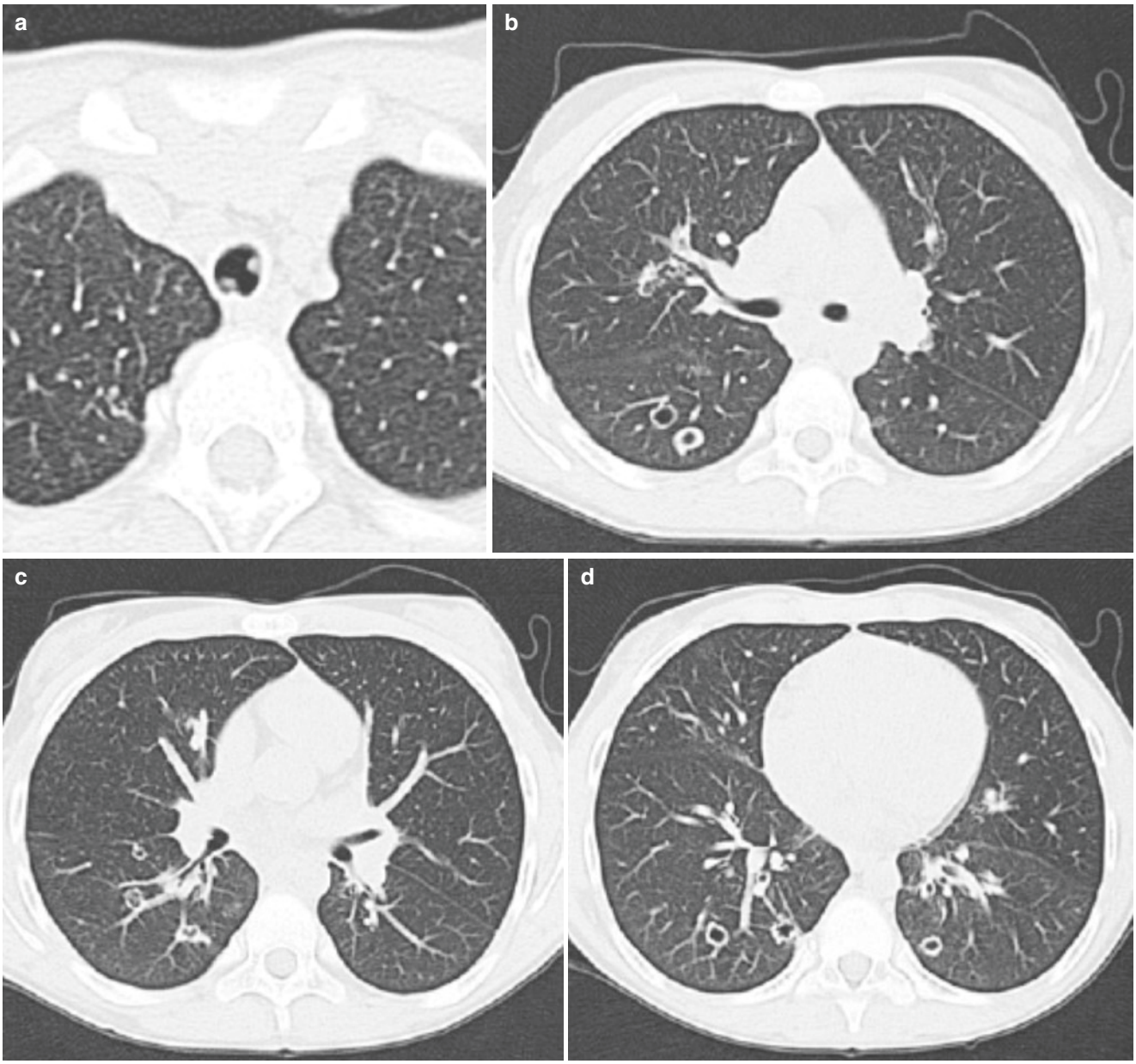

Fig. 7.32 A child with laryngotracheal papillomatosis. Axial lung window CT images (**a**–**d**) demonstrate multiple endotracheal soft tissue masses, as well as bilateral cavitary pulmonary nodules, typical for laryngotracheal papillomatosis

Pulmonary Angiitis and Granulomatosis

There are five distinctive syndromes of pulmonary angiitis and granulomatosis: granulomatosis with polyangiitis (Wegener granulomatosis), allergic angiitis and granulomatosis (AAG or Churg-Strauss), necrotizing sarcoid angiitis (NSA), bronchocentric granulomatosis, and lymphomatoid granulomatosis. These diseases cause necrosis of the small vessels anywhere in the body, including the lung, with resulting hemorrhage and granuloma formation [147, 148]. These rare diseases are most commonly seen in adults and only occasionally in children.

The classic triad of granulomatosis with polyangiitis (Wegener granulomatosis) consists of necrotizing lesions in the upper respiratory tract, lower respiratory tract, and kidneys [149, 150]. A limited and much less common form involves only the lungs. The radiographic appearance of pulmonary hemorrhage includes bilateral solid or cavitary nodules and small masses (Fig. 7.34). Confluent areas of hemorrhage may give the appearance of segmental or lobar consolidation [151].

Churg-Strauss is a systemic disorder characterized by asthma, transient pulmonary opacities, hypereosinophilia,

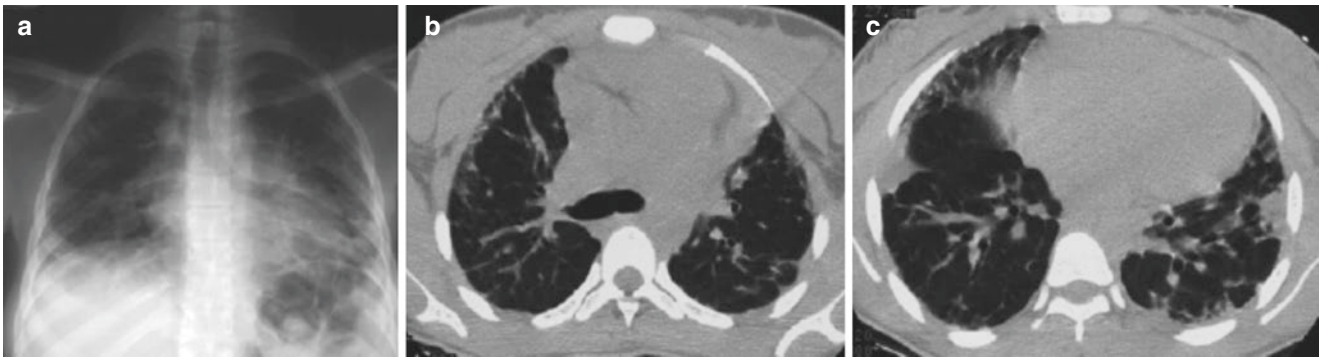

Fig. 7.33 A 16-year-old girl with scleroderma. Frontal chest radiograph (**a**) and axial CT images (**b**, **c**) demonstrate low lung volumes due to pulmonary fibrosis and pleural thickening

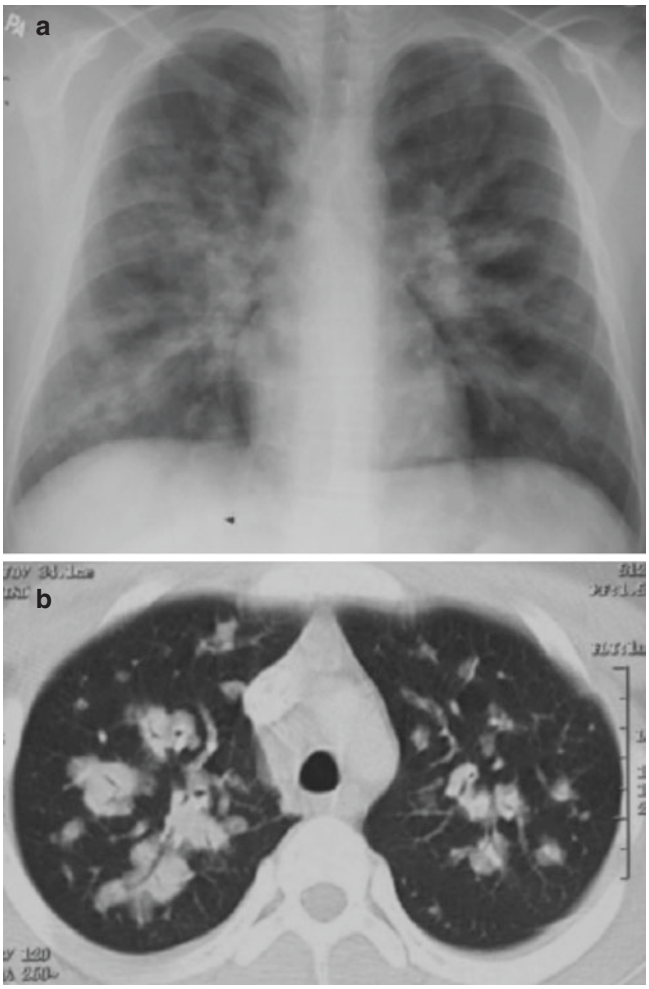

Fig. 7.34 A 14-year-old boy with granulomatosis with polyangiitis (Wegner granulomatosis) who presented with fever, shortness of breath, and rising creatinine. (**a**) Frontal chest radiograph demonstrates bilateral diffuse nodular opacities radiating from the hila. Axial lung window CT image (**b**) better demonstrates the size and distribution of bilateral pulmonary nodular opacities. Thoracoscopic biopsy and further pathologic evaluation demonstrated findings consistent with granulomatosis with polyangiitis

and systemic vasculitis [152]. The first phase of the disease is characterized by asthma and rhinitis; the lungs often appear normal on radiographs. In the second phase of the disease, eosinophilic infiltration of the lungs is characterized by fleeting peripheral pulmonary opacities. In the third phase of the disease, vasculitis may produce areas of pulmonary hemorrhage. Thus, the second and third phases of the disease show distinctly different findings in the chest [153]. In addition, HRCT shows thickening of the septal lines and bronchial walls, likely also representing eosinophilic infiltration [154]. Like Churg-Strauss, bronchocentric granulomatosis is always associated with asthma and may be associated with peripheral eosinophilia. Radiographic findings are varied and include bilateral pulmonary nodules, like the other entities in this group [147].

NSA is a variant of sarcoidosis that only involves the lungs; it is characterized by pulmonary vasculitis, granulomas, and pulmonary nodules on chest radiographs [155] (Fig. 7.35). Hilar adenopathy occurs in up to 60% of affected patients. The nodules are typically up to 1 cm in diameter and often cavitate [197].

Lymphoid granulomatosis is another rare disease, considered an Epstein-Barr virus-mediated variant of B-cell lymphoma. The lungs are the most common site of involvement; but the skin, central nervous system, kidneys, and liver are also commonly involved. On radiographs, lymphoid granulomatosis commonly shows bilateral nodules or occasionally migratory masses as well as pleural effusions. Thirty percent of the nodules or opacities cavitate [156].

Lymphocytic Interstitial Pneumonia

LIP is an uncommon syndrome which causes fever, cough, and dyspnea [157]. This disease is common among pediatric patients infected with the human immunodeficiency virus (HIV) type 1 and an AIDS-defining illness. In the era of aggressive use of antiretroviral therapy, LIP has become very rare with HIV. LIP is also associated with other viruses,

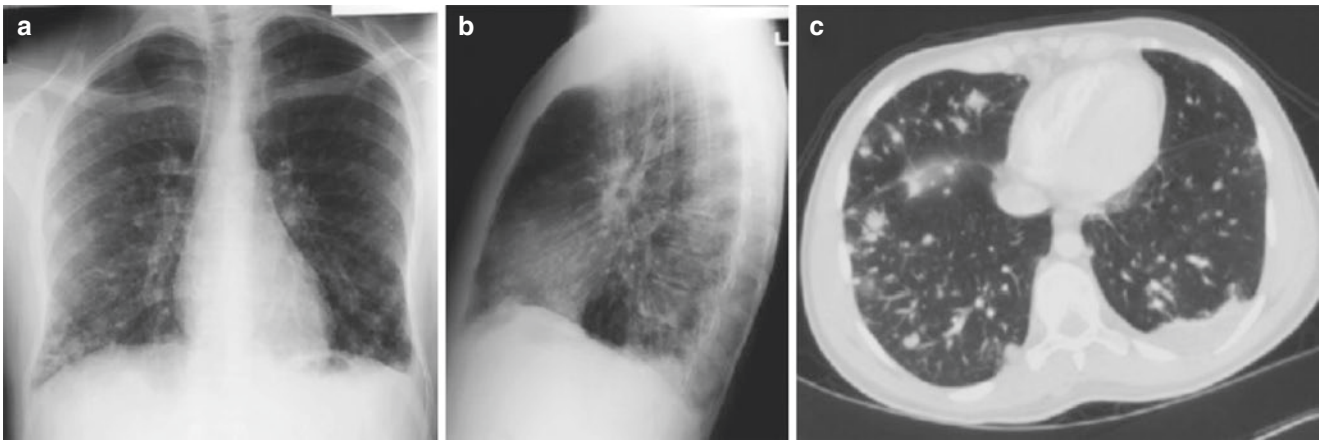

Fig. 7.35 A 16-year-old boy with sarcoid granulomatosis who presented to the emergency room with nonproductive cough and fever. Frontal (**a**) and lateral (**b**) chest radiographs show bilateral irregular pulmonary nodules and a left pleural effusion concerning for granulomatous disease. Axial lung window CT image (**c**) confirms the radiographic findings. A lung biopsy showed necrotizing sarcoid granulomatosis

Epstein-Barr virus, and the human T-cell leukemia virus (HTLV) type 1 [158], as well as autoimmune and lymphoproliferative disorders [159]. The radiographic findings of bilateral, mostly bibasilar, pulmonary nodules and opacities are due to dense interstitial accumulations of lymphocytes and plasma cells. The opacities may progress to cysts, honeycombing, and centrilobular nodules [160–163].

Noninfectious Inflammatory Lesions

Sarcoidosis

Sarcoidosis is an idiopathic inflammatory disorder in which non-necrotic, noncaseating granulomas comprised of epithelioid and multinucleate giant cells affect one or more organs. Childhood sarcoid is rare; there appear to be two different types [164, 165]. Most affected patients diagnosed with sarcoidosis present as teenagers (<18) with a multisystem disease similar to that observed in the adult form. Pulmonary findings, similar to those noted in the adult form of the disease, typically mimic those of tuberculosis. Paratracheal and subcarinal lymph node enlargement are the two most common features of intrathoracic disease [166]. Lung parenchymal abnormalities are less common and may include widespread parenchymal opacities simulating bronchopneumonia or bilateral, diffuse reticulonodular densities (Fig. 7.36) [167, 168].

The second childhood form of sarcoid typically occurs in children less than 4 years of age and is rarely associated with pulmonary abnormalities. These patients generally present with rash, uveitis, and arthritis/synovitis, a clinical presentation that can be confused with that of juvenile idiopathic arthritis [169].

Langerhans Cell Histiocytosis

LCH is also called histiocytosis X. It represents a disease spectrum which previously has been described as three distinct illnesses but which now are recognized as points on a spectrum. The classic terminology included Letterer-Siwe disease, Hand-Schuller-Christian disease, and eosinophilic granuloma. LCH is caused by a proliferation of histiocytes called Langerhans cells [170]. Letterer-Siwe disease is an aggressive, systemic disease that occurs in infants and young children, characterized by hepatosplenomegaly, lymphadenopathy, skin lesions, pancytopenia, and lung disease. Hand-Schuller-Christian disease is a milder form of the condition that occurs in older children and may present with the classic triad of exophthalmos, diabetes insipidus, and osteolytic lesions of the skull. Well-defined, lytic skeletal lesions are also common in this form of the disease. Finally, eosinophilic granuloma refers to disease affecting a single-organ system, typically the skeleton or lungs, usually encountered in adolescents or adults.

Although all forms of LCH may involve the lungs, the lungs are affected in only approximately 10% of cases involving children. Half of children with multisystem organ disease have lung involvement, usually interstitial lung disease, which may progress to fibrosis [42]. In cases of primary pulmonary Langerhans cell histiocytosis (PLCH) with involvement limited to the lungs, teenagers and adults are primarily affected, with a greater incidence among smokers. The Langerhans cells form granulomas in the peribronchial and perivascular interstitial tissues. Radiographically, these granulomas appear as diffuse nodules and predominate at the lung apices. Overtime, the nodules may cavitate and form cysts accompanied by fibrosis (Fig. 7.37) [43, 171–173].

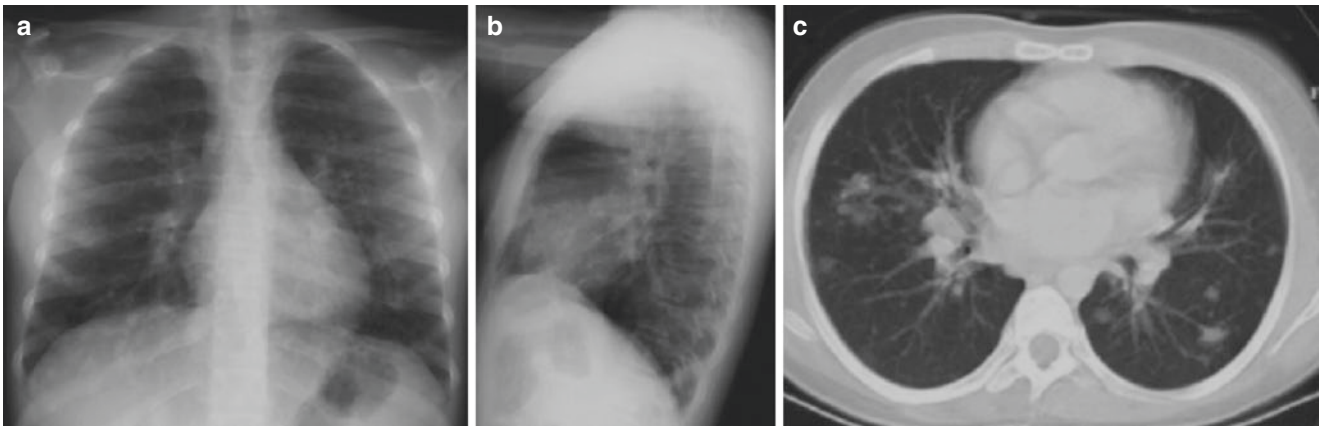

Fig. 7.36 A 20-year-old man with sarcoidosis who presented with pulmonary nodules. Frontal (**a**) and lateral (**b**) chest radiographs and axial lung window CT image (**c**) show multiple ill-defined pulmonary nodules in both lungs

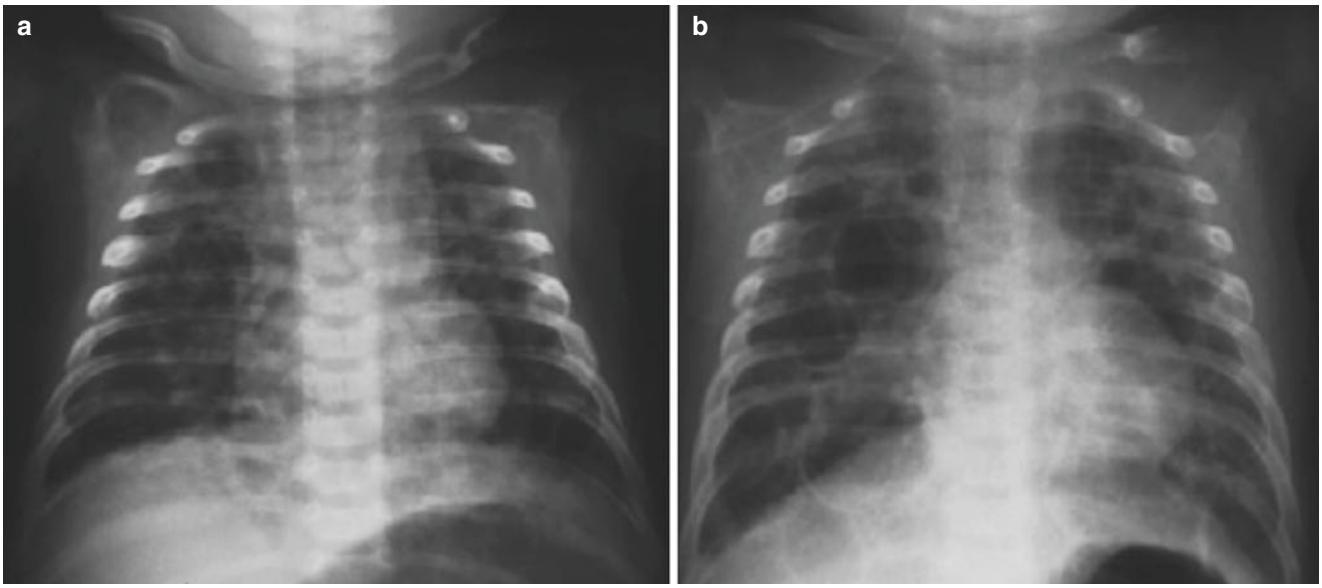

Fig. 7.37 A 3-month-old baby girl with Langerhans cell histiocytosis who presented with fever and lethargy. (**a**) Initial frontal chest radiograph demonstrates scattered pulmonary nodules. (**b**) Subsequently obtained frontal chest radiograph shows progression to bilateral pulmonary cysts of varying sizes, findings typical for Langerhans cell histiocytosis

Pulmonary Alveolar Microlithiasis

This nodular lung disease is of unknown etiology and is characterized by 1–3 mm-sized calcium phosphate microliths scattered throughout the lungs [174]. Pathologically, microliths are present in the alveolar airspaces and along interlobular septa, bronchovascular bundles, and the pleura. This rare disease has a characteristic radiographic pattern of small, calcified nodules, measuring approximately 1 mm in size, resembling sand; they are scattered diffusely throughout the lungs. On CT, the nodules can be seen in a background of ground glass attenuation, a finding especially common in children [175–178]. Chronic disease seen in adults may result in pulmonary fibrosis and induce right heart failure. Although the cause is unknown, the disease is known to be familial and especially common in Turkey [179].

Hyperlucent Lung and Lung Segments

There are many causes of overinflation of the lungs and increased lucency [18]. This may affect all of both lungs, all of one lung, or scattered segments of one or both lungs. These observations may be easily recognized from chest radiography or require dynamic imaging such as chest fluoroscopy, inspiratory/expiratory CT, or dynamic airway CT [180, 181].

Diffuse Air Trapping

Diffuse air trapping may be perceived as bilateral hyperlucent lungs. Air trapping is best confirmed by flattening of the diaphragms on all concurrent images. If even one image fails to reveal flattened diaphragms, then there is not air trapping. Counting the level of the hemidiaphragms in relation to the ribs may help, but this is complicated by variable degrees of lordotic projection which accompanies portable imaging. If rib and/or diaphragm relationship is used for assessment, the relationship of the anterior ribs is more reliable than the posterior ribs. The anterior rib ends are half as far from the dome of the diaphragms than the posterior ribs and therefore are affected by half as much by beam angle variance. There should be 6–6.5 right anterior ribs in the midclavicular line above the hemidiaphragm in a normally inflated child's chest. As in the adult, there should be ten posterior ribs above the hemidiaphragm. However, it is important to recognize that many young children, around ages 5–7 years, may take it as a challenge when asked to take a deep breath. This may produce high lung volumes and suggest air trapping.

In children less than 18 months of age, diffuse air trapping is most commonly encountered with acute lower airway viral infections (bronchiolitis). There may be accompanying bronchial wall thickening and atelectasis, but the hallmark of the disease is air trapping [28] (Fig. 7.38).

Also in children under 18 months of age, hyperventilation (the normal rate varies by age, sex, and activity) causes increase in lung volume and eventually hyperinflation. With increased respiratory rate in children of this age, the inspiratory constant exceeds the expiratory constant leading to breathing just below peak inspiratory volume and hence the high lung volume. The cause of the hyperventilation is irrelevant.

Children of any age with reactive airway disease or asthma, when experiencing an acute attack, potentially have hyperinflated lungs. The chest radiography may mimic the imaging appearance of viral bronchiolitis [28] (Fig. 7.38).

A former premature baby with chronic lung disease (CLD) of prematurity, also known as BPD, may present with diffusely overinflated, hyperlucent lungs. More commonly, however, the lungs are irregularly inflated, with multifocal areas of hyperinflation alternating with areas of atelectasis or fibrosis (Fig. 7.39).

Unilateral Hyperlucent Lung

The most common difficulty when encountering a unilaterally hyperlucent lung is to determine if the hyperlucent lung is overinflated or the other lung underinflated [18]. Corollary finding may provide the clue, or dynamic imaging may be required. If dynamic imaging is employed, fluoroscopy has several advantages. It is readily available and requires no sedation or anesthesia. In fact, it is important to have the child awake and actively breathing or crying to best assess

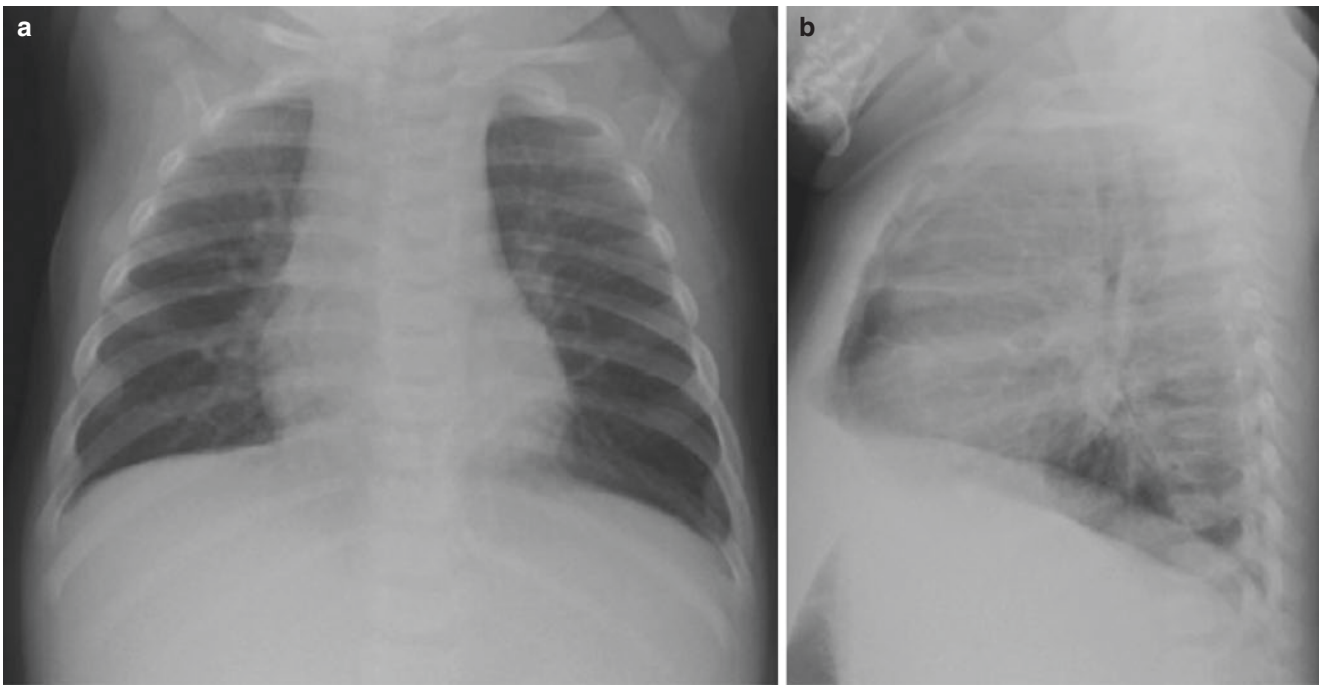

Fig. 7.38 A 3-month-old boy with RSV-positive bronchiolitis who presented with respiratory distress. Frontal (**a**) and lateral (**b**) chest radiographs show the flattening of the diaphragm which is the most reliable indicator of overinflation. There are also diffuse perihilar bronchial wall thickening and multifocal subsegmental atelectasis

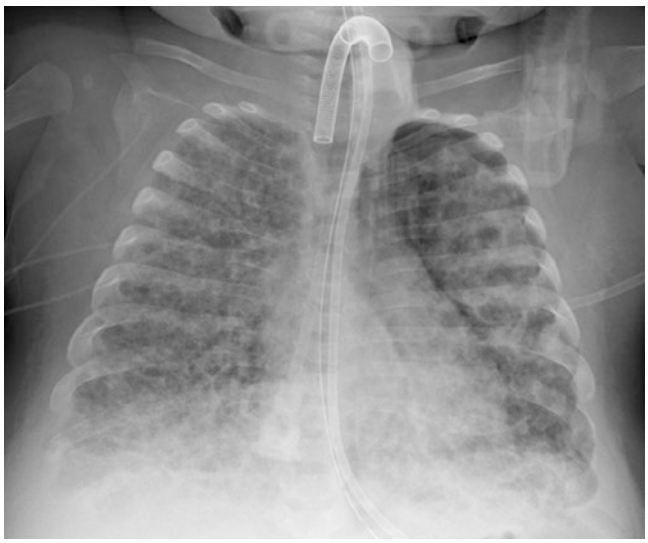

Fig. 7.39 An 8-month-old boy with history of prematurity and chronic lung disease of prematurity. Frontal chest radiograph shows coarse opacities and hyperinflation of both lungs in keeping with chronic lung disease of prematurity. Left-sided pneumothorax is also seen. In addition, tracheostomy, nasogastric tube, and feeding tube are seen

through a full and dynamic range of lung volumes. The brief fluoroscopy required exposes the child to less irradiation than inspiratory/expiratory CT, adhering to the "as low as reasonably achievable" (ALARA) concept of *imaging gently* [182, 183].

In toddlers and older children who are of an age capable of placing objects in their mouths and then aspirating them, an airway foreign body may produce either atelectasis or air trapping. In either case, a careful assessment for an airway foreign body is required. Fluoroscopy is preferred over decubitus images, as the commonly encountered oblique projection of the decubitus images makes comparison of lung volumes potentially inaccurate. Evaluation for a lucent foreign body may be greatly enhanced by CT, with or without *virtual bronchoscopy*. Extrinsic bronchial compression, as from a mass or vascular structure, if severe, may cause altered inflation. Rarely an intrinsic airway obstruction may be encountered, such as a tuberculoma.

Children may be born with a hypoplastic or absent lung [1–5]. With hypoplasia, the abnormal small lung is usually hyperlucent. This may be a part of a syndrome, such as venolobar or scimitar syndrome. In that specific instance, the abnormal, usually right sided, anomalously draining pulmonary vein should be recognized as a vertically oriented vessel coursing to the diaphragm through the smaller hyperlucent lung. With any cause of unilateral lung hypoplasia, the smaller lung should be relatively hyperlucent. The hypoplastic lung is hyperlucent partially because its vasculature is diminished. An additional, related observation is that the pulmonary vasculature of the normal lung is increased. This abnormally prominent vasculature of the normal lung may be the most obvious clue to the contralateral hypoplasia. Acquired underinflation, unless present for an extended period of time, should not have recognizably asymmetric pulmonary vasculature.

Bronchiolitis obliterans, also known as Swyer-James syndrome or McLeod syndrome, usually occurs after viral infection, although it can also arise from a bacterial or parasitic infection (i.e., *Mycoplasma*) [184]. In adults, bronchiolitis obliterans is characterized by unilateral hyperlucent small volume lung; but in children, by an overexpanded hyperlucent lung, a discrepancy is explained by diminished lung growth following onset of the disease. While air trapping is initially evident on imaging, proportionately less growth results in reduced lung volume compared to the more normal lung. In addition, it has been established that many cases of bronchiolitis obliterans feature diffuse and irregularly affected lungs. Specifically, on CT, both lungs may show abnormalities, including bronchiectasis, but one lung typically dominates (Fig. 7.40).

Children born with diaphragmatic hernia usually have hypoplasia of the ipsilateral lung [28]. If the amount of herniated bowel is large, the resultant shift of the mediastinum may cause hypoplasia of the contralateral lung. However, even in the latter case, the ipsilateral lung is more profoundly affected. Following repair of the hernia, the lungs continue to develop with increase in volume of the hypoplastic lung. However, in most cases, the ipsilateral lung remains smaller, more lucent, and with relatively diminished vasculature than the lung opposite to the side of the hernia. A clue to this diagnosis, postoperatively, is that the smaller, lucent lung is associated with a hemidiaphragm that is lower and flatter than the other. This is the result of the tension involved in plicating the diaphragmatic defect.

One lung may seem hyperlucent because the other hemithorax is of increased opacity [28]. This most commonly occurs when there is a pleural effusion or thickening. If the thickening is dominantly posterior or anterior, its presence may not be readily apparent on frontal projection radiographs. If the image is acquired with the patient supine, a relatively small effusion may be most easily appreciated as an apical cap, greater in degree than on the opposite side.

Asymmetric pulmonary edema may cause one lung to be more opaque than the other. In children, especially those with a history of complex congenital heart disease, this may be related to asymmetric pulmonary vasculature. Main branch pulmonary artery stenosis may be severe enough to cause decreased arterial flow on the affected side and "protect" that side from developing high-output pulmonary edema. Likewise, central pulmonary venous obstruction may raise the baseline venous pressure to above oncotic pressure

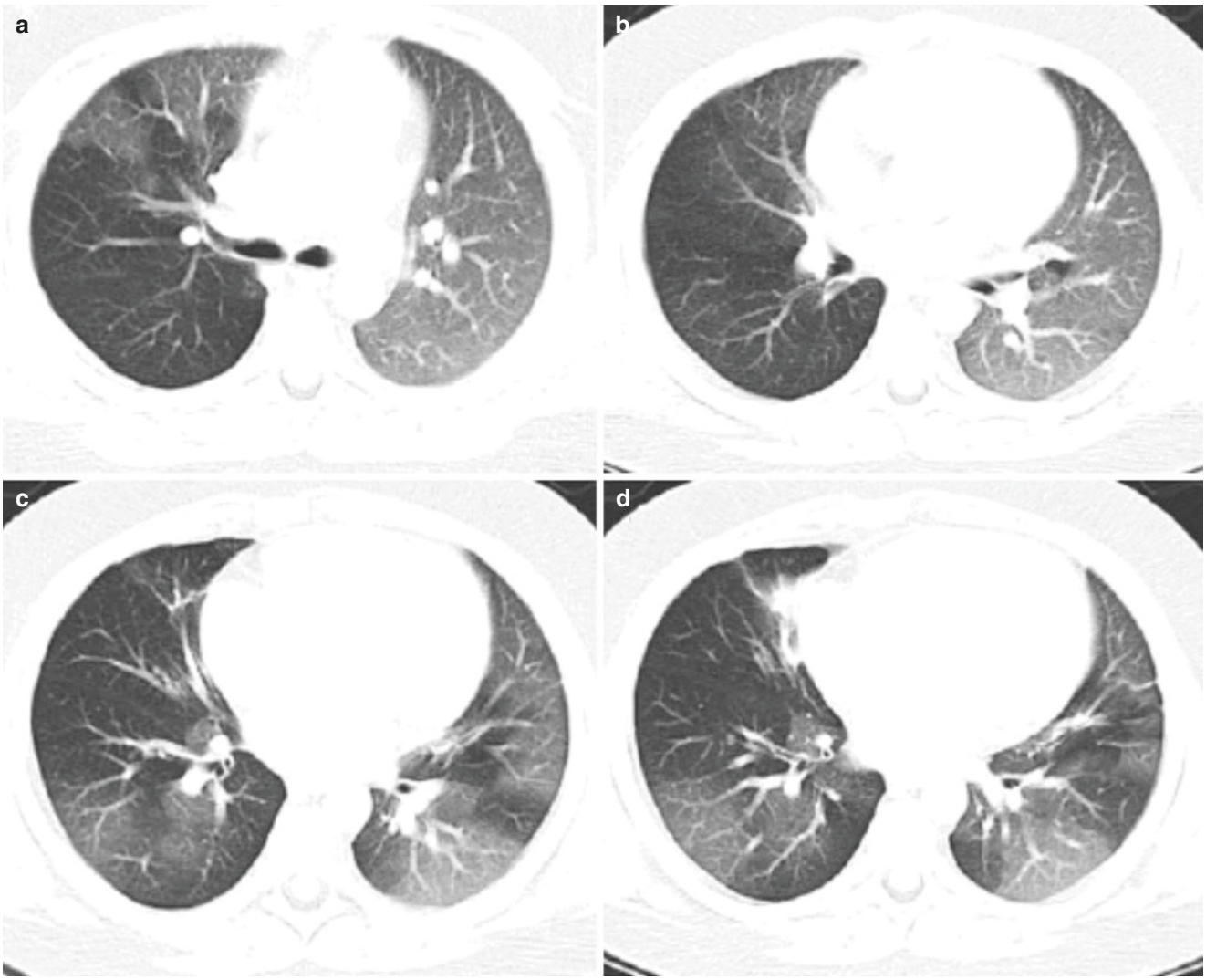

Fig. 7.40 A 15-year-old girl with bronchiolitis obliterans. Axial lung window CT images (**a-d**) show accentuated hyperlucent oligemic segments of lung, usually worse in one lung with associated mild to moderate bronchiectasis

and cause pulmonary edema or predispose to edema when left atrial pressure increases above baseline. Asymmetric lymphatic flow may be associated with asymmetric pulmonary lymphedema. Any of these situations may be a component of the congenital abnormality or acquired as a postoperative condition. In children, as adults, if the patient is left for a protracted period in a dominantly decubitus position, the dependent side can develop pulmonary edema.

Asymmetric increased size of the chest wall soft tissues can cause the affected side to be more opaque and therefore the other seem hyperlucent. This may occur with hemihypertrophy (congenital or acquired) or extensive chest wall masses such as lymphatic malformations or plexiform neurofibroma.

One lung may seem hyperlucent because of issues affecting that side than the other lung. This commonly is seen if the image is acquired in mild degrees of rotation. In small children, rotation may not be equal throughout the chest. On a perfectly straight frontal projection of the chest, not only should the medial ends of the clavicles be equidistant from the vertebral posterior spinous processes but also the anterior ends of all pairs of ribs.

A subtle pneumothorax may be perceived as an increased lucency of the hemithorax. This is most common with supine imaging. In the supine position, the pleural edge of a small pneumothorax is first encountered, medially adjacent to the inferior mediastinum or cardiac apex.

Asymmetrically decreased size of the chest wall soft tissues can cause the affected side to be hyperlucent. This may be congenital, as in Poland's syndrome (decrease in chest wall musculature and rarely ribs, sometimes associated with hypoplasia/absence of the radius or radial digits). The asymmetry may be acquired.

Hyperlucent Lung Segments

Possibly the most difficult observation is that of segmental hyperlucency (Table 7.3). Confirmation often requires CT, frequently performed in inspiration and expiration. This is especially true for demonstrating the irregular air trapping associated with interstitial lung disease.

A common cause of markedly irregular aeration is chronic lung disease of prematurity, as discussed earlier. As the child grows older, this observation may abate or occasionally resolve.

Obstruction of a segmental or subsegmental bronchus may cause altered aeration of the lung distal to the obstruction. This may be encountered with mucous plugging, allergic bronchopulmonary aspergillosis (ABPA), cast bronchitis, bronchial stenosis or atresia, foreign body, intrinsic obstruction (such as carcinoid tumors), or extrinsic compression.

Chronic lobar emphysema (CLE) may have some evidence of focal bronchial obstruction (in up to 50% of cases) that manifests itself as an overinflated, hyperlucent lobe [1–5]. In at least half of cases, no such obstruction is encountered. In the first few days of life, this may present with preferential trapping of fetal lung liquid in the abnormal lobe. This, in turn, produces an overinflated, opaque lobe, which slowly drains the fluid over ensuing days, subsequently becoming hyperlucent. The distribution of CLE is roughly 43% in the left upper lobe, 32% in the right middle lobe, 20% in the right upper lobe, and 5% in two lobes [1–5, 28]. With an overinflated hyperlucent lobe and associated mediastinal shift to the contralateral side, CLE may be mistaken as tension pneumothorax. When this occurs, CT is useful in visualizing the underlying, overinflated, and hyperlucent lung parenchyma.

Rarely peripheral pulmonary artery stenosis (PPS), with focally diminished pulmonary artery prominence, is perceived as a focal hyperlucent lung segment. PPS may be seen as an isolated phenomenon. It is encountered as a part of several conditions including congenital rubella, neurofibromatosis 1, Williams syndrome (congenital hypercalcemia), Ehlers-Danlos syndrome, and tetralogy of Fallot (most commonly the left main pulmonary artery) [185].

Pneumonia

Among the most common infections in children are those affecting the lower respiratory tract, lower respiratory tract infections (LRTIs) [186]. However, unfortunately, even in the most optimal circumstances, pediatric pneumonia is often difficult to diagnose [186, 187]. Patient history, physical findings, and laboratory results can all be elusive. Children with pneumonia do not necessarily present with the signs and symptoms typically associated with adult LRTI such as fever, cough, wheezing, tachypnea, and retractions. On physical examination, an accurate diagnosis may be further delayed by nonspecific complaints such as malaise, fever, and abdominal pain.

In addition, most clinicians attempt to distinguish bacterial pneumonias from viral pneumonias since bacterial pneumonias are treated with antibiotics and viral pneumonias are typically treated symptomatically. Unfortunately, signs and symptoms used to distinguish *typical* bacterial pneumonias from *atypical* viral or mycoplasmal pneumonias in adults do not reliably distinguish the two pneumonias in infants and young children [186, 187].

At present, no laboratory test can accurately diagnose pneumonia or differentiate bacterial from nonbacterial pneumonia. Among diagnostically relevant laboratory values, C-reactive protein level, which measures the concentration of a protein in serum, and the absolute neutrophil count which signals an increase in infection-fighting white blood cells, when elevated, are reliable indicators of acute infection and are clinically useful in distinguishing typical and atypical pneumonias [188–192].

One of the most common indications of imaging children arises from the need to evaluate suspected cases of LRTIs. In this setting, chest radiographs are the most specific test to evaluate for pneumonia and aid significantly in reaching diagnosis and in treating respiratory illnesses [186–192].

This chapter concentrates on the plain radiographic manifestations of community-acquired lower respiratory tract illnesses in immunocompetent children who have developed beyond the neonatal period (>30 days). In this chapter, the term *pneumonia* describes LRTI and inflammation [28].

Epidemiology of Lower Respiratory Tract Infections

Viruses are the most common cause of upper and LRTIs in children of all ages in the United States. They account for 65% of all pediatric pneumonias and for more than 90% of pneumonias in children under 2 [28]. Bacteria account for 5–10% of childhood pneumonias [28]. The single most common agent that produces pneumonia in childhood is *Mycoplasma pneumoniae*. *Mycoplasma* is a microorganism that, unlike a virus, does not need a host cell and, unlike a bacterium, does not have a cell wall.

In the United States, the most common viral pathogen is respiratory syncytial virus (RSV); this virus is responsible for at least 60% of severe LRTIs in children under the age of 5 [28]. Other common viral causes of LRTIs are influenza, types A and B, and parainfluenza, types 1 and 3. Adenoviruses and enteroviruses are other pathogens that are less common and/or more difficult to diagnose.

One of the most predictive indicators of pediatric pneumonia is age. The etiology of pneumonia may also be traced

seasonally and by the symptom complex that presents in individual patients. Certain viruses and bacteria, for example, are known to have higher prevalence rates in different age distributions – a largely unexplained phenomenon. For example, RSV, parainfluenza virus, influenza, and adenovirus account for most LRTIs in infants and toddlers (1–24 months). Among preschool-age children (2–5 years), these same viruses remain the most common cause of pneumonia, although viruses account for a smaller percentage of pneumonias than in the infant and toddler population. *Pneumococcus* is the most common cause of bacterial pneumonia in preschool-age children. Among school-age children (6–18 years), *M. pneumoniae*, *Streptococcus pneumoniae*, and *Chlamydia pneumoniae* (TWAR) are common pathogens for pneumonia [28]. *Mycoplasma* causes approximately 30% of respiratory infections in school-age children (6–18 years) [28]. *C. pneumoniae* is another common cause of pneumonia in elementary school-age children, causing 15–18% of community-acquired pneumonia among children aged 3–12 years [28]. Most infections are mild or asymptomatic with only 10% of cases resulting in clinically apparent pneumonia [193].

S. pneumoniae and *Haemophilus influenzae* (*H. influenzae*) have been implicated as common causes of bacterial pneumonia in children from infancy to early elementary school age [28]. However, the exact prevalence of these two pathogens is unknown because these organisms commonly live in the upper respiratory tract in asymptomatic individuals. The only way to truly isolate the organisms is to isolate them from the blood or pleural spaces by means of thoracentesis or directly from the lung through percutaneous aspiration. Finally, with the introduction of a heptavalent conjugated pneumococcal vaccine (PCV7, Prevnar) in 2000 and the widespread use of the *H. influenzae* type b (Hib) vaccine, the overall degree of invasive disease [194] has decreased, although the exact prevalence of *S. pneumoniae* and *H. influenza* has not been restudied [195].

Pathophysiology of Childhood Pneumonia with Radiographic Correlation

Infectious agents reach the lower respiratory tract through aspiration, hematogenous seeding of the lungs, and direct spread from extrapulmonary sites. The most common cause of pneumonia is from inhalation of airborne organisms or aspiration of infected secretions or gastric material. Less commonly, infections are carried by the bloodstream to the lungs through the pulmonary vasculature such as during diffuse blood infection (sepsis) or through infected thrombi. Infections from the mediastinum, chest wall, abdomen, and neck can also spread directly to the lungs.

The respiratory *tree* is composed of branching airways that terminate at the alveoli, the final gas exchange units between the outside world and the cells. The branching begins in the center of the chest at the hilum and extends peripherally. There are between 10 and 22 generations of branching airways before gas exchange occurs, with the largest airways called bronchi and the smaller airways called bronchioles. As the child grows, the length of the airways grow, but not the number. The airways complete their branching in fetal life at about the 16th week of gestation. The alveoli begin to mature at about the 29th week of gestation and continue to proliferate and mature until approximately 8 years of age [28]. Grossly, a normal right lung is divided into three lobes: the right upper lobe, right middle lobe, and right lower lobe. The left lung is divided into two lobes: the left upper lobe and left lower lobe. The left lung, unlike the right lung, does not have a middle lobe. although it does have a homologous structure, a projection of the upper lobe termed the lingula, which mean “little tongue”.

The inhaled or aspirated microorganisms giving rise to pneumonia cause distinctly different inflammatory reactions in the lungs; these differences, in turn, lead to three main distinctive pathologic patterns: interstitial pneumonia, lobar pneumonia, and lobular pneumonia (bronchopneumonia). The radiographic findings of pneumonia closely follow the pathologic processes.

Because viruses are the most common cause of childhood LRTIs, their pathologic process and radiographic manifestations are described first. Interstitial pneumonia is the typical pathologic description of viral infection in the lungs. Although there is some variation in the microscopic reaction produced in the lung by the various viruses, they produce generally similar pathological and radiographic patterns. Viruses infect the epithelial cells lining the small- and medium-sized airways causing destruction of the ciliated columnar epithelial cells, goblet cells, and mucus glands. The cell destruction triggers an inflammatory reaction that produces edematous bronchial walls infiltrated with mononuclear lymphocytic cells. The resulting sloughed cells, lymphocytic infiltrate, debris, and peribronchial edema cause occlusion of the small- and medium-sized airways. Thus, the pathologic hallmarks of viral pneumonia are peribronchial edema and occlusion of smaller airways.

On a frontal radiograph of the chest, normal-appearing small- and medium-sized airways are best seen near the hilum. The airways branch from the center to the periphery and are normally invisible in the outer one-third of the lungs. When the branching airways are seen on end, they appear as well-defined circles and are similar in diameter to the adjacent pulmonary artery (Fig. 7.41). Peribronchial edema causes irregularity and thickening of the normally sharply defined walls; this is described as peribronchial cuffing (Fig. 7.42). The relatively abundant overlapping thickened

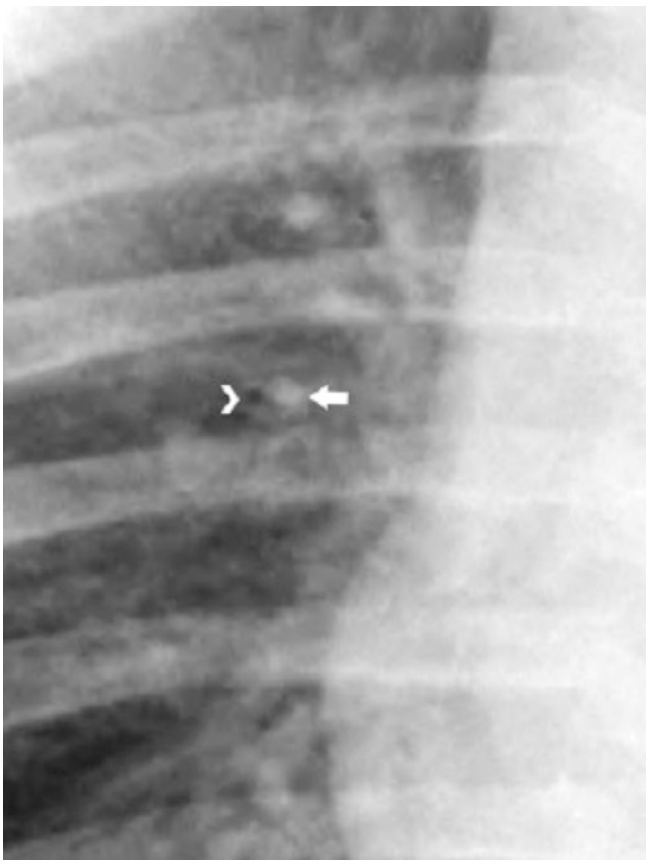

Fig. 7.41 This magnified anteroposterior (AP) view of the chest demonstrates a normal-appearing bronchus (*arrowhead*) and artery (*arrow*) on end. Notice how the edges of the bronchus are sharp and well defined

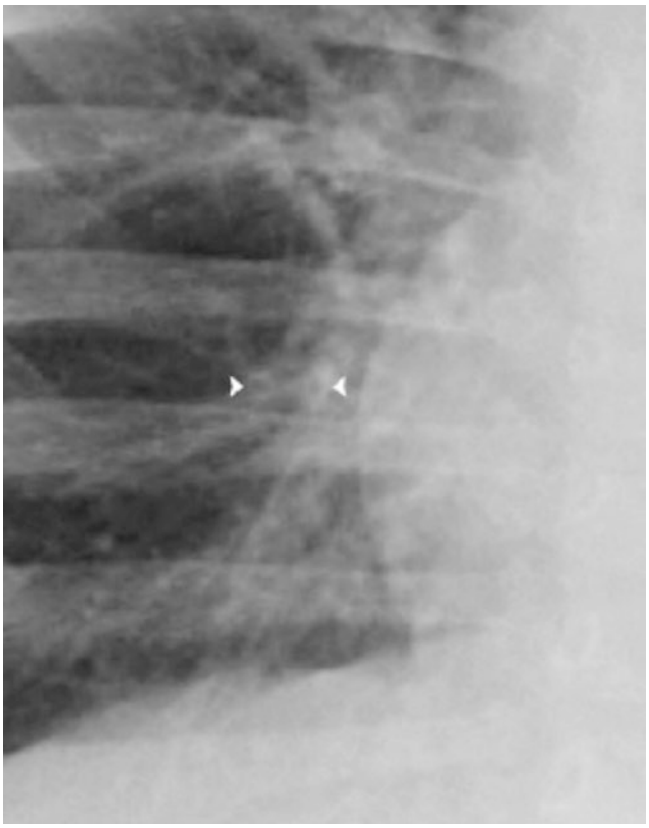

Fig. 7.42 This magnified view of the chest of an 8-month infant with severe respiratory distress demonstrates the radiographic finding of peribronchial cuffing. The margins of the bronchus (*arrowheads*) are thickened and irregular

bronchioles near the hilum can give the appearance of enhanced linear soft tissue at the hilum or hilar enlargement (Fig. 7.43a). Occlusion of small airways causes both atelectasis and hyperinflation, and both effects may occur simultaneously (Fig. 7.43b). Although it may be difficult to differentiate confluent atelectasis from consolidation, there are distinguishing characteristics. Atelectasis causes focal volume loss which may be recognized as bowing of fissures toward the opacified segment of the lung. With subsegmental atelectasis, there may be a linear margin to the opacification which cannot be attributed to a fissure. Also, frequently subsegmental atelectasis is often more clearly seen on either the frontal or lateral image than on the other. On frontal chest radiograph, with pectus excavatum, there is frequently obscuration of the right heart border with no lung abnormality demonstrated on lateral projection. Without the presence of the pectus deformity, this would suggest right middle lobe atelectasis.

The effect of small- and medium-sized airway occlusion is especially dramatic in infants and young children, especially in 18 months old and younger. Children are more susceptible to airway narrowing than adults because the diameter of their airways is smaller, mucus production is greater, and collateral pathways of aeration such as the channels of Lambert (bronchoalveolar channels) and pores of Kohn (intraalveolar pores) are poorly developed. These pathways, which allow collateral air drift between airspaces, become fully developed at approximately 8 years of age. One of the causes of air trapping is tachypnea; air trapping is one of the most sensitive indicators of LRTIs in young children [28].

Thus, the radiographic appearance of increased lung volumes, especially intermingled with areas of subsegmental atelectasis and peribronchial cuffing, offers compelling diagnostic evidence of viral LRTIs in young children [28]. Because young children are unable to follow commands regarding breath holds, images of their lungs, especially when they are not crying, are used to assess total lung volume. In older children (18 months of age) and adults with larger airways and mature collateral pathways of aeration, hyperinflation is no longer a useful tool in diagnosing viral pneumonia. In addition, older children and adults can follow the command to hold their breath at maximum inspiration requested during routine radiographs.

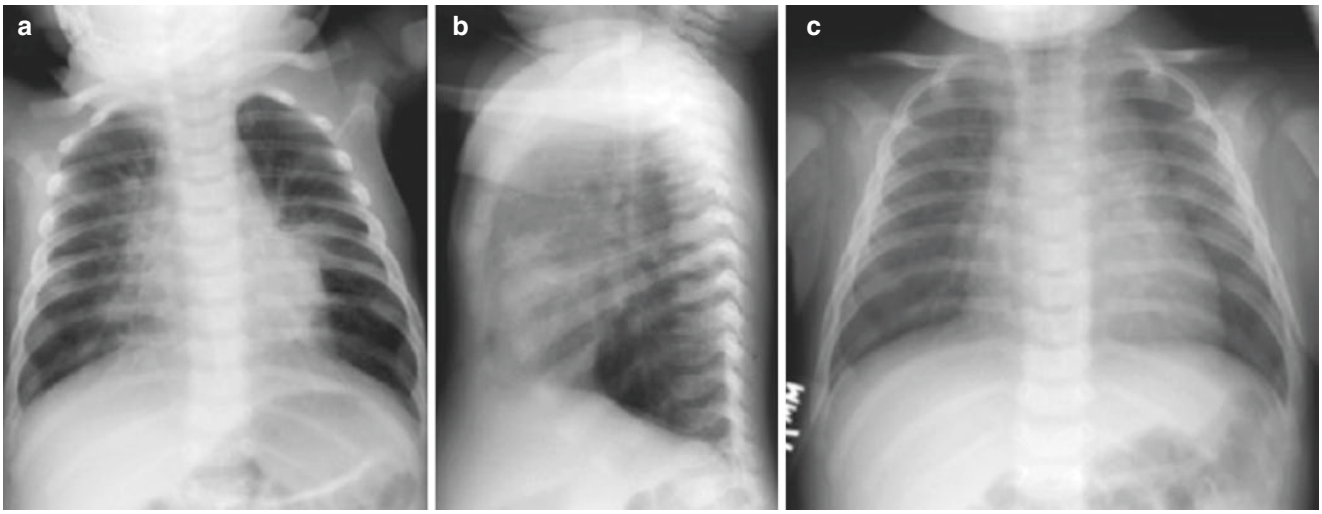

Fig. 7.43 A 2-month-old girl who presented with cough and coarse breath sounds. (**a**) AP view of the chest demonstrates coarse linear opacities radiating from the hilum consistent with peribronchial thickening. The (**b**) lateral radiograph demonstrates flattening of the hemidiaphragms (as does the AP view) and anterior bowing of the sternum, signs of hyperinflation. These findings are consistent with classical viral pneumonia. No microbial etiology was found. (**c**) Several weeks later, her radiographs had returned to normal

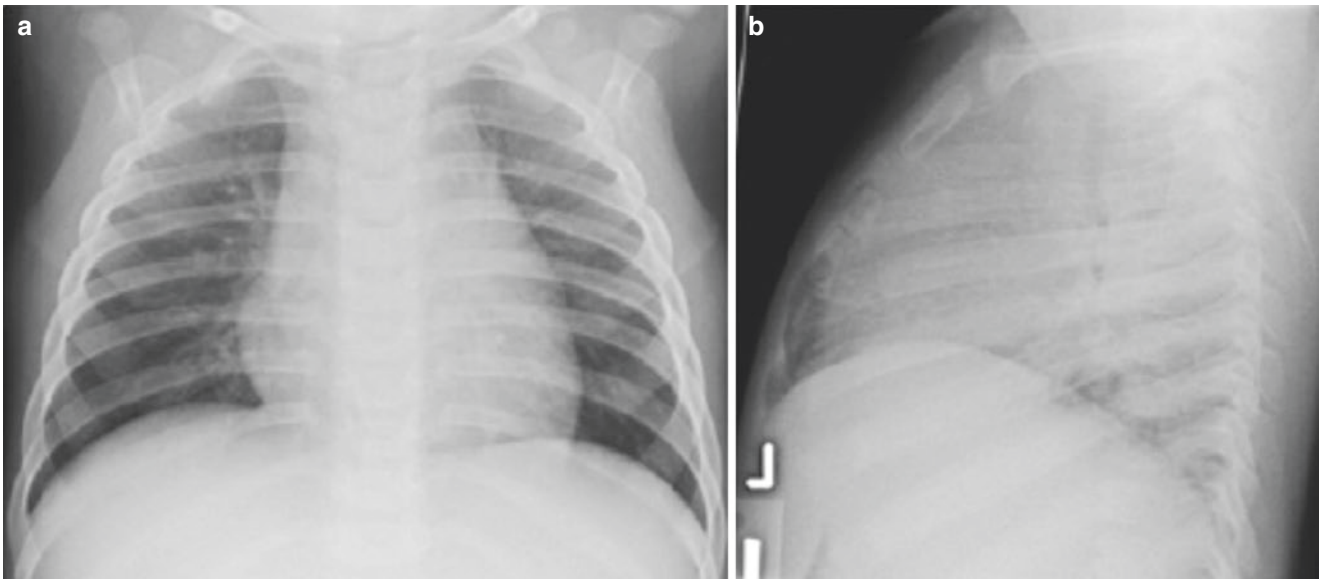

Fig. 7.44 Normal (**a**) AP and (**b**) lateral radiographs of an infant girl demonstrate that the anterior ribs curve downward relative to the posterior ribs and that the hemidiaphragms are curved on both the AP and lateral views

The shape of the chest wall and the orientation of the diaphragm change to accommodate increasing lung volume, and these changes can be clearly seen on radiographs. Normally, the anterior ribs are angled inferiorly relative to the posterior ribs (Fig. 7.44). As the chest expands to meet increasing lung capacity, the anterior ribs rise and become relatively horizontally oriented. Each hemidiaphragm is normally curved, with the apex of the curvature near the junction of the medial and middle thirds of each hemidiaphragm. As lung volume increases, the diaphragm flattens, and the apex of the diaphragm becomes positioned anteriorly. Flattening of the hemidiaphragms is especially easy to visualize on the lateral view radiograph. If accessory muscles of respiration are being used as a sign of severe respiratory distress, the upper sternum is bowed outwardly, and this can be visualized on the lateral view of a chest radiograph (Fig. 7.45).

The classical pathological description for bacterial pneumonia, specifically streptococcal pneumonia, is lobar consolidation. Unlike viruses, bacteria infect the alveoli. The inflammatory response initiated by the bacteria causes the normally aerated alveoli to become filled with fluid, cells,

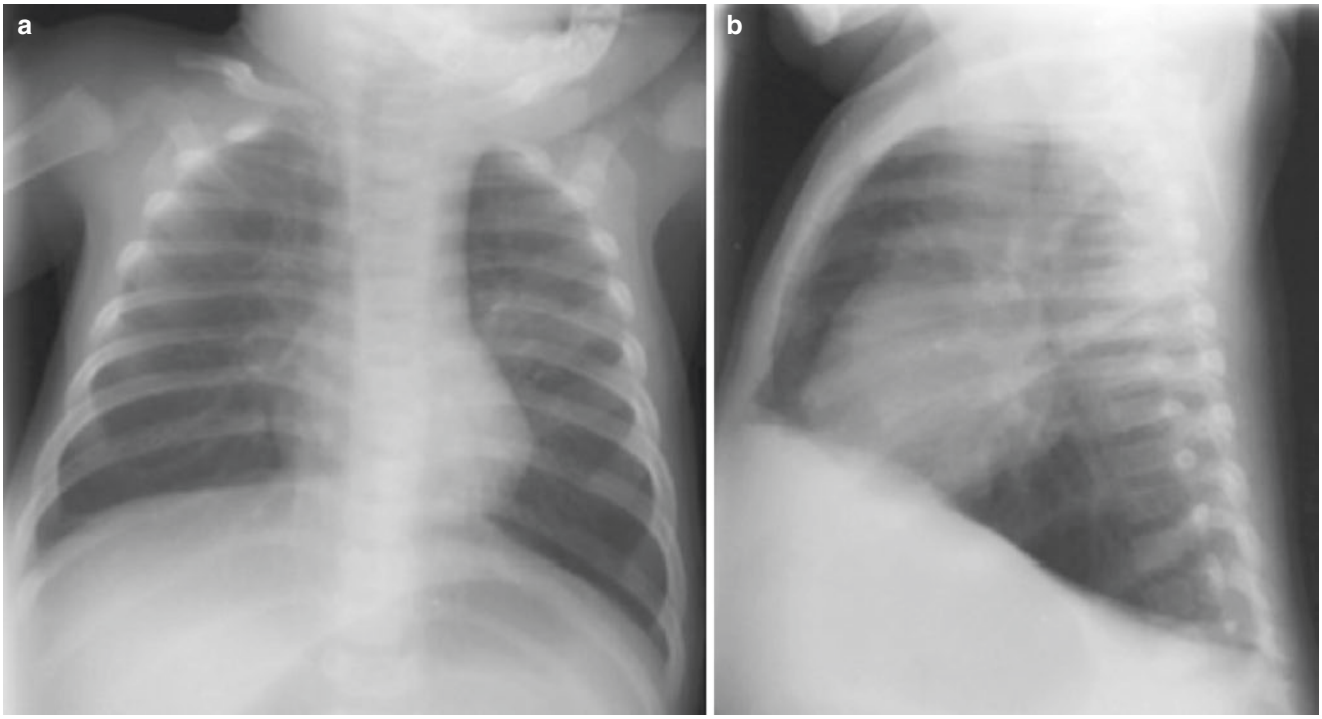

Fig. 7.45 A 4-month-old girl, who presented with tachypnea and fever, shows the typical manifestations of children with viral lower respiratory tract illness. Lungs are hyperinflated as evidenced by bilateral hyperlucent lungs, flattened hemidiaphragms, and anterior bowing of the sternum. There is a mild atelectasis in both perihilar regions. No microbial organism could be determined. (**a**) PA, (**b**) lateral projections

and inflammatory reactors. The bacteria also injure the alveolar walls so that the fluid and inflammation can easily spread to adjacent alveoli. Fully developed channels of Lambert and pores of Kohn also contribute to the spread of infection to nearby alveoli and groups of alveoli called lobules. The lumina of the bronchioles in the affected areas may be filled with inflammatory exudates, but not to the same degree as in viral infections. Moreover, the bronchial walls and interstitial tissues generally do not become inflamed, as the infection primarily affects the alveoli. Radiographically, the normally dark aerated lung becomes opacified with cells, cellular debris, and fluid, initially spreading from adjacent alveoli and lobules to encompass lung segments and eventually to the entire lobe (Fig. 7.46). The branching airways remain relatively aerated and appear lucent, in contrast to the adjacent opacified lung parenchyma. This appearance, referred to as an air bronchogram, is one of the radiographic hallmarks of pneumonia. However, air bronchograms are also seen in some cases of atelectasis when the larger airways remain air filled, as in compressive atelectasis.

Complete lobar consolidation is uncommon in children, probably because of underdeveloped channels of collateral airflow. The radiographic findings of classical lobar pneumonia are discussed briefly here. More in-depth discussion and descriptions can be found in other recent textbooks of pediatric radiology [28] and pediatric thoracic imaging [196].

In diagnosing lobar pneumonias, radiographic findings that show that airspace opacity is space occupying such as mediastinal shift away from the opacity and bowing of the fissures away from the airspace disease are important in distinguishing pneumonia from atelectasis, which causes volume loss. When an airspace consolidation abuts a fissure or is defined by a segment, the border of the opacity is straight. By contrast, opacities involving the central portions of the lobes or segments have more irregular borders. Infections which irritate the pleural surface are associated with pleural effusion. When an airspace opacity (e.g., lobar pneumonia) abuts a soft tissue structure, such as the mediastinum or diaphragm, the normal borders of the soft tissue structure blend in imperceptibly with the pneumonia. The addition of the lateral view to the frontal view is essential for accurately localizing airspace disease, as it provides three-dimensional information.

Lung infection by *M. pneumoniae*, as well as other bacteria including *Staphylococcus aureus* and gram-negative bacteria, presents a pathological pattern characteristic of bronchopneumonia or lobular pneumonia. The initial infection and injury occurs at the terminal and respiratory bronchioles and spreads to the peribronchial alveoli. The alveoli

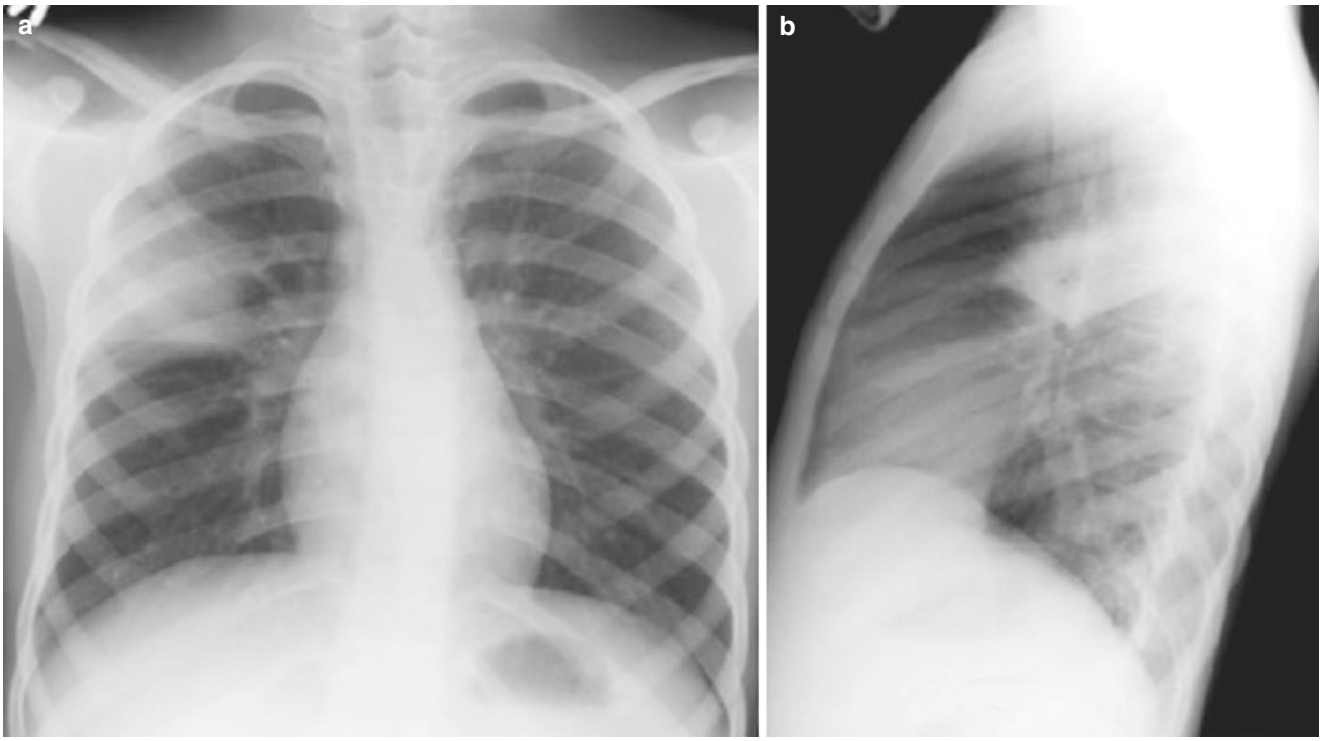

Fig. 7.46 A 13-year-old boy who presented with cough and fever. (**a**) PA and (**b**) lateral radiographs demonstrate a dense consolidation in the right upper lobe abutting the major and minor fissures. Sputum cultures grew *Pneumococcus*, and the patient became well on penicillin therapy

then become filled with fluid and inflammatory cells, and the reaction spreads to adjacent alveoli and acini. Peribronchial edema, interstitial thickening, small airway occlusion, and lobar consolidation may all occur [28, 196]. Thus, the radiographic pattern of bronchopneumonia may be a composite of the findings seen in interstitial pneumonia and lobar pneumonia.

The radiological manifestations of certain LRTIs are peculiar to children. In children younger than 8 years of age whose collateral pathways of circulation have not yet developed, some bacterial pneumonias are round and may mimic a mass. In a patient with a corresponding clinical history, a round mass in the chest should be considered pneumonia; and, in fact, when the illness presents in this way, it is typically called *round* pneumonia (Fig. 7.47) [28, 55, 56, 196]. Round pneumonia has a predilection for the lower lobes. The most common pathogen of round pneumonia is *S. pneumoniae* [28, 55, 56, 196]. Occasionally, lung cysts, called pneumatoceles, develop as a result of severe staphylococcal infections, but have also been reported in cases of *S. pneumoniae*, *H. Influenzae*, and *Escherichia coli*. Pneumatoceles are thin-walled, air-containing cavities that develop rapidly within the first week of infection (Fig. 7.48). Necrosis of the walls of small airways allows air to dissect into the interstitium causing these focal air collections. If pneumatoceles rupture into the pleural space, a pneumothorax may occur. Pneumatoceles typically resolve within 3 weeks.

The Usefulness of Chest Imaging in Diagnosing and Imaging Pneumonia

Despite the three distinct pathological and radiographic patterns of pneumonia, radiographic findings in pneumonia are broad, and the usefulness of chest radiographs in diagnosing pneumonia is controversial.

At best, the level of diagnostic certainty provided by radiological findings is quite high with respect to LRTI [28, 196]. Among young children, the most common cause of pneumonia is viral. In these patients, when a pattern of hyperinflation or uneven aeration and bronchial wall thickening is observed, its etiology is most likely viral. By contrast, older children, who have mature, adult-like airways and collateral pathways of air drift, lobar consolidations that may develop are most likely bacterial in origin [28, 196]. Radiographs are useful in diagnosing LRTIs at these two extremes of the pediatric spectrum.

However, many studies have shown that the radiographic patterns of pneumonias caused by different infectious agents overlap, making the findings on chest radiographs unreliable for predicting the etiology of pneumonia. For example, while

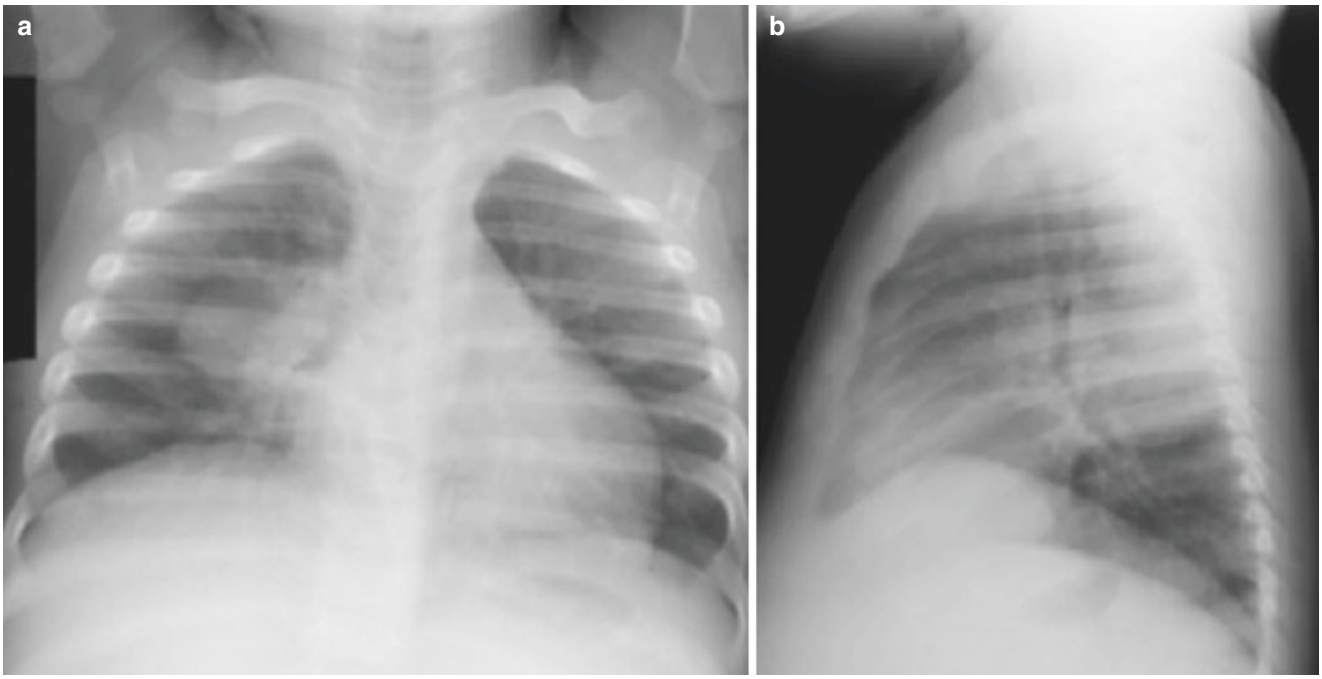

Fig. 7.47 A 9-month-old girl with a 3-week history of cough and fever (102 °F). (**a**) Frontal and (**b**) lateral radiographs demonstrate a round mass-like opacity in the superior segment of the right lower lobe. After antibiotic therapy, the mass resolved and the chest radiograph returned to normal

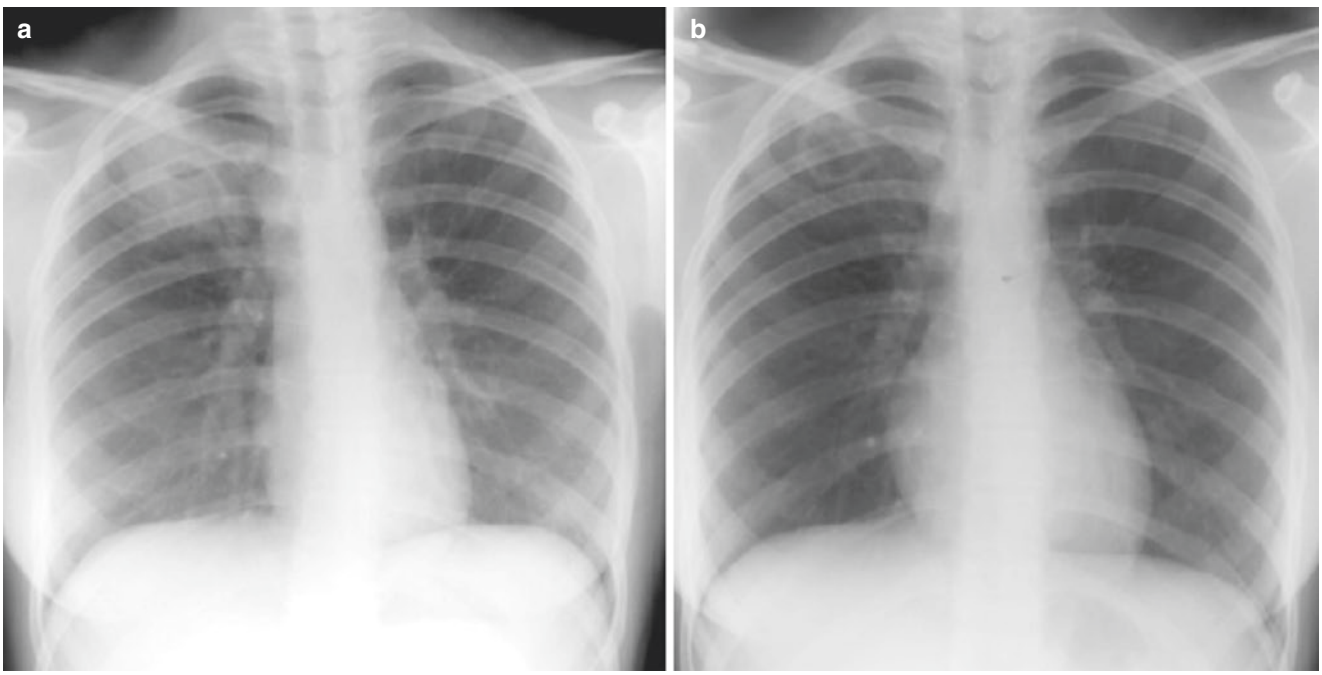

Fig. 7.48 A 14-year-old girl who presented with a fever of 104 °F, cough, and right upper chest pain. (**a**) Initial chest radiograph demonstrates right upper lobe opacity with an air-fluid level, consistent with a lung abscess. Sputum cultures revealed *Staphylococcus aureus*. (**b**) A chest radiograph obtained 1 week later shows that the abscess develops into a thin-walled lucent structure, a pneumatocele

RSV most commonly presents with the typical *viral pattern* characterized by hyperinflation, peribronchial cuffing, and perihilar opacities [28, 196], patients admitted to the hospital for adenovirus most often have lobar consolidation and pleural effusions, findings that are classically described for bacterial pneumonias [28, 196]. As mentioned previously, *Mycobacterium* is the most common cause of pneumonia in school-age children. Because *Mycobacterium* infects both the epithelial linings of the bronchioles and the alveoli, the radiographic pattern is mixed with the radiographic findings of both the alveolar and interstitial patterns [28, 196]. In addition, viral infections may be superimposed by bacterial infections, and a mixed radiographic pattern may reflect this.

Interobserver variation also affects diagnosis of an abnormal chest radiograph. Poor interobserver agreement and false-negative errors further complicate the use of plain radiographs in distinguishing bacterial and viral causes of pneumonia [189, 197]. This is especially true in young infants whose hyperinflation and interstitial abnormalities tend to be interpreted more subjectively [198]. The interobserver agreement in normal radiographs is much better than radiographs of pneumonia [199].

Not surprisingly, the *if and when* of ordering chest radiographs in the initial assessment of patients with suspected LRTIs remains controversial. In most cases of uncomplicated community-acquired pediatric pneumonia, imaging is not needed for initial diagnosis. Moreover, because LRTIs are routinely diagnosed and treated based on clinical findings, the addition of radiographs generally does not aid in diagnosis or result in more responsive treatment plans; nor is there any evidence that plain radiographs affect or hasten recovery [200]. For this reason, the World Health Organization does not recommend chest radiography in the management of acute LRTIs in children of developing countries. Likewise, the British Thoracic Society and the American National Guideline Clearinghouse do not advise routine radiographs for children suspected to have community-acquired pneumonia [201]. Despite these recommendations, in countries where radiographic imaging is readily available, respiratory tract infections remain one of the most common indications for imaging.

Perhaps chest radiographs are most useful in determining the diagnosis and affecting the management of children with suspected LRTIs when the clinical findings are ambiguous, failing to distinguish typical bacterial from atypical pneumonias. In suspected cases of LRTI, the purpose of a chest radiograph is to distinguish bacterial pneumonias from viral pneumonias and thereby distinguish which patients need antibiotic therapy. Chest radiography, in these circumstances, is generally useful. Only a small percentage of children with bacterial pneumonia have the clinical and radiographic appearance of lower viral respiratory infections. Thus, the high negative predictive value of radiography in excluding bacterial pneumonia is valuable in distinguishing those with bacterial pneumonia who should be treated with antibiotics from those with viral pneumonia who can be treated more expectantly [28, 196].

Routine follow-up chest radiographs are not needed in childhood community-acquired pneumonia if the child has a clinically uneventful recovery [28, 196]. Previously, healthy children with community-acquired pneumonia who have complete clinical resolution have normal chest radiographs 2–3 months after the initial infection. Prior to 3 months after the initial infection, radiographic abnormalities may still be present even if the infection is adequately treated [28, 196]. Thus, follow-up chest radiographs sooner than 2–3 months may give the mistaken impression of a lingering infection where one does not exist.

However, chest radiographs are indicated in children with persistent or worsening signs of pneumonia, particularly in circumstances where there may be complications of pneumonia or underlying problems such as a retained foreign body, congenital lung malformation, or atypical infections. In children with recurrent infections in the same location where an underlying congenital cause is suspected, the patient should be imaged during a well period.

Radiographs in patients with the clinical and radiographic picture of bacterial pneumonia can also help predict short-term mortality. Radiographs are very sensitive in detecting pleural effusions. As little as 50 cc of pleural fluid can be detected on a lateral radiograph [202]. Pneumonias associated with pleural effusions have a higher short-term mortality than pneumonias without effusions (Fig. 7.49) [203].

It is debatable whether children under 5 years of age with leukocytosis (>20,000/mm^3) and fever (temperature greater than 39 °C), but without signs of respiratory illness, should have chest radiographs to find occult pneumonias. Chest radiographs have been shown to reveal occult pneumonias in 26% of children without respiratory symptoms, but with high fever and an increased white blood cell count [204]. Although it is common practice in some institutions to obtain chest radiographs in all febrile infants, only those with respiratory symptoms are likely to have radiographic pneumonia. Pneumonia is typically found in only a minority of febrile infants without respiratory symptoms.

A final consideration on the use of imaging studies to diagnose and treat pneumonia is the harmful effect of radiation on children. Devices emitting ionizing radiation such as X-ray machines and CT should be operated under the ALARA principle [182, 183, 205]. Radiation exposure should be minimized in children because it is well known that for the same dose, children are more susceptible to radi-

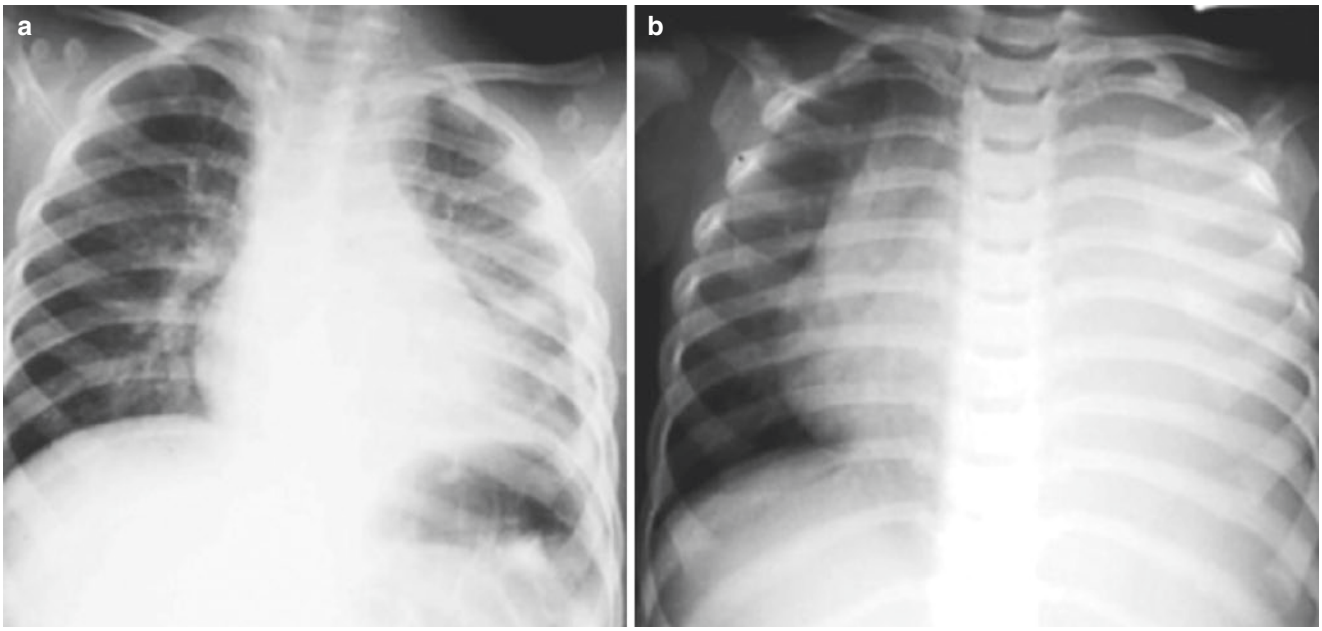

Fig. 7.49 An 18-month-old boy with progression of a left lower lobe pneumonia. (**a**) The initial chest radiograph shows a left lower lobe pneumonia and small effusion. (**b**) Three days later, the entire left lung is opacified. A chest tube was required to drain the left empyema, and the patient was hospitalized for 3 weeks

ation effects than adults. The 1-year-old *lifetime* cancer mortality rate from radiation is higher than in adults by an entire order of magnitude [206]. Children incur a far greater effective dose of radiation when undergoing CT than plain radiographs or fluoroscopy.

Traditionally, both frontal and lateral views have been considered standard views for evaluating the chest in children with pneumonia. The frontal radiograph is fundamental in creating a global picture of the chest. Most radiographic abnormalities can be visualized on this single view. The addition of the lateral view confirms the findings on the frontal radiograph and helps to locate any abnormalities in three dimensions. The lateral view also is more sensitive than the frontal view in detecting left lower lobe abnormalities in the retrocardiac region and in the pleural space [202] and in detecting hyperinflation. Two views have been shown to increase conspicuity of pneumonia compared to one view [207]. However, others have shown that the addition of a lateral radiograph did not improve sensitivity or specificity in the diagnosis of pneumonia [208]. The lateral radiograph more than doubles the dose of radiation per study of the chest. The radiation risks associated with the lateral radiograph as well as the costs that are incurred from ordering an additional study should be weighed against its usefulness in diagnosing pneumonia.

Because CT delivers a much greater radiation dose than plain radiographs, CT is reserved for only the most serious cases of pneumonia for which potential surgical intervention may be necessary or in cases of necrotizing pneumonia/empyema [205]. Like radiographs, CT is of limited value in determining the microbial etiology of pneumonia and should not be used to initially diagnose pneumonia. Even after optimizing techniques to reduce the dose of radiation in children, a chest CT delivers considerably more radiation than chest radiographs. CT is very helpful in better understanding complicated pneumonia, including cases of empyema, abscess or pulmonary cavitation, and bronchopulmonary fistula, complications which may require surgical or radiological intervention (Fig. 7.50) [209, 210]. CT and MRI are also helpful in diagnosing underlying developmental anomalies which may be causing recurrent pneumonias in the same location. Ultrasound, by contrast, delivers no ionizing radiation and is useful in evaluating pleural effusions, a common complication of pneumonia. A recent retrospective study consisting of 19 pediatric patients showed that chest ultrasound and chest CT were similar in their ability to detect loculated effusion and lung necrosis or abscess resulting from complicated pneumonia [211]. Ultrasound, however, cannot be used to diagnose or distinguish different types of pneumonia (Fig. 7.51).

An important look-alike of focal or multifocal alveolar or bacterial pneumonia occurs in sickle cell disease. The condition, referred to as acute chest syndrome, presents with alveolar disease and often a pleural effusion. Although this may, and sometimes does, represent pneumonia, it frequently represents venular thrombosis and pre-infarction.

In summary, community-acquired pneumonias of all etiologies are generally diagnosed without the need of chest

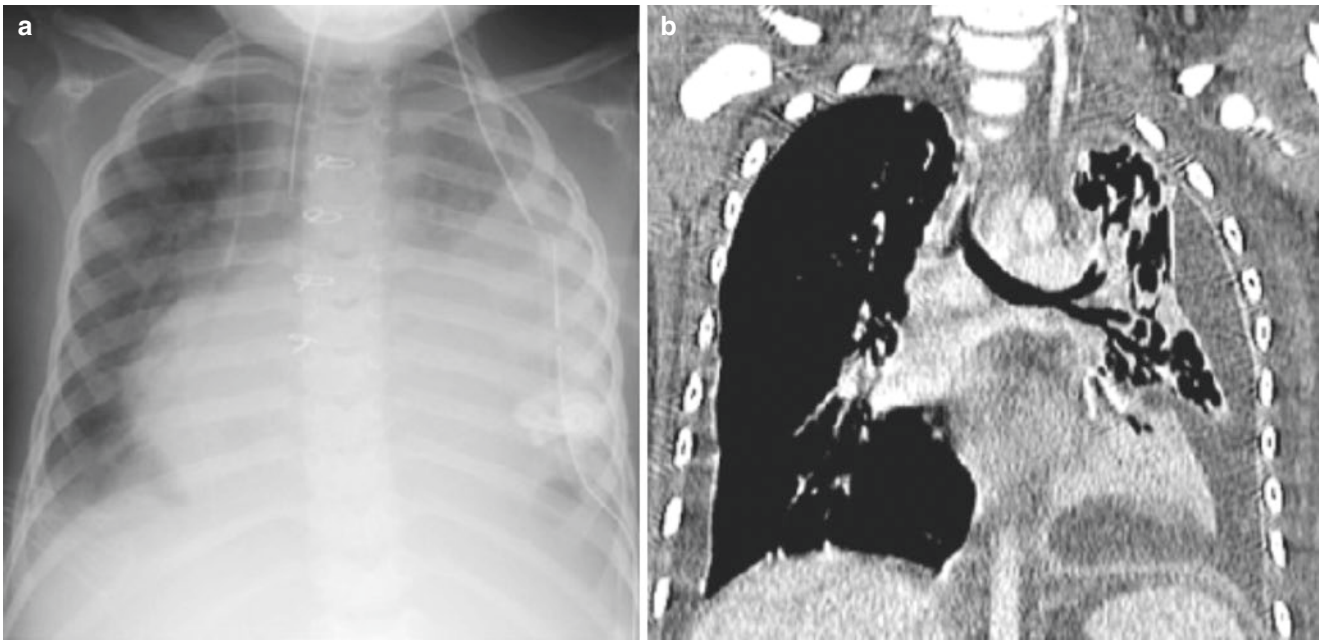

Fig. 7.50 A 3-year-old girl with a history of repaired tetralogy of Fallot who presented with high fever and left chest pain. Multiple radiographs demonstrated a left lower lobe pneumonia and pleural effusion. (**a**) Despite left chest tube placement, the left effusion persisted. (**b**) Coronal enhanced CT image better delineates the left empyema and cavitation of the left upper lobe and lingula

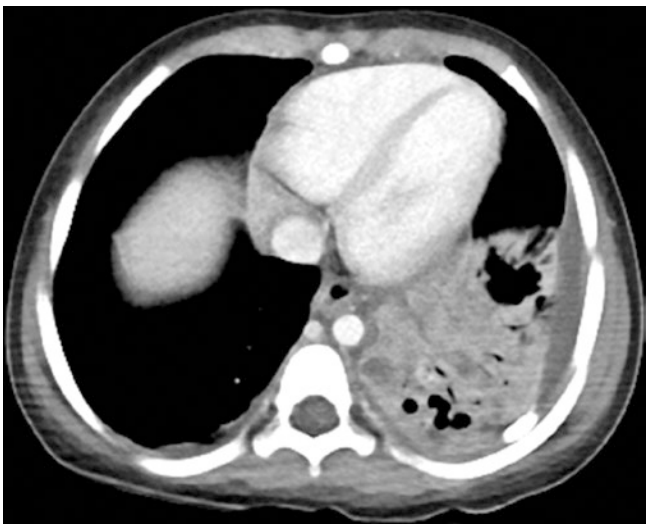

Fig. 7.51 A 3-year-old boy who presented with fever and cough. Axial enhanced CT image shows a left lower lobe pneumonia complicated by liquefaction/cavitation and empyema

radiographs. Radiography is helpful in cases where the initial clinical diagnosis is unclear, in eliciting the cause of recurrent pneumonias, or in evaluating pneumonias that do not resolve clinically despite treatment. Because computed tomography delivers a relatively high dose of ionizing radiation, CT is reserved for evaluating complicated pneumonias that may require surgical intervention or in cases of necrotizing pneumonia/empyema.

Necrotizing Pneumonia

Epidemiology

Necrotizing pneumonia (NP) is becoming an increasingly recognized complication of community-acquired pneumonia in children [212–214]. NP is also termed cavitary pneumonia or cavitary necrosis and has been associated with poor clinical outcomes in adults. Although NP has been recognized as a complication of pneumonia in adults for several decades, when initially described, NP was thought to be extremely rare in children. In fact, the first case series of NP including four children was published in 1994 [215]. Subsequently, there have been several additional case series of pediatric NP reported [216–222]. The incidence of NP appears to be increasing, similar to the observed rise in cases of complicated pneumonia overall [223]. Possible explanations for the increased incidence of NP include the emergence of particularly virulent microorganisms or simply the increased awareness and detection of this complication due to improved imaging techniques.

Pathophysiology and Microbiology of Necrotizing Pneumonia

The pathophysiology of NP is thought to be one of massive pulmonary gangrene and tissue liquefaction and necrosis secondary to bacterial infection and the resultant inflam-

matory response [224, 225]. The pathologic progression of pneumonia leads to resultant pulmonary parenchymal necrosis. The pathologic process is distinct from that of pulmonary abscess, in which bacterial infection leads to the development of a well-defined, often walled-off, area of infection. The most common causative bacteria isolated in cases of NP is *S. pneumoniae* [225, 226], though other bacterial organisms including *S. aureus* (both methicillin-sensitive and methicillin-resistant strains), other *Streptococcus* species such as *Streptococcus milleri*, *M. pneumoniae*, *C. pneumoniae*, *Pseudomonas aeruginosa*, and *Fusobacterium* species have also been reported as pathogens leading to NP [227–231]. Aspiration pneumonia leading to anaerobic infection may also lead to the development of NP. In recent years, more virulent strains of methicillin-resistant *Staphylococcus aureus* (MRSA), particularly MRSA strains producing Panton-Valentine leukocidin (PVL), have emerged in the community and may be driving the increasing incidence of pediatric NP [232–234]. Coinfection with respiratory viruses such as influenza A, including the novel H1N1 strain, has been also described in pediatric NP [235]. In addition, a recent report showed that NP can be caused by refractory mycoplasma pneumonia in children; however, it is often self-limiting and reversible with good outcomes when NP is appropriately managed [236].

Clinical Presentation

In its initial stages, the clinical presentation of necrotizing pneumonia is indistinguishable from community-acquired pneumonia. As such, NP is often diagnosed late in children who present to medical attention following treatment failure of pneumonia with oral antibiotics. Symptoms often include prolonged high fevers, cough, sputum production, tachypnea, dyspnea, and anorexia. However, many children may simply present with persistent fevers despite seemingly adequate treatment for community-acquired pneumonia. Hypoxia may be present although many children with NP do not require oxygen supplementation. NP results in the development of a pleural effusion in up to 70% of cases [226] and thus may also present with resultant pleuritic chest pain. Physical exam findings are consistent with other complicated pneumonias with parapneumonic effusion. Common laboratory findings are an elevated white blood cell count and low hemoglobin and low serum albumin. If pleural fluid is analyzed, parameters are consistent with empyema, with elevated white blood cell counts, decreased pleural pH, elevated pleural LDH, and decreased pleural fluid glucose.

Imaging of Necrotizing Pneumonia

Chest radiography, including PA, lateral, and, on occasion, decubitus views, constitute the initial imaging for diagnosis of NP [237]. The initial findings on chest radiography are variable. There may merely be an alveolar airspace disease. However, in many instances, there is an associated, ipsilateral pleural effusion, which may be free flowing or loculated. If free flowing, the concern for NP should be present. If the effusion is loculated (representing an organizing empyema), the presence of NP should be highly suspected (Fig. 7.52). Often by the time of initial imaging, there is air (or air and fluid)-containing cystic areas noted by chest radiography. This may represent necrotic regions within the lung parenchyma, loculated collections within an empyema, or both (Fig. 7.53). It is impossible to determine the location of these cystic areas by chest radiography alone. Therefore, even though the diagnosis of NP can be suspected by plain chest radiography, CT is necessary to clearly define the extent and nature of disease. CT should always be performed with contrast enhancement to clearly define the pleura and clarify the pleural or parenchymal location of cysts and potentially drainable pleural fluid (Fig. 7.53d). If characterization of the pleural process is required, usually prior to thoracostomy drainage, ultrasound can be employed to determine if the effusion is loculated and, if so, where the largest drainable collections are located. Ultrasound-guided drainage of the effusion may also be employed. It is possible that NP is underdiagnosed as CT may not always be obtained in the management of prolonged, complicated courses of pneumonia. This is particularly true when a significant pleural effusion is present and assumed to be the reason for persistent symptoms.

Radiographic CT criteria for NP have been established and include the loss of normal pulmonary parenchymal architecture, the presence of multiple small air- or fluid-filled cavities, and decreased parenchymal enhancement [237] (Figs. 7.52 and 7.53). CT generally reveals segments of the lung showing multiple areas of lung parenchyma containing air, air and fluid, or non-enhancing fluid surrounded by contrast-enhancing lung parenchyma without a defined rim of enhancement. This is distinguished from pulmonary abscess in which CT shows a well-defined enhancing rim outlining a single pulmonary cavity.

Management, Complications, and Long-Term Outcomes of Necrotizing Pneumonia

Since NP involves the presence of multiple fluid and subsequently air-filled cavities within the affected lung parenchyma, there is a heightened concern over the risk of

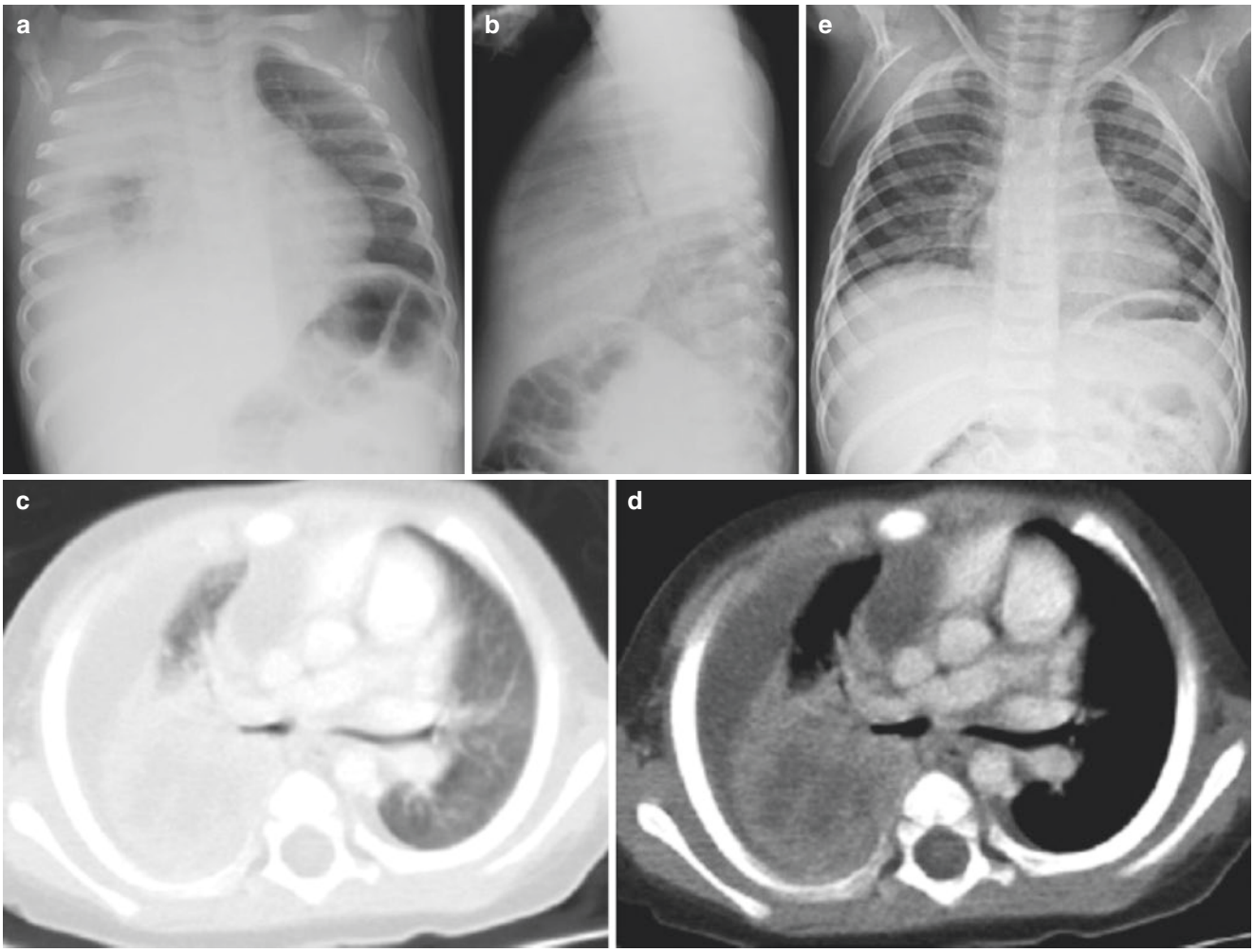

Fig. 7.52 A 9-month-old girl who presented with fever, cough, and respiratory distress. (**a**) PA chest radiograph shows a consolidation of the majority of the right lung and possible loculated pleural effusion. (**b**) The lateral chest radiograph confirms significant opacification. Neither suggests cavitation. (**c**) Axial lung window CT image suggests irregular areas of non-enhancing tissue, representing necrotic areas and surrounded by enhancing lung parenchyma. The necrotic areas have not yet drained their fluid and become air containing. There is a large partially located pleural effusion. (**d**) Axial enhanced soft tissue window CT image more clearly confirms areas of non-enhancing pulmonary necrosis with surrounding enhancing lung. The pleura is enhanced. (**e**) Follow-up PA chest radiograph obtained 9.5 months following the image in (**a**) is essentially normal

developing a bronchopleural fistula (BPF), defined as a persistent air leak lasting over 48 hours. In a small study of pediatric NP, five of the nine NP cases developed BPF following pleural intervention [238]. In a more recent larger series of cases, a smaller proportion of patients developed a fistula, and those who did develop a fistula had chest drains in place for over 7 days [226]. The observed decline may be attributed to awareness of the risk of a chest drain in the presence of NP, resulting in minimization of the drainage time. Therefore, it may be prudent to remove a pleural drain within 7 days of placement to decrease the risk of complication.

There have been no randomized trials of surgical intervention in pediatric NP; and in many cases, conservative management with antibiotics, chest drainage, and intrapleural thrombolytics such as urokinase or tissue plasminogen activator (tPa) may be sufficient. Video-assisted thoracoscopic surgery (VATS) may be indicated in certain situations and may reduce hospital length of stay [239]. However, although several small studies have suggested lobar resection as therapy for NP [240–243] without definitive scientific evidence, such surgery may not be necessary. In spite of the CT evidence of extensive and severe lung damage, follow-up studies have shown significant normalization of the previously affected parenchyma [226, 244] (Figs. 7.52e and 7.53e). The capacity of the young lung for repair is remarkable in its completeness and rapidity. Despite the extensive radiographic abnormalities

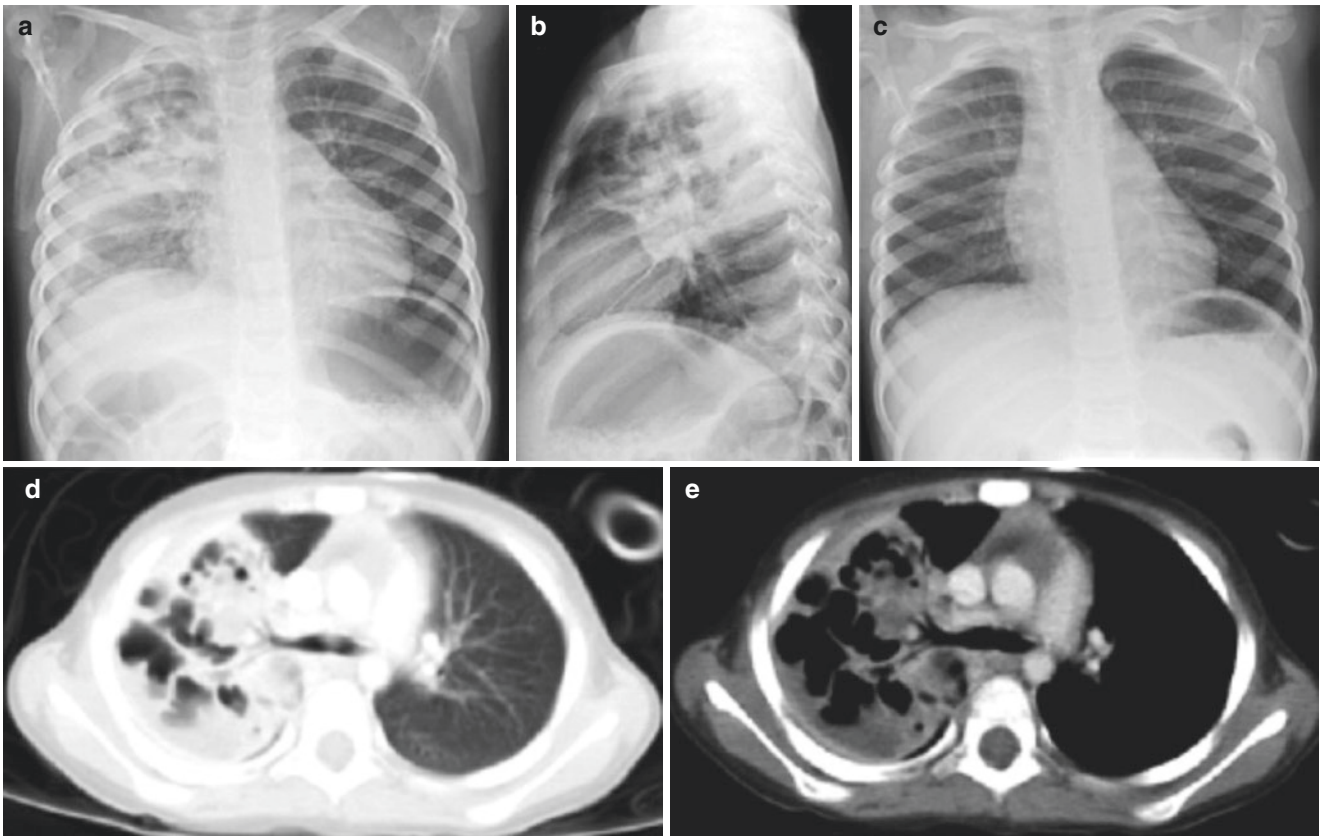

Fig. 7.53 A 14-month-old girl with fever, cough, and chest pain. (**a**) PA chest radiograph shows multiple cavities in the upper right hemithorax. It is unclear whether these are in the lung or pleura. There is a moderate-sized pleural effusion, questionably partially loculated. (**b**) Lateral chest radiograph confirms the PA chest radiograph observations. (**c**) Axial lung window CT image confirms the cavities within the lung parenchyma with an effusion. (**d**) Axial enhanced soft tissue window CT image more clearly delineates the enhanced pleura separating the fluid in the pleural space and the air- and fluid-filled lung cysts. (**e**) Follow-up PA chest radiograph obtained 3.5 months after the initial chest radiograph (**a**) reveals almost complete clearing of the affected lung

and significant short-term morbidity caused by NP, the long-term clinical and radiographic outcomes for patients seen in follow-up have been good. Clinical symptoms tend to resolve with therapy in 3–4 weeks. Significant normalization of pulmonary parenchyma seen on chest radiographs and CT also occurs within several months of acute illness. This pattern of improvement suggests the lung damage caused by NP in children is transient and that NP should be recognized as a severe, yet self-limiting and reversible, disease.

Acknowledgement The author of this chapter would like to sincerely thank the previous authors, Jeanne S. Chow, MD, Ellen M. Chung, MD, Andrew A. Colin, MD, Robert H. Cleveland, MD, and Gregory S. Sawicki, MD involved with previous edition of this chapter.

References

1. Winant AJ, Ngo AV, Phillips GS, Lee EY. Computed tomography of congenital lung malformations in children: a primer for radiologists. Semin Roentgenol. 2018;53(2):187–96.
2. Thacker PG, Schooler GR, Caplan MJ, Lee EY. Developmental lung malformations in children: recent advances in imaging techniques, classification system, and imaging findings. J Thorac Imaging. 2015;30(1):29–43.
3. Thacker PG, Rao AG, Hill JG, Lee EY. Congenital lung anomalies in children and adults: current concepts and imaging findings. Radiol Clin North Am. 2014;52(1):155–81.
4. Lee EY, Dorkin H, Vargas SO. Congenital pulmonary malformations in pediatric patients: review and update on etiology, classification, and imaging findings. Radiol Clin N Am. 2011;49(5):921–48.
5. Lee EY, Boiselle PM, Cleveland RH. Multidtector CT evaluation of congenital lung anomaies. Radiology. 2008;247(3):632–48.
6. Donnelly LF, Lucaya J, Ozelame V, et al. CT findings and temporal course of persistent pulmonary interstitial emphysema in neonates: a multiinstitutional study. AJR Am J Roentgenol. 2003;180(4):1129–33.
7. Pasha AB, Chen XQ, Zhou GP. Bronchopulmonary dysplasia: pathogenesis and treatment. Exp Ther Med. 2018;16(6):4315–21.
8. Taglauer E, Abman SH, Keller RL. Recent advances in antenatal factors predisposing to bronchopulmonary dysplasia. Semin Perinatol. 2018;42(7):413–24.
9. Liszewski MC, Stanescu AL, Phillips GS, Lee EY. Respiratory distress in neonates: underlying causes and current imaging assessment. Radiol Clin North Am. 2017;55(4):629–44.

10. Liszewski MC, Lee EY. Neonatal lung disorders: pattern recognition approach to diagnosis. AJR Am J Roentgenol. 2018;210(5):964–75.
11. Tracy MC, Mathew R. Complicated pneumonia: current concepts and state of the art. Curr Opin Pediatr. 2018;30(3):384–92.
12. Cevik M, Boleken ME, Kurkcuoglu IC, Eser I, Dorterler ME. Pulmonary hydatid disease is difficult to recognized in children. Pediatr Surg Int. 2014;30(7):737–41.
13. Yikilmaz A, Lee EY. CT imaging of mass-like nonvascular pulmonary lesions in children. Pediatr Radiol. 2007;37(12):1253–63.
14. Erdem CZ, Erdem LO. Radiological characteristics of pulmonary hydatid disease in children: less common radiological appearances. Eur J Radiol. 2003;45(2):123–8.
15. Haliloglu M, Saatci I, Akhan O, Ozmen MN, Besim A. Spectrum of imaging findings in pediatric hydatid disease. AJR Am J Roentgenol. 1997;169(6):1627–31.
16. Lee EY, Tracy DA, Mahmood SA, Weldon CB, Zurakowski D, Boiselle PM. Preoperative MDCT evaluation of congenital lung anomalies in children: comparison of axial, multiplanar, and 3D images. AJR Am J Roentgenol. 2011;196(5):1040–6.
17. Lee EY, Siegel MJ, Sierra LM, Foglia RP. Evaluation of angioarchitecture of pulmonary sequestration in pediatric patients using 3D MDCT angiography. AJR Am J Roentgenol. 2004;183(1):183–8.
18. Wasilewska E, Lee EY, Eisenberg RL. Unilateral hyperlucent lung in children. AJR Am J Roentgenol. 2012;198(5):W400–14.
19. Moore MA, Wallace EC, Westra SJ. Chest trauma in children: current imaging guidelines and techniques. Radiol Clin N Am. 2011;49(5):949–68.
20. Piccolo CL, Ianniello S, Trinci M, et al. Diagnostic imaging in pediatric thoracic trauma. Radiol Med. 2017;122(11):850–65.
21. Donnelly LF, Klosterman LA. Subpleural sparing: a CT finding of lung contusion in children. Radiology. 1997;204(2):385–7.
22. Manson D, Babyn PS, Palder S, Bergman K. CT of blunt chest trauma in children. Pediatr Radiol. 1993;23(1):1–5.
23. Lichtenberger JP 3rd, Biko DM, Carter BW, et al. Primary lung tumors in children: radiologic-pathologic correlation from the radiologic pathology archives. Radiographics. 2018;38(7):2151–72.
24. Abbo O, Pinnagoda K, Brouchet L, et al. Wilms tumor, pleuropulmonary blastoma, and DICER 1: case report and literature review. World J Surg Oncol. 2018;16(1):164. https://doi.org/10.1186/s12957-018-1469-4.
25. Lucia-Casadonte C, Kulkami S, Restrepo R, Gonzalez-Vallina R, Brathwaite C, Lee EY. An unusual case of pleuropulmonary blastoma in a child with jejunal hamartomas. Case Rep Pediatr. 2013;2013:140508. Epub 2013 July 22.
26. Zapala MA, Ho-Fung VM, Lee EY. Thoracic neoplasms in children: contemporary perspectives and imaging assessment. Radiol Clin North Am. 2017;55(4):657–76.
27. Chang AB, Bush A, Grimwood K. Bronchiectasis in children: diagnosis and treatment. Lancet. 2018;392(10150):866–79.
28. Laya BF, Amini B, Zucker EJ, Kilborn T, Vargas SO, Lee EY. Lung. In: Lee EY, editor. Pediatric radiology: practical imaging evaluation of infants and children. 1st ed: Wolters Kluwer; Philadelphia, USA. 2017.
29. Wasilewska E, Morris AD, Lee EY. Case of the season: Lemierre syndrome. Semin Roentgenol. 2012;47(2):103–5.
30. Rafati F, Bhalla V, Chillal V, Thyagarajan M. Lemierre syndrome: a diagnostic dilemma in paediatric patients. J Surg Case Rep. 2017;2017(12):rjx210. https://doi.org/10.1093/jscr/rjx210. eCollection 2017 Dec.
31. Kilborn T, Chu WCW, Kas KM, Laya B, Lee EY. Current updates on HIV-related pulmonary disease in children: what do radiologists and clinicians need to know? S Afr J Radiol. 2015;19(2):a928.
32. Griffith-Richards SB, Goussard P, Andronikou S, et al. Cavitating pulmonary tuberculosis in children: correlating radiology with pathogenesis. Pediatr Radiol. 2007;37(8):798–804.
33. Makrygianni EA, Palamidou F, Kaditis AG. Respiratory complictions following hydrocarbon aspiration in children. Pediatr Pulmonol. 2016;51(6):560–9.
34. Jariwala MP, Laxer RM. Primary vasculitis in childhood: GPA and MPA in childhood. Front Pediatr. 2018;226(6) https://doi.org/10.3389/fped.2018.00226. eCollection 2018.
35. Filocamo G, Torreggiani S, Agostoni C, Esposito S. Lung involvement in childhood onset granulomatosis with polyangiitis. Pediatr Rheumatol Online J. 2017;15(1):28. https://doi.org/10.1186/s12969-017-0150-8.
36. Wadsworth DT, Siegel MJ, Day DL. Wegener's granulomatosis in children: chest radiographic manifestations. AJR Am J Roentgenol. 1994;163(4):901–4.
37. Levine D, Akikusa J, Manson D, Silverman E, Schneider R. Chest CT findings in pediatric Wegener's granulomatosis. Pediatr Radiol. 2007;37(1):57–62.
38. Lohrmann C, Uhl M, Schaefer O, Ghanem N, Kotter E, Langer M. Serial high-resolution computed tomography imaging in patients with Wegener granulomatosis: differentiation between active inflammatory and chronic fibrotic lesions. Acta Radiol. 2005;46(5):484–91.
39. Kuhlman JE, Hruban RH, Fishman EK. Wegener granulomatosis: CT features of parenchymal lung disease. J Comput Assist Tomogr. 1991;15(6):948–52.
40. Seely JM, Jones LT, Wallace C, Sherry D, Effmann EL. Systemic sclerosis: using high-resolution CT to detect lung disease in children. AJR Am J Roentgenol. 1998;170(3):691–7.
41. Kramer SS, Wehunt WD, Stocker JT, Kashima H. Pulmonary manifestations of juvenile laryngotracheal papillomatosis. AJR Am J Roentgenol. 1985;144(4):687–94.
42. Braier J, Chantada G, Rosso D, et al. Langerhans cell histiocytosis: retrospective evaluation of 123 patients at a single institution. Pediatr Hematol Oncol. 1999;16(5):377–85.
43. Abbott GF, Rosado-de-Christenson ML, Franks TJ, Frazier AA, Galvin JR. From the archives of the AFIP: pulmonary Langerhans cell histiocytosis. Radiographics. 2004;24(3):821–41.
44. Forester CM, Terry J, Lee EY, Simoneau T, Haver K. Skin lesions and lung cyst in a neonate. J Pediatr. 2012;160(6):1061–.e1.
45. Odev K, Guler I, Altinok T, Pekcan S, Batur A, Ozbiner H. Cystic and cavitary lung lesions in children: radiologic findings with pathologic correlation. J Clin Imaging Sci. 2013;3:60. https://doi.org/10.4103/2156-7514.124087. eCollection 2013.
46. Grenier P, Valeyre D, Cluzel P, Brauner MW, Lenoir S, Chastang C. Chronic diffuse interstitial lung disease: diagnostic value of chest radiography and high-resolution CT. Radiology. 1991;179(1):123–32.
47. Brauner MW, Grenier P, Mouelhi MM, Mompoint D, Lenoir S. Pulmonary histiocytosis X: evaluation with high-resolution CT. Radiology. 1989;172(1):255–8.
48. Tateishi U, Hasegawa T, Kusumoto M, et al. Metastatic angiosarcoma of the lung: spectrum of CT findings. AJR Am J Roentgenol. 2003;180(6):1671–4.
49. Abbott GF, Rosado-de-Christenson ML, Frazier AA, Franks TJ, Pugatch RD, Galvin JR. From the archives of the AFIP: lymphangioleiomyomatosis: radiologic-pathologic correlation. Radiographics. 2005;25(3):803–28.
50. Newman B, Urbach AH, Orenstein D, Dickman PS. Proteus syndrome: emphasis on the pulmonary manifestations. Pediatr Radiol. 1994;24(3):189–93.
51. Biko DM, Schwartz M, Anupindi SA, Altes TA. Subpleural lung cysts in down syndrome: prevalence and association with coexisting diagnoses. Pediatr Radiol. 2008;38(3):280–4.

52. Gonzalez OR, Gomez IG, Recalde AL, Landing BH. Postnatal development of the cystic lung lesion of Down syndrome: suggestion that the cause is reduced formation of peripheral air spaces. Pediatr Pathol. 1991;11(4):623–33.
53. Zamora AC, Collard HR, Wolters PJ, Webb WR, King TE. Neurofibromatosis-associated lung disease: a case series and literature review. Eur Respir J. 2007;29(1):210–4.
54. Wood JR, Bellamy D, Child AH, Citron KM. Pulmonary disease in patients with Marfan syndrome. Thorax. 1984;39(10):780–4.
55. Liu YL, Wu PS, Tsai LP, Tsai WH. Pediatric round pneumonia. Pediatr Neonatolo. 2014;55(6):491–4.
56. Restrepo R, Palani R, Matapathi UM, Wu YY. Imaging of round pneumonia and mimics in children. Pediatr Radiol. 2010;40(12):1931–40.
57. Laya BF. Revisiting and redefining the standards in tuberculosis imaging. Pediatr Radiol. 2017;47(10):1235–6.
58. Fonseca-Santos J. Tuberculosis in children. Eur J Radiol. 2005;55:202–8.
59. Rottenberg GT, Shaw P. Radiology of pulmonary tuberculosis. Br J Hosp Med. 1996;56:195–9.
60. McAdams HP, Erasmus J, Winter JA. Radiologic manifestations of pulmonary tuberculosis. Radiol Clin N Am. 1995;33:655–78.
61. Agrons GA, Markowitz RI, Kramer SS. Pulmonary tuberculosis in children. Semin Roentgenol. 1993;28:158–72.
62. Leung AN, Muller NL, Pineda PR, FitzGerald JM. Primary tuberculosis in childhood: radiographic manifestations. Radiology. 1992;182:87–91.
63. McGuinness G, Naidich DP, Jagirdar J, Leitman B, McCauley DI. High resolution CT findings in miliary lung disease. J Comput Assist Tomogr. 1992;16:384–90.
64. Lamont AC, Cremin BJ, Pelteret RM. Radiological patterns of pulmonary tuberculosis in the paediatric age group. Pediatr Radiol. 1986;16:2–7.
65. Fischer GB, Mocelin H, Severo CB, Oliveira Fde M, Xavier MO, Severo LC. Histoplsmosis in children. Paediatr Respir Rev. 2009;10(4):172–7.
66. Gurney JW, Conces DJ. Pulmonary histoplasmosis. Radiology. 1996;199:297–306.
67. Wheat LJ, Wass J, Norton J, Kohler RB, French ML. Cavitary histoplasmosis occurring during two large urban outbreaks. Analysis of clinical, epidemiologic, roentgenographic, and laboratory features. Medicine (Baltimore). 1984;63:201–9.
68. Child DD, Newell JD, Bjelland JC, Spark RP. Radiographic findings of pulmonary coccidioidomycosis in neonates and infants. AJR Am J Roentgenol. 1985;145:261–3.
69. Davies SF, Sarosi GA. Epidemiological and clinical features of pulmonary blastomycosis. Semin Respir Infect. 1997;12:206–18.
70. Chuck SL, Sande MA. Infections with *Cryptococcus neoformans* in the acquired immunodeficiency syndrome. N Engl J Med. 1989;321:794–9.
71. Buff SJ, McLelland R, Gallis HA, Matthay R, Putman CE. *Candida albicans* pneumonia: radiographic appearance. AJR Am J Roentgenol. 1982;138:645–8.
72. Kassner EG, Kauffman SL, Yoon JJ, Semiglia M, Kozinn PJ, Goldberg PL. Pulmonary candidiasis in infants: clinical, radiologic, and pathologic features. AJR Am J Roentgenol. 1981;137:707–16.
73. Aquino SL, Kee ST, Warnock ML, Gamsu G. Pulmonary aspergillosis: imaging findings with pathologic correlation. AJR Am J Roentgenol. 1994;163:811–5.
74. Logan PM, Primack SL, Miller RR, Muller NL. Invasive aspergillosis of the airways: radiographic, CT, and pathologic findings. Radiology. 1994;193:383–8.
75. Knutsen AP, Slavin RG. Allergic bronchopulmonary aspergillosis in patients with cystic fibrosis. Clin Rev Allergy. 1991;9:103–18.
76. Jat KR, Vaidya PC, Mathew JL, Jondhale S, Singh M. Childhood allergic bronchopulmonary aspergillosis. Lung India. 2018;35(6):499–507.
77. Abramson S. The air crescent sign. Radiology. 2001;218:230–2.
78. Gefter WB, Weingrad TR, Epstein DM, Ochs RH, Miller WT. "Semi-invasive" pulmonary aspergillosis: a new look at the spectrum of *Aspergillus* infections of the lung. Radiology. 1981;140:313–21.
79. Zhang M, Zhang XY, Chen YB. Primary pulmonary actinomycosis: a retrospective analysis of 145 cases in mainland China. Int J Tuberc Lung Dis. 2017;21(7):825–31.
80. Cheon JE, Im JG, Kim MY, Lee JS, Choi GM, Yeon KM. Thoracic actinomycosis: CT findings. Radiology. 1998;209:229–33.
81. Hemmersbach-Miller M, Stout JE, Woodworth MH, Cox MG, Saullo JL. Norcadia infections in the transplanted host. Transpl Infect Dis. 2018;20(4):e12902. https://doi.org/10.1111/tid.12902. Epub 2018 May 7.
82. Yoon HK, Im JG, Ahn JM, Han MC. Pulmonary nocardiosis: CT findings. J Comput Assist Tomogr. 1995;19:52–5.
83. Feigin DS. Nocardiosis of the lung: chest radiographic findings in 21 cases. Radiology. 1986;159:9–14.
84. Camela F, Gallucci M, di Palmo E, et al. Pulmonary inflammatory myofibroblastic tumor in children: a case report and brief review of literature. Front Pediatr. 2018;6:35. https://doi.org/10.3389/fped.2018.00035. eCollection 2018.
85. Hajjar WA, Ashour MH, Al-Rikabi AC. Endobronchial inflammatory pseudotumor of the lung. Saudi Med J. 2001;22:366–8.
86. Kim JH, Cho JH, Park MS, et al. Pulmonary inflammatory pseudotumor – a report of 28 cases. Korean J Intern Med. 2002;17:252–8.
87. Kim TS, Han J, Kim GY, Lee KS, Kim H, Kim J. Pulmonary inflammatory pseudotumor (inflammatory myofibroblastic tumor): CT features with pathologic correlation. J Comput Assist Tomogr. 2005;29:633–9.
88. Kim I, Kim WS, Yeon KM, Chi JG. Inflammatory pseudotumor of the lung manifesting as a posterior mediastinal mass. Pediatr Radiol. 1992;22:467–8.
89. Hedlund GL, Navoy JF, Galliani CA, Johnson WH Jr. Aggressive manifestations of inflammatory pulmonary pseudotumor in children. Pediatr Radiol. 1999;29:112–6.
90. Berman M, Georghiou GP, Schonfeld T, et al. Pulmonary inflammatory myofibroblastic tumor invading the left atrium. Ann Thorac Surg. 2003;76:601–3.
91. Agrons GA, Rosado-de-Christenson ML, Kirejczyk WM, Conran RM, Stocker JT. Pulmonary inflammatory pseudotumor: radiologic features. Radiology. 1998;206:511–8.
92. Mas Estelles F, Andres V, Vallcanera A, Muro D, Cortina H. Plasma cell granuloma of the lung in childhood: atypical radiologic findings and association with hypertrophic osteoarthropathy. Pediatr Radiol. 1995;25:369–72.
93. Pichler G, Eber E, Thalhammer G, Muntean W, Zach MS. Arthralgia and digital clubbing in a child: hypertrophic osteoarthropathy with inflammatory pseudotumour of the lung. Scand J Rheumatol. 2004;33:189–91.
94. Messineo A, Mognato G, D'Amore ES, Antoniello L, Guglielmi M, Cecchetto G. Inflammatory pseudotumors of the lung in children: conservative or aggressive approach? Med Pediatr Oncol. 1998;31:100–4.
95. Genchellac H, Kirici MY, Basaran UN, et al. Successful sleeve lobectomy of pediatric inflammatory myofibroblastic tumor. Pediatr Iint. 2016;58(10):1087–9.
96. Sagel SS, Ablow RC. Hamartoma: on occasion a rapidly growing tumor of the lung. Radiology. 1968;91:971–2.
97. Davies MR, Cywes S, Rode H. Cystic pulmonary hamartoma simulating posterolateral diaphragmatic hernia. S Afr Med J. 1979;56:947–50.

98. Meza MP, Newman B, Dickman PS, Towbin RB. Pediatric case of the day. Pulmonary mesenchymal cystic hamartoma. Radiographics. 1992;12:843–4.
99. Carney JA, Sheps SG, Go VL, Gordon H. The triad of gastric leiomyosarcoma, functioning extra-adrenal paraganglioma and pulmonary chondroma. N Engl J Med. 1977;296:1517–8.
100. Green D. Incidental findings computed tomography of the thorax. Semin Ultrasound CT MR. 2005;26:14–9.
101. Davila DG, Dunn WF, Tazelaar HD, Pairolero PC. Bronchial carcinoid tumors. Mayo Clin Proc. 1993;68:795–803.
102. Nessi R, Basso Ricci P, Basso Ricci S, Bosco M, Blanc M, Uslenghi C. Bronchial carcinoid tumors: radiologic observations in 49 cases. J Thorac Imaging. 1991;6:47–53.
103. Balzer BWR, Loo C, Lewis CR, Tranhair TN, Anazodo AC. Adenocarcinoma of the lung in childhood and adolescence: a systemic review. J Thorac Oncol. 2018;13(12):1832–41.
104. Rosado de Christenson ML, Abbott GF, Kirejczyk WM, Galvin JR, Travis WD. Thoracic carcinoids: radiologic-pathologic correlation. Radiographics. 1999;19:707–36.
105. Shelley BE, Lorenzo RL. Primary squamous cell carcinoma of the lung in childhood. Pediatr Radiol. 1983;13:92–4.
106. Graham JM Jr, Boyle W, Troxell J, Cullity GJ, Sprague PL, Beckwith JB. Cystic hamartomata of lung and kidney: a spectrum of developmental abnormalities. Am J Med Genet. 1987;27:45–59.
107. Ishida Y, Kato K, Kigasawa H, Ohama Y, Ijiri R, Tanaka Y. Synchronous occurrence of pleuropulmonary blastoma and cystic nephroma: possible genetic link in cystic lesions of the lung and the kidney. Med Pediatr Oncol. 2000;35:85–7.
108. Senac MO Jr, Wood BP, Isaacs H, Weller M. Pulmonary blastoma: a rare childhood malignancy. Radiology. 1991;179:743–6.
109. Solomon A, Rubinstein ZJ, Rogoff M, Rozenman J, Urbach D. Pulmonary blastoma. Pediatr Radiol. 1982;12:148–9.
110. Tsai J, Lee EY. Case of the season: pulmonary arteriovenous malformation. Semin Roentgenol. 2012;47(1):4–6.
111. Mei-Zahav M, Letarte M, Faughnan ME, Abdalla SA, Cymerman U, MacLusky IB. Symptomatic children with hereditary hemorrhagic telangiectasia: a pediatric center experience. Arch Pediatr Adolesc Med. 2006;160:596–601.
112. McCue CM, Hartenberg M, Nance WE. Pulmonary arteriovenous malformations related to Rendu-Osler-Weber syndrome. Am J Med Genet. 1984;19:19–27.
113. Bartram O, Strickland B. Pulmonary varices. Proc R Soc Med. 1971;64:839.
114. Chilton SJ, Campbell JB. Pulmonary varix in early infancy: case report with 8-year follow up. Radiology. 1978;129:400.
115. Dinsmore BJ, Gefter WB, Hatabu H, Kressel HY. Pulmonary arteriovenous malformations: diagnosis by gradient-refocused MR imaging. J Comput Assist Tomogr. 1990;14:918–23.
116. Rankin S, Faling LJ, Pugatch RD. CT diagnosis of pulmonary arteriovenous malformations. J Comput Assist Tomogr. 1982;6:746–9.
117. Soysal N, Eyrices M, Verlhac S, et al. Non-invasive CT screening for pulmonary arteriovenous malformations in children with confirmed hereditary hemorrhagic telangiectasia: results from two pediatric centers. Pediatr Pulmonol. 2017;52(5):642–9.
118. Sharma SK, Mohan A. Miliary tuberculosis. Microbiol Spectr. 2017;5(2) https://doi.org/10.1128/microbiolspec.TNMI7-0013-2016.
119. Denny JT, Rocke ZM, McRae VA, et al. Varicella pneumonia: case report and review of a potentially lethal complication of a common disease. J Investig Med High Impact Case Rep. 2018;6:2324709618770230. https://doi.org/10.1177/2324709618770230. eCollection 2018 Jan-Dec.
120. Bozzola E, Gattinara GC, Bozzola M, et al. Varicella associated pneumoniae in a pediatric population. Ital J Pediatr. 2017;43(1):49. https://doi.org/10.1186/s13052-017-0366-8.
121. Somekh E, Maharashak N, Shapira Y, Greenberg D, Dagan R. Hospitalization for primary varicella-zoster virus infection and its complications in patients from southern Israel. Infection. 2000;28:200–4.
122. Saulsbury FT. Varicella pneumonia as the presenting manifestation of immunodeficiency. Clin Pediatr (Phila). 1991;30:555–8.
123. Mitnick J, Becker MH, Rothberg M, Genieser NB. Nodular residua of atypical measles pneumonia. AJR Am J Roentgenol. 1980;134:257–60.
124. Martin DB, Weiner LB, Nieburg PI, Blair DC. Atypical measles in adolescents and young adults. Ann Intern Med. 1979;90:877–81.
125. Markowitz LE, Chandler FW, Roldan EO, et al. Fatal measles pneumonia without rash in a child with AIDS. J Infect Dis. 1988;158:480–3.
126. Conte P, Heitzman ER, Markarian B. Viral pneumonia. Roentgen pathological correlations. Radiology. 1970;95:267–72.
127. Cook RJ, Ashton RW, Aughenbaugh GL, Ryu JH. Septic pulmonary embolism: presenting features and clinical course of 14 patients. Chest. 2005;128:162–6.
128. Gonzalez BE, Teruya J, Mahoney DH Jr, et al. Venous thrombosis associated with staphylococcal osteomyelitis in children. Pediatrics. 2006;117:1673–9.
129. Goldenberg NA, Knapp-Clevenger R, Hays T, Manco-Johnson MJ. Lemierre's and Lemierre's-like syndromes in children: survival and thromboembolic outcomes. Pediatrics. 2005;116:e543–8.
130. Wong KS, Lin TY, Huang YC, Hsia SH, Yang PH, Chu SM. Clinical and radiographic spectrum of septic pulmonary embolism. Arch Dis Child. 2002;87:312–5.
131. Dodd JD, Souza CA, Muller NL. High-resolution MDCT of pulmonary septic embolism: evaluation of the feeding vessel sign. AJR Am J Roentgenol. 2006;187:623–9.
132. Maile CW, Rodan BA, Godwin JD, Chen JT, Ravin CE. Calcification in pulmonary metastases. Br J Radiol. 1982;55:108–13.
133. Armstrong P, Dyer R, Alford BA, O'Hara M. Leukemic pulmonary infiltrates: rapid development mimicking pulmonary edema. AJR Am J Roentgenol. 1980;135:373–4.
134. Cohen M, Smith WL, Weetman R, Provisor A. Pulmonary pseudometastases in children with malignant tumors. Radiology. 1981;141:371–4.
135. Winer-Muram HT, Arheart KL, Jennings SG, Rubin SA, Kauffman WM, Slobod KS. Pulmonary complications in children with hematologic malignancies: accuracy of diagnosis with chest radiography and CT. Radiology. 1997;204:643–9.
136. Castellino RA, Bellani FF, Gasparini M, Musumeci R. Radiographic findings in previously untreated children with non-Hodgkin's lymphoma. Radiology. 1975;117:657–63.
137. Amini B, Huang SY, Tsai J, Benveniste MF, Robledo HH, Lee EY. Primary lung and large airway neoplasms in children: current imaging evalution with multidetector computed tomography. Radiol Clin North Am. 2013;51(4):637–57.
138. Soldatski IL, Onufrieva EK, Steklov AM, Schepin NV. Tracheal, bronchial, and pulmonary papillomatosis in children. Laryngoscope. 2005;115:1848–54.
139. Simma B, Burger R, Uehlinger J, et al. Squamous-cell carcinoma arising in a non-irradiated child with recurrent respiratory papillomatosis. Eur J Pediatr. 1993;152:776–8.
140. Godwin JD, Webb WR, Savoca CJ, Gamsu G, Goodman PC. Multiple, thin-walled cystic lesions of the lung. AJR Am J Roentgenol. 1980;135:593–604.
141. Smith L, Gooding CA. Pulmonary involvement in laryngeal papillomatosis. Pediatr Radiol. 1974;2:161–6.
142. Mayberry JP, Primack SL, Muller NL. Thoracic manifestations of systemic autoimmune diseases: radiographic and high-resolution CT findings. Radiographics. 2000;20:1623–35.
143. Yousefzadeh DK, Fishman PA. The triad of pneumonitis, pleuritis, and pericarditis in juvenile rheumatoid arthritis. Pediatr Radiol. 1979;8:147–50.

144. Richardson AE, Warrier K, Vyas H. Respiratory complications of the rheumatological diseases in childhood. Arch Dis Child. 2016;101(8):752–8.
145. Tanaka N, Newell JD, Brown KK, Cool CD, Lynch DA. Collagen vascular disease-related lung disease: high-resolution computed tomography findings based on the pathologic classification. J Comput Assist Tomogr. 2004;28:351–60.
146. Ramirez RE, Glasier C, Kirks D, Shackelford GD, Locey M. Pulmonary hemorrhage associated with systemic lupus erythematosus in children. Radiology. 1984;152:409–12.
147. Frazier AA, Rosado-de-Christenson ML, Galvin JR, Fleming MV. Pulmonary angiitis and granulomatosis: radiologic-pathologic correlation. Radiographics. 1998;18:687–710. quiz 727
148. Staples CA. Pulmonary angiitis and granulomatosis. Radiol Clin N Am. 1991;29:973–82.
149. Lee PY, Adil EA, Irace AL, et al. The presentation and management of granulomatosis with polyangiitis (Wegener's Granulomatosis) in the pediatric airway. Laryngoscope. 2017;127(1):233–40. https://doi.org/10.1002/lary.26013. Epub 2016 Apr 26.
150. Filocamo G, Torreggiani S, Agostoni C, Esposito S. Lung involvement in childhood onset aranulomatosis with polyangittis. Pediatr Rheumatol Online J. 2017;15(1):28. https://doi.org/10.1186/s12969-017-0150-8. Review.
151. Li J, Li C, Li J. Thoracic manifestation of Wegener's granulomatosis: computed tomography findings and analysis of misdiagnosis. Exp Ther Med. 2018;16(1):413–9.
152. Giovannini-Chami L, Blanc S, Hadchouel A, et al. Eosinophilic pneumonias in children: a review of the epidemiology, diagnosis, and treatment. Pediatr Pulmonol. 2016;51(2):203–16.
153. Abril A, Calamia KT, Cohen MD. The Churg Strauss syndrome (allergic granulomatous angiitis): review and update. Semin Arthritis Rheum. 2003;33:106–14.
154. Silva CI, Muller NL, Fujimoto K, Johkoh T, Ajzen SA, Churg A. Churg-Strauss syndrome: high resolution CT and pathologic findings. J Thorac Imaging. 2005;20:74–80.
155. Yeboah J, Afkhami M, Lee C, Sharma OP. Necrotizing sarcoid granulomatosis. Curr Opin Pulm Med. 2012;18(5):493–8.
156. Bolaman Z, Kadikoylu G, Polatli M, Barutca S, Culhaci N, Senturk T. Migratory nodules in the lung: lymphomatoid granulomatosis. Leuk Lymphoma. 2003;44:197–200.
157. Morris JC, Rosen MJ, Marchevsky A, Teirstein AS. Lymphocytic interstitial pneumonia in patients at risk for the acquired immune deficiency syndrome. Chest. 1987;91:63–7.
158. Nadal D, Caduff R, Frey E, et al. Non-Hodgkin's lymphoma in four children infected with the human immunodeficiency virus. Association with Epstein-Barr virus and treatment. Cancer. 1994;73:224–30.
159. Houghton KM, Cabral DA, Petty RE, Tucker LB. Primary Sjogren's syndrome in dizygotic adolescent twins: one case with lymphocytic interstitial pneumonia. J Rheumatol. 2005;32:1603–6.
160. Marks MJ, Haney PJ, McDermott MP, White CS, Vennos AD. Thoracic disease in children with AIDS. Radiographics. 1996;16:1349–62.
161. Johkoh T, Ichikado K, Akira M, et al. Lymphocytic interstitial pneumonia: follow-up CT findings in 14 patients. J Thorac Imaging. 2000;15:162–7.
162. Becciolini V, Gudinchet F, Cheseaux JJ, Schnyder P. Lymphocytic interstitial pneumonia in children with AIDS: high-resolution CT findings. Eur Radiol. 2001;11:1015–20.
163. Panchabhai TS, Farver C, Highland KB. Lymphocytic interstitial pneumonia. Clin Chest Med. 2016;37(3):463–74.
164. Shetty AK, Gedalia A. Sarcoidosis: a pediatric perspective. Clin Pediatr (Phila). 1998;37:707–17.
165. Passi GR, Arora K, Gokhale N. Childhood sarcoidosis presenting as recurrent facial palsy. Indian Pediatr. 2018;55(4):339–40.
166. Gorkem SB, Kose S, Lee EY, Doganay S, Koskun AS, Kose M. Thoracic MRI evaluation of sarcoidosis in children. Pediatr Pulmonol. 2017;52(4):494–9.
167. Merten DF, Kirks DR, Grossman H. Pulmonary sarcoidosis in childhood. AJR Am J Roentgenol. 1980;135:673–9.
168. Keesling CA, Frush DP, O'Hara SM, Fordham LA. Clinical and imaging manifestations of pediatric sarcoidosis. Acad Radiol. 1998;5:122–32.
169. Hafner R, Vogel P. Sarcoidosis of early onset. A challenge for the pediatric rheumatologist. Clin Exp Rheumatol. 1993;11:685–91.
170. Wang D, Cui L, Li ZG, et al. Clinical research of pulmonary Langerhans cell histocytosis in children. Chin Med J. 2018;131(15):1793–8.
171. Smets A, Mortele K, de Praeter G, Francois O, Benoit Y, Kunnen M. Pulmonary and mediastinal lesions in children with Langerhans cell histiocytosis. Pediatr Radiol. 1997;27:873–6.
172. Meyer JS, Harty MP, Mahboubi S, et al. Langerhans cell histiocytosis: presentation and evolution of radiologic findings with clinical correlation. Radiographics. 1995;15:1135–46.
173. Bano S, Chaudhary V, Narula MK, et al. Pulmonary Langerhans cell histocytosis in children: a spectrum of radiologic findings. Eur J Radiol. 2014;83(1):47–56.
174. Zhang XD, Gao JM, Luo JM, Zhao Y. Pulmonary alveolar microlithiasis: a case report and review of the literature. Exp Ther Med. 2018;15(1):831–7. https://doi.org/10.3892/etm.2017.5457. Epub 2017 Nov 7
175. Helbich TH, Wojnarovsky C, Wunderbaldinger P, Heinz-Peer G, Eichler I, Herold CJ. Pulmonary alveolar microlithiasis in children: radiographic and high-resolution CT findings. AJR Am J Roentgenol. 1997;168:63–5.
176. Sumikawa H, Johkoh T, Tomiyama N, et al. Pulmonary alveolar microlithiasis: CT and pathologic findings in 10 patients. Monaldi Arch Chest Dis. 2005;63:59–64.
177. Korn MA, Schurawitzki H, Klepetko W, Burghuber OC. Pulmonary alveolar microlithiasis: findings on high-resolution CT. AJR Am J Roentgenol. 1992;158:981–2.
178. Jankovic S, Pavlov N, Ivkosic A, et al. Pulmonary alveolar microlithiasis in childhood: clinical and radiological follow-up. Pediatr Pulmonol. 2002;34(5):384–7.
179. Proesmans M, Boon M, Verbeken E, et al. Pulmonary alveolar microlithiasis: a case report and review of the literature. Eur J Pediatr. 2012;171(7):1069–72.
180. Lee EY, Zucker EJ, Restrepo R, Daltro P, Boiselle PM. Advanced large airway CT imaging in children: evolution from axial to 4D assessment. Pediatr Radiol. 2013;43(3):285–97.
181. Lee EY, Greenberg SB, Boiselle PM. Multidetector computed tomography of pediatric large airway diseases: state-of-the-art. Radiol Clin N Am. 2011;49(5):869–93.
182. Sodhi KS, Lee EY. What all physicians should know about the potential radiation risk that computed tomography poses for paediatric patients. Acta Paediatr. 2014;103(8):807–11.
183. Sodhi KS, Krishna S, Saxena AK, Sinha A, Khandelwal N, Lee EY. Clinical application of "justification" and "optimization" principle of ALARA in pediatric CT imaging: "how many children can be protected from unnecessary radiation?". Eur J Radiol. 2015;84(9):1752–7.
184. Singh U, Vidhu A, Singh K, Singh A. Swyer-James-Macleod syndrome: a rare entity. Indian J Chest Dis Allied Sci. 2015;57(2):117–9.
185. Shah R, Cestone P, Mueller C. Congenital multiple peripheral pulmonary artery stenosis (pulmonary branch stenosis or supravalvular pulmonary stenosis). AJR Am J Roentgenol. 2000;175:856–7.

186. Boyd K. Back to the basics: community-acquired pneumonia in children. Pediatr Ann. 2017;46(7):e257–61.
187. Zar HJ, Andronikou S, Nicol MP. Advances in the diagnosis of pneumonia in children. BMJ. 2017;358:j2739. https://doi.org/10.1136/bmj.j2739.
188. Ponka A, Sarna S. Differential diagnosis of viral, mycoplasmal and bacteraemic pneumococcal pneumonias on admission to hospital. Eur J Respir Dis. 1983;64:360–8.
189. McCarthy PL, Spiesel SZ, Stashwick CA, Ablow RC, Masters SJ, Dolan TF Jr. Radiographic findings and etiologic diagnosis in ambulatory childhood pneumonias. Clin Pediatr (Phila). 1981;20:686–91.
190. Nohynek H, Valkeila E, Leinonen M, Eskola J. Erythrocyte sedimentation rate, white blood cell count and serum C-reactive protein in assessing etiologic diagnosis of acute lower respiratory infections in children. Pediatr Infect Dis J. 1995;14:484–90.
191. Korppi M, Kroger L. C-reactive protein in viral and bacterial respiratory infection in children. Scand J Infect Dis. 1993;25:207–13.
192. Korppi M, Heiskanen-Kosma T, Leinonen M. White blood cells, C-reactive protein and erythrocyte sedimentation rate in pneumococcal pneumonia in children. Eur Respir J. 1997;10:1125–9.
193. Hammerschlag MR. Atypical pneumonias in children. Adv Pediatr Infect Dis. 1995;10:1–39.
194. Black SB, Shinefield HR, Ling S, et al. Effectiveness of heptavalent pneumococcal conjugate vaccine in children younger than five years of age for prevention of pneumonia. Pediatr Infect Dis J. 2002;21:810–5.
195. Heiskanen-Kosma T, Korppi M, Leinonen M. Serologically indicated pneumococcal pneumonia in children: a population-based study in primary care settings. APMIS. 2003;111:945–50.
196. Liszewski MC, Laya BF, Zucker EJ, Restrepo R, Lee EY. Lung. In: Lee EY, editor. Pediatric thoracic imaging. 1st ed: Wolters Kluwer; Philadelphia, USA. 2018.
197. Courtoy I, Lande AE, Turner RB. Accuracy of radiographic differentiation of bacterial from nonbacterial pneumonia. Clin Pediatr (Phila). 1989;28:261–4.
198. Kiekara O, Korppi M, Tanska S, Soimakallio S. Radiological diagnosis of pneumonia in children. Ann Med. 1996;28:69–72.
199. Hopstaken RM, Witbraad T, van Engelshoven JM, Dinant GJ. Inter-observer variation in the interpretation of chest radiographs for pneumonia in community-acquired lower respiratory tract infections. Clin Radiol. 2004;59:743–52.
200. Swingler GH, Hussey GD, Zwarenstein M. Randomised controlled trial of clinical outcome after chest radiograph in ambulatory acute lower-respiratory infection in children. Lancet. 1998;351:404–8.
201. British Thoracic Society Standards of Care Committee. British Thoracic Society guidelines for the management of community acquired pneumonia in childhood. Thorax. 2002;57(Suppl 1):1–24.
202. Blackmore CC, Black WC, Dallas RV, Crow HC. Pleural fluid volume estimation: a chest radiograph prediction rule. Acad Radiol. 1996;3:103–9.
203. Grafakou O, Moustaki M, Tsolia M, et al. Can chest X-ray predict pneumonia severity? Pediatr Pulmonol. 2004;38:465–9.
204. Bachur R, Perry H, Harper MB. Occult pneumonias: empiric chest radiographs in febrile children with leukocytosis. Ann Emerg Med. 1999;33:166–73.
205. Andronikou S, Goussard P, Sorantin E. Computed tomography in children with community-acquired pneumonia. Pediatr Radiol. 2017;47(11):1431–40.
206. Brenner D, Elliston C, Hall E, Berdon W. Estimated risks of radiation-induced fatal cancer from pediatric CT. AJR Am J Roentgenol. 2001;176:289–96.
207. Ojutiku O, Haramati LB, Rakoff S, Sprayregen S. Radiology residents' on-call interpretation of chest radiographs for pneumonia. Acad Radiol. 2005;12:658–64.
208. Lynch T, Platt R, Gouin S, Larson C, Patenaude Y. Can we predict which children with clinically suspected pneumonia will have the presence of focal infiltrates on chest radiographs? Pediatrics. 2004;113:e186–9.
209. Tan Kendrick AP, Ling H, Subramaniam R, Joseph VT. The value of early CT in complicated childhood pneumonia. Pediatr Radiol. 2002;32:16–21.
210. Kosucu P, Ahmetoglu A, Cay A, et al. Computed tomography evaluation of cavitary necrosis in complicated childhood pneumonia. Australas Radiol. 2004;48:318–23.
211. Kurian J, Levin TL, Han BK, Taragin BH, Weinstein S. Comparison of ultrasound and CT in the evaluation of pneumonia complicated by parapneumonic effusion in children. AJR Am J Roentgenol. 2009;193(6):1648–54.
212. Masters IB, Isles AF, Grimwood K. Necrotizing pneumonia: an emerging problem in children? Pneumonia. 2017;9:11. https://doi.org/10.1186/s41479-017-0035-0. eCollection 2017.
213. Ramgopal S, Ivan Y, Medsinge A, Saladino RA. Pediatric necrotizing pneumoinia: a case report and review of the literature. Pediatr Emerg Care. 2017;32(2):112–5.
214. Nicolaou EV, Bartlett AH. Necrotizing pneumonia. Pediatr Ann. 2017;46(2):e65–8.
215. Kerem E, Bar Ziv Y, Rudenski B, Katz S, Kleid D, Branski D. Bacteremic necrotizing pneumococcal pneumonia in children. Am J Respir Crit Care Med. 1994;149:242–4.
216. Chen KC, Su YT, Lin WL, Chiu KC, Niu CK. Clinical analysis of necrotizing pneumonia in children: three-year experience in a single medical center. Acta Paediatr Taiwan. 2003;44:343–8.
217. Hacimustafaoglu M, Celebi S, Sarimehmet H, Gurpinar A, Ercan I. Necrotizing pneumonia in children. Acta Paediatr. 2004;93:1172–7.
218. McCarthy VP, Patamasucon P, Gaines T, Lucas MA. Necrotizing pneumococcal pneumonia in childhood. Pediatr Pulmonol. 1999;28:217–21.
219. Wong KS, Chiu CH, Yeow KM, Huang YC, Liu HP, Lin TY. Necrotising pneumonitis in children. Eur J Pediatr. 2000;159:684–8.
220. Schadeck T, Beckers D, Eucher P, deBilderling G, Tuerlinckx D, Bodart E. Necrotizing pneumonia in children: apropos 4 cases. Arch Pediatr. 2006;13:1209–14.
221. Ramphul N, Eastham KM, Freeman R, Eltringham G, Kearns AM, Leeming JP, et al. Cavitatory lung disease complicating empyema in children. Pediatr Pulmonol. 2006;41:750–3.
222. Sawicki GS, Lu FL, Valim C, Cleveland RC, Colin AA. Necrotizing pneumonia is increasingly detected as a complication of pneumonia in children. Eur Respir J. 2008;31(6):1285–91.
223. Schultz KD, Fan LL, Pinsky J, Ochoa L, Smith EO, Kaplan SL, et al. The changing face of pleural empyemas in children: epidemiology and management. Pediatrics. 2004;113:1735–40.
224. Curry CA, Fishman EK, Buckley JA. Pulmonary gangrene: radiologic and pathologic correlation. South Med J. 1999;91:957–60.
225. Hsieh YC, Hsiao CH, Tsao PN, Wang JY, Hsieh PR, Chiang BL, et al. Necrotizing pneumococcal pneumonia in children: the role of pulmonary gangrene. Pediatr Pulmonol. 2006;41:623–9.
226. Hsieh YC, Hsueh PR, Lu CY, Lee PI, Lee CY, Huang LM. Clinical manifestations and molecular epidemiology of necrotizing pneumonia and empyema caused by *Streptococcus pneumoniae* in children in Taiwan. Clin Infect Dis. 2004;38:830–5.
227. Oermann C, Sockrider MM, Langston C. Severe necrotizing pneumonitis in a child with *Mycoplasma pneumoniae* infection. Pediatr Pulmonol. 1997;24:61–5.
228. Wang RS, Wang SY, Hsieh KS, Chiou YH, Huang IF, Cheng MF, et al. Necrotizing pneumonitis caused by *Mycoplasma pneumoniae* in pediatric patients: report of five cases and review of literature. Pediatr Infect Dis J. 2004;23:564–7.

229. Cengiz AB, Kanra G, Caglar M, Kar A, Gucer S, Ince T. Fatal necrotizing pneumonia caused by group A streptococcus. J Paediatr Child Health. 2004;40:69–71.
230. Tsai MH, Huang YC, Chen CJ, Lin PY, Chang LY, Chiu CH, et al. Chlamydial pneumonia in children requiring hospitalization: effect of mixed infection on clinical outcome. J Microbiol Immunol Infect. 2005;38:117–22.
231. Sakamoto N, Tsuchiya K, Hikone M. Communicity-acquired necrotizing pneumonia with bacteremia caused by Psudomonas aeuginosa in a patient with emphysema: an autopsy case report. Respir Investig. 2018;56(2):189–94. https://doi.org/10.1016/j.resinv.2017.12.008. Epub 2018 Jan 12.
232. Gillet Y, Issartel B, Vanhems P, Lina G, Vandenesch F, Etienne J, et al. Severe staphylococcal pneumonia in children. Arch Pediatr. 2001;8(Suppl 4):742s–6.
233. Al-Tawfiq JA, Aldaabil RA. Community-acquired MRSA bacteremic necrotizing pneumonia in a patient with scrotal ulceration. J Infect. 2005;51:e241–3.
234. Labandeira-Rey M, Couzon F, Boisset S, Brown EL, Bes M, Benito Y, et al. *Staphylococcus aureus* Panton-Valentine leukocidin causes necrotizing pneumonia. Science. 2007;315(5815):1130–3.
235. Gilbert CR, Vipul K, Baram M. Novel H1N1 influenza A viral infection complicated by alveolar hemorrhage. Respir Care. 2010;55(5):623–5.
236. Wang X, Zhong LJ, Chen ZM, et al. Necrotipzing pneumonia caused by refractory mycoplasma pneumoniae pneumonia in children. World J Pediatr. 2018;14(4):344–9.
237. Hodina M, Hanquinet S, Cotting J, Schnyder P, Gudinchet F. Imaging of cavitary necrosis in complicated childhood pneumonia. Eur Radiol. 2002;12:391–6.
238. Hoffer FA, Bloom DA, Colin AA, Fishman SJ. Lung abscess versus necrotizing pneumonia: implications for interventional therapy. Pediatr Radiol. 1999;29:87–91.
239. Li ST, Gates RL. Primary operative management for pediatric empyema: decreases in hospital length of stay and charges in a national sample. Arch Pediatr Adolesc Med. 2008;162(1):44–8.
240. Ayed AK, Al-Rowayeh A. Lung resection in children for infectious pulmonary diseases. Pediatr Surg Int. 2005;21:604–8.
241. Eren S, Eren MN, Balci AE. Pneumonectomy in children for destroyed lung and the long-term consequences. J Thorac Cardiovasc Surg. 2003;126:574–81.
242. Kalfa N, Allal H, Lopez M, Counil FO, Forques D, Guibal MP, et al. An early thoracoscopic approach in necrotizing pneumonia in children: a report of three cases. J Laparoendosc Adv Surg Tech A. 2005;15:18–22.
243. Lai JY, Yang W, Ming YC. Surgical management of complicated necrotizing pneumonia in children. Pediatr Neonatol. 2017;58(4):321–7.
244. Donnelly LF, Klosterman LA. Cavitary necrosis complicating pneumonia in children: sequential findings on chest radiography. AJR Am J Roentgenol. 1998;171:253–6.

Pediatric Interstitial (Diffuse) Lung Disease

8

Edward Y. Lee

Introduction

Interstitial (diffuse) lung diseases in infants and children comprise a rare heterogeneous group of parenchymal lung disorders, with clinical syndromes characterized by dyspnea, tachypnea, crackles, and hypoxemia [1–5]. They arise from a wide spectrum of developmental, genetic, inflammatory, infectious, and reactive disorders. In the past, there has been a paucity of information and limited understanding regarding their pathogenesis, natural history, imaging findings, and histopathologic features, which often resulted in enormous diagnostic challenges and confusion.

In recent years, there has been a substantial improvement in the understanding of interstitial lung disease in pediatric patients due to the development of a structured classification system [1–7] based on the etiology of the lung disease, established pathologic criteria for consistent diagnosis, and the improvement of thoracoscopic techniques for lung biopsy [8, 9]. Imaging plays an important role in evaluating interstitial lung diseases in infants and children by confirming and characterizing the disorder, generating differential diagnoses, and providing localization for lung biopsy for pathological diagnosis.

In this chapter, the authors present the epidemiology, challenges, and uncertainties of diagnosis and amplify a recently developed classification system for interstitial lung disease in infants and children with clinical, imaging, and pathological correlation. It is not possible to review all of the conditions that are considered to be interstitial lung disorders in infants and children; individually, they are rare and collectively uncommon, but important conditions and particularly challenging ones are considered. The major aim of this chapter is to increase the understanding of interstitial lung disease among pediatric pulmonologists, neonatologists, radiologists, and pathologists who take care of affected infants and children. Increasing the understanding of these challenging disorders should result in early and correct diagnosis, which in turn will improve patient care.

E. Y. Lee (✉)
Department of Radiology, Boston Children's Hospital and Harvard Medical School, Boston, MA, USA
e-mail: Edward.Lee@childrens.harvard.edu

Epidemiology of Pediatric Interstitial (Diffuse) Lung Disease

Although the true prevalence of interstitial (diffuse) lung disease in infants and children is not clearly known, an estimated prevalence of chronic interstitial lung disease in the pediatric population of 3.6 cases per million in immunocompetent children younger than 17 years has been reported based on a national survey performed in the United Kingdom and Ireland from 1995 to 1998 [10]. This reported prevalence is likely to be substantially underestimated, particularly given the increased recognition of interstitial lung diseases in the pediatric population in recent years, due to (1) a recently developed classification system for categorizing pediatric interstitial lung disease, (2) increased recognition particularly of the unique interstitial lung diseases that occur in infants, and (3) increased use of thoracoscopic lung biopsy in pediatric patients for definitive diagnosis. Additionally, although the prevalence of any single-specific interstitial lung disease is low, the combination of the varied types of interstitial lung diseases in the pediatric population may be sizable as a collective group. A national registry or large prospective multicenter studies focusing on the evaluation of the true prevalence of interstitial lung disease in infants and children is currently needed.

Challenges and Uncertainties Regarding Diagnosis of Interstitial (Diffuse) Lung Disease in Infants and Children

There are many challenges and uncertainties for the early and correct diagnosis of interstitial (diffuse) lung disease in the pediatric patient. Three major challenges include, first,

R. H. Cleveland, E. Y. Lee (eds.), *Imaging in Pediatric Pulmonology*, https://doi.org/10.1007/978-3-030-23979-4_8

the fact that interstitial lung disease is less common in infants and children compared with adults. Therefore, most clinicians and radiologists are less familiar with considering and recognizing interstitial lung disease in this patient population. Second, the clinical manifestations of interstitial lung disease particularly in infants and the young child are often subtle, highly variable, and typically nonspecific, such as dyspnea, tachypnea, crackles, and hypoxemia. Lastly, there are currently no pathognomonic clinical or laboratory criteria for the diagnosis of interstitial lung disease in pediatric patients. Some of the major uncertainties involving interstitial lung disease in this population include (1) the paucity of information regarding the natural history of interstitial lung disease in childhood, (2) the lack of understanding of the role of specific host factors in the pathogenesis of interstitial lung disease, and (3) the absence of information on prognostic indicators in interstitial lung disease in childhood and more particularly in infants. Due to the above-stated challenges and uncertainties, evaluation and diagnosis of interstitial lung disease in childhood and particularly in infants has been markedly limited in the past.

New Pediatric Interstitial (Diffuse) Lung Disease Classification

Rationale and History Behind the Development of the New Childhood Interstitial (Diffuse) Lung Disease Classification

Rationale

Two main factors led to the development of a new classification for new childhood interstitial lung disease (ChILD). First, there has been substantial confusion and difficulty associated with the description and classification of specific interstitial lung diseases in infants and young children with multiple terms used for similar abnormalities and sometimes the same term used for differing conditions, and there has been a tendency to attempt to fit these pediatric disorders into the diagnostic schema used for adults. As the adult ILD classification became more refined and as more knowledge was gained about certain forms of infant ILD, it became clear that using the adult classification was both suboptimal and limiting as conditions common in adults are rare or nonexistent in infants and children and recently recognized infant conditions have no place in the adult classification. Second, the adult ILD classification system did not acknowledge the important role of heritable and genetic disorders that have become widely recognized as an important component of ChILD. The recognition of the role of genetic disorders of the surfactant system was pivotal in changing this understanding. And now genetic underpinnings are being sought for a wider group of ChILD. Classifying ILD in the pediatric patient based on the adult ILD classification system is no longer a viable approach.

History

Recognition of the substantial differences between pediatric and adult ILD led to the evolution of the current and evolving classification system for ChILD. A European Respiratory Society (ERS) Task Force addressed this issue in a retrospective review of 185 pediatric cases of chronic interstitial lung disease in immunocompetent patients; most, but not all, had lung biopsy and histologic material, which was not reviewed as part of this project; the diagnoses made at initial examination were accepted. The ERS review divided the diagnoses made clinically into four categories based on a proposal by Fan and Langston [11]: (1) diffuse lung parenchymal disease of unknown association (drug reaction, aspiration, connective tissue disorders, infection, environmental disorders); (2) idiopathic interstitial pneumonias (nonspecific interstitial pneumonia (NSIP)), cellular/fibrotic, desquamative interstitial pneumonitis (DIP), lymphoid interstitial pneumonia (LIP), diffuse alveolar damage/acute interstitial pneumonia (DAD/AIP), organizing pneumonia (OP), usual interstitial pneumonitis (UIP) to include familial cryptogenic fibrosing alveolitis, and chronic pneumonitis of infancy (CPI); (3) other forms of interstitial pneumonia to include lymphangioleiomyomatosis, Langerhans cell granulomatosis, pulmonary alveolar proteinosis (PAP), sarcoidosis, eosinophilic pneumonia, idiopathic/infantile pulmonary hemosiderosis; and (4) congenital disorders (DIP, LIP, lipoid pneumonia, NSIP/UIP, and surfactant deficiencies). Although this concept was an important step toward an improved understanding and diagnosis of ChILD, there was clearly a need for further refinement, particularly as diagnostic criteria were not provided for these entities, disorders of immunocompromised children were not addressed, and the requirement for chronicity excluded severe and rapidly progressive conditions. Additionally, adult terminology continued to be used in large part for quite different entities, including idiopathic pulmonary fibrosis (IPF) and usual interstitial pneumonia (UIP), conditions that are common in adults but vanishingly rare in childhood. This study was a major advance in redirecting thinking about ChILD, and it is important for this reason but does not truly present a new classification system, nor did it resolve many of the issues leading to diagnostic confusion.

A truly new classification system for pediatric interstitial lung disease [1–4, 12] evolved out of the recognition that clinical setting is an important consideration in the diagnosis of pediatric ILD and that combined clinical, imaging, and pathological correlation is a more powerful diagnostic tool than any one single component. This new pediatric interstitial lung disease classification system was validated for infants and very young children in a retrospective review of

186 lung biopsies done between 1999 and 2004 [7] with accompanying clinical histories and images from children under age 2 contributed by 11 pediatric institutions in North America. The importance of this new classification system lies in its acknowledgment of the unique nature of ILD in infants and the overlap of other lung disorders seen in infants and young children with the varied spectrum of conditions seen in older children and adults. Based on this new classification system, ChILD is classified into three main groups: (1) disorders of infancy, (2) other categories (not specific to infancy), and (3) unclassifiable. This expandable and flexible system for categorization has gained wide clinical recognition. This chapter uses this classification scheme (Table 8.1) as its organizing principal focusing initially on those disorders seen almost exclusively during infancy and not in older children or adults.

Table 8.1 Clinicopathologic classification of diffuse lung disease in childhood

I. Disorders of infancy
A. Diffuse developmental disorders
1. Acinar dysplasia
2. Congenital alveolar dysplasia
3. Alveolar capillary dysplasia with misalignment of pulmonary veins
B. Growth abnormalities
1. Prenatal conditions – Secondary pulmonary hypoplasia of varying degrees
2. Postnatal conditions – Chronic neonatal lung disease
(a) Prematurity-related chronic lung disease (also known as bronchopulmonary dysplasia (BPD))
(b) Term infants with chronic lung disease
3. Associated with chromosomal abnormalities
(a) Trisomy 21
(b) Others
4. Associated with congenital heart disease in chromosomally normal children
C. Surfactant dysfunction disorders and related abnormalities
1. Surfactant dysfunction disorders
(a) SpB genetic mutations (pulmonary alveolar proteinosis and variant histologies)
(b) SpC genetic mutations (chronic pneumonitis of infancy is the dominant histologic pattern; others include PAP, DIP, NSIP)
(c) ABCA3 genetic mutations (PAP-dominant histologic pattern; others include CPI, DIP, NSIP)
(d) Congenital GMCSF receptor deficiency (PAP histologic pattern)
(e) TTF1 genetic mutations
(f) Others with histology consistent with surfactant dysfunction disorder without an as yet recognized genetic disorder
2. Lysinuric protein intolerance (PAP histologic pattern)
D. Specific conditions of unknown/poorly understood etiology
1. Neuroendocrine cell hyperplasia of infancy (NEHI)
2. Pulmonary interstitial glycogenosis
(a) Primary
(b) Associated with other pulmonary conditions
II. Disorders of the normal host
A. Infectious and postinfectious processes
1. Postinfectious airway injury ranging from mild airway fibrosis to constrictive/obliterative bronchiolitis with and without preceding history of viral respiratory infection
2. Specific infections identified
(a) Bacterial
(b) Fungal
(c) Mycobacterial
(d) Viral
B. Disorders related to environmental agents
1. Hypersensitivity pneumonia
2. Toxic inhalation
C. Aspiration syndromes
D. Eosinophilic pneumonias
E. Acute interstitial pneumonia/Hamman–rich syndrome/ idiopathic diffuse alveolar damage
F. Nonspecific interstitial pneumonia
G. Idiopathic pulmonary hemosiderosis
H. Others
III. Disorders related to systemic disease processes
A. Immune-mediated disorders
1. Specific pulmonary manifestations
(a) Goodpasture's syndrome
(b) Acquired pulmonary alveolar proteinosis/autoantibody to GMCSF
(c) Pulmonary vasculitis syndromes
2. Nonspecific pulmonary manifestations
(a) Nonspecific interstitial pneumonia
(b) Pulmonary hemorrhage syndromes
(c) Lymphoproliferative disease
(d) Organizing pneumonia
(e) Nonspecific airway changes, including lymphocytic bronchiolitis, lymphoid hyperplasia, and mild constrictive changes
3. Other manifestations of collagen-vascular disease
B. Nonimmune-mediated systemic disorders
1. Storage disease
2. Sarcoidosis
3. Langerhans cell histiocytosis
4. Malignant infiltrates
5. Others
IV. Disorders of the immunocompromised host
A. Opportunistic infections
1. PCP
2. Fungal/yeast
3. Bacterial
4. Mycobacterial
5. Viral
6. Suspected
B. Disorders related to therapeutic intervention – Chemotherapeutic drug and radiation injury
1. Chemotherapeutic drug injury
2. Radiation injury
3. Combined
4. Drug hypersensitivity

(continued)

Table 8.1 (continued)

C. Disorders related to solid organ, lung and bone marrow transplantation, and rejection syndromes
1. Rejection
2. GVHD
3. PTLD
D. DAD of undetermined etiology
E. Lymphoid infiltrates related to immune compromise (for nontransplanted patients)
1. Nonspecific lymphoproliferation
2. With lymphoid hyperplasia
3. With poorly formed granulomas
4. Malignant
V. Disorders masquerading as interstitial disease
A. Arterial hypertensive vasculopathy
B. Congestive vasculopathy including veno-occlusive disease
C. Lymphatic disorders
1. Lymphangiectasis
2. Lymphangiomatosis
D. Pulmonary edema
E. Thromboembolic
VI. Unclassified
End-stage disease
Nondiagnostic
Inadequate tissue
Insufficient information

Modified from Deutsch et al. [7]. Reprinted with permission of the American Thoracic Society. Copyright American Thoracic Society. Official Journal of the American Thoracic Society.

SpB Surfactant protein B, *SpC* Surfactant protein C, *PAP* Pulmonary alveolar proteinosis, *DIP* Desquamative interstitial pneumonitis, *NSIP* Nonspecific interstitial pneumonia, *ABCA3* ATP-Binding Cassette subfamily A member 3 deficiency, *GMCSF* Granulocyte macrophage colony stimulating factor, *TTF1* Thyroid transcription factor-1, *PCP* Pneumocystis pneumonia, *GVHD* Graft-versus-host disease, *PTLD* Post-transplant lymphoproliferative disorder, *DAD* Diffuse alveolar damage

Interstitial (Diffuse) Lung Disorders in Infants

In the multicenter study, disorders of infancy comprised the largest portion of the 186 reviewed cases. These infant disorders are divided into four important subgroups: (1) diffuse developmental disorders, (2) growth abnormalities, (3) surfactant dysfunction mutations and related disorders, and (4) specific conditions of undefined etiology, currently including pulmonary interstitial glycogenosis (PIG) and neuroendocrine cell hyperplasia of infancy (NEHI). The clinical, imaging, and pathologic features of these different categories of infant ILD [13–21] are summarized in Table 8.2.

Diffuse Developmental Disorders

This category includes acinar dysplasia, congenital alveolar dysplasia (CAD) [22, 23], and alveolar capillary dysplasia with misalignment of pulmonary veins (ACDMPV) [24, 25].

Key Clinical Aspects

Infants with ILD in this category are typically term infants who present with rapidly and progressively worsening hypoxemia often associated with severe pulmonary hypertension (PHT) immediately following birth or early in the neonatal period. Due to their rapid clinical course of respiratory failure, most infants with this type of interstitial lung disease die during the first 2 months of life despite supportive management, including advanced ventilation support strategies, extracorporeal membrane oxygenation, and therapeutic interventions for PHT. Infants with acinar dysplasia, the rarest of these conditions, present at birth, and their survival is shortest. While most reported cases are female infants, male infants may be affected as well. Those with CAD typically present within hours of birth and require continuous and often maximal supportive measures for survival; with such support, they may survive weeks but cannot be weaned from these measures. Infants with ACD/MPV typically present within the first few days of birth, but a few have a delayed presentation at weeks or sometimes a few months of age. Once they present, their course with respiratory failure and PHT rarely ameliorates, and death by 1 month following presentation is the usual outcome.

Familial cases have been reported in all and account for about 10% of ACD/MPV cases; they have been identified rarely in each of the other disorders. This feature has suggested a genetic basis for all these disorders. In addition, the majority of infants with ACD/MPV have other congenital anomalies most commonly involving the cardiovascular, gastrointestinal (including absence of the gallbladder), and/or genitourinary system. A search for the genetic basis of ACD/MPV has resulted in the recent recognition of the mutation/microdeletion of the FOXF1 gene in a proportion of ACD/MPV cases, and the recognition of familial cases highlights the need for genetic testing and counseling in cases with suspected ACD/MPV. As genetic abnormalities have not been found for acinar dysplasia or CAD, and as all ACD/MPV cases have not yet had a genetic mechanism identified, the definitive diagnosis of these developmental disorders currently rests on the pathological analysis of the lung tissue from biopsy and/or postmortem specimens.

Imaging Features

Due to the rarity of these diffuse developmental disorders and the often precarious clinical status of these patients, detailed imaging findings for this category of ChILD are currently not available. Plain chest radiographs of affected infants with diffuse developmental abnormalities typically show normal to decreased lung volume associated with diffuse opacities related to hypoinflation resembling hyaline membrane disease (surfactant deficiency) (Fig. 8.1); however, with long-term ventilation support, as often occurs with CAD (Fig. 8.2) and ACD/MPV (Fig. 8.3), lung volume may be increased, and the increased size of the main pulmonary artery and increased

Table 8.2 Summary of clinical, imaging, and pathologic features of interstitial lung disease in infancy

Types of ILD	Clinical features	Imaging features	Pathologic features
Diffuse developmental disorders			
Acinar dysplasia	Term infants, mostly female, present at birth, severe hypoxemia, high morality (100%)	Diffuse opacity, hypoinflation	Small lung size, airway without acinar development, growth arrest late pseudoglandular phase
CAD	Term infants, present at birth, severe hypoxemia, high mortality (100%)	Diffuse opacity, hypoinflation, increased size of MPA/pulmonary blood flow if + PHT	Normal or increased lung size if chronic ventilatory support, growth arrest canalicular phase
ACDMPV	Term infants, present soon after birth, severe hypoxemia, associated with other congenital anomalies, high mortality (100%)	Diffuse opacity, hypoinflation, increased size of MPA/pulmonary blood flow if + PHT	Normal or increased lung size if chronic ventilatory support, reduced capillary density, malpositioned veins, arterial hypertensive changes
Growth abnormalities	Most common ILD, both preterm and term infants, variable clinical presentation, associated with underlying causes for growth abnormalities, moderate mortality (~ 30%)	Variable imaging findings, small cysts often located peripherally in the lungs with chromosomal abnormalities (e.g., trisomy 21)	Alveolar enlargement related to prenatal or postnatal defective alveolarization
Surfactant dysfunction mutations and related disorders			
SpB defect	Term infants, present at birth, severe hypoxemia, autosomal recessive, high mortality without transplant (100%)	Diffuse hazy or granular opacity on CXR, GGO with variable interlobular septal thickening on HRCT	Prominent diffuse alveolar epithelial hyperplasia, variable proteinosis material, foamy macrophages, lamellar body abnormalities on EM PAP or variant pattern
SpC defect	Term infants, present at birth, severe hypoxemia, autosomal-dominant, moderate early mortality	Diffuse hazy or granular opacity on CXR, GGO with variable interlobular septal thickening on HRCT	Prominent diffuse alveolar epithelial hyperplasia, variable proteinosis, foamy macrophages, no specific EM change CPI or DIP pattern
ABCA3 defect	Term infants, during postnatal period, persistent tachypnea and hypoxemia, autosomal recessive, moderate early mortality (~ 30%)	Diffuse hazy or granular opacity on CXR, GGO with variable interlobular septal thickening on HRCT	Prominent diffuse alveolar epithelial hyperplasia, variable proteinosis material, foamy macrophages, tiny lamellar bodies with dense inclusion on EM CPI or DIP pattern
Specific conditions of undefined etiology			
NEHI	Term infants, initially well, present by 3 months with persistent tachypnea, retractions, hypoxemia, and crackles without cough or wheeze, no steroid response no morality	Hyperinflation with variable increased perihilar opacity on CXR, geographic GGO with central predominance, especially in the lingula and RML on HRCT, air trapping in both the areas on HRCT	Essentially normal lung histology occasionally mild peri-airway lymphocytic inflammation, increased numbers bombesin for immunopositive cells in airways and prominent neuroepithelial bodies
PIG	Both preterm and term infants, presents at birth, severe tachypnea and hypoxemia, often associated with other conditions that affect lung growth, pulse steroid mortality related to associated disorders	Hyperinflation and diffuse increased interstitial markings on CXR, diffuse segmental or subsegmental GGO, interlobular septal thickening and reticular change predominantly subpleural with few centrilobular nodules on HRCT	Large clear rounded, glycogen-laden, vimentin immunopositive mesenchymal cells expand the lobular interstitium. Monoparticulate glycogen on EM

ILD interstitial lung disease, *CAD* congenital alveolar dysplasia, *MPA* main pulmonary artery, *PHT* pulmonary hypertension, *ACDMPV* alveolar capillary dysplasia with misalignment of pulmonary veins, *SpB* surfactant protein B, *CXR* chest radiographs, *GGO* ground glass opacity, *HRCT* high-resolution CT, *SpC* surfactant protein C, *ABCA3* ATP-binding cassette transport proteins (ABC), *NEHI* neuroendocrine cell hyperplasia of infancy, *RML* right middle lobe, *TX* treatment, *PAP* pulmonary alveolar proteinosis, *EM* electron microscopy, *CPI* chronic pneumonitis of infancy, *DIP* desquamative interstitial pneumonia

pulmonary blood flow may also be seen on plain chest radiographs in affected infants who have concurrent PHT.

Pathological Features

The diffuse developmental disorders are thought to originate early in lung development. On gross examination, the lungs in acinar dysplasia are small (Fig. 8.1); histologically, they suggest growth arrest in the pseudoglandular stage with only airway structures, bronchi, and larger bronchioles, embedded within loose mesenchyme, although occasionally there is minimal early acinar formation. For CAD (Fig. 8.2) and ACD/MPV (Fig. 8.3), lung size is typically normal or even large, particularly when there has been long-term ventilatory support. Histologically, CAD (Fig. 8.2) suggests growth arrest in the canalicular stage of lung development showing acinar formation with simplified lung structure and sometimes, but not

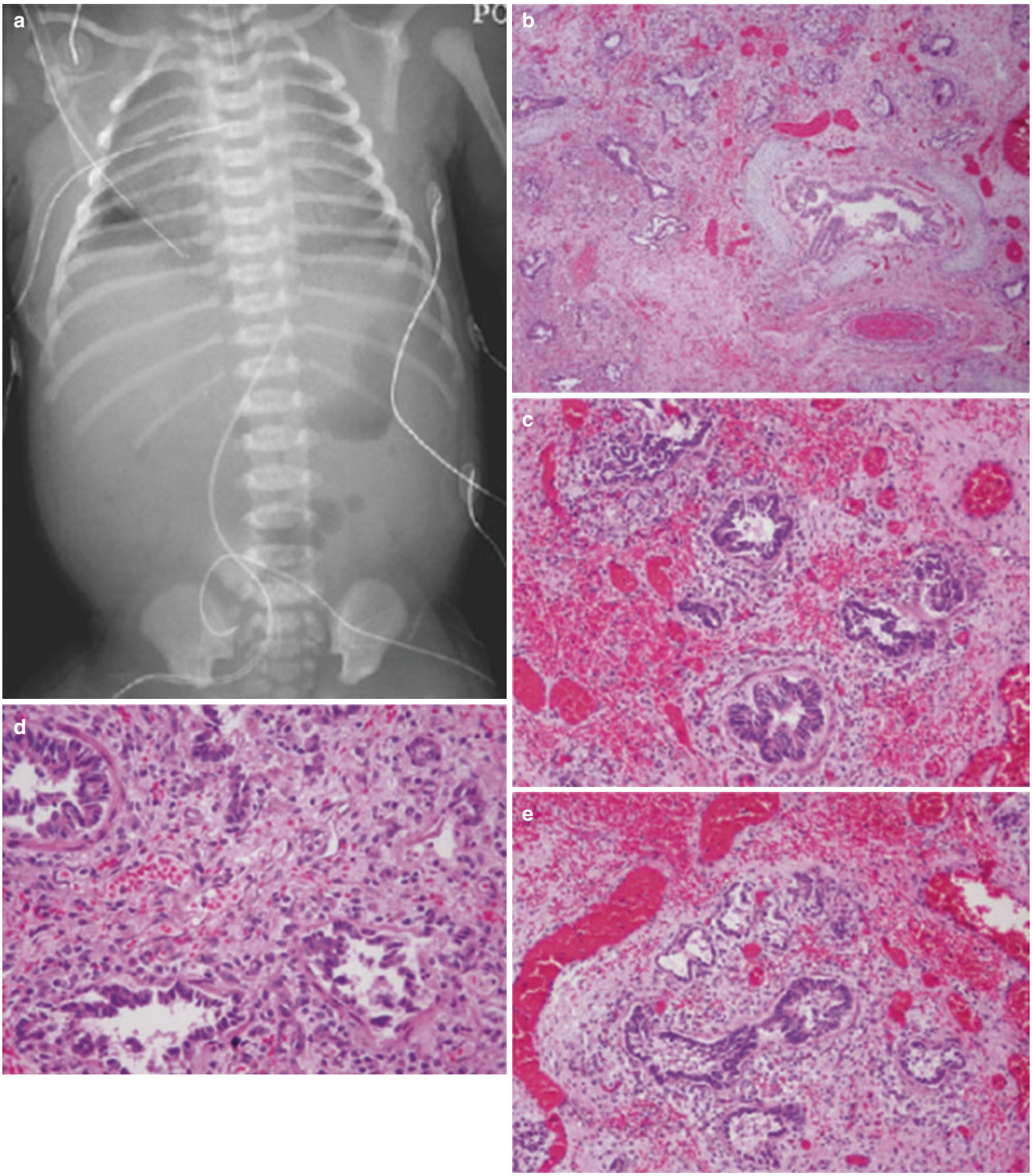

Fig. 8.1 (**a**) Acinar dysplasia: as is expected with the diffuse developmental disorders, the CXR on this baby with acinar dysplasia revealed nonspecific diffuse lung opacification resembling that seen with hyaline membrane disease. (Image courtesy of Dr. Paul Guillerman, Baylor College of Medicine, Texas Children's Hospital, Department of Radiology.) (**b**–**e**) Acinar dysplasia: the lung is from the autopsy of a near-term male infant who survived with continuous maximal support for only 14 h. The findings are typical for acinar dysplasia with arrest of development in the pseudoglandular stage. It shows multiple airways, both bronchi (**b**) and bronchioles (**b**–**e**), but very little acinar development (**e**) with only a very few airspaces among the prominent airways. A few airspaces seen are at the periphery of only a few lobular regions in the lower lobes. Bronchioles are surrounded by small amounts of smooth muscle (**c**, **e**) and are dispersed in loose mesenchyme. There is often prominent vascular dilatation and hemorrhage (**b**, **c**, **e**) related to hypoxia

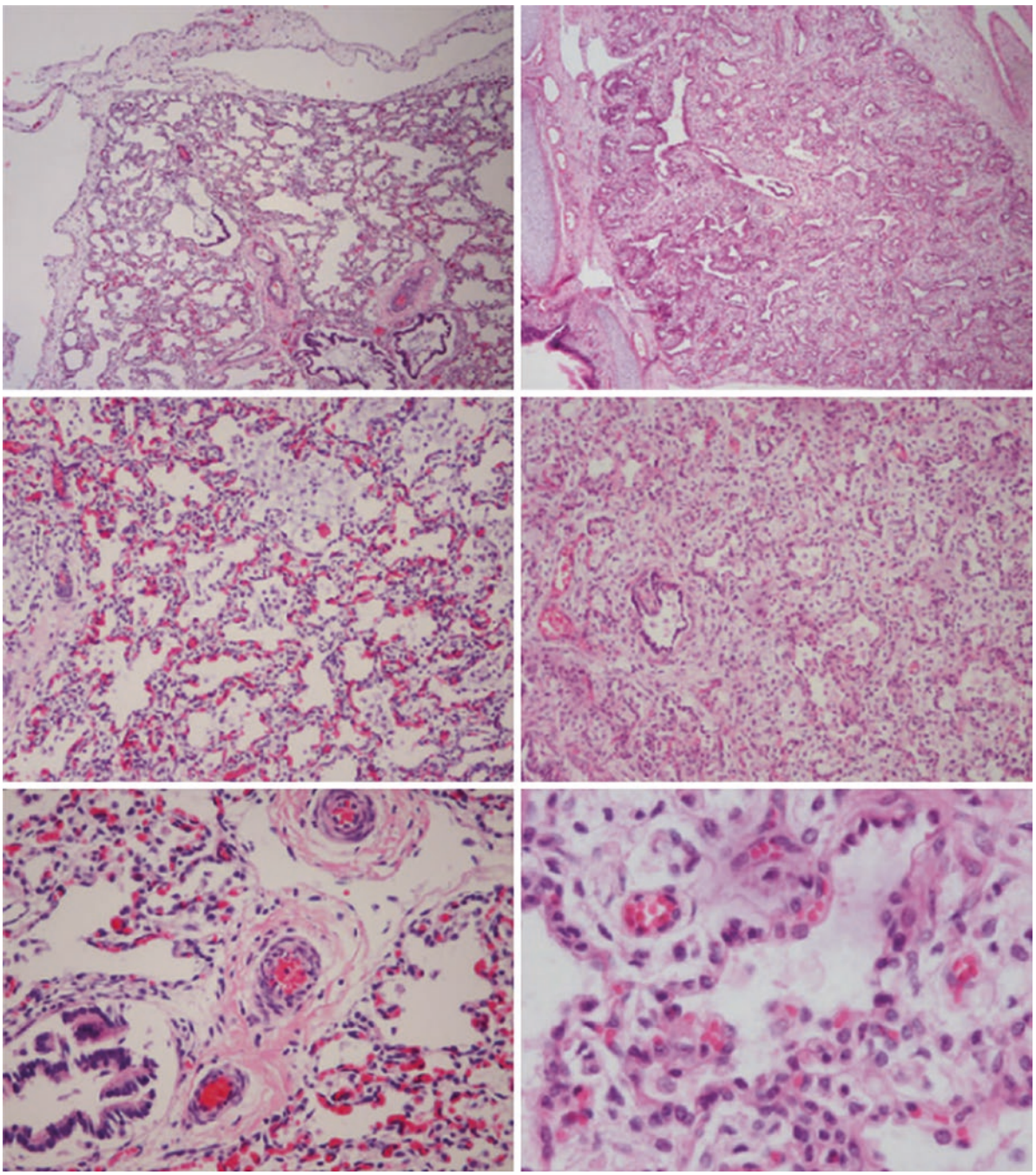

Fig. 8.2 Congenital alveolar dysplasia (CAD): the *left* and *right panels* are from two different examples of CAD and show the range of developmental delay that can be seen in this condition. CAD shows developmental arrest that ranges from the canalicular to the early saccular stage. The *left column* shows images from the lung of a near-term male infant who developed respiratory distress at a few hours of age and was supported with supplemental oxygen and mechanical ventilation for 2 weeks. An echocardiogram showed pulmonary hypertension. The *upper left panel* is an overview of the lung histology and also shows dilated lymphatic channels in the pleura and an interlobular septum, but not adjacent to airways and arteries. The lobules are composed of simple saccular structures that in the *left middle panel* are seen to have the somewhat irregular internal configuration seen with secondary crest formation and the wider airspace walls consistent with the early saccular stage of development. In the *lower left panel,* a well-developed pattern of capillaries is evident, oriented to the airspace epithelium in a normal fashion. There is no deficiency of capillary development in this case, although it may be seen occasionally in association with CAD. Small pulmonary arteries in the *lower left panel* have mildly increased medial smooth muscle. A single small bronchiole is also evident in the *lower left panel*. The *right hand panels* show images from the lung of a near-term female infant who developed hypoxia and respiratory failure shortly after birth. She survived 3 days. This lung shows an earlier developmental stage with far less advanced acinar development. Development is consistent with the canalicular stage. The *upper right panel* is an overview of lung with only small numbers of simple elongated airspaces disposed in loose mesenchyme. This is better seen in the *middle right panel* where somewhat irregular airspaces lined by cuboidal epithelium are separated by abundant mesenchyme. In the *lower right panel,* the airspace epithelium and capillary development are better seen with capillaries becoming apposed to the epithelium with the formation of small regions with thin air-blood barriers

always, reduced capillary density. Histologic changes in ACD/MPV (Fig. 8.3) are less clearly reminiscent of a specific stage in lung development, but there is lobular underdevelopment with variable and sometimes marked alveolar enlargement and reduced capillary density. In addition to the structural changes in the lobule, there are vascular changes, including prominent medial hyperplasia of small pulmonary arteries and malposition of pulmonary veins adjacent to arteries and small airways, as well as sometimes prominent regional or diffuse lymphangiectasis.

Growth Disorders

The commonest form of infant ILD is that related to alveolar growth disorders. These differ from diffuse developmental disorders in that the lung is not programmed to be abnormal; rather, some superimposed condition or event alters normal program development. Conditions in this category include (1) pulmonary hypoplasia associated with prenatal conditions such as oligohydramnios, space-occupying lesions, or neuromuscular disease; (2) postnatal conditions such as prematurity-related chronic lung disease (i.e., bronchopulmonary dysplasia) and term infants with chronic lung disease; (3) the structural pulmonary changes seen with chromosomal abnormalities, particularly Trisomy 21, as the genesis of their alveolar growth abnormalities is postnatal in origin, but this is a programmed abnormality; and (4) changes seen in some chromosomally normal infants with congenital heart disease.

Key Clinical Aspects

In the multicenter review, this was the most common of the infant interstitial lung disorders, accounting for 43% of diffuse lung disease in infants. Because of the varied underlying conditions and associations, clinical presentations of these infants vary substantially. If the clinical setting includes any of the various conditions associated with alveolar growth abnormality, including prematurity, oligohydramnios, chromosomal abnormality, or congenital heart disease, the possibility of a lung growth abnormality should be considered, and further investigations might include lung biopsy for diagnosis and prognosis as the mortality rate in this patient population is often substantial, being as high as 34% in the multicenter study.

Imaging Features

Variable imaging findings in infants with alveolar growth abnormalities are seen in both plain radiographs and high-resolution computed tomography (HRCT). However, small cysts, often located peripherally in the lungs, may suggest this diagnosis and are particularly common in infants with chromosomal abnormalities, such as Trisomy 21 (Fig. 8.4) or Turner syndrome.

Pathological Features

Histologically, the alveolar growth abnormalities share the common feature of alveolar enlargement and simplification, often marked and often more prominent at the lobular periphery and in subpleural regions (Fig. 8.5). This alveolar enlargement may be subtle or severe and is sometimes accompanied by vascular changes of pulmonary hypertensive arteriopathy with muscularization of alveolar wall vessels and medial thickening of small pulmonary arteries.

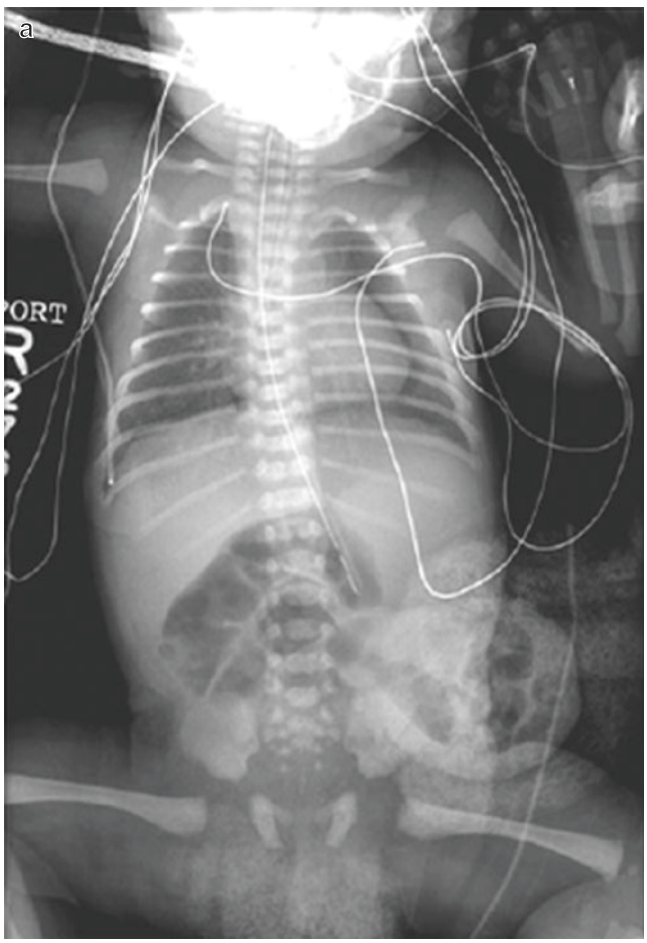

Fig. 8.3 (**a**) Alveolar capillary dysplasia: newborn with alveolar capillary dysplasia with misalignment of pulmonary veins. Even with the lung volumes increased with positive pressure ventilation, there is still evidence of a nonspecific diffuse granular interstitial opacification similar to that seen with hyaline membrane disease (surfactant deficiency). There is a left pneumothorax and an omphalocele. (Image courtesy of Dr. Paul Guillerman, Baylor College of Medicine, Texas Children's Hospital, Houston, TX.) (**b**) Alveolar capillary dysplasia with misalignment of pulmonary veins: all cases of alveolar capillary dysplasia with misalignment of pulmonary veins have a constellation of histologic features that include (1) medial thickening of small pulmonary arteries (*upper right* and *left* and *lower right panels*) with extension of arterial smooth muscle into small intralobular vessels (*middle right and left panels*); (2) abnormal position of pulmonary veins adjacent to small pulmonary arteries in their normal parabronchiolar location (*upper right* and *left* and *lower right*) and within the lobular parenchyma adjacent to small abnormally muscularized intralobar vessels (*middle left panel*); (3) lobular maldevelopment with enlarged, simple, and often thick-walled airspaces (*all panels*); (4) deficient numbers of normally positioned alveolar capillaries (*middle left* and *bottom right panels*); and (5), in some cases, there is also lymphangiectasis (*lower left panel*). Photographs are from two different cases of ACD/MPV, one in the *left panels* and another in the *right panels* and illustrate the variability in lobular maldevelopment, airspace size, and other associated changes

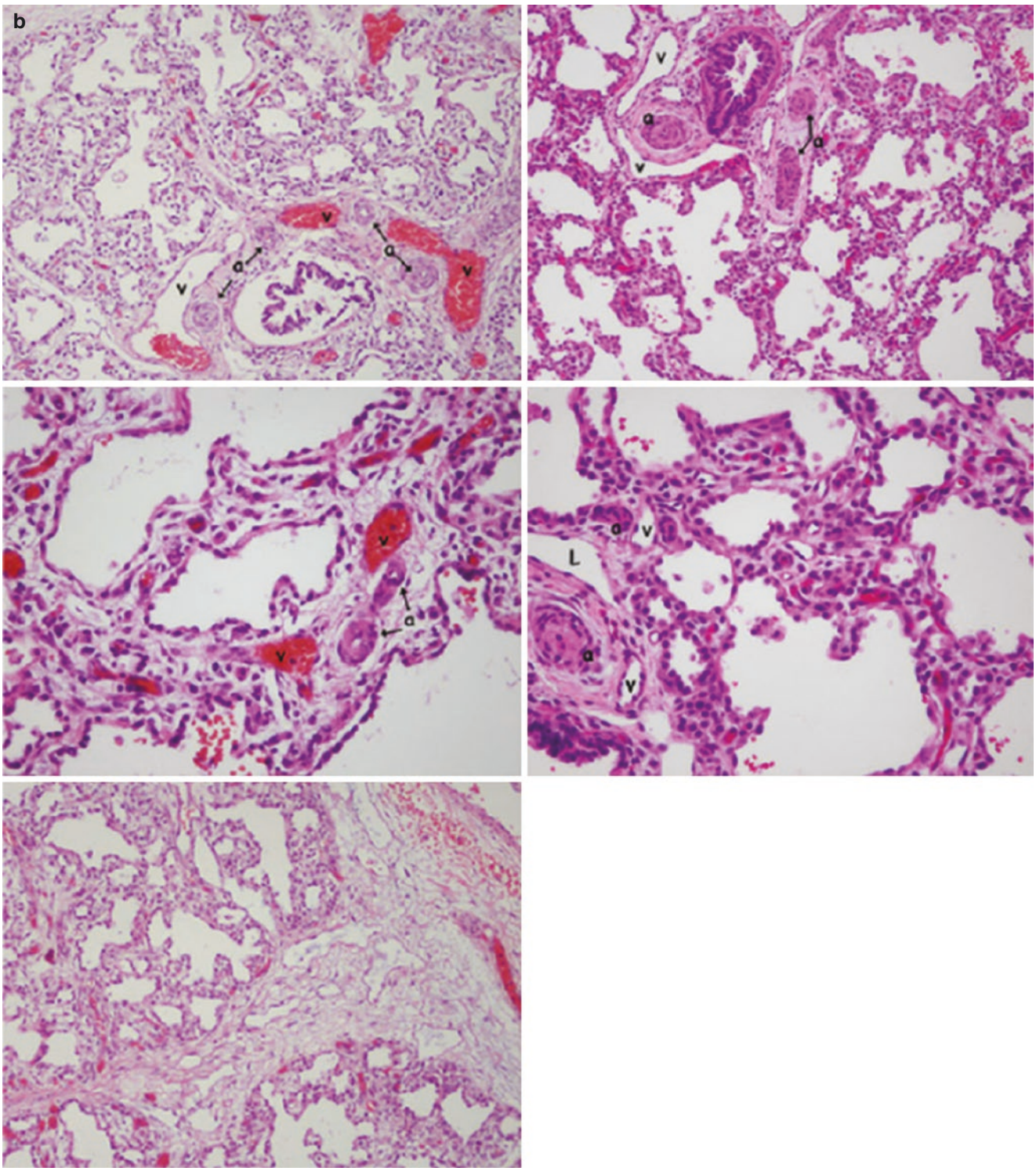

Fig. 8.3 (continued)

Surfactant Dysfunction Disorders

Interstitial (diffuse) lung diseases of infancy in this category include surfactant dysfunction disorders due to genetic abnormalities [26] in the surfactant proteins B (SpB) [27] and C (SpC) [28, 29] and in the ATP-binding cassette transporter protein A3 (ABCA3) [30, 31]. While inherited genetic mutations in SpB and ABCA3 are autosomal recessive, SpC mutations are autosomal-dominant loss of function mutations. Other rare genetic disorders also impact surfactant function and belong in this category, including abnormalities of TTF1 and lysinuric protein intolerance. There also may be other, as yet unrecognized, disorders in this category, and interstitial lung disease in infants with histology consistent with surfactant dysfunction disorder without a yet recognized genetic disorder is also included here.

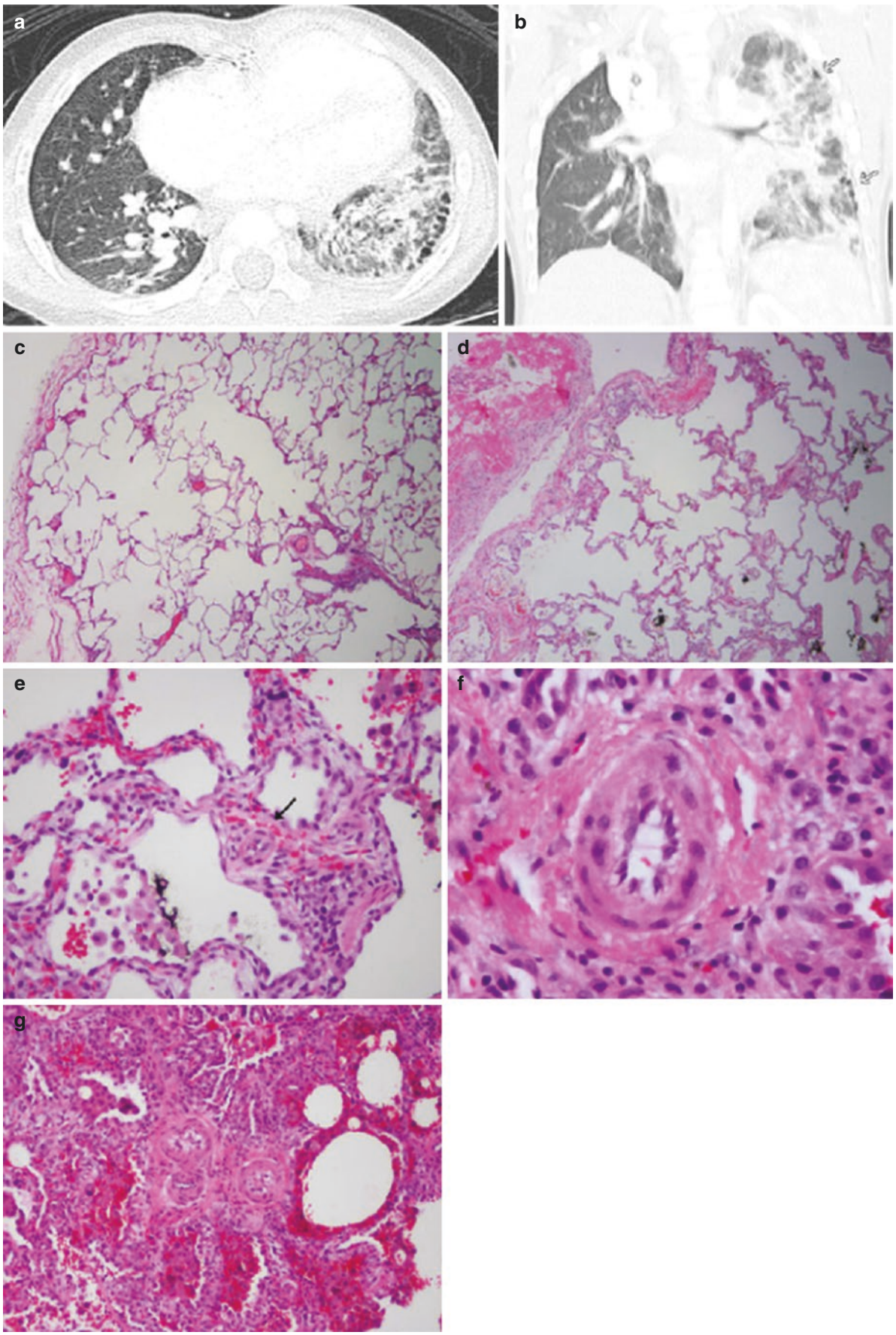
a
b
c
d
e
f
g

Fig. 8.4 (**a**) Trisomy 21: axial lung window CT image of a teenager with Trisomy 21 shows multiple peripheral cysts along the left posterolateral hemithorax. (**b**) Coronal lung window CT image again shows multiple peripheral cysts along the left lateral hemithorax (*arrows*). The lung in down syndrome (**c–g**) shows a distinctive form of pulmonary hypoplasia that is postnatally acquired and can be quite subtle (**c**) with mild-to-moderate alveolar enlargement, widening of alveolar ducts, and more prominent patchy enlargement of subpleural alveoli. This process may progress over early childhood, and the subpleural alveolar enlargement may become more prominent (**d**). This particular growth abnormality is generally accompanied, even in its early manifestations, by arterial changes with increased arterial smooth muscle, beginning with muscularization of alveolar wall vessels (**e**) and proceeding to more prominent arterial changes with increased medial smooth muscle (**f**) and evidence of tortuosity (**g**) with clustered profiles of a tortuous small artery

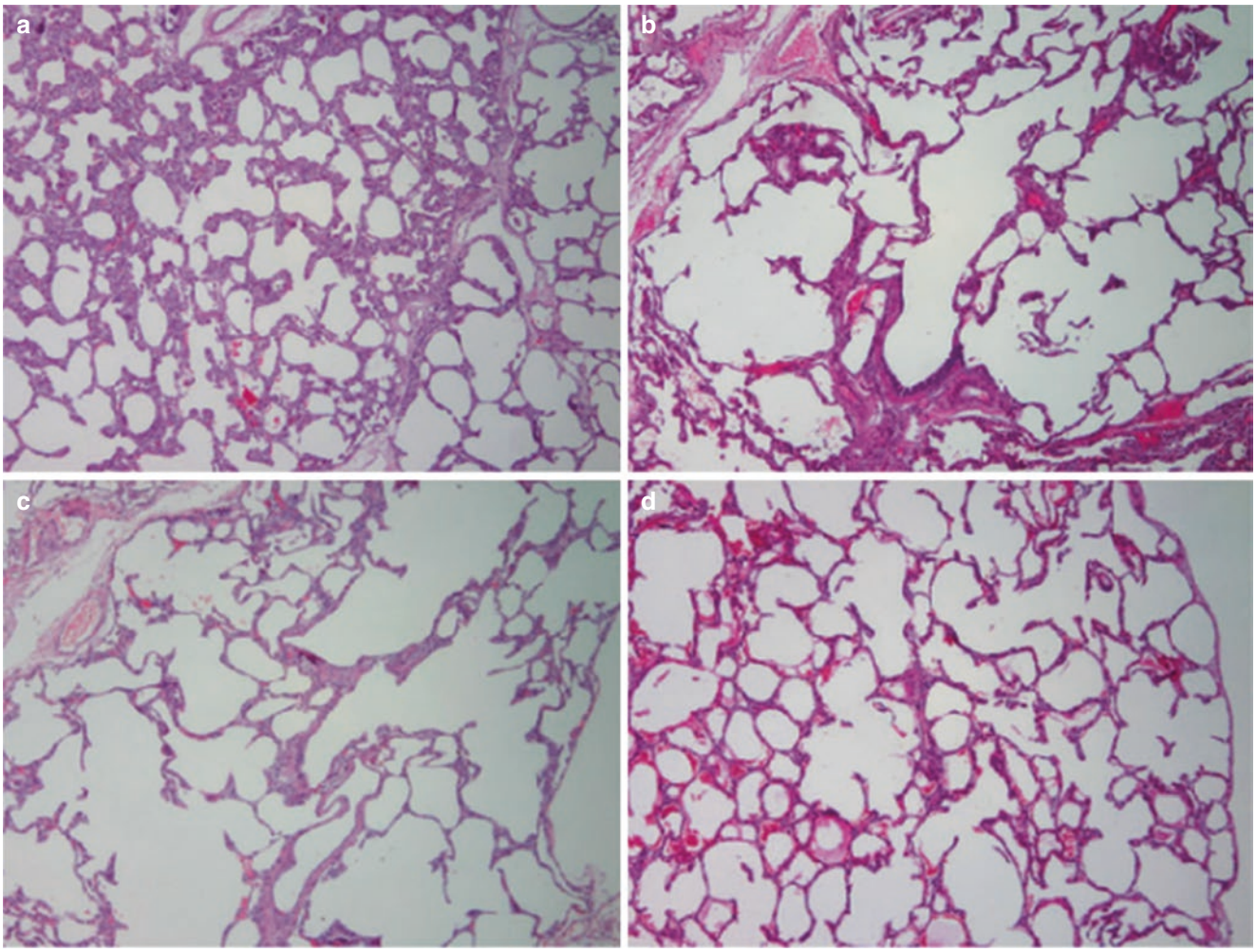

Fig. 8.5 (**a–j**) Alveolar growth abnormalities. All cases of alveolar growth abnormality show enlargement of alveolar spaces, which may vary in degree from mild (**a**) to extreme (**b**, **c**) and may be uniform (**a–f**) or variable (**b**, **c**, **g**). They may show a variety of associated changes, although none needs to be present, including typically mild pulmonary hypertensive arteriopathy (**h**) with muscularized alveolar wall vessels and/or the presence of PIG, typically in a patchy fashion, (**a**) which shows the patchy nature best, (**i**) with quite mild PIG. The appearance is similar regardless of the underlying condition, which may include various forms of pulmonary hypoplasia (**b**, **c**, **g**), chronic lung disease of prematurity (bronchopulmonary dysplasia) (**d**, **h–j**), or a combination of prenatal and postnatal insults (**a**, **e**, **f**). Comparison of alveolar size with that of small membranous bronchioles (**e**) can be useful in estimating alveolar size as alveoli should be much smaller than these distal airways

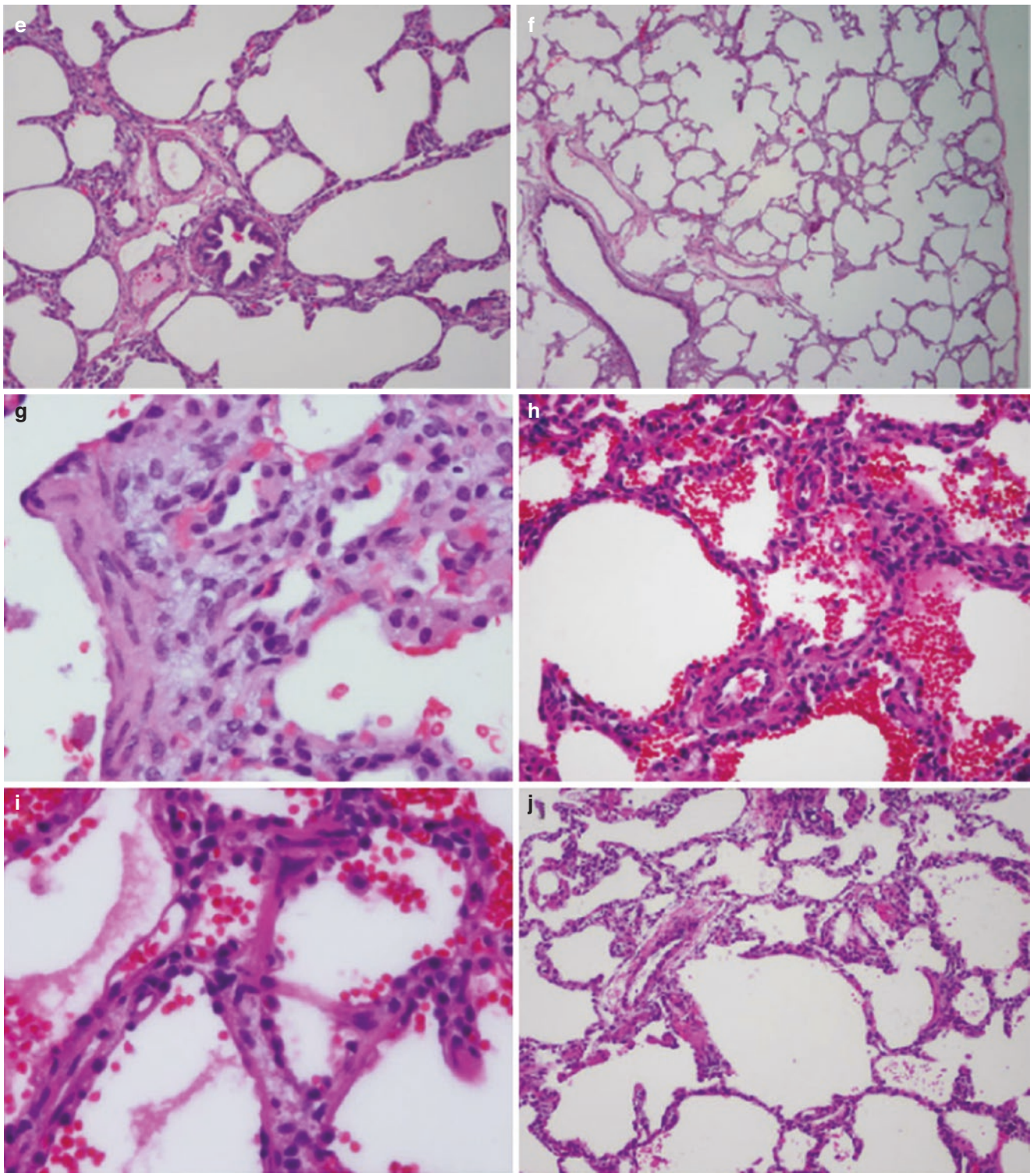

Fig. 8.5 (continued)

Key Clinical Aspects

Infants with surfactant dysfunction disorders typically present either immediately at birth with respiratory failure (SpB and ABCA3) or later postnatally with persistent tachypnea and hypoxemia (SpC and ABCA3). A family history of lung disease may be present in such infants and is common in those with SpC mutations. On laboratory examination, PAS-positive material identified in bronchoalveolar lavage (BAL) fluid and elevation of serum lactate dehydrogenase (LDH) can be potential clues in the diagnosis of surfactant dysfunction disorders. Genetic analysis is considered the definitive diagnostic test, although lung biopsy is often done for categorization and for prognosis and treatment considerations while awaiting the results of genetic testing. Lung biopsy is also definitive for those without as yet recognized genetic mutation and often guides the workup of those with rare genetic disorders in this

category. The current treatment for infants with surfactant dysfunction disorders presenting with interstitial lung disease varies based on the degree of clinical symptoms and the underlying genetic defect. Aggressive chronic ventilation for infants with respiratory failure is currently most often performed for infants with a SpC mutation, and lung transplant is the only effective therapeutic option for infants with SpB mutation. Those with ABCA3 mutations have a more varied presentation and course, at least in part depending on the specific mutation involved. In older children with ABCA3, there is a high incidence of pectus excavatum [32]. There are a few cases of SpB and ABCA3 mutations that have been noted anecdotally to respond to hydroxychloroquine therapy.

Imaging Features

The characteristic imaging findings of infants with surfactant dysfunction disorders are the early appearance of diffuse hazy or granular parenchymal opacities (ground glass opacities) on plain chest radiographs (Fig. 8.6). On HRCT, the most characteristic imaging findings of surfactant dysfunction disorders include ground glass opacity (GGO) with variable interlobular septal thickening. These imaging findings, however, can change over time.

Pathological Features

Surfactant dysfunction mutations in infants are histopathologically characterized (Fig. 8.6) by (1) prominent diffuse uniform alveolar epithelial hyperplasia, (2) variable amounts of proteinosis material, and (3) increased and often foamy macrophages with occasional cholesterol clefts, variable interstitial widening, and sometimes mild interstitial inflammation that may increase with age. These changes typically are described as one of several possible histologic patterns seen in these disorders, including PAP pattern, desquamative interstitial pneumonia (DIP) pattern, CPI pattern, and NSIP pattern, all of which in this setting suggest an underlying surfactant dysfunction mutation. While each of these patterns may be seen with any one of the specific surfactant dysfunction mutations, PAP is uncommon and when seen suggests an SpB abnormality, DIP is more often seen with SpC or ABCA3 abnormalities, and CPI is more characteristic of SpC but may also be seen with ABCA3 mutations. An NSIP pattern is more often seen in older infants and children with SpC or ABCA3 abnormalities. Histologic variants outside these typical definable patterns also occur, but all are marked by the key features of alveolar epithelial hyperplasia, an element of proteinosis and an element of lipid accumulation most often as a few scattered cholesterol clefts. Electron microscopic examination of the lung tissue can be helpful as well, as ABCA3 and SpB have specific ultrastructural abnormalities of lamellar bodies in type-2 alveolar epithelial cells. ABCA3 has tiny lamellar bodies with a prominent dense inclusion, and SpB shows reduced numbers of lamellar bodies with reduced lamellations and sometimes fusion of lamellar and multivesicular bodies.

Other Conditions in the Spectrum of the Surfactant Dysfunction Disorder

There are several rare conditions that should be considered in the differential of surfactant dysfunction disorders. These include mutations in TTF-1 (Fig. 8.7) [33–36], which may present with proteinosis in the neonate and in older infants and young children histology resembling that of surfactant dysfunction disorders often in combination with congenital hypothyroidism and benign chorea as part of the brain-thyroid-lung syndrome [37]. Lysinuric protein intolerance, another rare genetic disorder with mutation in the amino acid transporter gene *SLC7A7*, may also present with alveolar proteinosis in early infancy. Congenital deficiency of the GMCSF alpha receptor also results in alveolar proteinosis, although with presentation in early childhood rather than in infancy. It is also important to remember that in a proportion of infants with typical histologic and imaging findings for surfactant dysfunction disorders, no genetic abnormality may be identified and that other genetic disorders impacting surfactant function may yet be discovered.

Specific Conditions of Undefined Etiology

There are two important and relatively common interstitial lung disorders in this category of ILD in infancy, NEHI and PIG.

Key Clinical Aspects

Neuroendocrine cell hyperplasia of infancy (*NEHI*) [38–42] has also been known as persistent tachypnea of infancy or chronic idiopathic bronchiolitis of infancy and sometimes as follicular bronchitis [43]. This recently described entity accounts for a substantial portion of ILD in infants. Affected infants are usually term and typically present with clinical symptoms of persistent tachypnea, retractions, hypoxemia, and crackles without substantial cough or wheezing by 3 months of age often beginning after an initial period of well-being and sometimes following an uncomplicated viral respiratory infection. Infant pulmonary function test may show evidence of substantial hyperinflation, and bronchoscopy and BAL are usually normal.

The treatment for NEHI is currently supportive and aimed at preventing hypoxemia and infection while maintaining nutritional support. Many affected infants develop failure to thrive with time. Corticosteroids are not helpful for improving symptoms in infants with NEHI as an underlying inflammation is not a component of the disorder, evidenced by the lack of inflammatory cells on BAL or in the lung tissue at biopsy. Despite persistent symptoms and a prolonged need for oxygen therapy, infants with NEHI usually have a favorable long-term outcome with no reported deaths directly related to NEHI, no respiratory failure, and no progression to end-stage lung disease or lung transplantation. However, some patients with NEHI have long-term morbidity with persistent symptoms due to hyperinflation and reactive airway disease and may relapse with hypoxemia during intercurrent respiratory infection.

Pulmonary interstitial glycogenosis (*PIG*) [44, 45] has been previously known as infantile cellular interstitial pneumonitis and histiocytoid pneumonia and as such, has been recognized for many years. PIG may occur in both preterm and full-term infants who usually present with tachypnea and hypoxemia either immediately or soon after birth. It is very unusual for PIG to occur or persist beyond 6 months of age. Although PIG has been described as an isolated finding, it is more often associated with the variety of conditions that affect lung growth, the alveolar growth abnormalities. Most affected infants do not require specific treatment; however, in those more severely affected clinically, pulse steroids have been recommended. Clinical outcomes of infants with PIG are varied and are thought to be related to the underlying condition rather than to PIG itself.

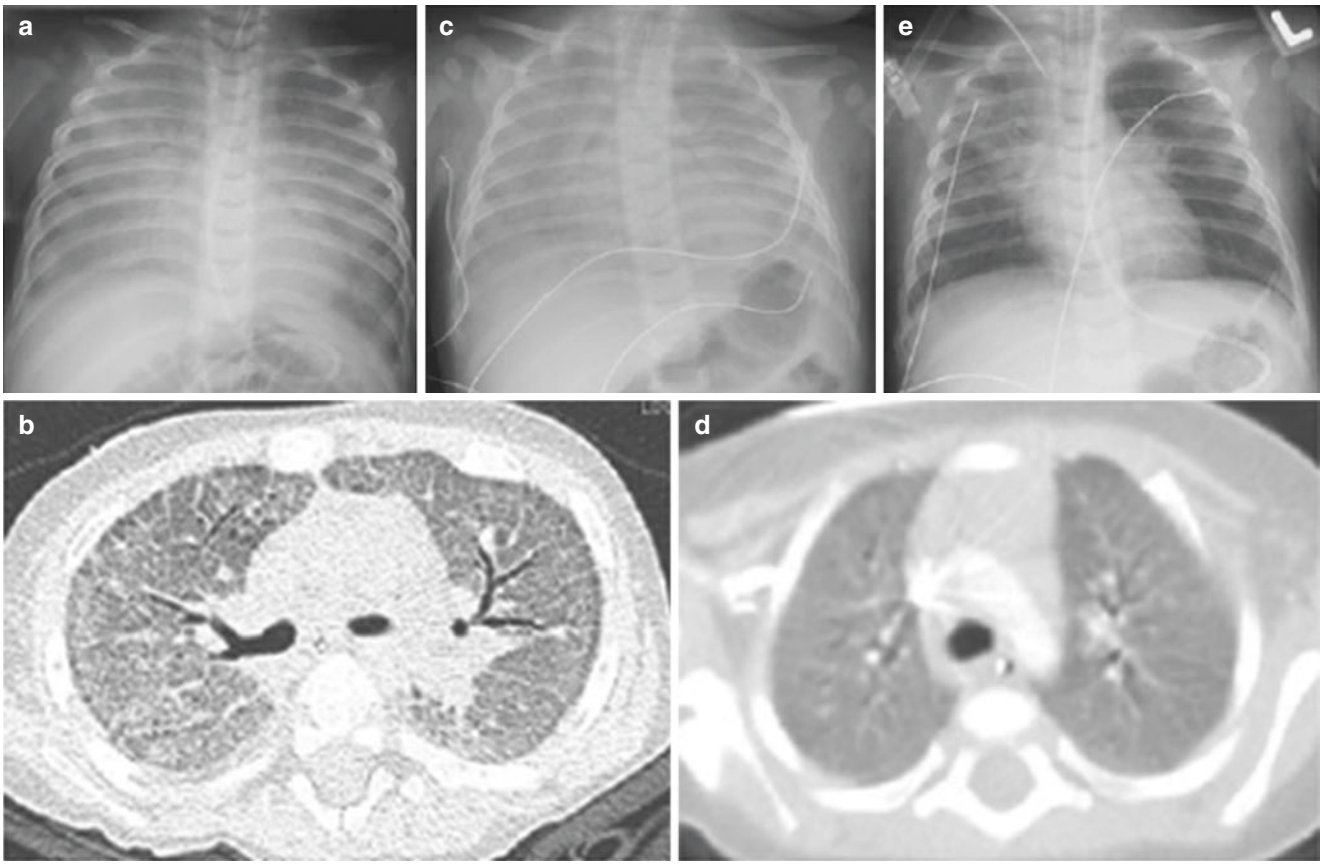

Fig. 8.6 (**a**) ABCA3 deficiency: newborn with ABCA3 deficiency. As is typical for the surfactant protein deficiencies, there is a hazy severe diffuse opacification. (**b**) Typical of the CT findings of the surfactant protein deficiencies, this image from the infant shown in Fig. 8.4 has diffuse ground glass opacity with intralobular septal thickening. (**c**) Another infant with ABCA3 shows similar findings by CXR. (Image courtesy of Dr. Mike Tsifansky, Advocate Lutheran General Children's Hospital, Pediatric Pulmonology and Critical Care Medicine, Park Ridge, IL.) (**d**) Axial lung window CT image of the infant shown in (**c**) has ground-glass opacity similar to that in Fig. 8.4b but less pronounced intralobular septal thickening. (Image courtesy of Dr. Mike Tsifansky, Advocate Lutheran General Children's Hospital, Pediatric Pulmonology and Critical Care Medicine, Park Ridge, IL.) (**e**) The baby shown in (**c**, **d**) was treated with aerosolized hydroxychloroquine with significant, but transient, improvement in respiratory and imaging conditions. (Image courtesy of Dr. Mike Tsifansky, Advocate Lutheran General Children's Hospital, Pediatric Pulmonology and Critical Care Medicine, Park Ridge, IL.) Surfactant dysfunction disorders and related abnormalities (**f**–**i**) are all surfactant B deficiency images, (**j**–**n**) are all surfactant C deficiency images, and (**o**–**t**) are all ABCA3 images. Surfactant dysfunction mutations: histologic changes in the infant lung in the surfactant dysfunction mutations are stereotypical with lobular remodeling (surfactant B (**h**)), surfactant C (**j**), ABCA3 (**q**) uniform diffuse alveolar epithelial hyperplasia (surfactant B (**i**)), surfactant C (**j**, **k**), ABCA3 (**o**), at least some element of proteinosis (surfactant B (**i**)), surfactant C (**j**–**m**), ABCA3 (**r**, **s**), and often at least a few cholesterol clefts (ABCA3 (**o**, **s**)). These changes are present in all cases regardless of the underlying abnormality or the histologic pattern. While a variety of histologic patterns have been described in surfactant dysfunction mutations, including pulmonary alveolar proteinosis (PAP), desquamative interstitial pneumonia, and chronic pneumonitis of infancy (surfactant C (**j**)), most cases do not present a single clearly defined pattern. An atypical proteinosis pattern is more frequent with surfactant B mutations (surfactant B (**h**, **i**)), a chronic pneumonitis of infancy pattern is more frequent with surfactant C mutations (surfactant C (**j**)), and ABCA3 shows proteinosis in a chunky fashion (**r**, **s**); however, no pattern is specific to a particular abnormality. While mutation analysis is the definitive diagnostic modality, ultrastructural changes in the lamellar bodies of type 2 pneumocytes can be quite helpful for more rapid categorization for prognosis and treatment decisions. These changes are quite specific for ABCA3 where there is a paucity of lamellar bodies (ABCA3 (**p**)), and those present are tiny, poorly lamellated and contain a dense central inclusion (ABCA3 (**t**)). SpB mutations also show characteristic ultrastructural changes with fusion of lamellar and multivesicular bodies (surfactant B (**f**)) and absence of tubular myelin (surfactant B (**g**)); there are also reduced numbers of lamellar bodies, which are typically poorly lamellated (not shown). There are no characteristic lamellar body ultrastructural findings with SpC mutations, the type 2 pneumocytes may appear normal (surfactant C (**m**)), or there may be mild changes in the size and distribution of lamellar bodies (surfactant C (**n**))

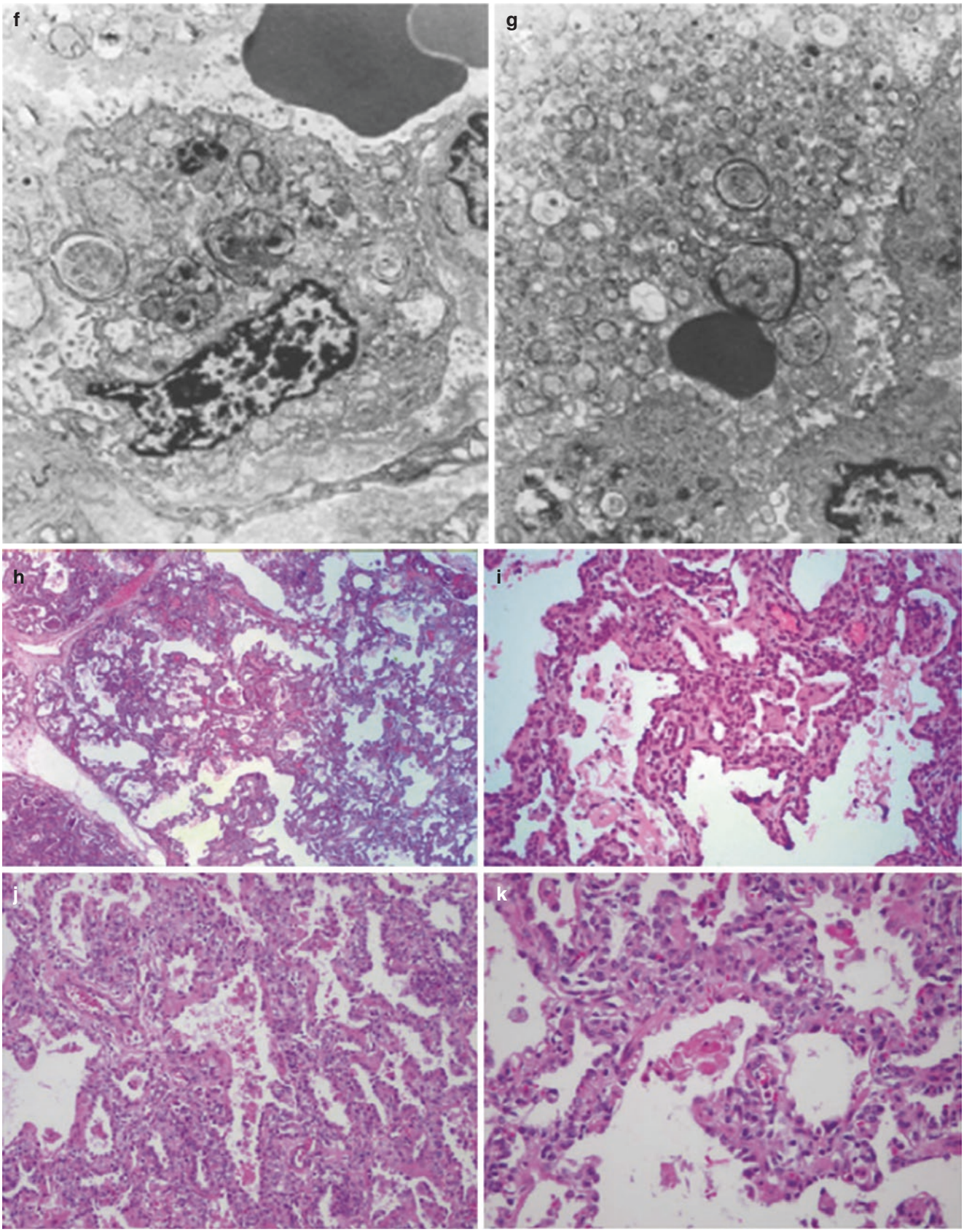

Fig. 8.6 (continued)

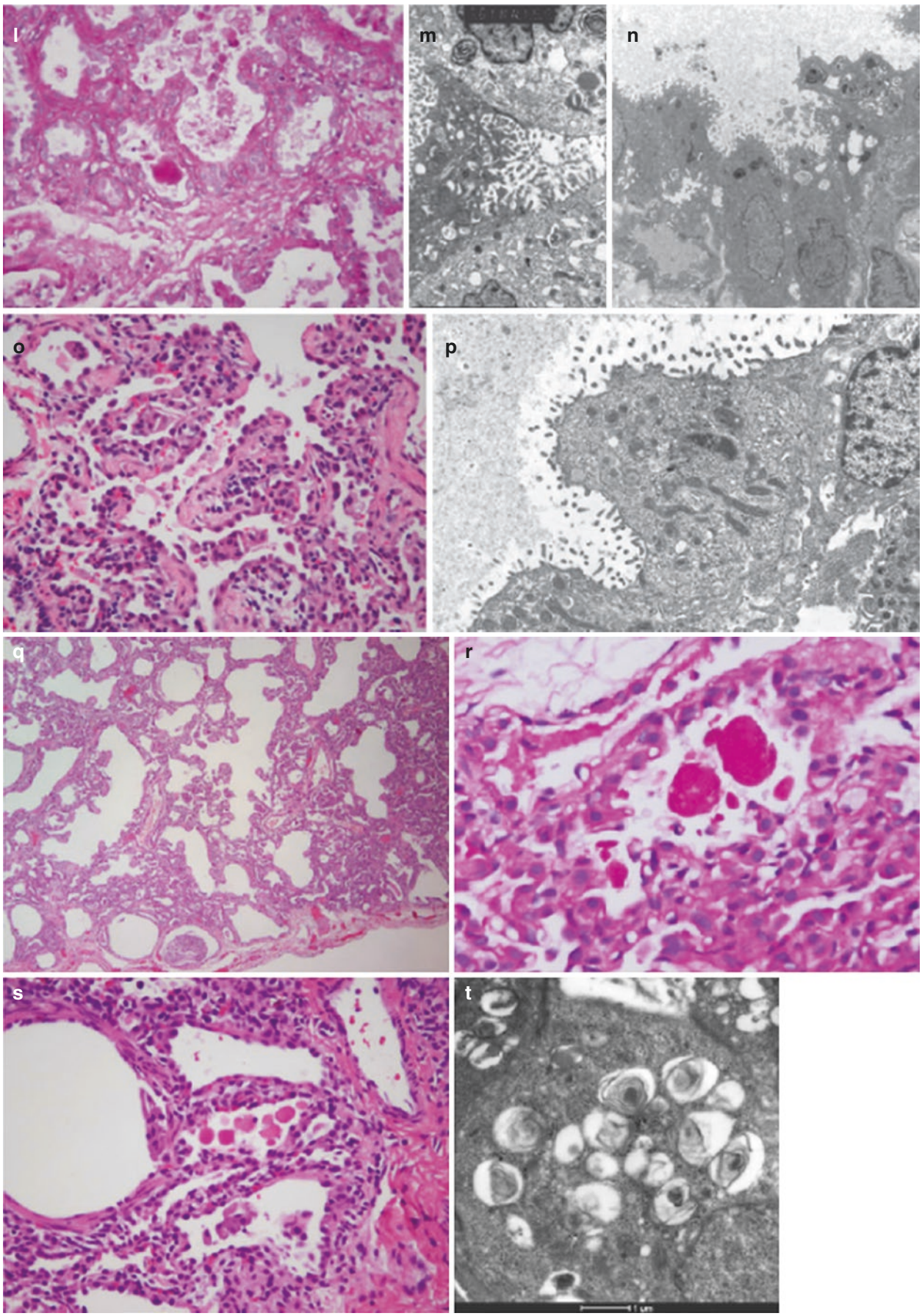

Fig. 8.6 (continued)

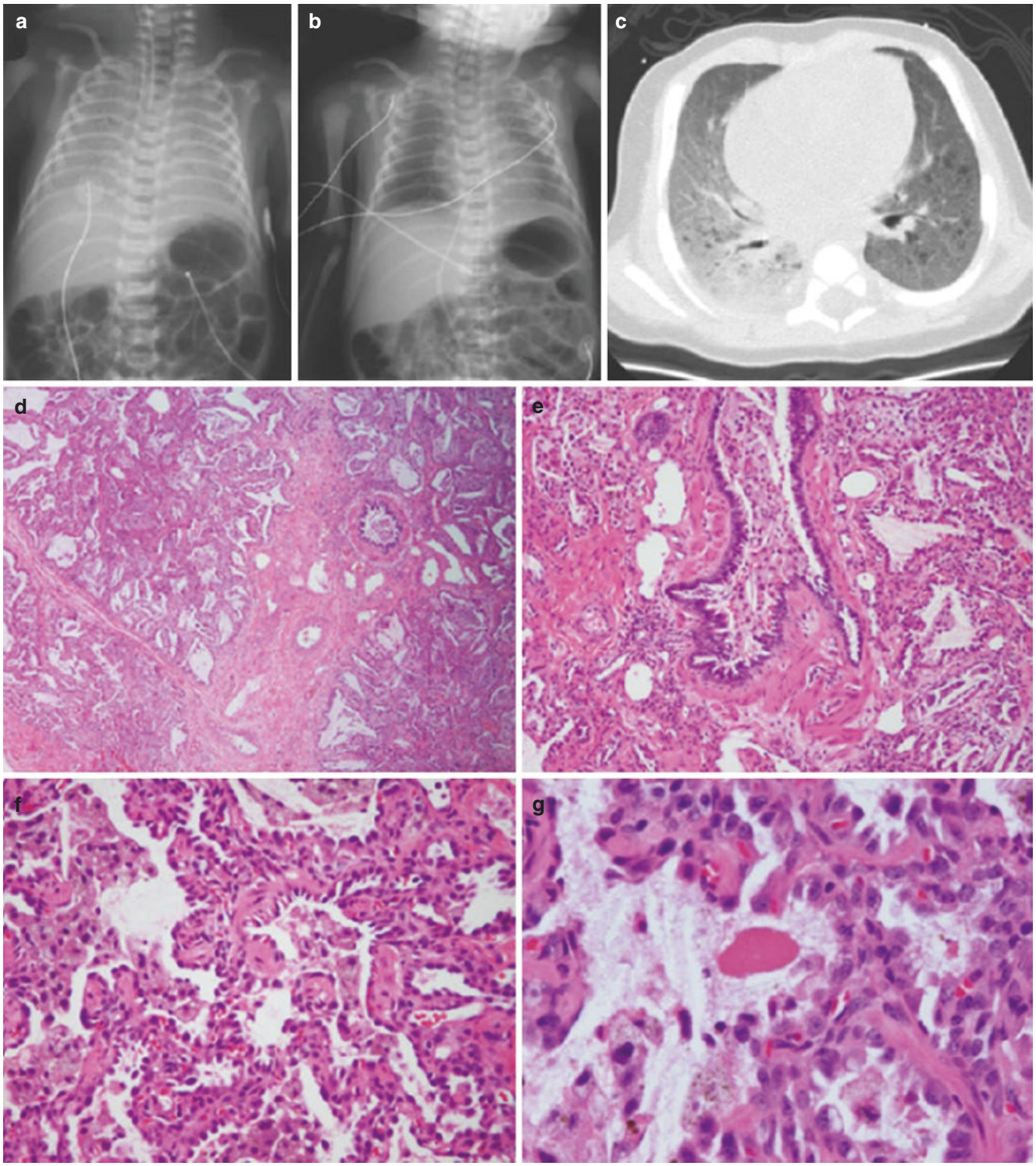

Fig. 8.7 (**a**) TTF-1: this infant with TTF-1 on the first day of life 1 has a severe nonspecific diffuse granular interstitial opacification similar to that seen with hyaline membrane disease. (**b**) TTF-1: with positive pressure ventilation, there is increased lung volume but persistent granular interstitial lung opacification. (**c**) TTF-1: axial lung window CT image obtained at 11 weeks reveals diffuse ground-glass opacification with multiple posterior cysts. (**a**–**c**, from Galambos et al. [36]. Reprinted with permission of the American Thoracic Society. Copyright American Thoracic Society. Official Journal of the American Thoracic Society.) TTF-1 histologic changes in the lung with TTF-1 mutations (**d**–**k**) clearly vary, but there is limited information on the variety of changes seen. These images are from one case with quite severe lung disease that shows histologic abnormalities within the spectrum of the surfactant dysfunction mutations with diffuse involvement with lobular remodeling (**d**), intraalveolar and distal airway debris with prominent numbers of cholesterol clefts (**e**), diffuse alveolar epithelial hyperplasia (**f**), proteinosis seen here as globular eosinophilic material (**g**), and mild patchy interstitial lymphoplasmacytic infiltrates (**h**). In addition to these changes that clearly link this disorder histologically with the surfactant dysfunction mutations, there may be other changes with metaplastic bronchiolar epithelium with lepidic spread (**i**), somewhat atypical features (**j**), and mucin content (Movat stain (**k**)) that suggest the possibility of bronchioloalveolar carcinoma

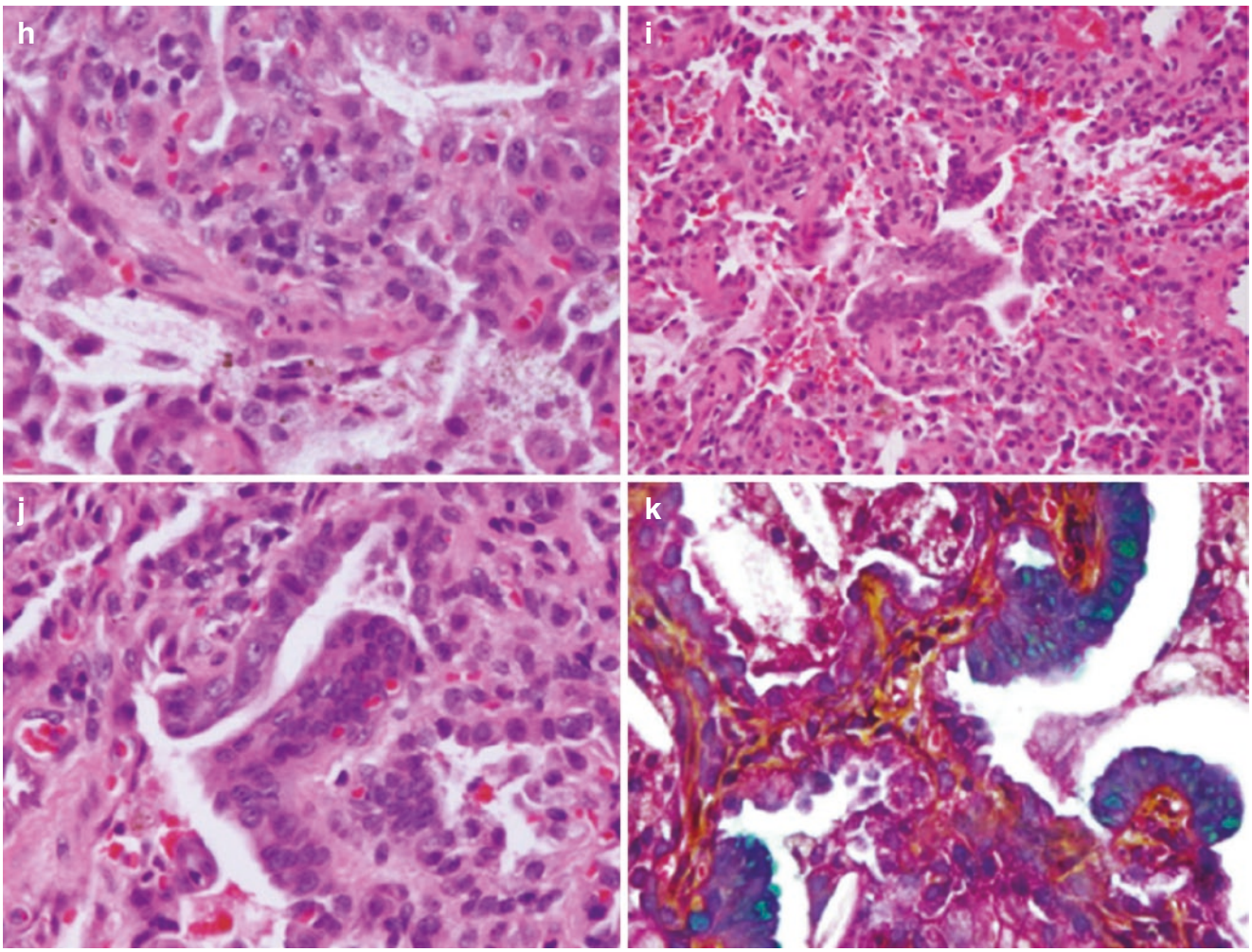

Fig. 8.7 (continued)

There has been no reported death in infants with pure diffuse PIG; however, death has been reported in infants with patchy PIG who also had underlying growth abnormalities and PHT.

Imaging Features

Neuroendocrine Cell Hyperplasia of Infancy (NEHI) The typical imaging findings of NEHI are hyperinflation with variable increased perihilar opacity on plain chest radiographs (Fig. 8.8). HRCT findings are quite characteristic with geographic GGO with central predominance, especially in the lingula and right middle lobe without other interstitial abnormalities. Additionally, marked air trapping often affecting both the areas of GGO and the remaining lung can be seen. It has been reported that the sensitivity and specificity of HRCT for the diagnosis of NEHI are 78 and 100%, respectively, based on a recent study of 29 CT examinations from 23 patients with biopsy-proven NEHI and 6 patients with other forms of pediatric interstitial lung disease.

Pulmonary Interstitial Glycogenosis (PIG) Similar to the imaging findings of NEHI, infants with PIG typically show changes of bilateral hyperinflation and diffuse interstitial markings on plain chest radiograph. On HRCT, diffuse, segmental, or subsegmental ground-glass opacities; interlobular septal thickening; and reticular change predominantly in a subpleural distribution with few centrilobular nodules have been reported. Recently, multiple small, variably sized scattered air-filled cystic changes in conjunction with diffuse ground-glass opacities, interlobular septal thickening, and reticular change have been reported in an infant boy with PIG in the setting of alveolar growth abnormality (Fig. 8.9) [46]; the contribution of PIG and of the growth abnormality to these changes cannot be apportioned with any certainty. The concomitant appearance of PIG with alveolar growth abnormalities suggests that imaging findings in these conditions typically share this uncertainty.

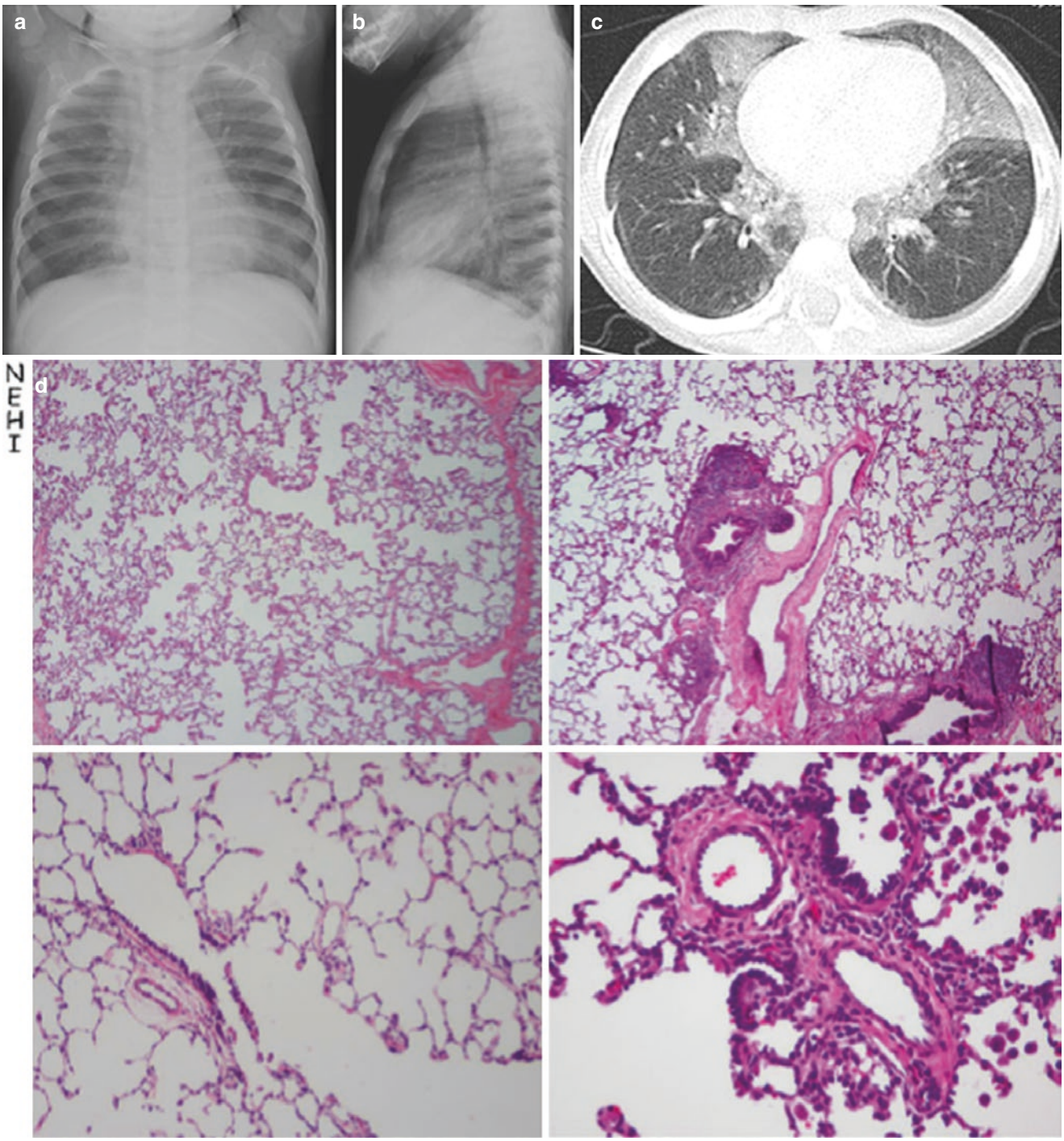

Fig. 8.8 (**a**) Neuroendocrine cell hyperplasia of infancy (NEHI): PA CXR of this baby with NEHI shows a centrally accentuated hazy interstitial opacification bilaterally with hyperinflation. (**b**) NEHI: lateral CXR confirms that the central opacifications are accentuated anteriorly. Hyperinflation is again evident. (**c**) Axial lung window CT image reveals the classic centrally, anteriorly accentuated ground-glass opacities of NEHI. (**d**) Neuroendocrine cell hyperplasia of infancy (NEHI): cases of NEHI generally have a near normal histologic appearance, illustrated in the *left upper two panels* with hematoxylin and eosin stain where there are mild nonspecific changes, including mild prominence of airway smooth muscle and a mild increase in alveolar macrophages; however, occasional cases may show prominence of airway-associated lymphoid tissue and mild peri-airway lymphocytic infiltrates, illustrated in the *right upper two panels* with hematoxylin and eosin stain, which overshadow the similar mild airway smooth muscle and macrophage increase. With this quite bland background, the histologic hallmark of NEHI is an increase in the proportion of neuroendocrine cells in small airways (*lower four panels* with immunostain for bombesin), where they often appear clustered in small groups and sheets, rather than as isolated cells; neuroepithelial bodies (*bottom right*) may be enlarged and/or numerous

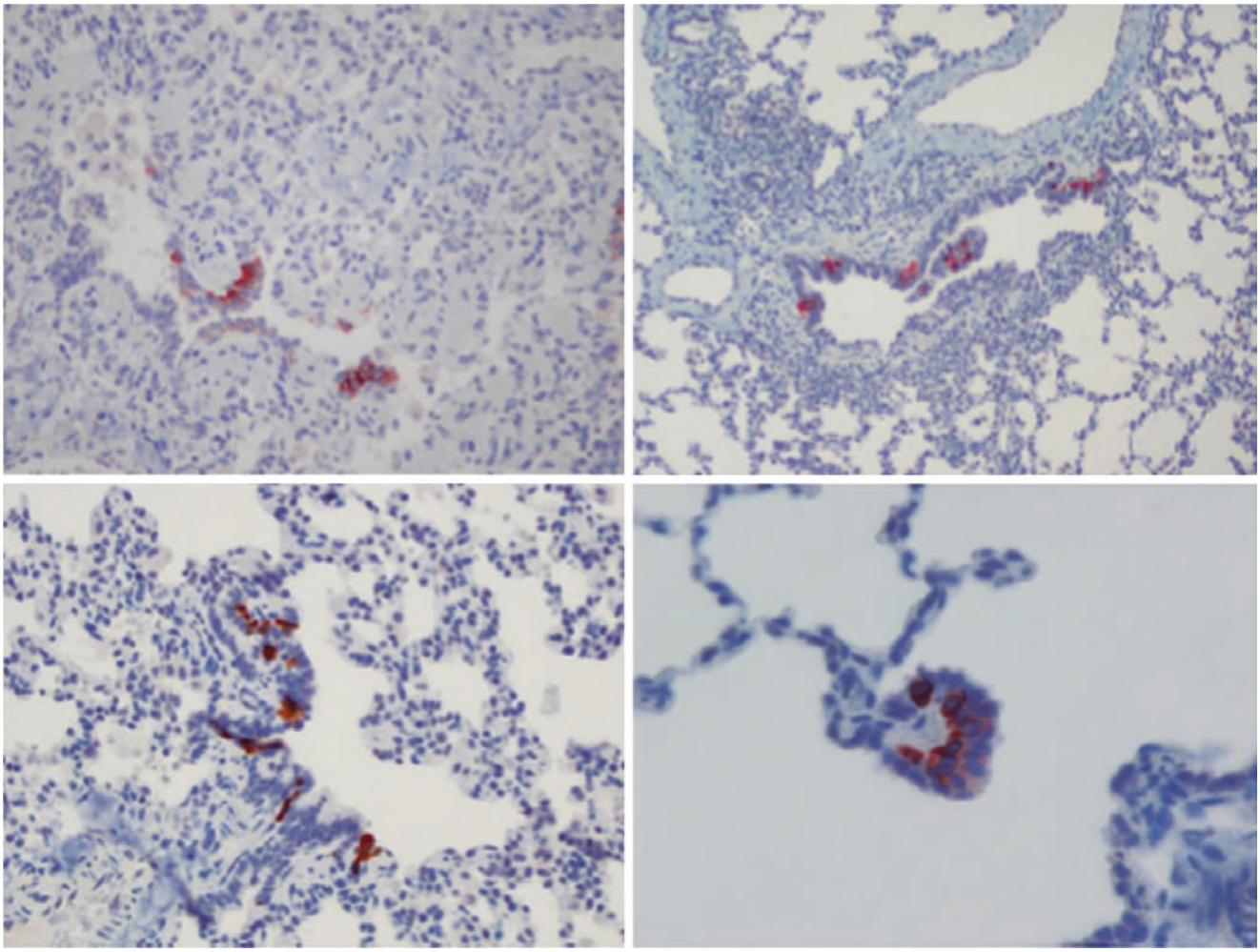

Fig. 8.8 (continued)

Pathological Features

Neuroendocrine Cell Hyperplasia of Infancy (NEHI) On routine histopathological evaluation, NEHI (Fig. 8.8) typically shows only minor and nonspecific changes, including mildly increased airway smooth muscle, mildly increased numbers of alveolar macrophages, and occasional mild peri-airway lymphocytic inflammation, although some biopsies also show mild and focal airway changes likely related to intercurrent infection. Histologic diagnosis rests on the identification of increased numbers of bombesin immunopositive neuroendocrine cells in bronchioles and prominent neuroepithelial bodies in the lobular parenchyma in the absence of other significant pathologic changes.

A recent study documents the absence of neuroendocrine cell hyperplasia in the focally injured airways sometimes seen within these biopsies, suggesting that NEHI is not an abnormal reaction to viral infection, and another documents familial association suggesting a genetic propensity for the development of NEHI. The pathophysiology of the disorder remains unknown, although the role of the neuroendocrine system in regulating bronchial and vasomotor tone in the lung may be central to disease manifestation.

Pulmonary Interstitial Glycogenosis (PIG) The diagnosis of PIG requires the examination of the lung tissue. It is characterized by the expansion of the lobular interstitium by rounded, glycogen-laden undifferentiated mesenchymal cells without fibrosis, airway disease, or underlying inflammation on pathological analysis (Fig. 8.9). The interstitial cells in patients with PIG are immunoreactive for vimentin and are negative for muscle, epithelial, macrophage, and leukocyte markers suggesting that they are poorly differentiated mesenchymal cells. The most reliable means of diagnosis is the ultrastructural identification of characteristic deposits of monoparticulate glycogen within these mesenchymal cells. These interstitial cells may rarely contain small amounts of lipid by ultrastructural examination. PIG has been classified as diffuse or patchy; the patchy form is more common and is typically seen in association with alveolar growth abnormalities of varied etiology.

Conclusions: Disorders More Prevalent in Infancy

The early and correct diagnosis of ILD in infants has been a major challenge for clinicians, radiologists, and pathologists mainly due to the rarity of these disorders, coupled with non-specific clinical symptoms and the absence of a coherent classification system. With the advent of the new ChILD classification system, our understanding of ILD in infants has markedly improved. Knowledge of clinical, imaging, and pathological features of ILD in infants will enhance accurate diagnosis and improve timeliness; both are crucial as prognosis and treatment vary considerably among the different infant interstitial lung disorders. Although the etiology is currently unknown, several of these abnormalities of lung parenchyma have been shown to have multiple cysts. This

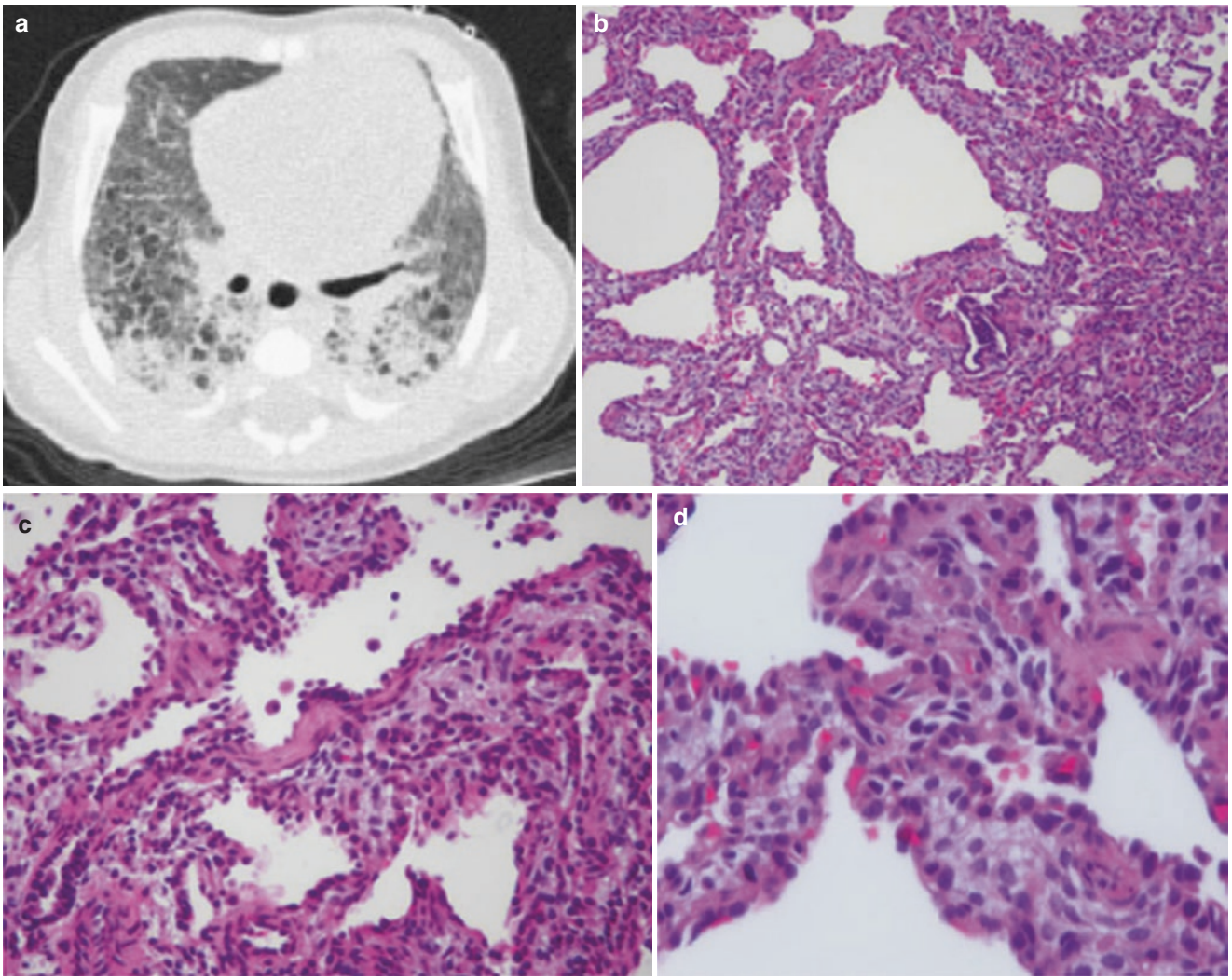

Fig. 8.9 (**a**) Pulmonary interstitial glycogenosis (PIG): axial lung window CT image of an infant with alveolar growth abnormality and PIG shows ground-glass opacities, intralobular septal thickening, reticular changes, and multiple posterior cysts. (Image courtesy of Dr. Paul Guillerman, Baylor College of Medicine, Texas Children's Hospital, Houston, TX.) Cases of PIG typically show at least some element of alveolar growth abnormality in the background, as seen in (**b**) with enlarged airspaces. In PIG, the lobular interstitium is widened by an accumulation of bland-appearing cells with abundant pale to bubbly cytoplasm (**b–d**). Other features vary depending on the underlying conditions affecting the infant. There may be mild and patchy alveolar epithelial hyperplasia (**b–d**); it is not a necessary feature and is almost never prominent and diffuse; there also may be pulmonary arterial changes of hypertensive vasculopathy (not illustrated). The large pale interstitial cells are immunopositive for vimentin (**e**) but not for macrophage or epithelial markers, suggesting that they are mesenchymal in type. Definitive diagnosis requires the identification of these large bland interstitial cells by electron microscopy. These cells widen the alveolar interstitium (**f**); they have bland nuclei and a paucity of cytoplasmic organelles (**g**), and their cytoplasm contains abundant monoparticulate glycogen (**e**). The cells stain similarly to the glycan-rich matrix of early fibrosis with Movat pentachrome stain (**h**) and as fibrous tissue with trichrome stain(not shown), although there is no actual collagen deposition by electron microscopy. While in occasional cases the intracellular glycogen may be demonstrated by PAS staining with PAS-positive, diastase-sensitive interstitial staining (not illustrated), in most the glycogen is washed out during processing and the PAS stain is not positive

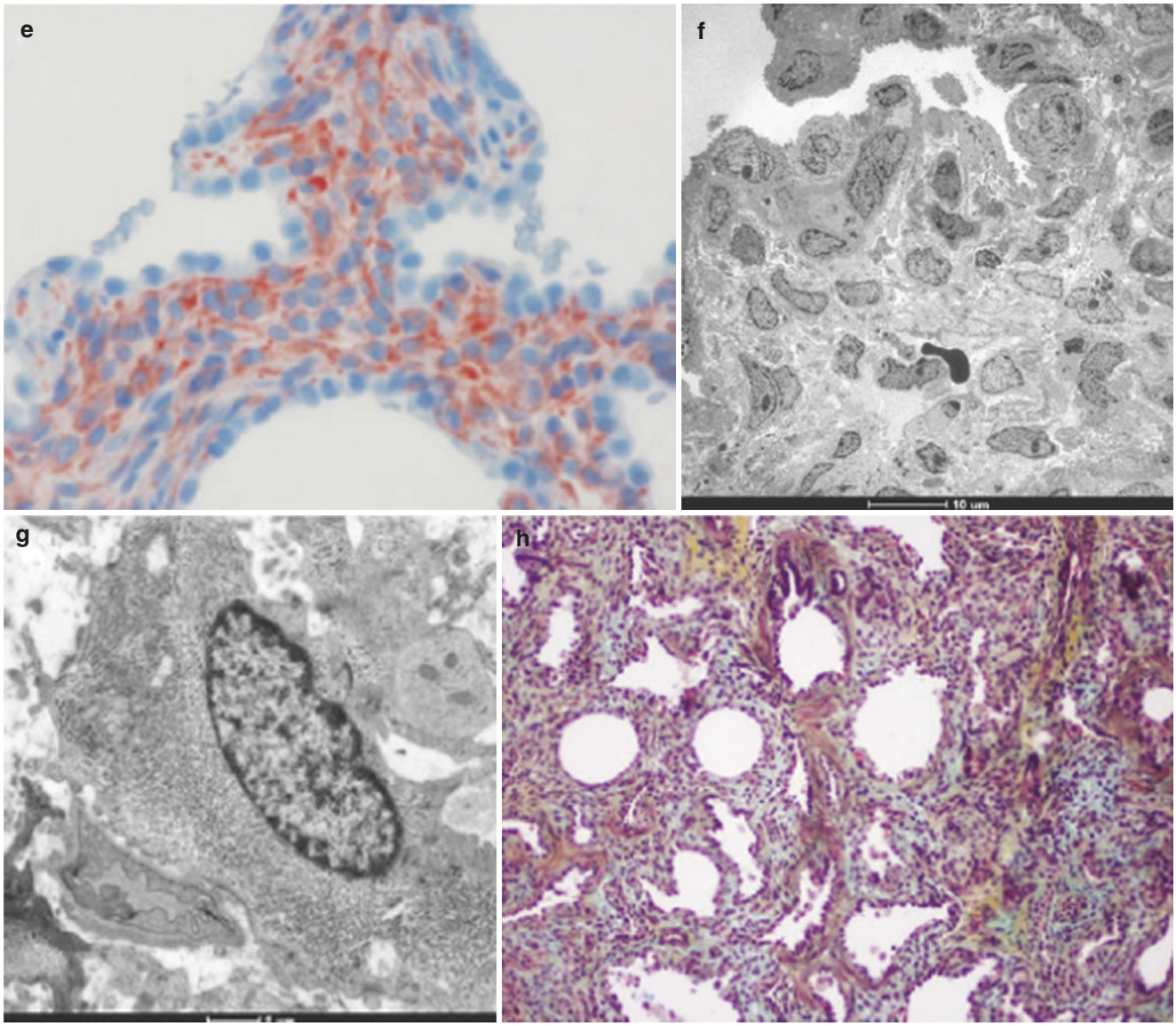

Fig. 8.9 (continued)

includes infants with TTF-1, alveolar growth disturbance, and PIG, as well as children with Trisomy 21 and Turner syndrome and in some chromosomally normal infants with congenital heart disease.

Other Childhood Interstitial (Diffuse) Lung Disorders

Infant lung disorders are only rarely seen in older children. Occasionally, children with alveolar growth disorders or NEHI may not come to biopsy until the third year, and some children with surfactant dysfunction mutations present later in childhood or as adolescents or young adults. While the lung disorders more specific to infancy predominate in infants and young children, almost 40% of the lung biopsies in the multicenter institutional study revealed diagnoses in other categories of ChILD (Table 8.1). This narrow predominance of lung disorders more specific to infancy was also documented in a single institutional study of diffuse lung disease in infancy [47]. The other categories for infants and also for older children are detailed below according to the ChILD classification system beginning with disorders of

the normal host and are supported by both the two multicenter studies [7] and by a multicenter review of almost 200 lung biopsies from children 2–18 years of age, similar to that done in infants and young children. In this older group, nearly equal numbers of biopsies were from immunocompetent as from immunocompromised children. Those from immunocompromised patients, the largest single group, account for nearly half the classifiable biopsies, followed by those from children with underlying systemic disorders, accounting for another quarter of the biopsies.

Disorders of the Normal Host

Previously, normal children are less likely to come to lung biopsy for the diagnosis of ILD than are those with immune compromise of underlying systemic disease [48]. In these normal children, infectious and postinfectious disorders predominate with noninfectious disorders including hypersensitivity pneumonia, aspiration syndromes, eosinophilic pneumonia, DAD, and idiopathic pulmonary hemosiderosis being individually uncommon.

Infectious Etiology

Acute Infectious Disease

Acute lower respiratory infections are common causes of pulmonary infections in children and continue to result in substantial morbidity and mortality globally. In immunocompetent pediatric patients, various pathogens, both viral and bacterial, can cause primary pulmonary infections. In fact, viruses are the cause of approximately 50% of all pneumonias in children less than 5 years old.

Table 8.3 lists common pathogens that can cause pulmonary infection in the pediatric population, categorized by age group. It is important to recognize that more than one pathogen can concomitantly cause pulmonary infection in children. For example, a recent review showed that approximately 23% of children with pneumonia have a viral infection together with a bacterial infection.

Imaging Features Although a characteristic imaging finding of pulmonary infection such as consolidation in pediatric patients with bacterial pneumonia can be easily recognized, various other imaging findings of pulmonary infections sometimes can be mistaken for interstitial lung disease in immunocompetent pediatric patients. Such imaging findings can result from abnormalities caused by an acute infectious process involving airways and interstitium. Airway abnormalities (e.g., bronchial wall thickening, irregular aeration, atelectasis) and interstitial abnormalities (e.g., fine linear markings, interlobular septal thickening, small nodular opacities) can mimic interstitial lung disease in children with normal immune function. In general, viral rather than bacterial pulmonary infection results in imaging findings similar to those of interstitial lung disease in children. Clinical history, laboratory findings, prior imaging studies, and follow-up imaging studies can provide helpful information to differentiate abnormal pulmonary imaging findings due to acute pulmonary infection from those of underlying interstitial lung disease.

Table 8.3 Common pathogens for pulmonary infections in pediatric patients by age group

	Pathogen	
Age group	Virus	Bacteria and mycoplasma
Neonates	Cytomegalovirus (CMV) Herpes simplex virus Respiratory syncytial virus (RSV)	Group B streptococcus Gram-negative bacilli *Escherichia coli* *Klebsiella pneumoniae* *Proteus*
1–3 months	RSV CMV	*Chlamydia* *Streptococcus pneumoniae* *Haemophilus influenzae* type B *Staphylococcus aureus*
4 months to 5 year	RSV Parainfluenza Adenovirus Influenza Rhinovirus	*S. pneumoniae* *H. influenzae* *S. aureus*
>5 year	–	*Myocoplasma* *S. pneumoniae*

Pathologic Findings Infection is a relatively common finding in diffuse lung disease in the normal host and is usually readily diagnosed by a consideration of the clinical history, imaging findings, and laboratory, particularly culture results. Sometimes diagnosis is elusive, and in such circumstances, BAL for culture and even lung biopsy may be obtained. In children who come to lung biopsy in such circumstances, viral and mycobacterial disease, sometimes atypical, as well as fungal infection, are more common findings than bacterial infection. The pathologic changes vary with the responsible organism from diffuse to patchy interstitial inflammation with associated airway epithelial changes for respiratory viral infections to granulomatous pneumonitis for mycobacterial and most fungal disorders.

Postinfectious Airway Injury

Postinfectious airway disease includes a spectrum of changes. This may be mild airway wall and peri-airway fibrosis with or without the organization of intraluminal contents as tufts of proliferated fibroblasts or granulation tissues within distal airways and streaming fibroblasts within distal airways and alveolar ducts. At the other end of the spectrum, there may be severe airway fibrosis with significant luminal narrowing to complete airway obliteration (constrictive/obliterative bronchiolitis).

For many, the term *constrictive/obliterative bronchiolitis* has replaced the terms bronchiolitis obliterans (BO) and bronchiolitis obliterans organizing pneumonia (BOOP), although none of these diagnostic terms convey the full spectrum of changes that may be seen. Within this context, what was previously called BO and BOOP are now considered points within a spectrum encompassed by the diagnosis of constrictive/obliterative bronchiolitis. Also, the radiology, pathology, and clinical use of the terms BO and BOOP differ from and are frequently at odds with each other. Consequently, these terms will not be used in this chapter.

Since historically within the pediatric imaging literature the terms BO [49] and BOOP [50] have been widely used, a brief discussion of them is warranted for clarity's sake. Historically, within the radiology community, BO and BOOP were described as secondary to a common set of predisposing conditions. These included pulmonary infection, Stevens–Johnson syndrome, connective tissue disease, toxic inhalation, hypersensitivity pneumonitis, drug-induced lung disease, rejection in lung or heart-lung transplantation, and graft-versus-host disease in bone marrow transplantation, among others. In the radiology literature, in children, most commonly BO was described as following previous lung infection and BOOP was often seen following organ transplantation. When BOOP was encountered as an idiopathic condition, many came to refer to it as cryptogenic organizing pneumonia. BO was considered irreversible, but BOOP often resolved, especially following a successful treatment of the underlying condition (such as acute rejection). The imaging findings described with BO were irregular hyperinflation and mosaic attenuation, usually with one lung dominantly affected and bronchiectasis (also referred to as Swyer–James or McLeod syndrome) (Fig. 8.10). BOOP was described as irregular hyperaeration, patchy interstitial lung disease, and scattered pulmonary nodules (often peripheral) (Fig. 8.11).

Nonetheless, postinfectious airway injury is the most common cause of irreversible chronic small airway disease in children. While there may be noninfectious etiologies for this pathologic process, in children it is most commonly a sequela of prior viral or bacterial infection. Rare cases follow inhalation of toxic gases or collagen-vascular disease or are seen in special settings complicating bone marrow and lung transplants. Among the many pulmonary infections known to have an association with the development of postinfectious airway injury, adenovirus pulmonary infection during early life (<5 years), especially with types 21 and 7, has been considered the most important cause of this condition.

Imaging Findings

Imaging plays an important role in the diagnosis of postinfectious airway injury with constrictive/obliterative bronchiolitis because the clinical findings are often nonspecific; however, a prior history of prolonged recovery from a pulmonary infection with subsequent development of wheezing and shortness of breath, as well as abnormal pulmonary function test characterized by fixed airway obstruction, should raise suspicion for postinfectious airway injury with constrictive/obliterative bronchiolitis.

The imaging appearance, particularly by CT, in affected children can be characteristic and may avoid subsequent invasive procedures, such as lung biopsy. On plain chest radiographs, the affected lung is hyperlucent and relatively underperfused while maintaining normal or decreased lung volume, although it can be normal in appearance. CT findings of constrictive/obliterative bronchiolitis are characterized by (1) air trapping, accentuated on expiration; (2) mosaic attenuation pattern; (3) bronchial wall thickening; (4) bronchiectasis; and (5) diminished small vessels. Although these CT findings should suggest a diagnosis of constrictive/obliterative bronchiolitis in children, other more common entities, such as acute viral bronchiolitis, should be considered unless air trapping and bronchiectasis are both present.

Follow-up imaging study can be helpful in differentiating the changes of chronic postinfectious airway injury from acute viral bronchiolitis. In cases of acute viral bronchiolitis, follow-up imaging studies will show normalization of the previously abnormal imaging findings after resolution of symptoms (although imaging abnormalities may persist for up to a few months), while persistent or worsening abnormalities will be present in cases of irreversible constrictive/obliterative bronchiolitis.

Pathologic Findings

Histologically, postinfectious airway injury is a patchy condition in which some, but not all, airways show signs of previous injury and repair with airway narrowing by subepithelial and peri-airway fibrosis. Typically, smaller membranous bronchioles and terminal bronchioles are affected, rarely larger airways. Such fibrosis may eventuate in marked luminal narrowing, and complete airway obliteration may occur. This can be difficult to identify histologically. Clues to its presence include the identification of small pulmonary arteries without associated airways and residual airway smooth muscle fibers embedded in the fibrotic tissue. This latter finding may be subtle, and may require special stains to highlight

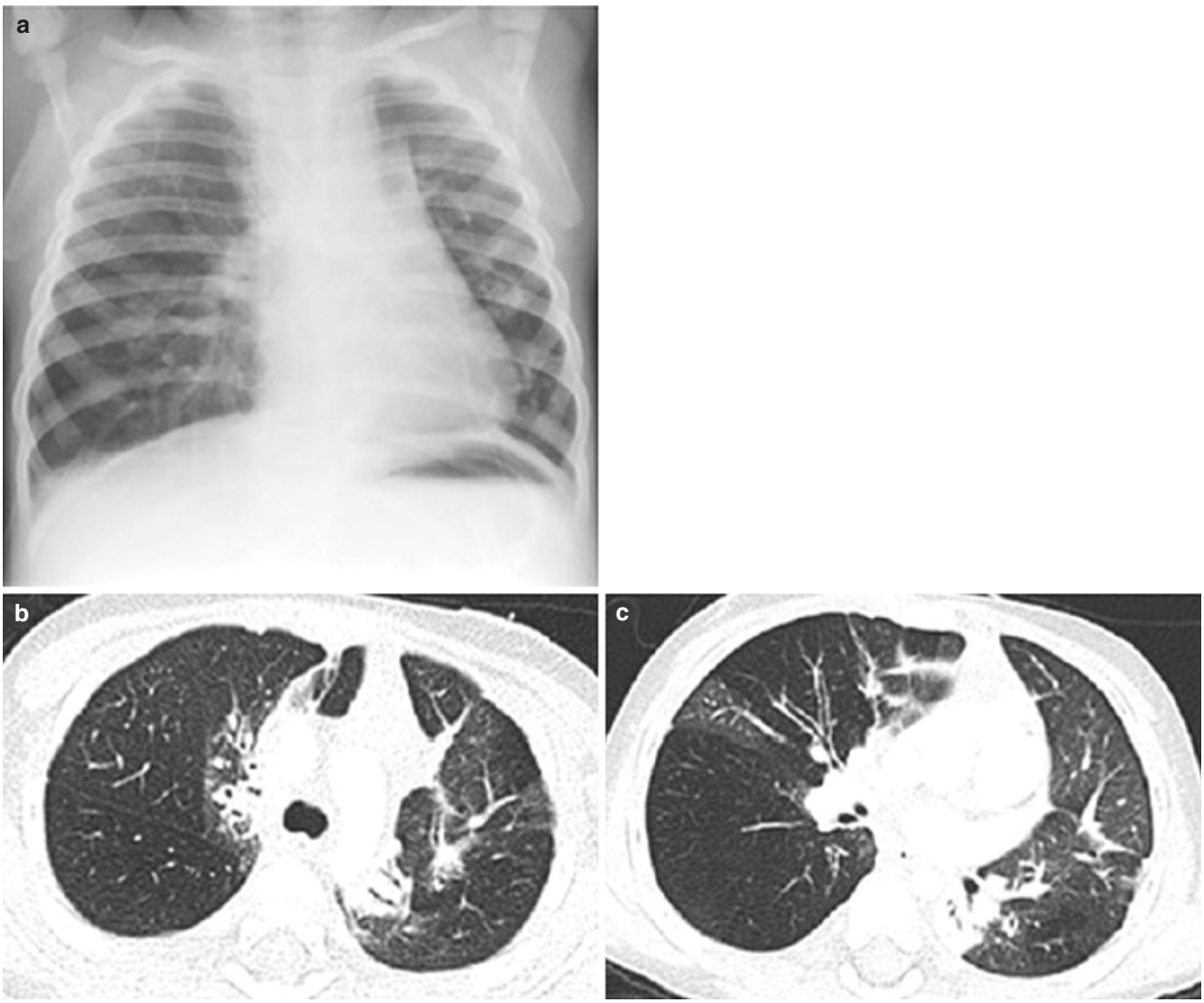

Fig. 8.10 (**a**) Bronchiolitis obliterans (BO): this 2.5-year-old boy had a normal CXR prior to an adenovirus type 3 infection several months previously. The current CXR shows asymmetric lung inflation with multifocal coarse parenchymal opacifications. Axial lung window CT images obtained at the level of the carina (**b**) and inferior hilus (**c**) both show a mosaic pattern of hyperlucent and overinflated lung segments with oligemia and segments of ground-glass interstitial lung disease. The right lung is again shown to be relatively more inflated than the left. There is diffuse bronchiectasis. The findings are those of BO

smooth muscle. There is often variable hyperexpansion of pulmonary lobules in affected regions. Inflammation may highlight affected airways, but late in the process or following steroid treatment this may not be a prominent feature.

Noninfectious Disorders

Hypersensitive Pneumonia

Hypersensitive pneumonia, also known as extrinsic allergic alveolitis, is characterized by the development of alveolar inflammation due to hypersensitivity to inhaled organic dusts. While it has been thought to be uncommon in childhood, it is more likely that it is rarely suspected and therefore poorly investigated. When children are affected, it is usually through an environmental exposure and only occasionally through close contact with family members who are exposed to an organic dust through their occupation or hobbies. Hypersensitivity pneumonia is traditionally classified into three forms based on the duration of illness: acute, subacute, and chronic.

The acute form of hypersensitivity pneumonia usually develops within 4–6 h after exposure to the causative dust antigen. Affected children typically present with nonspecific symptoms such as fever, chills, malaise, cough, dyspnea, and headache. These symptoms usually resolve within 12 h to several days after initial exposure. In children with the subacute form of hypersensitivity pneumonia, symptoms are

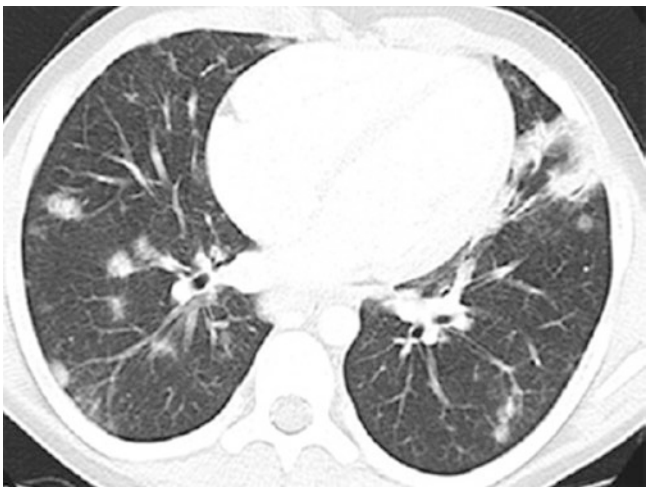

Fig. 8.11 Bronchiolitis obliterans organizing pneumonia (BOOP): axial lung window CT image shows diffuse nodules with mild intralobular septal thickening and mild patchy ground glass opacifications consistent with BOOP

similar to the acute form of hypersensitivity pneumonia, but usually less severe and more prolonged. The clinical presentation of children with the chronic form of hypersensitivity pneumonia is characterized by insidious onset of cough, progressive dyspnea, fatigue, and weight loss.

Imaging Findings On plain chest radiographs, the common imaging findings of the acute form of hypersensitivity pneumonia are diffuse micronodular interstitial prominence often with ground-glass opacities predominately in the middle and lower lung zones (Fig. 8.12). High-resolution CT (HRCT) can further characterize the chest radiographic findings of acute hypersensitivity pneumonia; these include small (1–3 mm), poorly defined centrilobular nodules representing bronchiolitis and ground-glass opacity representing alveolitis. Both chest radiographic and CT imaging findings of the subacute form of hypersensitivity pneumonia are similar to those of the acute form. In chronic hypersensitivity pneumo-

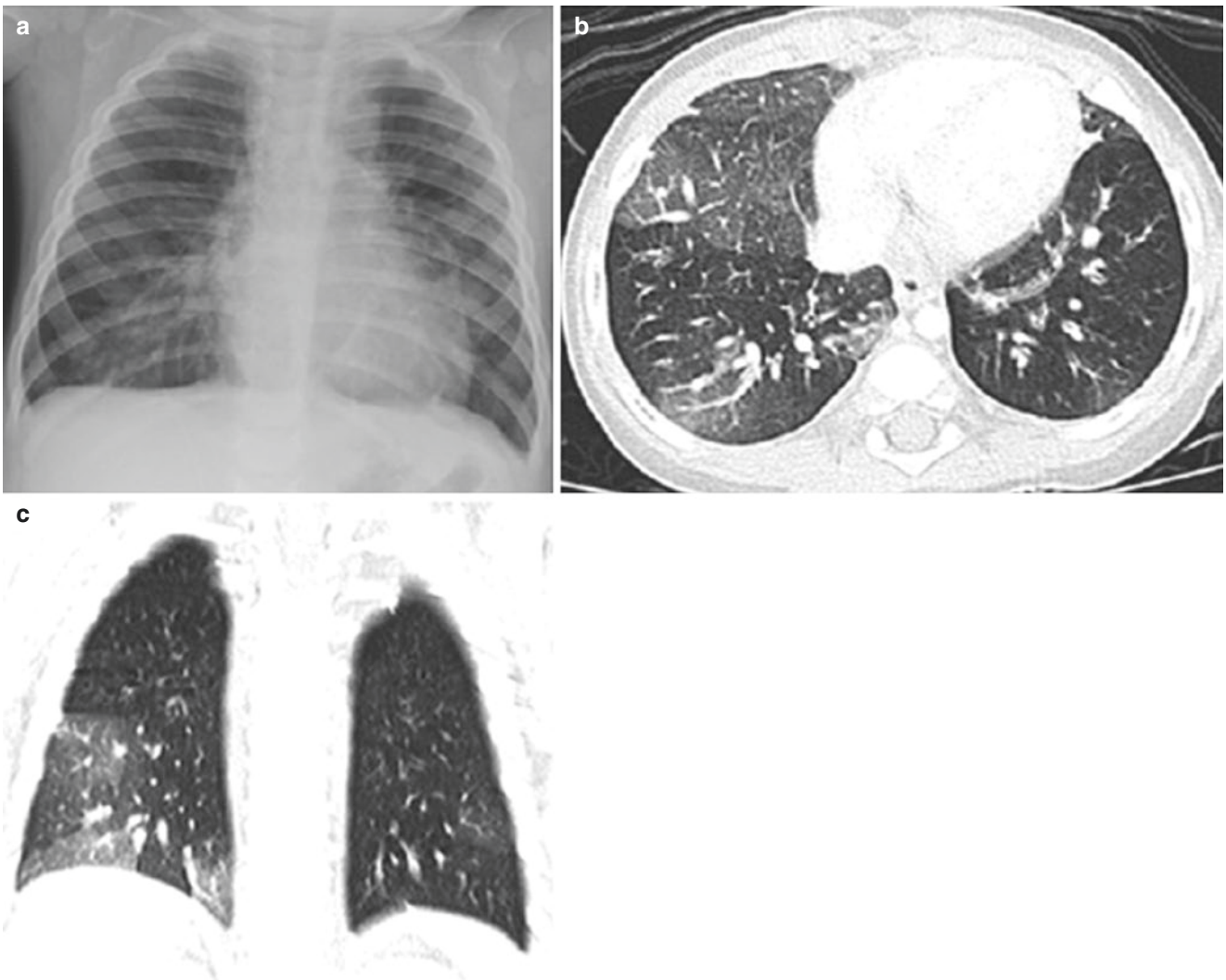

Fig. 8.12 (**a**) Acute hypersensitivity: frontal CXR reveals a coarse interstitial process accentuated in the bases. (**b**) Acute hypersensitivity: axial lung window CT image shows that there are scattered ground glass nodular-like opacities in both lung bases. (**c**) Acute hypersensitivity: coronal lung window CT image shows that the process is accentuated in the bases

nia, imaging findings on plain chest radiographs and CT include progressive fibrotic changes with volume loss without substantial nodular or ground-glass opacity predominately affecting the mid-lung zone (Fig. 8.13). The location of fibrotic lung changes can be helpful in differentiating this entity from IPF, which is predominately located in the lung bases.

Pathologic Findings Lung biopsy is rarely performed during acute disease, and there is limited information regarding pathologic findings at this stage. Histologic changes are similar in the subacute and chronic forms of hypersensitivity pneumonia with fibrosis supervening in chronic forms. The changes are characteristic and include lymphoplasmacytic inflammation centered around small airways and extending into alveolar walls with occasional multinucleate giant cells and small poorly formed granulomas in the walls of distal bronchioles and in alveoli and small airway lumens (Fig. 8.13).

For the diagnosis of hypersensitivity pneumonia, lung biopsy alone may be suggestive but is rarely diagnostic. A careful investigation of clinical history and imaging findings can provide important clues to the correct diagnosis, and serologic investigations for specific antigens, guided by the clinical history, may be diagnostic in cases of hypersensitivity pneumonia in children.

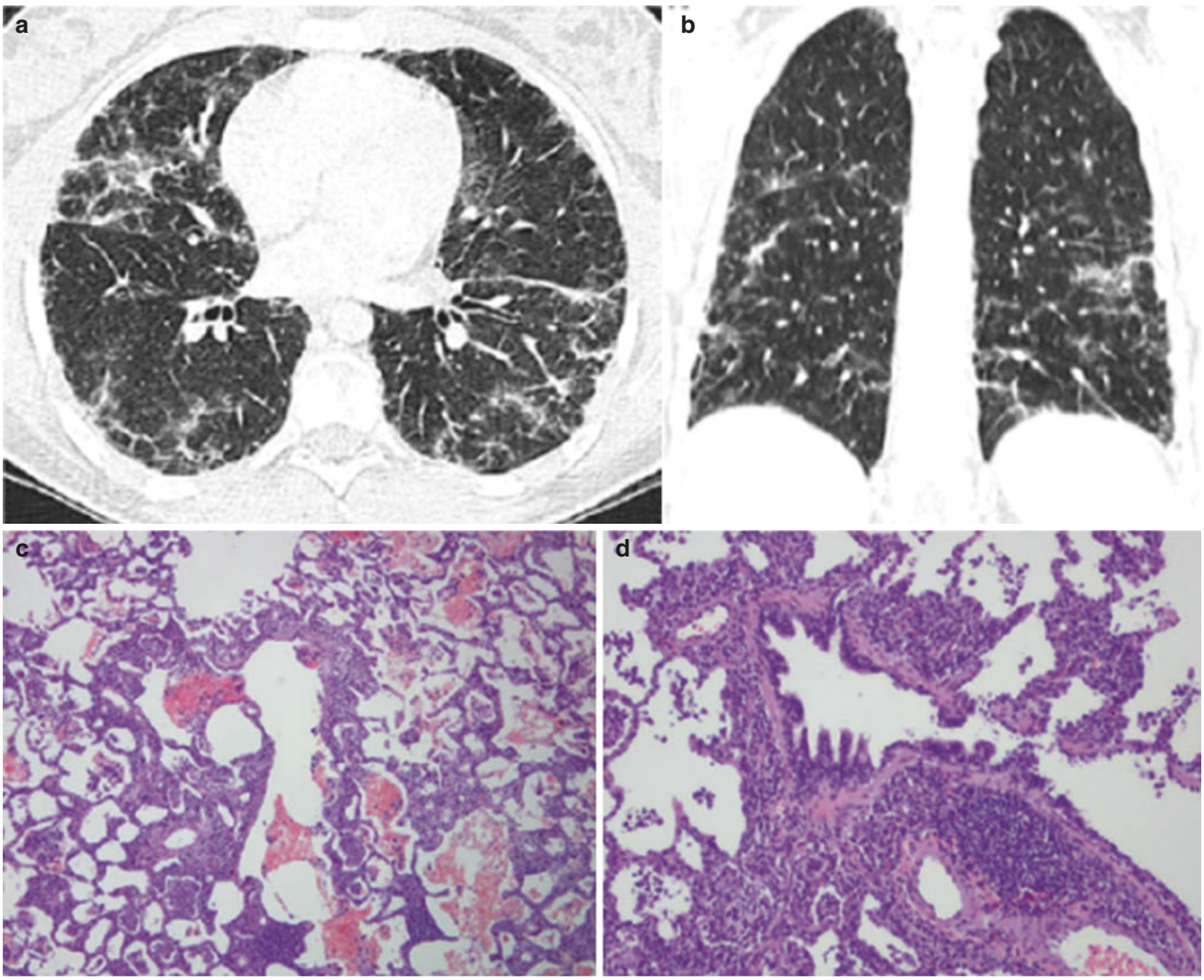

Fig. 8.13 (**a**) Chronic hypersensitivity: axial lung window CT image shows coarse diffuse fibrosis. (**b**) Chronic hypersensitivity: coronal lung window CT image reveals that the fibrosis is somewhat accentuated in the mid-lungs. Hypersensitivity pneumonia: hypersensitivity pneumonia or extrinsic allergic alveolitis is seen histologically in its subacute or chronic phase. It shows a picture of chronic interstitial pneumonia with bronchiolocentric lymphoplasmacytic infiltration (**c**) and lymphocytic bronchiolitis (**d**) with poorly formed granulomas (**e**) and giant cells (**f**) in airspaces and interstitial tissues, typically most prominent adjacent to small airways or at the lobular margins

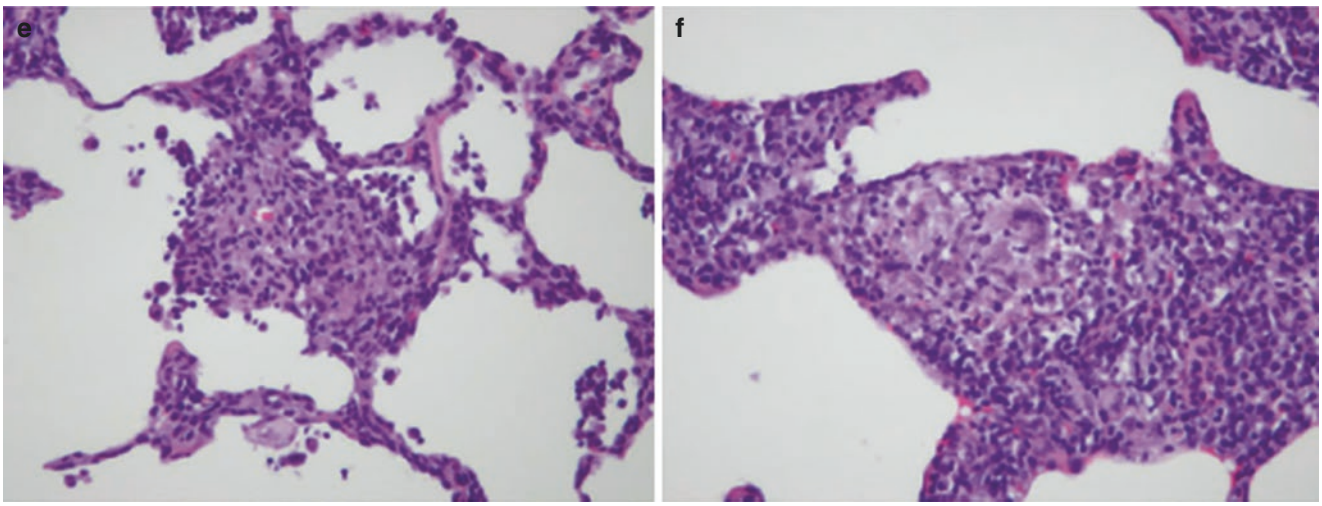

Fig. 8.13 (continued)

Aspiration Syndromes

Aspiration syndromes in children can result in acute and chronic lung changes. There are a wide variety of causes for aspiration in children, including (1) swallowing disorders (due to neurogenic abnormalities, neuromuscular disorders, immaturity, cleft palate, laryngeal cleft), (2) H-type fistula or bronchobiliary fistula, (3) esophageal stricture or obstruction (e.g., vascular ring, foreign body, achalasia), and (4) gastroesophageal reflux.

Imaging Findings

Imaging findings of aspiration syndromes largely depend on the timing and amount of aspiration. The typical plain radiographic and CT findings of aspiration syndromes are diffuse alveolar consolidations in the dependent portions of lungs, such as posterior lower lobes. In children with persistent aspiration syndrome, advanced lung disease such as abscess can also develop. For the evaluation of the causes of aspiration due to underlying swallowing disorders or anatomic malformation, barium swallow study is a useful imaging study. Chronic aspiration, without acute aspiration, may produce a diffuse but irregularly distributed interstitial prominence (Fig. 8.14).

Pathologic Findings

Except in its more extreme manifestations, such as prolonged chronic aspiration with H-type fistula, aspiration can be a difficult pathologic diagnosis; however, there should always be some degree of airway injury and repair, typically with reactive epithelial changes (hyperplasia or metaplasia), an element of inflammation (acute, chronic, and/or with foreign body giant cells and granuloma formation), and in severe cases often prominent lobular changes with inflammation and fibrosis.

Eosinophilic Pneumonia

Eosinophilic pneumonia is a component of eosinophilic lung diseases, a diverse group of pulmonary disorders characterized by peripheral or tissue eosinophilia. Eosinophilic lung diseases are traditionally classified into three groups: eosinophilic lung diseases of unknown cause, eosinophilic lung disease of known cause, and eosinophilic vasculitis.

Eosinophilic lung diseases of unknown cause include simple pulmonary eosinophilia, acute eosinophilic pneumonia, chronic eosinophilic pneumonia, and idiopathic hypereosinophilic syndrome. Eosinophilic lung diseases of known cause include allergic bronchopulmonary aspergillosis, bronchocentric granulomatosis, parasitic infections, and drug reactions. Eosinophilic vasculitis includes allergic angiitis and granulomatosis (i.e., Churg–Strauss syndrome). Churg–Strauss is now typically a clinical diagnosis made in the presence of a constellation of signs and symptoms in the setting of known asthma; it is not a pathologic diagnosis, although the histologic demonstration of extravascular eosinophils is one diagnostic sign. It may present with multiple pulmonary nodules but does not always do so (Fig. 8.15a, b). In this section, only acute eosinophilic pneumonia and chronic eosinophilic pneumonia are reviewed.

Acute eosinophilic pneumonia was first recognized in 1989, but its exact cause remains unknown. It is characterized by (1) an acute febrile illness of less than 5 days duration; (2) hypoxemia; (3) diffuse alveolar or mixed alveolar-interstitial opacities on chest radiographs; (4) BAL

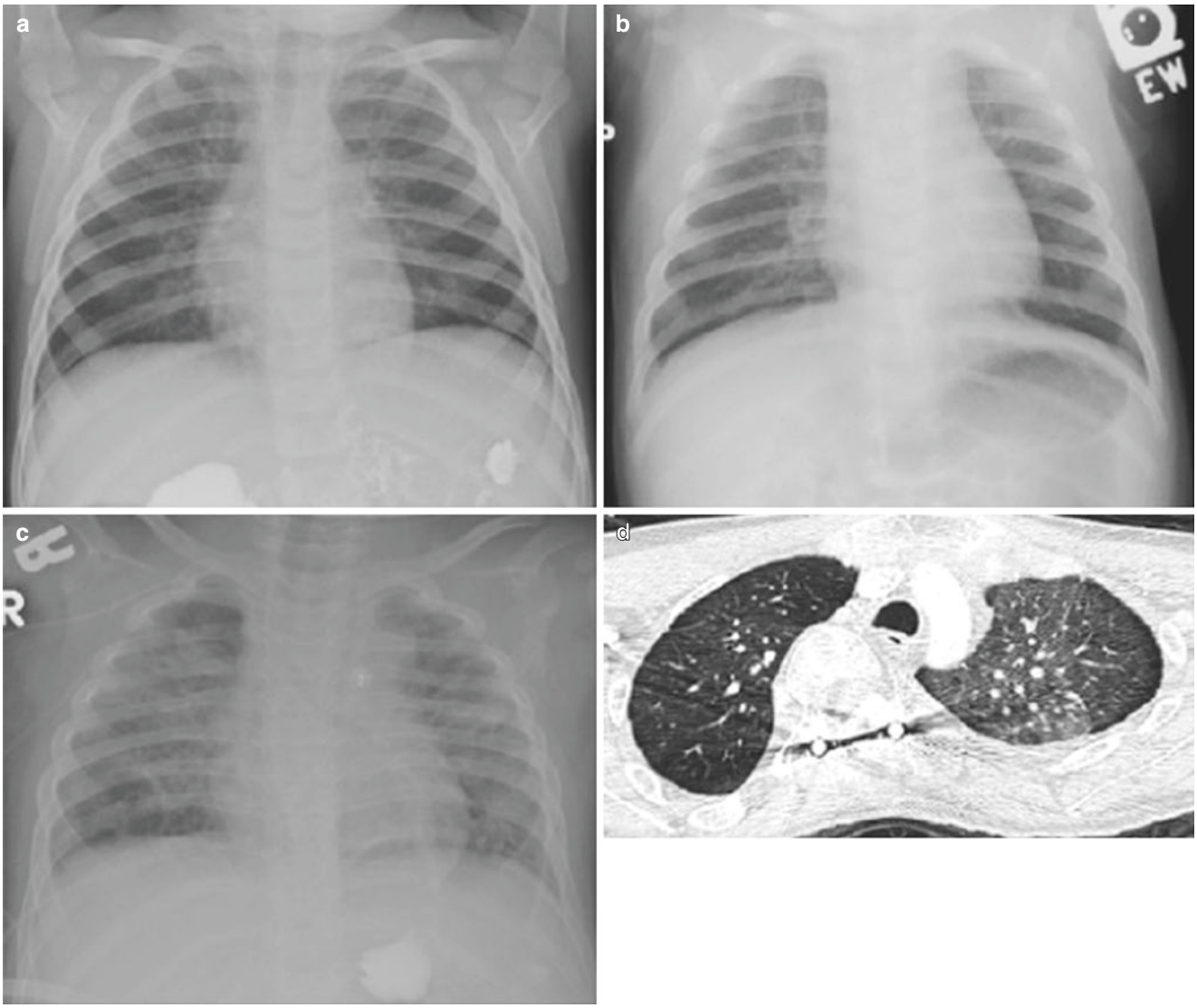

Fig. 8.14 (**a**) Chronic aspiration mild: 1-year-old with hypotonia and chronic cough and wheeze. There is diffuse peribronchial thickening (PBT), somewhat exaggerated in the right upper and lower lobes and the left perihilar region. The initial chronic manifestations of recurrent aspiration may mimic that seen in early CF or asthma. However, with aspiration, the PBT may be irregularly distributed, particularly in the right upper and lower lobes and left perihilar region as these are the locations most commonly affected when aspiration occurs in the supine position. (**b**) Chronic aspiration moderate: 4-month-old with chronic congestion and cough. There is moderately severe PBT accentuated in the same distribution as in (**a**). (**c**) Chronic aspiration severe: 2-year-old with seizures and aspiration. There is severe diffuse interstitial lung disease (ILD) with areas of atelectasis and/or fibrosis. (**d**) Axial lung window CT image in an 18-year-old with chronic aspiration shows a mosaic distribution of ground-glass ILD

fluid consisting of more than 25% eosinophils; (5) the absence of parasitic, fungal, or other infection; (6) a prompt and complete response to corticosteroids; and (7) the absence of relapse after discontinuation of corticosteroids. It is more often seen in adolescents than in young children.

Imaging Findings

Typical chest radiographic findings of children with acute eosinophilic pneumonia include bilateral reticular opacities with or without patchy consolidation and pleural effusion (Fig. 8.15e). On CT, there is bilateral patchy GGO frequently associated with interlobular septal thickening, consolidation, or poorly defined nodules (Fig. 8.15f). Due to its rarity and the similarity of its imaging findings to those of other more common entities such as hydrostatic pulmonary edema, acute respiratory distress syndrome, AIP, and atypical bacterial or viral pneumonia, correct diagnosis of acute eosinophilic pneumonia may be initially missed or delayed particularly in children. This delay may

be critical as failure to rapidly institute treatment may be accompanied by severe clinical deterioration and death. Peripheral blood eosinophilia is not a frequent feature of this disorder, although it may be present.

Pathologic Findings

On histology, acute eosinophilic pneumonia shows changes of DAD associated with interstitial and intraalveolar eosinophils.

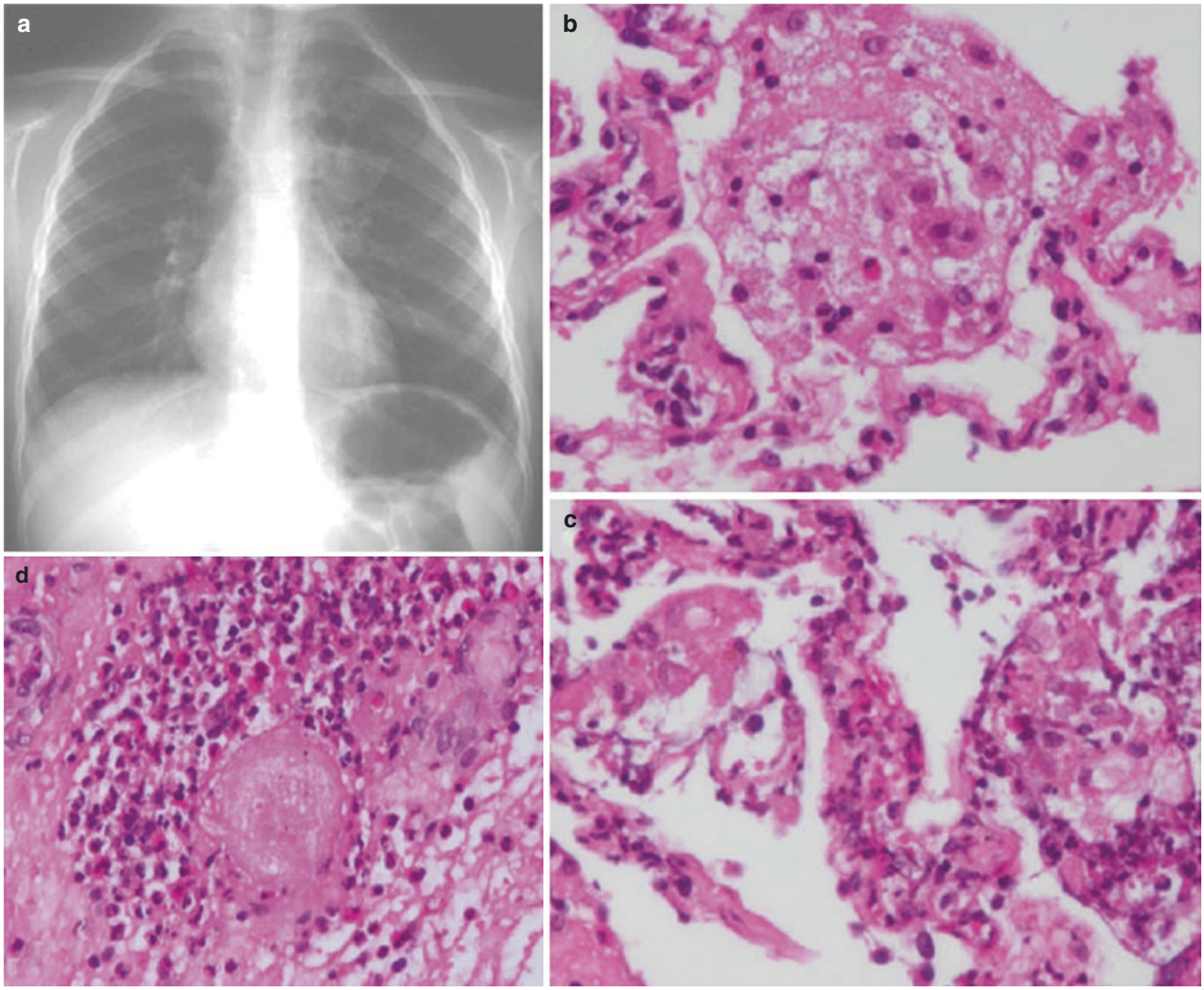

Fig. 8.15 (**a**) Churg–Strauss: this child presented with acute asthmatic symptoms. CXR reveals multiple nodules, most evident in the left perihilar region consistent with the diagnosis of Churg–Strauss syndrome. Churg–Strauss: histologic findings in Churg–Strauss syndrome depend on the stage of disease. Early, eosinophilic pneumonia is common (**b**, **c**) and eosinophils may appear extravascularly at other sites. In the vasculitic phase, there are also eosinophilic granulomas and eosinophilic vasculitis. The granulomas have a necrotic center of eosinophils with palisaded histiocytes. The vasculitis may involve any category of vessel and can include other inflammatory cells in addition to eosinophils (**d**). (**e**) Acute eosinophilic pneumonia: 4-year-old with acute onset of elevated temperature. There is severe reticular ILD accentuated centrally with the suggestion of a small left pleural effusion. (**f**) Axial lung window CT image in a different child with acute eosinophilic pneumonia shows multiple ground-glass peripheral opacifications. (**g**) CXR shows multiple peripheral nodules typical of chronic eosinophilic pneumonia. (**h**) Axial lung window CT image in a different patient with chronic eosinophilic pneumonia shows multiple peripheral airspace consolidations. In chronic eosinophilic pneumonia, there is multifocal consolidation (**i**) with interstitial and intralveolar collections (**j**) of eosinophils with associated macrophages and an often mild interstitial lymphoplasmacytic infiltrate. There may be associated small poorly formed granulomas (**k**), as well as variable interstitial fibrosis (**i**, **l**) and epithelial hyperplasia (**j**, **l**)

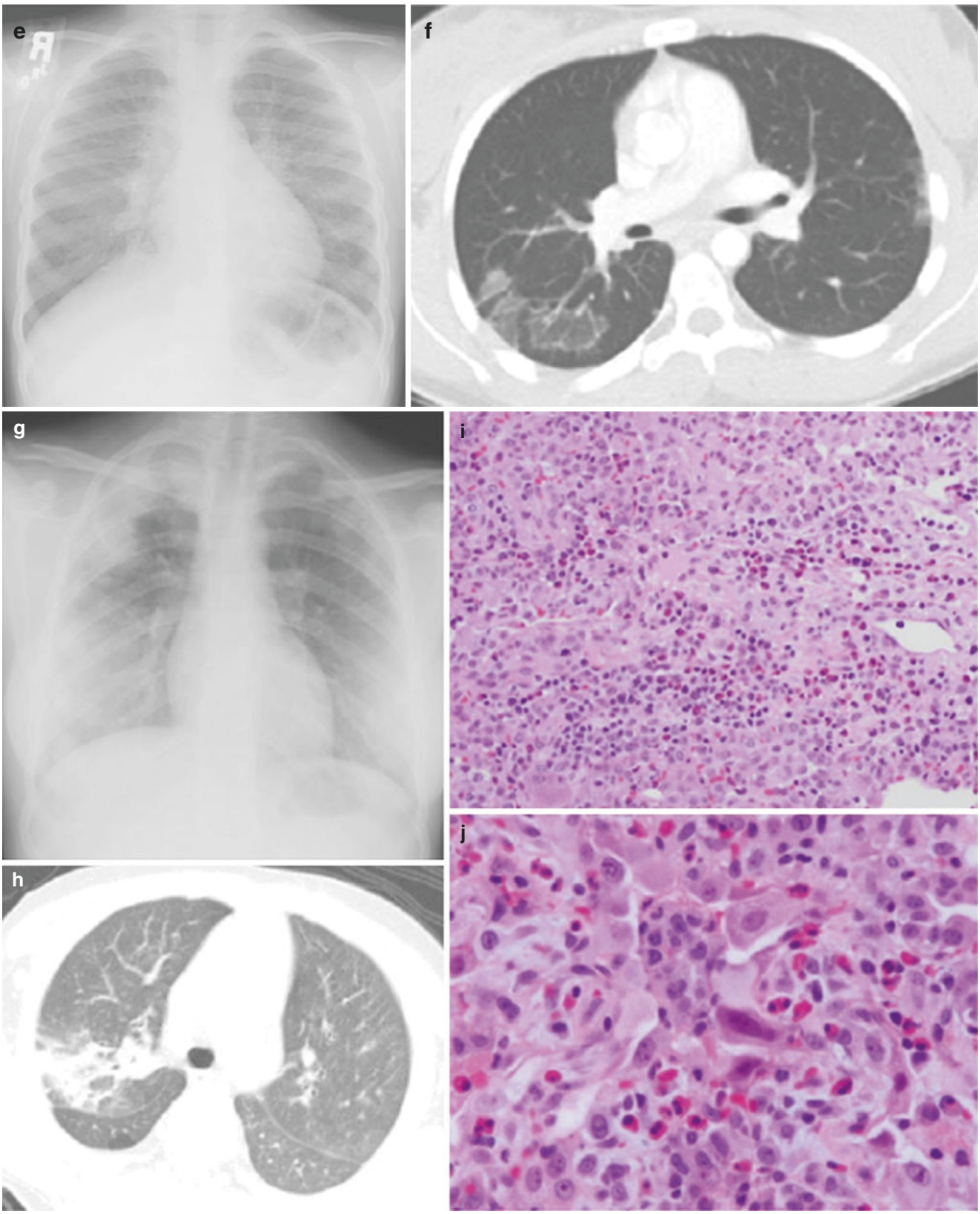

Fig. 8.15 (continued)

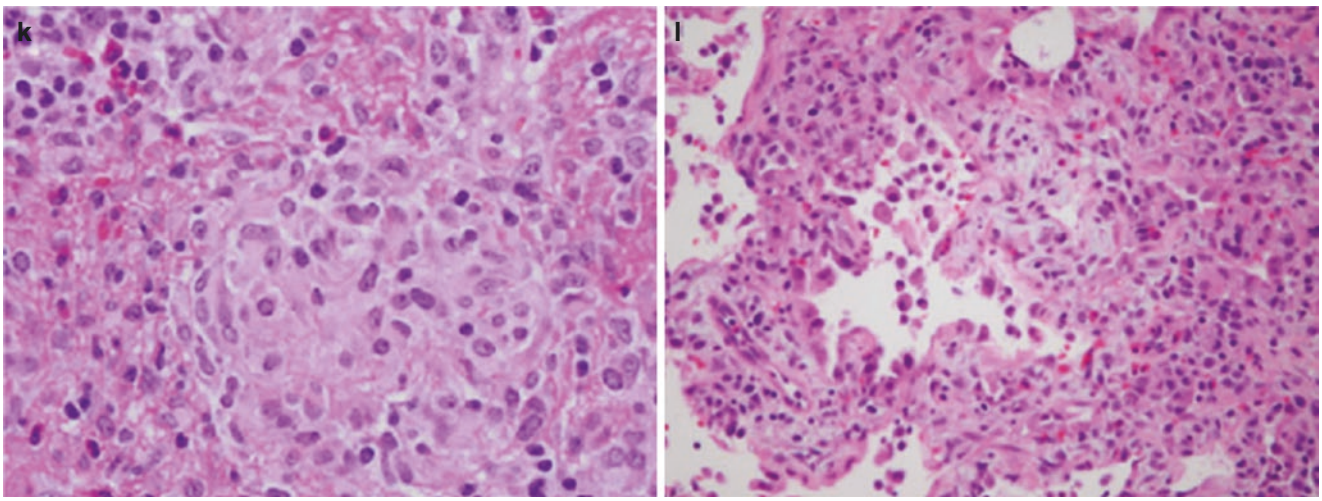

Fig. 8.15 (continued)

Chronic Eosinophilic Pneumonia

Chronic eosinophilic pneumonia is characterized by chronic and progressive respiratory and systemic symptoms. Although it is more common in middle-aged patients with asthma, chronic eosinophilic pneumonia can be seen in pediatric patients. In patients with chronic eosinophilic pneumonia, elevated peripheral blood eosinophilia, increased serum IgE levels, elevated erythrocyte sedimentation rate, and high percentage of eosinophils in the BAL fluid are typically present. Unlike patients with acute eosinophilic pneumonia, symptoms may relapse after discontinuation of corticosteroid treatment.

Imaging Findings

Plain chest radiographic findings in patients with chronic eosinophilic pneumonia are often characteristic and include nonsegmental peripheral airspace consolidation predominately affecting upper lobes (Fig. 8.15g). Peripheral infiltrates with a "reversed pulmonary edema pattern" is also considered highly suggestive of chronic eosinophilic pneumonia. On CT, typical nonsegmental areas of airspace consolidation with peripheral predominance are usually seen (Fig. 8.15h). Less common additional CT findings in patients with chronic eosinophilic pneumonia include ground-glass opacities, nodules, and reticulation.

Pathologic Findings

Histologic changes include dense accumulations of eosinophils, often with associated macrophages, which may contain eosinophil granules, in alveoli and in the interstitium, where the eosinophils are accompanied by lymphocytes and plasma cells (Fig. 8.15g). Eosinophils may be seen in the walls of blood vessels, but a true vasculitis with reactive vascular change or necrosis is never seen. Eosinophil abscesses with central necrosis and palisaded histiocytes with intermixed eosinophils may also be seen. There is usually organizing pneumonia and sometimes poorly formed granulomas; with continued chronicity, interstitial fibrosis may occur. Prebiopsy treatment with corticosteroids may strikingly diminish the numbers of eosinophils hampering accurate diagnosis.

Acute Interstitial Pneumonia/Hamman-Rich Syndrome/Idiopathic Diffuse Alveolar Damage

Acute interstitial pneumonia (AIP), also known as Hamman–Rich syndrome, was first described in 1935 by Louis Hamman and Arnold Rich. It is a rare lung disease of unknown etiology that typically affects adults older than 40 years old, but it can be seen in childhood and even occasionally in infancy resulting in severe lung disease in otherwise healthy children with intact immune function. Affected patients usually present with nonspecific symptoms such as cough, fever, and difficulty breathing. Unfortunately, these nonspecific symptoms can rapidly progress to severe respiratory failure requiring ventilatory support within days or weeks after symptom onset. Approximately half of the affected children recover, and half of those who recover do so without significant pulmonary sequelae. This improvement in survival is largely due to improved ICU care as there is not yet any clear understanding of the pathogenesis of this condition, and treatment remains supportive.

Imaging Findings

Due to its rarity, imaging findings of AIP are not well described; however, those reported are those of acute respiratory distress syndrome with diffuse bilateral alveolar opacities, septal thickening, and often pleural effusion.

Pathologic Findings

Biopsy of the lung in patients with AIP shows DAD usually in an exudative and early organizing stage.

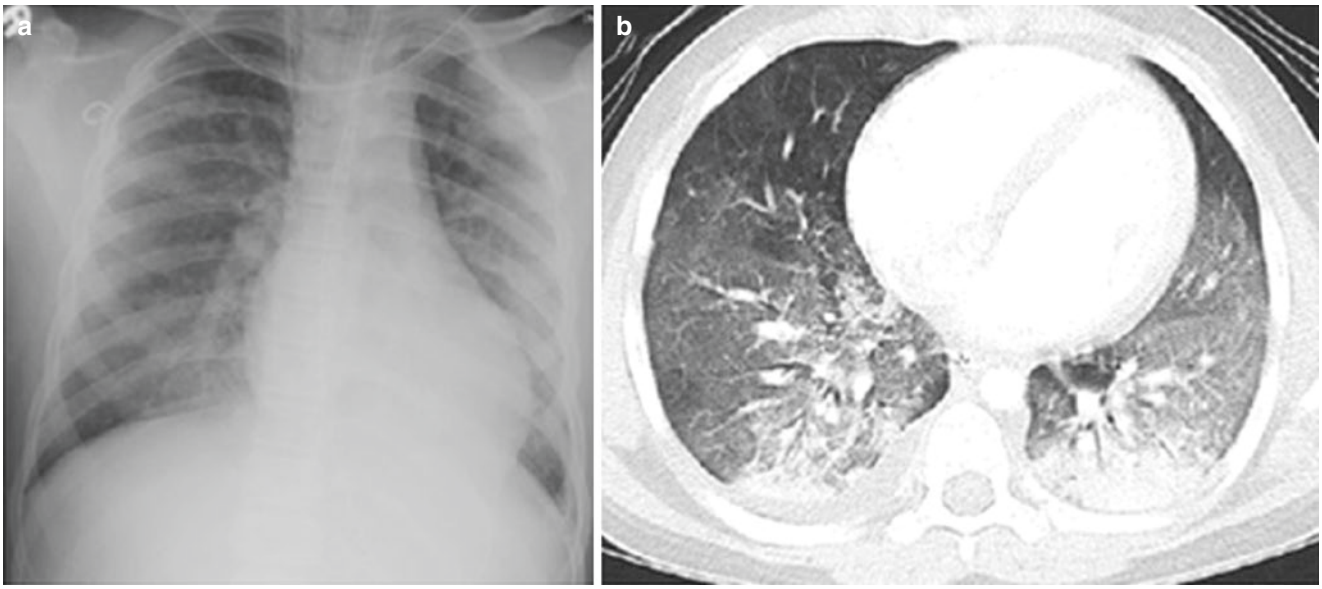

Fig. 8.16 (**a**) Idiopathic pulmonary hemosiderosis: 10-year-old with hemoptysis. There is diffuse moderate ILD increased in the right lower lobe and airspace opacification of the left lower lobe. There is a small left effusion. (**b**) Idiopathic pulmonary hemosiderosis: axial lung window CT image reveals diffuse patchy ground glass ILD with nodular/confluent airspace disease and a right effusion

Idiopathic Pulmonary Hemosiderosis

Idiopathic pulmonary hemosiderosis, first described by Virchow in 1864 as *brown lung induration*, is a rare lung disease that affects both children and adults. It is characterized by recurrent episodes of pulmonary hemorrhage with hemoptysis, iron deficiency anemia, and diffuse lung infiltrates on chest radiographs (Fig. 8.16). Due to recurrent concealed blood loss, the anemia of idiopathic pulmonary hemosiderosis is hypochromic, microcytic, and characteristic of iron deficiency. The clinical course of children with idiopathic pulmonary hemosiderosis is characterized by remissions and exacerbations of symptoms despite therapy. The causes of death in such patients include progressive pulmonary insufficiency resulting in chronic respiratory failure and acute pulmonary hemorrhage. With advances in early diagnosis and therapeutic management, 86% of patients now survive beyond 5 years after the diagnosis of idiopathic pulmonary hemosiderosis.

Imaging Findings

Imaging findings in idiopathic pulmonary hemosiderosis depend on the stage of disease progression. At early stages where pulmonary hemorrhage predominates pathologically, ground-glass opacity often associated with consolidation in a central distribution on CT is typically seen (Fig. 8.16b).

Pathologic Findings

In early stages on lung biopsy, there are prominent intraalveolar accumulations of hemosiderin-laden macrophages, usually without prominent associated hemorrhage. At later stages following recurrent clinical episodes, there are prominent reactive lung changes with a continuing abundance of hemosiderin-laden macrophages. In later stages, there is progression of these changes, including a deposition of hemosiderin in the interstitial tissue with a thickening of the interlobular septa and alveolar walls, as well as the bronchiolar and arterial walls, sometimes with prominent ferrocalcific deposits and with eventual progression to irreversible pulmonary fibrosis.

Disorders Related to Systemic Disease Process

Approximately one fourth of biopsies for ILD in a multicenter study in older children were from children with preexisting systemic disease, and in this study immune-mediated disorders with nonhemorrhagic parenchymal disease were slightly more common than immune-mediated hemorrhage syndromes. Other nonimmune-mediated systemic conditions were distinctly rare.

Immune-Related Disorders

Acquired Pulmonary Alveolar Proteinosis

Pulmonary alveolar proteinosis (PAP) is a rare lung disease, first described in 1958 by Rosen and his coworkers. It is characterized by an abnormal accumulation of surfactant, lipoproteinaceous material, within the alveoli, which prevents normal gas exchange.

PAP has been traditionally classified into congenital and acquired forms. Congenital PAP is discussed in the infant lung disorder section as it relates to surfactant dysfunction disorders. In older children and adults, PAP is an acquired disorder

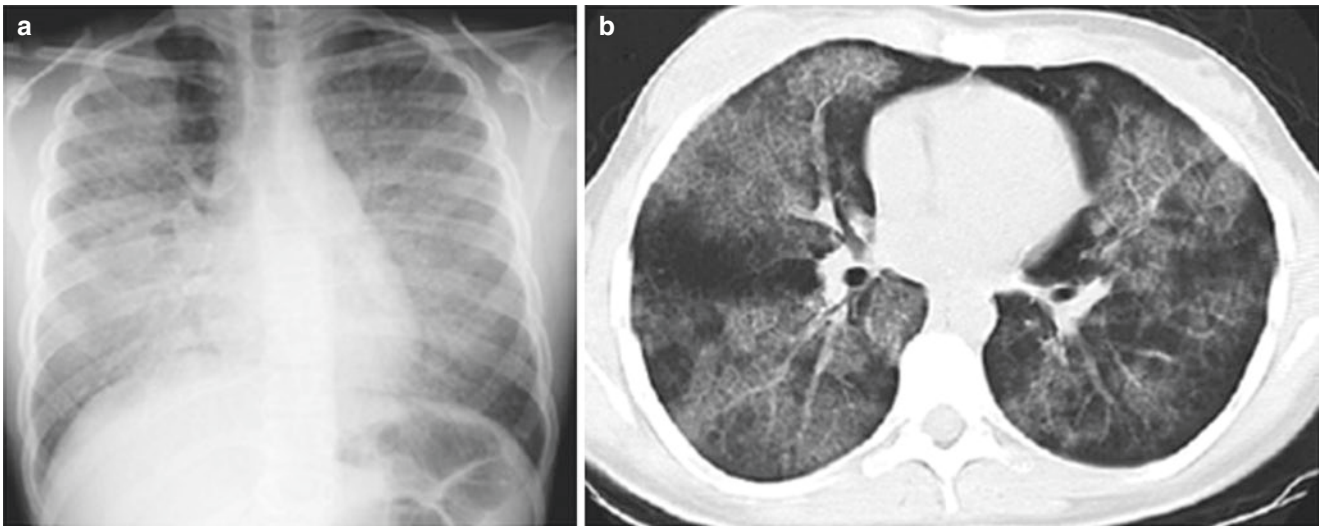

Fig. 8.17 (**a**) Pulmonary alveolar proteinosis (PAP): 13-year-old with known pulmonary alveolar proteinosis. There is diffuse severe *ground glass* opacification of both lungs typical of PAP. This CXR pattern is also frequently seen with subacute/chronic hemosiderosis. (**b**) PAP: axial lung window CT image shows diffuse ground glass opacification with septal thickening representing *crazy-paving* appearance

and is seen in two settings. The first is with macrophage dysfunction typically associated with chemotherapeutic drug use in malignancies. It is then categorized with disorders in the immunocompromised host. The form of PAP that belongs in this section on immune disorders is a manifestation of an autoimmune condition in which an autoantibody to GM-CSF is formed. It is not seen in early childhood but may affect school-age children or adolescents, as well as adults.

Affected children present with slowly progressive dyspnea and nonproductive cough. Diagnosis is by the demonstration of proteinosis material either on BAL or lung biopsy coupled with identification of the autoantibody. Current treatment for this acquired PAP is repeated lung lavage, which has been successful in older children and adults.

Imaging Findings Imaging studies do not differentiate among the various forms of PAP and show bilateral symmetric perihilar opacities that often extend into the peripheral portions of the lungs on plain chest radiographs. These opacifications are frequently not as consolidative and dense as those of a typical bacterial pneumonia (Fig. 8.17). On CT, particularly on HRCT, bilateral ground-glass opacities with smooth intra- and interlobular septal thickening in polygonal shapes, also known as a *crazy-paving* pattern, are commonly seen (Fig. 8.17b). After treatment with lung lavage, improvement of these CT findings has been reported in patients with autoimmune PAP.

Pathologic Findings Biopsy findings vary depending on the underlying etiology of the alveolar proteinosis, but all share the common feature of variably abundant PAS-positive granular-to-globular material with small cholesterol clefts filling alveolar spaces. The associated changes in infants with surfactant deficiency disorders are noted above. With PAP due to autoantibodies to GM-CSF, the background lung structure is relatively normal appearing, although there are often scattered interstitial plasma cells, and alveolar macrophages sometimes have atypical appearances.

Pulmonary Hemorrhage Syndromes

Immune-mediated pulmonary hemorrhage, usually with capillaritis [51], can be seen in a variety of disorders, including microscopic polyangiitis, collage-vascular disease (systemic lupus erythematosus, rheumatoid arthritis, systemic sclerosis, polymyositis, and mixed connective-tissue disease), Wegener's granulomatosis, and Goodpasture's syndrome. Not all pulmonary hemorrhage is immune mediated; other conditions leading to pulmonary hemorrhage include drug-induced coagulopathy and hemorrhage-associated malignancy. The clinical and imaging findings are often similar in all such disorders. Affected pediatric patients typically present with hemoptysis and dyspnea, as well as anemia.

Imaging Findings Bilateral symmetric geographic areas of ground-glass opacities with interlobular septal thickening are typical imaging findings of symptomatic patients with pulmonary hemorrhage syndrome. Focal, sometimes multifocal and nodular-like opacities, may also be present, representing sites of acute hemorrhage. Chest radiographic findings, particularly in the subacute phase, may be quite similar to that seen in PAP.

Pathologic Findings The definite diagnosis of pulmonary hemorrhage syndrome is based on the identification of blood within BAL fluid or the demonstration of abundant hemosiderin-laden alveolar macrophages. Serologic demonstration of antineutrophil cytoplasmic antibodies (ANCA) may avert lung biopsy to evaluate for the presence of capillaritis (Fig. 8.18), but when these are negative or not

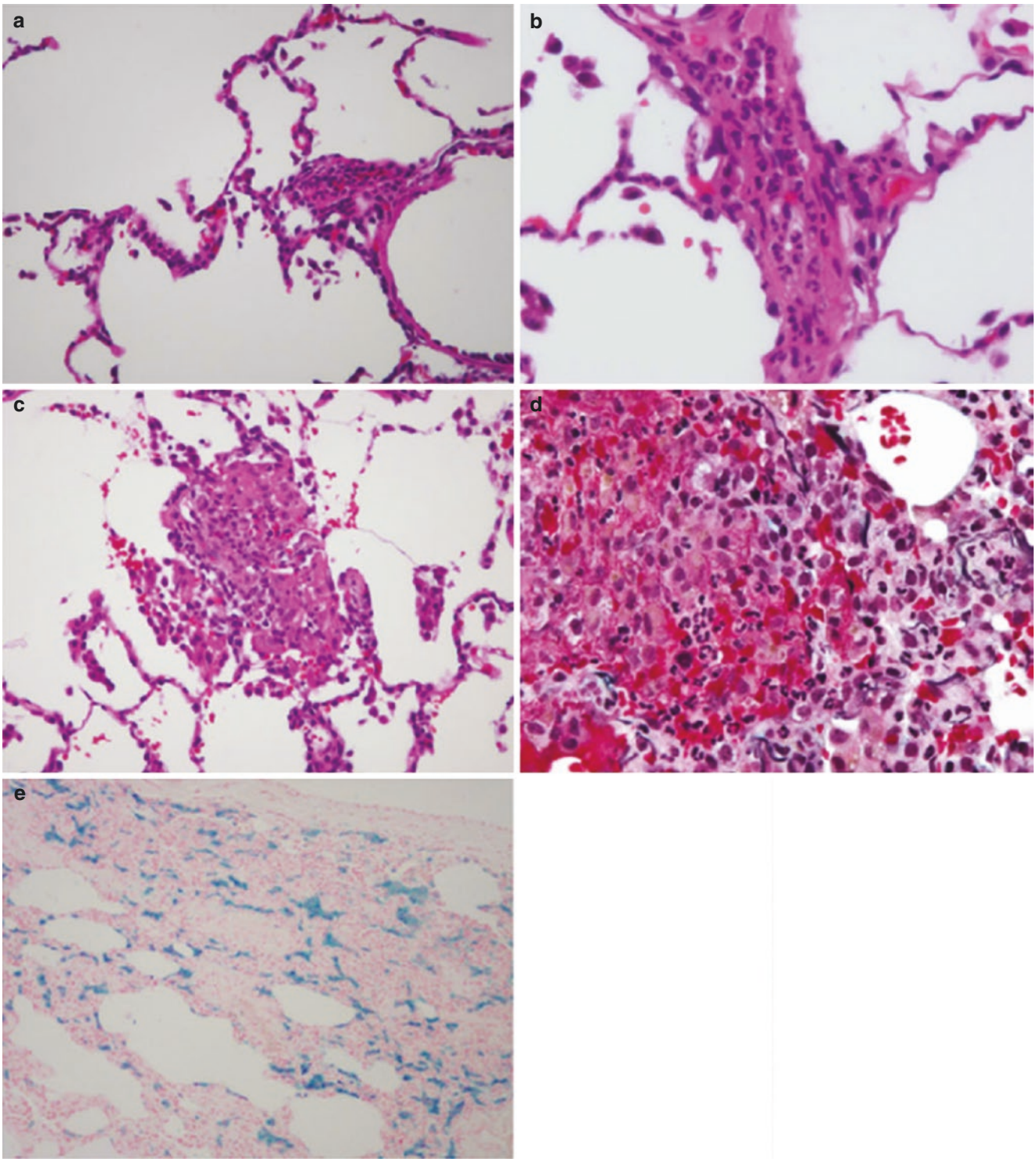

Fig. 8.18 Capillaritis: pulmonary capillaritis may be seen as a component of immune-mediated hemorrhage in a variety of situations. It may be seen in rheumatologic and autoimmune disorders, usually as a component of multicompartment involvement (see Fig. 8.19e, f), or it may be an isolated feature in microscopic polyangiitis or the only manifestation of Wegener's granulomatosis. In these situations, there may be foci of neutrophilic microvasculitis involving arterioles (**a**), small arteries (**b**), and capillaries often with regions of alveolar wall disruption (**c**) with focal fibrinous and cellular exudate in the region of alveolar wall disruption. Acute hemorrhage, neutrophils, and fibrin may be seen focally (Movat stain), (**d**) and there may be regionally prominent hemosiderin-laden macrophages (Iron stain) (**e**)

obtainable in an appropriate time frame, lung biopsy is often done. Active immune-mediated hemorrhage is associated with pulmonary capillaritis, often necrotizing.

Nonhemorrhagic Parenchymal Disease

Rheumatologic Disorders (Collagen-Vascular Disease) These conditions include systemic lupus erythematosus, rheumatoid arthritis, dermatomyositis, scleroderma, Sjogren's syndrome, and mixed connective tissue disease. The clinical presentation, physical findings, and laboratory findings of these collagen-vascular diseases vary; however, imaging findings of early disease are often those of NSIP.

Imaging Findings For collagen-vascular disease in general, early imaging findings include ground-glass opacity intermixed with septal thickening, while lower lobe-predominant ground-glass opacity, irregular septal thickening, honeycombing, and traction bronchiectasis are the usual imaging findings of later advanced disease or progressive collagen-vascular disease (Fig. 8.19). Characteristic CT findings of NSIP, a common histologic manifestation of many of these conditions, include ground-glass opacity with reticular abnormality, traction bronchiectasis, and lower lobe volume loss predominately located in the peripheral portions of the lower lobes in the absence of nodules, cysts, and areas of low attenuation (Fig. 8.19b). The presence of areas of low attenuation interspersed with areas of interstitial abnormality should raise the possibility of hypersensitivity pneumonitis rather than NSIP.

Pathologic Findings Although there are a variety of pathologic manifestation of these disorders in the lung, one of the commoner is of NSIP. Despite its name, this manifestation has a very specific histologic appearance with a mixture of lymphoplasmacytic inflammation and fibrosis and is typically divided into cellular and fibrotic subtypes (Fig. 8.19). It is seen in a variety of settings in childhood. It is one of the histologic patterns of the surfactant dysfunction disorders, particularly in patients with late-onset disease or prolonged survival. It is also a common manifestation of lung involvement by rheumatologic disorders (collagen-vascular disease) in children and adults and has been seen in the setting of systemic sclerosis, polymyositis and dermatomyositis, Sjogren syndrome, lupus, and rheumatoid arthritis.

Granulomatosis with Polyangiitis (Wegener's Granulomatosis)

Granulomatosis with polyangiitis (previously known as Wegener's granulomatosis) is a rare systemic disorder primarily affecting the upper and lower respiratory tract and the kidney. It is thought to be immunologically mediated via a T-cell reaction, and the frequent ANCA positivity suggests an autoimmune-mediated process. It is thought that immunologically mediated endothelial injury leads to the activation of inflammatory mediators and cellular inflammation with both vasculitis and parenchymal inflammation of various forms. Although this rare disorder is more common in adults, it is the most common necrotizing systemic vasculitis in the pediatric population. Affected children usually present with nonspecific symptoms such as fever, malaise, weight loss, arthralgias, and chronic rhinitis. Those with lung involvement may be asymptomatic or may present with hemoptysis, dyspnea, or chest pain. On laboratory studies, positive rheumatoid factor, elevated erythrocyte sedimentation rate, and c-ANCA (approximately 85% of patients with active disease) are usually present.

Imaging Findings The pulmonary changes in granulomatosis with polyangiitis are variable and range from discrete focal opacities to nodular masses (2–4 cm in diameter) with or without cavitation to ill-defined areas of consolidation on plain chest radiographs (Fig. 8.20). On CT, multiple pulmonary nodules typically ranging in size from 2 mm to several centimeters in diameter are often seen in both lungs. Associated cavitation within these nodules has been reported in 50% of nodules larger than 2 cm in diameter. Consolidation often due to pulmonary hemorrhage and/or ischemic necrosis is well evaluated with CT (Fig. 8.20).

Pathologic Findings Pulmonary involvement with granulomatosis with polyangiitis includes microabscesses, suppurative granulomas, and large geographic areas of necrosis in a background of interstitial inflammation that is typically regional (Fig. 8.20).

Nonimmune-Mediated Systemic Disorders

Sarcoidosis

Sarcoidosis is a systemic disease process of unknown etiology with multisystem involvement. Pulmonary sarcoidosis is traditionally classified into four different stages of disease progression: (1) isolated lymphadenopathy, (2) lymphadenopathy with pulmonary disease, (3) isolated pulmonary disease, and (4) pulmonary fibrosis. Affected patients present with a wide variety of symptoms related to specific end-organ damage. When sarcoid involves lungs, affected patients usually present with dyspnea, cough, and fever with a minority developing hemoptysis in advanced disease. Sarcoid does occur in childhood, although it is commoner in adults. The clinical presentation, imaging findings, and histologic features in the pediatric patient are not different from those seen in adults.

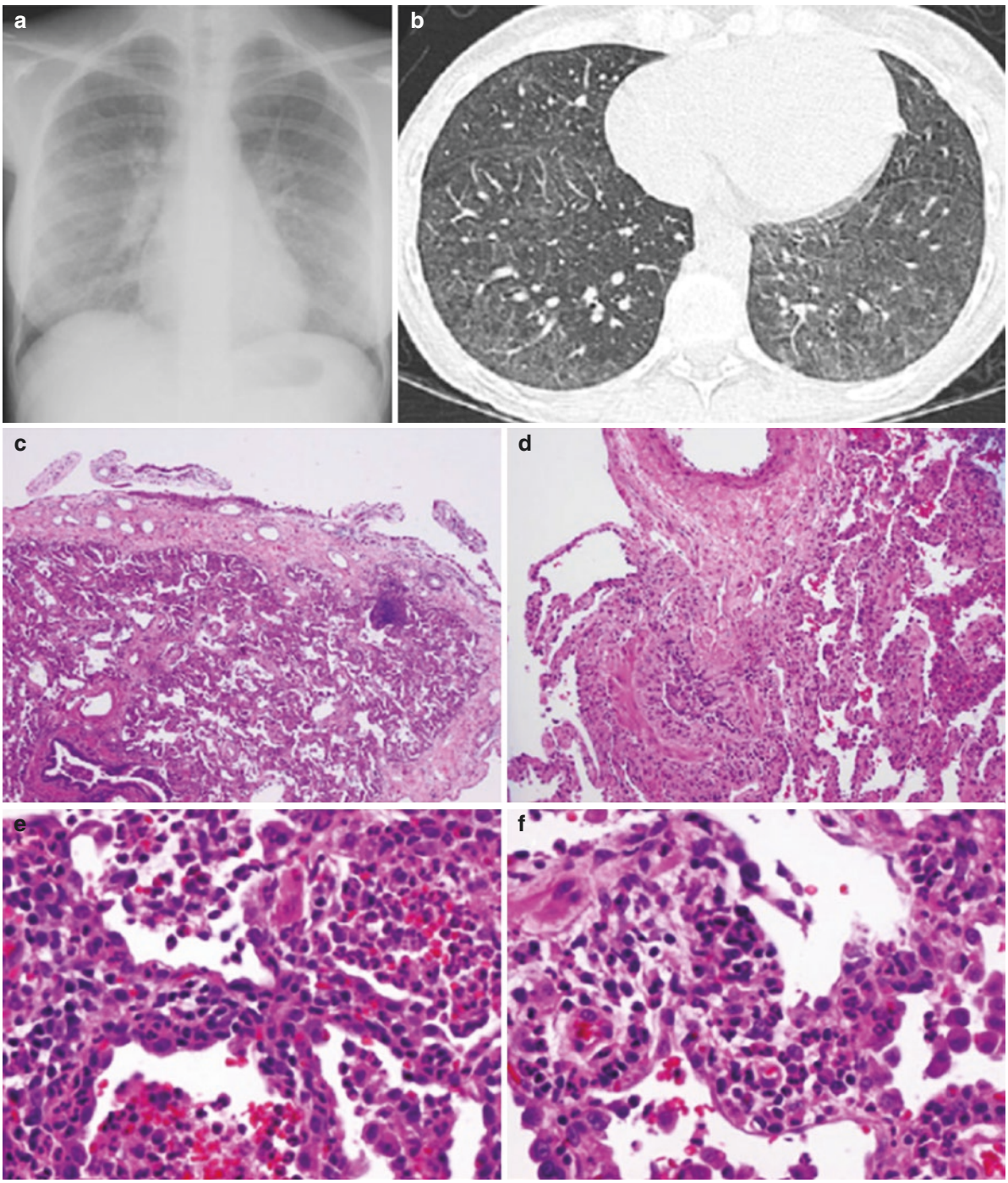

Fig. 8.19 (**a**) Nonspecific interstitial pneumonia (NSIP): 17-year-old with restrictive PFTs. There is moderate ILD worse in the lung bases. (**b**) NSIP: CT shows ground-glass ILD worse in the periphery of the lower lobes with associated mild bronchiectasis. The connective tissue diseases, now called rheumatologic disorders and auto immune disorders, have myriad manifestations in the lung with histologic changes in the interstitium, airways, vasculature, and pleura. It is this multicompartment involvement that characterizes such disorders histologically, sometimes with more specific lesions that implicate a specific disorder. Pleuritis (**c**) is a common feature of these disorders and may be active with cellular infiltrates or be present as pleural fibrosis with less prominent infiltrates. Airway changes may include lymphocytic or follicular bronchiolitis, constrictive bronchiolitis with subepithelial fibrosis narrowing the bronchiolar lumen (**d**) and bronchiectasis. Chronic interstitial pneumonia (**e**, **f**) with alveolar epithelial hyperplasia and interstitial lymphoplasmacytic infiltrates and exudates is common and may be patchy but is often widespread; acute alveolitis and capillaritis can be seen in this setting as well. Features of organizing pneumonia are also common in this setting (**g**) with streaming fibroblasts in alveolar ducts. In addition to capillaritis, other vascular changes, including thrombosis (**h**) and evidence of recent (**i**) and remote hemorrhage (**j**) (iron stain) with hemosiderin deposition, may also be seen. The pattern of interstitial pneumonia may vary, but in childhood it is most often nonspecific interstitial pneumonia with a variable mixture of cellular and fibrotic components or organizing pneumonia with intralveolar and bronchiolar organization of exudate by proliferated fibroblasts (**k**)

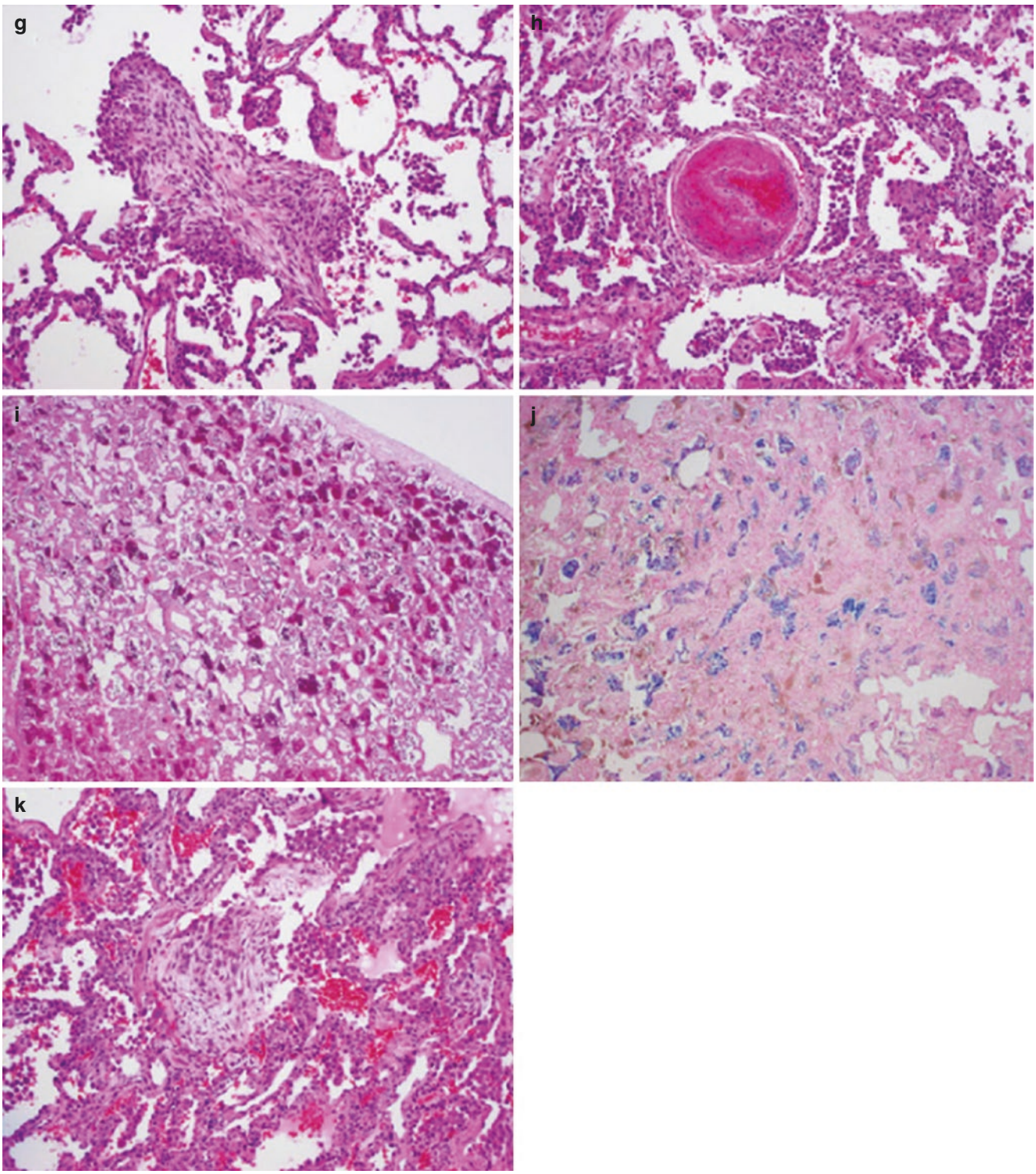

Fig. 8.19 (continued)

Imaging Findings Imaging findings of sarcoidosis depend on the stage of disease progression. Small peribronchial nodules (<3 mm in diameter) and interstitial thickening intermixed with the areas of ground-glass opacities and consolidation are typical imaging findings in patients with stage 1 to stage 3 pulmonary sarcoidosis (Fig. 8.21). In contrast, pulmonary fibrosis, architectural distortion, septal thickening, traction bronchiectasis, and honeycombing are predominant imaging findings on CT of patients with advanced stage 4 sarcoidosis. It has been reported that high-resolution CT (HRCT) is superior to

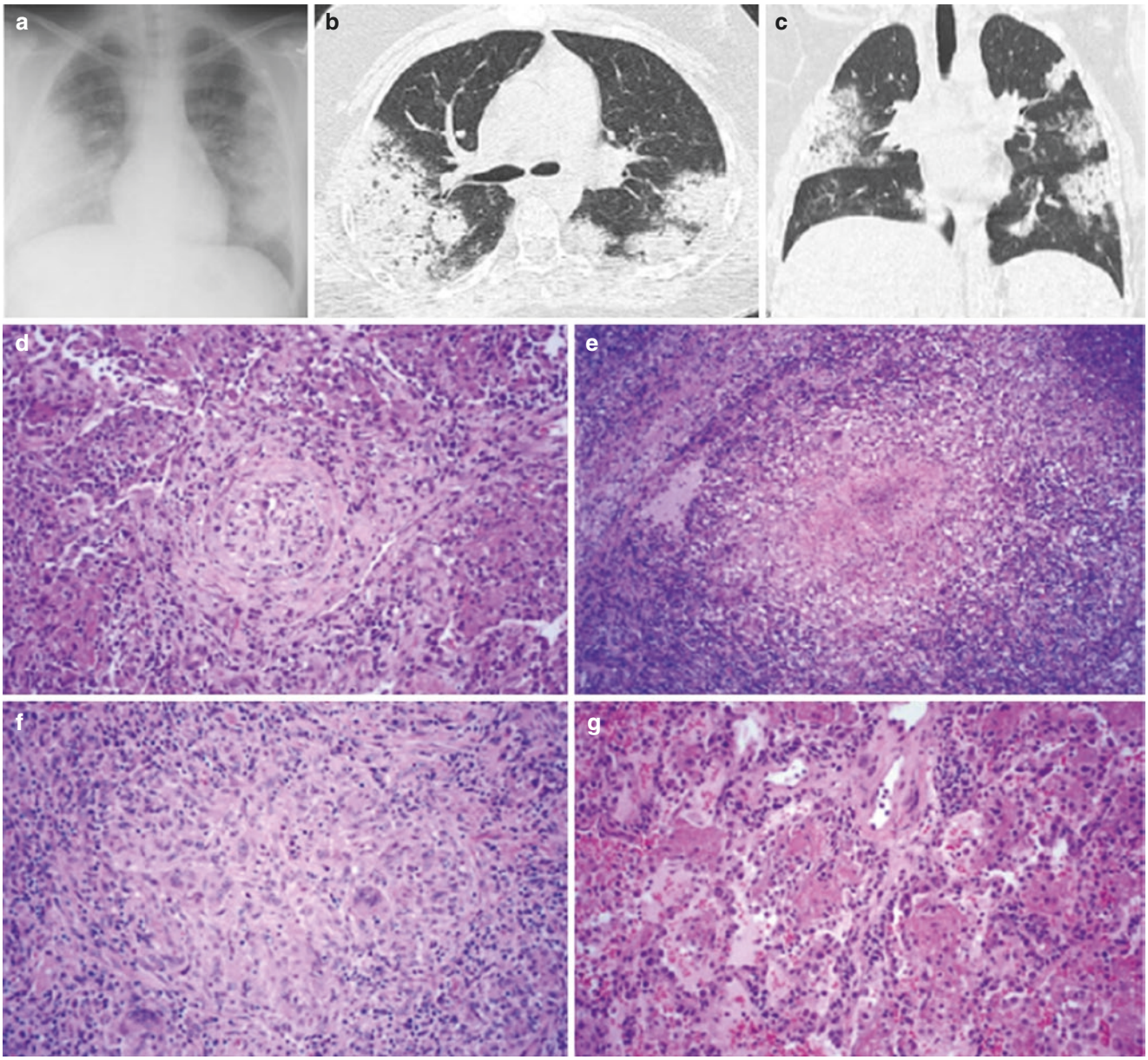

Fig. 8.20 (**a**) Granulomatosis with polyangiitis: CXR shows confluent peripheral opacities in both lungs. (**b**) Granulomatosis with polyangiitis: axial lung window CT image shows multiple ill-defined nodules, some of which are confluent. (**c**) Granulomatosis with polyangiitis: coronal lung window CT image again shows multiple ill-defined nodules, some of which are confluent. Granulomatosis with polyangiitis: the histologic picture in granulomatosis with polyangiitis includes vasculitis and necrosis with granulomatous inflammation and a widespread inflammatory background. The vasculitis, which is most often chronic, involves medium-sized and small pulmonary vessels (**d**), here seen involving a small pulmonary artery with lymphocytic infiltration of the perivascular tissue, media, and expanded intima. Large areas of both large geographic and more focal areas of necrosis as here (**e**) in a dense inflammatory background may be present, with scattered multinucleate giant cells and granulomas (**f**) within this inflammatory background. Regions of interstitial infiltrate with fibrinous exudate (**g**) and often hemorrhage are also present

conventional CT for detecting parenchymal detail and differentiating alveolitis from fibrosis in patients with sarcoidosis.

Pathologic Findings Sarcoid is characterized histologically by the presence of multiple small and well-circumscribed granulomas without necrosis. These granulomas are often located along lymphatic pathways and thus are seen in interlobular septa and around blood vessels. There is sometimes granulomatous vasculitis. Fibrosis occurs in advanced disease and may replace large regions of the lung parenchyma (Fig. 8.21).

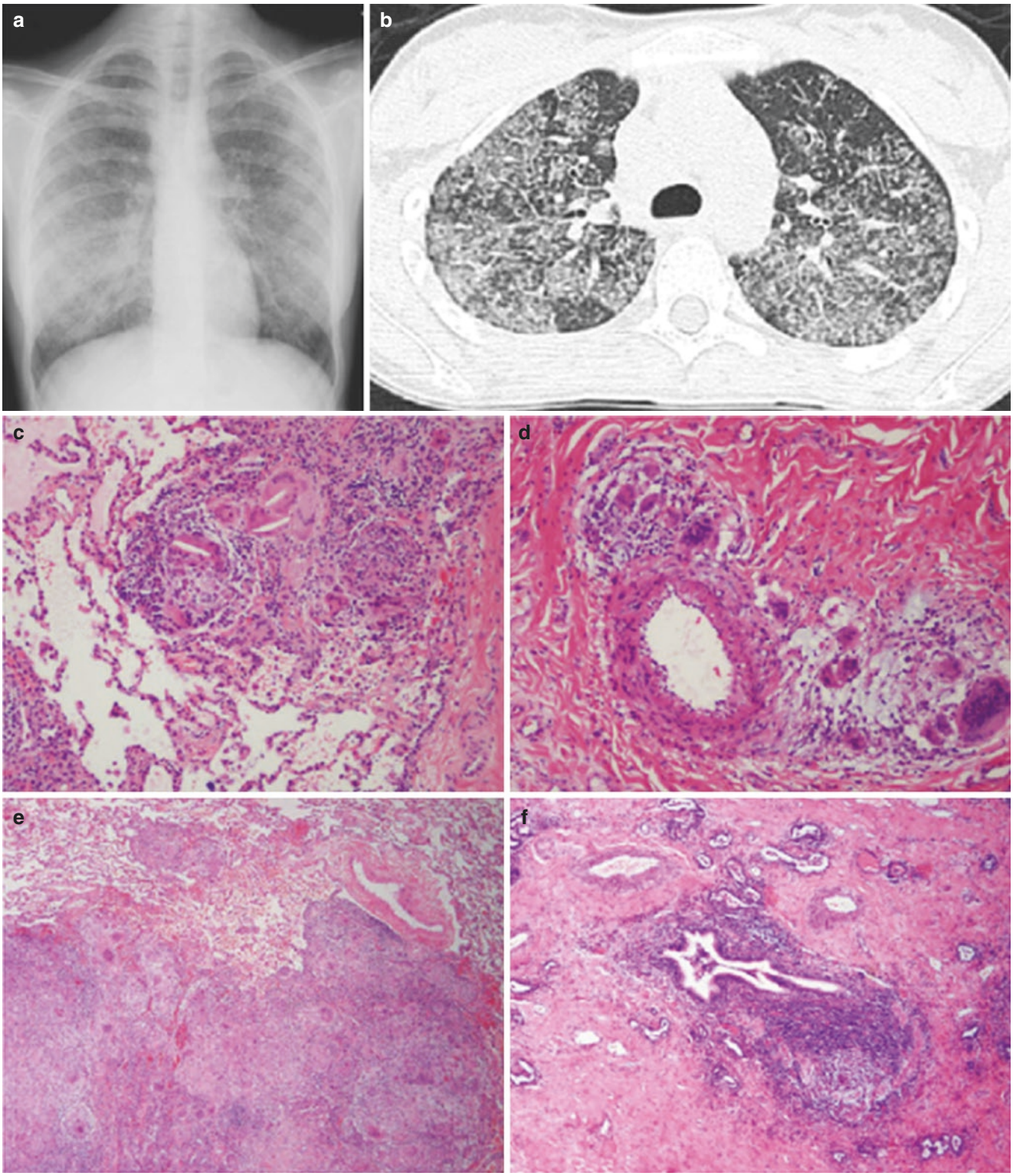

Fig. 8.21 (**a**) Sarcoid: 17-year-old with hypercalcemia, weight loss, fatigue, and chest pain. CXR shows diffuse coarse micronodular ILD with bilateral paratracheal adenopathy. (**b**) Axial lung window CT image, in another patient with sarcoidosis, shows diffuse nodular and confluent ground glass opacities. Sarcoid: the occurrence of multiple circumscribed nonnecrotizing granulomas (**c**, **d**) is the histologic hallmark of sarcoidosis. In the lung, these granulomas often are seen in perivascular regions (**d**) and along lymphatic pathways (**e**). The granulomas may be confluent (**e**). With time, granulomas may become hyalinized, and there may be dense interstitial fibrosis as in (**f**) where the remnant of a granuloma is seen in the wall of a narrowed and chronically inflamed small airway in a background of dense lobular fibrosis

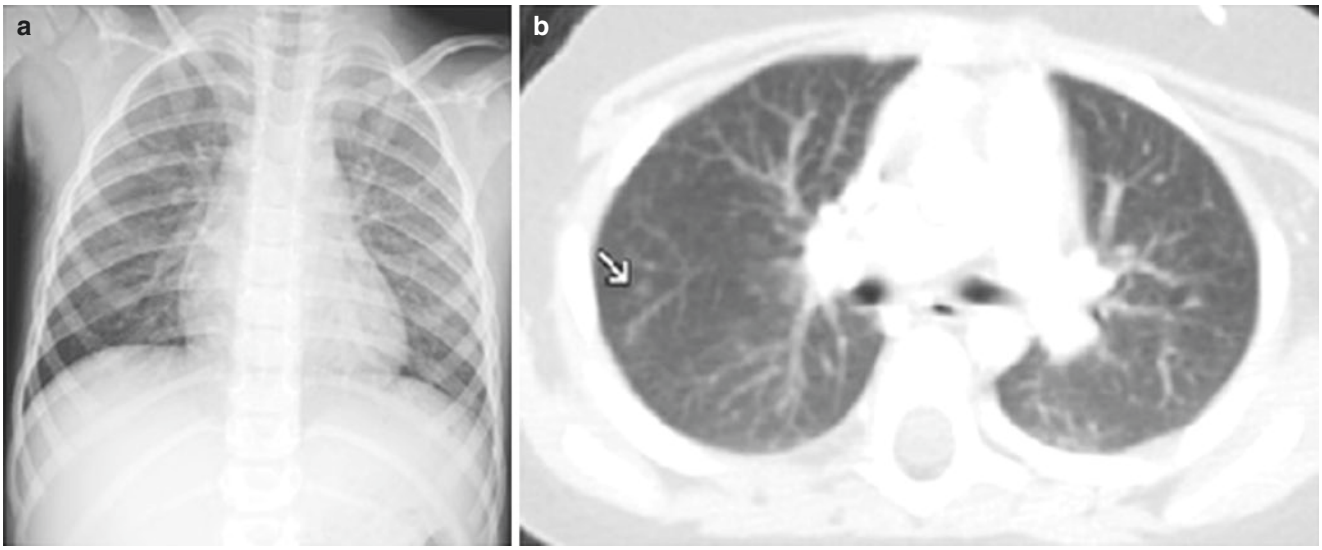

Fig. 8.22 (**a**) Acute Langerhans cell histiocytosis (LCH): CXR shows mild nonspecific ILD suggesting bronchial wall thickening, which is often the first imaging evidence of LCH. (**b**) Acute LCH: axial lung window CT image reveals multiple small nodules (*arrow*), dominantly in the upper lobes

Langerhans Cell Histiocytosis

Langerhans cell histiocytosis (LCH), previously known as eosinophilic granuloma or histiocytosis X, is a multisystem disease characterized by a clonal proliferation of Langerhans cells of bone marrow origin. It usually affects children between 1 and 15 years of age with a yearly incidence of one in 200,000. Although it is a sporadic and nonhereditary condition, familial clustering has been reported. In adults, but not in childhood, pulmonary LCH is known to be strongly associated with smoking. Affected patients typically present with nonspecific respiratory symptoms such as cough and dyspnea.

Imaging Findings On chest radiographs, indistinct nodular opacities intermixed with areas of reticular interstitial opacities predominately located in the upper lung zones are usually seen in patients with early-stage pulmonary involvement from LCH (Fig. 8.22). Pulmonary fibrosis with areas of architectural distortion and honeycombing can be observed on chest radiographs of patients with advanced and long-standing disease. HRCT is the preferred imaging modality for evaluating pulmonary disease caused by Langerhans cell histiocytosis because it can detect characteristic imaging features of small nodules (<5 mm in diameter) in a centrilobular or peribronchiolar distribution intermixed with thin-walled cysts in both lungs with sparing of the lung bases and costophrenic angles (Fig. 8.23).

Pathologic Findings Pulmonary LCH, previously known as pulmonary eosinophilic granuloma, is characterized by infiltration of the lung parenchyma by Langerhans cells. These CD1a and Langerin immunopositive histiocytes are generally seen in an airway-centered distribution that progresses to form symmetrical stellate nodules that also contain eosinophils, lymphocytes, and fibroblasts. In later stages, these nodules may become centrally cystic, but typically central scarring develops with later lesions showing associated honeycombing and surrounding emphysema. Ultrastructural examination shows the characteristic Birbeck granule of the Langerhans cell.

Cystic Fibrosis

Cystic fibrosis (CF), first recognized in 1930s, is the most common genetic disorder resulting in chronic pulmonary disease in children. It is an autosomal recessive disorder with mutations involving the cystic fibrosis transmembrane regulator (CFTR) gene located on the long arm of chromosome 7. Although CF is more common among children of European heritage with an estimated incidence of 1:2500 white live births, it can also affect children of Asian and African descent. Affected individuals are often discovered during infancy when they present with meconium ileus syndrome (18%), failure to thrive, malabsorption syndrome, or chronic recurrent respiratory infections. A definitive diagnosis of CF can be based on abnormal sweat test or via genetic testing, usually employing a panel of more common mutations in specific geographic groups.

Although CF may result in significant gastrointestinal and liver disease, involvement of the respiratory system is the major cause of morbidity and mortality in children, and nearly all affected children eventually develop progressive pulmonary disease. Pulmonary disease is the most common cause of death in patients with cystic fibrosis. Imaging findings of CF vary depending on several factors, including the age of the patient, the duration and severity of the disease, and associated infection.

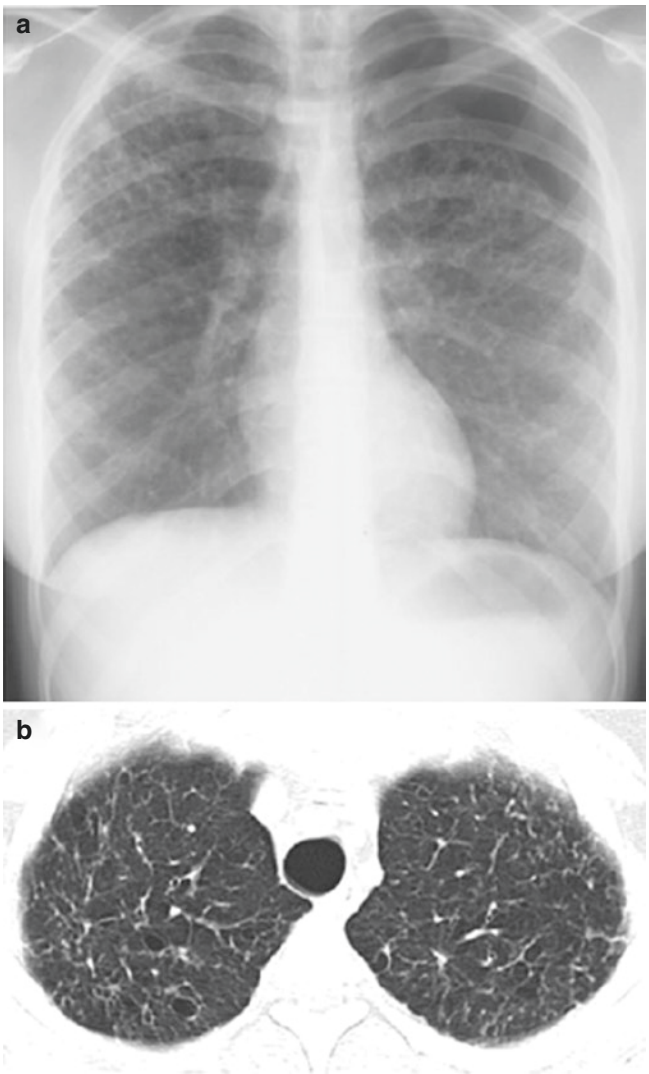

Fig. 8.23 (**a**) Chronic Langerhans cell histiocytosis (LCH): there is coarse ILD with multiple cysts, dominantly in the upper lobes. There is a left pneumothorax. (**b**) Chronic LCH: Axial lung window CT image reveals honeycombing with peripheral cysts and intralobular septal thickening

Imaging Lungs can be normal or show mild-to-moderate air trapping (hyperinflation) and/or bronchial wall thickening in children with early-stage CF. The hyperinflation in CF patients results from the obstruction of the small airways (i.e., terminal and respiratory bronchioles) by abnormally viscid mucus. Imaging findings of later or advanced disease are characterized by the presence of upper lobe predominant bronchiectasis (in 50% of patients with lobe dominate disease) [52], peribronchial wall thickening, centrilobular nodular and tree-in-bud opacities, and mucus plugging with air trapping best detected on expiratory CT images. The reason for upper lobe predominant lung changes in CF is not known, but it has been postulated that decreased ventilatory excursions in the upper lobe may exacerbate the already impaired drainage of bronchial secretions. Due to chronic and recurrent superimposed infection, concomitant hilar and mediastinal lymphadenopathy is often seen. Several CT scoring systems are available for an assessment of the extent and severity of CF disease, although they are not widely used clinically.

Pathologic Findings The lungs in cystic fibrosis show progressive changes that early on may be mistaken for ILD. Initially, there is mucus stasis with impaired clearance and supervening infection. The chronic inflammatory changes progress to the alteration of airway walls with epithelial erosion, partial replacement of the mucosa by granulation tissue, progressive airway dilatation resulting in bronchiectasis, and for small airways sometimes fibrotic and obliterative changes. With advanced disease there is progressive loss of lung parenchyma through lobular atrophy and fibrosis, as well as loss of access to the parenchyma due to airway obstruction.

Marfan-Associated Pulmonary Disorders

Marfan syndrome, first described in 1895, is an inherited disorder of connective tissue resulting from an abnormality in the fibrillin gene on chromosome 15. The estimated prevalence of Marfan syndrome is one in 5000 individuals. Although most serious complications of Marfan syndrome result from the involvement of the heart valves and aorta, it can also affect other organs, particularly the lungs, eyes, and skeleton. Affected patients are usually tall with long limbs and long thin fingers. Pulmonary involvement in Marfan syndrome is uncommon, occurring in only about 10% of affected patients. Such involvement may include congenital enlargement of the trachea and bronchi; later findings include pulmonary artery rupture and pneumothorax. A few patients with Marfan have an emphysema-like abnormality with pleural and subpleural bullae and parenchymal cysts.

Imaging The connective tissues that provide stability and elasticity for the lungs are affected by Marfan syndrome; this may uncommonly result in the development of emphysema, pleural and subpleural bullae, parenchymal cysts, and bronchiectasis. Pneumothorax is the only common respiratory disorder seen in Marfan syndrome and is the commonest imaging finding of pulmonary involvement in Marfan syndrome.

Pathologic Findings Marfan syndrome is a rare cause of spontaneous pneumothorax; the pathologic findings do not differ from those of pneumothorax in unaffected individuals.

Malignant Infiltrates

Malignant infiltrates of the lungs can be seen with a variety of underlying malignancies. In adults, this is commonly seen as lymphangitic carcinomatosis, resulting from the spread of malignant cells via the lymphatic system in the lung. In children, carcinoma is an uncommon form of malignancy, and infiltrative disease in the lung is more commonly related to hematologic malignancy with similar spread via pulmonary lymphatics. Such children usually have known and treated malignancy and present with shortness of breath, cough, or rarely hemoptysis.

Imaging It has been reported that the sensitivity of chest radiographs for detecting lymphangitic spread of malignancy is only approximately 25%. Therefore, the imaging modality of choice for evaluating lymphangitic tumor spread is CT. Smooth, irregular, or nodular interlobular septal thickening and peribronchial small nodules are the most common CT imaging findings of lymphangitic tumor dissemination. Malignant hilar or mediastinal lymphadenopathy and/or malignant pleural effusion are often concurrently present.

Pathologic Findings With lymphangitic tumor spread, there is typically regional permeation of malignant cells through the lymphatic system in interlobular septa and bronchovascular bundles. This may be coupled with early infiltration of the connective tissue of these regions and sometimes small nodular deposits of malignant cells.

Disorders of the Immunocompromised Host

In children beyond 2 years old who come to biopsy for the diagnosis of diffuse interstitial lung disease, disorders associated with immune compromise are commoner than any other single group, accounting for nearly half of biopsy diagnoses. In immunocompromised children with diffuse lung disease, opportunistic infection accounts for almost half of diagnoses with interstitial changes resulting from therapeutic intervention in the form of chemotherapeutic drugs and radiation accounting for perhaps another 20% of diagnoses.

Opportunistic Infection

The commonest pulmonary disorder in children with altered immunity on either a congenital or acquired basis is opportunistic infection, and in biopsied cases, fungal disease predominates. Opportunistic infection occurs with organisms that typically do not cause disease in the immunologically normal host. Immune compromise may occur from a variety of underlying conditions, including congenital immunodeficiency, malnutrition, the use of immunosuppressive agents in organ transplant and in chemotherapy for cancer, extensive skin damage, antibiotic treatment, and acquired immunodeficiency syndrome (AIDS). For immune-compromised children with diffuse lung disease leading to biopsy for diagnosis, the commonest underlying conditions are postbone marrow transplantation and in the setting of chemotherapy for malignancy. Common infectious agents in these children include *Pneumocystis jirovecii*, *Candida albicans*, *Aspergillus* sp., and viral agents such as *Cytomegalovirus* and *Respiratory syncytial virus*, but other organisms, including *Toxoplasma gondii*, *HHV6*, *Cryptosporidium*, and *Histoplasma capsulatum*, may also be implicated.

Imaging

Imaging findings with thoracic infection from these different pathogens widely vary from small pulmonary nodules to masses, ground-glass opacities to consolidations and increased interstitial markings/thickenings. However, there are sometimes characteristic imaging appearances of opportunistic pulmonary infections in children that can be helpful clues to early and correct diagnosis, which in turn can lead to optimal patient care.

Bilateral symmetric hazy ground-glass opacities and cystic lung changes are characteristic imaging findings in *Pneumocystis jirovecii* (Fig. 8.24) infection in children who are immunosuppressed secondary to organ transplantation, hematologic malignancy, or HIV infection (CD4 count <200/mm^3), or less commonly with an inflammatory condition requiring steroid therapy. Multiple small diffuse nodules in both lungs are common pulmonary imaging findings in children infected with *Candida albicans* (Fig. 8.25), *Toxoplasma gondii*, and *Cytomegalovirus*. Multiple lung nodules of various sizes often associated with calcification are common in children infected with *Histoplasma capsulatum* (Fig. 8.26). Parenchymal consolidation occasionally surrounded by ground-glass opacity representing alveolar hemorrhage, also known as a halo sign, is characteristic of invasive pulmonary aspergillosis infection (Fig. 8.27).

Pathologic Findings

Appropriate treatment of opportunistic infections depends on the identification of the infectious agent, so prompt and accurate diagnosis is paramount. When noninvasive means fail to identify an organism, lung biopsy may be done to provide tissues for both culture and histologic examination.

Congenital Immunodeficiency

In infants, the most common congenital immune deficiency leading to lung biopsy for the diagnosis of interstitial lung

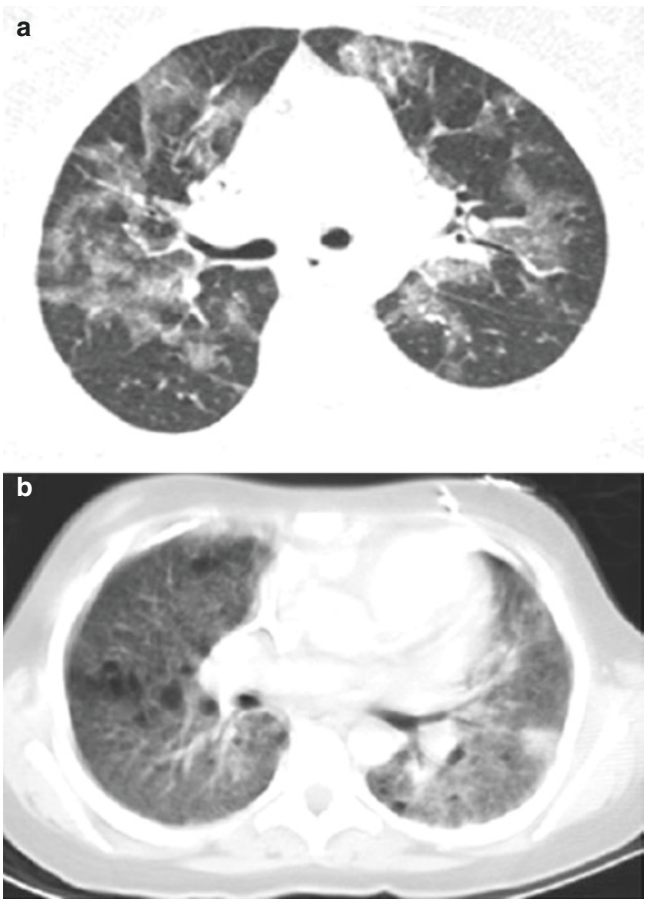

Fig. 8.24 (**a**) Pneumocystis: Axial lung window CT image of this child with *Pneumocystis jirovecli* pneumonia shows bilateral ground-glass opacifications, although no cysts were evident (which are often present). (**b**) Axial lung window CT image of another child with *Pneumocystis jirovecli* pneumonia shows diffuse coarse interstitial disease with areas of focal consolidation, intralobular septal thickening, and multiple scattered cysts

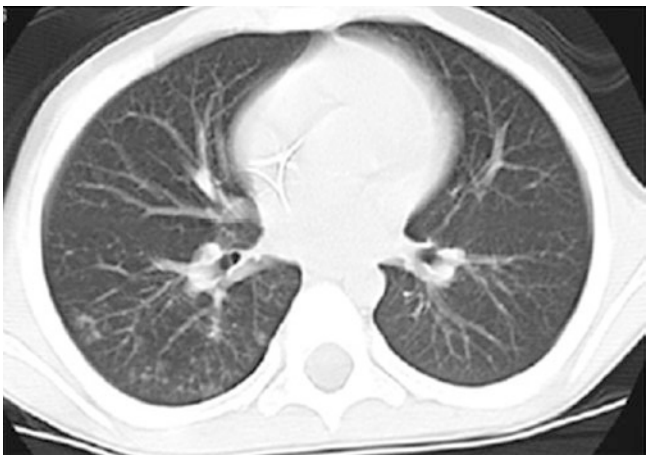

Fig. 8.25 Candida: axial lung window CT image shows multiple small nodules most accentuated in the right lower lobe. The patient had Candidal sepsis

disease is severe combined immunodeficiency syndrome (SCIDS). In older children, chronic granulomatous disease (CGD) and common variable immune deficiency (CVID), although rare, are the commonest associated inherited conditions. In all these settings, biopsy is most often done for suspected infection that has not been demonstrated by noninvasive methods. For CGD and CVID, there may also be noninfectious complications that should be considered [53].

Chronic Granulomatous Disease

Chronic granulomatous disease (CGD), first described in 1954, is a rare inherited immunodeficiency disorder due to genetic mutations in one of four genes encoding subunits of phagocyte nicotinamide adenine dinucleotide phosphate (NADPH). Most cases (75%) affect boys in an X-linked recessive inheritance pattern, and girls account for 25% of cases and show both autosomal recessive inheritance and sometimes skewed lyonization of the X-linked gene. The genetic mutations result in impaired phagocyte NADPH oxidase activity leading to reduced superoxide production and impaired oxidative burst. This impaired phagocyte oxidative function results in impaired intracellular killing of catalase-positive bacterial organisms, including *Staphylococcus*, *Burkholderia cepacia*, *Klebsiella*, and *Pseudomonas* sp., as well as fungal organisms, particularly *Aspergillus* and *Nocardia* and *Mycobacteria*. CGD affects approximately one in 200,000–250,000 live births in the United States.

Affected children typically present within the first 2 years of life with recurrent infections in various locations due to this inability in intracellular killing of catalase-positive organisms. In children with CGD, the lungs are the most common location of infection, followed by the skin and gastrointestinal tract. Liver or bones may also be affected resulting in hepatic abscess and osteomyelitis, respectively. Approximately 80% of patients with CGD present with recurrent pneumonia from *Aspergillus*, *Staphylococcus aureus*, and enteric bacteria.

The definitive diagnosis of CGD is based on the neutrophile oxidative burst test or previously on the nitroblue-tetrazolium (NBT) test; genetic testing is also available. Early diagnosis of CGD in children is important because they can then be placed on prophylactic antibiotics to prevent infection, and appropriate patient education can occur so that prompt and proper treatment can be achieved when infection does occur. With advances in the diagnosis and treatment of CGD in children, their prognosis has improved, and affected children now often survive into adulthood.

Imaging Pulmonary infections in children with CGD typically present as focal consolidation or multiple small pulmonary nodules in a military pattern in cases of hematogeneous spread. Development of abscess, pulmonary fibrosis, and honeycomb lung are eventual sequelae of long-standing

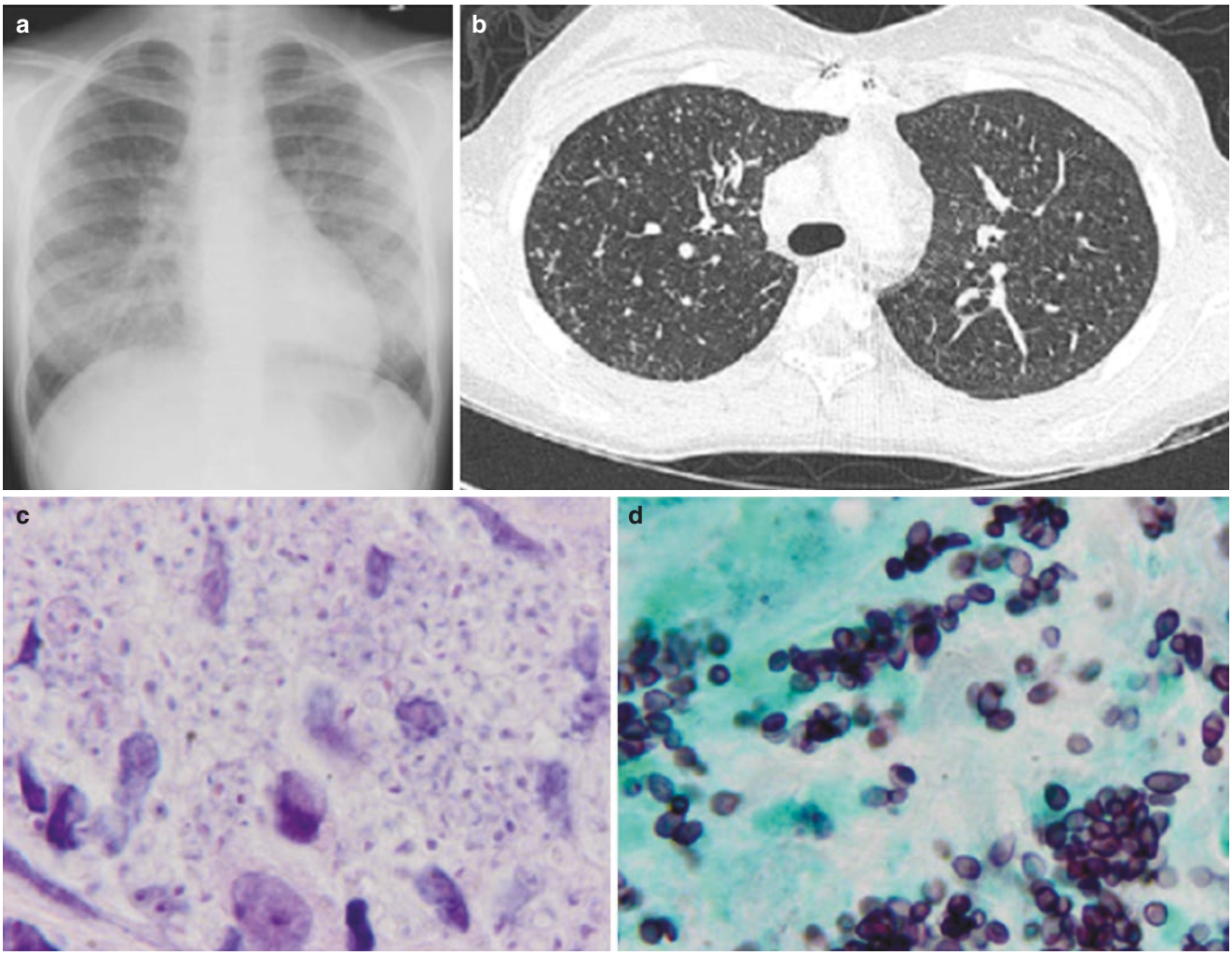

Fig. 8.26 (**a**) Histoplasma: PA CXR shows a diffuse coarse interstitial prominence in this 13-year-old girl with histoplasmosis 8 weeks following heart transplant with 2 weeks of fever. (**b**) Axial lung window CT image reveals diffuse small nodules. (**c**) Lung biopsy (H&E × 1000). Alveolar macrophages contain numerous yeast often with an artifactual halo as the cytoplasm retracts from the poorly stained cell wall giving the impression of an unstained capsule. This finding is suggestive of *H. capsulatum*. (**d**) Lung biopsy (Gomori methanamine silver ×1000). Ovoid yeast with occasional narrow-based budding (*upper right*) are most suggestive of *H. capsulatum*. This was confirmed by a urine antigen test and rising serum titres

recurrent pulmonary infections in children with CGD. In these children, additional thoracic involvement may include mediastinal or hilar lymphadenopathy, empyema, and osteomyelitis of adjacent ribs or vertebral bodies. Other common radiological manifestations of CGD in children include osteomyelitis of the small bones of the hands and feet, persistent lymphadenitis, soft-tissue calcification from healed infections (Fig. 8.28), and inflammatory obstruction of the gastrointestinal or urinary tract.

Pathologic Findings Histologically, there is granulomatous inflammation, often with necrosis, with surrounding chronic inflammation and fibrosis. It is this prominent granulomatous tissue reaction that has resulted in the name *chronic granulomatous disease*. Even though there is striking granulomatous reaction, the organism burden is typically quite low, and biopsy may be done to obtain tissues for culture even in known cases of CGD. Additionally, sometimes even with the eradication of the infectious agent, the granulomatous reaction is unchecked and may require immunomodulatory treatment for control.

Common Variable Immune Deficiency

Common variable immune deficiency (CVID) combines a group of varied disorders that result from defective or deficient immunoglobulin production. The estimated incidence of CVID is approximately one in 30,000 live births. Most cases are sporadic, but there are familial cases with varied inheritance pattern. The clinical presentation of CVID

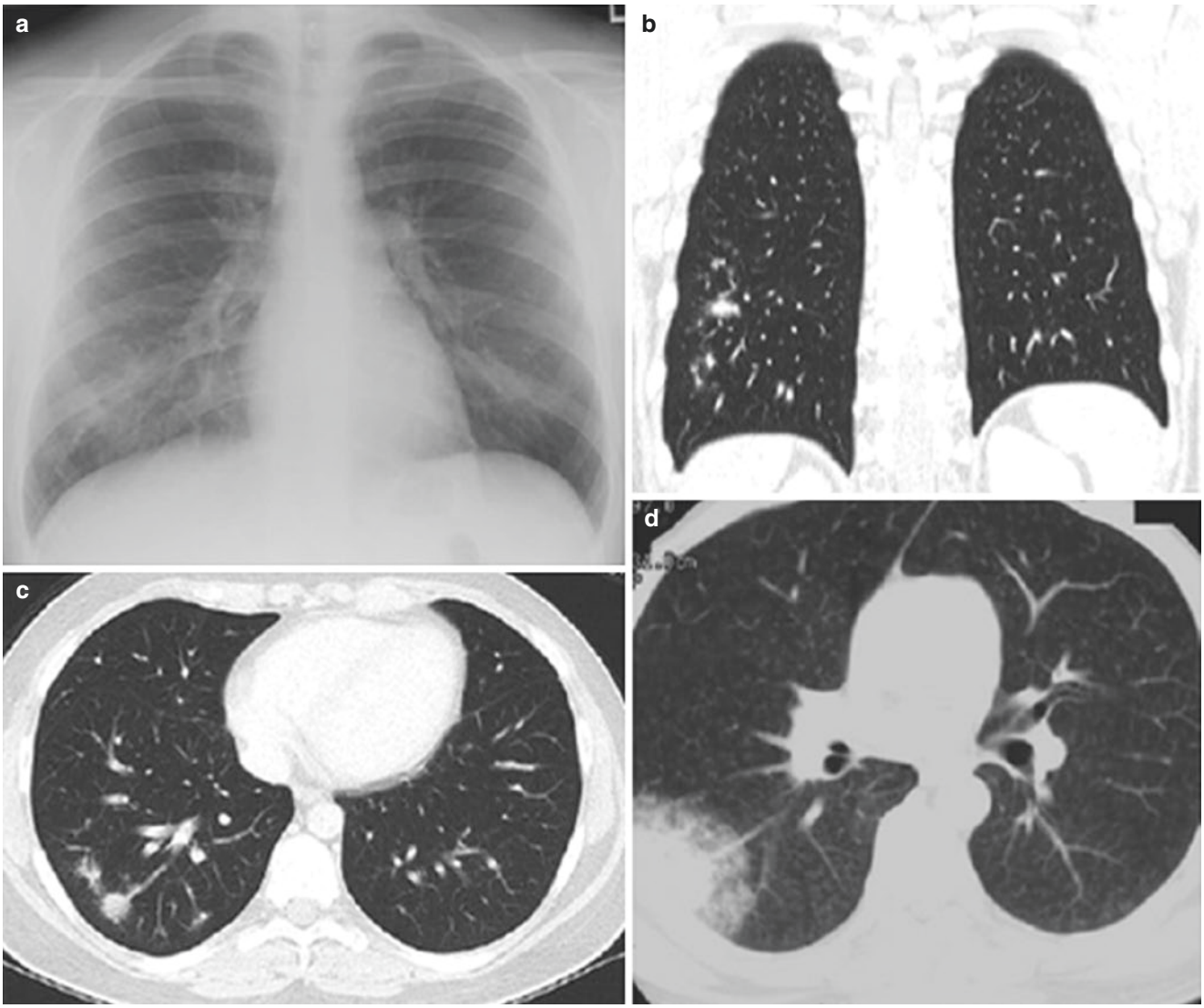

Fig. 8.27 (**a**) Aspergillus: there is an ill-defined right lung base airspace opacification. (**b**) Aspergillus: coronal lung window CT image shows multiple right lower lobe nodules, some with a questionable "halo" of ground-glass opacification. (**c**) Aspergillus: axial lung window CT image demonstrates the same as (**b**). (**d**) In another patient with diffuse nodular lesions, there is a classic "halo" sign surrounding a large right lower lobe nodule on axial lung window CT image. (Courtesy of Dr. Theresa McLoud, Department of Radiology, Massachusetts General Hospital, Harvard Medical School, Boston, MA.)

widely varies, but all have varying degrees of hypogammaglobulinemia resulting in recurrent pyogenic infections due to common bacteria, virus, and occasionally parasites and protozoa in children. In addition to impaired and immature B-cell function, there may be varied T cells, and other abnormalities and autoimmune phenomenon are seen in many patients. About one third of patients are diagnosed in childhood with a bimodal distribution of age of onset with peaks between 1 and 5 years and between 16 and 20. Other causes of humoral immune defects need to be excluded. Because of the difficulty in establishing the diagnosis, which rests on the exclusion of other causes of humoral immune deficiency, there is typically a 5-year delay between symptom onset and diagnosis. While recurrent pulmonary and sinus infections are the most common presentations, there may also be lymphoid hyperplasia, autoimmune disease, granulomatous inflammation, and malignancy.

Imaging Radiological findings of thoracic involvement from CVID are protean but typically include lymph node enlargement, pneumonia, bronchiectasis, and noncaseating granulomas in the lungs (Fig. 8.29).

Pathologic Findings Histologically, there are two major manifestations of pulmonary involvement with CVID: one is with infection often leading to chronic pulmonary infection and the development of bronchiectasis; the other is noninfectious diffuse lung disease characterized by lymphoproliferative and often associated granulomatous infiltration. These

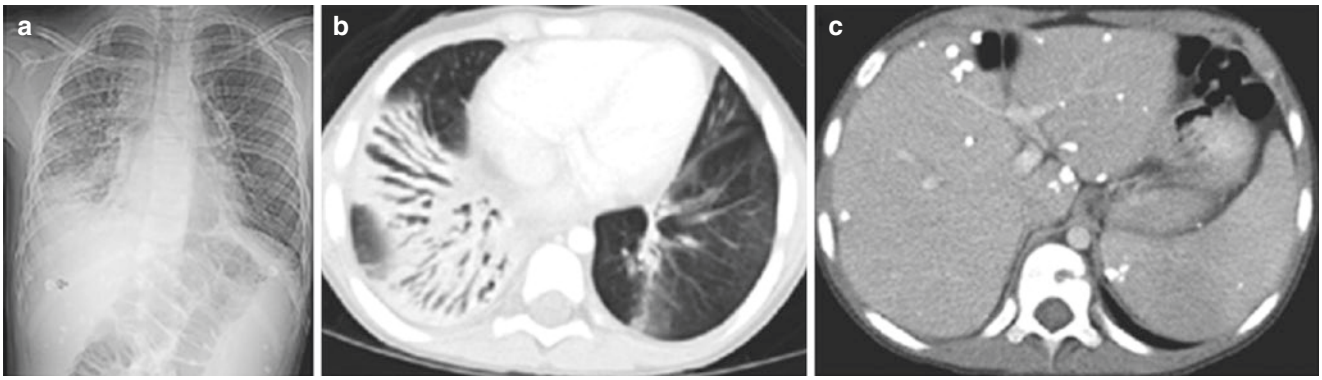

Fig. 8.28 (**a**) Chronic granulomatous disease (CGD) in an 8-year-old girl with recurrent infections. CXR shows diffuse, coarse irregularly distributed ILD with bibasilar airspace opacifications and bronchiectasis. The initial imaging manifestation of recurrent pneumonia is often diffuse ILD. As is also true for recurrent aspiration, the ILD frequently is irregular in its distribution. There are multiple soft tissue calcifications suggesting the diagnosis of CGD of childhood (arrows point to snaps on the patient's pajamas). (**b**) CGD: axial lung window CT image of the lung bases confirms the bronchiectasis. (**c**) CGD: axial enhanced soft tissue window CT image of the upper abdomen shows multiple calcifications

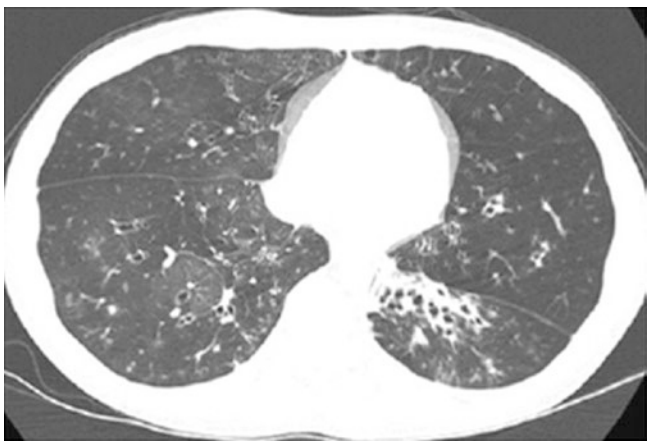

Fig. 8.29 Common variable immune deficiency (CVID): Axial lung window CT image reveals a mosaic attenuation with scattered nodules, bronchiectasis, and volume loss in this patient with CVID

may progress along the spectrum of lymphoid proliferations to malignancy, typically lymphoma. This latter manifestation is becoming more common as control of infection has been improved by high-dose intravenous gamma globulin administration in CVID patients. The development of granulomatous-lymphocytic lung disease is associated with increased morbidity and shortened survival; however, there are recent reports of response to TNF-alpha antagonists in patients with granulomatous involvement [54–56].

Acquired Immunodeficiency

Disorders Related to Therapeutic Intervention

Chemotherapeutic drug and radiation treatment, typically for the treatment of malignancy and also in other settings, leads to immune compromise and carries a risk of pulmonary complications, both infectious and noninfectious. Opportunistic infection is discussed above, but noninfectious complications of chemotherapeutic drug and radiation treatment may also be seen. Histologic manifestations of chemotherapeutic drug and radiation injury show many commonalities and may be difficult to separate with both showing DAD and varying degrees of organizing pneumonia and, for some chemotherapeutic agents, manifestations of hypersensitivity reactions. With certain drugs, specific histologic features may occur that permit their identification as the mechanism of lung injury, and for some hypersensitivity reactions poorly formed granulomas may occasionally occur.

Radiation injury in this setting is typically more prominent zonally and is often subpleural; in addition to the common features noted above, there are varying degrees of interstitial and alveolar fibrosis, as well as vascular changes with intimal fibrosis and foamy macrophages within vessel walls; veins are more affected than arteries. In addition, reactive changes affect a wide variety of cell types with nuclear enlargement and hyperchromasia, as well as bizarre nuclear forms. In both chemotherapeutic drug injury and radiation injury, changes may resolve spontaneously, or steroid therapy may be used in both to aid in this resolution. Or they may progress to chronic respiratory compromise with the degree of compromise being related to the degree of fibrosis. Death can occur in this setting, and risk depends on the agent and injury pattern.

Imaging Findings

During the early stage of lung injury from chemotherapeutic drugs and radiation, there is nonspecific interstitial prominence and alveolar opacities representing underlying alveolitis. These areas can eventually become fibrotic. Although any portion of the lung may be affected when pulmonary fibrosis resulting from chemotherapeutic drug injury, with radiation injury, changes are in geographic areas in the radiation field and are often zonal in the lung with subpleural

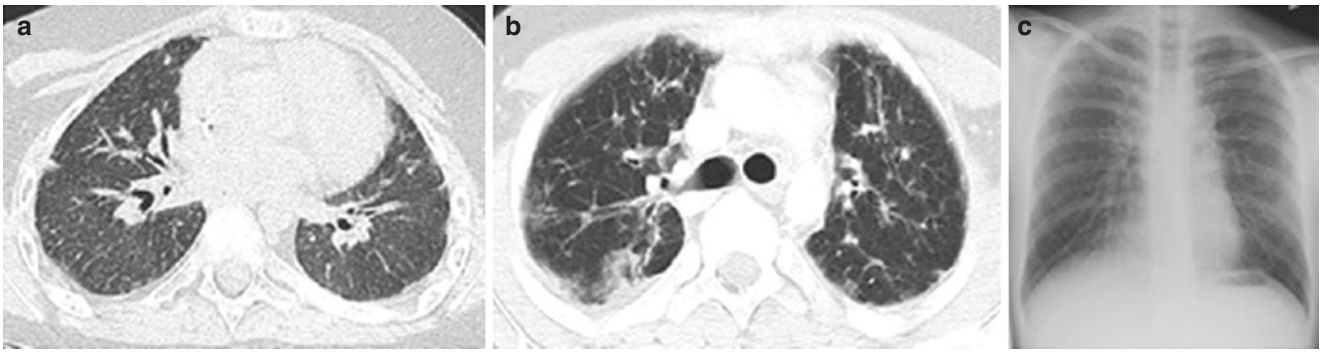

Fig. 8.30 (**a**) Fibrosis: the patient has had prior chemotherapy and bone marrow transplant (BMT). Axial lung window CT image reveals diffuse intralobular septal thickening consistent with pulmonary fibrosis. (**b**) Axial lung window CT image in a different patient also after remote chemotherapy and BMT. There is coarse interstitial thickening with intralobular septal thickening, pleural thickening, and focal airspace/nodular opacifications again consistent with pulmonary fibrosis. (**c**) CXR in this patient who received mantel radiation therapy for Hodgkin disease shows coarse interstitial prominence accentuated centrally in the region of mantel therapy

accentuation [33] (Fig. 8.30). Additional thoracic manifestations of high-dose radiation treatment include chest wall deformity associated with a loss in the lung volume and decreased functional lung capacity.

Disorders Related to Solid Organ, Lung, and Bone Marrow Transplantation

Rejection

Acute cellular rejection is a cell-mediated process with infiltration of the graft by host-derived lymphocytes targeting endothelial and epithelial cells with immune activation, inflammatory cytokine release, and up-regulation of adhesion molecules. In the lung, it may develop at almost any time in the posttransplant period from as early as 3 days to years later but is more common in the first year, particularly between 2 and 9 months. Presentation is with fever, cough, and dyspnea, and sometimes with hypoxemia and decrease in pulmonary function. It is thought that infection, and possibly aspiration, may precipitate rejection events, as may lack of compliance with immunosuppressive therapy. Lymphocytic bronchiolitis often accompanies higher grade pulmonary rejection (A2 and above). Acute cellular rejection is assessed by the evaluation of the lung tissue obtained by transbronchial biopsy.

In the lung, chronic rejection is manifested as constrictive/obliterative bronchiolitis. Its pathogenesis is incompletely understood, but the airway injury of acute rejection is thought to be an important factor. Clinically, there is a gradual onset of nonproductive cough and vague generalized symptoms, as well as progressive dyspnea and decline in pulmonary function tests. When this decline exceeds 10% of baseline, a diagnosis of bronchiolitis obliterans syndrome (BOS) can be made, and this is graded according to the degree of functional loss. When clinical diagnosis is uncertain, a lung wedge biopsy is done to confirm the clinical suspicion; transbronchial biopsies are considered to be inappropriate in this situation as diagnostic yield is low for airway pathology.

Imaging Findings

Acute Rejection Only approximately 40% of patients with acute lung transplant rejection have signs or symptoms of rejection. In these, noninvasive diagnostic tests, including HRCT, are notoriously insensitive and nonspecific. Consequently, patients are monitored by transbronchial biopsy. At this time, no imaging techniques are accepted as reliable in the diagnosis. There are experimental radionuclide techniques that have been reported [57].

Chronic Rejection Pulmonary imaging findings of BOS can be varied, but typical findings include subtle pulmonary nodules and GGO with mosaic patterns of lung attenuation. Such mosaic patterns of lung attenuation are due to the presence of areas of increased attenuation (from shunting of blood away from areas with diminished capacity for gas exchange) and decreased attenuation (from hypoxic pulmonary vasoconstriction and peripheral air trapping). CT, particularly high-resolution CT technique or thin section (<1 mm) technique with MDCT, is the best currently available imaging modality of choice for diagnosis. It is essential to perform expiratory CT imaging in addition to inspiratory because air trapping can be more accurately diagnosed with expiratory CT imaging.

Pathologic Findings

Acute Cellular Rejection Acute cellular rejection is characterized by lymphocytic infiltration, sometimes with associated eosinophils, neutrophils, and plasma cells, which begins in the perivascular region and extends into adjacent alveolar walls and other tissues. There is a well-defined system for the classification and grading of pulmonary allograft rejec-

tion based on the degree of lymphocytic infiltration and associated changes. This is monitored either on a protocol basis and/or in the face of clinical symptoms by transbronchial biopsy, often with associated BAL.

Chronic Rejection In chronic rejection, there is a spectrum of airway changes ranging from lymphocytic bronchiolitis to severe constrictive bronchiolitis and sometimes complete airway obliteration. The important change is subepithelial airway fibrosis, which may be patchy or concentric resulting in partial airway obstruction or progressive narrowing, eventuating in complete luminal obliteration. It may be accompanied by lymphocytic infiltration, but inflammatory infiltrates are not always seen. Concomitantly, there is intimal fibrosis and luminal narrowing of small blood vessels. Associated changes include mucus stasis, obstructive lipoid pneumonia, and focal acute bronchiolitis. All changes are patchy in their distribution and may range in severity in any given patient from mild to severe.

Graft-Versus-Host Disease

Graft-versus-host disease (GVHD) is seen in the lungs in two settings: in the postlung transplant patient where cells derived from host bone marrow react with the lung allograft and in the bone marrow transplant patient where cells derived from the allograft marrow react with the host lung. They have quite similar clinical, imaging, and histologic changes and are defined by the setting in which they occur.

In the past decade, bone marrow transplant has been increasingly performed to restore hematologic and immunologic competence after chemotherapy or radiation therapy in children with various neoplasms, immune deficiencies, and genetic disorders. In these children, as in children with lung transplantation, GVHD can develop when functional immune cells from the marrow recognize the patient as *foreign* and attack various organ systems in the setting of marrow transplant or only the lung in the setting of lung transplant.

Graft-versus-host disease has been classified traditionally into two forms: acute and chronic. The acute form of GVHD usually develops within the first 100 days after bone marrow transplant and is associated with high morbidity and mortality. In contrast, the chronic form of GVHD occurs later, more than 100 days after transplant. The current treatment of choice in children with both acute and chronic forms of GVHD is immune modulation with intravenous administration of corticosteroids.

Imaging The typical pulmonary imaging findings in children with acute GVHD following bone marrow transplant and lung transplant is diffuse bilateral alveolar opacities, which may be related to underlying diffuse alveolar hemorrhage, pulmonary edema, or an ARDS-like process. In chronic GVHD, changes are those of constrictive bronchiolitis described above in the setting of chronic rejection (Fig. 8.31).

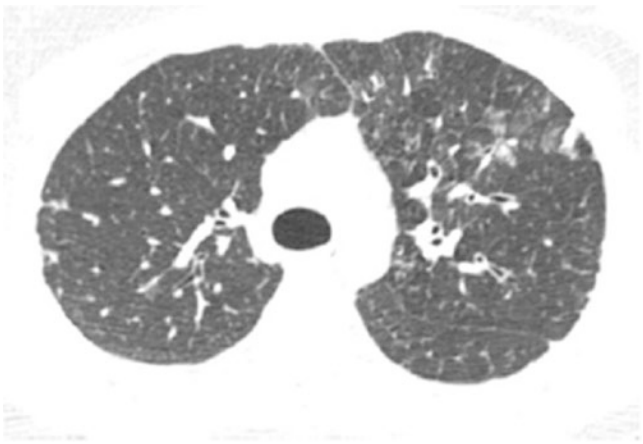

Fig. 8.31 Graft-versus-host disease (GVHD): this patient with GVHD shows changes of what the radiology literature refers to as BOOP on axial lung window CT image. There are multiple nodules, interlobular septal thickening, and bronchiectasis

Pathologic Findings Acute GVHD in the setting of bone marrow transplantation is rarely biopsied in the lung as more readily accessible sites, including the skin and gastrointestinal tract, are more often affected as well. In chronic GVHD in the setting of lung and bone marrow transplantation, the most prominent lung change is BO with constrictive bronchiolitis and organizing pneumonia (OP) as typical pathologic findings. The airway findings are similar to those seen in chronic rejection in the lung transplant patient with subepithelial airway fibrosis and lymphocytic infiltration.

Posttransplant Lymphoproliferative Disorder

In patients with lung and other solid organ transplants and bone marrow transplants, posttransplant lymphoproliferative disorder (PTLD) is a serious complication. Incidence varies with the organ transplanted, occurring in approximately 0.6% of patients after bone marrow transplantation, 1–5% of those with renal allografts, 2% of those with liver transplants, and in about 5% of heart transplant recipients. It is said to be higher, perhaps up to 10% in lung allograft recipients reflecting the degree of immunosuppression.

Lymphoproliferation in the setting of immunosuppression shows a predilection for extranodal sites, and a variety of organs, including the lung, may be affected. There is a strong association with EBV infection, and infection following transplant is a major risk factor. Early disease is treated by immune modulation, while more advanced disease is treated as lymphoma.

Imaging When occurring within the chest, PTLD presents as mediastinal adenopathy, pulmonary nodules, pulmonary parenchymal consolidation or effusion (pleural and pericardial), frequently in combination. The findings are nonspecific, and biopsy is required to confirm and stage the process. With lung transplants, pulmonary involvement is approximately four times as common as mediastinal, whereas with

other transplants, lung and mediastinal involvement is about equal. Nodules tend to be large, frequently in the range of 1–4 cm in diameter. There may be an associated *halo sign* with the nodules, as may be encountered with invasive aspergillosis (Fig. 8.27d), but most often the nodules are well defined. The nodules may have evidence of central necrosis with low attenuation on CT. Nodules may be single or multiple [58].

Pathologic Findings This B-cell disorder manifests a range of appearances from benign-appearing lymphoid proliferations that are shown to be polyclonal and polymorphous to monomorphic clonal lymphoid malignancy. It has an infiltrative appearance but may be focal and nodular or diffuse.

Disorders Masquerading as Interstitial (Diffuse) Lung Disease

As with any set of conditions defined by a common clinical presentation, there are conditions that show similar presentations but are clearly outside the boundaries of the defined disorder. With pediatric ILD, there are a variety of mimics or disorders that masquerade as ILD. It is important to correctly recognize these; they are individually important and require quite different management from ILD. Almost all such conditions seen in the pediatric patient with suspected ILD are vascular in their origin. In infants, congestive vasculopathy predominates, while in older children, arterial hypertensive vasculopathy, lymphatic disorders, and pulmonary edema, in addition to congestive vasculopathy, may also mimic ILD.

To identify underlying disorders and to differentiate among the various disorders masquerading as ILD, it is crucial to obtain high-quality, high-resolution CT images (either with conventional technique or with thin image reconstruction (<1 mm) from MDCT) often in conjunction with angiographic acquisitions in cases of conditions related to vasculopathy.

Arterial Hypertensive Vasculopathy

Pulmonary arterial hypertension is defined as a mean pulmonary artery pressure greater than 25 mmHg at rest or greater than 30 mmHg during exercise in the setting of an increased pulmonary vascular resistance. In children, pulmonary arterial hypertensive vasculopathy can be either idiopathic or in association with various other conditions, including parenchymal lung disease, liver disease, thromboembolic disease, and cardiac disease (i.e., left-to-right cardiac shunt lesions).

Imaging Findings

The common pulmonary imaging findings from various causes of pulmonary arterial hypertensive vasculopathy are similar. Enlargement of central pulmonary arteries, abrupt narrowing or tapering of peripheral pulmonary arteries, dilated bronchial arteries, and a mosaic pattern of lung parenchymal attenuation are commonly seen in patients with pulmonary arterial hypertensive vasculopathy. The mosaic pattern of lung parenchymal attenuation in children with arterial hypertensive vasculopathy is due to underlying variable lung perfusion and can sometimes be confused with interstitial lung disease in children. Additional imaging findings such as right ventricular hypertrophy and right ventricular and atrial enlargement in conjunction with information regarding the patient's underlying medical condition can be helpful in differentiating lung changes due to arterial hypertensive vasculopathy from true interstitial lung disease.

Pathologic Findings

Arterial hypertensive vasculopathy is characterized by progressive changes in the pulmonary arteries, which begin with extension of arterial smooth muscle into small, normally nonmuscularized, vessels in alveolar walls and progress to involve small pulmonary arteries with medial hypertrophy, followed by intimal cellular proliferation, vascular dilatation, and the development of plexiform lesions.

Congestive Vasculopathy

A variety of conditions related to pulmonary veins and the mitral valve may result in pulmonary venous hypertension and changes of congestive vasculopathy in children. These include pulmonary veno-occlusive disease, extrinsic pulmonary venous compression by mediastinal mass or fibrosis, left-sided cardiac disease, and pulmonary vein stenosis or atresia in pediatric patients.

Imaging

Pulmonary interstitial and alveolar edema are the most common imaging finding of congestive (venous) vasculopathy.

Pathologic Findings

Congestive vasculopathy is characterized pathologically by a thickening of the walls of pulmonary veins with sclerosis and arterialization, lymphatic dilatation, progressive peripheral lobular interstitial edema and fibrosis, and usually small numbers of hemosiderin-laden macrophages reflecting leakage of erythrocytes from the often dilated and congested alveolar capillaries. There are also changes involving the distalmost arteries with mild medial hyperplasia. The pleura and interlobular septa may also be widened by edema and progressive fibrosis. In pulmonary veno-occlusive disease, there will also be prominent cushions of expanded intima in veins that lead to marked luminal compromise or complete obliteration. With severe congestive vasculopathy, there may also be manifestations of pulmonary arterial hypertension

due to transmission of venous pressure through the alveolar capillaries into the arterial system.

Lymphatic Disorders

A variety of lymphatic disorders, including pulmonary lymphangiectasis and pulmonary lymphangiomatosis [59, 60], may mimic ILD. Pulmonary lymphatics play an essential role by removing extravascular lung fluid and protein. Lymphatics are located adjacent to the blood vessels in the bronchovascular spaces and in the connective tissues of interlobular septa and the pleura. In pulmonary lymphangiectasis, there is enlargement of these lymphatic channels on a congenital or acquired basis, and in some genetic syndromes. In pulmonary lymphangiomatosis, there is proliferation of lymphatic channels expanding the pleura, interlobular septa, and bronchovascular bundles. Both these lymphatic disorders may be isolated to the lung or associated with the involvement of other organs, sometimes limited to the thorax and sometimes extrathoracic as well.

Congenital pulmonary lymphangiectasis is a rare disorder of poorly understood etiology. It has been suggested that it results from failure of normal regression of lymphatic channels of the fetal lung at 20 weeks of gestation. Affected patients present at birth with severe respiratory distress, tachypnea, and cyanosis, often with pleural effusion that has limited late gestational lung growth. A proportion of affected fetuses are stillborn, and in those that are liveborn, there is early mortality within a few hours of birth likely due to lung hypoplasia. There are, however, less severely affected infants who may survive long term with variable degrees of respiratory compromise. These infants and young children are typically managed with fluid restriction and diet. Manifestations often improve with age. The diagnosis of congenital pulmonary lymphangiectasis should be strongly considered in term of neonates who present with severe respiratory distress and pleural effusion at birth. In older children with congenital pulmonary lymphangiectasis, the common clinical presentations include recurrent cough, wheeze, increased respiratory effort with inspiratory crackles, and sometimes congestive heart failure.

Imaging

Chest radiographs of affected infants usually show bilateral increased interstitial markings with hyperinflation and often with pleural effusion (Fig. 8.32). On CT, diffuse thickening of the peribronchovascular interstitium and interlobular septa is usually seen. On MRI, high-signal material within the pulmonary interstitium, often associated with pleural effusion, can be seen on T2-weighted images.

Pathologic Findings

Congenital pulmonary lymphangiectasis is characterized by the presence of dilated and tortuous lymphatic channels in normal numbers in their normal locations in the pleura, interlobular septa, and perivascular and peribronchial connective tissue. The pleural effusion, which often accompanies congenital pulmonary lymphangiectasis, is not chylous until enteric feeds are instituted but may contain prominent large lymphocytes of thoracic duct origin. Those who present later will show less prominent lymphatic dilatation but will have bland fibrosis of the pleura, interlobular septa, and bronchovascular bundles due to the presence of chronic edema in these regions (brawny edema).

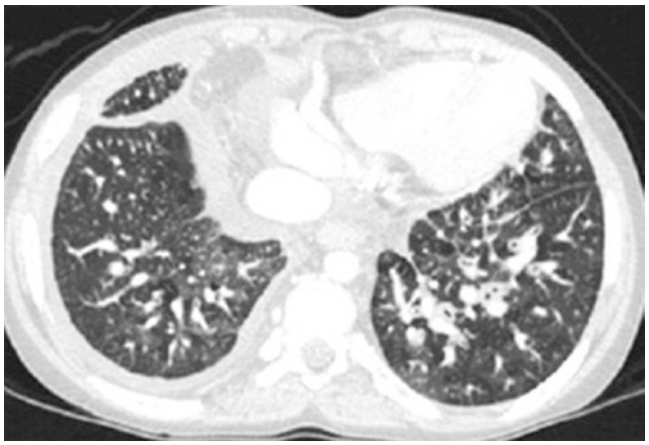

Fig. 8.32 Lymphangiectasis: Axial lung window CT image reveals diffuse bronchial wall thickening, intralobular septal thickening, mosaic opacifications, and bilateral pleural effusions in this child with lymphangiectasis. There is incidental fatty infiltration of the mediastinum

Pulmonary Edema

Pulmonary edema results from the excessive accumulation of fluid in lung tissues. It can be due to many causes but is traditionally categorized into three types: cardiogenic, noncardiogenic (capillary leak), and fluid overload (iatrogenic and renal causes).

In children, the majority of cardiogenic pulmonary edema is related to impaired left ventricular function or obstruction of pulmonary venous return. Noncardiogenic pulmonary edema can be due to upper airway obstruction, ARDS, and neurogenic causes (e.g., head trauma and seizures). Fluid overload due to either excessive administration of intravenous fluid or underlying renal dysfunction can result in fluid-overload-type pulmonary edema in children.

Clinical presentation of children with pulmonary edema varies based on the severity of the condition; however, they typically present with difficult breathing, desaturation, and excessive sweating.

Imaging

The imaging appearance of pulmonary edema usually follows the stages of increasing severity: (1) pulmonary vascular redistribution (on upright but not supine imaging), (2) interstitial edema, and (3) alveolar edema.

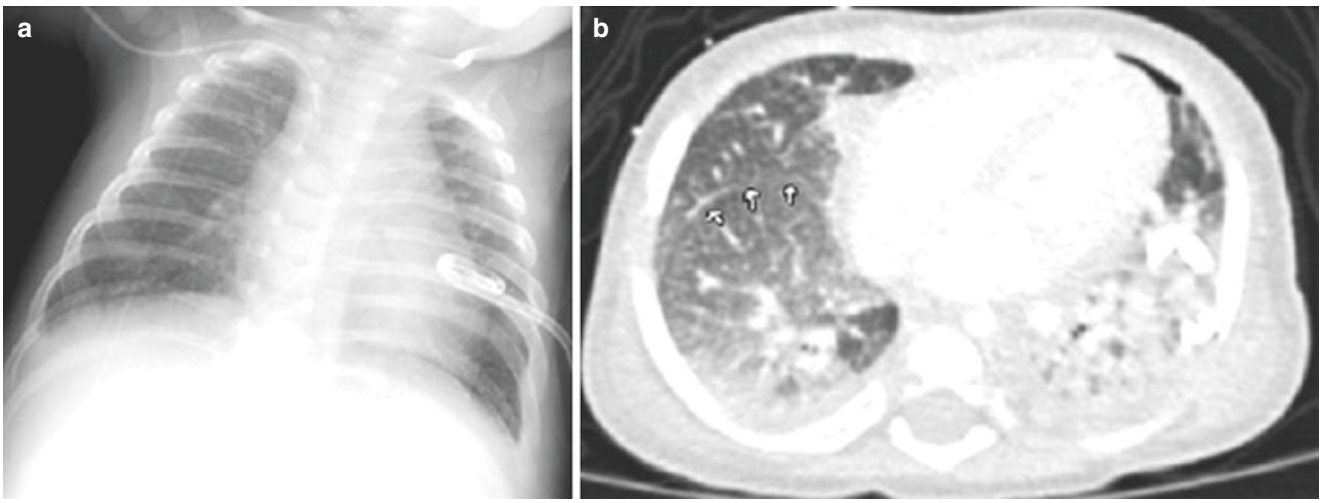

Fig. 8.33 (**a**) Edema: This infant is recently status post-PDA ligation with mild interstitial pulmonary edema. Note subtle Kerley B lines in the left costophrenic angle. (**b**) Axial lung window CT image reveals bibasilar atelectasis with dependent alveolar pulmonary edema. There is subpleural fluid accentuating the minor fissure (*arrows*). Mild intralobular septal thickening is present. Also noted is a small left pneumothorax

Characteristic radiographic findings of the early stage of pulmonary edema include vascular redistribution, fuzzy vascular and bronchial walls, Kerley's B lines (i.e., thickening of the interlobular septa presenting as thin, nonbranching lines abutting the pleura), and thickening of the pleural fissures (Fig. 8.33). More advanced degrees of pulmonary edema typically present as increased alveolar opacity and air bronchograms with ill-defined borders. On CT, areas of ground-glass opacity, smooth intralobular septal thickening, fissural thickening, and pleural effusion are often seen (Fig. 8.33). The presence of left atrial and ventricular enlargement on imaging studies can be helpful clues to cardiogenic pulmonary edema.

Pathologic Findings

It is rare for children with isolated pulmonary edema, particularly on an acute basis, to come to biopsy, but these would show protein-rich (pink) fluid within alveolar spaces. Occasionally, those with chronic edema mistaken for interstitial disease may have lung biopsy for diagnosis. Such biopsies show, in addition to protein-rich fluid within alveoli, capillary dilatation and congestion, leakage of erythrocytes, hemosiderin-laden macrophages, and widening of alveolar walls and the pulmonary interstitium by edema fluid. Advanced changes are those of congestive vasculopathy.

Acknowledgment The author of this chapter would like to sincerely thank the previous authors, Robert H. Cleveland, MD and Claire Langston, MD, involved with previous edition of this chapter.

References

1. Lee EY, editor. Pediatric radiology: practical imaging evaluation of infants and children. Philadelphia: Wolters Kluwer; 2018. p. 358–458.
2. Lee EY, editor. Pediatric thoracic imaging. Philadelphia: Wolters Kluwer; 2018. p. 1–113.
3. Thacker PG, Vargas SO, Fishman MP, Casey AM, Lee EY. Current update on interstitial lung disease in infancy: new classification system, diagnostic evaluation, imaging algorithms, imaging findings, and prognosis. Radiol Clin N Am. 2016;54(6):1065–76.
4. Lee EY. Interstitial lung disease in infants: new classification system, imaging technique, clinical presentation and imaging findings. Pediatr Radiol. 2013;43(1):3–13.
5. Liszewski MC, Lee EY. Neonatal lung disorders: pattern recognition approach to diagnosis. AJR Am J Roentgenol. 2018;210(5):964–75.
6. Deterding R. Evaluating infants and children with interstitial lung disease. Semin Respir Crit Care Med. 2007;28:333–41.
7. Deutsch GH, Young LR, Deterding RR, et al. Diffuse lung disease in young children: application of a novel classification scheme. Am J Respir Crit Care Med. 2007;176:1120–8.
8. Ponsky TA, Rothenberg SS, Tsao K, Ostlie DJ, St Peter SD, Holcomb GW III. Thoracoscopy in children: is a chest tube necessary? J Laparoendosc Adv Surg Tech A. 2009;19(Suppl 1):S23–5.
9. Ponsky TA, Rothenberg SS. Thoracoscopic lung biopsy in infants and children with endoloops allows smaller trocar sites and discreet biopsies. J Laparoendosc Adv Surg Tech A. 2008;18:120–2.
10. Dinwiddie R, Sharief N, Crawford O. Idiopathic interstitial pneumonitis in children: a national survey in the United Kingdom and Ireland. Pediatr Pulmonol. 2002;34:23–9.
11. Fan LL, Langston C. Pediatric interstitial lung disease: children are not small adults. Am J Respir Crit Care Med. 2002;165:1466–7.
12. Langston C, Dishop MK. Infant lung biopsy: clarifying the pathologic spectrum. Pathol Int. 2004;54:s419–21.
13. Fan LL, Mullen AL, Brugman SM, Inscore SC, Parks DP, White CW. Clinical spectrum of chronic interstitial lung disease in children. J Pediatr. 1992;121:867–72.
14. Fan LL, Kozinetz CA. Factors influencing survival in children with chronic interstitial lung disease. Am J Respir Crit Care Med. 1997;156:939–42.
15. Fan LL, Kozinetz CA, Deterding RR, Brugman SM. Evaluation of a diagnostic approach to pediatric interstitial lung disease. Pediatrics. 1998;101:82–5.
16. Brody AS. Imaging considerations: interstitial lung disease in children. Radiol Clin N Am. 2005;43:391–403.
17. Guillerman RP. Imaging of childhood interstitial lung disease. Pediatr Allergy Immunol Pulmonol. 2010;23:43–68.

18. Dishop MK. Diagnostic pathology of diffuse lung disease in children. Pediatr Allergy Immunol Pulmonol. 2010;23:69–85.
19. Popler J, Wagner BD, Accurso F, et al. Airway cytokine profiles in children's interstitial lung diseases. Am J Respir Crit Care Med. 2010;181:A3316.
20. Deterding RR, Wolfson A, Harris JK, Walker JJ, Accurso FJ. Aptamer proteomic analysis of bronchoalveolar lavage fluid yields different protein signatures from children with children's interstitial lung disease, cystic fibrosis and disease controls. Am J Respir Crit Care Med. 2010;181:A6722.
21. ATS Patient Education Series. What is interstitial lung disease in children? Am J Respir Crit Care Med. 2010;181:P1–2.
22. Sen P, Thakur N, Stockton DW, Langston C, Bejjani BA. Expanding the phenotype of alveolar capillary dysplasia (ACD). J Pediatr. 2004;145:646–51.
23. Licht C, Schickendantz S, Sreeram N, et al. Prolonged survival in alveolar capillary dysplasia syndrome. Eur J Pediatr. 2004;163:181–2.
24. Stankiewicz P, Sen P, Bhatt SS, et al. Genomic and genic deletions of the FOX gene cluster on 16q24.1 and inactivating mutations of FOXF1 cause alveolar capillary dysplasia and other malformations. Am J Hum Genet. 2009;84:780–91.
25. Eulmesekian P, Cutz E, Parvez B, Bohn D, Adatia I. Alveolar capillary dysplasia: a six-year single center experience. J Perinat Med. 2005;33:347–52.
26. Garmany TH, Wambach JA, Heins HB, et al. Population and disease-based prevalence of the common mutations associated with surfactant deficiency. Pediatr Res. 2008;63:645–9.
27. Cole FS, Hamvas A, Rubinstein P, et al. Population-based estimates of surfactant protein B deficiency. Pediatrics. 2000;105:538–41.
28. Gower WA, Popler J, Hamvas A, Deterding R, Nogee LM. Clinical improvement in infants with ILD due to mutations in the surfactant protein C gene (SFTPC). Am J Respir Crit Care Med. 2010;181:A6733.
29. Rosen DM, Waltz DA. Hydroxychloroquine and surfactant protein C deficiency. N Engl J Med. 2005;352:207–8.
30. Karjalainen MK, Haataja R, Hallman M. Haplotype analysis of ABCA3: association with respiratory distress in very premature infants. Ann Med. 2008;40:56–65.
31. Clement A, Corvol H, Epaud R, Feldman D, Fauroux B. Dramatic improvement by macrolides in surfactant deficiency with ABCA3 mutation. Am J Respir Crit Care Med. 2009;179:A3011.
32. Doan ML, Guillerman RP, Dishop MK, et al. Clinical, radiological and pathological features of ABCA3 mutations in children. Thorax. 2008;63:366–73.
33. Guillot L, Carre A, Szinnai G, et al. NKX2-1 mutations leading to surfactant protein promoter dysregulation cause interstitial lung disease in "brain-lung-thyroid syndrome". Hum Mutat. 2010;31:E1146–62.
34. Iwatani N, Mabe H, Devriendt K, Kodama M, Miike T. Deletion of NKX2.1 gene encoding thyroid transcription factor-1 in two siblings with hypothyroidism and respiratory failure. J Pediatr. 2000;137:272–6.
35. Deterding R, Dishop MK, Uchida DA, et al. Thyroid transcription factor 1 gene abnormalities: an under recognized cause of children's interstitial lung disease. Am J Respir Crit Care Med. 2010;181:A6725.
36. Galambos C, Levy H, Cannon CL, et al. Pulmonary pathology in thyroid transcription factor-1 deficiency syndrome. Am J Respir Crit Care Med. 2010;182:549–54.
37. Willemsen MA, Breedveld GJ, Wouda S, et al. Brain-thyroid-lung syndrome: a patient with a severe multi-system disorder due to a de novo mutation in the thyroid transcription factor 1 gene. Eur J Pediatr. 2005;164:28–30.
38. Kerby GS, Wilcox SL, Hay TC, et al. Infant pulmonary function testing in children neuroendocrine cell hyperplasia with and without lung biopsy. Am J Respir Crit Care Med. 2009;179:A3671.
39. Deterding RR, Pye C, Fan LL, Langston C. Persistent tachypnea of infancy is associated with neuroendocrine cell hyperplasia. Pediatr Pulmonol. 2005;40:157–65.
40. Popler J, Young LR, Deterding RR. Beyond infancy: persistence of chronic lung disease in neuroendocrine cell hyperplasia of infancy (NEHI). Am J Respir Crit Care Med. 2010;181:A6721.
41. Brody AS, Guillerman RP, Hay TC, et al. Neuroendocrine cell hyperplasia of infancy: diagnosis with high-resolution CT. AJR Am J Roentgenol. 2010;194:238–44.
42. Popler J, Gower WA, Mogayzel PJ Jr, et al. Familial neuroendocrine cell hyperplasia of infancy. Pediatr Pulmonol. 2010;45:749–55.
43. Bramson RT, Cleveland R, Blickman JG, Kinane TB. Radiographic appearance of follicular bronchitis in children. AJR Am J Roentgenol. 1996;166:1447–50.
44. Canakis AM, Cutz E, Manson D, O'Brodovich H. Pulmonary interstitial glycogenosis: a new variant of neonatal interstitial lung disease. Am J Respir Crit Care Med. 2002;165:1557–65.
45. Onland W, Molenaar JJ, Leguit RJ, et al. Pulmonary interstitial glycogenosis in identical twins. Pediatr Pulmonol. 2005;40:362–6.
46. Castillo M, Vade A, Lim-Dunham JE, Masuda E, Massarani-Wafai R. Pulmonary interstitial glycogenosis in the setting of lung growth abnormality: radiographic and pathologic correlation. Pediatr Radiol. 2010;40:1562–5.
47. Langston C, Dishop MK. Diffuse lung disease in infancy: a proposed classification applied to 259 diagnostic biopsies. Pediatr Dev Pathol. 2009;12:421–37.
48. Clement A. Task force on chronic interstitial lung disease in immunocompetent children. Eur Respir J. 2004;24:686–97.
49. Smith KJ, Dishop MK, Fan LL, et al. Diagnosis of bronchiolitis obliterans with computed tomography in children. Pediatr Allergy Immunol Pulmonol. 2010;23:253–8.
50. Al-Ghanem S, Al-Jahdali H, Bamefleh H, Khan AN. Bronchiolitis obliterans organizing pneumonia: pathogenesis, clinical features, imaging and therapy review. Ann Thorac Med. 2008;3:67–75.
51. Fullmer JJ, Langston C, Dishop MK, Fan LL. Pulmonary capillaritis in children: a review of eight cases with comparison to other alveolar hemorrhage syndromes. J Pediatr. 2005;146:376–81.
52. Cleveland RH, Neish AS, Zurakowski D, Nichols DP, Wohl ME, Colin AA. Cystic fibrosis: predictors of accelerated decline and distribution of disease in 230 patients. AJR Am J Roentgenol. 1998;171:1311–5.
53. Buckley RH. Pulmonary complications of primary immunodeficiencies. Paediatr Respir Rev. 2004;5(Suppl A):S225–33.
54. Bates CA, Ellison MC, Lynch DA, Cool CD, Brown KK, Routes JM. Granulomatous-lymphocytic lung disease shortens survival in common variable immunodeficiency. J Allergy Clin Immunol. 2004;114:415–21.
55. Thickett KM, Kumararatne DS, Banerjee AK, Dudley R, Stableforth DE. Common variable immune deficiency: respiratory manifestations, pulmonary function and high-resolution CT scan findings. QJM. 2002;95:655–62.
56. Martinez Garcia MA, deRojas MD, Nauffal Manzur MD, et al. Respiratory disorders in common variable immunodeficiency. Respir Med. 2001;95:191–5.
57. Blankenberg FG, Robbins RC, Stoot JH, et al. Radionuclide imaging of acute lung transplant rejection with annexin V. Chest. 2000;117:834–40.
58. Pickhardt PJ, Siegel MJ, Hayashi RJ, Kelly M. Posttransplantation lymphoproliferative disorder in children: clinical, histopathologic, and imaging features. Radiology. 2000;217:16–25.
59. Barker PM, Esther CR Jr, Fordham LA, Maygarden SJ, Funkhouser WK. Primary pulmonary lymphangiectasia in infancy and childhood. Eur Respir J. 2004;24:413–9.
60. Esther CR Jr, Barker PM. Pulmonary lymphangiectasia: diagnosis and clinical course. Pediatr Pulmonol. 2004;38:308–13.

Genetic Pediatric Pulmonary Disease

9

Megan H. Hawley, Peter P. Moschovis, T. Bernard Kinane, and Lael M. Yonker

Introduction

Recognition of underlying genetic etiologies of diseases is increasing at an exponential rate, likely due to greater access to and lower cost of genetic testing. Monogenic causes of disease, or conditions resulting from mutations in a single gene, are now well recognized in every subspecialty, including pediatric pulmonary medicine, and it is important to consider genetic conditions when evaluating pediatric pulmonary patients.

Detailed phenotyping, including close examination of radiographic findings, can help point to an underlying genetic condition. In the pediatric pulmonary clinic, genetic conditions should be considered when multiple family members present with similar or related clinical features and when individuals have unusual clinical presentations such as early-onset disease or complex, syndromic clinical features. This chapter discusses genetic conditions commonly seen in the pediatric pulmonary clinic that have pulmonary involvement as a main clinical feature. Many additional genetic syndromes require pediatric pulmonary care but are not discussed here as they are very rare or have predominantly nonpulmonary features.

Disease Outline

1. Surfactant related disorders
   - *Surfactant deficiencies*
   - *Pulmonary alveolar proteinosis*
2. Bronchiectasis
   - *Cystic fibrosis*
   - *Primary ciliary dyskinesia*
   - *Immune deficiencies*
3. Pulmonary fibrosis
   - *Short telomere syndromes*
   - *Hermansky Pudlak syndrome*
4. Vascular abnormalities
   - *Alveolar capillary dysplasia*
   - *Pulmonary arterial hypertension*
   - *Hereditary hemorrhagic telangiectasia*
5. Pneumothorax
   - *Connective tissue diseases*
   - *Birt-Hogg-Dubé syndrome*

Surfactant Related Disorders

Clinical Overview

Surfactant deficiency should be suspected when respiratory distress or failure occurs in a full-term infant. Symptoms include hypoxemia and retractions, with possible crackles on auscultation. Surfactant deficiency disorders occur when there is abnormal production or transport of the phospholipids and proteins that make up the pulmonary surfactant complex. Surfactant is required to reduce surface tension of the lungs, thus preventing alveolar collapse after exhalation [1, 2]. If the quantity or quality of surfactant in the lung is abnormal, the alveoli will collapse and there will be insufficient gas exchange resulting in hypoxia and hypercarbia, and symptoms will often develop shortly after birth.

In some cases, symptoms may be more subtle. Newborns may be well enough to be discharged home after delivery but then develop chronic tachypnea, retractions, and failure to thrive and may display hypoxia and crackles on exam. In milder disease, symptoms may not present until later in life, and occasionally even into adulthood. Symptoms may include

M. H. Hawley · P. P. Moschovis · L. M. Yonker (✉) · T. B. Kinane
Pediatric Pulmonary Division, Massachusetts General Hospital for Children, Boston, MA, USA
e-mail: lyonker@mgh.harvard.edu

R. H. Cleveland, E. Y. Lee (eds.), *Imaging in Pediatric Pulmonology*, https://doi.org/10.1007/978-3-030-23979-4_9

shortness of breath and exercise intolerance with the associated feature of digital clubbing. These patients may be diagnosed with interstitial lung disease or pulmonary fibrosis [2]. Patients may present with recurrent respiratory infections, and crackles or wheezing can be heard on physical exam.

Genetic Conditions

Surfactant Deficiencies

The three most common genetic causes of surfactant deficiency result from mutations in the *ABCA3*, *SFTPB*, and *SFTPC* genes. Mutations in the *NKX2–1* gene may also result in surfactant deficiency, although typically as part of a syndrome with additional features affecting the brain and thyroid. Each of these surfactant deficiency disorders have various inheritance patterns and clinical presentations depending on the underlying genetic defect.

Mutations in the *ABCA3* gene, which encodes a protein involved in surfactant production and transport, are the most common genetic cause of respiratory failure in the newborn period. Individuals with *ABCA3*-related surfactant deficiency can present in infancy, in childhood, or rarely in adulthood [2]. Disease severity and clinical outcome depend on the type of mutation with loss of function or null mutations in *ABCA3* resulting in a more severe clinical presentation [3]. Individuals with pathogenic changes in the *SFTPB* gene, which encodes surfactant protein B, present similarly to patients with severe forms of *ABCA3*-related surfactant deficiency, typically experiencing acute respiratory failure and death in the newborn period. *ABCA3* and *SFTPB*-related surfactant deficiencies are autosomal recessive disorders.

The *SFTPC* gene encoding surfactant protein C is associated with autosomal dominant inheritance, variable severity, and reduced penetrance. Individuals with *SFTPC* mutations can experience neonatal respiratory distress but more frequently present with interstitial lung disease at varying ages of onset [2, 4, 5].

Another condition associated with surfactant deficiency, known as brain-lung-thyroid syndrome, results from mutations in the *NKX2–1* gene, previously known as the thyroid transcription factor-1 (*TTF-1*) gene. In contrast to *ABCA3, SFTPB*, and *SFTPC*-related surfactant deficiencies, individuals with *NKX2–1* mutations can have a syndromic presentation resulting from the disruption of brain and thyroid development. About half of individuals exhibit involvement of all three organ systems, while the other half exhibit any combination of the associated features [6, 7]. Most individuals will have some neurological involvement, with childhood onset of chorea being one of the hallmark features of *NKX2–1*-related conditions, and some individuals have additional neurological involvment [8]. Thyroid manifestations may include congenital hypothyroidism or varying degrees of hypothyroidism [6, 9]. Lung disease accounts for the leading cause of mortality associated with *NKX2–1*-related conditions. Approximately 50% of individuals with *NKX2–1* mutations have some degree of pulmonary dysfunction, but the clinical presentation and onset of lung disease have a wide range [6, 10]. Respiratory distress syndrome may occur in the neonatal period [7, 11], while other patients can present with interstitial lung disease or pulmonary fibrosis at any age [6, 10]. Neuroendocrine cell hyperplasia of infancy (NEHI), a form of ILD characterized by tachypnea, crackles, retractions, and hypoxia in the newborn/infant period that generally improves with age, has been reported in one family with an NKX2–1 mutation [12]. Most cases of NEHI, however, do not have a clear genetic cause.

Pulmonary Alveolar Proteinosis

Pulmonary alveolar proteinosis (PAP) is another condition caused by a disruption of surfactant homeostasis that results from the accumulation of surfactant in the alveolar space; however, this disease usually does not present until late adolescence or adulthood. Individuals with PAP may develop signs of interstitial lung disease, including dyspnea, exercise intolerance, and dry cough, with crackles on exam and a "crazy paving" pattern on CT imaging of the chest. Lung biopsy reveals amorphous PAS-positive fluid filling the alveoli, and bronchoalveolar lavage would reveal copious frothy, creamy liquid. Additional clinical features can include tachypnea, clubbing, respiratory failure, fatigue, fever, weight loss, and chest pain. Treatment of PAP includes whole lung lavage, and success of treatment is dependent on the underlying etiology of the disease [13, 14].

Pulmonary alveolar proteinosis (PAP) can be secondary to toxic exposures, autoimmune disease, hematological disorders, malignancies, or infections. Autoimmune PAP is the most common cause of PAP and results from autoantibodies against the granulocyte macrophage colony–stimulating factors (GM-CSF), a protein that controls clearance of surfactant by airway macrophages [13]. Genetic causes of PAP are rare and include pathogenic changes in the *CSF2RA* and *CSF2RB* genes, which encode the target receptors for granulocyte macrophage colony–stimulating factors [15]. Other genetic syndromes that have PAP as a feature have been described [15, 16].

Radiographic Findings

In the newborn, chest X-rays often reveal low lung volumes with atelectasis and diffuse homogenous granular opacities [17]. Chest CT findings include ground-glass opacities, which evolve into cysts, infiltrates, atelectasis, and fibrosis in older patients [10, 18]. Figure 9.1 illustrates radiographic findings typical of a newborn infant with surfactant deficiency. In PAP, a "crazy paving" pattern, resulting from ground-glass infiltrates and interlobar septal thickening, may be seen on chest CT imaging.

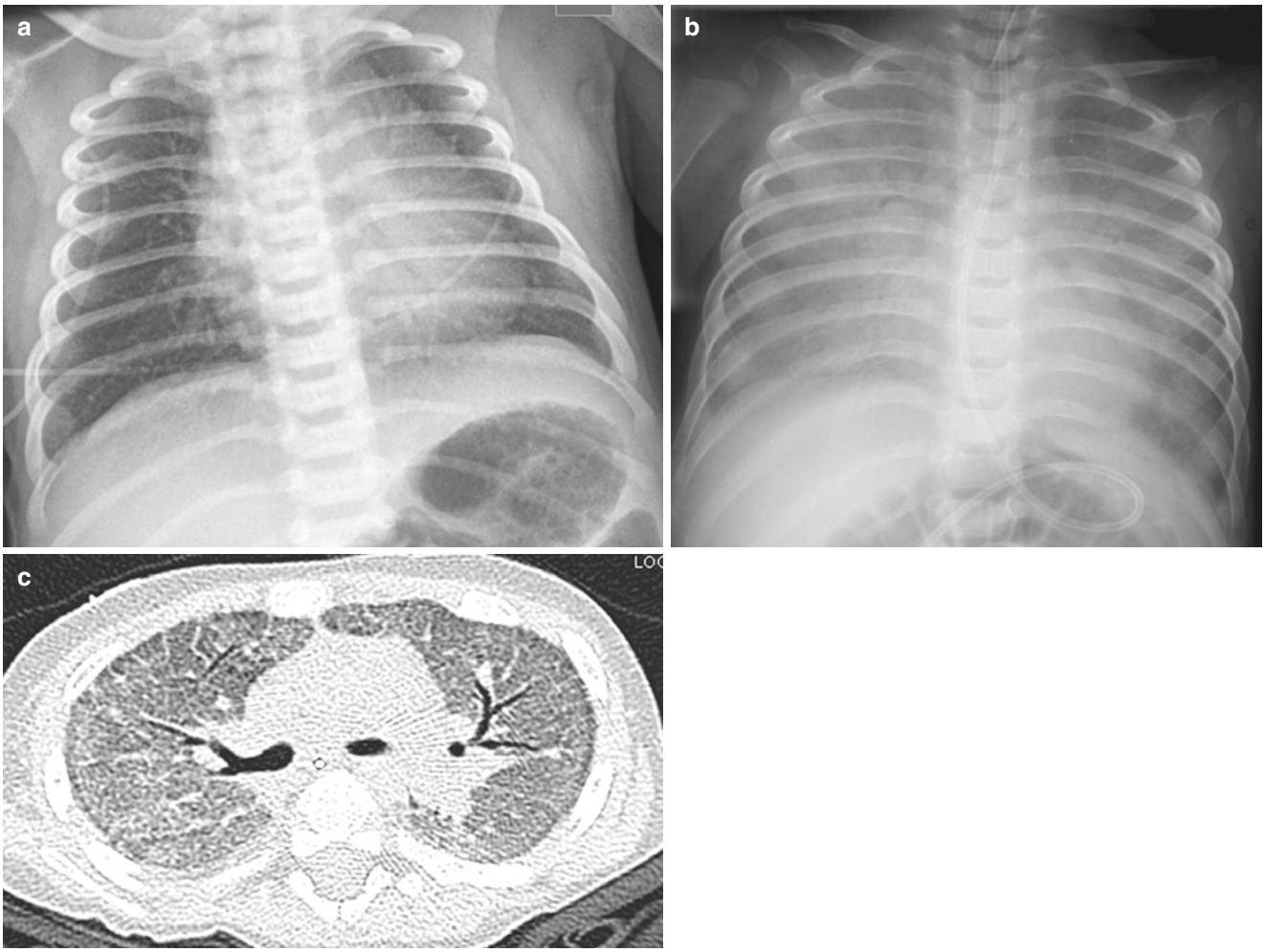

Fig. 9.1 (**a**) CXR of a newborn presenting within the first few hours of life with respiratory failure, later found to have two pathogenic mutations in the *ABCA3* gene. This full-term newborn girl was the product of a normal vaginal delivery without maternal risk factors for neonatal pneumonia. At a few hours of age, she was noted to have tachypnea and mild respiratory distress. There is a mild diffuse granular opacification that is nonspecific but could, in the correct clinical setting, represent TTN, HMD, or neonatal pneumonia. Lacking support for these diagnoses, the possibility of a surfactant deficiency syndrome was considered. (**b**) This full-term boy had a severe diffuse ground-glass opacification of both lungs and profound respiratory distress at birth. This scenario of severe involvement is frequently encountered with ABCA3, which this boy was found to have. (**c**) This CT is from the same infant as (**b**). There is diffuse severe ground-glass opacification and interlobular septal thickening

Bronchiectasis

Clinical Overview

Bronchiectasis is defined by a permanent dilation of the bronchial lumen, resulting in reduced mucus clearance. Bronchiectasis can be focal or diffuse, and affected lung tissue is at increased risk for inflammation and infection. Common clinical features include cough, sputum production, and recurrent respiratory infections. Many factors may lead to the development of bronchiectasis, including chronic aspiration, allergic hypersensitivity, severe lung infection, and inhalation injury. There are also several genetic conditions, including cystic fibrosis, primary ciliary dyskinesia, immune defects, and pseudohypoaldosteronism, that should be considered when a pediatric patient presents with bronchiectasis [19].

Genetic Conditions

Cystic Fibrosis

Cystic fibrosis (CF) is one of the most common pediatric pulmonary genetic conditions. It is characterized by obstructive lung disease with bronchiectasis, pancreatic insufficiency, recurrent sinopulmonary infections, and male infertility. The clinical and genetic characteristics of CF are discussed in detail in Chap. 18 of this book. Here, genetic causes of non-CF bronchiectasis will be discussed in further detail.

Primary Ciliary Dyskinesia

Primary ciliary dyskinesia (PCD), previously known as immotile cilia syndrome, is characterized by bronchiectasis, sinusitis, and chronic otitis media. Tachypnea and nasal congestion often develop in the newborn period, followed by chronic sinopulmonary infections beginning in early childhood. Bronchiectasis is common in PCD and often involves the right middle lobe. Additional pulmonary symptoms of PCD include chronic cough, wheezing, digital clubbing, and obstructive lung disease [20, 21]. Chronic ear infections sometimes lead to hearing loss and permanent scarring of the tympanic membrane. Additional features of PCD include male infertility due to abnormalities of sperm flagellar structure and laterality defects, including situs inversus and heterotaxy [20, 22].

Measurement of nasal nitric oxide levels and analysis of ciliary ultrastructure by transmission electron microscopy can aid in diagnosis [23], in addition to genetic testing. PCD is most frequently inherited in an autosomal recessive pattern, with pathogenic changes in the *DNAI1*, *DNAH5*, and *DNAH11* genes being the most common disease-causing mutations [24, 25]. Two genes, *OFD1* and *RPGR*, are associated with syndromic X-linked recessive forms of PCD. Many individuals with clinical diagnoses of PCD do not have identifiable pathogenic changes in PCD-related genes; however, detection rates are increasing as this area of research is expanding rapidly. Over 40 PCD genes having been identified to date [26].

Primary Immunodeficiencies

Primary immunodeficiencies (PID) encompass a group of over 180 genetic disorders in which there is an intrinsic defect in one or more components of the immune system and can present with varying clinical severity, depending on the underlying genetic defect. The pulmonary phenotype includes dyspnea, chronic cough, asthma, and recurrent pneumonia, which can result in bronchiectasis or features of ILD [27–29]. Individuals with immune defects may also develop infections from unusual bacteria, fungi, or mycobacteria that do not typically cause disease in the general population [30].

Severe combined immunodeficiency (SCID) is the most severe immunodeficiency resulting from a combined cellular and humoral immunodeficiency characterized by impaired B- and T-cell function that presents in infancy with life-threatening infections [31]. The most common type of SCID is inherited in an X-linked recessive pattern and caused by mutations in the *IL2RG* gene. The most common autosomal recessive causes of SCID result from mutations in the *ADA*, *CD3D*, *DCLRE1C*, *JAK3*, *RAG1*, and *RAG2* genes [32].

Common variable immune deficiency (CVID) is one of the most prevalent PID and is characterized by B-cell dysfunction resulting in low immunoglobulin levels. CVID can often be mild and may not be recognized until adulthood [28, 29]. The most commonly mutated gene is *TNFRSF13B* (previously known as *TACI*). *TNFRSF13B*-associated CVID can be inherited in an autosomal dominant or recessive pattern, although penetrance can be variable [33, 34]. Several syndromic genetic conditions, including DiGeorge syndrome, trisomy 21, Noonan syndrome, ataxia telangiectasia, and Wiskott-Aldrich syndrome, are also associated with immunodeficiency [35].

The majority of pediatric onset PID are inherited in autosomal recessive or X-linked recessive patterns; however, in a large proportion of individuals with suspected immune deficiencies, underlying genetic causes are not identified.

Radiographic Findings

Cystic fibrosis typically presents with progressive bronchiectasis, frequently starting in the upper lobes. Imaging of newborns with PCD will typically reveal lobular collapse, hypoxemia, and atelectasis [26]. As these individuals age, bronchiectasis will develop, usually within the middle and lower lobes. CT imaging of PCD-associated bronchiectasis is more likely to show middle lobe linear atelectasis and interlobular septal thickening when compared with scans from CF patients [36]. Figure 9.2 is a chest CT of an individual with PCD, revealing bronchiectasis predominantly of the right middle lobe, plus ground-glass opacities over the left lower lobe.

Individuals with immunodeficiency may have frank pneumonia, bronchiectasis, or signs of tree-in-bud formations suggesting an ongoing infection in the airway.

Pulmonary Fibrosis

Clinical Overview

Pulmonary fibrosis should be considered when pediatric patients present with restrictive lung disease, exercise intolerance, and hypoxia or desaturation with activity. Auscultation of the lungs reveals crackles, and pulmonary function testing reflects restrictive patterns with a decreased diffusion capacity. In the adult population, pulmonary fibrosis is often multifactorial, resulting from a combination of genetic and environmental risk factors [37, 38]. Pulmonary fibrosis is rare in the pediatric population, and underlying causes include genetic conditions, such as short telomere syndromes and Hermansky Pudlak syndrome.

Genetic Conditions

Short Telomere Syndromes

Short telomere syndromes result from defects in telomere elongation or maintenance that cause a reduction in telomere length [39]. The effects of excessively short telomeres for age can

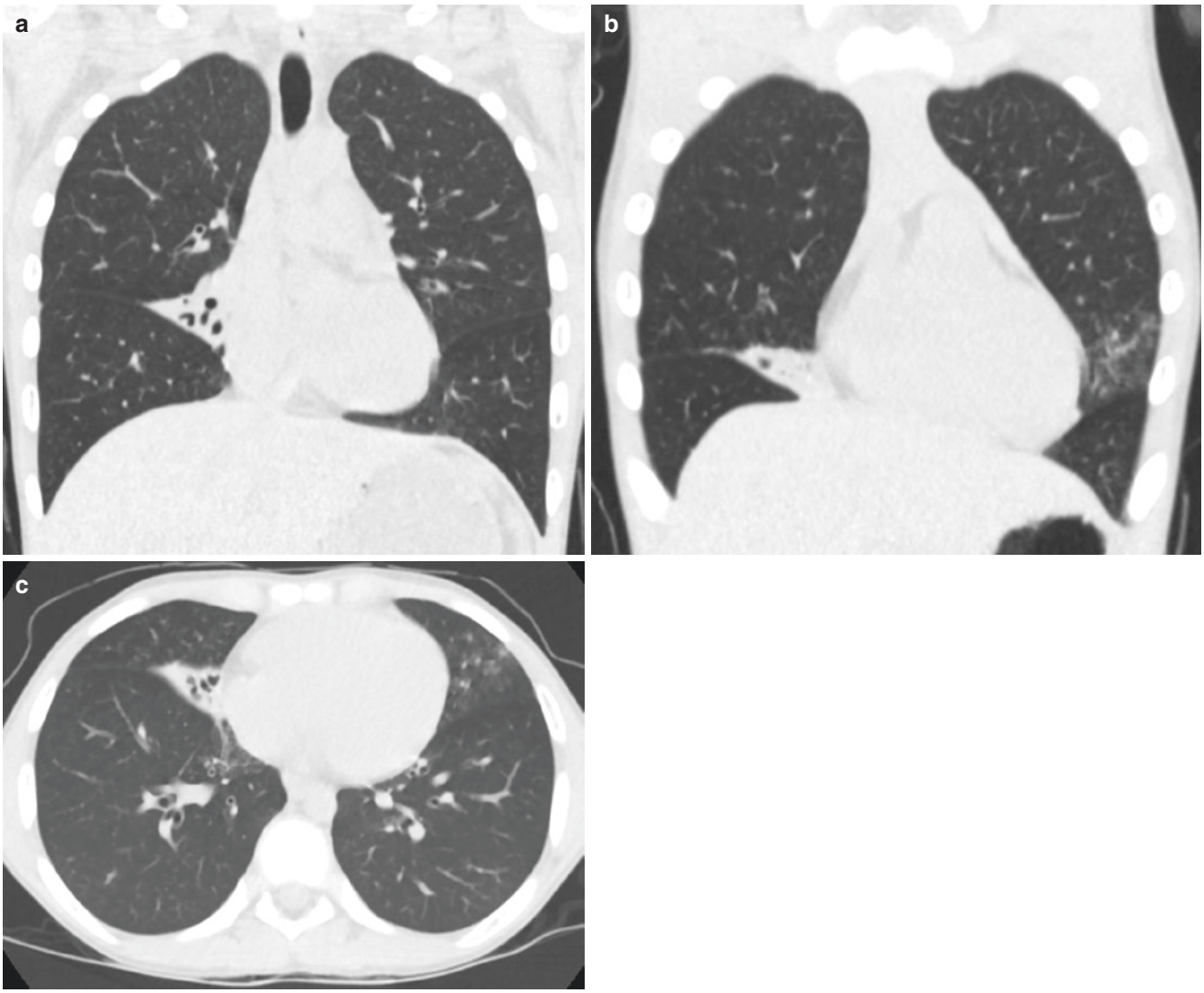

Fig. 9.2 (**a**) An adolescent boy presented with recurrent pneumonia, plus chronic otitis media. Coronal reconstructions on CT imaging highlights segmental collapse of the right middle lobe with tubular bronchiectasis. He was later found to have two pathogenic mutations resulting in primary ciliary dyskinesia. (**b**) In another coronal chest, CT image of the same patient as (**a**) with primary ciliary dyskinesia, patchy areas of airspace filling with centrilobular nodules can be seen, most notably in the lingual. (**c**) Axial views of this same young boy with primary ciliary dyskinesia reveal bilateral, central bronchiectasis with bilateral areas of tree-in-bud consolidation

impact multiple organ systems, and shorter telomere length correlates with a more severe phenotype, disproportionately impacting tissue types with high rates of cell proliferation, such as bone marrow and skin [40–42]. Telomere length is typically measured by automated multicolor flow cytometry fluorescence in situ hybridization (flow-FISH) in leukocytes [43, 44].

Short telomere syndromes can be quite variable in presentation, and variable expressivity leads to a wide range of clinical features and ages of onset. Dyskeratosis congenita is the more severe phenotype, while milder phenotypes may include isolated features of pulmonary fibrosis, aplastic anemia, or liver cirrhosis, which could present later in adulthood [40, 45, 46].

Dyskeratosis congenita classically includes a diagnostic triad of oral leukoplakia, nail dystrophy, and reticulated pigmentation. However, other features may include epiphora, lymphopenia, dental abnormalities, short stature, developmental delay, premature hair loss or graying, esophageal stricture or narrowing, hyperhidrosis, brain abnormalities, intrauterine growth restriction, and genitourinary abnormalities [44, 47]. In rare cases, pulmonary arteriovenous malformations have been reported [43]. Life-threatening complications of dyskeratosis congenita include bone marrow failure syndromes and pulmonary fibrosis [48]. Pulmonary fibrosis tends to present later than bone marrow failure; however, it can occur in childhood or adulthood and

may be the first life-threatening presentation of the disease [41, 49].

The most common genetic defects responsible for short telomere syndromes result in reduced activity of telomerase, the main enzyme involved in telomere elongation. The most frequently mutated genes are *TERC*, *TERT*, and *DKC1*, which encode the proteins that make up the major subunits of the telomerase complex. Mutations in the *TNIF2*, *RTEL1*, *CTC1*, *ACD*, *NOP10*, *NHP2*, *PARN*, *USB1*, and *WRAP53* genes have also been identified as rare causes of short telomere syndromes [41, 43, 44].

Hermansky Pudlak Syndrome

Hermansky Pudlak syndrome is a condition characterized by oculocutaneous albinism combined with a deficiency of platelet delta granules, which leads to bleeding diathesis [50]. Ocular features include nystagmus, photophobia, decreased visual acuity, and lack of visual attention. The albinism associated with Hermansky Pudlak syndrome is more accurately described as hypopigmentation, with individuals having lighter skin, hair, and eye color than other family members. Features of the bleeding diathesis include frequent bruising, epistaxis, prolonged bleeding after minor procedures, postpartum hemorrhage, colonic bleeding, gingival bleeding, and prolonged menstruation [51, 52].

Hermansky Pudlak syndrome (HPS) is due to mutations in the genes that encode proteins involved in the biogenesis of lysosome-related organelle complexes (BLOCs), which traffic lysosome-related organelles, including melanosomes and platelet dense granules. Improper trafficking of these organelles results in the albinism and bleeding diathesis observed in HPS [52, 53]. Pathogenic variants in the *AP3B1*, *AP3D1*, *BLOC1S3*, *BLOC1S6*, *DTNBP1*, *HPS1*, *HPS3*, *HPS4*, *HPS5*, and *HPS6* genes are associated with Hermansky Pudlak syndrome and are inherited in an autosomal recessive pattern [50].

The *HPS1*, *HPS4*, and *AP3B1* genes are associated with the development of early onset pulmonary fibrosis, typically occurring during the third decade of life. Histologically, pulmonary fibrosis in Hermansky Pudlak syndrome and adult-onset idiopathic pulmonary fibrosis have similar histological features; however, the pulmonary fibrosis associated with Hermansky Pudlak syndrome has a longer survival [50, 54].

Radiographic Findings

Typical pulmonary fibrosis CT findings include patchy peripheral reticular abnormalities with intralobular linear opacities, irregular septal thickening, subpleural honeycombing, and traction bronchiectasis. Figure 9.3 is a chest CT of a young child with short telomere syndrome. The chest CT reveals patchy ground-glass opacities and nodular subpleural opacities.

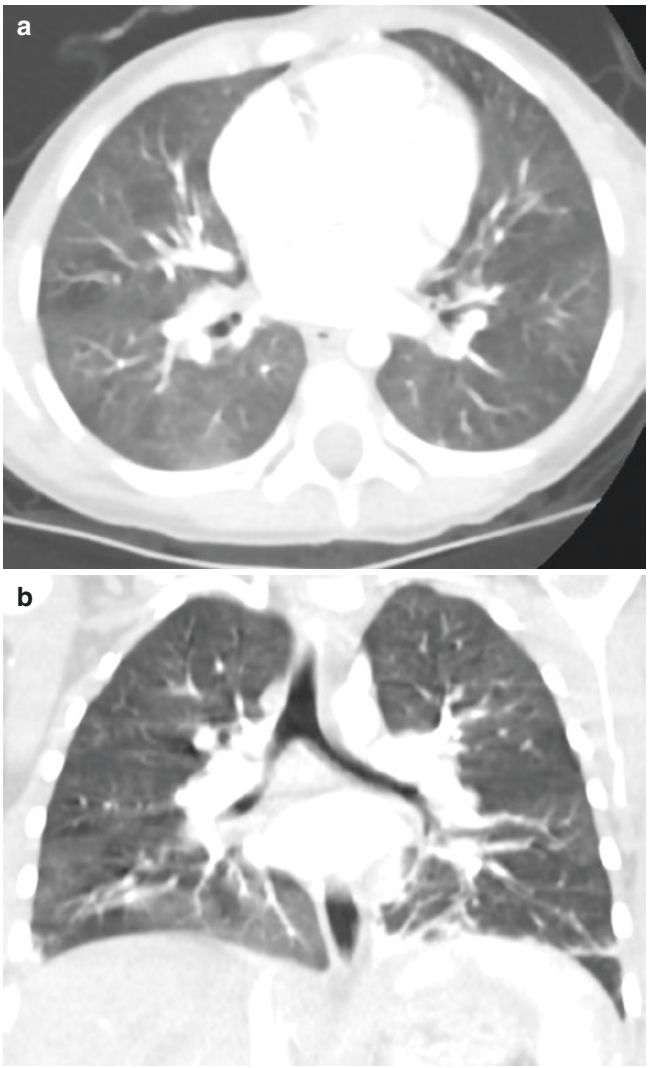

Fig. 9.3 (**a**) A young girl presented with anemia, recurrent infections, plus frequent cough and wheezing, was found to have short telomere syndrome due to a *TERT* mutation. Axial views of the chest CT reveal bilateral, patchy ground-glass opacities and atelectasis. (**b**) Coronal reconstructions of the chest CT imaging of this young girl with short telomere syndrome again show diffuse patchy ground-glass opacities and subsegmental atelectasis, underscoring the diffuse lung disease associated with the pulmonary fibrosis seen in this disease

Vascular Abnormalities

Clinical Overview

Genetic conditions associated with abnormalities of the pulmonary vasculature are a heterogeneous group of conditions affecting either the structure or function of pulmonary veins and arteries. They can be life threatening and are often associated with abnormalities of the vasculature in other parts of the body or additional syndromic features. Symptoms often include shortness of breath or exercise intolerance and may include hemoptysis. Exam findings can be variable, depending on the underlying condition.

Genetic Conditions

Alveolar Capillary Dysplasia

Alveolar capillary dysplasia with misalignment of pulmonary veins (ACD/MVP) is generally lethal within the first month of life or shortly thereafter. Affected individuals present shortly after birth with neonatal respiratory distress and pulmonary hypertension that is unresponsive to standard treatments. Respiratory issues result primarily from improperly positioned alveolar capillaries leading to defective transfer of oxygen from the alveoli to the circulation. Other developmental abnormalities, including cardiovascular, gastrointestinal, and genitourinary malformations, including atrial septal defects, intestinal malrotation, Hirschprung's disease, imperforate anus, doudenal atresia, and omphalocele, are common. [55, 56] In rare cases with a milder phenotype, later onset of a disease has been reported [57–59].

Histological features of pulmonary tissue include reduced and malpositioned alveolar wall capillaries, abnormally located pulmonary veins, deficient pulmonary lobular development, and thickening of the muscle walls of small pulmonary arteries. Some individuals also exhibit pulmonary lymphangiectasis [55].

ACD/MVP is an autosomal dominant condition resulting from mutations in the *FOXF1* gene, although often this disease occurs as a result of de novo change in this gene [60]. *FOXF1* encodes a transcription factor that impacts the function of many genes, including those involved in the development of the pulmonary mesenchyme.

Pulmonary Arterial Hypertension

Pulmonary arterial hypertension results from the narrowing and obstruction of the pulmonary arterioles, resulting in increasing pressure on the pulmonary artery as the right ventricle compensates for increased resistance in the lungs [61]. Onset of pulmonary arterial hypertension can occur at any age and is associated with a high mortality due to heart failure [62]. Initial symptoms can include dyspnea, fatigue, syncope, chest pain, palpitations, and leg edema [63, 64].

Hereditary pulmonary arterial hypertension has a similar disease course to isolated pulmonary arterial hypertension. Hereditary pulmonary arterial hypertension is characterized by markedly reduced penetrance of approximately 20% and variable expressivity [65]. Females are more likely to be affected than males; however, affected males generally have a more severe disease course [63, 66].

In the majority of cases, hereditary pulmonary arterial hypertension is caused by mutations in the *BMPR2* gene and is inherited in an autosomal dominant pattern [67]. In rare cases, pathogenic variants in other genes have been identified in individuals with pulmonary arterial hypertension. These genes include *ACVRL1*, *BMPR1B*, *CAV1*, *CBLN2*, *EIF2AK4*, *ENG*, *KCNA5*, *KCNK3*, and *SMAD9*. The *ACVRL1* and *ENG* genes are also associated with hereditary hemorrhagic telangiectasia, described below [63, 64].

Hereditary Hemorrhagic Telangiectasia

Hereditary hemorrhagic telangiectasia (HHT) is characterized by the development of multiple arteriovenous malformations (AVMs) of various sizes throughout the body. AVMs cause blood to flow directly from arteries into the veins without passing through the capillaries, which results in increased pressure on venous walls and hemorrhage. One of the most common features of HHT is recurrent epistaxis, usually beginning in childhood or adolescence and occurring in greater than 90% of HHT patients by age 30. Frequent or severe nosebleeds can lead to anemia and rarely may result in significant blood loss [68, 69].

Small AVMs, known as telangiectases, occur on the mucocutaneous surfaces of the body and can be appreciated on the lips, oral cavity, fingers, face, and chest. Telangiectases in the gastrointestinal mucosa can lead to gastrointestinal bleeding [69, 70]. Larger AVMs, most often occurring in the lungs, liver, and brain, can be life threatening. Pulmonary AVMs occur in 30–50% of individuals with HHT, and most individuals with pulmonary AVMs have HHT [71]. Features of pulmonary AVMs can include exercise intolerance, cyanosis, digital clubbing, migraine headache, pulmonary shunting, and polycythemia. Pulmonary AVMs generally increase in size over time, and serious complications include stroke, brain abscess, and transient ischemic attacks [72]. They occasionally rupture causing hemoptysis, and some individuals with pulmonary AVMs develop pulmonary arterial hypertension [71, 73]. Hepatic AVMs are common in individuals with HHT, although they are frequently asymptomatic [74, 75]. Cerebral AVMs, which can lead to hemorrhage, occur in approximately 10% of individuals and are often present from birth [69, 76].

HHT is inherited in an autosomal dominant pattern and is caused by pathogenic variants in the *ACVRL1*, *ENG*, *SMAD4*, and *GDF2* genes. A significant portion of individuals with clinical diagnoses of HHT do not have an identifiable mutation in one of these genes, suggesting that additional HHT genes may have yet to be discovered or that these individuals have another syndrome with overlapping features [70, 77].

Radiographic Findings

When suspecting abnormalities of the pulmonary vasculature, chest CT with IV contrast may offer the best view of the anatomy, although a CXR would reveal signs of enlarged cardiac silhouette or engorged pulmonary vessels. An echocardiogram is also helpful in assessing for pulmonary hypertension or, if performed in conjunction with an infusion of agitated saline, a shunt. ACD/MVP may reveal diffuse

haziness or subtle ground-glass opacities and on occasion may present with pneumothoraces [55].

Pulmonary arterial hypertension may have clear lung parenchyma but will often have a widened pulmonary artery and enlarged pulmonary vasculature.

In the case of HHT, CT imaging of the chest, completed with IV contrast, may reveal well-circumscribed areas of increased blood supply, occasionally with a feeding vessel visualized. However, the frequently very small telangiectases may not be apparent on CT. Figure 9.4a is a chest CT of an adolescent with HHT who presented with hemoptysis and was found to have numerous small AVMs, in addition to a larger AVM with a visualized feeding vessel. Figure 9.4b is a screening chest CT of a young child with HHT with small AVM in the left upper lobe.

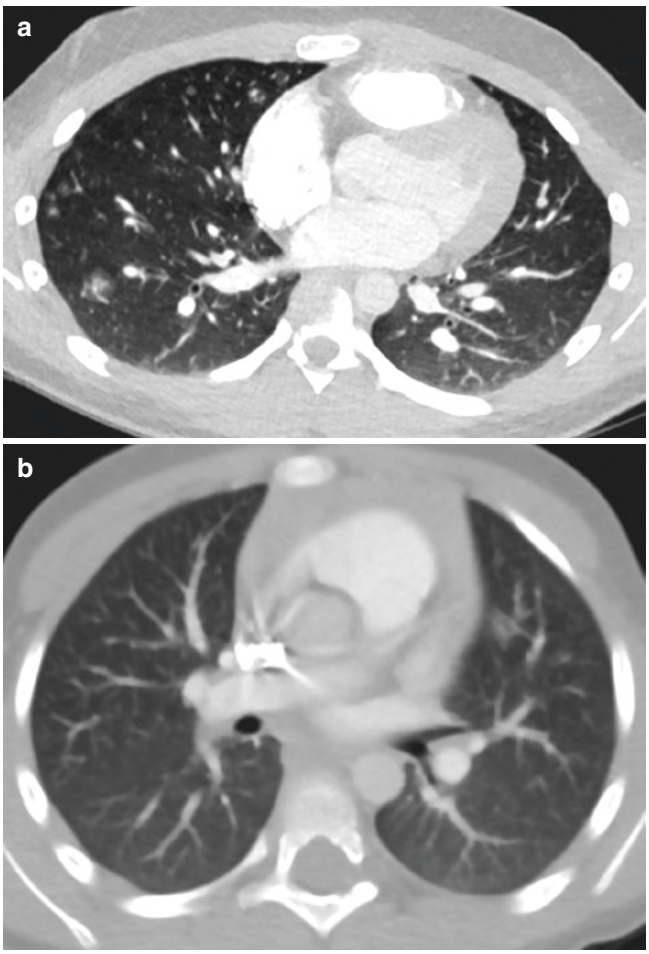

Fig. 9.4 (**a**) A teenage boy with a history of recurrent mild epistaxis presented with hemoptysis. Chest CT imaging reveals numerous nodular ground-glass opacities suggestive of small arteriovenous malformations. A feeding vessel is visualized with the posterior laterally located AV malformation. He was later found to have a de novo genetic mutation resulting in HHT. (**b**) A young child with a family history of HHT had screening chest CT imaging. This view shows an early AVM developing in the lingula

Pneumothorax

Clinical Overview

Pneumothorax is an abnormal collection of air in the pleural space of the lungs, and symptoms include dyspnea and chest pain. It is most commonly associated with emphysema, asthma, and tuberculosis. It may be spontaneous, traumatic, or related to an underlying pulmonary condition. Pneumothorax is more common in men than women. A family history of pneumothorax is present in about 10% of cases, and several genetic conditions, including various connective tissue disorders and Birt-Hogg-Dubé syndrome, can predispose individuals to pneumothorax. In these conditions, pneumothorax develops secondary to the presence of lung blebs or cysts [78].

Genetic Conditions

Connective Tissue Disorders

Connective tissue disorders are a large group of genetically and phenotypically heterogeneous disorders that commonly result in cutaneous, skeletal, and vascular abnormalities [79]. Connective tissue disorders result from mutations in genes involved in the structure or function of the primary proteins that comprise connective tissues, including collagen, elastin, and glycosaminoglycans. A subset of connective tissue disorders, including Marfan syndrome, Ehlers-Danlos syndrome, Loeys-Dietz syndrome and cutis laxa, are associated with the development of spontaneous pneumothorax.

Marfan syndrome is an autosomal dominant condition caused by mutations in the *FBN1* gene, which encodes the fibrillin protein. The condition can have variable features but is classically characterized by the involvement of the skeletal, ocular, and cardiovascular systems. Individuals with Marfan syndrome are often tall with long extremities, arachnodactyly, pectus deformities, scoliosis, and joint laxity as common skeletal features. Ocular manifestations include ectopia lentis, retinal detachment, and myopia. Cardiovascular issues, including aortic dilation, mitral valve prolapse, tricupsid valve prolapse, and enlargement of the pulmonary artery root can be life threatening [80, 81].

Ehlers-Danlos syndromes are a group of 13 disorders characterized by joint hypermobility, skin hyperextensibility, and tissue fragility [82]. Mutations in the *COL3A1* gene, which encoded type-3 collagen in the skin, lungs, intestinal walls, and vasculature walls, has been associated with an autosomal dominant form of the disease [83]. Common features of vascular Ehlers-Danlos syndrome include easy bruising; thin, translucent skin; characteristic facial features; and tissue fragility. Ruptures or dissection of arteries, gastrointestinal perforation, and organ rupture all lead to high mortality [83]. Individuals can also have hematomas and severe recurrent hemoptysis [84].

Loeys-Dietz syndrome is an autosomal dominant condition characterized by vascular, skeletal, craniofacial, and cutaneous features. Skeletal manifestations can be similar to those observed in Marfan syndrome patients and include pectus deformities, scoliosis, joint laxity, arachnodactyly, and talipes equinovarus. Vascular complications are the most common cause of death in Loeys-Dietz syndrome. Aortic dilation is present in more than 95% of individuals with Loeys-Dietz syndrome and can lead to aortic dissection. Arterial aneurysms and tortuosity can also be present in other parts of the body. Craniofacial features include hypertelorism, bifid uvula, cleft palate, and craniosynostosis, while cutaneous findings include velvety, translucent skin, easy bruising, and dystrophic scarring. Pneumothoraces and restrictive lung disease have also been reported, although the prevalence of these manifestations in Loeys-Dietz syndrome patients is unknown [85, 86]. Most cases of Loeys-Dietz syndrome are caused by mutations in the *TGFBR1* and *TGFBR2* genes [85].

Cutis laxa is a connective tissue disorder characterized by loose, saggy, inelastic skin, which is particularly noticeable around the neck, armpits, and groin. Additional features include inguinal, umbilical, and diaphragmatic hernia; visceral diverticula; joint hypermobility; developmental issues; and cardiovascular involvement. Pulmonary manifestations include neonatal or childhood onset emphysema, which can be severe and progressive, laryngomalacia, tracheomalacia, bronchomalacia, bronchiolitis, and pulmonary hypertension. Pneumothorax can occur secondary to emphysematous lung disease. The *FBLN5*, *EFEMP2*, *LTBP4*, and *ELN* genes are associated with cutis laxa with emphysema. *EFEMP2* and *LTBP4* are associated with autosomal recessive cutis laxa, while *FBLN5* mutations can be inherited in an autosomal dominant or recessive pattern [87–89]. Cutis laxa associated with the *ELN* gene can be caused by autosomal dominant sequence variants in the *ELN* gene or as part of Williams syndrome, which results from a microdeletion at 7q11.23 that encompasses the *ELN* gene [90].

Birt-Hogg-Dubé Syndrome

Birt-Hogg-Dubé syndrome is an autosomal dominant condition caused by mutations in the *FLCN* gene, which encodes the folliculin protein [91]. Birt-Hogg-Dubé syndrome primarily affects the skin, lungs, and kidneys. Although the penetrance of Birt-Hogg-Dubé syndrome is high, the clinical presentation and severity of disease is variable, and Birt-Hogg-Dubé syndrome is thought in general to be underdiagnosed [91, 92].

Skin manifestations consist of a spectrum of cutaneous hamartomas, including fibrofolliculomas, trichodiscomas, and acrochordons. Fibrofolliculomas are the most common skin finding and usually appear on the face, neck and upper trunk. Onset of skin lesions is usually in adulthood, and they are usually benign growths [93].

Individuals with Birt-Hogg-Dubé syndrome are at an estimated 15–30% risk for renal tumors, and thus the diagnosis of Birt-Hogg-Dubé syndrome should prompt kidney screening. Oncocytic hybrid tumors, chromophobe renal cell carcinoma, and renal oncocytomas are the most common tumors observed in Birt-Hogg-Dubé syndrome patients. The average age of diagnosis of kidney tumors is 48 years old, and kidney tumors associated with Birt-Hogg-Dubé syndrome are generally slow growing. In addition, many individuals with Birt-Hogg-Dubé syndrome are found to have renal cysts on imaging [91, 94].

Radiographic Findings

Pneumothorax is the most common radiographic finding in patients with genetic etiologies for each of the connective tissue disease, which can be spontaneous and recurrent. Approximately 5–10% of individuals with Marfan syndrome will develop pneumothorax. Imaging may also reveal the presence of apical blebs or bullae, connective tissue abnormalities in the lung parenchyma, or mechanical stress on the lung apices due to tall habitus [95]. Individuals with Marfan syndrome can also have additional pulmonary manifestations, including cystic changes, emphysema, bronchiectasis, congenital malformations, and fibrosis [96].

Hemothorax and hemopneumothorax have been reported in individuals with Ehlers-Danlos syndrome and are often associated with pulmonary blebs, cystic lesions, or lung nodules [82].

The majority of individuals with Birt-Hogg-Dubé syndrome have bilateral, multifocal basal lung cysts. Birt-Hogg-Dubé syndrome patients with lung cysts are often asymptomatic, but they are at high risk to develop pneumothoraces that can be recurrent. Pneumothoraces primarily occur in adulthood but can also occur in adolescence, in which case they are often the presenting feature of Birt-Hogg-Dubé syndrome. Some families with Birt-Hogg-Dubé syndrome present with isolated recurrent pneumothorax as the only disease manifestation [97, 98]. Figure 9.5 is a chest CT of an individual with Birt-Hogg-Dubé syndrome who presented with spontaneous pneumothorax. Chest tubes are in place, allowing the lung to reexpand, revealing an air-filled cyst along the right major fissure.

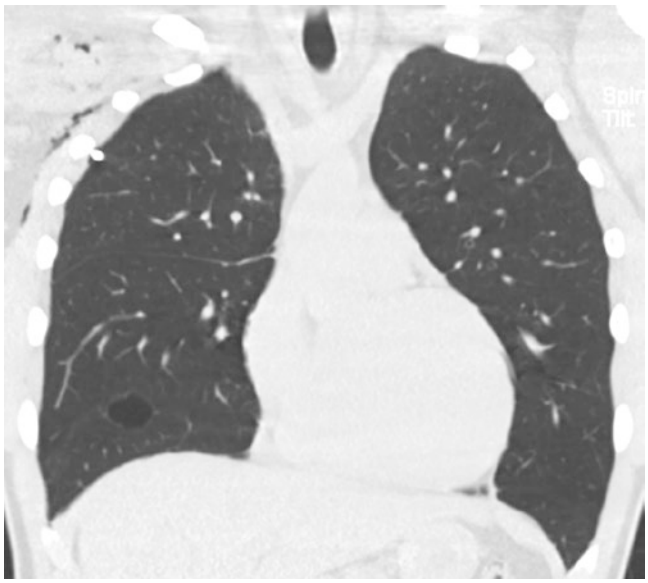

Fig. 9.5 A teenage boy with a family history of pneumothorax presented with acute pneumothorax requiring chest tube placement. Chest CT was completed upon reexpansion of his lungs, and he was found to have an air-filled cyst along the right major fissure. Given the family history, plus the location of the cyst, genetic testing for Birt-Hogg-Dubé was sent, which revealed a pathogenic mutation. Incidental note is made of subcutaneous air in the right axilla

Summary

As genetic mutations are becoming increasingly identified in pulmonary disease, clinical providers are better able to phenotype and characterize diseases. Understanding genetic etiologies of disease may aid the assessment of key diagnostic features. Conversely, improving phenotypic descriptions of gene-specific diseases may allow a better understanding of disease pathology. In summary, genetics is becoming an integral aspect to all medical specialties, including radiology. For an additional discussion of related issues, please refer to Chap. 6 (Pediatric Congenital and Miscellaneous Abnormalities), Chap. 8 (Pediatric Diffuse Lung Disorders), Chap. 11 (Pleural Effusion and Pneumothorax), Chap. 12 (Pulmonary Hypertension), Chap. 13 (Pulmonary Venous Drainage Disorders), and Chap. 18 (Cystic Fibrosis).

References

1. Griese M. Pulmonary surfactant in health and human lung diseases: state of the art. Eur Respir J. 1999;13:1455–76.
2. Whitsett JA, Wert SE, Weaver TE. Diseases of pulmonary surfactant homeostasis. Annu Rev Pathol. 2015;10:371–93. https://doi.org/10.1146/annurev-pathol-012513-104644.
3. Kroner C, et al. Lung disease caused by ABCA3 mutations. Thorax. 2017;72:213–20. https://doi.org/10.1136/thoraxjnl-2016-208649.
4. Turcu S, Ashton E, Jenkins L, Gupta A, Mok Q. Genetic testing in children with surfactant dysfunction. Arch Dis Child. 2013;98:490–5. https://doi.org/10.1136/archdischild-2012-303166.
5. Kroner C, et al. Genotype alone does not predict the clinical course of SFTPC deficiency in paediatric patients. Eur Respir J. 2015;46:197–206. https://doi.org/10.1183/09031936.00129414.
6. Gras D, et al. Benign hereditary chorea: phenotype, prognosis, therapeutic outcome and long term follow-up in a large series with new mutations in the TITF1/NKX2-1 gene. J Neurol Neurosurg Psychiatry. 2012;83:956–62. https://doi.org/10.1136/jnnp-2012-302505.
7. Patel NJ, Jankovic J. NKX2-1-related disorders. In Adam MP, et al., editors. GeneReviews. University of Washington. 2016.
8. de Gusmao CM, Kok F, Casella EB, Waugh JL. Benign hereditary chorea related to NKX2-1 with ataxia and dystonia. Neurol Genet. 2016;2:e40. https://doi.org/10.1212/NXG.0000000000000040.
9. Carre A, et al. Five new TTF1/NKX2.1 mutations in brain-lung-thyroid syndrome: rescue by PAX8 synergism in one case. Hum Mol Genet. 2009;18:2266–76. https://doi.org/10.1093/hmg/ddp162.
10. Nattes E, et al. Heterogeneity of lung disease associated with NK2 homeobox 1 mutations. Respir Med. 2017;129:16–23. https://doi.org/10.1016/j.rmed.2017.05.014.
11. Guillot L, et al. NKX2-1 mutations leading to surfactant protein promoter dysregulation cause interstitial lung disease in "brain-lung-thyroid syndrome". Hum Mutat. 2010;31:E1146–62. https://doi.org/10.1002/humu.21183.
12. Young LR, Deutsch GH, Bokulic RE, Brody AS, Nogee LM. A mutation in TTF1/NKX2.1 is associated with familial neuroendocrine cell hyperplasia of infancy. Chest. 2013;144:1199–206. https://doi.org/10.1378/chest.13-0811.
13. Trapnell BC, Whitsett JA, Nakata K. Pulmonary alveolar proteinosis. N Engl J Med. 2003;349:2527–39. https://doi.org/10.1056/NEJMra023226.
14. Carrington JM, Hershberger DM. Pulmonary Alveolar Proteinosis. StatPearls Publishing. 2019.
15. Griese M. Pulmonary alveolar Proteinosis: a comprehensive clinical perspective. Pediatrics. 2017;140 https://doi.org/10.1542/peds.2017-0610.
16. Nathan N, Borensztajn K, Clement A. Genetic causes and clinical management of pediatric interstitial lung diseases. Curr Opin Pulm Med. 2018;24:253–9. https://doi.org/10.1097/MCP.0000000000000471.
17. Liszewski MC, Stanescu AL, Phillips GS, Lee EY. Respiratory distress in neonates: underlying causes and current imaging assessment. Radiol Clin N Am. 2017;55:629–44. https://doi.org/10.1016/j.rcl.2017.02.006.
18. Hamvas A, et al. Heterogeneous pulmonary phenotypes associated with mutations in the thyroid transcription factor gene NKX2-1. Chest. 2013;144:794–804. https://doi.org/10.1378/chest.12-2502.
19. Schafer J, Griese M, Chandrasekaran R, Chotirmall SH, Hartl D. Pathogenesis, imaging and clinical characteristics of CF and non-CF bronchiectasis. BMC Pulm Med. 2018;18:79. https://doi.org/10.1186/s12890-018-0630-8.
20. Davis SD, et al. Clinical features of childhood primary ciliary dyskinesia by genotype and ultrastructural phenotype. Am J Respir Crit Care Med. 2015;191:316–24. https://doi.org/10.1164/rccm.201409-1672OC.
21. Zariwala MA, Knowles MR, Leigh MW. Cystic fibrosis and congenital absence of the vas deferens. In Adam MP, et al., editors. GeneReviews. University of Washington. 2017.
22. Zhu L, Belmont JW, Ware SM. Genetics of human heterotaxias. Eur J Hum Genet. 2006;14:17–25. https://doi.org/10.1038/sj.ejhg.5201506.
23. Shapiro AJ, et al. Diagnosis of primary ciliary dyskinesia. An official American Thoracic Society Clinical Practice Guideline. Am J

Respir Crit Care Med. 2018;197:e24–39. https://doi.org/10.1164/rccm.201805-0819ST.
24. Zariwala MA, Omran H, Ferkol TW. The emerging genetics of primary ciliary dyskinesia. Proc Am Thorac Soc. 2011;8:430–3. https://doi.org/10.1513/pats.201103-023SD.
25. Horani A, Ferkol TW. Primary ciliary dyskinesia and associated sensory ciliopathies. Expert Rev Respir Med. 2016;10:569–76. https://doi.org/10.1586/17476348.2016.1165612.
26. Horani A, Ferkol TW. Advances in the genetics of primary ciliary dyskinesia: clinical implications. Chest. 2018; https://doi.org/10.1016/j.chest.2018.05.007.
27. Boyle JM, Buckley RH. Population prevalence of diagnosed primary immunodeficiency diseases in the United States. J Clin Immunol. 2007;27:497–502. https://doi.org/10.1007/s10875-007-9103-1.
28. Nonas S. Pulmonary manifestations of primary immunodeficiency disorders. Immunol Allergy Clin N Am. 2015;35:753–66. https://doi.org/10.1016/j.iac.2015.07.004.
29. Picard C, et al. Primary immunodeficiency diseases: an update on the classification from the International Union of Immunological Societies Expert Committee for Primary Immunodeficiency 2015. J Clin Immunol. 2015;35:696–726. https://doi.org/10.1007/s10875-015-0201-1.
30. Raje N, Dinakar C. Overview of immunodeficiency disorders. Immunol Allergy Clin N Am. 2015;35:599–623. https://doi.org/10.1016/j.iac.2015.07.001.
31. Chinn IK, Shearer WT. Severe combined immunodeficiency disorders. Immunol Allergy Clin N Am. 2015;35:671–94. https://doi.org/10.1016/j.iac.2015.07.002.
32. Kwan A, et al. Newborn screening for severe combined immunodeficiency in 11 screening programs in the United States. JAMA. 2014;312:729–38. https://doi.org/10.1001/jama.2014.9132.
33. Resnick ES, Cunningham-Rundles C. The many faces of the clinical picture of common variable immune deficiency. Curr Opin Allergy Clin Immunol. 2012;12:595–601. https://doi.org/10.1097/ACI.0b013e32835914b9.
34. Sathkumara HD, De Silva NR, Handunnetti S, De Silva AD. Genetics of common variable immunodeficiency: role of transmembrane activator and calcium modulator and cyclophilin ligand interactor. Int J Immunogenet. 2015;42:239–53. https://doi.org/10.1111/iji.12217.
35. King JR, Hammarstrom L. Newborn screening for primary immunodeficiency diseases: history, current and future practice. J Clin Immunol. 2018;38:56–66. https://doi.org/10.1007/s10875-017-0455-x.
36. Robinson P, Morgan L. Bronchiectasis in PCD looks different to CF on CT scan. Multidiscip Respir Med. 2018;13:24. https://doi.org/10.1186/s40248-018-0139-2.
37. American Thoracic Society. Idiopathic pulmonary fibrosis: diagnosis and treatment. International consensus statement. American Thoracic Society (ATS), and the European Respiratory Society (ERS). Am J Respir Crit Care Med. 2000;161:646–64. https://doi.org/10.1164/ajrccm.161.2.ats3-00.
38. Gross TJ, Hunninghake GW. Idiopathic pulmonary fibrosis. N Engl J Med. 2001;345:517–25. https://doi.org/10.1056/NEJMra003200.
39. Herrmann M, Pusceddu I, Marz W, Herrmann W. Telomere biology and age-related diseases. Clin Chem Lab Med. 2018;56:1210–22. https://doi.org/10.1515/cclm-2017-0870.
40. Armanios M. Syndromes of telomere shortening. Annu Rev Genomics Hum Genet. 2009;10:45–61. https://doi.org/10.1146/annurev-genom-082908-150046.
41. Savage SA, Bertuch AA. The genetics and clinical manifestations of telomere biology disorders. Genet Med. 2010;12:753–64. https://doi.org/10.1097/GIM.0b013e3181f415b5.
42. Alter BP, et al. Telomere length is associated with disease severity and declines with age in dyskeratosis congenita. Haematologica. 2012;97:353–9. https://doi.org/10.3324/haematol.2011.055269.
43. Savage SA. Dyskeratosis congenita. In Adam MP et al., editors. GeneReviews. University of Washington. 2016.
44. Barbaro PM, Ziegler DS, Reddel RR. The wide-ranging clinical implications of the short telomere syndromes. Intern Med J. 2016;46:393–403. https://doi.org/10.1111/imj.12868.
45. Armanios MY, et al. Telomerase mutations in families with idiopathic pulmonary fibrosis. N Engl J Med. 2007;356:1317–26. https://doi.org/10.1056/NEJMoa066157.
46. Patnaik MM, Kamath PS, Simonetto DA. Hepatic manifestations of telomere biology disorders. J Hepatol. 2018;69:736–43. https://doi.org/10.1016/j.jhep.2018.05.006.
47. Vulliamy TJ, Dokal I. Dyskeratosis congenita: the diverse clinical presentation of mutations in the telomerase complex. Biochimie. 2008;90:122–30. https://doi.org/10.1016/j.biochi.2007.07.017.
48. Alter BP, Giri N, Savage SA, Rosenberg PS. Cancer in dyskeratosis congenita. Blood. 2009;113:6549–57. https://doi.org/10.1182/blood-2008-12-192880.
49. Alder JK, et al. Short telomeres are a risk factor for idiopathic pulmonary fibrosis. Proc Natl Acad Sci U S A. 2008;105:13051–6. https://doi.org/10.1073/pnas.0804280105.
50. El-Chemaly S, Young LR. Hermansky-Pudlak syndrome. Clin Chest Med. 2016;37:505–11. https://doi.org/10.1016/j.ccm.2016.04.012.
51. Huizing M, Helip-Wooley A, Westbroek W, Gunay-Aygun M, Gahl WA. Disorders of lysosome-related organelle biogenesis: clinical and molecular genetics. Annu Rev Genomics Hum Genet. 2008;9:359–86. https://doi.org/10.1146/annurev.genom.9.081307.164303.
52. Huizing M, Malicdan MCV, Gochuico BR, Gahl WA. Hermansky-Pudlak syndrome. In Adam MP, et al., editors. GeneReviews. University of Washington. 2017.
53. Di Pietro SM, Dell'Angelica EC. The cell biology of Hermansky-Pudlak syndrome: recent advances. Traffic. 2005;6:525–33. https://doi.org/10.1111/j.1600-0854.2005.00299.x.
54. Vicary GW, Vergne Y, Santiago-Cornier A, Young LR, Roman J. Pulmonary fibrosis in Hermansky-Pudlak syndrome. Ann Am Thorac Soc. 2016;13:1839–46. https://doi.org/10.1513/AnnalsATS.201603-186FR.
55. Bishop NB, Stankiewicz P, Steinhorn RH. Alveolar capillary dysplasia. Am J Respir Crit Care Med. 2011;184:172–9. https://doi.org/10.1164/rccm.201010-1697CI.
56. Goel D, Oei JL, Shand AW, Mowat D, Loo C. FOXF1 gene mutation in alveolar capillary dysplasia associated with Hirschsprung's disease and clinical review. J Paediatr Child Health. 2016;52:787–8. https://doi.org/10.1111/jpc.13191.
57. Antao B, Samuel M, Kiely E, Spitz L, Malone M. Congenital alveolar capillary dysplasia and associated gastrointestinal anomalies. Fetal Pediatr Pathol. 2006;25:137–45. https://doi.org/10.1080/15513810600908230.
58. Sen P, et al. Novel FOXF1 mutations in sporadic and familial cases of alveolar capillary dysplasia with misaligned pulmonary veins imply a role for its DNA binding domain. Hum Mutat. 2013;34:801–11. https://doi.org/10.1002/humu.22313.
59. Goel D, et al. Antenatal gastrointestinal anomalies in neonates subsequently found to have alveolar capillary dysplasia. Clin Case Rep. 2017;5:559–66. https://doi.org/10.1002/ccr3.888.
60. Nogee LM. Interstitial lung disease in newborns. Semin Fetal Neonatal Med. 2017;22:227–33. https://doi.org/10.1016/j.siny.2017.03.003.
61. Hoeper MM, et al. Definitions and diagnosis of pulmonary hypertension. J Am Coll Cardiol. 2013;62:D42–50. https://doi.org/10.1016/j.jacc.2013.10.032.

62. D'Alonzo GE, et al. Survival in patients with primary pulmonary hypertension. Results from a national prospective registry. Ann Intern Med. 1991;115:343–9.
63. Austin ED, Loyd JE, Phillips III JA. Heritable pulmonary arterial hypertension. In Adam et al., editors. GeneReviews. University of Washington. 2015.
64. Dodson MW, Brown LM, Elliott CG. Pulmonary arterial hypertension. Heart Fail Clin. 2018;14:255–69. https://doi.org/10.1016/j.hfc.2018.02.003.
65. Newman JH, et al. Mutation in the gene for bone morphogenetic protein receptor II as a cause of primary pulmonary hypertension in a large kindred. N Engl J Med. 2001;345:319–24. https://doi.org/10.1056/NEJM200108023450502.
66. Larkin EK, et al. Longitudinal analysis casts doubt on the presence of genetic anticipation in heritable pulmonary arterial hypertension. Am J Respir Crit Care Med. 2012;186:892–6. https://doi.org/10.1164/rccm.201205-0886OC.
67. Machado RD, et al. Genetics and genomics of pulmonary arterial hypertension. J Am Coll Cardiol. 2009;54:S32–42. https://doi.org/10.1016/j.jacc.2009.04.015.
68. Berg J, et al. Hereditary haemorrhagic telangiectasia: a questionnaire based study to delineate the different phenotypes caused by endoglin and ALK1 mutations. J Med Genet. 2003;40:585–90.
69. McDonald J, Bayrak-Toydemir P, Pyeritz RE. Hereditary hemorrhagic telangiectasia: an overview of diagnosis, management, and pathogenesis. Genet Med. 2011;13:607–16. https://doi.org/10.1097/GIM.0b013e3182136d32.
70. McDonald J, Pyeritz RE. Hereditary hemorrhagic telangiectasia. In Adam MP et al., editors. GeneReviews. University of Washington. 2017.
71. Ishiwata T, et al. Pulmonary arterial hypertension as the first manifestation in a patient with hereditary hemorrhagic telangiectasia. Intern Med. 2014;53:2359–63.
72. Kroon S, Snijder RJ, Faughnan ME, Mager HJ. Systematic screening in hereditary hemorrhagic telangiectasia: a review. Curr Opin Pulm Med. 2018;24:260–8. https://doi.org/10.1097/MCP.0000000000000472.
73. Dupuis-Girod S, Cottin V, Shovlin CL. The lung in hereditary hemorrhagic telangiectasia. Respiration. 2017;94:315–30. https://doi.org/10.1159/000479632.
74. Ianora AA, et al. Hereditary hemorrhagic telangiectasia: multi-detector row helical CT assessment of hepatic involvement. Radiology. 2004;230:250–9. https://doi.org/10.1148/radiol.2301021745.
75. Buscarini E, et al. Doppler ultrasonographic grading of hepatic vascular malformations in hereditary hemorrhagic telangiectasia – results of extensive screening. Ultraschall Med. 2004;25:348–55. https://doi.org/10.1055/s-2004-813549.
76. Kritharis A, Al-Samkari H, Kuter DJ. Hereditary hemorrhagic telangiectasia: diagnosis and management from the hematologist's perspective. Haematologica. 2018;103:1433–43. https://doi.org/10.3324/haematol.2018.193003.
77. Richards-Yutz J, Grant K, Chao EC, Walther SE, Ganguly A. Update on molecular diagnosis of hereditary hemorrhagic telangiectasia. Hum Genet. 2010;128:61–77. https://doi.org/10.1007/s00439-010-0825-4.
78. Scott RM, et al. Familial pneumothorax: towards precision medicine. Thorax. 2018;73:270–6. https://doi.org/10.1136/thoraxjnl-2017-211169.
79. Armon K, Bale P. Identifying heritable connective tissue disorders in childhood. Practitioner. 2012;256:19–23., 12–13.
80. Judge DP, Dietz HC. Marfan's syndrome. Lancet. 2005;366:1965–76. https://doi.org/10.1016/S0140-6736(05)67789-6.
81. Dietz H. Marfan syndrome. In Adam MP, et al., editors. GeneReviews. University of Washington. 2017.
82. Malfait F, et al. The 2017 international classification of the Ehlers-Danlos syndromes. Am J Med Genet C Semin Med Genet. 2017;175:8–26. https://doi.org/10.1002/ajmg.c.31552.
83. Pepin MG, Murray ML, Byers PH. Vascular Ehlers-Danlos syndrome. In Adam MP, et al., editors. GeneReviews. University of Washington. 2019.
84. Hatake K, et al. Respiratory complications of Ehlers-Danlos syndrome type IV. Leg Med (Tokyo). 2013;15:23–7. https://doi.org/10.1016/j.legalmed.2012.07.005.
85. Loeys BL, Dietz HC. Loeys-Dietz syndrome. In Adam MP, et al., editos. GeneReviews. University of Washington. 2018.
86. MacCarrick G, et al. Loeys-Dietz syndrome: a primer for diagnosis and management. Genet Med. 2014;16:576–87. https://doi.org/10.1038/gim.2014.11.
87. Berk DR, Bentley DD, Bayliss SJ, Lind A, Urban Z. Cutis laxa: a review. J Am Acad Dermatol. 2012;66(842):e841–17. https://doi.org/10.1016/j.jaad.2011.01.004.
88. Urban Z, Davis EC. Cutis laxa: intersection of elastic fiber biogenesis, TGFbeta signaling, the secretory pathway and metabolism. Matrix Biol. 2014;33:16–22. https://doi.org/10.1016/j.matbio.2013.07.006.
89. Vanakker O, Callewaert B, Malfait F, Coucke P. The genetics of soft connective tissue disorders. Annu Rev Genomics Hum Genet. 2015;16:229–55. https://doi.org/10.1146/annurev-genom-090314-050039.
90. Duque Lasio ML, Kozel BA. Elastin-driven genetic diseases. Matrix Biol. 2018; https://doi.org/10.1016/j.matbio.2018.02.021.
91. Toro JR. Birt-Hogg-Dubé syndrome. In Adam MP, et al., editors. GeneReviews. University of Washington. 2014.
92. Gupta N, Sunwoo BY, Kotloff RM. Birt-Hogg-Dube syndrome. Clin Chest Med. 2016;37:475–86. https://doi.org/10.1016/j.ccm.2016.04.010.
93. Tong Y, Schneider JA, Coda AB, Hata TR, Cohen PR. Birt-Hogg-Dube syndrome: a review of dermatological manifestations and other symptoms. Am J Clin Dermatol. 2018;19:87–101. https://doi.org/10.1007/s40257-017-0307-8.
94. Gupta S, et al. The ABCs of BHD: an in-depth review of Birt-Hogg-Dube syndrome. AJR Am J Roentgenol. 2017;209:1291–6. https://doi.org/10.2214/AJR.17.18071.
95. Hao W, et al. Marfan syndrome with pneumothorax: case report and review of literatures. J Thorac Dis. 2017;9:E1100–3. https://doi.org/10.21037/jtd.2017.11.66.
96. Dyhdalo K, Farver C. Pulmonary histologic changes in Marfan syndrome: a case series and literature review. Am J Clin Pathol. 2011;136:857–63. https://doi.org/10.1309/AJCP79SNDHGKQFIN.
97. Toro JR, et al. BHD mutations, clinical and molecular genetic investigations of Birt-Hogg-Dube syndrome: a new series of 50 families and a review of published reports. J Med Genet. 2008;45:321–31. https://doi.org/10.1136/jmg.2007.054304.
98. Frohlich BA, et al. Novel mutations in the folliculin gene associated with spontaneous pneumothorax. Eur Respir J. 2008;32:1316–20. https://doi.org/10.1183/09031936.00132707.

Pediatric Airway

10

Robert H. Cleveland, Edward Y. Lee,
Mary Shannon Fracchia, and Dennis Rosen

In addition to the various developmental and normal physiologic factors that influence the airway [1–4] (see Chap. 3), certain diseases and congenital defects may cause structural abnormalities. Many of these defects present with upper airway obstruction. The differential diagnosis for extrathoracic airway obstruction is extensive and includes obstructions of the nasal passages, oropharynx, larynx, and the glottis. Anatomic abnormalities of the chin and tongue include micrognathia and macroglossia, while obstruction of the nasopharynx may be caused by nasal polyps or persistence of the bucconasal membrane, as seen in choanal atresia (Fig. 10.1a) [5] or nasal piriform aperture stenosis (Fig. 10.1b). Within the oropharynx, adenotonsillar enlargement (Fig. 10.2), as well as peritonsillar and retropharyngeal abscesses, may obstruct the airway.

Obstructive sleep apnea (OSA) is a condition wherein the upper airway undergoes partial or total collapse during inspiration, resulting in a significant (greater than 50%) decrease in airflow [6]. The decrease in airflow during the obstructive event(s) may lead to a decrease in the hemoglobin oxygen saturation (SaO_2) or to an increase in end tidal carbon dioxide ($ETCO_2$) levels, prompting autonomic, physical, and electroencephalographic (EEG) arousals. OSA has been associated with a large array of short- and long-term behavioral and metabolic deficits and disorders.

R. H. Cleveland (✉)
Department of Radiology, Harvard Medical School, Boston Children's Hospital, Boston, MA, USA
e-mail: Robert.Cleveland@childrens.harvard.edu

E. Y. Lee
Department of Radiology, Boston Children's Hospital and Harvard Medical School, Boston, MA, USA

M. S. Fracchia
Department of Pediatric Pulmonary, Massachusetts General Hospital, Harvard Medical School, Boston, MA, USA

D. Rosen
Division of Pulmonary Medicine, Boston Children's Hospital and Harvard Medical School, Boston, MA, USA

There are many causes of OSA, often acting in combination, which can include adenotonsillar hypertrophy; gastroesophageal reflux disease (GERD) or environmental tobacco smoke exposure with resultant inflammation of the soft tissues of the upper airway, low muscle tone, attenuated upper airway reflexes to PCO_2 and negative pressure stimuli, craniofacial dysplasia, and mandibular hypoplasia. OSA is present in 2–4% [7] of the pediatric population and is more prevalent in obese children [8] and those with central hypotonia, craniofacial, and chromosomal abnormalities [9].

The diagnosis of OSA is made by a sleep study, also termed polysomnography, which entails parallel determination of multiple physiological parameters (EEG, EKG, EMG), eye movements, pulse oximetry, $ETCO_2$ levels, air flow, and respiratory effort while the subject sleeps [10]. A lateral neck film (Fig. 10.2) is sometimes used to assess for evidence of adenoidal or tonsillar hypertrophy, but this is not considered a sensitive modality for diagnosing OSA [11] since it does not account for sleep-related dynamic changes in airway patency.

In children, the first line of therapy for OSA is removal of the adenoids and tonsils. This is curative in as many as 85–90% of children with OSA [12]. However, in certain segments of the pediatric population, including older and obese children [13]; those with craniofacial abnormalities [14], chromosomal disorders, and central hypotonia; and some who are otherwise healthy children, this surgery is not sufficient, and further treatment is necessary. In these cases, continuous positive airway pressure (CPAP) while sleeping is usually prescribed.

Common causes of extrathoracic obstruction at the larynx include laryngomalacia and laryngostenosis. Laryngomalacia is the most common cause of stridor in children under two and results from delayed maturation of the supporting structures of the larynx [5]. A flaccid epiglottis, arytenoids, and aryepiglottic folds prolapse into the airway during inspiration. The malacia is pronounced when supine or agitated. Although this is a relatively common abnormality, it is difficult to accurately document with radiologic imaging, and so the diagnosis is

R. H. Cleveland, E. Y. Lee (eds.), *Imaging in Pediatric Pulmonology*, https://doi.org/10.1007/978-3-030-23979-4_10

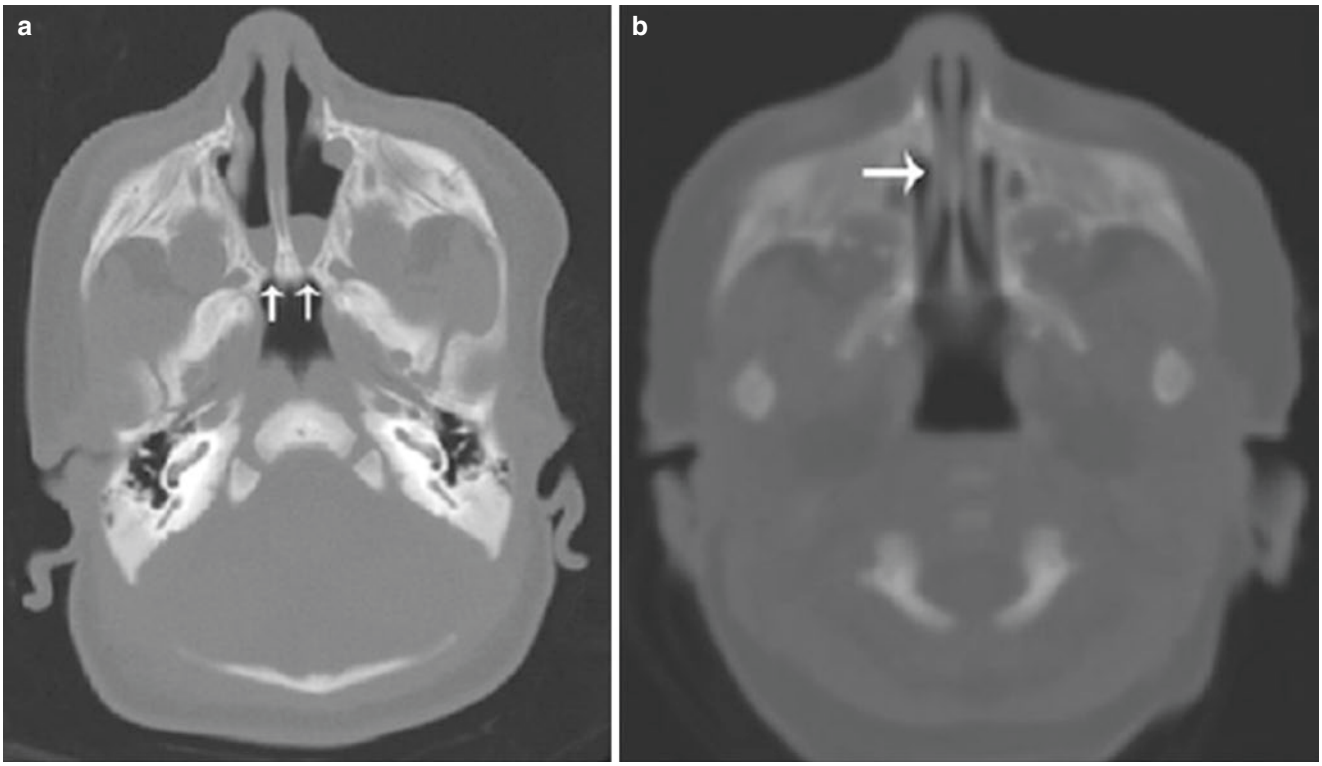

Fig. 10.1 (**a**) Choanal atresia is caused by bony or soft tissue obstruction of the posterior (*arrows*) nasopharynx. (**b**) Nasal piriform aperture stenosis causes relatively anterior (*arrow*) obstruction of the nasal passages

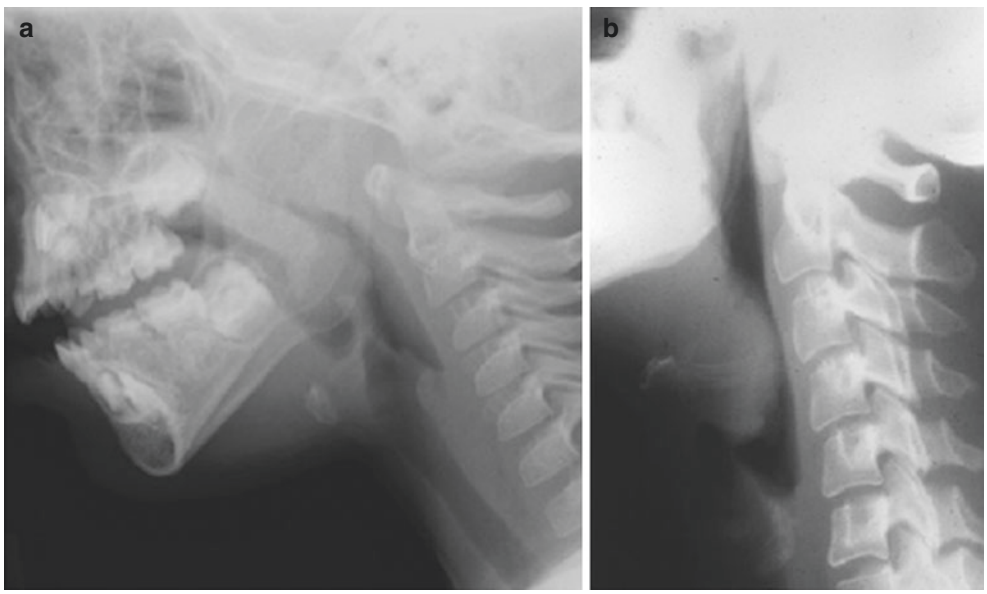

Fig. 10.2 (**a**) Large hypertrophied tonsils and adenoids are often the cause of obstruction in otherwise normal children. (**b**) There are enlarged pharyngeal tonsils in this child with infectious mononucleosis (similarly enlarged tonsils may be seen with lymphoma)

usually made by laryngoscopy. Laryngostenosis is a congenital or acquired narrowing of the airway, often termed subglottic stenosis. Although it may be congenital, it most commonly occurs after endotracheal intubation.

A lingual thyroid, due to failure of thyroid descent, may cause obstruction in the midline (Fig. 10.3). Remnants of the thyroglossal duct may form a cyst, which presents as a smooth mass in the midline of the neck and typically moves upward when the tongue is protruded [5]. Laryngoceles, webs, and cysts are rarer causes of midline obstruction. A web results from failure of the embryonic airway to recanalize, while a cyst occurs in the aryepiglottic fold and contains mucus from salivary glands. A laryngocele arises as a dilatation of the saccule of the laryngeal ventricle [5].

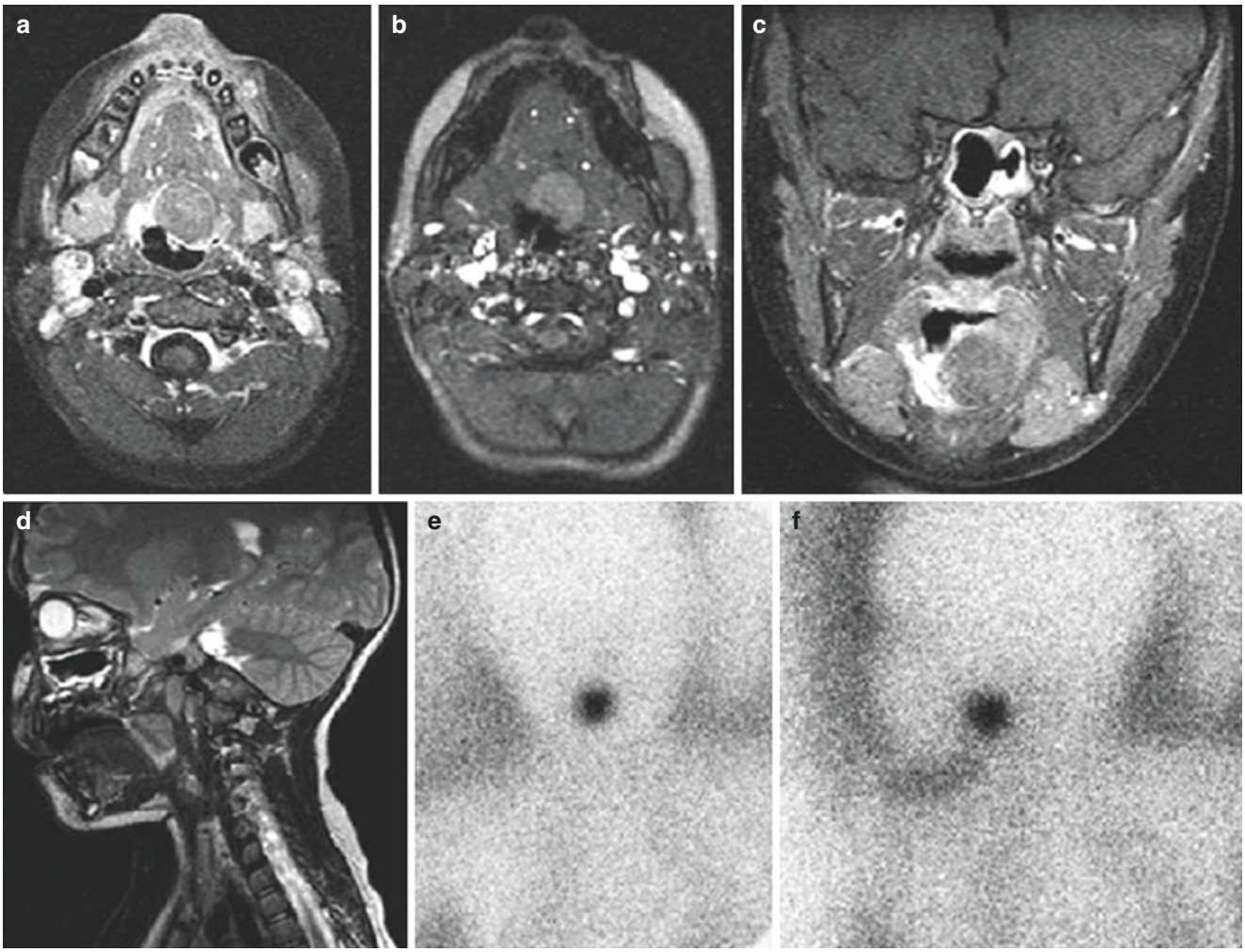

Fig. 10.3 A lingual thyroid is demonstrated posteriorly, slightly to the left of midline. (**a**) Cross-section MRI, T1 post gadolinium with fat suppression. (**b**) Cross-section MRI, SPGR. (**c**) Coronal MRI T1 postgadolinium with fat suppression. (**d**) Sagittal MRI T2 FSE with fat suppression. (**e**) 1^{123} radionuclide study in frontal projection. (**f**) 1^{123} radionuclide study in lateral projection

Vallecular cysts are rare causes of upper airway obstruction. They usually present at birth or within the first week of life. Presenting symptoms range from hoarse cry, inspiratory stridor, apnea, and cyanosis to chest retractions, feeding difficulties, reflux, and failure to thrive [15]. Laryngomalacia is a common association [16]. Vallecular cysts are usually assessed by laryngoscopy and are seen on the lingual surface of the epiglottis obstructing the upper airway [17, 18]. They may be detected by ultrasound (Fig. 10.4) or cross-sectional imaging. Careful visualization of the base of the tongue is imperative to visualize the cyst. The differential includes thyroglossal cysts, as well as dermoid cysts, hemangiomas, and lymphatic malformations (cystic hygromas) [19]. Lymphatic malformations are collections of lymphatic sacs that contain clear, colorless lymph, while a hemangioma is the collection of blood vessels located submucosally in the subglottic region.

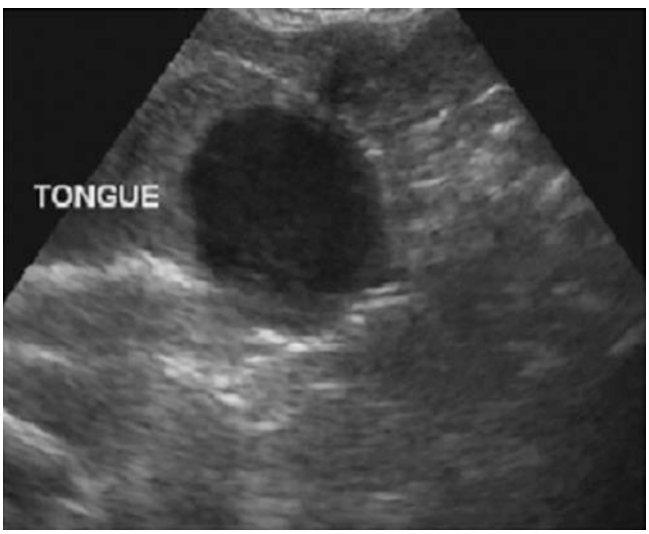

Fig. 10.4 This sagittal ultrasound image reveals a vallecular cystic mass at the base of the tongue

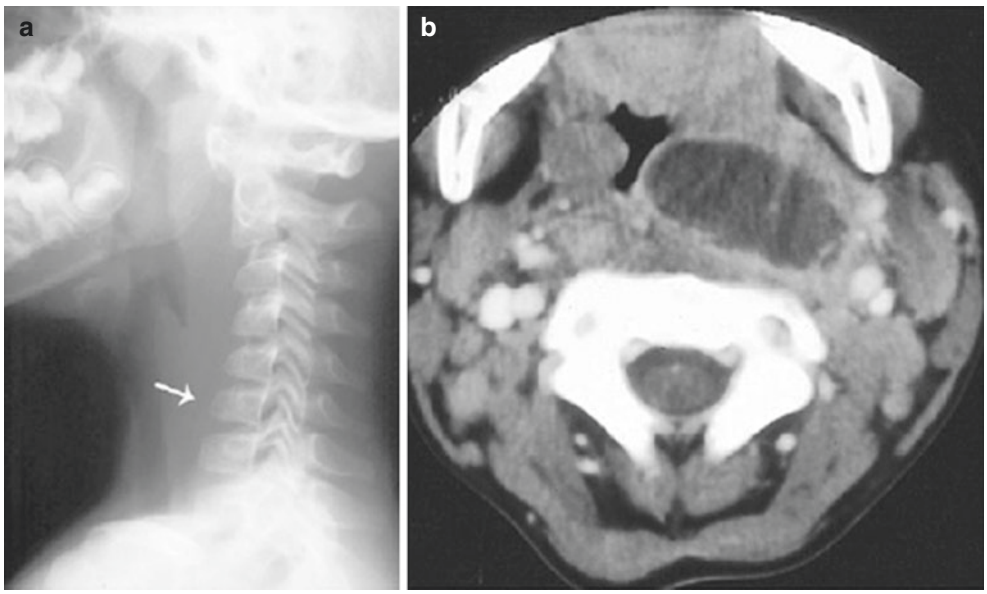

Fig. 10.5 (**a**) A focal soft-tissue prominence, which is out of proportion to the soft tissues inferior to it, is suggestive of a localized abnormality. Lending further evidence of a pathological process is obliteration of the normal fat planes (*arrow points to the normal fat plane below the level of the abnormality*) in the region of the soft-tissue prominence. (**b**) CT of the neck of the child imaged in Fig. 10.6a reveals a large left-sided retropharyngeal abscess. (From Cleveland [3], with permission of Lippincott Williams & Wilkins)

When there is incomplete development of the elastic and connective tracheal tissue (tracheomalacia), a *portion* of the intrathoracic trachea may collapse with expiration, while the remainder of the airway maintains normal in caliber during inspiration and expiration. In diagnosing tracheomalacia in infants and children, the gold standard is a flexible bronchoscopy, in which the airway can exhibit dynamic collapse. This study, however, is done under general anaesthesia, and as such radiographic diagnostic studies are often preferred. If bronchoscopy is not possible, conventional fluoroscopy-guided airway studies are typically recommended. Computed tomography (CT) may be more effective, however, in depicting the location, extent, and degree of tracheomalacia by utilizing a paired inspiratory-expiratory airway protocol that images the central airway at the end of inspiration and expiration. Further, multidetector CT (MDCT) with 3D central airway reconstruction produces exquisitely detailed images of the entire central airway [20]. Cervical tracheal size is affected by the pressure within its lumen. An excellent illustration of this is when the extrathoracic airway is obstructed or partially obstructed (as in croup). Under these circumstances, the entire cervical trachea may collapse with vigorous inspiration. Moreover, the cervical trachea may become significantly enlarged as the vocal cords close and there is a corresponding increase in positive pressure within the chest [21].

Disease processes such as prevertebral abscess, adenopathy, or tumor can also impact airway configuration. These pathologies are frequently characterized by prominent soft tissues (Fig. 10.5a) but without the angled configuration that takes place during normal expiration [1–4] (Chap. 3). Rhabdosarcoma, lymphoma, primitive neuroectodermal tumors (PNET), and mesenchymal cell sarcomas (including germ cell and yolk sac tumors) most commonly develop in this location. These lesions generally obscure the normal prevertebral soft tissue plains (Fig. 10.5a). Furthermore, if the retropharyngeal soft tissue fullness is more pronounced superiorly than inferiorly, it likely reflects pathology (Fig. 10.5a). Once retropharyngeal pathology is suspected on conventional imaging, CT should be performed to establish the extent of disease and the presence of a drainable abscess (Fig. 10.5b).

Laryngeal and Subglottic Airway

The junction of the underside of the true vocal cords and infraglottic larynx is less acute in infants and small children than it is in older children and adults; this results in a less prominent normal subglottic "shoulder" effect (Fig. 10.6a, b). However, subglottic narrowing can and should be distinguished from the normal sloping of the infraglottic larynx. In addition, during active breathing, the vocal cords are abducted, producing a normal loss of the infraglottic "shoulders" (Fig. 10.6c), which is recognized by the lack of vocal cord apposition.

The edema that causes subglottic narrowing, associated with "croup," is characterized by labored breathing and a hoarse, brassy cough. It is often associated with infection by a parainfluenza virus but may be brought on by other viruses as well. The term *croup* is used to refer to the expanded complex of laryngotracheobronchitis. This disease primarily affects children of 6 months to 3 years of age, during the fall and winter months. Whereas epiglottitis (see below) presents with high probability of life-threatening airway obstruction, croup is generally more benign and responsive to medical treatment like systemic steroids (Fig. 10.7). In severe circumstances, however, intubation may be necessary. In the most severe cases, intrathoracic pressure on inspiration may exceed oncotic pressure and result in pulmonary edema (Fig. 10.8).

Inflammation of the epiglottis (epiglottitis) is classically associated with infection by haemophilus influenza

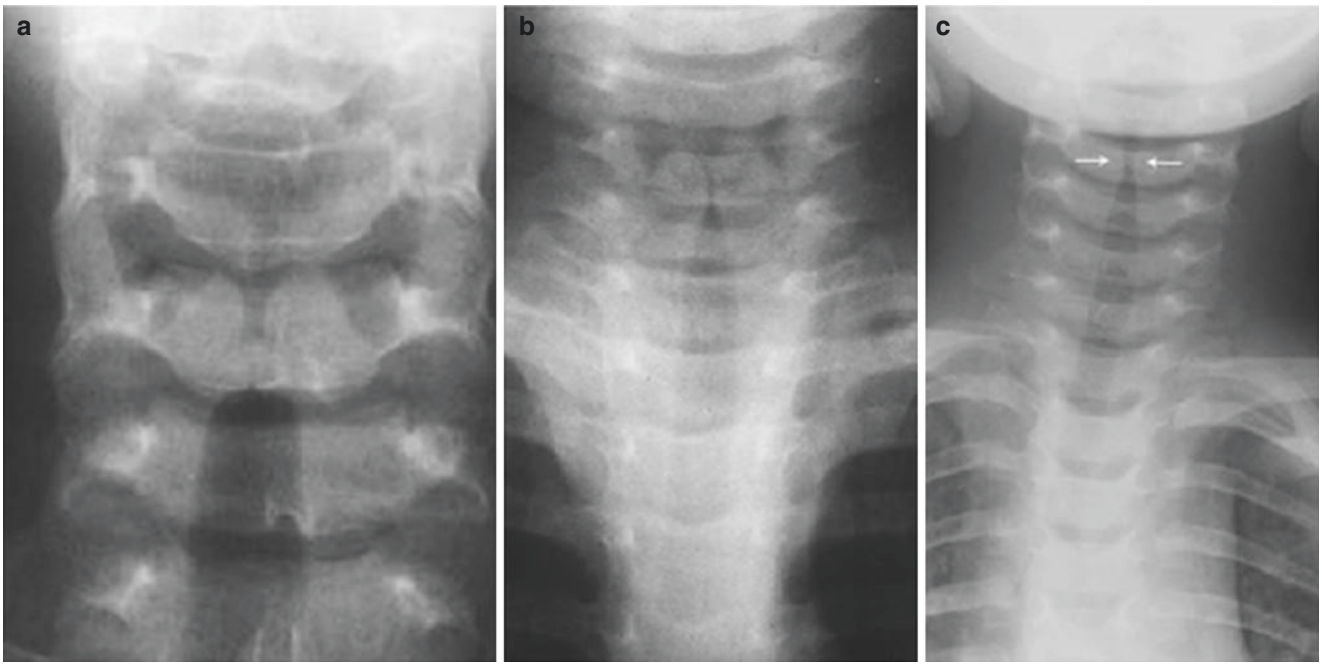

Fig. 10.6 (**a**) The normal adult subglottic airway (*shoulder*) is typically angularly squared off. (**b**) The normal subglottic "shoulder" in infants and small children is much less angular and squared off than in older children and adults. (**c**) With abduction of the vocal cords (*arrows*), there is normally a loss of the subglottic "shoulders." This should not be confused with croup, where the vocal cords will be apposed with a loss of the "shoulders"

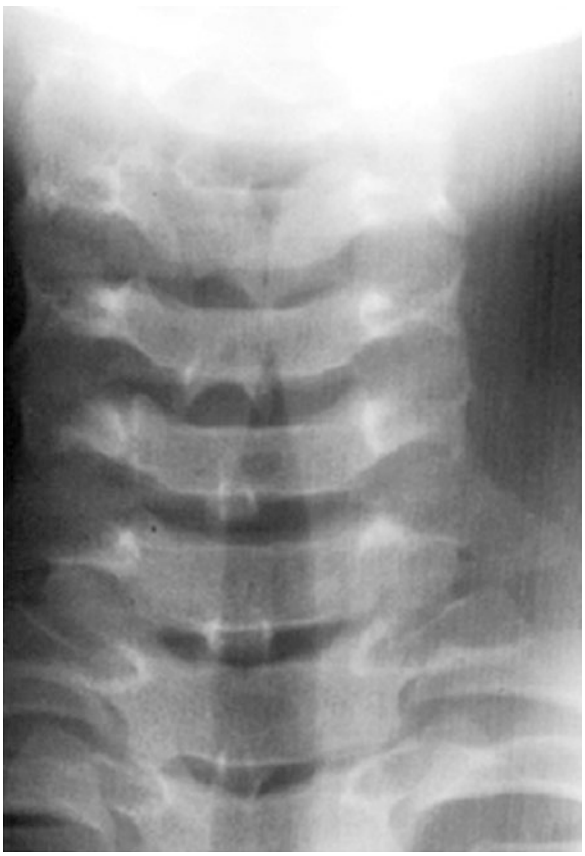

Fig. 10.7 Croup causes subglottic edema and narrowing, which is much better seen on frontal projection. Note that there is apposition of the vocal cords in conjunction with loss of the subglottic "shoulders" producing the typical "church steeple" or "pencil point" configuration

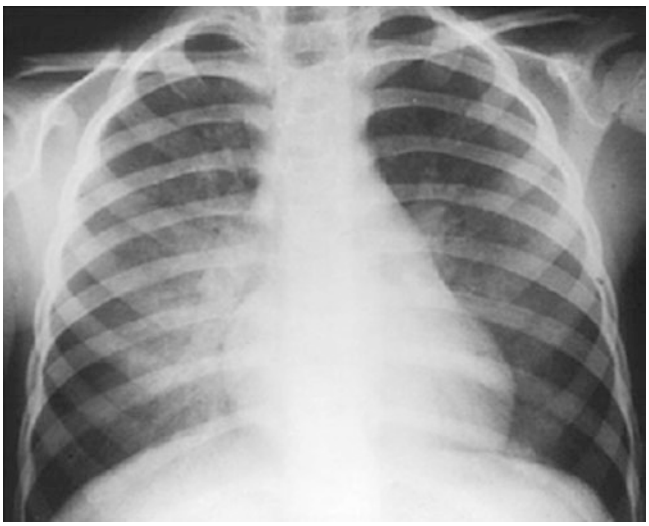

Fig. 10.8 The subglottic obstruction of croup may be so severe that attempts to inflate the lungs will produce such negative intrathoracic pressure that oncotic pressure will be exceeded producing pulmonary edema. (From Cleveland [3], with permission of Lippincott Williams & Wilkins)

type B (HIB) infection. Fortunately, relatively few cases of this disease are now reported since HIB vaccinations are widely available and strongly encouraged. Infections by non-type b haemophilus influenza, however, occasionally occur. Other types of bacteria may also give rise to epiglottitis. Edema caused by the ingestion of hot foods or liquids may also resemble epiglottitis. Edema that results from hypersensitivity (e.g., an allergic reaction) may also appear

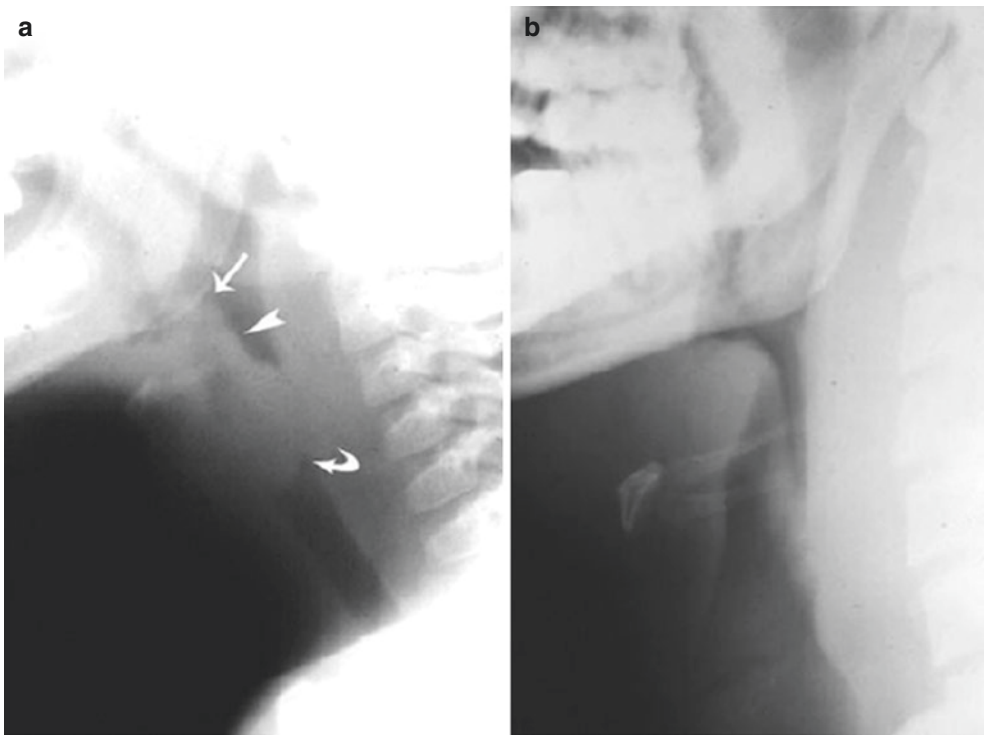

Fig. 10.9 (**a**) This child with H. flu disease exhibits swelling of the epiglottis (*arrow*), the aryepiglottic folds (*arrow head*), and the subglottic airway (*curved arrow*). This is an example of panglottitis. (**b**) More often the swelling will be limited mainly to the epiglottis. In this child with H. flu disease, there is also mild swelling of the aryepiglottic folds. (From Cleveland [3], with permission of Lippincott Williams & Wilkins)

anatomically similar to infection. Epiglottitis generally occurs in winter months and primarily affects children aged 3–6 years. The most clinically apparent symptom is epiglottic swelling, although the aryepiglottic folds and subglottic larynx may show evidence of inflammation as well.

Imaging by plain film or fluoroscopy may be used to definitively diagnose a suspected case of epiglottitis, but extreme caution must be exercised, and should be avoided if possible, because the child's airway may become completely obstructed during imaging. If the head and neck are moved or straightened, the airway may become completely occluded. At times, the aryepiglottic folds or subglottic airway are involved, further complicating an imaging study (Fig. 10.9). In certain cases, the epiglottis may be relatively spared, but the aryepiglottic folds and/or subglottic airway are affected (Fig. 10.10).

Bacterial organisms, frequently staphylococcal, may give rise to tracheal bacterial infections known as bacterial croup or pseudomembraneous tracheitis (Fig. 10.11). This process may present with pseudomembrane formation and croup-like symptoms.

In infants and children, focal masses may appear in the subglottic airway. Focal granulation tissues may develop secondary to previous intubation or tracheotomy (Fig. 10.12). Lesions may also be secondary to a subglottic hemangioma, which often arise concomitantly with cutaneous hemangiomata, often of the head or neck. Most often located posterolaterally, usually within 1–1.5 cm below the vocal cords,

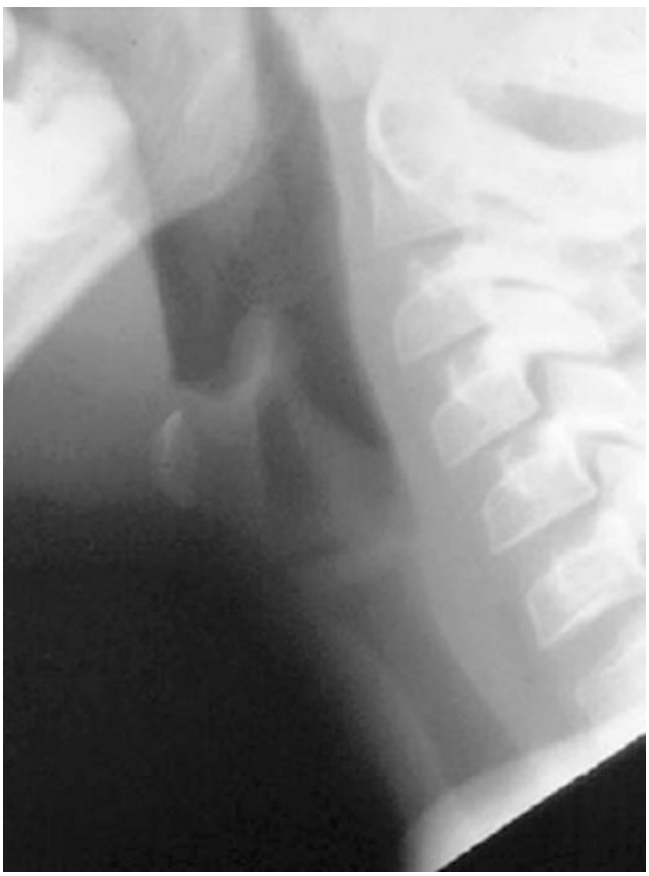

Fig. 10.10 Occasionally, the swelling will be primarily of the aryepiglottic folds, with a normal-appearing epiglottis

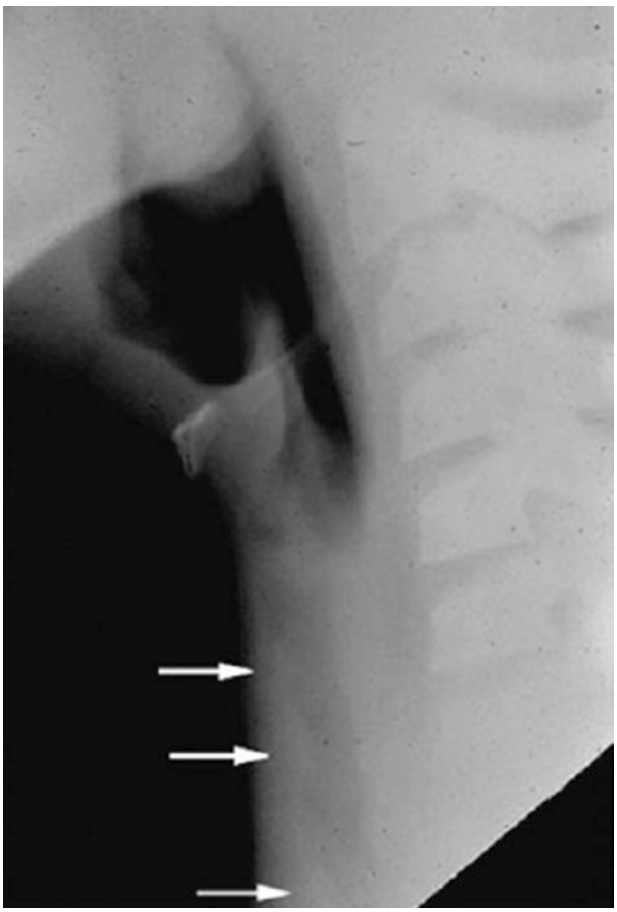

Fig. 10.11 Multifocal and irregular filling defects (*arrows*) may be seen in the infraglottic airway and upper trachea with pseudomembraneous tracheitis. This is caused by the presence of an apple peel configured pseudomembrane. The filling defect is usually more apparent on lateral projection than on the frontal projection

subglottic hemangiomas frequently involute spontaneously by age 5 or 6 years (Fig. 10.13). Although the detection of subglottic hemangioma can be accomplished by plain radiographs or conventional fluoroscopy-guided airway study, CT, especially MDCT with its multiplanar and 3D-imaging capabilities, can be helpful. Virtual tracheobronchoscopy is particularly useful for evaluating the degree of airway obstruction, which is proven to correlate well with the conventional tracheobronchoscopy (Fig. 10.14). After 5 years of age, it is more likely that an isolated subglottic mass is a papilloma (Fig. 10.15) than it is a hemangioma. The papillomata are caused by inoculation with the human papilloma virus, acquired during vaginal delivery. In up to 20% of patients, the viral infection may propagate down the airway and into the lung parenchyma producing nodular, cavitary lung lesions (Fig. 10.16) [22]. Other tumors of the subglottic airway and trachea are seen only rarely in children [23].

Trachea and Mainstem Bronchi

The most commonly found intraluminal airway abnormalities in children are aspirated foreign bodies. Among very young children, single aspirated foreign bodies are distributed nearly equally between the two lungs. By age 15, the bronchial angles subtended from the trachea acquire a more adult configuration; at this stage, twice as many foreign bodies localize to the right lung [24]. Even when a foreign body is suspected, an initial inspiratory chest film may not show this conclusively. In cases where the diagnosis is uncertain, different imaging strategies can be adopted. For example, an obstructed lung or segment of lung is usually clearly depicted

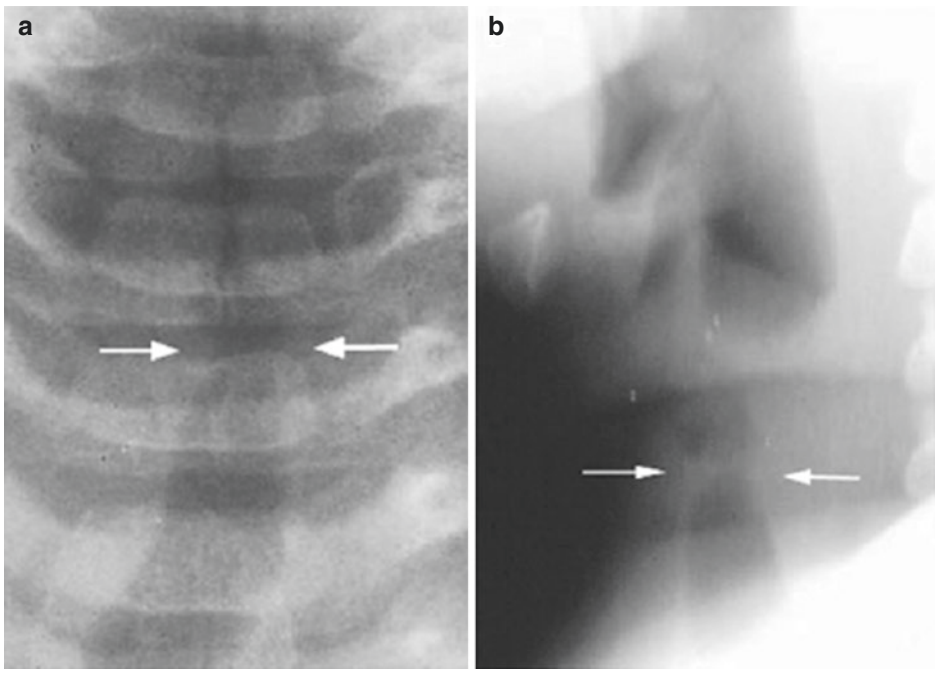

Fig. 10.12 (**a**) Postintubation granuloma causes moderate narrowing in AP projection (*arrows*). (**b**) The narrowing is more pronounced in AP direction, as seen in a comparison with this lateral projection (*arrows*)

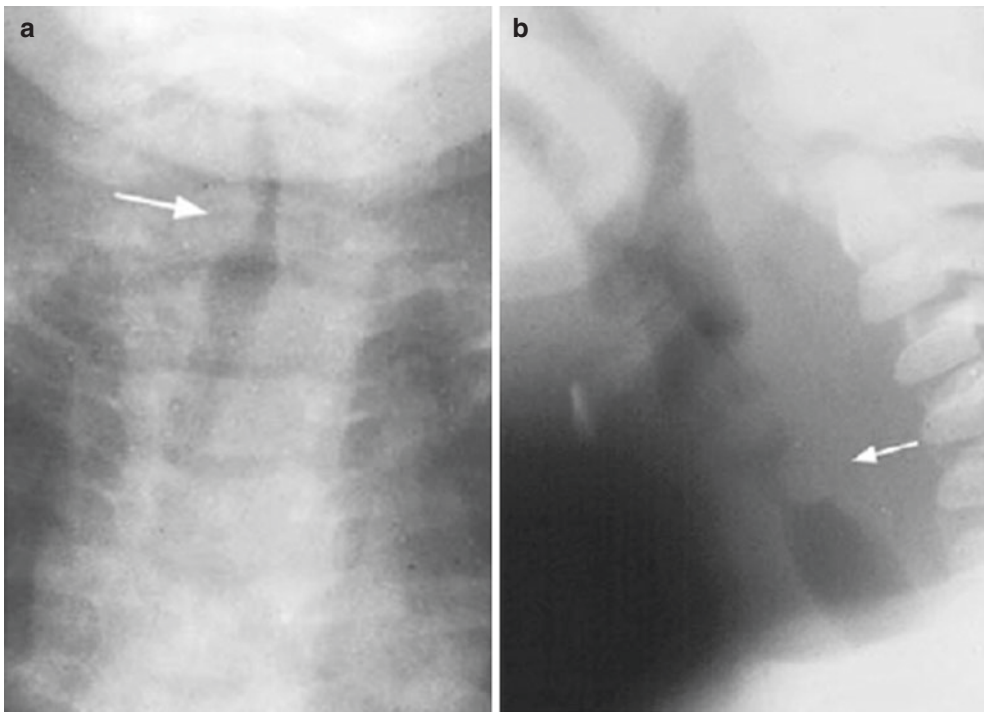

Fig. 10.13 Subglottic hemangiomas (*arrow*) typically arise 1–1.5 cm below the vocal cords. Symptoms of partially obstructing upper airway lesions may be confused with asthma. (**a**) AP projection, (**b**) lateral projection

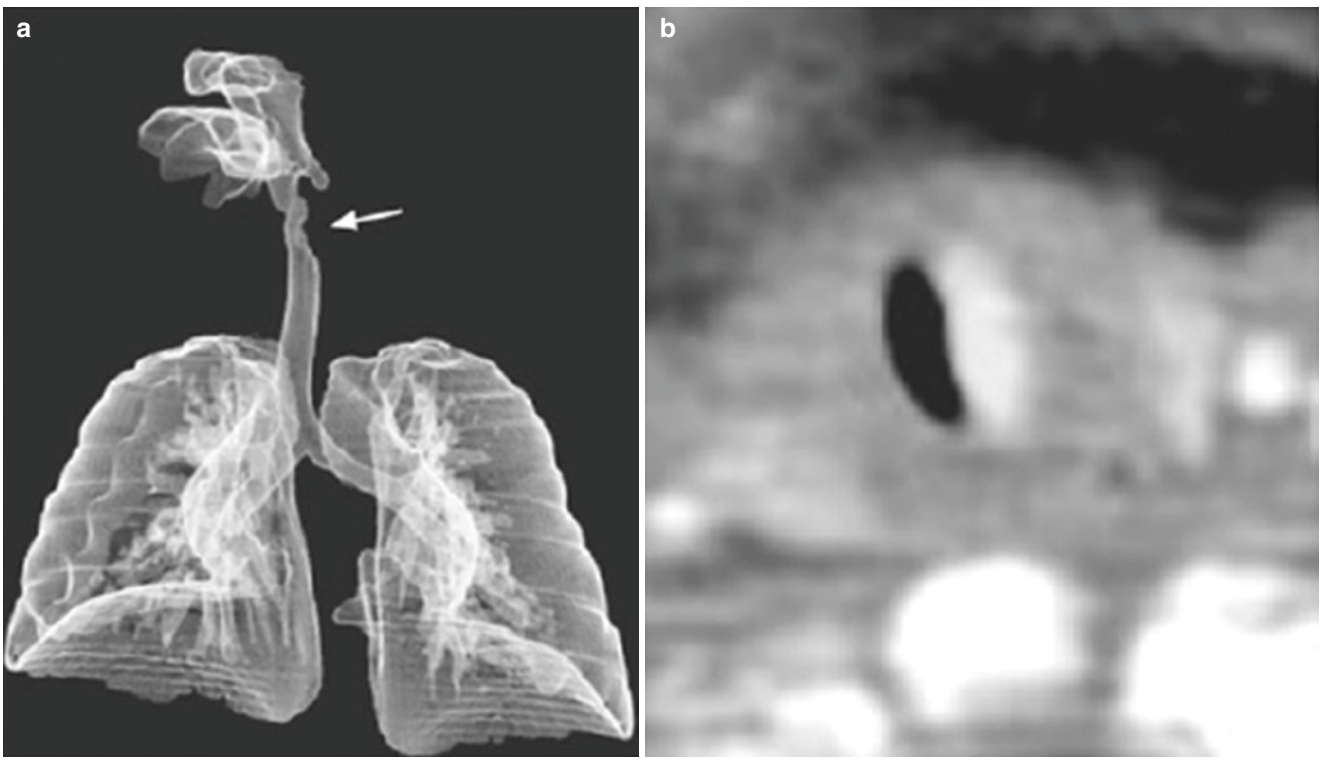

Fig. 10.14 (**a**) Contrast-enhanced CT shows enhancing intraluminal lesion located on the left lateral subglottic region. CT study was performed since the patient had cutaneous hemangiomas and respiratory distress. (**b**) 3D CT image better demonstrates location, extent, as well as degree of airway obstruction resulted from subglottic hemangioma (*arrow*) (**a** from Lee and Siegel [29], with permission). (**c**) 3D virtual tracheobronchoscopy shows the degree of subglottic narrowing in a patient with subglottic hemangioma. (**d**) Subglottic hemangioma seen on conventional tracheobronchoscopy correlates well with that of 3D virtual tracheobronchoscopy image (**c**)

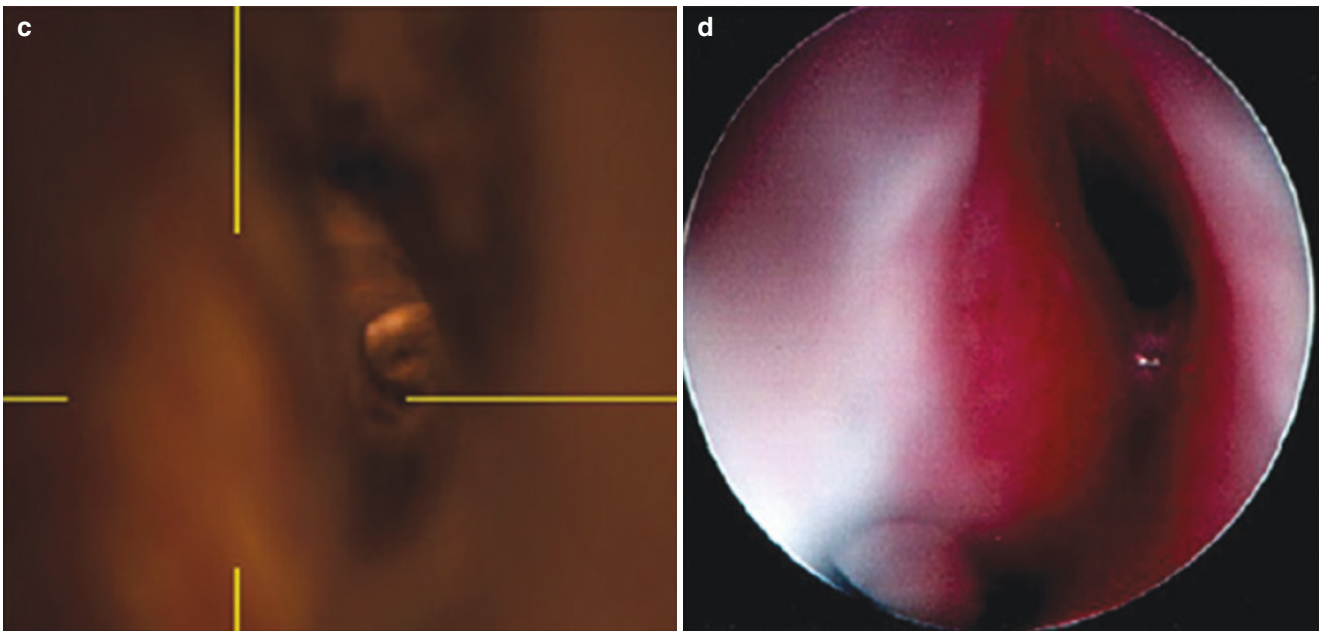

Fig. 10.14 (continued)

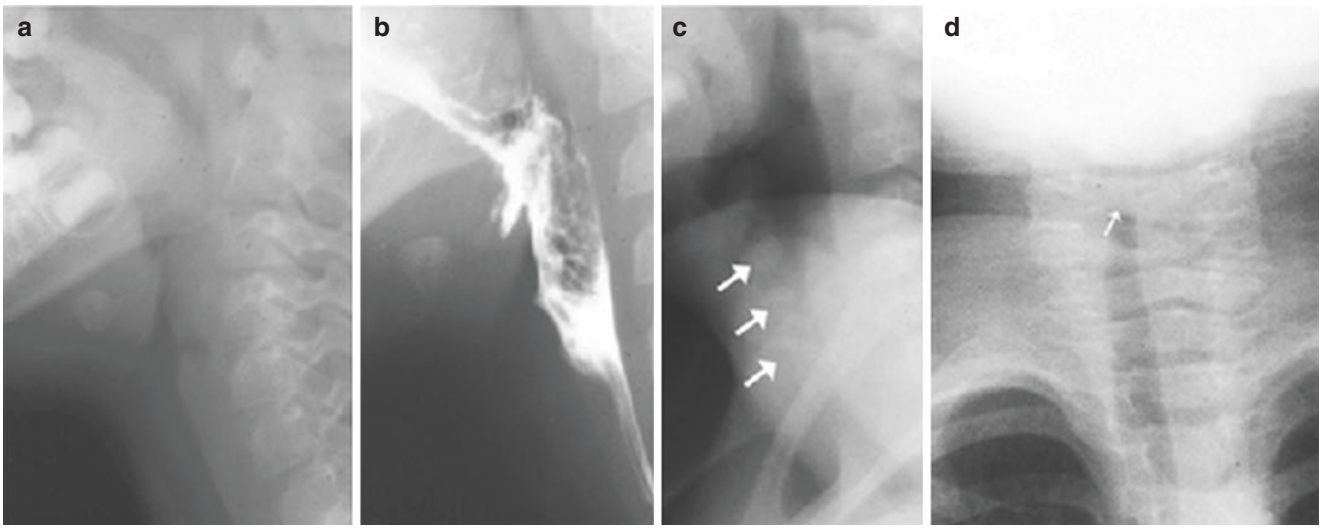

Fig. 10.15 (**a**) The verrucous lesions of laryngotracheal papillomatosis may present as a laryngeal mass, as seen in this lateral projection of the pharynx. (**b**) With oral contrast, the extent of the pharyngeal mass is better appreciated. (**c**) More commonly, the lesions will be encountered in the trachea, as in this girl, with multiple lesions (*arrows*). (From Cleveland [3], with permission of Lippincott Williams & Wilkins). (**d**) As with other focal lesions of the upper airway, papillomata may be more difficult to image in frontal projection (*arrow*) than the lateral (**c**)

with fluoroscopy. When the lung is obstructed, the abnormal side or lobe does not respond to respiration. In other words, a lung that is filled with trapped air may remain so even during expiration (Fig. 10.17a, b). Likewise, a partially collapsed lung may remain similarly collapsed throughout respiration. The failure of a lung, or a segment of a lung, to exhibit a change in volume through the respiratory cycle is the critical observation. Under these circumstances, diaphragmatic excursion is unequal. On inspiration, when there is air trapped in the obstructed lung, the mediastinum moves toward the abnormal side; on expiration, it is away from the side of obstruction. An alternative is to use bilateral decubitus chest images (Fig. 10.17c, d). However, this approach often provides less conclusive information since the decubitus images are often inadvertently obtained in an oblique position, which compromises the ability to accurately assess comparative lung volumes. When viewing right lateral or left lateral decubitus films, the normal dependent lung should appear deflated when compared to the normal nondependent lung. In older, more cooperative children, these altered

dynamics may be more clearly demonstrated with comparative inspiration and expiration X-rays.

Relatively radiolucent foreign bodies within the airway are sometimes visible in only one projection. Esophageal foreign bodies lodged for extended periods may result in significant edema and inflammation, creating, at times, obstruction of the adjacent airway (Fig. 10.18) [25]. Extrinsic compression on the airway may result from mediastinal masses such as bronchopulmonary foregut malformations (i.e., bronchogenic cysts, GI duplications, neuroenteric cysts), as well as abnormal mediastinal vessels (i.e., double aortic arch, aberrant subclavian artery, pulmonary sling, anomalous innominate artery) [26]. Central airway compression resulting from the abnormal mediastinal vessels may be identified [27, 28] with plain radiographs (Fig. 10.19); cross-sectional imaging by CT and MRI confirms this finding and provides useful preoperative data. The advantage of MRI is its ability to depict lung structure and function *without exposing* the patient to ionizing radiation. CT, on the other hand, offers more precise detail of the central airway and lung parenchyma. With the introduction of MDCT and its multiplanar and 3D-imaging capabilities, the diagnosis and preoperative assessment of mediastinal vascular anomalies resulting in central airway compression has been significantly enhanced [20]. Mediastinal vascular anomalies, central airway compression, and lung parenchyma can be separately evaluated with the same CT data by applying different CT reconstruction algorithms. The efficient use of imaging data thus minimizes exposure to the potentially harmful effects of radiation, which is of particular concern in evaluating children (Fig. 10.20).

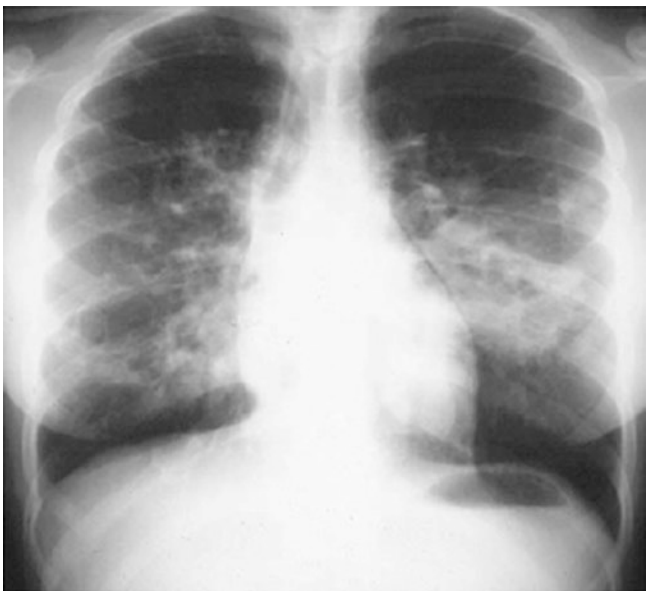

Fig. 10.16 In a few children, the papillomata may eventually spread to the lower airway presenting as multiple solid and eventually cavitating nodules. These predominate in the perihilar and posterior portions of the lungs, especially in the bases. (From Cleveland [3], with permission of Lippincott Williams & Wilkins)

When airway cartilage development is impaired in utero, bronchomalacic or tracheomalacic segments may develop. With esophageal atresia, the dilated upper pouch compresses the trachea, compromising tracheal cartilage development in the segment adjacent to the dilated upper

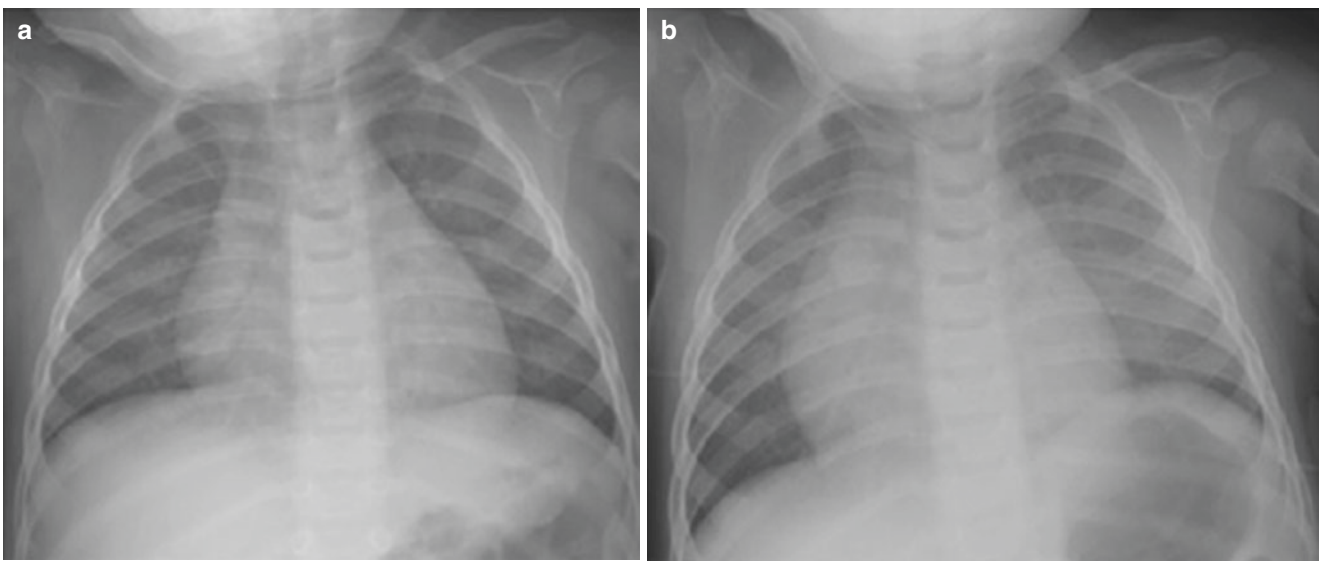

Fig. 10.17 (**a**) In this moderately inspiratory image, there is essentially equal lung inflation. (**b**) With expiration, it becomes clear that the right lung is trapping air, confirming the suspected foreign body in the right main bronchus. (**c**) In a separate child, this left lateral decubitus image shows deflation of the dependent left lung. (**d**) The right lateral decubitus image of the same child as (**c**) shows little change in the volume of the dependent right lung, confirming air trapping on the right

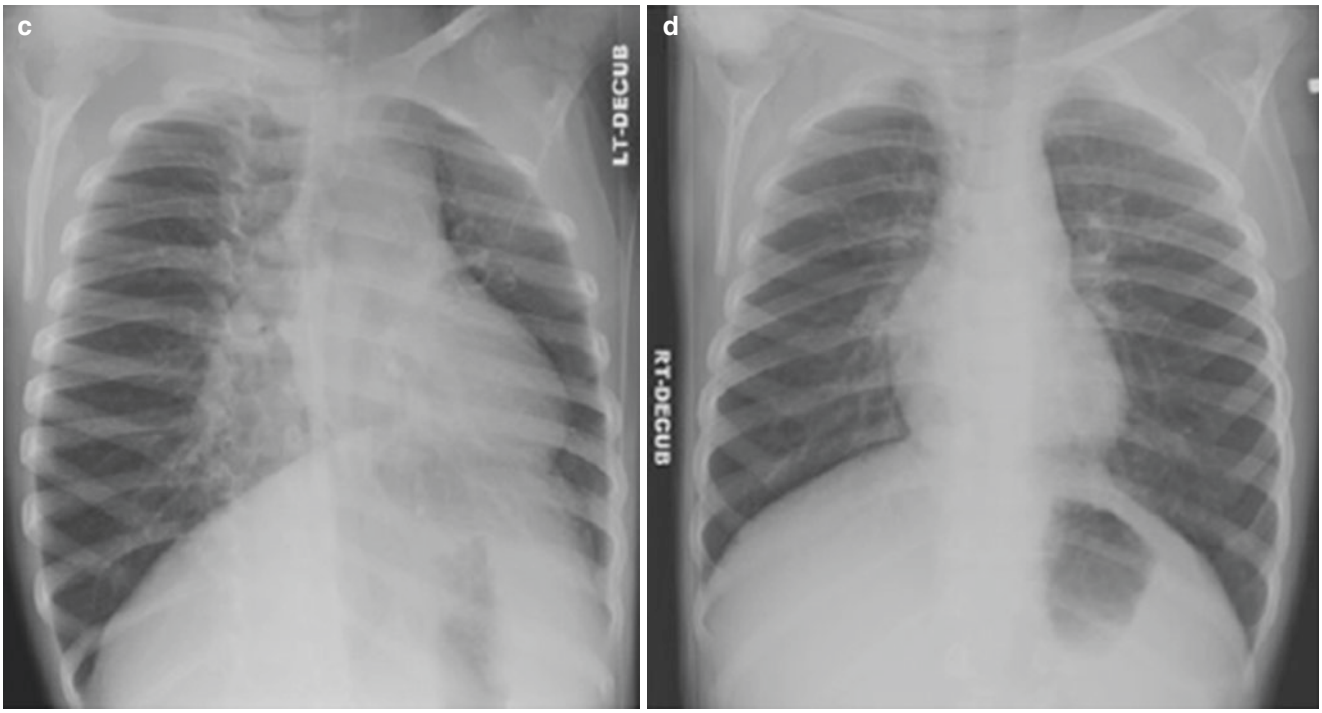

Fig. 10.17 (continued)

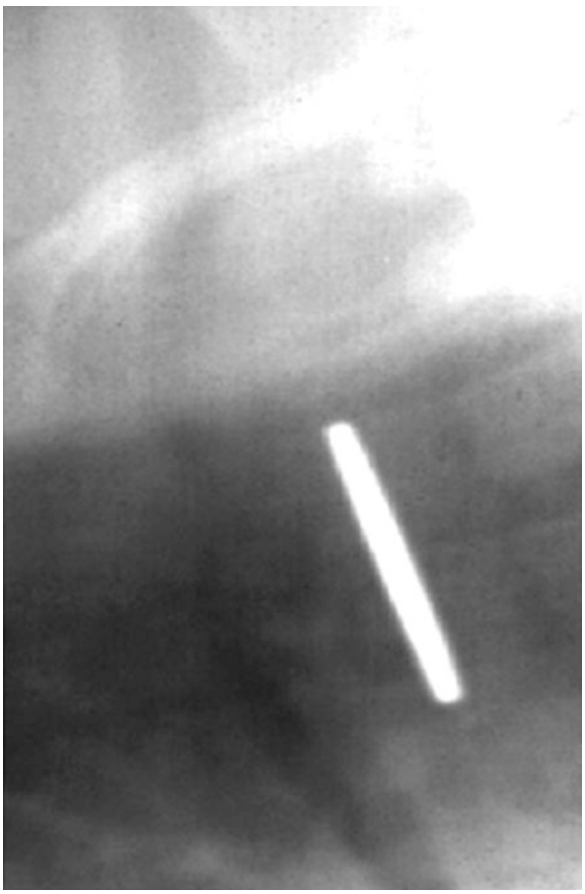

Fig. 10.18 This coin has been in the esophagus long enough to produce a degree of inflammatory response adequate to deviate the trachea anteriorly and to narrow it

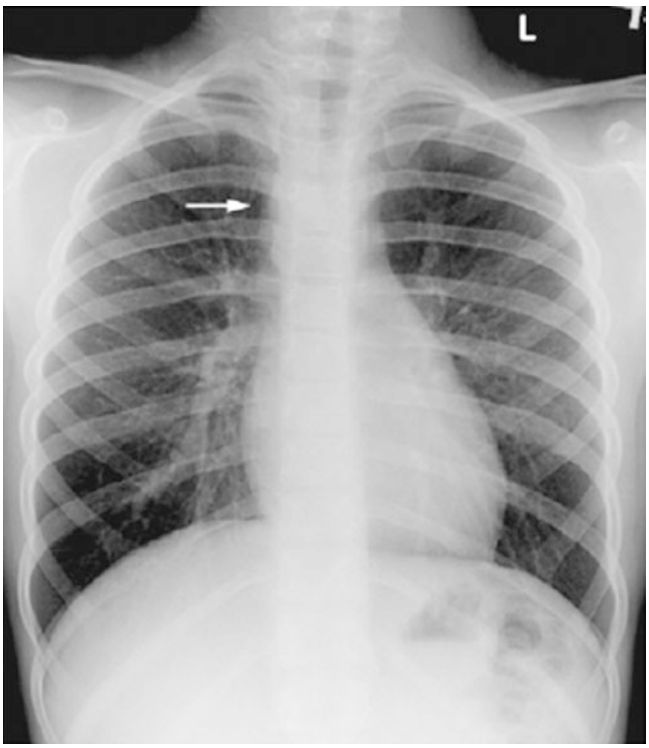

Fig. 10.19 Frontal radiograph of chest demonstrating tracheal narrowing due to right aortic arch (*arrow*)

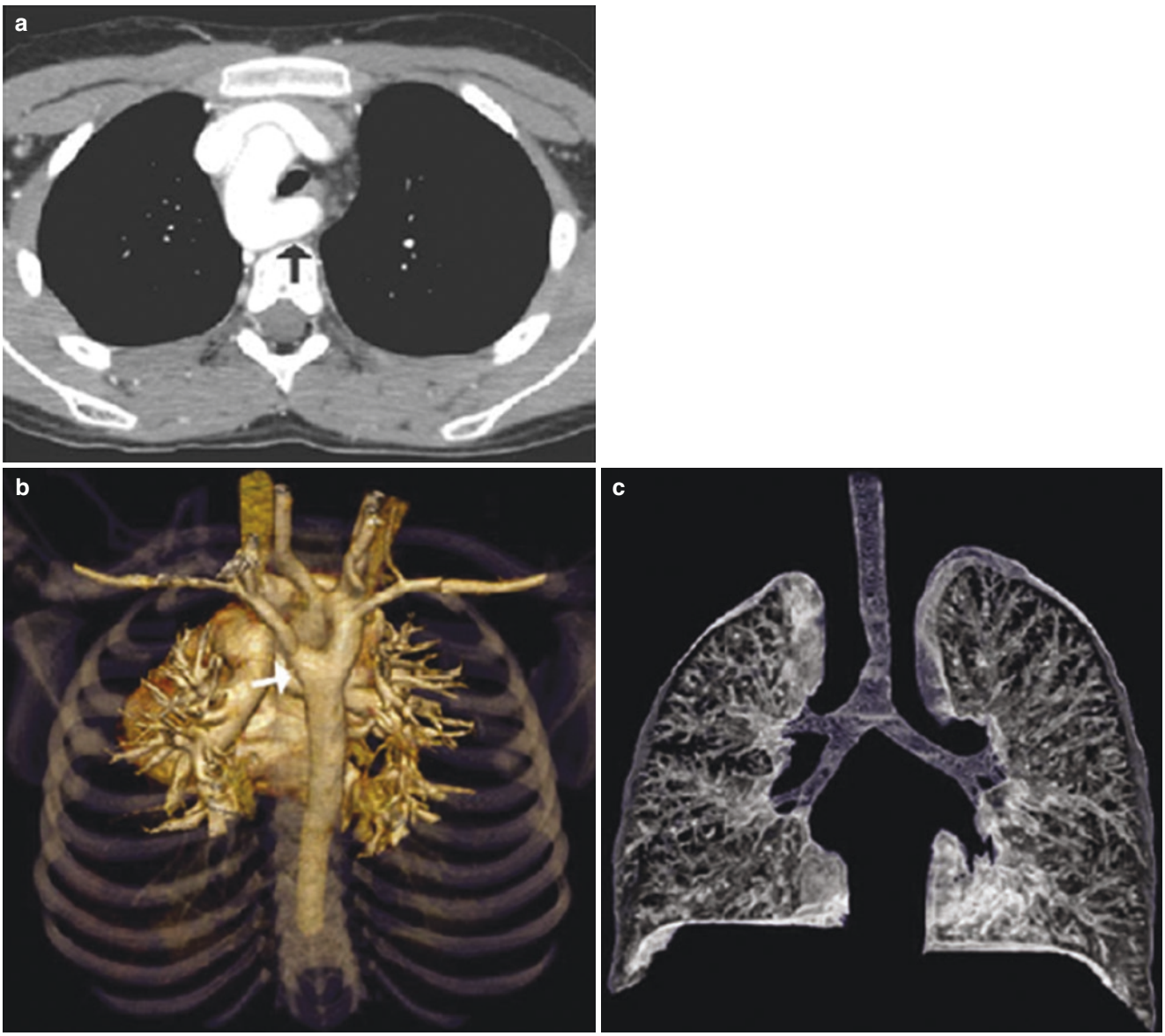

Fig. 10.20 (**a**) Contrast-enhanced CT study showing right aortic arch with aberrant left subclavian artery resulting in trachea compression in an infant girl who presented with respiratory distress. As is often the case, there is a diverticulum of Kommerell (*arrow*) at the origin of the aberrant left subclavian. This diverticulum may produce the dominant obstruction to the airway. (**b**) 3D-volume-rendered image of the mediastinal vessels from the posterior view shows right aortic arch with an aberrant left subclavian artery. The *arrow* indicates the diverticulum of Kommerell. (**c**) 3D-volume-rendered lumenogram of the central airway and lung demonstrates trachea compression due to the right aortic arch and an aberrant left subclavian artery. (From Lee and Siegel [29], with permission)

esophageal pouch. This structural aberration often produces significant tracheal narrowing and tracheomalacia (Fig. 10.21). The narrowed, malacic segment of the trachea may persist even after the esophageal atresia is surgically corrected. Less commonly, the entire esophagus may be distended by obstruction at the esphagogastric junction. This may relate to chalasia, ectopic tracheal cartilages, Chagas disease, or any other lesion causing relative obstruction at the gastroesophageal junction (Fig. 10.22). Significant tracheal narrowing is less common with these lesions than with esophageal atresia. Congenital tracheal or bronchial stenosis caused by a complete ring or "o" configuration of the cartilages is often associated with pulmonary sling, which passes between the esophagus and trachea (Figs. 10.23 and 10.24).

Peribronchial adenopathy that causes obstruction or endobronchial extension leading to obstruction is often associated with inflammatory processes, particularly tuberculosis

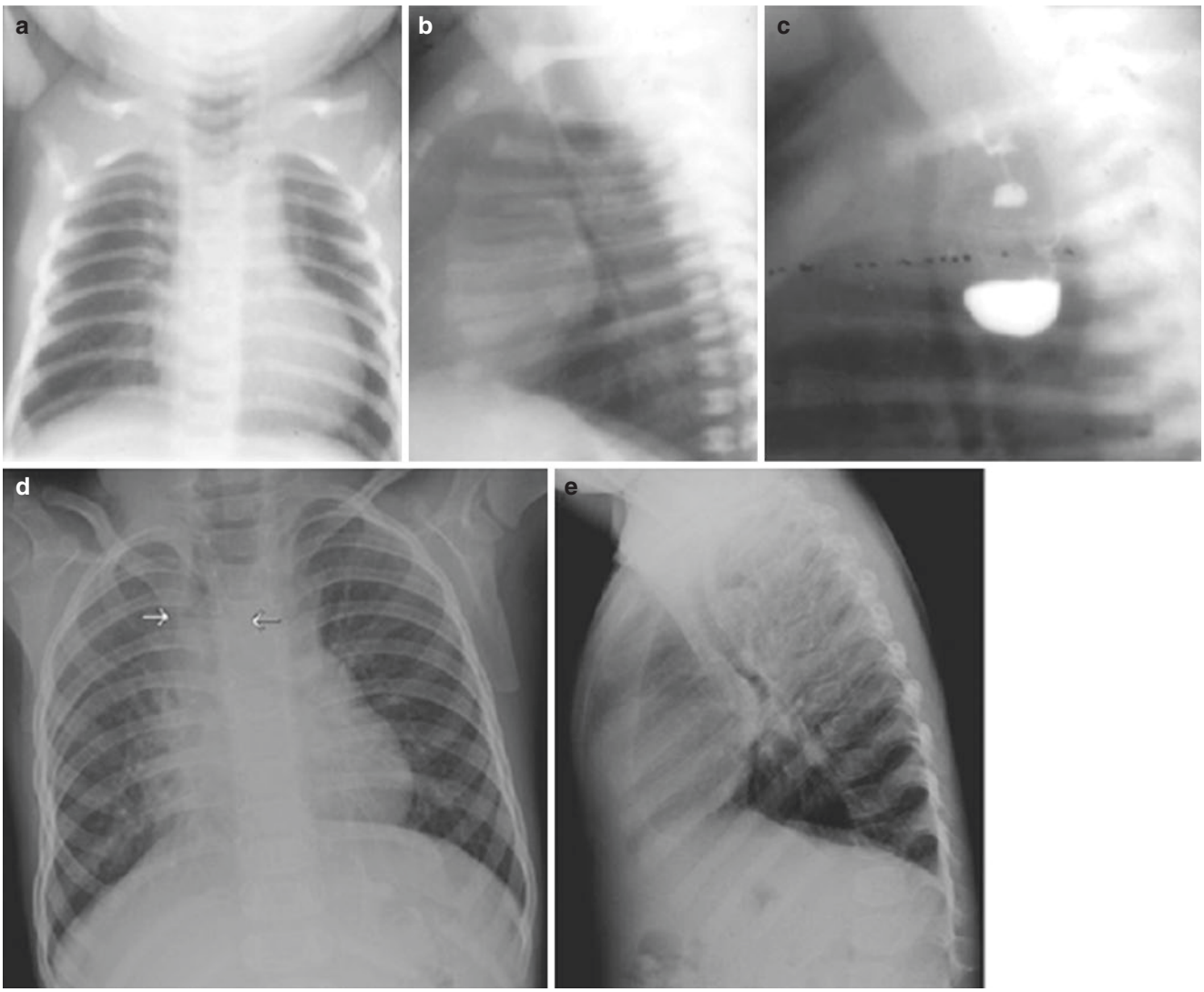

Fig. 10.21 The air-distended upper pouch of an esophageal atresia pushes upon the adjacent trachea from posteriorly. The trachea is deviated anteriorly and narrowed. (**a**) AP projection. (**b**) Lateral projection. (**c**) Lateral projection with barium in the blind-ending upper pouch. (**d**) When the obstruction is severe, there may be a demonstrable air fluid level above the obstruction (*arrows*). This child had repaired esophageal atresia; however, air fluid levels may result from esophageal obstruction at any level. (**e**) Lateral view in the same child as (**d**) also reveals an air fluid level in the dilated esophagus. The trachea is anteriorly displaced

(Fig. 10.25). CT may be especially useful in evaluating the location, extent, and associated airway compression or obstruction that arises from tuberculosis (Fig. 10.25) [29]. It is also important to evaluate airways that are distal to the obstruction. CT has an advantage over conventional tracheobronchoscopy for the evaluation of high-grade airway obstruction resulting from the peribronchial or mediastinal adenopathy. Although the airway distal to the obstruction can be evaluated with CT, conventional tracheobronchoscopy cannot be utilized if the obstruction is high-grade and the bronchoscope cannot be passed beyond the obstruction. Lymphoma, primary mediastinal tumors, or metastatic disease occurring in the mediastinum may cause similar extrinsic obstructions (Fig. 10.26).

Several congenital variations are viewed as failures of tracheoesophageal differentiation from the primitive foregut. There may be complete absence of differentiation of the trachea wherein the mainstem bronchi arise directly from the distal esophagus (Fig. 10.27). There may be laryngeotracheal clefts extending from the larynx to the carina of varying degrees, from type 1 to type 4 clefts (zipper-type opening varying from the cricoid down to the trachea). Type l, an H-type tracheoesophageal fistula (Fig. 10.28), is the least severe. Duplication of the trachea occurs rarely [30].

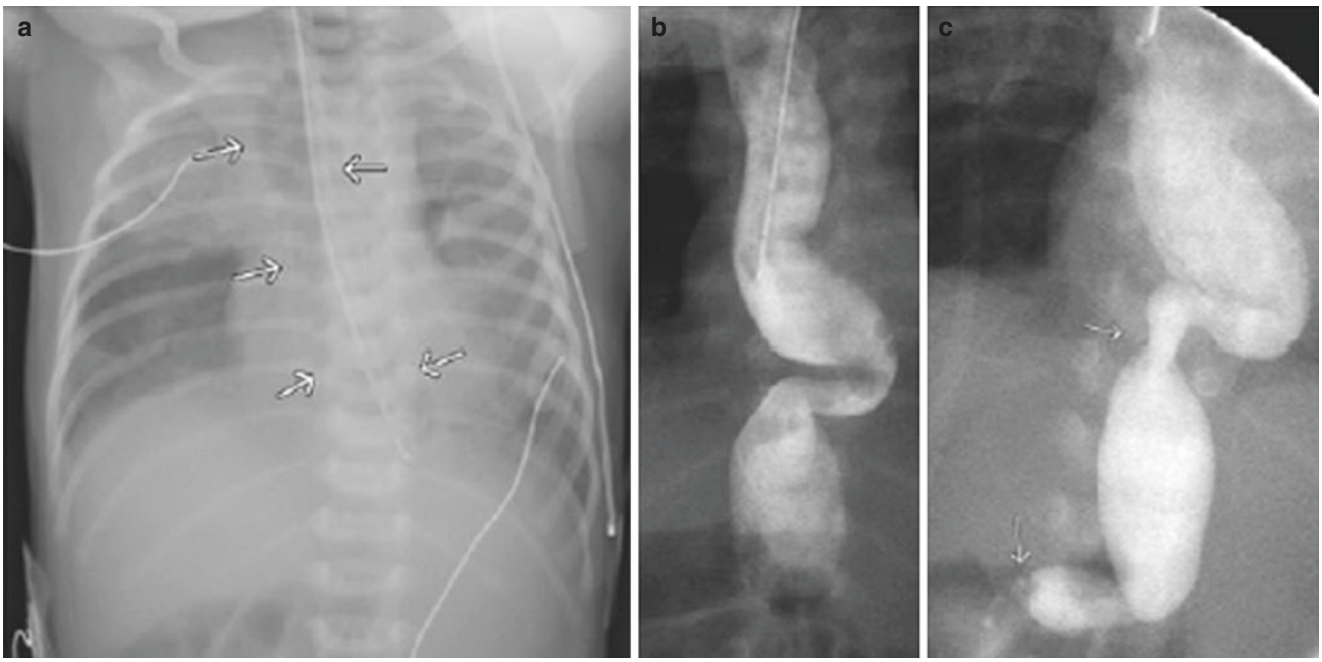

Fig. 10.22 (**a**) Portable AP CXR reveals gaseous distention of the entire esophagus (*arrows*). (**b**) Contrast injection via esophageal tube demonstrates a distended esophagus almost identical to that seen on CXR (**a**). (**c**) There is microgastria causing the esophageal dilatation. The *upper arrow* marks the gastroesophageal junction, the *lower arrow* points to the pylorus

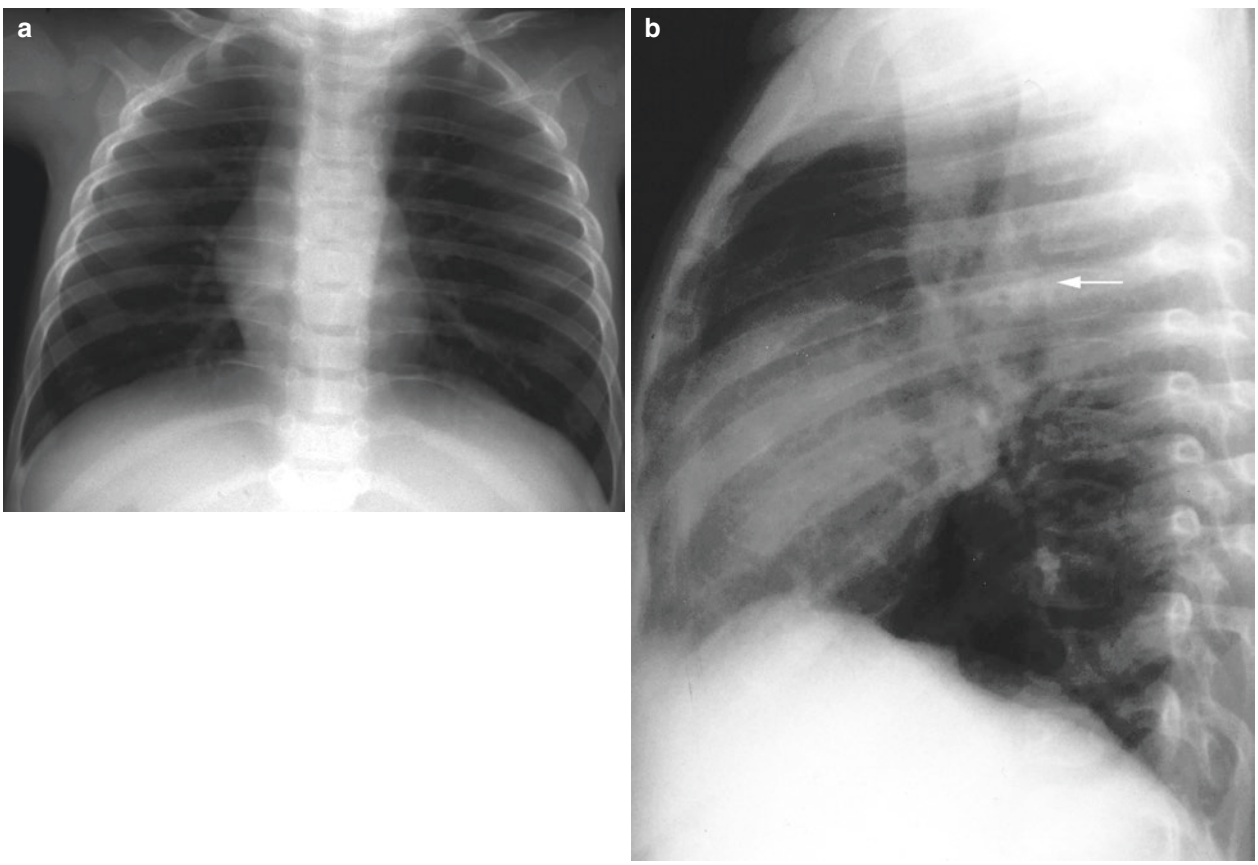

Fig. 10.23 (**a**) PA projection revealing findings of an aberrant left pulmonary artery, including a slightly inferiorly positioned right main bronchus, a leftward deviation of the distal, supracarinal portion of the trachea, partial obscuration of the distal, supracarinal portion of the trachea (tracheal cut-off sign), and a slightly hyperlucent, slightly enlarged left lung. (**b**) Lateral projection reveals a soft-tissue process (the aberrant left pulmonary artery) (*arrow*) posterior to the distal trachea deviating the trachea anteriorly and narrowing it

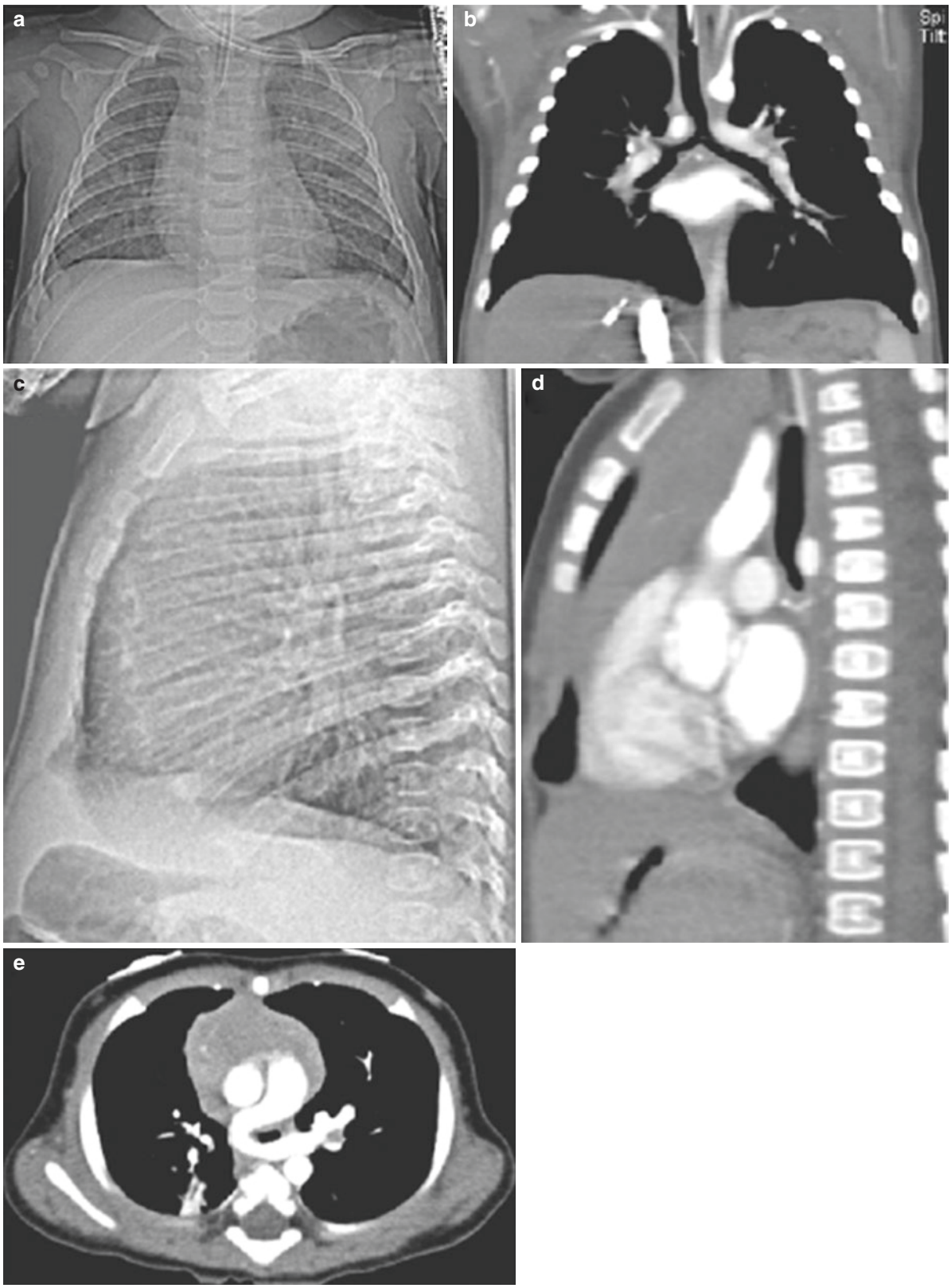

Fig. 10.24 Pulmonary sling. (**a**) PA CXR reveals a slight leftward deviation of the trachea just above the carina. (**b**) Coronal reconstruction from CT shows the aberrant left pulmonary artery adjacent to the inferior trachea causing the leftward deviation. (**c**) Lateral CXR reveals a slight anterior deviation of the inferior trachea. (**d**) Sagittal CT reconstruction reveals the aberrant left pulmonary artery causing the anterior bowing of the trachea. (**e**) Cross-sectional image shows the left pulmonary artery arising from the main pulmonary artery then coursing to the right of the trachea and then to the left between the trachea and esophagus

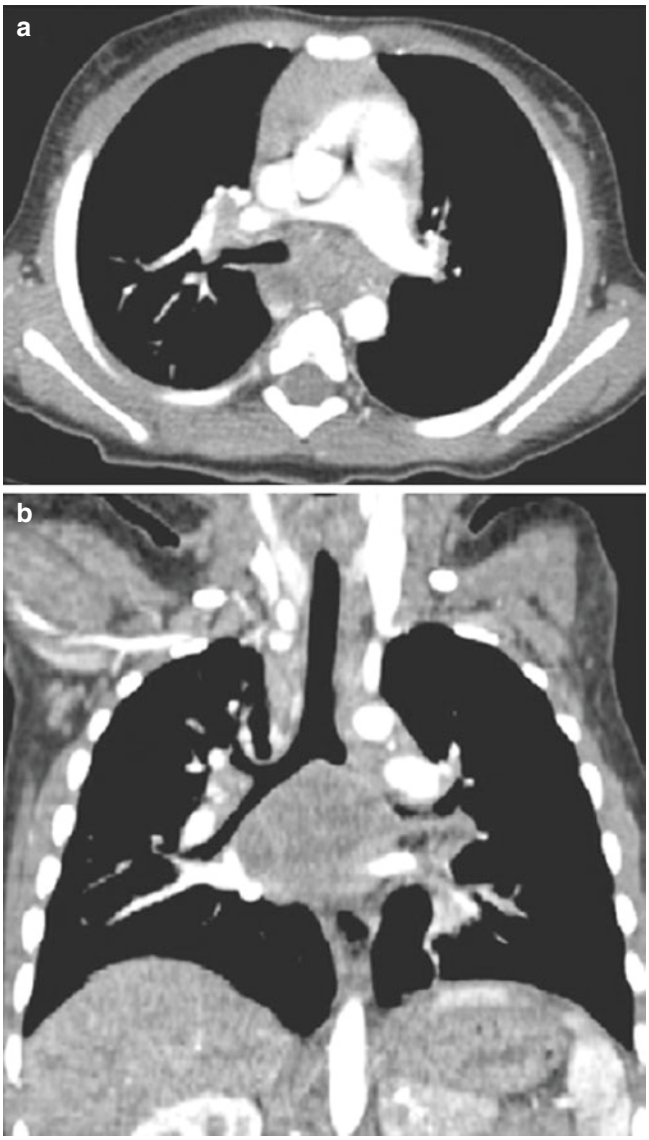

Fig. 10.25 (**a**) Contrast-enhanced CT demonstrates a heterogeneous posterior mediastinal mass obstructing the left mainstem bronchus. (**b**) The location, extent, and left mainstem bronchial obstruction resulting from the tuberculous mediastinal lymphadenopathy are better evaluated with coronal multiplanar CT image

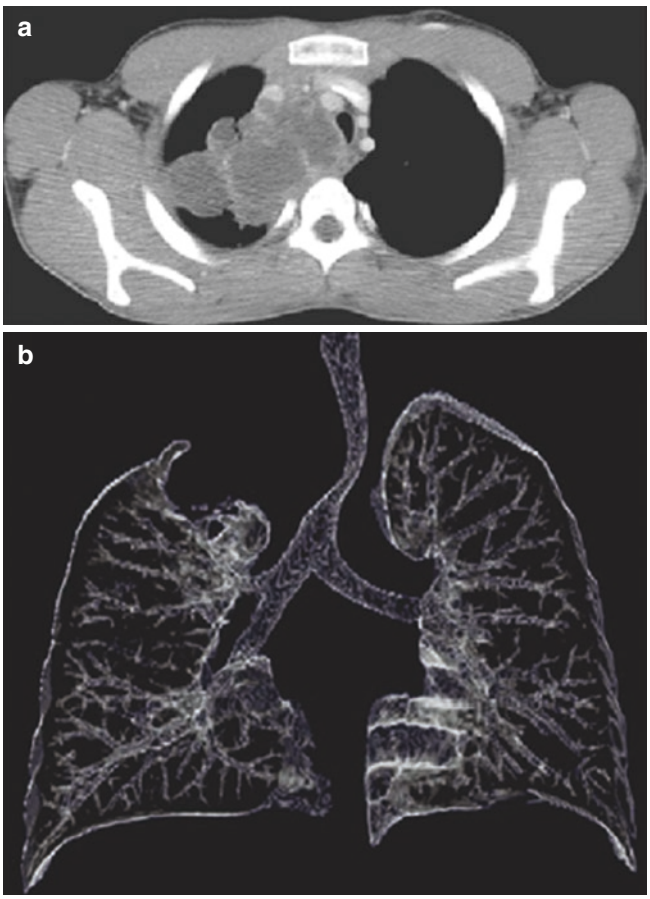

Fig. 10.26 (**a**) Contrast-enhanced CT shows heterogenous metastatic lymphadenopathy resulting in tracheal compression in a child with metastatic prostate rhabdomyosarcoma. (**b**) 3D-volume-rendered image shows a compressed trachea, which shifts to the contralateral side of the mass. Also noted is a metastatic mass compressing the right upper lung. (From Lee and Siegel [29], with permission)

Bronchial hypoplasia (or atresia), typically associated with pulmonary artery hypoplasia/atresia and congenitally hypoplastic/absent lung, are occasionally seen (predominantly on the right). In addition, "scimitar syndrome," a rare congenital disorder (1–3 in 100,000 live births), may also give rise to hypoplasia. This condition presents with an anomalous draining, usually right, upper lobe pulmonary vein emptying into the inferior vena cava. Although the crescent-shaped "scimitar" vein (Fig. 10.29) may be isolated and asymptomatic (scimitar sign), it may be associated with ipsilateral pulmonary, bronchial, and pulmonary artery hypoplasia (scimitar syndrome). There may also be associated congenital heart disease, especially atrial septal defect (ASD) and, less commonly, ventricular septal defect (VSD) [31]. Scimitar syndrome is also associated with pulmonary sequestration [32].

Yet another unusual condition known as "pig bronchus" occurs when the right upper lobe bronchus, multiple bronchi, or a bronchial segment arises directly from the trachea. Although this configuration is normal in pigs (and sheep), it can be problematic for human beings. While adults with this defect are generally asymptomatic, it may be the source of recurrent right upper lobe atelectasis or pneumonia in children (Fig. 10.30). This anatomic variant should be particularly suspected if a child is noted to develop right upper lobe atelectasis associated with the placement of an ET tube deep within the trachea but not with less advanced ET tubes. A small accessory cardiac bronchus rarely arises from the medial wall of the bronchus intermedius (Fig. 10.31). It may be associated with recurrent infection or hemoptysis and may trap debris [33].

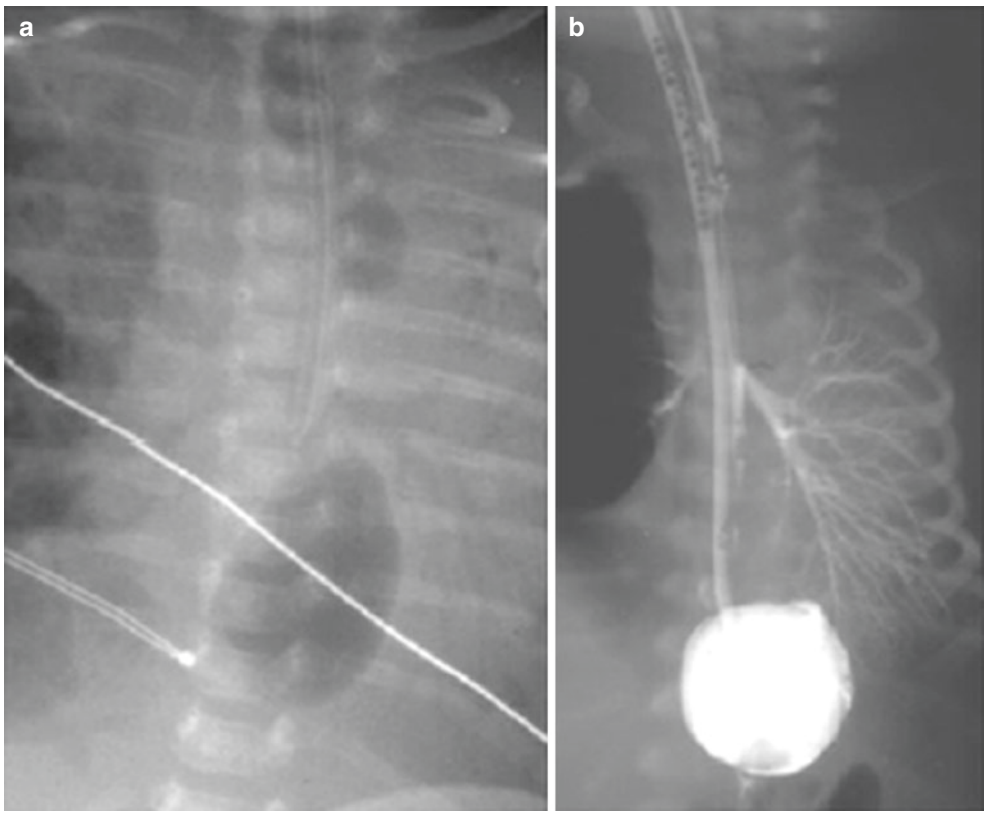

Fig. 10.27 (**a**) Attempts at intubation of this newborn consistently resulted in the tube being placed in the esophagus. This image shows the main bronchi abutting the esophageal tube at right angles. This scenario suggests an absent trachea. (From Cleveland [3], with permission of Lippincott Williams & Wilkins). (**b**) Postmortem injection of an esophageal tube confirms the origin of the bronchi from the distal esophagus

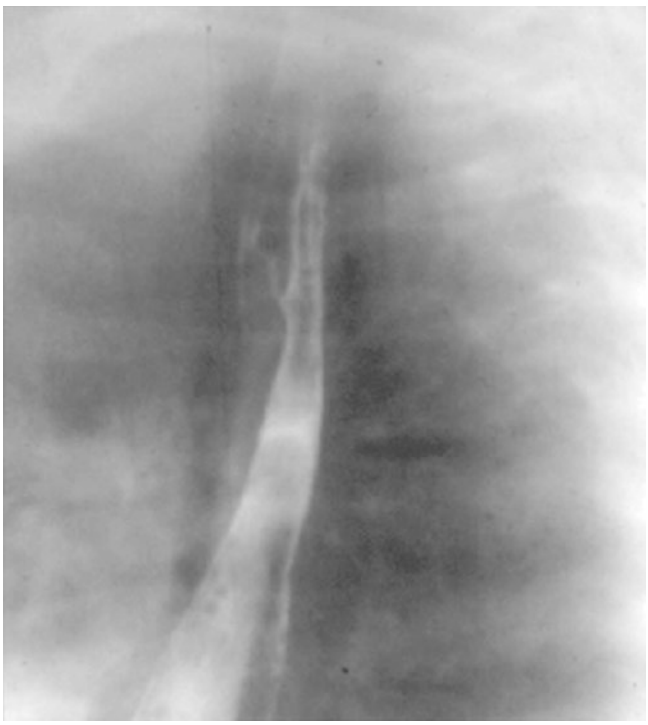

Fig. 10.28 "H" type tracheoesophageal fistula. The fistula courses upward from the esophagus to the trachea. This is a consistent finding suggesting that the abnormality possibly should be referred to as an "N" type fistula. Barium is the best contrast agent to use in assessing for this lesion with the patient positioned with the right side down on a horizontal fluoroscopy table

There are a few rare congenital abnormalities of the trachea and main bronchi, which may lead to atelectasis, pneumonia, and bronchiectasis. William-Campbell syndrome (deficient bronchial cartilages) may cause reduced airway clearance leading to recurrent atelectasis, infection, and bronchiectasis [34]. Congenital tracheobronchomegaly, Mounier-Kuhn syndrome, and acquired tracheomegaly/tracheobronchomegaly can also lead to recurrent atelectasis, pneumonia, and bronchiectasis. This may be associated with pulmonary fibrosis, Ehlers-Danlos syndrome, ankylosing spondyliltis, rheumatoid arthritis, or cystic fibrosis [35].

Peripheral Bronchi

Among the most common acute inflammatory processes that occur in infants and very young children is bronchiolitis, which is characterized by coughing, wheezing, and fever [2]. It is typically viral (most often respiratory syncytial virus) and primarily affects the peripheral bronchi. From a radiographic standpoint, bronchiolitis is depicted by "air trapping," often with little or no other radiographic abnormalities (Fig. 10.32). Diffuse bronchial wall thickening (peribronchial thickening), however, is frequently apparent. Atelectasis appears less often and on sequential imaging typically shows a shift in its distribution. Unfortunately, the radiographic course of bronchiolitis can create some confusion. Although

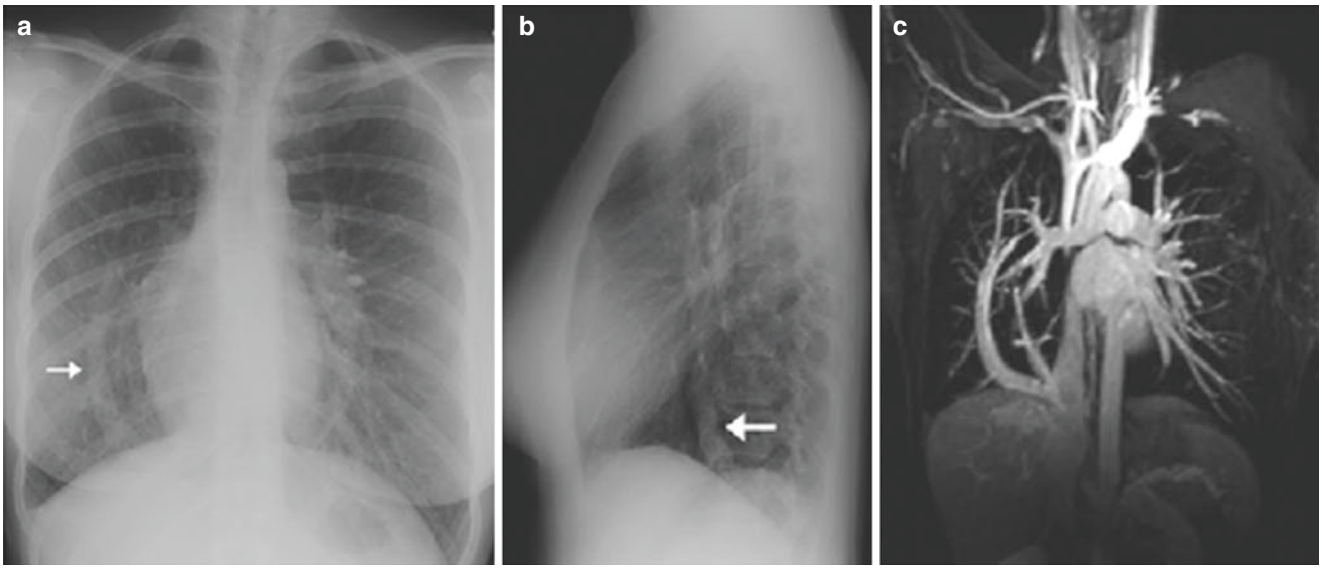

Fig. 10.29 An aberrant right upper lobe pulmonary vein, a scimitar vein, is easily recognized (*arrow*). (**a**) PA projection. (**b**) Lateral projection. (**c**) Coronal MRI

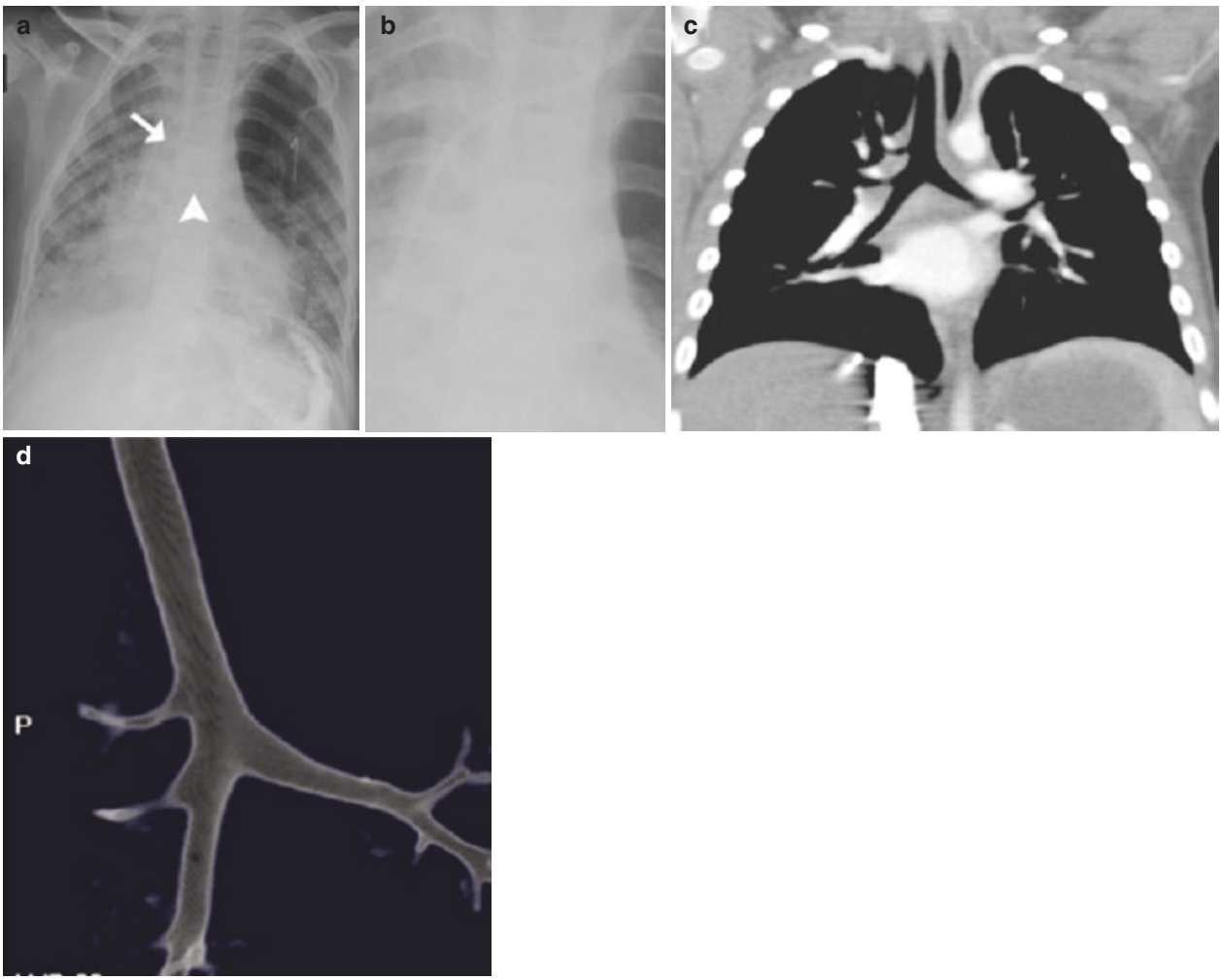

Fig. 10.30 (**a**) This frontal chest X-ray reveals a "pig" bronchus (*arrow*). The trachea distal to the anomalous bronchus is proportionately diminished in caliber (*arrow head* indicates the carina). (**b**) Coned image of the main intrathoracic airway from (**a**). (**c**) This coronal reconstruction from a CT of a different child shows a "pig" bronchus but without the associated narrowing of the distal trachea. (**d**) 3D rendering of the airway illustrated in (**c**)

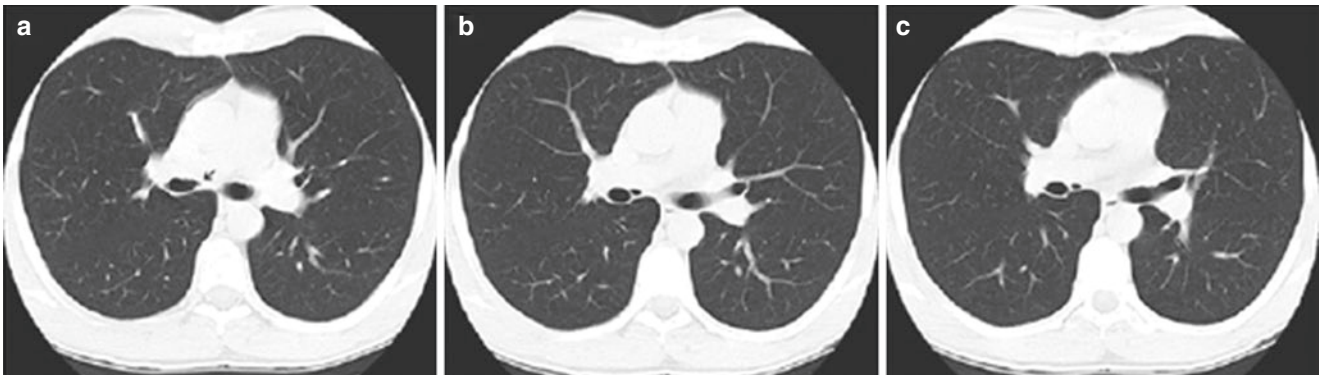

Fig. 10.31 Accessory cardiac bronchus. (**a**) CT image approximately 5 mm below the carina shows the orifice of an accessory cardiac bronchus (*arrow*) arising from the medial wall of the bronchus intermedius. (**b**) Five millimeters below the orifice of the accessory bronchus, the accessory bronchus is separated from the bronchus intermedius. (**c**) The accessory bronchus at approximately 1 cm below the site of its origin. It was no longer present on the next contiguous image

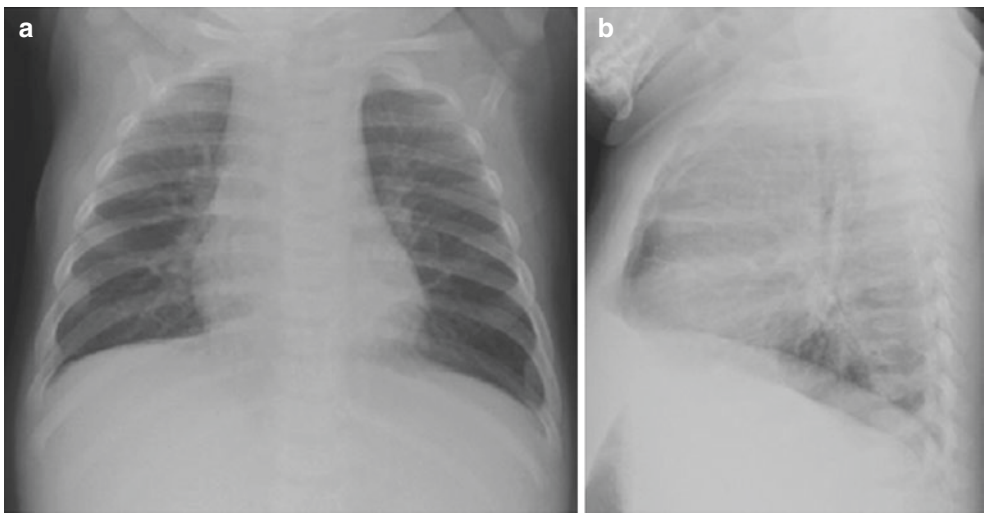

Fig. 10.32 (**a**, **b**) The chest radiograph on this infant with RSV positive bronchiolitis reveals diffuse air trapping. The flattening of the diaphragm is the most reliable indicator of overinflation (although it must be present on all images. If absent from one, it indicates air is not trapping). There is also multifocal subsegmental atelectasis and diffuse bronchial wall thickening

hyperinflation is the most prevalent initial finding, as the process resolves, the lungs generally show less air trapping but more atelectasis. Paradoxically, this apparent deterioration of multifocal lung disease is a sign that the inflammation is improving.

Bronchiolitis is the most common cause of acute bronchial wall thickening. Chronic bronchial wall thickening is most commonly seen in children with reactive airway disease or asthma. Radiographs of children with asthma or reactive airway disease generally show diffuse air trapping when acutely symptomatic. Diffuse bronchial wall thickening is present even when asymptomatic. The recognition of bronchial wall thickening is complicated since the prominence of the bronchial walls increases with age. As a guide, infants have only a minimal number of visible bronchial walls in the lung periphery, but many may be normally detected in the perihilar regions (Fig. 10.33). With pathologic bronchial wall thickening, more evidence of the process can be detected in the lung periphery, seen as "O rings" and "tram tracking" (Figs. 10.34 and 10.35). Since the process affects the bronchi, which converge on the hilar regions, the process may be most noticeably abnormal centrally, which may be recognized as large poorly marginated hilae, especially on the lateral image (Fig. 10.35a).

Diffuse bronchial wall thickening is also the most common initial radiographic indicator of cystic fibrosis in infants and young children [36, 37]. In older children and adults, this thickening often progresses to coarse bronchiectatic changes frequently perceived as nodules when fluid filled or as cysts when air filled (Fig. 10.36) [36, 37]. Less commonly, chronic recurrent pneumonia may result in bronchial wall thickening as a consequence of one of two processes: (1) it may be sec-

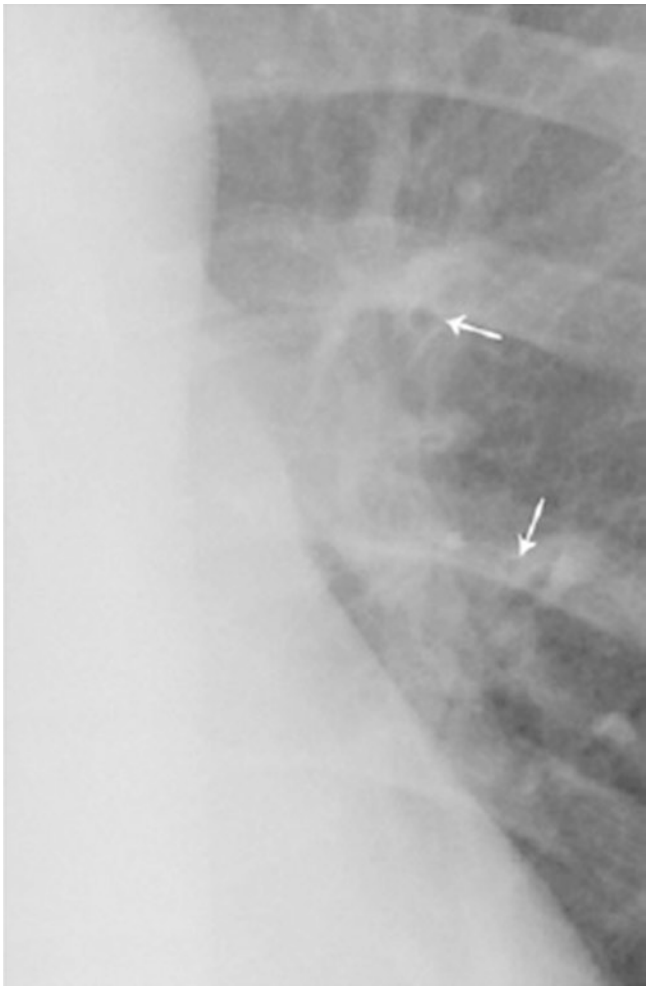

Fig. 10.33 Normal bronchial walls (*arrows*) in the perihilar regions are prominent enough to be easily recognized

ondary to recurrent aspiration associated with a swallowing abnormality or a tracheoesophageal fistula, or (2) it may relate to an immune deficiency. In these instances, the process may be uneven in distribution, as opposed to the more evenly distributed process seen with early CF and asthma/reactive airway disease. Other rarer causes include those entities discussed in the chapter on interstitial lung disease.

Also, inflammatory bowel disease (both Crohn's disease and ulcerative colitis) may have associated lung disease, most commonly affecting the airways. Entities include bronchiectasis, bronchitis, tracheobronchitis, and bronchiolitis, with symptoms suggesting asthma being the most common. Bronchiolitis is the most common and on CT may show irregular areas of air trapping. Airway symptoms may precede bowel symptoms but more commonly appear in patients with long-standing IBD and may occur with or without accompanying bowel systems. Tracheal and bronchial strictures may occur, as well as inflammatory nodules and circumferential mucosal infiltrates. Patients with Crohn's disease may develop colobronchial or esophago-pulmonary fistulas. Less commonly, patients will develop interstitial lung disease with focal opacities, especially frequent in those with organizing pneumonia. Pulmonary nodules may develop, which may be subpleural or cavitated. In patients with interstitial pneumonitis, CT will demonstrate ground-glass opacities, alveolar filling, or a reticular pattern. Also, bronchiectasis, air trapping, and a tree-in-bud pattern are common. In addition, pleural and pericardial effusions may occur [38, 39].

Although CT and MRI have become widely used in the imaging of the main airways, that is not yet the case for the smaller peripheral airways. For MRI, there has been continuing improvement in resolution and shortened image acquisition times. However, the degree of resolution is currently inadequate for peripheral airway assessment in children. For CT, the large airways, including the trachea and mainstem bronchi, can be accurately evaluated in conjunction with postprocessing techniques (2D and 3D imaging). However, distal branch airway evaluation can be particularly limited in pediatric patients due to small size. Currently 3D imaging is not completely reliable for the specific assessment of either congenital or acquired disorders of the small peripheral airways.

In congenital lobar emphysema (CLE), an estimated 50% of cases show some evidence of focal bronchial obstruction that manifests itself as an overinflated, hyperlucent lobe (Fig. 10.37) [40]. However, in the first few days of life, this may present with preferential trapping of fetal lung liquid in the abnormal lobe. This, in turn, produces an overinflated, opaque lobe (Fig. 10.38), which slowly drains the fluid over ensuing days, subsequently becoming hyperlucent. The distribution of CLE is roughly 43% in the left upper lobe, 32% in the right middle lobe, 20% in the right upper lobe, and 5% in two lobes [41]. With an overinflated, hyperlucent lobe and associated mediastinal shift to the contralateral side, CLE may be mistaken as tension pneumothorax. When this occurs, CT is useful in visualizing the underlying, overinflated, and hyperlucent lung parenchyma (Fig. 10.39).

Further complicating a definitive diagnosis is a condition known as "polyalveolar lobe," which is clinically and radio-

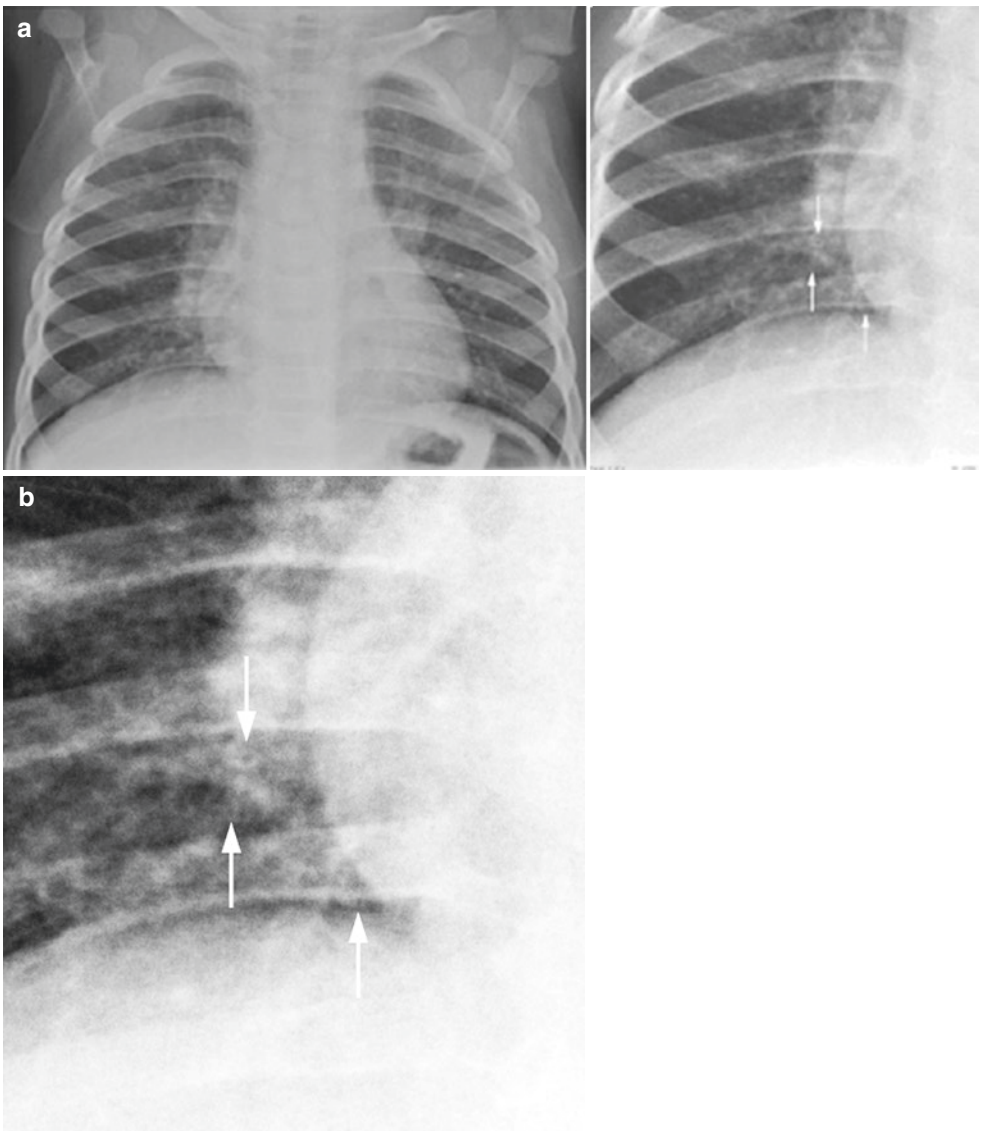

Fig. 10.34 (**a**) Peribronchial thickening (bronchial wall thickening) is seen diffusely on this PA chest X-ray in a child with bronchiolitis. (**b**) Coned image of the right lung base from (**a**) more clearly shows the "ring shadows" of thickened bronchial walls seen in cross-section (*arrows*)

graphically indistinguishable from CLE. Although polyalveolar lobe shares a similar distribution and demographics with CLE, it has a normal tracheobronchial tree but a greater number of alveoli [41]. It has been suggested that cases of suspected CLE that preferentially retain fetal lung liquid are actually polyalveolar lobe [41].

Chronic lung disease of prematurity (bronchopulmonary dysplasia) presents in premature infants with hyaline membrane disease, in which ciliated epithelial cells of the trachea and bronchi are destroyed and replaced with nonciliated cells. The replacement of ciliated cells with nonciliated cells leads to recurrent atelectasis and infections. There are also multifocal areas of atelectasis and fibrosis alternating with areas of focal overexpansion [40]. In premature infants with bronchopulmonary dysplasia who survive for several months or years, the radiographic and clinical depiction of the disease may closely resemble that of children with acute bronchiolitis or asthma. In addition, older children diagnosed with pulmonary disorders at birth, including hyaline membrane disease, meconium aspiration, neonatal pneumonia, and diaphragmatic hernia, frequently develop reactive airway disease that is clinically recognizable or confirmed by pulmonary function studies [42].

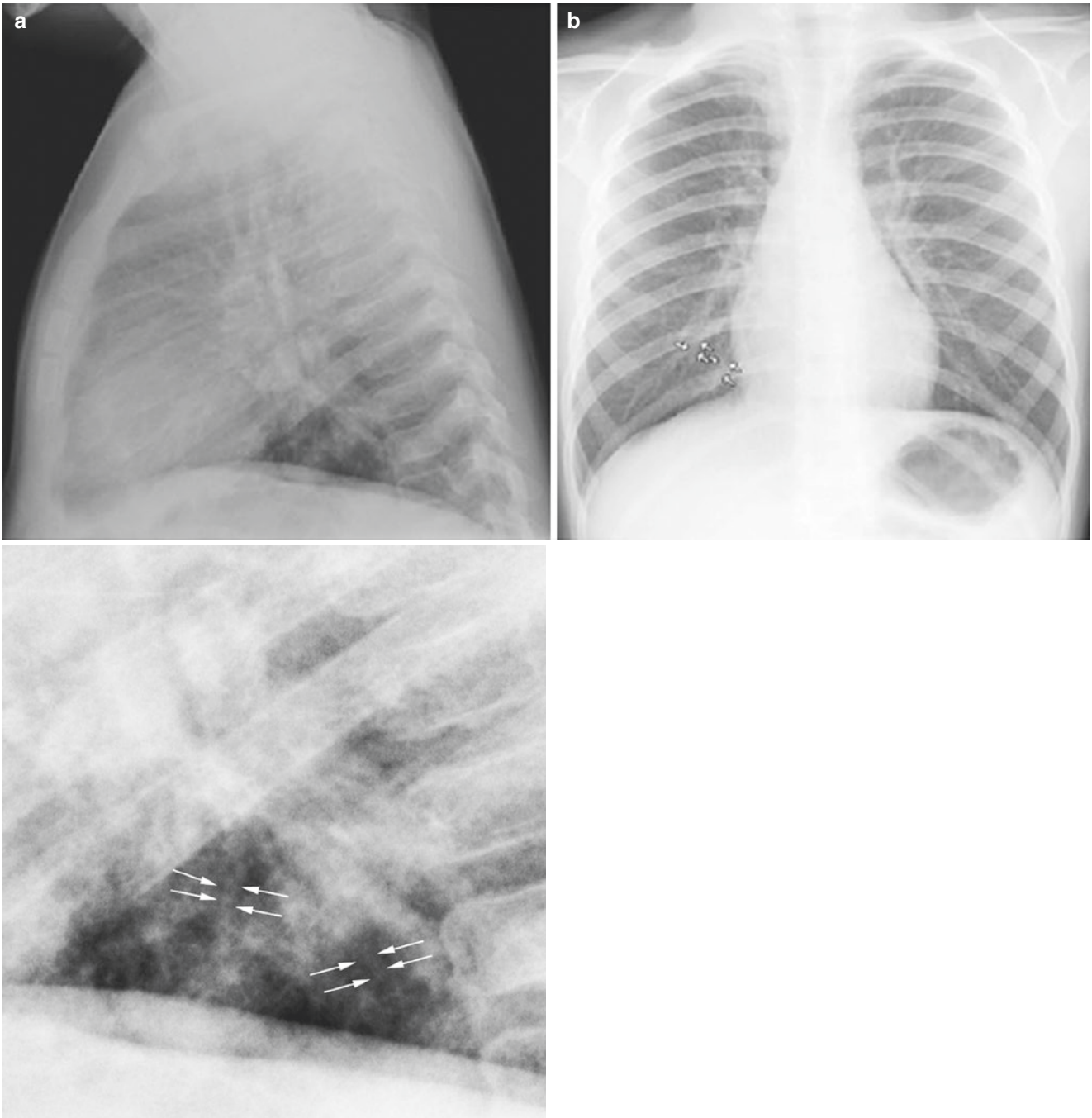

Fig. 10.35 (**a**) Lateral projection of the chest seen as Fig. 10.34 again reveals diffuse bronchial wall thickening. The convergence of the prominent bronchi has produced abnormally prominent hilar configuration, which is ill-defined (shaggy). (**b**) Tram tracking of thickened bronchial walls is seen in the right-lung base in a different patient (*arrows*) on PA projection and (**c**) lateral projection

Bronchiolitis obliterans (Swyer-James syndrome or McLeod syndrome) generally develops secondary to viral infection, although it can also arise from a bacterial or parasitic infection (i.e., mycoplasma). In adults, bronchiolitis obliterans is characterized by a hyperlucent small-volume lung, but in children by an overexpanded hyperlucent lung, a discrepancy explained by diminished lung growth following the onset of the disease. While air trapping is initially evident on imaging, proportionately less growth results in reduced lung volume compared to the more normal lung. In addition,

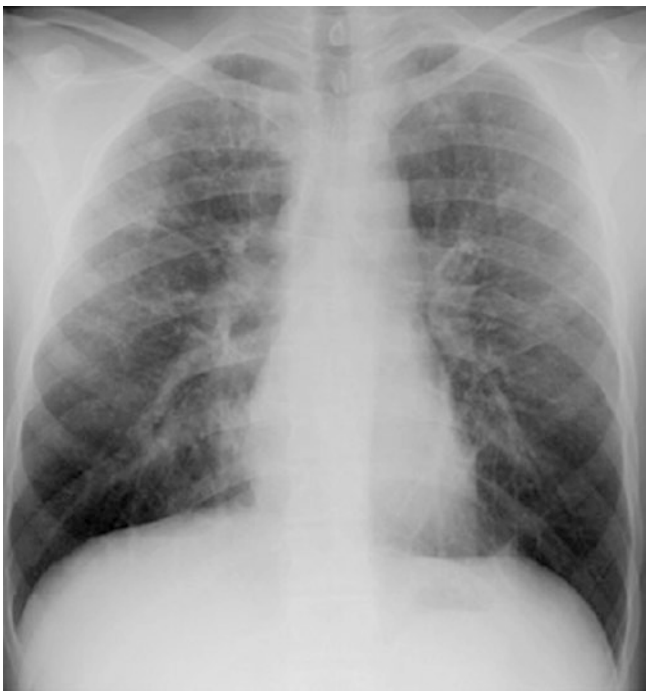

Fig. 10.36 This teenager with cystic fibrosis has the typical radiographic changes of her disease. There is diffuse bronchial wall thickening, with areas of bronchiectasis, prominent hilae, areas of atelectasis or fibrosis, and high lung volumes. In approximately 50% of patients with bronchiectasis, it will be most accentuated in the upper lobes

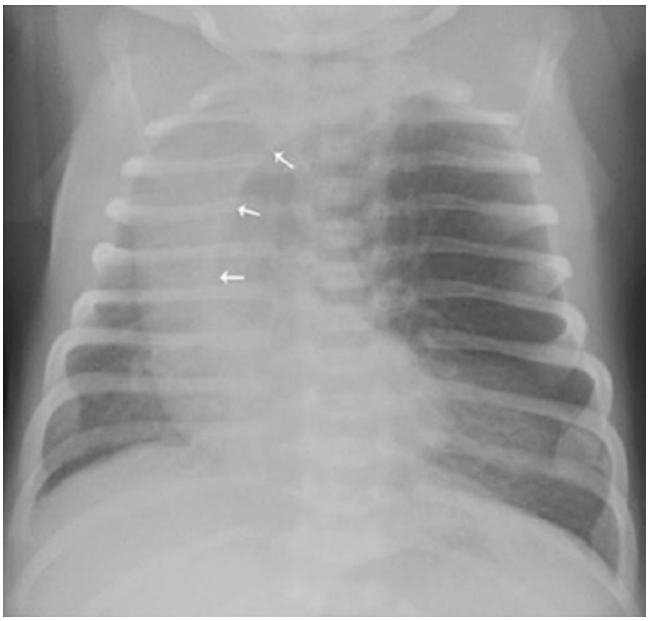

Fig. 10.37 There is congenital lobar emphysema of the left upper lobe with overinflation and increased lucency of the left upper lobe. This has resulted in mediastinal shift to the right and bilateral lower lobe atelectasis (left greater than the right). The *arrows* point the anterior junction line, where the pleural margins of the two lungs meet anteriorly. It is shifted to the right secondary to "herniation" of the overinflated left upper lobe

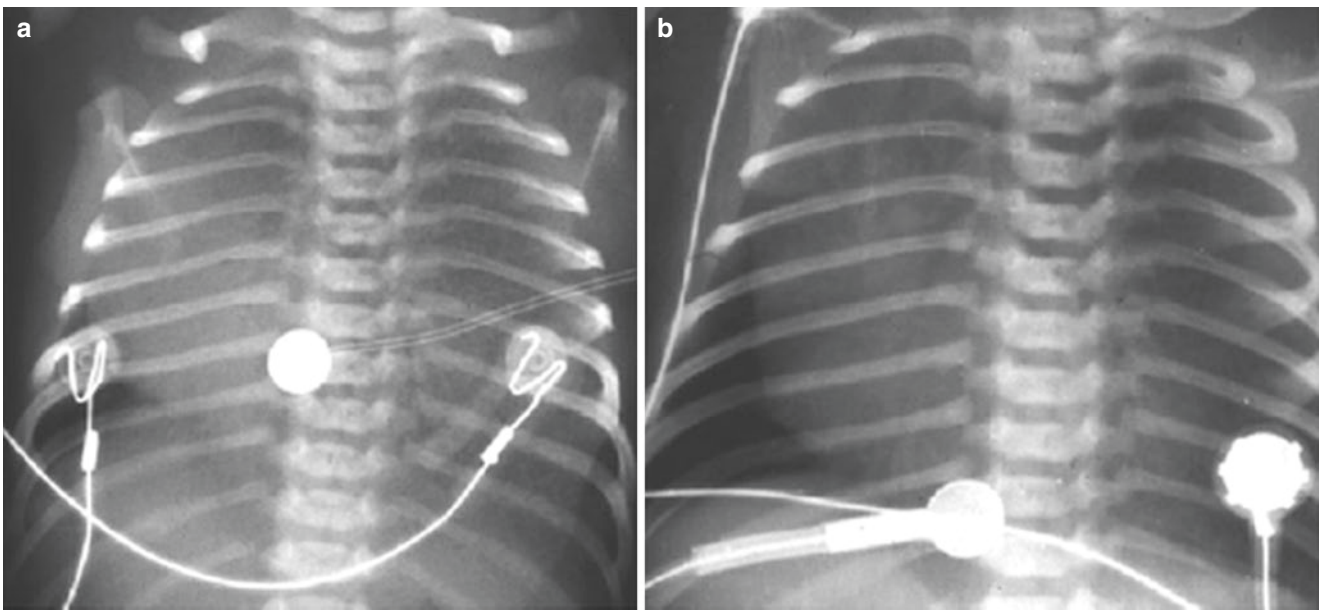

Fig. 10.38 (**a**) Polyalveolar left upper lobe with retained fetal lung liquid producing and overdistended and opaque left upper lobe in this 2 h old girl. (**b**) By 4 days of life, most of the fetal lung liquid has drained from the left upper lobe. (From Cleveland [3], with permission of Lippincott Williams & Wilkins)

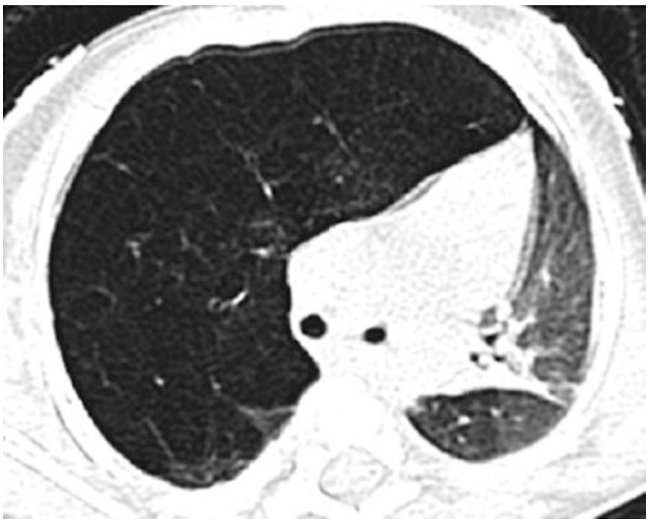

Fig. 10.39 Lung window CT image in an infant with right upper lobe congenital lobar emphysema demonstrates markedly hyperinflated right upper lobe resulting in mediastinal shift to the left side. Underlying lung parenchyma of the right upper lobe despite hyperinflation was well seen on lung window CT image

it has been established that many cases of bronchiolitis obliterans feature diffuse and irregularly affected lungs. Specifically, on CT, both lungs may show abnormalities, including bronchiectasis [43], but one lung typically dominates (Fig. 10.40).

Other inflammatory diseases may add to the diagnostic confusion. The early stages of follicular bronchitis [44] may radiographically and clinically resemble bronchiolitis. This disease, which some equate with "neuroendocrine cell hyperplasia" (NeHi), usually presents within the first 6–8 weeks of life. However, contrary to the typically short-lived clinical course of bronchiolitis, the tachypnea and wheezing characteristic of follicular bronchitis persist for 2–3 years. Radiographic findings initially suggest bronchiolitis because of air trapping, bronchial wall thickening, and occasional instances of atelectasis. By approximately 5 or 6 months of age, a diffuse, essentially interstitial process has evolved, and by 8 years of age, symptoms and radiographic indicators have generally reverted to normal. Recent work has identified a CT configuration specific for NeHi (Fig. 10.41) with anterior and perihilar dominant interstitial disease [45].

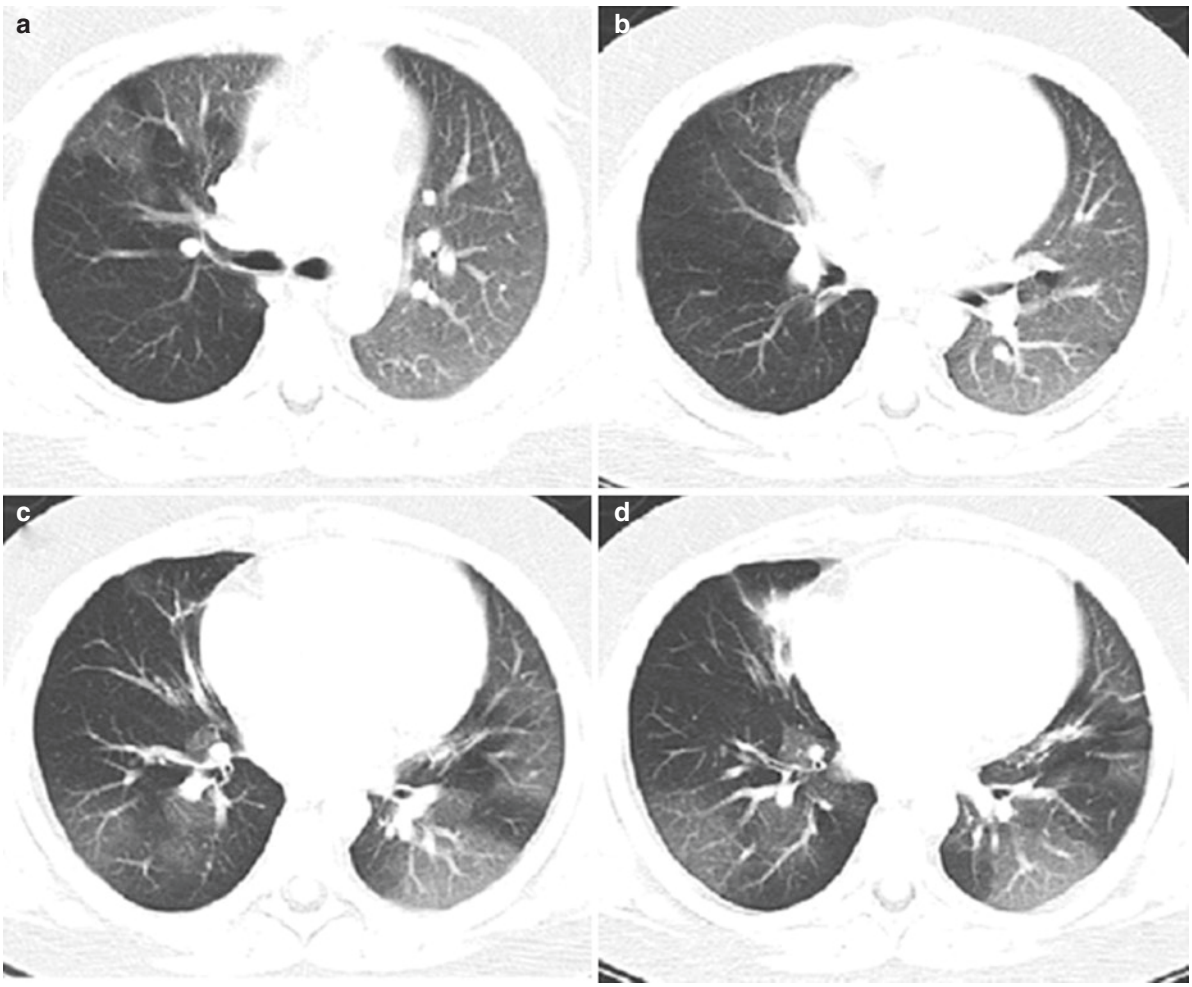

Fig. 10.40 CT of bonchiolitis obliterans presents with accentuated hyperlucent oligemic segments of lung, usually worse in one lung with associated mild-to-moderate bronchiectasis. (**a**–**d**) Images at discontiguous levels from cranial to caudal

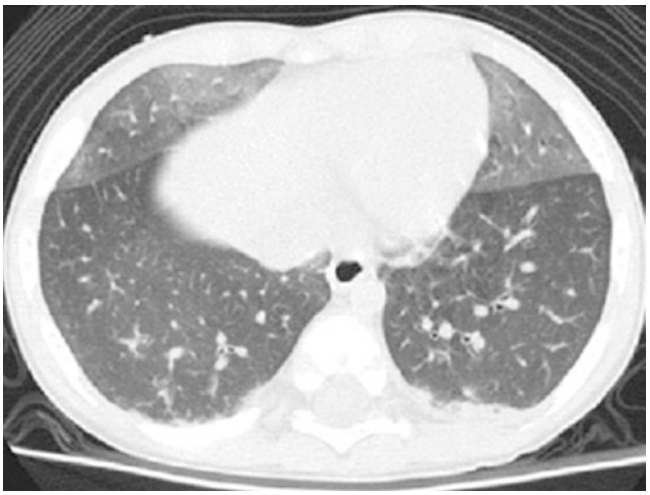

Fig. 10.41 CT study with lung window settings demonstrates ground-glass opacity in the right middle lobe and lingula in a 23-month-old infant with biopsy proven NeHi

References

1. Cleveland RH. The pediatric airway. Contemp Diagn Radiol. 1996;19:1–6.
2. Bramson RT, Griscom NT, Cleveland RH. Interpretation of chest radiographs in infants with cough and fever. Radiology. 2005;236:22–9.
3. Cleveland RH. The pediatric airway. In: Taveras JM, Ferrucci JT, editors. Radiology: diagnosis, imaging, intervention, vol. vol. 1., Chap. 48A. Philadelphia: JB Lippincott; 1997. p. 1–13.
4. Cleveland R. The pediatric airway. Syllabus IDKD: diseases of the heart, chest & breast. Milan: Springer-Verlag Italia; 2007. p. 204–8.
5. Leung KC, Cho H. Diagnosis of stridor in children. Am Fam Physician. 1999;60:2289–96.
6. AASM Manual for the Scoring of Sleep and Associated Events. Rules, terminology and technical specifications. Westchester: American Academy of Sleep Medicine; 2007.
7. Lumeng JC, Chervin RD. Epidemiology of pediatric obstructive sleep apnea. Proc Am Thorac Soc. 2008;5(2):242–52.
8. Redline S, Tishler PV, Schluchte M, Aylor J, Clark K, Graham G. Risk factors for sleep-disordered breathing in children. Associations with obesity, race, and respiratory problems. Am J Respir Crit Care Med. 1999;159:1527–32.
9. Dyken ME, Lin-Dyken DC, Poulton S, et al. Prospective polysomnographic analysis of obstructive sleep apnea in Down syndrome. Arch Pediatr Adolesc Med. 2003;157:655–60.
10. Chesson AL Jr, Ferber RA, Fry JM, Grigg-Damberger M, Hartse KM, Hurwitz TD, et al. The indications for polysomnography and related procedures. Sleep. 1997;20(6):423–87.
11. Brooks LJ, Stevens BM, Bacevice AM. Adenoid size is related to severity but not the number of episodes of obstructive apnea in children. J Pediatr. 1998;132(4):682–6.
12. Mitchell RB. Adenotonsillectomy for obstructive sleep apnea in children: outcome evaluated by pre- and postoperative polysomnography. Laryngoscope. 2007;117(10):1844–54.
13. Mitchell RB, Kelly J. Outcome of adenotonsillectomy for obstructive sleep apnea in obese and normal weight children. Otolaryngol Head Neck Surg. 2007;137(1):43–8.
14. Muntz H, Wilson M, Park A, et al. Sleep disordered breathing and obstructive sleep apnea in the cleft population. Laryngoscope. 2008;118(2):348–53.
15. Gutierrez JP, Berkowitz RG, Robertson C. Vallecular cysts in newborns and young infants. Pediatr Pulmonol. 1999;27:282–5.
16. Chow PY, Nag DK, Poon G, Hui Y. Vallecular cyst in a neonate. Hong Kong Med J. 2002;8:464.
17. Myer CH. Vallecular cyst in the newborn. Ear Nose Throat J. 1988;67:122–4.
18. Gluckman PG, Chu TW, Van-Hasselt CA. Neonatal vallecular cyst and failure to thrive. J Laryngol Otol. 1992;106:448–9.
19. Santiago W, Rybak LP, Bass RM. Thyroglossal duct cyst of the tongue. J Otolaryngol. 1985;14:261–4.
20. Lee EY, Siegel MJ, Hildebolt CF, Gutierrez FR, Fallah JH. MDCT evaluation of thoracic aortic anomalies in pediatric patients and young adults: comparison of axial, multiplanar, and 3D images. AJR Am J Roentgenol. 2004;182:777–84.
21. Wittenborg MH, Gyepes MT, Crocker D. Tracheal dynamics in infants with respiratory distress, stridor, and collapsing trachea. Radiology. 1967;88:653–62.
22. Gruden JF, Webb WR, Sides DM. Adult onset disseminated tracheobronchial papillomatosis: CT features. J Comput Assist Tomogr. 1994;18:640–2.
23. Mahboubi S, Behhah RD. CT evaluation of tracheobronchial tumors in children. Int J Pediatr Otorhinolaryngol. 1992;24:135–43.
24. Cleveland RH. Symmetry of bronchial angles in children. Radiology. 1979;133:89–93.
25. Jaramillo D, Cleveland RH, Blickman JG. Radiologic management of esophageal foreign bodies. Semin Intervent Radiol. 1991;8:198–203.
26. Berdon WE, Baker DH. Vascular anomalies and the infant lung: rings, slings, and other things. Semin Roentgenol. 1972;7:39–64.
27. van Son JA, Konstantinov IE, Burckhard F. Kommerell and Kommerell's diverticulum. Tex Heart Inst J. 2002;29:109–12.
28. Mossad E, Ibraim F, Youssef G, et al. Diverticulum of Kommerell: a review of a series and a report of a case with tracheal deviation compromising single lung ventilation. Anesth Analg. 2002;94:1462–4.
29. Lee EY, Siegel MJ. MDCT of tracheobronchial narrowing in pediatric patients. J Thorac Imaging. 2007;22:300–9.
30. Karcaaltincaba M, Haliloglu M, Ekinci S. Partial tracheal duplication: MDCT bronchoscopic diagnosis. AJR Am J Roentgenol. 2004;183:290–2.
31. Dupuis C, Charaf LA, Breviere GM, Abou P. "Infantile" form of the scimitar syndrome with pulmonary hypertension. Am J Cardiol. 1993;71:1326–30.
32. Horcher E, Helmer F. Scimitar syndrome and associated pulmonary sequestration: report of a successfully corrected case. Prog Pediatr Surg. 1987;21:107–11.
33. McGuinness G, Naidich DP, Garay SM, Davis AL, Boyd AD, Mizrachi HH. Accessory cardiac bronchus: CT features and clinical significance. Radiology. 1993;189:563–6.
34. Cleveland RH, Mark EJ. Case records of the Massachusetts General Hospital: case #31–1998. New Eng J Med. 1998;339:1144–52.
35. Woodring JH, Barrett PA, Rehm SR, Nurenberg P. Acauired tracheomegaly in adults as a complication of diffuse pulmonary fibrosis. AJR. 1989;152:743–7.
36. Cleveland RH, Neish AS, Nichols DP, Zurakowski D, Wohl MEB, Colin AA. Cystic fibrosis: a system for assessing and predicting progression. AJR Am J Roentgenol. 1998;170:1067–72.
37. Cleveland RH, Neish AS, Nichols DP, Zurakowski D, Wohl MEB, Colin AA. Cystic fibrosis: predictors of accelerated decline and distribution of disease in 230 patients. AJR Am J Roentgenol. 1998;171:1311–5.
38. Majewski S, Piotrowski W. Pulmonary manifestations of inflammatory bowel disease. Arch Med Sci. 2015;11:1179–88.
39. Mahadeva R, Walsh G, Flower CD, Shneerson JM. Clinical and radiological characteristic of lung disease in inflammatory bowel disease. Eur Respir J. 2000;15:41–8.
40. Cleveland R. Congenital lobar emphysema: case 4. In: Siegel MJ, Bisset GS, Cleveland RH, Donaldson JS, Fellows KE, Patriquin HB, editors. ACR pediatric disease (fourth series) test and syllabus. Reston: American College of Radiology; 1993. p. 96–130.

41. Cleveland RH, Weber B. Retained fetal lung liquid in congenital lobar emphysema: a possible predictor of polyalveolar lobe. Pediatr Radiol. 1993;23:291–5.
42. Cleveland RH. A radiologic update on medical diseases of the newborn chest. Pediatr Radiol. 1995;25:631–7.
43. Padley SP, Adler BD, Hansell DM, Muller NL. Bronchiolitis obliterans: high resolution CT findings and correlation with pulmonary function tests. Clin Radiol. 1993;47:236–40.
44. Bramson RT, Cleveland RH, Blickman JG, Kinane TB. The radiographic appearance of follicular bronchitis in children. AJR Am J Roentgenol. 1996;166:1447–50.
45. Brody AS, Crotty EJ. Neuroendocrine cell hyperplasia of infancy (NEHI). Pediatr Radiol. 2006;36:1328.

Pleural Effusion and Pneumothorax

11

Efraim Sadot and Edward Y. Lee

Pleural Effusion

The volume of normal pleural fluid is small and approximates 0.26 mL/kg body weight [2]. In the healthy pleura, about 10% of the volume is formed hourly and the same volume is absorbed to maintain steady state. Hydrostatic pressure opposed by counterbalancing osmotic pressure with an average of approximately 12 cmH_2O drives pressure for the movement of liquid into the pleural space.

Pleural fluid originates from systemic vessels that feed the pleura, and it is assumed that the parietal pleura is the major source for fluid formation [3]. Several mechanisms are suggested for fluid removal from the pleural space including reabsorption by mesothelial cells and passive flow of fluid into the low-pressure interstitial space of the lung. The most likely route of fluid removal is by lymphatic drainage via openings in the parietal portion of the pleural membrane, the stomata. Flow of lymphatic fluid is influenced both by contractility of the lymph vessels and by respiratory movements [4–6].

When balance between the entry and exit of fluid is disturbed, pleural effusion develops. Both mechanisms, increase in fluid entrance and decrease in fluid clearance, contribute to fluid accumulation [7]. Increase in fluid entry can be due to increase in fluid conductance through the pleura, elevated microvascular pressure (venous more than arterial), decrease in pleural pressure (as seen in substantial atelectasis), and decrease in plasma oncotic pressure. Decrease in fluid clearance is usually the result of reduction in lymphatic drainage as listed in Table 11.1.

E. Sadot (✉)
Department of Pediatric Intensive Care, Dana-Dwek Children's Hospital, Tel-Aviv Sourasky Medical Center and Sackler Faculty of Medicine, Tel-Aviv University, Tel-Aviv, Israel
e-mail: efraims@tlvmc.gov.il

E. Y. Lee
Department of Radiology, Boston Children's Hospital and Harvard Medical School, Boston, MA, USA

Normal pleural fluid is clear in appearance, slightly alkaline compared to serum, and has low protein content (1–2 g/dL), 1500–4500 white blood cells per cubic millimeter, mostly monocytes. Glucose content is similar to that of plasma, and lactate dehydrogenase level is less than 50% of plasma [8]. Abnormal pleural fluid should be characterized in order to distinguish different pathophysiologic processes. The Light criteria assist in differentiating transudate from exudate (Table 11.2) [9]. When none of the criteria are met, fluid accumulation is likely transudate.

Fluid pH, glucose concentration, white cell count, and differential, stains, cultures, specific serologic assays and polymerase chain reaction (PCR) assays are additional tests that assist in characterizing the fluid nature. When pleural fluid sample is milky in appearance, or a question of chylothorax is raised (e.g., congenital or following surgical intervention), triglyceride level should be checked to ascertain if it is elevated above 110 mg/dL. When fluid is bloody with a hematocrit of greater than 50% that in blood, hemothorax is likely the diagnosis.

Table 11.1 Factors altering pleural lymphatic drainage

Intrinsic	Extrinsic
Inflammation	Increase central venous pressure
Injury (e.g., iatrogenic during surgery, irradiation, etc.)	Pleural disease (pneumonia, malignancy) with decreased or blocked stomata
Congenital abnormality (e.g., lymphangiectasis)	Compression of the lymphatic vessels Decreased motion of the diaphragm (e.g., collapsed lung, diaphragmatic paralysis)

Table 11.2 Light's criteria to differentiate transudate from exudate

Protein ratio (pleural fluid/serum) less than 0.5
Lactic dehydrogenase (LDH) ratio (pleural fluid/serum) greater than 0.6
Pleural fluid LDH more than 2/3 the upper limit for serum

R. H. Cleveland, E. Y. Lee (eds.), *Imaging in Pediatric Pulmonology*, https://doi.org/10.1007/978-3-030-23979-4_11

Empyema is the presence of purulent material consisting typically of neutrophils and fibrin in the pleural space. Nearly one-half of all children with bacterial pneumonia develop parapneumonic effusions. Approximately 5% of the effusions complicating community-acquired pneumonia progress to empyema with an increase in the incidence of empyema over time [10]. Progression of a pleural effusion to empyema starts with the *exudative* phase, where most pleural effusions progress to and resolve with antibiotics alone [11, 12]. The *fibrinopurulent* phase is the next stage that starts when the pleural fluid becomes infected. White blood cells, mainly neutrophils, accumulate and fibrin deposition starts. The fluid becomes loculated, with decrease in pH and glucose concentration and increase in lactate dehydrogenase concentration. The most common pathogens in children are *Streptococcus pneumoniae*, *Staphylococcus aureus*, and *Streptococcus pyogenes* [11, 13–15]. The *organization* step takes place when fibroblasts migrate into the fluid and form membranes.

Complications of empyema include restriction of inspiration, bronchopleural fistula, bacteremia, pericarditis, and pneumothorax. In addition to infected pleural effusion, two other conditions commonly associated with organizing effusions are hemothorax and malignant effusions (other than lymphoma).

Imaging Studies

It is important to recognize even a small pleural effusion as it affects the differential diagnosis. In practice, this is most commonly relevant in differentiating bacterial pneumonia (may have an effusion) as opposed to viral infection (rarely has an effusion). In preterm neonates with respiratory distress, a small effusion suggests neonatal pneumonia or Transient Tachypnea of the Newborn (TTN) as opposed to uncomplicated surfactant deficiency syndrome.

Free pleural fluid accumulates in the dependent area. In the upright patient, a small amount of pleural fluid blunts the posterior costophrenic angle, often more apparent on a lateral chest X-ray (CXR) than on frontal projection (Fig. 11.1). With slightly larger effusions, a small amount of fluid can be noted in the lateral costophrenic angle (Fig. 11.2) and often in the medial costophrenic angle. As more fluid accumulates, the entire outline of the diaphragm on the affected side may become obscured with fluid extending upward around the

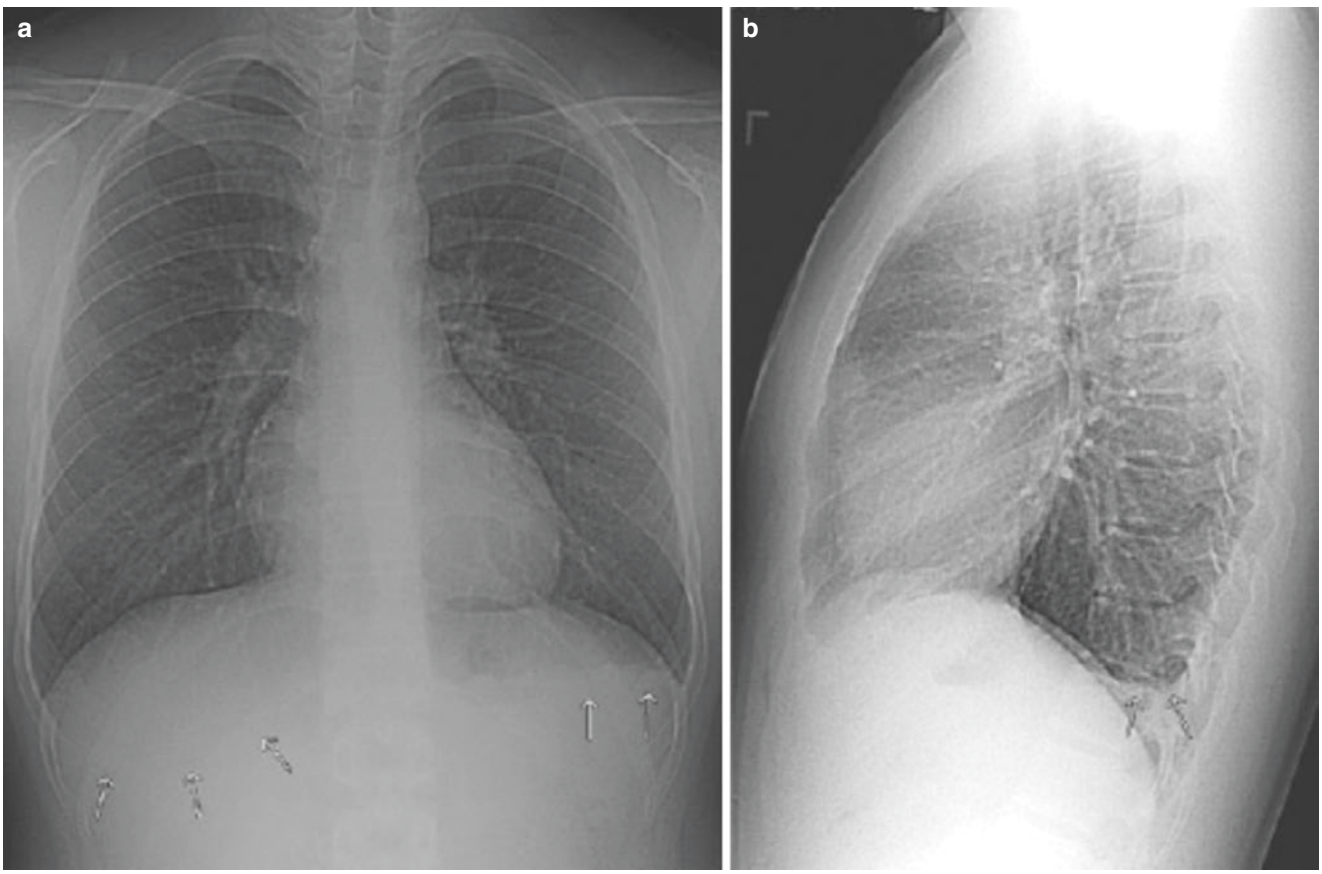

Fig. 11.1 (**a**) Frontal chest radiograph: *Right arrows* indicate the normal posterior costophrenic margin. *Left arrows* point to the stomach air/fluid level. No clear effusion is noted. (**b**) Lateral chest radiograph: *Arrows* indicate a small left-sided pleural effusion, obscured by the gastric content on the PA image

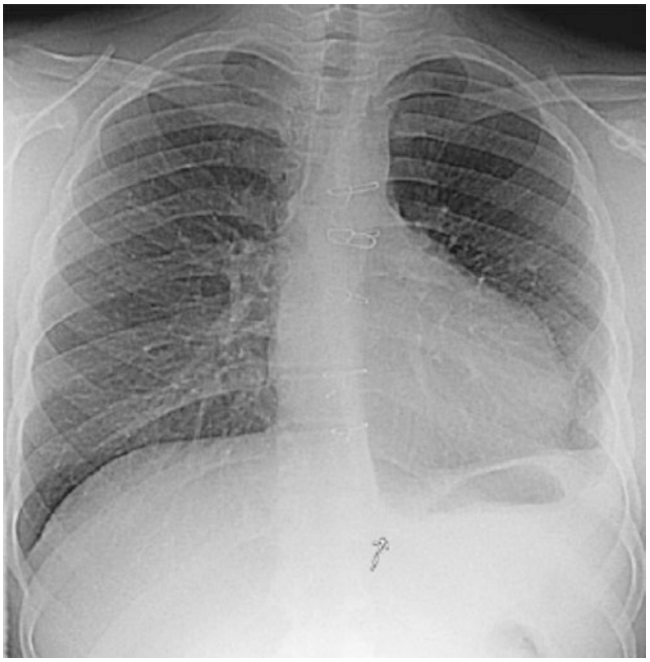

Fig. 11.2 A small effusion is noted in the lateral costophrenic angle, with a component in the inferior portion of the major fissure. The *arrow* indicates fluid in the medial costophrenic angle

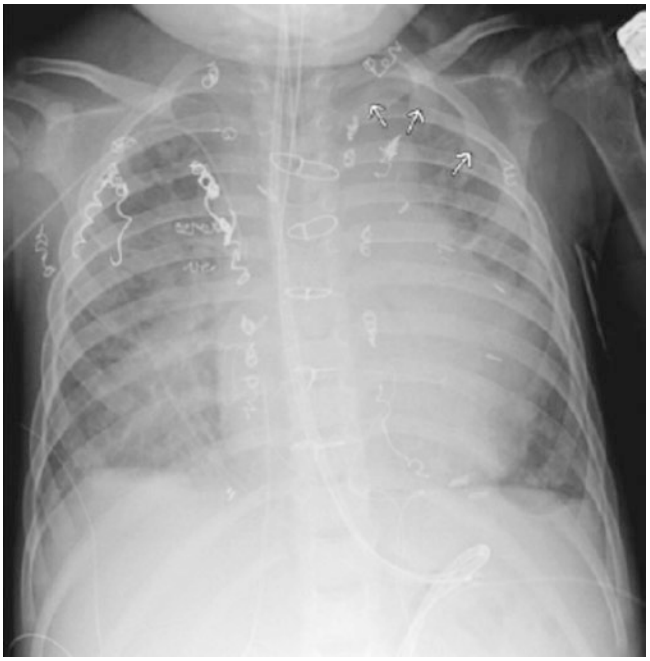

Fig. 11.4 *Arrows* indicate a small effusion extending over the left apex and somewhat laterally. A smaller effusion is also noted on the right

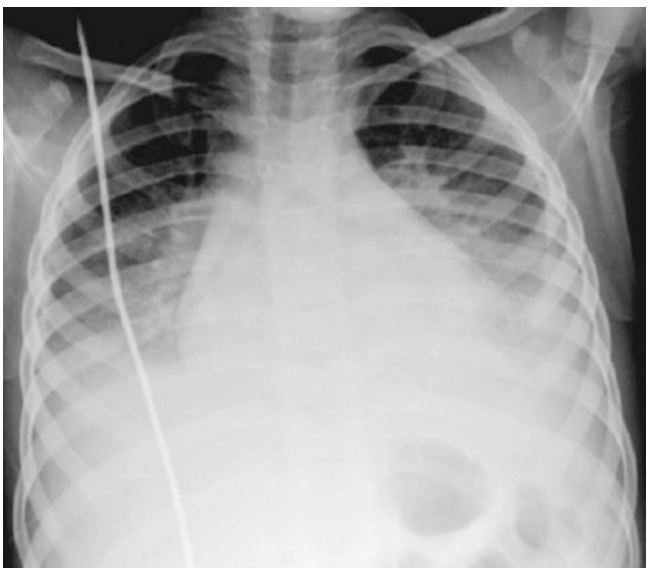

Fig. 11.3 There is a moderate effusion on the left extending up the lateral chest wall. A similarly distributed, smaller effusion is present on the right

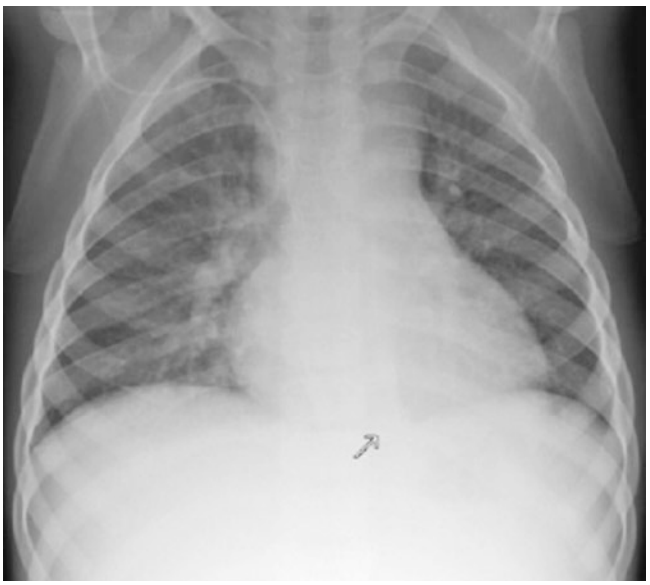

Fig. 11.5 *Arrow* indicates a small amount of fluid blunting the medial costophrenic angle

anterior, lateral, and posterior thoracic walls, producing opacification of the lung base with a smooth tapering meniscus narrowing superiorly (Fig. 11.3).

In the supine position, small effusions are often first seen as an apical cap (Fig. 11.4) and then, as it enlarges, as blunting of the inferior medial costophrenic sulcus (Fig. 11.5) and subsequently the lateral costophrenic angle (Fig. 11.6). As it enlarges further, it builds up around the lung, and extends into the fissures (Fig. 11.7) eventually causing the entire hemithorax to become opacified [16] (Fig. 11.8). Lateral decubitus radiograph, while lying on the affected side, can help in differentiating between the presence of fluid and other reasons for opacification such as large pneumonia or pleural thickening (Figs. 11.3 and 11.9). As little as 5 mL of pleural fluid can be detected with properly exposed decubi-

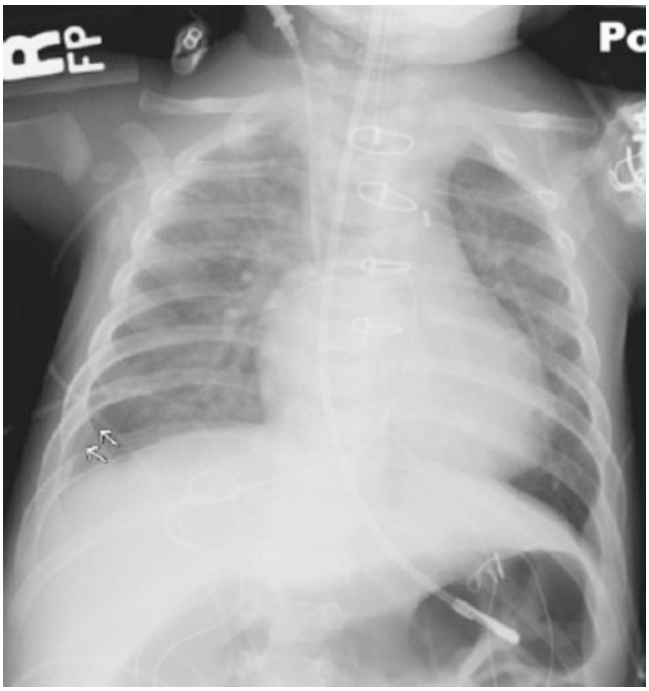

Fig. 11.6 There is blunting of the right lateral costophrenic angle with a small amount of fluid (*arrows*) in the major fissure

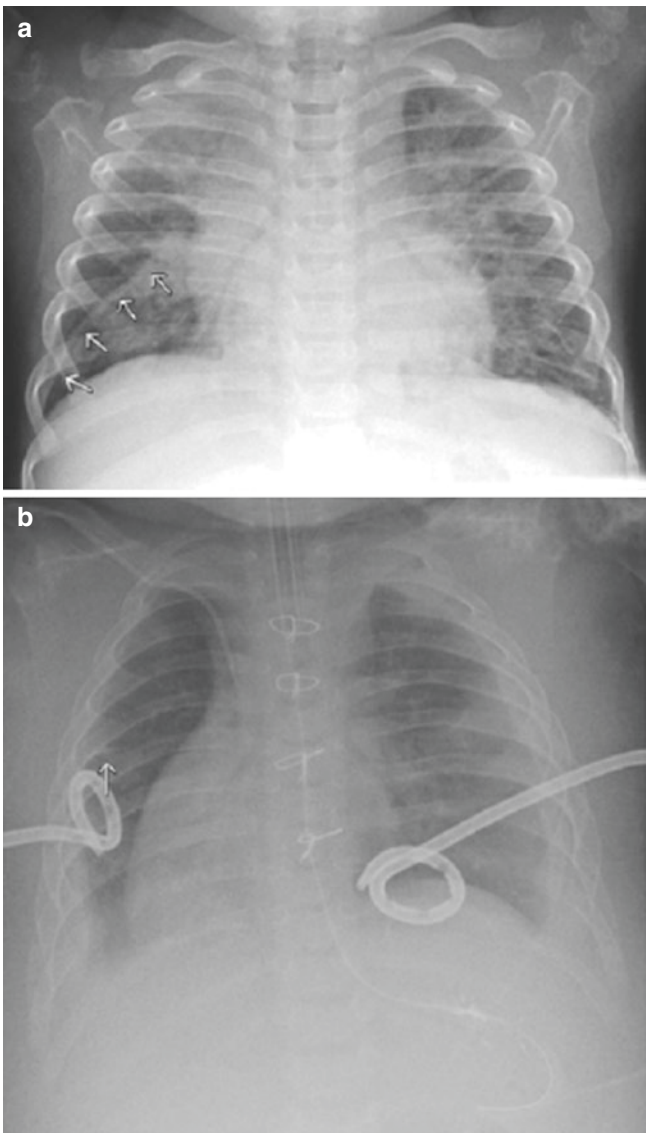

Fig. 11.7 (**a**) *Arrows* indicate a moderate amount of fluid in the right major fissure. (**b**) *Arrow* indicates a small amount of fluid in the minor fissure with effusions surrounding both lungs

tus radiographs [17]. When pleural fluid is loculated, the contour of the effusion may be irregular and not conform to gravitational forces. It does not change appreciably in distribution on decubitus imaging (Fig. 11.10). When the whole hemithorax is opacified, decubitus radiographs are of no use and ultrasonic examination or computed tomography (CT) should be obtained. The advantages of ultrasound over CT are the ease and speed with which the study can be done and the absence of irradiation. Both have the ability to provide real-time guidance for thoracocentesis when required [18] (Fig. 11.11).

CT is the best study to visualize the pleural space [19, 20] (Fig. 11.12). CT differentiates parenchymal and pleural lesions, such as lung abscess and necrotizing pneumonia from an air fluid level due to empyema, and in addition, CT has the ability to image the margins of the lesion well (Fig. 11.13). When pulmonary embolism is suspected, CT pulmonary angiography (CTPA) is the study of choice with high sensitivity and specificity for proximal or segmental pulmonary artery involvement [21–24].

Exudative Pleural Effusions

Exudative pleural effusions are common and may develop as a result of infection, inflammation, injury, or malignancy. They are all prone to becoming organized and loculated. Effusions caused by pus, blood, or malignancy often become loculated. Once this occurs, it is no longer free-flowing. If an effusion is irregular in its configuration or is not dominantly in the dependent portion of the hemithorax, it is either partly or completely loculated (Fig. 11.10).

Parapneumonic effusion is an effusion associated with an infection of the lung with the spread of inflammation and infection to the pleural space. These effusions are becoming more common in the pediatric population with an increase in incidence that coincides with the rise in antibiotic-resistant organisms [25–29]. It is more common to develop parapneumonic effusions in winter and spring, twice as often than in the rest of the year [30, 31]. The most common presenting symptoms are persistent fever, tachypnea, cough, dyspnea, chest pain, and decreased appetite [25, 30, 32, 33]. Usually,

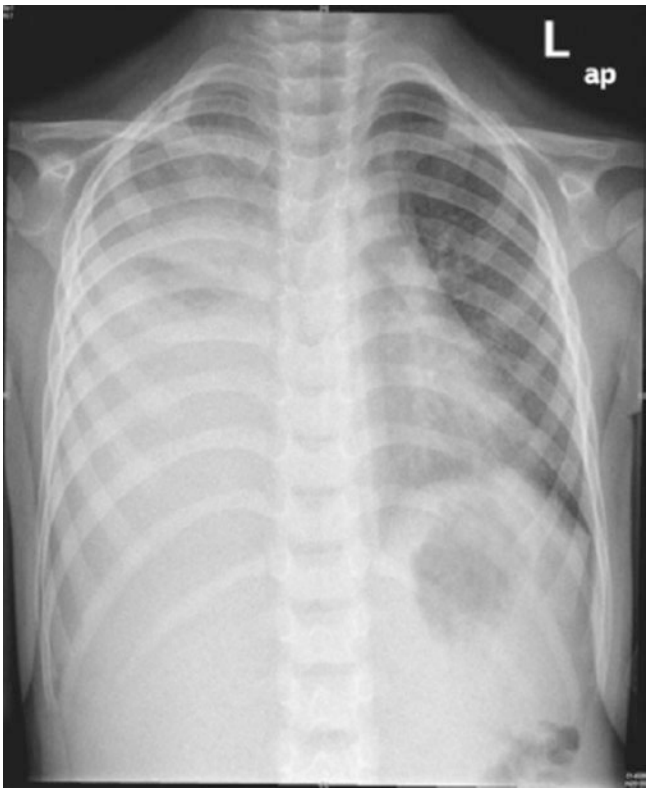

Fig. 11.8 There is almost complete opacification of the right hemithorax secondary to pneumonia and a large right effusion

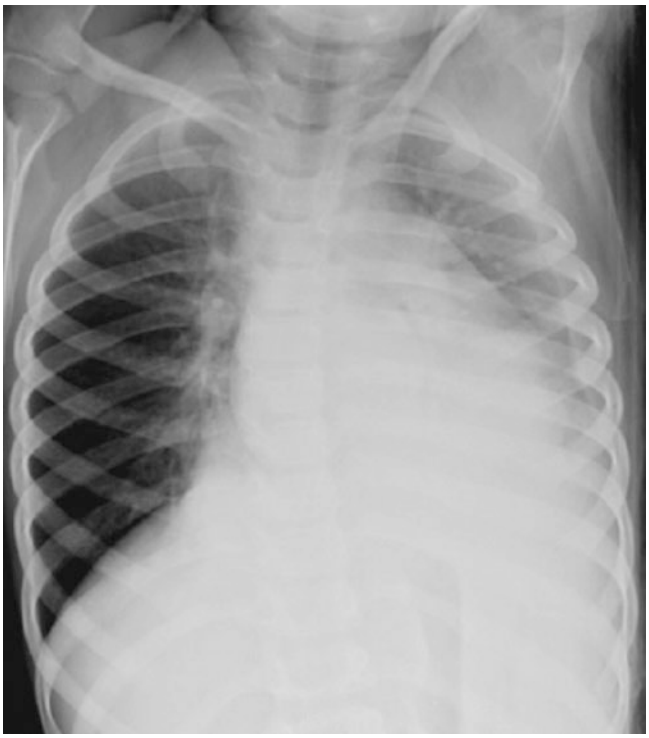

Fig. 11.9 Free-flowing effusion on supine is shown in Fig. 10.3. In this figure, the left decubitus radiograph reveals layering of the effusion dependent on the left. The right effusion has layered medially and is not convincingly seen

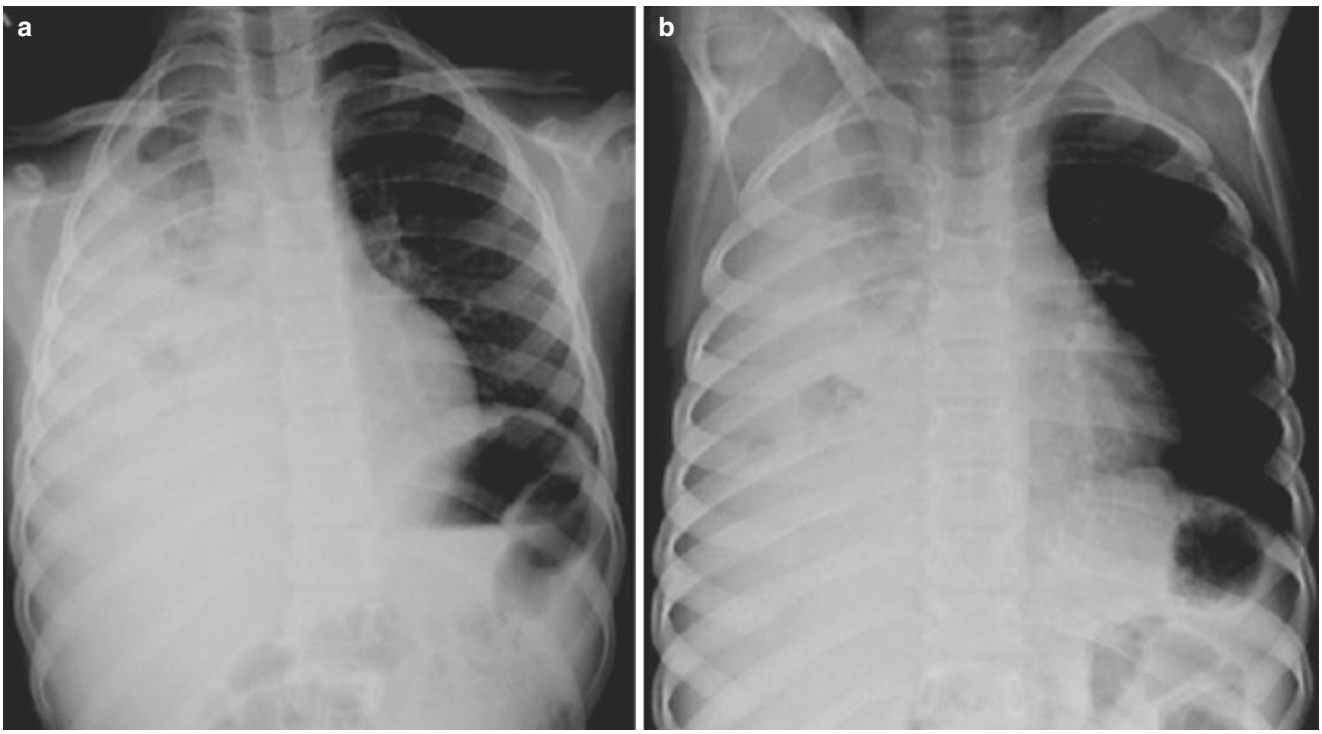

Fig. 11.10 Loculated pleural effusion on supine (**a**) and decubitus (**b**) radiographs with no significant change in the configuration or distribution of the effusion

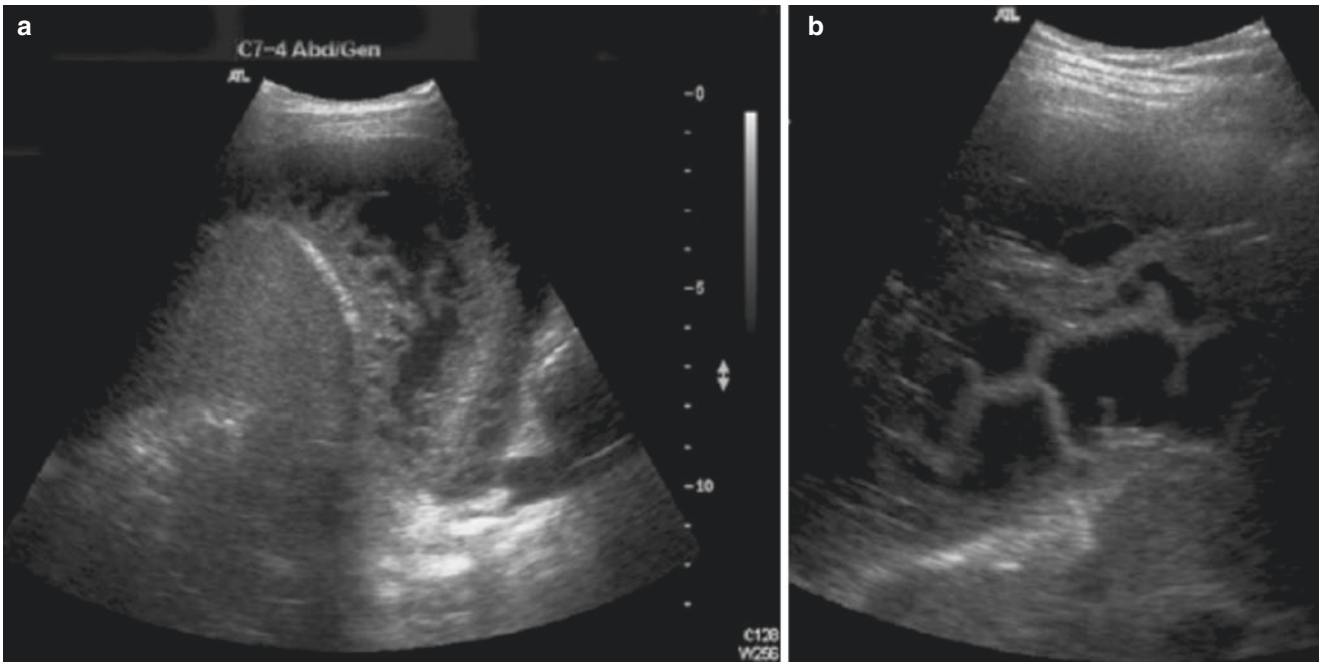

Fig. 11.11 Ultrasound of the chest demonstrates effusion with fine septae (**a**) and thick septae (**b**) with loculated fluid compartments

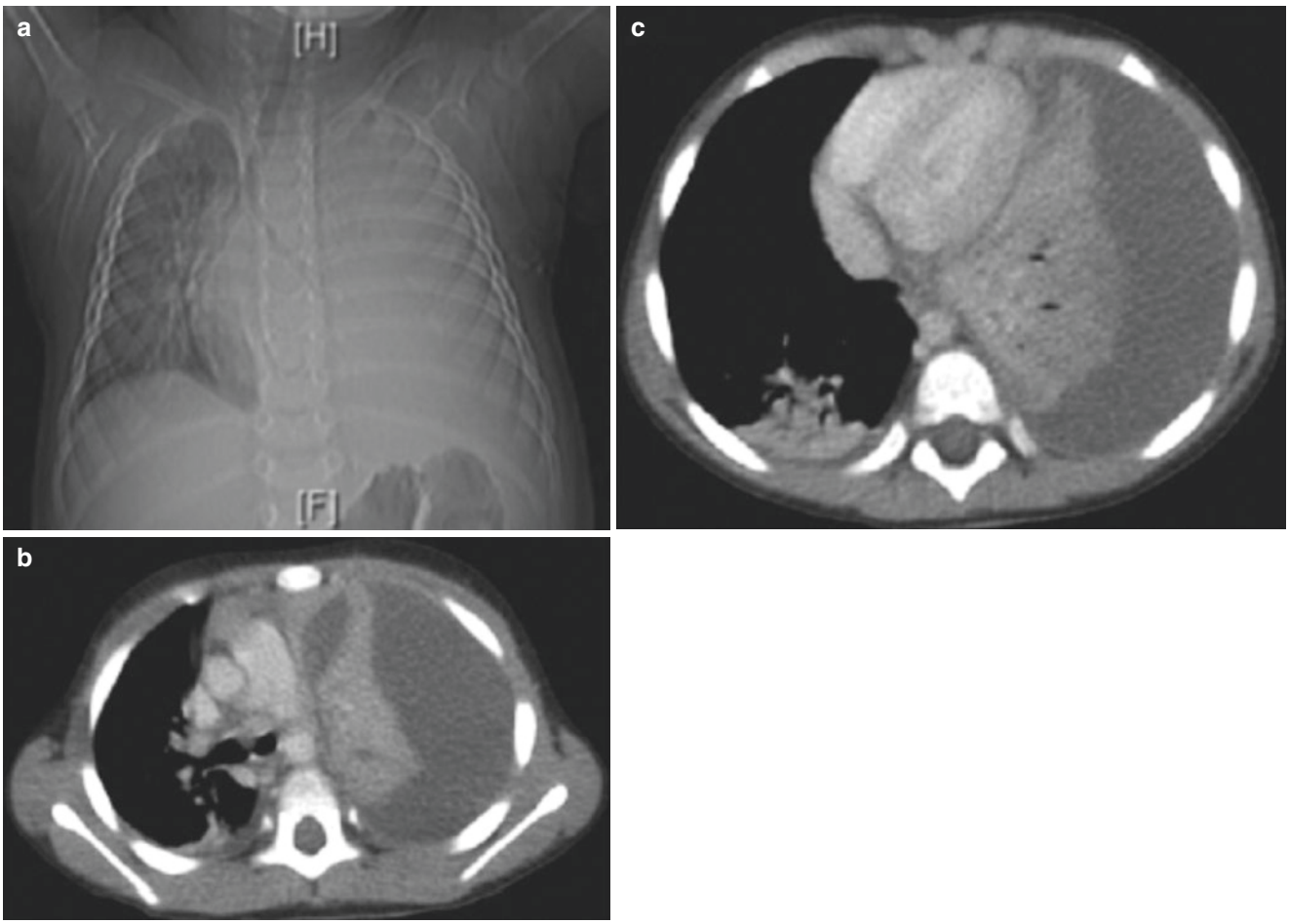

Fig. 11.12 Frontal chest radiograph (**a**) and CT images (**b**, **c**) demonstrate a large left pleural effusion with substantial deviation of the mediastinum to the right

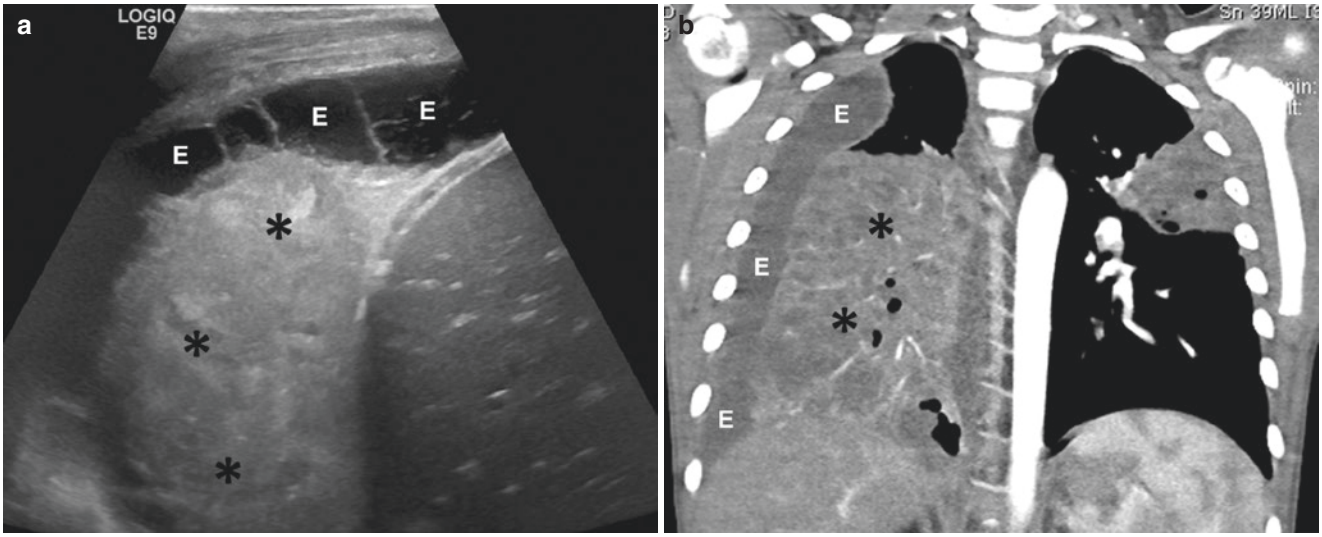

Fig. 11.13 An 8-year-old boy with loculated parapneumonic effusion (E) due to necrotizing pneumonia. Ultrasound image (**a**) and enhanced coronal CT image (**b**) show loculated effusion (E) with septations and adjacent necrotizing pneumonia (asterisks)

the child does not appear toxic, or in shock [34]. On exam, splinting toward the affected side could be noted; in addition, decrease in air entry and dullness to percussion are common findings.

Hypoalbuminemia, thrombocytosis, and leukocytosis are characteristics [35]. Hyponatremia secondary to inappropriate antidiuretic hormone (SIADH) secretion should be looked for. Chest radiograph does reveal the effusion, and with large volume of pleural fluid, mediastinal shift can occur (Fig. 11.8).

Blood, sputum, and pleural fluid, when available, should be sent for stains and cultures. Chest tube placement, intrapleural antifibrinolytic treatment, video-assisted thoracoscopic surgery (VATS), and pleurodesis are additional interventions to consider in cases of poor or no response to conventional antibiotic therapy.

In addition to pneumonia, there are other etiologies for exudative pleural effusions as previously discussed.

Pulmonary Embolism

Dyspnea and ipsilateral chest pain are the main symptoms and go along with pleural effusion in approximately 80% of cases. Associated conditions are hemoglobinopathies, nephrotic syndrome, and long bone fractures [36]. In the pediatric population, a recent study, focused on parenchymal and pleural abnormalities in children with and without pulmonary embolism at CTPA, showed that only wedge-shaped peripheral consolidation is significantly associated with pulmonary embolism on CTPA [37].

Pancreatitis

Cough, chest pain, and dyspnea accompany symptoms of pancreatitis. While free fluid is typically located adjacent to pancreas in acute cases, effusion, when present, is located in left hemithorax in chronic cases [38–41]. Effusion due to pancreatitis is often hemorrhagic, and amylase content is elevated [38–40].

Uremia

Chest pain, fever, cough as well as pericardial and pleural friction rub are common with uremia and resolve gradually with dialysis in most patients [42, 43]. The pleural fluid typically appears serosanguinous or hemorrhagic in 71% of patients and contains a predominance of lymphocytes more often than of neurtrophils [42].

Connective Tissue Disease

Pleural effusion is most commonly present in rheumatoid arthritis (RA) and systemic lupus erythematosus (SLE) among the connective tissue diseases. Immune complexes deposit in the pleural space and a consequent inflammatory response damages the pleural capillaries and causes capillary leak [44–46]. Pleurisy, dyspnea, and fever are common complaints, although pleural effusion can be asymptomatic. Spontaneous resolution can occur in cases of RA. Corticosteroids are often required in SLE cases. Decortication

is indicated in nonresponsive cases to avoid severe pleural thickening and trapped lung [47–50]. In cases of drug-induced lupus, discontinuation of the offending medication is recommended [51].

Mediastinal Injury

Esophageal perforation can be associated with pleural effusion and be accompanied by chest pain, dyspnea, fever, subcutaneous emphysema, and dysphagia. Pleuritic chest pain, fever, and dyspnea following cardiac injury are known as Dressler's syndrome and can develop within a few days to several months following injury [52–54].

Malignancy

Lymphoma is the most common childhood malignancy associated with pleural effusion [48]. In non-Hodgkin's lymphoma, effusion can be the presenting sign in contrast to Hodgkin's lymphoma where effusion is usually a late manifestation [55–57]. Large effusions are more common in non-Hodgkin's lymphoma. Leukemia, neuroblastoma, rhabdomyosarcoma, Ewing sarcoma, and Wilm's tumor are occasionally associated with pleural effusions (Fig. 11.14). Malignant effusion is usually unilateral. Most effusions resolve with chemotherapy and irradiation. In refractory cases, pleurodesis is recommended [58].

Chylous Effusion

These are most commonly due to injury to the thoracic duct either from trauma or following cardiothoracic surgery [59]. In newborns with pleural effusion and no history of birth trauma, chylothorax is common. Chyle appears milky, but has straw color appearance in malnourished patients and in newborns [60, 61]. Triglyceride content >110 mg/dl is diagnostic of chylothorax, whereas levels below 50 mg/dL make the diagnosis unlikely. Treatment includes drainage and nutritional support [62, 63]. However, if associated with pulmonary lymphangiectasia (which is usually not apparent), drainage may be prolonged, leading to depletion of lymphocytes and hypoproteinemia (Fig. 11.15). Therefore, drainage of a congenital chylous effusion should be approached cautiously.

Hemothorax

Collection of fluid in the pleural space with a hematocrit of at least 50% that of blood is considered as hemothorax [64]. The most common cause of hemothorax is trauma. Additional causes for hemothorax include erosion of a vessel by a central venous catheter, pulmonary infarction, rupture of a congenital vascular anomaly, bleeding diathesis, and spontaneous rupture of an intrathoracic blood vessel. The radiographic evidence of the presence of blood in the pleural space appears several hours after the bleed. Chest radiographs should be repeated in trauma cases particularly if the patient develops

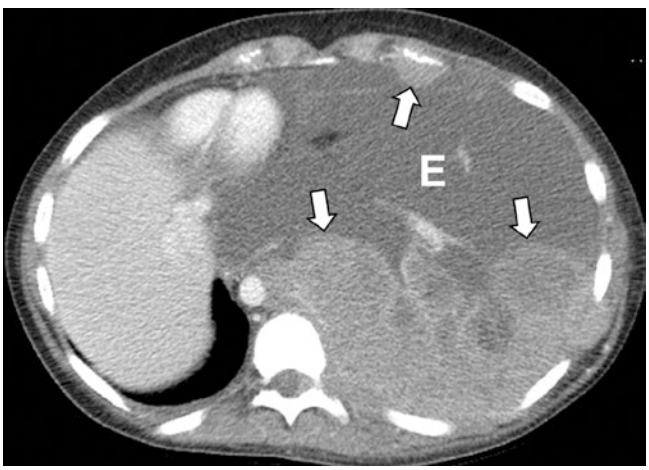

Fig. 11.14 A 16-year-old girl with malignant pleural effusion due to metastatic rhabdomyosarcoma. Enhanced axial CT image shows multiple pleural-based enhancing metastases (arrows) and large left effusion (E)

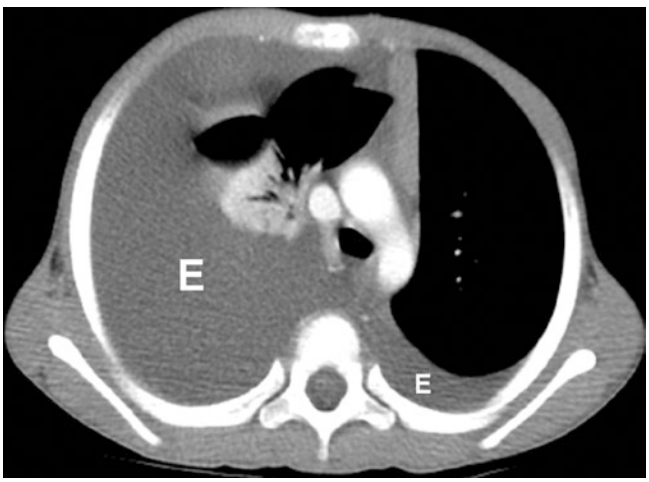

Fig. 11.15 A 4-year-old boy with effusion due to underlying Gorham disease. Enhanced axial CT image shows large right and moderate left effusions (E)

respiratory distress. Management consists of drainage of the bloody fluid, allowing re-expansion of the collapsed lung, and treatment of the underlying problem.

Transudative Pleural Effusions

Transudative pleural effusions frequently accompany common disease states. The primary abnormality originates, usually, from an organ other than the pleura.

Congestive Heart Failure

Clearance of the pleural fluid is decreased with heart failure. On chest radiography, cardiomegaly is apparent. Dyspnea on exertion and failure to gain weight are additional clinical signs. The effusion tends to be right sided or bilateral. Interstitial and alveolar edema can often be seen. Pleural fluid meets transudate characteristics according to Light's criteria, but can have higher protein and LDH concentration under diuretic therapy [65]. Treatment includes afterload reduction with diuretics and inotropes.

Nephrotic Syndrome

Approximately 20% of nephrotic syndrome patients have a concomitant pleural effusion [66]. The accumulation of fluid is due to the combination of decreased plasma oncotic pressure and increase in hydrostatic pressure secondary to salt retention.

Peritoneal Dialysis

Pleural effusion is well-documented in patients receiving continuous peritoneal dialysis. Fluid accumulates in the right hemithorax in most cases and is due to flow of dialysate from the peritoneal cavity into the pleural cavity [67].

Fontan Procedure

The final operation for single ventricle palliative repair is the anastomosis of the inferior vena cava to the pulmonary vessels. In Fontan physiology, central venous hydrostatic pressure is elevated and can contribute to the development of pleural effusion (Fig. 11.16). Reduction of the pulmonary vascular resistance pharmacologically is the initial treatment approach. In severe cases, pleuroperitoneal shunt and pleurodesis are optional treatments [68].

Pneumothorax

Pressure in the pleural space is lower than alveolar pressure and ambient pressure during the entire respiratory cycle. When communication develops between either an alveolus or through the chest wall, air flows into the pleural space. The main physiologic results of a pneumothorax (PTX) are decrease in vital capacity and decline in the PaO_2 secondary to ventilation perfusion mismatch, shunts, and alveolar hypoventilation [69]. PTX can be spontaneous but also can be due to underlying cysts or blebs as well as pulmonary metastasis (Fig. 11.17).

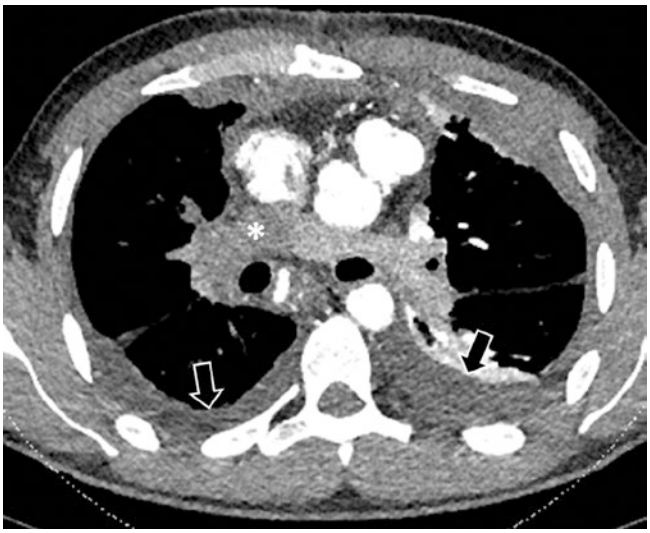

Fig. 11.16 An 18-year-old girl with bilateral small effusions due to underlying heart condition related to Fontan procedure (asterisk). Enhanced axial CT image shows bilateral effusions (arrows)

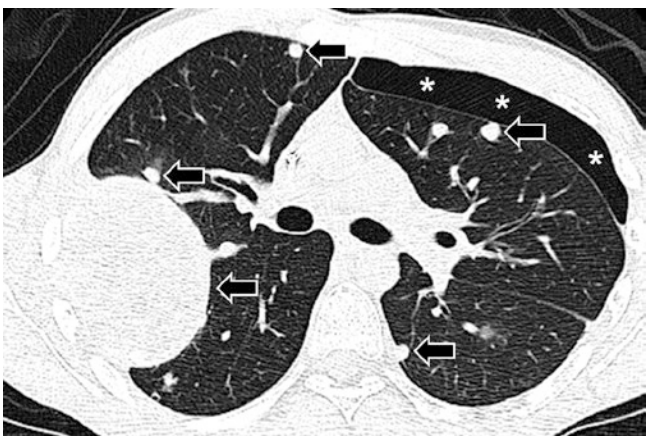

Fig. 11.17 A 15-year-old boy with pneumothorax due to metastatic osteosarcoma. Axial lung window CT image shows multiple pulmonary metastasis (arrows) with pneumothorax (asterisks)

Tension pneumothorax is present when intrapleural pressure exceeds the atmospheric pressure. Patients who develop tension pneumothorax commonly either are positive pressure ventilated (mechanical ventilation, bag mask ventilation) or have some type of one-way valve mechanism secondary to chest wall integrity defect, such as in penetrating trauma [70–72]. Causes of pneumothorax are listed in Table 11.3.

A small pneumothorax may be asymptomatic. Sudden chest pain and dyspnea are the two most common symptoms associated with the development of primary spontaneous pneumothorax. The pain is usually diffuse on the affected side of the chest with radiation to the ipsilateral shoulder. A non-productive cough is occasionally seen in association with pneumothorax.

Breath sounds and fremitus are diminished; hyperresonance with percussion is evident on the affected side. When tension pneumothorax develops, the affected patient appears distressed, with tracheal/mediastinal deviation toward the contralateral side, congestion of the jugular veins, narrow pulse pressure, and signs of shock. Subcutaneous emphysema can be extensive when air dissects into the mediastinum and the subcutaneous tissue. Chest radiograph can confirm even small volumes of intrapleural air in the upright position [73]. Outlining of the visceral pleura, hyperlucency, and attenuation of vascular and lung markings on the affected side are typical findings (Fig. 11.18). Collapsed lung and flattening of the diaphragm can be additional findings on the ipsilateral side with large amount of intrapleural air; mediastinal and tracheal shift away from the affected side are apparent when tension pneumothorax develops (Fig. 11.19).

Although on an upright chest radiograph, air first accumulates in the apical location, when the patient is supine, a small- or even moderate-sized PTX may only be apparent as a *medial pneumothorax* [73] adjacent to the mediastinum (Fig. 11.20). As the PTX enlarges, it may become apparent in the lateral costophrenic angle, then along the lateral chest and only finally, when moderately large, over the pulmonary apex. Commonly, a small medial PTX is suggested when actually not present. Normal retinal physiology produces an edge enhancement along the junction of lung and mediastinum, which is perceived as a faint lucent line adjacent to the mediastinum, remarkably simulating a small medial PTX. A simple process allows the observer to differentiate between this mock effect and a true PTX. An opaque object, such as a piece of paper, should be placed over the mediastinum, being careful not to cover the lucent line. If the lucent line disappears, it was a mock line (Fig. 11.21). If it remains, it is a PTX. When small pneumothorax is suspected, a lateral decubitus view, or cross-table lateral view, can provide additional information [74] (Fig. 11.22). Of these two, the decubitus view is preferred as it does not suffer from potential

Table 11.3 Causes for pneumothorax

Traumatic	Penetrating or blunt trauma
Airway disease	Asthma Cystic fibrosis
Interstitial lung disease	Langerhans' cell histiocytosis Sarcoidosis
Infectious	Bacterial Necrotizing pneumonia Pneumocystis jirovesi (carinii) Tuberculosis
Iatrogenic	Barotrauma Subclavian central venous catheter placement Laparoscopic procedures Airway procedures (intubation, bronchoscopy, etc.)
Congenital/familial	Marfan's syndrome Rheumatoid arthritis Homocystinuria Ehlers Danlos syndrome Polymyositis Dermatomyositis Alpha 1 antitrypsin deficiency Birt–Hogg–Dubé syndrome Subpleural cysts or blebs Congenital lung malformation (lobar emphysema, lung cyst, etc.)
Toxins	Cigarette smoking Marijuana smoking Cocaine snorting
Miscellaneous	Foreign body aspiration Catamenial pneumothorax Primary lung tumor Metastatic disease Irradiation

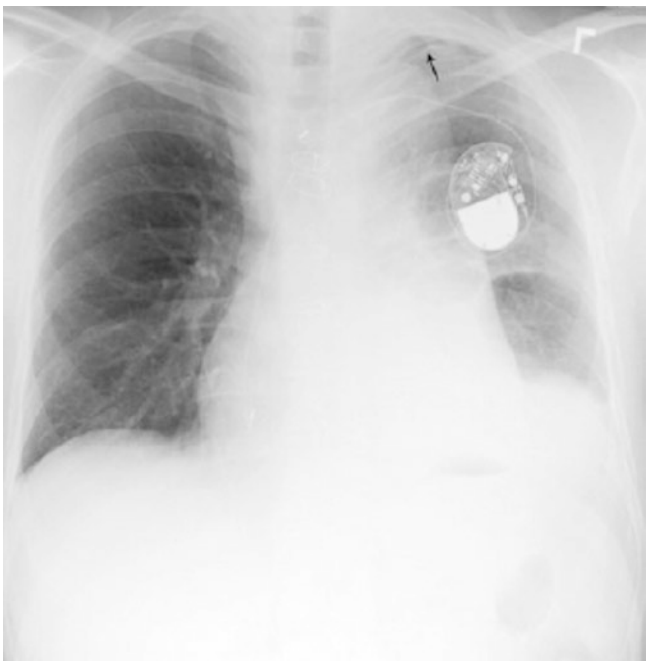

Fig. 11.18 Small left apical pneumothorax (*arrow*) with partially loculated hydropneumothorax noted elsewhere on the left

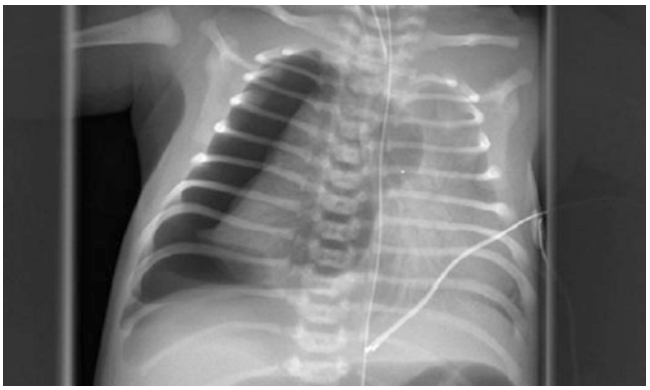

Fig. 11.19 Right tension pneumothorax

obscuring of the PTX by superimposed mediastinum and contralateral hemithorax. A pneumomediastinum or pneumopericardium should affect both sides, roughly to the same degree. In young children with persistence of the thymus, pneumomediastinum may not dissect into the neck. If there is air underneath the thymus, and lifting it away from the heart, it is mediastinal air, not a PTX (Fig. 11.23). A pneuomopericardium never ascends above the level of the main branch pulmonary arteries. In the upright patient, estimation of the pneumothorax size has been suggested by Collins by taking the sum of the distance between the ribs and the visceral pleura in millimeters, at three levels, apical, midthoracic, and base of the lung, and dividing by three which

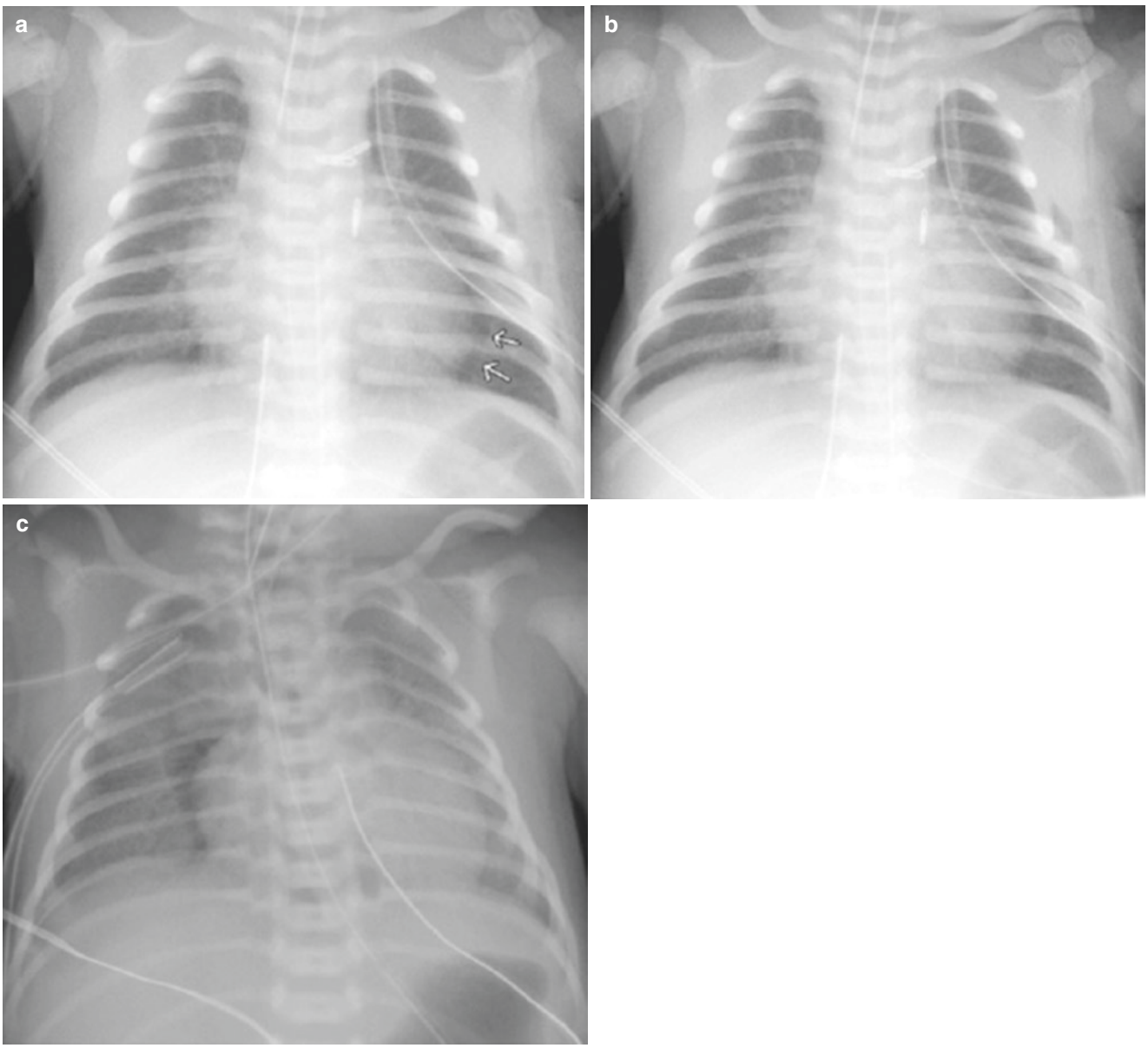

Fig. 11.20 Medial pneumothorax. (**a**) The *arrows* indicate a relatively small left medial pneumothorax, (**b**) same image as (**a**) but without the *arrows*, (**c**) a relatively large right medial pneumothorax

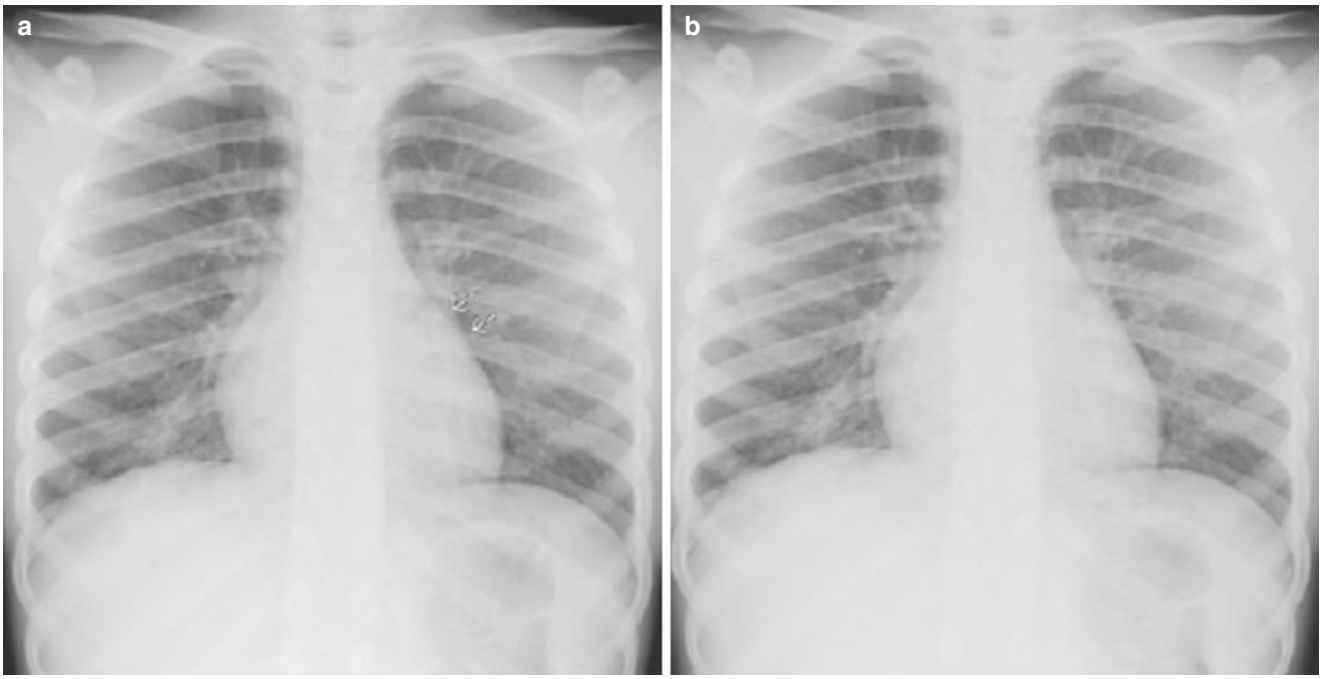

Fig. 11.21 (**a**) The *arrows* indicate a mock band adjacent to the left heart border. (**b**) Same image as (**a**) but without the *arrows*

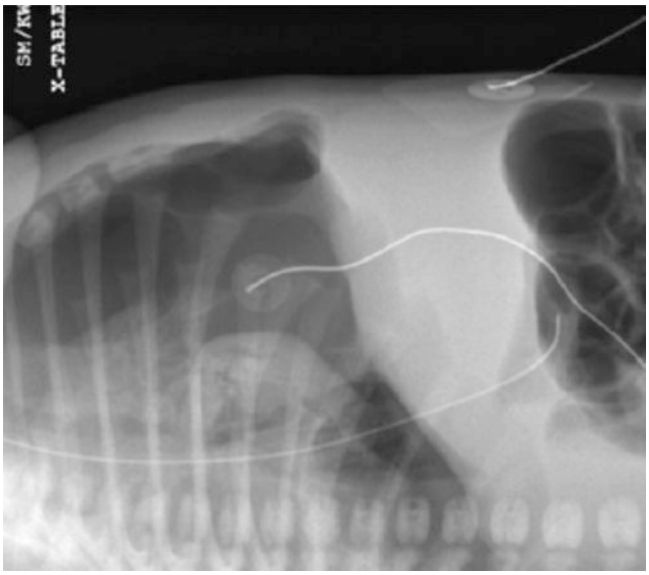

Fig. 11.22 Cross-table lateral chest radiograph shows a moderate-sized pneumothorax anteroinferiorly

expresses the percent of pneumothorax [75]. Other methods [51, 76] have also been proposed. However, opposed to these somewhat complicated calculations, the British Thoracic Society guidelines define the size by measuring the distance between the chest wall and the visceral pleura. A distance of 2 cm or more is considered a large pneumothorax [76].

Large subpleural bullae, stomach herniation through a diaphragmatic defect (congenital or traumatic), and skin folds are conditions that can mimic pneumothorax and should be looked for. The edge of a skin fold often is perceived as a thin line of increased density at the junction with the region of decreased density (i.e., the suspected pneumothorax).

The size of the pneumothorax dictates management. Small asymptomatic cases can be observed for spontaneous reabsorption. Administrating 100% oxygen to the patient accelerates the absorption of the pleural air [77].

Simple aspiration is indicated in cases with pneumothoraces greater than 15% in size and is successful in approximately 60% of cases [78]. When simple aspiration fails, tube thoracostomy is recommended, using small-diameter chest tubes or pigtail catheters [76, 79, 80]. In addition, negative pressure by suction (−20 cmH_2O) should be administered until it becomes evident that no air exists in the pleural space and no ongoing air leak is present. Pleurodesis, stapling of blebs, and pleural abrasion are indicated in cases of recurrent pneumothoraces or an ongoing air leak [81].

In cases of tension pneumothorax, a life-threatening situation, urgent needle application to the affected side in the second

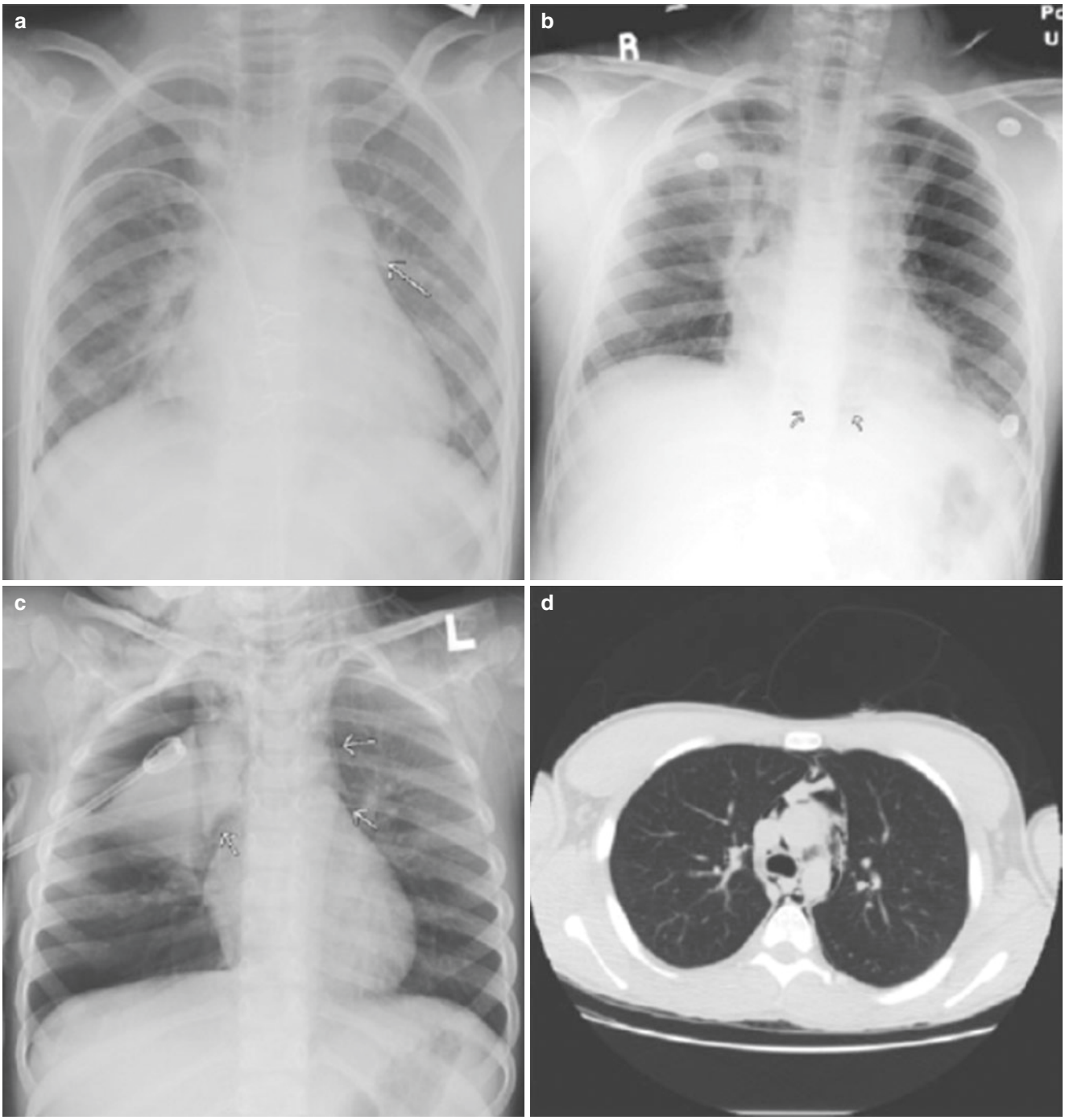

Fig. 11.23 (**a**) There is a pneumomediastinum seen only on the left. It is distinguished from a medial pneumothorax by the small amount of air lifting the left lobe of the thymus off the mediastinum (*arrow*). (**b**) In a different patient, there is a relatively large pneumomediastinum, with a larger right component. A small amount of air is noted beneath the heart (*arrows*). Air also has extended into the neck. A small right pneumothorax is present. (**c**) Portable AP chest radiograph shows air within the mediastinum (*upper arrow*) with both lobes of the thymus separated from the heart by air (*lower arrows*) (air separating the thymus from the heart occurs only with pneumomediastinum or pneumopericardium). Subcutaneous air is present within the neck. There is a moderately large right pneumothorax. (**d**) In another patient, CT easily shows an extensive pneumomediastinum with small left pneumothorax

intercostal space at the midclavicular line should be performed. Immediate air evacuation relieves the tension pneumothorax and allows time to perform thoracostomy safely.

Complications of thoracostomy include bleeding secondary to ruptured blood vessel and rarely infection of the pleural space. Re-expansion pulmonary edema is an additional possible complication.

Pneumoperitoneum

Free intraperitoneal air, with few exceptions, suggests bowel perforation, which may be life-threatening. It may be the consequence of recent abdominal surgery and of no clinical concern. Occasionally, a pneumomediastinum or pneumothorax may lead to a *benign* pneumoperitoneum.

Since well-performed frontal chest radiographs include a portion of the upper abdomen, it is important to assess for free intraperitoneal air. This is especially true in patients at risk for bowel ischemia as in an intensive care setting.

Identification of a pneumoperitoneum is simple on an upright image where the air outlines the inferior margin of the diaphragm (Fig. 11.24). In a supine patient, the manifestations of free intraperitoneal air may be much more difficult to perceive. Frequently, the only suggestion may be a subtle lucency over the abdomen with a faint margin defining the lateral peritoneal reflection (Fig. 11.25). If there are doubts concerning the observation, a cross-table lateral image (Fig. 11.26) or right-side down decubitus image should be performed.

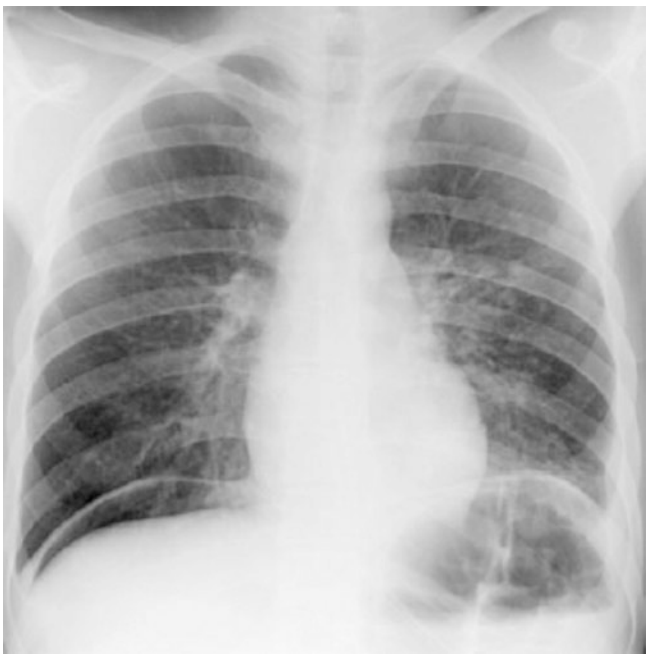

Fig. 11.24 Upright chest radiograph with pneumoperitoneum noted under the right hemidiaphragm

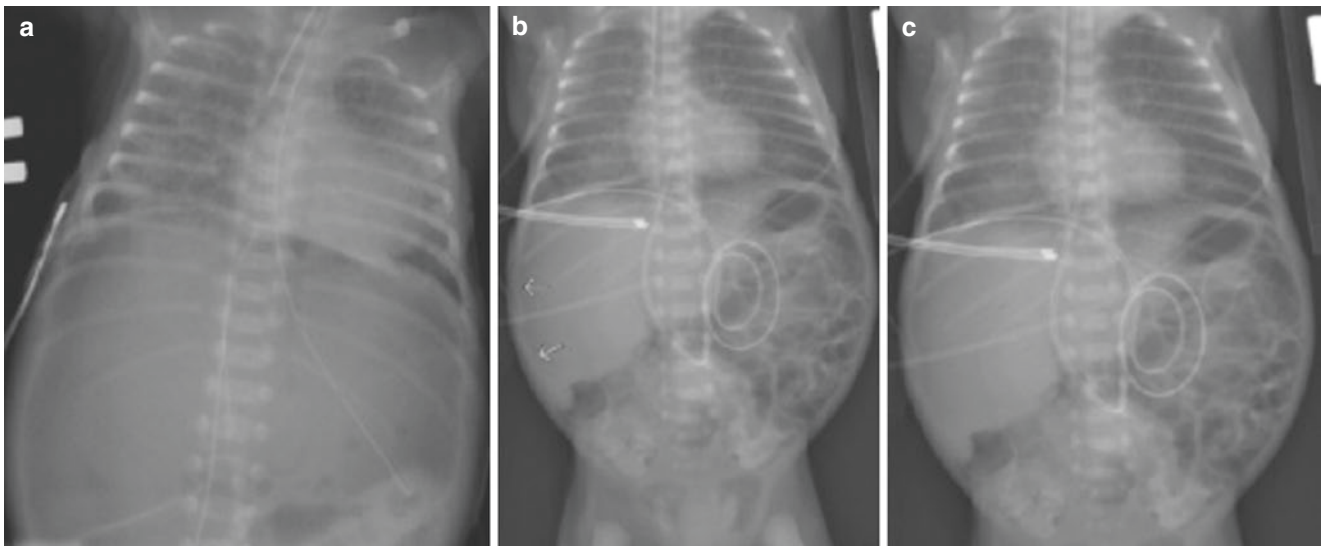

Fig. 11.25 (**a**) Supine radiograph with a large pneumoperitoneum, (**b**) the lateral extent of this relatively subtle pneumoperitoneum is indicated by the *arrows*, (**c**) same image as (**b**) without the *arrows*

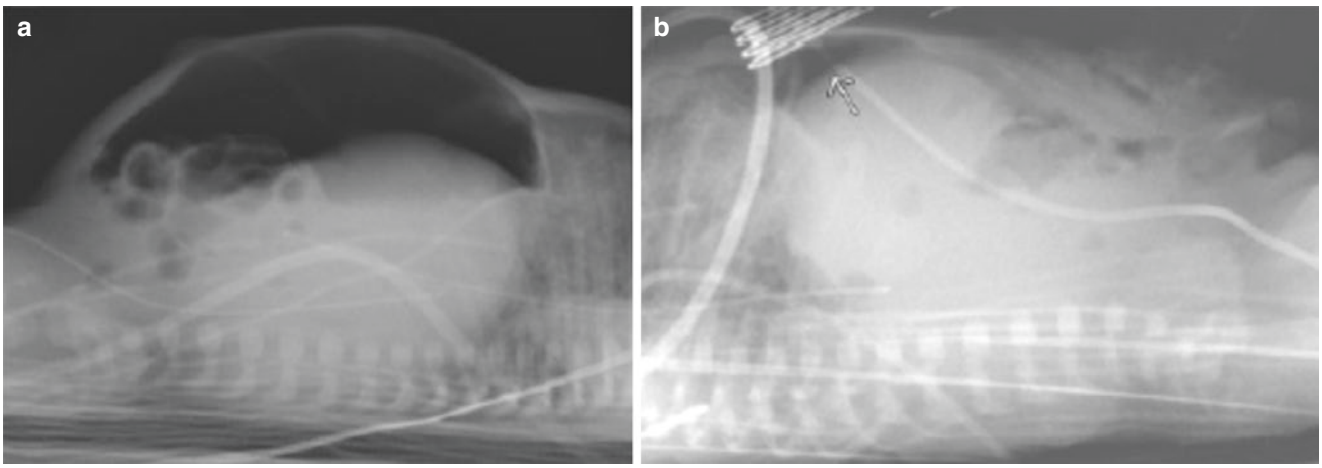

Fig. 11.26 (**a**, **b**) Cross-table lateral radiographs show anteriorly placed pneumoperitoneum (*arrow*)

References

1. Moore KL. The developing human. 2nd ed. Philadelphia: WB Saunders; 1977. p. 145–55.
2. Noppen M, De Waele M, Li R, et al. Volume and cellular content of normal pleural fluid in humans examined by pleural lavage. Am J Respir Crit Care Med. 2000;162:1023–6.
3. Staub NC, Wiener-Kronish JP, Albertine KH. Transport through the pleura: physiology of normal liquid and solute exchange in the pleural space. In: Chrétien J, Bignon J, Hirsch A, editors. The pleura in health and disease, lung biology in health and disease, vol. 30. New York: Marcel Dekker; 1985. p. 169–93.
4. Negrini D, Ballard ST, Benoit JN. Contribution of lymphatic myogenic activity and respiratory movements to pleural lymph flow. J Appl Physiol. 1994;76:2267–74.
5. Wang PM, Lai-Fook ST. Upward flow of pleural liquid near lobar margins due to cardiogenic motion. J Appl Physiol. 1992;73:2314–9.
6. Miserocchi G, Pistolesi M, Miniati M, et al. Pleural liquid pressure gradients and intrapleural distribution of injected bolus. J Appl Physiol. 1984;56:526–32.
7. Broaddus VC, Weiner-Kronish JP, Berthiaume Y, Staub NC. Removal of pleural liquid and protein by lymphatics in awake sheep. J Appl Physiol. 1988;64:384–90.
8. Wang NS. Anatomy and physiology of the pleural space. Clin Chest Med. 1985;6:3–16.
9. Light RW, MacGregor MI, Luchsinger PC, et al. Pleural effusions: the diagnostic separation of transudates and exudates. Ann Intern Med. 1972;77:507–13.
10. Kilbane BJ, Reynolds SL. Emergency department management of community-acquired methicillin-resistant Staphylococcus aureus. Pediatr Emerg Care. 2008;24(2):109–14.
11. Buckingham SC, King MD, Miller ML. Incidence and etiologies of complicated parapneumonic effusions in children 1996 to 2001. Pediatr Infect Dis J. 2003;22(6):499–504.
12. Kuhn J. Caffey's pediatric diagnostic imaging. 10th ed. Philadelphia: Mosby; 2004.
13. Chonmaitree T, Powell KR. Parapneumonic pleural effusion and empyema in children. Review of a 19-year experience, 1962–1980. Clin Pediatr (Phila). 1983;22(6):414–9.
14. Freij BJ, et al. Parapneumonic effusions and empyema in hospitalized children: a retrospective review of 227 cases. Pediatr Infect Dis. 1984;3(6):578–91.
15. Hardie W, et al. Pneumococcal pleural empyemas in children. Clin Infect Dis. 1996;22(6):1057–63.
16. Rudikoff JC. Early detection of pleural fluid. Chest. 1980;77:109–11.
17. Moskowitz H, Platt RT, Schachar R, et al. Roentgen visualization of minute pleural effusion. Radiology. 1973;109:33–5.
18. Tsai T-H, Yang P-C. Ultrasound in the diagnosis and management of pleural disease. Curr Opin Pulm Med. 2003;9:282–90.
19. Davies CL, Gleeson FV. Diagnostic radiology. In: Light RW, Lee GYC, editors. Textbook of pleural diseases. London: Arnold; 2003. p. 210–37.
20. Kohan JM, Poe RH, Israel RH, et al. Value of chest ultrasonography versus decubitus roentgenography for thoracentesis. Am Rev Respir Dis. 1986;133:1124–6.
21. Remy-Jardin M, Remy J, Deschildre F, et al. Diagnosis of pulmonary embolism with spiral CT: comparison with pulmonary angiography and scintigraphy. Radiology. 1996;200:699–706.
22. MacDonald SL, Mayo JR. Computed tomography of acute pulmonary embolism. Semin Ultrasound CT MR. 2003;24:217–31.
23. Kritsaneepaiboon S, Lee EY, Zurakowski D, Strauss KJ, Boiselle PM. MDCT pulmonary angiography evaluation of pulmonary embolism in children. AJR Am J Roentgenol. 2009;192(5):1246–52.
24. Victoria T, Mong A, Altes T, Jawad AF, Hernandez A, Gonzalez L, Raffini L, Kramer SS. Evaluation of pulmonary embolism in a pediatric patient with high clinical suspicion. Pediatr Radiol. 2009;39(1):35–41.
25. Byington CL, Spencer LY, Johnson TA, et al. An epidemiological investigation of a sustained high rate of pediatric parapneumonic empyema: risk factors and microbiological association. Clin Infect Dis. 2002;34:434–40.
26. Rees JH, Spencer DA, Parikh D, Weller P. Increase in incidence of childhood empyema in West Midlands. UK Lancet. 1997;349:402.
27. Playfor SD, Smyth AR, Stewart RJ. Increase in incidence of childhood empyema. Thorax. 1997;52:932.
28. Roxburgh CS, Youngson GG, Townend JA, Turner SW. Trends in pneumonia and empyema in Scottish children in the past 25 years. Arch Dis Child. 2008;93:316–8.
29. Schultz KD, Fan LL, Pinsky J, et al. The changing face of pleural empyemas in children: epidemiology and management. Pediatrics. 2004;113:1735–40.
30. Hardie W, Bokulic R, Garcia VF, et al. Pneumococcal pleural empyemas in children. Clin Infect Dis. 1996;22:1057–63.

31. Freij BJ, Kusmiesz H, Nelson JD, McCracken GH Jr. Parapneumonic effusions and empyema in hospitalized children: a retrospective review of 227 cases. Pediatr Infect Dis. 1984;3:578–91.
32. Balfour-Lynn IM, Abrahamson E, Cohen G, et al. BTS guidelines for the management of pleural infection in children. Thorax. 2005;60(Suppl 1):i1–21.
33. Rodgers BM, McGahren ED. Mediastinum and pleura. In: Oldham KT, Colombani PM, Foglia RP, Skinner MA, editors. Principles and practice of pediatric surgery. Philadelphia: Lippincott, Williams & Wilkins; 2005. p. 929–49.
34. Wheeler JG, Jacobs RF. Pleural effusions and empyema. In: Feigin RD, Cherry JD, Demmler GJ, Kaplan SL, editors. Textbook of pediatric infectious diseases. 5th ed. Philadelphia: Saunders; 2004. p. 320–30.
35. Wolach B, Morag H, Drucker M, Sadan N. Thrombocytosis after pneumonia with empyema and other bacterial infections in children. Pediatr Infect Dis J. 1990;9:718–21.
36. Bynum LJ, Wilson JE III. Characteristic of pleural effusions associated with pulmonary embolism. Arch Intern Med. 1976;136:159–62.
37. Lee EY, Zurakowski D, Diperna S, d'Almedia Bastos M, Strauss KJ, Boiselle PM. Parenchymal and pleural abnormalities in children with and without pulmonary embolism at MDCT pulmonary angiography. Pediatr Radiol. 2010;40(2):173–81.
38. Light RW, Ball WC Jr. Glucose and amylase in pleural effusions. JAMA. 1973;225:257–9.
39. Rockey DC, Cello JP. Pancreaticopleural fistula: report of 7 patients and review of the literature. Medicine. 1990;69:332–44.
40. Lankisch PG, Droge M, Becher R. Pleural effusions: a new negative prognostic parameter for acute pancreatitis. Am J Gastroenterol. 1994;89:1849–51.
41. Restrepo R, Hagerott HE, Kulkarni S, Yasrebi M, Lee EY. Acute pancreatitis in pediatric patients: demographics, etiology, and diagnostic imaging. AJR Am J Roentgenol. 2016;206(3):632–44.
42. Berger HW, Rammohan G, Neff MS, et al. Uremic pleural effusion: a study in 14 patients on chronic dialysis. Ann Intern Med. 1975;82:362–4.
43. Rodelas R, Rakowski TA, Argy WP, et al. Fibrosing uremic pleuritis during hemodialysis. JAMA. 1980;243:2424–5.
44. Halla JT, Schrohenloher RE, Volanakis JE. Immune complexes and other laboratory features of pleural effusion. Ann Intern Med. 1980;92:748–52.
45. Koster FT, McGregor DD, Mackaness GB. The mediator of cellular immunity: II. Migration of immunologically committed lymphocytes into inflammatory exudates. J Exp Med. 1971;133:400–9.
46. Horler AR, Thompson M. The pleural and pulmonary complications of rheumatoid arthritis. Ann Intern Med. 1959;51:1179–203.
47. Walker WC, Wright V. Pulmonary lesions and rheumatoid arthritis. Medicine. 1968;47:501–19.
48. Sahn SA. State of the art: the pleura. Am Rev Respir Dis. 1988;138:184–234.
49. Yarbrough JW, Sealy WC, Miller JA. Thoracic surgical problems associated with rheumatoid arthritis. J Thorac Cardiovasc Surg. 1975;68:347–54.
50. Vargas FS, Milanez JR, Filomeno LT, et al. Intrapleural talc for the prevention of recurrence in benign or undiagnosed pleural effusions. Chest. 1994;106:1771–5.
51. Light RW. Pleural diseases. 4th ed. Lippincott, Williams & Wilkins: Baltimore; 2001.
52. Stelzner TJ, King TE Jr, Antony VB, Sahn SA. The pleuropulmonary manifestations of the postcardiac injury syndrome. Chest. 1983;84:383–7.
53. Bladergroen MR, Lowe JE, Postlethwait RW. Diagnosis and recommended management of esophageal perforation and rupture. Ann Thorac Surg. 1986;42:235–9.
54. Reeder LB, DeFilippi VJ, Ferguson MK. Current results of therapy for esophageal perforation. Am J Surg. 1995;169:615–7.
55. Castellino RA, Bellani FF, Gasparini M, Musumeci R. Radiographic findings in previously untreated children with non-Hodgkin's lymphoma. Radiology. 1975;117:657–63.
56. Celikoglu F, Teirstein AS, Krellenstein DJ, Strauchen JA. Pleural effusion in non Hodgkin's lymphoma. Chest. 1992;101:1357–60.
57. Fisher AMH, Kendall B, VanLeuven BD. Hodgkin's disease: a radiological survey. Clin Radiol. 1962;13:115–27.
58. Keller SM. Current and future therapy for malignant pleural effusion. Chest. 1993;103:63s–7.
59. Teba L, Dedhia HV, Bowen R, Alexander JC. Chylothorax review. Crit Care Med. 1985;13:49–52.
60. Chernick V, Reed MH. Pneumothorax and chylothorax in the neonatal period. J Pediatr. 1970;76:624–32.
61. Yancy WS, Spock A. Spontaneous neonatal pleural effusion. J Pediatr Surg. 1967;2:313–9.
62. Strausser JL, Flye MW. Management of non traumatic chylothorax. Ann Thorac Surg. 1981;31:520–6.
63. Rubin JW, Moore HV, Ellison RG. Chylothorax: therapeutic alternatives. Am Surgeon. 1977;43:292–7.
64. Light RW. Pleural diseases. Philadelphia: Lea & Febiger; 1990.
65. Romero-Candeira S, Fernandez C, Martin C, et al. Influence of diuretics on the concentration of proteins and other components of pleural transudates in patients with heart failure. Am J Med. 2001;110:681–6.
66. Cavina G, Vichi G. Radiological aspects of pleural effusions in medical nephropathy in children. Ann Radiol Diagn. 1958;31:163–202.
67. Nomoto Y, Suga T, Nakajima K, et al. Acute hydrothorax in continuous ambulatory peritoneal dialysis: a collaborative study of 161 centers. Am J Nephrol. 1989;9:363–7.
68. Sade RM, Wiles HB. Pleuroperitoneal shunt for persistent pleural drainage after Fontan procedure. J Thorac Cardiovasc Surg. 1990;100:621–3.
69. Norris RM, Jones JG, Bishop JM. Respiratory gas exchange in patients with spontaneous pneumothorax. Thorax. 1968;23:427–33.
70. Baumann MH. Non-spontaneous pneumothorax. In: Light RW, Lee YCG, editors. Textbook of pleural diseases. London: Arnold; 2003. p. 464–74.
71. Murphy DG, Sloan EP, Hart RG, et al. Tension pneumothorax associated with hyperbaric oxygen therapy. Am J Emerg Med. 1991;9:176–9.
72. Mainini SE, Johnson FE. Tension pneumothorax complicating small-caliber chest tube insertion. Chest. 1990;97:759–60.
73. Moskowitz PS, Griscom NT. The medial pneumothorax. Radiology. 1976;120:143–7.
74. Carr JJ, Reed CJ, Choplin RH, et al. Plain and computed radiography for detecting experimentally induced pneumothorax in cadavers: implications for detection in patients. Radiology. 1992;183:193–9.
75. Collins CD, Lopez A, Mathie A, et al. Quantification of pneumothorax size on chest radiographs using interpleural distances: regression analysis based on volume measurements from helical CT. AJR Am J Roentgenol. 1995;165:1127–30.
76. Henry M, Arnold T, Harvey J. BTS guidelines for the management of spontaneous pneumothorax. Thorax. 2003;58(Suppl II):II39–52.
77. Northfield TC. Oxygen therapy for spontaneous pneumothorax. Br Med J. 1971;4:86–8.
78. Light RW. Manual aspiration: the preferred method for managing primary spontaneous pneumothorax? Am J Respir Crit Care Med. 2002;165:1202–3.
79. Ponn RB, Silverman HJ, Federico JA. Outpatient chest tube management. Ann Thorac Surg. 1997;64:1437–40.
80. Liu CM, Hang LW, Chen WK, et al. Pigtail tube drainage in the treatment of spontaneous pneumothorax. Am J Emerg Med. 2003;21:241–4.
81. Yim AP, Ng CS. Thoracoscopy in the management of pneumothorax. Curr Opin Pulm Med. 2001;7:210–4.

Pulmonary Hypertension

12

Edward Y. Lee and Gulraiz Chaudry

Introduction

Pulmonary hypertension (PHT) is a condition defined by a mean pulmonary arterial pressure (PAP) of 25 mmHg or greater at rest and 30 mmHg or greater during exercise. PHT can be idiopathic or associated with a wide spectrum of etiological factors and conditions in the pediatric population [1–4], often resulting in diagnostic and therapeutic challenges. Due to recent advances in treatment which have markedly decreased the mortality and morbidity in pediatric patients with PHT [5], early and correct diagnosis is particularly essential in optimally managing children with PHT.

In this chapter, we address the clinical presentation and the methods of evaluation of PHT in the pediatric population. Unique underlying pathophysiological processes and characteristic diagnostic study findings in idiopathic pulmonary arterial hypertension (IPAH) and common conditions typically associated with PHT in infants and children are also highlighted.

Clinical Presentation of Pulmonary Hypertension

Pediatric patients with PHT usually present with clinical symptoms which are often nonspecific. In addition, clinical symptoms somewhat differ between infants (<1 year old) and children. While infants with PHT typically present with failure to thrive, irritability and cyanotic spells with exertion, affected children usually present with chest pain, exertional dyspnea or syncope [6]. On physical examination, common findings in pediatric patients with PHT include: (1) left parasternal heave caused by the right ventricular enlargement, detected by placing the heel of the hand over the left parasternal region; (2) a prolonged P2 with paradoxical splitting of the second heart sound on auscultation; and (3) a murmur due to pulmonary regurgitation. Clinical signs of right-sided cardiac failure such as hepatomegaly or peripheral edema are uncommon in children.

E. Y. Lee (✉) · G. Chaudry
Department of Radiology, Boston Children's Hospital and Harvard Medical School, Boston, MA, USA
e-mail: Edward.Lee@childrens.harvard.edu

Evaluation of Pulmonary Hypertension

The overarching goal of evaluation in pediatric patients with PHT is to establish the diagnosis of PHT and determine the underlying cause [7, 8]. For infants and children with clinical suspicion of underlying PHT, initial diagnostic evaluation typically consists of chest radiographs (CXR), electrocardiogram (ECG), and echocardiography. Based upon findings on these studies, further evaluation can be performed with advanced diagnostic studies including (1) a 6-minute walk test, (2) cardiac catheterization, (3) computed tomography (CT), (4) ventilation-perfusion scan (V/Q scan), and (5) magnetic resonance imaging/angiography (MRI/MRA).

Initial Evaluation

Chest Radiographs (CXR)

Two views (posteroanterior and lateral views) of CXR are typically the first diagnostic imaging modality for evaluating infants and children with suspected PHT. The advantages of CXR in the evaluation of PHT include its widespread availability, relative low cost, and easy acquisition. However, associated ionizing radiation exposure is an important disadvantage particularly in the pediatric population. The most common chest radiographic imaging findings in children with PHT of any cause include (1) enlargement of the main and hilar pulmonary arteries, (2) tapering of the peripheral pulmonary arteries, and (3) right ventricular enlargement associated with loss of the retrosternal air space on the lateral view [5]. The CXR can also demonstrate lung parenchymal disease in some patients with PHT.

R. H. Cleveland, E. Y. Lee (eds.), *Imaging in Pediatric Pulmonology*, https://doi.org/10.1007/978-3-030-23979-4_12

Electrocardiogram (ECG)

The ECG in pediatric patients with PHT typically demonstrates right-sided cardiac strain associated with right ventricular hypertrophy and right axis deviation [9].

Echocardiography

Transthoracic echocardiography can be helpful in evaluating pediatric patients with PHT by demonstrating (1) left-sided cardiac disease; (2) valvular abnormalities, especially tricuspid regurgitation, which is known to be present in the majority of children with PHT [1]; and (3) intracardiac shunting (e.g., atrial septal defect, ventricular septal defect [VSD]). Estimation of right ventricular systolic pressure (RVSP) by Doppler interrogation has also been shown to correlate well with pressures measured at catheterization [9].

Advanced Evaluation

Six-Minute Walk Test

A 6-minute walk test is a type of pulmonary function test in which the distance a patient can walk over a 6-min period is measured, usually including pulse oximetry. In children (>6 years) with PHT who can follow the direction of a 6-minute walk test, this allows objective assessment of the degree of dyspnea [4, 10]. In addition, gas exchange capabilities can be evaluated with diffusing lung capacity for carbon monoxide (DLCO). The functional status is then classified according to the NYHA/WHO classification, with no limitation of physical activity seen in class I to patients unable to carry out any physical activity in class IV [11]. A 6-minute walk test combined with functional classification can play an important role in the initial evaluation, assessment of early response to treatment and response assessment following completion of therapy.

Cardiac Catheterization

Cardiac catheterization, which can directly measure the PAP, remains the gold standard for diagnosis of PHT in the pediatric population. In addition to PAP measurement, cardiac catheterization can also provide important information (regarding pulmonary capillary wedge pressure and pulmonary venous return) which can be used to determine the underlying etiology of PHT [11, 12]. Furthermore, catheterization can also be used to guide therapy by determining the response to selective pulmonary vasodilators.

Advanced Radiological Imaging Studies

In children diagnosed with PHT by cardiac catheterization or suspected of having PHT based on CXR and other evaluation studies, advanced imaging studies can be performed to determine the underlying cause. These include computed tomography, ventilation-perfusion scan, and magnetic resonance imaging/angiography [13]. The choice of specific advanced imaging studies and their characteristic imaging findings are discussed in detail under the discussion sections of idiopathic PHT and individual conditions associated with PHT.

Pulmonary Arterial Hypertension

Idiopathic Pulmonary Arterial Hypertension

IPAH is a diagnosis of exclusion when PHT occurs without identifiable underlying cause. Histologically, medial hypertrophy of pulmonary arterioles is commonly seen in children with IPAH without fixed changes (such as intimal fibrosis and plexiform lesions) typically present in adult patients with IPAH [14]. Although the exact incidence of IPAH is currently not known, particularly in the pediatric population, it is estimated to be 1–2 cases per million in all ages [6]. Despite the current uncertainty of the true incidence of IPAH, it is important to recognize that the incidence of IPAH in the pediatric population may be higher than it has been recognized in the past due to the increased awareness of IPAH in recent years [15]. This presumed higher incidence of IPAH, coupled with the recent advances in therapy for IPAH, underscore the importance of early and correct diagnosis of IPAH. With the improved therapy for IPAH in recent years, the 3-year survival rate now reaches as high as 94% at 1 year and 84% at 3 years after the initial diagnosis [16], up significantly from the abysmal prognosis of mean survival time of less than 1 year in the past [15].

CXR, ECG, and echocardiography are typically used in the initial evaluation of pediatric patients with IPAH. Common findings of these evaluation tests are included in the section of initial evaluation of PHT. Once the diagnosis of IPAH is suspected on the basis of these initial investigations, CT can provide further information on both pulmonary and extrapulmonary abnormalities associated with IPAH. With recent advances in CT technology, particularly with MDCT providing high-resolution images in a faster scanning time with 2D and 3D image reconstruction capability, CT is assuming an important role in evaluating IPAH in infants and children. A combined CT angiography protocol (which can provide detailed information of pulmonary vessels) and high-resolution technique (for lung parenchymal evaluation) should be utilized for complete evaluation of both pulmonary and extrapulmonary (e.g., vascular) abnormalities associated with IPAH. With a higher row MDCT (>16 MDCT) with very thin collimation (0.5–1.0 mm), diagnostic quality of thin-section CT images is almost equal to high-resolution CT images, with the added benefit of viewing in the transverse, sagittal, or coronal planes.

The most common extrapulmonary (vascular) finding in IPAH is central pulmonary artery enlargement (Fig. 12.1).

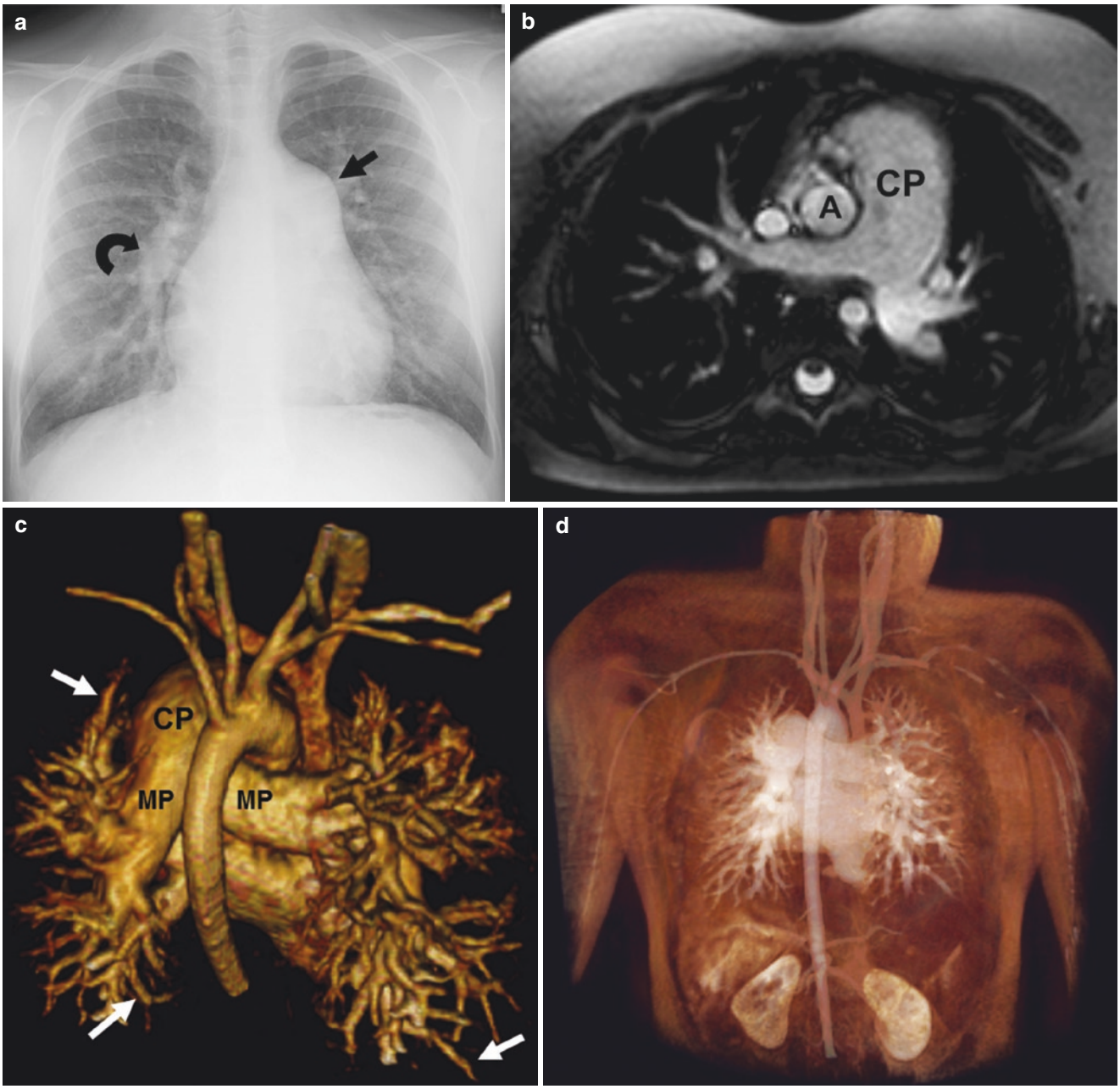

Fig. 12.1 Ten-year-old boy with idiopathic pulmonary hypertension (PHT) who initially presented with exertional dyspnea. (**a**) Frontal chest radiograph shows marked enlarged central (*straight arrow*) and main (*curved arrow*) pulmonary arteries. Also noted is mild cardiomegaly. (**b**) Axial T1-weighted MR image demonstrates an enlarged central pulmonary artery (CP), main pulmonary arteries (MP), and segmental pulmonary arteries (arrows). (**d**) Posterior view of the 3D volume-rendered image of the MRA shows the entire thoracic vascular structures

Distal main pulmonary artery exceeding the diameter of the ascending aorta has a specificity and positive predictive value of greater than 90% for PHT [17]. In addition, the ratio of the diameter of the right and left pulmonary arteries to their respective mainstem bronchi is invariably greater than 1:1, with a mean of 2:1 [18]. In some children, a peripheral vasculopathy is also identified, characterized by small tortuous vessels extending to the periphery (Fig. 12.2) [18]. The cause of this finding remains unknown, but possible etiologies include neovascularization or enlarged collateral vessels. Right-sided cardiac enlargement is also seen in the majority of these children (Fig. 12.3) [18]. In contrast, other extrapulmonary findings described in adults with IPAH, such as pericardial thickening and mural calcific deposits, are not commonly recognized in pediatric patients with IPAH [18].

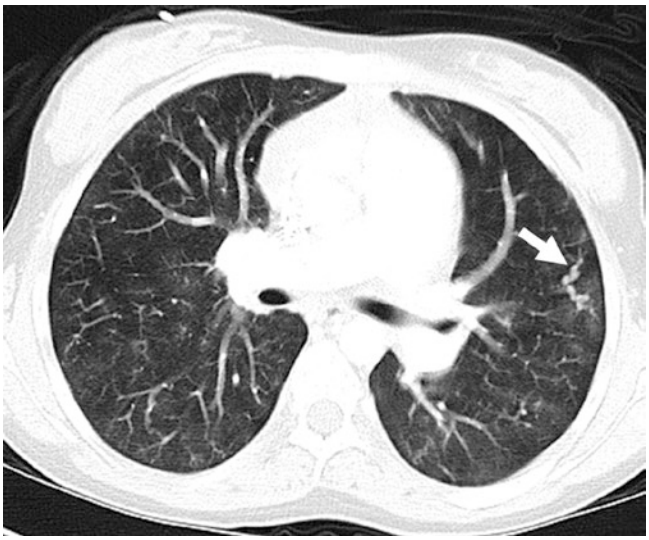

Fig. 12.2 Sixteen-year-old girl with idiopathic pulmonary hypertension who presented with shortness of breath. Axial lung window CT image demonstrates enlarged and tortuous peripheral pulmonary vessels (arrow)

The most common pulmonary parenchymal finding in infants and children with IPAH is the presence of well-defined centrilobular opacities (Figs. 12.3d and 12.4). However, this finding is also frequently seen in veno-occlusive disorder (VOD) and thromboembolic disease [19, 20]. Inhomogeneous ground-glass opacification and focal areas of hyperlucency are also frequently noted, but septal thickening is less common and extensive than that seen in VOD (Figs. 12.5 and 12.6) [18].

In addition to evaluating pulmonary and extrapulmonary findings associated with IPAH, CT is also helpful in identifying other conditions (e.g., thromboembolic and veno-occlusive disease) associated with PHT in infants and children.

Other radiological imaging studies currently available, including MRI and V/Q scan, have inherent limitations for evaluating IPAH in the pediatric population. However, a reported finding in pediatric patients with IPAH includes delayed contrast enhancement of the myocardium at the junction of the free wall of the right ventricle and the interventricular septum on MRI. This delayed contrast enhancement has been shown to be inversely related to right ventricular systolic function [21]. The main role of scintigraphy in the assessment of IPAH is the exclusion of possible underlying thromboembolic disease. Although there are no specific findings of IPAH on ventilation-perfusion scanning [22], it has been shown that nonspecific non-segmental patchy defect in perfusion with normal ventilation is the most common V/Q scan finding (Fig. 12.7) [23]. This finding is thought to be secondary to asymmetric vasoconstriction and occlusion of the pulmonary arterioles. In addition, quantitative assessment of these perfusion irregularities may also be useful in the assessment of severity of the disease [22].

Once the diagnosis of IPAH is established and treatment is initiated, follow-up imaging evaluation is primarily performed with ECG and echocardiography, including measurement of right ventricular pressures. Due to its relatively invasive

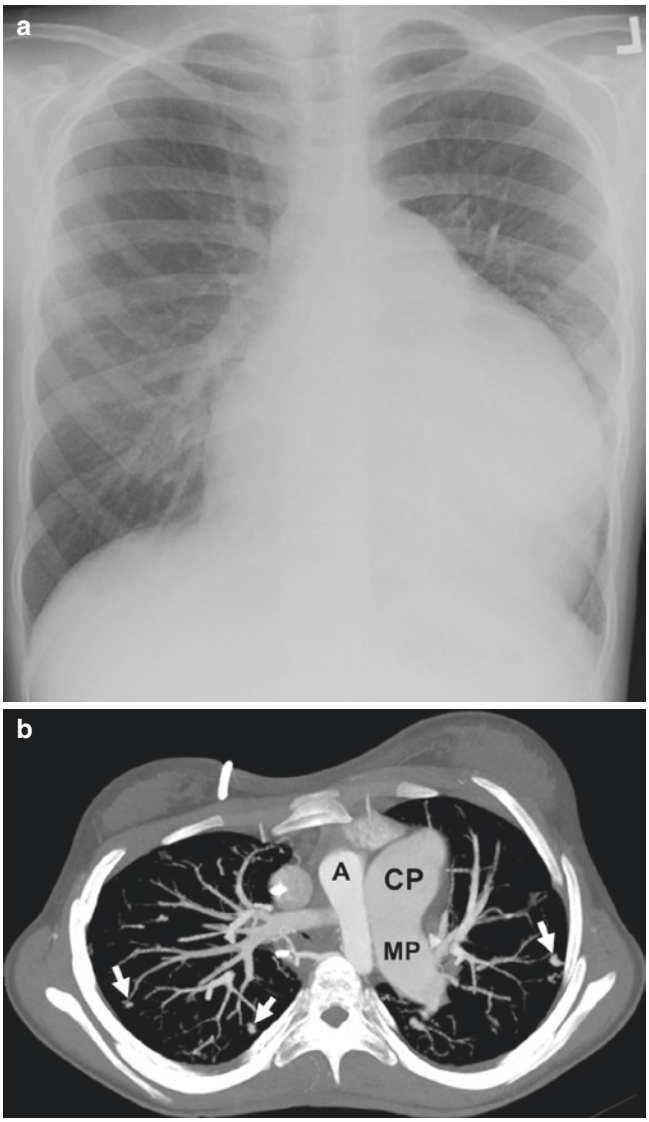

Fig. 12.3 Sixteen-year-old girl with idiopathic pulmonary hypertension who initially presented with syncope and chest pain. (**a**) Frontal chest radiograph demonstrates a markedly enlarged heart and aorto-pulmonary window region. (**b**) Enhanced axial maximum intensity projection CT image shows markedly enlarged central pulmonary artery (CP) and main pulmonary artery (MP). Also noted is development of small, enlarged, and tortuous vessels (arrows) within the periphery of the lungs *A* aorta. (**c**) Coronal multiplanar CT image demonstrates a markedly enlarged right atrium (RA) and right ventricle (RV). (**d**) High-resolution axial lung window CT image demonstrates relatively well-defined centrilobular opacities (arrows) associated with areas of inhomogeneous ground-glass opacification

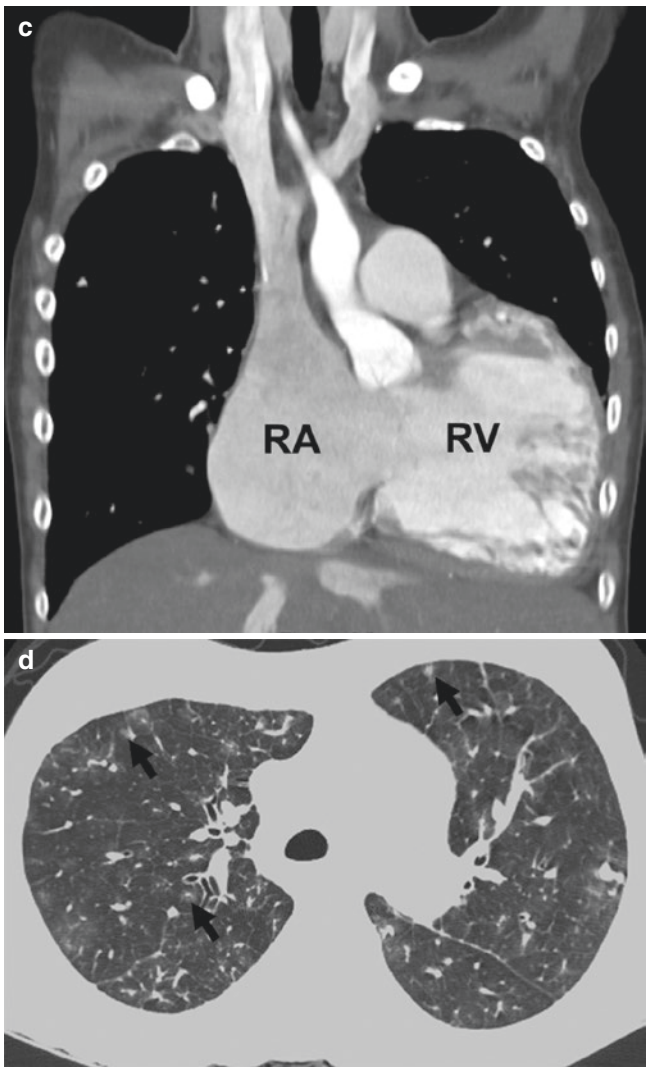

Fig. 12.3 (continued)

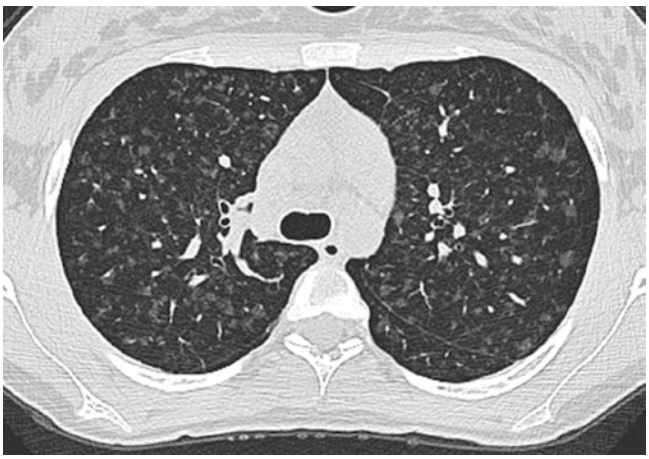

Fig. 12.4 Fifteen-year-old girl with idiopathic pulmonary arterial hypertension who presented with dyspnea and chest pain. High-resolution axial lung window CT image demonstrates diffuse centrilobular opacities bilaterally

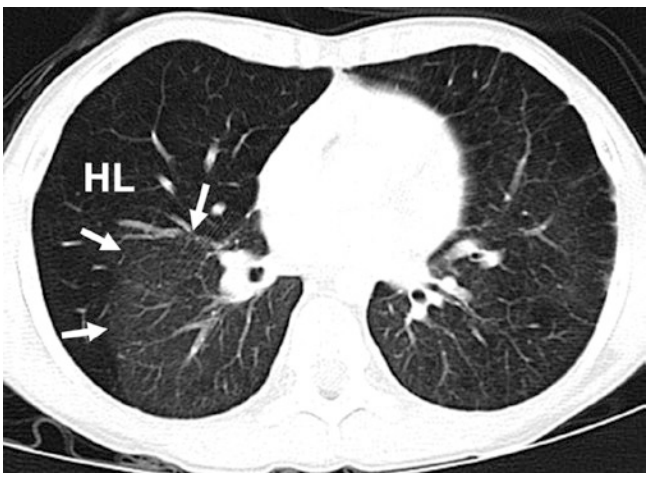

Fig. 12.5 Ten-year-old girl with idiopathic pulmonary hypertension who initially presented with syncope and shortness of breath. Axial lung window CT image demonstrates geographic areas of ground-glass opacification (arrows) and hyperlucency (HL)

nature, catheterization is seldom performed in pediatric patients with IPAH once diagnosis is made based on less invasive studies such as CT. However, catheterization with pulmonary vasodilator testing is useful for evaluating vascular responsiveness. Unfortunately, it has been reported that there is a wide variability of the results from catheterization with pulmonary vasodilator testing without accurate predictive factors, limiting its clinical utility [6].

Conditions Associated with Pulmonary Arterial Hypertension

It has long been recognized that a wide spectrum of conditions may be associated with pulmonary vascular disease that shares similar clinical, pathological, and imaging features with IPAH. These were previously termed *secondary pulmonary hypertension*, a potentially problematic nomenclature as it included conditions with pulmonary venous hypertension and altered respiratory function [7]. Thus in the revised Venice classification, the term associated with pulmonary arterial hypertension (APAH) was devised to describe pulmonary arterial hypertension associated with other conditions and risk factors. There is a wide spectrum of conditions associated with PAH as listed in Table 12.1, and several key conditions associated with PAH in pediatric population are reviewed in the following sections.

Congenital Systemic to Pulmonary Shunts

Infants and children with PAH secondary to congenital systemic to pulmonary shunts are a highly heterogeneous group

with regard to the underlying defect, as well as the timing and severity of PHT. Vicktor Eisenmenger published his report of pulmonary vascular disease associated with *congenital defects of the ventricular septum* in 1897. Eisenmenger syndrome was then further elucidated by Wood [24] and has come to encompass all systemic to pulmonary shunts that result in PHT and subsequent reversal or bidirectional shunt flow [7]. The low pulmonary vascular resistance and increased blood flow have a detrimental effect on the vascular bed, with suspected damage to the endothelial cells

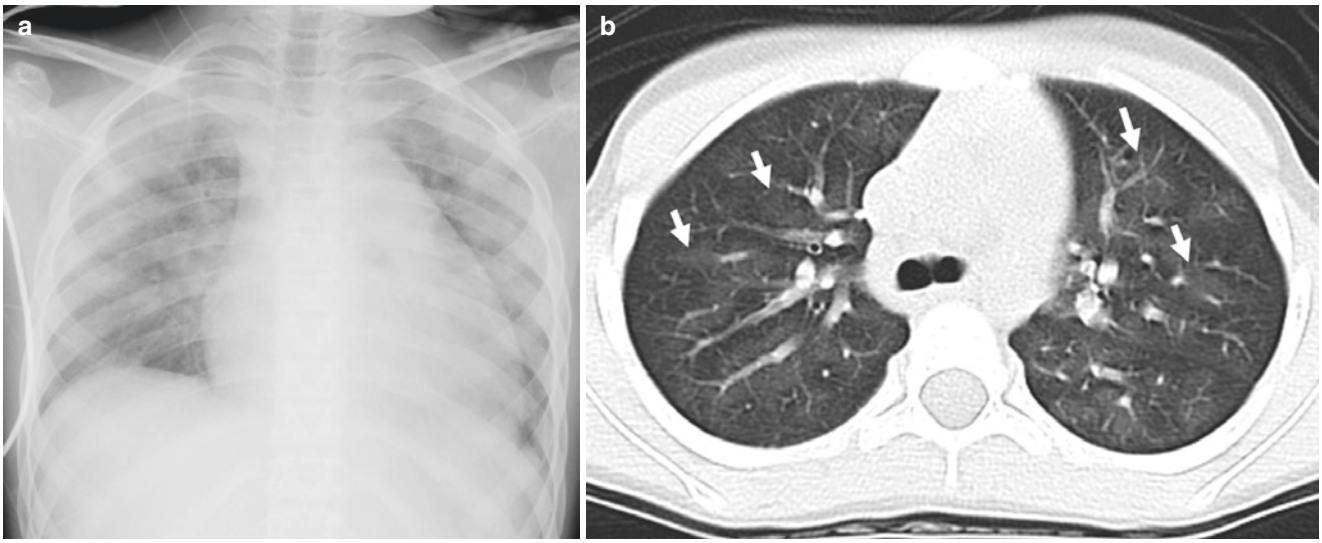

Fig. 12.6 Nine-year-old girl with idiopathic pulmonary hypertension who presented with chest pain. (**a**) Frontal chest radiograph shows mild diffuse opacities in both lungs. (**b**) Axial lung window CT image shows diffuse areas of both ground-glass opacification (arrows) surrounded by hyperlucency. In comparison to Fig. 12.3, these lung findings are more diffuse and symmetric

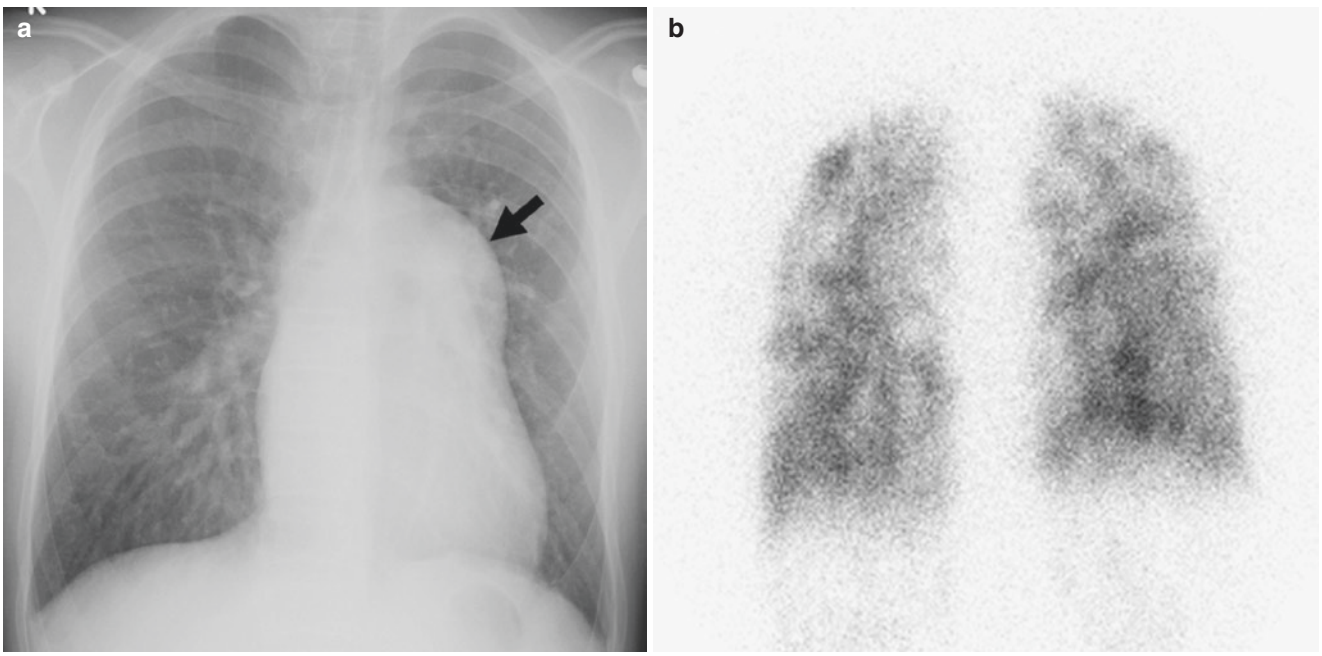

Fig. 12.7 Thirteen-year-old boy with known idiopathic pulmonary hypertension who presented with shortness of breath and decreasing oxygen saturation. V/Q scan was obtained for evaluation of possible pulmonary embolism. (**a**) Frontal chest radiograph shows a markedly enlarged central pulmonary artery (*arrow*) and cardiomegaly. (**b**) Posterior view of perfusion image from V/Q scan demonstrates diffusely patchy inhomogeneous uptake of tracer bilaterally compatible with innumerable subsegmental perfusion defects. (**c**) Posterior view of ventilation image shows relatively homogeneous tracer uptake without definite correlating matched ventilation and perfusion defects

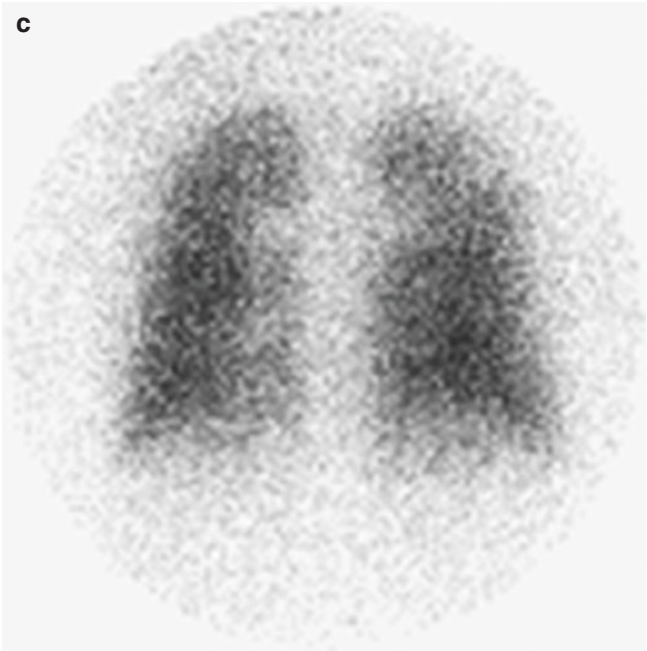

Fig. 12.7 (continued)

Table 12.1 Classification of pulmonary hypertension. (Based on the Venice 2003 clinical classification)

1. Pulmonary arterial hypertension
Idiopathic (IPAH)
Familial (FIPAH)
Associated with (APAH)
Connective tissue disease
Congenital systemic to pulmonary shunts
Portal hypertension
HIV
Drugs and toxins
Other
Associated with significant venous or capillary involvement
Pulmonary veno-occlusive disease (PVOD)
Pulmonary capillary hemangiomatosis (PCH)
Persistent pulmonary hypertension of the newborn (PPHN)
2. Pulmonary hypertension associated with left heart diseases
Left-sided atrial or ventricular disease
Left-sided valvular heart disease
3. Pulmonary hypertension associated with respiratory disease or hypoxia
Chronic obstructive pulmonary disease
Interstitial lung disease
Sleep-disordered breathing
Alveolar hypoventilation disorders
High altitude
Developmental abnormalities
4. Pulmonary hypertension due to chronic thrombotic and/or embolic disease
5. Miscellaneous

caused by shear stress [7]. Eventually, irreversible PHT develops with subsequent reversal of flow across the shunt and cyanosis. The histopathologic changes in the pulmonary vessels are identical to those seen in IPAH.

The likelihood of developing Eisenmenger syndrome depends on the location and size of the defect and the degree of the shunt [7]. Pediatric patients with a non-restrictive left-to-right shunt at the post-tricuspid level develop irreversible hypertension in over half of the cases and present in early childhood [25]. Examples of such conditions include large VSDs, atrioventricular septal defects (AVSD), and patent ductus arteriosus (PDA). In contrast, only 10–20% of patients with a hemodynamically significant pre-tricuspid level lesion, such as an atrial septal defect, develop PAH and generally not until the third or fourth decade [25]. The size of the defect is another critical factor in the development of PAH. While 3% of patients with a VSD less than 1.5 cm develop PAH, this increases to 50% if the defect is greater than 1.5 cm [7].

If detected early and the shunt closed, the PAH initially appears to be reversible [25]. Even without correction, patients with Eisenmenger syndrome appear to have a much longer life expectancy, up to the seventh decade, compared with 2.8 years in children with IPAH [26]. However, great variability exists and a small subgroup of patients continues to deteriorate even after correction of the defect [4]. This is believed to be due to the fact that there is a certain point of no return, following which pulmonary vascular remodeling progresses even after closure of the defect [25].

A further subgroup of children present with severe PHT early in life, associated with a cardiac defect with only mild hemodynamic effects [4, 25]. In these children, PAH due to another cause, such as IPAH, should be suspected and investigated accordingly.

A high index of suspicion is required for an early and timely diagnosis of a left-to-right shunt, which can allow closure of the defect prior to the development of irreversible pulmonary vascular changes. There may be evidence of left-to-right shunting on the CXR prior to the development of PHT characterized by increased pulmonary vascularity in a non-cyanotic child (Fig. 12.8). The most common location of the shunt is within the interventricular septum. A large VSD may show evidence of pulmonary artery enlargement associated with left ventricular hypertrophy. In contrast, pulmonary artery enlargement is uncommon in pediatric patients with an ASD, and cardiomegaly, if any, is predominantly right-sided. Increased pulmonary vascularity in an infant should raise the suspicion of a PDA or an AVSD. The aorta is often enlarged in the former condition, while commonly, there is evidence of congestive cardiac failure in children with an AVSD. Once the pulmonary vascular resistance has increased, the typical changes of PAH described earlier are seen. However, in Eisenmenger syndrome, small nodular

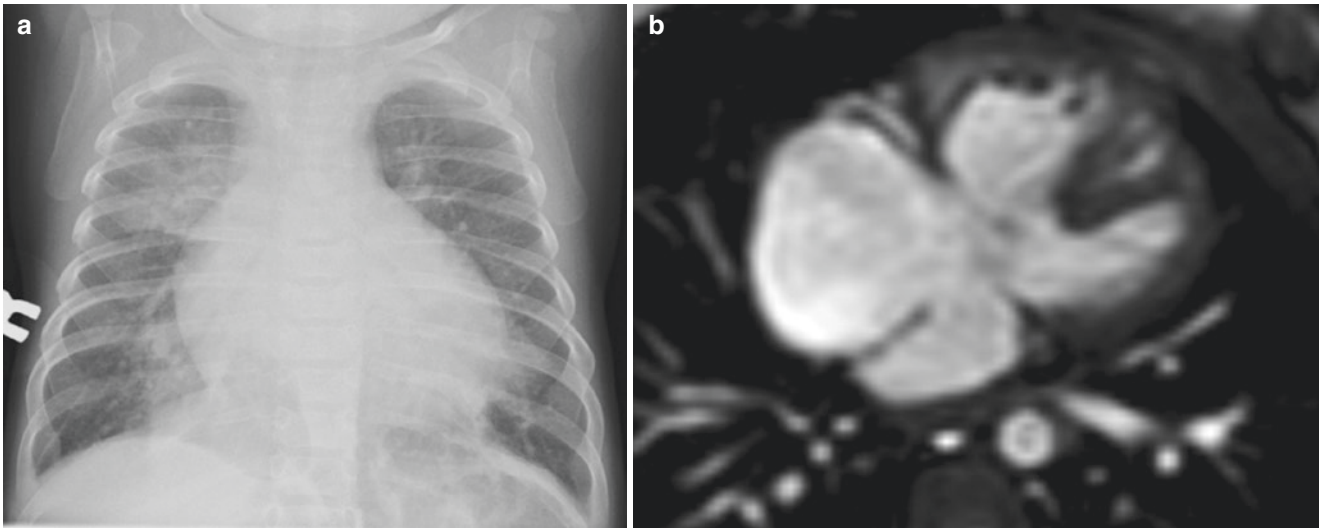

Fig. 12.8 A newborn girl with pulmonary hypertension secondary to atrioventricular defect. (**a**) Frontal chest radiograph shows increased pulmonary vascularity and cardiomegaly. (**b**) Axial T1 MR image demonstrates an atrioventricular septal defect

opacities, corresponding to neovascularity, appear to be much more common [27]. Intrapulmonary hemorrhage, also relatively common, may appear as focal areas of opacification [27].

The CT imaging findings of PAH in pediatric patients with congenital systemic to pulmonary shunts are similar to those seen in IPAH. However, in adults, several studies have highlighted some important differences in CT appearances in Eisenmenger vs. isolated IPAH. In particular, pulmonary neovascularity, characterized by peripheral serpiginous vessels, appears to be much more common in patients with Eisenmenger physiology [27, 28]. This is particularly the case with post-tricuspid defects. Lobular ground-glass opacity, which may be related to hemorrhage or dilated capillary networks, is also more frequently seen in these patients (Fig. 12.9) [27, 29]. Enlarged bronchial artery collaterals are often identified in both groups, but are more common in Eisenmenger syndrome [28]. Extrapulmonary findings that are particularly suggestive of Eisenmenger syndrome include aneurysmal dilatation of the pulmonary arteries and proximal pulmonary artery thrombosis [29].

MRI of the heart and great vessels can readily identify the anatomic defect and quantify the magnitude of the shunt. However, MR imaging of congenital heart disease is an extensive topic and outside of the scope of this chapter.

Scintigraphy is rarely performed in this setting as the other imaging modalities can accurately establish the diagnosis. However, it can be useful in excluding thromboembolic disease and often identify a hemodynamically significant shunt [30].

Most importantly, the key investigation in these infants and children is transthoracic or transesophageal echocardiography. This generally defines the size and location of the defect as well as the magnitude of the associated shunt. In addition, it provides an estimate of right ventricular and pulmonary artery systolic pressure. In cases of suspected irreversible hypertension, cardiac catheterization with vasodilator testing may be required prior to initiation of medical therapy.

Conditions Associated with Significant Venous or Capillary Involvement

Pulmonary Veno-Occlusive Disease

Pulmonary veno-occlusive disease (PVOD) is a rare cause of PHT [31]. It preferentially affects the post-capillary vasculature with fibrous obliteration of the pulmonary venous system [32]. The disease affects all ages with no sex predilection in the pediatric age group [33].

The clinical presentation is essentially the same as IPAH. However, differentiation from IPAH is critical, as vasodilator therapy, while effective for IPAH, can result in potentially fatal pulmonary edema in patients with PVOD [20]. Histological examination in PVOD demonstrates obliteration of venous lamina by fibrous tissue, particularly within the veins in the intralobular septa [32]. In this setting, pulmonary arteriolar dilatation induced by vasodilators significantly increases capillary hydrostatic pressure, with development of pulmonary edema [20].

Open surgical biopsy remains the only definitive method of diagnosing PVOD, but is often contraindicated due to the fragile clinical and hemodynamic status of these patients. Imaging, therefore, plays a critical role in early and correct diagnosis. The CXR findings reflect the PHT and post-capillary venous congestion [34]. Therefore, enlarged central

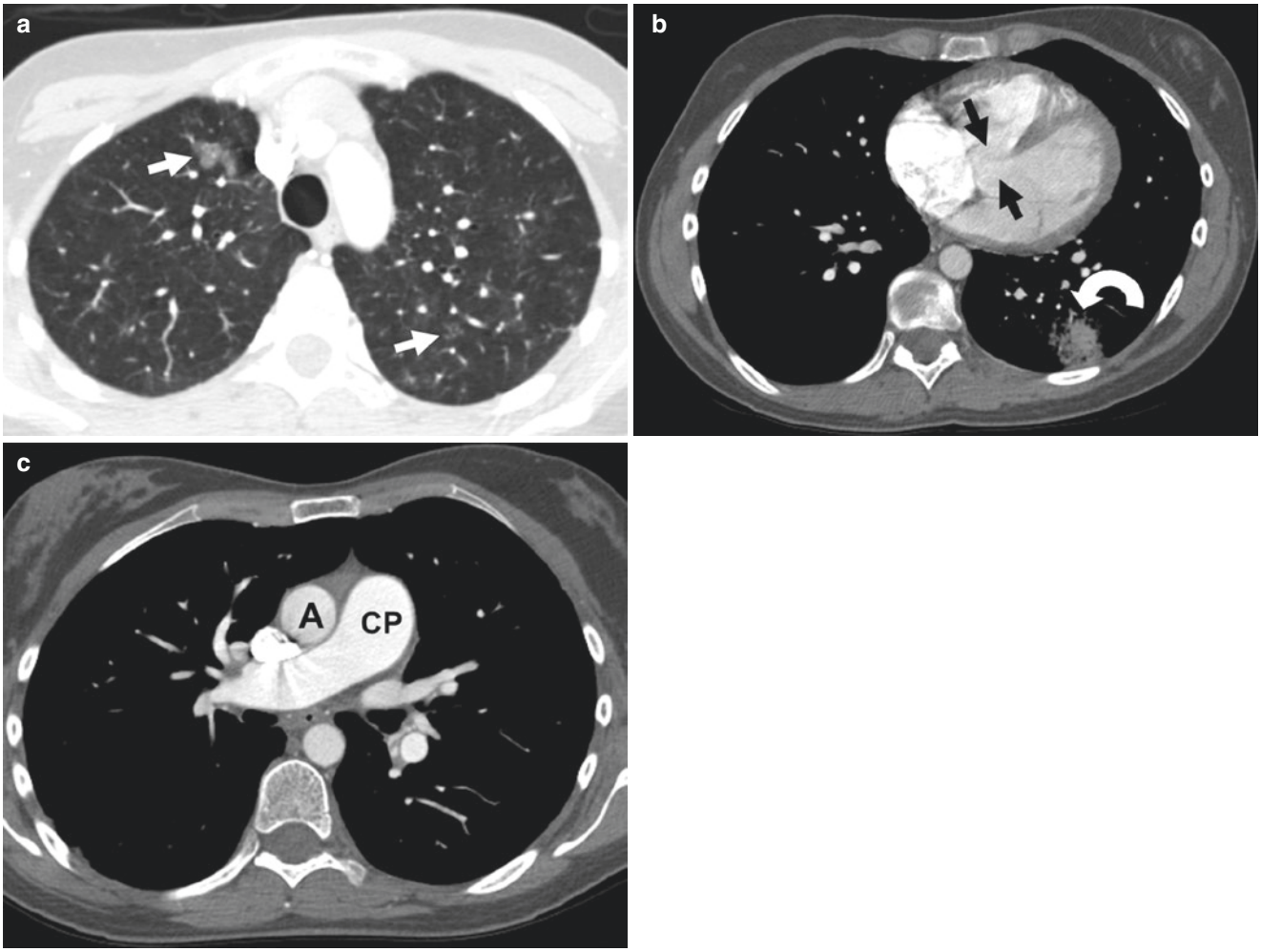

Fig. 12.9 Twenty-nine-year-old girl with Eisenmenger syndrome physiology who presented with pulmonary hypertension. (**a**) Axial lung window CT image shows areas of somewhat nodular and lobular ground-glass opacities (*arrows*). (**b**) Contrast-enhanced axial CT image demonstrates ventricular septal defect (arrows). Focal opacification consistent with an area of pulmonary hemorrhage is also noted in the left lower lobe (curved arrow). (**c**) Contrast-enhanced axial CT image shows an enlarged central pulmonary artery (CP). A aorta

pulmonary arteries with rapid tapering are seen in conjunction with increased interstitial markings, including Kerley B lines [34]. Absence of left-sided heart disease is also an important finding on CXR indicated by normal cardiac contours and size of pulmonary veins.

In recent years, several published studies have demonstrated that CT, in particular high-resolution CT, can be helpful in distinguishing PVOD from IPAH [18, 20, 32, 35]. While centrilobular opacities are more commonly seen in PVOD, these are also the most frequent intrapulmonary findings in IPAH [18, 20]. However, interlobular septal thickening is much more common and extensive in PVOD than in IPAH [20, 32]. Ground-glass opacity is also frequently seen and progresses from centrilobular to panlobular as the VOD worsens [20]. Of the extrapulmonary findings, the most specific imaging findings appear to be mediastinal lymphadenopathy in the absence of evidence for underlying chronic thromboembolic disease (CTED) or left-sided heart disease [20]. As with IPAH, central pulmonary artery and right-sided cardiac enlargement is identified, in the setting of normally sized left atrium and ventricle [34]. Pleural and pericardial effusions also appear to be nonspecific and are seen in both conditions [20]. Ventilation-perfusion scans in PVOD are very variable in appearance, ranging from normal to multiple mismatched perfusion defects [34].

Pulmonary Capillary Hemangiomatosis

Due to the similarities in clinical, pathological, and imaging features between PVOD and pulmonary capillary hemangiomatosis (PCH), in the most recent classification, these have been included in the same group [7, 36, 37]. Both conditions have similarly associated risk factors, such as systemic lupus erythematosis and scleroderma, but PCH has been reported much less frequently than PVOD [34]. It is

characterized pathologically by atypical proliferation of capillaries along both sides of the alveolar wall [38]. As this proliferation fills the alveolar septa, it compromises the gas exchange mechanism [39]. PCH occurs in a wide age range of patients (2–70 years) and is associated with rapid clinical deterioration [40]. Clinical presentation is similar to that of PVOD, with the exception that hemoptysis is much more common, reported in up to 30% of patients [38]. Laboratory testing may reveal thrombocytopenia, particularly in children [39].

On CXR, in addition to the typical findings of PHT, there is a diffuse bilateral reticulonodular pattern [39]. In contrast to PVOD, septal lines and pleural effusions are not commonly seen [34]. The CT findings in this condition are often characteristic. Central pulmonary enlargement is consistently accompanied by poorly defined centrilobular nodules of ground-glass density, mixed with lobular ground-glass opacification [34, 38–40]. In contrast to PVOD, septal thickening is much less prominent and may be nodular in PCH [38, 39]. Although V/Q scintigraphy may demonstrate a non-homogeneous pattern with radioisotope uptake in areas of capillary proliferation [41], it is usually not helpful as results varying from normal to high probability have been reported [34, 40, 42].

Persistent Pulmonary Hypertension of the Newborn

At birth, pulmonary vascular resistance decreases rapidly which is initiated by expansion of the lungs, increased oxygenation, and increased nitric oxide, PGI2, and bradykinin [43]. Over the course of 1 month, there is progressive remodeling of the airways with connective tissue deposition and smooth muscle maturation [44]. PPHN is a result of failure of normal pulmonary vascular relaxation at or shortly after birth [43, 45, 46]. It is characterized by high pulmonary vascular resistance, right to left shunting and severe hypoxemia [6]. Histologically, there is evidence of hyperplasia of the vascular smooth muscle combined with increased extracellular matrix deposition [47]. Persistent pulmonary hypertension of the newborn (PPHN) is frequently associated with perinatal stress (e.g., hypoglycemia, hypotension) and pulmonary parenchymal abnormalities, such as meconium aspiration, pneumonia, and congenital lung anomalies [6, 48]. Although fatal in some cases, in the vast majority, PPHN is transient with complete resolution [4].

There are no specific imaging findings of PPHN. However, CXR often shows the underlying etiology of PPHN. Meconium aspiration is the most common cause of PPHN in the United States. On CXR, meconium aspiration is characterized by coarse opacities in the affected lungs associated with hyperinflation and often pneumothorax (i.e., air leaks). Profound hypoxemia with clear lungs may reflect idiopathic (or *black-lung*) PPHN [49], named due to its CXR findings of clear, hyperlucent lungs. This is most common in term and near-term (34-week gestation) newborns.

PPHN should be differentiated from alveolar capillary dysplasia, a rare, likely congenital, disorder of pulmonary vascular development characterized by severe hypoxemia and PHT refractory to treatment in the newborn. There is a high incidence of associated congenital anomalies, particularly of the gastrointestinal tract such as a malrotation [50]. These infants present on the first day of life and the condition is universally fatal in the first few weeks [51].

Pulmonary Hypertension Associated with Left Heart Diseases

Left heart disease in pediatric patients is primarily associated with congenital heart disease. This includes conditions such as hypoplastic left heart syndrome and mitral stenosis [52, 53]. Similar findings can also be seen in partial (Scimitar) and total anomalous pulmonary venous return [54, 55]. The end result in all these conditions is the elevated left atrial pressure associated with subsequent pulmonary venous hypertension. This, in turn, often causes intimal fibrosis and medial hypertrophy of the arterioles resulting in increased PAPs [56]. However, pathologically, there is no evidence of plexiform lesions in these children, resulting in a significant degree of reversibility of the PAH following surgical correction of the cardiac abnormality [53]. The CXR and CT findings in the lungs can be very similar to PVOD, but with associated abnormalities in heart contour and configuration. The diagnosis is usually readily established by echocardiography.

Pulmonary Hypertension Associated with Respiratory Disease or Hypoxia

Alveolar hypoxia, by inducing pulmonary vasoconstriction, can reflexively result in elevated pulmonary pressures. If chronic, this typically results in pulmonary vascular remodeling and PHT [57]. Remodeling results in medial thickening in muscular arterioles and muscularization of previously non-muscular arterioles [58]. Although CXR has been the first-line imaging modality of initial investigation, high-resolution CT is currently the investigation of choice for evaluating chronic lung disease. Contrast-enhanced MDCT also demonstrates the vascular anatomy. In addition, ventilation-perfusion scans may be useful in the assessment of regional lung function.

Bronchopulmonary Dysplasia (Chronic Lung Disease of Infancy)

Bronchopulmonary dysplasia (BPD), also known as chronic lung disease of infancy, is characterized by the abnormal development of inflamed and scarred lung tissues, resulting from mechanical ventilation and oxygen therapy [59, 60]. Originally described by Northway in 1967, in the pre-surfactant era, this was seen in infants who underwent prolonged high-pressure ventilation with elevated oxygen concentrations. With the advent of surfactant and advancement in ventilation techniques, this is now predominantly seen in premature neonates of low birth weight. Consistent with the changing demographic pattern, the pathological changes seen in current cases of BPD are also substantially different. The classic progressive stages commonly seen with acute lung injury have now given way to findings consistent with impaired alveolar and vascular growth [61]. Prominent pathological features include alveolar simplification with decreased growth of the capillary bed.

In addition to the previously described changes seen with PHT, the CXR may also demonstrate hyperexpansion, interstitial opacities, and focal emphysema (Fig. 12.10) [62]. The lung findings tend to improve with age. HRCT demonstrates multifocal hyperlucent areas, linear opacities radiating from the periphery, and triangular subpleural opacities. The areas of low attenuation on CT are larger than a pulmonary segment and may reflect obstructive emphysema caused by destruction of small airways and arrest of acinar development [63, 64]. Large airway changes may also be noted with tracheobronchomalacia and decreased broncho-arterial diameter [63]. Thus in the setting of PHT, the broncho-arterial diameter should be interpreted with caution.

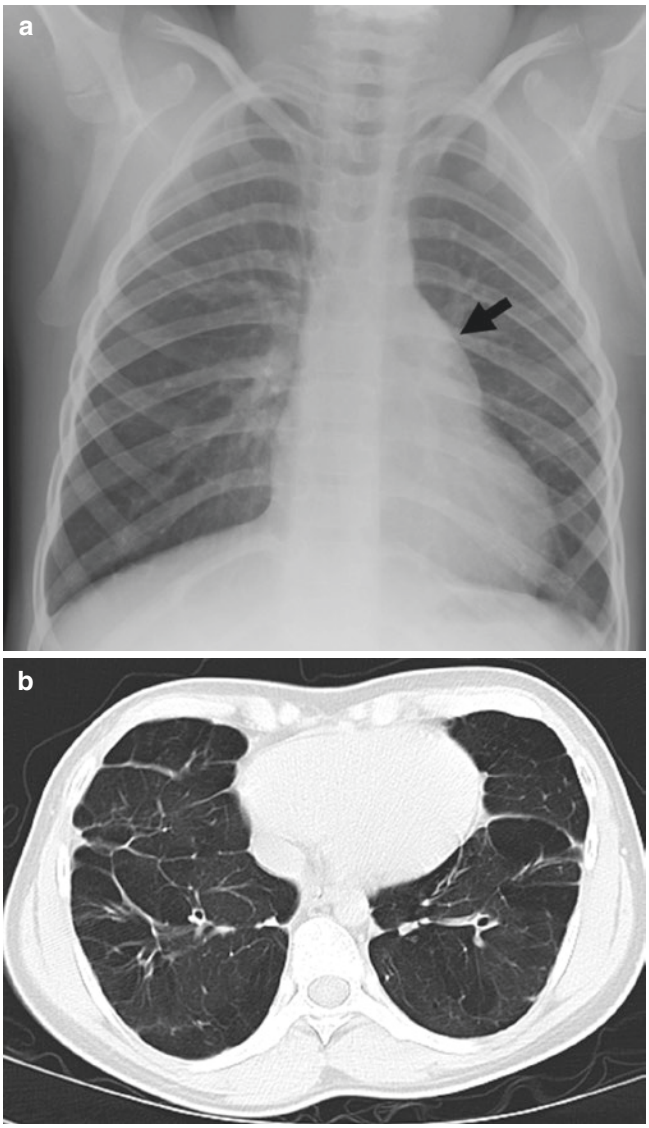

Fig. 12.10 Eight-year-old boy with prior history of prematurity and bronchopulmonary dysplasia who presented with pulmonary hypertension. (**a**) Frontal chest radiograph shows an enlarged central pulmonary artery (arrow). Mild hyperlucency is also noted within the bilateral lower lobes. (**b**) Axial lung window CT image demonstrates marked lung parenchymal damage characterized by the areas of coarse parenchymal thickening and air-trapping

Cystic Fibrosis and Bronchiectasis

PHT can be identified in up to a half of adolescents and young adults with cystic fibrosis (CF). PHT is particularly common in children with low peripheral oxygen saturation at rest [65]. Often subclinical, this is associated with thickening of the right ventricular wall on echocardiography [65]. Radiographic and CT findings of CF are discussed in detail elsewhere in this book, but evidence of PHT in the setting of upper lobe predominant bronchial wall thickening, bronchiectasis and "tree-in-bud" opacities representing superimposed bronchiolitis should strongly suggest the diagnosis of PHT associated with cystic fibrosis (Fig. 12.11).

Congenital Diaphragmatic Hernia

CDH is the most common developmental abnormality associated with PHT [4]. Bilateral pulmonary hypoplasia occurs early in fetal life with arrest of pre-acinar airway branching resulting in markedly decreased number of alveoli [66]. There is a similar arrest of the pulmonary vascular tree at 12–14 weeks of gestational age, with decreased cross-sectional area of the vascular bed and increased thickness of the muscular walls of the arterioles [67]. The PHT often abates in the first few weeks after birth but can persist and is associated with a significantly increased mortality [68].

The diagnosis of CDH is usually straightforward and often identified on prenatal imaging studies including prenatal ultrasound and MRI. Characteristic postnatal CXR

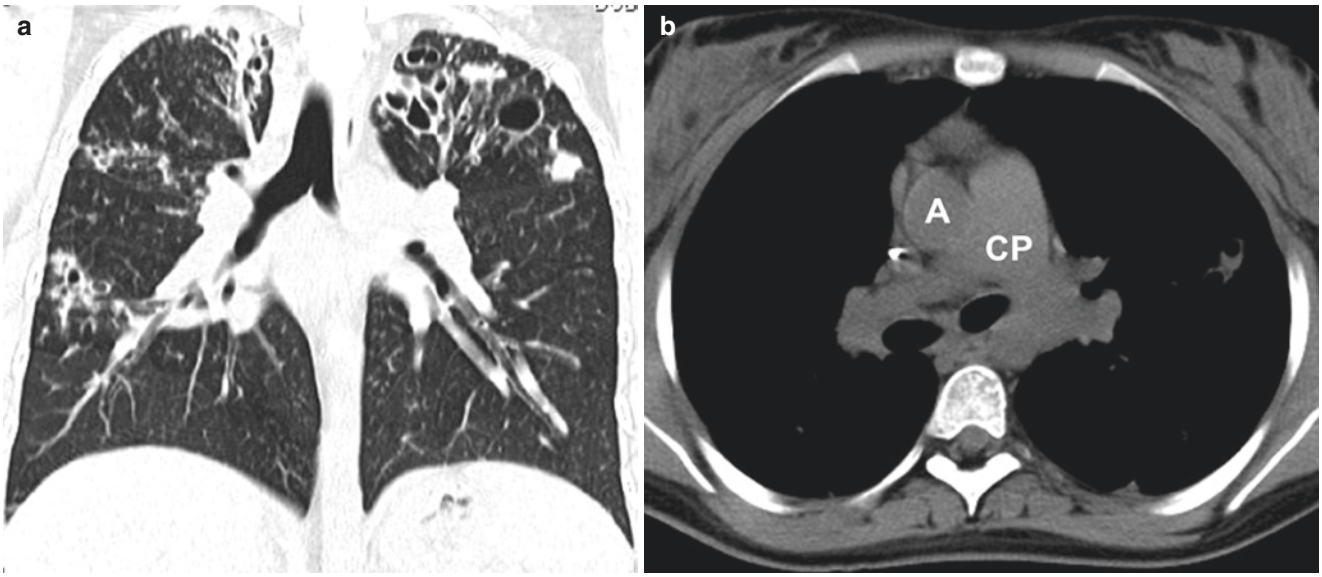

Fig. 12.11 Seventeen-year-old girl with pulmonary hypertension secondary to underlying lung disease (cystic fibrosis). (**a**) Coronal lung window CT image demonstrates advanced lung changes secondary to the patient's known cystic fibrosis characterized by bilateral upper lobe predominant bronchiectasis. (**b**) Axial non-enhanced CT image shows the enlarged central pulmonary artery (CP). A aorta

findings include mediastinal shift with bowel loops seen in the affected pleural cavity. Post-repair radiographs demonstrate resolution of the mediastinal shift with more marked hypoplasia of the ipsilateral lung. Similar findings are demonstrated on CT. Ventilation-perfusion scanning initially demonstrates decreased ventilation and perfusion in the affected ipsilateral lung. With increasing age, the ventilation normalizes but decreased perfusion persists, consistent with poor development of the pulmonary vascular tree [66].

Pulmonary Hypertension Due to Chronic Thrombotic and/or Embolic Disease

This is a rare cause of PHT in children [1]. Historically, the incidence of pulmonary embolism (PE) was believed to be much lower in children than in adults, in part because of a protective mechanism which decreases thromboembolism in children [69–72]. The incidence of deep venous thrombosis (DVT) and PE is greatest in adolescents and infants less than 1 year of age but still only accounts for 0.05–0.07 events per 10,000 children [69, 73]. However, in the hospital-based population, the incidence rises to 5.3 events per 10,000 hospital admissions. Much of this higher incidence is due to DVT/PE related to central venous lines. This accounts for almost 90% of embolic events in neonates and 60% in older children [69, 74]. Other less common risk factors for thromboembolic disease in children include cancer, cardiac disease, surgery, sickle cell disease, and tumor emboli. In fact, the recent study showed that it is unlikely for computed tomography pulmonary arteriography, which is the current gold standard for evaluating PE, to be positive in children with no underlying thromboembolic risk factors [75].

There is currently limited data on PHT associated with CTED in the pediatric population. In adults, in the vast majority of cases in which the patient survives a pulmonary embolic event, the thrombus is resorbed by fibrinolysis. However, in 0.1–0.4% of cases, the emboli evolve to an organized clot [76]. Contributing to the PHT is propagation of thrombus due to slow flow upstream from an occluded artery. In addition, there also appears to be a vasculopathy, similar to that seen in IPAH, in the unobstructed segments of the lung [76]. Histologically, medial hypertrophy, intimal thickening and plexiform lesion have all been identified [77].

Clinically, the patient may remain asymptomatic for many years, the so-called *honeymoon period*. Following obliteration of 60% of the pulmonary vascular bed, progressive dyspnea typically develops [78, 79].

Pulmonary angiography with right heart catheterization remains the gold standard investigation, providing a diagnosis as well as essential information on MPAP [80]. The aim of the investigation in CTED-related PHT is not only to establish the diagnosis but also to assess whether the hypertension is in proportion to the degree of vascular obstruction. Disproportionately high PHTN implies a significant degree of arteritis, with the condition less likely to respond to endarterectomy.

With the rapid advancement in MDCT technology in recent years, PE can now be identified to the sixth-order branches and is generally the investigation of choice in both the pediatric population and adults [81–86]. Recently, there

has also been growing interest in the use of MRI for evaluation of PE. It has been reported that MR angiography can be useful for evaluation of PE by demonstrating: (1) the visualization of pulmonary vessels to the subsegmental level; (2) the identification of the wedge-shaped lung parenchymal defects on MR perfusion sequences; and (3) the display of the extent of right heart impairment on cine MR sequences [78, 87]. Scintigraphic ventilation-perfusion scans show large segmental, often bilateral, perfusion defects associated with PE with normal ventilation.

Miscellaneous

Hemoglobinopathies

PHT is a well-documented sequela of sickle cell disease and accounts for 3% of the mortality [7, 88]. Elevated PAPs have been reported in almost half of children with sickle cell disease [89]. Historically, shear stress from the deformed erythrocytes passing through the pulmonary microvasculature has been proposed as the underlying cause of vascular injury. However, epidemiological evidence now suggests that hemolysis is the key factor in development of PHTN in sickle cell disease patients. The hemoglobin and arginase enzyme released from the hemolytic process produce a state of vascular proliferation and inflammatory stress [90] inducing a vasculopathy similar to that seen in IPAH, including the formation of plexiform lesions. In children, as in adults, the risk of developing PHTN appears to be related to the degree of hemolysis [89]. Co-existing underlying pulmonary disease such as asthma and obstructive sleep apnea also appear to play a contributing factor.

Transthoracic echocardiography plays a key role in diagnosis of elevated pressures and secondary cardiac changes. A V/Q scan is also usually performed to exclude CTED, a potentially treatable cause of PHTN which can occur in patients with sickle cell disease [91]. The CXR has a low overall sensitivity, but may indicate findings consistent with PHT in association with parenchymal disease and loss of volume consistent with fibrosis (Fig. 12.12). Fibrosis is better assessed on HRCT, characterized by predominantly basal interlobular septal thickening, traction bronchiectasis, and architectural distortion.

PHT has been described in virtually all hemoglobinopathies, especially beta-thalassemia [92]. The exact mechanism remains unclear, although chronic tissue hypoxia and hemolysis have been advocated as potential causes [92, 93]. The risk also appears to be elevated by splenectomy. This may be due to platelet activation resulting in microthrombi in the pulmonary vasculature or increased hemolysis due to the lack of removal of senescent cells [92]. The imaging appearances are generally nonspecific.

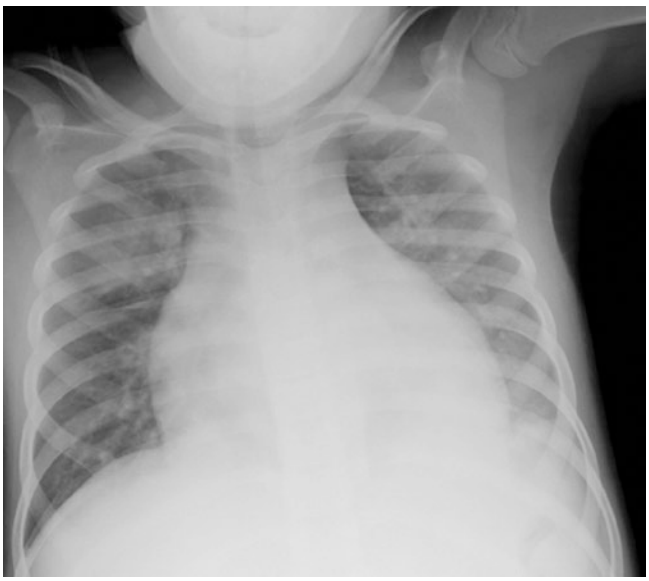

Fig. 12.12 Nine-year-old boy with known sickle cell disease who presented with shortness of breath and pulmonary hypertension. Frontal chest radiograph shows markedly enlarged heart and areas of mild patchy parenchymal opacities (worst in the left lower lobe) and surrounding lucencies in both lungs

Treatments

For IPAH, treatments may include:

- *Inhaled oxygen* to help raise the levels of oxygen in the bloodstream.
- *Nitric oxide* (NO) to help reduce the resistance in the lung blood vessels and improve heart function.
- *Calcium-channel blockers* to relieve constriction in the pulmonary arteries and improve the heart's ability to pump blood.
- *Intravenous prostacyclin*, *Flolan*, to help open up constricted lung blood vessels and reduce high blood pressure in the lungs.
- *Endothelin antagonists*, *prostacyclin analogs*, *and phosphodiesterase inhibitors* to reduce high blood pressure in the lungs.
- *Anticoagulants* to prevent blood clots in the lungs.
- *Diuretics* to help kidneys eliminate water.
- *Digoxin* to help support the ability of the heart to pump the blood.
- *Lung transplantation* for patients who do not respond to medication—a single-lung, double-lung or heart-lung transplant may be recommended.

For conditions associated with pulmonary arterial hypertension, treating the underlying disease or defect may have significant benefit. Use of many of the treatments listed above, in conjunction with treatment for the associated cause of the disease, may help ease the effects of PHT.

References

1. Abman SH, Hansmann G, Archer SL, et al. Pediatric pulmonary hypertension: guidelines from the American Heart Association and American Thoracic Society. Circulation. 2015;132(21):2037–99.
2. Nicholarsen J, Ivy D. Progress in the diagnosis and management of pulmonary hypertension in children. Curr Opin Pediatr. 2014;26(5):527–35.
3. Neptune E, Varghese N, Sockrider M. Pulmonary hypertension in children. Am J Respir Crit Care Med. 2017;196(8):15–6.
4. Haworth SG. The management of pulmonary hypertension in children. Arch Dis Child. 2008;93:620–5.
5. Rosenzweig EB, Barst RJ. Pulmonary arterial hypertension in children: a medical update. Curr Opin Pediatr. 2008;20:288–93.
6. Rosenzweig EB, Widlitz AC, Barst RJ. Pulmonary arterial hypertension in children. Pediatr Pulmonol. 2004;38:2–22.
7. Simonneau G, Galie N, Rubin LJ, et al. Clinical classification of pulmonary hypertension. J Am Coll Cardiol. 2004;43:5S–12.
8. Vorhies EE, Gajarski RJ, Yu S, Donohue JE, Figer CG. Echocardiographic evaluation of ventricular function in children with pulmonary hypertension. Pediatr Cardiol. 2014;35(5):759–66.
9. LaRaia AV, Waxman AB. Pulmonary arterial hypertension: evaluation and management. South Med J. 2007;100:393–9.
10. Zuk M, Migdal A, Jagiellowicz-Kowalska D, et al. Six-minute walk test in evaluation of children with pulmonary arterial hypertension. Pediatr Cardiol. 2017;38(4):754–61.
11. Gabbay E, Reed A, Williams TJ. Assessment and treatment of pulmonary arterial hypertension: an Australian perspective in 2006. Intern Med J. 2007;37:38–48.
12. Matsuura H. Cardiac catheterization in children with pulmonary arterial hypertension. Pediatr Int. 2017;59(1):3–9.
13. Johns CS, Kiely DG, Swift AJ. Novel imaging techniques in pulmonary hypertension. Curr Opin Cardiol. 2018;33(6):587–93.
14. Rosenzweig EB, Barst RJ. Idiopathic pulmonary arterial hypertension in children. Curr Opin Pediatr. 2005;17:372–80.
15. Widlitz A, Barst RJ. Pulmonary arterial hypertension in children. Eur Respir J. 2003;21:155–76.
16. Lammers AE, Hislop AA, Flynn Y, et al. Epoprostenol treatment in children with severe pulmonary hypertension. Heart. 2007;93:739–43.
17. Ng CS, Wells AU, Padley SP. A CT sign of chronic pulmonary arterial hypertension: the ratio of main pulmonary artery to aortic diameter. J Thorac Imaging. 1999;14:270–8.
18. Chaudry G, MacDonald C, Adatia I, et al. CT of the chest in the evaluation of idiopathic pulmonary arterial hypertension in children. Pediatr Radiol. 2007;37:345–50.
19. King MA, Ysrael M, Bergin CJ. Chronic thromboembolic pulmonary hypertension: CT findings. AJR Am J Roentgenol. 1998;170:955–60.
20. Resten A, Maitre S, Humbert M, et al. Pulmonary hypertension: CT of the chest in pulmonary venoocclusive disease. AJR Am J Roentgenol. 2004;183:65–70.
21. McCann GP, Gan CT, Beek AM, et al. Extent of MRI delayed enhancement of myocardial mass is related to right ventricular dysfunction in pulmonary artery hypertension. AJR Am J Roentgenol. 2007;188:349–55.
22. Fukuchi K, Hayashida K, Nakanishi N, et al. Quantitative analysis of lung perfusion in patients with primary pulmonary hypertension. J Nucl Med. 2002;43:757–61.
23. Ogawa Y, Nishimura T, Hayashida K, et al. Perfusion lung scintigraphy in primary pulmonary hypertension. Br J Radiol. 1993;66:677–80.
24. Wood P. The Eisenmenger syndrome or pulmonary hypertension with reversed central shunt. I. Br Med J. 1958;2:701–9.
25. van Albada ME, Berger RM. Pulmonary arterial hypertension in congenital cardiac disease – the need for refinement of the Evian-Venice classification. Cardiol Young. 2008;18:10–7.
26. Daliento L, Somerville J, Presbitero P, et al. Eisenmenger syndrome. Factors relating to deterioration and death. Eur Heart J. 1998;19:1845–55.
27. Sheehan R, Perloff JK, Fishbein MC, et al. Pulmonary neovascularity: a distinctive radiographic finding in Eisenmenger syndrome. Circulation. 2005;112:2778–85.
28. Griffin N, Allen D, Wort J, et al. Eisenmenger syndrome and idiopathic pulmonary arterial hypertension: do parenchymal lung changes reflect aetiology? Clin Radiol. 2007;62:587–95.
29. Perloff JK, Hart EM, Greaves SM, et al. Proximal pulmonary arterial and intrapulmonary radiologic features of Eisenmenger syndrome and primary pulmonary hypertension. Am J Cardiol. 2003;92:182–7.
30. Sun SS, Tsai MK, Yang CH, et al. Atrial septal defect with Eisenmenger's syndrome confirmed by Tc-99m MAA scintigraphy. Clin Nucl Med. 2002;27:219–20.
31. Woemer C, Cutz E, Yoo SJ, Grasemann H, Humpl T. Pulmonary veno-occlusive disease in childhood. Chest. 2014;146(1):167–74.
32. Ozsoyoglu AA, Swartz J, Farver CF, et al. High-resolution computed tomographic imaging and pathologic features of pulmonary veno-occlusive disease: a review of three patients. Curr Probl Diagn Radiol. 2006;35:219–23.
33. Holcomb BW Jr, Loyd JE, Ely EW, et al. Pulmonary veno-occlusive disease: a case series and new observations. Chest. 2000;118:1671–9.
34. Frazier AA, Franks TJ, Mohammed TL, et al. From the Archives of the AFIP: pulmonary veno-occlusive disease and pulmonary capillary hemangiomatosis. Radiographics. 2007;27:867–82.
35. Engelke C, Schaefer-Prokop C, Schirg E, et al. High-resolution CT and CT angiography of peripheral pulmonary vascular disorders. Radiographics. 2002;22:739–64.
36. O'Keefe MC, Post MD. Pulmonary capillary hemangiomatosis: a rare cause of pulmonary hypertension. Arch Pathol Lab Med. 2015;139(2):274–7.
37. Faria IM, Carmeiro LH, Tiradentes TA, Zanetti G, Marchiori E. Pulmonary capillary hemangiomatosis: an uncommon cause of pulmonary hypertension. J Bras Pneumol. 2013;29(3):390–2.
38. Lippert JL, White CS, Cameron EW, et al. Pulmonary capillary hemangiomatosis: radiographic appearance. J Thorac Imaging. 1998;13:49–51.
39. El-Gabaly M, Farver CF, Budev MA, et al. Pulmonary capillary hemangiomatosis imaging findings and literature update. J Comput Assist Tomogr. 2007;31:608–10.
40. Ito K, Ichiki T, Ohi K, et al. Pulmonary capillary hemangiomatosis with severe pulmonary hypertension. Circ J. 2003;67:793–5.
41. Rush C, Langleben D, Schlesinger RD, et al. Lung scintigraphy in pulmonary capillary hemangiomatosis. A rare disorder causing primary pulmonary hypertension. Clin Nucl Med. 1991;16:913–7.
42. Almagro P, Julia J, Sanjaume M, et al. Pulmonary capillary hemangiomatosis associated with primary pulmonary hypertension: report of 2 new cases and review of 35 cases from the literature. Medicine (Baltimore). 2002;81:417–24.
43. Dakshinamurti S. Pathophysiologic mechanisms of persistent pulmonary hypertension of the newborn. Pediatr Pulmonol. 2005;39:492–503.
44. Allen K, Haworth SG. Human postnatal pulmonary arterial remodeling. Ultrastructural studies of smooth muscle cell and connective tissue maturation. Lab Investig. 1988;59:702–9.
45. Bendapudi P, Rao GG, Greenough A. Diagnosis and management of persistent pulmonary hypertension of the newborn. Paediatr Respir Rev. 2015;16(3):157–61.
46. Steinhorn RH. Neonatal pulmonary hypertension. Pediatr Crit Care Med. 2010;11(2 Suppl):S79–84.
47. McLeod KA, Gerlis LM, Williams GJ. Morphology of the elastic pulmonary arteries in pulmonary hypertension: a quantitative study. Cardiol Young. 1999;9:364–70.
48. Atkinson JB, Ford EG, Kitagawa H, et al. Persistent pulmonary hypertension complicating cystic adenomatoid malformation in neonates. J Pediatr Surg. 1992;27:54–6.

49. Farrow KN, Fliman P, Steinhorn RH. The diseases treated with ECMO: focus on PPHN. Semin Perinatol. 2005;29:8–14.
50. Antao B, Samuel M, Kiely E, et al. Congenital alveolar capillary dysplasia and associated gastrointestinal anomalies. Fetal Pediatr Pathol. 2006;25:137–45.
51. Roy PG, Patel P, Vayalakkad A, et al. Alveolar capillary dysplasia presenting as pneumothorax: a case report and review of literature. Pediatr Surg Int. 2007;23:915–7.
52. Bardo DM, Frankel DG, Applegate KE, et al. Hypoplastic left heart syndrome. Radiographics. 2001;21:705–17.
53. Endo M, Yamaki S, Ohmi M, et al. Pulmonary vascular changes induced by congenital obstruction of pulmonary venous return. Ann Thorac Surg. 2000;69:193–7.
54. Gudjonsson U, Brown JW. Scimitar syndrome. Semin Thorac Cardiovasc Surg Pediatr Card Surg Annu. 2006;9:56–62.
55. Yamaki S, Tsunemoto M, Shimada M, et al. Quantitative analysis of pulmonary vascular disease in total anomalous pulmonary venous connection in sixty infants. J Thorac Cardiovasc Surg. 1992;104:728–35.
56. Yamaki S, Endo M, Takahashi T. Different grades of medial hypertrophy and intimal changes in small pulmonary arteries among various types of congenital heart disease with pulmonary hypertension. Tohoku J Exp Med. 1997;182:83–91.
57. Ghofrani HA, Voswinckel R, Reichenberger F, et al. Hypoxia- and non-hypoxia-related pulmonary hypertension – established and new therapies. Cardiovasc Res. 2006;72:30–40.
58. Howell K, Ooi H, Preston R, et al. Structural basis of hypoxic pulmonary hypertension: the modifying effect of chronic hypercapnia. Exp Physiol. 2004;89:66–72.
59. Tracy MC, Cornfield DN. The evolution of disease: chronic lung disease of infancy and pulmonary hypertension. Curr Opin Pediatr. 2017;29(3):320–5.
60. Nagiub M, Kanaan U, Simon D, Guglani L. Risk factors for development of pulmonary hypertension in infants with bronchopulmonary dysplasia: systematic review and meta-analysis. Paediatr Respir Rev. 2017;23:27–32.
61. Stenmark KR, Abman SH. Lung vascular development: implications for the pathogenesis of bronchopulmonary dysplasia. Annu Rev Physiol. 2005;67:623–61.
62. Griscom NT, Wheeler WB, Sweezey NB, et al. Bronchopulmonary dysplasia: radiographic appearance in middle childhood. Radiology. 1989;171:811–4.
63. Howling SJ, Northway WH Jr, Hansell DM, et al. Pulmonary sequelae of bronchopulmonary dysplasia survivors: high-resolution CT findings. AJR Am J Roentgenol. 2000;174:1323–6.
64. Husain AN, Siddiqui NH, Stocker JT. Pathology of arrested acinar development in postsurfactant bronchopulmonary dysplasia. Hum Pathol. 1998;29:710–7.
65. Rovedder PM, Ziegler B, Pinotti AF, et al. Prevalence of pulmonary hypertension evaluated by Doppler echocardiography in a population of adolescent and adult patients with cystic fibrosis. J Bras Pneumol. 2008;34:83–90.
66. Keller RL. Antenatal and postnatal lung and vascular anatomic and functional studies in congenital diaphragmatic hernia: implications for clinical management. Am J Med Genet C Semin Med Genet. 2007;145C:184–200.
67. Kitagawa M, Hislop A, Boyden EA, et al. Lung hypoplasia in congenital diaphragmatic hernia. A quantitative study of airway, artery, and alveolar development. Br J Surg. 1971;58:342–6.
68. Dillon PW, Cilley RE, Mauger D, et al. The relationship of pulmonary artery pressure and survival in congenital diaphragmatic hernia. J Pediatr Surg. 2004;39:307–12; discussion 307–12.
69. Andrew M, David M, Adams M, et al. Venous thromboembolic complications (VTE) in children: first analyses of the Canadian Registry of VTE. Blood. 1994;83:1251–7.
70. Anton N, Massicotte MP. Venous thromboembolism in pediatrics. Semin Vasc Med. 2001;1:111–22.
71. Babyn PS, Gahunia HK, Massicotte P. Pulmonary thromboembolism in children. Pediatr Radiol. 2005;35:258–74.
72. Chan AK, Deveber G, Monagle P, et al. Venous thrombosis in children. J Thromb Haemost. 2003;1:1443–55.
73. Revel-Vilk S, Massicotte P. Thromboembolic diseases of childhood. Blood Rev. 2003;17:1–6.
74. Schmidt B, Andrew M. Neonatal thrombosis: report of a prospective Canadian and international registry. Pediatrics. 1995;96:939–43.
75. Lee EY, Tse SK, Zurakowski D, et al. Children suspected of having pulmonary embolism: multidetector CT pulmonary angiography – thromboembolic risk factors and implications for appropriate use. Radiology. 2012;262(1):242–51.
76. Dartevelle P, Fadel E, Mussot S, et al. Chronic thromboembolic pulmonary hypertension. Eur Respir J. 2004;23:637–48.
77. Moser KM, Bloor CM. Pulmonary vascular lesions occurring in patients with chronic major vessel thromboembolic pulmonary hypertension. Chest. 1993;103:685–92.
78. Kreitner KF, Kunz RP, Ley S, et al. Chronic thromboembolic pulmonary hypertension – assessment by magnetic resonance imaging. Eur Radiol. 2007;17:11–21.
79. Elwing JM, Vaidya A, Auger WR. Chronic thromboembolic pulmonary hypertension: an update. Clin Chest Med. 2018;39(3):605–20.
80. Auger WR, Kim NH, Kerr KM, et al. Chronic thromboembolic pulmonary hypertension. Clin Chest Med. 2007;28:255–69. x.
81. Kritsaneepaiboon S, Lee EY, Zurakowoski D, et al. MDCT pulmonary angiography evaluation of pulmonary embolism in children. AJR Am J Roentgenol. 2009;192(5):1246–52.
82. Schoepf UJ. Diagnosing pulmonary embolism: time to rewrite the textbooks. Int J Cardiovasc Imaging. 2005;21:155–63.
83. Lee EY, Kritsaneepaiboon S, Arellano CM, et al. Unsuspected pulmonary emboli in pediatric oncology patients: detection with MDCT. AJR Am J Roentgenol. 2010;194(5):1216–22.
84. Lee EY, Zurakowski D, Boiselle PM. Pulmonary embolism in pediatric patients: survey of CT pulmonary angiography practices and policies. Acad Radiol. 2010;17(12):1543–9.
85. Thacker PG, Lee EY. Pulmonary embolism in children. AJR Am J Roentgenol. 2015;204(6):1278–88.
86. Thacker PG, Lee EY. Advances in multidetector CT diagnosis of pediatric pulmonary thromboembolism. Korean J Radiol. 2016;17(2):198–208.
87. Liszewski MC, Hersman FW, Altes TA, et al. Magnetic resonance imaging of pediatric lung parenchyma, airways, vasculature, ventilation, and perfusion: sate of the art. Radiol Clin N Am. 2013;51(4):555–82.
88. Shilo NR, Morris CR. Pathways to pulmonary hypertension in sickle cell disease: the search for prevention and early intervention. Expert Rev Hematol. 2017;10(10):875–90.
89. Onyekwere OC, Campbell A, Teshome M, et al. Pulmonary hypertension in children and adolescents with sickle cell disease. Pediatr Cardiol. 2008;29:309–12.
90. Machado RF. Sickle cell anemia-associated pulmonary arterial hypertension. J Bras Pneumol. 2007;33:583–91.
91. Machado RF, Gladwin MT. Chronic sickle cell lung disease: new insights into the diagnosis, pathogenesis and treatment of pulmonary hypertension. Br J Haematol. 2005;129:449–64.
92. Barnett CF, Hsue PY, Machado RF. Pulmonary hypertension: an increasingly recognized complication of hereditary hemolytic anemias and HIV infection. JAMA. 2008;299:324–31.
93. Aessopos A, Farmakis D. Pulmonary hypertension in beta-thalassemia. Ann N Y Acad Sci. 2005;1054:342–9.

Pulmonary Venous Drainage Disorders

13

Edward Y. Lee and Sanjay P. Prabhu

Pulmonary Venous Drainage Disorders

Congenital pulmonary venous drainage disorders, resulting from abnormal embryonic venous development, occur in a diverse spectrum in the pediatric population. Although echocardiography with pulsed Doppler remains the initial investigation of choice in the evaluation of pulmonary venous developmental anomalies particularly in infants and young children, noninvasive imaging studies such as multidetector computed tomography (MDCT) and magnetic resonance imaging (MRI) are currently playing increasing roles in the initial diagnosis and further characterization of this group of disorders. In this chapter, we review (1) embryology, (2) epidemiology, (3) anatomy, (4) clinical presentation, (5) preoperative imaging evaluation, (6) management, and (7) postoperative imaging evaluation of congenital pulmonary venous drainage disorders in the pediatric population.

Embryology of Congenital Pulmonary Venous Anomalies

A brief overview of the development of the pulmonary veins is a prerequisite to optimal understanding and ability to correctly classify various types of pulmonary venous anomalies.

Near the end of the fourth week of gestation, the primordial lung buds are surrounded by the splanchnic plexus. Multiple small connections exist between the splanchnic plexus and the umbilicovitelline and cardinal venous systems. But there is no direct connection to the heart at this stage. At this time, a single embryonic pulmonary vein develops as an outgrowth of the posterior left atrial wall, just to the left of the developing septum primum. This vein subsequently connects with veins of the developing lung buds and establishes a connection between the pulmonary venous plexus and the sinoatrial portion of the heart.

Historically, there is controversy with regard to the exact site of development of the common pulmonary vein. Some authors believe the common pulmonary vein originates from an evagination in the sinoatrial region of the heart [1]. Others believe that the common pulmonary vein results from a confluence of vessels emerging from the pulmonary plexus [2]. According to a third theory, the common pulmonary vein is formed by the confluence of capillaries growing into the mesocardium, located between the lung buds and the heart. Nevertheless, it is generally accepted that, by the end of the first month of gestation, the common pulmonary vein can be identified as a vessel draining the pulmonary plexus and entering the sinoatrial portion of the heart. The site of entry is above the junction of the left and right horns of the sinus venosus and to the left of the developing septum primum [3]. The two right-sided pulmonary veins develop first and the left-sided drainage enters the left atrium through a single trunk that eventually bifurcates to form two veins [4].

During further development, the common pulmonary vein becomes incorporated into the left atrium, forming the large smooth-walled part of the atrium at term. Consequently, the individual pulmonary veins connect separately and directly to the left atrium [4].

In summary, one common vein formed from two pulmonary veins from each lung initially enters the primitive left atrium. At the end of development, four separate major pulmonary veins (i.e., right and left superior and inferior pulmonary veins) enter the atrium as the branches are incorporated into the expanding atrial wall.

Epidemiology of Congenital Pulmonary Venous Anomalies

Total anomalous pulmonary venous return (TAPVR) is a rare and heterogeneous cardiac anomaly with an incidence of

E. Y. Lee (✉) · S. P. Prabhu
Department of Radiology, Boston Children's Hospital and Harvard Medical School, Boston, MA, USA
e-mail: Edward.Lee@childrens.harvard.edu

R. H. Cleveland, E. Y. Lee (eds.), *Imaging in Pediatric Pulmonology*, https://doi.org/10.1007/978-3-030-23979-4_13

0.6–1.2 per 10,000 live births and occurs in 0.7–1.5% of newborns with congenital heart disease [5, 6].

The prevalence of partial anomalous pulmonary venous return (PAPVR) is approximately 0.6% in anatomic specimens [2]. This is less than the number gleaned from clinical studies, which suggests that some patients with PAPVR are not recognized during life. The most common type of PAPVR is to the right superior vena cava (SVC), and the second most common is to the right atrium.

Pulmonary vein stenosis (PVS) is a rare condition, with reported prevalence of 1.7 per 100,000 children younger than 2 years of age [7]. Although PVS was considered a congenital abnormality, the term "primary PVS" is preferred as the recent literature indicates that PVS is a progressive abnormality and may not be present from birth [8]. Primary PVS occurs more frequently in the preterm population. Approximately 50% of pediatric patients with primary PVS have an associated cardiac defect. Secondary PVS in children occurs commonly after surgical treatment for TAPVR [8]. Clinically, significant PVS occurs in 10% of postoperative TAPVR patients [9].

Anatomy of Congenital Pulmonary Venous Anomalies

Normal Anatomy of Pulmonary Veins

Normally, there are four separate pulmonary veins draining into the left atrium: (1) right superior, (2) right inferior, (3) left superior, and (4) left inferior. The upper lobe pulmonary veins lie anterior to their respective pulmonary arteries. The left upper lobe vein enters the left atrium just posterior to the orifice of the left atrial appendage. The right upper lobe vein enters the left atrium immediately posterior to the entrance of the superior vena cava into the right atrium. The left lower lobe pulmonary vein courses anterior to the descending thoracic aorta before entering the left posterior aspect of the LA. The right lower lobe vein drains into the right posteroinferior aspect of the LA (Fig. 13.1).

Abnormalities of Pulmonary Veins

In anatomic terms, congenital pulmonary venous anomalies may be categorized as (1) anomalous connections, (2) anomalous drainage with normal connections, (3) PVS, and (4) abnormal numbers of pulmonary veins.

Anomalous Pulmonary Venous Connections

In this condition, one or more of the pulmonary veins may connect anomalously to one or more of the systemic veins. TAPVC encompasses a group of anomalies in which the pulmonary veins connect directly to the systemic venous circulation via persistent splanchnic connections (Fig. 13.2). The most common classification system described by Darling et al. consists of four types: supracardiac, cardiac, infracardiac, and mixed. If one or more, but not all, of the veins connect anomalously, the term PAPVR is currently used (Fig. 13.3 and Fig. 13.4).

Anomalous Drainage with Normal Connections

Normal pulmonary venous connections with abnormal drainage can also exist. This may occur in conditions such as a common atrium with complete absence of the interatrial septum or due to malposition of the septum primum. In this situation, pulmonary veins connect normally into the posterior wall of the atrium between the right and left horns of the sinus venosus, but absence of the interatrial septum or malposition of the septum primum results in anomalous pulmonary venous drainage into the morphologic right atrium (Fig. 13.5).

Pulmonary Vein Stenosis

Stenosis in one or more of the pulmonary veins or in the common pulmonary vein may occur either focally as a discrete shelf or as a longer segment of narrowing at the junction of the pulmonary vein to the left atrium that extends slightly into the pulmonary vein, or as diffuse hypoplasia of the pulmonary veins (Fig. 13.6). Veins with normal connections may exhibit stenoses, varying from stenosis of one or more of the individual pulmonary veins to cor triatriatum. These result in varying degrees of obstruction to pulmonary venous return to the left atrium. Anomalously connected veins may also be stenotic, with reduction of venous return to the right atrium.

Primary PVS without a history of prior surgery or catheterization is thought to result from abnormal incorporation of the common pulmonary vein into the left atrium in the later stages of cardiac development. PVS with no discernible preceding or concomitant cause of stenosis has been termed *congenital*. However, except in the small group of patients with diffusely hypoplastic pulmonary veins, the term *primary* PVS is preferred. The importance of making this distinction is that it is becoming more apparent that the *primary* form of the disease is often progressive and may not even be evident at birth and therefore not strictly *congenital*. Some authors believe that the rapidity of progression with no evidence of inflammation in many patients suggests an underlying neoproliferative process. This hypothesis is based on presence of apparently proliferative *myofibroblastic* cells that have been found in a small number of autopsy specimens [10, 11]. These cells show features of both myocytes and fibroblasts, consistent with a myofibroblast cell type. In other parts of the body, these types of cells retain the ability to differentiate into either myocytes or fibroblasts. Trials using antiproliferation therapy are currently underway to evaluate whether radiation or chemotherapy might affect the growth of these cells in patients with PVS. It is also not yet

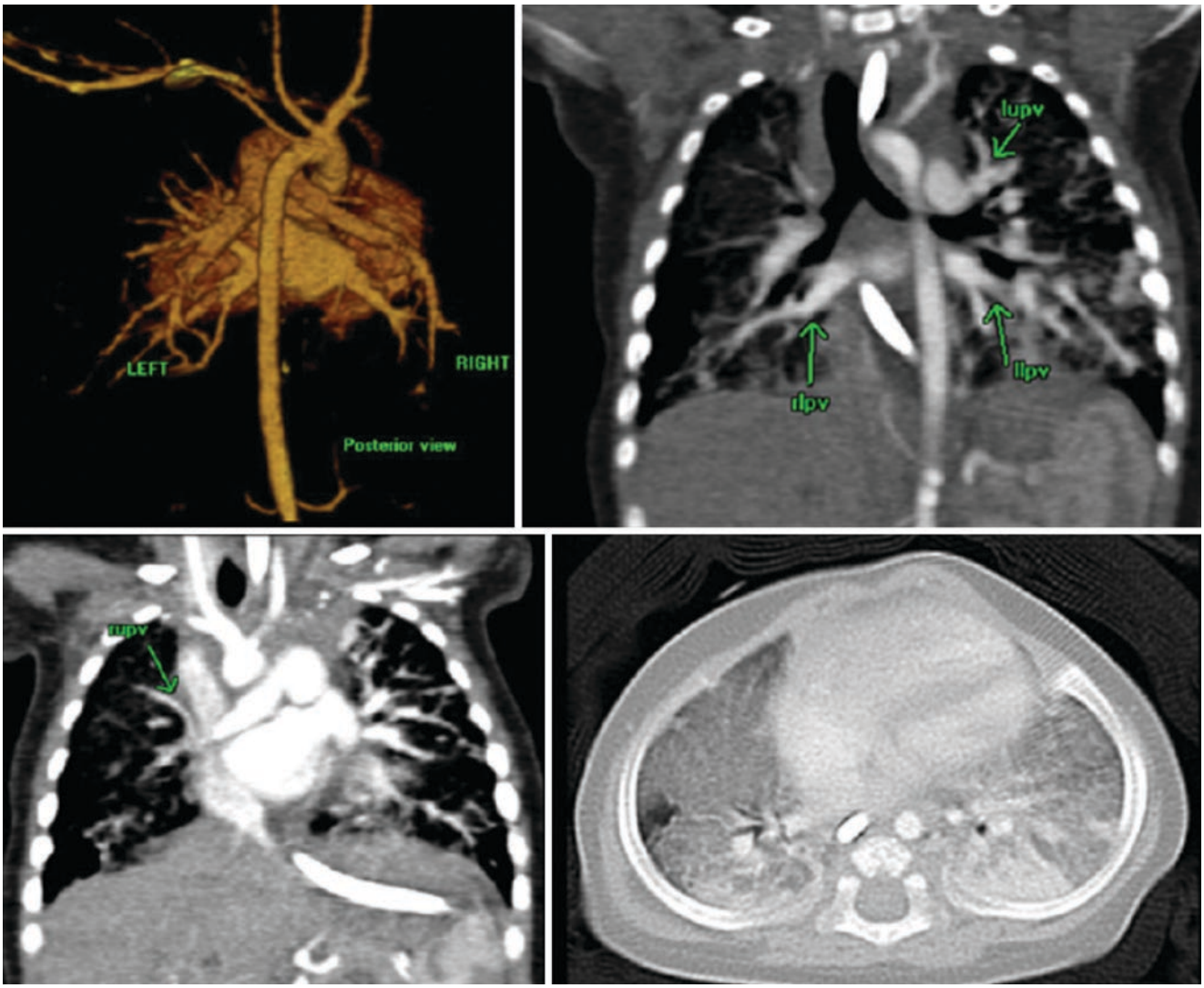

Fig. 13.1 A 5-month-old boy, former 28-week gestation infant. Posterior view of 3D volume-rendered CT image, coronal soft tissue window CT images, and axial lung window CT image show a normal pulmonary venous anatomy but with a markedly narrowed right upper lobe pulmonary vein, which is moderately to severely stenotic just proximal to the confluence. Lungs are abnormal secondary to chronic lung disease related to prematurity. Rupv right upper pulmonary vein, rlpu right lower pulmonary vein, lupv left upper pulmonary vein, llpv left lower pulmonary vein

clear whether these cell types may be more prevalent in the pulmonary veins of some patients and respond with excessive proliferation after a traumatic insult such as surgery or radiofrequency ablation.

Abnormal Numbers of Pulmonary Veins

Normally, there are four separate pulmonary veins: two on either side. The variations of pulmonary vein numbers include presence of a single vein on either side or all pulmonary veins entering a common pulmonary vein draining into the left atrium. A single left pulmonary vein is found more frequently than a single right [2]. A single common pulmonary vein, usually without stenosis, occurs almost exclusively in cases of visceral heterotaxy with asplenia. It is also possible to have an increased number of normally connecting pulmonary veins [2]. A fourth or even a fifth vein on one side has been reported as a rare finding. Abnormal numbers of pulmonary veins are not associated with any physiological problems.

Clinical Presentation of Congenital Pulmonary Venous Anomalies

Total Anomalous Pulmonary Venous Return

A number of anatomic patterns of total anomalous PV connection can result from persistence of splanchnic venous connections at almost any point in the cardinal or

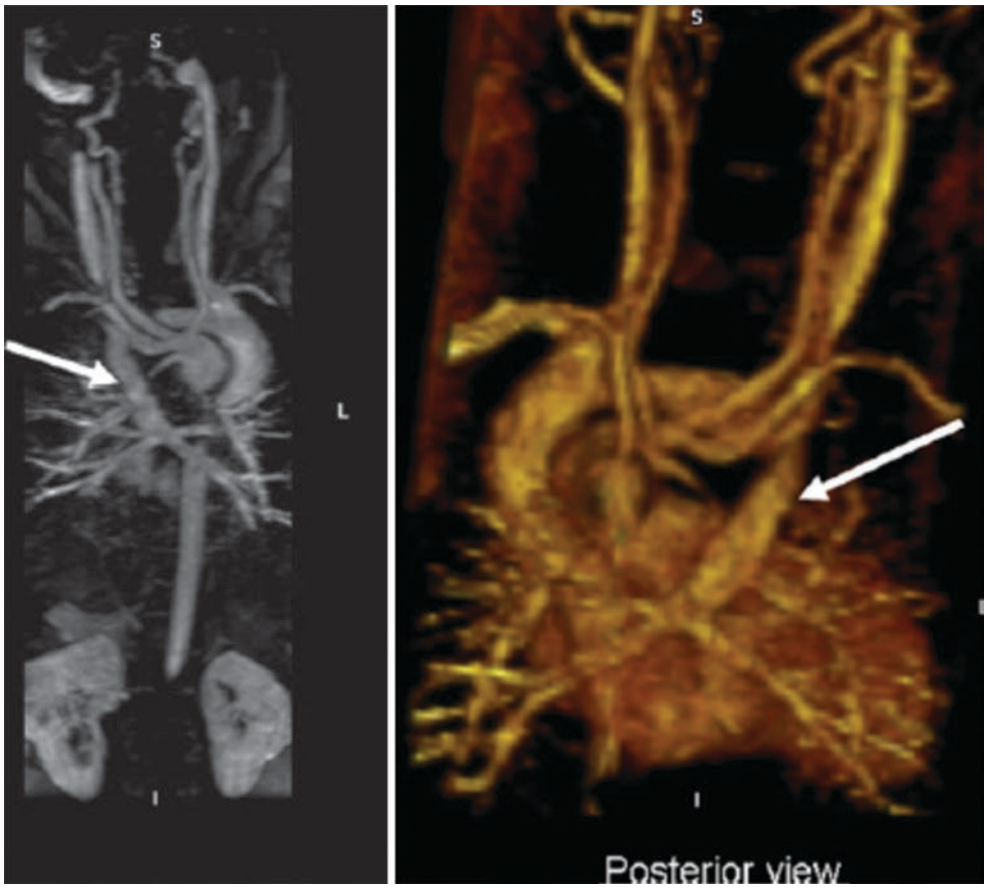

Fig. 13.2 A 5-month-old boy with total anomalous venous connection. Coronal and 3D volume-rendered CT images show patent all four pulmonary veins joining in the midline to a confluence, which extends to a right vertical vein (*arrow*), which continues to the innominate vein to left superior vena cava to a dilated structure that connects to the right side of a common atrial chamber

umbilicovitelline venous systems [12, 13]. This wide anatomical spectrum of TAPVR results in a variety of physiological and clinical presentation in postnatal life (Fig. 13.7), ranging from right-to-left shunts with mild cyanosis to pulmonary edema. Obstruction of the PV pathway is the most important predictor of adverse outcome and the tendency for PV obstruction in the infracardiac type of TAPVR is well-described, particularly in cases where infracardiac connections prevent the ductus venosus from bypassing the liver [14].

The overall natural history of TAPVR is poor, with up to 50% mortality in the first 3 months of life and a median survival of approximately 2 months. Therefore, early surgical repair is currently recommended, even before the onset of clinical symptoms and irrespective of anatomic subtype. Results of TAPVR repair in infancy have markedly improved in recent years.

Partial Anomalous Pulmonary Venous Return

Symptoms related to PAPVR are uncommon in childhood, but some dyspnea may occur on exertion. A small right-to-left shunt may exist, depending on the location of the PAPVR. The number of patients presenting with cyanosis increases during adult life as a result of changes in the pulmonary vascular bed, pulmonary hypertension, and increasing right-to-left shunt. Anomalous connection of a single pulmonary vein does not manifest clinically. If all except one of the veins connect anomalously, the clinical features mimic those of TAPVR. This is termed *subtotal TAPVR*. If all the veins of one lung connect anomalously, clinical symptoms result.

The age of presentation and severity of clinical symptoms in pediatric patients with PVS depends largely on the number of pulmonary veins involved and the severity of obstruction to each pulmonary vein. Most affected patients present in the first few months to years of life with significant respiratory symptoms. They have recurrent pneumonia and tachypnea. In later stages, signs related to pulmonary hypertension become prominent. Widespread or localized pulmonary edema may develop, and the degree and distribution of edema depends on whether single or more pulmonary veins are involved. Hemoptysis is a prominent symptom, especially in older patients. Evaluation for stenotic pulmonary veins is indicated in any young patient with severe pulmonary hypertension.

Pulmonary Vein Stenosis

PVS may occur as a secondary event in the pediatric age group, most often after surgical correction of anomalous pulmonary venous connection. Most series report clinically

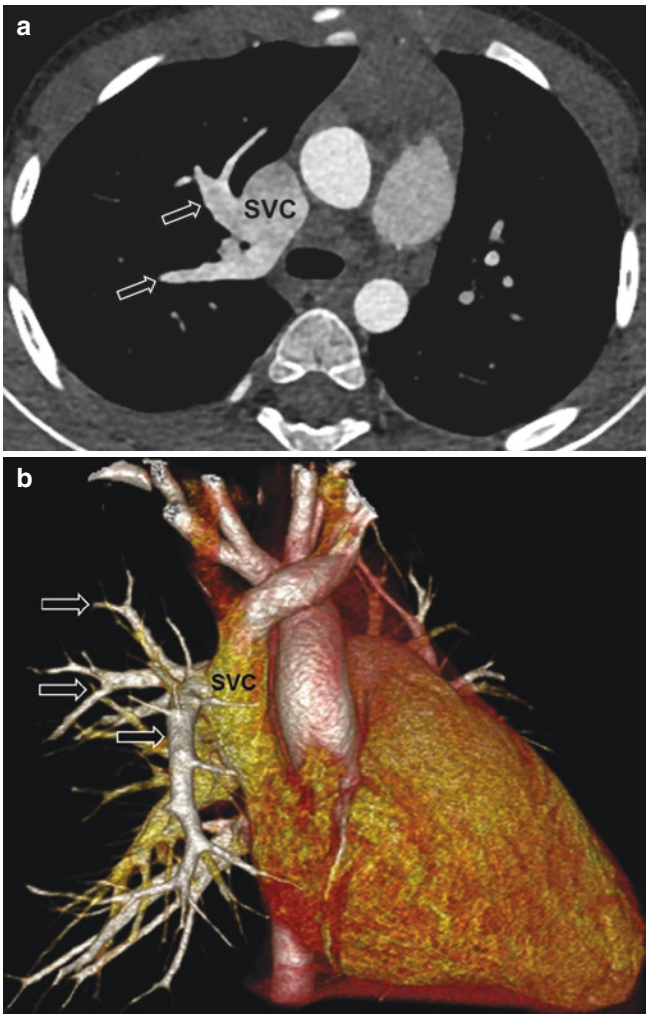

Fig. 13.3 A 5-year-old girl with right upper lobe partial anomalous pulmonary venous return. Axial enhanced CT image (**a**) and 3D volume-rendered CT image (**b**) show right upper lobe pulmonary veins (arrows) draining into the superior vena cava (SVC)

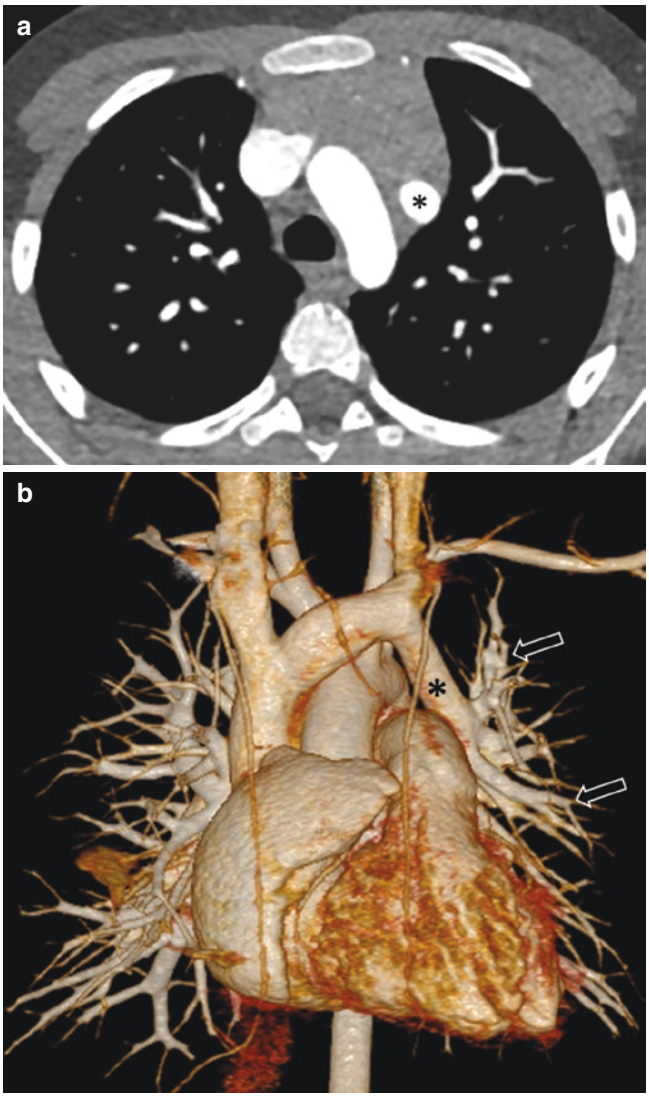

Fig. 13.4 A 6-year-old girl with left upper lobe partial anomalous pulmonary venous return. Axial enhanced CT image (**a**) and 3D volume-rendered CT image (**b**) show left upper lobe pulmonary veins (arrows) draining into the vertical vein (asterisk)

significant stenosis postoperatively in 10% of patients after repair of TAPVR [12]. The site of obstruction may be at the anastomotic site of the pulmonary venous confluence to the left atrium or may occur further into the central pulmonary veins. Cases of PVS have been described after cardiovascular surgical procedures for lesions not in proximity to the pulmonary veins [15].

Associated Cardiac Defects and Syndromes

Although PAPVR can present as an isolated structural abnormality, it commonly occurs with other cardiac abnormalities, most often an atrial septal defect (ASD). PAPVR or drainage has been seen in association with other congenital cardiac defects and syndromes. Most notably, patients with visceral heterotaxy and polysplenia have a high incidence of PAPVR secondary to malposition of the septum primum, and patients with asplenia have a high incidence of TAPVR. An increased incidence of PAPVR has been reported in association with Turner and Noonan syndromes. A rare but clinically important association is that of anomalous pulmonary venous connections with tetralogy of Fallot [16].

PVS occurs in the setting of various congenital heart diseases, the most common being patent ductus arteriosus and atrial, ventricular, and atrioventricular septal defects. Further, PVS is common after repair of TAPVR in patients with heterotaxy syndrome, may be diagnosed after infancy and is associated with poor outcomes [17].

Congenital Pulmonary Venolobar Syndrome

Special mention must be made in this context of the *scimitar syndrome*, which is a congenital anomaly affecting the right lung and the cardiovascular system (Fig. 13.8). It is also called

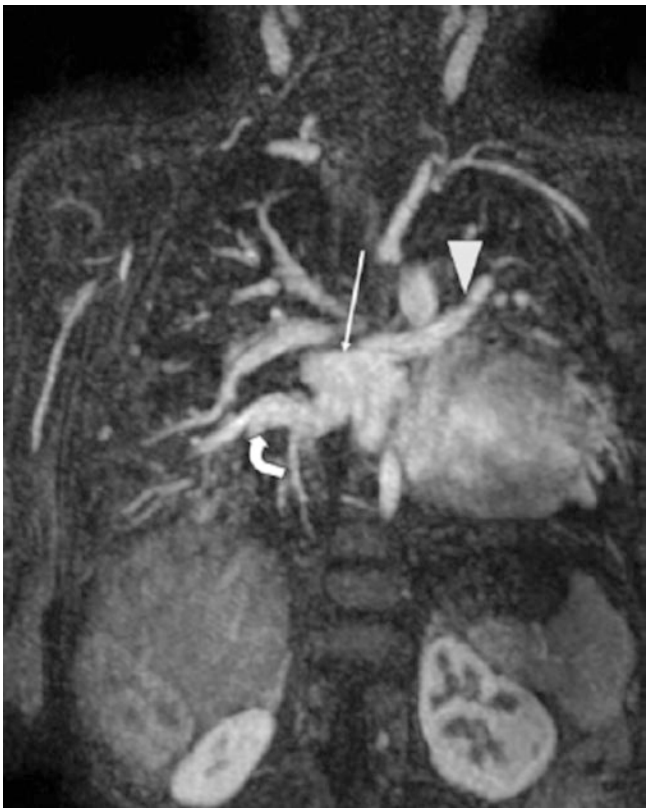

Fig. 13.5 A 3-month-old girl with cor triatriatum. Coronal MR angiography image shows the right lower pulmonary vein (*curved arrow*), left upper pulmonary vein (*arrowhead*), and left lower pulmonary vein (not seen on this image) that join a pulmonary venous chamber (*straight arrow*) that had two egresses: one to the supramitral portion of the left atrium and one through the sinus venosus defect

the *congenital pulmonary venolobar syndrome* and *hypogenetic lung syndrome*. The complete form of this syndrome consists of ipsilateral anomalous pulmonary drainage of part or all of the right pulmonary venous flow into the inferior vena cava, right lung hypoplasia, dextrocardia, hypoplasia or other malformation of the right branch pulmonary artery, and anomalous systemic arterial supply to the lower lobe of the right lung from the subdiaphragmatic aorta or its main branches [18]. The other features that may be seen include abnormal systemic blood flow to the right lung, abnormal bronchial anatomy, abnormal diaphragm, hemivertebrae, and anomalies of the genitourinary tract. Although most cases of scimitar syndrome are right-sided, rare cases have been reported involving the left side [19]. The three forms of this syndrome include the infantile form (with a large shunt between the abnormal artery that supplies the lower lobe of the right lung and the subdiaphragmatic aorta, sometimes called a sequestration), adult form (with a small shunt between the right pulmonary veins and IVC), and a third type with additional cardiac and extracardiac malformations [20].

Pulmonary Veno-occlusive Disease

A brief note may be relevant here regarding the term pulmonary veno-occlusive disease (PVOD). Previously, this term was used to refer to subgroups of patients with pulmonary venous stenoses. Currently, this entity is classified as a subgroup of pulmonary arterial hypertension (Figs. 13.9 and 13.10). It can be either idiopathic or as a complication of other conditions including bone marrow transplantation, connective tissue disease, pulmonary Langerhans cell

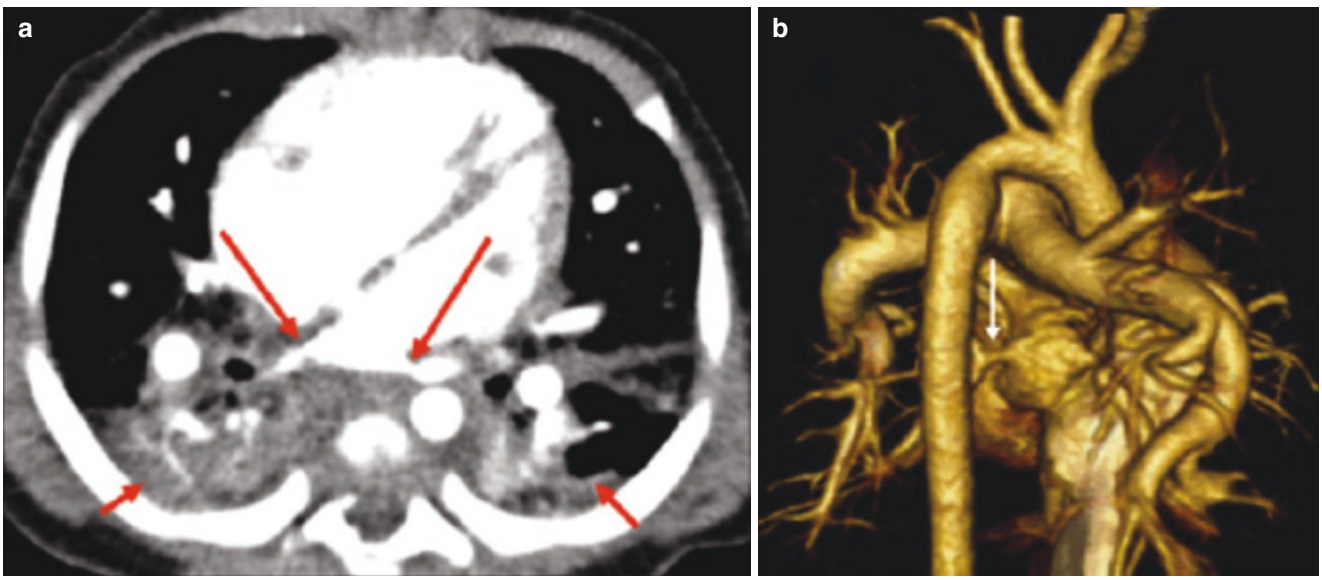

Fig. 13.6 A 4-month-old boy who presented with bilateral inferior pulmonary vein stenoses. (**a**) Axial enhanced CT image shows markedly narrowed bilateral inferior pulmonary veins (*long arrows*). Also noted are marked lung parenchymal changes (*short arrows*) due to pulmonary vein stenoses. (**b**) Posterior view of the 3D volume-rendered CT image shows markedly narrowed short segment pulmonary vein stenosis (*arrow*). 3D volume-rendered CT image is helpful for evaluation of the location, extent, and degree of the narrowing

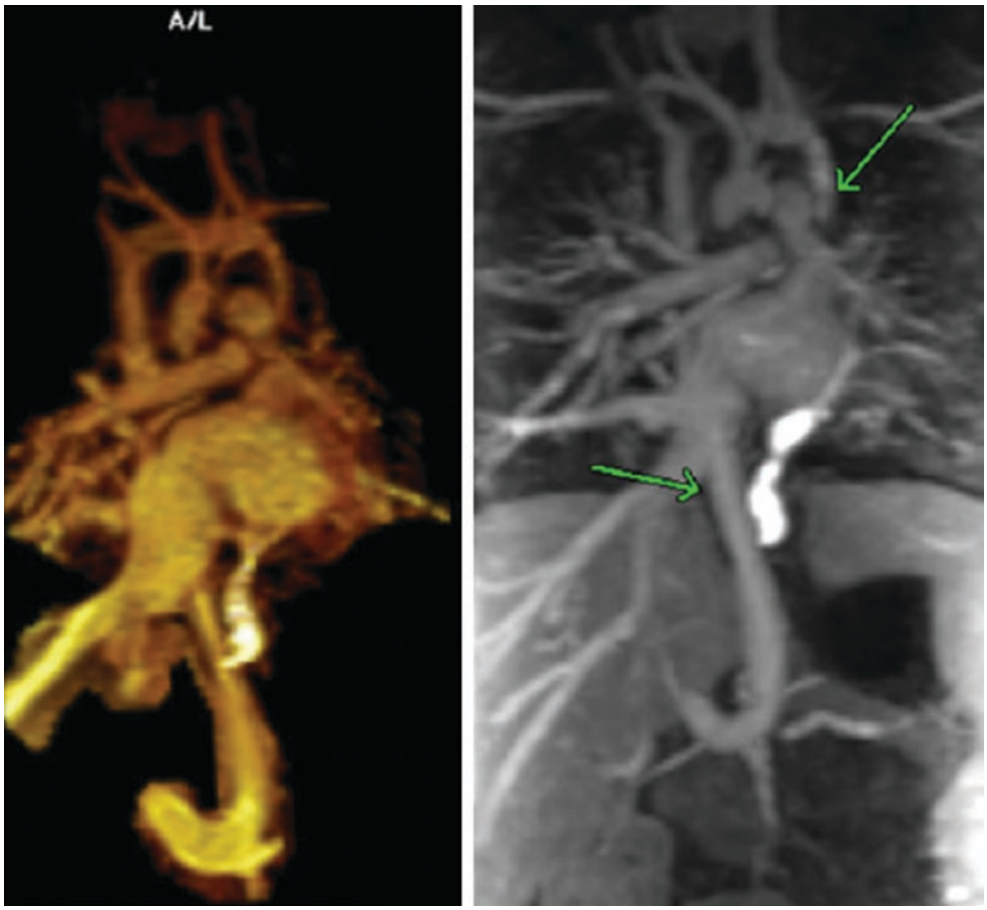

Fig. 13.7 A 7-day-old girl with mixed total anomalous pulmonary venous return. 3D volume-rendered and coronal MR angiography images show the right upper and right lower pulmonary veins drain infradiaphragmatically via a vertical vein (*arrow*) which courses inferiorly, behind the right atrium, and leftward past the midline to connect with a dilated left portal vein. This pathway is without discrete obstruction. A right middle and two left pulmonary veins drain to a small confluence posterior to the left atrium. This confluence is decompressed via a second vertical vein flowing inferiorly to connect with a different branch of the left portal vein. This vertical vein has a discrete narrowing within the liver. The umbilical venous catheter tip is located at this narrowing and may be contributing to the obstruction

histiocytosis, and sarcoidosis. The clinical presentation, genetic associations, and hemodynamics of PVOD are similar to pulmonary arterial hypertension. The diagnosis of this entity may be made from high-resolution CT in the presence of centrilobular opacities, septal lines, and lymphadenopathy in the appropriate clinical setting. Alveolar hemorrhage may be a feature of this condition [21].

Preoperative Evaluation of Congenital Pulmonary Venous Anomalies

Chest Radiography

In some instances of undiagnosed diffuse pulmonary venous obstruction, the signs and symptoms are nonspecific leading to a conundrum of whether the clinical problem is primarily pulmonary or cardiovascular. A CXR in this setting often merely suggests a nonspecific interstitial prominence. In these situations, an index of suspicion for venous obstructive disease should be entertained.

Echocardiography and Catheter Angiography

Two-dimensional (2D) echocardiography with color Doppler is usually the initial study of choice for evaluating the pulmonary veins particularly infants and young children. Although pulmonary venous obstruction, intracardiac defects, and functional variables are often well-assessed by echocardiography, the pulmonary veins cannot be identified and followed to their entry into the atria in all patients. Conventional angiography is still regarded as the gold standard to confirm the diagnosis after echocardiography. However, there are inherent risks of this invasive procedure technique especially in young infants and children whose vessels are smaller and weaker than adults.

MRI and MDCT

MRI and MDCT angiography can accurately define pulmonary venous connections in a vast majority of patients and presently, assuming a role of noninvasive modalities of choice for presurgical assessment of anomalous pulmonary venous connections in children. MRI and MRA can accurately demonstrate the abnormalities of pulmonary veins better than cardiac angiography and echocardiography.

The best MR images for pulmonary vein evaluation are obtained using a phased-array cardiac coil. Use of black blood and bright blood images may be obtained without IV contrast material [6]. Gradient-recalled echo (GRE) and 2D balanced steady-state free precession (SSFP) pulse sequences

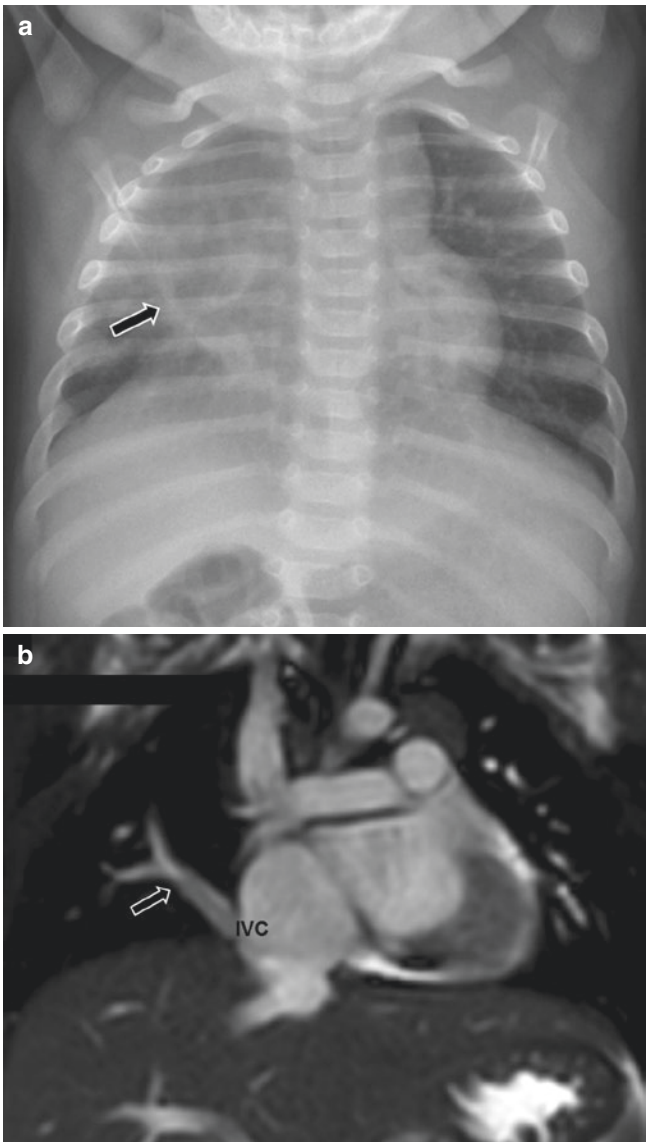

Fig. 13.8 A 2-month-old girl with Scimitar syndrome. (**a**) Frontal chest radiograph and (**b**) coronal MR image show a vertically oriented opacity (arrow), representing the Scimitar vein, in the hypoplastic right hemithorax draining into inferior vena cava (IVC)

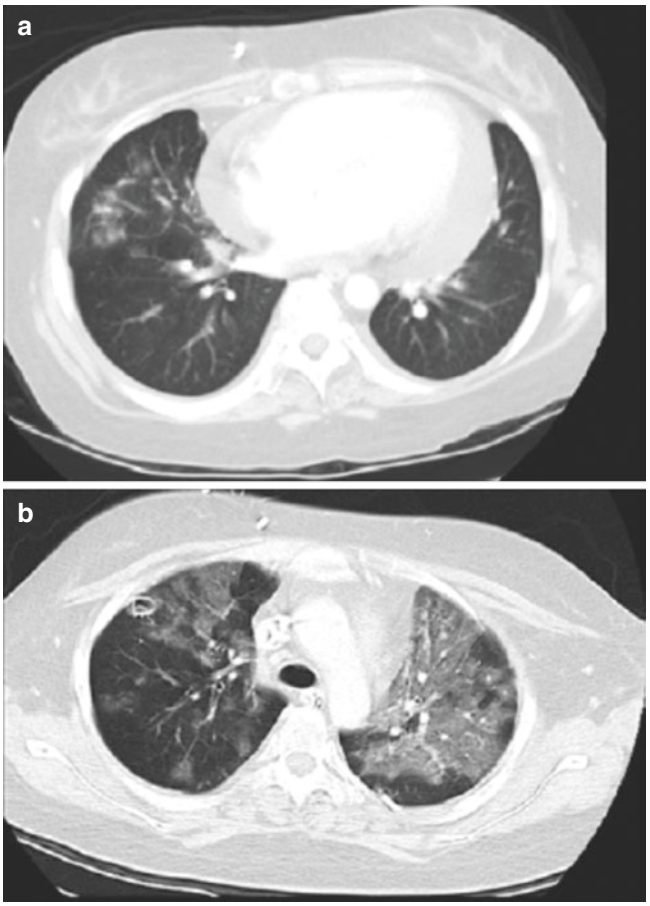

Fig. 13.9 A 17-year-old girl with aplastic anemia status-post bone marrow transplantation 6 months prior to admission who presented with chest pain. (**a**) Axial lung window CT image obtained on day 1 shows ill-defined nodular pattern that was initially interpreted as fungal infection. (**b**) On day 9, this developed into a widespread ground-glass pattern with septal lines. Biopsy was suggestive of pulmonary veno-occlusive disease characterized by fibrous obstruction of a septal vein and preseptal venules with pulmonary hemorrhage

used to evaluate the anatomy of the cardiac chambers and valvular function can also be used to evaluate the central pulmonary veins and the left atrium. In our institution, we use respiratory-triggered ECG-gated free breathing three-dimensional (3D) balanced SSFP pulse sequences that acquire near-isotropic volumetric data set that we then reformat in the various planes to define the pulmonary venous anatomy.

Postgadolinium MRA is also a useful technique. To obtain the best results, gadolinium-based contrast material is injected by hand or power-injected at a rate of 1–2 mL/s. Scans are obtained in the arterial and venous phases with multiple breath-holds or during quiet breathing using a non-ECG-gated 3D spoiled gradient recall echo imaging. After reviewing individual source images, multiplanar 2D reformats and 3D maximum-intensity-projection (MIP) or volume-rendered images are obtained to depict the pulmonary venous anatomy optimally.

Velocity-encoded phase contrast images perpendicular to the orientation of the vein are used to quantify the flow through the veins.

MDCT has the ability to demonstrate the vascular structures peripheral to the heart in the thorax exquisitely. 2D and 3D reconstructed CT images can define anomalous pulmonary venous structures with accuracy rates approaching 100%. The downsides of MDCT are the need for ionizing radiation and the requirement for iodinated contrast material, which may affect renal function. It is imperative that bolus timing is optimal to ensure a diagnostic study with good opacification of pulmonary venous structures. Image

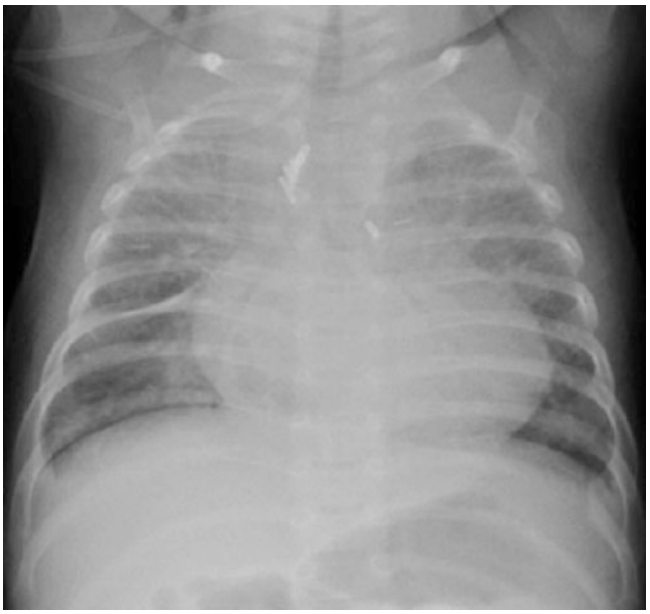

Fig. 13.10 An infant girl with pulmonary atresia, intact ventricular septum and right ventricular-dependent coronary circulation with left coronary stenosis, who presented 2 months after a modified Blalock Taussig shunt and PDA ligation. The frontal chest radiograph shows findings that are similar to cardiac failure, but the relative asymmetric vascularity and the patchy opacification of the lungs in the clinical context of prior surgery and congenital heart disease might suggest the presence of pulmonary vein stenosis. On further investigation with cardiac catheterization, the child was found to have left upper and lower lobe pulmonary vein stenosis

acquisition is optimized by using either bolus tracking or test injection depending on the age of the child. We prefer tracking of the injection bolus with low-dose monitoring scans in children with suspected pulmonary vein stenosis. A test bolus is typically not needed for non-gated CTA in children, although some authors have suggested test bolus may be helpful in evaluating cor triatriatum, central pulmonary vein hypoplasia, or stenosis. We reserve MDCT for imaging pulmonary venous structures in patients who are incompletely evaluated by echocardiography and who cannot undergo an MRI examination. Newer MDCT with ultrafast gantry rotation times, dual-source technology allowing acquisition of volume data, variable pitch (ability to increase pitch with rapid heart rates), and radiation dose modulation enable acquisition of CTA in young children with low radiation dose while avoiding sedation and breath-holding. This has increased the overall use of cardiac non-gated CTA in the last few years.

Thin section isotropic axial CT images are acquired and used to create multiplanar reformats and 3D volume-rendered images. Nonionic low-osmolality (or iso-osmolar) iodinated contrast material (<2.0 mL/kg up to a maximum of 100–150 mL maximum volume) is administered intravenously using a power injector at injection rates between 1 and 5 mL/s, depending on patient weight and size of the intravenous catheter. We prefer hand injection of contrast material in infants and small children with small caliber venous access.

In the evaluation of PAPVR, dual anomalous pulmonary venous drainage, and cor triatriatum in older patients, an initial test bolus may be used to optimize contrast opacification of the pulmonary venous system. For patients with suspected TAPVR as well as for small children, we image immediately after the injection of contrast material at our institution with visual triggering when contrast maximally opacifies the left ventricle. We do not recommend cardiac gating for the evaluation of pulmonary venous structures, although it may be useful if the patient is being specifically evaluated for cor triatriatum, central pulmonary vein hypoplasia, or stenosis.

Preoperative Evaluation of the Scimitar (Congenital Pulmonary Venolobar) Syndrome

Imaging studies form the mainstay of diagnosis of the Scimitar syndrome. A combination of chest radiography, echocardiography, CT, and/or MRI may be used in various combinations. On the plain radiograph, the characteristic appearance of the pulmonary vein descending along the right cardiac border resembles a Turkish sword or scimitar, thereby lending the name to the syndrome. Visualization of the vein may be difficult if it is small or obscured by the cardiac contour. The small hemithorax, bronchial anomalies, and pulmonary vein are delineated optimally on CT. The entrance of the anomalous vein into the inferior vena cava may be visible on echocardiography with Doppler. In the past decade, cine MR imaging and contrast-enhanced MRA has been used extensively in the evaluation of these patients as this allows optimal excellent visualization of pulmonary vasculature and also helps determine the hemodynamic significance of the anomalous pulmonary venous drainage [22].

Preoperative Evaluation of Pulmonary Vein Stenosis

Pulsed Doppler echocardiography is considered the first-line imaging tool in the evaluation of patients suspected of having congenital PVS (Fig. 13.11). Normal pulmonary venous flow into the atrium is laminar and triphasic. In cases of primary pulmonary vein stenosis, a high-velocity, continuous turbulent flow pattern is detected throughout systole and diastole, highest near the vein orifice. Diagnosis can be difficult and delayed in cases of total obstruction and when there is reduced flow due to pulmonary hypertension. Echocardiography is unable to assess the intrapulmonary venous stenosis due to its inherent inability to penetrate the aerated lung.

Therefore, there is a need for a noninvasive second-line test either to confirm echocardiographic and/or clinical

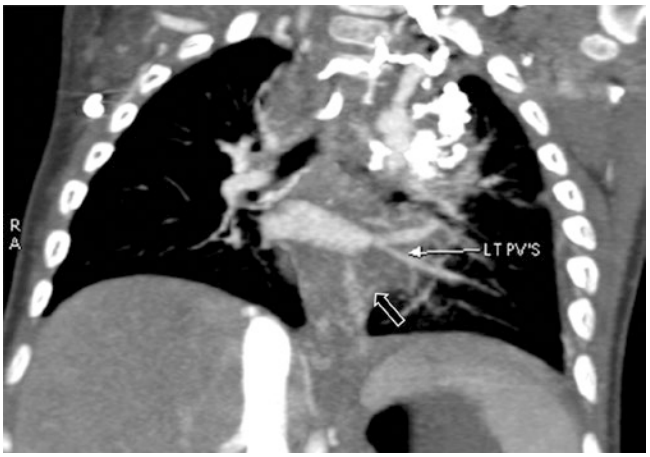

Fig. 13.11 A 10-month-old girl with a history of hypoplastic left heart syndrome. Status post stage I Norwood consisting of Stansel anastomosis, and bidirectional Glenn. Pulmonary vein stenosis treated with sutureless repair. Coronal enhanced CT image shows small caliber peripheral left upper lobe and left lower lobe pulmonary veins with completely atretic central segment. Diffuse mediastinal soft tissue induration with multiple serpiginous enhancing structures consistent with venous collateralization (arrow)

findings or define the exact anatomy. Although conventional angiography is still considered the gold standard for this purpose, MRI and MDCT can be used as noninvasive techniques.

MDCT has been described as a useful investigation in the diagnosis and evaluation of primary PVS in children in a few studies [23]. Diagnosing PVS early and obtaining accurate anatomical detail including the exact nature of the stenosis or atresia are invaluable in planning management.

MDCT angiography with multiplanar and 3D volume reformats allows detailed visualization of pulmonary venous drainage into the left atrium. Since MDCT examination can be typically completed within a few seconds in infants and children, it is possible to avoid intubating and anesthetizing the child for the procedure. Our own experience and the results of a few studies in the literature on this topic demonstrate that visualization of the pulmonary veins is possible even in young patients in most cases on MDCT angiography and optimal evaluation of PVS can be made in most cases. Postprocessing with 2D and 3D reformats aids in increasing the sensitivity and specificity of the exam. The recent study showed that the use of 3D CT images in the diagnosis of proximal PVS in children significantly improves accuracy, confidence level, added diagnostic value and interobserver agreement [24]. Therefore, the routine use of 3D CT images should be encouraged despite its increased interpretation time in the evaluation of PVS in children.

Conventional catheter angiography is currently reserved for infants and children in whom pulmonary pressure measurement is considered necessary or a percutaneous treatment is being considered. *Following* ALARA (As Low As Reasonably Achievable), we recommend low kilovoltage (80 kV in neonates and infants) and non-gated acquisitions with optimized settings to reduce the radiation dose in the pediatric population.

Magnetic resonance imaging can provide excellent tomographic and 3D views of the pulmonary veins with the use of contrast-enhanced multiphase MRA acquisition. It may show abnormalities of the flow patterns in the pulmonary veins and pulmonary arteries. But its use is limited by the relatively longer scan times, sensitivity to motion and arrhythmias, and the requirement of general anesthesia in young children.

The use of radionuclide studies to quantitate pulmonary flow allows fairly accurate determination of flow distribution between the lungs and must be considered as part of the preoperative workup in patients with PVS and also as part of the posttreatment follow-up.

Value of Imaging in Deciding Therapy

The value of cross-sectional imaging is especially important in cases where it is unclear from the clinical history and echocardiography findings whether the PVS is primary or secondary. For example, the presence of pulmonary changes of lung disease related to prematurity in a child with PVS suggests an acquired or secondary process. Similarly, the presence of diffuse intrapulmonary venous stenoses indicates a primary process. This differentiation between the primary and secondary type is important as the prognosis for the acquired type is considered better and the therapeutic approach is also modified accordingly.

Management of Congenital Pulmonary Venous Anomalies

Total and Partial Anomalous Pulmonary Venous Returns and Drainage

Medical Therapy

Infants and children with TAPVR with obstruction present immediately after birth with severe cyanosis and poor systemic perfusion and therefore need emergent treatment. Initial resuscitation measures instituted include sedation, assisted ventilation, high flow oxygen, prostaglandin infusion, and bicarbonate therapy. These are temporizing measures aimed at stabilizing the clinical condition of the patient and optimizing the preoperative state prior to surgical repair, which is currently the standard of care in this population. In neonates or young infants with unobstructed TAPVR, mild inotropic support, diuresis, and low-level oxygen therapy are instituted to treat right ventricular failure, hypoxia, and congestive heart failure. As the patients with PAPVR are most

commonly asymptomatic, treatment is initially required prior to surgical correction only in a small number of children who have arrhythmias or right heart failure.

Surgical Therapy

A number of techniques have been tried to surgically repair PAPVR and TAPVR. Surgical correction is aimed at creating unobstructed venous flow into the left-sided heart chambers. Associated anomalies like an ASD may be treated during the same procedure.

PAPVR is usually corrected surgically using patch repair of the anomalous vein to the atrium in most cases without complication. To correct supracardiac TAPVR, the vertical vein is ligated next to its connection to the systemic vein and the pulmonary venous confluence is identified. An incision is created in the pulmonary venous confluence and joined up with a similar incision in the posterior wall of left atrium extending into the atrial appendage. The aim is to create a large unobstructed anastomosis between the left atrium and the pulmonary venous confluence. The use of fine sutures decreases the potential for hyperplasia of the intimal lining, which can cause postrepair stenosis.

To correct cardiac TAPVR, the coronary sinus is unroofed by an incision between the coronary sinus and the foramen ovale, thus creating a large ASD. The pulmonary vein ostia are identified through the coronary sinus and its connection with the venous confluence. A patch is used to reconstruct the atrial septum. The end result of the procedure allows the pulmonary venous drainage to flow through the unroofed coronary sinus into the left atrium.

Treatment principles for infracardiac TAPVR are similar to that described for supracardiac TAPVR.

Mixed type of anomalous pulmonary venous drainage is corrected on an individual basis, depending on the exact nature and site of the abnormal venous connections. Surgical correction of mixed TAPVR depends on the exact anatomy and site of pulmonary venous connections. A combination of these procedures is required for the other types of TAPVR to successfully direct pulmonary venous blood to the left atrium.

The outcomes in the treatment of TAPVR are still poor, even in the hands of experienced surgeons, primarily due to the poor hemodynamic and metabolic state at presentation. Even in those patients who undergo a successful first procedure, a repeat surgical procedure may be required in up to 15%. Further, every repeat procedure carries an increasingly poor prognosis, and there is a high incidence of PVS in these patients following surgical repair.

The technique of *sutureless marsupialization* has been used to treat PVS that develops following surgical correction of anomalous pulmonary venous drainage. More recently, this technique is being tried to correct primary venous anomalies as well.

Pulmonary Vein Stenosis

The outcome of pediatric patients with PVS is relatively poor and prognostication in these cases must be guarded. In the absence of treatment, patients with stenosis of three or four pulmonary veins have progressive disease in the vast majority of cases and long-term survival is rare [25]. The terminal stage of illness in these patients is characterized by pulmonary hypertensive crises and may be complicated by concomitant infection or hemoptysis. Patients with only one or two pulmonary veins involved have a significantly more benign course. With the advances in cross-sectional imaging, there has been a recent increase in the early diagnoses of relatively asymptomatic children with milder forms of PVS. The natural history of the mild forms of PVS in these less symptomatic children needs to be studied in long-term studies.

The overall outcomes of both primary and secondary types of PVS have been similar, with similar techniques employed to treat both types [8, 26, 27]. Recurrence of PVS after repair of anomalous pulmonary venous return occurs in up to 10% of patients and this can prove to be a significant complication in patients with single-ventricle physiology [12]. Patients with stenosis of one or two veins and less marked stenosis have a better prognosis. When progressive PVS is unilateral, the patient may survive, even when there is no discernible flow to the affected lung on lung perfusion studies. Some patients need pneumonectomy to control hemoptysis.

The approaches to treating PVS can be broadly divided into three groups: (1) surgical repair, (2) catheter-based approaches (balloon dilatation or stenting), and (3) lung transplantation.

The currently accepted surgical technique employed in the surgical repair of PVS relies on minimizing trauma to the veins. The rationale behind this approach is that this may decrease the stimulus for recurrent growth of obstructive myofibroblastic tissue at the vein orifice. The technique is called *sutureless marsupialization*, wherein the pericardium around the pulmonary veins is attached to the left atrium and application of sutures is avoided along the cut edges of the pulmonary veins. This is now considered the best approach and early experience suggests that sutureless marsupialization may lead to better results compared to anastomosis following resection of stenotic segments and or patch insertion along the stenotic veins [28]. However, prognosis must be guarded, as even with the current advances in sutureless repair, up to 50% of patients may either need a second surgical procedure or die within 5 years of initial treatment [29].

Catheter-based approaches have been tried with limited success in patients with PVS [30]. Although high-pressure balloon dilatation appears to lead to an immediate angiographic response, recurrent stenosis occurs in the vast majority of patients. Cutting balloons have been found to be useful in cases with resistant stenoses. In our institution,

catheter angioplasty is often complementary to surgery. Further, catheter angioplasty can be potentially repeated a number of times. The outcome of stents has been universally poor with high occurrence of restenosis. Stent placement in a young child is technically challenging and even if stents are successfully deployed, subsequent surgical treatment approaches in these patients become limited. Intraoperative stent placement has been tried in a few patients and repeated stent dilation to relatively diameters >8 mm have resulted in some outcome improvement (Fig. 13.12) [31].

Lung transplantation is an option in patients with marked pulmonary hypertension and progressive PVS. Early studies have indicated favorable short-term results in patients with PVS undergoing bilateral sequential lung transplantations, but longer-term studies have not yet been carried out in this population [8, 32]. There is an ongoing search for agents that may help inhibit proliferation of myofibroblastic activity in the cases with progressive diffuse disease.

A recent study of drug therapies inhibiting tyrosine kinase pathways has shown promise in the treatment of young children with PVS as an adjunct to optimizing and maintaining pulmonary vein patency with surgical and transcatheter interventions. These agents (matinib mesylate and bevacizumab) targeted myofibroblast-like cell surface proteins (platelet-derived growth factor receptor (PDGFR)) and vascular endothelial growth factor receptor, respectively, in an effort to prevent or slow cell proliferation [33].

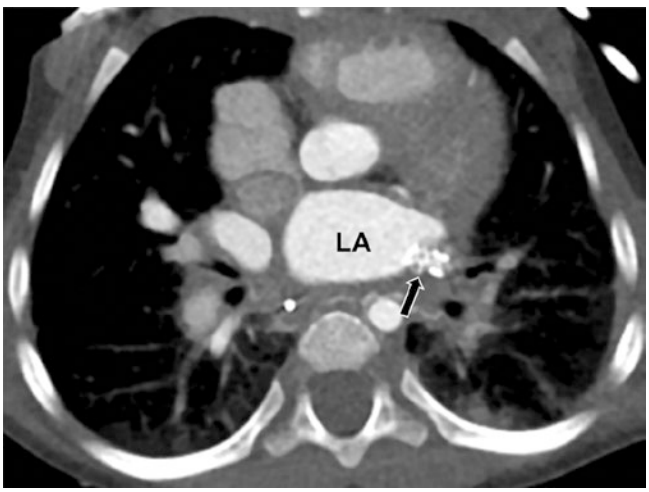

Fig. 13.12 A 2-month-old girl with pulmonary vein stenosis treated with stent placement. Axial enhanced CT image shows a metallic stent (arrow) in the proximal left lower pulmonary vein

Postoperative Imaging Evaluation of Congenital Pulmonary Venous Anomalies

As described above, the complications following surgical treatment of anomalous pulmonary venous connections and PVS are primarily due to the development of restenosis at the site of anastomosis. In a small number of patients with total anomalous pulmonary venous drainage, a diffuse stenotic process involving the entire length of the pulmonary veins including their intrapulmonary course may occur and may progress to almost complete vein occlusion. The prognosis in these cases, especially with bilateral involvement is poor. Transthoracic echocardiography is the first investigation in these patients. Presence of turbulence at the anastomotic site is the main diagnostic feature of restenosis. However, the echocardiogram may be limited in a number of cases (e.g., following an intracardiac patch baffle).

Both contrast-enhanced CTA and multiple phase acquisition contrast-enhanced MRA with multiplanar reconstructions and volume-rendered imaging are used for the postoperative evaluation of pediatric patients with anomalous pulmonary venous drainage and PVS. CT is particularly useful in cases where the echocardiogram is inconclusive, when MRI is either contraindicated or cannot be performed due to the need for sedation, and also in cases of diffuse restenosis to assess the intrapulmonary involvement and help assess the need for and to plan future diagnostic catheterization [34].

MRI may also be used to evaluate for restenosis following surgery and may be augmented by performing phase contrast imaging perpendicular to the plane of the vein just proximal to the veno-atrial junction [35]. Repaired veins usually show a greater diastolic flow component than normal veins, and often contain an abnormal downward deflection wave in the early systolic phase [36]. These findings are considered related to the decreased compliance of the left atrium due to either scar formation at the site of atrial incision or presence of patch graft material in the atrial wall.

As described in the previous section, radionuclide lung perfusion study allows a fairly accurate determination of flow distribution and helps determine the efficacy of treatment measures instituted. This recent study also showed that radionuclide lung perfusion study findings correlate well with angiographic findings in the detection of proximal PVS in pediatric patients [37]. Therefore, radionuclide lung perfusion study may have an important role in angiographically diagnosed PVS by noninvasively showing relative perfusion at the tissue level.

Conclusion

In this chapter, the embryology, epidemiology, anatomy, clinical presentation, preoperative imaging evaluation, management, and postoperative imaging evaluation of congenital pulmonary venous drainage disorders in the pediatric population are reviewed. Clear understanding of characteristic imaging findings of complex pulmonary venous drainage disorders has a great potential for early and accurate diagnosis and optimal pediatric patient management.

References

1. Neill CA. Development of the pulmonary veins; with reference to the embryology of anomalies of pulmonary venous return. Pediatrics. 1956;18(6):880–7.
2. Healey JE Jr. An anatomic survey of anomalous pulmonary veins: their clinical significance. J Thorac Surg. 1952;23(5):433–44.
3. Streeter GL. Developmental horizons in human embryos; a review of the histogenesis of cartilage and bone. Contrib Embryol. 1949;33(213–221):149–68.
4. Webb S, Kanani M, Anderson RH, et al. Development of the human pulmonary vein and its incorporation in the morphologically left atrium. Cardiol Young. 2001;11(6):632–42.
5. Reller MD, Strickland MJ, Riehle-Colarusso T, Mahle WT, Correa A. Prevalence of congenital heart defects in metropolitan Atlanta, 1998-2005. J Pediatr. 2008;153(6):807–13.
6. Hoffman JI, Kaplan S. The incidence of congenital heart disease. J Am Coll Cardiol. 2002;39(12):1890–900.
7. Drossner DM, Kim DW, Maher KO, et al. Pulmonary vein stenosis: prematurity and associated conditions. Pediatrics. 2008;122(3):e656–61.
8. Latson LA, Prieto LR. Congenital and acquired pulmonary vein stenosis. Circulation. 2007;115(1):103–8.
9. Hancock Friesen CL, Zurakowski D, Thiagarajan RR, Forbess JM, del Nido PJ, Mayer JE, Jonas RA. Total anomalous pulmonary venous connection: an analysis of current management strategies in a single institution. Ann Thorac Surg. 2005;79(2):596–606.
10. Saad EB, Marrouche NF, Saad CP, et al. Pulmonary vein stenosis after catheter ablation of atrial fibrillation: emergence of a new clinical syndrome. Ann Intern Med. 2003;138(8):634–8.
11. Sadr IM, Tan PE, Kieran MW, et al. Mechanism of pulmonary vein stenosis in infants with normally connected veins. Am J Cardiol. 2000;86(5):577–9.. A10
12. Michielon G, Di Donato RM, Pasquini L, et al. Total anomalous pulmonary venous connection: long-term appraisal with evolving technical solutions. Eur J Cardiothorac Surg. 2002;22(2):184–91.
13. Hancock Friesen CL, Zurakowski D, Thiagarajan RR, et al. Total anomalous pulmonary venous connection: an analysis of current management strategies in a single institution. Ann Thorac Surg. 2005;79(2):596–606; discussion 596–606.
14. van Son JA, Hambsch J, Kinzel P, et al. Urgency of operation in infracardiac total anomalous pulmonary venous connection. Ann Thorac Surg. 2000;70(1):128–30.
15. Ussia G, Marasini M, Zannini L, et al. Acquired pulmonary vein obstruction after open-heart surgery. Eur J Cardiothorac Surg. 2002;22(3):465–7.
16. Redington AN, Raine J, Shinebourne EA, et al. Tetralogy of Fallot with anomalous pulmonary venous connections: a rare but clinically important association. Br Heart J. 1990;64(5):325–8.
17. Foerster SR, Gauvreau K, McElhinney DB, et al. Importance of totally anomalous pulmonary venous connection and postoperative pulmonary vein stenosis in outcomes of heterotaxy syndrome. Pediatr Cardiol. 2008;29(3):536–44.
18. Berrocal T, Madrid C, Novo S, et al. Congenital anomalies of the tracheobronchial tree, lung, and mediastinum: embryology, radiology, and pathology. Radiographics. 2004;24(1):e17.
19. Hubbard AM, Adzick NS, Crombleholme TM, et al. Congenital chest lesions: diagnosis and characterization with prenatal MR imaging. Radiology. 1999;212(1):43–8.
20. Husain AN, Hessel RG. Neonatal pulmonary hypoplasia: an autopsy study of 25 cases. Pediatr Pathol. 1993;13(4):475–84.
21. Montani D, Price LC, Dormuller P, et al. Pulmonary veno-occlusive disease. Eur Respir J. 2009;33(1):189–200.
22. Henk CB, Prokesch R, Grampp S, et al. Scimitar syndrome: MR assessment of hemodynamic significance. J Comput Assist Tomogr. 1997;21(4):628–30.
23. Ou P, Marini D, Celermajer DS, et al. Non-invasive assessment of congenital pulmonary vein stenosis in children using cardiac-non-gated CT with 64-slice technology. Eur J Radiol. 2009;70(3):595–9.
24. Lee EY, Jenkins KJ, Muneeb M, Marshall AC, Tracy DA, Zurakowski D, Boiselle PM. Proximal pulmonary vein stenosis detection in pediatric patients: value of multiplanar and 3D VR imaging evaluation. Pediatr Radiol. 2013;43(8):929–36.
25. Breinholt JP, Hawkins JA, Minich LA, et al. Pulmonary vein stenosis with normal connection: associated cardiac abnormalities and variable outcome. Ann Thorac Surg. 1999;68(1):164–8.
26. Devaney EJ, Chang AC, Ohye RG, et al. Management of congenital and acquired pulmonary vein stenosis. Ann Thorac Surg. 2006;81(3):992–5; discussion 995–6.
27. van Son JA, Danielson GK, Puga FJ, et al. Repair of congenital and acquired pulmonary vein stenosis. Ann Thorac Surg. 1995;60(1):144–50.
28. Lacour-Gayet F, Rey C, Planche C. Pulmonary vein stenosis. Description of a sutureless surgical procedure using the pericardium in situ. Arch Mal Coeur Vaiss. 1996;89(5):633–6.
29. Yun TJ, Coles JG, Konstantinov IE, et al. Conventional and sutureless techniques for management of the pulmonary veins: evolution of indications from postrepair pulmonary vein stenosis to primary pulmonary vein anomalies. J Thorac Cardiovasc Surg. 2005;129(1):167–74.
30. Lock JE, Bass JL, Castaneda-Zuniga W, et al. Dilation angioplasty of congenital or operative narrowings of venous channels. Circulation. 1984;70(3):457–64.
31. Ungerleider RM, Johnston TA, O'Laughlin MP, et al. Intraoperative stents to rehabilitate severely stenotic pulmonary vessels. Ann Thorac Surg. 2001;71(2):476–81.
32. Mendeloff EN, Spray TL, Huddleston CB, et al. Lung transplantation for congenital pulmonary vein stenosis. Ann Thorac Surg. 1995;60(4):903–6; discussion 907.
33. Callahan R, Kieran MW, Baird CW, Colan SD, Gauvreau K, Ireland CM, Marshall AC, Sena LM, Vargas SO, Jenkins KJ. Adjunct targeted biologic inhibition agents to treat aggressive multivessel intraluminal pediatric pulmonary vein stenosis. J. Pediatr. 2018;198:29–35.e5.
34. Kasahara H, Aeba R, Tanami Y, Yozu R. Multislice computed tomography is useful for evaluating partial anomalous pulmonary venous connection. J Cardiothorac Surg. 2010;5:40.
35. Grosse-Wortmann L, Al-Otay A, Goo HW, et al. Anatomical and functional evaluation of pulmonary veins in children by magnetic resonance imaging. J Am Coll Cardiol. 2007;49(9):993–1002.
36. Valsangiacomo ER, Barrea C, Macgowan CK, et al. Phase-contrast MR assessment of pulmonary venous blood flow in children with surgically repaired pulmonary veins. Pediatr Radiol. 2003;33(9):607–13.
37. Drubach LA, Jenkins KJ, Stamoulis C, Palmer EL 3rd, Lee EY. Evaluation of primary pulmonary vein stenosis in children: comparison of radionuclide perfusion lung scan and angiography. AJR Am J Roentgenol. 2015;205(4):873–7.

Respiratory System Lymphatic Disorders

14

Annabelle Quizon, Edward Y. Lee, and Katie Krone

Lymphatic Disorders of the Respiratory System

Disorders of the respiratory lymphatic system encompass a variety of defects affecting the lymphatic vessels that are developmental and functional in nature [1–5]. They may lead to chronic and serious respiratory disease and manifest with a range of clinical presentations in the pediatric population. Congenital errors in lymphatic development are rare and their diagnoses and management are often difficult.

Review of Embryonic Development of the Lymphatic System

The lymphatic system begins to develop by the end of the sixth embryonic week. By the eighth week, six primary lymph sacs emerge as buds from the adjacent developing veins. The lymphatic vessels develop in a manner similar to that of the blood vessels and join the primitive lymph sacs. By the ninth week of gestation, there are two large lymphatic vessels (the right and left thoracic ducts) that subsequently merge to form the thoracic duct. Failure of the many connections to form between the embryonic lymphatic channels results in congenital malformations of the lymphatic system, alteration in lymphatic drainage, and development of lymphatic disease [6].

A. Quizon
Department of Respiratory Medicine, University of California San Diego- Rady Children's Hospital, San Diego, CA, USA

E. Y. Lee (✉)
Department of Radiology, Boston Children's Hospital and Harvard Medical School, Boston, MA, USA
e-mail: Edward.Lee@childrens.harvard.edu

K. Krone
Division of Pulmonary Medicine, Boston Children's Hospital, Harvard Medical School, Boston, MA, USA

The role of genetics in lymphatic anomalies is complex and beyond the scope of this chapter. Suffice to say, over 20 mutations have been reported thus far that encode proteins acting around vascular endothelial growth factor (VEGFR-3) signaling and also involving tyrosine kinase receptors [7]. These mutations account for the incidence mostly of the inherited forms.

Classification

In 1982, Mulliken and Glowacki proposed a classification schema for vascular anomalies as tumors and malformations, in infants and children, based on cellular characteristics [1–5, 8, 9]. Later, Faul et al. [10] modified an earlier classification by Hillard et al. [11] to describe lymphangiomas, lymphangiomatosis, lymphangiectasis, and lymphatic dysplasia syndrome. Borne out of evolving knowledge of vascular anomalies and response to treatment, this classification system was revised in 2014 by the International Society for the Study of Vascular Anomalies (ISSVA). While the original divisions remain, vascular malformations are further subdivided into simple malformations designated by the vascular element involved (capillary, arterial, venous, lymphatic) or combined elements, such as capillary-lymphatic-venous malformations [12, 13]. Lymphatic malformations (LM) comprise a heterogeneous group of entities, including cystic lymphatic anomalies, disordered lymphangiogenesis affecting bones (Gorham-Stout syndrome), and primary lymphedema, among others. For purposes of this chapter, the classification for vascular anomalies as they pertain to lymphatic malformations has been excerpted from the ISSVA Classification (Table 14.1).

Clinical Presentation

Common Lymphatic Malformations

Common LM, previously called lymphangiomas, occur in lymphatic-dense areas, with the majority affecting the head

R. H. Cleveland, E. Y. Lee (eds.), *Imaging in Pediatric Pulmonology*, https://doi.org/10.1007/978-3-030-23979-4_14

Table 14.1 ISSVA classification for vascular anomalies

Lymphatic malformations (LM)
Common (cystic) LM
Macrocystic LM
Microcystic LM
Mixed cystic LM
Generalized lymphatic anomaly (GLA)
LM in Gorham-Stout disease
Channel type LM
Primary lymphedema
Nonne-Milroy syndrome
Primary hereditary lymphedema
Lymphedema-distichiasis
Hypotrichosis-lymphedema-telangiectasia
Primary lymphedema with myelodysplasia
Primary generalized lymphatic anomaly (Hennekam lymphangiectasia-lymphedema syndrome)
Microcephaly with or without chorioretinopathy, lymphedema, or mental retardation syndrome
Lymphedema-choanal atresia

and neck region, as well as the axilla, mediastinum, and groin [1, 2, 14, 15]. There exist three morphologic types of common (cystic) LM: macrocystic (historically called cystic hygromas), microcystic (formerly termed lymphangioma circumscriptum) and combined. Macrocystic lesions are often large multilocular masses located below the mylohyoid muscle, distinguishable as fluid-filled collections involving the anterior and posterior cervical triangles [16]. Microcystic lesions appear as noncompressible masses generally located above the mylohyoid muscle and are often more infiltrative [17]. Histologically, cystic LM are composed of vascular spaces filled with eosinophilic, protein-rich fluid with walls of variable thickness and composed of abnormally formed smooth muscle. Hemorrhage within a cystic lesion is not uncommon.

Most common LM are evident within the first 2 years of life and present as swelling in the head, neck, or axilla. Approximately, 10% extend into the mediastinum and are equally distributed into the anterior, middle, and posterior compartments [18]. Intrapulmonary LM are rare [19, 20]. Thoracic LM are usually asymptomatic. When symptoms develop, they reflect a mass effect on vital structures and depending on the affected organ, manifest as cough, dyspnea, stridor, hemoptysis, Horner's syndrome, dysphagia, superior vena cava syndrome, constrictive pericarditis, phrenic nerve palsy, or of symptoms related to secondary infection of the cystic LM [21–25]. Chylous pleural and pericardial effusions may develop [21].

Typical LM cause no serious threat of morbidity or death. Large cystic LM may be diagnosed on prenatal ultrasound or MRI and pose potential morbidity in terms of airway obstruction. All cases of cervical cystic LM should have chest radiograph performed, at a minimum, in addition to ultrasound or MRI, to further define mediastinal extension. Whereas hemangiomas involute with time, LM generally increase in proportion to the size of the patient and may fluctuate in response to infections, inflammation, and intralesional bleeding. A scoring system, the Cologne Disease Score, has been used to predict outcomes [26].

Generalized Lymphatic Anomaly

Generalized lymphatic anomaly (GLA) is characterized by multisystem LM [10]. This disease entity, previously referred to as lymphangiomatosis, has now been renamed GLA in the ISSVA updated classification [12]. This condition is associated with diffuse proliferation of lymphatics with a particular pattern of visceral involvement and progressive course. It is frequently associated with other lymphatic abnormalities and involves multiple organs with a predilection for thoracic and neck involvement. Within the thorax, GLA may involve the lungs without extrathoracic lymphatic abnormalities, as in diffuse pulmonary lymphangiomatosis, as well as have a tendency to concomitantly involve the mediastinum, heart, chest wall, and thoracic duct [27–29].

GLA may present from birth to adulthood and most frequently presents in late childhood. Chylous effusions are common and chylopericardium and chylous ascites may occur [30, 31]. Affected pediatric patients may present with hemoptysis, wheezing, protein losing enteropathy, peripheral lymphedema, hemihypertrophy, lymphopenia, and disseminated intravascular coagulation [32]. Such nonspecific symptoms and the rarity of GLA may delay diagnosis. A majority have bony involvement, in contrast to Gorham-Stout disease as discussed briefly and separately, which is currently classified as a distinct entity and defined by progressive osteolysis with extensive cortical invasion [33]. In general, prognosis is poor and primarily determined by the progression of pulmonary dysfunction; neurological deficits have also been reported from involvement of the cervical vertebrae and impact on prognosis [31].

Lymphatic Malformation in Gorham-Stout Disease

Gorham-Stout disease is a rare skeletal condition characterized by the uncontrolled proliferation of distended, thin-walled vascular or lymphatic channels within bone which leads to resorption and replacement of bone with angiomas and/or fibrosis [34, 35]. It has also been called Gorham vanishing bone disease and phantom bone disease. Elevated plasma levels of interleukin-6 (IL-6) and VEGF have been detected in affected patients and speculated to contribute to osteolysis [36]. Disordered lymphagiogenesis as characteristic of the disease has been described [37].

While patients as young as 1 month have been reported, affected patients are generally younger than 40 years of age [38, 39]. The most typical presentation is osteolysis of a single bone or the bones connected by a shared joint, such as the shoulder, which is one of the most commonly involved areas along with the skull and the pelvic girdle. Spontaneous fractures are common and may be the first sign of the disease.

Symptoms of the disease vary depending on the bone involved. There may be acute onset of localized pain and swelling and over time, weakness and deformity of the affected area. Difficulty breathing and chest pain may occur if the disease is present in the ribs, scapula, or thoracic vertebrae. Extension of lesions into the chest may lead to development of chylous pleural and pericardial effusions [40].

Channel Type Lymphatic Malformation

Lesions are designated according to the predominant channel type as capillary malformation (CM), LM, venous malformation (VM), arterio-venous malformation (AVM), and arterio-venous fistula (AVF). Discussion of this category is beyond the scope of the chapter.

Primary Lymphedema

Primary lymphedema is the most common lymphatic anomaly in which developmental defects affecting maturation and function of the lymphatic system result in abnormal accumulation of interstitial fluid. This term includes primary hereditary lymphedema as well as associations with syndromic disorders, such as Turner syndrome, yellow nail syndrome, and others [41, 42]. Nonne-Milroy syndrome is a familial form of congenital lymphedema in which mutations in VEGFR-3 have been implicated in causing lymphatic hypoplasia; over 20 genes have been identified to date and there exists significant genetic heterogeneity [7]. Sporadic cases are more common than familial forms.

Primary lymphedema usually affects the lower extremities and rarely involves the arms, genitalia, or face [43–45]. Historically, primary lymphedema has been divided into three categories based on age of onset: (1) congenital lymphedema, present within the first 2 years of life, (2) lymphedema praecox, the most common subtype has a peripubertal onset and female predominance, and (3) lymphedema tarda, adult-onset [46]. Recent efforts have focused on deriving new classification systems for primary lymphedema that encompass the variability in phenotype, inheritance, and genetic defects to inform diagnosis, prognosis, and treatment decisions [47–49]. As there are many secondary causes of lymphedema and conditions that may mimic lymphedema, a thorough history and physical examination are paramount. Treatment focuses on minimizing risk of complications, such as recurrent lymphangitis/cellulitis, impaired limb function, and physical and psychosocial disability. Mortality from longstanding lymphedema may be attributed to life-threatening infection and malignancy, specifically the development of angiosarcoma, in rare cases [50].

Diagnosis

The diagnosis of lymphatic disorders is based primarily on the suggestive history and findings on physical examination. Prenatal detection of LM can be achieved with ultrasound [1–5, 51, 52]. Fetal MRI may improve diagnostic characterization and impact perinatal decisions, including termination of pregnancy [53]. Noninvasive imaging using Doppler ultrasound, computed tomography (CT), and magnetic resonance imaging (MRI) are critical in establishing the diagnosis, evaluating extent of malformation and planning appropriate treatment in infants and older children [1–5]. Conventional radiography such as chest radiographs play a limited role in diagnosis but may provide useful information about bone and joint involvement; pulmonary findings may yield diffuse reticular opacifications, soft tissue mass, and effusions. Ultrasound is not as informative as MRI but does not require sedation; it can differentiate between macrocystic and microcystic lesions and document intralesional bleeding [54]. MRI (MR-lymphangiography) overcomes technical limitations of traditional contrast lymphangiography in infants and small children [1–5]. Lymphedema can be diagnosed by lymphoscintigraphy.

Histologic confirmation is rarely necessary; moreover, histopathology is relatively nonspecific. Biopsy may be indicated if malignancy is suspected and if imaging is equivocal. In specific cases presenting with chylothorax, there is a risk of ongoing chylous leak at the time of lung biopsy from refractory leakage of lymph fluid from the incision site, such that there are no definitive criteria as to when this procedure should be performed [55, 56].

Imaging Evaluation

Plain chest radiographs may show bilateral pulmonary hyperinflation and a reticulonodular pattern throughout the lungs (Fig. 14.1a) and occasional fluid-filled cystic areas representing aerated distal bronchi or alveolar ducts as in pulmonary lymphangiectasia. In generalized LM, chest radiography may reveal an effusion and also shows reticular nodular shadowing throughout both lungs. The ribs, cervical spine, and humerus, when involved, show multiple lytic areas. Chest radiographs also confirm pleural effusions when present in lymphatic disorders.

Conventional oil-contrast lymphography has been the mainstay for lymphatic imaging; however, the emergence of CT and MRI has superseded the use of lymphography [1–5]. Improvements in direct lymphatic studies have enabled high-resolution imaging of peripheral lymphatic vessels and studies on lymphatic flow dynamics with lymphangioscintigraphy.

Lymphangioscintigraphy has replaced the conventional oil-contrast lymphography as standard of reference [57]. It allows high-resolution imaging of peripheral lymphatic vessels and provides insight into lymphatic flow dynamics. It is useful in patients with known or suspected lymphatic circulatory disorders in terms of (1) confirming the diagnosis and delineating the pathogenesis and evolution of lymphedema, (2) helping evaluate lymphatic truncal anatomy and radiotracer transport, (3) useful in evaluating the efficacy of

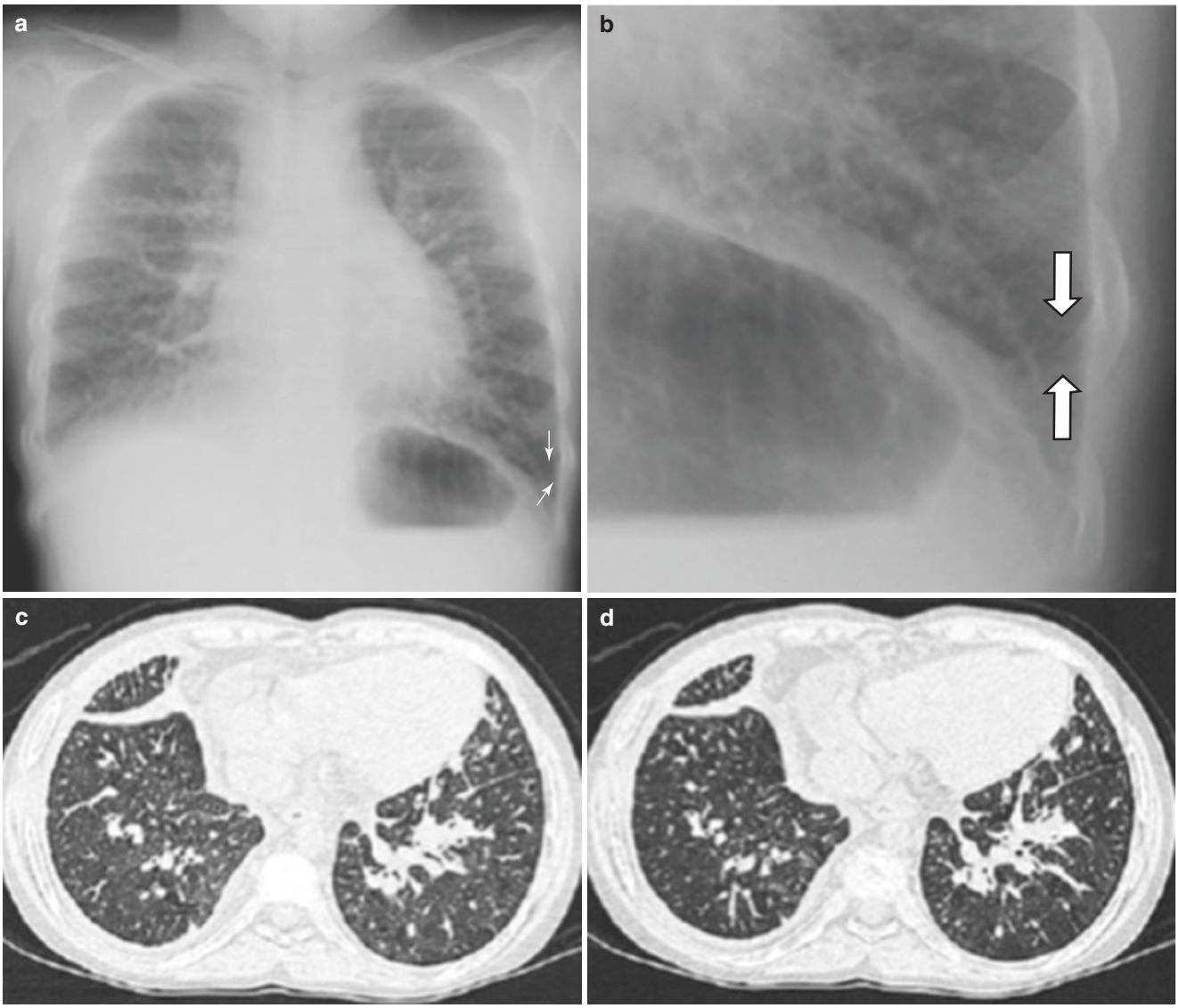

Fig. 14.1 17-year-old girl with Noonan's syndrome and pulmonary lymphangiectasis. (a) Frontal chest radiograph shows a diffuse coarse interstitial process and Kerley b lines (subpleural intralobular thickening) (*arrows*). There is a small right pleural effusion. As is usual for pulmonary lymphatic malformation, these findings are nonspecific. (**b**) Coned frontal chest radiograph of the costopherenic sulcus from fig a, more clearly demonstrates the Kerly b lines. (**c**, **d**) Axial lung window CT images show nonspecific findings with variable indicators of interstitial lung disease, in this case, subpleural septal thickening and a mild mosaic profusion pattern. There is bronchial wall thickening and a right pleural effusion. There is incidental bibasilar dependent minor atelectasis

various treatment options designed to facilitate lymph flow or reduce lymph formation. It is noninvasive in that it only requires intradermal injection of tracer (usually Tc-99 m albumin) into web space of the foot or hand. It is also repeatable and does not adversely affect lymphatic vascular endothelium. Given the limited treatment options especially for lymphedema, lymphatic imaging has not been utilized routinely and reliance on clinical history and physical examination has been emphasized.

CT and MRI have been used for examining lymph nodes for size rather than architecture [1–5]. It has been postulated that CT may show dilated subcutaneous lymphatics, although this is rarely if ever the case. Like CT, MRI may theoretically show pathologic dermal lymphatic vessels without added contrast material as well as more proximal lymph nodes and obstructing masses; it also allows visualization of the retroperitoneal ectatic lymphatic trunks and allows access for lymphatic truncal obliteration in the management of LM.

Specific Diagnostic Modalities

For common lymphatic malformations, plain radiographs (Fig. 14.2a), ultrasound (Fig. 14.2b), *CT* (Fig. 14.3), and *MRI* (Fig. 14.4) have been used to determine the number and extent of lesions. For these lesions, accurate anatomic

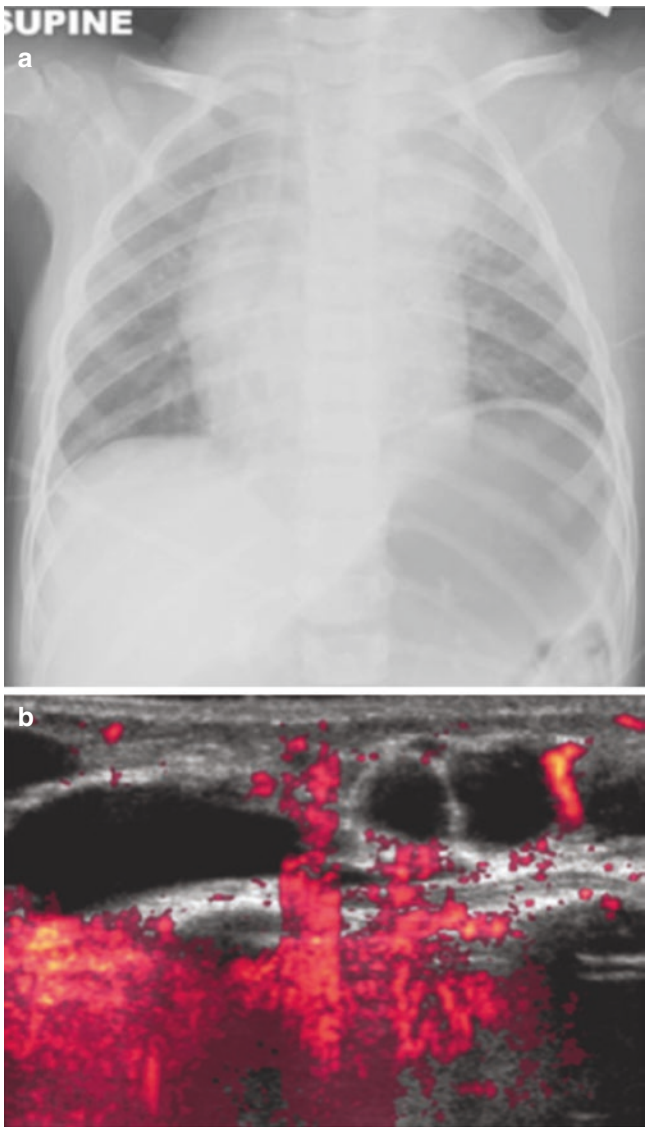

Fig. 14.2 *2-year-old boy who presented with shortness of breath.* (**a**) Frontal chest radiograph shows a fullness of the left aspect of the neck with a soft tissue mass in the left upper mediastinum with left apical pleural thickening. The constellation of findings is suggestive of a lymphatic malformation. (**b**) Ultrasound of the neck mass reveals a multicystic mass with no flow within the cysts, consistent with the suspected lymphatic malformation

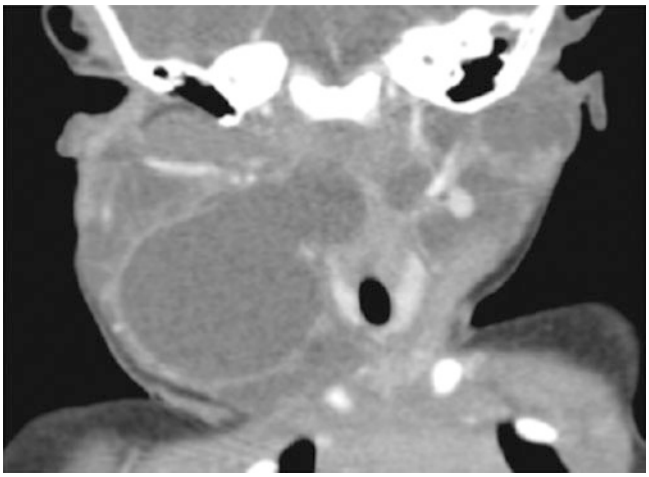

Fig. 14.3 3-month-old girl who presented with palpable bilateral neck masses, right side greater than left side. Coronal enhanced reformatted CT image shows bilateral lymphatic malformation of the neck. The walls of the cystic spaces enhance with contrast while the centers (i.e., cystic portions) do not

localization is important because the diagnosis is made postoperatively by means of histopathologic examination of the resected tissue. LM may be demonstrated by ultrasound with the typical pattern of multiple complex septations in a fluid-filled mass [1–5, 58]. CT shows the anatomical distribution and dimensions of the mass and their relationship to other organs. Most common LM appear as cystic masses of low attenuation value with or without septations; some of the septae show enhancement after a bolus injection of contrast material [59]. The advantages of MRI include more conclusive demonstration of cystic components, better demonstration of invasion of adjacent structures, and improved surgical planning with coronal or sagittal imaging planes [1–5, 60, 61].

In pulmonary LM, chest radiographs may show marked hyperinflation with interstitial opacifications that may be localized or diffuse [62] (Fig. 14.1a). Unilateral or bilateral pleural effusions may also be found. MRI may show cystic lesions and abnormal lymphatic vessels. High-resolution CT may demonstrate extensive bilateral septal and peribronchovascular interstitial thickening, areas of ground-glass attenuation and bilateral pleural effusions [63] (Fig. 14.1b). Lymphangiography shows abnormally dilated lymphatics with obstructive changes and collateral channels in the retroperitoneal, mediastinal, and cervical lymphatic system [64]. In generalized LM, chest radiography confirms pleural effusion and also shows reticular nodular opacity throughout both lungs [31]. The ribs, cervical spine, and humerus, when involved, may show multiple lytic areas. The combination of lytic bone lesions and chylothorax is an important diagnostic clue; diagnosis is sometimes made by bone biopsy. CT and MRI demonstrate generalized cystic lesions in parenchymal organs, lytic bone lesions, and diffuse thickening of pulmonary interstitium and mesenteries [65]. Specifically, with regard to chest CT findings, the combination of septal thickening (presumably related to dilated lymph vessels or veins in the interlobular septa of the lung) and pleural effusion or diffuse mediastinal infiltration strongly suggests LM. Moreover, ground-glass opacities are also demonstrated, and due to thickening of vascular structures within the alveolar interstitium [66]. Lymphangiography shows multiple lesions of the thoracic duct, dilated lymphatic channels, and lymphangiomas

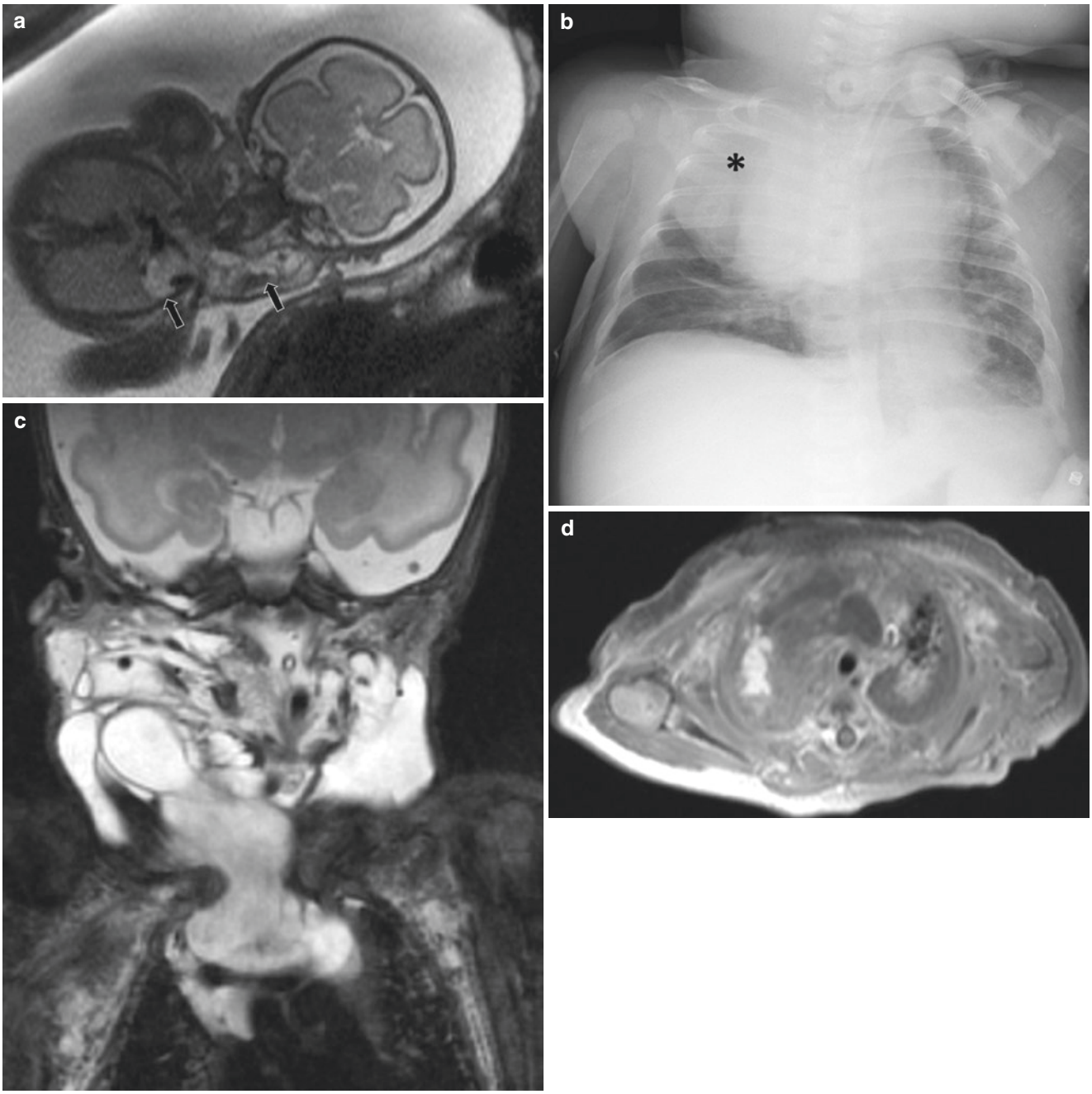

Fig. 14.4 4-week-old girl who presented with a palpable right sided neck mass on physical examination and abnormal prenatal MRI. (**a**) Prenatal MR image shows a large lymphatic malformation (arrows) of the neck and right chest. (**b**) Frontal chest radiograph demonstrates an opacity (asterisk) representing underlying intrathoracic portion of the lymphatic malformation. (**c**) Coronal T2-weighted MR image shows the lymphatic malformation involving the neck and intrathoracic components with multiple internal septations. (**d**) Axial T1-weighted and fat-suppressed MR image after administration of contrast shows areas of higher signal intensity of some cysts indicating blood within the cysts. The cyst walls enhance with contrast. The lymph containing cysts are of low signal intensity

throughout the bones and lungs. Lymphangioscintigraphy helps delineate lymphatic flow and relation between normal and abnormal lymphatics [67]. Lung biopsy demonstrates anastomosing endothelial lined spaces along pulmonary lymphatic routes accompanied by asymmetrically spaced bundles of spindle cells [21].

Management

Management of LM is challenging given their potential for rapid growth, disfigurement and functional impairment, intralesional bleeding and infection, and encroachment on vital structures such as the airway; they rarely resolve spon-

taneously and can recur post-treatment. A majority of the lesions occur in the head and neck region.

Aside from surgical resection, current therapeutic options include sclerotherapy, radiofrequency ablation, and laser therapy; newer modalities include use of drugs such as sildenafil, propranolol, and sirolimus, as well as vascularized lymph node transfer [68]. Treatment of LM continues to expand in light of biological and genetic discoveries. Treatment regimens are usually multimodal and should be individualized; selection of treatment modalities is dependent as well on available technology and expertise of specialists involved in the care and follow up of the patient.

Small or asymptomatic LM may be observed [54]. Prophylactic antibiotics are recommended when intralesional bleeding occurs due to the risk of secondary infection and when infected, intravenous antibiotics are often required. Lymphedema is managed with compression garments and pneumatic compression.

First line management of large or problematic LM consists of sclerotherapy that involves aspiration of the cysts followed by injection of an inflammatory substance that results in scarring of the cyst walls, thereby shrinking the lesion. Sclerotherapy is considered to have superior efficacy and a lower complication rate compared to resection [69]. It is the preferred treatment for macrocystic/combined lesions. Sclerosing agents used to treat LM include doxycycline, sodium tetradecyl sulfate (STS), ethanol, bleomycin, and OK-432 (killed group *Streptococcus pyogenes*) [70–72]. The most common complication of sclerotherapy is skin ulceration, which is managed with wound care [73]. LM may expand over time and may recur such that repeat sclerotherapy may be warranted; problematic recurrences will further warrant consideration of resection [74].

Surgical management or resection is recommended for symptomatic lesions that are associated with pain and significant deformity, or when encroaching on vital structures such as lesions that obstruct the airway, impede vision, or threaten the facial nerve. Green et al. further stated that resection is reserved for (1) small, well-localized LM (microcystic or macrocystic) that may be completely excised for cure, (2) symptomatic microcystic LM, and (3) symptomatic macrocystic/combined LM that no longer can be managed with sclerotherapy because all lesions have been treated [54].

Radiofrequency ablation also known as Coblation has been found to be a safe, viable alternative to existing techniques in the treatment of microcystic LM involving the upper aerodigestive tract; it achieves effective debulking of microcysts and avoids morbidities such as excessive bleeding and scarring [75–77]. Likewise, carbon dioxide laser has been described to be a safe and efficacious option for the treatment of microcystic LM, particularly if large and not amenable to surgical resection; adverse events were infrequent and included mild scarring and dyspigmentation [78, 79].

Medical therapies are emerging as part of multimodal management of LM. Sildenafil, a phosphodiesterase-5 inhibitor, given over several weeks, has been found to result in marked regression of LM in children with no significant adverse effects from treatment. The proposed mechanism for the therapeutic effect of sildenafil involves relaxation of smooth muscle followed by cystic decompression; it may also normalize lymphatic endothelial dysfunction [80, 81]. Sirolimus, also known as rapamycin, has been used for children and young adults with complicated vascular anomalies with significant lymphatic components refractory to other treatments. The effect of sirolimus on these lymphatic based lesions has been postulated to involve mammalian target of rapamycin (mTOR) inhibition. mTOR acts as master switch of numerous cellular processes including angiogenesis and cell growth; sirolimus thereby can inhibit lymphangiogenesis. It is also given over several months and proven to be safe with tolerable side effects [82–84]. There has been limited success associated with other immunotherapies, such as interferon, as well as traditional chemotherapy agents, in the management of some LM such as GLA and Gorham-Stout disease [85].

Finally, as regards other evolving modalities, human and animal studies report clear benefits of microsurgical procedures such as vascularized lymph node transfer for the treatment of lymphedema [86]. We mentioned the role of genetics in lymphatic anomalies. As research emerges around defective signaling pathways, new molecular targets will likely be discovered as alternatives to treat lymphatic diseases.

References

1. Lee EY, editor. Pediatric radiology: practical imaging evaluation of infants and children. Philadelphia: Wolters Kluwer; 2018. p. 609–39.
2. Lee EY, editor. Pediatric thoracic imaging. Philadelphia: Wolters Kluwer; 2018. p. 150–219.
3. White CL, Olivieri B, Restrepo R, McKeon B, Karakas SP, Lee EY. Low-flow vascular malformation pitfalls: from clinical examination to practical imaging evaluation – part 1, lymphatic malformation mimickers. AJR Am J Roentgenol. 2016;206(5):940–51.
4. Kollipara R, Dinneen L, Rentas KE, et al. Vascular anomalies in pediatric patients; updated classification, imaging, and therapy. Radiol Clin N Am. 2013;51(4):659–72.
5. Lowe LH, Marchant TC, Rivard DC, Scherbel AJ. Vascular malformation: classification and terminology the radiologist needs to know. Semin Roentgenol. 2012;47(2):106–17.
6. Semo J, Nicenboim J, Yaniv K. Development of the lymphatic system: new questions and paradigms. Development. 2016;143(6):924–35.
7. Brouillard P, Boon L, Vikkula M. Genetics of lymphatic anomalies. J Clin Invest. 2014;124(3):898–904.
8. Mulliken JB, Glowacki J. Hemangiomas and vascular malformations in infants and children: a classification based on endothelial characteristics. Plast Reconstr Surg. 1982;69(3):412–22.

9. Marler JJ, Mulliken JB. Current management of hemangiomas and vascular malformations. Clin Plast Surg. 2005;32(1):99–116. ix
10. Faul JL, et al. Thoracic lymphangiomas, lymphangiectasis, lymphangiomatosis, and lymphatic dysplasia syndrome. Am J Respir Crit Care Med. 2000;161(3. Pt 1):1037–46.
11. Hilliard RI, McKendry JB, Phillips MJ. Congenital abnormalities of the lymphatic system: a new clinical classification. Pediatrics. 1990;86(6):988–94.
12. Dasgupta R, Fishman SJ. ISSVA classification. Semin Pediatr Surg. 2014;23(4):158–61.
13. Wassef M, et al. Vascular anomalies classification: recommendations from the International Society for the Study of Vascular Anomalies. Pediatrics. 2015;136(1):e203–14.
14. Hochman M, Adams DM, Reeves TD. Current knowledge and management of vascular anomalies, II: malformations. Arch Facial Plast Surg. 2011;13(6):425–33.
15. Elluru RG, Azizkhan RG. Cervicofacial vascular anomalies. II. Vascular malformations. Semin Pediatr Surg. 2006;15(2):133–9.
16. de Serres LM, Sie KC, Richardson MA. Lymphatic malformations of the head and neck. A proposal for staging. Arch Otolaryngol Head Neck Surg. 1995;121(5):577–82.
17. Elluru RG, Balakrishnan K, Padua HM. Lymphatic malformations: diagnosis and management. Semin Pediatr Surg. 2014;23(4):178–85.
18. Brown LR, et al. Intrathoracic lymphangioma. Mayo Clin Proc. 1986;61(11):882–92.
19. Drut R, Mosca HH. Intrapulmonary cystic lymphangioma. Pediatr Pulmonol. 1996;22(3):204–6.
20. O TM, et al. Lymphatic malformations of the airway. Otolaryngol Head Neck Surg. 2013;149(1):156–60.
21. Hancock BJ, et al. Complications of lymphangiomas in children. J Pediatr Surg. 1992;27(2):220–4; discussion 224–6.
22. Mishra P, et al. Lymphangioma presenting as cardiac tamponade in a child. J Card Surg. 2015;30(7):613–6.
23. Khobta N, et al. Solitary cystic mediastinal lymphangioma. Eur Respir Rev. 2013;22(127):91–3.
24. Papsin BC, Evans JN. Isolated laryngeal lymphangioma: a rare cause of airway obstruction in infants. J Laryngol Otol. 1996;110(10):969–72.
25. Wright CC, et al. Intrathoracic cystic hygroma: a report of three cases. J Pediatr Surg. 1996;31(10):1430–2.
26. Wittekindt C, et al. Lymphatic malformations of the head and neck: introduction of a disease score for children, Cologne Disease Score (CDS). Int J Pediatr Otorhinolaryngol. 2006;70(7):1205–12.
27. Tazelaar HD, et al. Diffuse pulmonary lymphangiomatosis. Hum Pathol. 1993;24(12):1313–22.
28. Carlson KC, Parnassus WN, Klatt EC. Thoracic lymphangiomatosis. Arch Pathol Lab Med. 1987;111(5):475–7.
29. Takahashi K, et al. An adult case of lymphangiomatosis of the mediastinum, pulmonary interstitium and retroperitoneum complicated by chronic disseminated intravascular coagulation. Eur Respir J. 1995;8(10):1799–802.
30. Dunkelman H, et al. Generalised lymphangiomatosis with chylothorax. Arch Dis Child. 1989;64(7):1058–60.
31. Shah AR, et al. Generalized lymphangiomatosis and chylothorax in the pediatric age group. Pediatr Pulmonol. 1992;14(2):126–30.
32. Luisi F, Torre O, Harari S. Thoracic involvement in generalised lymphatic anomaly (or lymphangiomatosis). Eur Respir Rev. 2016;25(140):170–7.
33. Lala S, et al. Gorham-Stout disease and generalized lymphatic anomaly--clinical, radiologic, and histologic differentiation. Skelet Radiol. 2013;42(7):917–24.
34. Nikolaou VS, et al. Vanishing bone disease (Gorham-Stout syndrome): a review of a rare entity. World J Orthop. 2014;5(5):694–8.
35. Aviv RI, McHugh K, Hunt J. Angiomatosis of bone and soft tissue: a spectrum of disease from diffuse lymphangiomatosis to vanishing bone disease in young patients. Clin Radiol. 2001;56(3):184–90.
36. Dupond JL, et al. Plasma VEGF determination in disseminated lymphangiomatosis-Gorham-Stout syndrome: a marker of activity? A case report with a 5-year follow-up. Bone. 2010;46(3):873–6.
37. Radhakrishnan K, Rockson SG. Gorham's disease: an osseous disease of lymphangiogenesis? Ann N Y Acad Sci. 2008;1131:203–5.
38. Lee S, et al. Gorham Stout syndrome (disappearing bone disease): two additional case reports and a review of the literature. Arch Otolaryngol Head Neck Surg. 2003;129(12):1340–3.
39. Abrahams J, et al. Massive osteolysis in an infant. AJR Am J Roentgenol. 1980;135(5):1084–6.
40. Tie ML, Poland GA, Rosenow EC 3rd. Chylothorax in Gorham's syndrome. A common complication of a rare disease. Chest. 1994;105(1):208–13.
41. Toro-Sola MA. Distichiasis-lymphedema syndrome and the Turner phenotype. Bol Asoc Med P R. 1991;83(12):543–4.
42. Cordasco EM Jr, et al. Clinical features of the yellow nail syndrome. Cleve Clin J Med. 1990;57(5):472–6.
43. Szuba A, Rockson SG. Lymphedema: classification, diagnosis and therapy. Vasc Med. 1998;3(2):145–56.
44. Schirger A, Harrison EG Jr, Janes JM. Idiopathic lymphedema. Review of 131 cases. JAMA. 1962;182:14–22.
45. Kinmonth JB, et al. Primary lymphoedema; clinical and lymphangiographic studies of a series of 107 patients in which the lower limbs were affected. Br J Surg. 1957;45(189):1–9.
46. Browse NL, Stewart G. Lymphoedema: pathophysiology and classification. J Cardiovasc Surg. 1985;26(2):91–106.
47. Connell F, et al. A new classification system for primary lymphatic dysplasias based on phenotype. Clin Genet. 2010;77(5):438–52.
48. Connell FC, et al. The classification and diagnostic algorithm for primary lymphatic dysplasia: an update from 2010 to include molecular findings. Clin Genet. 2013;84(4):303–14.
49. Connell F, Brice G, Mortimer P. Phenotypic characterization of primary lymphedema. Ann N Y Acad Sci. 2008;1131:140–6.
50. Peyron N, Dandurand M, Guillot B. [Malignant tumors as complications of lymphedema]. J Mal Vasc. 1993;18(4):293–8.
51. Inde Y, et al. Morphological changes observed via fetal ultrasound in prenatally diagnosed and isolated congenital lymphangiomas: three case reports. J Med Ultrason (2001). 2013;40(3):265–9.
52. Adaletli I, et al. Anterior mediastinal lymphangioma: pre- and postnatal sonographic findings. J Clin Ultrasound. 2013;41(6):383–5.
53. Koelblinger C, et al. Fetal magnetic resonance imaging of lymphangiomas. J Perinat Med. 2013;41(4):437–43.
54. Greene AK, Perlyn CA, Alomari AI. Management of lymphatic malformations. Clin Plast Surg. 2011;38(1):75–82.
55. Esther CR Jr, Barker PM. Pulmonary lymphangiectasia: diagnosis and clinical course. Pediatr Pulmonol. 2004;38(4):308–13.
56. Dempsey EM, et al. Congenital pulmonary lymphangiectasia presenting as nonimmune fetal hydrops and severe respiratory distress at birth: not uniformly fatal. Pediatr Pulmonol. 2005;40(3):270–4.
57. Witte CL, et al. Advances in imaging of lymph flow disorders. Radiographics. 2000;20(6):1697–719.
58. Levine C. Primary disorders of the lymphatic vessels--a unified concept. J Pediatr Surg. 1989;24(3):233–40.
59. Caro PA, Mahboubi S, Faerber EN. Computed tomography in the diagnosis of lymphangiomas in infants and children. Clin Imaging. 1991;15(1):41–6.
60. Shaffer K, et al. Thoracic lymphangioma in adults: CT and MR imaging features. AJR Am J Roentgenol. 1994;162(2):283–9.
61. Siegel MJ, et al. Lymphangiomas in children: MR imaging. Radiology. 1989;170(2):467–70.
62. Bouchard S, et al. Pulmonary lymphangiectasia revisited. J Pediatr Surg. 2000;35(5):796–800.

63. Nobre LF, et al. Congenital pulmonary lymphangiectasia: CT and pathologic findings. J Thorac Imaging. 2004;19(1):56–9.
64. Jang HJ, Lee KS, Han J. Intravascular lymphomatosis of the lung: radiologic findings. J Comput Assist Tomogr. 1998;22(3):427–9.
65. Wunderbaldinger P, et al. CT and MR imaging of generalized cystic lymphangiomatosis in pediatric patients. AJR Am J Roentgenol. 2000;174(3):827–32.
66. Lynch DA, et al. Pediatric diffuse lung disease: diagnosis and classification using high-resolution CT. AJR Am J Roentgenol. 1999;173(3):713–8.
67. Pui MH, Yueh TC. Lymphoscintigraphy in chyluria, chyloperitoneum and chylothorax. J Nucl Med. 1998;39(7):1292–6.
68. Bagrodia N, Defnet AM, Kandel JJ. Management of lymphatic malformations in children. Curr Opin Pediatr. 2015;27(3):356–63.
69. Smith MC, et al. Efficacy and safety of OK-432 immunotherapy of lymphatic malformations. Laryngoscope. 2009;119(1):107–15.
70. Nehra D, et al. Doxycycline sclerotherapy as primary treatment of head and neck lymphatic malformations in children. J Pediatr Surg. 2008;43(3):451–60.
71. Burrows PE, Mason KP. Percutaneous treatment of low flow vascular malformations. J Vasc Interv Radiol. 2004;15(5):431–45.
72. Poldervaart MT, et al. Treatment of lymphatic malformations with OK-432 (Picibanil): review of the literature. J Craniofac Surg. 2009;20(4):1159–62.
73. Berenguer B, et al. Sclerotherapy of craniofacial venous malformations: complications and results. Plast Reconstr Surg. 1999;104(1):1–11; discussion 12–5.
74. Fliegelman LJ, et al. Lymphatic malformation: predictive factors for recurrence. Otolaryngol Head Neck Surg. 2000;123(6):706–10.
75. Goswamy J, et al. Radiofrequency ablation in the treatment of paediatric microcystic lymphatic malformations. J Laryngol Otol. 2013;127(3):279–84.
76. Grimmer JF, et al. Radiofrequency ablation of microcystic lymphatic malformation in the oral cavity. Arch Otolaryngol Head Neck Surg. 2006;132(11):1251–6.
77. Niti K, Manish P. Microcystic lymphatic malformation (lymphangioma circumscriptum) treated using a minimally invasive technique of radiofrequency ablation and sclerotherapy. Dermatol Surg. 2010;36(11):1711–7.
78. Savas JA, et al. Carbon dioxide laser for the treatment of microcystic lymphatic malformations (lymphangioma circumscriptum): a systematic review. Dermatol Surg. 2013;39(8):1147–57.
79. Glade RS, Buckmiller LM. CO2 laser resurfacing of intraoral lymphatic malformations: a 10-year experience. Int J Pediatr Otorhinolaryngol. 2009;73(10):1358–61.
80. Swetman GL, et al. Sildenafil for severe lymphatic malformations. N Engl J Med. 2012;366(4):384–6.
81. Danial C, et al. An open-label study to evaluate sildenafil for the treatment of lymphatic malformations. J Am Acad Dermatol. 2014;70(6):1050–7.
82. Hammill AM, et al. Sirolimus for the treatment of complicated vascular anomalies in children. Pediatr Blood Cancer. 2011;57(6):1018–24.
83. Adams DM, et al. Efficacy and Safety of Sirolimus in the Treatment of Complicated Vascular Anomalies. Pediatrics. 2016;137(2):e20153257.
84. Laforgia N, et al. Lymphatic malformation in newborns as the first sign of diffuse lymphangiomatosis: successful treatment with sirolimus. Neonatology. 2016;109(1):52–5.
85. Margolin JF, Soni HM, Pimpalwar S. Medical therapy for pediatric vascular anomalies. Semin Plast Surg. 2014;28(2):79–86.
86. Raju A, Chang DW. Vascularized lymph node transfer for treatment of lymphedema: a comprehensive literature review. Ann Surg. 2015;261(5):1013–23.

Pediatric Thoracic Oncology Disorders

15

Edward Y. Lee

Pediatric Lung, Central Airway, and Chest Wall Neoplasms

Primary thoracic neoplasms in children can arise within the lung, central airway, or chest wall [1–3]. Malignant lesions are much more common than benign processes. Metastatic tumors account for up to 80% of all lung tumors in children and more than 95% of the malignant ones. Due to the rarity and nonspecific presenting clinical symptoms of thoracic neoplasms in the pediatric population, a substantial delay in the diagnosis often occurs. Therefore, a high index of suspicion coupled with optimal imaging evaluation is of paramount importance in early and correct diagnosis. Early management can, in turn, result in decreased morbidity and mortality associated with the lung, central airway, and chest wall neoplasms in pediatric patients. The prognosis of thoracic tumors in children varies depending on the malignant nature of the tumor, evidence of metastasis, and amenability to surgical excision. In this section, we discuss pediatric lung, central airway, and chest wall neoplasms including (1) clinical presentation, (2) practical approach to diagnosis, (3) imaging findings, and (4) patient outcome.

Clinical Presentation and Practical Imaging Approach for Diagnosing Pediatric Lung, Central Airway, and Chest Wall Neoplasms in Pediatric Patients

There are some chief complaints and clinical presentations which ultimately lead to the discovery of a thoracic neoplasm. Because chest tumors are rare in the pediatric population, other more common diagnoses are often excluded before the actual diagnosis can be made. Frequently, thoracic tumors are inadvertently discovered when a pediatric patient undergoes an imaging study for some other unrelated complaint. Although history and physical examination can help to localize a mass, imaging is paramount in formulating a diagnostic and therapeutic plan.

More often than not, children with thoracic neoplasms do not complain of symptoms commonly associated with neoplastic processes such as fever, weight loss, and fatigue. Therefore, when pediatric patients do not respond to conventional therapies, other rarer diagnoses must be considered. Cough is one of the most common chief complaints that a pediatrician encounters in the office, which can be the presenting symptom of a thoracic malignancy. After excluding the common causes of cough such as asthma, postnasal drip, and gastroesophageal reflux, other entities must be considered. If the child has difficulty gaining weight or has evidence of malabsorption, he/she might need a sweat test or genetic testing to exclude cystic fibrosis. If there is a history of recurrent infections, an immune workup, placing a PPD, or sending a sputum sample looking for routine bacteria, acid fast bacilli, and fungus may be warranted. Sinusitis can be difficult to diagnose in young children due to lack of specific symptoms. Pulmonary function tests (PFTs) may aid in the diagnosis of cough, but almost all patients with unexplained cough need some form of an imaging study.

A posteroanterior (PA) and lateral chest radiographs (CXR) can reveal a great deal of information including signs of a possible infection, aspiration, persistent atelectasis, lymphadenopathy, or even a chest mass [4]. Lymphadenopathy can be secondary to infection, but could also be related to an underlying primary thoracic neoplasm and may be the only clue to a lymphoma. The chest drains into the supraclavicular nodes, therefore a thorough physical examination evaluating for lymphadenopathy is vital. External compression of the airway can be secondary to an enlarged lymph node or any type of mass in the thoracic cavity. Computed tomography (CT) is so warranted to obtain better visualization of the abnormality. CT can often detect abnormalities, that are not seen on CXR, by better delineating the anatomy and may aid-

E. Y. Lee (✉)
Department of Radiology, Boston Children's Hospital and Harvard Medical School, Boston, MA, USA
e-mail: Edward.Lee@childrens.harvard.edu

R. H. Cleveland, E. Y. Lee (eds.), *Imaging in Pediatric Pulmonology*, https://doi.org/10.1007/978-3-030-23979-4_15

ing in determining a surgical approach for biopsy [5]. Calcifications and lung parenchymal abnormalities are better elucidated via CT and, if present, may narrow the differential diagnosis. Magnetic resonance imaging (MRI), which is not associated with ionizing radiation exposure, has superior diagnostic capability when evaluating soft tissues. Therefore, MRI can be a valuable tool when evaluating certain abnormalities in the chest [6–10]. Although imaging studies can often narrow the differential, biopsy is typically required for a definitive diagnosis.

Wheezing, stridor, and noisy breathing are chief complaints associated with common pediatric disorders such as asthma, gastroesophageal reflux, laryngomalacia, and tracheomalacia [11–13]. However, children with endobronchial tumors may present in similar fashion. Therefore, it is crucial to obtain a thorough history and physical examination when assessing a pediatric patient with these common symptoms. A healthy, thriving child less than 1 year of age might need a very limited workup for noisy breathing. However, at the minimum, these children should have a CXR to ensure the symptoms are not secondary to a mass- or space-occupying lesion. In fact, one could argue that every child who wheezes for the first time should have a baseline CXR to exclude a mass in the thoracic cavity. For the child who has persistent noisy breathing, difficulty gaining weight, repeated respiratory infections, or anything else causing concern on history or physical examination, further workup is warranted. If the noisy breathing is associated with difficulty feeding or choking, then a barium swallow should be ordered to look for a vascular ring. If the child is old enough, a good place to start would be to obtain PFTs. PFTs can suggest a fixed intra- or extra-thoracic lesion. Total lung capacity and diffusing capacity of the lungs are also helpful when evaluating the patient. The next step in diagnosis is either a bronchoscopy to directly evaluate the airway or CT. Often this is determined by availability. CT is often much easier to obtain but has the disadvantage of exposing the child to radiation [14, 15].

A bronchoscopy allows assessment of the vocal cords for mobility and presence of any abnormal lesions which may be responsible for the clinical symptoms. Common diagnoses such as laryngomalacia and tracheomalacia can be excluded during bronchoscopy by assessing the dynamic movement of the larynx and trachea. Bronchoalveolar lavage fluid is tested for signs of infection, aspiration, and malignancy. It is important to look for an external compression-causing symptoms, such as an aberrant innominate artery, as well as any endobronchial lesions which may account for the presenting clinical symptoms. If there is evidence of external compression on the airway or if an endobronchial lesion is visualized, the next step must be CT or MRI [16–19]. A CT or MRI can sometimes suggest a specific diagnosis but almost always narrows the differential. Furthermore, the findings on imaging can demonstrate the extent of the lesion and dictate which service is most appropriate to attempt biopsy and/or removal of the lesion.

Dyspnea on exertion is another common complaint seen in the pediatric office and may be a clue to an underlying malignancy. It is important to take a careful cardiac history. After excluding a cardiac causes, exercise-induced bronchoconstriction, vocal cord dysfunction, and deconditioning, other possible entities should be carefully considered. In this scenario, PFTs are quite helpful, and some children need a full cardiopulmonary exercise test to determine the etiology of their symptoms. A CXR may show a mass, persistent atelectasis, or lymphadenopathy which could all be signs of an underlying malignancy and would therefore necessitate further examination. Symptoms often become apparent only after the tumor has grown large enough to cause a mass effect.

Inquiring about systemic complaints on a thorough review of systems is crucial as the lungs or chest wall may not be the primary source of the malignancy. Lung metastases are much more common that primary lung tumors in children and presenting symptoms are based on location. If the tumor load is large enough to replace parenchymal tissue, the patient will complain of dyspnea. Extension into the pleura causes pleuritic chest pain, and endobronchial metastases manifest as wheezing or hemoptysis. However, respiratory symptoms are often absent in patients with metastatic disease, making diagnosis much more difficult. Sputum cytologic analysis or lung biopsy may ultimately be necessary to make an accurate diagnosis when evaluating patients with metastatic disease, but imaging studies are always required, and a CXR is the first step. In fact, metastases are sometimes inadvertently picked up on a CXR obtained for other reasons. CT is more sensitive than a CXR in detecting pulmonary nodules, and when multiple nodules are seen, the clinician is obligated to look for a primary tumor. Common sites in this scenario would be the bones, testicles, kidneys, or soft tissues. The child may need to be screened with a bone scan, testicular ultrasound, evaluation of the peripheral blood smear, or a PET scan [20].

Pediatric Primary Lung Neoplasms

Benign Tumors

Inflammatory Myofibroblastic Tumor Inflammatory myofibroblastic tumor (IMT), also known as inflammatory pseudotumor of the lung or plasma cell granuloma, is a benign tumor of unknown origin. It was first described in 1939 and was thought to arise as a reaction to a previous insult [1, 2, 21]. Although IMT has been traditionally considered as a benign lesion, recent molecular analysis has raised suspicions to the contrary. The World Health Organization (WHO)

has currently defined this tumor as an intermediary neoplasm, characterized by a molecular rearrangement on chromosome locus 2p23 involving the tyrosine kinase receptor anaplastic lymphoma kinase (ALK), which is involved in other forms of malignancy [22]. This genetic rearrangement has been documented in some but not all IMTs.

IMT is the most common primary tumor of the lung in children less than 16 years of age [23]. It is estimated that IMTs account for approximately 20% of all primary lung tumors and 57% of all benign lesions [24]. They are typically slow-growing neoplasms and show signs of both reactive and neoplastic components [25]. Clubbing can be a presenting sign and often disappears after surgical removal [23, 26]. Patients with IMT are usually asymptomatic due to its predilection for occurring in the periphery. However, the tumor can grow in size over a long period of time and eventually lead to symptoms such as cough, hemoptysis, and dyspnea due to local invasion and/or mass effect on mediastinal structures. If allowed to grow substantially without treatment, IMTs can lead to significant morbidity as multiple deaths have been reported due to local invasion of this tumor [27–29]. IMTs are more likely to recur locally than to metastasize, and there is a 14% recurrence rate [30], which is highly correlated to the presence of local invasion. On gross inspection, they are usually firm and white to yellow in color. Microscopically, IMT is characterized by a localized proliferation of plasma cells, lymphocytes, and eosinophils with Russell bodies and reticuloendothelial cells supported by a stroma of granulation tissue [23, 26, 31].

Radiologically, IMTs are most often solitary, found in the periphery, and range from 1 to 12 cm in size. They are typically heterogeneously enhancing soft tissue masses often with calcification (Fig. 15.1). They are round- or oval-shaped circumscribed masses that are described as "coin lesions" [23, 26]. The potential differential should include infectious processes, other neoplasms, and congenital malformations. There seems to be two types of IMT. The first is noninvasive, often asymptomatic, and easily removed by wedge resection. The second type is larger, invasive, occurs in younger patients with systemic symptoms of fever, fatigue, or weight loss, and often requires a lobectomy or pneumonectomy [31]. Complete surgical resection when possible is the treatment of choice and the overall prognosis is excellent.

Leiomyoma A leiomyoma is a rare, benign, smooth muscle neoplasm which can present in the lung parenchyma or as an endobronchial lesion. Epstein–Barr virus is often associated with lymphoproliferative disorders in immunosuppressed children but is also linked to the development of pulmonary leiomyomas in children with HIV, recipients of solid organ transplants, and those with primary immunodeficiencies. Clinical presentation in children with leiomyoma depends on the location of the tumor. Endobronchial lesions may present with cough, hemoptysis, or repeated bouts of pneumonia, whereas peripheral lesions within the lung parenchyma may be asymptomatic [32]. Clubbing of the fingers may be the only presenting abnormality in children [33, 34]. Histologically, leiomyomas are composed of spindle-shaped cells and lack significant atypia and mitotic activity [32]. There is a spectrum from benign (leiomyoma) to malignant (leiomyosarcoma) morphology, and there is potential for regression with modulation of immunosuppression [35].

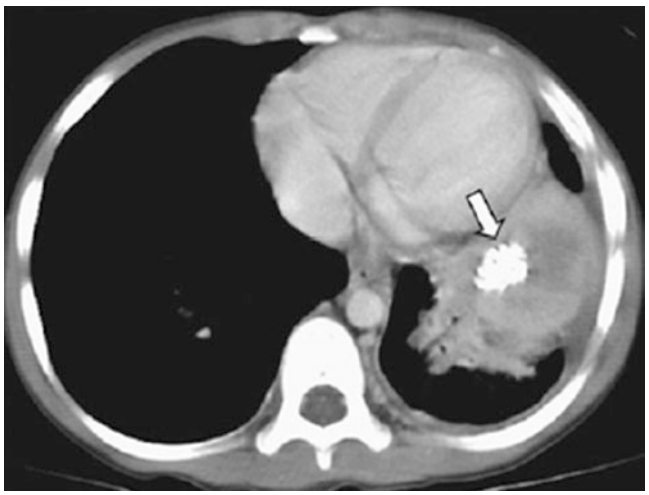

Fig. 15.1 A 6-year-old girl who presented with fever and abnormal chest radiographs. Enhanced axial CT image demonstrates a heterogeneously enhancing mass with associated chunky calcification (*arrow*) in the left lower lobe. Surgical pathology confirmed a diagnosis of inflammatory pseudotumor

Management of pediatric patients with leiomyoma is currently not well defined. However, benign tumors in noncritical locations may be observed, whereas endobronchial symptomatic lesions need to be removed by bronchoscopic resection or may even necessitate lobectomy or bronchial sleeve resection. Ultimately, management is tailored to the general clinical condition of the patient, the location of the tumor, and the effect of the tumor on the patient [35].

Congenital Pulmonary Myofibroblastic Tumor Congenital pulmonary myofibroblastic tumor (CPMT) is a very rare, congenital, benign lung tumor of the fetus and infant. It has been described under various terminologies, including massive congenital mesenchymal malformation of the lung, hamartoma of the lung, bronchopulmonary leiomyosarcoma, and primary bronchopulmonary fibrosarcoma (PBF) [36]. It is thought to arise from the pluripotent mesenchyme found around the developing bronchi at approximately 12 weeks gestation. Affected pediatric patients often present in utero or at birth with a unilateral lung mass with mediastinal shift resulting in polyhydramnios, hydrops, or immediate respiratory failure at delivery. Grossly, a large portion of the lung is

enlarged and replaced by a firm rubbery mass. Due to its cellularity and mitotic activity, it was originally thought to be malignant in nature. However, all reported cases have behaved in a benign fashion; no cases have shown tumor recurrence or metastases [37]. Karyotyping may show complex rearrangements involving chromosomes 4, 8, and 10, which can help to differentiate this lesion from other similar smooth muscle tumors. Although the lesion is benign, the large size may result in respiratory or hemodynamic compromise necessitating surgical removal. One series reported a mortality rate of 55% [38]. With early resection, typically by pneumonectomy or lobectomy, long-term survival is expected [37].

Lipoblastoma Lipoblastoma is a rare, benign, adipose tumor occurring exclusively in children. Eighty-eight percent of cases occur before the age of 3 and 40% before the first year of life [39]. Greater than 70% of all lipoblastomas arise in the superficial layers of the extremities; the rest are deeper and arise in the mediastinum, retroperitoneum, and the axilla [40]. Affected pediatric patients often present with rapidly growing asymptomatic masses; however, if involving the lung, the patient may develop respiratory distress. Two forms of this tumor have been described: a well-circumscribed, encapsulated type occurring superficially (lipoblastoma) and a diffuse, infiltrating type occurring in deep soft tissues (lipoblastomatosis) [41, 42]. Histology reveals mature fat cells mixed with mesenchymal and immature fat cells.

CT can often reveal the lipoid nature of the tumor, but cannot distinguish between other lesions made up of adipose tissue. Therefore, a biopsy is needed for a definitive diagnosis. The treatment for lipoblastomas is surgical resection, and the prognosis is excellent if complete surgical resection with clear margins can be achieved. Recurrence rates of 14%–25% have been reported for infiltrating tumors where complete surgical resection was not possible [40, 43–45].

Hamartoma A pulmonary hamartoma is a collection of disorganized tissues intrinsic to the lung with a peak incidence in the sixth decade. They are the most common benign pulmonary lesion in adults, and the second most common in children (18%–23%) [27, 46]. It is composed of normal cells in an abnormal pattern; however, there is some evidence that it is actually a benign neoplasm [47]. In a Dutch series, the annual incidence was found to be 1:100,000. Affected patients ranged from 14 to 74 years of age with a mean of 51. 92% of tumors are parenchymal with 8% being endobronchial in location [47]. Patients with parenchymal lesions are often asymptomatic at diagnosis; however, if they are large enough, they can cause respiratory distress. Endobronchial lesions often present with symptoms of obstruction such as cough, hemoptysis, and dyspnea on exertion. Pathology often reveals various mesenchymal components such as cartilage, fat, fibrous tissue, smooth muscle, and bone. Tumors with a single dominant component may be classified as a chondroma, fibroma, or lipoma depending on the mesenchymal component [25].

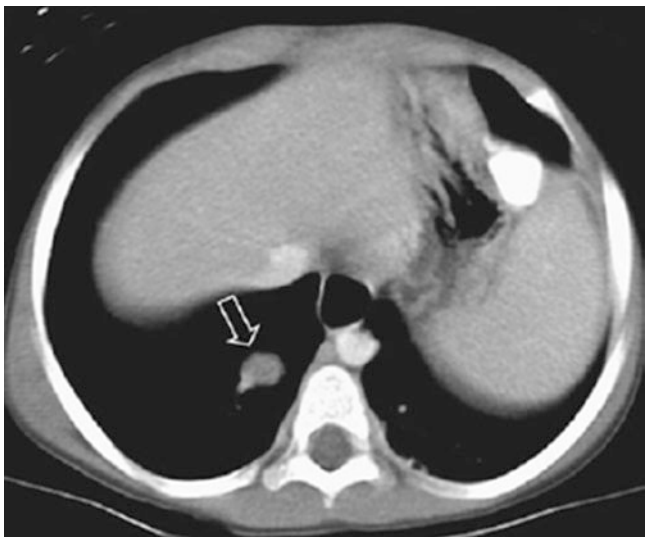

Fig. 15.2 A 5-year-old boy with a history of Wilm's tumor. Right lower lobe lung mass (arrow) was detected on chest CT examination performed for the evaluation of thoracic metastatic disease. Enhanced axial CT image demonstrates a round pulmonary mass (arrow) with areas of low attenuation consistent with a fat component. Surgical pathology was consistent with a diagnosis of a pulmonary hamartoma

Hamartomas of the lung are usually seen on CXR as a round homogenous opacity in the periphery of the lung. CT may show fat and "popcorn" calcifications which are pathognomonic for a hamartoma, but they are only seen in 10%–25% of cases (Fig. 15.2) [48, 49]. Management consists of surgical resection, and the prognosis is excellent; however, a 6.3 times increased risk of lung cancer has been described in patients with pulmonary hamartomas [50].

Malignant Tumors

Bronchogenic Carcinoma Primary lung carcinoma in children and adolescents is extremely rare, with 0.16% of all lung cancers occurring in the first decade and 0.7% in the second decade [51]. The overall incidence is difficult to determine precisely because reports are limited to case reports and small series. Most cases in the literature of pediatric lung carcinoma describe undifferentiated carcinomas followed by adenocarcinoma and squamous cell carcinoma. Primary lung carcinoma in children is often aggressive with evidence of metastatic disease at the time of diagnosis and carries a high mortality rate of up to 90% [27, 46]. Symptoms include cough, chest pain, pneumonia, and hemoptysis. However, affected pediatric patients can also present with bone pain, weight loss, or anemia due to metastatic disease. Radiologically, bronchogenic carcinoma typically presents as a large heterogeneously enhancing mass often invading adjacent thoracic structures (Fig. 15.3).

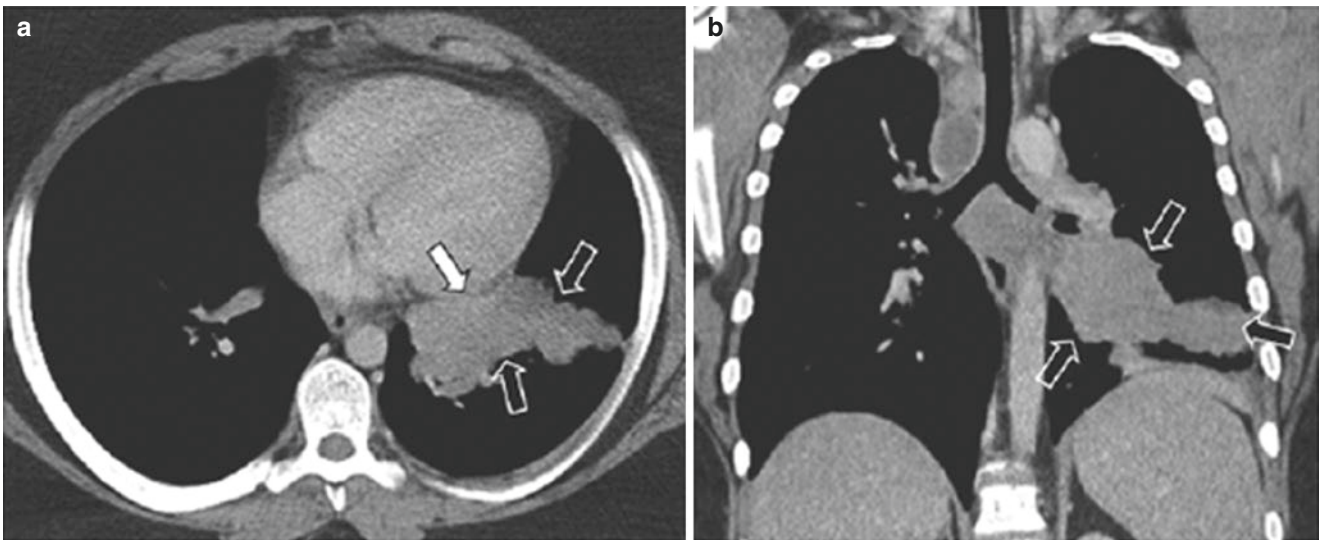

Fig. 15.3 A 15-year-old boy with bronchogenic carcinoma who presented with weight loss and progressively worsening shortness of breath. (**a**) Enhanced axial CT image demonstrates a large heterogeneous mass (*arrows*) with irregular borders located in the left lower lobe and abutting the left heart border. (**b**) Enhanced coronal CT image better demonstrates the entire extent of the mass (*arrows*)

NUT Midline Carcinoma NUT midline carcinoma (NMC) is a poorly differentiated neoplasm which is most common in children and pursues a highly aggressive course, usually resulting in death within weeks of diagnosis [52–58]. Affected pediatric patients with NMCs may present with constitutional symptoms or symptoms due to local mass effect from the tumor [55, 56, 59]. This tumor is characterized by rearrangement of the *NUT* gene (*nu*clear protein in *t*estis) on chromosome 15q14 [52–58]. In approximately two-thirds of cases, *NUT* (chromosome 15q14) is fused to the gene *BRD4* on chromosome 19p13.1, resulting in a novel *BRD4-NUT* fusion gene [53]. Such tumors have also been termed BRD4-NUT carcinoma or t(15;19) carcinoma. Anatomically, NMCs arise in or near the midline, most commonly in the head, neck, or mediastinum, as poorly differentiated carcinomas with variable degrees of squamous differentiation [52]. On imaging studies, NMC is usually a heterogeneously enhancing mass located within the mediastinum (Fig. 15.4). CT is the imaging modality of choice and can alert the surgical pathologist to submit tissue for karyotype analysis.

Surgical resection is the primary mode of therapy for bronchogenic carcinoma. Adjuvant therapy for local and disseminated disease utilizes both radio- and chemotherapy. Patients with disseminated disease at the time of diagnosis live on average less than 7 months [1, 2].

Pleuropulmonary Blastoma (Types I, II, III) Pleuropulmonary blastoma (PPB) is a rare, embryonal, mesenchymal neoplasm of the lung and pleura occurring almost exclusively in the pediatric population [1, 2, 24, 60, 61]. The actual incidence is unknown, but this is thought to be the most common malignant parenchymal tumor of childhood [62]. It is diagnosed mainly in infants and toddlers and rarely in

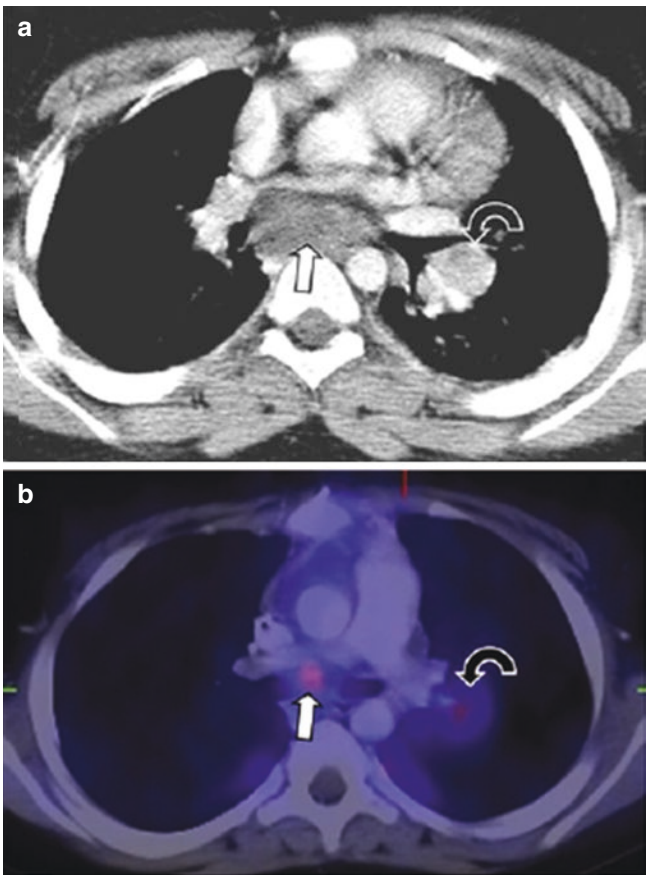

Fig. 15.4 A 10-year-old boy with NUT midline carcinoma (NMC) presented with multiple lower extremity arterial thromboses. Echocardiography showed a possible mediastinal mass, and CT was subsequently performed for further evaluation. (**a**) Enhanced axial CT image demonstrates a heterogeneously enhancing mass (*arrow*) located behind the heart with mass effect upon the right inferior pulmonary vein. Also noted is the left hilar lymphadenopathy (*curved arrow*). (**b**) Axial CT and PET fusion image shows an increased metabolism in the mediastinal mass (*arrow*) and left hilar lymphadenopathy (*curved arrow*)

those beyond 12 years of age. In the past, this specific entity had been referred to as an embryona of the lung, pulmonary blastoma, pulmonary sarcoma, embryonal sarcoma, and malignant mesenchymoma [62].

The tumor is thought to arise from pleuropulmonary germ cells and has been subclassified into three types based on gross morphological appearance. Type I tumors are exclusively cystic (Fig. 15.5); type II tumors contain both cystic and solid material, whereas type III lesions are predominantly solid (Fig. 15.6). As in bronchogenic carcinoma, PPB has been reported to arise from congenital malformations of the lung, including congenital pulmonary airway malformation (CPAM), pulmonary sequestrations, and bronchogenic cysts [63–66]. Pediatric patients with type I tumors present earlier than the other types with a mean age of 10 months compared to 34 and 44 months for types II and III, respectively [67]. Affected pediatric patients typically present with nonspecific respiratory symptoms, and spontaneous pneumothoraces have been described with cystic lesions. PPB may consist of solitary or multiple lesions and may even have a familial predisposition. They are often misdiagnosed as CPAM on imaging studies. Microscopically, these lesions are very similar to a CPAM in that PPBs have thin cyst walls lined by alveolar epithelium, but are distinguished by focal areas of hypercellularity and hypervascularity.

Complete surgical resection is the goal for children with PPB. Resection with clear margins may be adequate for type I lesions, but adjuvant therapy is required for higher-grade lesions after surgical resection, and radiation is recommended for any residual disease [1, 2, 61]. Metastases to the brain, bone, and liver are seen in up to 30% of patients with type II and III PPB. The outcome for children with PPB correlates with the grade. Type I lesions have an 83% long-term survival and cure rate, whereas this rate goes down to only 42% for those with type II and II lesions [60–67].

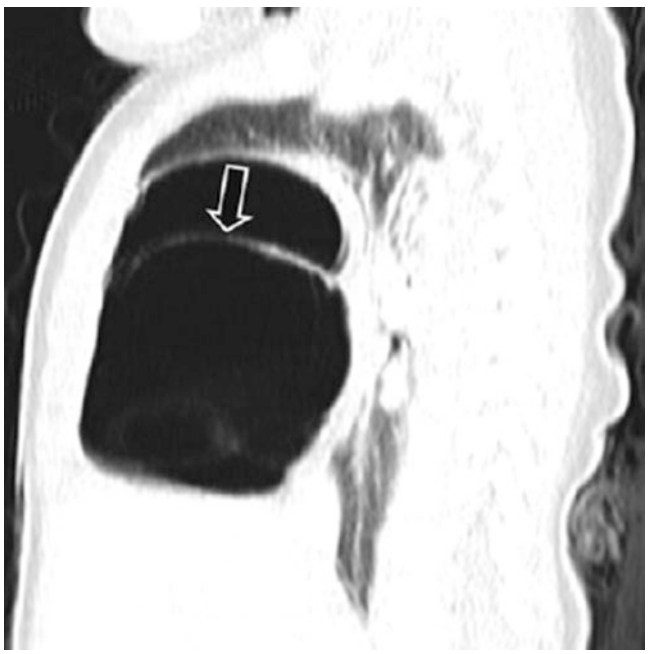

Fig. 15.5 A 2-month-old boy who presented with respiratory distress and abnormal chest radiographs. Sagittal lung window CT image shows a large cystic mass with internal septation (*arrow*) located in the right lung. Surgical pathology was consistent with type 1 pleuropulmonary blastoma (PPB)

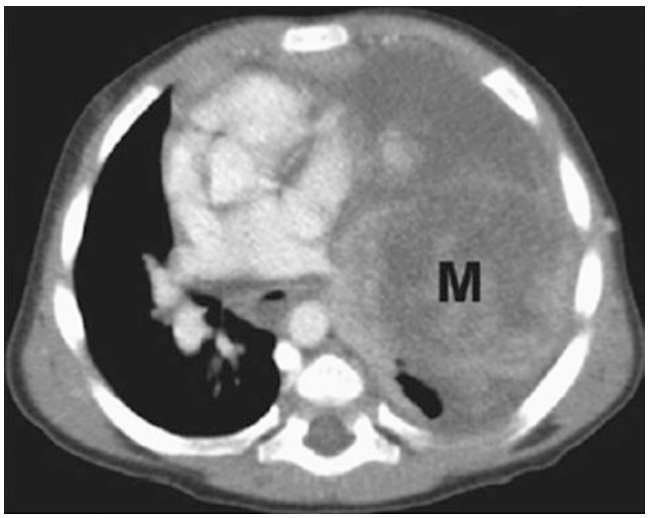

Fig. 15.6 A 1-month-old girl who presented with weight loss and respiratory distress. Enhanced axial CT image demonstrates a large heterogeneously enhancing mass (M) located in the left hemithorax with mediastinal shift to the right side. Surgical pathology was consistent with type 3 pleuropulmonary blastoma (PPB)

Bronchoalveolar Carcinoma Bronchoalveolar carcinoma (BAC) is classified as a subset of lung adenocarcinoma but has a distinct clinical presentation, tumor biology, response to therapy, and prognosis compared with other subtypes of non-small-cell lung carcinoma. It is characterized by growth along alveolar septae without evidence of stromal, vascular, or pleural invasion [68, 69]. BAC is much more common in adults than children. More than half of all patients with BAC are asymptomatic. Those who are symptomatic typically complain of cough, sputum production, shortness of breath, weight loss, hemoptysis, and fever. Later stages of BAC are associated with a greater likelihood of symptoms. When the patient is symptomatic, the tumor usually has a rapidly progressive downhill course [70]. Spread of the tumor tends to occur via the airways, but lymphogenous and hematogenous dissemination may occur in 50–60% of cases [71–73].

BAC can be classified into mucinous and nonmucinous lesions with the former accounting for 80% of cases [68–73]. Mucinous BAC originate from columnar mucus-containing cells, whereas nonmucinous tumors arise from Clara cells or type II pneumocytes. The prognosis for mucinous BAC is

worse than nonmucinous tumors with a 5-year survival rate of 26% vs. 72% [68–73]. Surgical resection is the only potentially curative treatment.

CPAMs are rare lesions characterized by the presence of an abnormal mass of pulmonary tissue that appears immature and malformed and may show varying degrees of cystic change. CPAMs can host metaplastic mucous cells, primitive mesenchymal cells, and differentiated but poorly organized striated muscle fibers. Therefore, these congenital malformations are viewed as a predisposing condition for possible oncogenesis [74]. Both BAC and rhabdomyosarcoma (RMS) have been reported in association with CPAMs, which justifies prompt surgical removal after diagnosis.

Leiomyosarcoma Leiomyosarcoma is a mesenchymal tumor with smooth muscle differentiation and is very rare in the pediatric population. The annual incidence is estimated to be less than two cases per 10 million children [75–78]. Primary leiomyosarcoma of the lung may arise from the smooth muscle coat of the bronchial tree [76] or the vascular smooth muscle. The presenting symptoms are similar to those of bronchogenic carcinoma including cough, chest pain, pneumonia, or hemoptysis. As is the case in pulmonary leiomyomas, immunosuppression after solid organ transplant, congenital immune deficiencies, and HIV are all predisposing conditions to developing leiomyosarcomas in children [77]. Furthermore, documented reports are available linking Epstein–Barr virus to the development of this malignancy [77]. As with a leiomyoma, there is a potential for regression of this tumor with modulation of immunosuppression.

Histologically, the tumor is made up of interlacing bundles of elongated cells, showing, in some cases, many mitotic figures and occasional tumor giant cells. Nuclear atypia, necrosis, and hemorrhage distinguish leiomyosarcoma from both leiomyomas and the myofibroblastic tumors. In spite of its anaplasia, this tumor has a much better prognosis than bronchogenic carcinoma. Metastases are uncommon but if present occur late and usually spare the lymphatics [78]. Most primary lesions are solitary, whereas multiplicity suggests metastasis from another site. Treatment consists of local excision when possible as well as chemotherapy and radiation [75–78].

Primary Bronchopulmonary Fibrosarcoma Primary bronchopulmonary fibrosarcoma (PBF) is an uncommon, mesenchymal tumor with less than 30 cases reported in the literature. They are low-grade tumors with a relatively good prognosis and should be regarded as the bronchopulmonary counterpart of the congenital infantile fibrosarcoma of the soft tissues [79, 80]. Affected pediatric patients with PBF typically present with cough, fever, chest pain, pneumonitis, and hemoptysis. Endobronchial and intraparenchymal tumors have both been described, with the former having a better prognosis, possibly due to earlier discovery because of obstructive symptoms. Endobronchial lesions are usually of a lower histologic grade, show less mitotic activity, and have a more uniform pattern of growth than the intraparenchymal tumors [79–81]. Histologically, these tumors are highly cellular and made up of interlacing bundles of densely packed spindle cells. Radiologically, PBF is a markedly heterogeneously enhancing large mass which typically occupies almost the entire hemithorax (Fig. 15.7). Metastases are uncommon and occur in 7% of affected patients. In the absence of metastases, complete resection can be curative. Bronchoscopic removal of endobronchial lesions is discouraged due to the possibility of endobronchial extension. Radiation and chemotherapy are reserved for unresectable lesions. There is a mortality rate of 21% [82–84] associated with PBF, but 5-year survival rates can reach as high as 84% [82–84].

Congenital/Infantile Fibrosarcoma Congenital fibrosarcoma most often occurs in children under 2 years of age, and almost half are present at birth. They most commonly affect the distal portions of the extremities, and most patients are asymptomatic other than a nontender swelling or mass. Fibrosarcoma is a tumor composed of anaplastic spindle-shaped cells that are arranged in a herringbone pattern. The degree of cellular differentiation and mitotic activity may be stratified into a specific grade and then used to predict the clinical behavior of the tumor [82–84]. However, fibrous proliferations in infants and children

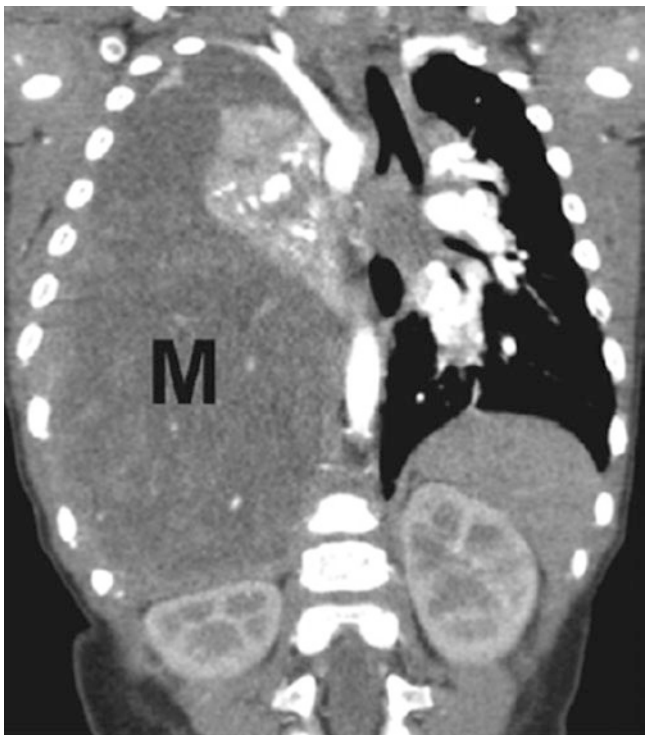

Fig. 15.7 A 2-month-old boy who presented with cough, fever, and hemoptysis. Enhanced coronal CT image demonstrates a large heterogeneously enhancing mass (M) almost completely occupying the right hemithorax. The mass was histologically confirmed as primary bronchopulmonary fibrosarcoma (PBF)

are often difficult to evaluate because their histologic features do not always correlate with clinical behavior [82–84]. Congenital fibrosarcomas are rapidly growing tumors composed of immature-appearing spindle-shaped cells with high cellularity and mitotic activity. Despite these features, they have a relatively good prognosis, especially compared with the adult form of fibrosarcoma. Approximately 8% of patients have evidence of metastases, and there is an 84% associated 5-year survival rate [82–84]. Wide local excision is the treatment of choice with radiation and chemotherapy being reserved for recurrent or metastatic lesions.

Pediatric Metastatic Lung Neoplasm

An overwhelming majority of lung tumors in the pediatric population are metastatic. Metastatic tumors account for 80% of all lung tumors in children and more than 95% of the malignant ones [1, 2]. In children, it is important to diagnose lung metastases at an early stage because early detection has important therapeutic and prognostic implications. Osteosarcoma and Wilms tumor are the two most common malignancies to metastasize to the lungs. Since lung metastases are far more common than primary lung tumors, the clinician is obligated to look for a primary source when suspicious lesions are detected by imaging studies.

Unfortunately, CXR often fails to detect a substantial number of thoracic metastases because most metastatic lesions are pleural based, subpleural, or in the outer one-third of the lung which is more difficult to detect. Therefore, CT is the image of choice for completely evaluating metastatic thoracic disease in the pediatric population. Metastases often appear as single or multiple circumscribed nodules, and preferentially involve the lower lobes [1, 2]. The current indications for using CT for evaluating metastatic thoracic disease include (1) searching for occult metastases for diagnostic and therapeutic reasons, (2) further evaluation when conventional studies are limited for a complete evaluation, (3) preoperative evaluation, (4) evaluation of prognostic indicators, (5) CT-directed transthoracic thin-needle aspiration, and (6) radiation planning [85].

It is important to recognize that no imaging modality has the ability to definitively distinguish between benign and malignant disease. Some metastatic lung nodules are excised in children for diagnostic purposes, but others are removed to achieve long-term survival and even cure [86]. Pulmonary metastasectomy is most common for osteosarcoma, but may also be beneficial in tumors resistant to chemotherapy and radiation. Surgical management of pulmonary metastases is uncommon and usually unnecessary for chemo- and radiosensitive tumors. However, when necessary, surgical resection of pulmonary metastases is always performed with a curative intent. In general, good surgical candidates meet all of the following five criteria:

- Primary tumor diagnosis
- Primary tumor site adequately controlled or resected
- No other known extrapulmonary metastases (if additional metastases are present, they should be considered amenable to surgery or some other form of therapy)
- Good surgical candidates from the standpoint of cardiopulmonary and other comorbid conditions
- Location of metastatic lesion is such that it can be completely resected with reasonable preservation of the remaining normal lung

Wilms Tumor

Wilms tumor is the most common childhood abdominal malignancy. It affects the kidney and is successfully treated in over 90% of affected pediatric patients. Pulmonary metastases are found in 12–15% of patients at the time of diagnosis [87, 88]. Metastases are typically asymptomatic and detected by imaging such as CXR or CT (Fig. 15.8). Pediatric patients with a favorable histology and lung

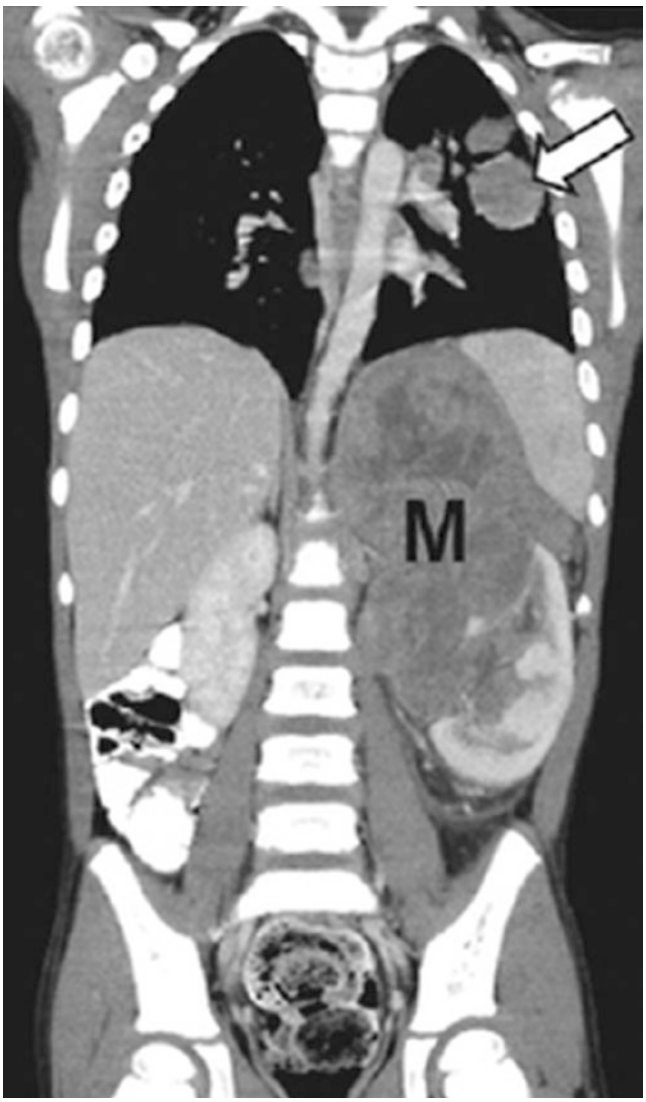

Fig. 15.8 A 4-year-old girl who presented with left flank pain and hematuria. Enhanced coronal CT image shows a large mass (M) arising from the left kidney and pulmonary metastasis (*arrow*). Surgical pathology of the left renal mass was consistent with Wilm's tumor

metastases have a 75% 4-year survival rate [89]. Metastases from a Wilms' tumor tend to be more chemo- and radiosensitive, so there is a limited role for metastasectomy. However, suspicious pulmonary lesions in the setting of a Wilms' tumor should be biopsied because up to 33% will be negative for tumor [90]. Thus, a biopsy can spare the patient extra radiation.

Hepatoblastoma

Hepatoblastoma is the most common malignant hepatic tumor in children, although it is relatively uncommon compared with other solid tumors in the pediatric age group. It accounts for 79% of all liver tumors in children and almost two-thirds of primary malignant liver tumors in the pediatric age group. Affected pediatric patients are most often diagnosed before 3 years of age with a median age of 1 year. In recent years, surgical techniques and adjuvant chemotherapy have markedly improved the prognosis of children with hepatoblastoma. Currently, complete surgical resection of the tumor at diagnosis, followed by adjuvant chemotherapy, is associated with 100% survival rates.

Although pediatric patients with hepatoblastoma are usually asymptomatic at diagnosis, approximately 40% of patients have advanced disease and 20% have pulmonary metastases. Surgical resection of pulmonary metastases is a preferred treatment option if local control of the primary tumor has been accomplished with preoperative chemotherapy and local resection [91]. Micrometastases at the time of diagnosis are treated by preoperative chemotherapy. Although the overall prognosis of patients with lung metastases is worse compared to those with localized involvement, metastasectomy may be curative with local control of the primary tumor (Fig. 15.9). The overall 5-year survival rate of patients with a positive CT and a negative CXR is 77% compared with 42% in patients who had positive findings on both CT and CXR [92].

Neuroblastoma

Neuroblastoma is the most common extracranial solid tumor in children accounting for 10% of all childhood cancers [93, 94]. It is an embryonal malignancy of the sympathetic nervous system arising from neuroblasts. Infants younger than 1 year of age have a good prognosis, even in the presence of metastatic disease, whereas older patients with metastatic disease fare poorly, even when treated with aggressive therapy. Infants more commonly present with thoracic and cervical tumors, whereas in older children, neuroblastomas are more likely abdominal in location.

Neuroblastoma can occur in the sympathetic ganglia in the chest wall in children. They manifest as palpable masses which may or may not be painful. Prognosis is variable and depends on the patient's age, stage of disease, and histologic findings. Most patients present with signs and symptoms related to tumor growth.

Pulmonary involvement in neuroblastoma can result from direct extension, hematogenous, or lymphangitic spread. Most large studies report an incidence of pulmonary metastases to be 5% or less [95–97]. Neuroblastoma lung metastases occur when the tumor is widely disseminated and is a poor prognostic factor. Patients with lung metastases are found to have N-MYC amplification and an unfavorable histopathology. Furthermore, children with lung metastases have a lower event-free survival (EFS) as compared to all other patients with stage IV disease, 15% vs. 50%, respectively, at 2 years after diagnosis [96].

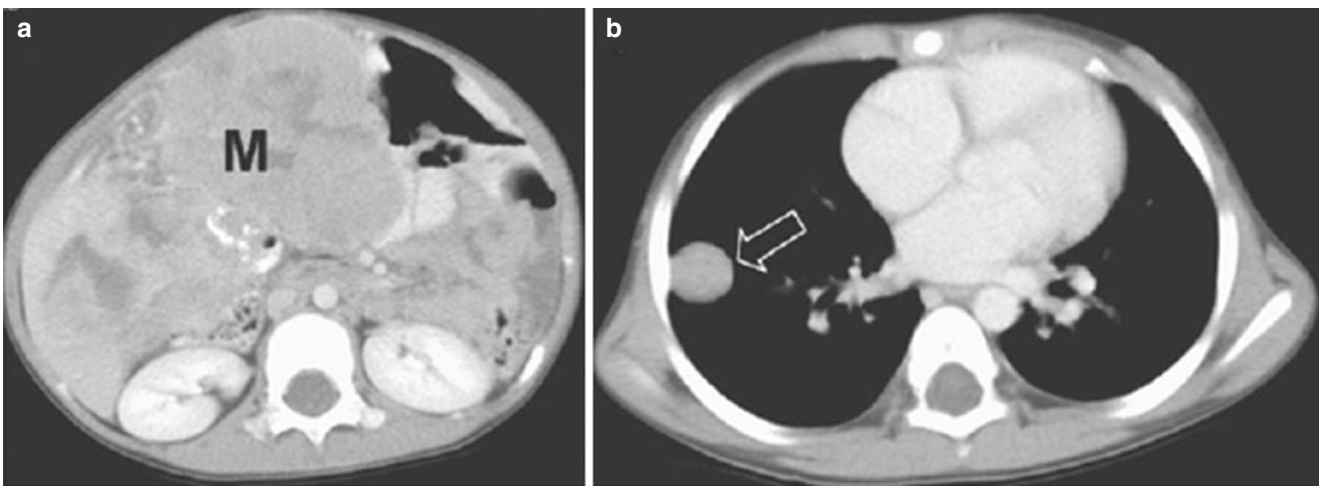

Fig. 15.9 A 3-year-old girl who presented with weight loss and a palpable right abdominal mass. Surgical pathology of the hepatic mass was consistent with hepatoblastoma. (**a**) Enhanced axial CT image of the upper abdomen shows a large heterogeneously enhancing (M) mass. (**b**) Enhanced axial CT image of the lung demonstrates a pulmonary mass (*arrow*) consistent with metastatic disease

A routine chest CT at the time of diagnosis is warranted to look for pulmonary metastases which can have a profound impact on prognosis. Due to the poor prognosis in patients with pulmonary metastases, pulmonary metastasectomy is not recommended. However, if there is concern about the nature of a pulmonary lesion after or during treatment, then a biopsy is warranted [98].

Osteosarcoma

Osteosarcoma is the third most common cancer in adolescence, occurring less frequently than lymphomas and brain tumors. It is thought to arise from a primitive mesenchymal bone-forming cell and is characterized by production of osteoid. The mainstay of therapy is removal of the lesion. Chemotherapy is also required to treat micrometastatic disease, which is present but not detectable in most patients at diagnosis.

Pulmonary metastases are found in approximately 10–15% of patients at the time of diagnosis [99]. They are usually asymptomatic and detected by imaging studies. The lung metastases are usually multiple, bilateral in over half the patients (Fig. 15.10), and calcified in 14% (Fig. 15.11) [100]. Both the number of nodules and number of lobes involved are significant predictors of survival. Each additional lobe that is affected signifies a 1.4 times increased risk of death. In patients with more than 3 nodules present at the time of diagnosis, the risk of death is 5.1 times greater [100]. Survival has been improved by metastasectomy which may require multiple thoracotomies. There is a 3-year survival rate of 45% vs. 5% with and without metastasectomy [101].

Ewing's Sarcoma

Ewing's sarcoma is the second most common primary osseous malignancy in childhood with an incidence of approximately 0.6 per million [102]. Twenty to twenty-five percent of patients with Ewing's sarcoma present with stage IV metastases with one-third having only lung or pleural nodules [103, 104]. This tumor is generally sensitive to both chemotherapy and radiation. Surgical excision of metastatic lesions is mainly for diagnostic purposes, and the role of metastasectomy is currently unclear.

Rhabdomyosarcoma

Rhabdomyosarcoma (RMS) is the most common soft tissue sarcoma in children [105]. Several distinct histologic groups have prognostic significance, including embryonal rhabdomyosarcoma (ERMS), which occurs in 55% of patients; the botryoid variant of ERMS, which occurs in 5% of patients; alveolar RMS, which occurs in 20% of patients; and undifferentiated sarcoma, which occurs in 20% of patients [106]. Although RMS is believed to arise from primitive muscle cells, tumors can occur anywhere in the body except the bone. The most common sites are the head and neck (28%), extremities (24%), and genitourinary (GU) tract (18%). Other notable sites include the trunk (11%), orbit (7%), and retroperitoneum (6%). Treatment responses and prognoses vary depending on tumor location and histology.

In patients with localized disease, overall 5-year survival rates have improved to more than 80% with the combined use of surgery, radiation, and chemotherapy [107]. Approximately 15% of patients present with metastatic disease, and the overall cure rate for these patients is below

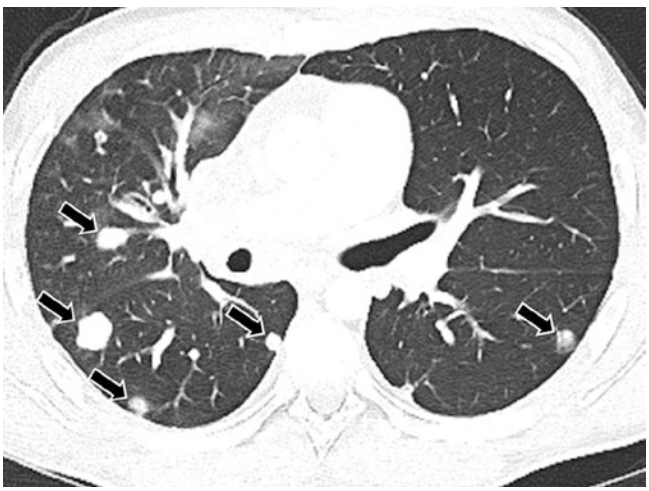

Fig. 15.10 A 13-year-old boy with right femoral osteosarcoma. Axial lung window CT image shows multiple pulmonary nodules (*arrows*) consistent with metastatic disease

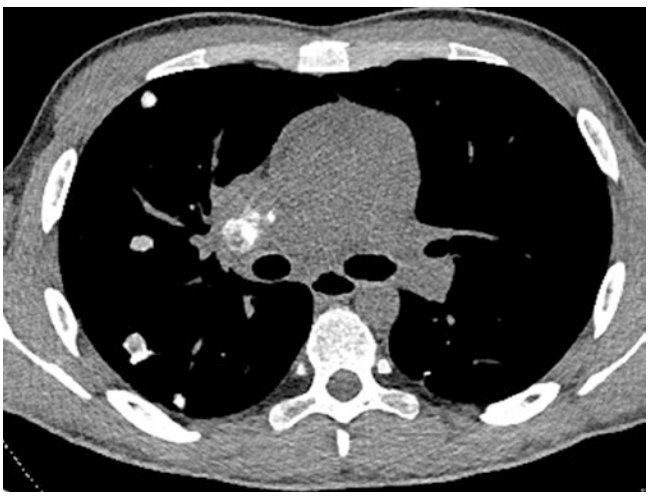

Fig. 15.11 A 16-year-old boy with metastatic osteosarcoma. Axial CT image demonstrates multiple calcified pulmonary nodules

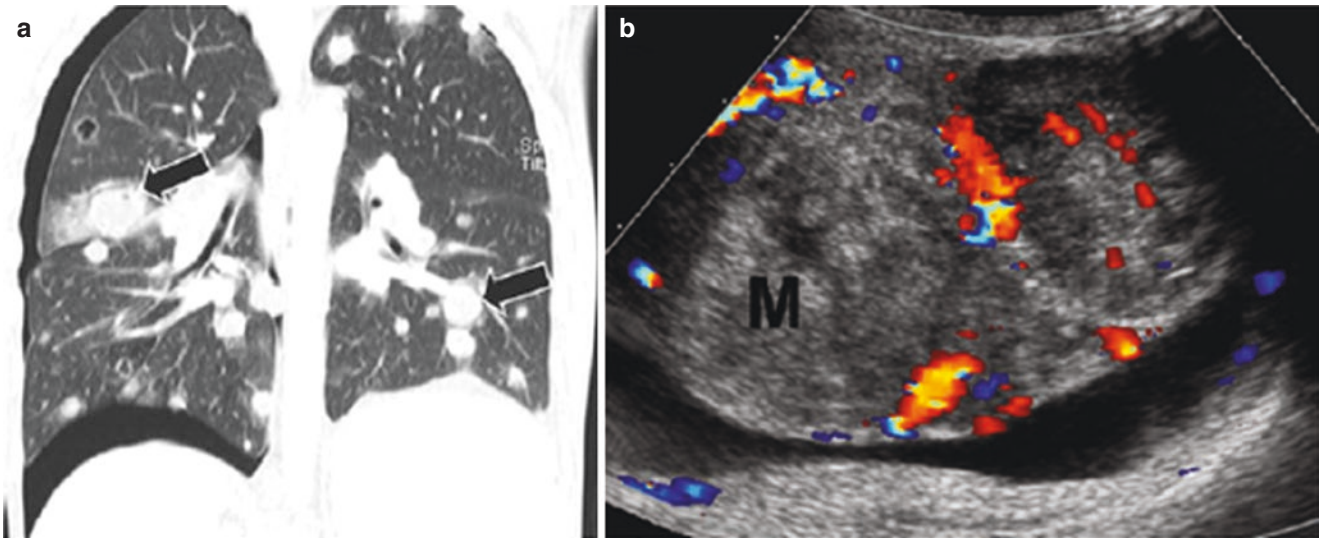

Fig. 15.12 A 12-year-old boy who presented with shortness of breath and enlarged scrotum on physical examination. Surgical pathology was consistent with testicular neoplasm. (**a**) Coronal lung window CT image shows multiple pulmonary masses (*arrows*). Also noted is a right-sided pneumothorax. (**b**) Transverse view of Doppler ultrasound of right testicle shows heterogeneous intratesticular mass (M)

30%. If metastatic disease is present, symptoms of bone pain, respiratory distress secondary to lung nodules, anemia, thrombocytopenia, and neutropenia may all be present. Currently, there is no standard role for metastasectomy.

Event-free survival (EFS) was found to correlate with certain risk factors: age less than 1 year or at least 10 years, unfavorable site of primary tumor (extremity), bone or bone marrow involvement, and three or more metastatic sites. EFS is 50% for patients without any of these four adverse factors and was, respectively, 42%, 18%, 12%, and 5% in patients with one, two, three, or four risk factors [108].

Synovial Sarcoma

Synovial sarcomas represent 5%–10% of all soft tissue sarcomas [108], which are rare tumors of connective tissue. Despite the name, synovial sarcomas are not thought to originate from the joint, but instead occur nearby. This lesion tends to affect young individuals within the age range of 15–40 and is divided into three histological types: biphasic, monophasic, and poorly differentiated [109]. Half of all patients develop metastatic disease with the lungs being the most common location [110, 111]. In one series [109], 74% of patients had developed metastatic disease by 5 years and 81% by 10 years. The median survival following a diagnosis of metastatic disease was 22 months. Prognostic factors correlate with an age less than 35 and response to first-line chemotherapy. There was no evidence that metastasectomy improved survival.

Germ Cell Tumors

Testicular cancer is the most common neoplasm in males under the age of 40 [112]. It constitutes about 2% of all malignancies, and 95% of all testicular tumors are of germ cell origin [113]. At the time of diagnosis, it is estimated that pulmonary metastases are present in 50% of patients with retroperitoneal involvement as opposed to only 10% of patients without retroperitoneal extension (Fig. 15.12) [114]. Germ cell tumors are chemosensitive lesions with a long-term survival rate of 90% [115]. Forty percent of patients harbor viable tumor cells within radiographically visible lesions post-therapy [115–119]. Therefore, the role of pulmonary metastasectomy is primarily to define the presence of viable tumor in lesions after chemotherapy and for determining further treatment regimens.

Pediatric Central Airway Neoplasms

Central airway tumors are rare in the pediatric population and often misdiagnosed leading to a delay in definitive treatment [1, 2]. Affected pediatric patients are symptomatic due to airway obstruction and present with common complaints such as cough, stridor, wheeze, recurrent pneumonia, or persistent atelectasis. Imaging is often not performed until it becomes evident that standard therapies are ineffective. Bronchoscopy can be useful for diagnosis of central airway neoplasms as it allows for direct visualization of the tumor. A biopsy of the lesion may provide a definitive diagnosis; however, the true extent of the tumor is often difficult to appreciate. Therefore, CT may be needed in conjunction with bronchoscopy.

Benign tumors occur more frequently in the larynx or upper trachea, while malignant tumors occur more distally [1, 2]. The most common benign tumors of the central airways are hemangiomas and papillomas in the pediatric population. Other benign central airway tumors include

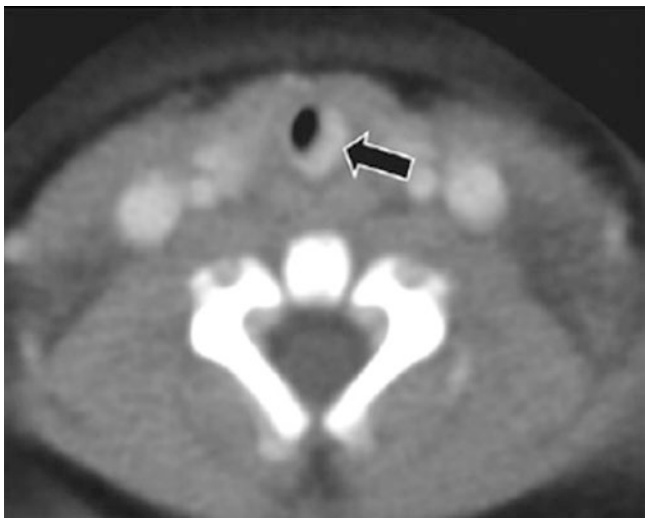

Fig. 15.13 A 2-month-old girl who presented with increasing respiratory distress. Enhanced axial CT examination shows markedly enhancing subglottic lesion (*arrow*), consistent with subglottic hemangioma

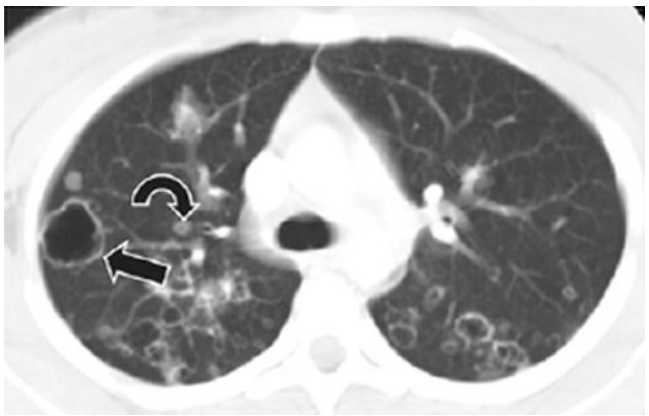

Fig. 15.14 A 17-year-old boy with known papillomatosis. Axial lung window CT image shows a combination of cavitary (*arrow*) and non-cavitary (*curved arrow*) nodules in both lungs

granular cell tumors, hamartomas, plasma cell granulomas, leiomyomas, and mucous gland tumors. Malignant central airway tumors in children include bronchial adenomas, a group of malignant tumors consisting of carcinoid tumor, mucoepidermoid carcinoma, and adenoid cystic carcinoma.

Benign Tumors

Hemangioma

Although airway hemangiomas are present at birth, symptoms usually develop between 1 and 6 months of age [120, 121]. Lesions are most often found in the subglottic area and present with symptoms of obstruction or recurrent hemoptysis. Hemangiomas appear as rounded soft tissue masses on CT with marked contrast enhancement (Fig. 15.13). Symptomatic pediatric patients can be treated with laser removal.

Papilloma

Recurrent respiratory papillomatosis (RRP) is a benign lesion of the larynx and trachea caused by human papillomavirus (HPV), usually types 6 and 11. RRP is the most common benign neoplasm of the larynx among children and the second most frequent cause of hoarseness in childhood [1, 2, 122]. The incidence in children is estimated at 4.3 cases per 100,000 persons. It is typically acquired during delivery through the birth canal and most commonly affects the larynx and trachea. However, in some cases, the distal bronchial tree and esophagus can be involved. Spread into the distal trachea and the lung parenchyma rarely occurs; however, if extension does occur, solid nodules or cystic air-filled cavities are seen (Fig. 15.14). As the papilloma grows, the airway becomes more obstructed leading to changes in a patient's voice or stridor which may progress from inspiratory to biphasic. The age of presentation is variable, but commonly occurs in patients between 2 and 3 years of age [1, 2, 122]. Papillomas of the larynx do not become symptomatic prior to 6 months of age.

Typical imaging findings of RRP are endotracheal or endobronchial lesions with pulmonary nodules or lobulated masses that enlarge and cavitate over time. The differential diagnosis includes asthma, croup, allergies, vocal cord nodules, and bronchitis. Diagnosis is made by flexible laryngoscopy in the office or rigid bronchoscopy in the operating room. Although considered a benign lesion, progression to squamous cell carcinoma has been reported. Therefore, it is essential to biopsy the lesion at the time of surgical excision.

Treatment consists of excision by a carbon dioxide laser. Younger age at diagnosis is associated with more aggressive disease and the need for more frequent surgical procedures to decrease the airway burden. Children may require surgical excision as frequently as every 2–4 weeks due to recurrence until the disease becomes quiescent in adolescence. There is currently no known effective medical adjuvant therapy.

Granular Cell Tumor

Granular cell tumors are uncommon benign lesions, although there are case reports of these tumors behaving in a malignant fashion. This entity has been described in patients as young as 6 months of age, with a median age of 31 years [123]. Granular cell tumors are often asymptomatic, thus can be present for up to 3 years before being diagnosed. Most cases are managed by bronchoscopic excision, but recurrent pneumonia has occasionally necessitated radical lobectomy or pneumonectomy (Fig. 15.15) [124].

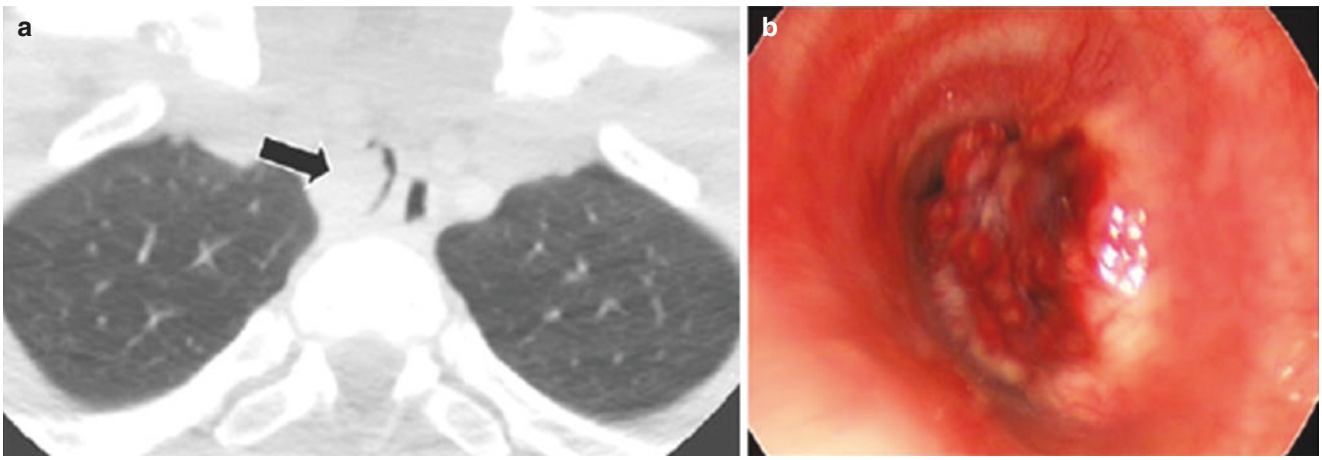

Fig. 15.15 A 5-year-old boy who presented with progressively worsening shortness of breath. (**a**) Axial lung window CT image demonstrates a large intratracheal mass (*arrow*) almost completely obstructing the trachea. (**b**) Bronchoscopy image shows a large lobulated intratracheal mass diagnosed as a granular cell tumor

Malignant Tumors

Bronchial Adenoma

Bronchial adenoma is a misnomer as this refers to a group of malignant lesions found in the airway. The most common tumors in this group are carcinoid tumors, mucoepidermoid carcinomas, and adenoid cystic carcinomas in decreasing order of frequency. The overall incidence is unknown, but bronchial adenomas may account for 5% of all primary pulmonary neoplasms in children [125]. However, they are the largest group (40%) of primary malignant lung lesions in the pediatric population [27, 46].

Carcinoid Tumor

Bronchial carcinoid tumors are characterized by neuroendocrine differentiation and a relatively indolent clinical course. Originally characterized as an adenoma, they are now classified as malignant tumors due to their potential to metastasize. Bronchial carcinoids are the most common primary malignant lung neoplasm in children and typically present in late adolescence. The incidence ranges from 0.2 to 2/100,000 population per year. The majority of carcinoid tumors arise in the proximal airways, and patients are symptomatic at presentation. The obstructive lesion manifests as cough, wheeze, chest pain, recurrent pneumonia, atelectasis, and even hemoptysis due to its hypervascularity. About 25% of carcinoid tumors originate peripherally and are detected on routine CXR. Pediatric patients with peripheral carcinoids are usually asymptomatic, which leads to a delay in diagnosis. Although bronchial carcinoids have the potential to metastasize, they rarely do so. In localized disease, carcinoid syndrome rarely occurs and only does so in tumors of larger size (>5 cm) [126]. However, carcinoid syndrome occurs in over 80% of patients with liver metastasis.

There are two types of bronchial carcinoids, and they are defined by their histological appearance. Typical carcinoids (90%) are low-grade, slow-growing neoplasms that rarely metastasize and have a more favorable prognosis. Atypical carcinoids (10%) are higher-grade lesions, present more often with hilar or mediastinal nodal metastases, and have a higher recurrence rate. Between 5% and 20% of typical carcinoids metastasize to lymph nodes compared to 30–70% of atypical lesions [127].

Diagnosis of a carcinoid tumor can be suggested by CXR and CT and then confirmed by bronchoscopy and biopsy (Fig. 15.16). Up to 75% of patients with a bronchial carcinoid have an abnormal CXR. CT is more sensitive and frequently shows marked enhancement of the lesion due to its hypervascularity. Treatment is primarily surgical; however, endoscopic resection is not recommended due to the risk of hemorrhage and incomplete resection. Local invasion or distant metastases have been reported in 27% of children, but overall survival is excellent and estimated to be approximately 90% [128, 129]. The 5-year survival rates for local, regional, and disseminated disease are 81%, 77%, and 26%, respectively [130].

Mucoepidermoid Carcinoma

Mucoepidermoid tumor (MET) is another "bronchial adenoma." These tumors typically arise from bronchial mucous glands in the main stem bronchus or in the proximal portion of lobar bronchi as an endobronchial polypoid growth covered by normal epithelium [131]. The true incidence is unknown, but the tumor is quite rare and usually presents with signs of obstruction such as cough, dyspnea, wheeze, hemoptysis, or obstructive pneumonia. CXR is usually abnormal showing a central mass or a nodule in 66% of cases (Fig. 15.17) [131]. Diagnosis is made most often by endobronchial biopsy. MET is classified as either low or high

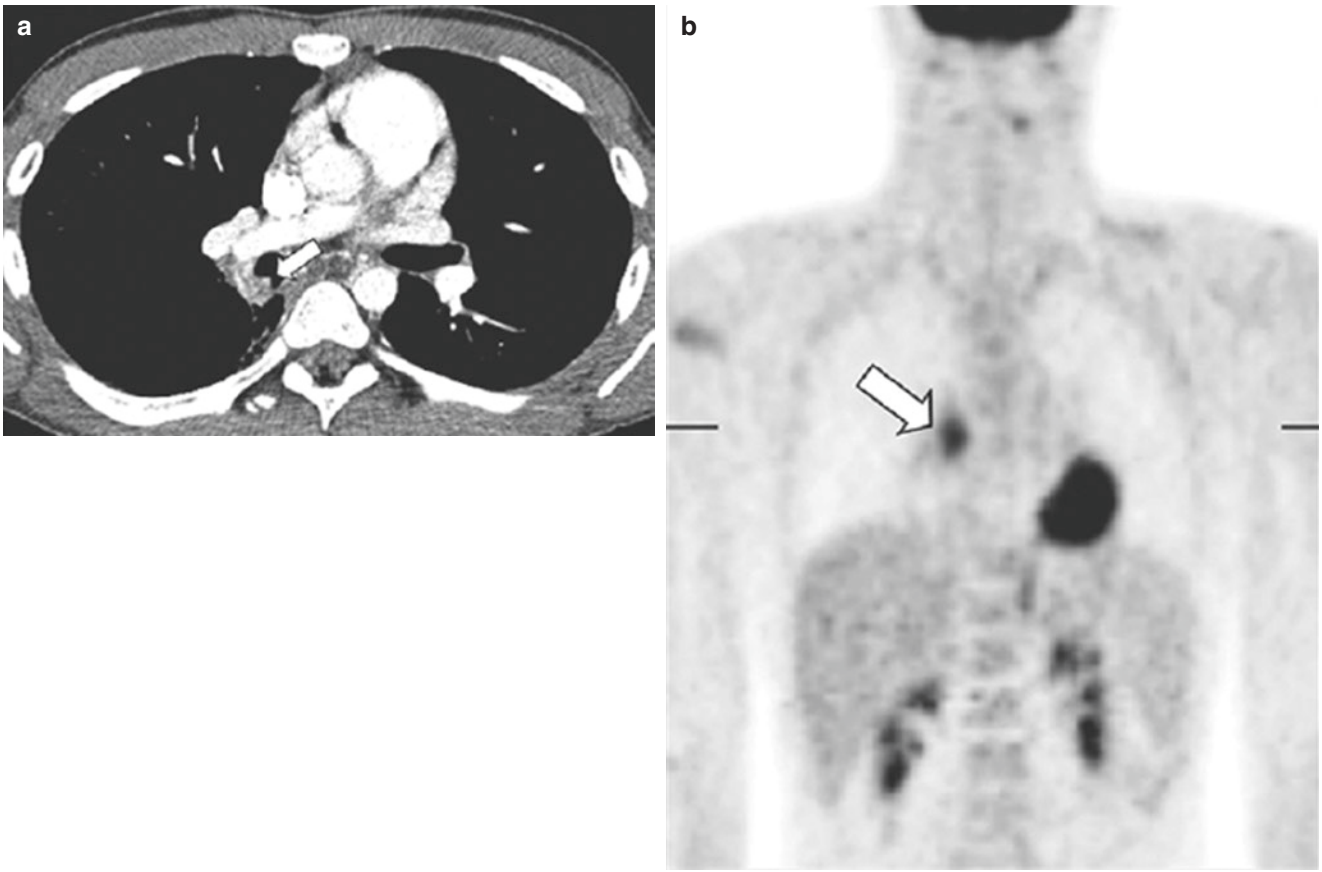

Fig. 15.16 A 15-year-old boy who presented with cough and one episode of hemoptysis. (**a**) Enhanced axial CT image demonstrates a heterogeneously enhancing endoluminal mass (*arrow*) in the proximal right lower lobe bronchus. (**b**) Coronal PET image shows an abnormal focus of uptake adjacent to the mediastinum in the right chest correlating with the site of the endobronchial mass seen in (**a**). Histologic diagnosis was carcinoid tumor

grade based on the histological appearance [132]. Low-grade tumors are mostly cystic and tend not to have local invasion into the parenchyma, and metastasis to lymph nodes is unusual. High-grade tumors have more solid areas of growth. Mitotic activity and necrosis are common in high-grade lesions and metastases to regional lymph nodes [133]. Low-grade tumors occur in patients younger than 30 years of age over 50% of the time, whereas high-grade tumors are more common in an older population [134]. Treatment is surgical resection. Low-grade METs have an excellent prognosis with a 5-year survival rate around 80%. However, high-grade tumors carry a significantly worse prognosis with 5-year survival rates as low as 31%. Survival seems to correlate with lymph node metastasis [133].

Adenoid Cystic Carcinoma

Adenoid cystic carcinoma is the last major tumor classified as a bronchial adenoma. It is a slow-growing, infiltrative, salivary gland-like tumor. It is rare in the pediatric population but has been reported in adolescents. There is often a long interval between onset of symptoms and diagnosis as the CXR is often negative. One series found a mean duration of symptoms before diagnosis to be 15 months. The most common presenting symptoms are shortness of breath, wheeze, cough, stridor, and hemoptysis [135]. This tends to be a locally invasive tumor that extends beyond the wall of the trachea, and it is often difficult to safely extend the surgical resection far enough to obtain tumor-free margins at the transected ends of the airway. Local recurrence may occur years after resection.

Adenoid cystic carcinoma has a higher likelihood of distant metastasis compared with MET and has a poorer prognosis. Hematogenous metastasis occur in over half of the patients, most often to the lungs, and rarely to the lymphatics. However, most patients do not have evidence of metastasis at the time of initial diagnosis. In fact, metastasis often occurs years after the diagnosis of the primary tumor. Treatment consists of both surgery and radiation. Many cases are amenable to segmental resection of the airway with removal of all gross disease and reconstruction by primary anastomosis. Most tumors respond to radiation, which may

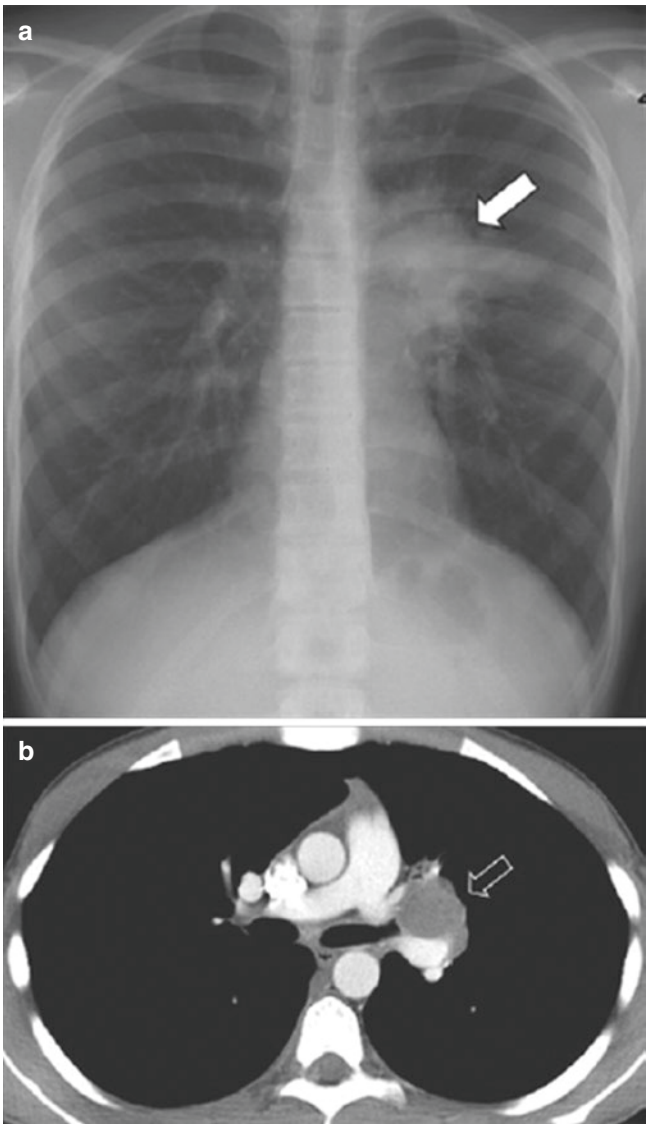

Fig. 15.17 An 11-year-old boy who presented with respiratory distress. Surgical pathology of the left hilar mass was consistent with mucoepidermoid carcinoma. (**a**) Frontal chest radiograph shows a large mass-like opacity (*arrow*) in the left hilar region. (**b**) Enhanced axial CT image demonstrates a mildly enhancing soft tissue mass (*arrow*) located in the left hilar region

be a reasonable adjuvant therapy to offer all patients with adenoid cystic carcinoma and definitely in those patients with residual tumor after surgical resection [135].

Pediatric Chest Wall Neoplasms

Benign chest wall tumors are uncommon lesions that originate from the blood vessels, nerves, bone, cartilage, or fat. Although radiologic characteristics of benign and malignant chest wall tumors often overlap, there are certain features that can suggest a specific diagnosis. Such features include the presence of mature fat tissue with little or no septation (lipoma), phleboliths and vascular enhancement (cavernous hemangioma), evidence of neural origin combined with a target-like appearance on MRI (neurofibroma), well-defined continuity of cortical and medullary bone with the site of origin (osteochondroma), or fusiform expansion and ground-glass matrix (fibrous dysplasia) [136].

Chest wall tumors are uncommon in the pediatric population, but when they do occur, they are usually malignant. Chest wall tumors typically present as a rapidly growing, palpable mass which may cause pain and respiratory distress. CXR is part of the initial evaluation, but most often a CT or even an MRI is required. CT is more sensitive than CXR for detecting calcification and cortical destruction. MRI can further characterize the soft tissue component of the tumor burden and help determine the extent of tumor invasion. Imaging techniques can often help to narrow the differential, but an incisional biopsy is often necessary because many of these lesions are malignant in nature. Malignant chest wall tumors are classified into eight diagnostic categories: muscular, vascular, fibrous and fibrohistiocytic, peripheral nerve, osseous and cartilaginous, adipose, hematologic, and cutaneous.

Osseous Neoplasms

Benign Tumors

Fibrous Dysplasia Fibrous dysplasia of the bone is a skeletal developmental anomaly in which mesenchymal osteoblasts fail to undergo normal morphologic differentiation and maturation [137]. Affected patients are most often asymptomatic but may present with pain from a pathologic fracture due to a weakened bone. Fifty percent of patients with fibrous dysplasia have a fracture [138]. Asymptomatic patients can be observed, whereas surgery is indicated for prevention or treatment of fractures or major deformities.

Osteochondroma Osteochondromas are the most common benign bone tumors. They are cartilage-capped bony projections on the external surface of a bone (Fig. 15.18). Whether sessile or pedunculated, the medullary canal of the stalk and the bone are in continuity by definition. Osteochondromas grow until skeletal maturity; growth generally stops once the growth plates fuse [139]. Most are diagnosed in patients younger than 20 years of age, usually as an incidental finding on CXR obtained for other reasons. The second most common presentation of osteochondroma is a palpable mass, which may or may not be associated with pain. Most of these lesions do not need to be treated, and asymptomatic lesions

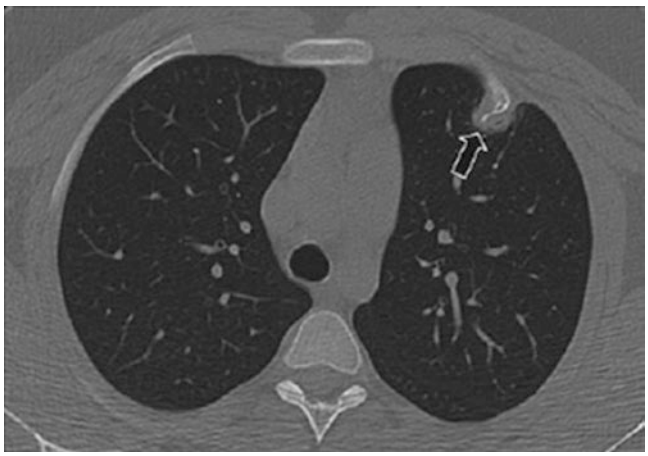

Fig. 15.18 A 17-year-old girl who presented with left chest pain. Axial bone window CT image demonstrates a cartilage-capped bony projection (*arrow*) arising from the inner surface of the left rib, consistent with osteochondroma

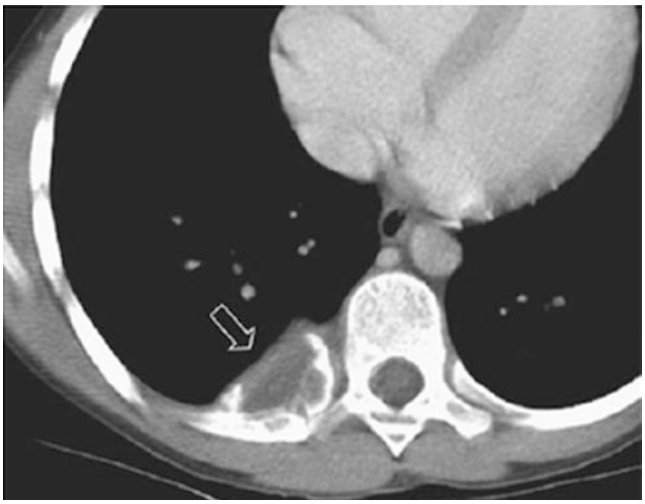

Fig. 15.19 A 12-year-old boy who presented with right lower thoracic pain. Enhanced axial CT image shows a mass (*arrow*) composed of both soft tissue and osseous components. Surgical pathology of this mass was consistent with osteosarcoma

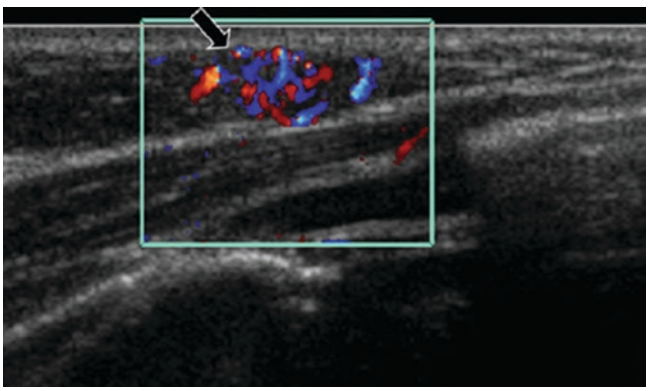

Fig. 15.20 A 2-year-old girl who presented with a palpable right-sided chest wall lesion. Ultrasound shows a subcutaneous soft tissue mass (*arrow*) with increased internal vascularity, consistent with hemangioma

can be safely ignored. However, when painful, they need to be evaluated properly. Complications include fractures, osseous deformity, vascular injury, neural compression, and malignant transformation. Pain at the lesion site, bone erosion, irregular calcification, or thickening of the cartilage cap depicted on radiographic imaging can indicate malignant transformation [137].

Malignant Tumors

Osteosarcoma Osteosarcomas in the thorax are rare and are usually osseous in origin. They tend to occur in the second and third decades of life and present as a painful mass. Sites of origin include ribs, scapula, and the clavicle (Fig. 15.19). Local recurrence and metastatic spread (up to 70% of patients) to the lungs and lymph nodes occur more frequently in osteosarcomas of the chest wall compared to those in the extremities. Treatment consists of preoperative chemotherapy followed by resection. Five-year survival rates are approximately 15% compared with osteosarcomas in the extremities which can reach 60–70%.

Ewing's Sarcoma Ewing sarcomas are associated with a chromosome 22 translocation and are composed of small round cells [140]. The Ewing sarcoma family of tumors includes Ewing sarcoma, peripheral primitive neuroectodermal tumor (PNET)/Askin tumor, neuroepithelioma, and atypical Ewing sarcoma. These tumors are treated similarly on the basis of their clinical presentation (e.g., metastatic or localized) rather than their histologic subtype. Tumors that arise in the chest wall usually do so from the rib or less commonly the scapula and account for 15% of Ewing sarcomas [141]. This is the most common tumor of the chest wall in children and young adults and usually presents as a painful chest mass. Treatment consists of chemotherapy followed by resection with or without radiation. Prognosis is determined by metastases which occur in 75% of patients. Five-year survival rates are less than 30% with metastatic involvement but can approach 100% with localized disease [141].

Soft Tissue Neoplasms

Benign Tumors

Hemangioma Cavernous hemangiomas consist of dilated, tortuous, thin-walled vessels. They are most often large cutaneous lesions which are poorly circumscribed (Fig. 15.20). These benign chest wall masses are either present at birth or appear before the age of 30.

Lipoma Lipomas are common benign mesenchymal tumors occurring in 1% of the population and are usually asymptomatic. They are slow-growing, benign fatty tumors that form soft, lobulated masses enclosed by a thin, fibrous capsule. Lipomas must be differentiated from other masses

or tumors. In the subcutaneous location, the primary differential diagnosis is a sebaceous cyst or an abscess. When they arise from fatty tissue between the skin and deep fascia, typical features include a soft, fluctuant feel, and free mobility of overlying skin. A characteristic *slippage sign* may be elicited by gently sliding the fingers off the edge of the tumor. The tumor will be felt to slip out from under your fingers, as opposed to a sebaceous cyst or an abscess that is tethered by surrounding induration. The overlying skin is typically normal. Most of lipomas are small subcutaneous tumors that are removed for the following reasons: (1) cosmetic reasons (>5 cm in size), (2) continuous growth resulting in symptoms, and (3) evaluation of their underlying histology.

Malignant Tumors

Rhabdomyosarcoma Primary thoracic sarcomas are rare and are classified by histological features. They occur in the lung, mediastinum, pleura, and chest wall. These tumors are large, heterogeneous masses that have a wide spectrum of radiologic appearances. Angiosarcoma, leiomyosarcoma, RMS, and mesothelioma are the four most common primary intrathoracic tumors [140]. RMSs are high-grade sarcomas characterized by skeletal muscle differentiation. Pulmonary RMS is more common in pediatric patients and represents approximately 0.5% of all RMSs in children [46]. It is the most common cardiac sarcoma in children.

RMS in the chest wall typically manifests as rapidly growing masses and may cause pain due to nerve compression (Fig. 15.21). Primary tumors invade the bone up to 20% of the time. The alveolar subtype is the most common and carries the worst prognosis, while the embryonal subtype typically occurs in children.

Pulmonary lesions tend to present with cough and dyspnea, whereas chest wall tumors present with pain. The mass is usually large on imaging studies with necrotic and cystic components. Focal invasion is common and treatment consists of chemotherapy. The prognosis is related to the histological subtype with embryonal and pleomorphic subtypes having a better prognosis than the alveolar RMS [142]. Well-differentiated tumors have the best prognosis, and survival may be greater than 80% if the tumor is localized [140].

Primitive Neuroectodermal Tumor (Askin Tumor) The Askin tumor is a rare, malignant small-cell neuroepithelioma that arises from the soft tissues of the chest wall or lung and is seen predominantly in children and young adults [143]. This neoplasm is now recognized as a type of PNET. They are undifferentiated small-round-cell sarcomas which develop from embryonal migrating cells of the neural crest. The Askin tumor must be differentiated from other tumors that have small round cells, such as undifferentiated neuroblastoma, ERMS, Ewing's sarcoma, and lymphoma [144]. Both Ewing's sarcoma and PNET carry the (11;22) translocation, but neurosecretory granules on electron microscopic examination are seen in the latter [143, 145, 146]. Clinically, the Askin tumor presents as a chest wall mass with or without pain. Rapid growth may result in destruction of adjacent anatomic structures [143], with bone destruction being the most common complication. Metastatic disease at presentation has been reported to range from 10% [143, 147, 148] to 38% [149]. MRI is useful in determining involvement of the chest wall muscle, whereas CT is better for detecting pulmonary metastases. Treatment consists of chemotherapy, surgery, and radiation. This tumor has a tendency to recur locally with direct extension into the pleura and lung or to develop pulmonary nodules [150]. This is a sign of initial treatment failure. One series showed a disease-free survival rate of 56% after 3 years for patients with localized PNET, whereas no curative approach seems available for patients with metastatic disease [151].

Pediatric Malignant Mediastinal Neoplasms

Malignant mediastinal masses are relatively uncommon in the pediatric population. Due to their rarity and often nonspecific clinical presentations, the correct diagnosis is unfortunately often initially missed or delayed in children. While these malignant mediastinal masses may be incidental findings in some children, they can also result in various symptoms depending on their size, location, mass effect upon adjacent mediastinal structures, and production of specific biochemical products. Imaging plays an important role for early and correct diagnosis, which in turn can improve patient care by guiding the next appropriate step in management [152–154]. In this section, we discuss malignant mediastinal masses in pediatric patients with an emphasis on reviewing (1) clinical presentation, (2) practical imaging approaches to diagnosis, and (3) radiological imaging findings.

Clinical Presentations of Malignant Mediastinal Masses in Pediatric Patients

Various clinical presentations may lead to the suspicion and detection of a mediastinal malignant neoplasm in pediatric patients. Often, tumors are incidentally found when a patient undergoes an imaging study for some other unrelated complaint. However, approximately one-half to two-thirds of mediastinal masses in children are symptomatic [152–156]. Clinical signs and symptoms with which patients present depend on the benignity or malignancy of the mass, its size, location, presence or absence of infection, production of specific biochemical products, and associated disease states [152–156]. When symptomatic, malignant mediastinal masses in children often present with lethargy, fever, and chest pain [152–156]. In affected infants and children, respi-

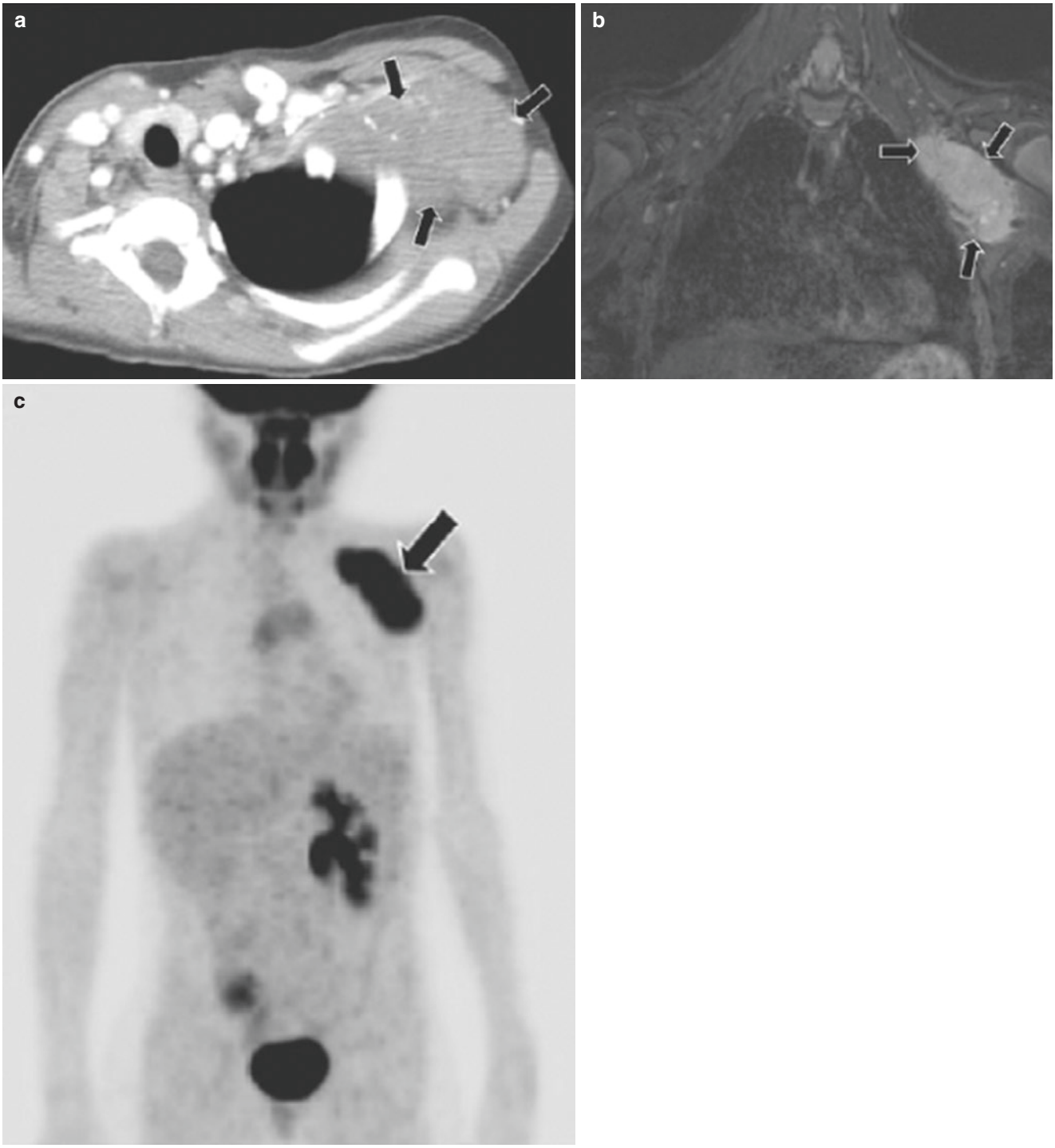

Fig. 15.21 A 6-year-old girl who presented with left chest and arm pain. Surgical pathology of the left chest wall mass was consistent with rhabdomyosarcoma (RMS). (**a**) Enhanced axial CT image shows a large heterogeneously enhancing mass (*arrows*) located in the left upper chest wall. (**b**) Coronal STIR MR image demonstrates a large left upper chest wall mass (*arrows*) with increased MR signal intensity. (**c**) Coronal PET image shows abnormally increased uptake (*arrow*) in the left chest wall area corresponding well with a large mass seen on CT (**a**) and MR (**b**) images

ratory symptoms such as dyspnea, cough, and stridor are common, particularly when there is an associated mass effect upon adjacent airways resulting in airway compression [152, 156]. Common diagnoses of these symptoms in children such as infection, reactive small airway disease, gastroesophageal reflux, and foreign body aspiration should first be carefully considered and evaluated, since mediastinal tumors are relatively rare compared with other more common causes.

When a malignant mediastinal neoplasm is present, invasion of adjacent structures such as the chest wall, pleura, and nerves can be also seen. Specific findings of chest pain, pleural effusion, hoarseness, Horner's syndrome (miosis, ptosis, and anhidrosis), superior vena cava syndrome, paraplegia, and diaphragmatic paralysis may occur. Constitutional symptoms such as weight loss and fever may also be present [152–156]. The onset of mediastinal malignancy may be slow and insidious. The initial physical finding may be enlarged lymph nodes in the neck or supraclavicular region. Although imaging evaluation is paramount in devising a diagnostic and therapeutic plan, tissue sampling is typically required for a definitive diagnosis for most malignant mediastinal masses in the pediatric population.

Practical Imaging Approach for Diagnosing Malignant Mediastinal Masses in Pediatric Patients

For diagnosing suspected malignant mediastinal masses on imaging, the first step is to localize the mass in three artificially divided mediastinal compartments (i.e., anterior, middle, or posterior mediastinal compartment) on the lateral CXR (Fig. 15.22). The anterior mediastinal compartment is defined by the space bordered anteriorly by the sternum and posteriorly by the pericardium [157–160]. The middle mediastinal compartment is located between the anterior border of the pericardium and an imaginary line drawn approximately 1 cm posterior to the anterior border of the thoracic vertebral bodies [157–160]. The posterior mediastinal compartment is defined as the space bordered anteriorly by an imaginary line drawn approximately 1 cm posterior to the anterior border of the vertebral bodies and posteriorly by the posterior paravertebral gutters [157–160]. Localizing the mediastinal masses in these three mediastinal compartments helps to generate possible diagnostic considerations and narrow them. Furthermore, it also helps in guiding the next appropriate imaging studies for further characterization of mediastinal masses for a correct diagnosis.

CXR is usually the first imaging modality used to determine the presence of a malignant mediastinal mass [156]. While CXR often demonstrates mediastinal masses with a reasonably high degree of accuracy, they are limited in their capacity to establish a specific diagnosis [156]. After a mediastinal mass has been identified and localized on the lateral chest radiograph, cross-sectional imaging such as CT or MRI can help confirm its location and further characterize the mass. CT is excellent for accurately diagnosing the nature, size, location, and organ involvement by mediastinal masses due to its high temporal and spatial resolution [156].

While CT is most often used in mediastinal mass assessment due to its wide availability and its ability to concomitantly assess airway and lung abnormalities, MRI can also provide important information. With its high contrast resolution and multiplanar capabilities, MR is the preferred modality in evaluating neurogenic tumors because it provides information regarding the nature and extent of intraspinal involvement from malignant mediastinal neoplasms. MRI can also help to characterize lesions as cystic or solid with more confidence than CT [156, 161, 162]. In pediatric patients with contraindications to iodinated contrast material, MR is a particularly useful alternative imaging modality to CT. The most important advantage of MR is the lack of ionizing radiation during image acquisition, an important consideration in pediatric patients. A disadvantage of MR, however, is the poor depiction of calcification, poorer spatial resolution, susceptibility to motion artifact, and longer scanning time often requiring sedation when compared to CT [155, 156,

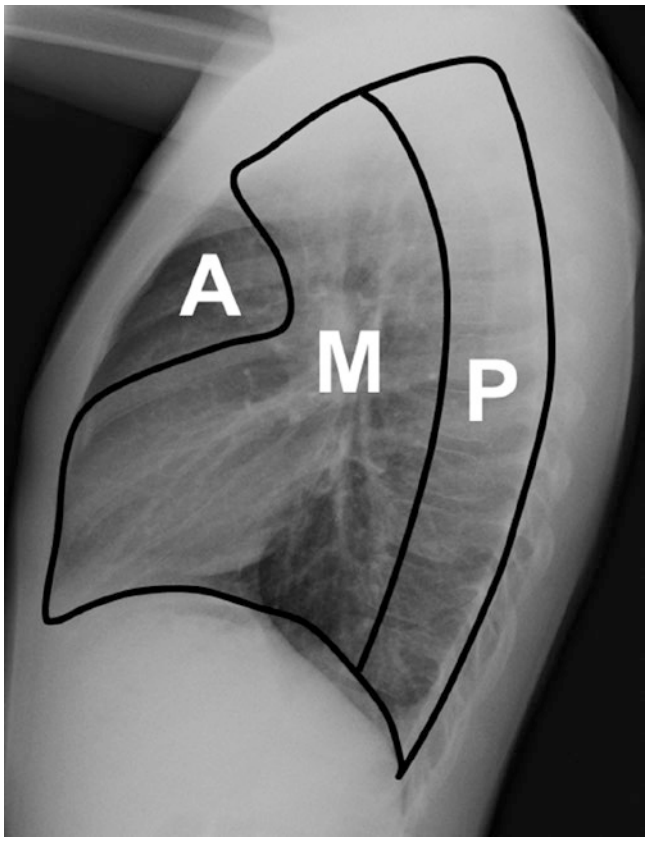

Fig. 15.22 Lateral chest radiograph depicting the three mediastinal compartments, anterior (A), middle (M), and posterior (P). The anterior mediastinal compartment is the space bordered anteriorly by the sternum and posteriorly by the pericardium. The middle mediastinal compartment is the space between the anterior border of the pericardium and an imaginary line drawn approximately 1 cm posterior to the anterior border of the thoracic vertebral bodies. The posterior mediastinal compartment is the space bordered anteriorly by an imaginary line drawn approximately 1 cm posterior to the anterior border of the vertebral bodies and posteriorly by the posterior paravertebral gutters

158, 163]. For MR, general anesthesia may be required in younger or cognitively impaired children to avoid motion artifact.

Of relevance for both CT and MR, when there is a large anterior mediastinal mass, there may be accentuated compression of the trachea when the patient is supine. This may be severe enough to cause physiologically significant airway obstruction which is not present if the patient is not supine. In this instance, it may be necessary to treat the disease and shrink the mass before performing cross-sectional imaging.

Anterior Mediastinal Compartment Masses

Lymphoma (Hodgkin and Non-Hodgkin)

Lymphoma is the most common anterior mediastinal mass in children and is traditionally classified into two types: Hodgkin and non-Hodgkin [154–156, 162–164]. Hodgkin lymphoma represents about 5% of cases, while non-Hodgkin lymphoma (NHL) accounts for the remaining 95% of mediastinal lymphoma in pediatric patients [165, 166]. Lymphadenopathy from lymphoma may be asymptomatic or cause symptoms such as cough, chest pain, dyspnea, dysphagia, hemoptysis, or superior vena cava syndrome [153–156]. Other more nonspecific symptoms, termed B symptoms, which include fever, weight loss, and night sweats, are more common in aggressive lymphomas [153–156].

Hodgkin lymphoma is histologically characterized by the presence of the Reed–Sternberg cell and has a good prognosis with an approximately 90% cure rate [154, 155, 162, 164]. It is traditionally classified into four types: (1) lymphocytic predominant, (2) nodular sclerosing, (3) mixed cellularity, and (4) lymphocyte depleted [166]. Hodgkin lymphoma often involves the anterior mediastinum, with the thymus reportedly involved in 40–50% of patients with the nodular sclerosing subtype of Hodgkin disease [162]. The Ann Arbor classification is currently the most widely used staging system which is based on the number of nodal sites and the location of lymphoma involvement [166]. Approximately 85% of Hodgkin lymphoma demonstrates intrathoracic involvement at presentation, most commonly involving the anterior superior mediastinal lymph nodes (Fig. 15.23) [154, 155, 162–164, 167]. The lymph nodes rarely calcify before treatment; approximately 5% calcify after treatment [162]. Associated findings, in addition to enlarged lymph nodes or conglomerations of nodes, include multiple pulmonary nodules or multifocal consolidation. Pleural effusions can be seen in approximately 15% of patients of Hodgkin lymphoma [154–156, 161, 164–168]. As is true for other malignancies, lymphoma is tracer avid for ^{18}F-fluorodeoxyglucose (FDG) which is used effectively to determine anatomic extent of disease.

NHL is traditionally classified into two categories based on histology: (1) lymphoblastic and (2) nonlymphoblastic. Nonlymphoblastic is further classified into histiocytic and undifferentiated, of which there are Burkitt and non-Burkitt types [166]. Unlike its adult manifestation, NHL is primarily extranodal in distribution [166]. T-cell-derived NHL is commonly found in the thorax, while the lineage of B-cell NHL usually occurs in the abdomen [166].

While Hodgkin lymphoma typically occurs in the first decade of life, NHL is common in both the first and second decades of life [156]. NHL has multiple manifestations but depends on the bulk of disease and histopathologic diagnosis, with the possibility of low-grade tumors evolving to higher-grade tumors [154, 155, 163, 164, 167]. Approximately, 50% of NHL cases demonstrate intrathoracic involvement [154–156, 161, 165, 168]. The CT appearance of NHL is varied and may demonstrate bulky mediastinal lymphadenopathy or extranodal disease. Involvement of anterior and posterior mediastinal nodes is equally likely, except for large B-cell lymphoma and lymphoblastic, which tend to exclusively involve the anterior mediastinum (Fig. 15.24a). Associated findings of lymphoma within the thorax also include pulmonary nodules, with or without cavitation, as well as airspace consolidation and diffuse interstitial thickening. Pleural involvement may manifest by effusions or pleural masses (Fig. 15.24b) [154–156, 161, 165, 168]. The presence of a large amount of pleural fluid is suggestive of NHL rather than Hodgkin lymphoma. Systemic involvement is typical at the time of diagnosis, obviating the need for radiographic staging. All patients receive chemotherapy, and the prognosis of children with lymphoma is worse if they have bone marrow and central nervous system involvement [166].

CXR of lymphoma usually demonstrate findings of an anterior mediastinal mass with obliteration of the retrosternal clear space and/or mediastinal widening (Fig. 15.23). Since it can be difficult to differentiate an anterior mediastinal mass from the normal thymus in children, the trachea should be carefully inspected, as the normal but prominent thymus does not usually cause mass effect on or displace the trachea. Ultrasound or airway fluoroscopy can also help differentiate the two, as the soft, pliable thymus appears distinct from a nonmobile mediastinal mass. On inspiration, the thymus will appear to shrink as its transverse diameter decreases with increasing lung volume. A pathologic mass does not change in apparent size.

Lymphoma often appears as homogeneous enlargement of the thymus from tumor infiltration on CT. However, larger nodal conglomerates often become heterogeneous from areas of necrosis or cystic change. While MRI is not typically used to evaluate mediastinal lymphoma since CT depicts anatomic extent of disease so well, PET is often used in the initial staging as well as to follow treatment response (Fig. 15.23d) [154–156, 161, 165, 168].

Eighty percent of patients with Hodgkin lymphoma have event-free survival prolonged by treatment regimens [166–168]. The preferred approach to treatment involves combined modalities, which limits toxicity of individual drugs and provides a synergistic effect. Currently both radiation therapy and chemotherapy are the modalities of treatment. Similar therapies are used for NHL, in addition to bone marrow transplantation [169]. With the initial treatment of NHL, there may be a rapid, significant increase in the size of the pleural effusion.

Thymoma

The thymus is normally seen in children up to 3 years of age but may be seen in older children up to 9 years of age [164, 165]. Rebound of the thymus, where there is unusually pronounced enlargement of the thymus following cessation of prolonged physiologic stress (such as treatment of malignancy), may be seen as late as the end of the second decade. The thymus' primary function is maturation of T-lymphocytes. A neoplasm that arises from thymic epithelium, a thymoma contains varying numbers of intermixed lymphocytes [161].

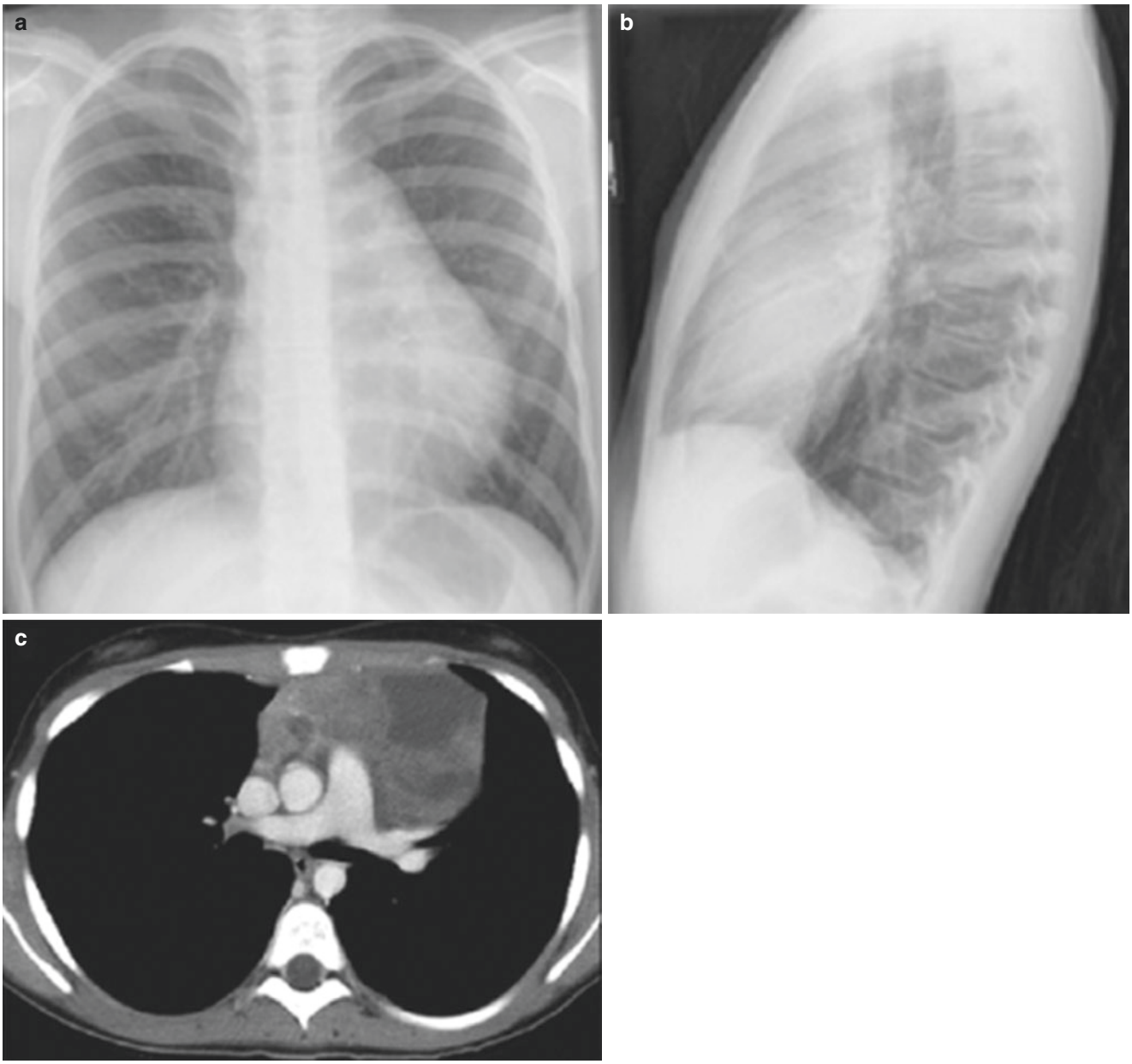

Fig. 15.23 An 11-year-old girl who presented with shortness of breath and weight loss. (**a**) Frontal chest radiograph shows a large mediastinal mass. (**b**) Lateral chest radiograph demonstrates the location of the mediastinal mass to be within the anterior mediastinal compartment. (**c**) Enhanced axial CT image shows a heterogeneously enhancing large anterior mediastinal mass. (**d**) Frontal PET image shows markedly increased FDG uptake in the anterior mediastinal mass and right supraclavicular lymph nodes in this patient with Hodgkin lymphoma

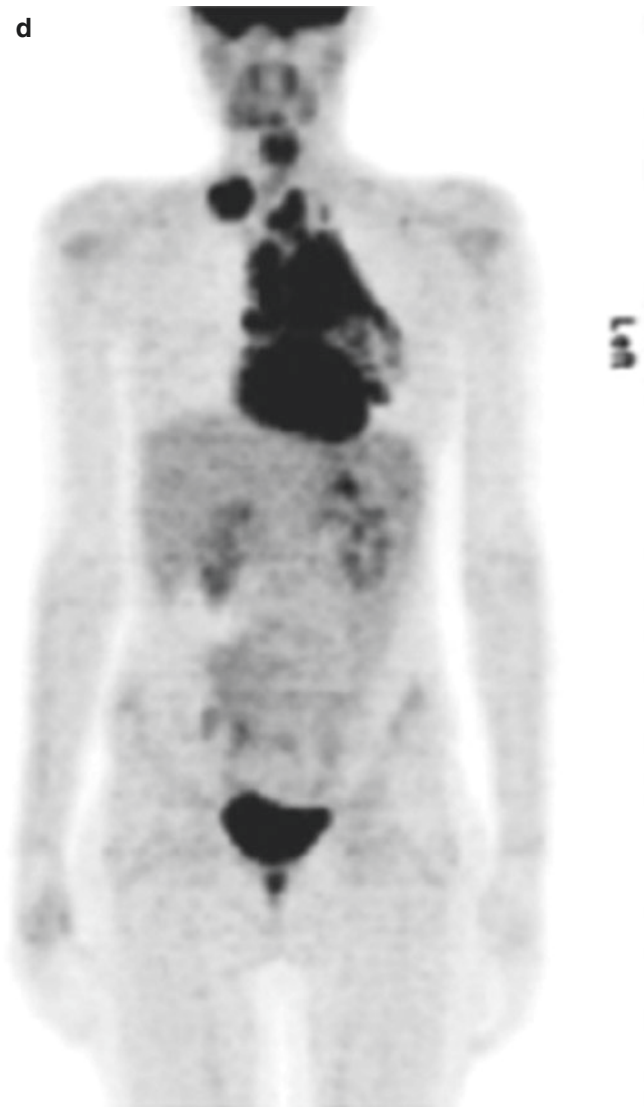

Fig. 15.23 (continued)

The admixture of epithelial cells and lymphocytes, which varies with each tumor, gives rise to the histologic subtyping of thymoma as predominantly lymphocytic, mixed lymphoepithelial, and predominantly epithelial types [161]. In the predominantly lymphocytic form, in which there are few interspersed epithelial tumor cells, the histologic differentiation from lymphoma may be difficult [161].

Thymomas represent approximately 20% of all mediastinal tumors. However, thymomas are quite infrequent in the pediatric population, accounting for approximately 1–2% of mediastinal tumors [160, 163–165]. Thymomas may be discovered incidentally, although approximately 25–30% cause symptoms related to local compression or invasion [154, 170–173]. Approximately 40% of patients with thymomas may present with a paraneoplastic syndrome such as hypogammaglobulinemia, red cell aplasia, or, most commonly, myasthenia gravis [170–174]. Of patients with myasthenia gravis, approximately 10–30% have a thymoma. Approximately 30–35% of patients with a thymoma develop myasthenia [161]. In patients with myasthenia gravis being evaluated for thymoma, CT can demonstrate small tumors that are invisible on CXR [161]. However, very small thymic tumors may not be distinguishable from a normal or hyperplastic gland with CT, particularly in younger patients who have a large amount of residual thymic tissue [161].

Thymomas are typically classified into two different types: (1) noninvasive thymoma and (2) invasive thymoma. Invasive thymoma refers to a thymoma that has invaded its fibrous capsule. Such lesions tend to spread locally, with invasion of adjacent mediastinal structures, as well as the chest wall [173]. In addition, invasive thymomas tend to spread contiguously along the pleural surface, usually unilaterally. Noninvasive thymomas tend to demonstrate well-defined margins on imaging studies, since they have not

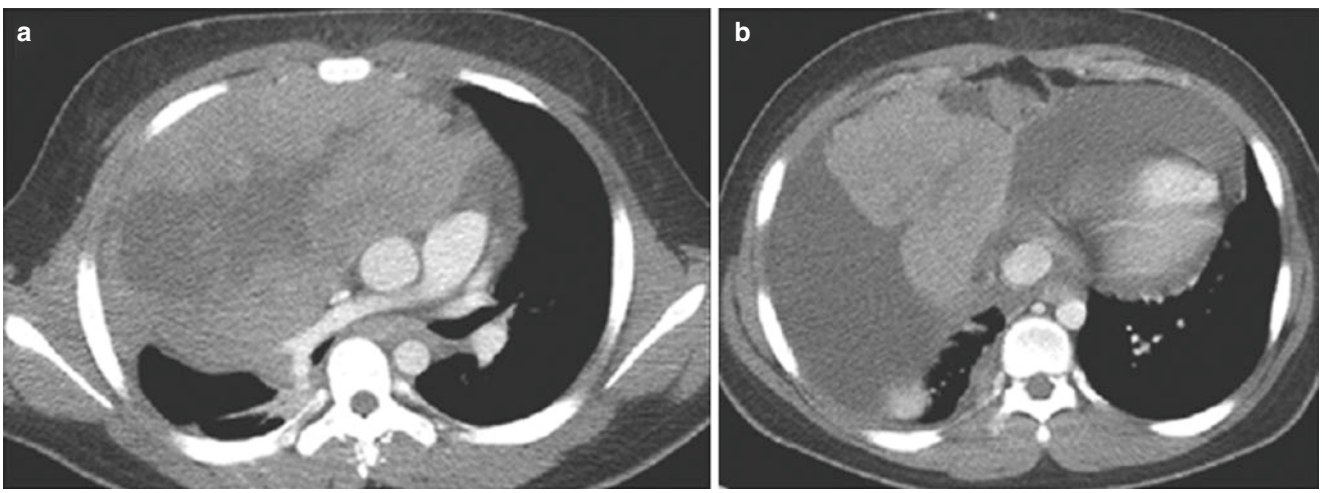

Fig. 15.24 A 15-year-old boy who presented with shortness of breath. (**a**) Enhanced axial CT image demonstrates a large, heterogeneous anterior mediastinal mass with central low density regions consistent with necrosis. (**b**) Enhanced axial CT image more inferiorly in the same patient shows a pleural effusion adjacent to this large mass in this patient with non-Hodgkin lymphoma (NHL)

extended past their fibrous capsules [173]. Because encapsulated and invasive thymomas are histologically the same, the diagnosis of invasive thymoma is based on visualizing gross or microscopic extension through the capsule. Because the capsule needs full evaluation, most thymomas require surgical excision [173, 174]. Therapy for myasthenia graves also includes thymectomy.

On CXR, thymomas most often appear as an oval mass within the mediastinum, usually projecting to one side [173, 174]. They are often seen best on lateral view, obliterating the retrosternal clear space. Invasive thymomas can present with pleural nodules or masses (Fig. 15.25). CT imaging confirms an oval or lobulated-enhancing mass within the anterior mediastinum, some with thin capsular calcification (Fig. 15.26). Cystic regions and necrosis are present in approximately 30%, particularly in larger tumors [161–165]. Signs of invasion include obliteration of mediastinal fat planes surrounding mediastinal vascular structures, pericardial thickening, chest wall, or diaphragmatic and pleural extension [155, 160, 164, 170–174]. MR typically demonstrates high signal intensity on T2-weighted images, but usually does not provide additional diagnostic information over CT.

Thymic Carcinoma

Thymic carcinomas usually present in the fifth or sixth decade of life and are exceedingly rare in the pediatric population [164, 165, 173, 174]. Thymic carcinoma is an aggressive epithelial carcinoma histologically characterized by malignant features of nuclear atypia, numerous mitotic figures, and necrosis [161]. Almost all patients are symptomatic at presentation, usually demonstrating constitutional symptoms such as weight loss, fatigue, night sweats, as well as chest pain [173, 174].

Thymic carcinomas usually present as large, irregular anterior mediastinal masses with aggressive local spread and mediastinal vascular invasion (Fig. 15.27) [153, 172, 175]. Often, these masses enhance heterogeneously with areas of necrosis, containing variable amounts of calcification. Thymic carcinoma may be indistinguishable from an invasive thymoma on imaging studies unless distant metastases are present. Unlike invasive thymomas, a thymic carcinoma tends to metastasize hematogenously [173, 174]. Prognosis is poor with progressive local growth and distant metastatic disease common [173, 174]. Treatment options include neoadjuvant chemotherapy to improve the resectability of the tumor, in addition to postoperative radiation therapy [176].

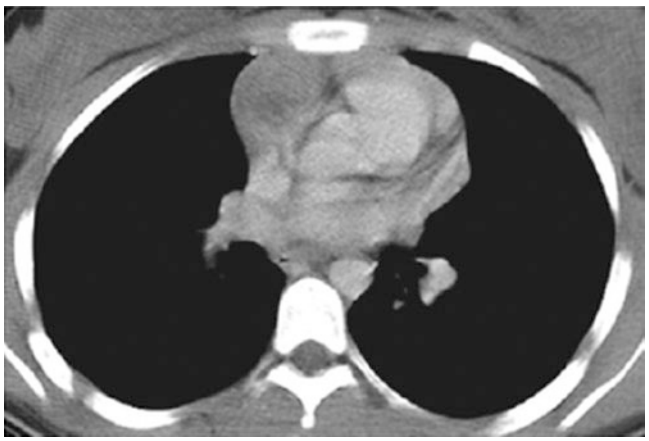

Fig. 15.26 A 14-year-old girl with a noninvasive thymoma who presented with fainting spell and abnormal chest radiographs. Enhanced axial CT image shows a relatively well-circumscribed lobulated mass in the anterior mediastinum abutting the right anterior heart

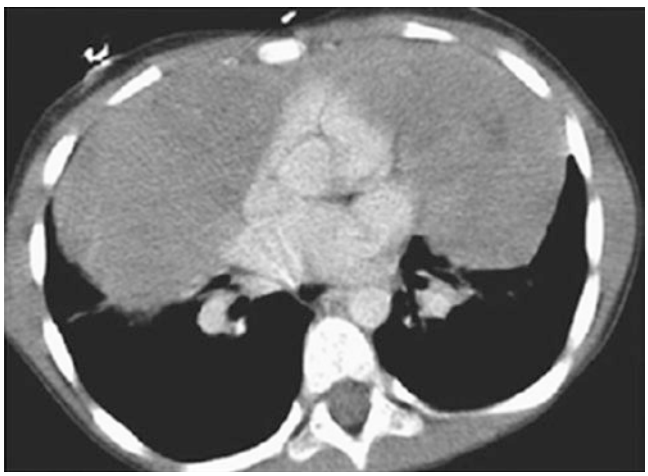

Fig. 15.25 A 5-year-old boy with a large invasive thymoma who presented with persistent cough. Enhanced axial CT image demonstrates a very large, heterogeneous pleural mass draped over the heart

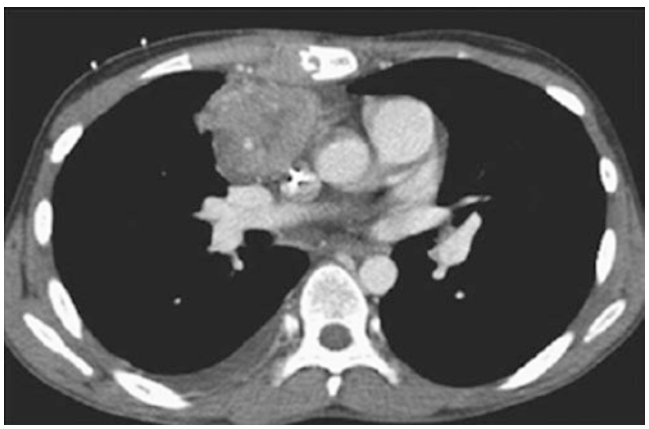

Fig. 15.27 A 6-year-old girl with thymic carcinoma who presented with chest pain. Enhanced axial CT image shows a heterogeneous mass in the anterior mediastinum with irregular borders and chest wall invasion, including sternal destruction

Germ Cell Tumor

Germ cell neoplasms arise from collections of primitive germ cells that arrest in the anterior mediastinum on their journey to the gonads during embryologic development [161, 170]. Because they are histologically indistinguishable from germ cell tumors arising in the testes and ovaries, the diagnosis of a primary malignant mediastinal germ cell neoplasm requires exclusion of a primary gonadal tumor as a source of mediastinal metastases [161].

Malignant germ cell tumors include immature teratomas, seminomas, and nonseminomatous germ cell tumors (NSGCT). Seminomas include germinoma and dysgerminoma, whereas NSGCT include embryonal cell, endodermal sinus/yolk sac tumors, choriocarcinoma, and mixed germ cell tumors [177, 178]. Seminoma, choriocarcinoma, and endodermal sinus/yolk sac tumors are malignant lesions seen primarily in young men [161, 170]. Seminoma is the most common malignant germ cell neoplasm, accounting for 30% of these tumors [161, 170]. Since these tumors may either be asymptomatic or present with nonspecific symptoms of dyspnea or chest pain, lab values are also useful for narrowing the diagnosis. Elevated serum alpha-fetoprotein (AFP) can be seen in NSGCTs, and human chorionic gonadotropin (hCG) is often elevated in both seminomas and NSGCTs [161, 170].

Malignant germ cell tumors usually appear as large anterior mediastinal masses arising either within or adjacent to the thymus. An immature teratoma is difficult to distinguish from its benign counterpart, the mature teratoma, as hallmarks of both include fat, fluid, and calcified components which differentiate from other mediastinal masses [164, 165]. One helpful feature is the presence of solid tissue, which is more prominent in immature teratomas [170, 178, 179]. While benign teratomas tend to displace adjacent structures, malignant teratomas tend to invade them [164, 165].

Seminomas often appear as large, lobulated masses of near homogenous soft tissue density and sometimes show internal necrosis. They often straddle the midline and may extend into the middle and posterior mediastinum or infiltrate fat planes (Fig. 15.28). NSGCTs are often large with heterogeneous density, often showing central areas of low density, and demonstrate irregular margins with obliterated fat planes. Lymphadenopathy and lung or liver metastases may also be present [153, 155, 162, 177].

While mature teratomas may be treated by surgery alone, malignant tumors must be treated with multimodality approaches. Seminomas are usually treated with chemotherapy followed by radiation for bulky tumors and surgery for residual disease. Nonseminomatous tumors are treated with a combination of chemotherapy and surgery [179].

Middle Mediastinal Compartment Masses

Metastatic Lymphadenopathy

Most middle mediastinal lymph node masses are malignant, representing metastases from various primary tumors or lymphoma or infectious in etiology [154, 155, 161]. In children, metastatic lymphadenopathy often results from primary tumors in the abdomen and pelvis, such as neuroblastoma, Wilms tumor, testicular neoplasms, and various sarcomas. Usually, these present as homogenous soft tissue masses which can be conglomerations of nodes (Fig. 15.29) [154, 155]. Lymphoma is also a common primary neoplasm that can manifest itself in any mediastinal compartment, including the middle mediastinum or as an extension from the anterior

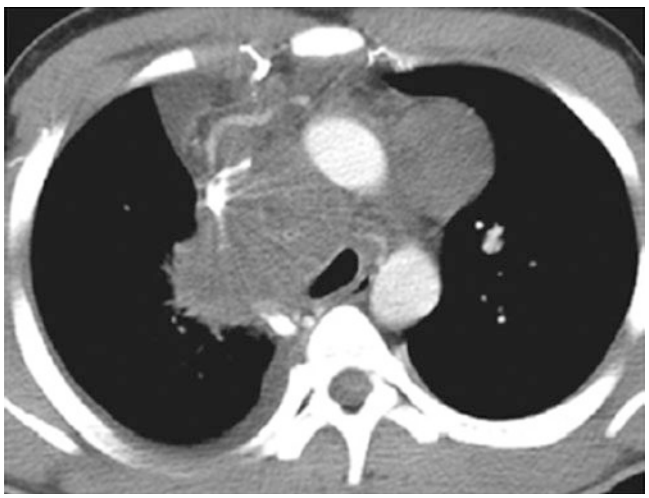

Fig. 15.28 A 10-year-old girl who presented with chest pain and weight loss. Enhanced axial CT image shows a heterogeneously enhancing mediastinal mass with ill-defined borders and mass effect upon trachea resulting in tracheal narrowing. This mass was proven to be a seminoma

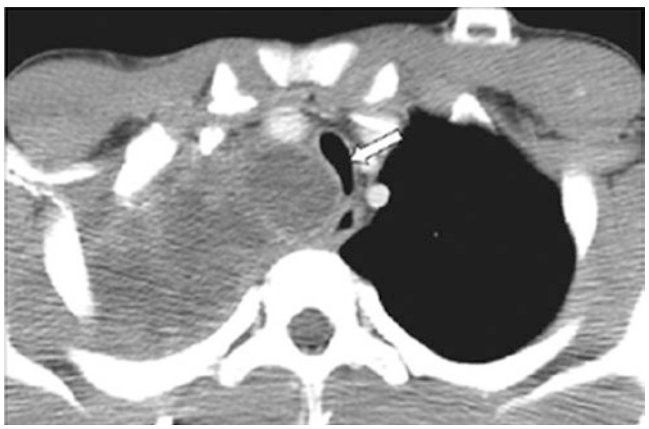

Fig. 15.29 A 14-year-old boy who presented with known metastatic prostate rhabdomyosarcoma. Enhanced axial CT image shows a large heterogeneously enhancing middle mediastinal mass causing tracheal narrowing (arrow)

mediastinum. While it is often difficult to determine which primary tumor is responsible for metastatic lymphadenopathy, one of the more helpful characteristics is lymph node calcification, which can be often seen in treated lymphoma or osteosarcoma metastases (Fig. 15.30) [155]. Similar to any other mediastinal mass, metastatic lymphadenopathy may be asymptomatic or cause a variety of symptoms including dyspnea or chest pain. Management of the adenopathy includes determining the site of primary disease and its appropriate treatment.

Posterior Mediastinal Compartment Masses

Neuroblastoma

Ninety percent of posterior mediastinal tumors are neurogenic, derived from the sympathetic chains which are located along the thoracic vertebral bodies [1, 2, 165, 180]. The vast majority of these neurogenic tumors are neuroblastomas in pediatric patients, while the rest are ganglioneuroblastoma or ganglioneuroma.

Neuroblastoma is a malignant tumor of primitive neural crest cells. Although it most commonly arises from the adrenal gland, it can arise from anywhere along the sympathetic chain, including the posterior mediastinum. Neuroblastoma is the third most common pediatric malignancy after leukemia and central nervous system tumors. Posterior mediastinal neuroblastoma accounts for approximately 20% of all neuroblastoma cases [181–184]. Common sites of metastases from neuroblastoma include the liver and the bone, with lung metastases being less common. Neuroblastoma, although malignant, holds a more favorable prognosis if diagnosed under the age of 1. Typical clinical presentation includes fever, irritability, weight loss, and anemia [165, 180]. Neural symptoms from cord compression may cause paraplegia, extremity weakness, and altered bowel or bladder function [165, 180].

CXR often shows soft tissue opacity in the paravertebral regions, sometimes demonstrating erosion or destruction of the ribs and/or vertebrae or widening of intercostal spaces (Fig. 15.31). Associated calcifications are common, reportedly occurring in up to 30% on CXR [181–183]. Bone metastases may also be seen and are usually permeative. CT provides further anatomic depiction of the mass and associated calcification and local extent of disease. Approximately 80% of neuroblastoma cases contain calcium on CT (Fig. 15.32a) [165, 170, 181–184]. In addition, tumor necrosis or hemorrhage can also be seen on CT.

As invasive mass tends to surround and encase vessels, neuroblastoma also tends to invade neural foramina and the spinal canal. Neural foramina invasion is important to recognize, as it can influence surgical planning and management [155, 160, 164, 167, 181–184]. MR often shows the tumor to be high in signal on T2-weighted images and low in signal on T1-weighted images and is the best modality for detecting extension of tumor into the spinal canal, as well as local disease extent (Fig. 15.32b) [185]. Neuroblastomas on MRI tend to enhance early, indicative of their high vascularity, and regions of necrosis or cystic change are well seen [155, 181–183, 185]. Imaging with metaiodobenzylguanidine (MIBG) is an excellent study for determining extent of disease, because there is avid uptake of MIBG related to catecholamine production by the tumor. Bone scan also helps stage neuroblastoma by providing information regarding local and distant osseous involvement from the tumor. The

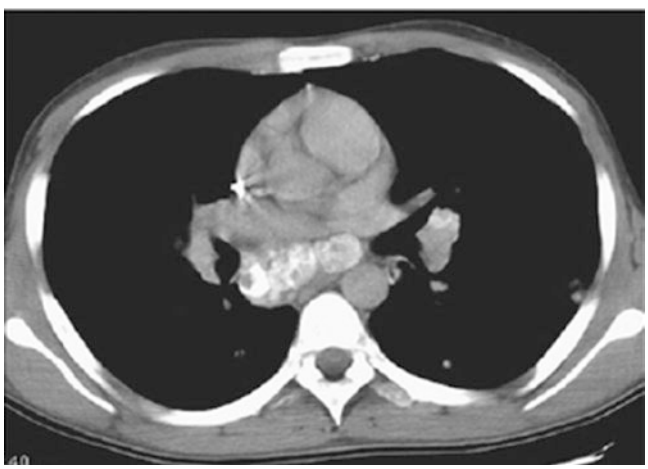

Fig. 15.30 A 17-year-old boy who presented with metastatic osteosarcoma. Non-enhanced axial CT image demonstrates multiple calcified mediastinal lymph nodes

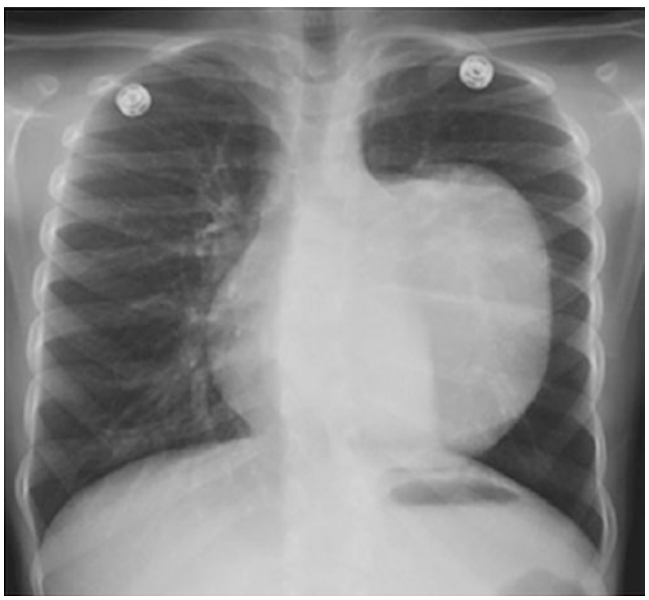

Fig. 15.31 A 7-year-old boy who presented with thoracic neuroblastoma. Note the thinning and spreading of the left seventh through ninth ribs immediately adjacent to the mass

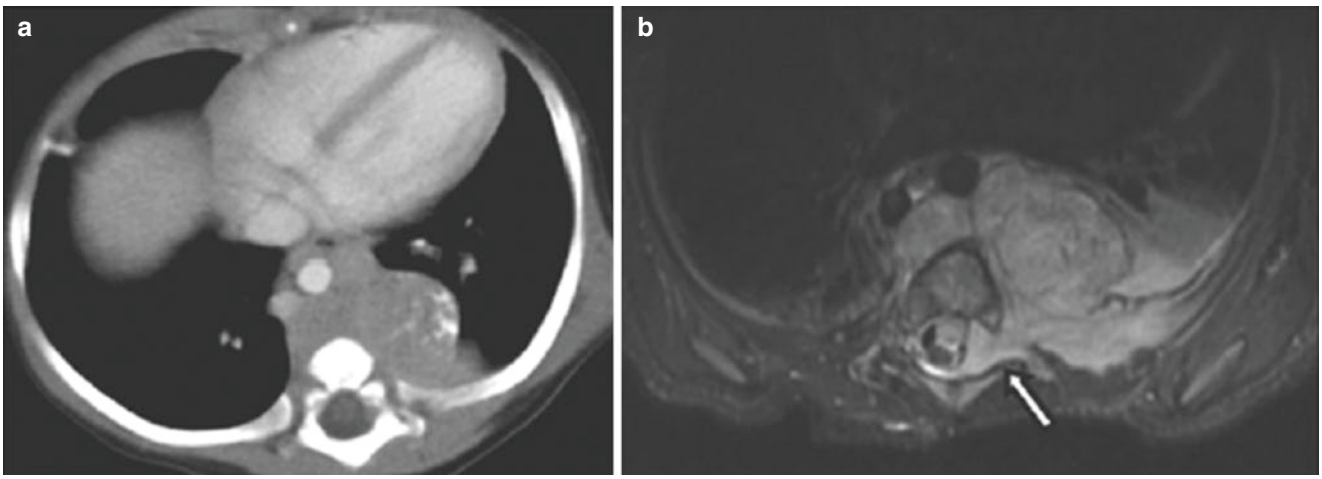

Fig. 15.32 A 3-month-old boy who presented with vomiting. After abdominal ultrasound failed to reveal the cause of his symptoms, a CT was performed after an abnormal CXR. (**a**) Enhanced axial CT image demonstrates a large left posterior mediastinal mass with regions of calcification. (**b**) MRI was also performed to evaluate for spinal involvement. Axial fluid-sensitive MRI image demonstrates extension of the neuroblastoma through the neural foramen and epidural extension (*arrow*)

current therapy of choice for neuroblastoma in pediatric patients is surgical resection with adjuvant chemotherapy and radiation therapy for advanced disease. The prognosis of neuroblastoma in children varies depending on the location of the tumor. Children with thoracic neuroblastoma have more favorable prognosis than those with abdominal tumor involvement [165, 180].

Ganglioneuroblastoma

Ganglioneuroma and ganglioneuroblastoma are less aggressive counterparts along the neuroblastoma spectrum. They are also tumors of primitive neural crest cells. Ganglioneuroma and ganglioneuroblastoma may arise in the posterior mediastinum, with ganglioneuromas considered benign and ganglioneuroblastomas considered malignant, the latter because of the possibility of distant metastases [1, 2, 165, 181–183]. Radiologically, ganglioneuroblastomas especially are difficult to differentiate from neuroblastomas, having similar characteristics on CT and MRI (Fig. 15.33). However, ganglioneuroblastoma and ganglioneuroma may have a more elongated (fusiform) configuration than usually encountered with neuroblastoma. Because the differential diagnosis for ganglioneuroblastoma includes neuroblastoma, surgical management is necessary.

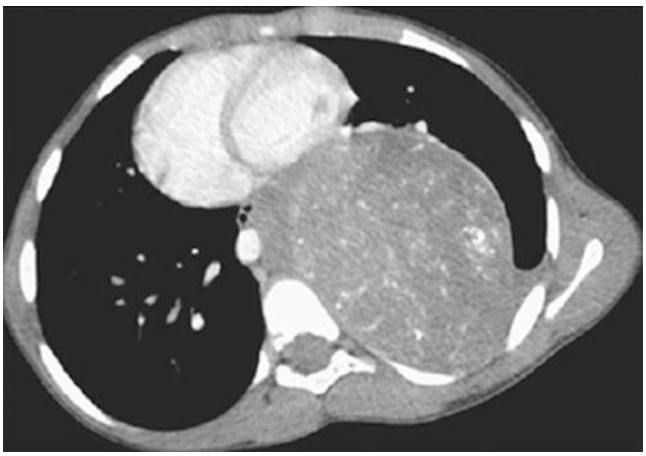

Fig. 15.33 A 7-year-old boy who presented with difficulty breathing. Enhanced axial CT image demonstrates a very large mass in the posterior mediastinum with regions of enhancement and calcification proven to be a ganglioneuroblastoma

Nerve Sheath Tumors

While most posterior mediastinal masses are neuroblastomas [1, 2, 165, 185], benign peripheral nerve sheath tumors such as schwannomas and neurofibromas and malignant peripheral nerve sheath tumors (MPNST) may also be seen. MPNSTs are spindle cell sarcomas of nerve sheath origin and are highly cellular with pleomorphic spindle cells. In pediatric patients, these masses most commonly arise from a preexisting plexiform neurofibroma, such as in patients with neurofibromatosis type 1 (NF-1). Less commonly, MPNSTs arise de novo or from preexisting schwannomas [154, 165, 185, 186]. Surgical removal for symptomatic or malignant lesions is the treatment of choice.

MPNSTs often appear as round or oblong posterior mediastinal masses with a widened neural foramen, following the axis of the involved nerve. On CT, these masses usually demonstrate decreased density due to lipid contents or cystic degeneration and can have variable enhancement (Fig. 15.34). Dumbbell extension into the spinal canal can be seen on both CT and MRI. Features of MPNST, whether arising de novo or from degeneration of a preexisting mass, include local invasion, osseous destruction, and pleural effusion [154, 185, 186].

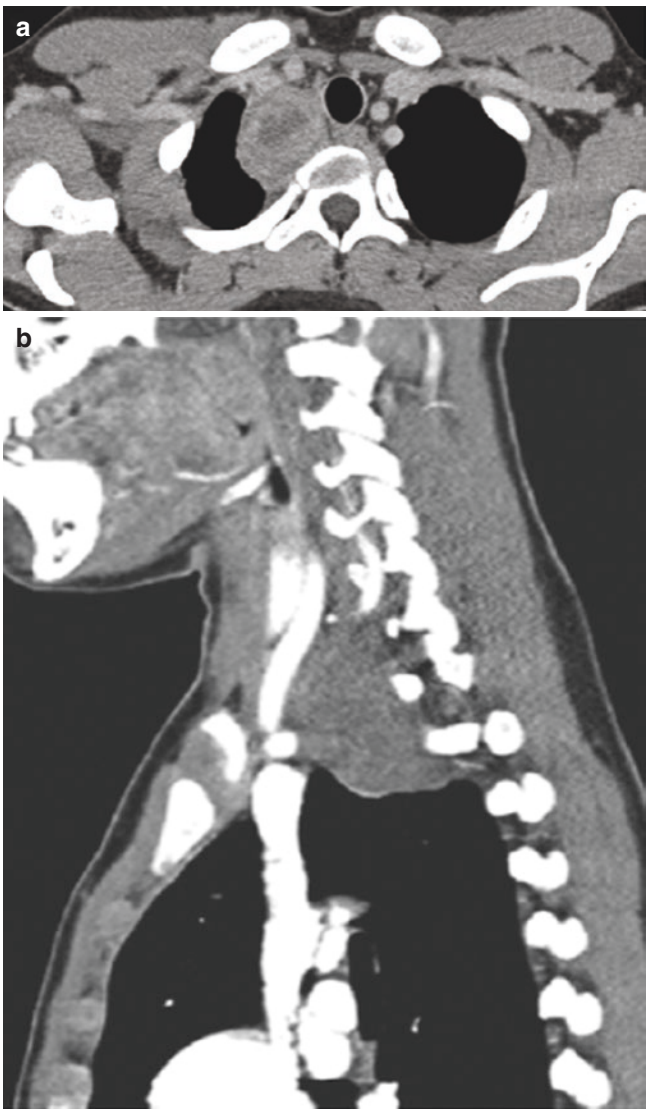

Fig. 15.34 A 17-year-old boy who presented with neurofibromatosis type 1 and new Horner's syndrome. (**a**) Enhanced axial CT image demonstrates a heterogeneously enhancing mass in the mediastinum adjacent to the right lung apex which had grown substantially since a prior CT, consistent with a MPNST. (**b**) Sagittal-enhanced CT image confirms that this mass is in the posterior mediastinum

Conclusion

Pediatric thoracic tumors are rare and present with nonspecific physical and radiographic findings. Therefore, a high index of suspicion is necessary to make the correct diagnosis when patients have persistent clinical symptoms. In general, malignant tumors are more common in children than benign lesions with the majority being metastatic in nature. Once a thoracic mass has been identified on CXR, cross-sectional imaging such as CT or MRI can be used for confirmation of findings and further characterization for generating differential diagnostic considerations. Although some malignant pediatric thoracic tumors may have characteristic imaging appearances, definitive diagnosis relies on histopathological analysis. Complete surgical resection is the mainstay of treatment in primary lesions and is becoming more defined in secondary malignancies. Some lesions are amenable to adjuvant therapy, and prognosis varies depending on tumor location, stage, and type.

Acknowledgment The author of this chapter would like to sincerely thank the previous authors, Benjamin A. Nelson, MD and Shashi H. Ranganath, MD, involved with previous edition of this chapter.

References

1. Zapala MA, Ho-Fung VM, Lee EY. Thoracic neoplasms in children: contemporary perspectives and imaging assessment. Radiol Clin N Am. 2017;555(4):657–76.
2. Amini B, Huang SY, Tsai J, Benveniste MF, Robeldo HH, Lee EY. Primary lung and airway neoplasms in children: current imaging evaluation with multidetector computed tomography. Radiol Clin North Am. 2013;51(4):637–57.
3. Sood S, Hryhorczuk AL, Rissmiller J, Lee EY. Spectrum of syndromic disorders associated with pediatric tumors: evolving role of practical imaging assessment. Radiol Clin North Am. 2017;55(4):869–93.
4. Schooler GR, Davis JT, Parente VM, Lee EY. Children with cough and fever: up-to-date imaging evaluation and management. Radiol Clin North Am. 2017;55(4):645–55.
5. Winant AJ, Ngo AV, Phillips GS, Lee EY. Computed tomography of congenital lung malformations in children: a primer for radiologists. Semin Roetgenol. 2018;53(2):187–96.
6. Liszewski MC, Ciet P, Sodhi KS, Lee EY. Updates on MRI evaluation of pediatric large airways. AJR Am J Roetgenol. 2017;208(5):971–81.
7. Gorkem SB, Kose S, Lee EY, Doganay S, Coskun AS, Kose M. Thoracic MRI evaluation of sarcoidosis in children. Pediatr Pulmolo. 2017;52(4):494–9.
8. Baez JC, Ciet P, Mulkern R, Seethamraju RT, Lee EY. Pediatric chest MR imaging: lung and airways. Magn Reson Imaging Clin N Am. 2015;23(2):337–49.
9. Sodhi KS, Sharma M, Lee EY, et al. Diagnostic utility of 3T lung MRI in children with interstitial lung disease: a prospective pilot study. Acad Radiol. 2018;35(3):380–6.
10. Liszewski MG, Gorkem S, Sodhi KS, Lee EY. Lung magnetic resonance imaging for pneumonia in children. Pediatr Radiol. 2017;47(11):1420–30.
11. Laya BF, Restrepo R, Lee EY. Practical imaging evaluation of foreign bodies in children: an update. Radiol Clin North Am. 2017;55(4):845–67.
12. Lee EY, Litmanovich D, Boiselle PM. Multidetector CT evaluation of tracheobronchomalacia. Radiol Clin N Am. 2009;47(2):261–9.
13. Lee EY, Boiselle PM. Tracheobronchomalacia in infants and children: multidetector CT evaluation. Radiology. 2009;25(1):7–22.
14. Ngo AV, Winant AJ, Lee EY, Phillips GS. Strategies for reducing radiation dose in CT for pediatric patients: how we do it. Semin Roentgenol. 2018;53(2):124–31.
15. Sodhi KS, Krishna S, Saxena AK, Singh A, Khandelwal N, Lee EY. Clinical application of "justification" and "optimization" principle of ALARA in pediatric CT imaging: "how many children can be protected from unnecessary radiation?". Eur J Radiol. 2015;84(9):1752–7.
16. Lee EY, Mason KP, Zurakowski D, Waltz DA, et al. MDCT assessment of tracheomalacia in symptomatic infants with medi-

astinal aortic vascular anomalies: preliminary technical experience. Pediatr Radiol. 2009;28(1):82–8.
17. Lee EY, Dorkin H, Vargas SO. Congenital pulmonary malformations in pediatric patients: review and update on etiology, classification, and imaging findings. Radiol Clin N Am. 2011;49(5):921–48.
18. Hellinger JC, Daubert M, Lee EY, Epleman M. Congenital thoracic vascular anomalies: evaluation with state-of-the-art MR imaging and MDCT. Radiol Clin N Am. 2011;49(5):969–96.
19. Kondrachuk O, Yalynska T, Tammo R, Lee EY. Multidetector computed tomography evaluation of congenital mediastinal vascular anomalies in children. Semin Roentgenol. 2012;47(2):127–34.
20. Kwatra NS, Grant FD, Lim R, Lee EY. Up-to-date review of nuclear medicine applications in pediatric thoracic imaging. Eur J Radiol. 2017;95:418–27. Umiker WO, Iverson L. Postinflammatory tumors of the lung; report of four cases simulating xanthoma, fibroma, or plasma cell tumor. J Thorac Surg. 1954;28(1):55–63.
21. Griffin CA, Hawkins AL, Dvorak C, Henkle C, Ellingham T, Perlman EJ. Recurrent involvement of 2p23 in inflammatory myofibroblastic tumors. Cancer Res. 1999;59(12):2776–80.
22. Bahadori M, Liebow AA. Plasma cell granulomas of the lung. Cancer. 1973;31(1):191–208.
23. Bumber Z, Jurlina M, Manojlovic S, Jakic-Razumovic J. Inflammatory pseudotumor of the trachea. J Pediatr Surg. 2001;36(4):631–4.
24. Dishop MK, Kuruvilla S. Primary and metastatic lung tumors in the pediatric population: a review and 25-year experience at a large children's hospital. Arch Pathol Lab Med. 2008;132(7):1079–103.
25. Monzon CM, Gilchrist GS, Burgert EO Jr, O'Connell EJ, Telander RL, Hoffman AD, et al. Plasma cell granuloma of the lung in children. Pediatrics. 1982;70(2):268–74.
26. Hartman GE, Shochat SJ. Primary pulmonary neoplasms of childhood: a review. Ann Thorac Surg. 1983;36(1):108–19.
27. Berardi RS, Lee SS, Chen HP, Stines GJ. Inflammatory pseudotumors of the lung. Surg Gynecol Obstet. 1983;156(1):89–96.
28. Warter A, Satge D, Roescin N. Angio-invasive plasma cell granuloma of the lung. Cancer. 1987;59:435–43.
29. Janik JS, Janik JP, Lovell MA, Hendrickson RJ, Bensard DD, Greffe BS. Recurrent inflammatory pseudotumors in children. J Pediatr Surg. 2003;38(10):1491–5.
30. Cerfolio RJ, Allen MS, Nascimento AG, Deschamps C, Trastek VF, Miller DL, et al. Inflammatory pseudotumors of the lung. Ann Thorac Surg. 1999;67(4):933–6.
31. Vera-Roman JM, Sobonya RE, Gomez-Garcia JL, Sanz-Bondia JR, Paris-Romeu F. Leiomyoma of the lung. Literature review and case report. Cancer. 1983;52(5):936–41.
32. Lynn RB, Macfadyen DJ. Solitary primary leiomyoma of the lung. Can J Surg. 1958;2(1):93–6.
33. Sherman RS, Malone BH. A roentgen study of smooth muscle tumors primary in the lung. Radiology. 1950;54:507–15.
34. De Chadarevian JP, Wolk JH, Inniss S, Lischner HW, D'Amore F, Faerber EN, et al. A newly recognized cause of wheezing: AIDS-related bronchial leiomyomas. Pediatr Pulmonol. 1997;24(2):106–10.
35. Warren JS, Seo IS, Mirkin LD. Massive congenital mesenchymal malformation of the lung: a case report with ultrastructural study. Pediatr Pathol. 1985;3(2–4):321–8.
36. Alobeid B, Beneck D, Sreekantaiah C, Abbi RK, Slim MS. Congenital pulmonary myofibroblastic tumor: a case report with cytogenetic analysis and review of the literature. Am J Surg Pathol. 1997;21(5):610–4.
37. McGinnis M, Jacobs G, el-Naggar A, Redline RW. Congenital peribronchial myofibroblastic tumor (so-called "congenital leiomyosarcoma"). A distinct neonatal lung lesion associated with nonimmune hydrops fetalis. Mod Pathol. 1993;6(4):487–92.
38. Coffin CM. Lipoblastoma: an embryonal tumor of soft tissue related to organogenesis. Semin Diagn Pathol. 1994;11(2):98–103.
39. O'Donnell KA, Caty MG, Allen JE, Fisher JE. Lipoblastoma: better termed infantile lipoma? Pediatr Surg Int. 2000;16(5–6):458–61.
40. Chung EB, Enzinger FM. Benign lipoblastomatosis. An analysis of 35 cases. Cancer. 1973;32(2):482–92.
41. Bertana S, Parigi GP, Giuntoli M, Pelagalli M, Battisti C, Bragheri R, et al. Lipoblastoma and lipoblastomatosis in children. Minerva Pediatr. 1999;51(5):159–66.
42. Hicks J, Dilley A, Patel D, Barrish J, Zhu SH, Brandt M. Lipoblastoma and lipoblastomatosis in infancy and childhood: histopathologic, ultrastructural, and cytogenetic features. Ultrastruct Pathol. 2001;25(4):321–33.
43. Chun YS, Kim WK, Park KW, Lee SC, Jung SE. Lipoblastoma. J Pediatr Surg. 2001;36(6):905–7.
44. Dilley AV, Patel DL, Hicks MJ, Brandt ML. Lipoblastoma: pathophysiology and surgical management. J Pediatr Surg. 2001;36(1):229–31.
45. Hancock BJ, Di Lorenzo M, Youssef S, Yazbeck S, Marcotte JE, Collin PP. Childhood primary pulmonary neoplasms. J Pediatr Surg. 1993;28(9):1133–6.
46. van den Bosch JM, Wagenaar SS, Corrin B, Elbers JR, Knaepen PJ, Westermann CJ. Mesenchymoma of the lung (so called hamartoma): a review of 154 parenchymal and endobronchial cases. Thorax. 1987;42(10):790–3.
47. Eggli KD, Newman B. Nodules, masses, and pseudomasses in the pediatric lung. Radiol Clin N Am. 1993;31(3):651–66.
48. Fudge TL, Ochsner JL, Mills NL. Clinical spectrum of pulmonary hamartomas. Ann Thorac Surg. 1980;30(1):36–9.
49. Karasik A, Modan M, Jacob CO, Lieberman Y. Increased risk of lung cancer in patients with chondromatous hamartoma. J Thorac Cardiovasc Surg. 1980;80(2):217–20.
50. Fontenelle LJ. Primary adenocarcinoma of lung in a child: review of the literature. Am Surg. 1976;42(4):296–9.
51. French CA. Demystified molecular pathology of NUT midline carcinomas. J Clin Pathol. 2010;63(6):492–6.
52. French CA, Miyoshi I, Kubonishi I, Grier HE, Perez-Atayde AR, Fletcher JA. BRD4-NUT fusion oncogene: a novel mechanism in aggressive carcinoma. Cancer Res. 2003;63(2):304–7.
53. French CA, Kutok JL, Faquin WC, Toretsky JA, Antonescu CR, Griffin CA, et al. Midline carcinoma of children and young adults with NUT rearrangement. J Clin Oncol. 2004;22(20):4135–9.
54. Mertens F, Wiebe T, Adlercreutz C, Mandahl N, French CA. Successful treatment of a child with t(15;19)-positive tumor. Pediatr Blood Cancer. 2007;49(7):1015–7.
55. Engleson J, Soller M, Panagopoulos I, Dahlen A, Dictor M, Jerkeman M. Midline carcinoma with t(15;19) and BRD4-NUT fusion oncogene in a 30-year-old female with response to docetaxel and radiotherapy. BMC Cancer. 2006;6:69.
56. French CA, Ramirez CL, Kolmakova J, Hickman TT, Cameron MJ, Thyne ME, et al. BRD-NUT oncoproteins: a family of closely related nuclear proteins that block epithelial differentiation and maintain the growth of carcinoma cells. Oncogene. 2008;27(15):2237–42.
57. Stelow EB, Bellizzi AM, Taneja K, Mills SE, Legallo RD, Kutok JL, et al. NUT rearrangement in undifferentiated carcinomas of the upper aerodigestive tract. Am J Surg Pathol. 2008;32(6):828–34.
58. Vargas SO, French CA, Faul PN, Fletcher JA, Davis IJ, Dal Cin P, et al. Upper respiratory tract carcinoma with chromosomal translocation 15;19: evidence for a distinct disease entity of young patients with a rapidly fatal course. Cancer. 2001;92(5):1195–203.
59. Teixeira MR. Recurrent fusion oncogenes in carcinomas. Crit Rev Oncog. 2006;12(3–4):257–71.
60. Miniati DN, Chintagumpala M, Langston C, Dishop MK, Olutoye OO, Nuchtern JG, et al. Prenatal presentation and out-

come of children with pleuropulmonary blastoma. J Pediatr Surg. 2006;41(1):66–71.
61. Manivel JC, Priest JR, Watterson J, Steiner M, Woods WG, Wick MR, et al. Pleuropulmonary blastoma. The so-called pulmonary blastoma of childhood. Cancer. 1988;62(8):1516–26.
62. Weinblatt ME, Siegel SE, Isaacs H. Pulmonary blastoma associated with cystic lung disease. Cancer. 1982;49(4):669–71.
63. Federici S, Domenichelli V, Tani G, Sciutti R, Burnelli R, Zanetti G, et al. Pleuropulmonary blastoma in congenital cystic adenomatoid malformation: report of a case. Eur J Pediatr Surg. 2001;11(3):196–9.
64. Tagge EP, Mulvihill D, Chandler JC, Richardson M, Uflacker R, Othersen HD. Childhood pleuropulmonary blastoma: caution against nonoperative management of congenital lung cysts. J Pediatr Surg. 1996;31(1):187–9; discussion 190.
65. Holland-Moritz RM, Heyn RM. Pulmonary blastoma associated with cystic lesions in children. Med Pediatr Oncol. 1984;12(2):85–8.
66. Pleuropulmonary blastoma registry [homepage on the Internet]; 2005. www.ppbregistry.org. Accessed 25 May 2011.
67. Priest JR, McDermott MB, Bhatia S, Watterson J, Manivel JC, Dehner LP. Pleuropulmonary blastoma: a clinicopathologic study of 50 cases. Cancer. 1997;80(1):147–61.
68. Raz DJ, He B, Rosell R, Jablons DM. Bronchioloalveolar carcinoma: a review. Clin Lung Cancer. 2006;7(5):313–22.
69. Lee KS, Kim Y, Han J, Ko EJ, Park CK, Primack SL. Bronchioloalveolar carcinoma: clinical, histopathologic, and radiologic findings. Radiographics. 1997;17(6):1345–57.
70. Storey CF, Knudtson KP, Lawrence BJ. Bronchiolar (alveolar cell) carcinoma of the lung. J Thorac Surg. 1953;26(4):331–406.
71. Greenberg SD, Smith MN, Spjut HJ. Bronchiolo-alveolar carcinoma-cell of origin. Am J Clin Pathol. 1975;63(2):153–67.
72. Liebow AA. Bronchiolo-alveolar carcinoma. Adv Intern Med. 1960;10:329–58. Manning Jr JT, Spjut HJ, Tschen JA. Bronchioloalveolar carcinoma: the significance of two histopathologic types. Cancer. 1984;54(3):525–534.
73. Clayton F. Bronchioloalveolar carcinomas. Cell types, patterns of growth, and prognostic correlates. Cancer. 1986;57(8):1555–64.
74. Granata C, Gambini C, Balducci T, Toma P, Michelazzi A, Conte M, et al. Bronchioloalveolar carcinoma arising in congenital cystic adenomatoid malformation in a child: a case report and review on malignancies originating in congenital cystic adenomatoid malformation. Pediatr Pulmonol. 1998;25(1):62–6.
75. Lack EE. Leiomyosarcomas in childhood: a clinical and pathologic study of 10 cases. Pediatr Pathol. 1986;6(2–3):181–97.
76. Havard CW, Hanbury WJ. Leiomyosarcoma of the lung. Lancet. 1960;2(7156):902–4.
77. Timmons CF, Dawson DB, Richards CS, Andrews WS, Katz JA. Epstein-barr virus-associated leiomyosarcomas in liver transplantation recipients. Origin from either donor or recipient tissue. Cancer. 1995;76(8):1481–9.
78. Guillan RA, Wilen CJ, Zelman S. Primary leiomyosarcoma of the lung. Dis Chest. 1969;56(5):452–4.
79. Tateishi U, Gladish GW, Kusumoto M, Hasegawa T, Yokoyama R, Tsuchiya R, et al. Chest wall tumors: radiologic findings and pathologic correlation: Part 2. Malignant tumors. Radiographics. 2003;23(6):1491–508.
80. Pettinato G, Manivel JC, Saldana MJ, Peyser J, Dehner LP. Primary bronchopulmonary fibrosarcoma of childhood and adolescence: reassessment of a low-grade malignancy. Clinicopathologic study of five cases and review of the literature. Hum Pathol. 1989;20(5):463–71.
81. Guccion JG, Rosen SH. Bronchopulmonary leiomyosarcoma and fibrosarcoma. A study of 32 cases and review of the literature. Cancer. 1972;30(3):836–47.
82. Enzinger FM, Weiss SW. Soft tissue tumors. 2nd ed. St. Louis: CV Mosby; 1988. p. 213–20.
83. Soule EH, Pritchard DJ. Fibrosarcoma in infants and children: a review of 110 cases. Cancer. 1977;40(4):1711–21.
84. Chung EB, Enzinger FM. Infantile fibrosarcoma. Cancer. 1976;38(2):729–39.
85. Wellner LJ, Putman CE. Imaging of occult pulmonary metastases: state of the art. CA Cancer J Clin. 1986;36(1):48–58.
86. Kayton ML. Pulmonary metastasectomy in pediatric patients. Thorac Surg Clin. 2006;16(2):167–83. vi
87. Green DM. The treatment of stages I–IV favorable histology Wilms' tumor. J Clin Oncol. 2004;22(8):1366–72.
88. Mitchell C, Jones PM, Kelsey A, Vujanic GM, Marsden B, Shannon R, et al. The treatment of Wilms' tumour: results of the United Kingdom children's cancer study group (UKCCSG) second Wilms' tumour study. Br J Cancer. 2000;83(5):602–8.
89. Gatta G, Capocaccia R, Coleman MP, Ries LA, Berrino F. Childhood cancer survival in Europe and the United States. Cancer. 2002;95(8):1767–72.
90. Ehrlich PF, Hamilton TE, Grundy P, Ritchey M, Haase G, Shamberger RC, et al. The value of surgery in directing therapy for patients with Wilms' tumor with pulmonary disease. A report from the national Wilms' tumor study group (national Wilms' tumor study 5). J Pediatr Surg. 2006;41(1):162–7; discussion 162–167
91. Schnater JM, Aronson DC, Plaschkes J, Perilongo G, Brown J, Otte JB, et al. Surgical view of the treatment of patients with hepatoblastoma: results from the first prospective trial of the international society of pediatric oncology liver tumor study group. Cancer. 2002;94(4):1111–20.
92. Perilongo G, Brown J, Shafford E, Brock P, De Camargo B, Keeling JW, et al. Hepatoblastoma presenting with lung metastases: treatment results of the first cooperative, prospective study of the international society of paediatric oncology on childhood liver tumors. Cancer. 2000;89(8):1845–53.
93. Young JL Jr, Ries LG, Silverberg E, Horm JW, Miller RW. Cancer incidence, survival, and mortality for children younger than age 15 years. Cancer. 1986;58(2. Suppl):598–602.
94. Matthay KK, Villablanca JG, Seeger RC, Stram DO, Harris RE, Ramsay NK, et al. Treatment of high-risk neuroblastoma with intensive chemotherapy, radiotherapy, autologous bone marrow transplantation, and 13-cis-retinoic acid. Children's cancer group. N Engl J Med. 1999;341(16):1165–73.
95. Cowie F, Corbett R, Pinkerton CR. Lung involvement in neuroblastoma: incidence and characteristics. Med Pediatr Oncol. 1997;28(6):429–32.
96. DuBois SG, Kalika Y, Lukens JN, et al. Metastatic sites in stage IV and IVS neuroblastoma correlate with age, tumor biology, and survival. J Pediatr Hematol Oncol. 1999;21:181–9.
97. Kammen BF, Matthay KK, Pacharn P, Gerbing R, Brasch RC, Gooding CA. Pulmonary metastases at diagnosis of neuroblastoma in pediatric patients: CT findings and prognosis. AJR Am J Roentgenol. 2001;176(3):755–9.
98. Weldon CB, Shamberger RC. Pediatric pulmonary tumors: primary and metastatic. Semin Pediatr Surg. 2008;17(1):17–29.
99. Kager L, Zoubek A, Potschger U, Kastner U, Flege S, Kempf-Bielack B, et al. Primary metastatic osteosarcoma: presentation and outcome of patients treated on neoadjuvant cooperative osteosarcoma study group protocols. J Clin Oncol. 2003;21(10):2011–8.
100. Kaste SC, Pratt CB, Cain AM, Jones-Wallace DJ, Rao BN. Metastases detected at the time of diagnosis of primary pediatric extremity osteosarcoma at diagnosis: imaging features. Cancer. 1999;86(8):1602–8.

101. Price CH, Jeffree GM. Incidence of bone sarcoma in SW England, 1946–74, in relation to age, sex, tumour site and histology. Br J Cancer. 1977;36(4):511–22.
102. Patricio MB, Vilhena M, Neves M, Raposo S, Catita J, DeSousa V, et al. Ewing's sarcoma in children: twenty-five years of experience at the instituto portuges de oncologia de francisco gentil (I.P.O.F.G.). J Surg Oncol. 1991;47(1):37–40.
103. Sandoval C, Meyer WH, Parham DM, Kun LE, Hustu HO, Luo X, et al. Outcome in 43 children presenting with metastatic Ewing sarcoma: the St. Jude children's research hospital experience, 1962 to 1992. Med Pediatr Oncol. 1996;26(3):180–5.
104. Arndt CACW. Common musculoskeletal tumors of childhood and adolescence. N Engl J Med. 1999;341(5):342–52.
105. Pappo AS, Shapiro DN, Crist WM, Maurer HM. Biology and therapy of pediatric rhabdomyosarcoma. J Clin Oncol. 1995;13(8):2123–39.
106. Punyko JA, Mertens AC, Baker KS, Ness KK, Robison LL, Gurney JG. Long-term survival probabilities for childhood rhabdomyosarcoma. A population-based evaluation. Cancer. 2005;103(7):1475–83.
107. Oberlin O, Rey A, Lyden E, Bisogno G, Stevens MC, Meyer WH, et al. Prognostic factors in metastatic rhabdomyosarcomas: results of a pooled analysis from United States and European cooperative groups. J Clin Oncol. 2008;26(14):2384–9.
108. Enzinger W. Soft tissue tumours. 4th ed. Chicago: Mosby; 2001.
109. Spurrell EL, Fisher C, Thomas JM, Judson IR. Prognostic factors in advanced synovial sarcoma: an analysis of 104 patients treated at the royal marsden hospital. Ann Oncol. 2005;16(3):437–44.
110. Hajdu SI, Shiu MH, Fortner JG. Tendosynovial sarcoma: a clinicopathological study of 136 cases. Cancer. 1977;39(3):1201–17.
111. Cadman NL, Soule EH, Kelly PJ. Synovial sarcoma; an analysis of 34 tumors. Cancer. 1965;18:613–27.
112. Gerl A, Clemm C, Schmeller N, Hartenstein R, Lamerz R, Wilmanns W. Advances in the management of metastatic non-seminomatous germ cell tumours during the cisplatin era: a single-institution experience. Br J Cancer. 1996;74(8):1280–5.
113. Anyanwu E, Krysa S, Buelzebruck H, Vogt-Moykopf I. Pulmonary metastasectomy as secondary treatment for testicular tumors. Ann Thorac Surg. 1994;57(5):1222–8.
114. Pizzocaro G. Cancer of the testis. In: Veronesi U, Arnesjo B, Burn I, et al., editors. Surgical oncology – a European handbook. Berlin: Springer; 1989. p. 758.
115. Cagini L, Nicholson AG, Horwich A, Goldstraw P, Pastorino U. Thoracic metastasectomy for germ cell tumours: long term survival and prognostic factors. Ann Oncol. 1998;9(11):1185–91.
116. Liu D, Abolhoda A, Burt ME, Martini N, Bains MS, Downey RJ, et al. Pulmonary metastasectomy for testicular germ cell tumors: a 28-year experience. Ann Thorac Surg. 1998;66(5):1709–14.
117. Horvath LG, McCaughan BC, Stockle M, Boyer MJ. Resection of residual pulmonary masses after chemotherapy in patients with metastatic non-seminomatous germ cell tumours. Intern Med J. 2002;32(3):79–83.
118. Kesler KA, Wilson JL, Cosgrove JA, Brooks JA, Messiha A, Fineberg NS, et al. Surgical salvage therapy for malignant intrathoracic metastases from nonseminomatous germ cell cancer of testicular origin: analysis of a single-institution experience. J Thorac Cardiovasc Surg. 2005;130(2):408–15.
119. Pfannschmidt J, Zabeck H, Muley T, Dienemann H, Hoffmann H. Pulmonary metastasectomy following chemotherapy in patients with testicular tumors: experience in 52 patients. Thorac Cardiovasc Surg. 2006;54(7):484–8.
120. McCarthy MJ, Rosado-de-Christenson ML. Tumors of the trachea. J Thorac Imaging. 1995;10(3):180–98.
121. Pransky SM, Kang DR. Tumors of the larynx, trachea, and bronchi. In: Bluestone CD, Stool SES, Alper CM, et al., editors. Pediatric otolaryngology. 4th ed. Philadelphia: Saunders; 2002. p. 1558–72.
122. Derkay CS, Wiatrak B. Recurrent respiratory papillomatosis: a review. Laryngoscope. 2008;118(7):1236–47.
123. Khansur T, Balducci L, Tavassoli M. Granular cell tumor. Clinical spectrum of the benign and malignant entity. Cancer. 1987;60(2):220–2.
124. Majmudar B, Thomas J, Gorelkin L, Symbas PN. Respiratory obstruction caused by a multicentric granular cell tumor of the laryngotracheobronchial tree. Hum Pathol. 1981;12(3):283–6.
125. Andrassy RJ, Feldtman RW, Stanford W. Bronchial carcinoid tumors in children and adolescents. J Pediatr Surg. 1977;12(4):513–7.
126. Fischer S, Kruger M, McRae K, Merchant N, Tsao MS, Keshavjee S. Giant bronchial carcinoid tumors: a multidisciplinary approach. Ann Thorac Surg. 2001;71(1):386–93.
127. Gustafsson BI, Kidd M, Chan A, Malfertheiner MV, Modlin IM. Bronchopulmonary neuroendocrine tumors. Cancer. 2008;113(1):5–21.
128. McCahon E. Lung tumours in children. Paediatr Respir Rev. 2006;7(3):191–6.
129. Lack EE, Harris GB, Eraklis AJ, Vawter GF. Primary bronchial tumors in childhood. A clinicopathologic study of six cases. Cancer. 1983;51(3):492–7.
130. Raut CP, Kulke MH, Glickman JN, Swanson RS, Ashley SW. Carcinoid tumors. Curr Probl Surg. 2006;43(6):383–450.
131. Al-Qahtani AR, Di Lorenzo M, Yazbeck S. Endobronchial tumors in children: institutional experience and literature review. J Pediatr Surg. 2003;38(5):733–6.
132. DiAgostino RS, Ponn RB, Stern H. Adenoid cystic carcinoma, mucoepidermoid carcinoma, and mixed salivary gland-type tumors. In: Shields T, editor. General thoracic surgery. Philadelphia: Lea and Febiger; 1994. p. 1298–305.
133. Vadasz P, Egervary M. Mucoepidermoid bronchial tumors: a review of 34 operated cases. Eur J Cardiothorac Surg. 2000;17(5):566–9.
134. Yousem SA, Hochholzer L. Mucoepidermoid tumors of the lung. Cancer. 1987;60(6):1346–52.
135. Maziak DE, Todd TR, Keshavjee SH, Winton TL, Van Nostrand P, Pearson FG. Adenoid cystic carcinoma of the airway: thirty-two-year experience. J Thorac Cardiovasc Surg. 1996;112(6):1522–31; discussion 1531–1532.
136. Tateishi U, Gladish GW, Kusumoto M, Hasegawa T, Yokoyama R, Tsuchiya R, et al. Chest wall tumors: radiologic findings and pathologic correlation: Part 1. Benign tumors. Radiographics. 2003;23(6):1477–90.
137. Ippolito E, Bray EW, Corsi A, De Maio F, Exner UG, Robey PG, et al. Natural history and treatment of fibrous dysplasia of bone: a multicenter clinicopathologic study promoted by the European pediatric orthopaedic society. J Pediatr Orthop B. 2003;12(3):155–77.
138. Nogier A, De Pinieux G, Hottya G, Anract P. Case reports: enlargement of a calcaneal osteochondroma after skeletal maturity. Clin Orthop Relat Res. 2006;447:260–6.
139. Gladish GW, Sabloff BM, Munden RF, Truong MT, Erasmus JJ, Chasen MH. Primary thoracic sarcomas. Radiographics. 2002;22(3):621–37.
140. Burt M. Primary malignant tumors of the chest wall. The memorial Sloan-Kettering cancer center experience. Chest Surg Clin N Am. 1994;4(1):137–54.
141. Rosai J, In e S t. Ackerman's surgical pathology. 7th ed. St. Louis: Mosby; 1989. p. 1547–633.

142. Askin FB, Rosai J, Sibley RK, Dehner LP, McAlister WH. Malignant small cell tumor of the thoracopulmonary region in childhood: a distinctive clinicopathologic entity of uncertain histogenesis. Cancer. 1979;43(6):2438–51.
143. Dehner LP. Peripheral and central primitive neuroectodermal tumors. A nosologic concept seeking a consensus. Arch Pathol Lab Med. 1986;110(11):997–1005.
144. Jaffe R, Santamaria M, Yunis EJ, Tannery N, Medina J, Goodman M. Neuroendocrine tumor of bone: its distinction from Ewing's sarcoma (abstr). Lab Investig. 1984;50:5P.
145. Linnoila RI, Tsokos M, Triche TJ, Marangos PJ, Chandra RS. Evidence for neural origin and PAS-positive variants of the malignant small cell tumor of thoracopulmonary region ("askin tumor"). Am J Surg Pathol. 1986;10(2):124–33.
146. Cohen MD. Imaging of children with cancer. St. Louis: Mosby; 1992. p. 247–51.
147. Saifuddin A, Robertson RJ, Smith SE. The radiology of askin tumours. Clin Radiol. 1991;43(1):19–23.
148. Winer-Muram HT, Kauffman WM, Gronemeyer SA, Jennings SG. Primitive neuroectodermal tumors of the chest wall (askin tumors): CT and MR findings. AJR Am J Roentgenol. 1993;161(2):265–8.
149. Fink IJ, Kurtz DW, Cazenave L, Lieber MR, Miser JS, Chandra R, et al. Malignant thoracopulmonary small-cell ("askin") tumor. AJR Am J Roentgenol. 1985;145(3):517–20.
150. Jurgens H, Bier V, Harms D, Beck J, Brandeis W, Etspuler G, et al. Malignant peripheral neuroectodermal tumors. A retrospective analysis of 42 patients. Cancer. 1988;61(2):349–57.
151. Shields TW. General thoracic surgery. 7th ed. Philadelphia: Lippincott Williams and Wilkins; 2009.
152. Grosfeld JL. Primary tumors of the chest wall and mediastinum in children. Semin Thorac Cardiovasc Surg. 1994;6:235–9.
153. Grosfeld JL, Skinner MA, Rescorla FJ, et al. Mediastinal tumors in children: experience with 196 cases. Ann Surg Oncol. 1994;1:121–7.
154. Son JK, Lee EY, Eisenberg RL. Focal nonvascular thoracic masses in children. AJR Am J Roentgenol. 2011;196(3):W224–39.
155. Lee EY. Evaluation of non-vascular mediastinal masses in infants and children: an evidence-based practical approach. Pediatr Radiol. 2009;39 Suppl 2:S184–90.
156. Williams PL, Warwick R, Dyson M, Bannister LH, editors. Splanchnology. In: Gray's anatomy. 37th ed. New York: Churchill Livingstone; 1989. p. 1245–475.
157. Zylak CJ, Pallie W, Jackson R. Correlative anatomy and computed tomography: a module on the mediastinum. Radiographics. 1982;2(4):555–92.
158. Lee EY, editor. In Mediastinum. Pediatric thoracic imaging. Philadelphia: Wolters Kluwer; 2018. p. 150–217.
159. Aquino SL, Duncan G, Taber KH, Sharma A, Hayman LA. Reconciliation of the anatomic, surgical, and radiographic classifications of the mediastinum. J Comput Assist Tomogr. 2001;25(3):489–92.
160. Laurent F, Latrabe V, Lecesne R, et al. Mediastinal masses: diagnostic approach. Eur Radiol. 1998;8:1148–59.
161. Brant W, Helms C. Fundamentals of diagnostic radiology. 2nd ed. Philadelphia: Lippincott Williams & Wilkins; 1999.
162. Whitten CR, Khan S, Munneke GJ, Grubnic S. A diagnostic approach to mediastinal abnormalities. Radiographics. 2007;27:657–71.
163. Piira T, Perkins SL, Anderson JR, et al. Primary mediastinal large cell lymphoma in children: a report from the Children's Cancer Group. Pediatr Pathol Lab Med. 1995;15:561–70.
164. Merten DF. Diagnostic imaging of mediastinal masses in children. AJR Am J Roentgenol. 1992;158:825–32.
165. Lee EY, editor. Pediatric radiology: practical imaging evaluation of infants and children. Philadelphia: Wolters Kluwer; 2018. p. 609–39.
166. Montravers F, McNamara D, Landman-Parker J, et al. 18F FDG in childhood lymphoma: clinical utility and impact on management. Eur J Nucl Med Mol Imaging. 2002;29:1155–65.
167. Williams HJ, Alton HM. Imaging of paediatric mediastinal abnormalities. Paediatr Respir Rev. 2003;4:55–66.
168. DeVita VT. A selective history of the therapy of Hodgkin's disease. Br J Haematol. 2003;122:718–27.
169. Ansell SM, Armitage J. Non-Hodgkin lymphoma: diagnosis and treatment. Mayo Clin Proc. 2005;80(8):1087–97.
170. Rosado-de-Christenson ML, Galobardes J, Moran CA. Thymoma: radiologic-pathologic correlation. Radiographics. 1992;12(1):151–68.
171. Morgenthaler TI, Brown LR, Colby TV, Harper CM Jr, Coles DT. Thymoma. Mayo Clin Proc. 1993;68(11):1110–23.
172. Kim DJ, Yang WI, Choi SS, Kim KD, Chung KY. Prognostic and clinical relevance of the World Health Organization schema for the classification of thymic epithelial tumors: a clinicopathologic study of 108 patients and literature review. Chest. 2005;127(3):755–61.
173. Freundlich IM, McGavaran MH. Abnormalities of the thymus. J Thorac Imaging. 1996;1:58–65.
174. McLoud TC, Boiselle PM. Thoracic radiology: the requisites. 2nd ed. Philadelphia: Mosby; 2010. p. 427–9, 452–453.
175. Yaris N, Nas Y, Cobanoglu U, Yavuz MN. Thymic carcinoma in children. Pediatr Blood Cancer. 2006;47(2):224–7.
176. Lucchi M, Mussi A, Basolo F, Ambrogi MC, et al. The multimodality treatment of thymic carcinoma. Eur J Cardiothorac Surg. 2001;19(5):566–9.
177. Ueno T, Tanaka YO, Nagata M, et al. Spectrum of germ cell tumors: from head to toe. Radiographics. 2004;24:387–404.
178. Khan AN. Mediastinal germ cell tumor imaging. http://emedicine.medscape.com/article/359110-overview; 2008.
179. Sakurai H, Asamura H, Suzuki K, et al. Management of primary malignant germ cell tumor of the mediastinum. Jpn J Clin Oncol. 2004;34(7):386–92.
180. Reed JC, Hallet KK, Feigin DS. Neural tumors of the thorax: subject review from the AFIP. Radiology. 1978;126:9–17.
181. Mehta K, Haller JO, Legasto AC. Imaging neuroblastoma in children. Crit Rev Comput Tomogr. 2003;44(1):47–61.
182. Lonergan GJ, Schwab CM, Suarez ES, Carlson CL. Neuroblastoma, ganglioneuroblastoma, and ganglioneuroma: radiologic-pathologic correlation. Radiographics. 2002;22(4):911–34.
183. Donnelly LF, Frush DP, Zheng JY, Bisset GS III. Differentiating normal from abnormal inferior thoracic paravertebral soft tissues on chest radiography in children. AJR Am J Roentgenol. 2000;175(2):477–83.
184. Temes R, Allen N, Chavez T. Primary mediastinal malignancies in children: report of 22 patients and comparison to 197 adults. Oncologist. 2000;5:179–84.
185. Strollo DC, Rosado-de-Christenson ML, Jett JR. Primary mediastinal tumors: part II. Tumors of the middle and posterior mediastinum. Chest. 1997;112:1344–57.
186. Levine E, Huntrakoon M, Wetzel LH. Malignant nerve-sheath neoplasms in neurofibromatosis: distinction from benign tumors by using imaging techniques. AJR Am J Roentgenol. 1987;149(5):1059–64.

Pediatric Pulmonary Embolism

16

Abbey J. Winant and Edward Y. Lee

Clinical Considerations

Epidemiologic Characteristics

Previously considered rare in pediatric patients, pulmonary embolism (PE) has a higher incidence in children than previously thought [1]. Several studies have demonstrated a prevalence ranging from 14% to 17% of PE among children with clinical suspicion of PE [2–4]. This prevalence approaches the 23.3% prevalence of PE in adults reported in the adult PIOPED II trial [5]. The exact incidence of pediatric PE is unknown because many cases are misdiagnosed as other cardiopulmonary diseases, without cross-sectional imaging evaluation [2]. Consequently, most epidemiologic studies are based on autopsy findings or children with known venous thromboembolism (VTE) [2]. For example, a large retrospective review of 3600 pediatric autopsies demonstrates a 3.7% incidence of PE, contributing to death in 31% of cases [6]. Furthermore, the incidence of hospital-associated venous thromboembolism, including deep venous thrombosis and PE, has increased in pediatric patients [7, 8].

Clinical Presentation

PE presents differently in children than in adults. The classic symptoms of PE in adults, including dyspnea, hemoptysis, and pleuritic chest pain, are often not present in pediatric patients with PE unless there is a very large clot burden. Most children have a significant cardiopulmonary reserve allowing them to compensate for PE [1]. Therefore, affected pediatric patients typically present with more subtle, vague symptoms, mimicking other pulmonary disease processes. In fact, pediatric pulmonary emboli that obstruct less than 50% of the pulmonary circulation are often clinically silent unless the patient has coexisting cardiopulmonary disease [9]. Consequently, high clinical suspicion is important for the prompt detection and management of PE in pediatric patients. It is important to note that pediatric PE is not correlated with patient age or sex, and can affect even very young children, including infants and neonates [2, 10]. Symptomatic children often present with tachypnea, syncope, dysrhythmia, hypotension, and right heart failure. Of note, persistent tachypnea is a particularly important indicator of PE in pediatric patients [11]. Interestingly, adolescents with PE most often present with pleuritic chest pain (84%) [12].

Pathophysiology

The pathophysiology of PE in children is also different than adults. First, in adults, the vast majority of PE originate from the lower extremity venous valve pockets, with upper extremity thrombosis only accounting for 4–10% of adult PE [13, 14]. However, in children, the upper extremity veins are an important source of PE, accounting for almost two-thirds of cases in children (60%) [15]. In fact, a large study of pediatric PE found that lower extremity Doppler venous ultrasound was positive for lower extremity DVT in only 10% of pediatric PE cases [2].

Risk Factors

Another important difference between adult and pediatric PE is the presence of risk factors. In adults, PE is idiopathic in up to 31% of cases, whereas children with PE almost always have an identifiable risk factor (96–98% of cases) [15, 16]. A large study identified five statistically significant independent risk factors for PE in pediatric patients: immobilization, hypercoagulable state, excess estrogen state, indwelling central venous catheters (CVC),

A. J. Winant (✉) · E. Y. Lee
Department of Radiology, Boston Children's Hospital and Harvard Medical School, Boston, MA, USA
e-mail: abbey.winant@childrens.harvard.edu

R. H. Cleveland, E. Y. Lee (eds.), *Imaging in Pediatric Pulmonology*, https://doi.org/10.1007/978-3-030-23979-4_16

and prior deep venous thrombosis or prior pulmonary thromboembolism (Fig. 16.1) [10]. Furthermore, the vast majority of pediatric patients with PE had two or more risk factors (75–89%) [10, 15]. Of these risk factors, the presence of an indwelling CVC may be the most important risk factor (Fig. 16.2). Indeed, a large study demonstrated that all children who died as a result of PE had CVC-related upper extremity thrombosis [15]. Of note, positive D-dimer result did not have a statistically significant relationship with the presence of pediatric PE; however, inpatient status did have a significant relationship with the presence of pediatric PE [10].

Thromboembolic risk factor assessment is an important first-line triage tool for the utilization of advanced imaging in pediatric patients with clinical suspicion of PE [10]. In children with clinically suspected PE, utilizing the presence of two or more thromboembolic risk factors (previously described) as a clinical threshold for CTPA results in high sensitivity (89%) and specificity (94%) for the detection of pediatric PE (Figs. 16.3 and 16.4) [10]. In summary, in pediatric patients with no thromboembolic risk factors, CTPA is very unlikely to be positive for PE, despite clinical suspicion of PE (Fig. 16.3) [10].

Of note, thromboembolic risk factor assessment for PE should be tailored to patient age. For example, in older children and young adults (19–25 years), a unique set of three statistically significant independent risk factors for PE have been identified: immobilization, history of prior PE or DVT, and cardiac disease [17]. In contrast to younger children, hypercoagulable state, excess estrogen state, and the presence of CVC were not found to be statistically significant risk factors for PE in older children and young adults [17]. Utilizing the presence of two or more of the unique risk factors as a clinical threshold for CTPA in older children and young adults results in high sensitivity (75%) and specificity (99%) for the detection of PE [17].

Another important consideration in risk factor assessment for pediatric PE is the presence of an underlying malignancy. A significant fraction (25–40%) of children with venous thromboembolism have a coexisting neoplasm [18]. Of note, pediatric oncology patients are at risk of both tumor emboli and bland venous thromboembolism. In fact, a large retrospective study found that PE is an unexpected finding on nearly 2% of routine contrast-enhanced chest CT examinations in pediatric oncology patients (Fig. 16.5) [18]. This prevalence approaches the reported prevalence

Variable	Patients with PE ($n = 36$)	Patients without PE ($n = 191$)	*P* Value*
Age (y)†	13.6 ± 5.4	14.1 ± 4.0	.529
Sex			.623
Male	18 (50)	87 (46)	
Female	18 (50)	104 (54)	
Clinical signs and symptoms			
Tachycardia	22 (61)	101 (53)	.466
Pleuritic chest pain	15 (42)	104 (54)	.203
Shortness of breath	17 (47)	96 (50)	.856
Increased oxygen requirement	9 (25)	48 (25)	.987
Pulmonary hypertension	7 (19)	7 (4)	.999
Hemoptysis	0	3 (2)	.999
Referral setting			
Inpatient	33 (92)	43 (23)	<.0001
Outpatient	2 (06)	68 (36)	
Emergency Department	1 (3)	80 (42)	
Multidetector CT scanner			
16 Detector row	7 (19)	42 (22)	.457
32 Detector row	7 (19)	53 (28)	
64 Detector row	22 (62)	96 (50)	
Risk factors			
Immobilization	27 (75)	10 (5)	<.0001
Indwelling CVL	20 (56)	24 (13)	<.0001
Prior PE and/or DVT	16 (44)	22 (12)	<.0001
Hypercoagulable state	8 (22)	13 (7)	.003
Excess estrogen state	8 (22)	12 (6)	.002
Malignancy	9 (25)	32 (17)	.243
Cardiac disease	3 (8)	18 (9)	.998

Fig. 16.1 Comparison of data in pediatric patients with and those without PE. Note: Unless otherwise specified, data are numbers of patients, with percentages in parentheses. Percentages may not add up to 100% owing to rounding. CVL central venous line, DVT deep venous thrombosis. *Calculated with the Fisher exact test (except the *P* value for age, which was calculated with the Student *t* test). †Data are means ± standard deviations. (Reprint with permission from Lee et al. [10])

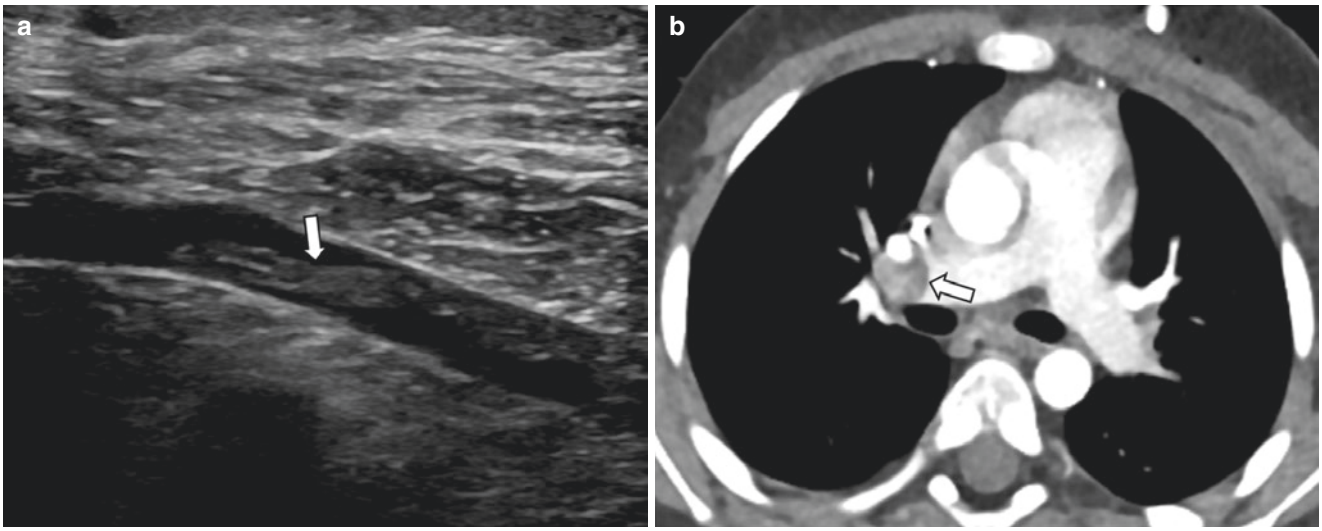

Fig. 16.2 A 4-year-old boy with leukemia with left upper extremity PICC presenting with tachycardia and shortness of breath. (**a**) Sagittal gray-scale image from a left upper extremity Doppler venous ultrasound demonstrates linear echogenic material (arrow) within an expanded left subclavian vein, reflecting acute deep venous thrombosis. (**b**) Axial CTPA image demonstrates expansile filling defect (arrow) with the right main pulmonary artery, suspicious for acute PE

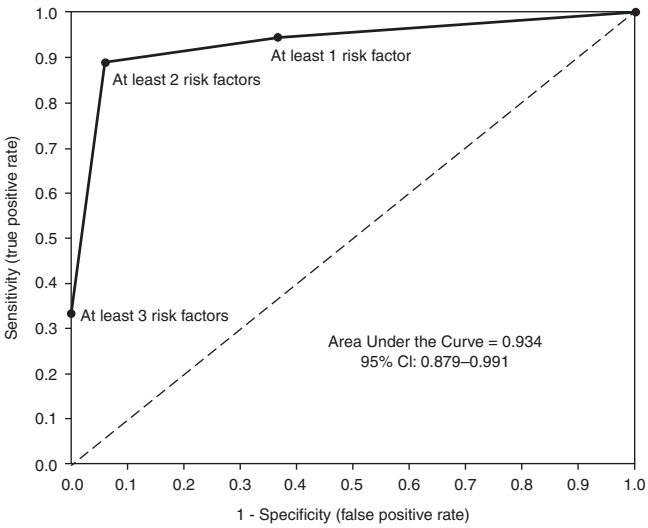

Fig. 16.3 ROC curve for differentiating patients with PE from those without PE on the basis of the total number of risk factors (immobilization, indwelling CVL, prior PE and/or DVT, hypercoagulable state, and excess estrogen state). Dashed line = 45° line of nondiscrimination (equivalent to coin tossing). The AUC of 0.934 indicates excellent discrimination ($P < 0.0001$). (Reprint with permission from Lee et al. [10])

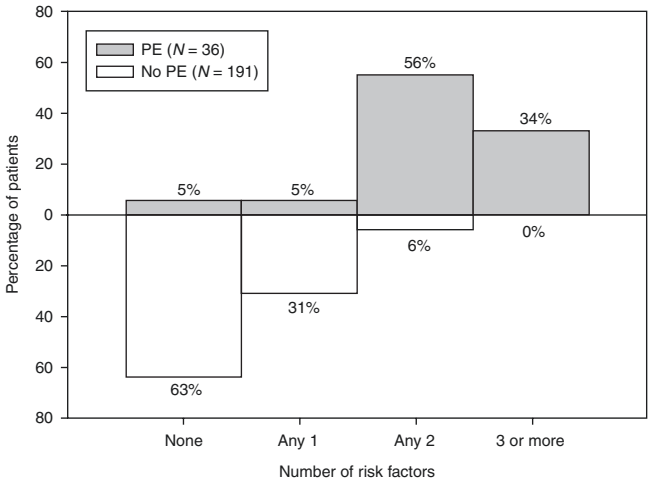

Fig. 16.4 Histogram shows a number of risk factors (immobilization, indwelling CVL, prior PE and/or DVT, hypercoagulable state, and excess estrogen state) in patients with PE and those without PE. Among the 36 patients with PE, 34 (94%) had at least two risk factors. Among the 191 patients without PE, 180 (94%) had no or only one risk factor. (Reprint with permission from Lee et al. [10])

of unsuspected PE in adult oncology patients (2.6–4.0%) [19–21]. The majority of unsuspected PE in pediatric oncology patients were located in the segmental (53%) and lobar (29%) pulmonary arteries, which is slightly less central than the adult oncology population in which unsuspected PE frequently extended into the main pulmonary arteries [18, 19, 21]. Similar to the adult oncology population, the majority of unsuspected PE in pediatric oncology patients were located in the lower lobes (91%) [18]. More than half of these unsuspected PE were not identified prospectively [18]. All the missed unsuspected PEs in pediatric oncology patients were solitary and the majority were in smaller segmental pulmonary arteries [18]. Risk factors for unsuspected PE in pediatric oncology patients include underlying coagulopathy and history of deep venous thrombosis or prior PE. Pediatric oncology patients are a unique subset of patients, in whom it is important to have a high clinical suspicion for PE.

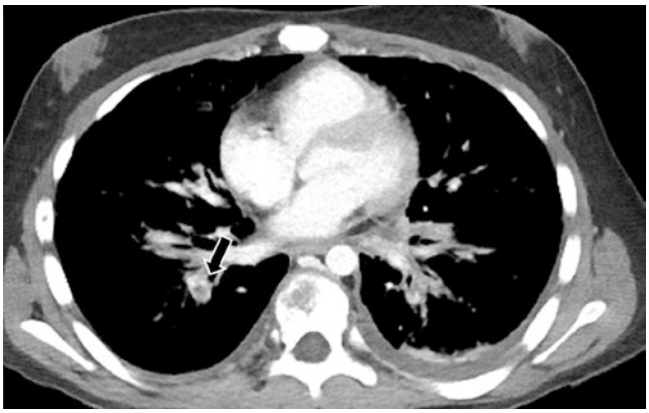

Fig. 16.5 Incidental PE in a 13-year-old boy with metastatic adenocarcinoma, unknown primary, who presented with dyspnea and left shoulder pain. Axial image from a routine contrast-enhanced CT chest demonstrates an expansile filling defect (arrow) in a right lower lobe segmental pulmonary artery. Trace right and small left pleural effusions are also visualized. Bilateral gynecomastia is also incidentally noted

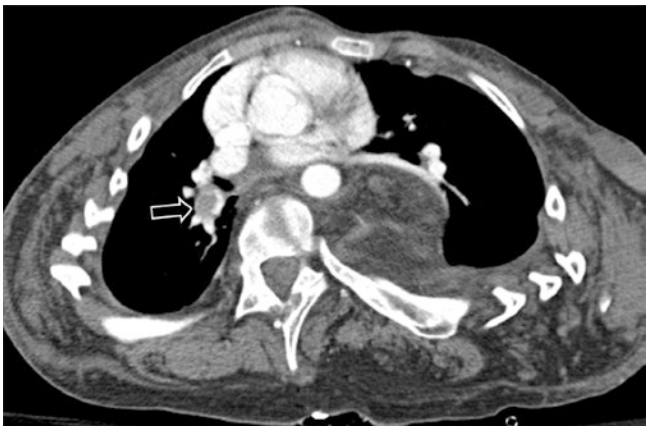

Fig. 16.6 A 10-year-old boy with CLOVES syndrome and known thoracic phlebectasia (not visualized on this image) with shortness of breath and right chest pain after the procedure. Axial CTPA image demonstrates an expansile filling defect (arrow) in a right lower lobar pulmonary artery, suspicious for acute PE

Lastly, there is an increased risk of PE in patients with complex vascular anomalies with overgrowth, including Klippel-Trenaunay syndrome and Proteus syndrome [22]. In particular, in patients with CLOVES syndrome (congenital lipomatous overgrowth, vascular malformations, epidermal nevi, and skeletal/scoliosis and spinal abnormalities), central and thoracic ectatic veins (phlebectasia) can predispose to PE (Fig. 16.6) [22]. The risk for PE is highest during the perioperative period [22]. In particular, the intraoperative prone position in CLOVES patients with innominate-subclavian phlebectasia is especially dangerous and is considered one of the few indications for preoperative placement of an SVC filter [22].

Imaging Techniques

Radiography

Chest radiographs are often the first imaging test performed in pediatric patients with clinical suspicion of PE. Chest radiographic findings are neither sensitive nor specific for the detection of PE, and advanced imaging is almost always required to make the diagnosis of PE. However, chest radiographs should be performed before CTPA in pediatric patients with suspected PE, because radiographs may sometimes identify an alternative diagnosis, such as pneumothorax, and obviate the need for CTPA [23].

Chest radiographs are frequently abnormal (up to 88%) in pediatric PE, with cardiomegaly being the most common chest radiographic abnormality associated with acute PE [24, 25]. In addition, chronic PE can also present with radiographic features of pulmonary arterial hypertension, including large central pulmonary arteries with rapid pruning and cardiomegaly, especially right heart enlargement. [26] Additional common radiographic abnormalities seen in PE include unilateral pleural effusion, elevated hemidiaphragm, atelectasis, and pulmonary parenchymal opacities. Classic radiographic signs of PE, such as the Hampton hump (pleural-based wedge-shaped opacification), Westermark sign (pulmonary oligemia), and Fleischner sign (prominent central pulmonary artery) are seen in a small subset of patients with PE (up to 20%), however not significantly different from control patients without PE (Figs. 16.7 and 16.8) [25]. Consequently, although chest radiographs are essential to the evaluation of pediatric PE, their main value is to exclude alternative diagnoses that may mimic PE, as well as to aid in interpretation of V/Q scans [25].

Multidetector CTPA

Multidetector CT pulmonary angiography (CTPA) is the imaging modality of choice for detection of pediatric PE, due to its widespread availability, fast scanning time, high spatial resolution, and high sensitive and specificity [9]. CTPA is performed with the patient in the supine position, with the scan field of view extending from the thoracic inlet through the diaphragm. Infants and children less than 5 years of age often require sedation for CTPA; however, the faster scanning times of newer scanners are making sedation less frequent [1]. In sedated patients, image acquisition may be performed at resting lung volumes. Scanning in the caudal-cranial direction may be helpful given the higher prevalence of PE in the lower lobes, with the goal of reducing respiratory motion artifact in the lower lobes in dyspneic patients [1]. Collimation depends on the number of detectors: 0.75 mm collimation for a 16-MDCT, 0.625 mm collimation

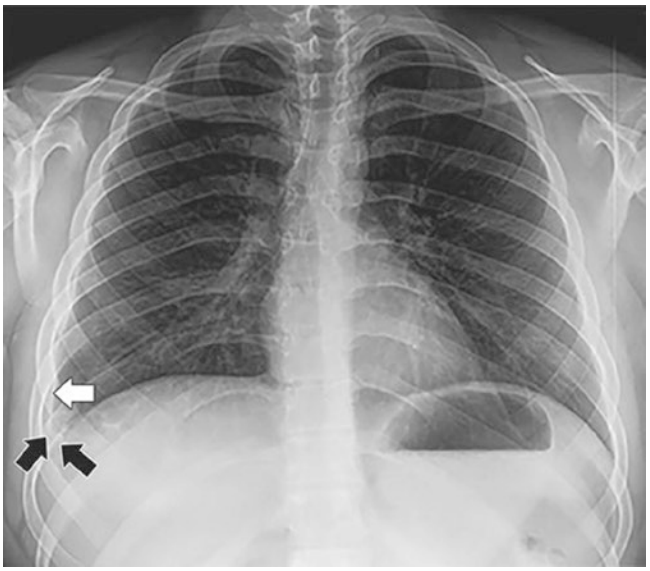

Fig. 16.7 A 17-year-old boy with prolonged immobilization after a motor vehicle collision, with acute onset of tachycardia. Frontal radiograph shows small right pleural effusion (white arrow) and pleural-based opacity (black arrow) in the right costophrenic angle, with triangular opacity, with superomedial margin pointing toward the hilum (Hampton hump), representing small pulmonary infarct. (Reprint with permission from Lee et al. [9])

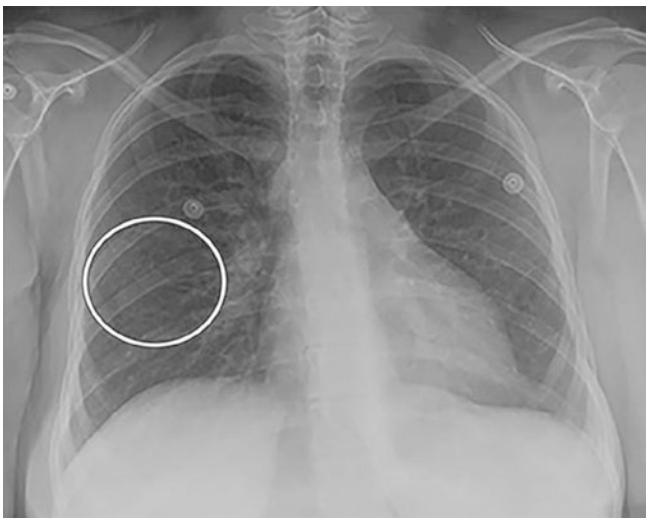

Fig. 16.8 A 17-year-old girl presenting with acute onset of shortness of breath. Frontal chest radiograph demonstrates subtle decreased vascularity (white circle) in the midportion of the right lung (Westermark sign). (Reprint with permission from Lee et al. [9])

for a 32-MDCT, and 0.60 mm collimation for a 64-MDCT. Weight-based low-kilovoltage scanning has been shown to increase the detection of central and peripheral pulmonary emboli while simultaneously decreasing radiation dose [27]. High pitch is recommended, ranging between 1.0 and 1.5. From the initial axial dataset, sagittal and coronal multiplanar reformats and 3D reconstruction of the pulmonary vasculature should be generated. The use of multiplanar reformats has been shown to significantly increase reader confidence and interobserver agreement for the detection of PE in both children and adults [3, 28].

Optimization of pulmonary arterial enhancement on CTPA is critical for the detection of pulmonary emboli. A large study of pediatric PE found that 80% of CTPA studies in children were limited in the evaluation of the subsegmental pulmonary arteries [2]. CTPA utilizes nonionic iodinated intravenous contrast (2–4 mL/kg, with total volume not exceeding 125 cc), which is preferably power injected at a rate dependent on IV catheter size (3.0 cc/sec for a 20-gauge catheter, 1.5–2.0 cc/sec for a 22-gauge catheter). Very small catheters (less than 22-gauge) or catheters in the hand or foot may be manually injected at a rate of approximately 1.0 cc/sec [1]. Larger catheter sizes and higher rates of power injection are preferred for optimal pulmonary arterial enhancement [1].

Pulmonary arterial enhancement is also affected by scan timing. Bolus tracking methods are preferred: a region of interest (ROI) placed over the pulmonary outflow tract triggers scan initiation when ROI reaches attenuation >150 Hounsfeld units [1, 23]. Alternatively, some institutions utilize a weight-based empiric scan delay of 12–25 seconds from the end of injection; however, given the wide variability in pediatric heart rates, this technique is likely to result in a higher frequency of scans with suboptimal pulmonary arterial enhancement [1].

Lastly, pulmonary arterial enhancement may be affected by respiratory cycle. Full inspiration may result in dilution of contrast secondary to differential flow rates in the superior vena cava and inferior vena cava, as well as decreased pulmonary blood flood secondary to Valsalva maneuver that often accompanies full inspiration [1, 29, 30]. Consequently, shallow free-breathing is recommended to optimize pulmonary arterial enhancement on CTPA [1, 29, 30].

CTPA technique should be slightly altered in children who have undergone Fontan procedure for congenital heart disease. CTPA studies are often technically inadequate in Fontan patients, often with suboptimal pulmonary arterial enhancement due to slow-flowing blood in the Fontan pathway and lack of mixing in the right atrium, which can lead to misdiagnosis of PE when no PE is actually present (Fig. 16.9) [1, 31]. One technique to overcome the challenges of CTPA in Fontan patients recommends simultaneous contrast injection through both upper and lower extremity veins, with the use of a second delayed-phase scan if there is a suboptimal pulmonary arterial enhancement on the initial images, especially in patients with a bilateral Glenn shunt and very sluggish flow in the Fontan pathway [31]. In addition, bolus tracking to initiate scan when enhancement is optimal in the Fontan pathway or pulmonary artery may also be helpful [31].

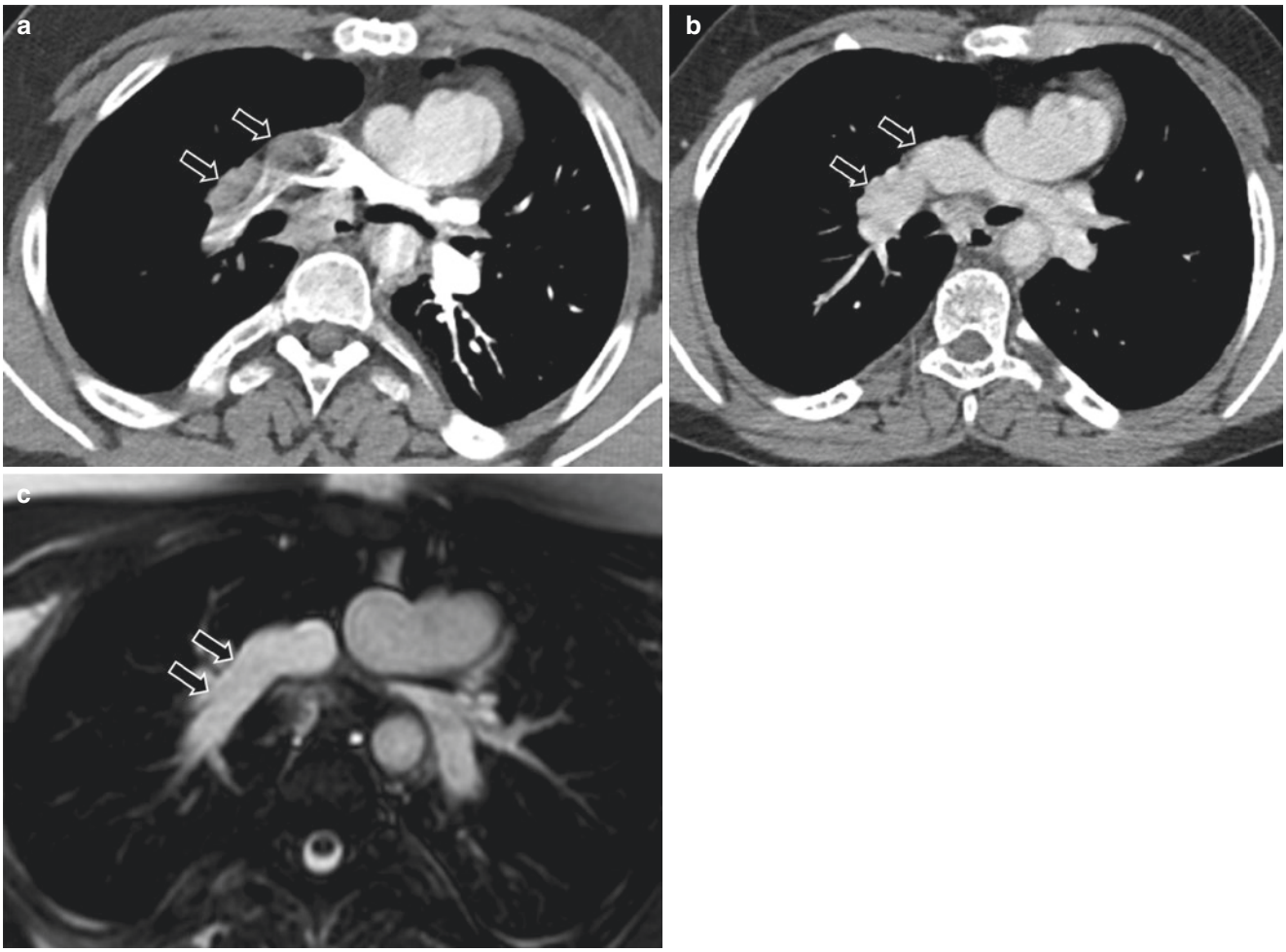

Fig. 16.9 A 14-year-old girl with Fontan with indeterminate CTPA study. (**a**) CTPA demonstrates suboptimal pulmonary arterial enhancement and apparent filling defects (arrows) in the right main pulmonary artery, which are indeterminate and may reflect pulmonary emboli and/or slow flow with mixing artifact in the Fontan pathway. (**b**) Delayed CT images demonstrate resolution of previously seen apparent filling defects in the right main pulmonary artery, which now appears nearly homogenously opacified (arrows). (**c**) Axial T2 fat-saturated MR image from a pulmonary MRA also demonstrates homogenous signal intensity in the right pulmonary artery (arrows), without filling defect, confirming that no pulmonary embolus is present

Magnetic Resonance Imaging

In the past, pediatric chest MRI has been limited by respiratory and cardiac motion, long acquisition time, low spatial resolution, and low signal-to-noise ratio due to air within the pulmonary parenchyma. However, recent technologic advances, including parallel imaging and time-resolved MRA, have significantly shortened acquisition times and improved spatial resolution [32]. Although CTPA is the current standard of care for detection of PE, mainly because it can be performed and interpreted rapidly MRI, MRI may be a viable imaging technique for pediatric PE in the appropriate clinical circumstance. For example, patients with contraindications to iodinated contrast, pregnant patients, and young patients in which radiation exposure is a concern, may be candidates for pulmonary MRA [32]. The patient's clinical condition should be assessed prior to pulmonary MRA. Critically ill patients are not candidates for pulmonary MRA, due to scan time and the need to move patients out of the magnet for resuscitative efforts [32].

Contrast-enhanced MRA (CE-MRA) is the MRI technique best suited to evaluate the pulmonary arteries for emboli [32]. Similar to CTPA, the goal in pulmonary CE-MRA is to enhance the pulmonary arteries to the subsegmental level to allow for the detection of intraluminal filling defects [32]. CE-MRA utilizes a gadolinium-based contrast agent (GBCA), with a common adult CE-MRA protocol for PE detection utilizing 0.1 mmol/kg gadobenate dimeglumine (Multihance), diluted with normal saline to a volume of 30 cc, injected at a rate of 1.5 cc/sec, for uniform bolus throughout the pulmonary arteries during k-space acquisition [32].

In addition, dynamic contrast-enhanced pulmonary perfusion MRI may be used to evaluate the perfusion of the pulmonary parenchyma to assess for perfusion defects. Following intravenous administration of GBCA, rapid volumetric imaging sequences, such as 3D spoiled gradient time-resolved MRI, can be used to assess pulmonary perfusion, either during long breath hold or shallow free breathing [32]. Dynamic contrast-enhanced pulmonary perfusion MRI may be used in conjunction with CE-MRA to improve detection of pulmonary emboli.

Although there are noncontrast techniques for pulmonary MRA, including time of flight, steady-state free precession, and phase contrast sequences, there is less evidence supporting their use for routine clinical use for detection of pulmonary emboli [32]. Time of flight and phase contrast sequences are frequently degraded by respiratory and cardiac motion. Some studies have shown that bright blood-balanced steady-state free precession may perform similarly to CE-MRA when evaluated the central and lobar pulmonary arteries; however, these sequences are often limited by respiratory motion and decreased signal in the segmental and smaller pulmonary arteries [32]. Overall, CE-MRA is the preferred technique when clinically feasible.

Nuclear Medicine

Lung ventilation-perfusion scintigraphy (V/Q scan) has historically played an important role in the diagnosis of PE. With a relatively low radiation dose, V/Q scanning remains a safe and helpful problem-solving tool when results are definitive. A normal perfusion scan essentially results out the diagnosis of clinically significant pulmonary embolus, while a high-probability scan confers an approximately 85% chance of PE (Fig. 16.10) [33, 34]. The major limitation of V/Q scintigraphy is the large number of low or intermediate probability scans. A current chest radiograph is required for the interpretation of the V/Q scan, and a normal chest radiograph decreases the number of nondiagnostic V/Q scans [34].

Perfusion scintigraphy is performed with technetium-99 m-labeled macroaggregated albumin (MAA) particles, with a recommended activity of 0.03 mCi/kg [9]. MAA particles are injected intravenously with the patient supine to prevent false positives. The injected MAA particles temporarily occlude the pulmonary arterial vasculature with regional particle distribution proportional to blood flow to that region of the lung. Portions of the lung with decreased radiotracer activity appear photopenic and correspond to areas of decreased pulmonary arterial perfusion. Imaging is performed with the patient upright if possible, with the goal of eight views: bilateral anterior and posterior oblique, anterior, posterior, and bilateral lateral. All eight views may not be obtainable in critically ill patients; however, a minimum of one anterior and bilateral oblique views are required for interpretation [9].

Ventilation scans are more technically challenging in pediatric patients, especially in young children, because they require the child's active participation with aerosol inhalation. A variety of ventilation agents can be used, including technetium-99 m-labeled DTPA, Xenon-133, and Krypton-81 m. Perfusion scan is often performed first, given that a normal perfusion scan obviates the need for a ventilation scan [35].

V/Q scans in children are interpreted with the Modified PIOPED II V/Q scan interpretation criteria [9, 36]. These criteria classify V/Q scans into five categories: high probability, intermediate probability, low probability, very low probability, and normal. High probability scans are characterized by: two or more large segmental perfusion defects, without corresponding ventilation or radiographic abnormalities; 1 large segmental perfusion defect and at least two moderate segmental perfusion defects, without corresponding ventilation or radiographic abnormalities; or at least 4 moderate segmental perfusion defects without corresponding ventilation or radiographic abnormalities. A normal scan is when there are no perfusion defects. Normal scans generally exclude clinically significant PE. High probability and normal scans are seen in only 25% of cases [35]. All other scan categories are classified as nondiagnostic [9].

Catheter-Based Conventional Angiography

Conventional pulmonary angiography is the historic gold standard test used to diagnose PE [34, 37]. Angiography, however, is an invasive, expensive, time-consuming procedure, associated with a high radiation dose, which is suboptimal for pediatric patients. In addition, the procedure itself is associated with the risk of complications, including infection, bleeding, heart block, renal dysfunction, and even death. Patients with pulmonary hypertension have the highest risk of major complications [38].

Conventional pulmonary angiography technique utilized weight-based low-osmolar non-ionic contrast, injected through a pigtail catheter placed within the left or right main pulmonary artery. Depending on patient weight, a total of 10–50 cc of contrast may be injected, at a rate of 10–25 cc/sec. Diagnosis is made by detection of an intraluminal pulmonary arterial filing defect (Fig. 16.11). Although no studies have documented sensitivity and specificity of angiography in children, adult studies have found a high sensitivity and high negative predictive value (>99%) with non-diagnostic studies in only 3% of cases [9, 39]. Similarly, no studies have specifically evaluated the risks of conventional pulmonary angiography in pediatric patients. However, in

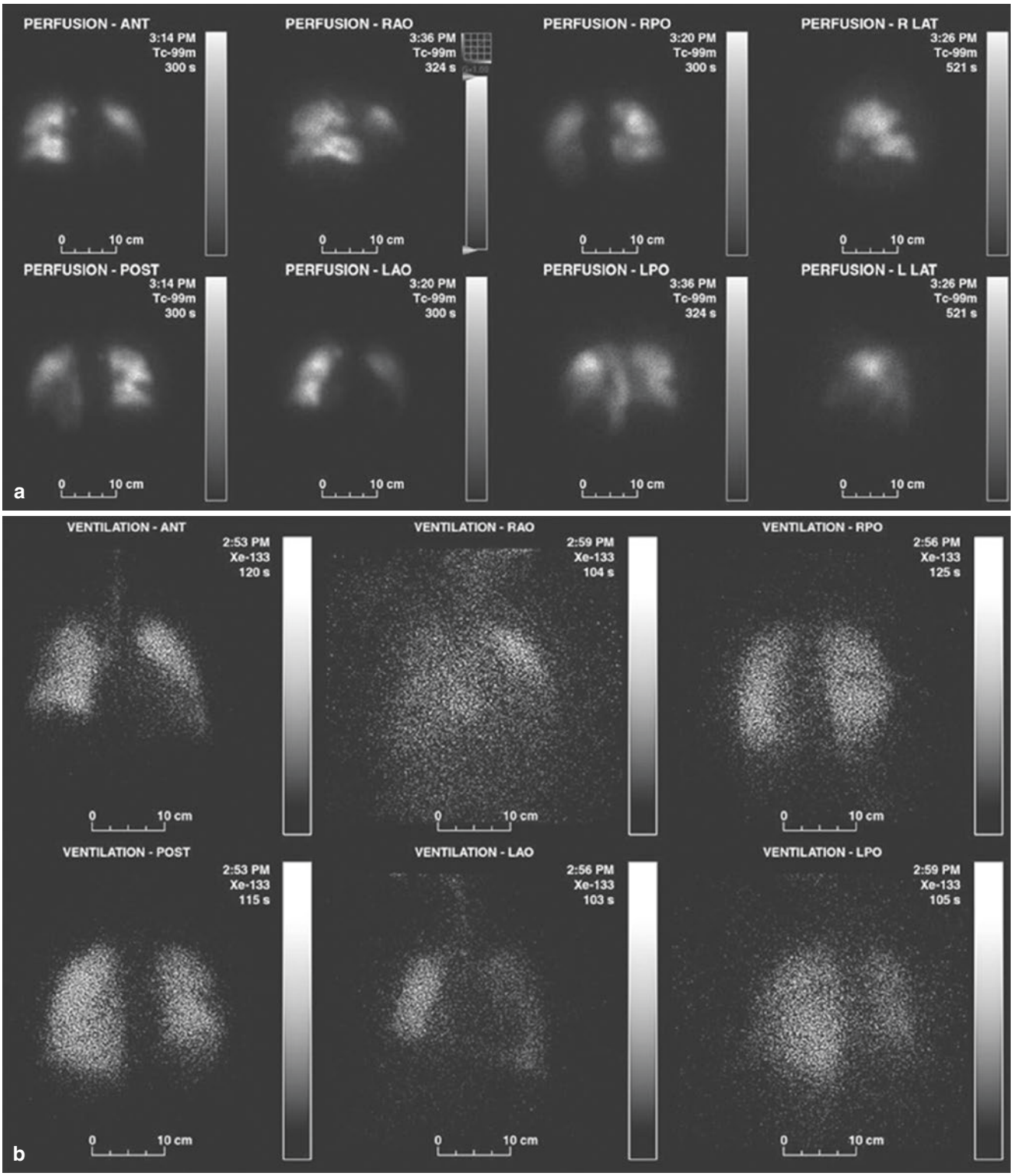

Fig. 16.10 An 18-year-old female with a history of allergy to iodinated contrast presenting with chest pain. Chest radiograph (not shown) was normal. ANT anterior, RAO right anterior oblique, RPO right posterior oblique, R LAT right lateral, POST posterior, LAO left anterior oblique, LPO left posterior oblique, L LAT left lateral. (**a**) Planar perfusion images from a V/Q scan demonstrate multiple peripheral wedge-shaped perfusion defects throughout the right lung. (**b**) Planar ventilation images from the same V/Q scan demonstrate a single ventilation defect in the right middle lobe. No other ventilation defects were identified. The findings of multiple mismatched perfusion defects, including a large perfusion defect in the left lower lobe, are consistent with a high probability of PE. (Reprint with permission from Lee et al. [9])

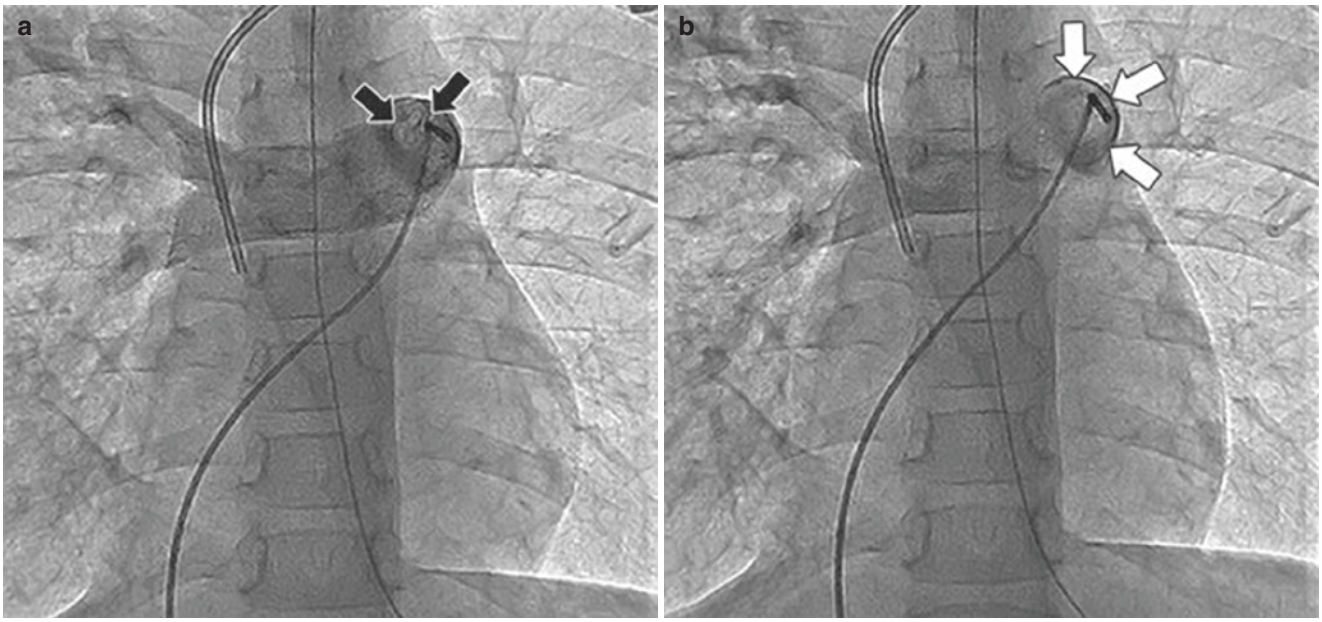

Fig. 16.11 A 12-year-old boy with left chest wall port and clinically suspected PE. (**a**) AP spot fluoroscopic image demonstrates percutaneously placed catheter tip in the main pulmonary artery. Contrast opacifies the right main pulmonary artery; however, the left main pulmonary artery is not opacified. Subtle irregular filling defect just to the right of the catheter tip (black arrows) presents the most proximal portion of a large left main pulmonary artery embolus. (**b**) AP spot fluoroscopic image obtained seconds after image A shows contrast meniscus (white arrows) outlining the periphery of the left main pulmonary artery, which is completely occluded by a clot. (Reprint with permission from Lee et al. [9])

the PIOPED study, death occurred in 0.5% of adult patients, major complications occurred in 1%, and minor complications in 5% [39]. Given this risk profile, as well as the wide availability of alternative imaging modalities, conventional pulmonary angiography is only recommended in pediatric patients with appropriate clinical indications, including the planning of invasive treatment, such as interventional embolectomy [9].

Imaging Findings

There are both vascular and avascular findings in pediatric PE.

Vascular Findings

The most direct imaging finding of acute PE is pulmonary arterial occlusion. Specifically, on CTPA and CE-MRA, PE appears as a nonenhancing filling defect, corresponding to the thromboembolus, within the pulmonary arterial lumen, resulting in partial or complete pulmonary arterial nonopacification (Fig. 16.12) [1]. The affected pulmonary artery may be enlarged relative to the other nonaffected pulmonary arteries of the same branching order.

Pediatric PE demonstrates a similar anatomic distribution to adult PE, most commonly occurring in the lobar pulmonary arteries (39%) and segmental (35%) arteries. Approximately one-quarter of pulmonary PE occur in the subsegmental (16%) and main pulmonary arteries (10%) [2]. The vast majority of pediatric pulmonary emboli are multifocal, distributed bilaterally (61%) more frequently than unilaterally (39%) [2]. Pediatric PE demonstrates a predilection for the lower lobes (>60%): right lower lobe (37%), left lower lobe (24%), right upper lobe (15%), right middle lobe (12%), and left upper lobe (12%) [2]. In summary, pulmonary emboli in children demonstrate an anatomic distribution similar to adults, including a predilection for the lobar and segmental pulmonary arteries, and the lower lobes [40, 41].

In addition, on nuclear medicine perfusion scans, as well as dynamic contrast-enhanced pulmonary perfusion MRI, there is decreased pulmonary perfusion in the pulmonary segments perfused by the affected pulmonary arteries containing thromboembolus.

Avascular Findings

There has been much research into the avascular imaging findings of PE. Many nonspecific pulmonary parenchymal and pleural changes have been described in association with

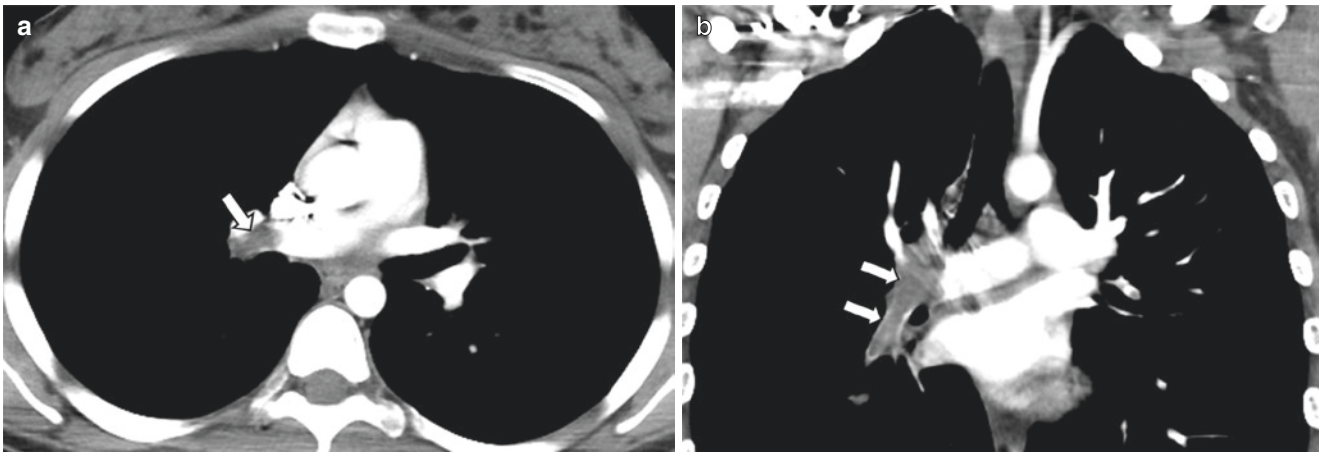

Fig. 16.12 A 17-year-old girl on oral contraceptive pills. Axial (**a**) and coronal (**b**) images from chest CTPA demonstrate a large filling defect (white arrows) in the right main pulmonary artery, with a prominent inferior extension on coronal images, consistent with PE

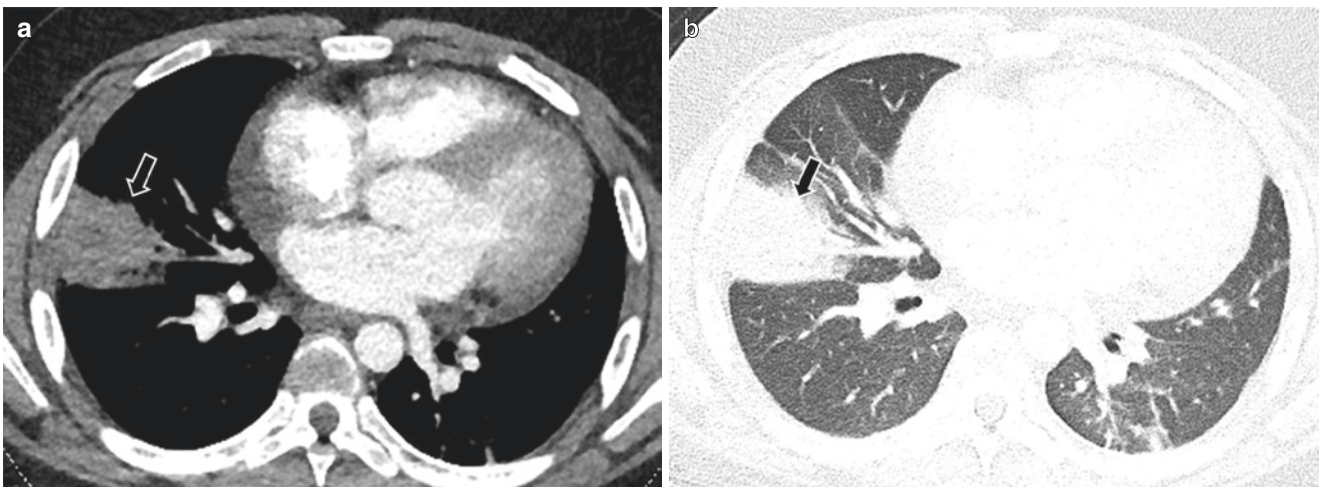

Fig. 16.13 A 15-year-old boy with acute lymphocytic leukemia. Axial CT images from a CTPA study in soft tissue (**a**) and lung (**b**) windows demonstrate a peripheral wedge-shaped consolidative opacity (black arrow) in the right lower lobe, suspicious for pulmonary infarction

pediatric PE, including wedge-shaped peripheral consolidation, linear opacities, pleural effusions, ground-glass opacities, atelectasis, nodules, and patchy areas of increased attenuation [42]. Most of these findings are nonspecific, with limited clinical utility for the detection of pediatric PE. However, wedge-shaped areas of peripheral consolidation are the only nonvascular pulmonary abnormality that has been shown to be significantly more common in children with PE (Fig. 16.13) [42].

Similar to adults, wedge-shaped peripheral consolidations are significantly associated with the presence of PE on CTPA studies in children [42]. In a large series of pediatric PE, the most common pleural and parenchymal findings associated with PE were: atelectasis, peripheral wedge-shaped consolidation, and pleural effusion [42]. However, the most common radiologic findings in a control group of pediatric patients without PE were atelectasis, ground-glass opacities, and pleural effusion [42]. Consequently, the only radiologic finding significantly associated with pediatric PE on CTPA was wedge-shaped peripheral consolidation, which was seen in approximately one-third of pediatric PE cases [42]. These wedge-shaped peripheral opacities typically demonstrate a board base abutting the peripheral pleural surface and a truncated apex. Furthermore, peripheral wedge-shaped consolidations occurred in a vascular distribution corresponding to identified PE in the majority of cases (75%), most likely reflecting pulmonary infarction [42]. Indeed, CT-pathologic correlation has demonstrated that in these wedge-shaped peripheral consolidations, the increased attenuation reflects secondary pulmonary lobules filled with

red blood cells, with or without frank pulmonary tissue necrosis, corresponding to pulmonary infarction [42–44].

Alternative Diagnoses

Unlike other imaging modalities to evaluate for PE, CTPA is unique and preferred because it provides a comprehensive evaluation of additional intrathoracic structures, including the pulmonary parenchyma, pleura, and mediastinum, allowing for detection of alternative etiologies of patient symptoms. In both adult and pediatric patients, CTPA frequently identifies an alternative diagnosis in patients with clinically suspected PE when PE is excluded (59% of children and 25% of adults) [4, 45]. In particular, in pediatric patients with clinically suspected but excluded PE, the most common alternative diagnoses are pneumonia (39%) and atelectasis (39%), which are also the most common alternative diagnoses in the adults with suspected but excluded PE [4, 44, 46]. Pleural effusions were a relatively common finding (30%); however, these were almost always associated with pneumonia or atelectasis. Rare alternative diagnoses discovered on CTPA in children with excluded PE included malignancy, congenital heart disease, pulmonary hypertension, pulmonary nodules, rib fractures, right atrial thrombus, and fat emboli [4]. Of note, pulmonary MRA has also been shown to identify alternative, actionable findings in patients suspected but excluded PE, with an incidence similar to that reported for CTPA [47]. Consequently, it is important to comprehensively search beyond the pulmonary arteries on cross-sectional imaging studies to identify common alternative diagnoses.

Conclusion

PE is a life-threatening condition that more commonly affects pediatric patients than previously thought and requires prompt diagnosis and treatment. Unique pediatric thromboembolic risk factor assessment is an important first-line triage tool for the utilization of imaging in pediatric patients with clinical suspicion of PE. CTPA is the current standard of care for detecting PE in pediatric patients; however, additional complementary modalities, including MRA, are available. Imaging of patients with suspected PE frequently identifies alternative etiologies for patient symptoms, with the most common alternative diagnoses in pediatric patients with clinical suspicion of PE being pneumonia and atelectasis. Up-to-date knowledge of imaging techniques, and characteristic vascular and avascular radiologic findings of pediatric PE is important for timely diagnosis and treatment.

References

1. Thacker PG, Lee EY. Advances in multidetector CT diagnosis of pediatric pulmonary thromboembolism. Korean J Radiol. 2016;17(2):198–208.
2. Kritsaneepaiboon S, Lee EY, Zurakowski D, Strauss KJ, Boiselle PM. MDCT pulmonary angiography evaluation of pulmonary embolism in children. AJR Am J Roentgenol. 2009;192(5):1246–52.
3. Lee EY, Zucker EJ, Tsai J, et al. Pulmonary MDCT angiography: value of multiplanar reformatted images in detecting pulmonary embolism in children. AJR Am J Roentgenol. 2011;197(6):1460–5.
4. Lee EY, Kritsaneepaiboon S, Zurakowski D, Arellano CM, Strauss KJ, Boiselle PM. Beyond the pulmonary arteries: alternative diagnoses in children with MDCT pulmonary angiography negative for pulmonary embolism. AJR Am J Roentgenol. 2009;193(3):888–94.
5. Stein PD, Fowler SE, Goodman LR, et al. Multidetector computed tomography for acute pulmonary embolism. N Engl J Med. 2006;354(22):2317–27.
6. Buck JR, Connors RH, Coon WW, Weintraub WH, Wesley JR, Coran AG. Pulmonary embolism in children. J Pediatr Surg. 1981;16(3):385–91.
7. Mahajerin A, Branchford BR, Amankwah EK, et al. Hospital-associated venous thromboembolism in pediatrics: a systematic review and meta-analysis of risk factors and risk-assessment models. Haematologica. 2015;100(8):1045–50.
8. Raffini L, Huang YS, Witmer C, Feudtner C. Dramatic increase in venous thromboembolism in children's hospitals in the United States from 2001 to 2007. Pediatrics. 2009;124(4):1001–8.
9. Thacker PG, Lee EY. Pulmonary embolism in children. AJR Am J Roentgenol. 2015;204(6):1278–88.
10. Lee EY, Tse SK, Zurakowski D, et al. Children suspected of having pulmonary embolism: multidetector CT pulmonary angiography--thromboembolic risk factors and implications for appropriate use. Radiology. 2012;262(1):242–51.
11. van Ommen CH, Heyboer H, Groothoff JW, Teeuw R, Aronson DC, Peters M. Persistent tachypnea in children: keep pulmonary embolism in mind. J Pediatr Hematol Oncol. 1998;20(6):570–3.
12. Bernstein D, Coupey S, Schonberg SK. Pulmonary embolism in adolescents. Am J Dis Child. 1986;140(7):667–71.
13. Spiezia L, Simioni P. Upper extremity deep vein thrombosis. Intern Emerg Med. 2010;5(2):103–9.
14. Montiel FS, Ghazvinian R, Gottsäter A, Elf J. Treatment with direct oral anticoagulants in patients with upper extremity deep vein thrombosis. Thromb J. 2017;15:26.
15. Monagle P, Adams M, Mahoney M, et al. Outcome of pediatric thromboembolic disease: a report from the Canadian Childhood Thrombophilia Registry. Pediatr Res. 2000;47(6):763–6.
16. Andrew M, David M, Adams M, et al. Venous thromboembolic complications (VTE) in children: first analyses of the Canadian Registry of VTE. Blood. 1994;83(5):1251–7.
17. Lee EY, Neuman MI, Lee NJ, et al. Pulmonary embolism detected by pulmonary MDCT angiography in older children and young adults: risk factor assessment. AJR Am J Roentgenol. 2012;198(6):1431–7.
18. Lee EY, Kritsaneepaiboon S, Arellano CM, Grace RF, Zurakowski D, Boiselle PM. Unsuspected pulmonary emboli in pediatric oncology patients: detection with MDCT. AJR Am J Roentgenol. 2010;194(5):1216–22.
19. Sebastian AJ, Paddon AJ. Clinically unsuspected pulmonary embolism--an important secondary finding in oncology CT. Clin Radiol. 2006;61(1):81–5.
20. Gladish GW, Choe DH, Marom EM, Sabloff BS, Broemeling LD, Munden RF. Incidental pulmonary emboli in oncology patients: prevalence, CT evaluation, and natural history. Radiology. 2006;240(1):246–55.

21. Storto ML, Di Credico A, Guido F, Larici AR, Bonomo L. Incidental detection of pulmonary emboli on routine MDCT of the chest. AJR Am J Roentgenol. 2005;184(1):264–7.
22. Alomari AI, Burrows PE, Lee EY, Hedequist DJ, Mulliken JB, Fishman SJ. CLOVES syndrome with thoracic and central phlebectasia: increased risk of pulmonary embolism. J Thorac Cardiovasc Surg. 2010;140(2):459–63.
23. Lee EY, Zurakowski D, Boiselle PM. Pulmonary embolism in pediatric patients survey of CT pulmonary angiography practices and policies. Acad Radiol. 2010;17(12):1543–9.
24. Elliott CG, Goldhaber SZ, Visani L, DeRosa M. Chest radiographs in acute pulmonary embolism. Results from the International Cooperative Pulmonary Embolism Registry. Chest. 2000;118(1):33–8.
25. Worsley DF, Alavi A, Aronchick JM, Chen JT, Greenspan RH, Ravin CE. Chest radiographic findings in patients with acute pulmonary embolism: observations from the PIOPED Study. Radiology. 1993;189(1):133–6.
26. Woodruff WW 3rd, Merten DF, Wagner ML, Kirks DR. Chronic pulmonary embolism in children. Radiology. 1986;159(2):511–4.
27. Schueller-Weidekamm C, Schaefer-Prokop CM, Weber M, Herold CJ, Prokop M. CT angiography of pulmonary arteries to detect pulmonary embolism: improvement of vascular enhancement with low kilovoltage settings. Radiology. 2006;241(3):899–907.
28. Espinosa LA, Kelly AM, Hawley C, et al. Clinical utility of multiplanar reformation in pulmonary CT angiography. AJR Am J Roentgenol. 2010;194(1):70–5.
29. Renne J, Falck C, Ringe KI, Raatschen HJ, Wacker F, Shin HO. CT angiography for pulmonary embolism detection: the effect of breathing on pulmonary artery enhancement using a 64-row detector system. Acta Radiol. 2014;55(8):932–7.
30. Bauer RW, Schell B, Beeres M, et al. High-pitch dual-source computed tomography pulmonary angiography in freely breathing patients. J Thorac Imaging. 2012;27(6):376–81.
31. Prabhu SP, Mahmood S, Sena L, Lee EY. MDCT evaluation of pulmonary embolism in children and young adults following a lateral tunnel Fontan procedure: optimizing contrast-enhancement techniques. Pediatr Radiol. 2009;39(9):938–44.
32. Benson DG, Schiebler ML, Nagle SK, Francois CJ. Magnetic resonance imaging for the evaluation of pulmonary embolism. Top Magn Reson Imaging. 2017;26(4):145–51.
33. Papanicolaou N, Treves S. Pulmonary scintigraphy in pediatrics. Semin Nucl Med. 1980;10(3):259–85.
34. Patocka C, Nemeth J. Pulmonary embolism in pediatrics. J Emerg Med. 2012;42(1):105–16.
35. Babyn PS, Gahunia HK, Massicotte P. Pulmonary thromboembolism in children. Pediatr Radiol. 2005;35(3):258–74.
36. Worsley DF, Alavi A. Comprehensive analysis of the results of the PIOPED Study. Prospective Investigation of Pulmonary Embolism Diagnosis Study. J Nucl Med. 1995;36(12):2380–7.
37. Van Ommen CH, Peters M. Acute pulmonary embolism in childhood. Thromb Res. 2006;118(1):13–25.
38. Zuckerman DA, Sterling KM, Oser RF. Safety of pulmonary angiography in the 1990s. J Vasc Interv Radiol. 1996;7(2):199–205.
39. Stein PD, Athanasoulis C, Alavi A, et al. Complications and validity of pulmonary angiography in acute pulmonary embolism. Circulation. 1992;85(2):462–8.
40. Oser RF, Zuckerman DA, Gutierrez FR, Brink JA. Anatomic distribution of pulmonary emboli at pulmonary angiography: implications for cross-sectional imaging. Radiology. 1996;199(1):31–5.
41. Ritchie G, McGurk S, McCreath C, Graham C, Murchison JT. Prospective evaluation of unsuspected pulmonary embolism on contrast enhanced multidetector CT (MDCT) scanning. Thorax. 2007;62(6):536–40.
42. Lee EY, Zurakowski D, Diperna S, d'Almeida Bastos M, Strauss KJ, Boiselle PM. Parenchymal and pleural abnormalities in children with and without pulmonary embolism at MDCT pulmonary angiography. Pediatr Radiol. 2010;40(2):173–81.
43. Balakrishnan J, Meziane MA, Siegelman SS, Fishman EK. Pulmonary infarction: CT appearance with pathologic correlation. J Comput Assist Tomogr. 1989;13(6):941–5.
44. Shah AA, Davis SD, Gamsu G, Intriere L. Parenchymal and pleural findings in patients with and patients without acute pulmonary embolism detected at spiral CT. Radiology. 1999;211(1):147–53.
45. van Strijen MJ, Bloem JL, de Monye W, et al. Helical computed tomography and alternative diagnosis in patients with excluded pulmonary embolism. J Thromb Haemost. 2005;3(11):2449–56.
46. Tsai KL, Gupta E, Haramati LB. Pulmonary atelectasis: a frequent alternative diagnosis in patients undergoing CT-PA for suspected pulmonary embolism. Emerg Radiol. 2004;10(5):282–6.
47. Schiebler ML, Ahuja J, Repplinger MD, et al. Incidence of actionable findings on contrast enhanced magnetic resonance angiography ordered for pulmonary embolism evaluation. Eur J Radiol. 2016;85(8):1383–9.

Asthma

17

Annabelle Quizon, Katie Krone, and Marilynn Chan

Definition and Pathophysiology

Asthma is a common chronic disease of the airways that is complex and characterized by variable and recurring symptoms, airflow obstruction, bronchial hyperresponsiveness, and underlying inflammation. The interaction of these features determines the clinical manifestations and severity of the disease and response to treatment [1].

Airflow limitation is secondary to a number of mechanisms: (1) bronchoconstriction arising from bronchial smooth muscle contraction in response to stimuli or triggers such as viral infections especially in children, allergens, and irritants; (2) airway edema from mucus hypersecretion; (3) airway hyperresponsiveness to a variety of stimuli and secondary to interplay of inflammation, abnormal neuroregulation, and structural changes; and (4) airway remodeling [1–3]. The latter is associated with permanent changes in the airways that further impact on airflow obstruction and response to treatment.

Airway inflammation plays a central role in the pathophysiology of asthma. It involves the interaction of a number of cells such as mast cells, eosinophils, T lymphocytes, macrophages, neutrophils, and epithelial cells. These cells release chemokines and cytokines resulting in further recruitment of inflammatory cells and modification of the inflammatory response. Recent advances in the treatment of asthma have focused on targeted therapies against inflammatory mediators.

A. Quizon (✉)
Department of Respiratory Medicine, University of California San Diego- Rady Children's Hospital, San Diego, CA, USA
e-mail: anquizon@ucsd.edu

K. Krone
Division of Pulmonary Medicine, Boston Children's Hospital, Harvard Medical School, Boston, MA, USA

M. Chan
Department of Pediatric Pulmonology, University of California San Francisco Medical Center, San Francisco, CA, USA

Factors Influencing Asthma Manifestations

Host factors, notably genetic susceptibility and environmental exposures, play important roles in the clinical manifestations of asthma. Several genes have been linked to asthma and atopy, and aggregates in families [4–6]. Genome-wide association study (GWAS) discoveries have identified several genes or loci associated with asthma susceptibility [7–9]. Genetic factors have also been studied as regards severity and progression of the disease, specifically addressing biomarkers, pharmacogenetics, and gene-environment interactions [10–14].

Environmental factors that are associated with disease prevalence are legion and include diet, microbial exposure and viral respiratory tract infections, airborne allergens and irritants, tobacco smoke exposure, and outdoor pollution [15–18]. Significant allergen exposure especially to rodent, cockroach, and dust mite allergens has been shown to underlie the high prevalence of asthma in inner city populations [19]. Respiratory viruses have been associated as well with the development of asthma and its recurrences or exacerbations. Respiratory syncytial virus (RSV) and rhinovirus infections have been associated with recurrent and persistent wheezing into late childhood [20–22]. The *hygiene hypothesis,* however, suggests that exposure to infection and endotoxins early in life shapes the pattern of development of immune function along a nonallergic pathway and thereby reduces the risk of asthma and other allergic diseases [23–25]. Research has also focused on the association of the lung and gut microbiome with allergy and asthma; studies have been done regarding the use of antibiotics early in life and increased susceptibility of asthma [26, 27]. *The biodiversity hypothesis* extends the *hygiene hypothesis* such that disturbances in the composition of the gut microbiome disrupt immunological tolerance [28, 29].

Nutritional deficiencies and excesses have likewise been shown to impact on asthma morbidity and the development of allergies. Specifically, vitamin D has been linked to immune system and lung development in utero; its defi-

R. H. Cleveland, E. Y. Lee (eds.), *Imaging in Pediatric Pulmonology*, https://doi.org/10.1007/978-3-030-23979-4_17

ciency is associated with increased risk of asthma, allergies, and obesity [30, 31]. Conversely, supplementation early in life including higher maternal intake during pregnancy decreases the risk for recurrent wheeze in childhood [32]. The increasing prevalence of obesity has been associated with a concomitant increase in respiratory complications such as sleep disordered breathing and asthma. The nature of the association with asthma is complex and transcends the effect of obesity on chest wall mechanics to include complex inflammatory pathways shared by both conditions [33–36].

Diagnosis of Asthma

Asthma is typically a clinical diagnosis. The presence of risk factors is helpful in diagnosis especially in a young child with recurrent or persistent respiratory symptoms. Predictive risk factors have been described notably from the Tucson Birth cohort; both the original and modified versions of the Asthma Predictive index were developed from this cohort and have included personal history of eczema and allergic rhinitis, parental history of asthma, allergic sensitization to aeroallergens and to food products, as well as blood eosinophilia [37, 38]. A number of tests including radiographic studies as described in this chapter can be helpful to support the diagnosis of asthma and, for that matter, identify complications and alternative diagnosis. This said, following the adage that "not everything that wheezes is asthma," it is important to consider alternative diagnoses for recurrent cough and wheeze that can be extensive based on age.

Clinical Presentation

Typically, asthma presents with cough, wheezing, and dyspnea. Older patients may describe chest tightness. In some patients, cough may be a more prominent symptom than wheezing such that the term cough-variant asthma has been used. These symptoms are recurrent, worse at night, and may occur or worsen in the presence of known triggers such as exercise, viral infections, and exposure to airborne allergens or irritants.

During acute exacerbations, patients exhibit increased work of breathing with tachypnea and tachycardia. Physical exam findings include diffuse wheezing, usually expiratory, prolonged expiration, chest retractions, and use of accessory muscles of respiration. The absence of wheezing may, however, be an ominous sign of critical airway obstruction. Hypoxemia results from ventilation–perfusion mismatching; airway obstruction may progress to respiratory failure with hypercarbia.

Pulmonary Function Testing

Objective assessment of airflow obstruction and its severity should be performed in patients with the diagnosis of asthma. Spirometry is usually applicable for children over 4 years of age and measures the maximal volume of air forcibly exhaled from the point of maximal inhalation (FVC), the volume of air exhaled during the first second of the maneuver (FEV_1), and the ratio of FEV_1 to FVC. The most widely used parameter to define the severity of airflow obstruction is FEV_1 as a percentage of predicted. Reversibility of airflow obstruction is also ascertained by the improvement in FEV_1 of >12% or 200 mL after inhalation of a short-acting bronchodilator. Periodic monitoring of pulmonary function with the use of spirometry is recommended.

Forced oscillation technique (FOT) is preferred for young children who are unable to perform spirometry as it is noninvasive and requires the patient to simply breathe normally into the apparatus. FOT applies small oscillations of pressure, and thus flow, on the patient's airway in order to determine the resistance and reactance, otherwise known as the impedance, of the respiratory system. The impedance is a reflection of airway resistance and airflow limitation. As such, it can be applied to diagnose reversible airway obstruction by noting a significant decrease in resistance after bronchodilator administration [39, 40]. A notable limitation of FOT is the lack of reference standards due to variations in technique and studied populations [41].

Additional Diagnostic Tests

Bronchial Challenge and Exercise Challenge Tests

These tests are used to document bronchial hyperreactivity by inducing bronchospasm in asymptomatic patients. Bronchial challenge tests with inhalation of methacholine, hypertonic saline, histamine, or adenosine are utilized to elicit hyperresponsiveness. Exercise challenge tests are used in patients with exercise-induced symptoms. The test involves treadmill, cycle, or other standardized exercise. In some laboratories, a cold air inhalation challenge is used in lieu of the exercise challenge and involves hyperventilation of subfreezing dry air for about 4 min. In these challenge tests, a positive result is a standardized level of decline in FEV_1 from a predetermined baseline [42, 43].

Exhaled Nitric Oxide

Endothelial nitric oxide is generated from vascular endothelium in the lung and is present in exhaled breath [44]. Measurement of fractional exhaled nitric oxide (FeNO) utilizing commercial devices provides a rapid and noninvasive marker of airway inflammation. Elevated levels have been found to correlate with airway eosinophilia, and a reduction

of FeNO after using inhaled corticosteroids can suggest response and adherence to medications. It is useful as an adjunctive tool for the diagnosis of asthma and in the assessment of asthma control. A limitation is that elevated values are not specific for asthma and can be seen in allergic rhinitis and gastroesophageal reflux, among other conditions.

Normal values are based on age. For children under 12 years of age, FeNO less than 20 parts per billion (ppb) is normal and suggests that eosinophilic inflammation, and response to steroids is less likely. Conversely, values greater than 35 ppb suggests eosinophilic inflammation and response to steroids. Intermediate values require clinical correlation [45].

Blood Eosinophilia and Immunoglobulin E

Elevated circulating eosinophil count may suggest atopy, although there are other causes of peripheral eosinophilia such as parasitic infection and eosinophilic syndromes. The Asthma Predictive Index (API) includes blood eosinophilia >4% as a minor criterion for persistent wheezing in children [37, 38]. Similarly, elevated total serum immunoglobulin E (IgE) >100 IU/ml has been found to correlate with aeroallergen sensitization and early development of asthma.

Allergy Testing

Confirmation of allergy is usually recommended for patients in whom allergic factors or triggers are deemed by history to contribute significantly to asthma symptoms. This is done by demonstration of specific IgE by percutaneous skin prick testing or by serum-specific IgE measurement.

Sputum Cytology

Sputum induction by hypertonic saline inhalation has been utilized to identify the presence of eosinophils or other inflammatory cells in the airways. Eosinophilic asthma is defined as greater than normal eosinophils (>2% of the viable sputum cell count) and is usually responsive to steroid therapy [46, 47]. Inflammatory subtypes based on airway cytology are further described in the following subsection.

Bronchoscopy with Bronchoalveolar Lavage and Biopsy

Bronchoscopy is an invasive technique but can be indicated in the evaluation and management of difficult to control or severe asthma; it is also helpful in identifying airway abnormalities or lesions insofar as alternative diagnoses are concerned. When performed with bronchoalveolar lavage (BAL), cytology of BAL can reveal the inflammatory cellular profile (eosinophilic, neutrophilic, or paucigranulocytic); such provides further insight into immunopathology, asthma severity, and response to treatment [48–50]. Biopsy of the airway in asthmatic patients is performed infrequently and primarily for research purposes. However, when endobronchial biopsies are taken, the histopathology tends to reveal increased airway smooth muscle, basement membrane thickening, and intraepithelial cells such as eosinophils, neutrophils, and lymphocytes, compared to normal [51–54]. Lung autopsies in fatal cases of pediatric asthma have found thickened reticular basement membrane and increased eosinophils and mucus plugs [55].

Genetic Studies

GWAS have identified several genes or loci that are associated with asthma susceptibility. A number of asthma susceptibility genes have been replicated in some but not all populations, implying heterogeneity in the genetic risk in populations of different ethnic backgrounds [7–9]. Genetic factors have also been studied linking asthma to other allergic phenotypes and affecting progression and severity of the disease including those that confer additional risk for future lung function decline [56, 57].

Radiographic Studies

Radiographic findings in asymptomatic children with intermittent asthma episodes often reveal a chronic, stable presence of bronchial wall thickening with normal lung volumes or the chest radiograph may be normal. A chest radiograph is not a requisite to establish a diagnosis of asthma but is useful when complications such as pneumothorax or acute pneumonia are suspected or an alternative diagnosis such as foreign body is being considered (see Section on Alternative Diagnoses). Considering the variability in the severity of the disease, there are radiographic findings considered typical of asthma. Most commonly, during an acute episode, hyperinflation and peribronchial thickening are demonstrated. Hyperinflation is demonstrated by hyperlucent lungs and findings of flat or low hemidiaphragms on the frontal view. Lateral view also will show flattening of the hemidiaphragms and hyperlucency in the retrosternal and retrocardiac areas (Fig. 17.1). Hyperinflation must be present on all images to be abnormal. If lacking on one image, there is no air trapping. Subsegmental atelectasis is also encountered and may be severe enough to involve a lobe. In infants who develop viral bronchitis or bronchiolitis, it is difficult to distinguish radiographic findings consistent with viral lower respiratory tract infections and asthma, which may coexist. In both cases, atelectasis occurs and may present as ill-defined opacities which are frequently overinterpreted as representing bacterial consolidation (Fig. 17.1). Bronchial wall thickening is found in either condition and may be perceived as increased in the para hilar regions. However, the bronchial wall thickening is diffuse throughout the lungs and only seems worse centrally because of the convergence of the bronchi toward the hila. The term para hilar peribronchial thickening has been used to describe this observation but is actually a misnomer.

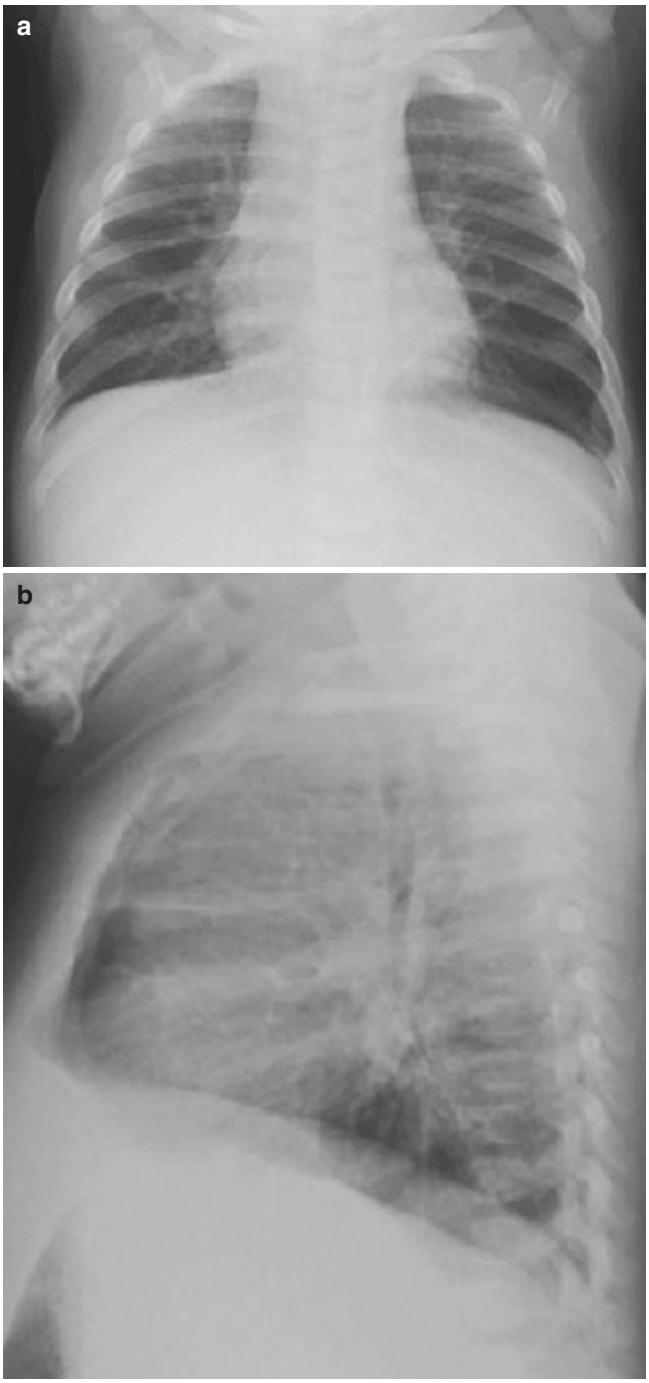

Fig. 17.1 PA (**a**) and lateral (**b**) chest radiographs show diffuse bronchial wall thickening, multifocal subsegmental atelectasis, and hyperinflation. Hyperinflation must be present on all images to be abnormal. If lacking on one image, there is no air trapping. Bronchial wall thickening or peribronchial thickening (PBT) is a common manifestation of asthma and is indistinguishable from that seen in lower airway viral infections. However, PBT often will be recognizable in known asthmatics who are currently asymptomatic. This scenario is also the initial imaging manifestation in many children with cystic fibrosis. Hyperaeration is seen in asthmatics who are acutely symptomatic as is true for infants with bronchiolitis. Subsegmental atelectasis is often present in acutely ill asthmatics as well as infants with bronchiolitis

Intrathoracic air leaks occur as complications of asthma and in the setting of acute exacerbations. Pneumomediastinum presents as lucency adjacent to the mediastinal structures (Fig. 17.2). Patients may be asymptomatic but may complain of chest pain or dysphagia. Subcutaneous emphysema may be appreciated as gas dissects into the neck and soft tissues of the upper neck (Fig. 17.2) and sometimes even into the retroperitoneum. Pneumothoraces also occur, but a tension pneumothorax is rare in asthma.

Allergic bronchopulmonary aspergillosis (ABPA) is an uncommon complication of childhood asthma and is discussed in the section on Comorbid Conditions. Radiographically, ABPA manifests with central bronchiectasis more prominent in the upper lobes (Fig. 17.3).

Bronchial casts are uncommon and nonspecific and can be found in the airways of patients with asthma, cystic fibrosis (CF), plastic bronchitis, cardiac abnormalities, ABPA, among other entities. Bronchial casts are mucoid plugs that form within the tracheobronchial tree in the form of a branching tubular cast of the airway. They have been histologically characterized as inflammatory or non-inflammatory as discussed in Chap. 6 of this textbook. Inflammatory casts are associated mostly with asthma and CF. Chest radiographs and high-resolution computed tomography often reveal atelectasis and consolidation due to obstruction of the affected airway (Fig. 17.4a, b) [58, 59]. Chest CT can be useful to guide targeted bronchoscopic removal of these casts.

Alternative Diagnosis

The diagnosis of asthma can usually be made by history, physical examination findings, and response to treatment. Adjunctive tools and laboratory testing as described in the preceding section are also helpful. Because of the high prevalence of asthma worldwide, alternative diagnoses tend to be missed. Such diagnoses must be explored if there is doubt about the diagnosis of asthma. Based on age, diagnoses to consider for wheezing, cough, or labored breathing are detailed below; note that some conditions overlap age groups [60].

In preschool age children, if symptoms do not respond to appropriate therapy, the following diagnoses should be considered: structural airway anomalies such as congenital or secondary airway malacia (tracheal and/or bronchial); tracheoesophageal fistula or from compression of the airway from congenital cysts or aberrant vessels (e.g., vascular ring or slings); aspiration syndromes, bronchopulmonary dysplasia, and diseases with airway complications such as CF, primary ciliary dyskinesia (PCD), immune deficiency or alpha-1-anti-trypsin deficiency, foreign body in the airway,

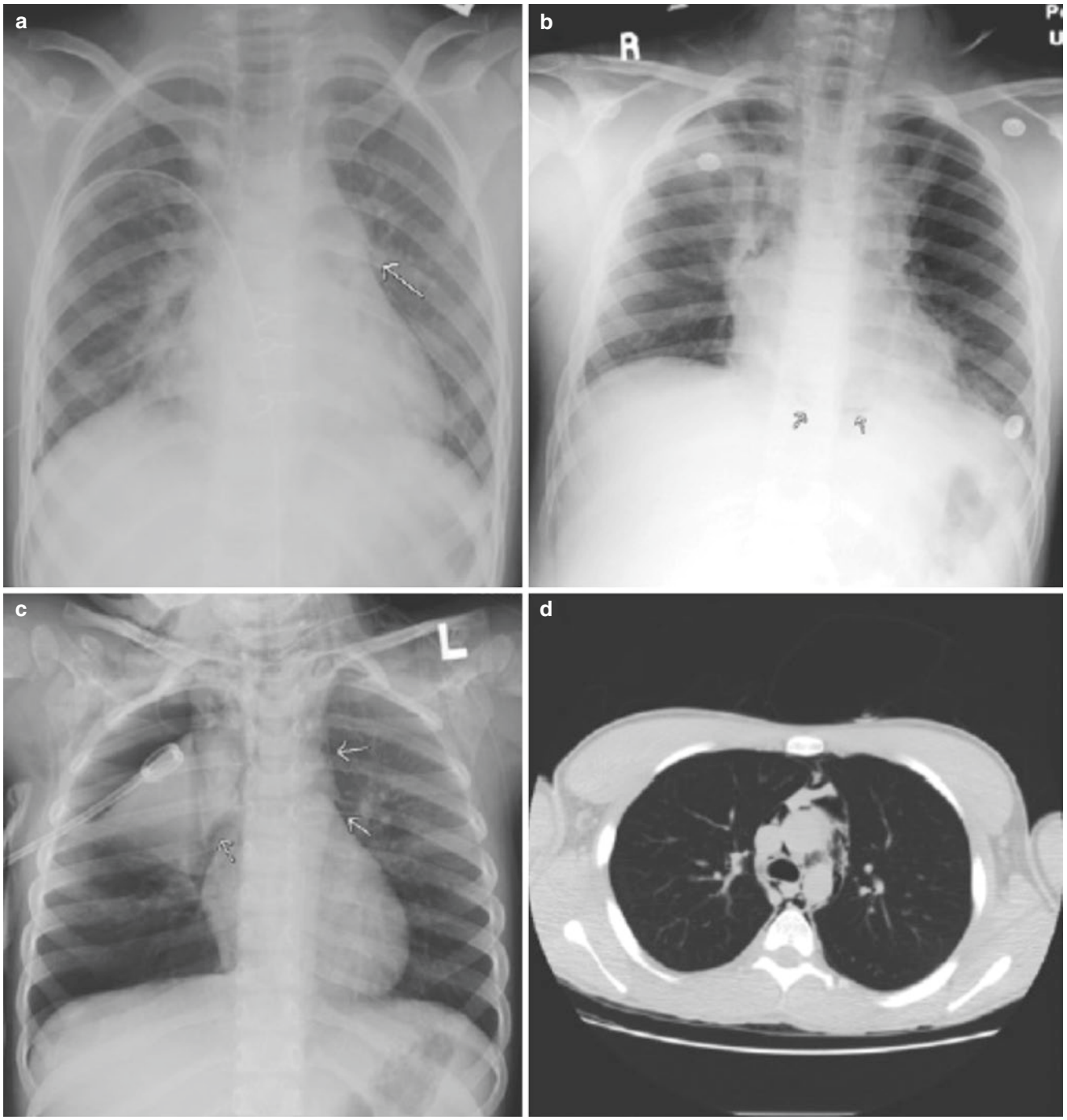

Fig. 17.2 Pneumomediastinum and subcutaneous air may be hallmarks of previously undiagnosed asthma or may be clinically suspected in children with known asthma. (**a**) There is a pneumomediastinum seen only on the left. It is distinguished from a medial pneumothorax by the small amount of air lifting the left lobe of the thymus off the mediastinum (*arrow*). (**b**) In a different patient, there is a relatively large pneumomediastinum, with a larger right component. A small amount of air is noted beneath the heart (*arrows*). Air also has extended into the neck. A small right pneumothorax is present. (**c**) Portable AP CXR reveals air within the mediastinum (*upper arrow*) with both lobes of the thymus separated from the heart by air (*lower arrows*) (air separating the thymus from the heart occurs only with pneumomediastinum or pneumopericardium). Subcutaneous air is present within the neck. There is a moderately large right pneumothorax. (**d**) In another patient, CT imaging easily shows an extensive pneumomediastinum with small left pneumothorax

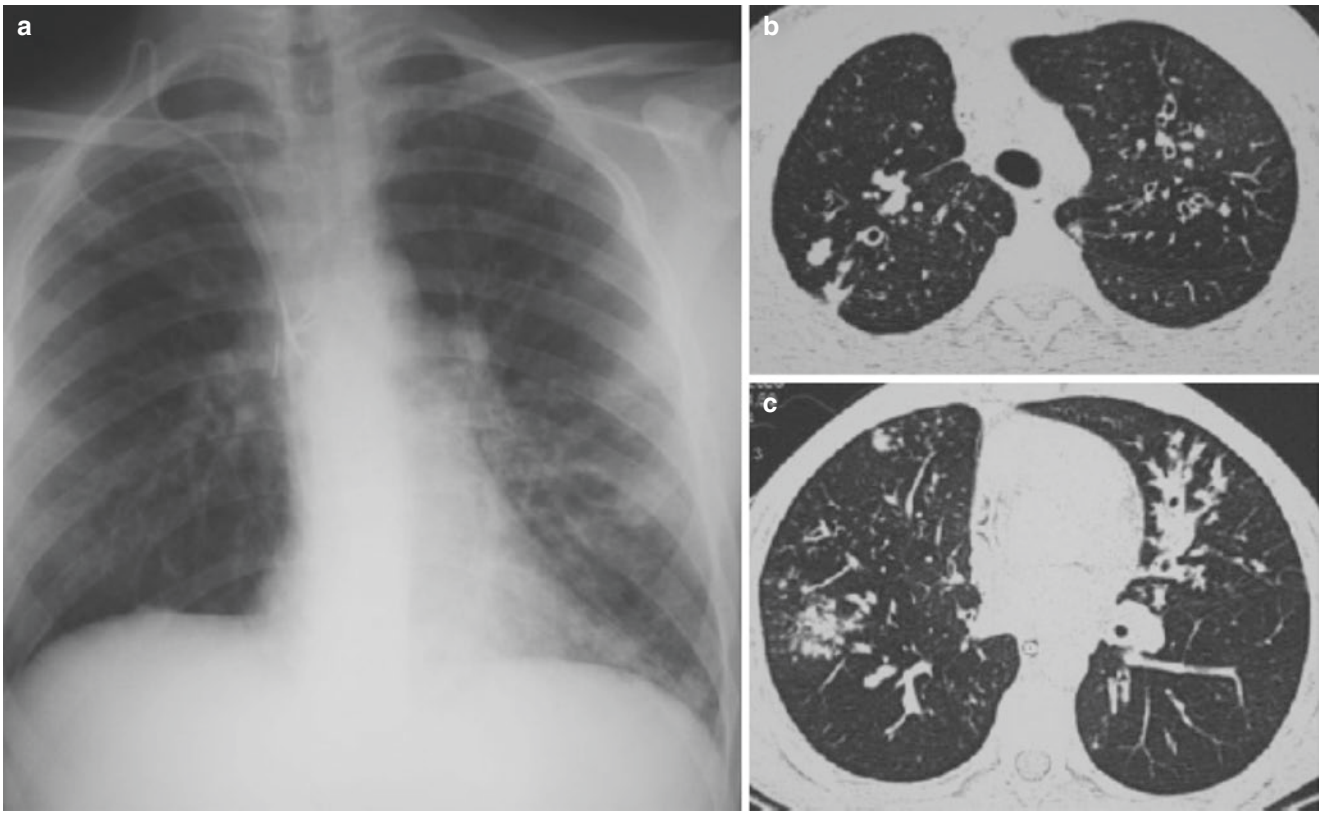

Fig. 17.3 (**a**–**c**) Allergic bronchopulmonary aspergillosis occurs in children with asthma, as well as those with cystic fibrosis (frequently those with a known asthmatic component). A 16-year-old boy with allergic bronchopulmonary aspergillosis (ABPA) in the setting of CF. (**a**) Chest x-ray shows ill-defined patchy opacification in the left lower and right upper lobes. (**b**) CT chest shows moderate to severe bronchial wall thickening with bronchiectasis. (**c**) On the left side there is a linear branching opacification suggestive of fluid filled dilated bronchi. There are ill-defined slightly lobulated masses in the right lung

and foreign body in the esophagus compressing the airway; and respiratory infections such as recurrent viral infections, pertussis and persistent purulent bronchitis (PBB), and other pathology within the airways such as tracheal polyps, laryngeal webs or hemangioma.

In older patients with recurrent or chronic wheezing, the following should be considered: angioedema and vocal cord dysfunction (VCD), intraluminal obstruction or compression of the airway as from congenital or acquired lesions (as from papillomatosis, granulation tissue, carcinoid, lymphoma, enlarged lymph nodes, bronchogenic cyst, vascular ring or slings), untreated respiratory infections or postinfectious as from mycoplasma, PBB, or sequela of viral infections notably from adenovirus, inhalation of irritant substances (smoke, illicit drugs), aspiration/gastroesophageal reflux (GER) diseases (e.g., CF, PCD, immune deficiency, sarcoidosis, hypersensitivity pneumonitis, and eosinophilic syndromes), vasculitides (e.g., granulomatosis with polyangiitis), and alpha-1-antitrypsin deficiency.

Pulmonary congestion manifesting with wheeze, cough, or labored respiration from congestive heart failure or from congenital heart lesions such as septal defects can affect any age group. Similarly, upper airway conditions such as recurrent or chronic rhinitis and/or sinusitis resulting in cough and wheeze must also be considered.

Comorbid Conditions

While the majority of the 8.4% of US children with asthma achieve control with currently available therapies, a subset are classified as having difficult-to-treat or severe asthma [61, 62]. Adherence to therapy to include appropriate technique in using inhaled medications must be ascertained. Comorbid conditions that can mimic asthma, underlie airway reactivity, or exacerbate veritable asthma must also be considered. Identification and treatment of the following conditions may improve asthma management: allergic bronchopulmonary aspergillosis (ABPA), gastroesophageal reflux (GER), obesity, obstructive sleep apnea (OSA), rhinitis/sinusitis, vocal cord dysfunction (VCD), and anxiety and depression [63, 64]. Of note, despite the epidemiologic association of vitamin D deficiency and asthma symptoms, with vita-

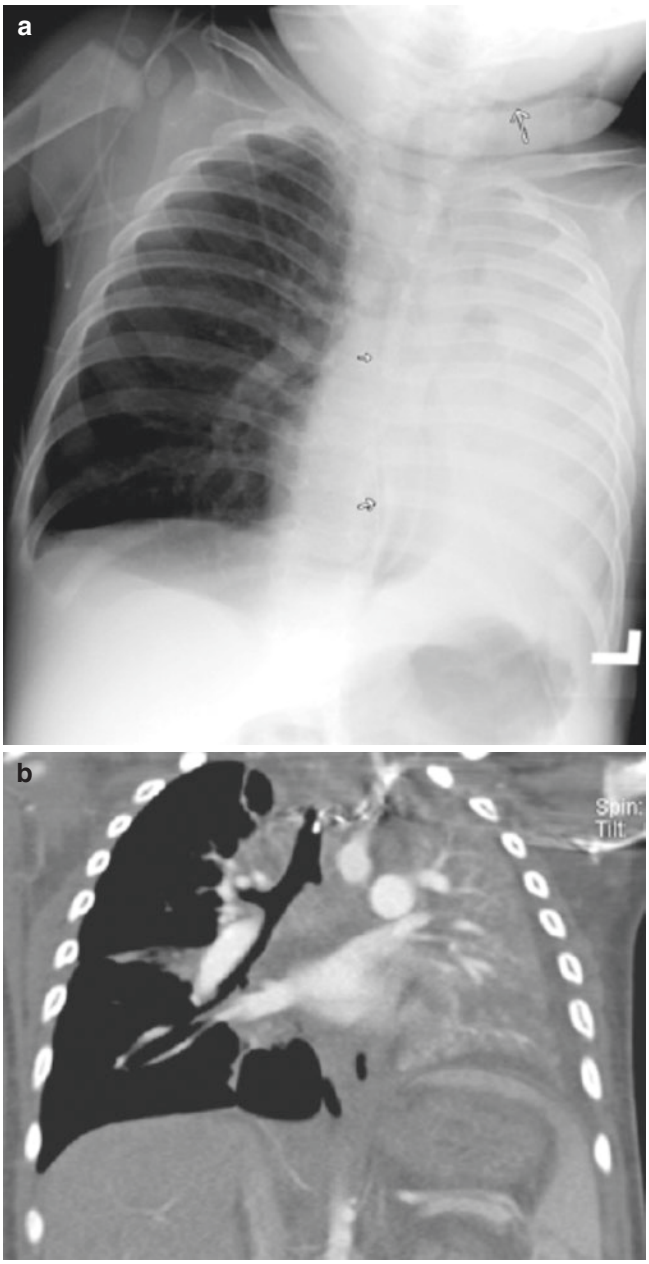

Fig. 17.4 (**a**) CXR reveals collapse of the left lung. There is subcutaneous air in the left aspect of the neck (large arrow) consistent with a pneumomediastinum (small arrows). There is compensatory overinflation of the right lung, the mediastinum is shifted to the left. (**b**) CT confirms a complete obstruction of the proximal left main bronchus, but did not determine the exact nature of the obstructing process, a bronchial cast which was removed at bronchoscopy

min D hypothesized to augment glucocorticoid sensitivity, evidence of therapeutic benefit from vitamin D supplementation is lacking [65–67]. Frequently, comorbid conditions coexist such as obesity, GER and OSA, or OSA and rhinitis. In a bidirectional manner, asthma can impact on GER and OSA, and discussion is beyond the scope of this chapter.

Allergic Bronchopulmonary Aspergillosis

A wide variation in the range of 16–38% has been observed in Aspergillus sensitization among asthmatics [68]. ABPA is an immunologically mediated, disease and criteria for diagnosis are evolving and based on a combination of clinical, laboratory, and radiologic findings. Elevated serum IgE levels and Aspergillus-specific IgE and/or IgG are obligatory criteria [69]. Radiologically, patients demonstrate transient migratory infiltrates on chest X-ray or bronchiectasis on chest CT; high-attenuation mucous (HAM), present in approximately 20% of ABPA, is considered pathognomonic (Fig. 17.3) [70–72]. Bronchocele density measurement of 36 Hounsfield units or over specifically has been proposed as indicative of APBA [73]. Oral steroids are the mainstays of treatment with antifungal agents playing an adjunctive role.

Gastroesophageal Reflux

GER represents a potential masquerading diagnosis as a cause of nocturnal cough as well as a relatively common comorbid diagnosis with asthma [74]. Symptoms of cough and wheeze can be caused by direct aspiration of gastric contents into the airway resulting in bronchoconstriction and airway inflammation, but the symptoms can also be triggered via vagally mediated reflexes by acid and possibly nonacid reflux of gastric contents into the distal esophagus. While the diagnosis of GER is often elusive in childhood, presenting without gastrointestinal symptoms, treatment of this entity is controversial. Treatment of asymptomatic GER in the setting of poorly controlled asthma has failed to improve asthma symptoms or lung function [75, 76]. However, children with steroid-dependent asthma and documented GER refractory to medical management show improvement in respiratory status and ability to wean off steroids after laparoscopic Nissen fundoplication [77].

Obesity

Obesity is associated with difficult to control asthma though the exact mechanism remains incompletely understood [78]. The association of obesity with asthma appears to be stronger in nonallergic children, varies with gender, and may lead to alterations in lung function such as increased airway closure [79–81]. This said, obesity is thought to (1) adversely impact lung mechanics secondary to chronic lung compression by a restrictive obese chest wall as well as (2) contribute to a pro-inflammatory state with implications for the allergic asthma phenotype [82, 83]. Interestingly, obesity is associated with dysanapsis (incongruence between the growth of the lungs and the airways) with obese patients having greater

lung volumes but reduced expiratory flows, as well as severe asthma exacerbations [84]. Obesity also contributes to comorbid conditions such as GER and OSA. Of note is that weight loss interventions lead to an improvement in asthma measures [85].

Obstructive Sleep Apnea

Obstructive sleep apnea and asthma may coexist. Systemic and local airway inflammation and neuromechanical effects of upper airway collapse have been invoked in the association of OSA with asthma [86]. Patients with both conditions present with arousals, changes in airflow and ventilatory effort, and hypoxemia during sleep. Moreover, obesity, GER, and chronic rhinitis with nasal obstruction contribute to both OSA and poor asthma control and must be addressed. The Pediatric Sleep Questionnaire (PSQ) is validated to screen for OSA in children with asthma [87]. Administration of continuous positive airway pressure (CPAP) may improve symptoms of OSA in patients with unstable asthma [88]. Of note is that there is a significant association between adenoidal hypertrophy and nasal obstruction especially in atopic patients [89]; moreover, adenoidal (with or without tonsillar) hypertrophy is a major cause of OSA in children. Adenotonsillectomy is the first-line treatment for children with OSA. A systematic review of asthma outcomes following adenotonsillectomy showed significant reductions in markers of asthma severity [90, 91].

Rhinitis and Sinusitis

Allergic rhinitis contributes to asthma morbidity and invokes the concept of the upper and lower airways as a continuum. The association of rhinitis and asthma symptoms has been described in the united airway disease theory, and putative mechanisms include postnasal dripping, naso-bronchial reflex, and systemic inflammatory response [92]. Underlying allergy appears to be a major driver of this association. Sinus infections also trigger the release of inflammatory mediators in the bronchial mucosa. The treatment of inflammatory processes of the upper airway such as the use of nasal steroids and/or leukotriene antagonists often alleviates asthma symptoms [93].

Vocal Cord Dysfunction

VCD is characterized by paradoxical vocal cord adduction during inspiration and sometimes exhalation resulting in dyspnea, wheeze, cough, stridor, and throat or chest tightness. It is a functional disorder that can mimic asthma. Laryngoscopic demonstration of vocal cord adduction has been considered the gold standard but is oftentimes difficult to perform during symptoms or during simulation of events such as exercise leading to symptoms. Historical, clinical, and spirometry findings may provide adequate clues; as regards the latter, blunting of the inspiratory loop suggests extrathoracic obstruction [94]. Noninvasive quantification of laryngeal movement has been described using dynamic CT imaging. Measurement of the ratio of vocal cord to tracheal diameter using CT has also been reported; this method is however not easily available [95, 96]. It is important to recognize VCD as management involves addressing known triggers, avoiding unnecessary asthma medications and initiating speech therapy, and, in some patients, use of biofeedback [97].

Anxiety and Depression

The presence of anxiety and depression negatively impact asthma; their co-occurrence is associated with greater asthma severity, including more frequent exacerbations, hospitalizations, and medication use [98, 99]. Over-perception of symptoms result in poorer outcomes and may falsely inform treatment decisions resulting in increased asthma healthcare costs [100]. Psychological stress has also been implicated in the pathogenesis of airway inflammation in asthmatics under chronic stress [101]. Interventions to screen for and treat these comorbid conditions are important in the management of asthma.

Management

Asthma is a chronic condition, and the key points of management are divided into two major categories: (1) reducing impairment via reduction of symptoms and maintenance of normal activity level and (2) reducing risk by preventing loss of lung function and possibly lung growth and minimizing adverse effects of therapy.

The medical management of asthma is two-pronged and revolves around two parallel concepts: (1) chronic administration of controller medications represented by inhaled corticosteroids, combination inhaled corticosteroids and long-acting beta-agonists, and/or leukotriene pathway modifiers and (2) provision of rapid-acting or short-acting reliever medications for acute exacerbations represented predominantly by beta-agonists such as albuterol [1].

A majority of pediatric patients achieve asthma control with the aforementioned management strategies. After establishment of a veritable diagnosis of asthma, assessment of medication delivery and adherence, addressing comorbid illness as impactful to a more severe asthma phenotype, and

eliminating alternative diagnoses, a small subset of patients will emerge with difficult-to-control asthma. In these cases, biologic agents may be considered [102]. Measurement of serum IgE level and absolute eosinophil count is important in determining their therapeutic role and indications. Biologic agents in the form of humanized monoclonal antibodies currently approved for use in pediatric severe asthma include (1) omalizumab (anti-IgE), (2) mepolizumab (anti-IL-5), and (3) reslizumab (anti-IL-5). Outcome data have shown a reduction in exacerbation frequency as well as corticosteroid dose and improvement in symptoms and quality of life [103, 104].

Details of medical regimens for asthma control and for exacerbations as well as inpatient evaluation and management of acute asthma are beyond the scope of this chapter.

References

1. National Asthma Education and Prevention Program. Expert Panel Report 3 (EPR-3): Guidelines for the Diagnosis and Management of Asthma-Summary Report 2007. J Allergy Clin Immunol. 2007;120(5 Suppl):S94–138.
2. Ward C, et al. Airway inflammation, basement membrane thickening and bronchial hyperresponsiveness in asthma. Thorax. 2002;57(4):309–16.
3. Woodruff PG, et al. Relationship between airway inflammation, hyperresponsiveness, and obstruction in asthma. J Allergy Clin Immunol. 2001;108(5):753–8.
4. Daniels SE, et al. A genome-wide search for quantitative trait loci underlying asthma. Nature. 1996;383(6597):247–50.
5. Cookson W, Moffatt M. Making sense of asthma genes. N Engl J Med. 2004;351(17):1794–6.
6. Jenmalm MC, Bjorksten B. Cord blood levels of immunoglobulin G subclass antibodies to food and inhalant allergens in relation to maternal atopy and the development of atopic disease during the first 8 years of life. Clin Exp Allergy. 2000;30(1):34–40.
7. Moffatt MF, et al. A large-scale, consortium-based genomewide association study of asthma. N Engl J Med. 2010;363(13):1211–21.
8. Moore WC, et al. Identification of asthma phenotypes using cluster analysis in the Severe Asthma Research Program. Am J Respir Crit Care Med. 2010;181(4):315–23.
9. Li X, et al. Genome-wide association study of asthma identifies RAD50-IL13 and HLA-DR/DQ regions. J Allergy Clin Immunol. 2010;125(2):328–335.e11.
10. Wechsler ME. Managing asthma in the 21st century: role of pharmacogenetics. Pediatr Ann. 2006;35(9):660–2, 664–9.
11. Tantisira KG, et al. Genomewide association between GLCCI1 and response to glucocorticoid therapy in asthma. N Engl J Med. 2011;365(13):1173–83.
12. Bleecker ER, et al. Beta2-receptor polymorphisms in patients receiving salmeterol with or without fluticasone propionate. Am J Respir Crit Care Med. 2010;181(7):676–87.
13. Colilla S, et al. Evidence for gene-environment interactions in a linkage study of asthma and smoking exposure. J Allergy Clin Immunol. 2003;111(4):840–6.
14. Ege MJ, et al. Gene-environment interaction for childhood asthma and exposure to farming in Central Europe. J Allergy Clin Immunol. 2011;127(1):138–44, 144.e1–4.
15. Pearce N, Pekkanen J, Beasley R. How much asthma is really attributable to atopy? Thorax. 1999;54(3):268–72.
16. Warner JO. The early life origins of asthma and related allergic disorders. Arch Dis Child. 2004;89(2):97–102.
17. Litonjua AA, et al. A longitudinal analysis of wheezing in young children: the independent effects of early life exposure to house dust endotoxin, allergens, and pets. J Allergy Clin Immunol. 2002;110(5):736–42.
18. Butland BK, Strachan DP, Anderson HR. The home environment and asthma symptoms in childhood: two population based case-control studies 13 years apart. Thorax. 1997;52(7):618–24.
19. Rosenstreich DL, et al. The role of cockroach allergy and exposure to cockroach allergen in causing morbidity among inner-city children with asthma. N Engl J Med. 1997;336(19):1356–63.
20. Martinez FD. Viral infections and the development of asthma. Am J Respir Crit Care Med. 1995;151(5):1644–7; discussion 1647–8.
21. Stein RT, et al. Respiratory syncytial virus in early life and risk of wheeze and allergy by age 13 years. Lancet. 1999;354(9178):541–5.
22. Rossi GA, Colin AA. Infantile respiratory syncytial virus and human rhinovirus infections: respective role in inception and persistence of wheezing. Eur Respir J. 2015;45(3):774–89.
23. Strachan DP. Family size, infection and atopy: the first decade of the "hygiene hypothesis". Thorax. 2000;55 Suppl 1:S2–10.
24. Brooks C, Pearce N, Douwes J. The hygiene hypothesis in allergy and asthma: an update. Curr Opin Allergy Clin Immunol. 2013;13(1):70–7.
25. Liu AH, Szefler SJ. Advances in childhood asthma: hygiene hypothesis, natural history, and management. J Allergy Clin Immunol. 2003;111(3 Suppl):S785–92.
26. Penders J, Kummeling I, Thijs C. Infant antibiotic use and wheeze and asthma risk: a systematic review and meta-analysis. Eur Respir J. 2011;38(2):295–302.
27. Marra F, et al. Antibiotic use in children is associated with increased risk of asthma. Pediatrics. 2009;123(3):1003–10.
28. Huang YJ, Boushey HA. The microbiome in asthma. J Allergy Clin Immunol. 2015;135(1):25–30.
29. Riiser A. The human microbiome, asthma, and allergy. Allergy Asthma Clin Immunol. 2015;11:35.
30. Litonjua AA, Weiss ST. Is vitamin D deficiency to blame for the asthma epidemic? J Allergy Clin Immunol. 2007;120(5):1031–5.
31. Gupta A, et al. Relationship between serum vitamin D, disease severity, and airway remodeling in children with asthma. Am J Respir Crit Care Med. 2011;184(12):1342–9.
32. Camargo CA Jr, et al. Maternal intake of vitamin D during pregnancy and risk of recurrent wheeze in children at 3 y of age. Am J Clin Nutr. 2007;85(3):788–95.
33. Romieu I, et al. Dietary intake, physical activity, body mass index, and childhood asthma in the Third National Health And Nutrition Survey (NHANES III). Pediatr Pulmonol. 2004;38(1):31–42.
34. Beuther DA, Sutherland ER. Overweight, obesity, and incident asthma: a meta-analysis of prospective epidemiologic studies. Am J Respir Crit Care Med. 2007;175(7):661–6.
35. Forno E, et al. Overweight, obesity, and lung function in children and adults-a meta-analysis. J Allergy Clin Immunol Pract. 2018;6(2):570–581.e10.
36. Forno E, Quizon A. The relationship between asthma, sleep apnea, and other respiratory disorders and childhood metabolic syndrome. In: Lipshultz MS, SE MTL, editors. Pediatric metabolic syndrome. London: Springer; 2012. p. 159–81.
37. Castro-Rodriguez JA, et al. A clinical index to define risk of asthma in young children with recurrent wheezing. Am J Respir Crit Care Med. 2000;162(4 Pt 1):1403–6.
38. Guilbert TW, et al. Atopic characteristics of children with recurrent wheezing at high risk for the development of childhood asthma. J Allergy Clin Immunol. 2004;114(6):1282–7.
39. Marotta A, et al. Impulse oscillometry provides an effective measure of lung dysfunction in 4-year-old children at risk for persistent asthma. J Allergy Clin Immunol. 2003;112(2):317–22.
40. Nielsen KG, Bisgaard H. Discriminative capacity of bronchodilator response measured with three different lung function tech-

niques in asthmatic and healthy children aged 2 to 5 years. Am J Respir Crit Care Med. 2001;164(4):554–9.
41. Frei J, et al. Impulse oscillometry: reference values in children 100 to 150 cm in height and 3 to 10 years of age. Chest. 2005;128(3):1266–73.
42. Haby MM, et al. An exercise challenge protocol for epidemiological studies of asthma in children: comparison with histamine challenge. Eur Respir J. 1994;7(1):43–9.
43. Popa V. ATS guidelines for methacholine and exercise challenge testing. Am J Respir Crit Care Med. 2001;163(1):292–3.
44. Kharitonov SA, Barnes PJ. Exhaled biomarkers. Chest. 2006;130(5):1541–6.
45. Dweik RA, et al. An official ATS clinical practice guideline: interpretation of exhaled nitric oxide levels (FENO) for clinical applications. Am J Respir Crit Care Med. 2011;184(5):602–15.
46. Spanevello A, et al. Induced sputum cellularity. Reference values and distribution in normal volunteers. Am J Respir Crit Care Med. 2000;162(3 Pt 1):1172–4.
47. Simpson JL, et al. Inflammatory subtypes in asthma: assessment and identification using induced sputum. Respirology. 2006;11(1):54–61.
48. Bossley CJ, et al. Pediatric severe asthma is characterized by eosinophilia and remodeling without T(H)2 cytokines. J Allergy Clin Immunol. 2012;129(4):974–82.e13.
49. de Blic J, et al. Difficult asthma in children: an analysis of airway inflammation. J Allergy Clin Immunol. 2004;113(1):94–100.
50. Snijders D, et al. Markers of eosinophilic and neutrophilic inflammation in bronchoalveolar lavage of asthmatic and atopic children. Allergy. 2010;65(8):978–85.
51. O'Reilly R, et al. Increased airway smooth muscle in preschool wheezers who have asthma at school age. J Allergy Clin Immunol. 2013;131(4):1024–32, 1032.e1–16.
52. Gordon IO, et al. Endobronchial biopsy: a guide for asthma therapy selection in the era of bronchial thermoplasty. J Asthma. 2013;50(6):634–41.
53. Chakir J, et al. Effects of bronchial thermoplasty on airway smooth muscle and collagen deposition in asthma. Ann Am Thorac Soc. 2015;12(11):1612–8.
54. Andersson CK, et al. Intraepithelial neutrophils in pediatric severe asthma are associated with better lung function. J Allergy Clin Immunol. 2017;139(6):1819–1829.e11.
55. Malmstrom K, et al. Immunohistology and remodeling in fatal pediatric and adolescent asthma. Respir Res. 2017;18(1):94.
56. Imboden M, et al. Genome-wide association study of lung function decline in adults with and without asthma. J Allergy Clin Immunol. 2012;129(5):1218–28.
57. Slager RE, et al. Genetics of asthma susceptibility and severity. Clin Chest Med. 2012;33(3):431–43.
58. Seear M, et al. Bronchial casts in children: a proposed classification based on nine cases and a review of the literature. Am J Respir Crit Care Med. 1997;155(1):364–70.
59. Goo HW, et al. CT findings of plastic bronchitis in children after a Fontan operation. Pediatr Radiol. 2008;38(9):989–93.
60. Wilmott RW, Boat T, Bush A, Chernick V, Deterding RR, Ratjen F. Kendig and Chernick's disorders of the respiratory tract in children. 8th ed. Philadelphia, PA: Elsevier Saunders; 2012.
61. Centers for Disease Control and Prevention. Current asthma prevalence percents by age, United States: National Health Interview Survey, 2015. [cited 2017 Nov 26]; Available from: https://www.cdc.gov/asthma/nhis/2015/data.htm.
62. Lang A, et al. Severe asthma in childhood: assessed in 10 year olds in a birth cohort study. Allergy. 2008;63(8):1054–60.
63. Lodrup Carlsen KC, et al. Assessment of problematic severe asthma in children. Eur Respir J. 2011;37(2):432–40.
64. Chung KF, et al. International ERS/ATS guidelines on definition, evaluation and treatment of severe asthma. Eur Respir J. 2014;43(2):343–73.
65. Gupta A, et al. Vitamin D and asthma in children. Paediatr Respir Rev. 2012;13(4):236–43; quiz 243.
66. Castro M, et al. Effect of vitamin D3 on asthma treatment failures in adults with symptomatic asthma and lower vitamin D levels: the VIDA randomized clinical trial. JAMA. 2014;311(20):2083–91.
67. Pfeffer PE, Hawrylowicz CM. Vitamin D in Asthma: mechanisms of action and considerations for clinical trials. Chest. 2018;153(5):1229–39.
68. Agarwal R, et al. Allergic bronchopulmonary aspergillosis: review of literature and proposal of new diagnostic and classification criteria. Clin Exp Allergy. 2013;43(8):850–73.
69. Shah A, Panjabi C. Allergic bronchopulmonary aspergillosis: a perplexing clinical entity. Allergy Asthma Immunol Res. 2016;8(4):282–97.
70. Muldoon EG, Strek ME, Patterson KC. Allergic and noninvasive infectious pulmonary aspergillosis syndromes. Clin Chest Med. 2017;38(3):521–34.
71. Knutsen AP, Slavin RG. Allergic bronchopulmonary aspergillosis in asthma and cystic fibrosis. Clin Dev Immunol. 2011;2011:843763.
72. Agarwal R, et al. Clinical significance of hyperattenuating mucoid impaction in allergic bronchopulmonary aspergillosis: an analysis of 155 patients. Chest. 2007;132(4):1183–90.
73. Occelli A, et al. Bronchocele density in cystic fibrosis as an indicator of allergic broncho-pulmonary aspergillosis: a preliminary study. Eur J Radiol. 2017;93:195–9.
74. Hancox RJ, et al. Associations between respiratory symptoms, lung function and gastro-oesophageal reflux symptoms in a population-based birth cohort. Respir Res. 2006;7:142.
75. Mastronarde JG, et al. Efficacy of esomeprazole for treatment of poorly controlled asthma. N Engl J Med. 2009;360(15):1487–99.
76. Holbrook JT, et al. Lansoprazole for children with poorly controlled asthma: a randomized controlled trial. JAMA. 2012;307(4):373–81.
77. Rothenberg S, Cowles R. The effects of laparoscopic Nissen fundoplication on patients with severe gastroesophageal reflux disease and steroid-dependent asthma. J Pediatr Surg. 2012;47(6):1101–4.
78. Quinto KB, et al. The association of obesity and asthma severity and control in children. J Allergy Clin Immunol. 2011;128(5):964–9.
79. Forno E, et al. Adiposity and asthma in a nationwide study of children and adults in the United States. Ann Am Thorac Soc. 2018;15(3):322–30.
80. Tantisira KG, et al. Association of body mass with pulmonary function in the Childhood Asthma Management Program (CAMP). Thorax. 2003;58(12):1036–41.
81. Collins LC, et al. The effect of body fat distribution on pulmonary function tests. Chest. 1995;107(5):1298–302.
82. Bates JHT, et al. Pathophysiology to phenotype in the asthma of obesity. Ann Am Thorac Soc. 2017;14(Supplement_5):S395–s398.
83. Grossman DC, et al. Screening for obesity in children and adolescents: US preventive services task force recommendation statement. JAMA. 2017;317(23):2417–26.
84. Forno E, et al. Obesity and airway dysanapsis in children with and without asthma. Am J Respir Crit Care Med. 2017;195(3):314–23.
85. Eneli IU, Skybo T, Camargo CA Jr. Weight loss and asthma: a systematic review. Thorax. 2008;63(8):671–6.
86. Prasad B, Nyenhuis SM, Weaver TE. Obstructive sleep apnea and asthma: associations and treatment implications. Sleep Med Rev. 2014;18(2):165–71.
87. Ehsan Z, et al. Validation of the pediatric sleep questionnaire in children with asthma. Pediatr Pulmonol. 2017;52(3):382–9.
88. Trivedi M, et al. Pediatric obstructive sleep apnea and asthma: clinical implications. Pediatr Ann. 2017;46(9):e332–5.
89. Pagella F, et al. Adenoids and clinical symptoms: epidemiology of a cohort of 795 pediatric patients. Int J Pediatr Otorhinolaryngol. 2015;79(12):2137–41.

90. Kohli N, et al. Asthma outcomes after adenotonsillectomy: a systematic review. Int J Pediatr Otorhinolaryngol. 2016;90:107–12.
91. Bhattacharjee R, et al. Association of adenotonsillectomy with asthma outcomes in children: a longitudinal database analysis. PLoS Med. 2014;11(11):e1001753.
92. Papadopoulou A, Tsoukala D, Tsoumakas K. Rhinitis and asthma in children: comorbitity or united airway disease? Curr Pediatr Rev. 2014;10(4):275–81.
93. de Groot EP, et al. Allergic rhinitis is associated with poor asthma control in children with asthma. Thorax. 2012;67(7):582–7.
94. Hseu A, et al. Paradoxical vocal fold motion in children presenting with exercise induced dyspnea. Int J Pediatr Otorhinolaryngol. 2016;90:165–9.
95. Low K, et al. Abnormal vocal cord function in difficult-to-treat asthma. Am J Respir Crit Care Med. 2011;184(1):50–6.
96. Low K, et al. Abnormal vocal cord movement in patients with and without airway obstruction and asthma symptoms. Clin Exp Allergy. 2017;47(2):200–7.
97. Hoyte FC. Vocal cord dysfunction. Immunol Allergy Clin N Am. 2013;33(1):1–22.
98. Katon W, et al. The prevalence of DSM-IV anxiety and depressive disorders in youth with asthma compared with controls. J Adolesc Health. 2007;41(5):455–63.
99. Sundbom F, et al. Effects of poor asthma control, insomnia, anxiety and depression on quality of life in young asthmatics. J Asthma. 2016;53(4):398–403.
100. Apter AJ, et al. Perception of airway obstruction in asthma: sequential daily analyses of symptoms, peak expiratory flow rate, and mood. J Allergy Clin Immunol. 1997;99(5):605–12.
101. Rosenkranz MA, et al. Mind-body interactions in the regulation of airway inflammation in asthma: a PET study of acute and chronic stress. Brain Behav Immun. 2016;58:18–30.
102. Krishnan JA, et al. Adherence to inhaled corticosteroids: an ancillary study of the Childhood Asthma Management Program clinical trial. J Allergy Clin Immunol. 2012;129(1):112–8.
103. Farne HA, et al. Anti-IL5 therapies for asthma. Cochrane Database Syst Rev. 2017;9:Cd010834.
104. Chipps BE, et al. Omalizumab in children with uncontrolled allergic asthma: review of clinical trial and real-world experience. J Allergy Clin Immunol. 2017;139(5):1431–44.

Cystic Fibrosis

18

Katie Krone and Alicia Casey

Introduction

Cystic fibrosis is a life-limiting hereditary disorder of the cystic fibrosis transmembrane conductance regulator (CFTR) characterized by recurrent sinopulmonary infections and progressive obstructive lung disease. There are also common manifestations affecting the gastrointestinal, hepatobiliary, endocrine, and reproductive systems. It is most common among non-Hispanic whites of Northern European descent, with a carrier frequency of 1/25. The incidence varies according to population but is estimated at approximately 1 in 2500–3500 white newborns. Clinical findings vary according to age though common features include recurrent sinopulmonary infections and failure to thrive secondary to pancreatic exocrine insufficiency. Therapeutic strategies are focused on preserving lung function, optimizing nutritional status, and managing manifestations of extrapulmonary disease. Astounding progress over the past decade has resulted in mutation-specific pharmacologic interventions, and optimism remains for the future development of medications to treat all patients. Since the initial identification of this autosomal recessive disorder 80 years ago, there has been a dramatic increase in the median age of survival.

Clinical Presentation

The clinical presentation of cystic fibrosis varies according to age though the common phenotype includes recurrent sinopulmonary infections and failure to thrive secondary to pancreatic exocrine insufficiency. Eighty-five percent of those affected with cystic fibrosis are pancreatic insufficient and, without pancreatic enzyme treatment, manifest with fat malabsorption, poor weight gain, abdominal cramps and distention, and steatorrhea. Fifteen to twenty percent of neonates with cystic fibrosis present with delayed meconium passage or meconium ileus; 50% of cases are complicated by bowel obstruction, perforation, and peritonitis. Older children and adolescents may present with respiratory symptoms and recurrent infections, bronchiectasis, nasal polyps, sinusitis, and digital clubbing. Details of clinical presentation according to age categories are outlined in Table 18.1.

Genetics

Cystic fibrosis is an autosomal recessive disorder caused by mutations in a single gene on the long arm of chromosome 7 that encodes the cystic fibrosis transmembrane regulator (CFTR) protein [1–3]. It is most common in northern European populations; Phe508del (known as f508del), a 3 bp deletion, causing a loss of phenylalanine at position 508 of the protein, is the predominant mutation, comprising ~70% of mutations worldwide, followed by G542X and G551D at 5% and 4%, respectively [4]. The prevalence of different CFTR mutations varies considerably within populations throughout the world. To date, more than 2000 mutations have been identified and genotype-phenotype correlations described for more than 300 genetic variants [5, 6]. There is a wide spectrum of disease severity, with complex interactions from modifier genes and the environment hypothesized to play a role [7–9]. Heterozygotes are asymptomatic.

Mutations in CFTR result in alterations in protein structure and function. Historically, CFTR mutations have been divided into six major classes based on the cellular defect and effect on CFTR function. Classes I, II, and III are the most severe, whereas classes IV, V, and VI are less severe, with some preserved CFTR function. CFTR is expressed in many cells and has many functions, not all of which have been linked with disease. CFTR protein functions primarily as an ion (Cl^-) channel in the apical membrane of exocrine

K. Krone · A. Casey (✉)
Division of Pulmonary Medicine, Boston Children's Hospital, Harvard Medical School, Boston, MA, USA
e-mail: Alicia.Casey@childrens.harvard.edu

R. H. Cleveland, E. Y. Lee (eds.), *Imaging in Pediatric Pulmonology*, https://doi.org/10.1007/978-3-030-23979-4_18

Table 18.1 Presentations of cystic fibrosis

Age	Frequent presentation	Less frequent presentation
Antenatal	Chorionic villous sampling Amniocentesis in high risk families Fetal echogenic bowel wall	
Neonatal	Newborn cystic fibrosis screening Meconium ileus	Prolonged neonatal obstructive jaundice
Infant and young child	Recurrent respiratory tract infections Failure to thrive secondary to pancreatic exocrine insufficiency Screening of siblings of child with CF	Rectal prolapse Dehydration plus electrolyte abnormality Triad of anemia, edema and hypoproteinemia Deficiencies of fat-soluble vitamins: vitamin K (bleeding disorder), vitamin E (hemolytic anemia), vitamin A (raised intracranial pressure)
Older children and adolescents	Recurrent respiratory tract infections Failure to thrive/fat malabsorption Finger clubbing Nasal polyps or sinusitis Screening of siblings of child with CF (in countries with no neonatal screening)	Liver disease Dehydration plus electrolyte abnormality Acute pancreatitis Chronic constipation/ abdominal pain

epithelial cells that regulates liquid volume on epithelial surfaces through chloride secretion and inhibition of sodium absorption [1].

CFTR Dysfunction

Depletion of the periciliary liquid layer (the *low volume hypothesis*), and not abnormal ion composition, is generally accepted as the explanation for airway disease in cystic fibrosis [10]. The primary pathology in the lung is chronic inflammation due to (1) ineffective clearance of microorganisms, and (2) a hyperinflammatory immune cell response. CFTR transports chloride and bicarbonate ions across epithelial cells in the respiratory tract, gastrointestinal tract, and the reproductive and endocrine systems [11, 12]. CFTR resorption of sodium is also modulated by epithelial sodium channel (ENaC) [13, 14]. Dysfunction of CFTR results in altered ion conductance with consequent reduced volume of airway surface liquid (ASL), thickened mucus and impaired mucociliary clearance [15]. Additionally, increased ASL acidity contributes to ineffective bactericidal activity [16, 17]. While chronic infection produces an inflammatory microenvironment, there is data to suggest that intrinsic immune defects of the CF respiratory epithelium potentiate a proinflammatory state, and possibly even drive a hyperinflammatory state in the absence of infection [18–20]. The functional consequences of CFTR mutations culminate in inspissated secretions and mucus obstruction, recurrent infections, bronchiectasis, fibrosis, and respiratory failure [21]. Similarly, abnormal ion transport in other epithelial-lined organs results in inspissated secretions and leads to obstruction, inflammation and ultimately fibrosis. Complex genetic-environmental interactions determine disease severity, and work to identify potential genetic modifiers of disease progression and survival is ongoing [22].

Diagnosis

The diagnostic algorithm was revised by the Cystic Fibrosis Foundation Consensus Panel in 2015 and is based on a (1) clinical presentation consistent with CF, including the presence of a characteristic phenotype, positive newborn screen, or positive family history, and confirmed by (2) evidence of CFTR dysfunction, including two abnormal sweat chloride results (sweat chloride ≥60 mmol/l) or one abnormal sweat chloride and two CFTR mutations or abnormal CFTR physiologic testing (nasal potential difference or intestinal current measurement). If diagnostic criteria are not met, CFTR-related disorder, or CFTR-related metabolic syndrome/CF screen positive, inconclusive diagnosis (CRMS/CFSPID) for newborns (following NBS) should be considered [23].

Newborn screening for cystic fibrosis has been widely implemented and was universally adopted in the United States in 2010. Antenatal diagnosis can be made with chorionic villous sampling or amniocentesis in high risk families. An echogenic fetal bowel on ultrasound, though a nonspecific finding, is suggestive of cystic fibrosis [24]. Diagnosis of CF in nonscreened individuals may be more challenging due to symptom variability and age of onset [25]. Patient registry data and the expanding number of identified CFTR mutations have contributed to our rapidly evolving knowledge of genotype-phenotype correlations [6].

Imaging

The imaging findings are variable and depend on the age at diagnosis and the severity of the disease. In infants and young children, the chest radiograph may be normal. However, air trapping and obstruction appear to precede infection on computed tomography (CT) scans [26]. With regard to monitoring presymptomatic infants, magnetic resonance imaging (MRI) may emerge as a safe and sensitive

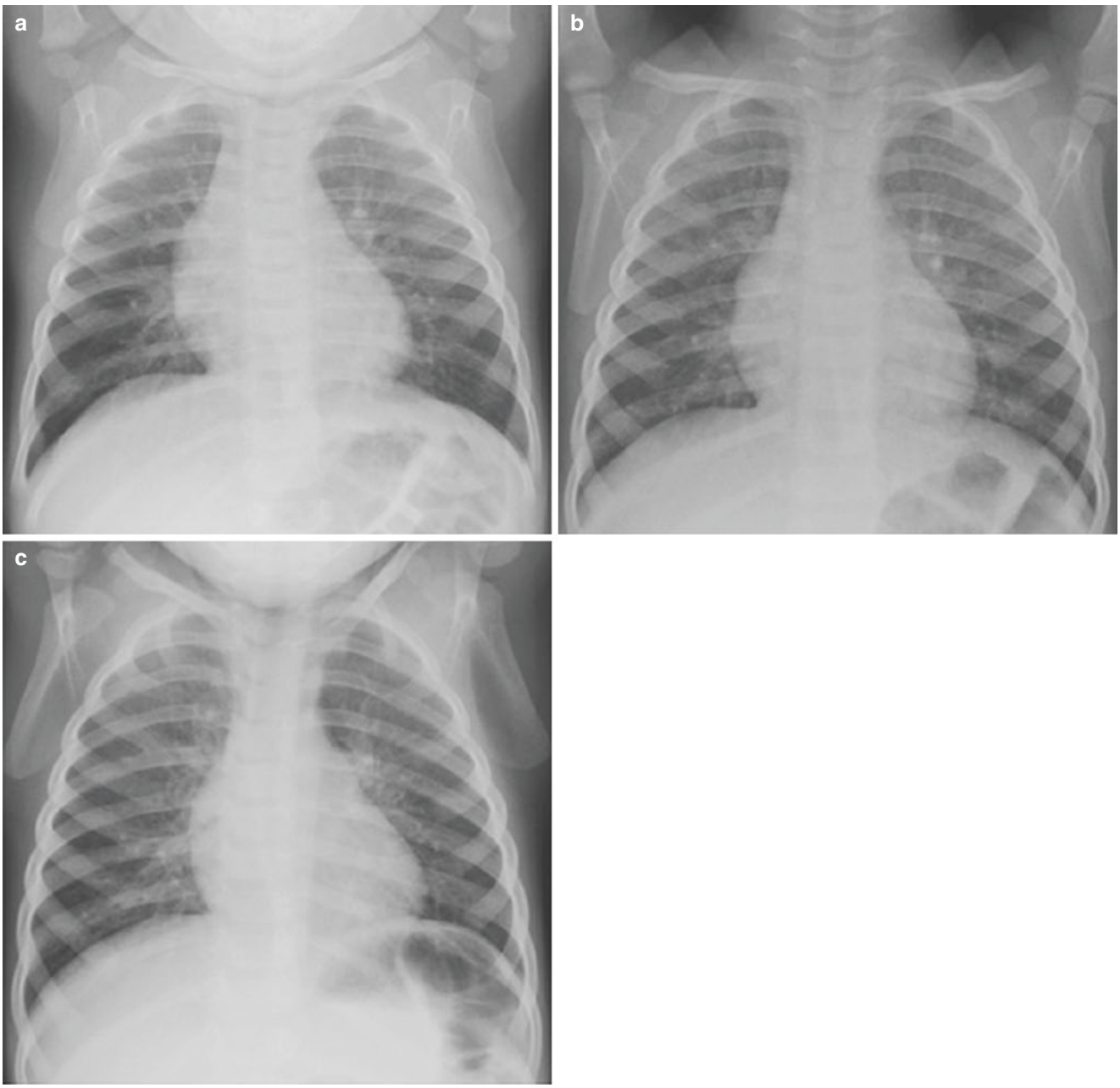

Fig. 18.1 (**a**) 8 months, (**b**) from 13 months, and (**c**) from 21 months. All show a very similar pattern of bronchial wall thickening. The presenting symptoms at each encounter was *fever, cough, and wheeze*. Two subsequent sweat tests were positive

tool [27]. The initial imaging abnormality generally seen in infancy is diffuse bronchial wall thickening [28]. Occasionally, there may be some degree of hyperinflation [28]. There may be areas of atelectasis, mimicking bronchiolitis or asthma. If a young child has serial chest X-rays (CXR) over several months with unchanging bronchial wall thickening and does not have reactive airways (asthma), this may represent early findings of cystic fibrosis, and a sweat test should be performed (Fig. 18.1). As the disease progresses, the bronchial wall thickening will progress to bronchiectasis (Fig. 18.2). The latter can be suggested on radiography when the bronchus is larger than the adjacent pulmonary vessel. Areas of ill-defined opacification suggest mucous impaction or allergic bronchopulmonary aspergillosis (Fig. 18.3). Ill-defined areas of focal opacification may relate to acute pneumonia or pulmonary hemorrhage. Although cystic fibrosis has been reported as an upper lobe dominant disease, this is the case in only approximately 50% of patients [28]. Hilar lymphadenopathy is common and can occur during an episode of acute infection. Lobar pneumonia and pleural effusions are uncommon. In very severe disease, there may be evidence of right-sided cardiac failure.

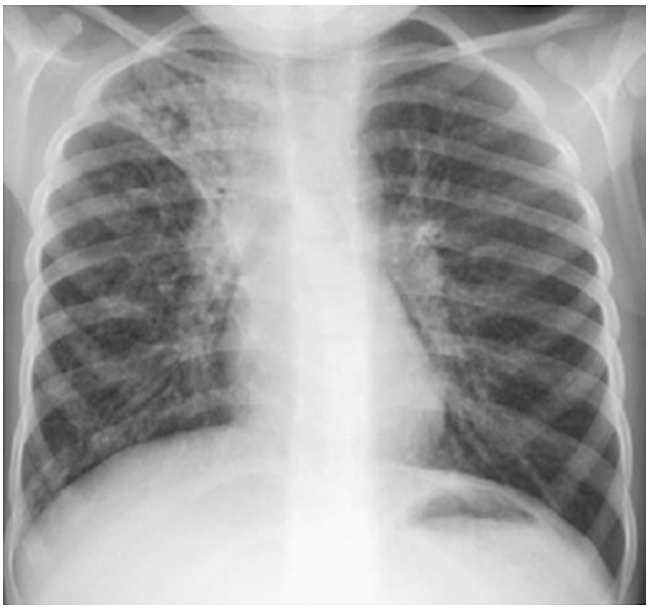

Fig. 18.2 Chest X-ray in a 7-year-old girl with cystic fibrosis. The lungs are hyperinflated. There is right upper lobe atelectasis. There is course bronchial wall thickening and the beginning of bronchiectasis. There is bilateral hilar enlargement suggesting adenopathy

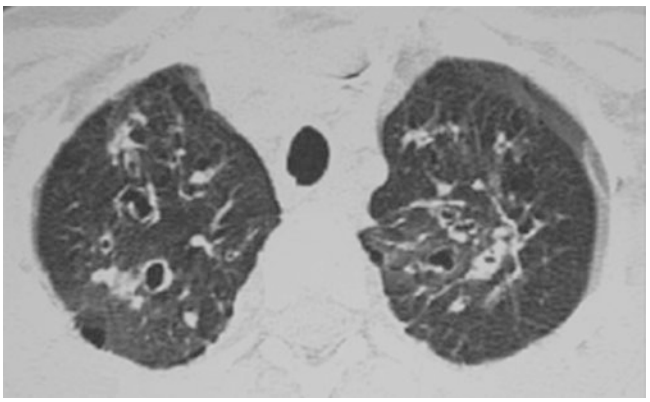

Fig. 18.3 CT chest on a 14-year-old boy showing typical findings of cystic fibrosis. There is bronchial wall thickening, bronchiectasis, and areas of mucous plugging

The severity and extent of the various radiographic features have been scored by several methods. However, the Brasfield system is often used as it correlates closely with pulmonary function. It uses scores of 0–5 to assess air trapping, linear shadows, nodular cystic lesions, large pulmonary shadows and general severity. Cleveland et al. [28] reported a radiography-based database which scored changes over time in patients with cystic fibrosis to provide comparison for groups undergoing new treatments such as aerosolized tobramycin [29]. Although these scoring systems have proven useful for research purposes, their use for clinical patient care is uncommon. Computed tomography (CT) studies are the most accurate method of evaluating the changes in lung disease. It is more sensitive than radiography in detecting the extent of bronchiectasis, bronchial wall thickening, mucous plugging, infiltration, and hilar adenopathy. At present, however, there is no consensus on when to use CT in the various pediatric age groups with cystic fibrosis. There is also the issue of cumulative radiation dose in patients with any lifelong condition. This has become even more important since the introduction of multi-slice CT which has a much higher dose burden than high-resolution thin slices at intervals. At present, the lowest doses required to identify lung disease on high-resolution CT are still not available from the various manufacturers of CT scanners, and there is still no consensus on when a volume sequence is required instead of high-resolution images. In 1991, Bhalla et al. introduced a CT-based system where they scored the severity and extent of bronchiectasis, the severity of bronchial wall thickening, mucous plugging, bullous disease, emphysema, collapse and consolidation together with the involvement of the number of bronchial divisions [30]. Since then other scoring systems have been published and adopted by several clinicians. MRI may provide a functional alternative to CT for assessing disease severity in CF [31].

Management

Management goals for cystic fibrosis focus on optimizing nutrition, preserving lung health, and preventing CF-related complications. The Cystic Fibrosis Foundation (CFF) specifies that children with cystic fibrosis require multidisciplinary care, with routine quarterly visits, provided by a center accredited by the CFF. CFF clinical care guidelines were updated in 2013 to provide guidance on long-term therapies to maintain maximal pulmonary function [32]. These guidelines address management of chronic airway infection and inflammation, including (1) treatment of initial *Pseudomonas aeruginosa* infection with the goal of eradication, (2) alternate month antibiotics for chronic *P. aeruginosa* infection, (3) airway clearance maneuvers and concomitant use of mucolytic agents, and (4) use of anti-inflammatory therapies such as azithromycin and high-dose ibuprofen.

More recently, there has been exponential growth in the development of oral small molecule mutation-specific therapies: ivacaftor for individuals with at least one copy of G551D and/or other responsive mutations [33–36], ivacaftor/lumacaftor for patients homozygous for the F508 del mutation [37–39], and tezacaftor/ivacaftor for patients homozygous for the F508del mutation or who have at least one responsive mutation based on in vitro data and/or clinical evidence [40]. The positive response to these mutation-specific therapies provides optimism for an overall improved prognosis in those eligible for treatment and supports the

development of additional targeted therapies [41, 42]. Optimization of nutritional status remains paramount to maintaining lung function [43]. A high-calorie, high-fat diet is instituted in conjunction with pancreatic enzyme replacement and administration of fat-soluble vitamins (A, D, E, and K) in those who are pancreatic insufficient. Lastly, vaccination against preventable respiratory illness, e.g., influenza, pneumococcal, and varicella, in accordance with immunization schedules, is important.

Prognosis

Although new therapies have emerged and life expectancy continues to improve, cystic fibrosis remains a life-limiting disorder with significant morbidity. Complications such as chronic airway infections leading to exacerbations, sinus disease, gastroenterologic disease, and cystic fibrosis-related diabetes contribute significantly to morbidity. According to the Cystic Fibrosis Foundation Patient Registry (CFFPR), the median predicted survival of CF patients in the US increased to 40.6 years from 2009 to 2013, whereas the median age of survival in Canada increased to 50.9 years during this time period [44]. While country-specific differences related to healthcare delivery systems may account for this survival gap, increased survival of patients with CF is attributed to continual improvements in nutrition and quality of care. Despite these advances, CF disease progression inevitably leads to respiratory failure and mortality.

Lung Transplant

Lung transplantation is indicated for individuals with CF who develop end-stage lung disease despite maximal therapy. It is key to refer patients for transplant when there is a clinical trajectory that portends a poor prognosis while also allowing for sufficient time for lung transplant evaluation and listing [45]. Given advances in care, respiratory failure requiring lung transplantation is more frequent in adults as compared to children. For some centers, infections with *Burkholderia cenocepacia* or *Mycobacterium abscessus* are contraindications to transplant due to the association with poorer outcomes [45]. Further detail is outside of the scope of this chapter and discussed in Chap. 19, Lung Transplant in Pediatric Patients.

Respiratory Tract Disease

The respiratory tract extends from the mouth and nose to the alveoli, lined throughout with pseudostratified ciliated epithelium.

Respiratory Viruses

Respiratory viruses may precipitate up to 65% of pulmonary exacerbations, with rhinovirus being the predominant cause [46–50]. The same viruses affect children with cystic fibrosis as children without, e.g., respiratory syncytial virus (RSV); adenovirus; influenza A and B; para-influenza types 1, 2, and 3; rhinovirus [51]; and likely metapneumovirus.

There is no evidence to suggest that individuals with cystic fibrosis have an increased risk of contracting a viral infection following exposure, but there is evidence of increased morbidity for patients with cystic fibrosis who develop viral respiratory infections, including precipitating pulmonary exacerbations and initial *P. aeruginosa* infection [46, 51–53].

Risk factors for the development of RSV bronchiolitis in all infants include being born during the winter RSV season (October to March in the northern hemisphere), siblings attending day care, and smokers at home.

Clinical presentation of bronchiolitis in an infant with cystic fibrosis is the same as any infant with bronchiolitis, although the presentation may be more severe. Investigations may include a nasopharyngeal swab checking for RSV, influenza, para-influenza, adenovirus, as well as oxygen saturation measurement in room air and, if clinically indicated, a chest radiograph. Further investigations are not usually required, but this decision depends on the clinical state of the infant.

Chest radiography may not be required in patients with a typical presentation of bronchiolitis, particularly if the symptoms are mild, but may be necessary if there is more severe respiratory difficulty or diagnostic uncertainty, in order to identify other conditions which may mimic bronchiolitis. Typically, there are varying degrees of hyperinflation with flattening of the diaphragms (Fig. 18.4). There may be associated atelectasis. Viral infections may cause localized or diffuse interstitial disease and rarely hilar lymphadenopathy. However, it may be difficult to distinguish bacterial from non-bacterial infection on chest radiography.

Inpatient hospital treatment includes supportive therapy with oxygen, fluids (either nasogastric or intravenous—the latter if vomiting), and attention to nutrition. Intravenous antibiotics may be added if there is an associated secondary bacterial infection. The first isolation of *Pseudomonas aeruginosa* in cystic fibrosis often follows a viral infection [54, 55]. Whether this is due to epithelial damage and airway inflammation caused by the virus or because the bacteria are simply isolated at the time of increased mucus production is not clear.

Viral infections may lead to increased frequency and duration of hospitalization for respiratory exacerbations and deterioration in clinical status and lung function which may persist for several months [51, 56]. RSV bronchiolitis in

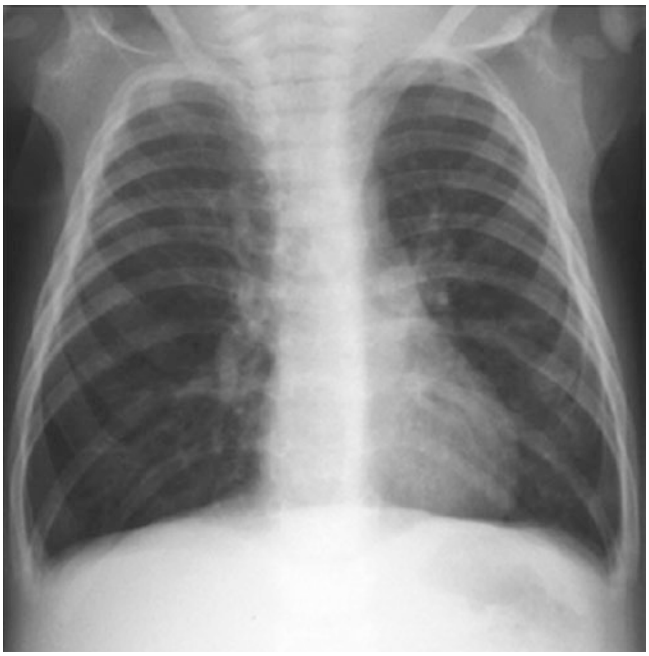

Fig. 18.4 Ten-month-old boy with bronchiolitis, subsequently diagnosed with CF. There is flattening of the diaphragms and bilateral perihilar streaky opacification and bronchial wall thickening

infants with cystic fibrosis may cause prolonged hospitalization and hypoxemia, requiring mechanical ventilation. Studies suggest that infants with cystic fibrosis who had RSV bronchiolitis experienced prolonged hospitalizations, increased respiratory symptoms, and pulmonary exacerbations over the subsequent 2 years of follow-up [47, 56]. Evidence does suggest that palivizumab may potentially reduce RSV hospitalization in children less than age 2 years with CF, but further study is needed [57]. In older children, studies demonstrate that influenza may result in significant deterioration in lung function and clinical status; influenza A is linked to increased rate of hospital admission [58–60]. Annual influenza vaccine is recommended in children (>6 months of age) and adults with cystic fibrosis. Interestingly, a Cochrane review did not find evidence that administration of influenza vaccine is beneficial to patients with cystic fibrosis [61].

Respiratory Bacterial Infections

Bronchoscopic studies have demonstrated that respiratory infection occurs early in life. While *Staphylococcus aureus*, *Haemophilus influenza*, and *P. aeruginosa* [62, 63] predominate in the first few years of life, *P. aeruginosa* becomes the most common pathogen in the second decade. Other bacteria include *Stenotrophomonas maltophilia*, *A. xylosoxidans*, and *Burkholderia cepacia*. The presence of non-tuberculous mycobacteria should be assessed in patients with established lung disease. Fungi may cause infection and allergy in the airways.

A cycle of infection, inflammation, and lung injury is established in cystic fibrosis. The presence of bacteria in the airways incites a host response of neutrophil inflammation and proinflammatory cytokines and chemokines [64]. An exaggerated inflammatory response occurs in the presence of infection, although immune dysregulation in the setting of cystic fibrosis may exist independent of infection [20, 62, 65, 66]. Thick tenacious secretions block the airways. These secretions are particularly viscous secondary to dehydration of ASL, mucins and DNA from necrotic neutrophils and bacteria [67]. Chronic inflammation, infection, and airway obstruction lead to ongoing lung injury and ultimately bronchiectasis.

Criteria used to define a pulmonary exacerbation are varied and may include increased cough with increased sputum production and purulence, shortness of breath, dyspnea on exertion, hemoptysis, fatigue, anorexia with or without weight loss, sinus pain, or change in sinus discharge [68–70]. Examination varies from more subtle exam changes with decreased lung function to hypoxia, weight loss, stigmata of acute respiratory distress and new crackles on auscultation. A decline in baseline forced expiratory volume in one second (FEV_1) and new changes on chest radiography may be seen.

Patients with pancreatic exocrine insufficiency tend to have poorer lung function than those with pancreatic exocrine sufficiency [71].

Sputum culture and sensitivity, pulmonary function tests, chest radiograph and blood tests are useful in the setting of pulmonary exacerbations. Prior pathogen surveillance data is useful to guide selection of antibiotic treatment. In children who are unable to expectorate sputum, sputum induction is a reliable surrogate for bronchoalveolar lavage, and superior to throat swab [72].

Chest radiography findings are non-specific, and bacterial infection must be considered in patients who have an acute increase in pulmonary opacification. Lobar consolidation is uncommon.

While evidence guiding specific treatment recommendations in the management of pulmonary exacerbations is lacking, the components of treatment include IV antibiotics, chest physiotherapy, airway clearance techniques, nebulized rhDNAse (*pulmozyme*), hypertonic saline, nebulized bronchodilators, and attention to nutrition [73, 74]. Many patients receive intravenous antibiotic treatment and aggressive airway clearance at home.

Pseudomonas aeruginosa

P. aeruginosa is the most common organism causing chronic lung disease in patients with cystic fibrosis. It is the

most important cause of morbidity and an important predictor of survival [75, 76]. Chronic *Pseudomonal* infection with the mucoid form is impossible to permanently eradicate and is associated with a decline in lung function and poorer prognosis [77]. The mucoid phenotype contributes to biofilm formation, allowing for antibiotic resistance, and results in airway damage by frustrated neutrophil-release of proteases and free radicals [78]. The initial isolation of *P. aeruginosa* (usually non-mucoid and detected during routine surveillance) should be treated with inhaled tobramycin for 28 days, which achieves high eradication rates [79–82]. Eradication of initial *Pseudomonas* infection is standard of care due to the association of this organism with increased pulmonary exacerbations and significant decline in lung function compared to other organisms [83]. Once persistently colonized with *P. aeruginosa,* chronic nebulized antibiotics are used, such as inhaled tobramycin, aztreonam, and colistin. *Pseudomonas* has a propensity to develop resistance, so dual anti-pseudomonal antibiotic therapy is employed in the setting of pulmonary exacerbations when oral antibiotics fail.

Staphylococcus aureus

Methicillin-Sensitive *S. aureus*

Methicillin-sensitive *S. aureus* (MSSA) is the most common pathogen isolated in sputum of children with cystic fibrosis during the first decade [44, 45]. Flexible bronchoscopy studies demonstrate up to 40% of children aged <3 years cultured *S. aureus* on bronchoalveolar lavage. MSSA often co-infects patients chronically infected with *P. aeruginosa*, *B. cepacia* complex, and other gram-negative organisms [46, 47]. UK guidelines recommend prophylaxis for *S. aureus* starting in infancy; however, US guidelines do not recommend this approach based on evidence suggesting the association of prophylactic anti-staphylococcal treatment with the acquisition of *Pseudomonas* [84].

Methicillin-Resistant *S. aureus*

Methicillin-resistant *S. aureus* (MRSA) may be healthcare or community acquired, and patient-to-patient spread is well documented [52, 53]. Prevalence among CF patients in the United States has been reported as high as 26% [85]. Patients with MRSA infection have been shown to have lower lung function compared to MSSA as well as increased hospitalizations and antibiotic use [86–88]. Controversy exists in the literature regarding the potential association of persistent MRSA infection and increased mortality [89]. While previously there has been insufficient data to recommend eradication of early MRSA infection, recent studies suggest microbiological efficacy of this approach [90, 91].

Burkholderia cepacia Complex

Burkholderia cepacia complex comprise a group of 22 gram-negative bacteria widely distributed in the environment [92]. The majority of infections in cystic fibrosis patients are caused by *B. cenocepacia* (previously genomovar III) and *B. multivorans* (genomovar II), followed by *B. vietnamiensis.* Accurate identification is crucial. Appropriate selective medium is required [93]. If identified, the organism should be sent to a specialized laboratory for confirmation because high false-positive (10%) and false-negative rates (30%) have been reported [94]. While infections by *Burkholderia cepacian* complex bacteria are relatively rare in cystic fibrosis patients, the pathogenicity and multidrug resistance of these organisms, paired with severe declines in lung function and reduced survival, make these organisms a clinical challenge [95, 96]. Some patients may experience "cepacia syndrome" with these organisms, characterized by fevers, bacteremia, and necrotizing pneumonia resulting in death. This syndrome has been described more frequently with *B. cenocepacia* but can also be seen with other *Burkholderia cepacian* complex organisms. Infection with *B. cenocepacia* is considered a contraindication to lung transplant at many centers due to increased mortality post-transplant [97–99]. Infection with *B. multivorans* is less severe, and a significant proportion subsequently clear the organism [95].

Non-tuberculous Mycobacterial Infection

Mycobacterium avium complex (MAC) is the most common non-tuberculous mycobacterial (NTM) infection in patients with cystic fibrosis, accounting for approximately 61% of isolates while *Mycobacterium abscessus* accounts for 39% [100]. Clinical sequelae of NTM infection may vary, from asymptomatic to progressive inflammatory lung disease [101]; however, patients with *M. abscessus* usually manifest with significant decline in pulmonary function compared to other species of NTM [102]. All patients with cystic fibrosis should be screened annually with sputum AFB and culture, with positive cultures undergoing molecular identification. If an NTM isolate is detected and the patient is on chronic azithromycin therapy, this should be held pending further evaluation given the risk for developing resistance on macrolide monotherapy. While diagnostic criteria have been outlined by the American Thoracic Society and Cystic Fibrosis Foundation expert panel, diagnosis can be challenging given the overlap of NTM pulmonary disease with increased pulmonary symptoms of cystic fibrosis. Diagnosis is suggested by: (1) clinical findings consistent with NTM pulmonary disease, such as worsening pulmonary symptoms and a decline in pulmonary function, (2) two or more positive sputum cultures for the same NTM species, and (3) radiologic changes

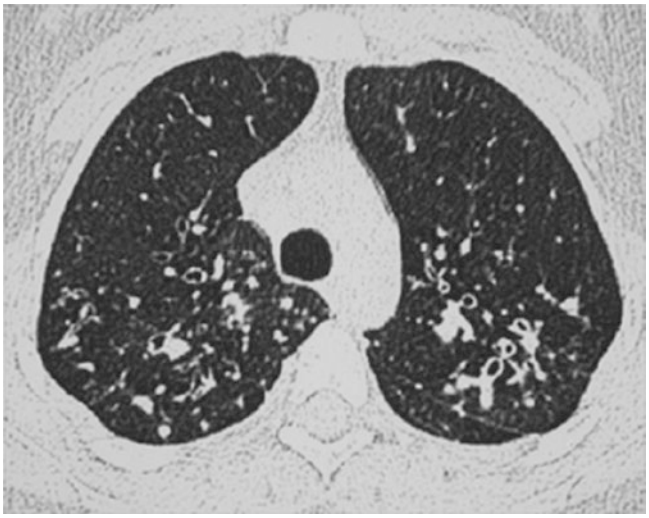

Fig. 18.5 Fifteen-year-old girl with non-TB mycobacteria. There is bronchiectasis with ill-defined densities. *Tree in bud* opacification is seen in the left lower lobe

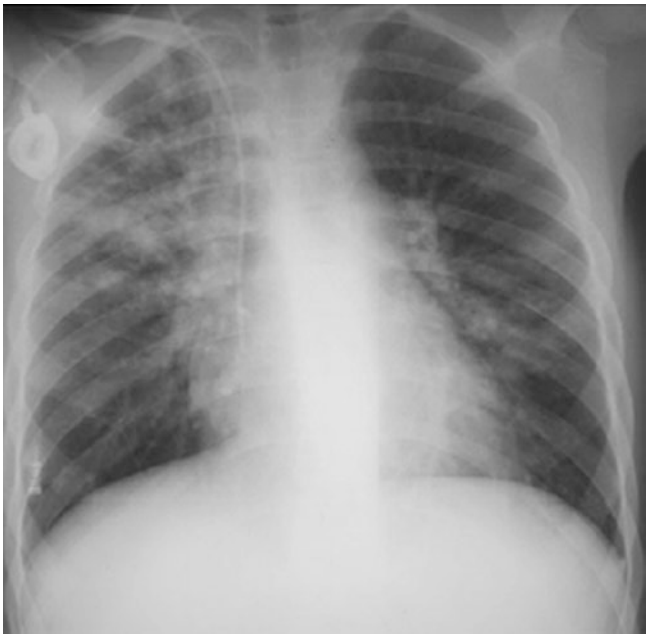

Fig. 18.6 Thirteen-year-old boy with CF. Admitted with hemoptysis. There is ill-defined right upper lobe and lingular opacifications

on HRCT, despite optimization of CF care and treatment of non-NTM infection [103, 104]. In the case in which less than two sputum cultures are positive for NTM species, though clinical suspicion remains for NTM pulmonary disease, bronchoalveolar lavage should be considered. Antibiotic regimens for the treatment of *M. abscessus* and MAC include an intensive and continuation phase with combinations of oral, inhaled, and intravenous antibiotics, often with drug toxicity necessitating medication changes. Despite intensive and prolonged treatment, there is only a single case report presenting eradication of *M. abscessus* in a patient with cystic fibrosis [105, 106].

The chest radiographic features in NTM may be indistinguishable from those in tuberculosis. There may be cavitation which tends to be more thin walled than the cavitation seen in tuberculosis. There may also be peribronchial or nodular opacification. The nodules may be single or in clusters, and they may occur bilaterally. Computed tomography can better delineate cavity formation and demonstrate bronchiectasis with *tree in bud* opacification, centrilobular nodules and pleural thickening [107] (Fig. 18.5).

Non-infectious Complications of Cystic Fibrosis Respiratory Disease

Hemoptysis

Hemoptysis usually occurs in established lung disease or pulmonary exacerbation and is more common in older patients. Massive hemoptysis is a serious, albeit rare, complication of cystic fibrosis, affecting 0.87% of patients annually [108]. Bleeding usually originates from the bronchial arteries, although other collateral vessels may also be a source of hemorrhage. In CF chronic infection and inflammation leads to increased angiogenesis of the bronchial arteries [109]. Hemoptysis occurs when there is rupture of the abnormally formed vessels into the lumen of the airways sometimes associated with coughing.

Clinical presentation varies from mild blood streaked sputum (usually of no large significance) to large volumes of fresh blood with clots. Severe hemoptysis is defined as more than 240 mL in 24 hours or 100 mL daily for several days, though these volumes are arbitrary and significant bleeding less than these amounts should be treated seriously. Evaluation of hemoptysis, in addition to quantity, should include (1) acuity (whether frank bright red blood or older brown-coffee ground appearing blood), (2) presence or absence of clots, and (3) patient perception of localization/laterality of bleeding source.

Investigations include a full blood count to rule out anemia and thrombocytopenia, a coagulation screen looking for a prolonged prothrombin time, blood group and cross match, liver function tests, venous blood gas, chest radiograph, and sputum for culture and sensitivity. Epistaxis and hematemesis are confounders that need to be excluded. If there is large volume hemoptysis or chronic hemoptysis then interventional radiology should be consulted to determine further imaging and interventions needed.

The chest radiograph may not reveal any specific abnormality, or non-specific ill-defined airspace opacification may be evident (Fig. 18.6).

The CFF has provided hemoptysis management guidelines based on expert consensus [110]. Consensus was not reached for the management of mild to moderate hemoptysis with regard to continuation of airway clearance and aerosolized therapies, whereas consensus was reached with regard to discontinuation of NSAIDs and treatment with antibiotics. Treatment of massive hemoptysis involves stabilization of the patient, establishing robust intravenous access (two large bore cannulas), providing fluid resuscitation, oxygen supplementation, placing the patient in the lateral position with affected side down (to prevent aspiration into the upper lobe) and vitamin K administration. Unstable patients should emergently undergo bronchial artery embolization (BAE) whereas embolization for a spontaneously resolved episode of massive hemoptysis is less clear. Although BAE may be lifesaving in the acute situation, this intervention does carry the potential for substantial morbidity, including paralysis, if the spinal arteries are occluded, organ infarction or death, as well as the need to repeat embolization [111, 112]. For further discussion of BAE, see Chap. 20: Percutaneous Chest Intervention in Infants and Children. Intubation with endobronchial tamponade with balloon catheters, ligation of the bronchial artery, and lobectomy are therapeutic options if embolization fails.

The CFF expert consensus guidelines for management of massive hemoptysis do not identify any particular imaging modality for the pre-embolization assessment to aid in anatomic assessment and case planning. However, others suggest that for the stable patient with massive hemoptysis, multidetector computed angiography (MDCT-A) may be of considerable value in identification of the bleeding culprit pre-procedure [113–115].

Massive hemoptysis is a poor prognostic indicator due to its association with advanced lung disease and can be life-threatening. CFF patient registry data demonstrated that patients with massive hemoptysis were older (mean age 24 years) and had more severe lung disease, as well as increased morbidity and mortality after massive hemoptysis; more than 1/3 died within 12 months [108].

Pneumothorax

Pneumothorax is a common non-infectious complication of cystic fibrosis, occurring more frequently in adult patients with advanced lung disease, and affecting approximately 3.4% of patients with cystic fibrosis during their lifetime [116]. The pathophysiology is presumed to be a consequence of obstruction and air trapping in cystic fibrosis pulmonary disease such that the alveolar pressure becomes larger than the interstitial pressure resulting in air leak into the interstitium and mediastinal structures. Rupture of a subpleural bleb in the visceral pleura is likely a less common etiology for CF-associated pneumothorax given the lack of connection between observed blebs/cysts and pneumothorax in patients with cystic fibrosis [117].

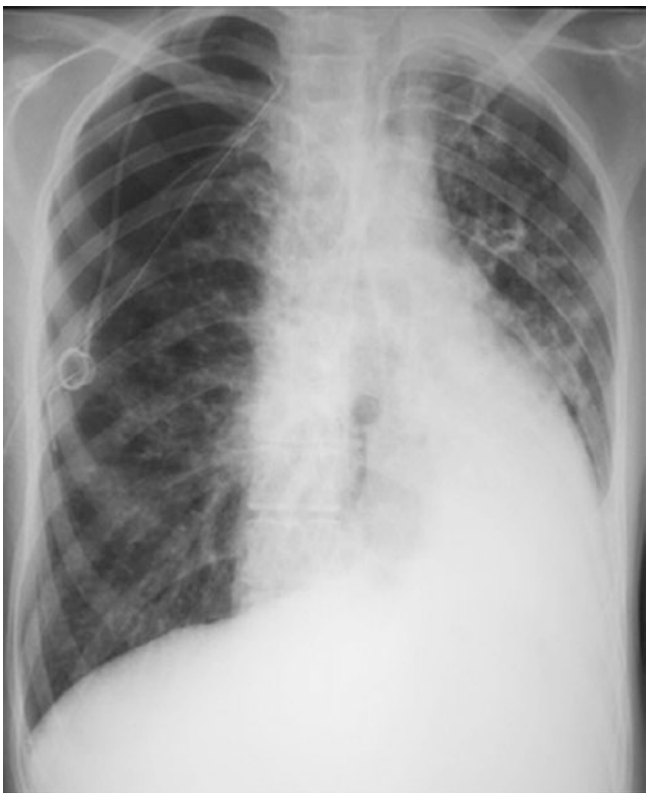

Fig. 18.7 Sixteen-year-old boy with extensive changes of CF with left lower lobe atelectasis. He developed a right apical pneumothorax requiring drainage. The chest X-ray demonstrates a residual pneumothorax. The chest drain tip is projected over the apex of the lung medially

While small pneumothoraces may be asymptomatic, larger pneumothoraces may present with pleuritic chest pain, sudden onset dyspnea, hypoxia, hemoptysis, pallor, cyanosis, tachypnea, increased resonance to percussion, and diminished breath sounds. It is important to have a high index of clinical suspicion in patients with established lung disease or a previous pneumothorax.

A chest radiograph confirms the diagnosis (Fig. 18.7). Air in the pleural space is evident, and the degree of mediastinal shift is related to the size of the pneumothorax. Following drainage, a CT of the thorax may be useful to identify the presence of subpleural bullae as a cause (Fig. 18.8).

Small and asymptomatic pneumothoraces may often be observed in the outpatient setting in many circumstances, whereas large pneumothoraces require the insertion of a chest tube connected to suction to achieve re-expansion. Pleurodesis should not be offered for an initial occurrence unless re-expansion has not occurred after 4–5 days. Surgical pleurodesis is the preferred approach, compared to chemical pleurodesis, due to the potential eventual requirement of

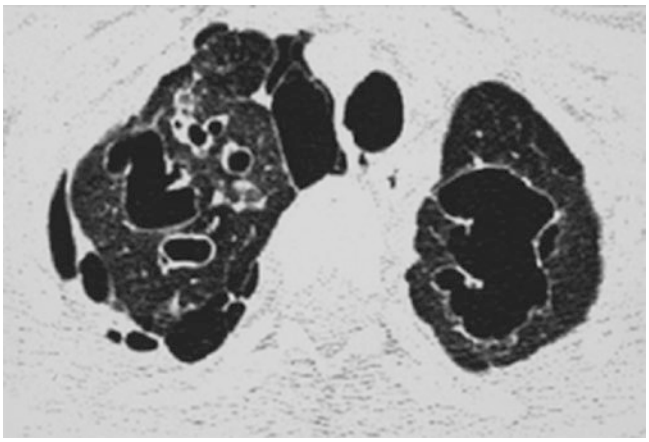

Fig. 18.8 CT post drainage of right apical pneumothorax in patient in Fig. 18.7. There are large bullae in both lung apices

lung transplant. Prolonged chest tube insertion carries the risk of bronchopleural fistula.

Although delivery of high FiO2 (up to 10 L) via a non-rebreather mask may promote resolution, given that many patients with cystic fibrosis retain CO_2, $PaCO_2$ must be carefully monitored. By reducing the total pressure of gas (particularly nitrogen) in the capillaries, high-flow oxygen creates a higher gradient between the pleural capillaries and pleural cavity, and therefore air is resorbed: up to four times faster than without oxygen therapy [118]. Temporary use of a Heimlich valve may be an option, particularly in a patient with end-stage lung disease, who is unsuitable for general anesthesia and in the situation in which pleurodesis under local anesthetic has failed. Maintenance airway clearance therapies that do not contribute to increased airway pressure may be continued in the setting of pneumothorax.

Pneumothoraces in cystic fibrosis carry a poor prognosis. The median survival after pneumothorax is 30 months [119]. Post pneumothorax, an increased rate and duration of hospital admissions was documented in the U.S.A. together with an increased 2-year mortality: 49 vs. 12% when compared to patients who never had a pneumothorax [116]. Pneumothoraces carry a recurrence risk in patients with cystic fibrosis.

Allergic Bronchopulmonary Aspergillosis

Allergic bronchopulmonary aspergillosis (ABPA) is a hypersensitivity response of the lung to *Aspergillus fumigatus* antigens and occurs predominately in patients with asthma and CF. The prevalence of ABPA in CF has been reported as high as 9%, although wide variation exists in the diagnostic criteria used for ABPA [120]. In patients with CF, abnormal mucociliary clearance as well as an impaired innate immune defense results in accumulation and persistence of inhaled spores that then germinate and form mycelia. This in turn triggers an IgE-mediated hypersensitivity reaction due to an exaggerated T helper type-2 lymphocyte response with the release of interleukin (IL) 3, IL-4, IL-5, and IL-6. Eosinophils, which contain Fc receptors, are recruited by IL-5 and IL-6; *A. fumigatus* IgG, IgA, and IgE binding to these Fc receptors results in eosinophil degranulation and consequent inflammation and damage to the airway epithelium [121]. Risk factors include male gender, adolescence, poor lung function, *P. aeruginosa*, and poor nutritional status [122]. Atopy is a significant risk factor: ABPA occurs in 22% of atopic cystic fibrosis patients versus 2% of non-atopic cystic fibrosis patients. ABPA is less common in young children (<6 years of age).

The presentation of ABPA may be acute or chronic. In an acute presentation, patients may present with wheeze, shortness of breath, cough, increased production of sputum which contains brown/blacks specks, chest pain, mild fever, and myalgia similar to an *influenza-like* illness. Alternatively, patients may present similar to a subacute pulmonary exacerbation, with worsening pulmonary function and new infiltrates on chest imaging, and exercise intolerance, but not respond to intravenous antibiotics.

Diagnosis of ABPA in patients with CF is challenging due to the overlap of symptoms with CF pulmonary exacerbations. In 2003, the CFF established consensus criteria for the diagnosis of ABPA in CF patients [123]. These criteria include (1) clinical deterioration that is not attributable to an alternative etiology, (2) elevated total IgE>1000 IU/mL, (3) elevated serum IgE antibody to *A. fumigatus* or immediate cutaneous reactivity to *Aspergillus*, and one of the following: (4) precipitins to *A. fumigatus*, *A. fumigatus*-specific IgG, or new abnormalities on chest radiography or CT which does not clear with antibiotics and physiotherapy [123]. A sputum culture with *A. fumigatus* is non-specific.

The chest radiographic features tend to be non-specific. There may be evidence of bronchiectasis with patchy opacification, compatible with mucous plugging (Fig. 18.9a). The opacification may involve the perihilar regions and extend toward the lung periphery. On CT, there is evidence of central bronchiectasis of a moderate to severe degree, bronchial wall thickening, and lobulated opacification (Fig. 18.9b, c). The radiographic findings described in ABPA include (1) ring sign, circumferential bronchial wall thickening; (2) tram-track sign, appearance of non-tapered parallel dilated bronchi; and (3) finger-in-glove sign, mucous impaction in dilated bronchi. Radiographic findings that are more frequently seen in ABPA are central (within the central two-thirds of the lung) varicose bronchiectasis and high-attenuation mucus plugs [124, 125]. Additionally, infiltrates or opacities that resolve with steroid treatment are suggestive of ABPA. Bronchocele density (>36 Hounsfield units) has been shown to correlate with ABPA in patients with CF, though larger studies are

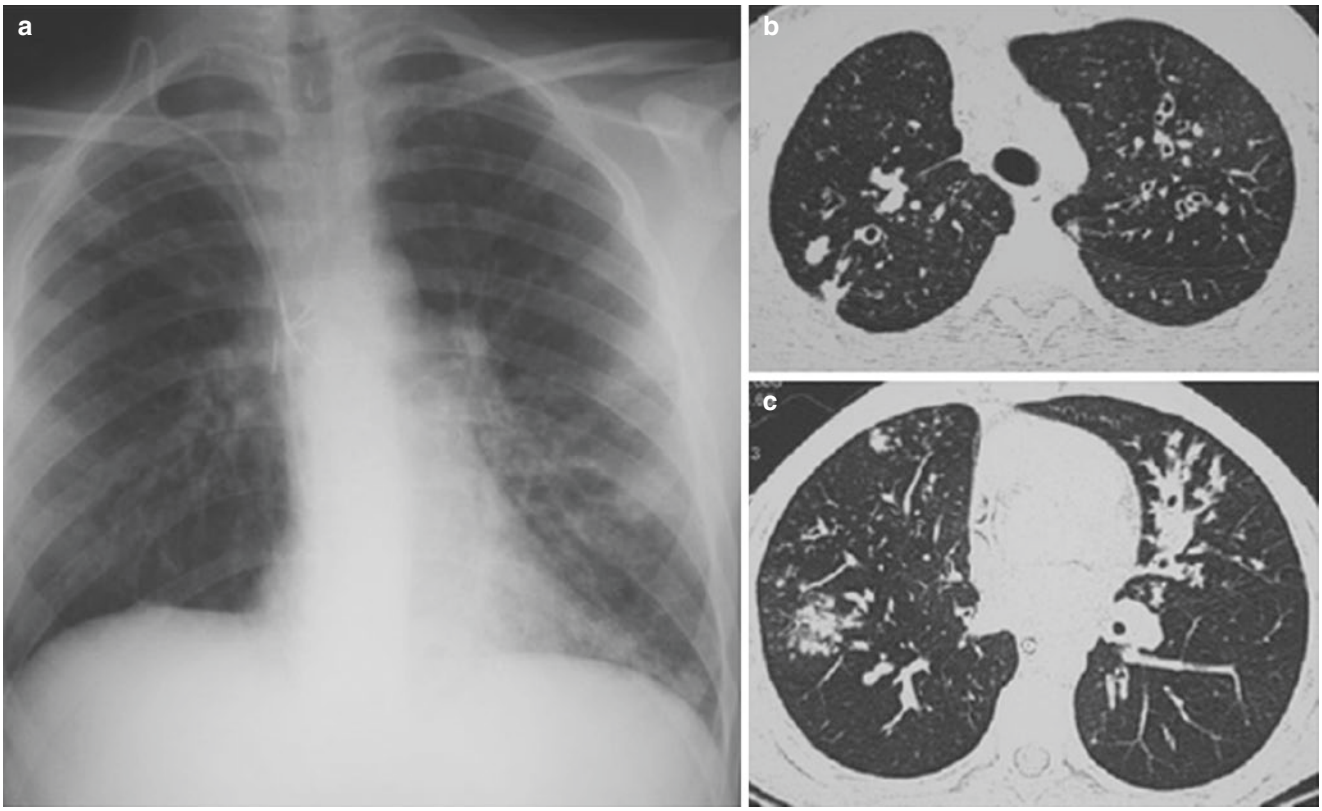

Fig. 18.9 Sixteen-year-old boy with allergic bronchopulmonary aspergillosis (ABPA). (**a**) Chest X-ray shows ill-defined patchy opacification in the left lower and right upper lobes. (**b**) CT chest shows moderate to severe bronchial wall thickening with bronchiectasis. (**c**) On the left side there is linear branching opacification suggestive of fluid-filled dilated bronchi. There are ill-defined slightly lobulated masses in the right lung

needed to confirm density thresholds for the diagnosis of ABPA [126].

A total IgE should be performed annually on all patients over 6 years of age (CFF guidelines), and if >500 IU/mL, immediate cutaneous reactivity to *A. fumigatus* or IgE-specific *A. fumigatus* should be determined; if total IgE is 200–500 IU/mL, the total IgE should be repeated in 1–3 months.

ABPA is associated with progressively worsening pulmonary function, and the goal of therapy is to prevent permanent fibrotic damage and irreversible decline in pulmonary function [127]. Management strategies rely on observational evidence as large randomized-controlled trial data are lacking at present. Oral corticosteroids are a mainstay of ABPA treatment (prednisone 0.5–2 mg/kg per day for 1–2 weeks with tapering over 2–3 months) and are used to attenuate the inflammatory and immunological reaction [123]; however, their impact on long-term progression of the disease is unclear [128]. The addition of antifungal azole drugs is generally reserved for patients who respond poorly to corticosteroids, relapse, become steroid-dependent or develop adverse effects related to steroid exposure. Small observational studies have suggested a role for omalizumab, anti-IgE monoclonal antibody, as a steroid-sparing agent in the treatment of ABPA, though it is not yet recommended for the treatment of ABPA in CF patients due to the lack of substantial data [129, 130].

Sinus Disease

Nasal polyposis is a feature of cystic fibrosis, affecting 50% of pediatric [131] and 32–45% of adult cystic fibrosis patients [132–134]. The majority of CF patients have radiographic evidence of pansinusitis. The pathophysiology of nasal polyposis and chronic rhinosinusitis is thought to result from mechanical sinus ostial obstruction by thick secretions, leading to chronic neutrophilic Th-1-mediated inflammation, secondary ciliary dyskinesia, and superimposed infection, usually with the same bacteria that have colonized the lower airway, i.e., *S. aureus*, *H. influenza*, and later *P. aeruginosa.*

Clinical manifestations of chronic sinusitis include, most commonly, headache and peri-orbital pain [135]. Other symptoms may include pressure across the forehead (frontal sinuses) or below the eyes (maxillary sinuses), nasal obstruction, rhinorrhea, snoring, voice change, cough and post nasal

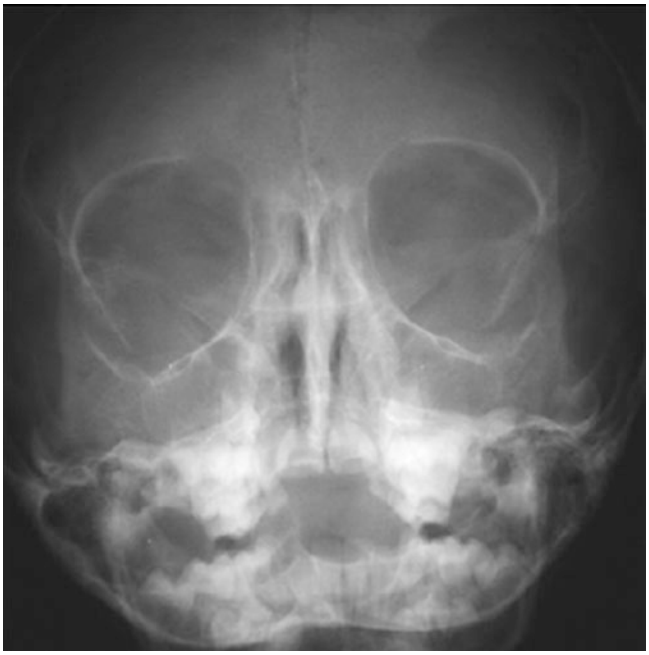

Fig. 18.10 Sinus radiograph in a 7-year-old girl demonstrating complete opacification of the maxillary sinuses, compatible with sinusitis

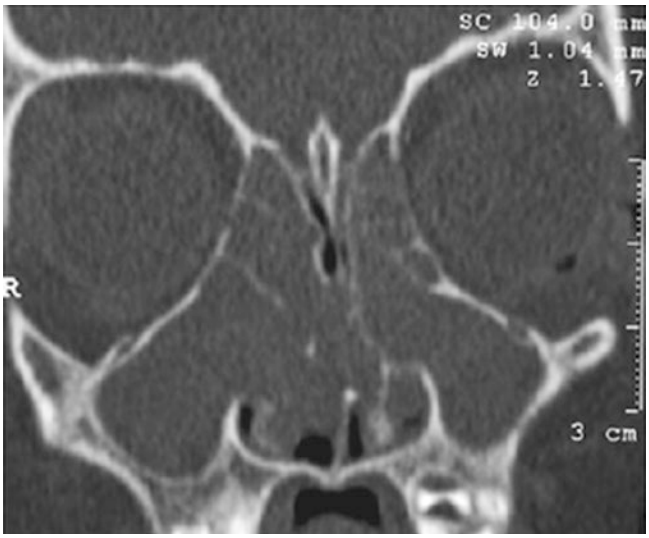

Fig. 18.11 Coronal CT of sinuses in a 4-year-old girl. There is complete opacification of both maxillary sinuses and ethmoid sinuses compatible with sinusitis. The medial wall of the right antrum is thinned and displaced. On endoscopic examination polyps were identified requiring functional endoscopic sinus surgery (FESS)

drip. Anosmia is the most frequent symptom in those with nasal polyposis [135]. Nasal obstruction may result in mouth breathing and widening of the nasal bridge giving rise to the impression of hypertelorism. Tenderness to palpation over the affected sinuses is present in one-third of patients with acute sinusitis. While large polyps may be visible on direct examination of the nose, up to 25% may be missed [136]. In case of suspected nasal polyps, referral to an Ear, Nose and Throat (E.N.T.) specialist for examination with flexible endoscopy is recommended. There is data to suggest that lower airway colonization with *P. aeruginosa* is associated with nasal polyposis in CF patients [137]. *Aspergillus* allergy is more common in patients with cystic fibrosis who have polyps than those who do not [138].

Imaging of the sinuses is recommended only in CF patients who are symptomatic since pansinusitis is an almost universal finding in CF regardless of the presence of absence of symptoms. Sinus radiographs may demonstrate sinus opacification (Fig. 18.10) or air fluid level. If imaging is indicated, sinus CT is the investigation of choice to identify the extent of mucosal thickening, polyposis, sinus wall displacement and obstruction of the osteomeatal complex (Fig. 18.11). Imaging may also benefit surgical planning. Classically, the frontal and sphenoidal sinuses are hypoplastic in CF.

Management of CF sinusitis is generally conservative, relying on medical management, and reserving surgical intervention for severe, symptomatic cases. Chronic rhinosinusitis may be treated with antibiotics, anti-inflammatory agents and nasal irrigations, e.g., nasal saline irrigations either hyper or hypotonic. Single polyps causing mild symptoms can be treated conservatively with intranasal steroid sprays but should be used for short periods only because of the risk of systemic side effects, e.g., adrenal suppression [139].

Symptomatic sinus disease refractory to medical management is often an indication for functional endoscopic sinus surgery (FESS), although significant variation exists among the frequency with which FESS is used in CF patients [140]. FESS usually includes maxillary antrostomy, anterior and posterior ethmoidectomy, sphenoidotomy, and frontal sinusotomy. While CF patients report improved symptoms after FESS, radiographic and endoscopic scores are rarely impacted. Additionally, data on lung function improvement following FESS is inconclusive [141–143]. While 50% of a pediatric patient group had an average symptom-free period of 11.3 years after sinus surgery, endoscopic review demonstrated a 50% chance of reverting to preoperative state within 18–24 months [144]. Preoperative grading of polyps using a modified Malm scale may help predict the likelihood of revision sinus surgery [145]. Prophylactic FESS prior to lung transplant does not appear to influence allograft recolonization or survival [146].

Non-respiratory Conditions of Cystic Fibrosis

CF patients are often affected by gastrointestinal, pancreatic, and hepatobiliary disease; however, a detailed discussion of non-respiratory CF conditions is beyond the scope of this book.

References

1. Riordan JR, et al. Identification of the cystic fibrosis gene: cloning and characterization of complementary DNA. Science. 1989;245(4922):1066–73.
2. Kerem B, et al. Identification of the cystic fibrosis gene: genetic analysis. Science. 1989;245(4922):1073–80.
3. Rommens JM, et al. Identification of the cystic fibrosis gene: chromosome walking and jumping. Science. 1989;245(4922):1059–65.
4. Consortium, C.F.G.A. Cystic fibrosis mutation database. 2010. 27 Feb 2018. Available from: http://www.genet.sickkids.on.ca/app.
5. The Clinical and Functional TRanslation of CFTR (CFTR2). 2011. Available from: http://cftr2.org.
6. Sosnay PR, Cutting GR. Interpretation of genetic variants. Thorax. 2014;69(3):295–7.
7. Cutting GR. Modifier genes in Mendelian disorders: the example of cystic fibrosis. Ann N Y Acad Sci. 2010;1214:57–69.
8. Ong T, et al. Socioeconomic status, smoke exposure, and health outcomes in young children with cystic fibrosis. Pediatrics. 2017;139(2):e20162730.
9. Oates GR, Schechter MS. Socioeconomic status and health outcomes: cystic fibrosis as a model. Expert Rev Respir Med. 2016;10(9):967–77.
10. Matsui H, et al. Evidence for periciliary liquid layer depletion, not abnormal ion composition, in the pathogenesis of cystic fibrosis airways disease. Cell. 1998;95(7):1005–15.
11. Sheppard DN, Welsh MJ. Structure and function of the CFTR chloride channel. Physiol Rev. 1999;79(1 Suppl):S23–45.
12. Hanrahan JW, Wioland MA. Revisiting cystic fibrosis transmembrane conductance regulator structure and function. Proc Am Thorac Soc. 2004;1(1):17–21.
13. Rauh R, Hoerner C, Korbmacher C. δβγ-ENaC is inhibited by CFTR but stimulated by cAMP in Xenopus laevis oocytes. Am J Physiol Lung Cell Mol Physiol. 2017;312(2):L277–87.
14. Stanke F, et al. The TNFalpha receptor TNFRSF1A and genes encoding the amiloride-sensitive sodium channel ENaC as modulators in cystic fibrosis. Hum Genet. 2006;119(3):331–43.
15. Pilewski JM, Frizzell RA. Role of CFTR in airway disease. Physiol Rev. 1999;79(1 Suppl):S215–55.
16. Pezzulo AA, et al. Reduced airway surface pH impairs bacterial killing in the porcine cystic fibrosis lung. Nature. 2012;487(7405):109–13.
17. Coakley RD, et al. Abnormal surface liquid pH regulation by cultured cystic fibrosis bronchial epithelium. Proc Natl Acad Sci U S A. 2003;100(26):16083–8.
18. Keiser NW, et al. Defective innate immunity and hyperinflammation in newborn cystic fibrosis transmembrane conductance regulator-knockout ferret lungs. Am J Respir Cell Mol Biol. 2015;52(6):683–94.
19. Verhaeghe C, et al. Early inflammation in the airways of a cystic fibrosis foetus. J Cyst Fibros. 2007;6(4):304–8.
20. Cohen-Cymberknoh M, et al. Airway inflammation in cystic fibrosis: molecular mechanisms and clinical implications. Thorax. 2013;68(12):1157–62.
21. Cutting GR. Cystic fibrosis genetics: from molecular understanding to clinical application. Nat Rev Genet. 2015;16(1):45–56.
22. Agrawal PB, et al. The epithelial sodium channel is a modifier of the long-term nonprogressive phenotype associated with F508del CFTR mutations. Am J Respir Cell Mol Biol. 2017;57(6):711–20.
23. Farrell PM, et al. Diagnosis of cystic fibrosis: consensus guidelines from the Cystic Fibrosis Foundation. J Pediatr. 2017;181S:S4–S15.e1.
24. Monaghan KG, Feldman GL. The risk of cystic fibrosis with prenatally detected echogenic bowel in an ethnically and racially diverse North American population. Prenat Diagn. 1999;19(7):604–9.
25. Sosnay PR, et al. Diagnosis of cystic fibrosis in nonscreened populations. J Pediatr. 2017;181S:S52–S57.e2.
26. Adam RJ, et al. Air trapping and airflow obstruction in newborn cystic fibrosis piglets. Am J Respir Crit Care Med. 2013;188(12):1434–41.
27. Mall MA, et al. Early detection and sensitive monitoring of CF lung disease: prospects of improved and safer imaging. Pediatr Pulmonol. 2016;51(S44):S49–60.
28. Cleveland RH, et al. Cystic fibrosis: predictors of accelerated decline and distribution of disease in 230 patients. AJR Am J Roentgenol. 1998;171(5):1311–5.
29. Slattery DM, et al. CF: an X-ray database to assess effect of aerosolized tobramycin. Pediatr Pulmonol. 2004;38(1):23–30.
30. Bhalla M, et al. Cystic fibrosis: scoring system with thin-section CT. Radiology. 1991;179(3):783–8.
31. Amaxopoulou C, et al. Structural and perfusion magnetic resonance imaging of the lung in cystic fibrosis. Pediatr Radiol. 2018;48(2):165–75.
32. Mogayzel PJ Jr, et al. Cystic fibrosis pulmonary guidelines. Chronic medications for maintenance of lung health. Am J Respir Crit Care Med. 2013;187(7):680–9.
33. Ramsey BW, et al. A CFTR potentiator in patients with cystic fibrosis and the G551D mutation. N Engl J Med. 2011;365(18):1663–72.
34. Accurso FJ, et al. Effect of VX-770 in persons with cystic fibrosis and the G551D-CFTR mutation. N Engl J Med. 2010;363(21):1991–2003.
35. Davies JC, et al. Safety, pharmacokinetics, and pharmacodynamics of ivacaftor in patients aged 2–5 years with cystic fibrosis and a CFTR gating mutation (KIWI): an open-label, single-arm study. Lancet Respir Med. 2016;4(2):107–15.
36. McGarry ME, et al. In vivo and in vitro ivacaftor response in cystic fibrosis patients with residual CFTR function: N-of-1 studies. Pediatr Pulmonol. 2017;52(4):472–9.
37. Milla CE, et al. Lumacaftor/ivacaftor in patients aged 6–11 years with cystic fibrosis and homozygous for F508del-CFTR. Am J Respir Crit Care Med. 2017;195(7):912–20.
38. Konstan MW, et al. Assessment of safety and efficacy of long-term treatment with combination lumacaftor and ivacaftor therapy in patients with cystic fibrosis homozygous for the F508del-CFTR mutation (PROGRESS): a phase 3, extension study. Lancet Respir Med. 2017;5(2):107–18.
39. Ratjen F, et al. Efficacy and safety of lumacaftor and ivacaftor in patients aged 6–11 years with cystic fibrosis homozygous for F508del-CFTR: a randomised, placebo-controlled phase 3 trial. Lancet Respir Med. 2017;5(7):557–67.
40. Rowe SM, et al. Tezacaftor-ivacaftor in residual-function heterozygotes with cystic fibrosis. N Engl J Med. 2017;377(21):2024–35.
41. Wainwright CE, et al. Lumacaftor-ivacaftor in patients with cystic fibrosis homozygous for Phe508del CFTR. N Engl J Med. 2015;373(3):220–31.
42. Quon BS, Rowe SM. New and emerging targeted therapies for cystic fibrosis. BMJ. 2016;352:i859.
43. Yen EH, Quinton H, Borowitz D. Better nutritional status in early childhood is associated with improved clinical outcomes and survival in patients with cystic fibrosis. J Pediatr. 2013;162(3):530–535.e1.
44. Stephenson AL, et al. Survival comparison of patients with cystic fibrosis in Canada and the United States: a population-based cohort study. Ann Intern Med. 2017;166(8):537–46.
45. Snell G, et al. The evolution of lung transplantation for cystic fibrosis: a 2017 update. J Cyst Fibros. 2017;16(5):553–64.
46. Wang EE, et al. Association of respiratory viral infections with pulmonary deterioration in patients with cystic fibrosis. N Engl J Med. 1984;311(26):1653–8.

47. Abman SH, et al. Role of respiratory syncytial virus in early hospitalizations for respiratory distress of young infants with cystic fibrosis. J Pediatr. 1988;113(5):826–30.
48. Smyth AR, et al. Effect of respiratory virus infections including rhinovirus on clinical status in cystic fibrosis. Arch Dis Child. 1995;73(2):117–20.
49. Wark PA, et al. Viral infections trigger exacerbations of cystic fibrosis in adults and children. Eur Respir J. 2012;40(2):510–2.
50. Asner S, et al. Role of respiratory viruses in pulmonary exacerbations in children with cystic fibrosis. J Cyst Fibros. 2012;11(5):433–9.
51. Wat D, Doull I. Respiratory virus infections in cystic fibrosis. Paediatr Respir Rev. 2003;4(3):172–7.
52. Ramsey BW, et al. The effect of respiratory viral infections on patients with cystic fibrosis. Am J Dis Child. 1989;143(6):662–8.
53. Hiatt PW, et al. Effects of viral lower respiratory tract infection on lung function in infants with cystic fibrosis. Pediatrics. 1999;103(3):619–26.
54. Petersen NT, et al. Respiratory infections in cystic fibrosis patients caused by virus, chlamydia and mycoplasma--possible synergism with Pseudomonas aeruginosa. Acta Paediatr Scand. 1981;70(5):623–8.
55. Collinson J, et al. Effects of upper respiratory tract infections in patients with cystic fibrosis. Thorax. 1996;51(11):1115–22.
56. Abman SH, et al. Early bacteriologic, immunologic, and clinical courses of young infants with cystic fibrosis identified by neonatal screening. J Pediatr. 1991;119(2):211–7.
57. Kua KP, Lee SWH. Systematic review of the safety and efficacy of palivizumab among infants and young children with cystic fibrosis. Pharmacotherapy. 2017;37(6):755–69.
58. Pribble CG, et al. Clinical manifestations of exacerbations of cystic fibrosis associated with nonbacterial infections. J Pediatr. 1990;117(2 Pt 1):200–4.
59. Conway SP, Simmonds EJ, Littlewood JM. Acute severe deterioration in cystic fibrosis associated with influenza A virus infection. Thorax. 1992;47(2):112–4.
60. Ortiz JR, et al. Influenza-associated cystic fibrosis pulmonary exacerbations. Chest. 2010;137(4):852–60.
61. Dharmaraj P, Smyth RL. Vaccines for preventing influenza in people with cystic fibrosis. Cochrane Database Syst Rev. 2014;3:CD001753.
62. Armstrong DS, et al. Lower airway inflammation in infants and young children with cystic fibrosis. Am J Respir Crit Care Med. 1997;156(4 Pt 1):1197–204.
63. Rosenfeld M, et al. Early pulmonary infection, inflammation, and clinical outcomes in infants with cystic fibrosis. Pediatr Pulmonol. 2001;32(5):356–66.
64. Cantin AM, et al. Inflammation in cystic fibrosis lung disease: pathogenesis and therapy. J Cyst Fibros. 2015;14(4):419–30.
65. Balough K, et al. The relationship between infection and inflammation in the early stages of lung disease from cystic fibrosis. Pediatr Pulmonol. 1995;20(2):63–70.
66. Bartlett JA, et al. Newborn cystic fibrosis pigs have a blunted early response to an inflammatory stimulus. Am J Respir Crit Care Med. 2016;194(7):845–54.
67. Chmiel JF, Berger M, Konstan MW. The role of inflammation in the pathophysiology of CF lung disease. Clin Rev Allergy Immunol. 2002;23(1):5–27.
68. Bradley J, McAlister O, Elborn S. Pulmonary function, inflammation, exercise capacity and quality of life in cystic fibrosis. Eur Respir J. 2001;17(4):712–5.
69. Rosenfeld M, et al. Defining a pulmonary exacerbation in cystic fibrosis. J Pediatr. 2001;139(3):359–65.
70. Bilton D, et al. Pulmonary exacerbation: towards a definition for use in clinical trials. Report from the EuroCareCF Working Group on outcome parameters in clinical trials. J Cyst Fibros. 2011;10(Suppl 2):S79–81.
71. Cleveland RH, et al. Cystic fibrosis genotype and assessing rates of decline in pulmonary status. Radiology. 2009;253(3):813–21.
72. Ronchetti K, et al. The CF-Sputum Induction Trial (CF-SpIT) to assess lower airway bacterial sampling in young children with cystic fibrosis: a prospective internally controlled interventional trial. Lancet Respir Med. 2018;6(6):461–71.
73. Flume PA, et al. Cystic fibrosis pulmonary guidelines: treatment of pulmonary exacerbations. Am J Respir Crit Care Med. 2009;180(9):802–8.
74. Bhatt JM. Treatment of pulmonary exacerbations in cystic fibrosis. Eur Respir Rev. 2013;22(129):205–16.
75. Lyczak JB, Cannon CL, Pier GB. Lung infections associated with cystic fibrosis. Clin Microbiol Rev. 2002;15(2):194–222.
76. Demko CA, Byard PJ, Davis PB. Gender differences in cystic fibrosis: Pseudomonas aeruginosa infection. J Clin Epidemiol. 1995;48(8):1041–9.
77. Parad RB, et al. Pulmonary outcome in cystic fibrosis is influenced primarily by mucoid Pseudomonas aeruginosa infection and immune status and only modestly by genotype. Infect Immun. 1999;67(9):4744–50.
78. Watt AP, et al. Neutrophil cell death, activation and bacterial infection in cystic fibrosis. Thorax. 2005;60(8):659–64.
79. Mogayzel PJ Jr, et al. Cystic Fibrosis Foundation pulmonary guideline. Pharmacologic approaches to prevention and eradication of initial Pseudomonas aeruginosa infection. Ann Am Thorac Soc. 2014;11(10):1640–50.
80. Langton Hewer SC, Smyth AR. Antibiotic strategies for eradicating Pseudomonas aeruginosa in people with cystic fibrosis. Cochrane Database Syst Rev. 2017;4:CD004197.
81. Ratjen F, et al. Treatment of early Pseudomonas aeruginosa infection in patients with cystic fibrosis: the ELITE trial. Thorax. 2010;65(4):286–91.
82. Treggiari MM, et al. Comparative efficacy and safety of 4 randomized regimens to treat early Pseudomonas aeruginosa infection in children with cystic fibrosis. Arch Pediatr Adolesc Med. 2011;165(9):847–56.
83. Emerson J, et al. Pseudomonas aeruginosa and other predictors of mortality and morbidity in young children with cystic fibrosis. Pediatr Pulmonol. 2002;34(2):91–100.
84. Smyth AR, Rosenfeld M. Prophylactic anti-staphylococcal antibiotics for cystic fibrosis. Cochrane Database Syst Rev. 2017;4:CD001912.
85. Foundation CF. Patient registry 2016 annual data report. Cystic Fibrosis Foundation, Bethesda, MD.
86. Sawicki GS, Rasouliyan L, Ren CL. The impact of MRSA on lung function in patients with cystic fibrosis. Am J Respir Crit Care Med. 2009;179(8):734–5; author reply 735.
87. Ren CL, et al. Presence of methicillin resistant Staphylococcus aureus in respiratory cultures from cystic fibrosis patients is associated with lower lung function. Pediatr Pulmonol. 2007;42(6):513–8.
88. Muhlebach MS, et al. Treatment intensity and characteristics of MRSA infection in CF. J Cyst Fibros. 2011;10(3):201–6.
89. Dasenbrook EC, et al. Association between respiratory tract methicillin-resistant Staphylococcus aureus and survival in cystic fibrosis. JAMA. 2010;303(23):2386–92.
90. Muhlebach MS, et al. Microbiological efficacy of early MRSA treatment in cystic fibrosis in a randomised controlled trial. Thorax. 2017;72(4):318–26.
91. Kappler M, et al. Eradication of methicillin resistant Staphylococcus aureus detected for the first time in cystic fibrosis: a single center observational study. Pediatr Pulmonol. 2016;51(10):1010–9.
92. Vandamme P, Dawyndt P. Classification and identification of the Burkholderia cepacia complex: past, present and future. Syst Appl Microbiol. 2011;34(2):87–95.

93. Henry DA, et al. Identification of Burkholderia cepacia isolates from patients with cystic fibrosis and use of a simple new selective medium. J Clin Microbiol. 1997;35(3):614–9.
94. McMenamin JD, et al. Misidentification of Burkholderia cepacia in US cystic fibrosis treatment centers: an analysis of 1,051 recent sputum isolates. Chest. 2000;117(6):1661–5.
95. Jones AM, et al. Burkholderia cenocepacia and Burkholderia multivorans: influence on survival in cystic fibrosis. Thorax. 2004;59(11):948–51.
96. Courtney JM, et al. Clinical outcome of Burkholderia cepacia complex infection in cystic fibrosis adults. J Cyst Fibros. 2004;3(2):93–8.
97. De Soyza A, et al. Lung transplantation for patients with cystic fibrosis and Burkholderia cepacia complex infection: a single-center experience. J Heart Lung Transplant. 2010;29(12):1395–404.
98. De Soyza A, et al. Burkholderia cepacia complex genomovars and pulmonary transplantation outcomes in patients with cystic fibrosis. Lancet. 2001;358(9295):1780–1.
99. Meachery G, et al. Outcomes of lung transplantation for cystic fibrosis in a large UK cohort. Thorax. 2008;63(8):725–31.
100. Adjemian J, Olivier KN, Prevots DR. Epidemiology of pulmonary nontuberculous mycobacterial sputum positivity in patients with cystic fibrosis in the United States, 2010–2014. Ann Am Thorac Soc. 2018;15(7):817–26.
101. Leung JM, Olivier KN. Nontuberculous mycobacteria in patients with cystic fibrosis. Semin Respir Crit Care Med. 2013;34(1):124–34.
102. Esther CR Jr, et al. Chronic Mycobacterium abscessus infection and lung function decline in cystic fibrosis. J Cyst Fibros. 2010;9(2):117–23.
103. Griffith DE, et al. An official ATS/IDSA statement: diagnosis, treatment, and prevention of nontuberculous mycobacterial diseases. Am J Respir Crit Care Med. 2007;175(4):367–416.
104. Floto RA, et al. US Cystic Fibrosis Foundation and European Cystic Fibrosis Society consensus recommendations for the management of non-tuberculous mycobacteria in individuals with cystic fibrosis: executive summary. Thorax. 2016;71(1):88–90.
105. Mussaffi H, et al. Nontuberculous mycobacteria in cystic fibrosis associated with allergic bronchopulmonary aspergillosis and steroid therapy. Eur Respir J. 2005;25(2):324–8.
106. Colin AA. Eradication of mycobacterium abscessus in a chronically infected patient with cystic fibrosis. Pediatr Pulmonol. 2000;30(3):267–8.
107. Martinez S, McAdams HP, Batchu CS. The many faces of pulmonary nontuberculous mycobacterial infection. AJR Am J Roentgenol. 2007;189(1):177–86.
108. Flume PA, et al. Massive hemoptysis in cystic fibrosis. Chest. 2005;128(2):729–38.
109. Charan NB, Baile EM, Pare PD. Bronchial vascular congestion and angiogenesis. Eur Respir J. 1997;10(5):1173–80.
110. Flume PA, et al. Cystic fibrosis pulmonary guidelines: pulmonary complications: hemoptysis and pneumothorax. Am J Respir Crit Care Med. 2010;182(3):298–306.
111. Flight WG, et al. Outcomes following bronchial artery embolisation for haemoptysis in cystic fibrosis. Cardiovasc Intervent Radiol. 2017;40(8):1164–8.
112. Barben J, et al. Bronchial artery embolization for hemoptysis in young patients with cystic fibrosis. Radiology. 2002;224(1):124–30.
113. Monroe EJ, et al. An interventionalist's guide to hemoptysis in cystic fibrosis. Radiographics. 2018;38(2):624–41.
114. Giron Moreno RM, Caballero P, Friera A. Multidetector computed tomography angiography for pre-embolization assessment in cystic fibrosis patients with massive haemoptysis. Respir Med. 2014;108(5):816–7.
115. Hayes D Jr, et al. Preprocedural planning with prospectively triggered multidetector row CT angiography prior to bronchial artery embolization in cystic fibrosis patients with massive hemoptysis. Lung. 2012;190(2):221–5.
116. Flume PA, et al. Pneumothorax in cystic fibrosis. Chest. 2005;128(2):720–8.
117. Tomashefski JF Jr, et al. Pulmonary air cysts in cystic fibrosis: relation of pathologic features to radiologic findings and history of pneumothorax. Hum Pathol. 1985;16(3):253–61.
118. Northfield TC. Oxygen therapy for spontaneous pneumothorax. Br Med J. 1971;4(5779):86–8.
119. Spector ML, Stern RC. Pneumothorax in cystic fibrosis: a 26-year experience. Ann Thorac Surg. 1989;47:204–7.
120. Maturu VN, Agarwal R. Prevalence of Aspergillus sensitization and allergic bronchopulmonary aspergillosis in cystic fibrosis: systematic review and meta-analysis. Clin Exp Allergy. 2015;45(12):1765–78.
121. Janahi IA, Rehman A, Al-Naimi AR. Allergic bronchopulmonary aspergillosis in patients with cystic fibrosis. Ann Thorac Med. 2017;12(2):74–82.
122. Geller DE, et al. Allergic bronchopulmonary aspergillosis in cystic fibrosis: reported prevalence, regional distribution, and patient characteristics. Scientific Advisory Group, Investigators, and Coordinators of the Epidemiologic Study of Cystic Fibrosis. Chest. 1999;116(3):639–46.
123. Stevens DA, Moss RB, Kurup VP. Allergic broncho-pulmonary aspergillosis in cystic fibrosis: state of the art: cystic Fibrosis Consensus Conference. Clin Infect Dis. 2003;37(Suppl 3):S225–64.
124. Agarwal R. High attenuation mucoid impaction in allergic bronchopulmonary aspergillosis. World J Radiol. 2010;2(1):41–3.
125. Logan PM, Muller NL. High-attenuation mucous plugging in allergic bronchopulmonary aspergillosis. Can Assoc Radiol J. 1996;47(5):374–7.
126. Occelli A, et al. Bronchocele density in cystic fibrosis as an indicator of allergic broncho-pulmonary aspergillosis: a preliminary study. Eur J Radiol. 2017;93:195–9.
127. Kraemer R, et al. Effect of allergic bronchopulmonary aspergillosis on lung function in children with cystic fibrosis. Am J Respir Crit Care Med. 2006;174(11):1211–20.
128. Wark P. Pathogenesis of allergic broncho-pulmonary aspergillosis and an evidence-based review of azoles in treatment. Respir Med. 2004;98:915–23.
129. Nove-Josserand R, et al. Case series of omalizumab for allergic bronchopulmonary aspergillosis in cystic fibrosis patients. Pediatr Pulmonol. 2017;52(2):190–7.
130. Jat KR, Walia DK, Khairwa A. Anti-IgE therapy for allergic bronchopulmonary aspergillosis in people with cystic fibrosis. Cochrane Database Syst Rev. 2018;3:CD010288.
131. Slieker MG, et al. Children with cystic fibrosis: who should visit the otorhinolaryngologist? Arch Otolaryngol Head Neck Surg. 2002;128:1245–8.
132. Brihaye P, Jorissen M, Clement PA. Chronic rhinosinusitis in cystic fibrosis (mucoviscidosis). Acta Otorhinolaryngol Belg. 1997;51:323–37.
133. Coste A, Gilain L, Roger G. Endoscopic and CT-scan evaluation of rhinosinusitis in cystic fibrosis. Rhinology. 1995;33:152–6.
134. Hadfield PJ, Rowe-Jones JM, Mackay IS. The prevalence of nasal polyps in adults with cystic fibrosis. Clin Otolaryngol Allied Sci. 2000;25(1):19–22.
135. Nishioka GJ, Cook PR. Paranasal sinus disease in patients with cystic fibrosis. Otolaryngol Clin. 1996;29:193–205.
136. Brihaye P, et al. Pathological changes of the lateral nasal wall in patients with cystic fibrosis (mucoviscidosis). Int J Pediatr Otorhinolaryngol. 1994;28(2–3):141–7.
137. Henriksson G, Westrin KM, Karpati F. Nasal polyps in cystic fibrosis: clinical endoscopic study with nasal lavage fluid analysis. Chest. 2002;121:40–7.

138. Cimmino M, Cavaliere M, Nardone M. Clinical characteristics and genotype analysis of patients with cystic fibrosis and nasal polyposis. Clin Ololaryngol Allied Sci. 2003;28:125–32.
139. Hadfield PJ, Rowe-Jones JM, Mackay IS. A prospective treatment trial of nasal polyps in adults with cystic fibrosis. Rhinology. 2000;38(2):63–5.
140. Virgin FW, et al. Inter-hospital variation in the frequency of sinus surgery in children with cystic fibrosis. Pediatr Pulmonol. 2015;50(3):231–5.
141. Macdonald KI, et al. Endoscopic sinus surgery in patients with cystic fibrosis: a systematic review and meta-analysis of pulmonary function. Rhinology. 2012;50(4):360–9.
142. Khalfoun S, et al. Improved lung function after sinus surgery in cystic fibrosis patients with moderate obstruction. Otolaryngol Head Neck Surg. 2018;158(2):381–5.
143. Jarrett WA, et al. Endoscopic sinus surgery in cystic fibrosis: effects on pulmonary function and ideal body weight. Ear Nose Throat J. 2004;83(2):118–21.
144. Rowe-Jones JM, Mackay IS. Endoscopic sinus surgery in the treatment of cystic fibrosis with nasal polyposis. Laryngoscope. 1996;106(12):1540–4.
145. Rickert S, et al. Cystic fibrosis and endoscopic sinus surgery: relationship between nasal polyposis and likelihood of revision endoscopic sinus surgery in patients with cystic fibrosis. Arch Otolaryngol Head Neck Surg. 2010;136(10):988–92.
146. Leung MK, et al. Effects of sinus surgery on lung transplantation outcomes in cystic fibrosis. Am J Rhinol. 2008;22(2):192–6.

Pediatric Lung Transplantation

19

Gary Visner and Edward Y. Lee

Introduction

Lung and heart–lung transplantation are established therapies for children with end-stage lung or congenital heart disease (CHD)/pulmonary vascular disease (PVD) in which there are no other therapeutic options. Lung transplantation was first successfully performed in 1983. Since 1986, there have been more than 2330 pediatric lung transplant and 730 pediatric heart–lung transplant procedures performed in children worldwide [1]. Based on the current age definition of the United Network for Organ Sharing (UNOS) and the International Society for Heart and Lung Transplantation (ISHLT) for transplantation, *children* are identified as being under 18 years of age. The majority of lung or heart–lung transplants in children are from age 12–17. As of March 2018, there are more than 40 children on the lung transplant waiting list in the USA (Organ Procurement and Transplantation Network (OPTN)).

The most common indications for transplantation differ by age group (Table 19.1). Cystic fibrosis is the most common overall indication at 57.6% and is the diagnosis for nearly 66.7% of the lung recipients for the 12–17-year age group. In children younger than 1 year, the most common indications are CHD/PVD and diffuse lung disease from surfactant abnormalities. Additional diagnoses include transplant and nontransplant bronchiolitis obliterans and pulmonary fibrosis/interstitial pneumonitis.

Survival in pediatric patients following lung transplantation is approximately 80% after 1 year and approximately 57% after 5 years [1]. Multiorgan failure is the major cause of early mortality (<1 month), while infection is the most common cause of death within the first year [1]. Infection remains a significant complication throughout the life of the pediatric lung transplant patient. The major complication for long-term survival in lung transplantation in both adult and pediatric patients is bronchiolitis obliterans, which is believed to be the manifestation of chronic lung rejection.

Fewer than 5% of the procedures have been single lung transplants. In the USA, heart–lung transplantation is primarily for patients with complex CHD or pulmonary vascular abnormalities or a small number of patients with primary pulmonary hypertension. From 1995 to 2005, living lobar donor surgeries made up approximately 10% of pediatric lung transplantation mostly in older children who had a better size match with the two lower lobes from adult donors. With the new lung allocation system in 2005 in which lung allocation is based on a number of factors such as lung function rather than time on the list, there has been a decrease in the number of living lobar donor transplantations.

This chapter review pretransplant, donor, and posttransplant imaging evaluation.

Pretransplant Imaging Evaluation

Imaging evaluation plays a crucial role in all phases of the lung transplant process from evaluation of the recipient and donor lungs to early and late posttransplant management. Imaging studies in the evaluation process is usually dependent upon the disease indication; however, all patients have some form of lung imaging.

Chest radiographs and computed tomography (CT) of the chest are typically performed to assess lung pathology as to the extent of the disease process and assessment of chest and lung size in virtually all patients undergoing lung transplant evaluation. With the development and widespread availability of multidetector CT (MDCT), CT has assumed a greater role in the prelung transplant evaluation in children. MDCT provides high-resolution images, faster scan times, and high-quality multiplanar (MPR) and three-dimensional (3D) images of the airways and vascular structures. The high-quality MPR

G. Visner
Boston Children's Hospital, Harvard Medical School, Boston, MA, USA

E. Y. Lee (✉)
Department of Radiology, Boston Children's Hospital and Harvard Medical School, Boston, MA, USA
e-mail: Edward.Lee@childrens.harvard.edu

R. H. Cleveland, E. Y. Lee (eds.), *Imaging in Pediatric Pulmonology*, https://doi.org/10.1007/978-3-030-23979-4_19

Table 19.1 Indications for pediatric lung transplants by recipient age group (Transplants: January 1, 2000–June 30, 2016)

	<1 year	1–5 years	6–10 years	11–17 years
Diagnosis	No. (%)	No. (%)	No. (%)	No. (%)
Cystic fibrosis	0	4 (3.7)	116 (50.0)	814 (66.7)
Non-cystic fibrosis-bronchiectasis	0	0	2 (0.9)	23 (1.9)
ILD	5 (8.3)	9 (8.3)	6 (2.6)	37 (3.0)
ILD other	6 (10.0)	10 (9.3)	21 (9.1)	46 (3.8)
PH/pulmonary arterial hypertension	7 (11.7)	28 (25.9)	24 (10.3)	100 (8.2)
PH				
Eisenmenger syndrome	0	1 (0.9)	2 (0.9)	6 (0.5)
Other	15 (25.0)	21 (19.4)	8 (3.4)	20 (1.6)
Obliterative bronchiolitis (non-retransplant)	0	10 (9.3)	26 (11.2)	58 (4.8)
Bronchopulmonary dysplasia	4 (6.7)	4 (3.7)	3 (1.3)	3 (0.2)
ABCA3 transporter mutation	5 (8.3)	4 (3.7)	1 (0.4)	1 (0.1)
Surfactant protein B deficiency	13 (21.7)	4 (3.7)	1 (0.4)	0
Surfactant protein C deficiency	0	1 (0.9)	0	1 (0.1)
Retransplant				
Obliterative bronchiolitis	0	4 (3.7)	8 (3.4)	41 (3.4)
Not obliterative bronchiolitis	0	4 (3.7)	6 (2.6)	41 (3.4)
COPD, with or without A1ATD	2 (3.3)	1 (0.9)	3 (1.3)	10 (0.8)
Other	3 (5.0)	3 (2.8)	5 (2.2)	20 (1.6)

A1ATD α-1-anti-trypsin deficiency, *ABCA3* adenosine 5′-triphosphate-binding cassette subfamily A member 3, *COPD* chronic obstructive pulmonary disease, *ILD* interstitial lung disease, *PH* pulmonary hypertension

and 3D images have enhanced the display of airways and vascular structures which improves communication among patients, patients' parents, clinicians, and surgeons before and after lung transplantation. In older adult patients, chest CT scans are also useful to screen for occult lung cancer, which is less of an issue in the pediatric population. Ventilation–perfusion (V/Q) scans can give some indication of lung function and assist in deciding which lung to transplant for single lung transplantation. The vast majority of pediatric patients receive bilateral lung transplants, and a V/Q scan may help decide which lung to transplant first if the procedure is not performed using cardiopulmonary bypass. V/Q scans may also be indicated in evaluating underlying pulmonary hypertension and chronic thromboembolic pulmonary hypertension.

Additional studies may include sinus CT scans especially for patients with cystic fibrosis to assess severity of chronic sinusitis and possible need for intervention. Imaging the abdomen most commonly by ultrasound is valuable to evaluate for abdominal organ pathology. Most patients with cystic fibrosis have an abdominal ultrasound. Echocardiography and/or cardiac catheterization is used to assess cardiac function and for pulmonary vascular disease. Bone densitometry may be performed especially in patients with chronic steroid use or limited physical activity. Patients receive chronic steroid therapy post transplantation, which may aggravate their bone disease and increase the risk for fractures.

Donor Imaging Evaluation

A chest radiograph is standard evaluation of donor lungs to assess lung size and potential pulmonary pathology. The ideal donor has a clear CXR with no evidence of lung pathology along with other parameters such as PaO_2 of >300 mmHg on and FiO_2 1.0 and a normal bronchoscopy. Although a normal CXR is considered ideal for the donor lung, there is no data in regard to the use of abnormal CXRs. It is common to find atelectasis in donors, and CXR is valuable in identifying atelectasis which may clear with increased airway clearance and/or bronchoscopy to clear mucus plugging, thereby potentially salvaging an otherwise unusable lung. On occasion, chest CT scan may help in delineating lung pathology and the feasibility of the lung for organ donation (Fig. 19.1).

Posttransplant Imaging Evaluation

Early complications of postlung transplantation include hyperacute rejection and primary graft dysfunction (Table 19.2). Hyperacute rejection is an uncommon complication occurring minutes to hours after transplantation as a result of recipient antibody response to donor vascular endothelium [2]. This results in respiratory failure with CXR showing severe pulmonary edema and diffuse consolidation. This has a very poor survival. Primary graft dysfunction (PGD) has been classified as PGD 1, 2, or 3 based on CXR abnormalities and oxygenation index (PaO_2/FiO_2) within the first 72 hours [3]. Contributing factors that may need to be excluded include hyperacute rejection, cardiogenic pulmonary edema, pulmonary venous obstruction, pneumonia, and possibly transfusion-related acute lung injury. Based on this classification, the incidence of severe PGD (PGD3 with P/F <200 after 48 hours posttransplant) appears to be ~15%, and more importantly PGD3 is associated with an increase in both early and late graft failure and mortality [4]. CXR typically shows bilateral pulmonary edema and basal air-space consolidation (Fig. 19.2) [5].

Mechanical complications may occur when there is a size mismatch between donor lungs and recipients thoracic cavity. Lungs that are too large may result in distortion of the airways and atelectasis, which may progress to scarring. Lungs that are too small may result in hemodynamic compromise, exercise limitations, and pulmonary hypertension from an inadequate pulmonary vascular circulation. There may also be delayed filling of the entire thoracic cavity with persistent pleural air. Another possible complication is injury to the phrenic nerve resulting in diaphragmatic dysfunction.

As a result of the transplant procedure, pleural abnormalities are seen which include pneumothorax and pleural effusions, and chest tubes are routinely placed upon completion of the lung transplant surgery. With increased capillary permeability and impaired lymphatic clearance, pleural effusions are commonly seen and usually self-limiting within approximately 2 weeks. Persistent or delayed effusions may result from complications such as empyema, rejection, or vascular abnomalities.

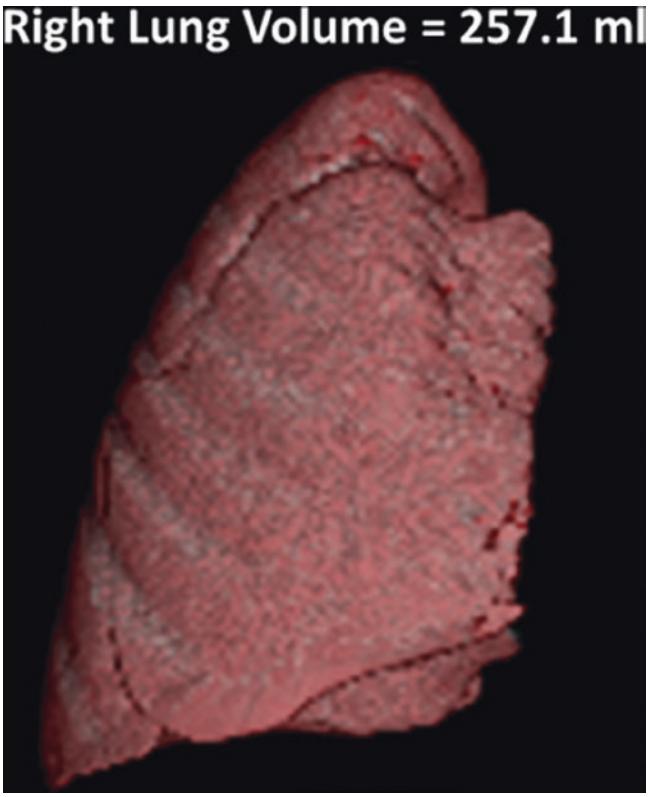

Fig. 19.1 3D CT imaging evaluation of feasibility of the lung for organ donation. 3D volume-rendered CT image shows the right lung volume of 257.1 ml

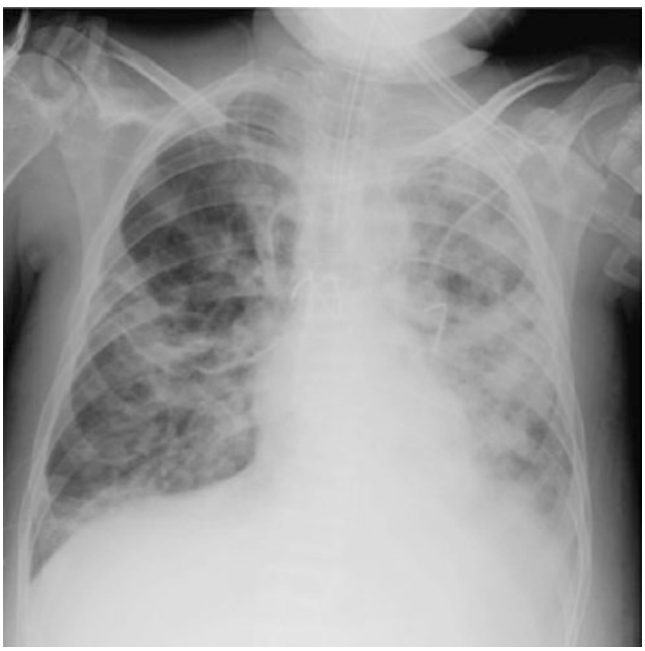

Fig. 19.2 A 14-year-old girl with bilateral lung transplantation for cystic fibrosis. Chest radiograph shows pulmonary edema associated with patchy air-space opacities in both lungs immediately after lung transplantation, compatible with primary graft dysfunction

Table 19.2 Cause of death for pediatric lung recipients (Deaths: January 1, 2000–June 30, 2016)

	0–30 days	31 days–1 year	>1–3 years	>3–5 years	>5 years
	(*n* = 89)	(*n* = 145)	(*n* = 222)	(*n* = 120)	(*n* = 146)
Cause of death	No. (%)	No. (%)	No. (%)	No. (%)	No. (%)
OB/BOS	0	15 (10.3)	73 (32.9)	48 (40.0)	65 (44.5)
Acute rejection	3 (3.4)	3 (2.1)	6 (2.7)	3 (2.5)	1 (0.7)
Lymphoma	0	4 (2.8)	4 (1.8)	3 (2.5)	5 (3.4)
Malignancy, non-lymphoma	0	3 (2.1)	1 (0.5)	1 (0.8)	7 (4.8)
CMV	0	2 (1.4)	0	0	0
Infection, non-CMV	14 (15.7)	40 (27.6)	36 (16.2)	17 (14.2)	13 (8.9)
Graft failure	13 (14.6)	34 (23.4)	68 (30.6)	28 (23.3)	35 (24.0)
Cardiovascular	14 (15.7)	7 (4.8)	3 (1.4)	1 (0.8)	1 (0.7)
Technical	15 (16.9)	3 (2.1)	3 (1.4)	3 (2.5)	2 (1.4)
Multiple organ failure	17 (19.1)	23 (15.9)	14 (6.3)	5 (4.2)	8 (5.5)
Other	13 (14.6)	11 (7.6)	14 (6.3)	11 (9.2)	9 (6.2)

BOS bronchiolitis obliterans syndrome, *CMV* cytomegalovirus, *OB* obliterative bronchiolitis

In the early period of lung transplantation, bronchial complications were frequent and limited the utility of this procedure. With improved donor preservation, surgical techniques, and immunosuppression, these are much less frequent; however, the incidence of airway complications is still estimated to be 10% [6]. Since the bronchial circulation is not reconnected with the transplant procedure, the airway circulation is dependent upon retrograde perfusion through the pulmonary circulation. Bronchial dehiscence is an early complication which is best detected by CT scan with the presence of extraluminal air around the anastomosis site. New or persistent pneumothorax or pneumomediastinum may be indirect evidence of a bronchial air leak. Bronchial stenosis, which is a complication of surgical anastomotic healing or dehiscence, is a serious complication that can occur after lung transplantation [5]. Although diagnosis of bronchial stenosis can be made with bronchoscopy, MDCT with 3D imaging of the central airways is a useful noninvasive imaging modality. On CT, focal or diffuse narrowing of the airway, typically at the site of surgical anastomosis, is seen (Fig. 19.3). Vascular complications are less common and can be evaluated by perfusion scan and visualized by angiographic studies. However, MDCT with 3D imaging can also be used as an alternative noninvasive imaging modality to detect vascular complications in children after lung transplantation (Fig. 19.4).

Infections and acute cellular rejection (ACR) are common complications in lung transplant patients and difficult to differentiate based on clinical or radiographic parameters. Bronchoscopy with bronchoalveolar lavage and transbronchial biopsy is currently the procedure to differentiate infection and rejection. ACR may occur without CXR changes, or the CXR may show new or persistent infiltrates or pleural effusion. CT findings of ACR include areas of ground-glass attenuation, interlobular septal thickening, small nodules (<1 mm), decreased vascularity, and air-space disease (Fig. 19.5) [5]. In addition to detecting ACR, CT may be useful for localizing the site of disease for biopsy to confirm the diagnosis.

Because of immunosuppression, lung denervation, loss of cough reflex, and impaired lymphatic drainage, lung transplant patients are at increased risk for infections and may not present with the usual clinical signs and symptoms. Bacterial

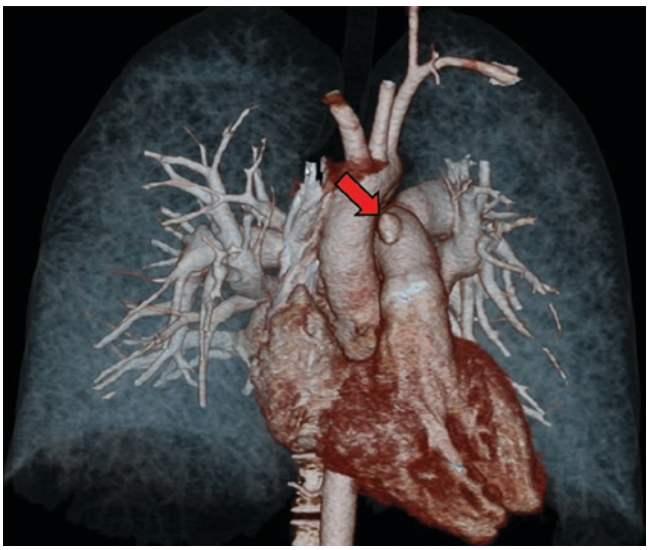

Fig. 19.4 A 15-year-old girl with bilateral lung transplantation for cystic fibrosis. 3D volume-rendered CT image of the vascular structure shows a large aneurysm (arrow) arising from the main pulmonary artery as a vascular complication from the lung transplant

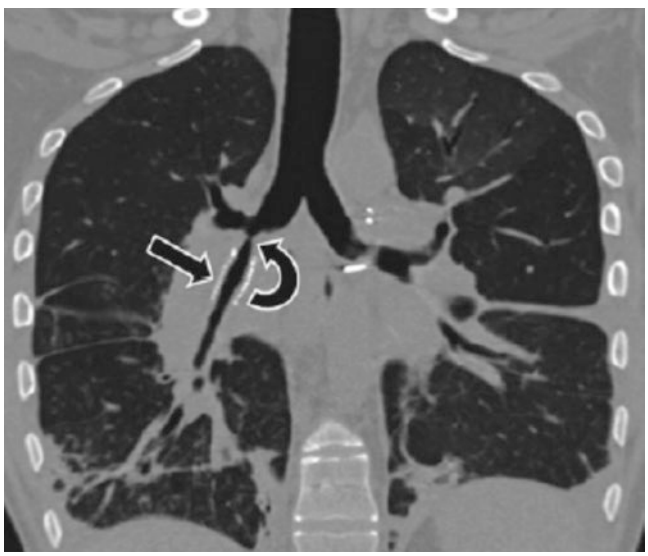

Fig. 19.3 An 18-year-old girl with bilateral lung transplantation for cystic fibrosis. Coronal reformatted CT demonstrates right-sided bronchial narrowing (*curved arrow*). Also noted is a metallic stent (*straight arrow*) located in the right lower lobe bronchus

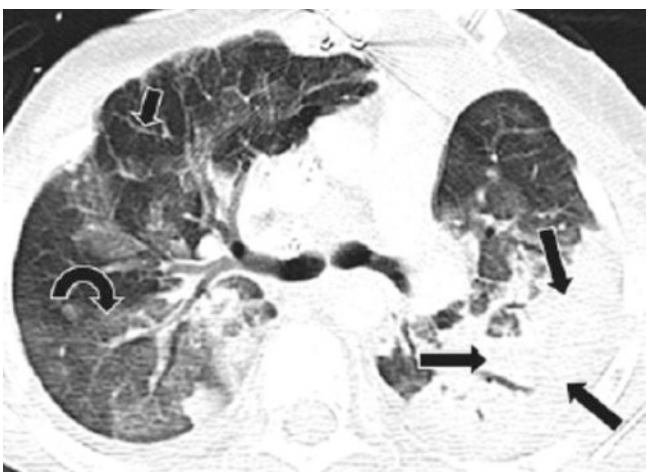

Fig. 19.5 A 15-year-old girl with bilateral lung transplantation for cystic fibrosis. Axial lung window CT image shows ground-glass opacification (*curved arrow*), septal thickening (*short arrow*), and air-space consolidation (*long arrows*) compatible with acute cellular rejection

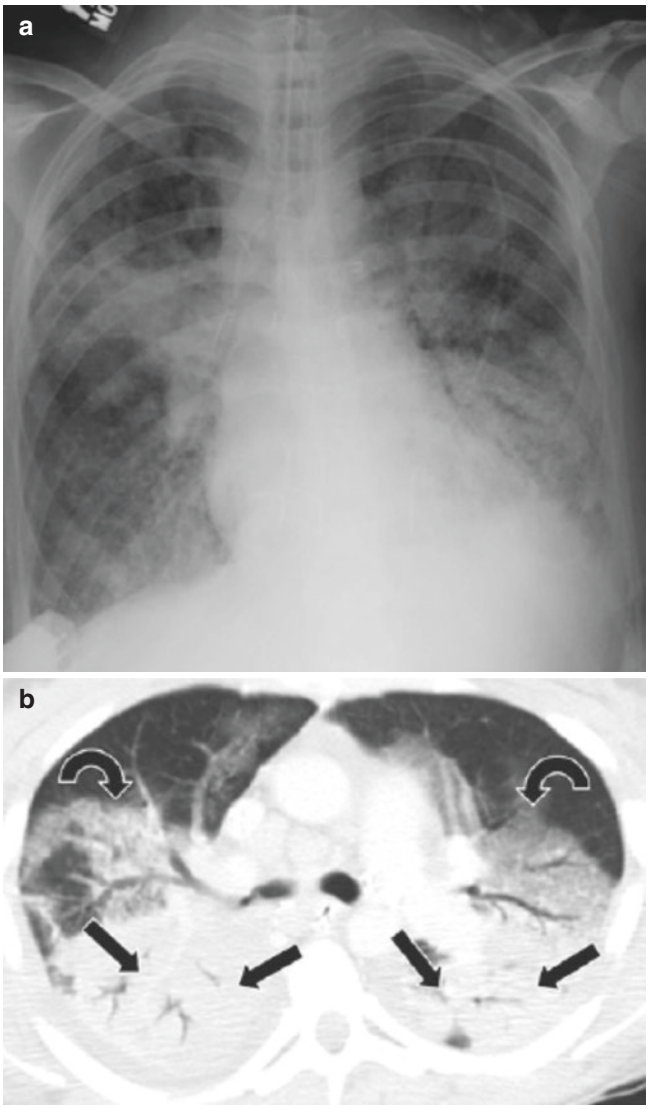

Fig. 19.6 A 17-year-old girl with bilateral lung transplantation for cystic fibrosis who presents with fever and elevated white blood cell counts. *Staphylococcus aureus* pneumonia was confirmed on bronchoalveolar lavage. (**a**) Chest radiograph shows multifocal air-space consolidations in both lungs. (**b**) Axial lung window CT image demonstrates ground-glass opacifications (*curved arrows*) and air-space consolidations (*straight arrows*) in both lungs. Also noted are several air bronchograms within the consolidated portions of lungs

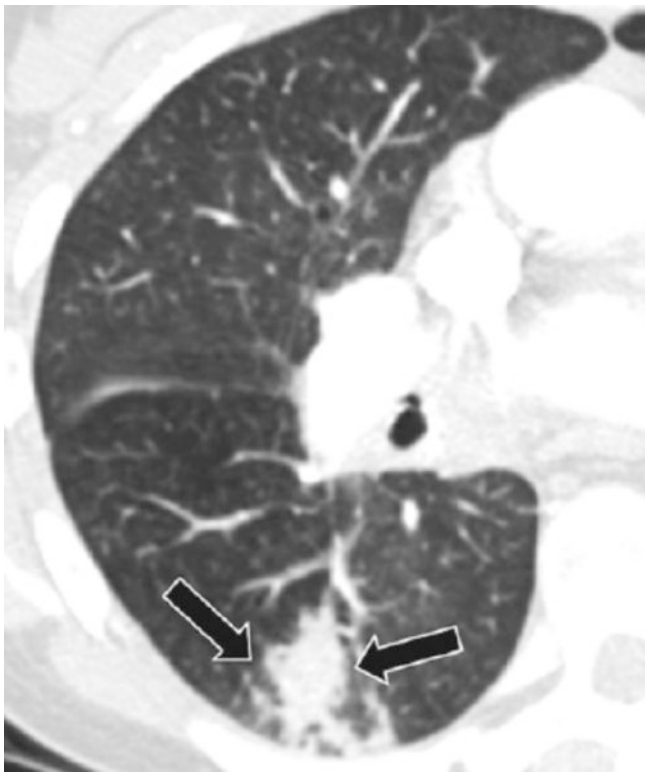

Fig. 19.7 A 15-year-old girl with bilateral lung transplantation for cystic fibrosis. Axial CT lung window image shows nodular air-space opacity (*arrows*), which was found to be aspergillous infection

infections are most frequent within the first month, but in pediatric patients, this is one of the more common complications of morbidity and mortality. The common bacterial pathogens which affect children with lung transplantation include *Enterobacter*, *Pseudomonas*, and *Streptococcus pneumoniae* [5]. Radiologic presentation may include lobar or multifocal infiltrates, consolidation, ground-glass opacities, cavitation, or lung nodules (Fig. 19.6) [5]. Rarely, pulmonary or mediastinal abscess can be also seen. Fungal infections, which can occur within the first few postoperative weeks or as late as several years after transplantation, are less common, although there is a higher mortality associated with invasive fungal infections. *Candida albicans* and *Aspergillus* are the two most common causes of fungal infection in children with lung transplantation [5]. Radiographic findings may include consolidation, ground-glass or cavitary opacities, and ill-defined nodules. CT typically shows nodular air-space disease, cavitary lesions, and mediastinal adenopathy (Fig. 19.7) [5].

Viral infections are also a frequent complication in the pediatric transplant population [7]. Cytomegalovirus (CMV) pneumonitis and respiratory viral infection are the most common viral infections in children with lung transplantation, followed in frequency by herpes simplex and Epstein–Barr virus infections. CMV infection previously was a common cause of pneumonia in the posttransplant period and highest incidence in donor (+)/recipient (−) CMV exposure in lung transplant patients. With the use of CMV prophylaxis in patients that are donor or recipient (+), CMV pneumonia is much less frequent. CXR may show diffuse parenchymal haziness or reticulonodular interstitial opacities, and CT scan may show ground-glass attenuation, interlobular septal thickening, micronodules, or consolidation [5]. Diagnosis of CMV infection can be definitively made when CMV inclusion bodies are detected within pneumocytes microscopically.

Posttransplant lymphoproliferative disorder (PTLD) typically occurs within the first year after transplantation [8]. However, it can also manifest months to years posttransplantation. In the majority of patients, it is associated with EBV infection/reactivation and is thought to be secondary to B-cell proliferation although there are EBV negative cases and even reports of T-cell abnormalities. PTLD can vary from polyclonal lymphoid proliferation to aggressive high-grade lymphoma. Early detection of PTLD is paramount because most cases of PTLD are reversible with reduction of the immunosuppressants. The incidence in pediatric lung transplant recipients is ~15% and most commonly seen as solitary or multiple pulmonary nodules or masses in addition to often necrotic mediastinal lymphadenopathy (Fig. 19.8) [9]. However, it also occurs in extrapulmonary sites especially of the head and neck region as well as abdomen and pelvis with a relatively high rate (34%) of abdominal involvement by PTLD in children with allograft lung transplantation [8].

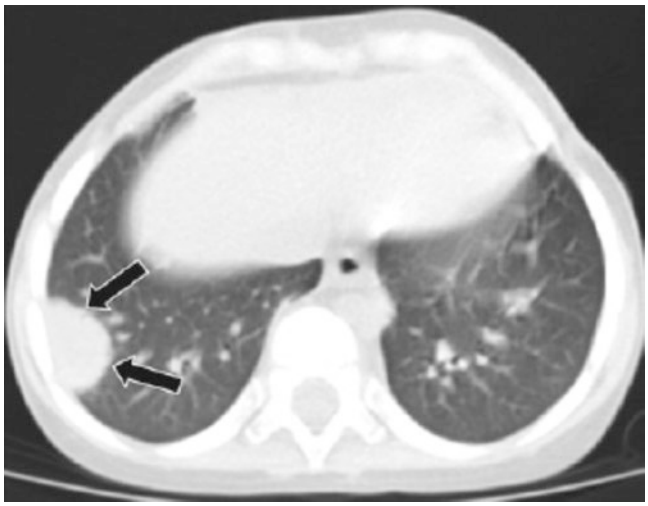

Fig. 19.8 A 6-year-old boy who is status post-bilateral lung transplant approximately 8 months ago. Follow-up chest radiographs showed an opacity in the right lung base, and CT was subsequently obtained for confirmation and further characterization. Axial lung window CT image showed round pleural-based mass (*arrows*) located in the right lower lobe. Biopsy of this mass confirmed posttransplant lymphoproliferative disorder

Bronchiolitis obliterans (BO) is the major limitation for long-term survival and a frequent complication in both adult and pediatric patients. It is a histologic diagnosis, although transbronchial biopsy is not a very sensitive study and frequently misses the diagnosis since it is initially a heterogeneous lesion. The clinical correlate is bronchiolitis obliterans syndrome which is an unexplained drop in lung function after infection, ACR, and airway complications have been excluded. Early in the course, the CXR may be normal and later may show attenuated vessels, bronchial cuffing, subsegmental atelectasis, and irregular linear opacities. CT scan is a more sensitive imaging modality showing mosaic attenuation, bronchial dilatation, and bronchial wall thickening, and the most sensitive study may be with the addition of an expiratory CT showing air trapping (Fig. 19.9) [10]. It has been reported that the sensitivity of inspiratory CT for enabling diagnosis of BO was 71%; the specificity, 78%; the positive predictive value, 62%; and the negative predictive value, 84% [11]. By contrast, the sensitivity of expiratory CT for enabling diagnosis of BO was 100%; the specificity, 71%; the positive predictive value, 64%; and the negative predictive value, 100% [10]. Furthermore, it has been shown that expiratory CT scores correlated more strongly with pulmonary function test-based scores than did inspiratory CT scores in children diagnosed with BO after lung transplantation [11].

Imaging study plays an important role in managing all phases of the pediatric lung transplant patient. It is useful in defining the severity of the disease process of the lung trans-

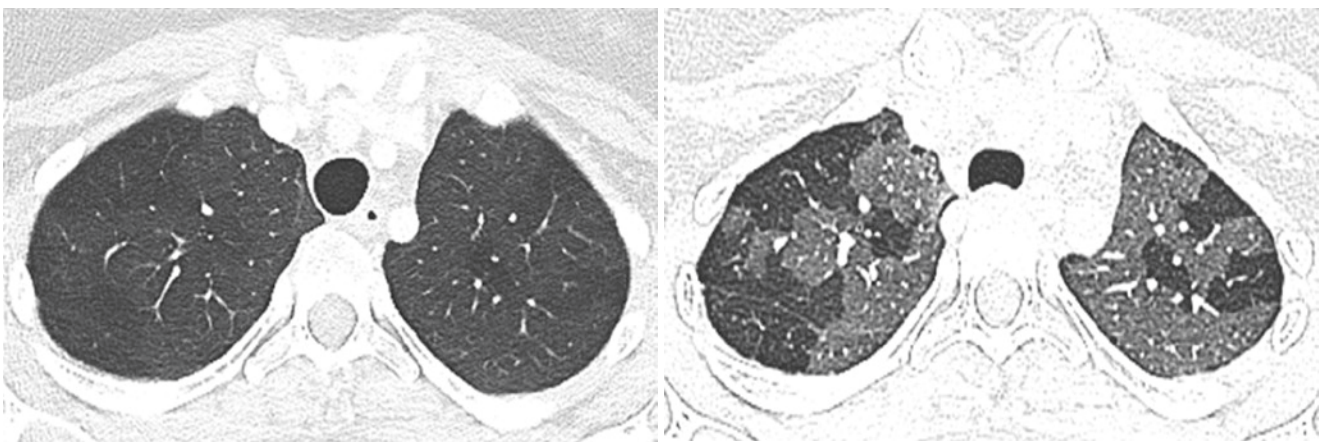

Fig. 19.9 A 17-year-old girl who is status post-bilateral lung transplant 2 years ago and presented with worsening shortness of breath. Axial lung window CT image obtained at end-inspiration (left) shows relatively normal attenuation of well-aerated lungs. However, axial lung window CT image obtained at end-expiration (right) demonstrates substantial underlying air-trapping consistent with bronchiolitis obliterans

Table 19.3 Lung transplant imaging protocol

Prelung transplant imaging evaluation
Plain chest radiographs (PA and lateral views)
CT angiogram (with 2D and 3D reconstruction of airway and vascular structures)
Postlung transplant imaging evaluation
Plain chest radiographs (AP view of the chest)—every day during hospitalization
Plain chest radiographs (PA and lateral views)—on the day of discharge from the hospital
Plain chest radiographs (PA and lateral views)—1 month F/U clinic visit
CT angiogram (with 2D and 3D reconstruction of airway and vascular structures)—1 month F/U clinic visit
Chest CT with expiratory cuts—3 month F/U and 6 month F/U clinic visit
Chest CT with expiratory cuts—yearly F/U

PA posteroanterior, *CT* computed tomography, *D* dimensional, *AP* anterioposterior, *F/U* follow-up

plant candidate, assessing donor quality and size, and in monitoring the postlung transplant process. Our program has established protocols for both the evaluation and posttransplant monitoring as outlined in Table 19.3.

References

1. Goldfarb SB, Levvey BJ, Cherikh WS, Chambers DC, Khush K, Kucheryavaya AY, et al. Registry of the International Society for Heart and Lung Transplantation: eleventh official pediatric lung and heart/lung transplantation report–2017. J Heart Lung Transplant. 2017;36(10):1070–9.
2. Zander DS, Baz MA, Visner GA, Staples ED, Donnelly WH, Faro A, et al. Analysis of early deaths after isolated lung transplantation. Chest. 2001;120:225–32.
3. Christie JD, Carby M, Bag R, Corris P, Hertz M, Weill D. Report of the ISHLT working group on primary lung graft dysfunction part II: definition. A consensus statement of the International Society for Heart and Lung Transplantation. J Heart Lung Transplant. 2005;24:1454–9.
4. Prekker ME, Nath DS, Walker AR, Johnson AC, Hertz MI, Herrington CS, et al. Validation of the proposed International Society for Heart and Lung Transplantation grading system for primary graft dysfunction after lung transplantation. J Heart Lung Transplant. 2006;25:371–8.
5. Medina LS, Siegel MJ. CT of complications in pediatric lung transplantation. Radiographics. 1994;14:1341–9.
6. Choong CK, Sweet SC, Zoole JB, Guthrie TJ, Mendeloff EN, Haddad FJ, et al. Bronchial airway anastomotic complications after pediatric lung transplantation: incidence, cause, management, and outcome. J Thorac Cardiovasc Surg. 2006;131:198–203.
7. Liu M, Wortey S, Arrigain S, Aurora P, Ballmann M, et al. Respiratory viral infections within one year after pediatric lung transplant. Transpl Infect Dis. 2009;11(4):304–12.
8. Siegel MJ, Lee EY, Sweet SC, Hildebolt C. CT of posttransplantation lymphoproliferative disorder in pediatric recipients of lung allograft. AJR Am J Roentgenol. 2003;181:1125–31.
9. Boyle GJ, Michaels MG, Webber SA, Knisely AS, Kurland G, Cipriani LA, et al. Posttransplantation lymphoproliferative disorders in pediatric thoracic organ recipients. J Pediatr. 1997;131:309–13.
10. Lau DM, Siegel MJ, Hildebolt CF, Cohen AH. Bronchiolitis obliterans syndrome: thin-section CT diagnosis of obstructive changes in infants and young children after lung transplantation. Radiology. 1998;208:783–8.
11. Siegel MJ, Bhalla S, Gutierrez FR, Hildebolt C, Sweet S. Postlung transplantation bronchiolitis obliterans syndrome: usefulness of expiratory thin-section CT for diagnosis. Radiology. 2001;220:455–62.

Pediatric Percutaneous Chest Intervention

20

Frédéric Thomas-Chaussé, Mohammad Amarneh, Ashraf Thabet, and Raymond Liu

The development and advancement of interventional tools and image guidance has allowed for expansion of the use of percutaneous interventions in pediatric thoracic disorders. In this chapter, we discuss the main thoracic pathologies for which percutaneous interventional procedures offer a safe, minimally invasive therapeutic alternative. Integration of interventional procedures into the management of many of these disorders has become the standard of care at many institutions and a key component of a successful, interdisciplinary treatment plan.

Pre-intervention Evaluation

A thorough review of the patient's chart is necessary to obtain information such as allergies, prior interventions, and current medical status. A standard laboratory work-up is obtained including INR (sometimes referred to as prothrombin time), platelets, and aPTT (activated partial thromboplastin time). Consensus guidelines for periprocedural management of coagulation status and hemostatic risk have been published [1, 2] for the adult population and may be carefully applied to the pediatric population, yet the final decision on the appropriate coagulation values must be tailored to each individual patient's clinical situation. Table 20.1 summarizes the recommendations (adapted from [1, 2]).

Considering that most procedures will require either moderate sedation or general anesthesia, obtaining an anesthesia evaluation and ensuring the patient has adequate NPO status is recommended. Less invasive procedures, often performed in older patients, may be performed with local anesthesia.

Whether the procedure is performed at the bedside, dedicated interventional radiology suite, or hybrid operating room, standard monitoring for the patient is required and should include at least oxygen saturation, heart rate, and ECG. Ensuring adequate temperature control is paramount as children lose body heat rapidly. Depending on the procedure, antibiotic prophylaxis can be considered. A summary of the most recent guidelines published by the Society of Interventional Radiology (SIR) is summarized in Table 20.2 [3]. This table summarizes the recommendations pertinent to chest interventions.

Also, considering that the procedure will be image-guided (i.e., fluoroscopy, CT), it is important to respect the ALARA principle [4]. As such, imaging guidance with ultrasound is employed whenever possible given the lack of ionizing radiation.

Once the procedure is complete, the patient is usually observed on bed rest from 1 to 4 hours depending on the procedure. Vital signs are typically monitored every 15 minutes for the first hour, every 30 minutes for another 1 hour, and then every 60 minutes for 2 hours. The patient can then either be sent back to the unit or discharged home.

Pneumothorax

A pneumothorax refers to the presence of air or gas in the pleural cavity (Fig. 20.1a). It may be spontaneous or secondary to a wide variety of etiologies. Most of the spontaneous pneumothorax are caused by the rupture of an apical bleb. The secondary causes include pneumonia,bronchopleural fistula and chest trauma. Tension pneumothorax refers to progressive

F. Thomas-Chaussé (✉)
Department of Radiology, Radiation Oncology and Nuclear Medicine, University of Montreal, CHU Sainte-Justine, Montréal, QC, Canada
e-mail: frederic.thomas-chausse@umontreal.ca

M. Amarneh
Department of Pediatric and Interventional Radiology, University of Iowa Carver College of Medicine, Iowa City, IA, USA

A. Thabet
Department of Interventional Radiology, Massachusetts General Hospital, Harvard Medical School, Boston, MA, USA

R. Liu
Department of Radiology, Massachusetts General Hospital, Boston, MA, USA

R. H. Cleveland, E. Y. Lee (eds.), *Imaging in Pediatric Pulmonology*, https://doi.org/10.1007/978-3-030-23979-4_20

Table 20.1 Periprocedural management of coagulation parameters in chest interventions

Category	Category 1 (low bleeding risk)	Category 2 (moderate bleeding risk)	Category 3 (significant bleeding risk/ bleeding difficult to detect)
Procedure	Thoracentesis Abscess aspiration, drainage, and/or biopsy (remaining extra-thoracic)	Biopsy (lung or mediastinum) Angiography (arterial intervention with access size up to 7Fr) Abscess aspiration, drainage, and/or biopsy (intra-thoracic)	Radiofrequency ablation
Test	INR: recommended aPTT: recommended Platelet count: not routinely recommended	INR: recommended aPTT: recommended Platelet count: recommended	INR: recommended aPTT: recommended Platelet count: recommended
Threshold	INR: correct to <2.0 Platelets: if <50,000/ml recommend transfusion aPTT: no consensus	INR: correct to <1.5 Platelets: if <50,000/ml recommend transfusion aPTT: no consensus	INR: correct to <1.5 Platelets: if <50,000/ml recommend transfusion aPTT: correct so that value is <1.5 control

Table 20.2 Society of Interventional Radiology (SIR) recommendations for antibiotic prophylaxis in chest interventions

Procedure	Recommendation
Thoracentesis/tube thoracostomy	No antibiotic prophylaxis recommended
Percutaneous abscess drainage (empyema)	If a patient is not on antibiotics, antibiotic initiation is recommended
Percutaneous biopsy	No antibiotic prophylaxis recommended (liver biopsy in the setting of biliary dilatation may be an exception)
Angiography	Prophylactic antibiotics targeted to skin flora could be considered
Vascular malformation treatment	Prophylactic antibiotics are not routinely administered. However, if the lesion is in a dirty or contaminated location (i.e., oropharynx), antibiotic prophylaxis is usually recommended

accumulation of air under pressure in the pleural space resulting in serious cardiopulmonary compromise. Regardless of the etiology, a symptomatic pneumothorax can be effectively drained with a chest tube.

Indications

There are several therapeutic options for managing a pneumothorax including observation, oxygen therapy, thoracentesis, image-guided tube thoracostomy, or open thoracostomy. The type of therapy employed depends on the severity of the symptoms, the degree of lung collapse, and the presence of underlying lung disease. A small pneumothorax, not infrequently seen post-lung biopsy, typically resolves spontaneously. A tension pneumothorax requires immediate decompression and placement of chest tube.

Technique: Tube Thoracostomy

Tube thoracostomy (or chest tube placement) in pediatric patients is often performed under sedation or general anesthesia. Fluoroscopy is used for treating a pneumothorax, while sonographic guidance is used for treating a fluid collection in the pleural space and, at times, computed tomography (CT) for loculated pleural collections or small refractory pneumothorax. In selected patients, chest tubes can be inserted using local anesthesia.

Standard pre-interventional evaluation as described in section "Pre-intervention Evaluation" is performed. The site and size of drainage catheter are determined before the procedure, guided by the imaging findings and clinical situation. Typically, an 8–12 Fr drainage catheter is sufficient to treat a pneumothorax.

A fluoroscopic examination in a supine position is initially performed, and an entry site is chosen and marked. Under sterile conditions, local anesthetic agent (e.g., buffered 1% lidocaine) is administered to the skin and chest wall. A small dermatotomy is made with a scalpel. Under collimated fluoroscopic guidance, a needle (e.g., 5 Fr Yueh) attached to an empty syringe is advanced above the rib and through the intercostal space into the pleural space while gentle aspiration is applied with the syringe. Once air is withdrawn into the syringe, a guide wire is advanced through the needle into the pleural space. Over the wire, the tract is dilated sequentially to the desired diameter. A pigtail drainage catheter is placed over the wire under fluoroscopic guidance and its pigtail is formed (Fig. 20.1b). The catheter is appropriately secured to the skin and connected to continuous underwater seal suction device (e.g., Atrium or Pleurovac drainage system) at −20 cm water.

Post-procedure Management

The patient is usually observed in a post-procedure recovery room on bed rest for 2–4 hours and is typically transferred to the medical floor or ICU. The drainage catheter may be connected to continuous suction at −20 cm of water. After the patient is discharged from the recovery room, the drainage catheter is flushed with 5 to 15 ml of

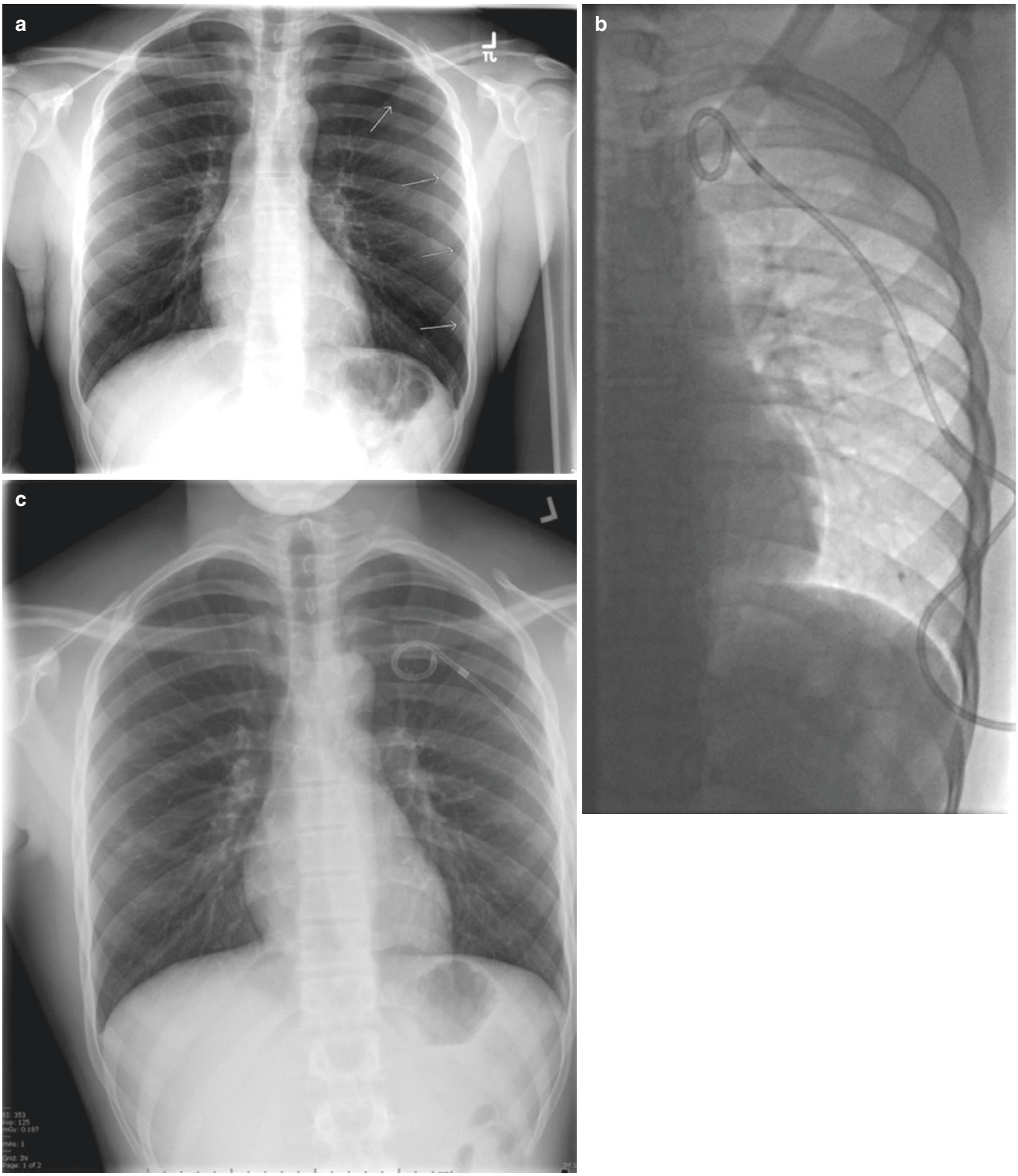

Fig. 20.1 A 17-year-old patient presented to the ED with acute onset of shortness of breath. A chest X-ray revealed a moderate left pneumothorax (**a**). The patient was brought to the IR suite, and an 8 Fr pigtail catheter was inserted under fluoroscopic guidance using only local anesthesia (**b**). After a 24-hour water seal test, the pneumothorax had resolved completely (**c**) and the chest tube was removed at the bedside

sterile saline solution twice per day and monitored for air leakage. When air is no longer aspirated, the drainage catheter is switched to underwater seal drainage, and a chest radiograph is obtained. The drainage catheter may be removed unless there is a recurrent pneumothorax that occurs while on underwater seal for 24 hours.

Results and Complications

When there is no longer evidence of an air leak, the tube is switched from suction to water seal. The chest tube is then removed if chest radiograph confirms no recurrence of pneumothorax. For patient with spontaneous pneumothorax, further evaluation is recommended in order to identify an underlying etiology [5].

Removal of Chest Tube

A chest radiograph should be taken and assessed before removing the chest tube, to confirm the expansion of the lung (Fig. 20.1c). The chest tube can be removed at the patient's bedside, typically without any sedation.

The operator should cut the hub of the pigtail drainage catheter in order to release the locking loop prior to removing the catheter. When the catheter is removed, the patient is asked to hold breath at maximum inspiration, if possible, to avoid inadvertent aspiration of air into the pleural cavity. Gentle pressure should be applied immediately to the skin insertion site upon removal of chest tube, which then is sterilely dressed. A chest radiograph is typically obtained after removal of chest tube.

Pleural Effusion: Hydrothorax, Empyema, Hemothorax, Chylothorax, and Malignant Pleural Effusion

A pleural effusion refers to the presence of a fluid collection in the pleural space (Fig. 20.2a). Among the many causes of pleural effusion, bacterial pneumonia is still the most common culprit. It can be divided into two main types: transudate or exudate based on several biochemical and physical characters of the fluid (Tables 20.3 and 20.4).

Hydrothorax (transudative, non-inflammatory fluid) is often associated with an accumulation of fluid in the peritoneal cavity or in the subcutaneous tissues, caused mostly by cardiac, renal, or hepatic diseases. An exudate typically results from a local aggressive, inflammatory etiology, has a specific gravity of >1.020, and contains more cells and proteins than a transudate.

Table 20.3 Various causes of transudate and exudate

Transudate	Exudate
Congestive heart failure	Hemothorax
Cirrhosis	Lung infection
Nephritic syndrome	Neoplasm
Iatrogenic hydrothorax (central catheters, VP shunts)	Chylothorax
Pulmonary embolism	
Peritoneal dialysis	
Pericardial disease	
Collagen vascular disease	

Table 20.4 Characteristic laboratory findings of transudative and exudative fluids

Fluid type	Transudate	Exudate
Specific gravity	<1.020	>1.020
pH	>7.2	<7.2
Protein: pleural/serum	<0.5	≥0.5
LDH (IU)	<200	>200
LDH: pleural/serum	<0.6	>0.6
Amylase: pleural/serum	<1	>1
Glucose (mg/dl)	>40	<40
RBC	<5000	>5000
WBC	<1000 (monos)	>10,000 (polys)

Thoracentesis can elucidate the type of effusion, thereby directing treatment to the underlying etiology. Large compressive effusions with symptoms should be drained to provide symptomatic relief.

Thoracentesis and Tube Thoracostomy (see section "Technique: Tube Thoracostomy" for Technique)

Sonographic guidance is typically the preferred imaging guidance technique for thoracentesis and tube thoracostomy for pleural effusions (Fig. 20.2a, b). An adjuvant fluoroscopic guidance can also be used, though it is difficult to differentiate between fluid and consolidated or collapsed lung tissue on fluoroscopy. A pigtail drainage catheter is the most frequently used. Larger pigtail catheters are preferred for thick, exudative fluids. Continuous drainage of the effusion is aided by treatment of the primary etiology (e.g., intravenous antibiotics).

Empyema

Empyema refers to the presence of pus in the pleural space. Three stages of empyema formation are classically described:

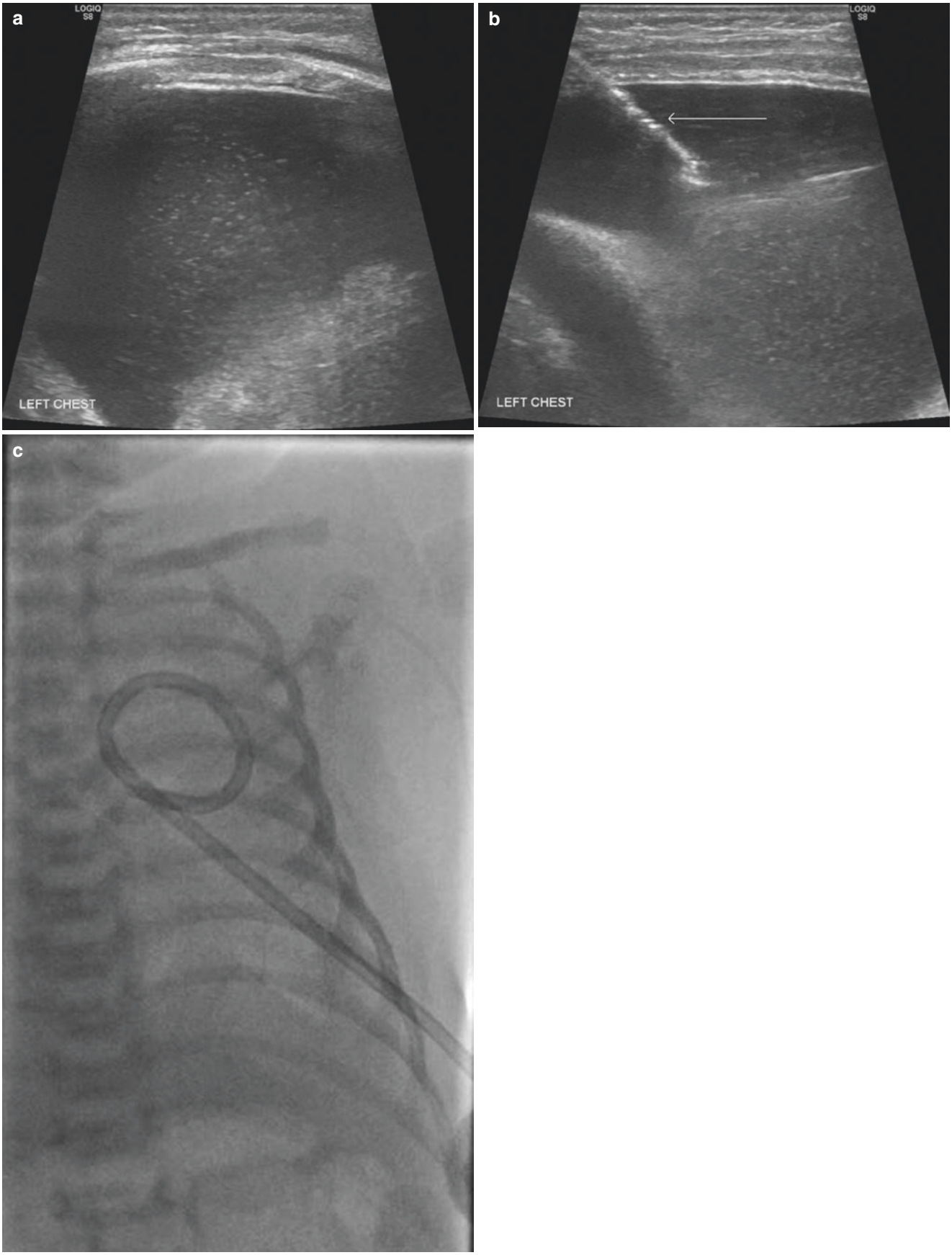

Fig. 20.2 A 20-day-old patient with a left-sided congenital chylothorax. Initial ultrasound evaluation revealed a small to moderate effusion minimally complex effusion (**a**). Under ultrasound guidance, a 5 Fr Yueh access needle was inserted (**b**) to allow for the placement of an 8 Fr pigtail drainage catheter (**c**)

- *Exudative*: Accumulation of free-flowing protein-rich fluid with rapidly increasing neutrophils. Glucose and pH levels are normal.
- *Fibropurulent*: The viscosity of the pleural fluid increases the appearance of pus and coating of the pleural membrane with an adhesive meshwork of fibrin. Glucose and pH levels are lower than normal. Fluid loculation may be seen.
- *Organizing*: Fluid loculation and formation of fibrous inelastic membrane (pleural peel) encasing the lung occur [6].

If untreated, an empyema in the last stage could spontaneously drain into the lung through a bronchopleural fistula or out through the chest wall (empyema necessitans).

Multi-loculated collections are often seen in empyemas in the fibropurulent and organizing stages. Treatment options include tube thoracostomy with or without the instillation of fibrinolytics, video-assisted thoracoscopic surgery (VATS), or open thoracotomy and decortication. Fibrinolytic agents can be used to optimize the drainage of loculated pleural collections [7].

Fibrinolytic Therapy for Empyema

Empyema is associated with fibrinous, hemorrhagic, and suppurative processes, leading to fibrous organization, adhesions, and fibrous pleural thickening. The rationale to instill fibrinolytic agents (such as tissue plasminogen activator (t-PA), streptokinase, or urokinase) into the pleural cavity is based on the idea that these agents break down fibrinous tissues, thereby promoting drainage.

The fibrinolytic agent can be infused via the chest tube into the pleural space. There are several formulas to prepare the fibrinolytic solution. Examples are:

1. t-PA (2–6 mg in a 50–250 ml of normal saline, depending on the size of the effusion)
2. Streptokinase (250,000 units in 100 ml normal saline once per day for 1–3 days)
3. Urokinase (80,000 units every 8 hours for 1–3 days)

After instillation, the chest tube is closed for 1–2 hours to allow the fibrinolytic agent to spread throughout the pleural space. After 1–2 hours, the tube is then opened for drainage.

Results of fibrinolytic therapy in children have demonstrated high success rates (as high as 99%) [8]. Although retrospective studies showed efficacious results of these agents, only urokinase has been evaluated in a randomized controlled trial in children, and more controlled randomized studies are needed [8].

Hemothorax

Hemothorax (blood in the pleural space) in children is often associated with chest trauma and surgical procedures. It may occur from erosion of a blood vessel associated with inflammatory processes in the lungs or rarely from rupture of a pulmonary arteriovenous malformation. Thoracentesis is the gold standard to make a diagnosis of hemothorax.

Chylothorax

A chylothorax refers to chyle (milky lymph rich in fat and nutrients absorbed from the intestines) in the pleural space. In children, it is usually a sequela of injury of the thoracic duct during cardiothoracic surgery with a reported incidence of 0.89–6.6% [9, 10] or can be congenital [11]. Chylothorax may also occur due to malformation of the central conducting lymphatic channels. Management of chylothorax is challenging which may require progressive escalation of therapy if it is not resolving [12, 13]. If suspected, thoracentesis should be performed to confirm the presence of chylous fluid in the thoracic cavity. Conservative treatment includes low-fat, high-protein diets with medium chain triglycerides supplemented with fat-soluble vitamins A, D, E, and K, total parenteral nutrition, or somatostatins. Spontaneous recovery has been reported in infants less than 1 year old [14]. Thoracentesis or tube thoracostomy may be required in case of significant respiratory distress or persistent chylous effusions. Repeated drainage of large volumes of chyle can lead to protein loss, lymphopenia, hypogammaglobulinemia, and abnormal lymphocyte function [13]. Iatrogenic chylothorax refractory to medical therapy may require alternate interventions such as pleurodesis, a pleuroperitoneal shunt, embolization, or surgical ligation of the thoracic duct.

Malignant Effusion

Management of malignant pleural effusions in pediatric oncology patients is not well established. Respiratory benefit from pleurodesis using doxycycline for terminal pediatric oncology patients with malignant effusions has been reported [15] and so is the use of an indwelling tunneled catheter [16].

Pleurodesis

Pleurodesis refers to obliteration of the pleural space by administration of sclerosing agents via a chest tube. The resulting fibrosis and adhesion prevent the accumulation of fluid or air between the pleural layers. It can be performed to treat persistent or recurrent pneumothoraces or pleural effusions. In pediatric oncology patients, the use of pleurodesis should be preceded by a multidisciplinary discussion as the long-term effect of pleurodesis on lung development is still unclear. The procedure can be quite painful and typically performed under general anesthesia.

Technique

Prior to chemical pleurodesis, a large chest tube has already been placed. In cases of pleural effusions, the fluid in the pleural space should be aspirated via the indwelling drainage catheter as much as possible. Next, a sclerosing agent is injected into the pleural space via the chest tube. A specimen of the pleural fluid should be obtained to confirm or exclude evidence of malignancy.

The chest tube can be removed when the pleural drainage is persistently minimal. Several sclerosing agents can be used, including talc, doxycycline, and bleomycin.

Removal of Chest Tube

See section "Removal of Chest Tube."

Bronchopleural Fistula

A bronchopleural fistula (BPF) refers to an abnormal communication between the bronchial tree and the pleural space. The most common cause by far is a postoperative complication following a pulmonary resection. The reported incidence is between 1.5% and 28% after pulmonary resection [17–20]. Other recognized etiologies include lung necrosis complicating a pulmonary infection, spontaneous pneumothorax, and chemotherapy or radiotherapy for lung cancer and tuberculosis [17]. A BPF is a rare entity that carries a high morbidity and mortality. Therapeutic options include various medical, surgical, and now gaining more acceptance, endoscopic procedures to deliver various embolic agents to occlude the fistulous communication. However, there are only a few reports describing bronchoscopic or fluoroscopically guided embolization of a BPF in pediatric patients. Therefore, various procedures should be considered as complementary and treatment should be individualized.

Indications

The location and size of the BPF will guide whether surgery or an endoscopic procedure is performed. Bronchoscopic or fluoroscopically guided embolization has typically been performed on the patients who are too high risk for surgery. A distal small fistula is more suitable for bronchoscopic or fluoroscopic therapy, while a large or central fistula is best managed with surgery or bronchoscopic stent placement.

Technique

Patients with a bronchopleural fistula typically have a pneumothorax, with or without pleural effusion (usually empyema). The presence of bronchopleural fistula can be suspected when air leakage is prolonged via a chest tube for more than 4 days. CT scan, instillation of nontoxic dye (e.g., methylene blue), bronchography, and inhalation of 133 Xe gas may also be used to identify the fistula.

The American College of Chest Physicians recommendations for the management of patients with persistent pneumothorax is helpful for further management: continue observation for 4 days. If an air leak persists longer than 4 days, intervention may be considered. Thoracoscopy is the preferred management procedure. If surgery is contraindicated, bronchoscopy intervention with pleurodesis can be considered [21].The use of several sealing or sclerosing agents has been reported including lead shots, ethanol, polyethylene glycol, cyanoacrylate glue [22], fibrin glue, blood clot, antibiotics, albumin-glutaraldehyde tissue adhesive, cellulose, gel foam, coils, balloon catheter occlusion, silver nitrate, and even muscle flap transfer [23]. Successful embolization of BPF under fluoroscopic guidance using a microcatheter has also been reported.

Post-procedural evaluation includes observation of air leakage via the chest tube and serial chest radiographs.

Local Tumor Therapy: Thermal Ablation

Thermal ablative therapy is a minimal invasive technique used to treat focal tumors, either through hyperthermic injury—radiofrequency (RF), microwave (MW), and laser ablation—or through hypothermic injury, cryoablation. Radiofrequency ablation (RFA) has been the most commonly used thermal ablative therapy, but microwave and cryoablation are becoming more commonly used. RFA was initially established as an effective therapy to treat primary and metastatic malignancies of the liver; then, it was rapidly used to treat focal tumors in other organs. The liver and the lung are the most common sites for metastases. Following the initial experience by Dupuy et al. in 2000, there have been several studies demonstrating the effectiveness of RFA in treating primary and metastatic malignancies in the lung [24]. One such large study demonstrated that it has low morbidity, negligible mortality, and improved quality of life [25, 26]. A recent review (2017) by Mouli et al. concludes that "numerous studies have reported safety and efficacy for the treatment of both primary and metastatic disease of the lungs in select patients" [27].

In children, primary lung malignancies are rare, accounting for only 0.19% of all pediatric malignancies. However, metastatic pulmonary tumors are approximately 12 times more common than primary lung cancer [28]. Several studies report survival benefit in excision of osteosarcoma pulmonary metastases [28–31]. Metastasectomy can play a role in other tumors resistant to chemotherapy and radiotherapy such as adrenocortical carcinoma and chondrosarcoma.

The use of RFA in children is not a novel therapy as it is commonly used to treat cardiac conduction abnormalities and osteoid osteomas. While RFA and other thermal ablation modalities performed in adults can be potentially extended to children, the currently available experience is limited. Some small series have been published demonstrating that RFA ablation can be used with success to treat lung metastases of osteosarcoma with satisfying results [32, 33]. The use of thermal ablation in interventional oncology has significantly increased in the last few years. In addition to primary and secondary lung lesions, cryoablation has been shown to be effective in controlling pain related to osseous metastases without any relevant side effects and with a decreased use of opioids [34]. In the chest, cryoablation has been used to treat sternal metastasis [35] and as an option for pain control after surgery for pectus excavatum (Nuss procedure) [36].

Airway Obstruction

In both adults and children, airway obstruction causes significant morbidity and mortality. However, the underlying etiologies are quite different. In adults, malignant causes predominate, while in children, airway obstructions are attributed mainly to benign stenoses or malacia [37, 38]. In general, tracheobronchomalacia occurring in infancy has a good long-term prognosis as most resolve at about 18 months–24 months of age [39].

Management of airway obstruction in children is challenging due to the small and soft airways and the required long-term tolerance and adaption to growth [38]. Treatment options include surgical and endoscopic procedures; operative management is the first-line therapy for treating congenital abnormalities of the airway including cardiac anomalies causing airway narrowing [39].

However, there is a cohort of patients that may benefit from balloon dilatation or stenting of airway stenoses. There have been several reports describing the role of endoscopic procedures, such as balloon tracheobronchoplasty and airway stenting, in treating airway obstruction in children [38–45].

Indications

Balloon tracheobronchoplasty refers to balloon dilatation of an airway narrowing with an angioplasty balloon under bronchoscopic or fluoroscopic guidance. A stent refers to an artificial hollow structure inserted into tracheobronchial tree with the goal to maintain airway patency.

Treatment is guided by the location and etiology of the airway narrowing. Children with focal malacia, unlike diffuse disease, will benefit from the surgical intervention or even external airway splint. Diffuse malacia usually respond to long-term CPAP delivered via a tracheostomy [46].

Balloon dilatation is often used to treat recurrent stenoses following surgery or airway stenting [39]. In cases of resistant stenoses, the use of cutting balloons may decrease the rate of re-stenosis [47].

The types of airway stents available are plastic (silicon or silastic), metallic (balloon-expandable or self-expanding), and bioabsorbable stents. The main indications for airway stenting in children are recurrent stenoses after surgery and/or stenoses that do not respond to balloon dilatation. In addition, stents have been used to treat incompletely surgically treated focal malacia and extrinsic compression, not correctable by surgery. Stents should only be considered when conservative and surgical options have been exhausted. In children with malignant disease or severe congenital anomalies, stents may be used with palliative intent to improve quality of life [38, 39].

Results and Complications

There have been no randomized trials evaluating balloon dilatation or airway stenting in children, but the success rates in pediatric patients have been reported in several case series. Analysis of published case series demonstrated the calculated initial success rate of 92.6% (112 patients among 121) and mortality rate of 11.6% (14 patients among 121). Most of these 121 children were in critical situation before stent placement and had no other therapeutic choices.

Complications during balloon dilatation and airway stenting are uncommon. Minor complications seen are migration and tissue granulation formation. Major complications reported to date include death from bleeding, erosion into aorta, stent fracture, erosion into adjacent tissues, and mucous retention. Lethal complications have been reported with an estimated mortality from these case series of 12.9% [38].

Percutaneous Needle Biopsy of Pulmonary and Mediastinal Lesions

Management of pulmonary, mediastinal, pleural, and chest wall lesions are similar to adults. In the past, particularly in children, surgeons obtained tissue through open or transthoracic procedures but, more recently, through video-assisted thoracoscopic biopsies (VATS). Less invasive methods such as image-guided percutaneous or transbronchial approaches have gained favor due to the decreased procedural morbidity. The safety and efficacy of percutaneous image-guided biopsy in children have been reported in the literature [48–56]. The various methods used to obtain tissue should be considered

complementary with preference for more minimally invasive procedures.

Indications [48, 51, 57]

- Focal pulmonary lesion or multiple pulmonary focal opacities [55]
- Focal infectious lung lesion, particularly when bronchoscopy is unsuccessful [51]
- Mediastinal masses or lymphadenopathy
- Focal or diffuse pleural thickening
- Chest wall masses or fluid collections
- Staging of tumors (lung cancer and extra-thoracic malignancy)
- Needle localization for small pulmonary lesions [54, 56]

Suitability for transbronchial versus percutaneous biopsy depends on the size and location of the lesion. Central lesions adjacent to major bronchi may be more amenable to a transbronchial approach. However, the size of the airway in children may preclude a transbronchial biopsy. Imaging modalities used to guide percutaneous biopsies include computed tomography (CT), ultrasonography, and fluoroscopy.

Contraindications [57]

Similar to the adult population, contraindications to biopsy may include:

- Severe underlying pulmonary disease
- Contralateral pneumonectomy or severely limited function in the contralateral lung
- Patients on positive pressure ventilation
- Abnormal coagulation parameters
- Pulmonary arterial hypertension that are at higher risk of hemorrhage

Technique

Pre-procedural imaging studies including chest radiographs and contrast-enhanced chest CT scan should be reviewed to determine the safest approach—transbronchial versus image-guided percutaneous biopsy. Standard pre-intervention evaluation should be done (see section "Pre-intervention Evaluation"). One important point is that general anesthesia should be administered when respiratory control is required to stabilize the lesion during the biopsy [48, 52]. In selected cooperative children, biopsies may be performed with local anesthesia, especially for superficial lesions in the chest wall, large peripheral lung, or mediastinal lesions.

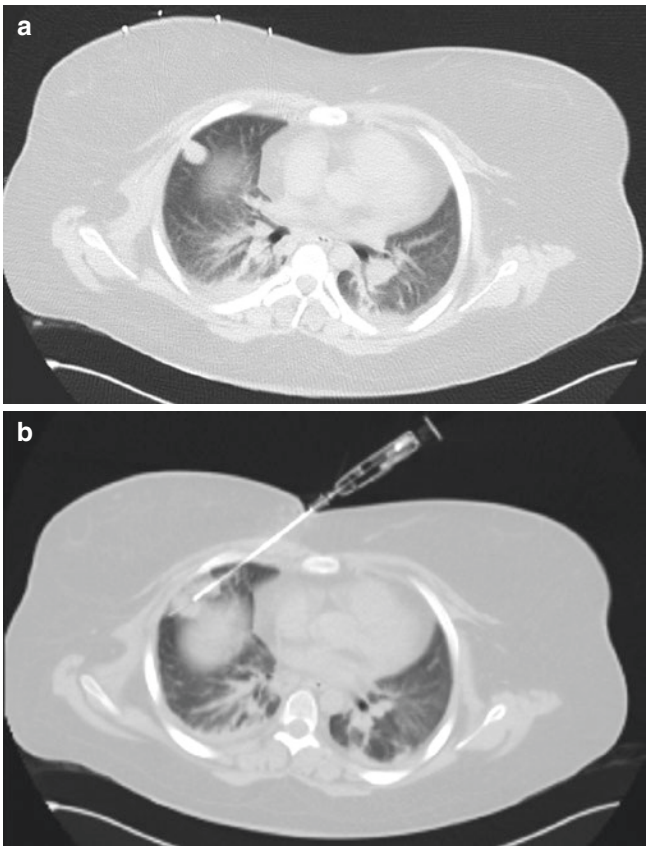

Fig. 20.3 A 17-year-old female with a biopsy-proven Ewing sarcoma of the sacrum (not shown) and a suspicious pulmonary nodule. (**a**) A 19–20 gauge coaxial technique was used to biopsy the nodule under CT guidance (**b**). Pathology confirmed a metastasis of the Ewing sarcoma

For deeper lung lesions with intervening aerated tissue, CT guidance is the most often used imaging modality. It clearly delineates structures to avoid during the biopsy such as lung tissue, fissures, large vessels, bullae, and vital cardiovascular structures (Fig. 20.3). Ultrasound guidance may be suitable for chest wall, pleural, superior mediastinal, and peripheral lung lesions [50]. Fluoroscopy can be used if the lesion can be visualized in two projections. The main advantage of fluoroscopic and ultrasound guidance is real-time imaging and less radiation exposure. The most direct route to the lesion should be used. Avoiding traversing other structures such as pulmonary vessels, fissures, and major bronchi decreases the risk of complications.

The patient is positioned prone or supine. The lesion is reimaged for proper localization. For CT guidance, a radiopaque skin marker can be placed over the area of interest, and thin axial sections are obtained through the lesion and skin marker. The appropriate lesion, size, depth, safest trajectory, and skin entry site are determined. After a sterile preparation and applying local anesthetics, the biopsy needle is advanced incrementally to its predetermined position. The position of the needle is confirmed with CT imaging before a biopsy is

taken. A coaxial biopsy system is used if multiple biopsies are to be taken. Temporary suspension of breathing is valuable for lesions that move with respiration. The lung is then reimaged after needle placement and following the biopsy. An occlusive patch can be placed over the puncture site [48].

The sample type (needle aspiration or core biopsy) is often dictated by the type, size, and location of the lesion.

Samples are obtained using either an aspiration or core biopsy needle via a single-needle (Chiba, Franseen, or Westcott needle), coaxial needle, or tandem needle technique. A coaxial needle system is most commonly employed and can be used to obtain multiple samples using a single pleural puncture. Core samples are usually obtained from 18–20 gauge core biopsy needles, but a large bore needle, such as 14 gauge needle, has been shown to be safe and effective in children [53].

Large pleural-based lesions or parenchymal lesions with no intervening aerated lung can be biopsied with a large bore needle with direct puncture. A single pass technique is recommended for parenchymal lesions with intervening aerated lung, with or without the formation of a saline window [48]. A 1 cm throw should be used for small <2 cm lesion and a 2 cm throw for >2 cm lesions. For smaller lesion, <1 cm, wire localization can assist a thoracoscopic resection of small pulmonary nodules in children [54, 56].

Postoperative Management

An immediate post-biopsy scan is typically obtained to evaluate for a pneumothorax. Standard postoperative monitoring should be done (see section "Pre-intervention Evaluation") with special attention to signs of pneumothorax and hemothorax. As previously discussed (see section "Post-procedure Management"), a small, stable pneumothorax in an asymptomatic patient may not need any treatment. However, drainage should be performed if the child develops a large (or enlarging) pneumothorax or symptoms (dyspnea or chest pain). The rare tension pneumothorax requires immediate needle decompression followed by chest tube placement under image guidance.

Results and Complications

The safety and efficacy of percutaneous lung biopsy in children have been reported only in retrospective case series of small numbers of patients. Diagnostic yields of CT-guided or US-guided percutaneous lung biopsy in children have been reported between 85% and 95% [48, 50–55]. Percutaneous biopsies are less time-consuming and less invasive, require shorter post-procedural stay, and are less costly than transthoracic procedures [49].

The most common complication is pneumothorax (12–30%) and hemoptysis (4%). The risk is higher in small (<2 cm) and deep lesions [58]. Significant pneumothoraxes requiring treatment usually occur within 1 hour after the biopsy. Fungal lesions seem to have a higher incidence of hemorrhage spontaneously and at time of biopsy [48]. Fatal pericardial tamponade, tension pneumothorax, air embolism, and pulmonary hemorrhage have been reported in the literature, but the risk is quite low.

Pulmonary Angiography and Hemodynamic Assessment in Children

Recent advances in noninvasive CT and MR pulmonary angiography have made the need for invasive diagnostic pulmonary angiography less frequent. However, conventional pulmonary angiography is still considered the definitive test in evaluating some of the diseases involving the pulmonary vasculature. In addition, invasive pulmonary angiography allows for hemodynamic measurements and therapeutic intervention.

Indications

In pediatric patients, similar to adult patients, recognized indications for pulmonary angiography include [57]:

- Evaluation of pulmonary hypertension [59]
- Evaluation and treatment of pulmonary arteriovenous malformations (PAVM) [60]
- Evaluation of cardiopulmonary disorders pre- or post-cardiac surgery
- Assessment and intervention for congenital cardiac anomalies
- Pre-retrieval foreign body in pulmonary arterial tree
- Evaluation of clinically suspected pulmonary embolism or foreign body
- Evaluation of massive hemoptysis and hemothorax, especially with a negative bronchoscopy

Acute pulmonary embolism is uncommon in pediatric patients. Despite recent advances in CT imaging of the pulmonary artery vasculature, in selected cases, pulmonary angiography can still be considered a gold standard to evaluate patients with suspected pulmonary embolism.

In many children, pulmonary angiograms are performed under general anesthesia in order to minimize the effect of respiratory and cardiac motion on the digitally subtracted images. Prolonged breath-holding needed for diagnostic quality images is often not possible in infants and small children, especially if they have underlying cardiopulmonary

disease. Recently, jet ventilation techniques have been utilized in these cases to obtain high-quality images in pulmonary angiography without the need for breath-holds.

Relative Contraindications [57]

- Coexisting severe pulmonary hypertension. Echocardiography may be helpful.
- Left bundle branch block on a 12-lead electrocardiogram (ECG). Placement of a temporary transvenous pacing catheter will prevent complete heart block that may occur due to catheter-induced right bundle branch block.
- Ventricular irritability.
- Other concomitant life-threatening illness (e.g., decompensated congestive heart failure).
- Severe contrast allergy.

Preoperative Management

Standard pre-evaluation protocols should be performed (see section "Pre-intervention Evaluation"), and renal function should be evaluated. The patient's ECG and echocardiography studies should be evaluated prior to pulmonary angiography to exclude a left bundle branch block. A temporary prophylactic pacemaker can be inserted before the catheter is introduced into the right atrium and ventricle for the patients with a left bundle branch block.

Technique

Procedures are usually performed under general anesthesia with continuous cardiac monitoring. Evaluation of the pulmonary vasculature requires venous access with the femoral vein being most frequently used. Alternate access includes the jugular veins.

Pressure measurements are performed with simultaneous tracing of the ECG prior to contrast injections. The commonly recorded pressures are those of the central veins, right atrium, right ventricle, pulmonary artery, and pulmonary capillary wedge pressure. The latter typically requires a Swan-Ganz catheter. Continuous ECG monitoring should be performed while introducing a catheter into the right atrium and, subsequently, the right ventricle.

Different types of catheters can be used to select the main pulmonary artery. A pigtail or angled-tip catheter is advanced into the main pulmonary artery under fluoroscopic guidance. Larger special catheters (such as 6 Fr modified Grollman catheter) can also be utilized while less likely to be needed in smaller children. A tip deflecting wire inserted into any catheter can help the operator advance into the right atrium, through the right ventricle, and into the main pulmonary artery. The catheter will typically show a preference for the left main pulmonary artery, and a 0.035″ Glidewire may be needed to negotiate into the right main pulmonary artery. Digital subtraction angiography is performed with breath-holding. Nonionic low osmolality contrast agents are used.

Pulmonary arteriography should be performed with extreme caution in patients with pulmonary AVM and pulmonary hypertension. Meticulous technique is required to remove air bubbles from all injections to prevent paradoxical emboli.

Results and Complications

There has been no evaluation of the safety and efficacy of pulmonary angiography in children. The reported mortality of pulmonary angiography is between 0.1% and 0.5% [61, 62]. Retrospective studies have shown that mortality due to acute cor pulmonale was associated with severely elevated pulmonary artery and right ventricular end-diastolic pressures [62, 63]. Nonfatal major and minor complications are 1% and 5%, respectively. They include right ventricular perforation (1%), significant arrhythmia (0.8%), contrast reaction (0.8%), and renal dysfunction (1%) [61–63]. Paradoxical emboli can be the cause of embolic stroke and require careful technique to avoid.

Pulmonary Artery Embolization and Pulmonary Arteriovenous Malformations

Pulmonary arteriovenous malformations (PAVMs) refer to an abnormal direct communication between a pulmonary artery and vein resulting in a high-flow right-to-left shunt and with subsequent symptoms of hypoxemia, cyanosis, dyspnea, platypnea, or orthodeoxia. The lack of a capillary plexus can result in paradoxical embolization with neurological complications such as stroke or cerebral abscess [64]. AVMs may also result in serious hemoptysis or hemothorax due to spontaneous rupture, although this represents a less common occurrence. Patients may have symptoms of dizziness, syncope, or polycythemia and may eventually develop symptoms of congestive heart failure and/or respiratory failure [65].

Idiopathic congenital PAVMs are congenital pulmonary AVMs that are not associated with hereditary hemorrhagic telangiectasia (HHT). These PAVMs tend to be single with fewer associated physical findings. However, approximately 70% of PAVMs are associated with HHT, and 15–30% of individuals with HHT have a PAVM [64–66]. PAVMs may be acquired due to trauma, occurring in patients with hepato-

pulmonary syndrome—47% patients with end-stage liver disease acquire abnormal arterial venous communications—or following surgery for congenital cyanotic heart disease such as a Glenn or modified Fontan procedures.

Hereditary Hemorrhagic Telangiectasia

Hereditary hemorrhagic telangiectasia, also known as Osler-Weber-Rendu syndrome, is an autosomal dominant disorder manifested by mucocutaneous telangiectasias and arteriovenous malformations that can affect the nasopharynx, CNS, lung, liver, and spleen, including the urinary and GI tracts. Majority of patients, up to 90%, manifest by the fourth decade of life with epistaxis being the most frequent clinical manifestation. HHT is diagnosed clinically based on the Curaçao criteria, established in 2000 by the HHT Foundation's Scientific Advisory Board (Table 20.5) [67]. Due to delayed manifestation of the typical features of HHT, the use of Curaçao criteria to establish the diagnosis of HHT in children is less reliable than in adults.

There are at least four gene defects implicated in HHT that affect the signaling of transforming growth factor beta (TGF-b), an important pathway in vascular formation and repair [65]. However, genetic abnormalities may be present in patients with PAVMs who do not have HHT. The first two genetic mutations linked to HHT were a mutation in the endoglin (ENG) protein (chromosome 9, 9q33-34) called HHT type 1 and a mutation for encoding activin receptor-like kinase (ALK1; also called ACVRL1, activin receptor-like kinase, type II), resulting in HHT type 2 [68, 69]. PAVMs are more frequently seen in patients with HHT type 1 mutation. In the last few years, two other gene mutations have been implicated—HHT type 3, a mutation of chromosome 5 (5q31.1-32), and HHT-juvenile polyposis overlap syndrome (JPHT), a mutation in SMAD4 of chromosome 18 (part of a TGF-beta signaling pathway). JHPT is autosomal dominant with clinical features of HHT and juvenile polyposis [70, 71].

The vast majority of PAVMs are simple (single feeding pulmonary branch and single draining vein), located in the lower lobes, and have a fusiform aneurysm with an immediate draining vein. Around one fifth of PAVMs are complex (two or more feeding arteries or draining veins). The size of the PAVMs may vary from microscopic to the typical size of 1–5 cm [60]. Multiple lesions occur in more than one third of the patients and bilateral disease in one half.

Table 20.5 *Curacao criteria*: diagnosis is classified as definite if at least three criteria are present, possible or suspected if two criteria are present, and unlikely if fewer than two criteria are present [67]

Criterion	Description
Epistaxis	Spontaneous, recurrent nosebleeds
Telangiectases	Multiple at characteristic sites such as the lips, oral cavity, fingers, and nose
Visceral lesions	Such as gastrointestinal (GI) telangiectasia (with or without bleeding), pulmonary, hepatic, cerebral or spinal AVM
Family history	A first-degree relative with HHT

Indications

Several retrospective series have demonstrated the severe disabling and life-threatening complications of PAVMs, such as stroke, TIA, cerebral abscess, massive hemoptysis, and spontaneous hemothorax [60, 72–74]. These complications have also been reported in the pediatric literature [60, 74, 75]. Rationale for treatment is to prevent any potential complications, especially in cases of diffuse PAVMs [76]. Likewise, screening of asymptomatic patients including children and family members with PAVM or HHT should be performed to determine individuals requiring treatment.

Treatment should commence if there is evidence of:

- History of paradoxical embolization
- Signs and symptoms: hypoxemia, dyspnea, fatigue, poor growth, etc.
- The presence of large or enlarging feeding artery [74–77].

Historically, feeding arteries with a minimum size of >3 mm were considered an indication for treatment, to prevent future potential paradoxical embolizations.

Noteworthy, the standard recommendation for embolotherapy for PAVMs with feeding artery >3 mm may not be relevant in children with multiple small symptomatic PAVMs. For asymptomatic children, the decision to treat smaller shunts should be made on a case-by-case basis [75].

Transarterial catheter-directed embolization, rather than lung resection, is the preferred choice for treating PAVMs, especially in patients with multiple or bilateral PAVMs. The safety and efficacy of embolization have been demonstrated in several large series in adults and one series in children [73, 74, 77–79]. Diagnostic angiography and embolization should be performed on the same day in children.

Of note, since patients with pulmonary AVMs are at higher risk of brain abscess due to the pulmonary right-to-left shunt, lifelong prophylactic antibiotic treatment is advised [75].

Technique

General anesthesia is preferred to intravenous sedation for children as it allows for better quality digital subtraction images during pulmonary angiography (controlled breath-

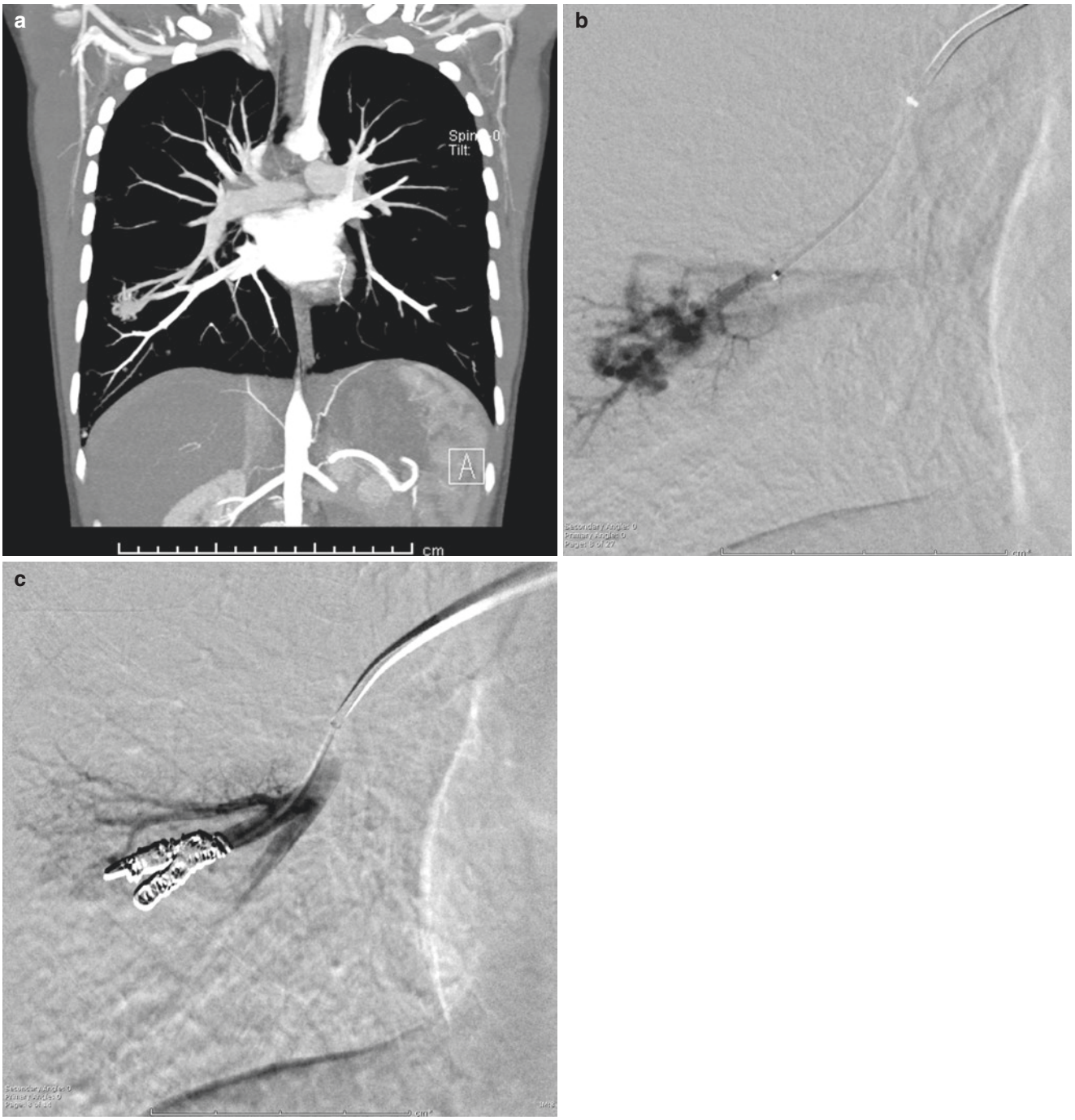

Fig. 20.4 A 12-year-old male with a history of hereditary hemorrhagic telangiectasia (HHT) and multiple pulmonary arteriovenous malformations. The patient is symptomatic with epistaxis, exercise intolerance, and hypoxia (**a**). CT angiogram MIP demonstrated the largest PAVM in the right lower lobe (**b**). Selective pulmonary arterial angiogram demonstrated a complex PAVM with multiple small arterial feeders and draining veins (**c**). The lesion was embolized with multiple coils

holds) and for continuous monitoring for potentially protracted procedures. As mentioned, jet ventilation techniques have also been utilized recently to acquire high-quality images, without the need for breath-holds.

Imaging studies (chest radiograph, contrast-enhanced CT studies, and prior pulmonary angiograms) are reviewed (Fig. 20.4a). The use of air filters for all vascular access is essential.

Diagnostic pulmonary angiography as previously described is performed. Pulmonary hemodynamic measurements and angiography via a femoral vein route are initially performed. Selective pulmonary angiography helps illustrate the feeding

artery and determine the size of the embolic tools needed for complete permanent occlusion. (Fig. 20.4b, c). Typically, a triaxial system is utilized, with a larger (6 Fr) sheath placed in the right/left main pulmonary artery for stability. A coaxial system with an angled diagnostic catheter (5 Fr) combined with a microcatheter (3 Fr) helps achieve distal access, as close as possible to the nidus of the pulmonary AVM.

The choice of embolic agents is often operator dependent. The most important element in choosing the correct embolic agent is local control, so that the embolic material does not become the source of paradoxical emboli. For this reason, detachable coils and plugs have evolved to be an embolic device of choice in treating pulmonary AVMs.

Embolization should be performed as close to the malformation nidus as possible, without placement of embolic materials within the actual nidus itself. Embolization of the actual nidus, rather than the feeding artery, increases the risk of paradoxical emboli with the embolic material. The distal segment of the feeding artery is selectively cannulated, and embolic material is placed to avoid obliteration of normal branches or venous aneurysm. For smaller shunts, the use of microcatheters facilitates the procedure. This is especially important in multiple complex PAVMs in symptomatic children. Techniques such as anchoring, scaffolding, or balloon-assisted embolization can help prevent coil paradoxical embolization, especially in large PAVMs [60]. Post-embolization angiography is subsequently performed to confirm the occlusion of the feeding arteries.

Postoperative Management

The patient is observed in the recovery room as previously described (see section "Pre-intervention Evaluation"). The patient should be monitored for hemorrhage, vascular disruption due to balloon dilatation, chest pain due to pulmonary infarction, and arterial or venous obstruction due to thrombosis or vasospasm. Typically, pulmonary AVM treatment can be considered an outpatient procedure, and recovery observation can be less than 4 hours.

Follow-up assessment in pediatric patients is not standardized. A follow-up CTA scan is often obtained within 1–3 months for evaluation of procedure success. CTA is used to detect reperfusion, as evidenced by non-involution of aneurysmal sac/fistulous communication. Transthoracic contrast echocardiography has been shown to not be useful post-embolization, given that it remains positive in approximately 90% of post-embolization [80]. Follow-up patients with small untreated PAVMs or with suspected microscopic PAVMs should be determined on a case-by-case basis (approximately every 1–5 years) with CTA [75]. If recanalization is suspected, pulmonary angiography and additional treatments should be performed.

Results and Complications

Several case series have shown transarterial catheter-directed embolization to be efficacious and safe with complications being rare in long-term follow-up [73, 77–79]. Faughnan et al. reviewed several case series and demonstrated high rates of PAVM involution (85–97%) and improved oxygen saturation. In the longitudinal period, reperfusion was seen in 15% of treated PAVMs and growth of small PAVMS in up to 18% [75]. Recurrences occurred due to incompletely occluded arteries or accessory arteries, reflecting the need to embolize as close to the nidus as possible. Recurrent lesions can be treated with re-embolization. There have been a few case reports and case series of PAVM embolization in pediatric populations. Faughnan et al. evaluated transarterial catheter-directed embolization in 42 pediatric patients (aged 4–18 years) with 172 PAVMs—71% with focal and 21% with diffuse PAVMs. There was improved oxygen saturation and absence of complications noted in 100% and 83% of patients, respectively [74]. A recent series by Tau et al. [81] compared the use of detachable Amplatzer plugs to coils for PAVM embolization. A total of 37 PAVM were embolized with Amplatzer plug and 21 PAVM with coils with a median follow-up time of 7.7 years (range 1.4–18.9). Recanalization was detected in seven vessels, all treated with coils, and there were no cases of recanalization in the vessels occluded with Amplatzer plug ($p = 0.0413$).

There is little experience with embolization of PAVMs in children under the age of 4 years.

Potential complications of blood vessel rupture, tachyarrhythmias, bradyarrhythmias, and nontarget vascular occlusion have been reported but are uncommon. Likewise, long-term complications were rare. The most common complication was self-limiting pleuritic chest pain, observed in up to 12% of patients. Also reported was paradoxical air embolization in up to 5% of patients and paradoxical device embolization, in less than 1 to 4%. Complication rates in children were similar to adults [74].

Acute Pulmonary Embolism

Acute pulmonary embolism (PE) is uncommon in the pediatric population. The exact incidence is unknown, but pediatric autopsy studies have estimated an incidence of 0.73–4.2% [82, 83]. According to data from the National Hospital Discharge Survey published in 2004, the incidence of PE was 0.9/100,000 children/year [84].

Children may be protected from thromboembolism due to decreased capacity to generate thrombin, increased capacity of alpha-2 macroglobulin to inhibit thrombin, and enhanced antithrombotic potential by the vessel wall [85, 86]. Despite

this, pulmonary embolism can be potentially life-threatening when it occurs.

Multiple etiologic and risk factors have been implicated in the pathogenesis of pulmonary embolism—burns, central venous line and catheters, deep vein thrombosis, dehydration, heart disease, hematologic disorders, immunosuppression, neoplasia, obesity, renal disease, sepsis, shock, stem cell transplantation, surgery, thrombophilia/hypercoagulable, trauma, or vascular malformation (such as Klippel-Trenaunay syndrome) [87]. However, the most important acquired risk factor in children is central venous lines [88]. With advances in pediatric care, the incidence of pulmonary embolism is likely to increase.

Clinical presentation is variable depending on the degree of pulmonary artery occlusion, amount of liberated vasoactive amines, and underlying cardiopulmonary studies of the child [87]. Pulmonary embolism is often silent in children with dyspnea and tachycardia being less common reflecting the better physiologic reserve in children. With a large degree of pulmonary artery obstruction, clinical symptoms and signs may be similar to adults. Although not validated in children, diagnostic algorithms for the evaluation of pulmonary embolism are similar to adults.

Treatment of Acute Pulmonary Embolism

Large clinical trials evaluating the safety and efficacy of thrombolysis for acute PE in children have not been done. Therefore, children are treated according to recommendations based on small pediatric studies and clinical trials in the adult population [89].

Treatment should be guided by the risk associated with pulmonary embolism in the setting of other comorbid conditions. Treatment options for children with pulmonary embolism include supportive care, anticoagulant therapy with heparin or low molecular weight heparin and warfarin, systemic thrombolysis, IVC filtration, and surgical or interventional thrombolysis [87]. Anticoagulation therapy should be considered in patients with stable hemodynamics in order to prevent thrombus extension and development of late complications. However, hemodynamically unstable patients, such as those in shock, need more aggressive therapy to reduce thrombus burden to improve right ventricular function [89]. More aggressive therapy includes thrombolysis or thrombectomy.

Systemic or catheter-directed pharmacologic thrombolysis can be considered in cases of massive or submassive (acute pulmonary embolism without systemic hypotension but with either right ventricular dysfunction or myocardial necrosis) pulmonary embolism or thrombus not responding to anticoagulants; however, the latter is less often used. In addition, surgical or interventional thrombectomy/thrombolysis may be considered. There are several catheter-directed thrombectomy techniques: aspiration thrombectomy, fragmentation thrombectomy, and rheolytic thrombectomy [90, 91]. Effective fragmentation and rheolytic thrombectomy have been reported in infants and children [91–95]. Combined thromacute pulmonary embolism without systemic hypotension but with either right ventricular dysfunction or myocardial necrosis bolysis and thrombectomy technique have been reported. It involves fragmentation of central thrombus and dislodging of the fragments to the periphery resulting in relative gain of non-obstructed cross-sectional artery area and increased surface area of the thrombus fragments accessible for thrombolysis [89, 91]. The decision to treat pulmonary embolism with catheter-directed thrombolysis should be made by a multidisciplinary team familiar with the treatment alternatives and risks.

Contraindications to pharmacologic thrombolysis include active bleeding, history of internal or intracranial bleeding, recent intracranial or intraspinal surgery or trauma, intracranial neoplasm, arteriovenous malformation (AVM) or aneurysm, known coagulation disorders, or severe, uncontrolled hypertension. Many of these contraindications are relative, and the potential risk of treatment should be evaluated with respect to the risk of not treating the thrombosis.

Preoperative Management

There needs to be documentation of the site and extent of thrombosis with imaging modalities deemed satisfactory by the experienced interventional radiologists. The risk and time window should be assessed between the interventionalists, referring service, intensivists, and hematologists. Baseline clinical and laboratory documentation is required, which includes complete blood cell counts and disseminated intravascular coagulopathy (DIC) panel (including fibrinogen and D-dimer) and kidney and liver function tests. Clinical signs of PE must be documented. For prolonged infusion of lytic agents, the patients stay in the ICU with adequate hydration and monitoring of the vital signs, coagulation parameters, and access sites.

Technique

Appropriate informed consents with detailed discussion of the benefits and serious bleeding risk are mandatory. If indicated, an inferior vena cava (IVC) filter is placed under the same setting. Initially, venography and IVC filter placement are performed. If the patient has a lower extremity DVT, a jugular approach is preferable. Pulmonary arteriography and pressure measurements are performed before thrombolysis. A catheter is placed within the thrombus with fluoroscopic guidance.

Among thrombolytic agents, tissue plasminogen activator (tPA) is the most widely used and can be given through a pigtail catheter which is left in place for an extended period of time. Typically, tPA may be given at a weight-based dosage for approximately 12 hours, along with concurrent administration of heparin. The typical pediatric dose for tPA is 0.03–0.06 mg/kg/hr (maximum of 1 mg/hr).

Mechanical thrombectomy is an adjuvant tool in selected patients. With large residual embolus, prolonged transcatheter infusion of lytic agents can be considered. If so, the patient is transferred to the ICU and monitored per ICU protocol. Coagulation parameters are obtained as follows:

- CBC, fibrinogen, and D-dimer every 4–6 hours.
- Maintain fibrinogen >100 (neonates should maintain fibrinogen >150) and platelet count >100,000.
- Check stool for occult blood and urine dipstick with each void and for 8 hours after the infusion.

If major bleeding occurs, lytic agent and heparin must be discontinued immediately. Appropriate consults and imaging are obtained. Aminocaproic acid (Amicar®), cryoprecipitate, and packed red blood cells can be administered.

In case of moderate bleeding, i.e., bleeding without significant hemodynamic changes, the tPA and heparin doses should be lowered. Minor bleeding, i.e., oozing of blood around venous sheaths, is frequent and does not constitute an indication for treatment change. Gentle manual and/or compression dressing can be administered around the puncture site.

Often, the catheter is subsequently removed without additional imaging at the end of the tPA administration. Echocardiogram can be used to assess the degree of success in alleviating submassive or massive pulmonary embolism.

Results

Mortality rate of acute pulmonary embolism in pediatric patients is lower than that in adults. Mortality rates in children with pulmonary embolism have been reported up to 10% [89]. In adult patients, mortality of PE in the high-risk population is 65% if untreated and 10–40% when treated with catheter-directed thrombolysis.

Limited numbers of cases have been reported in pediatric patients for whom rheolytic or pharmacomechanical thrombectomy successfully removed a pulmonary thrombosis.

Complications

Complications of thrombolysis include bleeding within the lungs or GI tract or within the intracranial ventricular system. Complications of rheolytic thrombectomy include vessel perforation, particularly <6 mm, and transient bradycardia and hypotension, presumably by stretching the vessel wall, have been reported in adult patients who received pharmacomechanical thrombectomy [92].

Hemoptysis and Bronchial Artery Embolization

Hemoptysis refers to the expectoration of blood from the respiratory tract. It poses a potentially life-threatening respiratory emergency with major hemoptysis warranting prompt investigation and intervention. Conservative management of massive hemoptysis has a 50–100% mortality rate [96–98]. The most common etiology in children is tuberculosis and other chronic lung infections or cystic fibrosis. Episodes of major hemoptysis occur in 1% of all patients with cystic fibrosis, more frequently with severe lung disease and rarely seen in children less than 10 years old [99]. Other recognized potential causes of life-threatening hemoptysis in children are summarized in Table 20.6 [100].

There is no consensus for grading the severity of hemoptysis. A commonly used definition of major hemoptysis is acute large volume bleeding of greater than 240 ml/d, recurrent bleeding of substantial volume (>100 ml/d) for a few days or weeks, or chronic recurrent small-volume hemoptysis (<100 ml/d) that interferes with a person's lifestyle and/or prevents effective physical therapy [101]. The cause of death is due to asphyxiation rather than exsanguination—approximately 400 ml of blood in the alveolar space is sufficient to significantly prevent gaseous exchange [96, 97]. In children, hemoptysis tends to be mild and self-limiting. Life-threatening hemoptysis in a child can be defined as >8 ml/kg in a 24-hour period [102]. Nevertheless, the decision to intervene does not rely solely on these numbers, and the overall clinical picture must likewise be taken into consideration.

Table 20.6 Causes of life-threatening hemoptysis in children [98]

Cystic fibrosis
Inflammatory conditions
Tuberculosis
Other causes of bronchiectasis
Other infections (necrotic lung, lung abscess, fungal)
Tumors and tumorlike conditions
Congenital heart disease and pulmonary artery interruption
Iatrogenic causes
Tracheostomy and other airway surgery
Airway stenting
Lung biopsy (percutaneous, transbronchial)
Pulmonary arteriovenous malformations
Vasculitis
Foreign body aspiration

Bronchial artery embolization is now considered the initial intervention for major refractory hemoptysis, either as first line or as an adjunct to surgery. In addition, a large portion of patients are not suitable for surgery due to existing comorbidity, poor pulmonary reserve, and high mortality rates (up to 40%) following emergency surgery [103]. Bronchial artery embolization is considered a safe procedure but requires knowledge of the anatomy, pathophysiology, and procedural pitfalls in order to minimize the risks and improve the outcome.

Bronchial Artery Anatomy and Pathophysiology

The bronchial arteries have variable origins, branching patterns, and course. They typically originate between the superior margin of T5 and the inferior margin of T6 in 70–83% [104]. Non-orthotopic bronchial feeders originating outside this zone are frequent. They may originate from the aortic arch, brachiocephalic artery, subclavian artery, internal mammary artery, thyrocervical trunk, costocervical trunk, inferior phrenic artery, or abdominal aorta. These variants extend along the course of the major bronchi which distinguishes them from non-bronchial systemic arteries that do not course parallel to the major bronchi and enter the lung parenchyma through adherent pleura or pulmonary ligaments [104, 105]. Four common branching patterns have been described based on a large cadaveric study [104] (Fig. 20.5). The medullary arteries supplying the spinal cord most commonly arise from the intercostal arteries at multiple levels. The medullary arteries supply the anterior spinal artery, which supplies 80% of the anterior spinal cord. The artery of Adamkiewicz is the largest anterior medullary artery supplying the anterior spinal artery, which supplies the spinal cord from T8 to the conus medullaris. The artery of Adamkiewicz has a characteristic hairpin appearance as it joins the anterior spinal artery. The artery is most commonly a single artery with left-sided origin (80%) between T9 and T12 (74%) and less commonly between T5 and T8 (15%). It is important to recognize this artery and other spinal cord arterial supply during bronchial embolization. Inadvertent embolization of anterior spinal artery can result in cord infarction and paralysis.

There is a dual arterial supply to the lungs from the pulmonary and bronchial arteries that are connected by numerous anastomoses at the level of the bronchi and pulmonary lobules [107]. The pulmonary arteries account for 99% of the arterial supply (deoxygenated blood) and are responsible for gaseous exchange. The bronchial arteries (oxygenated blood) account for the remaining 1% and supply nutrient branches to the bronchi, vasa vasorum to the pulmonary arteries and veins, and smaller bronchopulmonary branches to the lung parenchyma [106]. There is a physiological right-to-left shunt in the anastomoses that accounts for approximately 5% of the total cardiac output [108].

Pulmonary circulation compromise, such as in hypoxic vasoconstriction or in chronic inflammation, results in bronchial arteries proliferation and enlargement to replace the pulmonary circulation. The inflammatory process causes release of angiogenic growth factors that stimulate neovascularization and recruitment of collateral vessels from the systemic circulation. These new vessels are prone to rupture into the airways as they are thin-walled and fragile and exposed to the high systemic arterial pressure or eroded by an infective process [103, 109]. While the bronchial arteries are the most common source for major hemoptysis (>90%), in a minority of cases, the pulmonary arteries (5%) or non-bronchial systemic arteries (5%) may be the source of the hemorrhage [103].

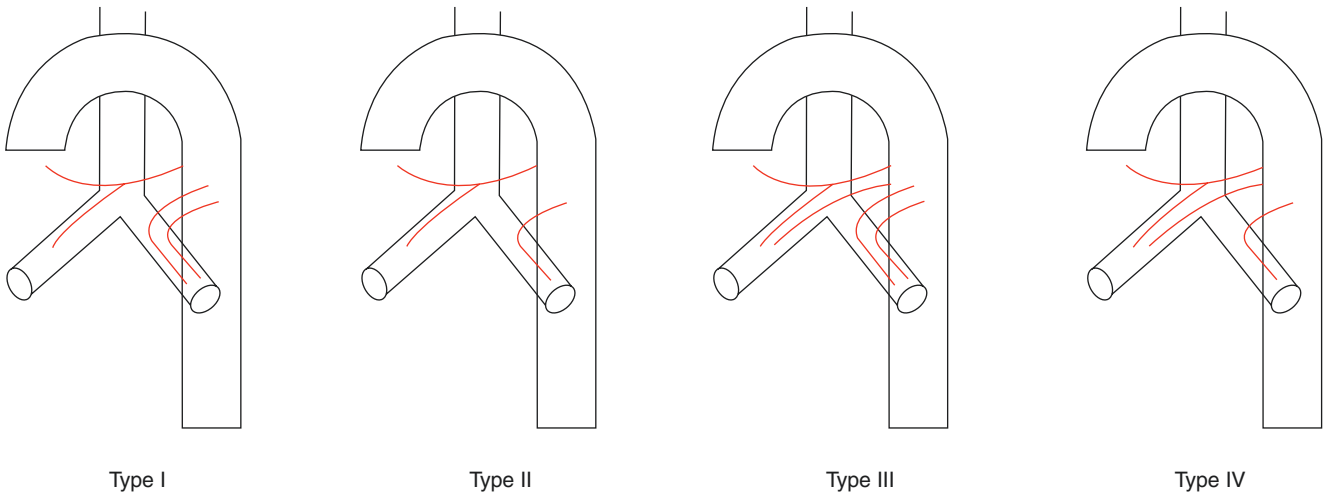

Fig. 20.5 Four main types of bronchial artery anatomy. Type I: one right bronchial artery from right bronchointercostal trunk, two left bronchial arteries (40.6%). Type II: one on the right from bronchointercostal trunk, one on the left (21.3%). Type III: two on the right (one from bronchointercostal trunk and one bronchial artery), two on the left (20.6%). Type IV: two on the right (one from bronchointercostal trunk and one bronchial artery), one on the left (9.7%) [104, 106]

Indications

In children, mild hemoptysis tends to be mild and self-limiting. Life-threatening hemoptysis in a child has been defined as >8 ml/kg volume in a 24-hour period [102].

While bleeding often stops spontaneously within a few days, other conservative treatments may control symptoms such as bed rest, intensive intravenous antibiotic treatment, vitamin K therapy, blood transfusion, and temporary discontinuation of physical therapy [100]. Pharmacologic treatment has not been proven; however, vasopressin, an intravenous octreotide infusion (a selective bronchial vasoconstrictor), or oral or intravenous tranexamic acid, an antifibrinolytic agent utilization, has been described.

In general, bronchial artery embolization is recommended when other measures have failed to control a major or life-threatening hemoptysis episode. Recurrent hemoptysis, even post-bronchial artery embolization, warrants a repeat procedure to evaluate for recanalization and bleeding from a non-bronchial artery.

Preoperative Management

Initial evaluation should be focused on identifying the source of bleeding and determining the underlying cause. Diagnostic evaluation includes sputum examination, chest radiograph, CTA scan, and bronchoscopy. A chest radiograph may lateralize the bleeding and underlying parenchymal abnormality; however, the reported diagnostic yield is only 50% [110]. Multidetector CTA has increased the localization of hemorrhage and demonstrated 100% of bronchial and 62% of non-bronchial artery hemoptysis [111]. In adults, according to the American College of Physicians, clinicians favored early bronchoscopy within the first 24 hours [112]. However, bronchoscopy detected the site of hemorrhage in only 50% of the cases and is less likely to determine the underlying cause [103, 113]. Due to the smaller airways in children, routine bronchoscopic examination prior to bronchial artery embolization is controversial. The advantage of bronchoscopy is that it may treat bleeding from larger airways with cautery, laser, topical adrenaline, or rarely an occlusion balloon in severe cases [100]. In addition, bronchoscopy may help provide diagnostic localization information for subsequent bronchial artery embolization.

Technique

General anesthesia is typically required in children. General anesthesia has the advantage of respiratory control for better imaging quality, particularly in younger children, and lengthy procedures. However, there are some concerns about the effects of intubation itself on hemoptysis and respiratory efforts in advanced lung disease. Arterial access is usually via the common femoral artery. A 5 Fr selective catheter (such as a Cobra, Sos, or Michelson) is used to evaluate the bronchial arteries, intercostal arteries, and non-bronchial arteries. When performing the angiography care must be taken to identify the artery of Adamkiewicz (also called the great anterior radiculomedullary artery) which usually originates from a left intercostal or lumbar artery (in almost 2/3 of patients) at the level of the 9th to 12th intercostal artery. It has a caracteristic « hairpin » appearance and supplies the lower one-third of the spinal cord. A microcatheter is often used to catheterize as distal as possible in the bronchial artery to ensure avoidance of nontarget embolization. Typical findings of bronchial arteries which should be targeted for embolization include marked tortuosity and evidence of small pseudoaneurysms. Frank extravasation is rarely noted in typical cases. Target bronchial arteries are generally embolized using particles, polyvinyl alcohol particles (350–500 micrometer in diameter), or Embospheres® Microspheres (300–500 micron) (Merit Medical). Liquid embolics such as nBCA or onyx have been utilized as well. Coil embolization is contraindicated, because coils in the proximal portion of the artery allow for the development of collateral flow in the distal area and make subsequent embolization difficult when the patient needs repeated endovascular occlusion for recurrent hemoptysis in the future, which is commonly encountered.

If a bleeding vessel and a spinal artery arising from bronchial arteries are identified, a microcatheter should be advanced distal to the spinal artery.

Results and Complications

Immediate success rates, defined as no bleeding within 24 hours, have been reported as high as 95% in some reports for cystic fibrosis patients with hemoptysis. However, 55% of the patients required repeated embolization during the long-term follow-up [100]. Early rebleeding can be attributed to incomplete embolization which may be due in part to the extensive underlying pulmonary disease or incomplete evaluation of non-bronchial vessels. Later rebleeding events can be attributed to recanalization of previously embolized vessels or revascularization of collateral vessels secondary to progression of the underlying pulmonary disease [37].

Several complications have been reported in the literature. Minor complications such as chest pain, fever, and dysphagia have been reported. Severe hemoptysis during a procedure is thought to be related to the positive pressure during general anesthesia; however, it may be fatal. Neurological complications have been reported. Phrenic nerve palsy has been attributed to embolization of the internal thoracic artery pericardiophrenic branch. Spinal cord ischemia has been reported to occur in <1% of bronchial artery embolization procedures, but it is often temporary, with only a small risk of permanent paraplegia [100]. Brain injury may occur because embolic agents inadvertently com-

municate to the left circulation through a shunt or aberrant communication with the vertebral arteries. Other complications that have been reported include myocardial injury, fingertip ischemia, bowel ischemia, and bronchoesophageal fistula [100]. Although severe complications of bronchial artery embolization have been reported, bronchial artery embolization, as performed by experienced interventional physicians, is a safe and effective treatment for hemoptysis.

Vascular Anomalies

Vascular malformations and tumors of the thorax are frequently encountered. These lesions can impact the development of the chest wall, spinal column, and lungs with potential impact on respiratory function. Management of children with vascular anomalies requires the interdisciplinary expertise at specialized centers.

The widely accepted classification of vascular anomalies distinguishes between two types of vascular anomalies: vascular tumors and vascular malformations [114]. Infantile hemangiomas are the prototype of the former, while vascular malformations are represented by the slow-flow (lymphatic, capillary, and venous), high-flow (arteriovenous), and combined types. In addition, some of the overgrowth syndromes with complex vascular anomalies may present with peculiar thoracic involvement. In this chapter, we will focus on the two most common malformations affecting the chest wall: venous and lymphatic malformations.

Slow-Flow Malformations

Venous Malformations

Venous malformations (VMs) are congenital vascular anomalies that result from abnormal development of venous channels. These lesions can occur anywhere in the body and can extend from the dermis to the bone, but the muscle is the most commonly involved structure. The superficial lesions are bluish and compressible and may contain palpable phleboliths. Deeper lesions of the chest wall may involve the skin, subcutaneous fat, muscles, and bones or extend into the thoracic cavity. Larger VMs of the chest wall may be associated with scoliosis. Phlebectasia refers to dilated orthotopic or accessory veins which can be associated with altered flow dynamics and thromboembolism. Central and thoracic phlebectasia in CLOVES (Congenital Lipomatous Overgrowth, Vascular malformations, Epidermal nevi, and Skeletal/Scoliosis/Spinal anomalies) syndrome is common and increases the risk of pulmonary embolism [115].

Lymphatic Malformations

Lymphatic malformations (LM) can be divided into two major types: macrocystic (identifiable fluid-containing cyst) and microcystic. In addition, a combination of both types frequently exists. Macrocystic LMs manifest as cystic masses and microcystic lesions as diffuse tissue swelling and overgrowth. LMs are prone to recurrent flare-ups due to infections and intralesional bleeding. Less common manifestations include deformity of the chest wall and cutaneous vesicles and, with the rare involvement of the conducting lymphatic channels, chylothorax, chylous reflux, and interstitial lung disease.

Thoracic involvement can be isolated or, more commonly, part of an extensive cervicofacial or axillary disease. Large cervical LMs frequently extend into the superior mediastinum via the thoracic inlet. Chest wall and mediastinal lymphatic malformations are common in CLOVES syndrome [116].

Sclerotherapy

Sclerotherapy refers to instillation of a toxic agent into an abnormal cavity with the goal of inducing intralesional fibrosis and shrinkage. Sclerotherapy has been documented in the literature as an effective primary treatment modality of lymphatic and venous malformations. MRI is superior to other imaging modalities to assess the soft tissue extension of the malformation. For VMs, the most common indications for treatment are pain and size of the lesion. Small, painless lesions can be observed though many will eventually become symptomatic. A combination of embolization, sclerotherapy, and surgical resection is often used with large lesions. Treatment, when indicated, is preferably initiated early in life.

For LMs, the major indications for treatment are size of lesion and recurrent infections. Skin vesicles may cause leakage, bleeding, and hygienic problems.

Sclerotherapy is typically performed under anesthesia with the access planned based on the imaging studies. Percutaneous access is common. Sonographic (with high-resolution probes) or fluoroscopic guidance directs the access into the malformation. Multiple needles are carefully placed within the lesion, and, for VMs, venography is performed after intralesional placement is confirmed by free blood return. Sclerosants with or without contrast opacification are then injected into the malformation. Other portions of the malformation can be treated similarly.

In treating VM, several sclerotherapy agents have been used including pure ethanol, detergents such as sodium tetradecyl sulfate (STS), and bleomycin. The choice of the sclerosing agent depends heavily on the institutional practice and the experience of the treating physician. However, the most commonly used sclerosing agent used is the STS that is most often injected into the venous malformation as a foam created by mixing the STS with air and iodine contrast or Lipiodol® (Guerbet Group); a lipid based contrast agent.

For LMs, the macrocysts are cannulated with small gauge needles, the lymphatic fluid is aspirated, and the sclerosant is

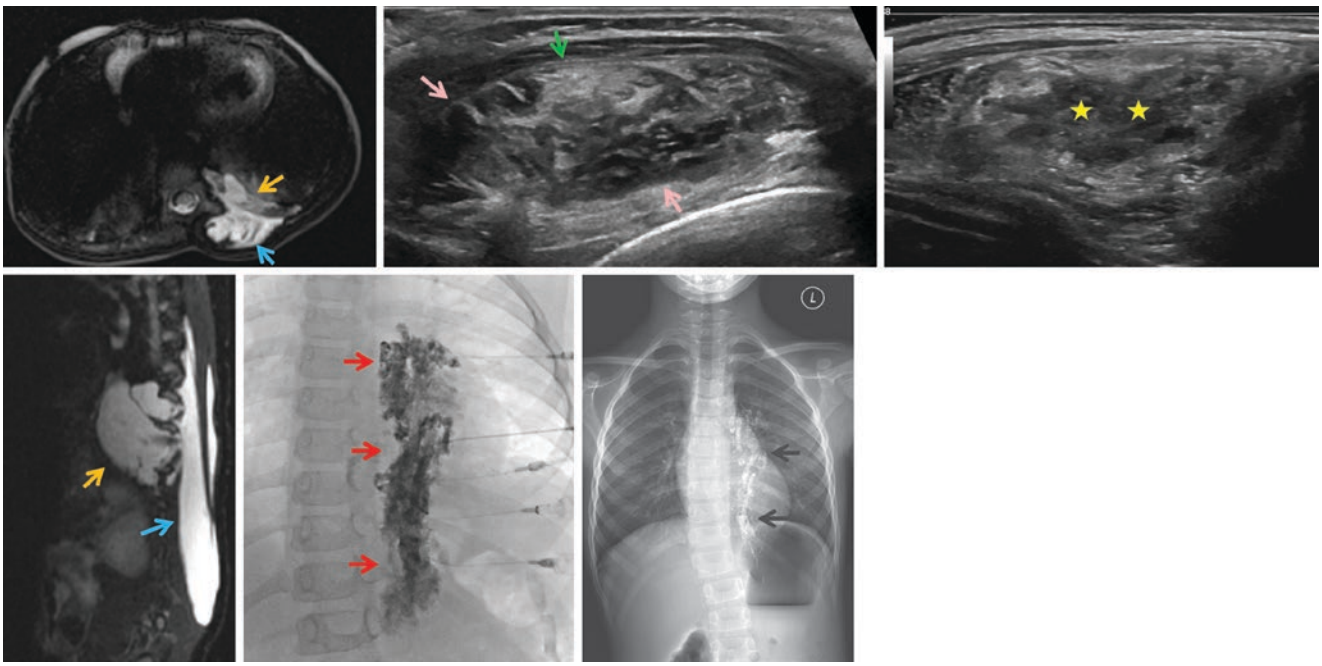

Fig. 20.6 A 6-year-old male with a history of right paraspinal intramuscular venous malformation (blue arrows) with pleural involvement (orange arrows). Ultrasound after one sclerotherapy treatment with STS (sodium tetradecyl sulfate) foam demonstrates partial closure of the superficial portion of the malformation (green arrow) and significant residual open channels (pink arrows) with multiple open channels. Glue (Histoacryl) was used to treat the deeper portions of the malformation (red arrows). Follow-up chest X-ray demonstrates the glue cast (black arrows) and scoliosis due to long-term paraspinal involvement. Six months post-treatment follow-up ultrasound demonstrates a significant decrease in size of the venous malformation and minimal residual open channels (yellow stars)

then injected. Several sclerosants have been used to treat macrocystic lymphatic malformations including pure ethanol, doxycycline, sodium tetradecyl sulfate, bleomycin, and OK32. However, the most commonly used sclerosing agent used for macrocystic lymphatic malformation is doxycycline. It is first mixed with iodine contrast (most often in a 1:1 ratio) and is injected directly into the cysts under fluoroscopic guidance after the lymphatic fluid has been aspirated. Microcystic LMs typically respond poorly to traditional sclerotherapy agents. However, intralesional bleomycin has been reported effective in treating microcystic LMs [117]. In addition to sclerotherapy, diffuse and extensive LMs may benefit from medical treatment using sirolimus (mTOR inhibitor) [118].

Post-sclerotherapy swelling is maximal within the first 24 hours after the procedure. Appropriate analgesics are used when needed. Hemoglobinuria secondary to hemolysis is a frequent complication of sclerotherapy for VMs and is managed by hydration and alkalization of urine. Clinical assessment is scheduled 2 months after the procedure (Fig. 20.6). The procedure can be repeated if the residual lesion is significant.

References

1. Patel IJ, Davidson JC, Nikolic B, Salazar GM, Schwartzberg MS, Walker TG, et al. Consensus guidelines for periprocedural management of coagulation status and hemostasis risk in percutaneous image-guided interventions. J Vasc Interv Radiol. 2012;23(6):727–36.
2. Patel IJ, Davidson JC, Nikolic B, Salazar GM, Schwartzberg MS, Walker TG, et al. Addendum of newer anticoagulants to the SIR consensus guideline. J Vasc Interv Radiol. 2013;24(5):641–5.
3. Chehab MA, Thakor A, Tulin-Silver S, Connolly BL, Cahill AM, Ward TJ, et al. Adult and pediatric antibiotic prophylaxis during vascular and IR procedures: a Society of Interventional Radiology practice parameter update endorsed by the Cardiovascular and Interventional Radiological Society of Europe and the Canadian Association for Interventional Radiology. J Vasc Interv Radiol. 2018;29:1483–1501.e2.
4. Strauss KJ, Kaste SC. The ALARA (as low as reasonably achievable) concept in pediatric interventional and fluoroscopic imaging: striving to keep radiation doses as low as possible during fluoroscopy of pediatric patients--a white paper executive summary. Radiology. 2006;240(3):621–2.
5. Dotson K, Johnson LH. Pediatric spontaneous pneumothorax. Pediatr Emerg Care. 2012;28(7):715–20; quiz 21–3.
6. Balfour-Lynn IM, Abrahamson E, Cohen G, Hartley J, King S, Parikh D, et al. BTS guidelines for the management of pleural infection in children. Thorax. 2005;60(Suppl 1):i1–21.
7. Sahn SA. Diagnosis and management of parapneumonic effusions and empyema. Clin Infect Dis. 2007;45(11):1480–6.
8. Wells RG, Havens PL. Intrapleural fibrinolysis for parapneumonic effusion and empyema in children. Radiology. 2003;228(2):370–8.
9. Milonakis M, Chatzis AC, Giannopoulos NM, Contrafouris C, Bobos D, Kirvassilis GV, et al. Etiology and management of chylothorax following pediatric heart surgery. J Card Surg. 2009;24(4):369–73.
10. Nath DS, Savla J, Khemani RG, Nussbaum DP, Greene CL, Wells WJ. Thoracic duct ligation for persistent chylothorax after pediatric

cardiothoracic surgery. Ann Thorac Surg. 2009;88(1):246–51; discussion 51–2.
11. Attar MA, Donn SM. Congenital chylothorax. Semin Fetal Neonatal Med. 2017;22(4):234–9.
12. Soto-Martinez M, Massie J. Chylothorax: diagnosis and management in children. Paediatr Respir Rev. 2009;10(4):199–207.
13. Epaud R, Dubern B, Larroquet M, Tamalet A, Guillemot N, Maurage C, et al. Therapeutic strategies for idiopathic chylothorax. J Pediatr Surg. 2008;43(3):461–5.
14. Jernite M, Donato L, Favre R, Haddad J, Esposito M, Messer J. Medical treatment of chylous effusions in newborn infants. Apropos of 3 cases. Arch Fr Pediatr. 1992;49(9):811–4.
15. Hoffer FA, Hancock ML, Hinds PS, Oigbokie N, Rai SN, Rao B. Pleurodesis for effusions in pediatric oncology patients at end of life. Pediatr Radiol. 2007;37(3):269–73.
16. den Hollander BS, Connolly BL, Sung L, Rapoport A, Zwaan CM, Grant RM, et al. Successful use of indwelling tunneled catheters for the management of effusions in children with advanced cancer. Pediatr Blood Cancer. 2014;61(6):1007–12.
17. Lois M, Noppen M. Bronchopleural fistulas: an overview of the problem with special focus on endoscopic management. Chest. 2005;128(6):3955–65.
18. McManigle JE, Fletcher GL, Tenholder MF. Bronchoscopy in the management of bronchopleural fistula. Chest. 1990;97(5): 1235–8.
19. Cerfolio RJ. The incidence, etiology, and prevention of postresectional bronchopleural fistula. Semin Thorac Cardiovasc Surg. 2001;13(1):3–7.
20. Sirbu H, Busch T, Aleksic I, Schreiner W, Oster O, Dalichau H. Bronchopleural fistula in the surgery of non-small cell lung cancer: incidence, risk factors, and management. Ann Thorac Cardiovasc Surg. 2001;7(6):330–6.
21. Cundiff WB, McCormack FX, Wikenheiser-Brokamp K, Starnes S, Kotloff R, Benzaquen S. Successful management of a chronic, refractory bronchopleural fistula with endobronchial valves followed by talc pleurodesis. Am J Respir Crit Care Med. 2014;189(4):490–1.
22. Iwata T, Iida S, Hanada S, Inoue H, Morikawa Y, Inoue K, et al. Transbronchial occlusion of a malignant bronchopleural fistula with cyanoacrylate glue. J Bronchology Interv Pulmonol. 2011;18(2):176–8.
23. Jester I, Nijran A, Singh M, Parikh DH. Surgical management of bronchopleural fistula in pediatric empyema and necrotizing pneumonia: efficacy of the serratus anterior muscle digitation flap. J Pediatr Surg. 2012;47(7):1358–62.
24. Dupuy DE, Zagoria RJ, Akerley W, Mayo-Smith WW, Kavanagh PV, Safran H. Percutaneous radiofrequency ablation of malignancies in the lung. AJR Am J Roentgenol. 2000;174(1):57–9.
25. Steinke K, Sewell PE, Dupuy D, Lencioni R, Helmberger T, Kee S, et al. Pulmonary radiofrequency ablation--an international study survey. Anticancer Res. 2004;24(1):339–43.
26. Sano Y, Kanazawa S, Gobara H, Mukai T, Hiraki T, Hase S, et al. Feasibility of percutaneous radiofrequency ablation for intrathoracic malignancies: a large single-center experience. Cancer. 2007;109(7):1397–405.
27. Mouli SK, Kurilova I, Sofocleous CT, Lewandowski RJ. The role of percutaneous image-guided thermal ablation for the treatment of pulmonary malignancies. AJR Am J Roentgenol. 2017;209(4):740–51.
28. Dishop MK, Kuruvilla S. Primary and metastatic lung tumors in the pediatric population: a review and 25-year experience at a large children's hospital. Arch Pathol Lab Med. 2008;132(7):1079–103.
29. Tronc F, Conter C, Marec-Berard P, Bossard N, Remontet L, Orsini A, et al. Prognostic factors and long-term results of pulmonary metastasectomy for pediatric histologies. Eur J Cardiothorac Surg. 2008;34(6):1240–6.
30. Chen F, Miyahara R, Bando T, Okubo K, Watanabe K, Nakayama T, et al. Repeat resection of pulmonary metastasis is beneficial for patients with osteosarcoma of the extremities. Interact Cardiovasc Thorac Surg. 2009;9(4):649–53.
31. Hacker FM, von Schweinitz D, Gambazzi F. The relevance of surgical therapy for bilateral and/or multiple pulmonary metastases in children. Eur J Pediatr Surg. 2007;17(2):84–9.
32. Saumet L, Deschamps F, Marec-Berard P, Gaspar N, Corradini N, Petit P, et al. Radiofrequency ablation of metastases from osteosarcoma in patients under 25 years: the SCFE experience. Pediatr Hematol Oncol. 2015;32(1):41–9.
33. Yevich S, Gaspar N, Tselikas L, Brugieres L, Pacquement H, Schleiermacher G, et al. Percutaneous computed tomography-guided thermal ablation of pulmonary osteosarcoma metastases in children. Ann Surg Oncol. 2016;23(4):1380–6.
34. Ferrer-Mileo L, Luque Blanco AI, Gonzalez-Barboteo J. Efficacy of cryoablation to control cancer pain: a systematic review. Pain Pract. 2018;18:1083.
35. Hegg RM, Kurup AN, Schmit GD, Weisbrod AJ, Atwell TD, Olivier KR, et al. Cryoablation of sternal metastases for pain palliation and local tumor control. J Vasc Interv Radiol. 2014;25(11):1665–70.
36. Keller BA, Kabagambe SK, Becker JC, Chen YJ, Goodman LF, Clark-Wronski JM, et al. Intercostal nerve cryoablation versus thoracic epidural catheters for postoperative analgesia following pectus excavatum repair: preliminary outcomes in twenty-six cryoablation patients. J Pediatr Surg. 2016;51(12):2033–8.
37. Chin CS, Litle V, Yun J, Weiser T, Swanson SJ. Airway stents. Ann Thorac Surg. 2008;85(2):S792–6.
38. Nicolai T. Airway stents in children. Pediatr Pulmonol. 2008;43(4):330–44.
39. McLaren CA, Elliott MJ, Roebuck DJ. Tracheobronchial intervention in children. Eur J Radiol. 2005;53(1):22–34.
40. Pillai JB, Smith J, Hasan A, Spencer D. Review of pediatric airway malacia and its management, with emphasis on stenting. Eur J Cardiothorac Surg. 2005;27(1):35–44.
41. Anton-Pacheco JL, Cabezali D, Tejedor R, Lopez M, Luna C, Comas JV, et al. The role of airway stenting in pediatric tracheobronchial obstruction. Eur J Cardiothorac Surg. 2008;33(6):1069–75.
42. Filler RM, Forte V, Chait P. Tracheobronchial stenting for the treatment of airway obstruction. J Pediatr Surg. 1998;33(2):304–11.
43. Hebra A, Powell DD, Smith CD, Othersen HB Jr. Balloon tracheoplasty in children: results of a 15-year experience. J Pediatr Surg. 1991;26(8):957–61.
44. Kumar P, Bush AP, Ladas GP, Goldstraw P. Tracheobronchial obstruction in children: experience with endoscopic airway stenting. Ann Thorac Surg. 2003;75(5):1579–86.
45. Maeda K, Yasufuku M, Yamamoto T. A new approach to the treatment of congenital tracheal stenosis: balloon tracheoplasty and expandable metallic stenting. J Pediatr Surg. 2001;36(11): 1646–9.
46. Jacobs IN, Wetmore RF, Tom LW, Handler SD, Potsic WP. Tracheobronchomalacia in children. Arch Otolaryngol Head Neck Surg. 1994;120(2):154–8.
47. Watters K, Russell J. The cutting balloon for endoscopic dilatation of pediatric subglottic stenosis. Int J Pediatr Otorhinolaryngol. 2008;3(1):39–43.
48. Cahill AM, Baskin KM, Kaye RD, Fitz CR, Towbin RB. CT-guided percutaneous lung biopsy in children. J Vasc Interv Radiol. 2004;15(9):955–60.
49. Hayes-Jordan A, Connolly B, Temple M, Chait P, Weitzman S, Njere I, et al. Image-guided percutaneous approach is superior to the thoracoscopic approach in the diagnosis of pulmonary nodules in children. J Pediatr Surg. 2003;38(5):745–8.
50. Fontalvo LF, Amaral JG, Temple M, Chait PG, John P, Krishnamuthy G, et al. Percutaneous US-guided biopsies of peripheral pulmonary lesions in children. Pediatr Radiol. 2006;36(6):491–7.

51. Heyer CM, Lemburg SP, Kagel T, Mueller KM, Nuesslein TG, Rieger CH, et al. Evaluation of chronic infectious interstitial pulmonary disease in children by low-dose CT-guided transthoracic lung biopsy. Eur Radiol. 2005;15(7):1289–95.
52. Bendon AA, Krishnan BS, Korula G. CT-guided lung biopsies in children: anesthesia management and complications. Paediatr Anaesth. 2005;15(4):321–4.
53. Wilkinson AG, Paton JY, Gibson N, Howatson AG. CT-guided 14-G cutting needle lung biopsy in children: safe and effective. Pediatr Radiol. 1999;29(7):514–6.
54. Waldhausen JH, Shaw DW, Hall DG, Sawin RS. Needle localization for thoracoscopic resection of small pulmonary nodules in children. J Pediatr Surg. 1997;32(11):1624–5.
55. Connolly BL, Chait PG, Duncan DS, Taylor G. CT-guided percutaneous needle biopsy of small lung nodules in children. Pediatr Radiol. 1999;29(5):342–6.
56. Partrick DA, Bensard DD, Teitelbaum DH, Geiger JD, Strouse P, Harned RK. Successful thoracoscopic lung biopsy in children utilizing preoperative CT-guided localization. J Pediatr Surg. 2002;37(7):970–3; discussion 970–3.
57. Kandarpa K, Hagspiel K. Pulmonary arteriography. In: Kandarpa K, Aruny J, editors. Handbook of interventional radiologic procedures. 3rd ed. Philadelphia: Lippincott Wiliams & Wilkins; 2002. p. 35–42.
58. Yeow KM, Su IH, Pan KT, Tsay PK, Lui KW, Cheung YC, et al. Risk factors of pneumothorax and bleeding: multivariate analysis of 660 CT-guided coaxial cutting needle lung biopsies. Chest. 2004;126(3):748–54.
59. Hofmann LV, Lee DS, Gupta A, Arepally A, Sood S, Girgis R, et al. Safety and hemodynamic effects of pulmonary angiography in patients with pulmonary hypertension: 10-year single-center experience. AJR Am J Roentgenol. 2004;183(3):779–86.
60. White RI Jr, Pollak JS, Wirth JA. Pulmonary arteriovenous malformations: diagnosis and transcatheter embolotherapy. J Vasc Interv Radiol. 1996;7(6):787–804.
61. Stein PD, Athanasoulis C, Alavi A, Greenspan RH, Hales CA, Saltzman HA, et al. Complications and validity of pulmonary angiography in acute pulmonary embolism. Circulation. 1992;85(2):462–8.
62. Perlmutt LM, Braun SD, Newman GE, Oke EJ, Dunnick NR. Pulmonary arteriography in the high-risk patient. Radiology. 1987;162(1 Pt 1):187–9.
63. Mills SR, Jackson DC, Older RA, Heaston DK, Moore AV. The incidence, etiologies, and avoidance of complications of pulmonary angiography in a large series. Radiology. 1980;136(2):295–9.
64. Kjeldsen AD, Oxhoj H, Andersen PE, Elle B, Jacobsen JP, Vase P. Pulmonary arteriovenous malformations: screening procedures and pulmonary angiography in patients with hereditary hemorrhagic telangiectasia. Chest. 1999;116(2):432–9.
65. Shovlin CL, Letarte M. Hereditary haemorrhagic telangiectasia and pulmonary arteriovenous malformations: issues in clinical management and review of pathogenic mechanisms. Thorax. 1999;54(8):714–29.
66. De Cillis E, Burdi N, Bortone AS, D'Agostino D, Fiore T, Ettorre GC, et al. Endovascular treatment of pulmonary and cerebral arteriovenous malformations in patients affected by hereditary haemorrhagic teleangiectasia. Curr Pharm Des. 2006;12(10):1243–8.
67. Shovlin CL, Guttmacher AE, Buscarini E, Faughnan ME, Hyland RH, Westermann CJ, et al. Diagnostic criteria for hereditary hemorrhagic telangiectasia (Rendu-Osler-Weber syndrome). Am J Med Genet. 2000;91(1):66–7.
68. McAllister KA, Grogg KM, Johnson DW, Gallione CJ, Baldwin MA, Jackson CE, et al. Endoglin, a TGF-beta binding protein of endothelial cells, is the gene for hereditary haemorrhagic telangiectasia type 1. Nat Genet. 1994;8(4):345–51.
69. Johnson DW, Berg JN, Baldwin MA, Gallione CJ, Marondel I, Yoon SJ, et al. Mutations in the activin receptor-like kinase 1 gene in hereditary haemorrhagic telangiectasia type 2. Nat Genet. 1996;13(2):189–95.
70. Cole SG, Begbie ME, Wallace GM, Shovlin CL. A new locus for hereditary haemorrhagic telangiectasia (HHT3) maps to chromosome 5. J Med Genet. 2005;42(7):577–82.
71. Gallione CJ, Repetto GM, Legius E, Rustgi AK, Schelley SL, Tejpar S, et al. A combined syndrome of juvenile polyposis and hereditary haemorrhagic telangiectasia associated with mutations in MADH4 (SMAD4). Lancet. 2004;363(9412):852–9.
72. Moussouttas M, Fayad P, Rosenblatt M, Hashimoto M, Pollak J, Henderson K, et al. Pulmonary arteriovenous malformations: cerebral ischemia and neurologic manifestations. Neurology. 2000;55(7):959–64.
73. Pollak JS, Saluja S, Thabet A, Henderson KJ, Denbow N, White RI Jr. Clinical and anatomic outcomes after embolotherapy of pulmonary arteriovenous malformations. J Vasc Interv Radiol. 2006;17(1):35–44; quiz 5.
74. Faughnan ME, Thabet A, Mei-Zahav M, Colombo M, Maclusky I, Hyland RH, et al. Pulmonary arteriovenous malformations in children: outcomes of transcatheter embolotherapy. J Pediatr. 2004;145(6):826–31.
75. Faughnan ME, Palda VA, Garcia-Tsao G, Geisthoff UW, McDonald J, Proctor DD, et al. HHT Foundation International - Guidelines Working Group. International guidelines for the diagnosis and management of hereditary haemorrhagic telangiectasia. J Med Genet. 2011;48(2):73–87.
76. Lacombe P, Lagrange C, Beauchet A, El Hajjam M, Chinet T, Pelage JP. Diffuse pulmonary arteriovenous malformations in hereditary hemorrhagic telangiectasia: long-term results of embolization according to the extent of lung involvement. Chest. 2009;135(4):1031–7.
77. Gupta P, Mordin C, Curtis J, Hughes JM, Shovlin CL, Jackson JE. Pulmonary arteriovenous malformations: effect of embolization on right-to-left shunt, hypoxemia, and exercise tolerance in 66 patients. AJR Am J Roentgenol. 2002;179(2):347–55.
78. Prasad V, Chan RP, Faughnan ME. Embolotherapy of pulmonary arteriovenous malformations: efficacy of platinum versus stainless steel coils. J Vasc Interv Radiol. 2004;15(2 Pt 1):153–60.
79. Mager JJ, Overtoom TT, Blauw H, Lammers JW, Westermann CJ. Embolotherapy of pulmonary arteriovenous malformations: long-term results in 112 patients. J Vasc Interv Radiol. 2004;15(5):451–6.
80. Lee WL, Graham AF, Pugash RA, Hutchison SJ, Grande P, Hyland RH, et al. Contrast echocardiography remains positive after treatment of pulmonary arteriovenous malformations. Chest. 2003;123(2):351–8.
81. Tau N, Atar E, Mei-Zahav M, Bachar GN, Dagan T, Birk E, et al. Amplatzer vascular plugs versus coils for embolization of pulmonary arteriovenous malformations in patients with hereditary hemorrhagic telangiectasia. Cardiovasc Intervent Radiol. 2016;39(8):1110–4.
82. Byard RW, Cutz E. Sudden and unexpected death in infancy and childhood due to pulmonary thromboembolism. An autopsy study. Arch Pathol Lab Med. 1990;114(2):142–4.
83. Buck JR, Connors RH, Coon WW, Weintraub WH, Wesley JR, Coran AG. Pulmonary embolism in children. J Pediatr Surg. 1981;16(3):385–91.
84. Stein PD, Kayali F, Olson RE. Incidence of venous thromboembolism in infants and children: data from the National Hospital Discharge Survey. J Pediatr. 2004;145(4):563–5.
85. Chan AK, Deveber G, Monagle P, Brooker LA, Massicotte PM. Venous thrombosis in children. J Thromb Haemost. 2003;1(7):1443–55.

86. Anton N, Massicotte MP. Venous thromboembolism in pediatrics. Semin Vasc Med. 2001;1(1):111–22.
87. Babyn PS, Gahunia HK, Massicotte P. Pulmonary thromboembolism in children. Pediatr Radiol. 2005;35(3):258–74.
88. Andrew M, David M, Adams M, Ali K, Anderson R, Barnard D, et al. Venous thromboembolic complications (VTE) in children: first analyses of the Canadian Registry of VTE. Blood. 1994;83(5):1251–7.
89. Van Ommen CH, Peters M. Acute pulmonary embolism in childhood. Thromb Res. 2006;118(1):13–25.
90. Uflacker R. Interventional therapy for pulmonary embolism. J Vasc Interv Radiol. 2001;12(2):147–64.
91. Robinson A, Fellows KE, Bridges ND, Rome JJ. Effectiveness of pharmacomechanical thrombolysis in infants and children. Am J Cardiol. 2001;87(4):496–9, A8.
92. Sur JP, Garg RK, Jolly N. Rheolytic percutaneous thrombectomy for acute pulmonary embolism in a pediatric patient. Catheter Cardiovasc Interv. 2007;70(3):450–3.
93. Peuster M, Bertram H, Windhagen-Mahnert B, Paul T, Hausdorf G. Mechanical recanalization of venous thrombosis and pulmonary embolism with the Clotbuster thrombectomy system in a 12-year-old boy. Z Kardiol. 1998;87(4):283–7.
94. Feldman JP, Feinstein JA, Lamberti JJ, Perry SB. Angiojet catheter-based thrombectomy in a neonate with postoperative pulmonary embolism. Catheter Cardiovasc Interv. 2005;66(3):442–5.
95. Vincent RN, Dinkins J, Dobbs MC. Mechanical thrombectomy using the AngioJect in a child with congenital heart disease. Catheter Cardiovasc Interv. 2004;61(2):253–5.
96. Crocco JA, Rooney JJ, Fankushen DS, DiBenedetto RJ, Lyons HA. Massive hemoptysis. Arch Intern Med. 1968;121(6):495–8.
97. Jean-Baptiste E. Clinical assessment and management of massive hemoptysis. Crit Care Med. 2000;28(5):1642–7.
98. Najarian KE, Morris CS. Arterial embolization in the chest. J Thorac Imaging. 1998;13(2):93–104.
99. FitzSimmons SC. The changing epidemiology of cystic fibrosis. J Pediatr. 1993;122(1):1–9.
100. Roebuck DJ, Barnacle AM. Haemoptysis and bronchial artery embolization in children. Paediatr Respir Rev. 2008;9(2):95–104.
101. Barben J, Robertson D, Olinsky A, Ditchfield M. Bronchial artery embolization for hemoptysis in young patients with cystic fibrosis. Radiology. 2002;224(1):124–30.
102. Batra PS, Holinger LD. Etiology and management of pediatric hemoptysis. Arch Otolaryngol Head Neck Surg. 2001;127(4):377–82.
103. Yoon W, Kim JK, Kim YH, Chung TW, Kang HK. Bronchial and nonbronchial systemic artery embolization for life-threatening hemoptysis: a comprehensive review. Radiographics. 2002;22(6):1395–409.
104. Cauldwell EW, Siekert RG, et al. The bronchial arteries; an anatomic study of 150 human cadavers. Surg Gynecol Obstet. 1948;86(4):395–412.
105. Botenga AS. The role of bronchopulmonary anastomoses in chronic inflammatory processes of the lung. Selective arteriographic investigation. Am J Roentgenol Radium Therapy, Nucl Med. 1968;104(4):829–37.
106. Chun JY, Morgan R, Belli AM. Radiological management of hemoptysis: a comprehensive review of diagnostic imaging and bronchial arterial embolization. Cardiovasc Intervent Radiol. 2010;33(2):240–50.
107. Pump KK. Distribution of bronchial arteries in the human lung. Chest. 1972;62(4):447–51.
108. Deffebach ME, Charan NB, Lakshminarayan S, Butler J. The bronchial circulation. Small, but a vital attribute of the lung. Am Rev Respir Dis. 1987;135(2):463–81.
109. McDonald DM. Angiogenesis and remodeling of airway vasculature in chronic inflammation. Am J Respir Crit Care Med. 2001;164(10 Pt 2):S39–45.
110. Hirshberg B, Biran I, Glazer M, Kramer MR. Hemoptysis: etiology, evaluation, and outcome in a tertiary referral hospital. Chest. 1997;112(2):440–4.
111. Khalil A, Fartoukh M, Tassart M, Parrot A, Marsault C, Carette MF. Role of MDCT in identification of the bleeding site and the vessels causing hemoptysis. AJR Am J Roentgenol. 2007;188(2):W117–25.
112. Haponik EF, Fein A, Chin R. Managing life-threatening hemoptysis: has anything really changed? Chest. 2000;118(5):1431–5.
113. Hsiao EI, Kirsch CM, Kagawa FT, Wehner JH, Jensen WA, Baxter RB. Utility of fiberoptic bronchoscopy before bronchial artery embolization for massive hemoptysis. AJR Am J Roentgenol. 2001;177(4):861–7.
114. Mulliken JB, Glowacki J. Hemangiomas and vascular malformations in infants and children: a classification based on endothelial characteristics. Plast Reconstr Surg. 1982;69(3):412–22.
115. Alomari AI, Burrows PE, Lee EY, Hedequist DJ, Mulliken JB, Fishman SJ. CLOVES syndrome with thoracic and central phlebectasia: increased risk of pulmonary embolism. J Thorac Cardiovasc Surg. 2010;140(2):459–63.
116. Alomari AI. Characterization of a distinct syndrome that associates complex truncal overgrowth, vascular, and acral anomalies: a descriptive study of 18 cases of CLOVES syndrome. Clin Dysmorphol. 2009;18(1):1–7.
117. Chaudry G, Guevara C, Rialon J, Kerr K, Mulliken L, Greene C, et al. Safety and efficacy of bleomycin sclerotherapy for microcystic lymphatic malformation. Cardiovasc Intervent Radiol. 2014;37(6):1476–81.
118. Adams D, Trenor C, Hammill A, Vinks A, Patel M, Chaudry G, et al. Efficacy and safety of sirolimus in the treatment of complicated vascular anomalies. Pediatrics. 2016;137(2):E20153257.

Pediatric Thoracic MRI

21

Mark C. Liszewski, Pierluigi Ciet, Giuseppe Cicero, and Edward Y. Lee

Introduction

MRI of the pediatric thorax has historically been constrained by technical factors including artifact from respiratory and cardiac motion, rapid signal dephasing at air-tissue interfases, and relatively low proton density within the lung. Advances in MRI scanner technology have made it possible to overcome many of these constraints. The current generation of MRI scanners available in most imaging centers is capable of performing imaging studies of diagnostic quality to evaluate many conditions of the pediatric thorax. In this chapter, MR imaging techniques for imaging the pediatric chest are presented. The MR imaging findings in a spectrum of anomalies and abnormalities of the pediatric chest are then presented and illustrated.

Imaging Techniques

The main advantage of chest MRI is its ability of integrating excellent anatomical as well as physiologic information under a single examination. Nonetheless, chest MRI faces many challenges.

M. C. Liszewski
Department of Radiology, Division of Pediatric Radiology, Montefiore Medical Center, Bronx, NY, USA

P. Ciet
Department of Radiology and Nuclear Medicine, Sophia Children Hospital – Erasmus Medical Center, Rotterdam, The Netherlands

G. Cicero
Department of Radiology and Nuclear Medicine, Sophia Children Hospital – Erasmus Medical Center, Rotterdam, The Netherlands

Department of Biomedical Sciences and Morphological and Functional Imaging, University of Messina, Messina, Italy

E. Y. Lee (✉)
Department of Radiology, Boston Children's Hospital and Harvard Medical School, Boston, MA, USA
e-mail: Edward.Lee@childrens.harvard.edu

Signal-to-Noise Ratio (SNR) in Chest MRI

The lung parenchyma is an organ with a relatively small number of water protons and high content of air. These two conditions result in intrinsically low signal on chest MRI.

Due to the low proton content of the healthy lung parenchyma, the voxel size in chest MRI is usually adjusted to be significantly larger than that of CT in order to maximize signal. The slice thickness achieved with chest MRI protocols generally range between 3 and 5 mm, which is 3–5 times thicker than that of CT. However, the newest ultrashort (UTE) and zero echo time (ZTE) MRI readout schemes provide higher SNR with thinner slices enabling submillimeter isotropic resolution [1]. These acquisition schemes are usually acquired in free-breathing conditions with respiratory triggering and a long acquisition time. However, breath-hold acquisition can be obtained by using parallel imaging [2]. With parallel imaging techniques, the spatial information related to each phased array coil element is utilized for reducing the amount of conventional encoding lines in order to gain spatial or temporal resolution [2]. The higher parallel imaging factor or "acceleration" utilized, the higher the penalty in SNR due to a higher noise. The most appropriate parallel imaging techniques for chest MRI are those that reconstruct the image in the frequency domain, before the Fourier transform, from the frequency signals of each coil such as in the case of GRAPPA (GeneRalized Autocalibrating Partially Parallel Acquisition) or ARC (Autocalibrating Reconstruction for Cartesian imaging) [2]. Using GRAPPA or ARC, comfortable breath-hold acquisition can be achieved (6–15 s), which can be easily performed in children older than 5 years.

Signal loss in chest MRI is directly related to the T2 star (T2∗) effect of air-tissue interfaces, which are particularly strong with gradient recalled echo (GRE) techniques. When using GRE sequences, the shortest TE achievable should be employed to ensure optimal SNR. This can be obtained with MR scanners that have powerful slew rate of 200 T/m/ms or more. Independent of the sequence used, imaging at

R. H. Cleveland, E. Y. Lee (eds.), *Imaging in Pediatric Pulmonology*, https://doi.org/10.1007/978-3-030-23979-4_21

end-inspiration provides lower SNR than scanning performed at end-expiration due to the larger amount of air within the lung.

Breathing and Cardiac Motion Compensation

Image quality in chest MRI is influenced by cardiac and breathing motion, which determines SNR dephasing. This problem is more severe in children, who have higher respiratory and cardiac rates than adults. To eliminate these motion effects, image acquisition can be synchronized with the motion itself (respiratory or ECG gating), or data can be averaged over many respiratory cycles without any specific form of synchronization. Respiratory and cardiac triggering are performed using navigator echoes or cardiac and respiratory monitoring devices, such as pneumobelts and ECG leads. Navigator echo techniques detect the diaphragm position in real time and trigger the image acquisition prospectively, most often selecting the diaphragm position at end-expiration. Navigator echo-based techniques improve image quality, but this is at the expense of longer acquisition times, especially in patients with irregular breathing patterns [2]. Pneumobelts are external devices placed around the rib cage, which monitor chest excursion and trigger image acquisition at end-expiration. Multiple averaging techniques are used during free breathing to reduce image ghosting. An advantage of this technique over techniques using respiratory and cardiac triggering is constant scan times. A drawback of this technique is image blurring. Some or all of these motion compensation techniques are routinely employed when imaging children under 5 years of age, who cannot follow breathing instructions.

Patient Preparation

Children younger than 5 years of age are usually scanned under moderate sedation or total anesthesia in combination with free-breathing MRI techniques. For infants, many pediatric centers use the "feed and wrap" method, where the child is fed immediately before the MRI scan and placed in the gantry after being swaddled [3].

Children older than 5 years can be coached to perform specific breathing maneuvers before or during the MRI scan. This coaching is crucial in children, who are less capable to follow instructions than adults. The training can be performed in a mock MRI scanner, which reproduces the noisy environment of a true MRI system and acquaints the child with the MRI setting. Depending on the examination performed, the patients are asked to maintain a breath-hold at inspiration or expiration, to breathe regularly, or to perform rapid expiratory and inspiratory or coughing maneuvers in order to study the response of the airways to stress situations.

MRI Protocols

Selection of an appropriate chest MRI protocol requires one to consider several factors including the type of contrast needed, SNR, contrast-to-noise ratio (CNR), and spatial and temporal resolution. Two groups of sequences can be used for chest MRI: spin echo (SE) or gradient echo (GRE). These sequences may collect imaging data during breath-hold conditions using ultrafast bidimensional (2D) and three-dimensional (3D) MR pulse sequences, which are usually preferred for chest MRI and MR angiography (MRA). These sequences freeze respiratory and/or cardiac motion allowing short acquisition times, which are indispensable in pediatric patients, who are not capable of long apnea times. In the group of 2D SE, several single-shot turbo SE (TSE) sequences are used. A typical 2D T2-weighted single-shot TSE scan is the Half-Fourier-Acquired Single-shot Turbo spin Echo (HASTE; RARE or SSFSE depending on the MRI scan manufacturer). One particular TSE non-breath-hold readout is the Periodically Rotated Overlapping ParallEL Lines with Enhanced Reconstruction (PROPELLER) sequence, which collects imaging data using rotating k-space bands or blades and is relatively insensitive to respiratory movement [4]. This sequence is more suitable for patients who are unable to comply with breathing instructions, such as children. TSE techniques have high sensitivity and SNR for fluid detection, evaluation of nodules, consolidation, and bronchial wall thickening [2].

2D or 3D GRE acquisitions include spoiled RF GRE readouts (SPGR, FLASH) or steady-state free precession SSFP readouts (trueFISP, FIESTA). Both of these sequences allow for high SNR and CNR in young noncooperative children. Short and ultrashort TE GRE scans are usually collected with very short TRs when compared to TSE scans, which is important for children who can only hold their breaths for a short time. 3D GRE acquisitions are more advantageous than the 2D scans, because they provide better SNR and are less sensitive to susceptibility artifacts than 2D scans [2]. In general, 3D GRE acquisitions can scan the entire thorax with isotropic voxels of 2–3 mm in less than 15 seconds. Isotropic voxels enable multiplanar reformats (MPR) which are important in the evaluation of vascular and airway structures. FLASH/SPGR sequence can be proton density weighted, which is most helpful for evaluating the lung parenchyma, vascular structures, and airways without the use of contrast agents (using a low flip angle) or T1-weighted, which is most helpful for MRA studies. SSFP/

TruFISP sequences generate a T1-/T2-weighted contrast with medium to high flip angle settings enhancing tissues in the lung with more water-like behavior, such as mucus plugs in the airways. SSFP has been used to assess relevant structural abnormalities, such as bronchiectasis, mucus plugging, and consolidation.

Functional Imaging

MRI has several techniques that can be used to assess multiple functional aspects of the lung and airways. Contrast-enhanced MRI has been used in pulmonary vasculature assessment and lung perfusion [2]. Cine-MRI has proven to be useful to assess central airway mechanics [5, 6]. Diffusion-weighted imaging (DWI) has been used to assess lung inflammation [7]. Fourier decomposition (FD) can be used to assess lung perfusion and lung ventilation without the use of contrast media [8].

Magnetic Resonance Angiography (MRA)

Magnetic resonance angiography (MRA) of the chest can be obtained without and with intravenous contrast agents [2]. The noncontrast studies are based on SSFP sequences ("bright blood") and SSFSE/HASTE sequences ("black blood"). The sequences are particularly advantageous in children, because they do not require the use of gadolinium. Therefore, these techniques can be repeated numerous times without concern about gadolinium deposition, which has been recently raised as a concern [9]. SSFSE dark blood sequences are usually applied to study the anatomy of the heart, great vessels, and mediastinum.

Contrast-enhanced MRI (CEMRI) provides higher temporal and spatial resolution than noncontrast-enhanced techniques [2]. CEMRI uses high temporal resolution 2D/3D T1-weighted GRE imaging and an acquisition rate of one image every 1.0–1.5 s with short TR (3–5 ms), short TE (1–2.5 ms), flip angle >15–60°, and resolution and coverage adjusted to breath-hold. For safety reasons, macrocyclic non-ionic agents (Gd-HP-DO3A [Dotarem] or Gd-BT-DO3A [Gadovist]) are preferred in pediatric patients, with doses ranging between 1 and 2 ml/kg and injection rates of up to 2 ml/sec [2]. In pediatric patients, CEMRI is used to study congenital vascular anomalies.

Perfusion MR Imaging

Perfusion defects can be assessed on MRI by administering contrast and performing dynamic contrast-enhanced (DCE) imaging or with FD [2]. DCE is obtained by fast imaging of the first pass of contrast agent through the lungs after intravenous bolus injection. 3D GRE sequences with high spatial and temporal resolution (e.g., FLASH, TREAT, TWIST, and TRICKS) are used.

FD is a recent technique that supplies perfusion and ventilation maps without intravenous or gaseous contrast agents. FD is based on a 2D SSFP/SPGR sequence with high temporal resolution without cardiac or respiratory gating. After data collection, image registration techniques are applied to compensate for respiratory motion. Fourier transform is eventually used to decompose the signal intensity changes of the lung parenchyma related to the cardiac and respiratory cycle and to obtain the perfusion- and ventilation-weighted images. Upgraded versions of the post-processing software for FD have shown an improvement of SNR and image quality [10], making this technique superior to nuclear medicine studies to assess ventilation/perfusion defects. This technique has been tested in patients with cystic fibrosis, chronic pulmonary embolism, and COPD [11].

Cine MR Imaging

Cine-MRI allows evaluation of the lung in dynamic conditions. Fast temporal resolution techniques, such as 3D GRE FLASH, have been used to delineate the diaphragmatic domes and chest wall during active breathing. Campbell et al. has proposed cine-MRI to assess and monitor pediatric patients after spinal surgery for scoliosis [12]. 2D SSFP multiphase or 3D TRICKS can be used to assess airways in dynamic conditions. Typical breathing maneuvers are forced expiration or coughing, which are used to reproduce the breathing condition occurring during exercise. Ciet et al. used a cine-MRI protocol to assess tracheobronchomalacia (TBM) in a group of pediatric patients and in a cohort of adult with saber-sheath TBM [5, 6].

In short, chest MRI, by combining functional and structural information, can be a powerful tool in pediatric thoracic imaging by providing information about ventilation, inflammation, perfusion, and structure (VIPS-MRI) [13]. A summary of VIPS-MRI protocol is presented in Table 21.1.

Spectrum of Thoracic Anomalies and Abnormalities

Since MRI and CT are both cross-sectional imaging modalities, the basic MR imaging findings in disorders of the pediatric chest are similar to the findings on CT. A practitioner familiar with CT of the pediatric chest should have little difficulty identifying the same pathology on MRI. In addition, MRI often provides the opportunity to obtain more information than CT. Because MRI does not involve the use of ionizing radiation, multiple MRI sequences with different tissue weighting, multiphase contrast-enhanced imaging, and

Table 21.1 Imaging protocols for ventilation, inflammation, perfusion, and structural (VIPS) MRI (lung, static airway, and dynamic airway)

Sequence	Manufacturer acronyms	Typical contrast	Average acquisition time (for entire chest, otherwise stated)	Spatial resolution/scan plane	Temporal resolution	Scan parameters	Field strength
Ventilation							
2D steady-state free precession gradient echo – SSFP	**FIESTA** (GE) **TruFISP** (SIEMENS) **Balanced FFE** (PHILIPS)	T1-/T2-weighted Inflow enhancement Bright blood	3–9 minutes Free-breathing	FOV = 450 × 450 mm SL =12 mm Matrix = 128 × 128 coronal or sagittal	3–4 images/s	TR = shortest (1.8–2.2 ms) TE = shortest (0.7–0.9 ms) FA = 65° BW = medium – high	1.5 T
2D RF-spoiled gradient echo	**SPGR** (GE) **FLASH** (SIEMENS) **FFE** (PHILIPS)	T1-weighted Inflow enhancement Bright blood	3–9 minutes Free-breathing	FOV = 500 × 500 mm SL = 15 mm Matrix = 256 × 192 coronal or sagittal	3–4 images/s	TR = shortest (1.8–2.2 ms) TE = shortest (0.7–0.9 ms) FA = low (<5°) BW = medium – high	1.5 T and 3.0 T
Inflammation							
2D single-shot echo-planar imaging sequence (EPI)	**EPI – DWI** (GE,SIEMENS, PHILIPS)	T2-weighted Diffusion weighted Black blood	5–7 minutes Free-breathing	FOV = 420 × 210 mm SL = 6 mm Matrix = 100 × 128 Axial	Low	TR = long (>4000 ms) TE = medium – long (>60 ms) FA = 90°/180° b = 0 and 600 s/mm^2 BW = high Fat suppressed	1.5 T and 3.0 T
2D single-shot echo-planar imaging (EPI) sequence	**EPI – DWI** (GE,SIEMENS, PHILIPS)	T2-weighted Perfusion and diffusion weighted Black blood	5–7 minutes Free-breathing	FOV = 420 × 210 mm SL = 6 mm Axial	Low	TR = long (>4000 ms) TE = medium – long (>60 ms) FA = 90°/180° b = 0, 10, 20, 30, 50, 70, 100, 150, 200, 400, 800 s/mm^2 BW = high Fat suppressed	1.5 T and 3.0 T
2D fast spin echo	**FSE** (GE) **TSE** (SIEMENS) **TSE** (PHILIPS)	T2-weighted Black blood	5–7 minutes Free-breathing	FOV = 400 mm SL = 5–7 mm Matrix = 256 × 192 axial and coronal	Low	TR = long (2000–4000 ms) TE = medium – long (>60 ms) FA = 90°/110° – 160° BW = low – medium Fat suppression	1.5 T and 3.0 T
Perfusion/angiography							
2D steady-state free precession gradient echo – SSFP	**FIESTA** (GE) **TruFISP** (SIEMENS) **balanced FFE** (PHILIPS)	See scan parameters above					
2D RF-spoiled gradient echo	**SPGR** (GE) **FLASH** (SIEMENS) **FFE** (PHILIPS)	See scan parameters above					
3D RF-spoiled gradient echo	**SPGR** (GE) **FLASH** (SIEMENS) **FFE** (PHILIPS)	T1-weighted, after contrast injection Bright blood	12–20 seconds End-expiratory breath-hold, shallow breathing	FOV = 460 mm Matrix = 40 × 192 × 256 Voxel size (<8 mm^3) sagittal or coronal	Low	TR = short (2.5–3 ms) TE = short (1.0–1.5 ms) FA = 30–40° BW = medium – high	1.5 T and 3.0 T

3D RF spoiled gradient echo	**TRICKS** (GE) **TWIST** (SIEMENS) **TRACK** (PHILIPS)	T1-weighted, after contrast injection k-space shared acquisition Bright blood	Breath-hold (end-expiratory)/ shallow breathing	FOV = 460 mm Matrix = 32 × 96 × 128 Voxel size (<12 mm^3) sagittal or coronal	Medium, 0.5–1 s/ volume	TR = short (2.0–2.5 ms) TE = shortest (0.8–1.1 ms) FA = 8–20° BW = medium – high	1.5 T and 3.0 T
Structure (including static airways)							
2D fast spin echo	**PROPELLER** (GE) **BLADE** (SIEMENS) **MultiVane** (PHILIPS)	T2-weighted Black blood	End-expiratory with navigator echo triggering 3–7 minutes according respiratory pace and pattern	FOV = 380–400 mmMatrix = 200 × 200 SL = 5–6 mm axial and coronal	Low	TR = respiratory rate (2–5 seconds) TE = short – medium (25–60 ms) FA = 90°/150° ± FAT Saturation BW = low – medium	1.5 T and 3.0 T
2D SSFP	**FIESTA** (GE) **TRUFISP** (SIEMENS) **Balanced FFE** (PHILIPS)	T1-/T2-weighted Bright blood	12–20 seconds Breath-hold	FOV = 400 mmMatrix = 160 × 160 SL = 2.5–5 mm axial and coronal	High	TR = shortest (<4 ms) TE = shortest (<2 ms) FA = 40° BW = high	1.5 T
3D fast spin echo	**CUBE** (GE) **SPACE** (SIEMENS) **VISTA** (PHILIPS)	T2-weighted Black blood	End-expiratory with pencil-beam navigator triggering 5–7 min	FOV = 320 mmMatrix = 160 × 160SL = 2 mm sagittal or coronal	Low	TR = respiratory rate (2–5 seconds)TE = medium (60 ms~) FA = 90°/variable flip train BW = medium – high Echo train length = 80–140 Fat saturation	1.5 T and 3.0 T
3D RF-spoiled gradient echo	**SPGR** (GE) **VIBE** (SIEMENS) **THRIVE** (PHILIPS)	PD- to T1-weighted	Breath-hold 10–12 seconds (inspiratory and expiratory)	FOV = 400 mmMatrix = 200 × 200 SL = 2 mm Isotropic voxel, as low as 8 mm^3 sagittal or coronal	High	TR = shortest (<1.7 ms) TE = shortest (<0.7 ms) FA = 2° BW = medium – high	1.5 T and 3.0 T
3D RF-spoiled gradient echo	**STARVIBE** (SIEMENS) clinically not available for GE or PHILIPS	PD- to T1-weighted	Free-breathing3–5 min	FOV = 400 mm Matrix = 320 × 320 SL = 1.2–4 mm voxel (2–5 mm^3) axial	Low	TR = 7.46 ms TE = 2.46 ms FA = 9° BW = medium	1.5 T and 3.0 T
3D 2-point Dixon RF-spoiled gradient echo	**LAVA FLEX** (GE)	PD to T1-weighted Water-only, fat-only, in-phase and out-of-phase contrast	Breath-hold (10s) Free-breathing (pencil-beam navigator)	FOV = 260 mm Matrix = 128 × 128 SL = 3 mm Voxel (<3 mm^3) axial	High	TR = 3.7–4.5 ms TE = min full (<2.0 ms) FA = 2–10° BW = medium – high	1.5 T and 3.0 T
3D ultrashort TE gradient echo	**UTE/VNAV(GE)** **PETRA/ SPIRALVIBE (SIEMENS)** **MultiVane** (PHILIPS)	PD-weighted, slight T1-weighting depending on readout flip angle chosen UTE	7–10 min Free-breathing	FOV = 360 mmvoxel size = 1–8 mm^3 Sagittal or coronal	Low	TR = short (<5 ms) TE = 0.07 msBW = medium – high	1.5 T and 3.0 T

(continued)

Table 21.1 (continued)

Sequence	Manufacturer acronyms	Typical contrast	Average acquisition time (for entire chest, otherwise stated)	Spatial resolution/scan plane	Temporal resolution	Scan parameters	Field strength
3D ultrashort TE gradient echo	**ZTE** (GE)	PD-weighted Slight T1-weighting depending on readout flip angle chosen **Silent**	7–10 min Free-breathing	FOV = 360 mmMatrix = 360 × 360 × 360 sagittal or coronal	Low	TR = shortest (<1.3 ms) TE = 0 ms BW = medium – High	1.5 T and 3.0 T
Dynamic airways							
2D steady-state free precession gradient echo – SSFP	**FIESTA** (GE)**TruFISP** (SIEMENS) **balanced FFE** (PHILIPS)	T1-/T2-weighted Inflow enhancement	3–4 minutes Hyperventilation Coverage larynx to carina ~ 4 seconds per slice position	FOV = 450 × 160 mm SL = 8 mm Matrix = 128 × 128 axial	4–5 images/s	TR = shortest (1.8 ms – 2.4 ms) TE = shortest (<1.2 ms) FA = 35° BW = medium – high	1.5 T
3D RF-spoiled gradient echo	**TRICKS** (GE) **TWIST** (SIEMENS) **4D TRACK** (PHILIPS)	PD- to T1-weighted	20 seconds Forced expiration, free-breathing or hyperventilation	FOV = 300 mm Matrix = 80 × 100 SL = 3.2 mm sagittal	<400 ms/ volume	TR = shortest (<2 ms) TE = minimum (<1.1 ms) FA = 2° BW = medium – high	1.5 T and 3.0 T

Reprinted from pending MRI Clinics Article, permission pending

dynamic imaging are routinely performed in MRI of the chest. This often allows MRI to provide greater information about tissue composition than CT. MR imaging findings in the spectrum of anomalies and abnormalities of the pediatric chest are presented and illustrated in the following section.

Vascular Thoracic Anomalies and Abnormalities

In children, echocardiography is often the first imaging modality used to evaluate mediastinal vascular anomalies, as it is often able to provide diagnostic images without the use of ionizing radiation or intravenous contrast [14]. Cross-sectional imaging with MRI or CT is often indicated to further characterize lesions first detected on echocardiography [15]. MRI has a well-established role in the evaluation of mediastinal vascular anomalies and abnormalities in children. MRA is typically able to provide excellent depiction of the mediastinal vasculature and provide necessary information for diagnosis and surgical planning. In many centers, contrast-enhanced MRI with MRA has replaced contrast-enhanced CT angiography for this indication. Although MRI has the advantage of not requiring ionizing radiation, MRI requires longer acquisition times compared to CT and is more susceptible to motion artifact. Therefore sedation or anesthesia is often needed to perform MRI in pediatric patients. In this scenario, the risks of ionizing radiation must be balanced with the risks of sedation when choosing between CT and MRI.

MR imaging findings of several commonly encountered mediastinal vascular anomalies and abnormalities associated with congenial lung malformations are illustrated in the following sections.

Obstructive Lesions

Interrupted Aortic Arch

Interrupted aortic arch (IAA) is a congenital condition defined by discontinuity between the ascending and descending thoracic aorta. IAA is rare, occurring in approximately 2 per 100,000 live births [15]. IAA is classified into type A (arch interruption is distal to the origin of the left subclavian artery), type B (arch interruption is between the origins of the left common carotid and left subclavian arteries), and type C (arch interruption is between the origins of the brachiocephalic and left common carotid arteries). In a review of 95 cases by Schreiber et al., 13% were type A, 84% were type B, and 3% were type C [16]. The right subclavian artery may arise normally (subtype 1), distal to left subclavian artery (subtype 2), or from a right ductus arteriosus (subtype 3). IAA is often associated with other congenital cardiac lesions, most commonly ventriculoseptal defect (VSD), patent ductus arteriosus and truncus arteriosus, and specific associations vary depending on the type of IAA [15]. IAA typically causes symptoms soon after birth with heart failure or shock, which typically worsens with closure of the ductus arteriosus [15, 17]. Initial treatment is with IV prostaglandin to maintain patency of the ductus arteriosus, followed by surgical correction in the first few days of life [15, 17].

Imaging evaluation of IAA is essential to surgical planning. Traditionally, this was achieved with a combination of echocardiography and catheter angiography [17]. However echocardiography can sometimes be limited in the evaluation of the aorta, and catheter angiography is invasive; therefore CTA and MRA may be utilized [17, 18]. MRA may be preferable to CTA given the lack of associated ionizing radiation, although MRA does often require sedation or anesthesia. The characteristic imaging finding of IAA on MRI is nonvisualization of a portion of the aortic arch [17]. This is typically well visualized on both unenhanced and contrast-enhanced MRA sequences.

Coarctation of Aorta

Aortic coarctation is characterized by focal narrowing of the aorta in the region of the aortic isthmus, defined as the portion of the aorta between the origin of the left subclavian artery and the ductus arteriosus [15]. Coarctation of the aorta is relatively common, occurring in approximately 4 of 10,000 live births [19]. Aortic coarctation may be associated with other congenital heart defects, most commonly VSD and bicuspid aortic valve [15, 20]. Within the first few months of life, collateral arteries begin to form between the proximal and distal aorta in order to allow blood flow to bypass the aortic narrowing [15]. Clinical presentation is usually during infancy, with heart murmur, decreased femoral pulses, and supine arm-leg blood pressure gradient of greater than 20 mmHg [21]. Early diagnosis and treatment is important to reduce development of long-term sequelae. Surgical treatment is preferred in infants and young children, and percutaneous transcatheter treatment is preferred in older patients [21].

The primary imaging modality used for initial diagnosis of aortic coarctation in the newborn and infant is echocardiography [14]. However, poor sonographic windows to this region often limit complete evaluation and advanced imaging with CT or MRI are routinely utilized for further characterization and surgical planning. CTA offers the advantage of excellent temporal resolution but requires ionizing radiation and is not able to provide hemodynamic information [21]. Therefore, MRI with three-dimensional contrast-enhanced MRA is often the preferred cross-sectional imaging modality for evaluation of aortic coarctation. The primary imaging finding in aortic coarctation on MRA is focal narrowing of the aorta in the region of the aortic isthmus (Fig. 21.1). In addition, large collateral vessels are often visible on

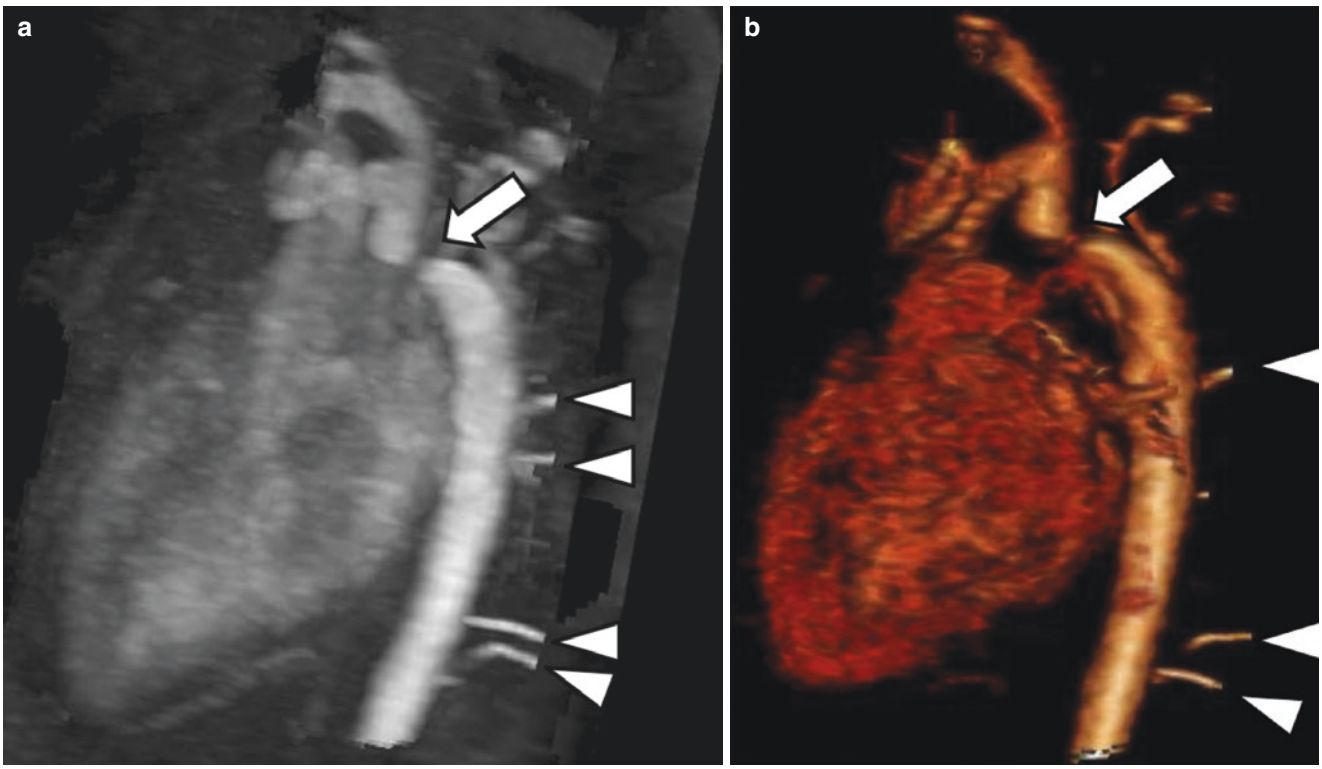

Fig. 21.1 A 2-year-old girl with aortic coarctation. (**a**) Maximum intensity projection image from enhanced T1-weighted MR angiogram with fat suppression shows narrowing (arrow) of the aortic isthmus and multiple collateral arteries (arrowheads) arising from the descending thoracic aorta. (**b**) 3D volume-rendered image from enhanced T1-weighted MR angiogram with fat suppression shows narrowing of the aortic isthmus (arrow) and multiple collateral arteries (arrowheads) arising from the descending thoracic aorta

MRA. Phase-contrast sequences can be used to estimate the pressure gradient across the coarctation and quantify collateral flow [21]. Given the lack of ionizing radiation, MRI is ideal for follow-up imaging. Long-term complications which may be seen on follow-up MRI include recoarctation, aneurysm, and dissection [21].

Vascular Rings and Sling

Double Aortic Arch

Double aortic arch occurs during embryonic development when the right arch does not regress and both the right and left arches persist [15]. The result is two aortic arches that encircle the trachea and esophagus, causing a vascular ring [15]. Signs and symptoms of double aortic arch are primarily due to mass effect on the trachea and esophagus. Compression of the trachea may cause wheezing, stridor, and tachypnea, and compression of the esophagus may cause dysphagia [22]. The aortic arches are often asymmetric in size. Dominant right arch with small left arch is most common (80%), while dominant left arch (10%) and balanced aortic arches (10%) are less common [23]. Preoperative imaging assessment is essential, as the smaller arch is typically resected [22, 24].

The imaging evaluation of double aortic arch often begins with echocardiography, which may depict the double arch and also evaluates for associated congenital heart disease, which is present in 12% of cases [22, 23]. Definition of the precise anatomy of double aortic arch is highly important for surgical planning, and advanced imaging with contrast-enhanced CTA or MRA is essential. Both CT and MRI have similar performance when depicting the double aortic arch [25]. MRI can often be successfully performed without sedation or anesthesia in infants, utilizing a "feed and swaddle" technique, and when possible MRI is preferred given the lack of ionizing radiation [26]. When the "feed and swaddle" technique is not successful, the risks of ionizing radiation with CT must be weighed against the risks of sedation and anesthesia with MRI. Imaging findings of double aortic arch include right and left aortic arches which both arise from the ascending aorta, encircle the trachea and esophagus, and then join to form a single descending thoracic aorta [15, 24] (Fig. 21.2). It is particularly important to define the arch anatomy in each case, identifying the smaller arch or depicting the balanced arch to aid in surgical planning and define which aortic arch to resect [22].

Right Aortic Arch with an Aberrant Left Subclavian Artery

Right aortic arch with an aberrant left subclavian artery is the most common type of right aortic arch and the second most common type of vascular ring after double aortic arch [15].

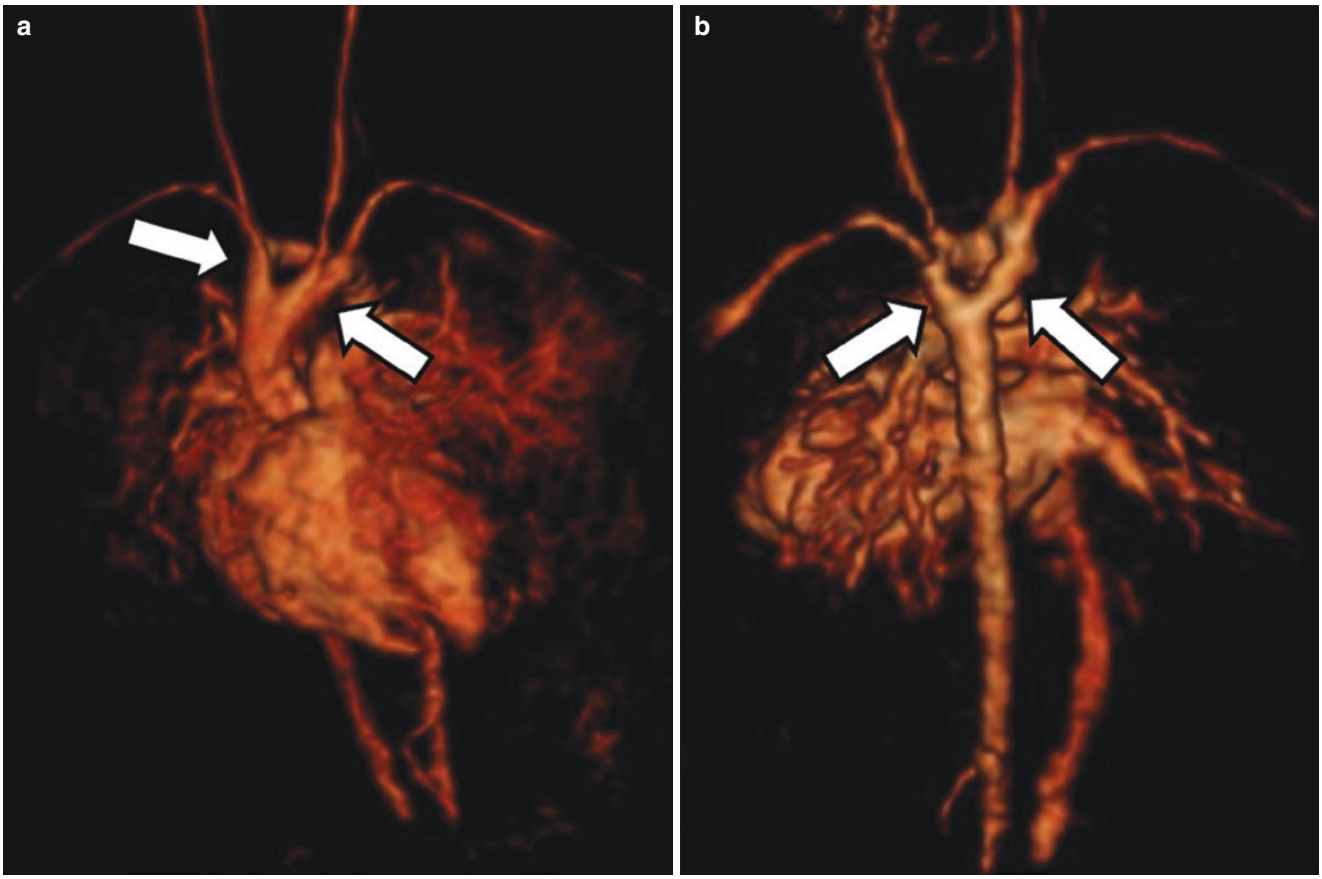

Fig. 21.2 A 1-year-old boy with double aortic arch. (**a**) Anterior oblique 3D volume-rendered image from contrast-enhanced time-resolved imaging of contrast kinetics (TRICKS) MR angiogram shows a double aortic arch (arrows). (**b**) Posterior 3D volume-rendered image from contrast-enhanced time-resolved imaging of contrast kinetics (TRICKS) MR angiogram shows a double aortic arch (arrows)

In this condition, the aortic arch is on the right, the left subclavian artery passes posterior to the esophagus, and the vascular ring is completed by a left-sided ductus arteriosus [15]. Most commonly, the left subclavian artery arises from a retroesophageal diverticulum of Kommerell [15]. The vascular ring in this condition is "looser" than the ring in a double aortic arch, and symptoms are typically less severe [22]. Treatment is with surgical division of the ligamentum arteriosus, and the diverticulum of Kommerell may also be resected [22].

Right-sided aortic arch may first be detected on chest radiography, demonstrating the aortic shadow to the right of the trachea, with leftward deviation of the trachea. Echocardiography typically also demonstrates the right-sided aortic arch. Cross-sectional imaging with CTA or MRA is indicated to evaluate the branching pattern. As previously discussed, MRA may be attempted with a "feed and swaddle" technique, but when not successful, the risks of ionizing radiation with CT must be weighed against the risks of sedation and anesthesia with MRI. On MRA of right aortic arch with an aberrant left subclavian artery, a single aortic arch is seen on the right, and the left subclavian artery typically arises from a dilated retroesophageal diverticulum of Kommerell [15, 24] (Fig. 21.3). The left ligamentum arteriosus may not be visible on MRI, although its presence may be inferred [27].

Pulmonary Artery Sling

Pulmonary artery sling is a rare vascular anomaly characterized by anomalous origin of the left pulmonary artery from the right pulmonary artery. The left pulmonary artery is located between the trachea and esophagus as it passes to the left hilum and typically causes compression of the right main bronchus and trachea. Extrinsic airway compression may lead to tracheobronchomalacia and air trapping [22, 27, 28]. In addition, intrinsic airway anomalies are associated with pulmonary artery sling including tracheobronchial branching anomalies and complete tracheal rings causing tracheobronchial stenosis [27, 28]. Pediatric patients with pulmonary artery sling typically present with respiratory symptoms within the first year of life, including stridor, wheezing, and recurrent pneumonia [22, 27, 28]. Surgical repair is recommended soon after diagnosis is established [22].

Diagnosis of pulmonary artery sling is typically made on MRI or CT, which are both well-suited to define the vascular anatomy and associated airway anomalies [27, 28]. The pri-

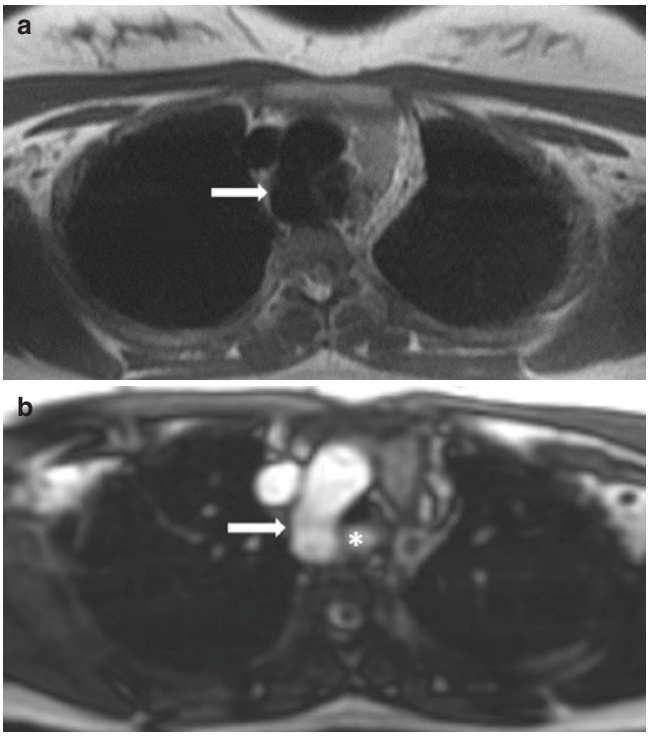

Fig. 21.3 A 12-year-old girl with right-sided aortic arch and aberrant left subclavian artery. (**a**) Axial 2D BB SSFSE MR image shows the abnormal position of arch the aortic (arrow), located on the right side of the mediastinum, consistent with the right aortic arch. (**b**) Axial 2D SSFP MR image demonstrates the right aortic arch (arrow) with an aberrant left subclavian artery (asterisk) passing posterior to the trachea and esophagus

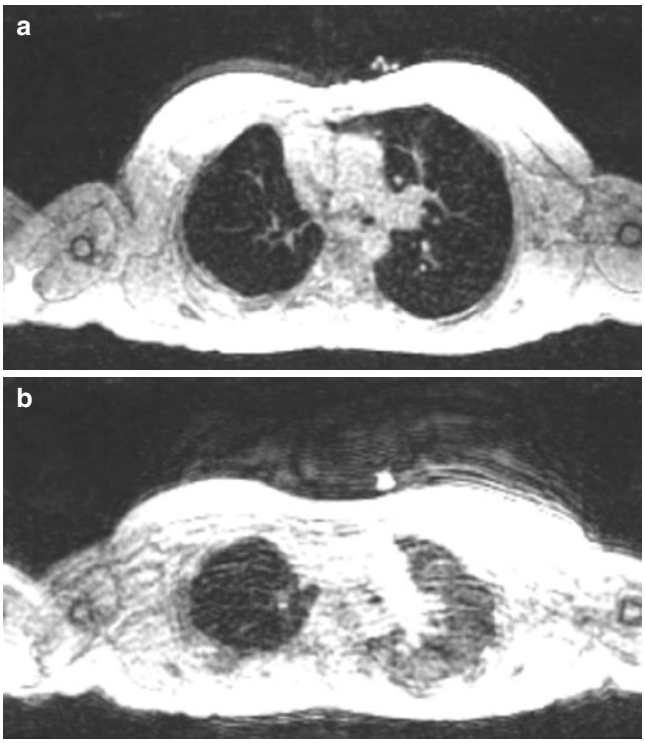

Fig. 21.4 A 11-year-old girl with pulmonary hypoplasia. (**a**) Axial 3D SPGR MR image obtained at end-inspiration demonstrates a smaller right lung compared to the left. (**b**) Axial 3D SPGR MR image obtained at end-inspiration shows a diffuse hypointensity of the right hypoplastic lung due to air trapping

mary advantage of MRI is its lack of ionizing radiation. However this benefit must be weighed against the risks of anesthesia, which is often required for MRI. Imaging is essential for surgical planning, and key elements to be assessed on MRI include pulmonary artery location and course, pulmonary artery caliber, airway branching pattern, airway caliber, and lung size to evaluate for air trapping [27]. 3D MRA sequences are ideal for characterization of the vascular anatomy. Nonfat-suppressed T1-weighted images are also excellent for depicting airway anatomy and assessing associated airway anomalies [27].

Congenital Lung Malformations

Pulmonary Hypoplasia

Pulmonary hypoplasia is a congenital anomaly of the pulmonary vasculature, airways, and parenchyma. Pulmonary hypoplasia is the least severe subtype of a larger group of pulmonary underdevelopment disorders which also include pulmonary agenesis and pulmonary aplasia [29]. Pulmonary agenesis is characterized by absent lung, airways, and vessels. Pulmonary aplasia has absent lung parenchyma and vessels, but a rudimentary bronchus is present. In pulmonary hypoplasia, the lung parenchyma, vessels, and airways are all present, but they are fewer and smaller than normal. The secondary form of pulmonary hypoplasia, in which a space-occupying process impedes pulmonary development, is most common. Primary pulmonary hypoplasia is encountered less frequently and can occur in isolation or in association with other conditions such as scimitar syndrome or horseshoe lung [30–33].

In the more common secondary form, pulmonary hypoplasia is often first appreciated on imaging studies in the context of the underlying space-occupying process. For example, in pulmonary hypoplasia secondary to congenital diaphragmatic hernia, the diagnosis is most often first appreciated on prenatal ultrasound or neonatal chest radiograph when intra-abdominal viscera are seen within the thorax. In these cases, postnatal MRI has less of a role in the diagnosis of pulmonary hypoplasia, but MRI may occasionally be performed to evaluate the hernia and visualize the size of the hypoplastic lung. In the less common primary form, thoracic MRI can play a large role in the diagnosis and management of pulmonary hypoplasia. In this scenario, a small lung may first be detected on chest radiograph, prompting work-up with cross-sectional imaging. MRI may then be obtained and show a small lung with small airways on standard T1- and T2-weighted images, and MRA may show small pulmonary arteries and veins (Fig. 21.4). MRI is also useful to evaluate

for associated conditions including scimitar syndrome, horseshoe lung, and congenital heart disease [34, 35].

Pulmonary Sequestration

Pulmonary sequestration is a congenital lung lesion characterized by an abnormal arterial supply from the systemic circulation and an abnormal tracheobronchial connection [36]. Pulmonary sequestration may be intralobar, in which the lesion shares a pleural covering with the adjacent normal lung and typically has venous drainage to the left atrium, or extralobar, in which the lesion has its own pleural covering and typically has venous drainage to a systemic vein [37–39]. Intralobar sequestration typically occurs in the lower lobes, and extralobar sequestration may occur in the lower lobes, below the diaphragm or within the mediastinum [37–39]. Pulmonary sequestration is at increased risk for pneumonia, and historically diagnosis was often established during the work-up of recurrent pneumonia. In current medical practice, most cases of pulmonary sequestration are first detected on prenatal sonogram as an incidental finding, in which a focal lung lesion is detected on gray-scale images and color Doppler demonstrates a systemic feeding artery [40]. Treatment for symptomatic pulmonary sequestration is surgical resection. Treatment for incidentally detected asymptomatic pulmonary sequestration is more variable and may involve watchful waiting or elective surgical resection due to concern about subsequent infection and small risk for malignancy [41, 42].

Cross-sectional imaging is indicated prior to resection in order to aid in surgical planning. In current practice, the preferred modality for this indication is most often CTA with 2D and 3D reformations rather than MRA given the superior temporal and spatial resolution without the need for sedation or anesthesia. The issue of spatial resolution is particularly important in pulmonary sequestration, as anomalous vessels are often small and better depicted on CTA than MRA. However, in cases where ionizing radiation is of significant concern, MRA is a potential alternative to CTA. On MRI, pulmonary sequestration typically appears as a cystic or solid mass-like lesion within the lung, which is hyperintense on fluid-sensitive sequences [43] (Fig. 21.5). MRA typically demonstrates a systemic feeding artery from the aorta and venous drainage to the left atrium (in intralobar sequestration) or a systemic vein (in extralobar sequestration) [43].

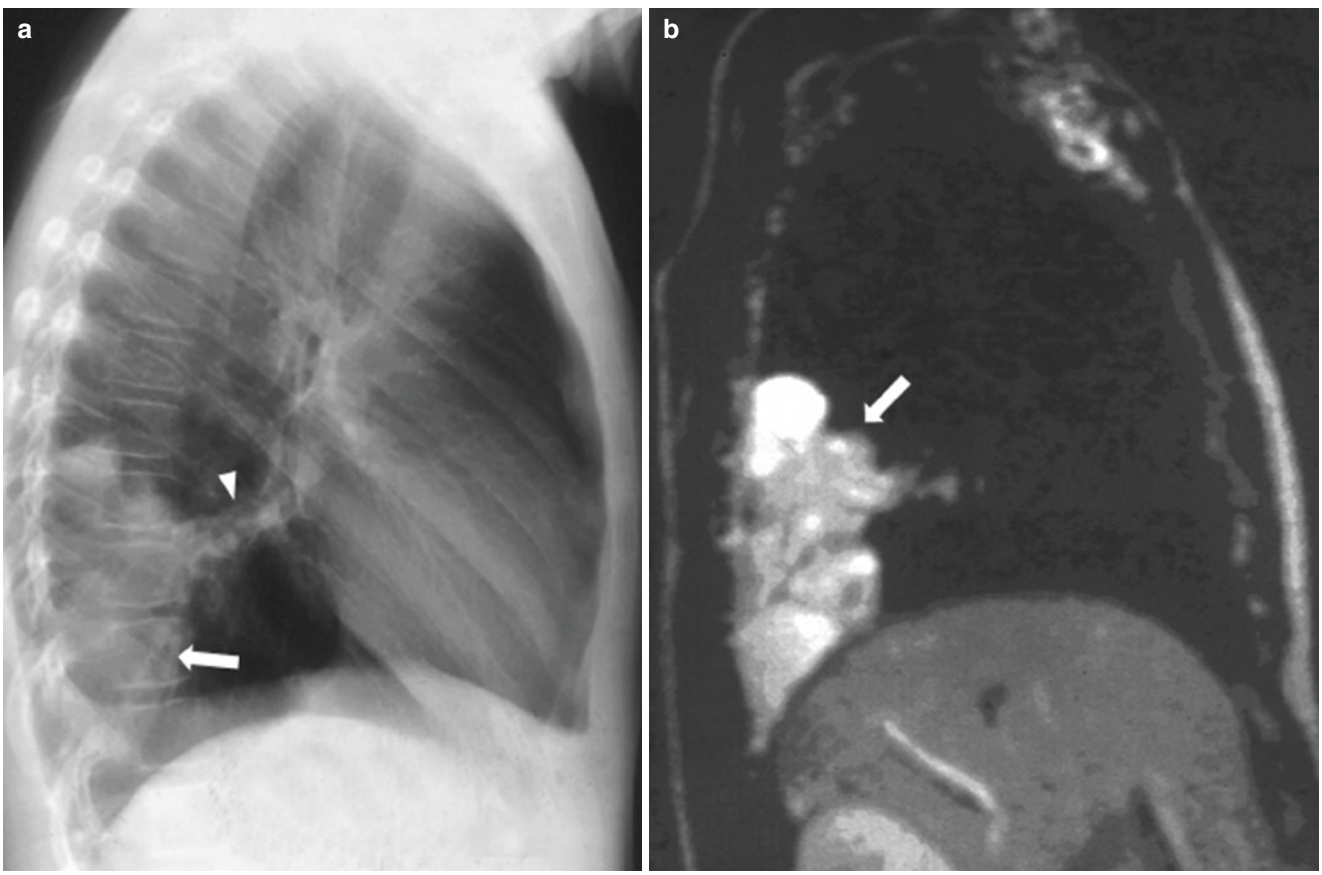

Fig. 21.5 Teenage boy with pulmonary sequestration. (**a**) Chest radiograph on left lateral view shows a large opacity (arrow) involving the dorsal region of the right lower lobe with a vascular connection (arrowhead) to the right hilum. (**b**) Sagittal T2-weighted fat-suppressed MR image shows a heterogeneous hyperintense mass-like lesion (arrow) confirmed after surgical resection as pulmonary sequestration. (Courtesy of Dr G Morana, Treviso, Italy)

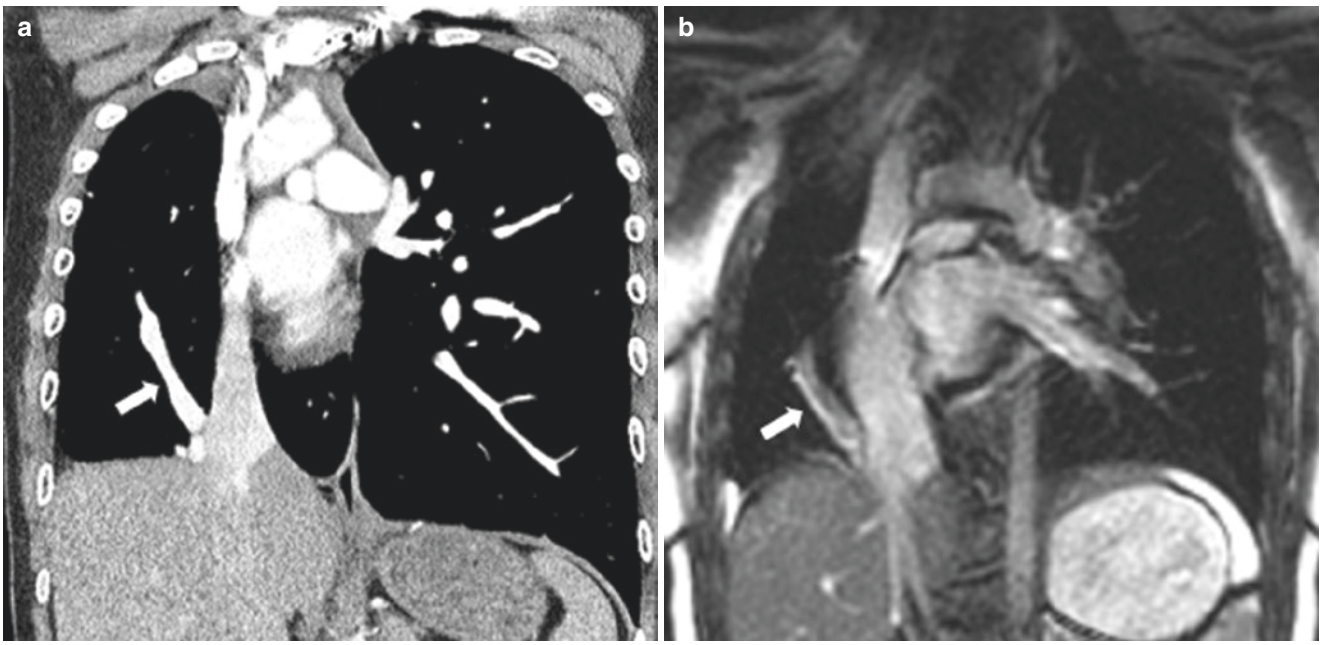

Fig. 21.6 A 11-year-old girl with scimitar syndrome. (**a**) Coronal contrast-enhanced CT image demonstrates a hypoplastic right lung drained by an anomalous vein (arrow) which is connected to the inferior vena cava. (**b**) Coronal 2D FIESTA MR image shows a hypoplastic right lung drained by an anomalous vein (arrow) which is connected to the inferior vena cava

Scimitar Syndrome

Scimitar syndrome, also known as congenital venolobar syndrome, is a congenital condition characterized by right lung hypoplasia and partial anomalous pulmonary venous return in which the anomalous vein drains the right lung into the inferior vena cava [44]. The name scimitar syndrome is derived from the appearance of the anomalous vein on chest radiography, which resembles a Turkish sword. Patients with scimitar syndrome may present to medical attention due to symptoms related to left-to-right shunting, associated congenital heart disease, or the findings may be incidentally noted on chest radiographs or other imaging tests. Patients presenting in infancy have more symptoms, aortopulmonary collaterals, coexisting congenital heart disease, extracardiac anomalies, and pulmonary hypertension than patients presenting later in life [45]. The optimal management strategy is controversial. Asymptomatic patients without significant shunting may be managed medically to prevent or control pulmonary hypertension [44]. Symptomatic patients with significant shunting may be treated surgically by reimplanting the scimitar vein into the left atrium or creating an intracardiac baffle between the scimitar vein ostium and the left atrium [44]. Mortality and vein stenosis/obstruction after baffle repair or scimitar vein reimplantation are higher for patients with infant-onset disease than for patients who present later [46].

When scimitar syndrome is suspected, cross-sectional imaging with CT or MRI with 2D and 3D angiographic reconstructions is recommended for confirmation of the diagnosis, mapping the anomalous vein, and surgical planning. MRI provides an advantage over CT, as it is able to quantify the Qp/Qs shunt ratio with phase-contrast sequences, and Qp/Qs >1.5 is an indication for surgery [44]. Both MRA and CTA are well-suited to depict the anatomy of the scimitar vein or veins, which may show a scimitar vein or veins draining one, two, or three lobes of the lung into the supradiaphragmatic or infradiaphragmatic IVC [44] (Fig. 21.6). Additional findings associated with scimitar syndrome that may be detected on MRI include pulmonary sequestration, accessory diaphragm, diaphragmatic hernia, variant lobar anatomy, right lung hypoplasia, right pulmonary artery hypoplasia, enlarged pulmonary arteries, congenital heart disease, aortic arch anomalies, right ventricular enlargement, dextroposition of the heart, and vertebral anomalies [44].

Nonvascular Thoracic Anomalies and Abnormalities

With increased utilization of cardiac MRI, most appreciate the potential role for MRI of the chest to evaluate the heart and mediastinal vasculature. MRI of the thorax for nonvascular lesions has been less widely adopted, largely because of the widespread availability and excellent imaging quality of CT for these indications. CT often provides the additional advantage of not requiring sedation or general anesthesia, which are often required for MRI in young uncooperative children. MRI provides the distinct advantage of not utilizing

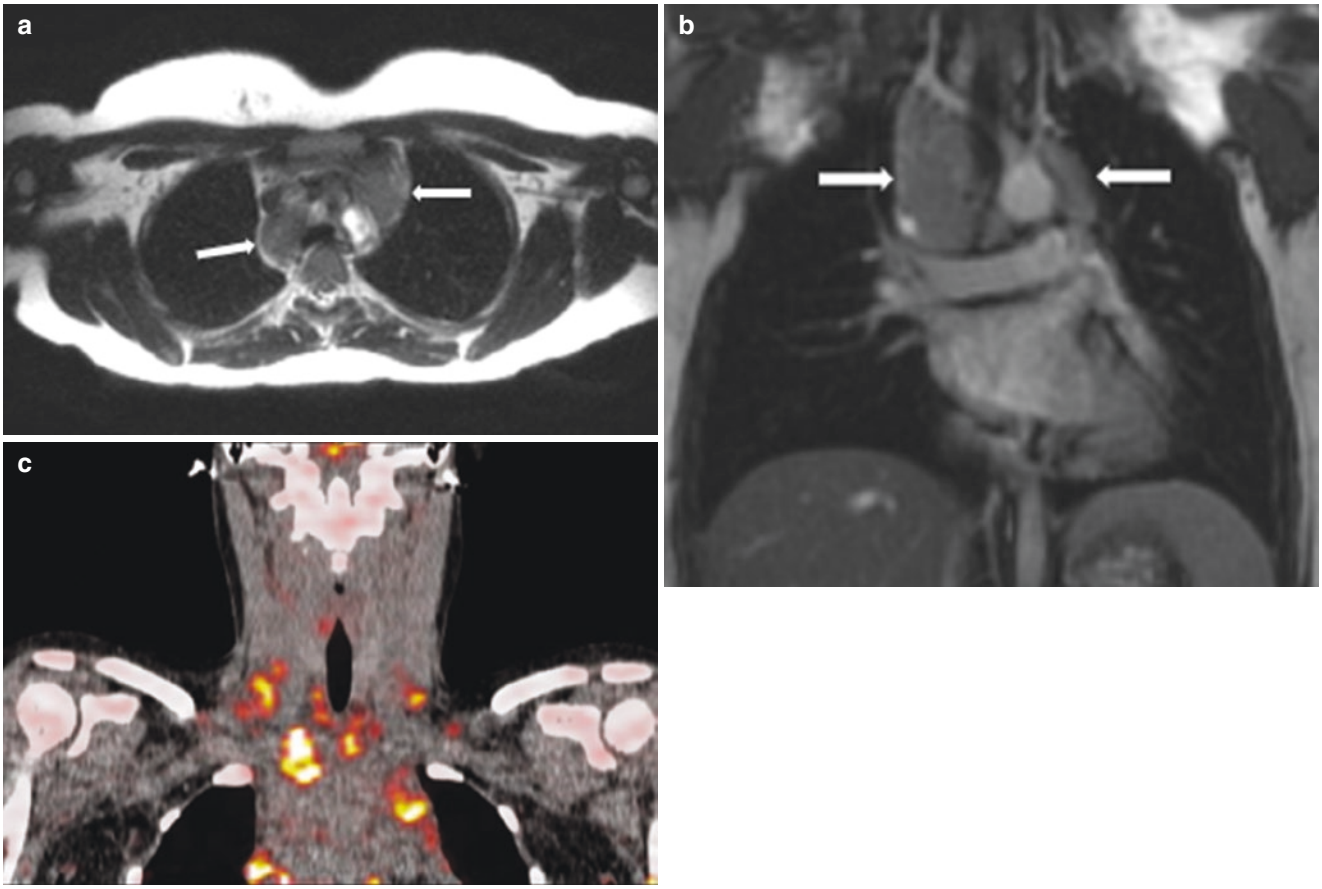

Fig. 21.7 A 12-year-old girl with Hodgkin lymphoma. (**a**) Axial T2-weighted HASTE MR image shows mediastinal lymphadenopathy (arrows). (**b**) Coronal contrast-enhanced T1-weighted FIESTA MR image shows mediastinal lymphadenopathy (arrows). (**c**) Fluoro-deoxyglucose (FDG) PET/CT MR image shows intense FDG uptake by the mediastinal lymph nodes

ionizing radiation, and as the imaging quality of MRI has improved in recent years, there has been increased interest in performing more imaging studies of the chest with MRI rather than CT. This might be most pertinent to children who can cooperate for MRI without sedation and would therefore potentially reap the benefit of a diagnostic study without risks of exposure to ionizing radiation or sedating medications. Potential nonvascular applications for MRI of the thorax described here include mediastinal masses, infectious disorders, lung anomalies, and airway disorders.

Mediastinal Masses

Lymphoma

Lymphoma is the third most common malignancy among patients aged 0–19 years [47]. It is the most common cause of an anterior mediastinal mass in a child [48, 49]. The currently recommended modality for staging of lymphoma is FDG-PET/CT [50]. However, FDG-PET/CT requires the use of ionizing radiation, which is of particular concern in children who require multiple staging examinations through the course of treatment. Due to these concerns, there is increased interest in whole-body MRI as a potential alternative for staging lymphoma [50]. Recommended protocols include T1-weighted, T2-weigthed STIR, and diffusion-weighted sequences [50]. Initial studies suggest good agreement between FDG-PET/CT and whole-body MRI for the staging of lymphoma [50].

Anesthesia is often required for MRI in young children who are unable to cooperate with instructions, but this can be a risk in lymphoma. Large anterior mediastinal masses may cause airway compression, obstruction of venous return, or obstruction of cardiac output, which may be exacerbated by general anesthesia [51]. When imaging an anterior mediastinal mass, it is essential to do so carefully and with as little sedation as possible. Furthermore, surgical procedures must also be approached with caution, and assessment of airway and vascular compression on cross-sectional imaging is essential to surgical and anesthesia planning [48, 49, 51].

The most common intrathoracic findings of lymphoma on MRI include an anterior mediastinal mass and lymphadenopathy (Fig. 21.7). When an anterior mediastinal mass is present due to thymic involvement, MRI typically shows an enlarged heterogeneous thymus on T1- and T2-weighted

images and increased signal intensity on diffusion-weighted images [50]. On T1- and T2-weighted images, lymph nodes can be assessed in a similar fashion as on CT and are considered enlarged when measuring greater than 1 cm in short-axis diameter. As discussed previously, assessment of airway compression is essential and is well evaluated on nonfat-suppressed T1-weighted MR images [52].

Teratoma

Germ cell tumors are the second most common anterior mediastinal mass in children after lymphoma [53]. Germ cell tumors are thought to derive from pluripotential primitive germ cells. Germ cell tumors most commonly occur in the gonads, but can occur outside the gonads along the midline of the body, 4% of which arise in the mediastinum [54]. The majority of mediastinal germ cell tumors are benign mature teratomas [53, 55]. Malignant mediastinal germ cell tumors include seminoma, embryonal carcinoma, teratocarcinoma, choriocarcinoma, and endodermal sinus tumor. Mediastinal teratomas may present with symptoms of respiratory distress, cough, chest pain, and weight loss, but approximately half of benign mature teratomas are incidentally detected on imaging performed for another reason [56]. The treatment for benign mature cystic teratoma is surgical resection, which is curative [53, 55, 56]. Treatment of malignant germ cell tumors depends on the type and extent of disease, but may include resection, chemotherapy, radiation therapy, or a combination [53, 55, 56].

Mature teratomas contain tissues from all three embryological layers, and the imaging appearance reflects the presence of multiple tissue types. Masses are most often located in the anterior mediastinum, demonstrate well-demarcated borders, and may contain cystic elements, fat, and calcification [57]. Although CT is most often utilized in the evaluation of mature teratomas, MRI is also well suited to characterize the different tissue compositions of the mass, given its superior contrast resolution. MRI findings may include a heterogeneous mass with cystic elements that are hyperintense on T2-weighted images and hypointense on T1-weighted images [57] (Fig. 21.8). Fat is often present and appears hyperintense on T1-weighted nonfat-suppressed images [57]. In and out of phase imaging demonstrates chemical shift artifact at fat-soft tissue interfaces, and fat-suppressed sequences may confirm presence of fat by showing signal loss compared to nonfat-suppressed sequences [58]. Malignant mediastinal germ cell tumors typically appear as solid enhancing mediastinal masses, which may invade adjacent structures. Superior contrast resolution makes MRI ideal for demonstrating violation of adjacent fat planes and extension to adjacent structures [57].

Lipoma

Lipomas are benign fat-containing masses, which are rare in children. Thoracic lipomas may occur in the mediastinum or chest wall. Mediastinal lipomas most often occur in the anterior mediastinum. They are most often asymptomatic and incidentally noted on chest radiography [58]. Symptoms may rarely occur due to mass effect and may include dysphagia, dyspnea, cough, jugular distention, and cardiac arrhythmias [58]. Surgical excision is curative and only necessary in patients with symptoms. The appearance on MR is a homogenous well-demarcated mass which is hyperintense on T1-weighted nonfat-suppressed sequences with signal loss on fat-suppressed sequences (Fig. 21.9).

Mediastinal lipomas should not be confused with lipoblastomas, which are also benign fat containing masses but have a different imaging appearance. Lipoblastomas are masses seen in young children, most detected before 3 years of age [59]. Unlike lipomas which are uniformly composed of fat, lipoblastomas contain prominent stromal elements. The MR imaging appearance of lipoblastoma is a mass which contains fat that is hyperintense on T1-weighted nonfat-suppressed sequences and loses signal on fat-suppressed sequences along with linear areas of soft tissue and fluid signal representing the fibrovascular network and cystic changes [58].

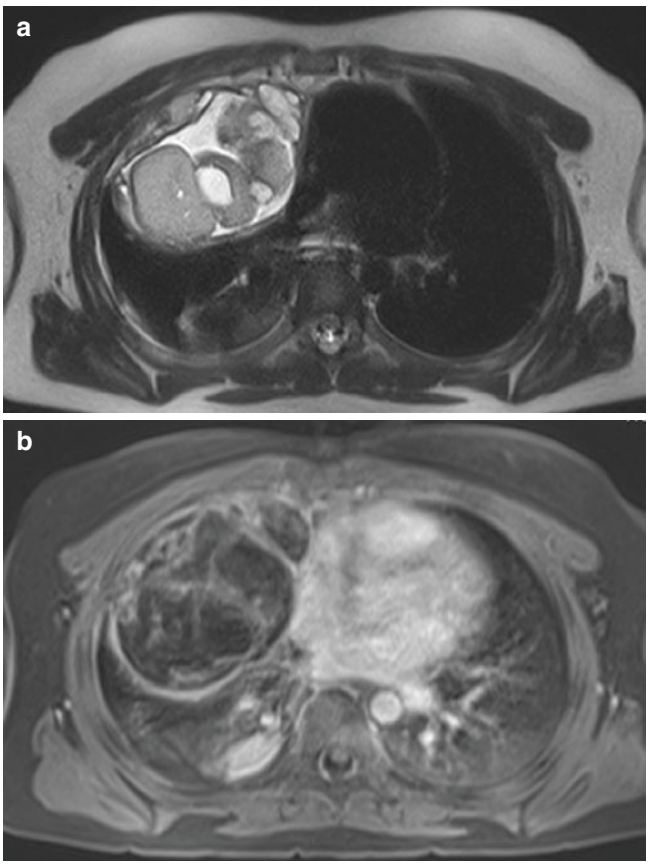

Fig. 21.8 A 14-year-old girl with mediastinal teratoma. (**a**) Axial T2-weighted HASTE MR image demonstrates a mediastinal mass with inhomogeneous signal intensity due to cystic and solid components. (**b**) Axial contrast-enhanced T1-weighted THRIVE MR image with fat suppression shows hyperenhancement of the wall and soft tissue components of the mass

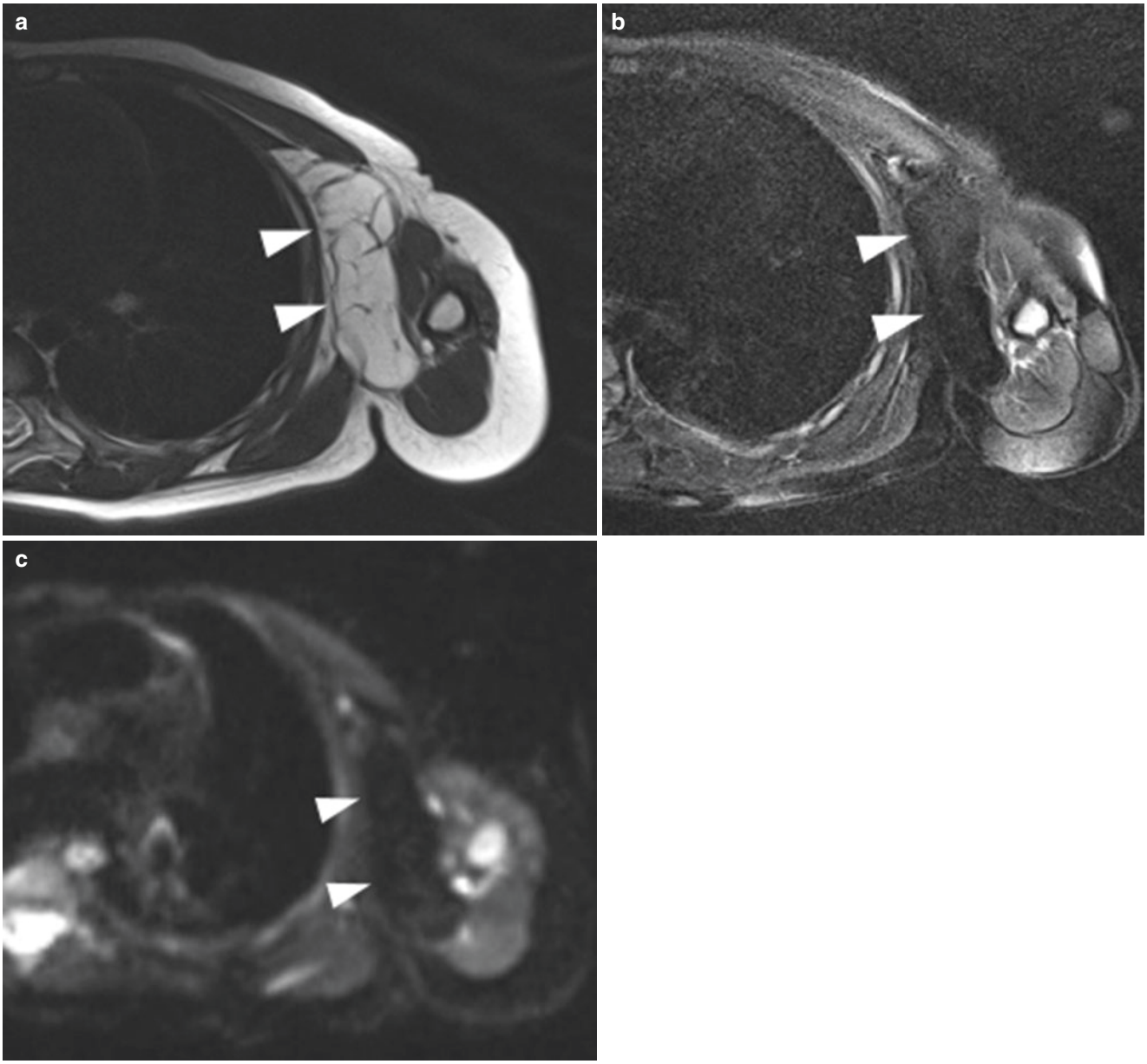

Fig. 21.9 A teenage boy with chest wall lipoma. (**a**) Axial T1-weighted BLADE MR image demonstrates a hyperintense multiseptated well-circumscribed mass (arrowheads) located in the left chest-wall. (**b**) Axial T2-weighted BLADE MR image with fat suppression shows a loss of signal within the mass (arrowheads), indicating fat. (**c**) Axial DWI MR image does not show restricted diffusion within the mass (arrowheads), indicating low cellularity

Neuroblastoma

Approximately 90% of posterior mediastinal masses in children are neurogenic tumors arising from the paraspinal sympathetic chains [60, 61]. Most of these are neuroblastomas, which are malignant tumors derived from neural crest cells. The majority of neuroblastomas occur in the adrenal glands; however, up to 20% occur within the posterior mediastinum [60]. Signs and symptoms may include fever, irritability, weight loss, anemia, and Horner syndrome if in the superior mediastinum [60]. Differential considerations for a posterior mediastinal mass include related neurogenic tumors that also arise from the sympathetic chain, including ganglioneuroblastoma and ganglioneuroma. Nerve sheath tumors are another differential consideration and include neurofibroma and schwannoma. The preferred treatment for neuroblastoma is surgical resection and chemotherapy [60].

MRI is the preferred imaging modality for the diagnosis and staging of mediastinal neuroblastoma due to its lack of ionizing radiation and superior ability to depict neuroforaminal and extradural intraspinal extension [61]. MRI is also well suited to detection of metastatic disease, which most commonly involves the liver, bone, bone marrow, and local

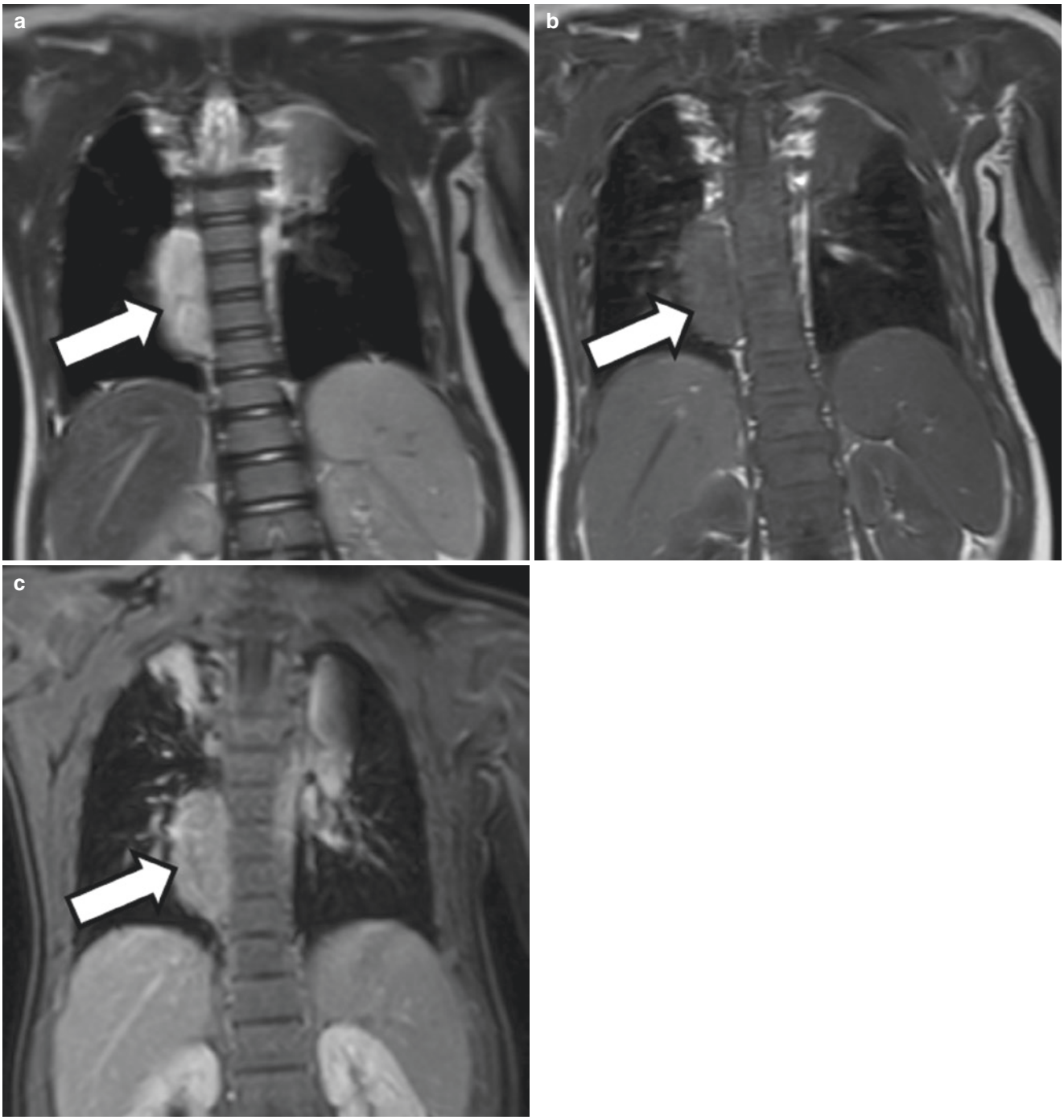

Fig. 21.10 A 19-month-old girl with thoracic neuroblastoma. (**a**) Coronal T2-weighted MR image shows a right paraspinal mass (arrow), which is hyperintense to the adjacent skeletal muscle. (**b**) Coronal T1-weighted MR image shows a right paraspinal mass (arrow), which is mildly hyperintense to the adjacent skeletal muscle. (**c**) Coronal enhanced T1-weighted MR image with fat suppression shows a right paraspinal mass (arrow), which is hyperenhancing compared to the adjacent skeletal muscle

lymph nodes. MRI does not depict calcification as well as CT, which is present in up to 30% of cases [60]. The typical appearance of neuroblastoma is an infiltrating mass which surrounds and encases vessels and adjacent structures. On MRI, neuroblastoma is typically heterogeneously hyperintense to skeletal muscle on T2-weighted images, mildly hyperintense on T1-weighted images, and heterogeneously enhances on contrast-enhanced images (Fig. 21.10).

Infectious Disorders

Tuberculosis

Although tuberculosis (TB) has become rare in the developed world, it continues to be a major cause of morbidity and mortality in the developing world. Worldwide, 12 million people are estimated to have active TB, and 1.5 million deaths are attributed to TB every year [62]. In the developed

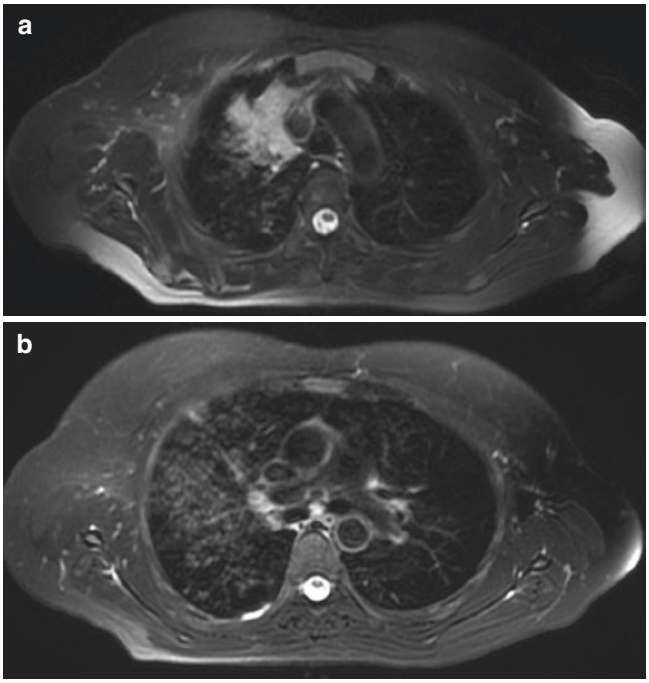

Fig. 21.11 A 16-year-old girl with tuberculosis. (**a**) Axial T2-weighted FRFSE MR image with fat suppression shows parenchymal consolidation in the right upper lobe. (**b**) Axial T2-weighted FRFSE MR image with fat suppression acquired at a lower level demonstrates mucus plugging with "tree in bud" appearance in the right lung

world, TB most often affects those with lower income, migrants, and immunodeficiency [63]. The initial infection is referred to as primary TB and occurs when an exposed individual inhales respiratory droplets, and infection occurs within the lung. Primary infection most often causes mild symptoms of fever and cough. Symptoms can be more severe in progressive primary TB and may lead to significant airspace disease and intrathoracic adenopathy which may compress the airway [64, 65]. After primary infection the symptoms often improve, and infection becomes dormant. Reactivation TB can occur when infection worsens, and symptoms may include fever, weight loss, night sweats, productive cough, chest pain, and hemoptysis.

Imaging plays an important role in the management of TB, and chest radiography and CT are the main modalities used. MRI is less often utilized given the higher cost, more limited availability, and technical challenges, but can be considered in children who may require multiple imaging studies in order to reduce exposure to ionizing radiation, such as those with immunodeficiency. MRI findings in pulmonary TB may include consolidation with or without cavitation, ground-glass signal abnormality, pulmonary nodules, lymphadenopathy, and pleural effusion [66, 67] (Fig. 21.11). It has been suggested that MRI may be superior to CT for evaluation of nodal disease and pleural effusion in TB infection [66]. T2- and STIR-weighted sequences may show pulmonary necrosis in TB as a region of low signal intensity centered within a region of consolidation [67]. However, MRI is known to be less sensitive than CT for ground-glass and tree-in-bud signal abnormalities [66].

Histoplasmosis

Histoplasmosis is endemic to many regions and infection is common. Infection most often causes only mild symptoms [68]. However, immunocompromised children may experience severe infection [68]. Infection may lead to intrathoracic lymphadenopathy, pulmonary consolidation, pulmonary nodules, cavitation, and bronchiectasis. A potential complication of histoplasmosis infection is mediastinal fibrosis.

MRI is not utilized in the routine management of histoplasmosis, though it may be considered in patients with concern about ionizing radiation, such as immunocompromised children who may require multiple imaging studies over their lifetimes. There is very little published literature describing the findings of pulmonary histoplasmosis on MRI. MRI findings may include enlarged intrathoracic lymph nodes, ill-defined pulmonary nodules, and pulmonary consolidation, all of which are hyperintense on T2-weighted images [69] (Fig. 21.12).

Aspergillosis

Aspergillus fumigatus is an airborne fungus that is ubiquitous within the environment [70]. In normal immunocompetent children, inhalation of the fungus most often causes no symptoms or illness. *Aspergillus*-related lung disease may occur in children with immunodeficiency or underlying lung disease, and the manifestations depend on the immunologic status of the child [70]. Three different forms of pulmonary aspergillosis include aspergilloma within a preexisting cavity, allergic bronchopulmonary aspergillosis (ABPA), and invasive aspergillosis.

Pulmonary aspergillosis is most often diagnosed and managed on the basis of chest radiographs and CT. MRI might be considered for children in whom there is concern about the effects of ionizing radiation, although there are few descriptions of MRI findings in pulmonary aspergillosis in the medical literature. Pulmonary aspergilloma appears as a "fungus ball" within a cavity that is hypointense on both T1- and T2-weighted images [71]. ABPA appears as dilated bronchi and bronchioles containing impacted material which is hyperintense on T1-wieghted images and hypointense on T2-wieghted images [72, 73] (Fig. 21.13). The signal characteristics of the impacted material are the opposite of water, and this pattern is called the inverted mucoid impaction signal sign, which is characteristic for ABPA [72, 73]. Invasive aspergillosis appears as round and nodular areas of signal abnormality, which classically have the appearance of a "target." The "target" is formed by an outer portion demonstrating high signal intensity on T1- and T2-weighed images and enhancement on post-contrast images surrounding a central area of hypointensity [74, 75].

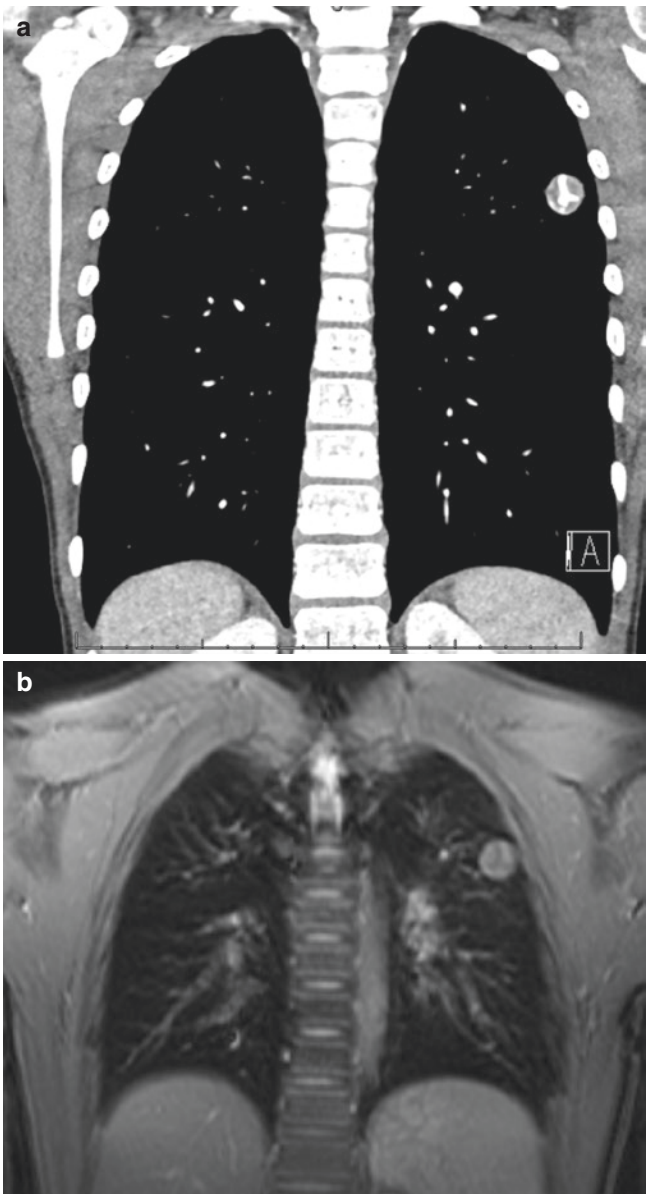

Fig. 21.12 A 9-year-old boy with histoplasmosis. (**a**) Coronal contrast-enhanced CT image in soft tissue window setting shows a round nodule within the left upper lobe with central calcification. (**b**) Coronal contrast-enhanced LAVA MR image shows the left upper lobe nodule with a hypointense non-enhancing central portion at the site of calcification

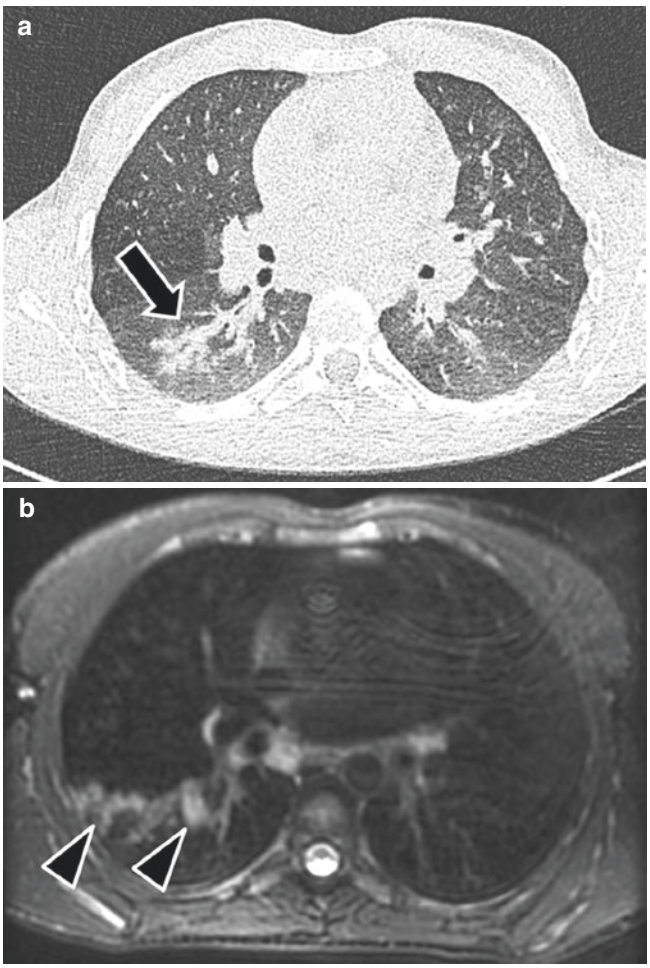

Fig. 21.13 A 12-year-old boy with cystic fibrosis and *Aspergillus* infection. (**a**) Axial non-enhanced lung window setting CT image shows right lower lobe bronchiectasis containing impacted material (arrow). (**b**) Axial T2-weighted MR image with fat suppression shows right lower lobe bronchiectasis containing impacted hyperintense mucus (black arrowheads) due to *Aspergillus*

Lung Anomalies and Abnormalities

Congenital Pulmonary Airway Malformation

Congenital pulmonary airway malformations (CPAMs) (previously known as congenital cystic adenomatoid malformations (CCAMs)) are malformations of the lung which are composed of cysts and bronchiolar overgrowth without a normal connection with the airway [37, 39]. Cysts may range in size from microscopic to large. Large cysts are visible on gross inspection and imaging. When composed of microscopic cysts, the appearance is that of a solid mass on gross inspection and on imaging. CPAMs are frequently diagnosed on prenatal ultrasound and are asymptomatic at birth. CPAMs are at risk for superinfection and may present with infectious symptoms at the time of superinfection. Surgical resection is the preferred treatment for symptomatic CPAMs. Asymptomatic CPAMs may be removed due to risk for subsequent superinfection and small risk of malignancy or may be managed conservatively with a watchful waiting approach [76–81].

Radiologists most commonly use the updated and modified Stocker classification system when describing CPAMs [37, 39, 82–86]. In this system, there are five types of CPAM.

Type 0 CPAMs are incompatible with life and cause diffuse acinar dysgenesis or tracheobronchial dysplasia. Type 1 CPAMs are macrocytic, containing one or more cysts measuring >2 cm. Type 2 lesions are composed of

smaller macrocysts measuring <2 cm. Type 3 CPAMs are microcystic and appear as solid masses on gross inspection and imaging, but small cysts <5 mm are evident at microcopy. Type 4 lesions are characterized by large cysts located within the periphery of the lung and appear similar to Type 1 CPAMs.

CPAMs may be visible on neonatal chest radiograph as an air-filled cystic lesion or a solid mass, depending on the type [87]. Alternatively, a CPAM detected on prenatal ultrasound may not be visible on chest radiographs after birth [38–40]. When surgical resection is being considered, cross-sectional imaging is required to localize and evaluate the lesion. Although classic CPAMs are not associated with anomalous vascular supply, cross-sectional imaging with 2D and 3D angiographic technique is advised since pulmonary sequestration and hybrid lesions (combined CPAM and sequestration) are often differential considerations. In current practice this is most often achieved with contrast-enhanced CTA. Contrast-enhanced MRI with MRA can be considered as an alternative to CTA in certain situations, such as when there is substantial concern for radiation exposure. Fluid-filled Type 1, 2, and 4 CPAMs are well-seen on T2-weighted images as hyperintense cysts, which on contrast-enhanced images demonstrate a thin enhancing wall [43]. Air-filled Type 1, 2, and 4 CPAMs are not as easily seen on MRI, since the air-filled cyst may appear similar to the adjacent aerated lung [43]. Type 3 CPAMs are well visualized on contrast-enhanced images as a solid enhancing mass (Fig. 21.14).

Lymphangiectasia

Pulmonary lymphangiectasia is a congenital condition characterized by dilated pulmonary lymphatics and chylous pleural effusions [88, 89]. It is associated with congenital heart disease, trisomy 21 and Noonan syndrome [90]. Newborns with pulmonary lymphangiectasia typically present with severe respiratory symptoms. In the past, pulmonary lymphangiectasia was considered to be a fatal condition, but mortality rates have decreased due to improvements in treatment and better survival among affected patients with a late-onset form of the condition [89–91]. Pulmonary lymphangiectasia is often challenging to diagnose, but may be suggested by performing thoracentesis after a fatty meal, and pleural fluid will be chylous.

Imaging findings are somewhat nonspecific in pulmonary lymphangiectasia, but imaging is essential to the evaluation and work-up of the condition. Radiographs and CT are the most commonly utilized modalities in this condition. Chest radiographs typically show interstitial thickening and pleural effusion, and CT typically shows interlobular septal thickening, ground-glass opacities, and pleural effusion [91, 92]. MRI is not routinely performed for this indication, but patients with congenital heart disease-related pulmonary lymphangiectasia may have an MRI during the work-up of cardiac disease, and findings may be detected. Findings on MRI are similar to the findings on CT and include interlobular septal thickening which is hyperintense on T2-weighted images and pleural effusion [43].

Cystic Fibrosis

Cystic fibrosis (CF) is an inherited autosomal recessive disease caused by mutations in the CF transmembrane regulator (CFTR) gene. CF is the most common autosomal recessive disease in Caucasians [93]. The mutation leads to decreased transmembranous chloride transport causing secretions to be thick and viscous, leading to manifestations with the lung, gastrointestinal tract, and exocrine systems. In the neonatal period, affected patients may be asymptomatic, have respiratory symptoms, or present with meconium ileus. Screening blood tests for CF are now included with newborn screening in all 50 states in the USA, and diagnosis is often established before substantial symptoms occur.

Pulmonary manifestations of CF include air trapping, mucus impaction, airway wall thickening, and bronchiectasis [94–96]. Imaging plays a key role in monitoring disease progression and offers many advantages over pulmonary function tests (PFTs) alone [96]. CT has served as the reference standard for CF, and established advantages of CT over PFTs include evaluation of regional disease severity, greater sensitivity for detection of disease progression, and detection of structural changes before PFTs become abnormal [96]. However, CF is a lifelong disease, and numerous imaging tests are required over a patient's lifetime. Repeated CTs have the potential to lead to large cumulative radiation doses. As a result, MRI has emerged as an alternative imaging modality that does not require ionizing radiation [97]. Although the spatial resolution of MRI is lower than CT, increased signal associated with bronchiectasis, mucus plugging, and consolidation on MRI leads to improved contrast resolution, and sensitivity of MRI for these findings is comparable to CT [96, 98–100] (Fig. 21.15). Advanced MRI techniques including contrast-enhanced perfusion imaging and hyperpolarized gas ventilation imaging can provide functional information not available on CT [96]. New ultrashort echo time (UTE) sequences which overcome issues of rapid signal dephasing and low spatial resolution to produce "CT-like" images of the lung will likely further enhance the role of MRI in the evaluation of CF-related lung disease in the future [96, 101].

Common Variable Immunodeficiency

Common variable immunodeficiency (CVID) is a primary immunodeficiency syndrome characterized by low immunoglobulin levels. The syndrome may be caused by a variety of different genetic mutations. Clinical manifestations in a cohort of 473 patients described by Resnick et al. include recurrent

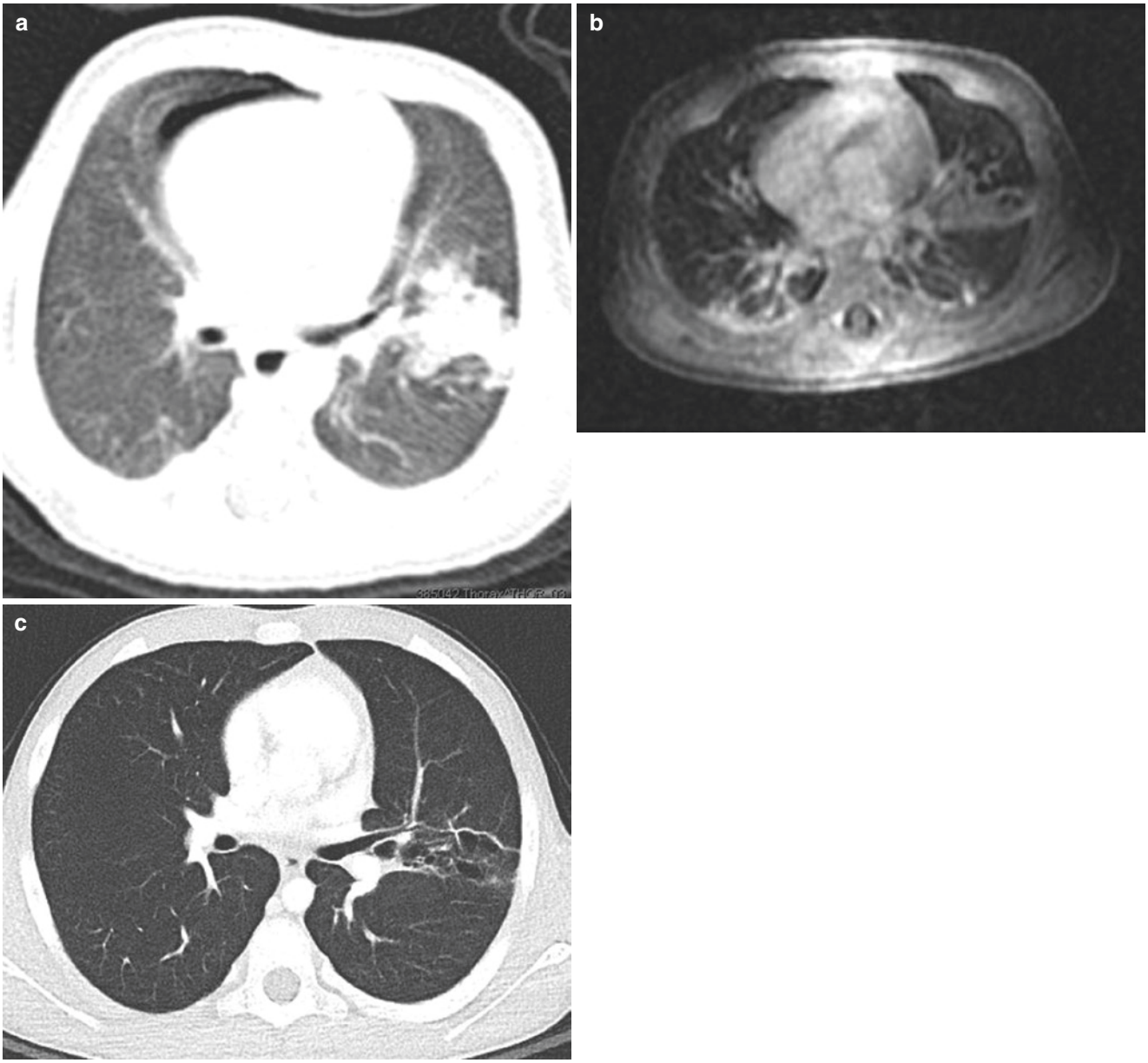

Fig. 21.14 A 3-year-old girl with congenital pulmonary airway malformation (CPAM) imaged at three different time points. (**a**) Axial non-enhanced lung window CT image obtained at day 1 of life shows consolidation within the left lower lobe. Small right pneumothorax is incidentally noted. (**b**) Axial contrast-enhanced SPGR MR image obtained at 6 months of age shows persistent consolidation within the left lower lobe. (**c**) Axial contrast-enhanced lung window setting CT image obtained at 8 years of age shows cystic appearance of left lower lobe CPAM after clearance of consolidation

infections (94%) and noninfectious complications including hematologic or organ-specific autoimmunity (28.6%), chronic lung disease (28.5%), bronchiectasis (11.2%), gastrointestinal inflammatory disease (15.4%), malabsorption (5.9%), granulomatous disease (9.7%), liver diseases and hepatitis (9.1%), lymphoma (8.2%), and other cancers (7.0%) [102]. Most cases of CVID are diagnosed in adulthood, but as many as 34% are diagnosed during childhood [103].

Pulmonary manifestations of CVID include pneumonia, chronic lung disease, and bronchiectasis. Imaging plays a key role in the diagnosis and management of these complications. Although CT is an excellent modality for the evaluation of these findings, patients with CVID are more susceptible to radiation-induced malignancy making MRI an attractive alternative [104, 105]. MRI findings in CVID may include consolidation, bullae, nodules, air trapping, and bronchiectasis with bronchial wall thickening and mucus plugging (Fig. 21.16).

In studies of patients with CVID, lung MRI was similar to CT for detection of moderate-to-severe disease including consolidation, bullae, mucus plugging, nodules, bronchial

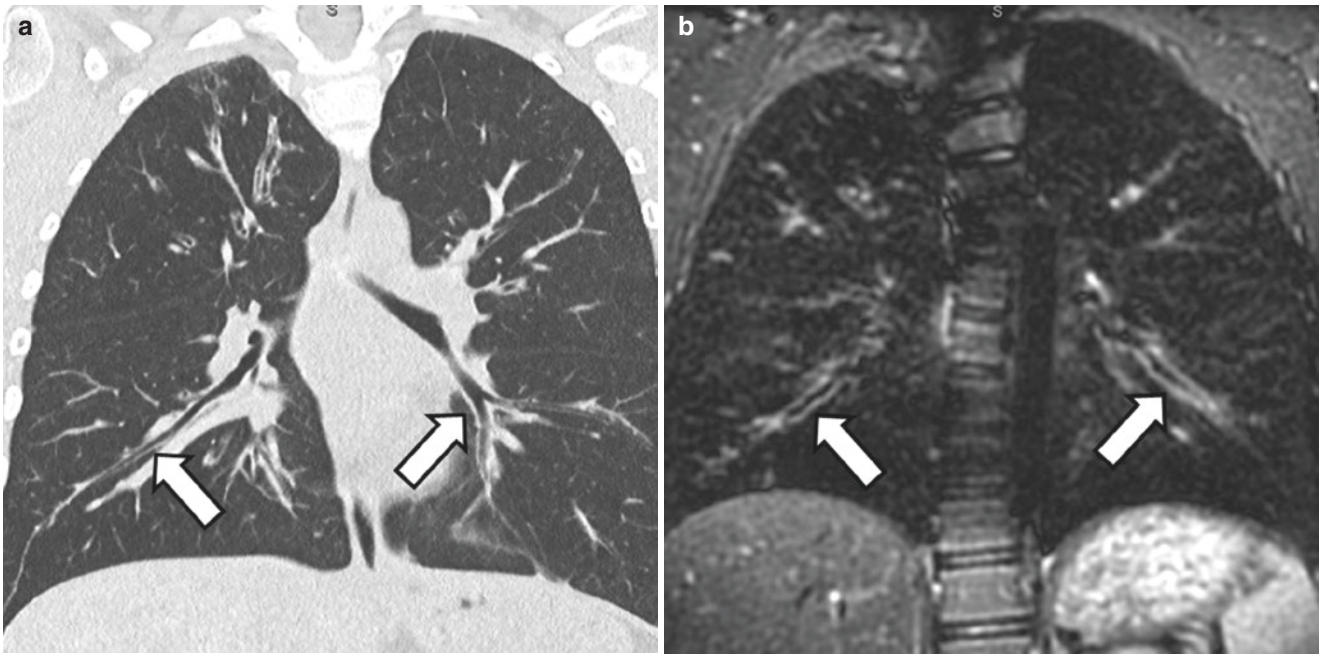

Fig. 21.15 A 13-year-old boy with cystic fibrosis. (**a**) Coronal non-enhanced lung window setting CT image shows bronchiectasis and bronchial wall thickening (arrows) in both lower lobes. (**b**) Coronal T2-weighted MR image with fat suppression shows bronchiectasis and hyperintense bronchial wall thickening (arrows) in both lower lobes

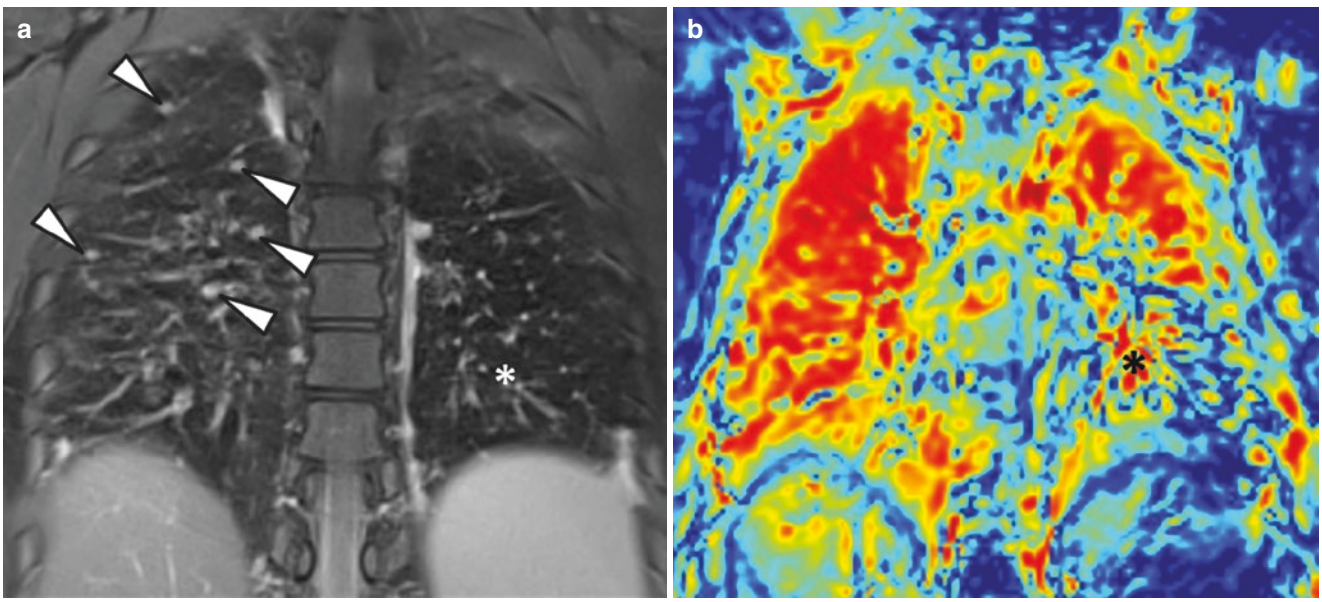

Fig. 21.16 A 19-year-old-girl with common variable immunodeficiency. (**a**) Coronal T2-weighted MR image with fat suppression shows multiple nodules in the right lung (arrowheads) representing lung granulomas and a large area of low signal intensity in the left lower lobe (white asterisk) representing air trapping. (**b**) Coronal ventilation map with Fourier decomposition shows region of hypoventilation (black asterisk) in the left lower lobe, matching then area of air trapping on the morphological image. (Courtesy of Dr G Morana, Treviso, Italy)

wall thickening, and bronchiectasis but was inferior to CT for detection of mild bronchial abnormalities [104, 105]. Despite the lower performance for detection of mild disease, MRI should be considered an important alternative to CT in patients with CVID given their increased sensitivity to ionizing radiation [104].

Dynamic Large Airway Disorder

Tracheomalacia

Tracheomalacia is a condition in which the cartilage of the airway becomes soft and losses its normal stiffness. When the intrathoracic pressure increases during normal expira-

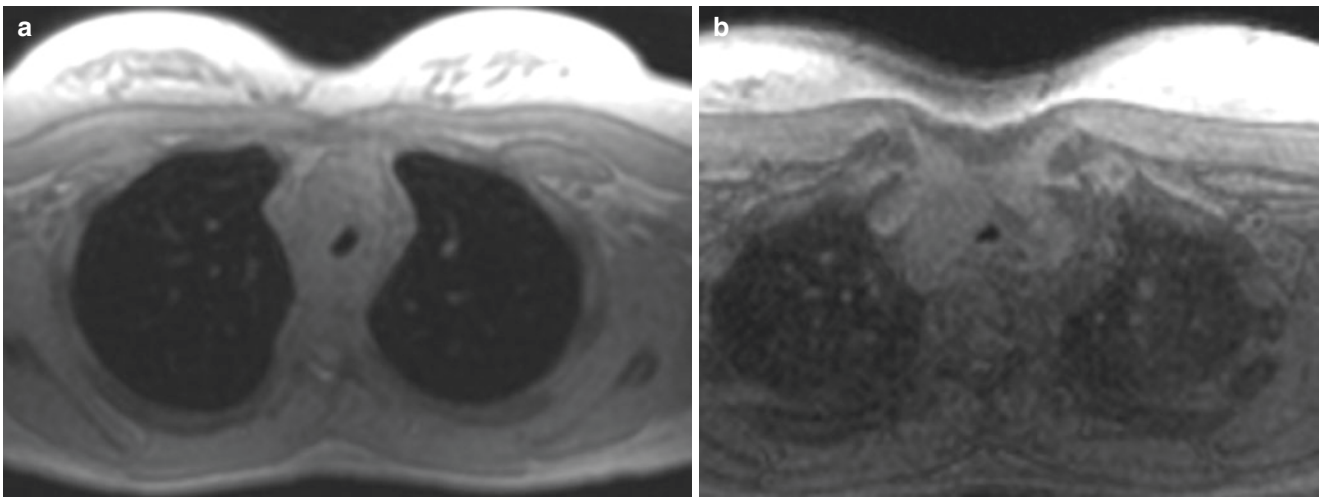

Fig. 21.17 A 8-year-old girl with tracheomalacia. (**a**) Axial 3D SPGR MR image obtained at end-inspiration shows narrowed caliber of the trachea. (**b**) Axial 3D SPGR MR image obtained at end-expiration shows further collapse of the trachea

tion, the weakened cartilage collapses, leading to airway narrowing and obstruction. The airway may be normal in caliber during inspiration when the intrathoracic pressure is negative. Tracheomalacia may be primary, due to intrinsic disorder of cartilage development, or secondary, due to acquired injury to the airway cartilage. The secondary form is more common and causes include trauma, intubation, infection, inflammation, and compression (e.g., by a dilated esophagus in cases of esophageal atresia) [106, 107]. Tracheomalacia is a relatively common cause of respiratory symptoms in children; 15–30% of children undergoing bronchoscopy for respiratory distress are diagnosed with tracheomalacia [108–110].

The gold standard for diagnosis of tracheomalacia is bronchoscopy; however noninvasive imaging is often preferred as a first step in the diagnostic work-up. In addition to being noninvasive, cross-sectional imaging provides the advantage of visualizing extraluminal structures which may be associated with tracheomalacia, such as vascular rings and pulmonary sling. When choosing an imaging test to evaluate tracheomalacia, it is important to consider the dynamic nature of the condition. The airway may appear normal during inspiration; therefore tracheomalacia is often incompletely evaluated on standard radiographs, CT or MRI which are routinely performed at end-inspiration. Therefore, imaging of tracheomalacia requires imaging during both inspiration and expiration or dynamic imaging through the respiratory cycle. Historically, this was achieved with fluoroscopy of the airway during breathing. However, detailed evaluation of the airway is often limited on fluoroscopy, and CT with inspiratory and expiratory image acquisition has become the preferred noninvasive imaging test by many given its ability to evaluate cross-sectional airway diameter and morphology and create 3D/4D reformations [107]. Although image quality is typically excellent with CT, there is concern about radiation exposure, and CT exams require scanning during multiple phases of respiration. This has motivated the development of new MRI techniques that allow dynamic imaging of the airway during breathing [5, 6]. By utilizing an MRI-compatible spirometer that is integrated with the image acquisition, images of the airway and end-inspiration, end-expiration, and cine images throughout the respiratory cycle can be obtained [5, 6]. MR imaging findings of tracheomalacia are similar to findings on CT and include excessive reduction in airway diameter during expiration, which may appear as a "frown" shape or complete collapse [107, 111] (Fig. 21.17). Dynamic spirometer-controlled MRI of the airways is not currently available outside of the research setting, but it is a practical application that may become more widely available in upcoming years.

References

1. Dournes G, Menut F, Macey J, et al. Lung morphology assessment of cystic fibrosis using MRI with ultra-short echo time at submillimeter spatial resolution. Eur Radiol. 2016;26:3811.
2. Ciet P, Tiddens HA, Wielopolski PA, et al. Magnetic resonance imaging in children: common problems and possible solutions for lung and airways imaging. Pediatr Radiol. 2015;45(13):1901–15.
3. Baez JC, Seethamraju RT, Mulkern R, Ciet P, Lee EY. Pediatric chest MR imaging: sedation, techniques, and extracardiac vessels. Magn Reson Imaging Clin N Am. 2015;23(2):321–35.
4. Ciet P, Serra G, Bertolo S, et al. Assessment of CF lung disease using motion corrected PROPELLER MRI: a comparison with CT. Eur Radiol. 2016;26(3):780–7.
5. Ciet P, Wielopolski P, Manniesing R, et al. Spirometer-controlled cine magnetic resonance imaging used to diagnose tracheobronchomalacia in paediatric patients. Eur Respir J. 2014;43(1):115–24.
6. Ciet P, Boiselle PM, Heidinger B, et al. Cine MRI of tracheal dynamics in healthy volunteers and patients with tracheobronchomalacia. AJR Am J Roentgenol. 2017;209(4):757–61.

7. Ciet P, Bertolo S, Ros M, et al. Detection and monitoring of lung inflammation in cystic fibrosis during respiratory tract exacerbation using diffusion-weighted magnetic resonance imaging. Eur Respir J. 2017;50(1):1601437.
8. Bauman G, Puderbach M, Heimann T, et al. Validation of Fourier decomposition MRI with dynamic contrast-enhanced MRI using visual and automated scoring of pulmonary perfusion in young cystic fibrosis patients. Eur J Radiol. 2013;82(12):2371–7.
9. Mithal LB, Patel PS, Mithal D, Palac HL, Rozenfeld MN. Use of gadolinium-based magnetic resonance imaging contrast agents and awareness of brain gadolinium deposition among pediatric providers in North America. Pediatr Radiol. 2017;47(6):657–64.
10. Voskrebenzev A, Gutberlet M, Kaireit TF, Wacker F, Vogel-Claussen J. Low-pass imaging of dynamic acquisitions (LIDA) with a group-oriented registration (GOREG) for proton MR imaging of lung ventilation. Magn Reson Med. 2017;78(4):1496–505.
11. Voskrebenzev A, Gutberlet M, Klimes F, et al. Feasibility of quantitative regional ventilation and perfusion mapping with phase-resolved functional lung (PREFUL) MRI in healthy volunteers and COPD, CTEPH, and CF patients. Magn Reson Med. 2018;79(4):2306–14.
12. Campbell RM Jr. VEPTR: past experience and the future of VEPTR principles. Eur Spine J. 2013;22(Suppl 2):S106–17.
13. Tiddens HA, Stick SM, Wild JM, et al. Respiratory tract exacerbations revisited: ventilation, inflammation, perfusion, and structure (VIPS) monitoring to redefine treatment. Pediatr Pulmonol. 2015;50(Suppl 40):S57–65.
14. Goudar SP, Shah SS, Shirali GS. Echocardiography of coarctation of the aorta, aortic arch hypoplasia, and arch interruption: strategies for evaluation of the aortic arch. Cardiol Young. 2016;26(8):1553–62.
15. Hanneman K, Newman B, Chan F. Congenital variants and anomalies of the aortic arch. Radiographics. 2017;37(1):32–51.
16. Schreiber C, Mazzitelli D, Haehnel JC, Lorenz HP, Meisner H. The interrupted aortic arch: an overview after 20 years of surgical treatment. Eur J Cardiothorac Surg. 1997;12(3):466–9; discussion 469–70.
17. Dillman JR, Yarram SG, D'Amico AR, Hernandez RJ. Interrupted aortic arch: spectrum of MRI findings. AJR Am J Roentgenol. 2008;190(6):1467–74.
18. Yang DH, Goo HW, Seo DM, et al. Multislice CT angiography of interrupted aortic arch. Pediatr Radiol. 2008;38(1):89–100.
19. Bjornard K, Riehle-Colarusso T, Gilboa SM, Correa A. Patterns in the prevalence of congenital heart defects, metropolitan Atlanta, 1978 to 2005. Birth Defects Res A Clin Mol Teratol. 2013;97(2):87–94.
20. Warnes CA. Bicuspid aortic valve and coarctation: two villains part of a diffuse problem. Heart. 2003;89(9):965–6.
21. Dijkema EJ, Leiner T, Grotenhuis HB. Diagnosis, imaging and clinical management of aortic coarctation. Heart. 2017;103(15):1148–55.
22. Backer CL, Monge MC, Popescu AR, Eltayeb OM, Rastatter JC, Rigsby CK. Vascular rings. Semin Pediatr Surg. 2016;25(3):165–75.
23. Backer CL, Mavroudis C, Rigsby CK, Holinger LD. Trends in vascular ring surgery. J Thorac Cardiovasc Surg. 2005;129(6):1339–47.
24. Kellenberger CJ. Aortic arch malformations. Pediatr Radiol. 2010;40(6):876–84.
25. Leonardi B, Secinaro A, Cutrera R, et al. Imaging modalities in children with vascular ring and pulmonary artery sling. Pediatr Pulmonol. 2015;50(8):781–8.
26. Fogel MA, Pawlowski TW, Harris MA, et al. Comparison and usefulness of cardiac magnetic resonance versus computed tomography in infants six months of age or younger with aortic arch anomalies without deep sedation or anesthesia. Am J Cardiol. 2011;108(1):120–5.
27. Dillman JR, Attili AK, Agarwal PP, Dorfman AL, Hernandez RJ, Strouse PJ. Common and uncommon vascular rings and slings: a multi-modality review. Pediatr Radiol. 2011;41(11):1440–54; quiz 1489–1490.
28. Lee KH, Yoon CS, Choe KO, et al. Use of imaging for assessing anatomical relationships of tracheobronchial anomalies associated with left pulmonary artery sling. Pediatr Radiol. 2001;31(4):269–78.
29. Biyyam DR, Chapman T, Ferguson MR, Deutsch G, Dighe MK. Congenital lung abnormalities: embryologic features, prenatal diagnosis, and postnatal radiologic-pathologic correlation. Radiographics. 2010;30(6):1721–38.
30. Berrocal T, Madrid C, Novo S, Gutierrez J, Arjonilla A, Gomez-Leon N. Congenital anomalies of the tracheobronchial tree, lung, and mediastinum: embryology, radiology, and pathology. Radiographics. 2004;24(1):e17.
31. Tilea B, Garel C, Delezoide AL, et al. Prenatal diagnosis of horseshoe lung: contribution of MRI. Pediatr Radiol. 2005;35(10):1010–3.
32. Jeewa A, Culham JA, Human DG. A case of horseshoe lung and complex congenital heart disease in a term newborn. Pediatr Radiol. 2010;40(2):206–9.
33. Hwang HK, Chen MR, Chen SJ, Kao HA, Lee KS, Shih SL. Horseshoe lung with pseudo-ring-sling complex. Pediatr Pulmonol. 2002;34(5):402–4.
34. Festa P, Lamia AA, Murzi B, Bini MR. Tetralogy of fallot with left heart hypoplasia, total anomalous pulmonary venous return, and right lung hypoplasia: role of magnetic resonance imaging. Pediatr Cardiol. 2005;26(4):467–9.
35. Mahani MG, Morani AC, Lu JC, et al. Non-cardiovascular findings in clinical cardiovascular magnetic resonance imaging in children. Pediatr Radiol. 2016;46(4):473–82.
36. Pryce DM. Lower accessory pulmonary artery with intralobar sequestration of lung; a report of seven cases. J Pathol Bacteriol. 1946;58(3):457–67.
37. Lee EY, Dorkin H, Vargas SO. Congenital pulmonary malformations in pediatric patients: review and update on etiology, classification, and imaging findings. Radiol Clin N Am. 2011;49(5):921–48.
38. Lee EY, Boiselle PM, Cleveland RH. Multidetector CT evaluation of congenital lung anomalies. Radiology. 2008;247(3):632–48.
39. Epelman M, Daltro P, Soto G, Ferrari CM, Lee EY. Congenital lung anomalies. In: Coley BD, editor. Caffey's pediatric diagnostic imaging. 12th ed. Philadelphia: Elsevier; 2013. p. 550–66.
40. Epelman M, Kreiger PA, Servaes S, Victoria T, Hellinger JC. Current imaging of prenatally diagnosed congenital lung lesions. Semin Ultrasound CT MR. 2010;31(2):141–57.
41. Eber E. Antenatal diagnosis of congenital thoracic malformations: early surgery, late surgery, or no surgery? Semin Respir Crit Care Med. 2007;28(3):355–66.
42. Laje P, Liechty KW. Postnatal management and outcome of prenatally diagnosed lung lesions. Prenat Diagn. 2008;28(7):612–8.
43. Liszewski MC, Hersman FW, Altes TA, et al. Magnetic resonance imaging of pediatric lung parenchyma, airways, vasculature, ventilation, and perfusion: state of the art. Radiol Clin N Am. 2013;51(4):555–82.
44. Masrani A, McWilliams S, Bhalla S, Woodard PK. Anatomical associations and radiological characteristics of Scimitar syndrome on CT and MR. J Cardiovasc Comput Tomogr. 2018;12:286.
45. Dusenbery SM, Geva T, Seale A, et al. Outcome predictors and implications for management of scimitar syndrome. Am Heart J. 2013;165(5):770–7.
46. Wang H, Kalfa D, Rosenbaum MS, et al. Scimitar syndrome in children and adults: natural history, outcomes, and risk analysis. Ann Thorac Surg. 2018;105(2):592–8.

47. Li J, Thompson TD, Miller JW, Pollack LA, Stewart SL. Cancer incidence among children and adolescents in the United States, 2001–2003. Pediatrics. 2008;121(6):e1470–7.
48. Garey CL, Laituri CA, Valusek PA, St Peter SD, Snyder CL. Management of anterior mediastinal masses in children. Eur J Pediatr Surg. 2011;21(5):310–3.
49. Acker SN, Linton J, Tan GM, et al. A multidisciplinary approach to the management of anterior mediastinal masses in children. J Pediatr Surg. 2015;50(5):875–8.
50. Littooij AS, Kwee TC, Barber I, et al. Whole-body MRI for initial staging of paediatric lymphoma: prospective comparison to an FDG-PET/CT-based reference standard. Eur Radiol. 2014;24(5):1153–65.
51. Hack HA, Wright NB, Wynn RF. The anaesthetic management of children with anterior mediastinal masses. Anaesthesia. 2008;63(8):837–46.
52. Liszewski MC, Ciet P, Sodhi KS, Lee EY. Updates on MRI evaluation of pediatric large airways. AJR Am J Roentgenol. 2017;208(5):971–81.
53. Yalcin B, Demir HA, Tanyel FC, et al. Mediastinal germ cell tumors in childhood. Pediatr Hematol Oncol. 2012;29(7):633–42.
54. Schneider DT, Calaminus G, Koch S, et al. Epidemiologic analysis of 1,442 children and adolescents registered in the German germ cell tumor protocols. Pediatr Blood Cancer. 2004;42(2):169–75.
55. De Backer A, Madern GC, Hakvoort-Cammel FG, Oosterhuis JW, Hazebroek FW. Mediastinal germ cell tumors: clinical aspects and outcomes in 7 children. Eur J Pediatr Surg. 2006;16(5):318–22.
56. Takeda S, Miyoshi S, Ohta M, Minami M, Masaoka A, Matsuda H. Primary germ cell tumors in the mediastinum: a 50-year experience at a single Japanese institution. Cancer. 2003;97(2):367–76.
57. Drevelegas A, Palladas P, Scordalaki A. Mediastinal germ cell tumors: a radiologic-pathologic review. Eur Radiol. 2001;11(10):1925–32.
58. Gaerte SC, Meyer CA, Winer-Muram HT, Tarver RD, Conces DJ Jr. Fat-containing lesions of the chest. Radiographics. 2002;22 Spec No:S61–78.
59. Samuel M, Moore IE, Burge DM. Thoracic wall lipoblastoma: a case report and review of histopathology and cytogenetics. Eur J Pediatr Surg. 2000;10(1):53–7.
60. Ranganath SH, Lee EY, Restrepo R, Eisenberg RL. Mediastinal masses in children. AJR Am J Roentgenol. 2012;198(3):W197–216.
61. Lee EY. Evaluation of non-vascular mediastinal masses in infants and children: an evidence-based practical approach. Pediatr Radiol. 2009;39(Suppl 2):S184–90.
62. de Almeida CPB, Ziegelmann PK, Couban R, Wang L, Busse JW, Silva DR. Predictors of in-hospital mortality among patients with pulmonary tuberculosis: a systematic review and meta-analysis. Sci Rep. 2018;8(1):7230.
63. Lobato MN, Hopewell PC. Mycobacterium tuberculosis infection after travel to or contact with visitors from countries with a high prevalence of tuberculosis. Am J Respir Crit Care Med. 1998;158(6):1871–5.
64. Goussard P, Gie RP, Janson JT, et al. Decompression of enlarged mediastinal lymph nodes due to mycobacterium tuberculosis causing severe airway obstruction in children. Ann Thorac Surg. 2015;99(4):1157–63.
65. Goussard P, Gie R. Airway involvement in pulmonary tuberculosis. Paediatr Respir Rev. 2007;8(2):118–23.
66. Rizzi EB, Schinina V, Cristofaro M, et al. Detection of pulmonary tuberculosis: comparing MR imaging with HRCT. BMC Infect Dis. 2011;11:243.
67. Peprah KO, Andronikou S, Goussard P. Characteristic magnetic resonance imaging low T2 signal intensity of necrotic lung parenchyma in children with pulmonary tuberculosis. J Thorac Imaging. 2012;27(3):171–4.
68. Kleiman MB. Histoplasmosis. In: Cherry JD, Harrison GJ, Kaplan SL, Steinbach WJ, Hotez PJ, editors. Feigin and Cherry's textbook of pediatric infectious diseases. 7th ed. Philadelphia: Elsevier; 2014. p. 2807–32.
69. Cohen MD, Eigen H, Scott PH, et al. Magnetic resonance imaging of inflammatory lung disorders: preliminary studies in children. Pediatr Pulmonol. 1986;2(4):211–7.
70. Chabi ML, Goracci A, Roche N, Paugam A, Lupo A, Revel MP. Pulmonary aspergillosis. Diagn Interv Imaging. 2015;96(5):435–42.
71. Fujimoto K, Meno S, Nishimura H, Hayabuchi N, Hayashi A. Aspergilloma within cavitary lung cancer: MR imaging findings. AJR Am J Roentgenol. 1994;163(3):565–7.
72. Dournes G, Berger P, Refait J, et al. Allergic bronchopulmonary aspergillosis in cystic fibrosis: MR imaging of airway mucus contrasts as a tool for diagnosis. Radiology. 2017;285(1):261–9.
73. Garg MK, Gupta P, Agarwal R, Sodhi KS, Khandelwal N. MRI: a new paradigm in imaging evaluation of allergic bronchopulmonary aspergillosis? Chest. 2015;147(2):e58–9.
74. Blum U, Windfuhr M, Buitrago-Tellez C, Sigmund G, Herbst EW, Langer M. Invasive pulmonary aspergillosis. MRI, CT, and plain radiographic findings and their contribution for early diagnosis. Chest. 1994;106(4):1156–61.
75. Herold CJ, Kramer J, Sertl K, et al. Invasive pulmonary aspergillosis: evaluation with MR imaging. Radiology. 1989;173(3):717–21.
76. MacSweeney F, Papagiannopoulos K, Goldstraw P, Sheppard MN, Corrin B, Nicholson AG. An assessment of the expanded classification of congenital cystic adenomatoid malformations and their relationship to malignant transformation. Am J Surg Pathol. 2003;27(8):1139–46.
77. d'Agostino S, Bonoldi E, Dante S, Meli S, Cappellari F, Musi L. Embryonal rhabdomyosarcoma of the lung arising in cystic adenomatoid malformation: case report and review of the literature. J Pediatr Surg. 1997;32(9):1381–3.
78. Domizio P, Liesner RJ, Dicks-Mireaux C, Risdon RA. Malignant mesenchymoma associated with a congenital lung cyst in a child: case report and review of the literature. Pediatr Pathol. 1990;10(5):785–97.
79. Ozcan C, Celik A, Ural Z, Veral A, Kandiloglu G, Balik E. Primary pulmonary rhabdomyosarcoma arising within cystic adenomatoid malformation: a case report and review of the literature. J Pediatr Surg. 2001;36(7):1062–5.
80. Federici S, Domenichelli V, Tani G, et al. Pleuropulmonary blastoma in congenital cystic adenomatoid malformation: report of a case. Eur J Pediatr Surg. 2001;11(3):196–9.
81. Burge D, Wheeler R. Increasing incidence of detection of congenital lung lesions. Pediatr Pulmonol. 2010;45(1):103; author reply 104.
82. Langston C. New concepts in the pathology of congenital lung malformations. Semin Pediatr Surg. 2003;12(1):17–37.
83. Holder PD, Langston C. Intralobar pulmonary sequestration (a nonentity?). Pediatr Pulmonol. 1986;2(3):147–53.
84. Riedlinger WF, Vargas SO, Jennings RW, et al. Bronchial atresia is common to extralobar sequestration, intralobar sequestration, congenital cystic adenomatoid malformation, and lobar emphysema. Pediatr Dev Pathol. 2006;9(5):361–73.
85. Stocker JT, Madewell JE, Drake RM. Congenital cystic adenomatoid malformation of the lung. Classification and morphologic spectrum. Hum Pathol. 1977;8(2):155–71.
86. Stocker J. The respiratory tract. In: Stocker JT, LP D, editors. Pediatric pathology. 2nd ed. Philadelphia: Lippincott, Williams & Wilkins; 2001. p. 466–73.
87. Alamo L, Gudinchet F, Reinberg O, et al. Prenatal diagnosis of congenital lung malformations. Pediatr Radiol. 2012;42(3):273–83.
88. Esther CR Jr, Barker PM. Pulmonary lymphangiectasia: diagnosis and clinical course. Pediatr Pulmonol. 2004;38(4):308–13.

89. Malone LJ, Fenton LZ, Weinman JP, Anagnost MR, Browne LP. Pediatric lymphangiectasia: an imaging spectrum. Pediatr Radiol. 2015;45(4):562–9.
90. Yao LC, Testini C, Tvorogov D, et al. Pulmonary lymphangiectasia resulting from vascular endothelial growth factor-C overexpression during a critical period. Circ Res. 2014;114(5):806–22.
91. Cleveland RH, Rhein L. Newborn chest. In: Cleveland RH, editor. Imaging in pediatric pulmonology. New York: Springer; 2012. p. 81–97.
92. Chung CJ, Fordham LA, Barker P, Cooper LL. Children with congenital pulmonary lymphangiectasia: after infancy. AJR Am J Roentgenol. 1999;173(6):1583–8.
93. Dodge JA, Lewis PA, Stanton M, Wilsher J. Cystic fibrosis mortality and survival in the UK: 1947–2003. Eur Respir J. 2007;29(3):522–6.
94. Mott LS, Park J, Murray CP, et al. Progression of early structural lung disease in young children with cystic fibrosis assessed using CT. Thorax. 2012;67(6):509–16.
95. Sly PD, Gangell CL, Chen L, et al. Risk factors for bronchiectasis in children with cystic fibrosis. N Engl J Med. 2013;368(21):1963–70.
96. Wielputz MO, Mall MA. Imaging modalities in cystic fibrosis: emerging role of MRI. Curr Opin Pulm Med. 2015;21(6):609–16.
97. Wielputz MO, Eichinger M, Puderbach M. Magnetic resonance imaging of cystic fibrosis lung disease. J Thorac Imaging. 2013;28(3):151–9.
98. Puderbach M, Eichinger M, Gahr J, et al. Proton MRI appearance of cystic fibrosis: comparison to CT. Eur Radiol. 2007;17(3):716–24.
99. Puderbach M, Eichinger M, Haeselbarth J, et al. Assessment of morphological MRI for pulmonary changes in cystic fibrosis (CF) patients: comparison to thin-section CT and chest x-ray. Investig Radiol. 2007;42(10):715–25.
100. Murphy KP, Maher MM, O'Connor OJ. Imaging of cystic fibrosis and pediatric bronchiectasis. AJR Am J Roentgenol. 2016;206(3):448–54.
101. Dournes G, Grodzki D, Macey J, et al. Quiet submillimeter MR imaging of the lung is feasible with a PETRA sequence at 1.5 T. Radiology. 2015;276(1):258–65.
102. Resnick ES, Moshier EL, Godbold JH, Cunningham-Rundles C. Morbidity and mortality in common variable immune deficiency over 4 decades. Blood. 2012;119(7):1650–7.
103. Gathmann B, Mahlaoui N, Gerard L, et al. Clinical picture and treatment of 2212 patients with common variable immunodeficiency. J Allergy Clin Immunol. 2014;134(1):116–26.
104. Arslan S, Poyraz N, Ucar R, Yesildag M, Yesildag A, Caliskaner AZ. Magnetic resonance imaging may be a valuable radiation-free technique for lung pathologies in patients with primary immunodeficiency. J Clin Immunol. 2016;36(1):66–72.
105. Serra G, Milito C, Mitrevski M, et al. Lung MRI as a possible alternative to CT scan for patients with primary immune deficiencies and increased radiosensitivity. Chest. 2011;140(6):1581–9.
106. Carden KA, Boiselle PM, Waltz DA, Ernst A. Tracheomalacia and tracheobronchomalacia in children and adults: an in-depth review. Chest. 2005;127(3):984–1005.
107. Lee EY, Boiselle PM. Tracheobronchomalacia in infants and children: multidetector CT evaluation. Radiology. 2009;252(1):7–22.
108. Jacobs IN, Wetmore RF, Tom LW, Handler SD, Potsic WP. Tracheobronchomalacia in children. Arch Otolaryngol Head Neck Surg. 1994;120(2):154–8.
109. Mair EA, Parsons DS. Pediatric tracheobronchomalacia and major airway collapse. Ann Otol Rhinol Laryngol. 1992;101(4):300–9.
110. Holinger LD. Etiology of stridor in the neonate, infant and child. Ann Otol Rhinol Laryngol. 1980;89(5 Pt 1):397–400.
111. Boiselle PM, Ernst A. Tracheal morphology in patients with tracheomalacia: prevalence of inspiratory lunate and expiratory "frown" shapes. J Thorac Imaging. 2006;21(3):190–6.

Pulmonary Incidentaloma

22

Thomas Carraway, Anne C. Coates, and Charles K. Grimes

Case Presentation

A 1.5 cm nodule (Fig. 22.1) was discovered at the base of the right lung in an otherwise healthy 17-year-old girl during an emergency room evaluation of abdominal pain. The radiologist recommended a follow-up chest CT be performed. This was completed 4 months later and was found to be normal. The abdominal pain resolved spontaneously while she was in the emergency room.

Definition

The pulmonary incidentaloma refers to a pulmonary lesion discovered on a radiographic study which is unrelated to the primary process. With the advent of high-resolution CT, pulmonary nodules as small as 1–2 mm are routinely diagnosed leading to a conundrum for clinicians as there are no formal guidelines, such as the Fleischner Society Guidelines, for those under 35 years of age. Furthermore, with the advent of the Image Gently campaign [1], more consideration is being given to avoiding unnecessary radiographic studies in the pediatric population. Since the prior edition of this chapter was published, this issue has garnered more attention culminating in the publication of recommendations from the Thoracic Imaging Committee of the Society for Pediatric Radiology (SPR) [2, 3] regarding the management of the incidental pulmonary nodule.

T. Carraway (✉)
Department of Radiology, Maine Medical Center, Portland, ME, USA
e-mail: tcarraway@mmc.org

A. C. Coates
Department of Pediatrics, Stanford School of Medicine/Lucille Packard Children's Hospital, Palo Alto, CA, USA

C. K. Grimes
Department of Radiology, Maine Medical Center, Portland, ME, USA

Where the Issue Stands Today

The incidence of pulmonary nodules in children is not known. One study of roughly 5000 pediatric patients undergoing *abdominal* CT scan diagnosed pulmonary nodules in only 1.2% [4]. Importantly, of the 1.2% of children with a nodule, only two were malignant, and both occurred in patients with a known malignancy and in nodules greater than, or equal to, 7 mm. Another study of 72 children undergoing trauma CT of the chest diagnosed nodules in 38% of patients [5]. These two studies very nearly represent all that is known about the incidence of the incidental pulmonary nodule in children.

When found, what do we know about the clinical importance of a nodule? Does it represent underlying malignancy? The available data to answer those questions is limited. A retrospective study of biopsied pulmonary nodules rendered a ratio of 1.4 benign to 1 primary malignancy of the lung to 11.6 metastatic lesions [6]. However, only nodules and masses which were excised were studied; therefore these patients likely had an increased risk profile necessitating the removal of the nodule or mass in the first place. This information cannot be extrapolated to the general population. This study suggests metastatic nodules or masses are relatively more common than primary lung cancer in the pediatric population. A retrospective single-institution study [7] of primary lung cancers concluded they are extremely rare (40 cases in 90 years) and almost always symptomatic at presentation.

The prognostic implications of the imaging characteristics of pulmonary nodules are also limited. A review of the available data by the Thoracic Imaging Committee of the SPR [2] reveals linear or ground-glass opacifications are more likely to represent infection or inflammation rather than underlying malignancy. They conclude, however, not enough is known about the natural course of the solid pulmonary nodule to confidently state how size, shape, margin, or calcification speaks to the risk of underlying malignancy. There are some findings classically considered benign

R. H. Cleveland, E. Y. Lee (eds.), *Imaging in Pediatric Pulmonology*, https://doi.org/10.1007/978-3-030-23979-4_22

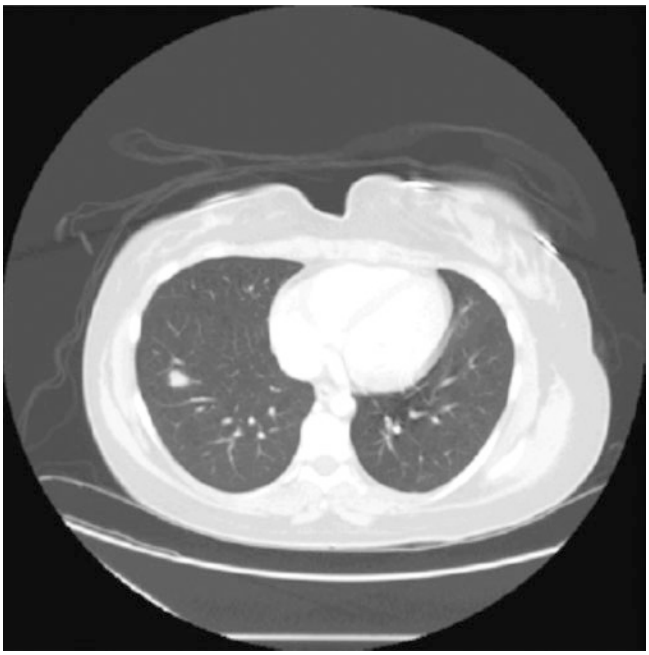

Fig. 22.1 Imaging of the lung bases, obtained as part of an abdominal CT, reveals an approximately 1.5 cm nodule in the right lower lobe

which can enter into a holistic evaluation of the patient when a nodule is diagnosed such as uniform calcification, features consistent with a pleural lymph node or macroscopic fat containing lesion representing a hamartoma. However, these imaging features should take on a secondary role relative to the clinical history of the patient. Although there are no clear numbers, it is suspected radiologists are over-recommending follow-up studies for pulmonary nodules which are almost certainly benign. Prior to making a recommendation, one should consider radiation is not benign and has demonstrable risks associated with it [8]. Furthermore there are no clear guidelines to follow. The 2017 update of the Fleischner Society guidelines [9] state for children and adults under 35 years of age, "these guidelines are not appropriate for such patients…management decisions should be made on a case-by-case basis." Thus without clear guidelines, it is reasonable for the radiologist to be the driving force behind the initial management of these incidentalomas as they are likely among the few providers familiar (within the bounds of our current limited knowledge) with the likelihood serious disease lurks in the background. Given the medical literature is not definitive about the incidence, natural course, characteristics, or appropriate follow-up criteria for pulmonary incidentalomas, it is incumbent upon the radiologist to first ensure the right study is being ordered for the child and will answer the clinical question posed. Reasonable consideration should be given to alternatives that do not utilize ionizing radiation such as ultrasound or MRI. A 2009 study of pediatric chest CTs in a tertiary care center [10] noted the chest CT had a low yield of clinically relevant findings in patients with diffuse lung disease and in acquired focal lung disease. However, it was more useful in further evaluation of congenital lung disease. If a CT scan is clinically indicated, tissue not relevant to the clinical question should not be imaged. Finally, when a nodule is diagnosed, members of the Society for Pediatric Radiology (SPR) Thoracic Imaging Committee have supplied a flow chart for consideration (Fig. 22.2). They note that although "all authors are members of the Society for Pediatric Radiology (SPR) Thoracic Imaging Committee, the opinions expressed … are solely those of the authors and are not endorsed by the SPR" [3].

The primary branch point is based on the history of the patient. If there is any history of respiratory symptomatology, malignancy, immunocompromise, or risk factors for infectious or inflammatory etiologies, care and imaging follow-up should be individualized. If the nodule is truly incidental, the patient has none of the above risk factors, and if the nodule contains classically benign features, the members of the Society for Pediatric Radiology (SPR) Thoracic Imaging Committee recommend no further work-up [3]. If the nodule does not contain classically benign imaging features, the patient is placed in the individualized care category, and a discussion with the patient's provider and the patient's family should ensue.

Ideally this discussion will discuss the paucity of data regarding incidental pulmonary nodules, the lack of an evidence-based guideline, the real risk associated with repeat imaging or tissue sampling, and the risk factors the patient carries for malignancy (if any). Only after this discussion should a recommendation for follow-up evaluation be rendered.

Conclusion

The pulmonary incidentaloma remains a quandary for clinicians. There is a marked lack of data regarding their natural course yet a heightened risk of over-radiating or over-sampling children for a lesion which, in the correct patient population, is overwhelmingly likely to be benign. The incidentaloma provides an ideal opportunity for the radiologist to practice the ALARA (as low as reasonably achievable) principle following a discussion with the stakeholders in the patient's care and ultimately utilize the consultant function of a Radiologist or Pulmonologist for the benefit of the patient. Chest CT should not be used merely to avoid medicolegal risk because of the potential harm to the patient. Medicine is both art and science. For now, the evaluation of the pulmonary incidentaloma is more art than science.

Acknowledgment Dedicated to Robert Zwerdling, MD

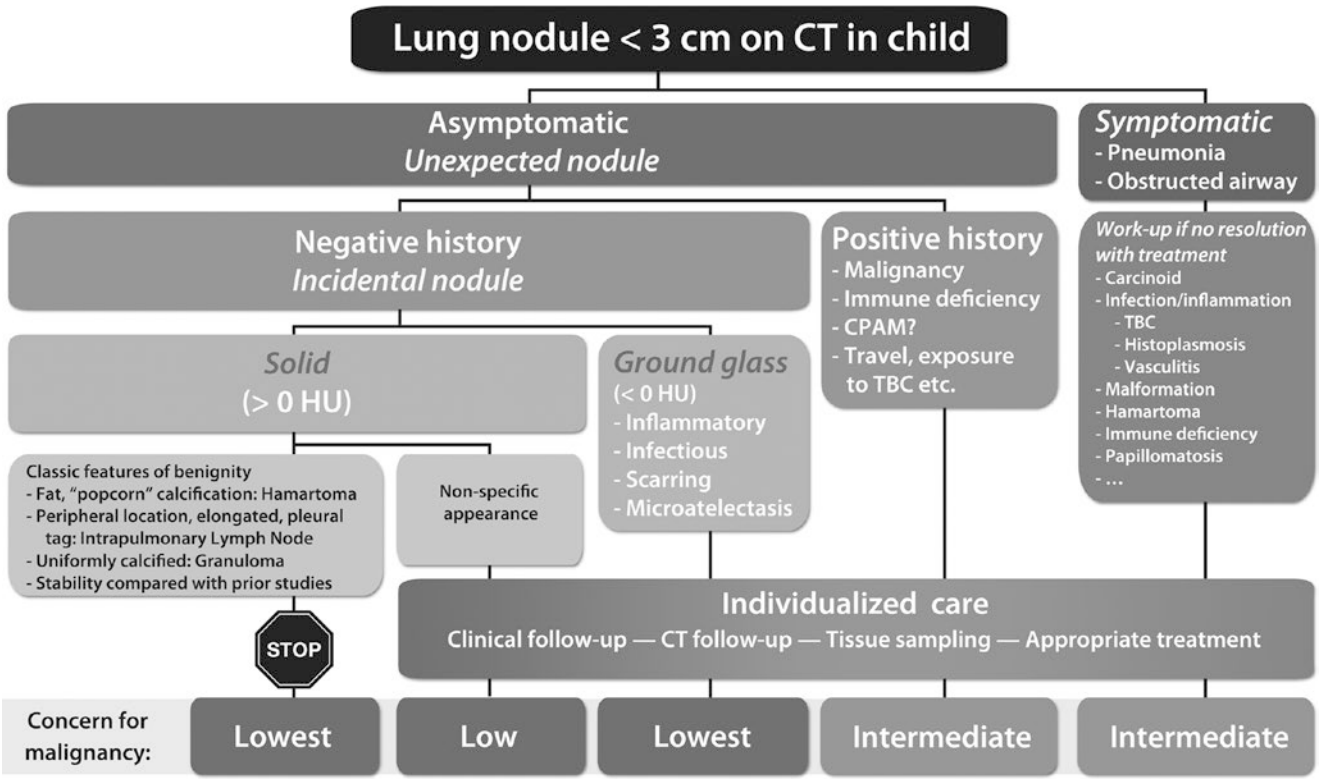

Fig. 22.2 This flow chart was published by members of the Society for Pediatric Radiology (SPR) Thoracic Imaging Committee as a "conceptual framework for the diagnostic management of a lung nodule measuring up to 3 cm in diameter on CT in a child" [3]. It is provided here with permission of the authors who note that it is provided as the authors' personal opinion and is not endorsed by the SPR

References

1. Goske MJ, Applegate KE, Bulas D, et al. Image gently: progress and challenges in CT education and advocacy. Pediatr Radiol. 2011;41:461–6.
2. Westra SJ, Brody AS, Mahani MG, et al. The incidental pulmonary nodule in a child. Part 1: recommendations from the SPR Thoracic Imaging Committee regarding characterization, significance and follow-up. Pediatr Radiol. 2015;45:628–33.
3. Westra SJ, Thacker PG, Podberesky DJ, et al. Part 2: commentary and suggestions for clinical management, risk communication and prevention. Pediatr Radiol. 2015;45:634–9.
4. Breen M, Zurakowski D, Lee EY. Clinical significance of pulmonary nodules detected on abdominal CT in pediatric patients. Pediatr Radiol. 2015;45:1753–60.
5. Samim A, Littooij AS, van den Heuvel-Eibrink MM, et al. Frequency and characteristics of pulmonary nodules in children at computed tomography. Pediatr Radiol. 2017;47:1751. [Epub ahead of print].
6. Dishop MK, Kuruvilla S. Primary and metastatic lung tumors in the pediatric population: a review and 25-year experience at a large children's hospital. Arch Pathol Lab Med. 2008;132:1079–103.
7. Yu DC, Grabowski MJ, Kozakewich HP, et al. Primary lung tumors in children and adolescents: a 90-year experience. J Pediatr Surg. 2010;45:1090–5.
8. Brenner D, Elliston C, Hall E, Berdon W. Estimated risks of radiation-induced fatal cancer from pediatric CT. Am J Roentgenol. 2001;176:289–6.
9. MacMahon H, Naidich DP, Goo JM, et al. Guidelines for management of incidental pulmonary nodules detected on CT images: from the Fleischner Society 2017. Radiology. 2017;284:228–43.
10. Schneebaum N, et al. Use and yield of chest computed tomography in the diagnostic evaluation of pediatric lung disease. Pediatrics. 2009;124:472–9.

Index

R. H. Cleveland, E. Y. Lee (eds.), *Imaging in Pediatric Pulmonology*, https://doi.org/10.1007/978-3-030-23979-4